Libro de resúmenes

XXXVIII Reunión Bienal de la Real Sociedad Española de Física

Murcia, 11-15 de julio de 2022

Editores: Rafael García Molina, Miguel Ortuño

Real Sociedad Española de Física

R.S.E.F.

XXXVIII Reunión Bienal Murcia, 11-15 julio 2022 Real Sociedad Española de Física

ISBN: 978-84-09-46885-0 (no comercial)

Editorial: Real Sociedad Española de Física

Título: XXXVIII Bienal de Física de la Real Sociedad Española de Física

Subtítulo: Libro de resúmenes

Editado por: Real Sociedad Española de Física

Editores del volumen: García Molina, Rafael; Ortuño Ortín, Miguel

Formato: Digital

Número de páginas: 592

Idioma: Inglés, Español/Castellano

Cubierta: Basada en el diseño del cartel de la Bienal realizado por Gonda de Goa Knaack

Contracubierta: Fotografía realizada por Rafael García Molina

Logotipo de la Bienal de Física en Murcia: Pedro M. Prieto Corrales

Publicado en: Diciembre de 2022

Índice de contenidos

Comités

Patrocinadores

Actos sociales

Compendio fotográfico

Textos preliminares

Conferencias plenarias

XXXI Encuentro Ibérico de Enseñanza y Divulgación de la Física

Mujeres en Física

Didáctica e Historia de la Física

Física Médica

Termodinámica y Análisis Térmico

Física de la atmósfera y el océano

Información y Computación Cuánticas

Tecnologías Cuánticas

Óptica Cuántica y Óptica No Lineal

Inteligencia Artificial en Física de la Materia Condensada

Fronteras en Materia Blanda Condensada

Nuevos retos en superconductividad

Sistemas interactuantes de baja dimensionalidad fuertemente correlacionados

Avances en la caracterización de nanomateriales mediante Microscopía de Fuerzas Atómicas

Nuevas fronteras y retos en magnetismo

Energía y Sostenibilidad

Física Teórica y de Partículas

Nanociencia y Materiales Moleculares

Física de Plasmas y sus Aplicaciones

Astrofísica y Astropartículas

Física de Sistemas Complejos

Tópicos Avanzados en Óptica

Física Nuclear

Ampliando horizontes: interdisciplinariedad, física general e investigación novel

Otros actos

Comités

Presidentes:
Pablo Artal Soriano, Universidad de Murcia
Miguel Ortuño Ortín, Universidad de Murcia

Comité organizador:
Enrique Josua Fernández Martínez
José Juan Fernández Melgarejo
Rafael García Molina
Sonia Jerez
Pedro Jiménez Guerrero
María Luisa López Ibáñez
Rosa Maria Martinez Ojeda
Mario Navarro Rodríguez
Alba Paniagua Díaz
Pedro Prieto Corrales
Pablo de Vera Gomis

Comité científico:
Eva Acosta, Universidade de Santiago de Compostela
Bárbara Álvarez González, Universidad de Oviedo (DFTP)
Pablo Ares García, Universidad Autónoma de Madrid
Rosa María Benito Zafrilla, Universidad Politécnica de Madrid (GEFENOL)
Jorge Bravo-Abad, Universidad Autónoma de Madrid (DFMC-GEFES)
Juan Manuel Bueno, Universidad de Murcia
María José Calderón, ICMM, CSIC (DFMC-GEFES)
Pedro Carpena Sánchez, Universidad de Málaga (GEFENOL)
Dolores Cortina, Universidad de Santiago de Compostela (GRFN)
Alexander Dauphin, ICFO (DFMC-GEFES)
Antonio Dobado González, Universidad Complutense de Madrid (DFTP)
Enrique Josua Fernández Martínez, Universidad de Murcia
A. Fernandez-Nieves, Universitat de Barcelona - UBICS (DFMC-GEFES)
Jose Angel Fernández-Roldán, Universidad de Oviedo
Ricardo García Herrera, Universidad Complutense de Madrid (GEFAO)
Pascuala García Martínez, Universitat de València (GEMF)
Roberto Gomez-Calvet (GEE)
Isabel Guillamón, Universidad Autónoma de Madrid (DFMC-GEFES)
Antonio Guirao Piñero, Universidad de Murcia
Carlos Hernández-García, Universidad de Salamanca (GEOCONL)
Miriam Jaafar, Universidad Autónoma de Madrid
Gabriela Llosá Llácer, Instituto de Física Corpuscular (CSIC-Univ. València) (GEFM)
Joaquín López Herraiz, Universidad Complutense de Madrid (GEFM)
María José Martínez-Pérez, Universidad de Zaragoza (DFMC-GEFES)
Manuel Martínez Piñeiro, Universidad de Vigo (GECAT-GET)
Mariela Menghini, IMDEA (DFMC-GEFES)
Gabriel Molina Terriza, Material Physics Center, San Sebastián (GEOCONL)
Luis Moreno Martínez (GEDH)
Román Orús, Donostia International Physics Center, San Sebastián (GEIC)
Ignacio Pagonabarraga, Universitat de Barcelona - UBICS (DFMC-GEFES)

Comité de honor

Presidente: S. M. el Rey Don Felipe VI

Fernando López Miras, Presidente de la Comunidad Autónoma de Murcia
Diana Morant Ripoll, Ministra de Ciencia e Innovación
José Antonio Serrano Martínez, Alcalde de Murcia
María del Valle Miguélez Santiago, Consejera de Empresa, Empleo, Universidades y Portavocía de la Comunidad Autónoma de Murcia
Eloísa del Pino Matute, Presidenta del Consejo Superior de Investigaciones Científicas
José Luján Alcaraz, Rector Magnífico de la Universidad de Murcia
Perla Wahnón Benarroch, Presidenta de la Confederación de Sociedades Científicas de España
Luis Viña Liste, Presidente de la Real Sociedad Española de Física
David Christian de la Fe Rodríguez, Director General de Universidades de la Comunidad Autónoma de Murcia
María Isabel Fortea Gorbe, Directora General de Investigación e Innovación Científica de la Comunidad Autónoma de Murcia
María Senena Corbalán García, Vicerrectora de Investigación de la Universidad de Murcia
Ángel Pérez Ruzafa, Presidente Academia de Ciencias de la Región de Murcia
Pedro Lozano Rodríguez, Decano de la Facultad de Química de la Universidad de Murcia

Patrocinadores

HAMAMATSU
PHOTON IS OUR BUSINESS

mtb
TECNOLOGÍA DE PRECISIÓN

UAM | IfiMAC

SPIE.

FUNDACIÓN CIUDAD DE REQUENA

innova scientific

LASING

Materials Advances

Journal of Materials Chemistry C

Patrocinadores institucionales

UNIVERSIDAD DE MURCIA

PREMIOS REI JAUME I

ACADEMIA DE CIENCIAS de la REGIÓN DE MURCIA

IDE INSTITVTO D ESPAÑA

IUPAP Centenary YEARS 1922 - 2022

IYBSSD2022
International Year of Basic Sciences for Sustainable Development

Actos sociales

11/07 Lunes por la noche: Cóctel de bienvenida
Hora: 20:30
Lugar: Hotel Occidental Siete Coronas

12/07 Martes por la noche: Física para tod@s
Hora: 20:00
Lugar: Patio Campus de la Merced

13/07 Miércoles por la noche: Cena de gala
Hora: 20:30
Lugar: Finca Buenavista

15/07 Jueves al mediodía
Hora: 13:30
Lugar: Patio Campus de la Merced

15/07 Viernes al mediodía: Cóctel de despedida
Hora: 13:30
Lugar: Patio Campus de la Merced

Compendio fotográfico

Quantum physics: from theory to technologies
XXXVIII Reunión Bienal de la Real Sociedad Española de Física

Ondas electromagnéticas
Ciencia de materiales
Microelectrónica
Óptica
Relatividad (especial y general)
...
XXXVIII Reunión Bienal de la Real Sociedad Española de Física

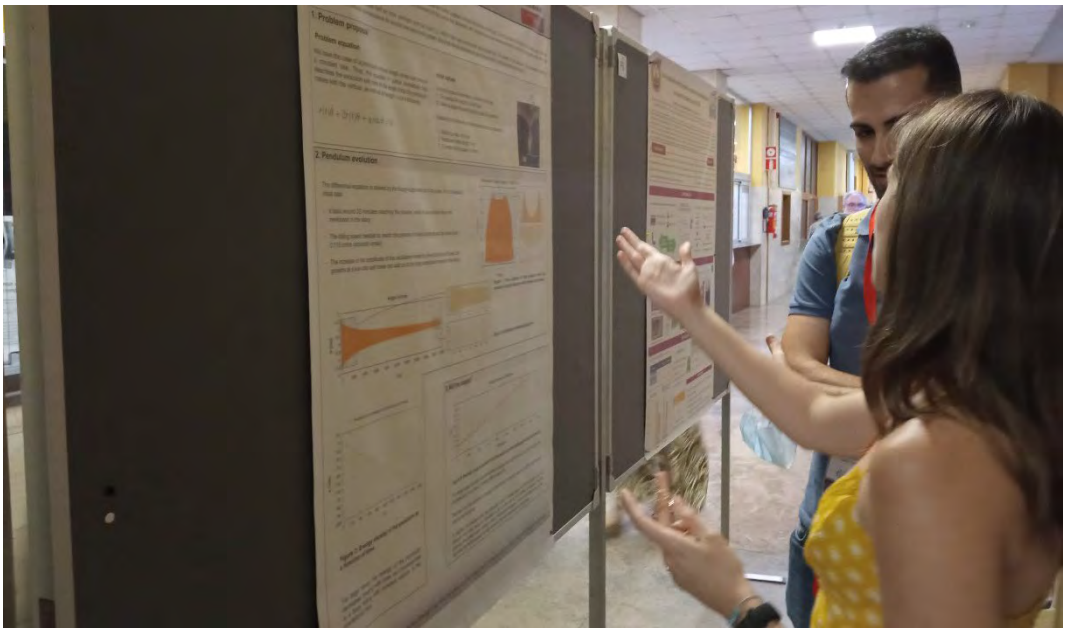

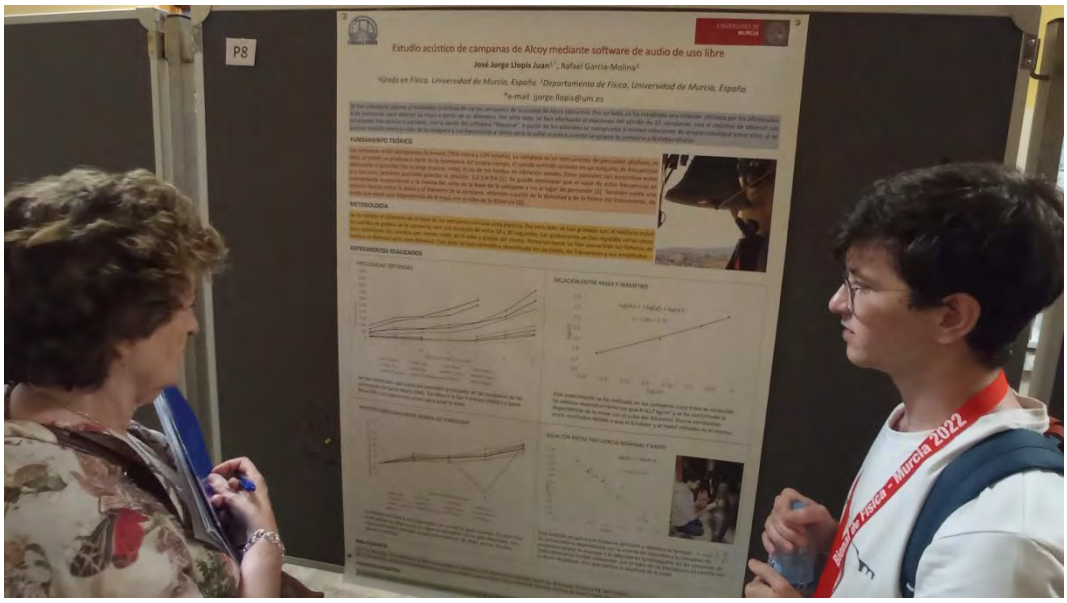
P8
Estudio acústico de campanas de Alcoy mediante software de audio de uso libre
José Jorge Llopis Juan[1*], Rafael García-Molina[2]
[1]Grado en Física, Universidad de Murcia, España. [2]Departamento de Física, Universidad de Murcia, España.
*e-mail: jjorge.llopis@um.es
FUNDAMENTO TEÓRICO
METODOLOGÍA
EXPERIMENTOS REALIZADOS
Joven Física - Murcia 2022

Prólogo del presidente de la RSEF

Luis Viña

Finalmente, la *XXXVIII Reunión Bienal de la Real Sociedad Española de Física* se celebra en el Campus de la Merced de la Universidad de Murcia en la semana del 11 al 15 de julio de 2022. Esto corresponde a tres años (menos una semana) de la última Bienal celebrada en Zaragoza en julio de 2019, rompiendo la periodicidad de dos años que se venía manteniendo desde el año 1985 en que tuvo lugar la XX Reunión en Sitges (Barcelona). La pandemia, que todavía no parece estar totalmente superada, ha obligado a cambiar los planes originales y posponer la celebración en un año para así poder celebrar la Bienal de forma presencial, lo que indudablemente contribuye a una mejor comunicación de ideas, a la interacción entre los participantes y a la creación de nuevas colaboraciones, ingrediente esencial para el avance de la Ciencia. Con toda seguridad, este aplazamiento tendrá sus frutos.

En esta ocasión, la Bienal está compuesta por 24 simposios, que se celebrarán por las tardes, cuatro de ellos transversales: "XXXI Encuentro Ibérico de Enseñanza y Divulgación de la Física", "Mujeres en Física", "Didáctica e Historia de la Física" y "Ampliando horizontes: interdisciplinariedad, física general e investigación novel". Los otros veinte, organizados por las distintas divisiones y grupos especializados de la RSEF tratan temas en la frontera de los distintos campos de la Física (no se mencionan aquí en aras de la brevedad). El programa cuenta con eminentes y destacados oradores que impartirán las conferencias plenarias por las mañanas, ofreciendo a los asistentes una panorámica de temas punteros de investigación en Física, y con cuatro mesas redondas, una de ellas sobre "Energía y Sostenibilidad" en perfecto alineamiento con el aprobado por consenso en la Asamblea General de la Naciones Unidas "Año Internacional de las Ciencias Básicas para el Desarrollo Sostenible", cuya ceremonia de apertura se celebrará el 8 de julio de 2022 en la sede de la UNESCO en París. A última hora de la tarde del martes 12 de julio, también habrá un atractivo programa abierto para una audiencia general llamado "Física para tod@s". Este libro contiene las más de 500 comunicaciones presentadas en forma oral y póster en las sesiones de los diferentes simposios, cubriendo un amplio rango de especialidades, superando el número de contribuciones de las ediciones previas.

La Universidad actual que nos acoge, fundada en 1915 por el Ministerio de Instrucción Pública y Bellas Artes, en realidad es una de las más antiguas de España pues sus orígenes se remontan a 1272 (60 años después de la instauración de la primera universidad española, el Studium Generale de Palencia), coincidiendo con la concesión por parte de Alfonso X el Sabio de unas casas y una huerta a los dominicos para que construyesen su convento en el que se ubicó un centro de estudios e investigación de nivel superior. La RSEF aprecia la calurosa acogida de esta región, bien conocida como la "Huerta de Europa" por su fértil huerta, de su milenaria universidad y de la ciudad de Murcia en la que la cultura y la ciencia han ocupado un papel muy importante desde sus orígenes durante la dominación musulmana, para celebrar nuestra *XXXVIII Reunión Bienal*. Los participantes se beneficiarán no sólo de las comunicaciones científicas, técnicas y docentes de la Reunión sino también del amplio acervo cultural de la ciudad con su incomparable Catedral de Santa María en la Plaza del Cardenal Belluga, su gran conjunto de edificios barrocos y el patrimonio escultórico único de Francisco Salzillo. Estoy seguro de que no olvidaremos esta Bienal de Murcia.

Prólogo de los presidentes del comité organizador

Pablo Artal, Miguel Ortuño

La *XXXVIII Reunión Bienal de la Real Sociedad Española de Física* (RSEF) se celebra en la ciudad de Murcia del 11 al 15 de julio de 2022. Tras 120 años, es la primera vez que esta reunión de los físicos españoles viene a Murcia. Los físicos que organizamos esta reunión estamos ilusionados y agradecidos a la RSEF por su confianza y esperamos que la Bienal sea todo un éxito.

Aprovechamos estas líneas para agradecer el trabajo de todos los que han contribuido en el comité local, a las entidades colaboradoras por sus contribuciones y a la Universidad de Murcia por el uso de sus instalaciones. Tenemos 20 conferenciantes plenarios, incluyendo dos sesiones especiales de premiados Rey Jaime I y de medallistas de la RSEF. Numerosos simposios simultáneos por las tardes, además de mesas redondas sobre temas de actualidad e interés para todos los participantes.

Esta reunión bienal es un gran ejemplo de la enorme diversidad y riqueza de la física en España y de sus posibilidades para mejorar la vida de las personas en muchos aspectos. Desde aquí damos la bienvenida a la RSEF y a todos los participantes, esperando que disfruten tanto de la ciencia y tecnología que se presente como de los atractivos de nuestra ciudad.

Prefacio

Rafael García Molina, Miguel Ortuño

Este libro contiene los resúmenes correspondientes a las comunicaciones (plenarias, orales y pósteres) presentadas en la *XXXVIII Bienal de la Real Sociedad Española de Física* que se ha celebrado en Murcia en 2022. Con el propósito de uniformizar el formato de estos resúmenes, se proporcionaron plantillas en LaTeX y Word para que las emplearan los autores de los trabajos presentados a la *Bienal*. Aun así, hemos tenido que revisar y reformatear un gran número de los documentos enviados, para conseguir que el libro tenga un aspecto homogéneo, lo cual redunda en la mejora de su legibilidad y en la comodidad de su manejo. A pesar de las múltiples revisiones que hemos realizado antes de dar por acabada la composición del libro, siempre se pueden escapar pequeños detalles. Rogamos que se nos disculpe por las posibles deficiencias de maquetación que pudieran detectarse en algunos resúmenes, aunque estamos seguros de que Titivillus (el demonio burlón responsable de introducir errores en las labores de los escribas) no habrá estado ocioso durante la preparación de este libro.

Si la forma de un escrito es importante para que su mensaje llegue de manera eficiente a los lectores, lo que realmente importa en un documento de las características que nos ocupan es el fondo (esto es, su contenido), cuya responsabilidad recae exclusivamente en los autores de los casi 550 resúmenes que aparecen en este volumen, los cuales abarcan las principales áreas de la física.

Los resúmenes de las comunicaciones presentadas durante la *XXXVIII Reunión Bienal de la RSEF* están agrupados siguiendo el esquema de simposios organizados por las divisiones y los grupos especializados de la RSEF, precedido por las conferencias plenarias. Al principio de cada simposio aparece el correspondiente programa de la *Bienal*. A continuación, se presentan los resúmenes de las comunicaciones, agrupadas en las categorías de orales y de pósteres, siguiendo el orden de dicho programa.

Dado que este documento está disponible en formato electrónico, no hemos creído necesario dotarlo de un índice de autores, puesto que las contribuciones de cada persona (o sobre alguna temática concreta) pueden localizarse sencillamente, empleando la herramienta de búsqueda propia del visor de documentos que cada individuo emplee.

Conferencias plenarias

Conferencias plenarias

Lunes 11/07:

Presidenta de sesión: Perla Wahnon

09:00-09:35 Welcome / Acto de bienvenida

09:35-10:10 Pedro Miguel Echenique Landiribar (Donostia International Physics Centre). *Ciencia después de la pandemia. La sublime utilidad de la ciencia inútil*

10:10-10:45 Pilar Hernández Gamazo (IFIC, Universitat de Valencia-CSIC). *On the matter-antimatter asymmetry*

10:45-11:15 **Café**.

11:15-11:50 María Ángeles Chamarro Calvo (Sorbonne Université-- Institut de Nanosciences de Paris). *Lo que siempre quiso saber sobre los excitones y las perovskitas a base de halógenos pero nunca se atrevió a preguntar...*

11:50-13:20 Mesa redonda. *Promoting Gender Equality in Physics in Europe*

GENERA (Gender Equality Network in Physics in the European Research Area): Lisa Kamlade (Deutsches Elektronen-Synchrotron DESY, Germany).

WIDERA project (Horizon Europe) and QUANTERA project (European partnership on Quantum technologies): Lydia González (Spanish Foundation for Science and Technology, Spain).

JUNO Project: Jane Smith and Fiona Dorrington (Institute of Physics, UK).

Moderadora: Pas García Martínez (Universitat de València)

Martes 12/07:

Presidenta de sesión: María Ángeles Chamarro Calvo

09:00-09:35 Àngels Ramos Gómez (Universitat de Barcelona). *Strangeness Nuclear Physics and astrophysical implications*

09:35-10:10 Alejandro González-Tudela (Instituto de Física Funsamental, CSIC). *Nanophotonics for quantum technologies*

10:10-10:45 Rafael Garcia-Molina (Universidad de Murcia). *Physics in everyday life*

10:45-11:15 **Café**.

11:15-11:50 María Luisa Castaño Marín (CIEMAT). *¿De que hablamos cuando decimos Transición Energética?*

11:50-13:20 Mesa redonda. *Energía y sostenibilidad*

Mercedes Ballesteros (CIEMAT).

Roberto Gomez Calvet (Universida Europea de Valencia).

Antonio Gonzalez Jiménez (Director de Estudios y Apoyo Técnico en Foro Nuclear).

Maria de la Mercedes Vazques (Sostenibilidad y Medio Ambiente en Red Eléctrica Española).

Moderadora: María Luisa Castaño Marín (CIEMAT)

Miércoles 13/07:

Sesión de Medallas de la RSEF

Presidente de sesión: Luis Viña

09:00-09:50 Eugenio Coronado Miralles (Universitat de Valencia). *Molecular Control Over the Properties of 2D Materials*

09:50-10:40 Pablo Artal Soriano (Universidad de Murcia). *Peripheral optics in the eye: from myopia to cataracts*

10:45-11:15 **Café**.

11:15-11:50 Florian Macquardt (Max Planck Institute for the Science of Light). *Physical Self-Learning Machines*

11:50-13:20 Mesa redonda. *Agencia Estatal de Investigación*

Domènec Espriu Climent, Director de la AEI (Universitat de Barcelona).

Francisco J. García Vidal, Presidente del área de Ciencias físicas de la AEI (Universidad Autónoma de Madrid).

Moderador: Pablo Artal Soriano (Universidad de Murcia)

Jueves 14/07:

Sesión de Premiados Jaume I

Presidente de sesión: Pablo Artal

09:00-09:05 Javier Quesada (Secretario General de la Fundación). *Presentación*

09:05-09:35 Laura Lechuga Gómez (Catalan Institute of Nanoscience and Nanotechnology). *Nanophotonic biosensors for ultrasensitive and decentralised diagnostics at the point-of-need*

09:35-10:10 Francisco J. García Vidal (Universidad Autónoma de Madrid). *Nanophotonics: the first 30 years*

10:10-10:45 Licia Verde (Universitat de Barcelona). *Precision Cosmology, when the party is over*

10:45-11:15 **Café**.

11:15-11:50 Rafael Rebolo (Instituto de Astrofísica de Canarias). *High precision spectroscopy in astrophysics: implications on fundamental physics and the characterization of Earth-like planets*

11:50-13:20 Mesa redonda. *Presente y Futuro de las Grandes Instalaciones Científico-Técnicas*

Ángela Fernández Curto (Subdirectora General Adjunta de Grandes Instalaciones Científico-Técnicas, Madrid).

Caterina Biscari (Sincrotrón ALBA, Barcelona).

Luis Roso (Centro de Láseres Pulsados de Salamanca).

Martín Guerrrero (Instituto de Astrofísica de Andalucía, Granada).

Carlos Peña (Laboratorio Subterráneo de Canfranc, Huesca).

Moderador: Juan M. Bueno (Universidad de Murcia)

Viernes 15/07:

Presidente de sesión: Miguel Ortuño

09:00-09:40 Boris Altshuler (Columbia University). *Many-body localization*

09:40-10:20 Pablo Jarillo-Herrero (Massachussetts Institute of Technology). *The Magic of Moiré Quantum Matter*

10:20-10:45 Entrega de Premios de los concursos de Estudiantes y de Jóvenes Doctores.

10:45-11:15 **Café**.

11:15-12:00 Centenario de la IUPAP

Luis Viña, Presidente del Comité de Enlace Español de la IUPAP, Universidad Autónoma de Madrid.

Raúl Toral, Miembro de la Comisión C3-Física Estadística, Universitat de les Illes Balears.

Hermann Suderow, Miembro de la Cosmisión C5-Física de Bajas Temperaturas, Universidad Autónoma de Madrid.

Gloria Platero, Secretaria de la Comisión C8-Semiconductores, Instituto de Ciencia de Materiales de Madrid-CSIC.

Alfonso Muñoz, Miembro de la Comisión C20-Física Computacional, Universidad de La Laguna.

12:00-13:15 Junta General Ordinaria de la Real Sociedad Española de Física

13:15-14:30 Cóctel de despedida

Conferencia plenaria

Ciencia después de la pandemia. La sublime utilidad de la ciencia inútil

Pedro Miguel Echenique

Fundación DIPC, Pº Manuel de Lardizabal 4, 20018 Donostia - San Sebastián, España.

e-mail: pedromiguel.echenique@ehu.es

La pandemia del Covid ha puesto a la ciencia en el escaparate y ha revelado su importancia decisiva para el futuro de la humanidad. También ha revelado la importancia de la comunicación científica, y la necesidad de entender correctamente cómo funciona la ciencia.

La ciencia actual no contesta a todo, está en una fase primitiva e infantil, pero es lo mejor que tenemos, la gran esperanza de la humanidad.

Más importante, y sobre todo más rentable que fijar objetivos a la ciencia, es crear una atmósfera, un caldo de cultivo donde la creatividad pueda florecer. Los cambios cualitativos, los grandes avances de la Humanidad, han surgido de preguntas fundamentales de la Ciencia Básica.

Sería un error centrarnos solamente en lo biomédico, o en lo aplicado. Si así lo hacemos podemos avanzar en problemas conocidos, pero seremos sorprendidos cuando aparezcan nuevos frentes. No sabemos lo que va a venir por lo que tenemos que tener un arsenal de posibilidades que solo puede venir de la ciencia básica.

Incluso en la práctica médica el desarrollo de la curiosidad acerca de los hechos básicos de la naturaleza ha demostrado ser la ruta más eficiente para conseguir medicinas y aparatos con éxito.

La preeminencia en investigación requiere mucho, no puede adquirirse en pocos años, pero puede dañarse rápidamente.

On the matter-antimatter asymmetry

Pilar Hernández

Instituto de Física Corpuscular, Universidad de Valencia and CSIC, Catedrático José Beltrán 2, E-46980 Paterna, Spain.

e-mail: m.pilar.hernandez@uv.es

The existence of ordinary matter in the Universe remains an unsolved mystery. The possibility that it might be understood from the fundamental properties of particle interactions is under intensive investigation, both from a theoretical as well as an experimental point of view. Three essential ingredients are required: violation of the charge conjugation and parity symmetries of fundamental interactions, the non-conservation of baryon number, and a cosmological evolution that is not fully thermal. I will review recent progress in this area and explain what are the future measurements that can reveal the origin the matter-antimatter asymmetry.

Conferencia plenaria

Lo que siempre quiso saber sobre los excitones y las perovskitas a base de halógenos pero nunca se atrevió a preguntar

Maria Angeles Chamarro Calvo

Sorbonne Université - Institut de Nanosciences de Paris, Paris, France.

e-mail: Maria.Chamarro@insp.jussieu.fr

Las perovskitas a base de halógenos han sido durante estos últimos años, y continúan siendo, el centro de la atención de una multitud de estudios y conferencias sobre los temas de la optoelectrónica y las aplicaciones fotovoltaicas. Estos materiales aparecen como una nueva clase de semiconductores que han permitido una sorprendente y fulgurante evolución del rendimiento fotovoltaico en las células solares y que presentan una eficiencia de emisión excepcional. A la base de estas propiedades se encuentra el "exciton", la pareja formada por un electrón y un hueco, que aparece en el material semiconductor después de una absorción de fotones de energía superior a la energía de la banda prohibida.

En esta charla nos centraremos sobre la descripción de las principales características de los excitones en las perovskitas a base de halógenos y discutiremos su íntima relación con el rendimiento fotovoltaico y con la eficiencia de emisión de estos materiales.

Strangeness Nuclear Physics and astrophysical implications

Àngels Ramos

Departament de Física Quàntica i Astrofísica i Institut de Ciències del Cosmos, Universitat de Barcelona, Marti i Franquès 1, 08028 Barcelona, Spain.

e-mail: ramos@fqa.ub.edu

Strangeness Nuclear Physics extends the scope of conventional nuclear physics to a new degree of freedom (strangeness) and accommodates a variety of new phenomena which have fascinating consequences in various fields of research.

Hypernuclei are bound systems composed of neutrons, protons, plus one or more strange baryons, like the hyperons Λ, Σ or Ξ. Spectroscopic studies of hypernuclei permit constraining the properties of the hyperon-nucleon and hyperon-hyperon interactions. These are crucial ingredients for understanding the physics of neutron star interiors, where the extreme density conditions favor the presence of hyperons which reduce the maximum mass the star can support, challenging many of the present models of the nuclear equation-of-state.

Strangeness in nuclear matter can also be present in the form of mesons, like the antikaons. Provided their nuclear interactions are attractive enough, it has been argued that negatively charged antikaons could replace energetic electrons inside a neutron star, giving rise to the phenomenon of kaon condensation. Although still a matter of debate, the more modern theories do not support this claim, but new information on the antikaon nuclear interaction from kaonic atoms experiments or heavy-ion collisions might soon resolve this issue.

In this talk I will review the progress, challenges, and state-of-the art developments in the field of strangeness nuclear physics, paying a special attention to problems and phenomena of astrophysical relevance.

Nanophotonics for quantum technologies

Alejandro González-Tudela

Instituto de Física Fundamental. Consejo Superior de Investigaciones Científicas.
C/ Serrano 113bis, CP 28006. Madrid. Spain.

e-mail: a.gonzalez.tudela@csic.es

Recent experimental advances in the integration of quantum emitters with nanophotonic structures opens up unprecedented for quantum technologies [1]. In particular, the low dimensionality of the photons enables to obtain longer ranged interactions than with free-space setups that can be harnessed for quantum simulation purposes [2], as well as for improving the figures of merit of non-classical light-generation [3]. Besides, the possibility to engineer topologically non-trivial photonic band structures [4] opens the realization of topological light-matter interfaces [5], opening a path to engineer robust quantum devices based on such effects [6]. In this talk, I will review some of my main contributions to this field [2,3,6].

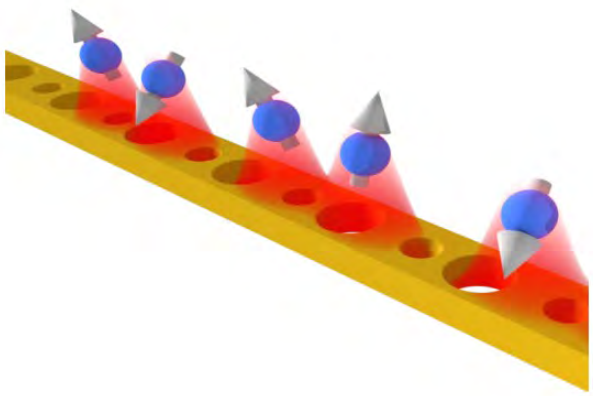

Figure 1. Quantum emitters interacting with the confined photonic modes propagating in photonic crystals

[1] D. E. Chang, J. S. Douglas, A. Gonzalez-Tudela, C. L. Hung, H. J. Kimble, *Reviews of Modern Physics* **90** (3), 031002 (2018).
[2] A. Gonzalez-Tudela *et al*., *Nat. Photonics* **9** (5), 320 (2015); J. Douglas *et al.*, *Nat. Photonics* **9** (5), 326 (2015).
[3] A. Gonzalez-Tudela *et al*., *Phys. Rev. Lett.* **115** (16), 163603 (2015); *Phys. Rev. Lett.* **118** (21), 213601 (2017).
[4] T. Ozawa *et al*., *Rev. Mod. Phys.* **91**, 015006 (2019).
[5] S. Barik *et al*., *Science* **359,** 666 (2018).
[6] M. Bello, G. Platero, I. Cirac, A. Gonzalez-Tudela, *Science Advances* **5** (7), eaaw0297e (2019); I. García-Elcano, A. Gonzalez-Tudela, J. Bravo-Abad, *Phys. Rev. Lett.* **125** (16), 163602 (2020); E. Kim *et al.*, *Phys. Rev. X* **11** (5), 011015 (2021); C. Vega *et al*., Phys. Rev. A **104** (5), 053522 (2021).

Acknowledgements: AGT acknowledges support from CSIC Research Platform on Quantum Technologies PTI-001, from Spanish project PGC2018-094792-B-100 (MCIU/AEI/FEDER, EU), and from the Proyecto Sinérgico CAM 2020 Y2020/TCS-6545 (NanoQuCo-CM).

Physics in everyday life

Rafael Garcia-Molina

Departamento de Física – Centro de Investigación en Óptica y Nanofísica, Universidad de Murcia, E-30100 Murcia, Spain.

e-mail: rgm@um.es

We can find numerous phenomena and activities in everyday life where physics is present. In addition to the technological devices that make our lives easier (such as GPS, lasers, computers…, which will not be discussed in this talk), it is enough to look around us to be acquainted how physics permeates our daily lives, in circumstances as diverse as sports events (curved trajectories of ball throws, reduction of friction through the design of sportswear...) [1], circus shows (risky balances and synchronization of trapeze artists...) [2], visits to amusement parks (where conservation of energy is present in roller coaster rides, or how you can perform experiences of weightlessness during free fall…) [3], magic shows (with challenges to the laws of nature that are nothing more than a consequence of optical, mechanical, magnetic effects...) [4]. Physics is also at the foundations of toys (from classic ones as the spinning top or the yo-yo, to more recent innovations, such as the Levitron) [5], after-lunch conversations can be enriched with physics entertainments, the (un)plausibility of physics laws can be checked in the storyline of many science fiction films and novels [6], and even references to physics appear in opera [7]. These are just a few examples of the many cases in which physics can be appreciated and enjoyed just around us. But to perceive these manifestations of physics all over we need to open our eyes (as well as all of our senses) and especially our minds.

Throughout this plenary talk different topics (and even historical periods) will be covered where I will present various examples of the role that physics has had and has in our daily lives, showing that this scientific discipline is everywhere and can also be fun (two important points to raise awareness in society of the importance of physics in our daily lives).

[1] J. E. Goff, *Gold Medal Physics. The Science of Sports*, The Johns Hopkins University Press (2010).
[2] *The Science Behind the Circus with Imperial Opa*, https://scienceatl.org/the-science-behind-the-circus-with-imperial-opa/Authors (December 18, 2017); A. Volfson, H. Eshach, Y. Ben-Abu, *Physical Review Physics Education Research* **16**, 010134 (2020).
[3] C. Escobar, *The Physics Teacher* **28**, 446 (1990); J. R. Dennison, *Amusement Park Physics Curriculum Manual*, Utah State University (1996).
[4] Robert-Houdin, *Magia y física recreativa (obra póstuma)*, Pascual Aguilar Editor (1887). [Reproducción facsímil en la editorial Alta Fulla, Barcelona, 1998].
[5] R. Garcia-Molina, *Revista de Física (Societat Catalana de Física)* **2**, 34 (1998); H. Biezeveld, R. Garcia-Molina, *Physics on Stage 2000*, p. 28, ESA Publications Division (2001); J. Güémez, C. Fiolhais, M. Fiolhais, *Physics Education* **44**, 53 (2009).
[6] M. Moreno Lupiáñez, J. José Pont, *De King Kong a Einstein. La física en la ciencia ficción*, Edicions UPC, 1999; R. Flack, *Physics Education* **44**, 430 (2009).
[7] R. Garcia-Molina, Un físico en la ópera (Círculo de Bellas Artes de Madrid, 10 de marzo de 2016), https://www.youtube.com/watch?v=OM7h68n3iSA

What are we talking about when we say energy transition?

Maria Luisa Castaño

Centro de Investigaciones Energeticas, medioambientales y tecnológicas. CIEMAT, Spain.

e-mail: mluisa.castano@ciemat.es

There is no doubt about the most important challenge facing the planet: global warming caused by human activity. The development of modern society and its industrialization linked to the use of enormous amounts of fossil fuels have caused an increase in the concentration of greenhouse gases (GHG) in the earth's atmosphere, the main consequence of which is the increase in the planet's temperature.

Global warming, as a consequence of the use of fossil fuels, is causing a deterioration of the planet of such magnitude that, if the energy paradigm was not radically changed immediately, the effects would be irreparable

The historic Paris Agreement on Climate Change in 2015 confirms a growing interest in achieving viable energy solutions with low or zero CO2 emissions, economically competitive and integrated into the energy system. In the case of the European Union (EU), the legislative package "Clean Energy for all Europeans" and the European Green Deal, establish binding objectives for the EU to 2030.

One of the obligations established by this proposal is that the Member States have to carry out “Integrated National Energy and Climate Plans” with objectives, goals and contributions until 2030 and 2050, and frame them in their national legislation. Spain, immersed in this process, has drawn up its National Integrated Energy and Climate Plan (PNIEC), with the commitment to reduce greenhouse gas emissions by 23% compared to the 1990 level, to reach 42% renewable energy on the use of final energy in the country, a 74% penetration of renewable energies in the electrical system and an improvement in energy efficiency of 39.5%.

These objectives represent a radical change in the way of generating and consuming energy, with a direct impact on residential and services use of energy, on the electrical system, on the mobility of people and goods, as well as the energy use of industry.

In this process of energy transition you can be an actor or a spectator. Being a protagonist means taking advantage of opportunities to achieve national energy, technological and industrial sovereignty

Molecular Control Over the Properties of 2D Materials

E. Coronado

Instituto de Ciencia Molecular, Universitat de Valencia, C/ Catedrático José Beltrán 2, Paterna, Spain.

e-mail: eugenio.coronado@uv.es

Graphene and other 2D materials are almost exclusively based on inorganic lattices. Except for the chemical functionalization of the surface of the 2D material, molecules have been scarcely considered in this area. Here I will focus on the association of functional molecules with 2D materials with the aim of creating smart molecular/2D heterostructures in which the properties of the "all surface" 2D material are tuned *via* an active control of the hybrid interface. This new class of heterostructures may be at the origin of a novel generation of hybrid materials and devices of direct application in highly topical fields like electronics, spintronics and straintronics. To reach this goal I propose to interface stimuli-responsive molecular systems with graphene and semiconducting transition metal dichalcogenides (MoS_2 and WSe_2). As smart-molecular systems I will choose magnetic spin-crossover materials able to switch between two spin states upon the application of an external stimulus (temperature, light or pressure) [2]. This spin transition is always accompanied by a significant change of volume in the material (by ca. 10%), so it can generate strain in its surroundings. I will show that in these heterostructures the electronic properties of graphene and the optical photoluminescence of monolayers of semiconducting metal dichalcogenides can be switched by light or by varying the temperature due to the strain concomitant to the spin transition [3, 4].

[1] J. Lopez-Cabrelles *et al*, *J. Am. Chem. Soc.* **143**, 18502 (2021).
[2] E. Coronado, *Nature Rev. Mater.* **5**, 87 (2020).
[3] R. Torres-Cavanillas *et al*, *Nature Chem.* **13**, 1101 (2021).
[4] C. Boix-Constant *et al*, *Adv. Mater.* **34**, 2110027 (2022).

Peripheral optics in the eye: from myopia to cataracts

Pablo Artal

Laboratorio de Óptica de la Universidad de Murcia (LOUM)
Departamento de Física, Universidad de Murcia, Spain.

e-mail: pablo@um.es

The optical quality of the images formed by the eye in the retina imposes a physical limit to our vision. For decades, the eye's optics has been mainly studied on axis, typically at the fovea where the eye has its maximum spatial resolution. However, beyond the fovea, the quality of the eye in the periphery of the retina presents special characteristics. In the last years, there has been a renewed interest in this area fueled by two important applications. On the one hand, it was suggested that optical errors in the periphery could trigger the development of myopia in children. On the other hand, it was discovered that the crystalline lens have a protective effect for the peripheral optics that was missed after cataract surgery when intraocular lenses were implanted. In this talk, I will revise the state of the art of this area with special emphasis in the results of my lab including the design and clinical result of a new intraocular lens to improve peripheral optics in pseudophakic patients.

Physical Self-Learning Machines

Víctor José López Pastor[1], **Florian Marquardt**[1,2,*]

[1]*Max Planck Institute for the Science of Light, Erlangen, Germany.*
[2]*Friedrich-Alexander-Universität Erlangen-Nürnberg, Erlangen, Germany.*

*e-mail: Florian.Marquardt@mpl.mpg.de

Machine learning using artificial neural networks is revolutionizing many areas of science and technology. This increases the urgency for exploring alternatives to artificial neural networks running on digital hardware. These alternatives might eventually be faster and/or more power-efficient. With this in mind, we ask the question whether one can identify a general principle that would enable a nonlinear physical system to become a self-learning machine – i.e. a physical information-processing device where internal degrees of freedom self-adjust by physical interactions to learn a desired input-output relation.

In this talk, I will present our recent idea on how this might be achieved for arbitrary time-reversal-invariant Hamiltonian systems. I will introduce the principle of 'Hamiltonian Echo Backpropagation', and demonstrate how efficient learning could be possible in a wide class of physical systems. The main idea is to apply a time-reversal operation to the output of the device (e.g. waves emerging from the device) before adding a small error term that reflects the deviation from the desired output. As we show in our manuscript, the subsequent physical dynamics (independent of its details) will produce a change in some persistent, arbitrary 'learning degrees of freedom' that eventually ensures minimization of the cost function during training. Thus, using this approach, arbitrary nonlinear time-reversal-invariant Hamiltonian systems can be trained to achieve some desired input-output relation. These systems include in particular nonlinear optical wave fields as well as superconducting microwave circuits in the classical regime.

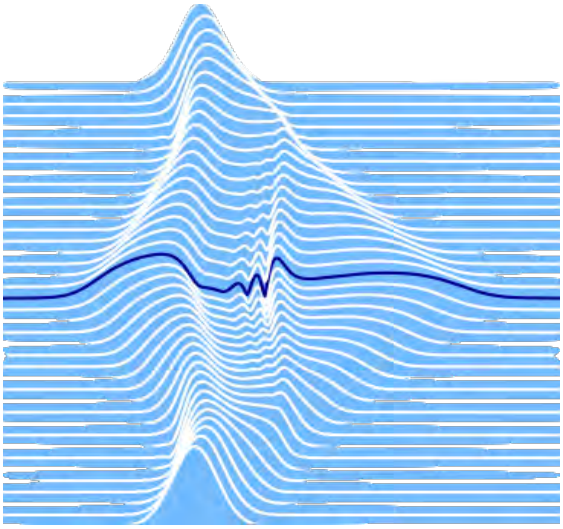

Figure 1. Schematic depiction of a nonlinear wave field evolving forward in time, getting subjected to a time-reversal operation, and continuing to evolve afterwards. Hamiltonian Echo Backpropagation injects an "error signal" right before the time-reversal operation.

[1] Victor Lopez-Pastor, Florian Marquardt, *Self-learning Machines based on Hamiltonian Echo Backpropagation*, arXiv 2103.04992 (2021).

Nanophotonic biosensors for ultrasensitive and decentralised diagnostics at the point-of-need

Laura M. Lechuga

Nanobiosensors and Bioanalytical Applications Group,
Catalan Institute of Nanoscience and Nanotechnology (ICN2), CSIC, BIST and CIBER-BBN,
Campus UAB, Bellaterra, 08193 Barcelona, Spain.

e-mail: Laura.lechuga@icn2.cat

COVID-19 pandemics has evidenced the urgent need of having portable diagnostic tools that enable rapid testing and screening of the population with sensitivity and specificity levels comparable to laboratory techniques. Biosensor technology is one of the best prepared to tackle the challenging goal of offering fast and user-friendly diagnostics tests than can be employed at the point-of-need. In particular, nanophotonic biosensors based on eveanescent wave detection can provide sensitive, reliable and selective analysis, while reducing test and therapeutic turnaround times, decreasing and/or eliminating sample transport, and using low sample volume. Our main objective is to achieve ultrasensitive Point-of-care (POC) platforms for label-free analysis using nanophotonics biosensing technologies and custom-designed biofunctionalization protocols, accomplishing the requirements of disposability and portability.

Photonic biosensors are systems that seize different light-based phenomena for the fast detection and quantification of substances. We have demonstrated cutting-edge nanophotonic biosensors based on Nanoplasmonics and in Silicon photonics technologies that enables ultrasensitive analysis of body fluids in few minutes. By custom tailoring the biochemistry of the sensor biochips, our POC nanophotonic biosensor technology can perform direct detection of proteins, genetic biomarkers or pathogens within <15 min, with high sensitivity and selectivity. The diagnostic potential has been demonstrated and validated among others, for the drug monitoring of anticoagulants in plasma, antibiotic allergy diagnosis in plasma, early cancer diagnosis (colorectal and lung cancer) and bacterial, and viral infectious diseases [1-3]. During COVID-19 pandemic, our POC biosensor has been fully validated with hundreds of clinical samples for the direct detection of anti-SARS-CoV-2 immunoglobulins in COVID-19 patients, confirming excellent diagnostic performance [4].

Our nanophotonic biosensor approach paves the way for modern decentralised disease diagnostics. The nanobiosensor POC devices could be employed by non-expert personnel at the bed-side of patients and could have a strong impact in guiding quick medical decisions across various clinical scenarios.

[1] C. S. Huertas, D. Fariña and L.M. Lechuga, *ACS Sensors* **1**, 748 (2016).
[2] J. Maldonado, M. C. Estévez, A. Fernández-Gavela, J. J. González-López, A. B. González-Guerrero, L. M. Lechuga, *Analyst* **145** (2), 497 (2020).
[3] M. Soler, M.-C. Estevez, M.C. Cardenosa-Rubio, A. Astua, and L.M. Lechuga, *ACS Sensors* **5** (9), 2663 (2020).
[4] O. Calvo-Lozano,….and L.M. Lechuga. *Anal. Chem*. **94**, 2, 975 (2022).

Nanophotonics: the first 30 years

Francisco J. García Vidal

Departamento de Física Teórica de la Materia Condensada and Condensed Matter Physics Center (IFIMAC), Universidad Autónoma de Madrid, Spain.

e-mail: fj.garcia@uam.es

During the last thirty years, a new area of research within Physics has emerged, aiming to control the flow of light at length scales of the order or even smaller than the wavelength. This new frontier is named Nanophotonics and has become an interdisciplinary field of research that combines expertise from Condensed Matter Physics, Classical and Quantum Optics and Materials Science. The basic idea of Nanophotonics is to tune the material properties of the medium in which light flows to devise its propagation at will. To frame our own research, in the first part of my talk I will briefly introduce the three main developments that have emerged in Nanophotonics during these thirty years: Photonic Crystals, Plasmonics and Metamaterials.

The main part of the presentation will be devoted to describing two main findings achieved in our theoretical group in this field of research: the phenomenon of the transmission of light through subwavelength apertures [1] and the concept of spoof surface plasmons [2]. First, we will show how surface plasmons can be utilized to overcome the two main limitations that diffraction imposes to light when passing through subwavelength apertures: low transmission and propagation into all directions. Next, we will discuss how structuring metallic surfaces allows for the support of surface electromagnetic modes at low frequencies that mimic the behavior of surface plasmons at optical frequencies. We will also illustrate how these spoof surface plasmon modes can be used in applications that require the manipulation of electromagnetic fields at microwave and terahertz frequencies.

Finally, we will briefly show how light-matter interaction can be used not only to control light propagation as classical Nanophotonics does but, by taking advantage of the quantum hybrid nature of the polaritons formed when light-matter coupling is strong enough, to modify material and chemical properties by tailoring vacuum electromagnetic fields [3].

[1] F. J. García-Vidal, L. Martín-Moreno, T.W. Ebbesen, and L. Kuipers, *Reviews of Modern Physics* **82**, 729 (2010).
[2] Francisco J. García-Vidal *et al*., *Reviews of Modern Physics* **94**, 025004 (2022).
[3] Francisco J. García-Vidal, Cristiano Ciuti and Thomas W. Ebbesen, *Science* **373**, eabd0336 (2021).

Precision Cosmology, when the party is over

Licia Verde

ICREA Institució Catalana de Recerca i Estudi Avançat & Universitat de Barcelona, Spain.

e-mail: liciaverde@gmail.com

Over the past 20 years cosmology has made the transition to a precision science. Synergies between cosmology and particle physics have been pivotal in this progress and in the theoretical interpretation of the experimental evidence. The standard cosmological model (the LCDM model) has been established and its parameters are now measured with unprecedented precision. This relatively simple model successfully describes observations from widely different epochs of the Universe, from the early Universe all the way to the present day. The "unreasonable effectiveness" of the LCDM model offers challenges and opportunities.

Firstly, precision is not enough: accuracy is also crucial. In addition, there is a big difference between modelling and understanding. This is further complicated by the fact that cosmology only makes observations not experiments, so virtually every inference is heavily model dependent.

This brings to mind what Feynman said: "The first principle is that you must not fool yourself and you are the easiest person to fool."

The next decade will see the era of large surveys; a large coordinated effort of the scientific community in the field is on-going to map the cosmos producing an exponentially growing amount of data. I will explore some examples of how I think we can proceed as not to fool ourselves in the interpretation of forthcoming data.

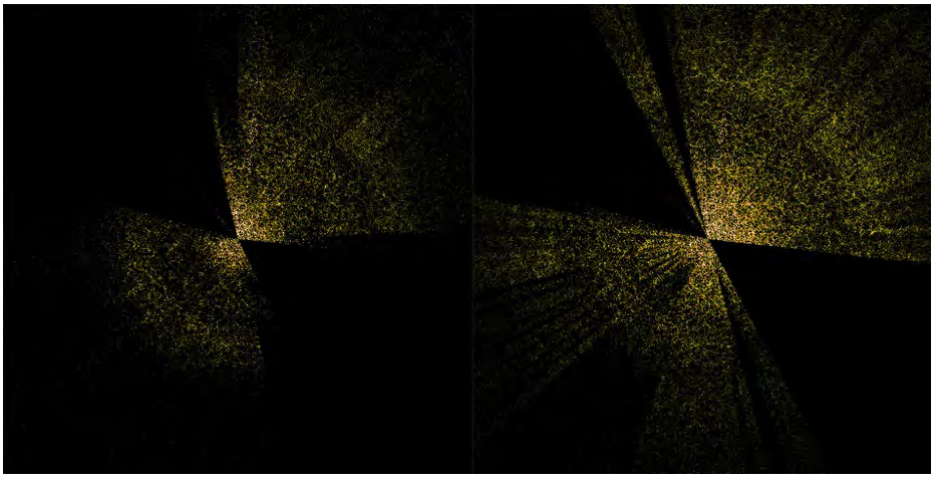

A slice through the 3-D map of galaxies from the completed Sloan Digital Sky Survey (left) and from the first few months of the Dark Energy Spectroscopic Instrument (DESI; right). The earth is at the center, with the furthest galaxies plotted at distances of 10 billion light years. Each point represents one galaxy. This preliminary version of the DESI map shows only 400,000 of the 35 million galaxies that will be in the final map. **Credit:** D. Schlegel/Berkeley Lab using data from DESI.

Acknowledgements: I would like to thank all my collaborators and the members of my research group. Without them, this work would not have been possible: "It takes a village" as they say. I acknowledge support from the European Union's Horizon 2020 research and innovation programme ERC (BePreSysE, grant agreement 725327), project PGC2018-098866-B-I00 MCIN/AEI/ 10.13039/501100011033 y FEDER "Una manera de hacer Europa", and the "Center of Excellence Maria de Maeztu 2020-2023" award to the ICCUB (CEX2019-000918-M funded by MCIN/AEI/ 10.13039/501100011033).

High precision spectroscopy in astrophysics: implications on fundamental physics and the characterization of Earth-like planets

Rafael Rebolo

Instituto de Astrofísica de Canarias, C/ Vía Láctea s/n, 38201 La Laguna, Tenerife, Spain.

e-mail: rrl@iac.es

New high-resolution astronomical spectrographs designed for ultra-high radial velocity precision and extreme spectral fidelity are leading to significant advances in exoplanet research and allow to perform astrophysical experiments on gravitational redshift and stability of the fundamental physical constants with unprecedented precision and accuracy. Progress on laser frequency combs, as new calibration systems, was essential to achieve few cm s^{-1} Doppler precision as required to measure masses of Earth-like planets in solar-type stars and sub-Earth mass planets around low-mass stars. For planets eclipsing their host stars, the radius is known and determination of masses provide densities which set constrains and give insight on the overall chemical composition of these exoplanets.

I will review recent observations of terrestrial planets with ultra-stable spectrographs, new progress on the measurement of the solar gravitational redshift and on-going efforts to measure any variations in the value of the fine-structure constant on cosmological timescales via observations of absorption systems towards high redshift quasars.

XXXI Encuentro Ibérico de Enseñanza y Divulgación de la Física

Presentaciones orales

Lunes 11/07:

15:30-17:00 Mesa redonda. *La enseñanza de la Física en el primer curso de las carreras científicas*

Benito Vázquez Dorrio, U. Vigo:. *La Física y los estudiantes de Ingeniería*

M.ª Jesús Hernández Lucas, U Valencia:. *La Física y los estudiantes de grado de Física*

Luis Roca Zamora, U. Murcia:. *¿Qué nos dicen las pruebas EBAU en los estudiantes de Física?*

Miguel Ángel Fernández Sanjuan, U. Rey Juan Carlos de Madrid. *La Física en el Grado de Ciencias Experimentales*

Moderadora: Chantal Ferrer Roca, U. Valencia

17:00-18:00 **Pósteres y café**.

18:00-18:12 Antonio Ángel Moya Molina. *Laboratorio de Física General basado en Arduino*

18:12-18:24 Manuel Iván González Martín. *Video aids at the students' lab: a proposal for a Renewable Energy Laboratory*

18:24-18:36 Juan F. González Hernández. *Teaching Physics with Physmatics: ideas from Mathematics, Astronomy and Theoretical Physics*

18:36-18:48 José Antonio García Gamuz. *Experiencia docente post-confinamiento: la clase invertida en Grados de Ciencias de la Salud*

18:48-19:00 Germán Ros Magán. *Formación científica inicial de maestros basada en el aula invertida y la indagación*

19:00-19:12 Íñigo Rodríguez-Arteche. *El centro de gravedad a través de una Secuencia de Enseñanza-Aprendizaje centrada en contextos cotidianos*

19:12-19:24 Juan Tomé Escribano. *Los relojes y el significado de sus medidas*

Martes 12/07:

15:30-17:00 Mesa redonda. *La divulgación de la Física en contextos no formales (ferias, museos...)*

Chantal Ferrer Roca, U. Valencia. *Feria Experimenta*

José González López de Guereñu. *Director de la Feria Madrid es Ciencia*

Rosa Martínez Martínez. *Directora Museo Didáctico e Interactivo de Ciencias, Vega Baja del Segura, Alicante*

Isabel Abril Sánchez, U. Alicante. *El Pati de la Ciència. Divulgar Ciencia en el Siglo XXI*

Pablo Contreras Vélez, profesor IES. *La Semana de la Ciencia y la Tecnología de Murcia*

Moderadora: Carmen Carreras Béjar, vicepresidenta DEDF

17:00-17:30 **Café**.

17:30-18:00 Benito Vázquez Dorrio, U. Vigo. *Enseñar Color con actividades experimentales*

18:00-18:12 Manuel Alonso Sánchez. *Estudio de la iridiscencia en 2° Bachillerato*

18:12-18:24 Manuel Alonso Orts. *Cristales fotónicos en 2° Bachillerato*

18:24-18:36 Emma Torró Pastor. *Masterclasses Internacionales "HandsonParticle- Physics" en el IFIC*

18:36-18:48 Marília Peres. *The Physics Collection of the Instituto Maynense*

18:48-19:00 Matilde Ariza. *Physics sounds through heritage: Study of sonorous scientific-historical instruments and bells*

19:00-19:12 Luis Afonso. *Eyes Protection Against UV*

19:12-19:24 Ana Cros Sttoter. *8 vídeos y 32 experimentos en un Kit: experimentos de física de la RSEF sección local de Valencia*

19:24-19:36 Isabel Abril Sánchez. *Dos propuestas para divulgar ciencia entre los más jóvenes*

Miércoles 13/07:

15:30-17:00 Mesa redonda. *Nuevos currículos de Física (y Química) de la ESO y Bachillerato en la LOMLOE*

Rafael López-Gay, U. Almería. *Análisis del currículo de Física y Química en la ESO*

Pablo Nacenta Torres, JdG DEDF. *Los ámbitos, un modelo de organización de las materias en la ESO. El caso de la Física y Química*

Patricio Gómez de Lesarri, IES Ramiro de Maeztu, Madrid. *Propuesta de la Física (y de la Química) en los nuevos Bachilleratos*

Marisa Amieva Suárez, IES Leopoldo Alas Clarín, Oviedo, JdG DEDF. *El modelo de evaluación por competencias La competencia científica*

Moderador: José María Pastor Benavides, presidente DEDF

17:00-18:00 **Café**.

17:30-18:00 Teresa Seixas, U. Porto. *Students judgment of learning strategies effectiveness: a case study in an undergraduate physics course at the University of Porto*

18:00-18:12 Beatriz Padín Romero. *Herramientas computacionales de software libre en la Física de Secundaria*

18:12-18:24 Ernesto Pastor Lebrero. *Estudio de la fuerza eléctrica entre dos esferas cargadas*

18:24-18:36 Daniel Aguirre Molina. *Los laboratorios remotos para la enseñanza de la Física en Secundaria*

18:36-18:48 Miguel Ángel Queiruga Dios. *Análisis de la implementación de proyectos STEAM en el aula de la Educación Secundaria Obligatoria*

18:48-19:00 Ángel Ávila Freire. *Quantum break – Exploiting a scape room to reinforce Physics and Chemistry among Bachillerato Students*

19:00-19:12 Manuel Fiolhais. *On the experience of 25 years in writing textbooks for middle and high school in Portugal*

19:12-19:24 Jesús M.ª Marcos Merino. *La Física de la Formula 1*

19:30-20:30 Asamblea General de la DEDF.

Pósteres

- S. Pinto, L. Santos, J. Couto, F. Leal y G. Barbosa. *Collisions in the Macroscopic World: Billiard Balls*
- J. Daza, L. Escoda, M. Soler, J. Planella y J.J. Suñol. *Teaching/Learning experiences in Physics: engineering degrees*
- D. Montagud-Martínez, V. Ferrando, L. Remón, A. Martínez-Espert, W.D. Furlan y J.A. Monsoriu. *Laboratorio virtual para estudiar la caracterización de lentes multifocales*
- J. Güémez y J.A. Mier. *On teaching thermodynamics in 21st century*
- María J. Hernández Lucas y J.C. Jiménez Muñoz. *The challenge of teaching Physics to unmotivated undergraduate students: a case study of Health and Food Sciences degrees at the University of Valencia*
- E. Baradit, I. Sánchez y R. Aedo. *Una Propuesta de Enseñanza de las Condiciones de Frontera para los Campos Electromagnéticos*
- T.P. Iglesias, J.L. Legido y M.A. Rivas. *Online examination procedure with a tool developed in Visual .NET*
- M. Villaplana Pérez, S. González de la Hoz y F. Ballester. *Uso de calcme (Wiris) como recurso didáctico en la enseñanza y evaluación de matemáticas y física*
- P. Palacios, J.C. Jiménez-Sáez, F.J. Sánchez, J. Gaite y S. Muñoz. *Experiencia de aula invertida y gamificación en la docencia de un laboratorio de física de primer curso*
- J.J. Miralles Canals. *Elaboration of calculated questions using Moodle and Wolfram language*

- D. González y J. Gil. *La Óptica en la historia militar*
- E. Yubero, A. Clemente, A. López-Caravaca, N. Galindo y J.F. Nicolás. *The use of discussion boards in undergraduate physics courses in experimental science degrees*
- M. Peres, I. Bruno y V. Silva. *Improving the Teaching of Physics with Space Projects*
- C. Marín Sepúlveda, J. Castro-Palacio y J. Monsoriu. *Los teléfonos inteligentes: un laboratorio de bolsillo*
- Ives Torriente García, Juan C. Castro-Palacio, Juan A. Monsoriu. *The Smartphone as a Variable Voltage Supply: Cases of the RC, RL and RLC Series Circuits*
- Camila Marín, Juan Castro-Palacio, Juan Monsoriu. *Acoustic Determination of the Gravitational Acceleration*
- K. Kristiani, L. Sirqueira, M.G. Silva, S. Francisco, M.A. Salgueiro da Silva y T.M. Seixas. *Social-emotional learning: a case study in academic institutions of Portuguese speaking countries*
- A. Sotto Díaz, J.M.ª Arsuaga Ferreras y P. Melón Jiménez. *La situación de la Física en los nuevos currículos de ESO y Bachillerato*
- A. Sotto, J.M. Arsuaga y P. Melón. *Diseñando un átomo. Un ejemplo de abproblemas*
- María Consolación Rodríguez-Palazón, Rafael Garcia-Molina. *Propuesta práctica para la enseñanza-aprendizaje de los espectros atómicos en el último curso de secundaria*
- Irene Carrión, Ana Teresa Gea, Mercedes Contreras, Gema María Muñoz, Rafael Garcia-Molina. *Análisis físico de una obra literaria: El pozo y el péndulo de E. A. Poe*
- José Jorge Llopis Juan, Rafael Garcia-Molina. *Estudio acústico de campanas de Alcoy mediante software de audio de uso libre*
- J. M. Cámara-Zapata, H. Puerto, A. Conesa, J. M. Brotons. *Multidisciplinary collaborative learning. Application to the analysis of citrus cultivation in the Vega Baja del Segura against rising energy prices*

Laboratorio de Física General basado en Arduino

A. A. Moya

Departamento de Física, Universidad de Jaén, Paraje Las Lagunillas, s/n, 23071-Jaén, Spain.

e-mail: aamoya@ujaen.es

Las asignaturas de Física General de primer curso de universidad incluyen una competencia específica relativa a la comprensión y dominio de los conceptos básicos sobre las leyes generales de la Física y su aplicación para la resolución de problemas, en la que las prácticas de laboratorio juegan un papel primordial. Hoy en día, el desarrollo de nuevas tecnologías ha dado lugar a la aparición de una gran cantidad de sensores y sistemas electrónicos de adquisición automática de datos experimentales de bajo coste, tal como Arduino, cuyo uso está internacionalmente recomendado como actividad docente de tipo STEM.

Este trabajo, basado en un proyecto de innovación docente desarrollado con estudiantes de los grados de Química, Ciencias Ambientales e Ingeniería Informática, así como diferentes grados de la rama de Ingeniería Industrial, describe las líneas básicas que permiten introducir las plataformas electrónicas de bajo coste en el laboratorio de Física General [1-5].

Se seleccionan varias prácticas de laboratorio cuyos cuadernos de instrucciones incluirán los programas de Arduino básicos para su seguimiento automatizado. En el campo de la mecánica se consideran, mediante el uso de sensores de ultrasonidos, los movimientos rectilíneo y circular, el movimiento de caída libre, el movimiento armónico simple y la determinación de la velocidad del sonido en aire. En el campo de la termodinámica se considerará el estudio de las leyes de los gases, las escalas de temperatura, experimentos de calorimetría y cambio de fase, así como curvas de enfriamiento de líquidos y aspectos prácticos de meteorología, fundamentalmente mediante el uso de sensores de presión barométrica y sondas de temperatura. Los aspectos a considerar relativos al electromagnetismo serán, por una parte, el estudio de circuitos de corriente continua, medida de la resistencia interna de pilas y baterías, y carga y descarga de condensadores, que se estudiarán con las fuentes de corriente continua y los multímetros incorporados en el propio Arduino. Por otra parte, se considerará la medida de campos magnéticos y el estudio de la inducción electromagnética, que se realizará mediante sensores de efecto Hall. En relación con la óptica se estudiará la intensidad luminosa mediante el uso de fotorresistencias, el efecto fotoeléctrico, las características de los diodos LED, así como la generación y determinación de colores.

En todos los casos, los cuadernos de laboratorio incluirán también la presentación de resultados en forma de tablas y gráficos. La realización de las prácticas, optimizando los códigos de programación en Arduino, el tratamiento de los datos experimentales mediante ordenador, y la presentación del trabajo correspondiente constituye la herramienta necesaria para la evaluación del alumno de las actividades STEM realizadas, fomentando así la evaluación por competencias. Se prestará, en todo caso, una especial atención a la identificación de los errores instrumentales que acompañan a los diferentes sensores utilizados.

El uso de plataformas electrónicas de bajo coste puede ayudar a los estudiantes universitarios a una mejor comprensión de los principios básicos de la Física. Además, parece razonable y deseable que los estudiantes de primer curso universitario adquieran habilidades y competencias en el manejo de sistemas de adquisición automática de datos experimentales, y particularmente en el uso de sensores para la medida de magnitudes físicas. Las prácticas de laboratorio constituyen una excelente oportunidad para introducir actividades de tipo STEM sin reducir el tiempo para tratar con el contenido propio de un curso universitario de Física General.

[1] A. A. Moya, *Phys. Teach.* **55**, 228 (2017).
[2] A. A. Moya, *Phys. Educ.*, **53**, 035006 (2018).
[3] A. A. Moya, *Phys. Educ.*, **53**, 055020 (2018).
[4] A. A. Moya, *Phys. Educ.*, **54**, 015005 (2019).
[5] A. A. Moya, *Phys. Teach.* **57**, 621 (2019).

Agradecimientos: Se agradece la financiación del trabajo al Proyecto de Innovación Docente PIMED45_201921 de la Universidad de Jaén.

Video aids at the students' lab: a proposal for a Renewable Energy laboratory

Manuel I. González

Departamento de Física – Universidad de Burgos, Escuela Politécnica, Avda. Cantabria s/n, 09006 Burgos, España.

*e-mail: miglez@ubu.es

New technologies constitute a revolution that profoundly affects all areas of teaching practice. This paper describes a proposal based on new technologies, recently implemented in the Department of Physics of the University of Burgos. It is a part of a course in Renewable Energies, which is taught in various Engineering degrees.

A hundred students, approximately, enter our Renewable Energies laboratory every year. The way of working in the laboratory is, in principle, rather traditional: each pair of students is assigned a different experiment, with its own material and written script.

Few months ago, however, new complementary, audio-visual material, has been added to the scripts, in the form of brief video clips, which aim to help the students in one of these three areas:

- Handling of specific measuring devices.
- Description of delicate experimental procedures, difficult to communicate in writing.
- Data processing techniques.

For the convenience of the students, the video clips are supplied in several ways: as video files uploaded to the virtual classroom, through links in the electronic version of the scripts and by means of in-situ QR codes. Students can consult them freely during the execution of the experiment and at the time of preparing their laboratory reports.

In the few months elapsed since the launch of this initiative, the results are very encouraging. Autonomy and "experimental productivity" of the students have increased significantly, whereas waiting times for consultations to the teacher have nearly disappeared.

[1] Repositorio Institucional de la Universidad de Burgos. Teaching materials prepared by the author, at https://riubu.ubu.es/handle/10259/2684/browse?authority=255&type=author. Consult the entries starting with "Laboratorio de EERR".

Teaching Physics with Physmatics: ideas from Mathematics, Astronomy and Theoretical Physics

Juan F. González H.*

Department of Physics and Chemistry, I.E.S. Humanejos, Parla, Madrid, España.

* e-mail: jfgh.teorfizikisto@gmail.com

Teaching Physics is challenging and hard. Following the approach of Physmatics [1, 2] (the integrated and simultaneous teaching of Physics and Mathematics), we present several ideas, references and activities (not all are new) for High School (normal and advanced) students and University level students coming from pure Mathematics, the attractive world of Astronomy and the abstract world of Theoretical Physics, using the Physmatics framework. The mathematical language prerequisites are diverse, but they can be adjusted to the target class and the different age and background of the students. Topics included will be: proportion, dimensions and geometry, algebra, differential and vector calculus, integrals, dimensional analysis, power laws, black holes, gravitation, field theory, relativity, quantum physics, particle physics, cosmology, computational tools and several reference websites.

[1] Eric Zaslow, Public lecture given at The Fields Institute, June 2, 2005. Also available in *ArXiv: https://arxiv.org/abs/physics/0506153* .
[2] Eric Zaslow, *Physmatics*, paper that accompanies the public lecture given at The Fields Institute, June 2, 2005, as part of the Clay Senior Scholars program.
[3] *The Spectrum of Riemannium*, website dedicated to Science, Physics, Physmatics and their teaching (yet, mainly), URL: http:\www.thespectrumofriemannium.com

Experiencia docente post-confinamiento: la clase invertida en Grados de Ciencias de la Salud

José A. García-Gamuz[1,2,*], M. Alcaraz-Baños[2], A. Olivares-Rueda[2], R. Valerdi-Pérez[2], A. Candel-Ramón[2]

[1] *Colegio Diocesano Santo Domingo, Orihuela, 03300, Alicante, España.*
[2] *Dpto. Radiología y Medicina Física. Fac. Medicina. Campus de Espinardo. Universidad de Murcia, 30071, Murcia.*

*e-mail: jagarcia@cdsantodomingo.com

En las últimas décadas, la educación ha pretendido adaptarse a los rápidos cambios surgidos en la sociedad, especialmente en el mercado laboral, debido a factores como el avance tecnológico y otros. Por ello, se ha ido introduciendo diversas técnicas o métodos de trabajo diferentes en las distintas etapas, comenzando por la educación primera hasta la universitaria.

Esto ha causado, durante varios años, una auténtica "fiebre" por la innovación educativa, tratada por diversas corrientes pedagógicas y a través de distintas metodologías. Con el paso del tiempo, todo ello ha podido ser comprobado y estudiado, existiendo una variada bibliografía al respecto, en la que muchos trabajos actuales coinciden en la idea de que todas las técnicas o métodos puedes ser válidos dependiendo del objetivo que se persiga. No se trata de enfrentarlas, sino de emplear cada una en aquello para lo que es más eficaz [1].

En el año 2020, con la llegada repentina de un confinamiento estricto, el mundo educativo se vio obligado a modificar el método de trabajo programado en tiempo récord, generalizándose la utilización de medios audiovisuales y distintas plataformas poco usadas anteriormente, especialmente en los grados universitarios. Estos cambios, que debieron mantenerse en el tiempo por la situación sanitaria, han dado lugar a replanteamientos en distintas asignaturas, combinando los recursos utilizados tradicionalmente con aquellos que se han incorporado.

En la asignatura de Biofísica Aplicada del Grado de Fisioterapia, de la Universidad de Murcia, se ha pretendido aprovechar esta situación, para proporcionar al alumnado un rol más determinante en su proceso de enseñanza, fomentado el aprendizaje activo, utilizando como metodología para ello la "clase invertida". Se ha creado un grupo de innovación docente aprobado por la Universidad de Murcia para llevarlo a cabo.

Se pretende mostrar el enfoque que se ha dado a la asignatura, el tipo de actividades planteadas, así como el sistema de evaluación diseñado. También los resultados obtenidos, haciendo un análisis realista, cuantitativo y cualitativo, del proceso de aprendizaje seguido.

[1] J. Tourón, *Revista de Educación* **391**, 11 (2021).

Formación científica inicial de maestros basada en el aula invertida y la indagación

Germán Ros[1,*], Iñigo Rodríguez-Arteche[1], M. Teresa Rodríguez-Laguna[2]

[1]*Departamento de Física y Matemáticas. Universidad de Alcalá. España.*
[2]*Departamento de Química Analítica, Química Física e Ingeniería Química. Universidad de Alcalá. España.*

*e-mail: german.ros@uah.es

En este trabajo se presenta y analiza el proceso de enseñanza-aprendizaje desarrollado en la asignatura de Ciencias de la Materia y la Energía en el Grado de Magisterio en Educación Primaria en la Universidad de Alcalá. En esta asignatura se pretende como objetivos principales: *i)* propiciar una mejor comprensión de los conceptos físicos; *ii)* fomentar la experimentación y concienciar de su importancia en el aula; *iii)* impulsar al alumnado hacia estrategias de aprendizaje activo y; *iv)* mejorar las actitudes hacia las ciencias y sus expectativas como futuros docentes de ciencias.

Para todo ello, se ha elegido un doble enfoque metodológico (Figura 1). Por un lado, la asignatura se organiza de acuerdo con el modelo indagativo de las 5E [1] combinado con la metodología del aula invertida [2]. Así, las fases de Empezamos, Exploramos y Explicamos parten del estudio previo del alumnado, cuya reflexión y comprensión iniciales se recoge en cuestionarios sobre los que se profundiza en el aula, junto con actividades de ampliación y conectando con fenómenos cotidianos. La fase de Elaboramos se desarrolla en las sesiones prácticas de laboratorio (50% del total), donde el alumnado profundiza, amplia y construye el conocimiento de forma compartida a través de experiencias de indagación y resolución de problemas.

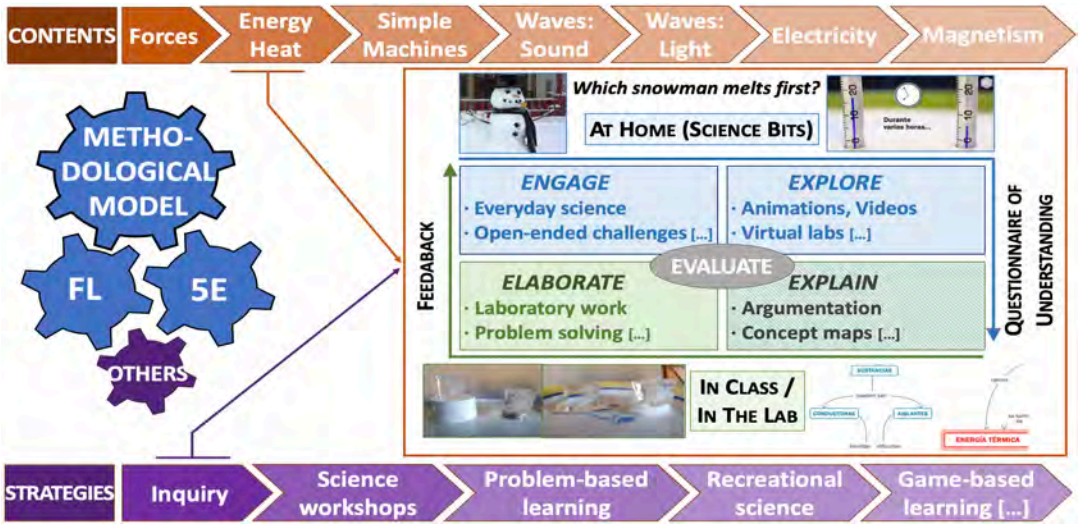

Figura 1. Enfoque metodológico de la asignatura basado en las 5E y el aula invertida.

Se han demostrado los beneficios de este enfoque a nivel conceptual y actitudinal a través de cuestionarios validados [2]. Además, mediante el análisis cualitativo con ATLAS.ti 9 de las encuestas del alumnado, se ha comprobado que éstos expresan emociones como entusiasmo y diversión asociados a la asignatura, y su satisfacción con la adquisición de habilidades manipulativas y de herramientas útiles para su futura labor docente.

[1] Bybee, R. W., Taylor, J. A., Gardner, A., Van Scotter, P., Powell, J. C., Westbrook, A., Landes, N. The BSCS 5E instructional model: Origins and effectiveness. *Colorado Springs, Co: BSCS* **5**, 88 (2006).
[2] Ros, G., Rodríguez Laguna, M. T. Influencia del aula invertida en la formación científica inicial de Maestros/as: beneficios en el proceso de enseñanza-aprendizaje, actitudes y expectativas hacia las ciencias. *Revista de Investigación Educativa* **39**(2), 463 (2021).

El centro de gravedad a través de una Secuencia de Enseñanza-Aprendizaje centrada en contextos cotidianos

Iñigo Rodríguez-Arteche*, Germán Ros

Departamento de Física y Matemáticas. Universidad de Alcalá. España

*e-mail: inigo.rodrigueza@uah.es

La implementación y evaluación de Secuencias de Enseñanza-Aprendizaje (SEA) en el ámbito de la física cuenta con un amplio respaldo de la comunidad dedicada a la didáctica de esta disciplina. Entre los beneficios de estas propuestas alineadas con la investigación educativa, se destaca su contribución al desarrollo de competencias científicas y a la construcción gradual del conocimiento, además de la viabilidad de ser refinadas en iteraciones sucesivas [1,2]. No obstante, su transferencia al aula demanda el desarrollo de prácticas docentes en la selección de objetivos didácticos, en la conexión con las ideas previas del alumnado y en la inclusión de contextos que la estimulen, entre otras [3]. Así pues, se requiere una adecuada formación del profesorado, que incluya la vivencia de experiencias de aprendizaje a través de SEA y la reflexión sobre sus bondades y desafíos.

Este trabajo se centra en una SEA para abordar el concepto de Centro de Gravedad (CG) en la asignatura de Ciencias de la Materia y la Energía del Grado de Magisterio en Educación Primaria. Esta propuesta didáctica se implementa con futuros maestros para promover su aprendizaje sobre la mecánica y hacerlos partícipes del diseño de la SEA. Por todo ello, los objetivos de la comunicación son: *i)* Caracterizar la SEA sobre el CG: contextos, interrogantes guía y actividades. *ii)* Analizar la percepción del futuro profesorado sobre la SEA, a partir de cuestiones de respuesta abierta.

Objetivo 1. Se parte de un contexto de enganche como es la arquitectura singular (miradores, torres, balcones, etc.), las acrobacias de circo y la magia para dotar de sentido a la SEA. Así, se comienza por abordar el concepto de peso y la idea de CG como punto imaginario donde se aplica la resultante de la fuerza gravitatoria. A continuación, la SEA se divide en tres bloques que responden a varios interrogantes: *a)* ¿Cómo se puede determinar el CG en cuerpos 1-D y 2-D? ¿Y en sistemas más complejos? (3 actividades); *b)* ¿Cómo afecta el CG al equilibrio de las estructuras? (2 actividades); *c)* ¿Qué efectos tiene alterar la posición vertical y/o horizontal del CG? (3 actividades).

En el primer bloque se recurre a varas, escobas (Actividad 1), bandejas, taburetes (Actividad 2) y sistemas complejos como cubiertos y palillos acoplados (Actividad 3) para indagar sobre la determinación del CG. En el segundo bloque se trabaja con bloques diversos, más o menos apilados a un lado u otro, hasta conseguir torres inclinadas (Actividad 4). A continuación, se reconstruye una Torre de Pisa que incluye una plomada, para explicar su equilibrio (Actividad 5). En el tercer bloque se comienza simulando a bailarines/as de ballet (Actividad 6) y equilibristas en la cuerda floja (Actividad 7) a través de materiales como latas, corchos, alfileres y palitos de brocheta. Se busca comprender los efectos de variar la altura del CG en el equilibrio de los cuerpos. Finalmente, la SEA concluye con un toque mágico, donde una caja de galletas –con un cuerpo oculto en uno de los extremos de su interior– es capaz de ascender una rampa desafiando a la gravedad (Actividad 8). Según se observa, a lo largo de la propuesta se consideran situaciones cotidianas y materiales de bajo coste, con el fin de acercar la física a los estudiantes e invitarles a indagar sobre sus fundamentos.

Objetivo 2. La valoración de la propuesta se recaba a través de varias preguntas abiertas sobre los aspectos más destacables de la SEA. El análisis del contenido de las respuestas se realiza a través de ATLAS.ti 9, obteniéndose como categorías principales las de «aprendizaje» a través de la SEA y «emociones» suscitadas en el proceso. En ambos casos, se obtienen resultados muy positivos. En la primera categoría, se pone en valor la contribución de la propuesta al aprendizaje de conceptos científicos, explicación de fenómenos cotidianos y desarrollo de destrezas experimentales. En la segunda, se destacan emociones como el entusiasmo, la diversión y la satisfacción ligada a la comprensión de contenidos de física.

[1] Guisasola, J., Zuza, K., Ametller, J., Gutierrez-Berraondo, J. Evaluating and redesigning teaching learning sequences at the introductory physics level. *Physical Review Physics Education Research* **13**(2), 020139 (2017).
[2] Greca, I. M., Ortiz, J., Arriassecq, I. Diseño y evaluación de una secuencia de enseñanza-aprendizaje STEAM para Educación Primaria. *Revista Eureka sobre Enseñanza y Divulgación de las Ciencias* **18**(1), 1802 (2021).
[3] Grossman, P., *Teaching Core Practices in Teacher Education.* Cambridge, MA: Harvard Education Press (2018).

Los relojes y el significado de sus medidas

Juan Tomé Escribano*

Catedrático de Enseñanza Secundaria, jubilado

*e-mail: casa@amonaria.com

Toda medida supone siempre una comparación, más o menos directa, de entidades homogéneas con el fin de cuantificar una propiedad física de las entidades comparadas. Entonces, al hacer medidas con relojes, ¿qué entidades se comparan?, ¿qué propiedad física de esas entidades es la que se cuantifica al hacerlas? Y otra pregunta que subyace a esas dos: ¿qué es un reloj?

Se pueden contestar consistentemente esas preguntas si se admite que la realidad física es cambiante (ubicua y permanentemente) e intrínsecamente cuadridimensional. Más concretamente, si se admite que los cambios se concatenan causalmente en procesos, que los procesos son las entidades básicas de la realidad física, y que se relacionan entre sí en una maraña que puede llamarse *universo de procesos*. Cambios, procesos y *universo de procesos* (realidades físicas) encuentran su correlato formal en sucesos, líneas de universo y espaciotiempo.

En esa concepción de la realidad física, las repuestas a aquellas preguntas serían:

1. Las medidas con relojes son comparaciones de procesos.
2. Los relojes son los procesos patrón en esas comparaciones. Los relojes modernos, que repiten automáticamente el proceso patrón, son ritmos patrón.
3. La propiedad física que se cuantifica al medir con relojes es la *duración*. Es propiedad del proceso comparado con el reloj y viene dada por el número de veces que el proceso patrón cabe en él.

Para realizar la medida directa de la duración de un proceso basta que un reloj lo acompañe. De esta forma, el reloj, un proceso pautado por repetición, se tiende junto al proceso con el que se compara (la línea de universo del reloj y la del proceso se superponen), y se pueden contar los tictacs que el reloj deja a lo largo del proceso. Las medidas de reloj, todas, se pueden interpretar entonces como la longitud cuadridimensional de la línea de universo que representa al proceso en el espaciotiempo e identificarlas con la magnitud física correspondiente: el tiempo propio relativista. Entendidas así, todas las medidas de reloj son medidas de tiempos propios (duraciones propias de procesos concretos) y todas son absolutas (todos los observadores coincidirán en asignar la misma duración al mismo proceso).

La consideración de los relojes como patrones y el carácter absoluto de la duración hacen que sea razonable adoptar la hipótesis de que los ritmos de los relojes se mantienen mientras miden. De cara a la introducción y divulgación de la TRE, la consecuencia más inmediata es que las explicaciones de fenómenos de desincronización de relojes no se refieren a relojes que atrasan o adelantan ni a tiempos que pasan más despacio o más deprisa, sino que remiten a la comparación de las duraciones medidas por los relojes que se desincronizan: si dos relojes de calidad empiezan a medir marcando lo mismo y terminan de medir marcando distinto, lo más inmediato es pensar que han estado midiendo cosas distintas. Así planteada, la tarea de explicar fenómenos de desincronización de relojes consiste en mostrar, en cada caso, qué midió cada uno de los relojes cuya desincronización se constata. En [1] pueden verse ejemplos concretos de este tipo de explicación.

[1] J. Tomé, Relatividad Especial: una interpretación del fenómeno de la “dilatación temporal”, *Revista Española de Física* **35**(2), 7 (2021).

Aprender color con actividades experimentales

José Benito Vázquez Dorrío[1,*], Miguel Ángel Queiruga-Dios[2]

[1]*Departamento de Física Aplicada, Universidade de Vigo, España.*
[2]*Departamento de Didácticas Específicas, Universidad de Burgos, España.*

*e-mail: bvazquez@uvigo.es

El conocimiento asociado al color, aun teniendo una gran importancia en nuestra vida cotidiana así como en innumerables contextos de investigación, innovación y transferencia no tiene posteriormente una correspondencia similar en los saberes básicos de las materias del ámbito científico-tecnológico de la Educación Secundaria Obligatoria y del Bachillerato. Como ya ocurría en anteriores currículos, una búsqueda del término "color" en los recientes decretos de enseñanzas mínimas de estos niveles muestran una treintena de resultados asociados exclusivamente a materias del ámbito de la educación plástica, artística y audiovisual. Así mismo, una revisión de libros de texto actuales en esos niveles muestra que en la mayoría de los casos la teoría del color enfocada a la síntesis aditiva como una sensación, cuanto menos, fisiológica y psicológica se presenta, si es el caso, de manera muy somera y tangencial en Física de 2º de Bachillerato. Esta descompensación entre la dedicación formal a la síntesis sustractiva y aditiva del color puede estar en la causa de la escasa comprensión conceptual y una fuerte persistencia de modelos que difieren del paradigma aceptado actualmente cuando se realizan estudios sobre las ideas previas sobre el color [1-3].

El color con el que se perciben los objetos depende, por lo menos, de su iluminación, reflectancia, entorno, sistema de fotodetección y sistema de procesado [4]. En situaciones cotidianas con variaciones de iluminación natural incluso relevantes nuestra percepción es firme [5], lo que puede ser el origen de las ideas previas que permanecen a lo largo del tiempo y el conflicto cognitivo que producen las denominadas ilusiones ópticas relacionadas con el color cuando algunas de las variables que se ponen en juego se modifican.

En este trabajo se presentan algunas actividades experimentales [6-8] que fomentan la curiosidad, el interés y la creatividad, al mismo tiempo que propician el aprendizaje del color *haciendo* color, combinado materiales simples y de bajo coste (Fig. 1) con otras aplicaciones y herramientas TIC. Se muestran los valores de ganancia de aprendizaje [9] con el empleo de las mismas en cursos de formación de profesorado de secundaria. El patrón de conocimiento inicial similar al de su futuro alumnado [2], podría interferir en el proceso posterior de enseñanza-aprendizaje del cual serán responsables.

Figura 1. Actividades relacionadas con el color [8].

[1] Martínez-Borreguero, G., Pérez-Rodríguez, Á. L., Suero-López, M. I., Pardo-Fernández, P. J., *International Journal of Science Education* **35**, 1299 (2013).
[2] Correa, F.L.N., Borreguero, G.M., Rodríguez, A.L.P., López, M.I.S., Fernández, P.J.P., *Color Research and Application* **41**, 325 (2016).
[3] Haagen-Schützenhöfer, C., *Physics Education* **52**, 044003 (2017).
[4] Albright T.D., Stoner, G.R., *Annual Review of Neuroscience* **25**, 339 (2002).
[5] Foster D. H., *Vision Research* **51**, 674 (2011).
[6] Vázquez-Dorrío, B., García-Parada, E., González-Fernández, P.M, *Enseñanza de las Ciencias: Revista de Investigación y Experiencias Didácticas* **12**, 63 (1994).
[7] Vázquez-Dorrío, B., Rúa-Vieites A., *Revista Iberoamericana de Educación* **42/7**, 1 (2007).
[8] http://www.clickonphysics.es/cms/
[9] Hake R.R., *American Journal of Physics* **66**, 64 (1998).

Estudio de la iridiscencia en 2º Bachillerato

Manuel Alonso Sánchez[1,*], Manuel Alonso Orts[2]

[1]*Sección Local de Alicante de la RSEF, Alicante, España.*
[2]*Institute of Solid State Physics, University of Bremen, 28030, Bremen, Alemania.*

*e-mail: manoloalonsosanchez@gmail.com

En esta comunicación mostraremos actividades y experiencias pertenecientes a la primera parte de una secuencia de enseñanza-aprendizaje sobre conceptos relativos el estudio de la luz y el color. Estos conceptos son adecuados para que el alumnado, en primer lugar, comprenda el fenómeno de la iridiscencia, y, en segundo término, pueda se adentre en un estudio elemental de los cristales fotónicos.

La secuencia se dirige principalmente al alumnado de Bachillerato, pero también se puede implementar provechosamente en primeros cursos de Universidad. La primera parte de ella, que presentaremos aquí, comienza recordando y ampliando algunos conceptos sobre la luz y el color que forman parte de la enseñanza habitual en esta etapa educativa, prosigue desarrollando un modelo físico básico adecuado para que el alumnado comprenda el fenómeno de la iridiscencia a partir de la interferencia, y acaba con un conjunto variado de experiencias a realizar en el aula sobre este fenómeno.

En primer lugar, veremos algunas actividades destinadas a que los estudiantes recuerden cómo se obtiene la mayoría de los colores del mundo natural que nos rodea (color pigmento), pudiendo entender, por ejemplo, por qué nuestro color de piel puede ser más claro u oscuro, por qué la mayoría de las hojas de las plantas son verdes, los tomates son rojos, etc.

Después de haber repasado estos conceptos, los alumnos ya están en buena situación para percatarse de que (al contrario de lo que ocurre con los ejemplos anteriores), los mosaicos de colores que se producen en los fenómenos iridiscentes no pueden tener un origen químico, pues una misma sustancia, como, por ejemplo, el jabón en el agua, da lugar a diversos colores según la pompa observada, el ángulo de observación, etc. Comprendido esto, la secuencia prosigue con algunas actividades en las que los estudiantes, usan conocimientos básicos de óptica para interpretar satisfactoriamente la iridiscencia.

La comunicación terminará con un breve recorrido por algunas experiencias sencillas y atractivas para realizar en clase, mediante las cuales los estudiantes producen e interpretan iridiscencias generadas por láminas delgadas. Algunos ejemplos son: lámina de aceite usado derramado sobre asfalto húmedo; capa fina de polvos de talco formada encima de un espejo [1] (Figura 1), película jabonosa recogida con el borde de un recipiente de plástico [2]; lámina iridiscente formada después de dejar caer una gotita de laca en un recipiente lleno de agua [3], etc.)

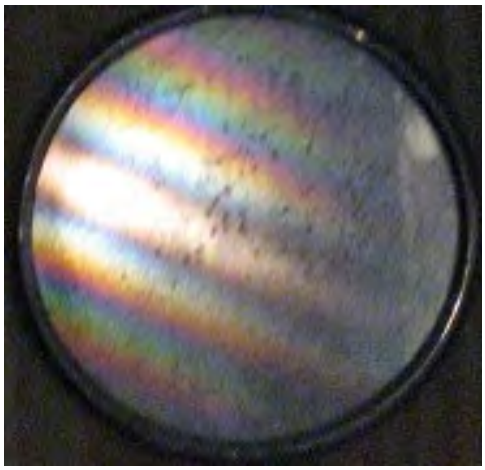

Figura 1. Iridiscencia producida en un espejo "manchado" con polvos de talco [1].

Veremos cómo se pueden realizar en clase estas experiencias y mostraremos algunos desarrollos elementales, cálculos y diagramas básicos, que puede realizar el alumnado para interpretarlas.

Decir finalmente que el estudio de la iridiscencia a este nivel tiene una gran utilidad para el alumnado de Bachillerato más allá de la de reforzar conceptos básicos de Física. Además de estar presente en nuestro entorno, el estudio de este fenómeno puede hacer de puente para conectar con investigaciones y aplicaciones actuales relevantes en el campo de la fotónica. En particular, nos permite adentrarnos en el apasionante mundo de los cristales fotónicos, a los que se dedica la segunda parte de la anteriormente mencionada secuencia de enseñanza-aprendizaje, la cual presentamos en otra comunicación.

[1] A. Luis Aina. "Un interferómetro de talco", en la Web *Fenómenos ópticos cotidianos*. (https://webs.ucm.es/info/gioq/fenopt/imagenes/interferenciatalco/index.htm).
[2] B. Vázquez Dorrío, "Uno de los interferómetros más sencillos del mundo: nanotecnología de salón, en la Web *Ciencia en Acción* (2021) (https://cienciaenaccion.org/experimento/uno-de-los-interferometros-mas-sencillos-del-mundo-nanotecnologia-de-salon)
[3] R. García-Molina y H. Pérez García, "Iridiscencias caseras", en la Web *Ciencia en Acción* (2003) (http://anteriores.cienciaenaccion.org/es/2003/experimento-186/iridiscencias-caseras.html)

Cristales fotónicos en 2º Bachillerato

Manuel Alonso Orts[1,*], Manuel Alonso Sánchez[2]

[1]*Institute of Solid State Physics, University of Bremen, 28030 Bremen, Alemania.*
[2]*Sección Local de Alicante de la RSEF, Alicante, España.*

*e-mail: manalo01@ucm.es

En esta comunicación se presenta una propuesta didáctica para introducir al alumnado de Bachillerato y de primeros cursos de Universidad en el apasionante mundo de los cristales fotónicos, unas estructuras periódicas que reflejan de manera selectiva ciertas longitudes de onda gracias al fenómeno de la interferencia. Los cristales fotónicos se encuentran tanto en el mundo natural como en el tecnológico, y se basan en fenómenos básicos de óptica, por lo que tiene sentido motivar al profesorado de Bachillerato y de primeros cursos de Universidad a que los incorporen (de forma introductoria) en sus programaciones.

En la otra comunicación para este mismo congreso, se expone la primera parte de nuestra propuesta didáctica. En ella, se repasa en primer lugar la generación del color más habitual, debida al color pigmento, y se continua estudiando con bastante detalle el fenómeno de la iridiscencia, tanto de forma teórica como mediante una variedad de experiencias con ejemplos cotidianos de interferencia de lámina delgada.

Llegados a este punto, es decir, a partir de que el alumnado comprende el proceso de iridiscencia debido a la interferencia en una lámina delgada, comienza la segunda parte de esta secuencia, referida en esta comunicación. En primer lugar, se introduce el concepto de cristal fotónico 1D, que no es más que la repetición sucesiva de láminas delgadas de dos materiales distintos, realizada de tal modo que se maximice la interferencia constructiva en aquellas longitudes de onda (colores) que se desee reflejar según la aplicación buscada. Este es el puente que usamos para introducir de forma sencilla los cristales fotónicos canónicos; aquellos con patrones periódicos en 2D y 3D, que reflejan el rango deseado de longitudes de onda en un gran número de orientaciones.

Una vez ha entendido el alumnado el fundamento básico de los cristales fotónicos, es muy interesante adentrarse en el conocimiento de algunos que ya existían en la naturaleza antes de que el ser humano desarrollara los suyos propios. Uno de ellos, es el de las mariposas *Morpho*, cuyo brillo azul en sus alas está basado en estructuras periódicas en las mismas, y les permite identificarse a grandes distancias [1]. Otro ejemplo, aún más llamativo, lo brinda el camaleón pantera (Figura 1), que presenta una estructura ordenada de cristales de guanina en las células cromatóforas de su piel. Investigaciones recientes [2] han mostrado que el cambio de dicha estructura periódica es el responsable del cambio de color del animal, utilizado tanto para el camuflaje como para la competición entre los machos.

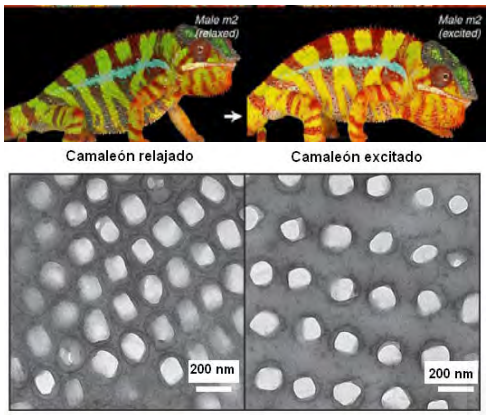

Figura 1. Cambio de color en el camaleón pantera al excitarse, debido al cambio en la periodicidad de la estructura fotónica en su piel [2].

Finalmente veremos que estos y otros ejemplos de la naturaleza son, a su vez, un perfecto vínculo con la investigación actual en cristales fotónicos, ya que, de hecho, algunas de las estructuras fotónicas naturales han servido de inspiración para el estudio teórico y aplicado de cristales fotónicos "artificiales" [3]. En relación con esto, presentaremos algunos de ejemplos del desarrollo científico-tecnológico actual en este campo, como las fibras ópticas de cristal fotónico bidimensional, que ya se pueden adquirir comercialmente [4] para aplicaciones ópticas y de sensado.

[1] F. P. Barrows, M. H. Bartl, Photonic structures in biology: a possible blueprint for nanotechnology, *Nanomaterials and Nanotechnology* **4**, 1 (2014).
[2] J. Teyssier, S. V. Saenko, D. van der Marel, M. C. Milinkovitch, Photonic crystals cause active colour change in chameleons, *Nature Communications* **6**, 6368 (2015).
[3] R. K. Cersonsky, J. Antonaglia, B. D. Dice, S. C. Glotzer, The diversity of three-dimensional photonic crystals, *Nature Communications* **12**, 2543 (2021).
[4] Catálogo de fibras de cristal fotónico de la compañía *Thorlabs*, https://www.thorlabs.com/navigation.cfm?guide_id=2092

Masterclasses Internacionales "Hands on Particle Physics" en el IFIC

Alberto Aparici, Santiago González de la Hoz, Fernando Martínez Vidal, Ángela Molina Ruiz, **Emma Torró Pastor***, Mª Amparo Tórtola Baixauli

Instituto de Física Corpuscular (IFIC) Centro mixto Universidad de Valencia – CSIC, Valencia.

*e-mail: emma.torro@ific.uv.es

Desde hace más de diez años, el IFIC participa en las Masterclasses Internacionales "Hands on Particle Physics" [1] para estudiantes de secundaria, organizadas por el International Particle Physics Outreach Group [2]. Esta es una actividad divulgativa internacional que pretende estimular las vocaciones científicas. Esta contribución detalla la evolución de la participación del IFIC en las Masterclasses haciendo hincapié en la organización de las cuatro Masterclasses que se han celebrado en el IFIC durante el año 2022.

La primera sesión tuvo lugar el 11 de febrero coincidiendo con la celebración del Día de la Mujer y la Niña en la Ciencia. Se organizó una Masterclass destinada a fomentar las vocaciones científicas femeninas para alumnas de 3º y 4º de la ESO. La sesión fue dedicada al experimento ATLAS del CERN [3] y seguida de un coloquio sobre el papel de la mujer en la ciencia. Las otras tres sesiones estuvieron dedicadas a distintos grandes experimentos de física de partículas en los que el IFIC tiene participación: los experimentos ATLAS y LHCb en el Gran Colisionador de Hadrones (LHC) del CERN, y el experimento Minerva, en Fermilab [4].

En estas cuatro sesiones han participado un total de alrededor de 280 alumnos y alumnas de 80 institutos de la Comunidad Valenciana. Cada sesión fue precedida de seminarios sobre física de partículas, el funcionamiento de un acelerador y de los experimentos cuyos datos manejaron los estudiantes. Estos eventos se celebran en 220 laboratorios de 55 países con más de 13.000 participantes en todo el mundo. Entre ellos, el IFIC es un centro pionero en la realización de esta actividad. Durante las jornadas los alumnos y alumnas de secundaria y bachillerato han podido formar parte de la comunidad científica por un día experimentando una aproximación al trabajo del personal investigador de nuestro centro, esperando que les resulte atractivo y les anime a convertirse en parte de nuestros equipos en un futuro próximo.

[1] http://ific.uv.es/masterclass/index.php
[2] https://ippog.web.cern.ch/
[3] https://home.cern/
[4] https://www.fnal.gov/

The Physics Collection of the Instituto Maynense

Marília Peres[1,2,*], Maria Inês Alves[3]

[1]*Sociedade Portuguesa de Física,* [2]*Escola Secundária José Saramago-Mafra, Portugal.*
[3]*Academia das Ciências de Lisboa, Portugal.*

*e-mail: mariliaperes@esjs-mafra.net

Historians of science have increasingly been using the collections of scientific instruments available in museums and other scientific institutions as primary sources in their research. There is, in the Maynense Museum (Lisbon Academy of Sciences), a collection of Physics devices from the 18th and 19th centuries, which were used in the teaching of Physics in this institution.

In 2021, the Lisbon Academy of Sciences inaugurated an exhibition of these instruments, with the aim of disseminating them amongst historians, teachers, and the general public, while simultaneously paying tribute to Professor Rómulo de Carvalho, who dedicated a part of his life to studying this collection, and was one of the directors of the Museum [1].

To prepare such an exhibition is a challenge which cannot fail to consider the state of conservation of the instruments, the selection of those deemed most representative or even the information available on their origin [2,3].

We intend in this presentation to make known the importance of this collection, as a remarkable example of the chief agent in the transition from the so-called ancient Physics into modern Physics, as we know it today; namely, experimental demonstration [4].

[1] Rómulo Carvalho, *A Actividade Pedagógica da Academia das Ciências de Lisboa nos Séculos XVIII e XIX*. Lisboa: Academia de Ciências de Lisboa (1981

[2] M. C. Elvas, I. M. Peres, S. Gessner, The Laboratorio Chimico of the Museum of Science, University of Lisbon: Reflections on documenting a collection. In M. C. Lourenco, A. Carneiro (Eds.), *Spaces and collections in the history of science. The Laboratorio Chimico ouverture* (pp. 185–194). Museum of Science of the University of Lisbon (2009).

[3] M. Lourenço, S. Gessner, Documenting Collections: Cornerstones for More History of Science in Museums. *Science & Education* **23**(4), 727 (2014).

[4] Isabel M. Malaquias, A Física nos finais do século XVIII. In *Ciência e experiência: formação de médicos, boticários, naturalistas e matemáticos: homenagem a Rómulo de Carvalho (1906-2006)* (pp. 21-32) Imprensa da Universidade de Coimbra (2006). DOI: http://dx.doi.org/10.14195/978-989-26-0413-8_2. Accessed: 13-Apr-2022,

Acknowledgements: Academia de Ciências de Lisboa, Sociedade Portuguesa de Física.

Physics sounds through heritage: Study of sonorous scientific-historical instruments and bells

Mª Matilde Ariza Montes

IES "Pedro Espinosa", Antequera (Málaga). España.

e-mail: matiariza@iespedroespinosa.es

This research makes it possible to bring the heritage of the sound scientific-historical instruments from the IES "Pedro Espinosa", as well as the bells, to the teaching and dissemination of Physics. An unprecedented perspective within the study of these genuine treasures.

Introduction Sound has accompanied the human being since its existence for communication, hence the need to design instruments that serve both for its study and for its use. This is the case of the ancient instruments from the IES "Pedro Espinosa" and the bells used since antique times as a means of communication, informing the population of all kinds of events. Both are at the same time magnificent scientific instruments for the study of multitudes of physical magnitudes and their corresponding laws. Its design and mass or its dimensions, among others, are crucial for the study of mechanics, acoustics or even astronomy.

Methodology This work tries to research the centuries-old instruments that the heritage of this school houses and the bells of the religious and civil buildings from the Antequera area.

Various written works have consulted and work has done with the heritage of the aforementioned high school. All the nearby buildings that house bells have visited and the greatest number of physical magnitudes of the bells, their dimensions or their frequencies have measured. Finally, a catalogue has made that will serve to delve into the aspects that define their sound.

The positions of the bell towers or belfries with respect to the orientation of the churches have explored and the liturgical celebrations have used to measure the natural frequency of the bells, the sound sensation in the decibel scale and the angular frequency of rocking or turning. A file has made with all the characteristics to the study of the mechanics and acousticS of each bell. Finally, the comparison of the most characteristic values with those of other Spanish bells has made.

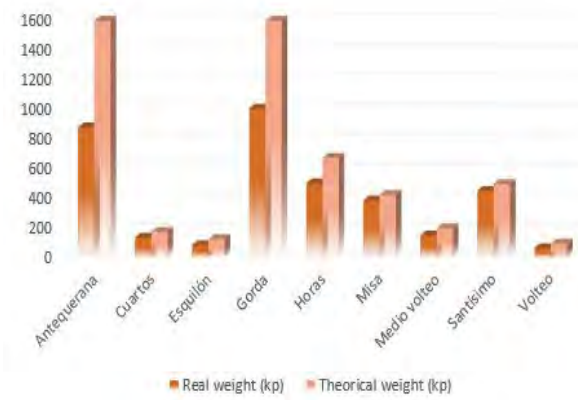

Figure 1. Real and theoretical weights from the church of San Sebastian´s bells in Antequera (Málaga).

Results and Discussion Scientific-historical instruments are key in the daily teaching of physics and promote the dissemination of science.

The result of the investigation from the physics of the bells, as a scientific testimony, has generated more data of bibliographic origin than experimental, due to the difficulty of accessing the bell towers because they are in poor condition.

Each bell has a different frequency according to its composition, design and dimensions. An outstanding fact is that no relationship found between the position of the bell towers and the type of temple or its orientation.

[1] M. M. Ariza Montes, Virtual Museum of Heritage from the IES "Pedro Espinosa". Antequera, 2015. Available at the web http://museovirtualiespedroespinosa.blogspot.com/. Consulted on April 18th, 2022.
[2] S. Ivorra Chorro, Acciones dinámicas introducidas por las vibraciones de las campanas sobre las torres-campanario. Valencia, 2002.

Acknowledgements: To all the students from the IES "Pedro Espinosa", religious and neighbors participating in the research.

Eyes Protection Against UV

L. Afonso[1,2,*], L. Peralta[1,3]

[1]*Laboratório de Instrumentação e Física Experimental de Partículas, Lisboa, Portugal.* [2]*Agrupamento de Escolas de Benfica, Lisboa, Portugal.* [3]*Faculdade de Ciências, Universidade de Lisboa, Portuga.l*

*e-mail: lafonso@lip.pt

The use of sunglasses is important on bright days. They protect eyes from visible radiation and ultraviolet (UV) radiation. UV radiation can damage retina, so it is important to prevent its passage. The eyes have protective mechanisms, such as closing the eyelids or decreasing the pupil diameter. These mechanisms are activated in the presence of intense visible light, so filtering only this component can leave eyes unprotected from UV radiation.

In this work we reconstructed and improved a device built by one of the authors [1]. The device makes it possible to assess the reduction in visible and near UV light intensity introduced by colored lenses. The key component of this assembly is an integrated light-voltage converter with a sensitivity window that spans from near UV to infrared. As light sources, LEDs of different wavelengths are used. Branded eyeglass lenses purchased from optical stores and eyeglasses purchased from sports stores were used.

We applied the experimental activity to high school students in physics class in 12th grade.

Tests did not reveal significant differences between the two batches or between the various lens colours. In general, the experience carried out showed that the protection offered by the tested colored lenses is adequate for the critical UV region.

[1] L. Peralta, *Revista Brasileira de Ensino de Física* **42**, e20200144 (2020).

8 vídeos y 32 experimentos en un Kit: experimentos de física de la RSEF sección local de Valencia

Javier Reig-Navarro, Núria Falcó, Chantal Ferrer-Roca, **Ana Cros***

Departamento de Física Aplicada y Electromagnetismo e Instituto de Ciencia de los Materiales (ICMUV), Universidad de Valencia, España.

*e-mail: Ana.Cros@uv.es

Presentamos aquí el contenido de un Kit de experimentos de física, divulgativo y de carácter no comercial, elaborado por la Sección Local de Valencia de la Real Sociedad Española de Física (RSEF-Valencia). El conjunto de 32 experimentos se presenta en una caja transparente de tamaño reducido (15x35x25 cm^3), fácilmente transportable y que contiene diversos elementos para su uso experimental. Se incluye también un libro con explicaciones sobre la realización de los experimentos y con enlaces a 8 vídeos depositados en YouTube. La duración de cada vídeo es de unos 10 minutos. La temática tratada abarca conceptos de Electricidad (12 experimentos), Magnetismo (6), Aire, agua y presión (8), Equilibrio mecánico (6), Óptica (8) y Vibraciones (2). En su mayor parte, estos experimentos están basados en el material desarrollado en el proyecto de innovación educativa *Demostraciones de Física para el aula* de la Facultad de Física de la Universidad de Valencia (ver enlace en www.uv.es/fisicademos[1,2]), así como en el material desarrollado en la feria Experimenta dentro del taller "Fisicalandia".

Las explicaciones de los experimentos se realizan a un nivel accesible para el público general, pero se han incluido referencias a diversos artículos educativos que permiten ampliar conocimientos hasta llegar a nivel universitario. El público objetivo al que va dirigido el contenido del Kit corresponde a alumnos de ESO, Bachiller y primeros cursos de grados científicos, así como a los profesores de asignaturas relacionadas con la física de estos niveles educativos.

En la Figura 1 incluimos los enlaces a los vídeos. El libro con explicaciones puede descargarse del siguiente enlace: https://links.uv.es/GB7FTOP

Figura 1. Link a los ocho videos desarrollados para el Kit.

[1] Ch. Ferrer-Roca, Demostraciones de Física para todos los grados de la UVEG, *Revista Española de Física* **33**(3), 31 (2019)
[2] Ch. Ferrer-Roca et al., Physics demos for all UVEG degrees: a unique project in Spain, *Procedia-Social and Behavioral Sciences*, **228**, 628 (2016).

Dos propuestas para divulgar ciencia entre los más jóvenes

Isabel Abril[1,*], Rafael Garcia-Molina[2]

[1]*Departament de Física Aplicada, Universitat d'Alacant, E-03080 Alacant, España.*
[2]*Departamento de Física, Universidad de Murcia, E-30100 Murcia, España.*

*e-mail: ias@ua.es

Conscientes de la transcendencia de la Ciencia en la sociedad y su contribución al estado del bienestar, consideramos imprescindible la divulgación científica para fomentar el interés por la ciencia, así como su positiva valoración, a fin de crear una cultura científica entre la población, independientemente del grupo social al que pertenezca y de su formación académica.

Presentamos dos propuestas de divulgación científica dirigidas a niños y a jóvenes: *El Pati de la Ciència* y el *Certamen d'Experiències Científiques*, ambas desarrolladas en la Universitat d'Alacant (UA). El contacto con la ciencia desde edades tempranas es una excelente forma de impulsar vocaciones científicas, contribuir a aumentar la visibilidad de la ciencia y favorecer la alfabetización científica.

El Pati de la Ciència se inició en el año 2005, integrado en la Escuela de Verano de la UA, y su objetivo es acercar la ciencia a los más jóvenes en un ambiente educativo informal, atractivo y lúdico, demostrando que se puede aprender divirtiéndose. A continuación, se detallan de las actividades de que consta. *Espectáculos Científicos* de física, química y matemáticas (realizados por reconocidos divulgadores), donde se presentan experimentos sorprendentes que estimulan la curiosidad. *Talleres científicos* (tutelados por estudiantes de la Facultad de Ciencias de la UA), donde los niños desarrollan sus propios experimentos, lo cual sirve para promover actitudes críticas a través de la interrogación, la observación y la experimentación, introduciendo el método científico como una herramienta eficaz para encontrar respuestas a cada pregunta. *Camisetas con la caricatura de científicos ilustres*, donde se presentan personajes que son referentes prestigiosos, así como acontecimientos científicos históricos, y, en particular, se destaca el papel de las mujeres científicas. Regalo de *juguetes científicos*, para resaltar el carácter lúdico de la ciencia. *Grabación y edición* de los espectáculos científicos (disponibles en https://rua.ua.es/dspace/handle/10045/15064), con la finalidad de que estas actividades sean accesibles a cualquier persona interesada por la ciencia.

El *Certamen d'Experiències Científiques* está pensado para que grupos de estudiantes no universitarios (dirigidos por sus profesores), preparen y realicen experimentos científicos para explicarlos al público asistente a una feria de la ciencia que se realiza en las instalaciones de la UA. En este proyecto los protagonistas son alumnos de preescolar, primaria, secundaria y bachillerato, quienes exponen sus experimentos de una manera próxima, atractiva y participativa, y son capaces de entusiasmar con su creatividad y gracia a familiares y amigos. Hay que destacar que la lengua vehicular de este proyecto es el valenciano (variante dialectal del catalán), lo cual ha supuesto que en ocasiones los tutores sean profesores de ciencias y de valenciano, proporcionando un acercamiento entre ciencias y letras, y fomentando la idea de que la ciencia es cultura. En el enlace https://www.youtube.com/watch?v=LPuBLoieOgg puede verse un vídeo que resume el ambiente de este certamen y algunas de las presentaciones. Este evento de divulgación científica ha tenido un enorme éxito, ya que al primer certamen se presentaron 15 proyectos, mientras que en la segunda edición se presentaron 57 proyectos, desarrollados por alumnos de todas las edades. Y es que la creatividad y la innovación de las presentaciones cautivó a todos los asistentes, estimulando el interés y la curiosidad por la ciencia. Como resultado de estos certámenes se publicó el libro *Certàmens d'Experiències Científiques (2015 i 2016) Universitat d'Alacant*, donde se recogen todos los experimentos presentados para que puedan ser utilizados por otros docentes como material didáctico.

QUANTUM BREAK - exploiting an escape room to reinforce physics and chemistry concepts among bachillerato students

Angel Avila[1,*], Pablo de Vera[2], Jesus Martinez-Asencio

[1]*IES Severo Ochoa, Elche, Spain.* [2]*Departamento de Física - Centro de Investigación en Óptica y Nanofísica, Universidad de Murcia, Murcia, Spain.*

*e-mail: innovadoc.gid@gmail.com

Schrödinger's cat thought experiment is one of the most popular paradoxes in quantum physics. The counterintuitive fact that the cat locked up in the box is in fact dead and alive at the same time, until the box is opened, very easily catches the imagination of scientists and students alike, and has become one of the most recognizable scientific facts in popular culture. This reasoning led INNOVADOC (a group of secondary school and university teachers, science disseminators and students interested in teaching innovation [1]) to use this famous experiment as a storytelling premise to elaborate the project QUANTUM BREAK, in the vein of the popular recreational science activities that have proven so effective for stimulating the interest of students for science [2].

QUANTUM BREAK is a scientific escape room game aimed at Bachillerato level (university preparatory courses in Spain). Players, i.e. the students, reinforce the concepts they have learnt in physics and chemistry lessons, putting them in practice through a set of intellectual riddles and puzzling challenges. They have to complete them in time to beat the game victoriously. In QUANTUM BREAK, students need to work as a team to face the mission of infiltrating Schrödinger's lab in order to find and rescue a cat trapped inside a box and, thereby, solving the experiment paradox. To accomplish their task, they have to solve different physics and chemistry enigmas, such as adjusting the coefficients of a chemical reaction, deducing the wavelength of a light source, finding the pH of various solutions, or making an electrical circuit work (see figure 1).

Figure 1. QUANTUM BREAK project: examples of some of the scientific challenges the students have to solve.

In this contribution, the QUANTUM BREAK activity will be explained, as well as how it has been implemented in the classroom. The impact it had on the students' learning process and the interest it has sparked in them will be estimated.

[1] INNOVADOC social media: Facebook - innovadoc.gid; Instagram - innovadoc.gid; Twitter - @innovadoc_gid.
[2] R. García-Molina, Ciencia recreativa: un recurso didáctico para enseñar deleitando, *Revista Eureka sobre Enseñanza y Divulgación de las Ciencias* **8** (Número Extraordinario) (2011) 370.

Acknowledgements: The authors would like to thank the students of IES Severo Ochoa in Elche (Spain) for their participation in this activity. PdV acknowledges the Teaching Innovation Group "Enseñanza Práctica de la Física" and the Knowledge Transfer Group "PaCienciaLaNuestra" of the Universidad de Murcia, for encouraging his participation in teaching innovation and science popularisation activities.

On the experience of 25 years in writing textbooks for middle and high school in Portugal

Manuel Fiolhais

Department of Physics and Centre for Physics of the University of Coimbra (CFisUC), P-3004-516 Coimbra, Portugal.

e-mail: tmanuel@uc.pt

We describe our experience, already over more than two decades, in the production of textbooks and other educational resources for the middle and secondary levels of the Portuguese educational system, in Physics.

The changes of the political-educational contexts, that shape the genesis of these materials, are highlighted. In particular, the different ways the syllabuses have been introduced, along the years, to the stakeholders, including textbook authors, are presented, as well as the process of certification of the contents of the books and the process of their selection by the teachers in the schools.

The main technological developments applied to the educational resources since the beginning of the century are also stressed in a time-line perspective. In a not so far future, the textbook is likely to exist only in digital form, accompanied with a plenty of complementary digital materials. Nowadays, both the traditional books and the digital ones co-exist, though the tendency favouring only the digital form turns out to be increasingly stronger.

The principal focal points in the elaboration of these pedagogical materials are presented, including the vision of the historical evolution and the inevitable reference to the current situation, with references to the state-of-the art in the various fields of physics and their technological applications. Other pedagogical aspects, including the role of exercise books are discussed as well as the increasing role of the publishers in providing the necessary didactical support to the physics teachers, a situation which is very much appreciated and recognized.

We deem that the exchange of experiences, on this domain of physics textbooks at non-university levels, between teachers of our both countries − Portugal and Spain −, is highly important, and the Encuentro Ibérico de Enseñanza y Divulgación de la Física is an adequate forum for such a discussion.

Including reformulated editions, which occur very often due to the frequent modifications of the syllabuses, the speaker co-authored more than fifty textbooks (manuals), exercise books, teacher support notebooks and other material intended for the 7th, 8th and 9th grades (ages 12-14 years) of basic school (Physics-Chemistry) and for the 10th, 11th and 12th grades (ages 15-17 years) of secondary school (Physics) in Portugal.

Students judgment of learning strategies effectiveness: a case study in an undergraduate physics course at the University of Porto

T. M. Seixas[1,2,*], M. A. Salgueiro da Silva[1,2]

[1]*Department of Physics and Astronomy, Faculty of Sciences, University of Porto, Rua do Campo Alegre, 687, 4169-007 Porto, Portugal.* [2]*Centre for Earth and Space Research of the University of Coimbra (CITEUC), Portugal.*

*e-mail: tmseixas@fc.up.pt

Giving college students more control on one's own learning experiences is a common practice at higher education. Students establish goals and action plans to manage their academic learning, requiring a considerable engagement in academic self-regulated learning. Self-regulation refers to the control students have over their cognition, motivation, emotions, and behaviour, based on their personal learning strategies, to achieve their established goals regarding academic performance and success. There are different theories to explain how self-regulated learning (SRL) works, but the two most recognized models that have received considerable attention are the Zimmerman's [1] and Pintrich's [2] models of SRL. According to Zimmerman's model, SRL covers key processes, involving cognitive, behavioural and motivational aspects to the attainment of personal goals. In this model, SRL can be organized in three phases: forethought, performance and self-reflection. Pintrich's model of SRL presents a ground and a clarification of SRL through a conceptual framework organized in four phases: forethought/planning/activation, monitoring, control, reaction/reflection. Each of these phases have four different areas for regulation (cognition, motivation/affect, behaviour, context), where motivation and behaviour roles in SRL are emphasized.

Even though higher education students engaged in academic self-regulated learning are prone to successful performance, instructor role in scaffolding students in the different phases and areas of SRL is seen as a way to close achievement gaps and activating learning strategies. Students differ in their learning methods and in their metacognitive analysis. In practice, how instructors guide students in their SRL depends on the situation and must be adapted accordingly.

This study examines data collected through a questionnaire about the Students Judgment of Learning Strategies Effectiveness (SJLSE) in order to explore students' cognitive and metacognitive strategies. A sample of 66 out of 71 students of an undergraduate physics course on Digital Electronics and Circuits, at the Faculty of Sciences of the University of Porto (2020/2021), participated in the survey. Students were asked to report their use (yes or no) of seven provided common learning strategies and their perceived effectivenesses (scale: 1-5). For each of the strategies, we calculated the sample average and standard deviation of the following quantities: strategy use (SU), strategy perceived effectiveness (SE), strategy used effectiveness (SUE), and strategy effectiveness loss (SEL). We also calculated the correlation matrix of the strategies' perceived effectivenesses and found that the correlations are generally low. The correlation between students' final grades and strategies' use or strategies' perceived effectivenesses are also very small.

Previous research [3] revealed that students often do not develop effective learning strategies, using instead unaware low effective learning strategies, and making poor and inaccurate assumptions of their effectiveness. Such ineffective SRL, which partially corroborates our findings, requires teacher scaffolding in different phases and areas, to guide students in their choice of learning strategies, thereby promoting their academic success.

[1] B. J. Zimmerman, *Handbook of self-regulation* (pp.13–39). San Diego, CA, US: Academic Press. M. Boekaerts, P. Pintrich, M. Zeidner (Eds.) (2000).
[2] P. R. Pintrich, *Handbook of self-regulation* (pp. 451–502). Academic Press. M. Boekaerts, P. R. Pintrich, M. Zeidner (Eds.) (2000) https://doi.org/10.1016/B978-012109890-2/50043-3
[3] R. A. Bjork, J. Dunlosky, N. Kornell, *Annual Review of Psychology* **64**, 417 (2013) https://doi.org/10.1146/annurev-psych-113011-143823.

Acknowledgements: This work was carried out under project UID/Multi/00611/2020, funded by FCT/MEC (PIDDAC) and FEDER — European Regional Development Fund through COMPETE 2020 — Operational Programme Competitiveness and Internationalization (project: POCI-01-0145-FEDER-006922).

Herramientas computacionales de software libre en la Física de Secundaria

Beatriz Padín

Colexio M. Peleteiro, Santiago de Compostela, España.

e-mail: beatrizpadin@peleteiro.com

Saber programar es una habilidad esencial en la práctica de la Física [1]. Sin embargo, la programación científica no está incluida en el currículo de las asignaturas de ciencias en Enseñanza Secundaria, a pesar de ser una herramienta que aparece de una u otra manera en los primeros cursos de todas las carreras de ciencias.

En la presente ponencia se muestran varias herramientas de software libre que permiten introducir la programación científica en la enseñanza de la Física en ESO y Bachillerato. Con este enfoque no solo se enriquece enormemente la enseñanza de la asignatura, sino que además se fomenta que los alumnos adquieran unas competencias en las TIC que serán absolutamente fundamentales en su futuro trabajo como científicos, y se promueve el uso del software libre.

Las herramientas presentadas abarcan tres campos diferentes. En primer lugar se muestra el entorno SageMath, que agrupa decenas de programas matemáticos bajo una interfaz única, para usarlo en la resolución computacional de problemas. A continuación se presenta el software estadístico R, una completísima herramienta que permite hacer el tratamiento de los datos experimentales en las prácticas de laboratorio. Por último se verá cómo se puede utilizar la plataforma Arduino para programar sensores y montar prototipos que ilustren de manera práctica diferentes aspectos teóricos tratados en el aula. Junto con cada herramienta se presenta una variedad de actividades sobre temas curriculares que se pueden llevar a cabo en el aula de Secundaria.

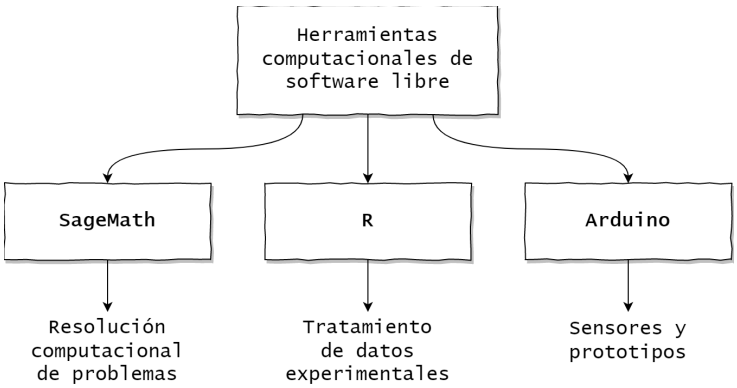

Los ejemplos analizados son solo una muestra de cómo el uso de un lenguaje de programación posibilita adoptar enfoques didácticos que de otra manera no serían posibles. Aparte de la ventaja que esto supone, es de resaltar el factor motivador que puede tener para los alumnos afrontar retos más interesantes y realistas que los habitualmente tratados en el aula. Sin embargo, a nadie se le escapa que las condiciones para usar la programación en el aula son adversas: su uso no es inmediato ni intuitivo; aprenderlas y dominarlas lleva tiempo; la mayoría de los profesores no tienen formación en este campo y, sobre todo, los temarios oficiales son de por sí muy extensos como para introducir nuevos contenidos. Para empeorar aún más la situación, no hay apenas bibliografía con recursos de calidad enfocados a la programación científica en Secundaria. Es por esto que la principal intención de la presente ponencia es, por un lado, dar a conocer estas herramientas computacionales y los beneficios didácticos que ofrecen y, por otro, compartir materiales didácticos con la comunidad educativa para que aquellos profesores que decidan utilizar la programación científica en el aula dispongan de actividades concretas con las que complementar la manera tradicional de enseñar Física.

[1] American Association of Physics Teachers, *AAPT Recommendations for Computational Physics in the Undergraduate Physics Curriculum* (2016).

Estudio de la fuerza eléctrica entre dos esferas cargadas

Guadalupe Grande Alcalde[1], Ernesto Pastor Lebrero[2,*]

[1]*Estudiante 2º IB, IES Castilla (Soria), España.* [2]*Departamento de Física y Química, IES Castilla (Soria), España.*

*e-mail: ernesto.pasleb@educa.jcyl.es

Los modelos que se estudian en secundaria y bachillerato definen situaciones ideales, que en la mayoría de los casos se ajustan razonadamente bien a la realidad. El objetivo principal de nuestro estudio es mostrar a los alumnos que estos modelos devuelven soluciones aproximadas mientras nuestro sistema sea similar a los conceptos ideales en los que se sustentan. Uno de estos conceptos ideales es el de carga puntual.

Para su estudio se crean esferas de distintos tamaños (1, 2 y 4 cm de diámetro) y se recubren con pintura conductora. A continuación, se introducen en una balanza de precisión como se muestra en la figura 1. Se cargan con ayuda de un Van der Graaf. La esfera superior está conectada a un tornillo sin fin con el que se varía la distancia. La balanza nos muestra, de forma indirecta, la fuerza entre las esferas. Se mide la fuerza en función de la distancia entre los centros y se estudia para esferas de distinto tamaño.

Los resultados obtenidos muestran que la relación entre fuerza eléctrica y distancia entre esferas no se ajusta del todo al modelo de cargas puntuales de Coulomb. Evidenciando que, en algunas distribuciones, la fuerza es ligeramente inferior a la esperada teóricamente. Se decide a continuación añadir al modelo un término de corrección que proponen Slisko y Brito-Orta [1]. En la figura 2 se representa la fuerza eléctrica en función del parámetro $A = (1-4\beta^3)/d^2$. Donde $\beta=R/d$, es la relación entre el radio de las esferas R y la distancia entre sus centros d. Se puede confirmar que la aproximación propuesta para la fuerza entre dos esferas cargadas es válida siempre que la distancia entre sus centros sea mayor a 2,5 veces el radio. La pendiente de las rectas es directamente proporcional al cuadrado de carga acumulada en el sistema, observamos que a mayor radio de las esferas mayor es la carga acumulada, como era de esperar.

En conclusión, se ha estudiado la repulsión entre esferas cargadas, comprobando que no se ajusta al modelo ideal de cargas puntales de Coulomb, pero sí a la aproximación propuesta por Slisko y Brito-Orta. Además, resulta muy ilustrativo usar el montaje diseñado, en sesiones de 2º de bachillerato para mostrar de forma cualitativa la variación de la fuerza en función de la distancia entre cargas.

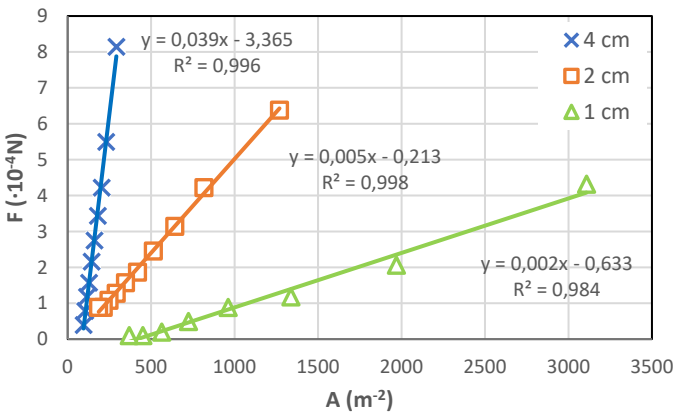

Figura 2. Fuerza eléctrica frente a *A*, para esferas cargadas de distinto diámetro, como se muestra en la leyenda.

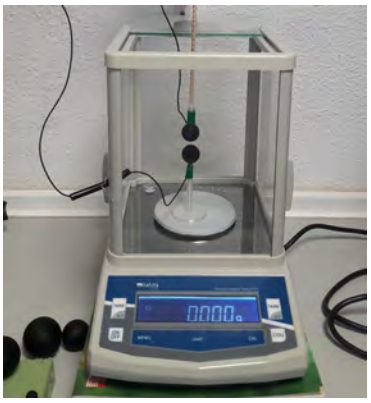

Figura 1. Detalle del montaje. Esferas en la balanza de precisión.

[1] Slisko J., Brito-Orta R. A., On approximate formulas for the electrostatic force between two conducting spheres. *Am. J. Phys.* **66**(4) 352 (1998).

Los laboratorios remotos para la enseñanza de la Física en Secundaria

Daniel Aguirre Molina

Colegio Pedro Poveda, Jaén, España.

e-mail: d.aguirre3@gmail.com

El uso de laboratorios remotos es algo habitual en la docencia universitaria online. Pero este tipo de situación didáctica también ofrece interesantes opciones en la Educación Secundaria. Se analizan varias opciones que ofrece la plataforma LabsLand para el uso de laboratorios remotos para cualquier nivel.

También se analizan las ventajas e inconvenientes que ofrecen frente a los laboratorios virtuales o simulaciones, así como frente a la realización de experimentos reales en el laboratorio de la escuela.

Se describe la experiencia realizada en 4º ESO en el Colegio Pedro Poveda de Jaén (España) el curso 2020-2021 donde se utilizaron laboratorios remotos en varias situaciones como por ejemplo para la obtención del valor de la aceleración de la gravedad g y otros ejemplos utilizados en la asignatura de tecnología por el autor, como el uso de la placa Arduino y robots programables a distancia.

Se detallan las posibilidades que ofrece la plataforma LabsLand para la gestión de estudiantes y el uso que realizan los mismos de los laboratorios y se comentan otros laboratorios interesantes para los estudiantes de secundaria en el ámbito de las ciencias y la tecnología.

Finalmente se detallan otras opciones para el uso de experimentos remotos y virtuales, como los desarrollados por el proyecto NextLab (y su antecesor GoLab), donde existen además desarrollos didácticos listos para usar en el aula.

Análisis de la implementación de proyectos STEAM en el aula de la Educación Secundaria Obligatoria

Miguel Ángel Queiruga-Dios[1,*], José Benito Vázquez Dorrío[2]

[1]*Departamento de Didácticas Específicas, Universidad de Burgos, España.*
[2]*Departamento de Física Aplicada, Universidade de Vigo, España.*

*e-mail: maqueiruga@ubu.es

Los currículos educativos se están orientando hacia un enfoque integrativo de las disciplinas [1,2]. Así, de un tiempo a esta parte, se habla del enfoque educativo STEAM, que busca la integración de las disciplinas STEM (*Science*, *Technology*, *Engeeniering and Mathematics*) y el arte, el lenguaje, los estudios sociales y las humanidades [3]. Esta integración de las disciplinas permite abordar, además, la comprensión y resolución de problemas actuales, desde una mayor interdisciplinariedad [4]. Con esto, se contribuye a desarrollar la alfabetización científica del alumnado preparándolo para la ciudadanía global, a la par que enriqueciendo las experiencias de aprendizaje mejorando los aspectos afectivos del proceso de enseñanza-aprendizaje y disminuyendo el abandono escolar. La metodología de Aprendizaje Basado en Proyectos (ABP) [5] puede proporcionar al alumnado oportunidades para aplicar conceptos STEAM, involucrándolos en actividades que se asemejan a las situaciones familiares que pueden encontrar en sus vidas y para las que existen múltiples soluciones. Así, el ABP involucra al alumnado en el diseño, resolución de problemas, toma de decisiones y procesos de investigación cuasiautónoma, habitualmente en pequeños grupos en los que cada uno asume un rol, establecido por el profesor o que surge como consecuencia del crecimiento del proyecto, y que finaliza con un producto o una presentación. El alumnado participa controlando muchos de los aspectos del proyecto, desde las preguntas que se generan, los recursos que utilizan para encontrar respuestas, las tareas y roles que asumen dentro del grupo, así como los productos que van a desarrollar como conclusión.

En esta comunicación se analizarán los resultados, ventajas y dificultades de algunos ejemplos de proyectos STEAM realizados en la Enseñanza Secundaria Obligatoria utilizando la metodología ABP con conexiones o sinergias con el entorno (Fig. 1).

Figura 1. Exposiciones de los proyectos realizados por el alumnado.

[1] MEFP, *Ley Orgánica 3/2020, de 29 de diciembre, por la que se modifica la Ley Orgánica 2/2006, de 3 de mayo, de Educación* (2021).
[2] G. Oliveira, *O perfil dos alunos à saída da escolaridade obrigatória*, Ministério da Educação (2017).
[3] M. Á. Queiruga-Dios, E. López-Iñesta, M. Diez-Ojeda, M. C. Sáiz-Manzanares, J. B. Vázquez-Dorrío, *Journal for the Study of Education and Development* **44**, 871 (2021).
[4] A. Nistor, A. Gras-Velazquez, N. Billon, G. Mihai, *Science, Technology, Engineering and Mathematics Education Practices in Europe. Scientix Observatory Report*, European Schoolnet (2018).
[5] M. Á. Queiruga-Dios, M. C. Sáiz-Manzanares, E. Montero-García, *Research in Education and Learning Innovation Archives*, **23**, 1 (2019).

La Física de la Fórmula 1

J. M. Marcos*, Julia Gil

Departamento de Física, Universidad de Extremadura, España.

*e-mail: jesusmm@unex.es

La Fórmula 1 cuenta cada vez con más espectadores y cada vez más jóvenes. El estreno de la serie de Netflix "Drive to Survive" a partir de la temporada 2018 de la Fórmula 1 no ha hecho sino aumentar esta tendencia. Es por eso, que consideramos que la introducción de esta temática en un aula puede resultar atractiva para introducir a los estudiantes en algunos conceptos sencillos relacionados con la física de fluidos como la presión de un fluido o para que comprendan mejor la ecuación de conservación de la energía de un fluido en el caso ideal (Ecuación de Bernouilli).

Para empezar, creemos que sería adecuado introducir una analogía entre las alas de los aviones y los alerones de un monoplaza de Fórmula 1 (Figura 1). Esto ayudará a entender mejor cómo funcionan los alerones, y cuáles son las fuerzas que intervienen en el sistema.

En el caso más sencillo, solo hay que tener en cuenta 4 fuerzas sobre el ala de un avión. El peso del avión (vertical y hacia abajo), la sustentación del ala (vertical y hacia arriba), el empuje que hacen los motores (horizontal y en el sentido del movimiento) y la fuerza de rozamiento con el aire (horizontal y en el sentido contrario al movimiento). (Figura 2)

Todas estas fuerzas salvo la sustentación son fácilmente entendibles por el alumnado [1]. Para entender de donde sale esta fuerza de sustentación lo más sencillo es hacerles ver que el ala del avión divide el flujo de aire en dos secciones (superior e inferior) que tienen presiones diferentes. Esta diferencia de presiones es la que genera esta fuerza de sustentación (al igual que una diferencia de presiones mueve un pistón).

Figura 1: Alerón trasero de un monoplaza de Fórmula 1. Es fácil observar las similitudes entre el perfil del alerón y el ala de un avión.

Explicar el motivo de la existencia de esta diferencia de presiones entre ambas secciones es probablemente el mayor problema que se nos presenta ante una clase de secundaria. Este problema se puede afrontar de varias maneras. La primera de ellas consiste en introducir la ecuación de conservación de la energía para un fluido en el caso ideal (Ecuación de Bernouilli) y a partir de ahí ver como una diferencia de velocidades en las distintas secciones implica una diferencia de presiones en las mismas. Este planteamiento, aunque muy sencillo para estudiantes de secundaria no es correcto al contener algunos errores [2] que hacen que sea mejor elegir otras explicaciones para el mismo.

Figura 2: Análisis simplificado de las fuerzas que actúan sobre el ala de un avión.

Otro planteamiento más sencillo incluso y conceptualmente correcto consiste en utilizar la tercera Ley de Newton y ver que si el ala deflecta aire hacia abajo entonces el ala debe sufrir una fuerza en el sentido contrario a la que sufre el aire.

Como habíamos partido de que los alerones de un monoplaza de Fórmula 1 son esencialmente un ala de un avión del revés, es fácil que los alumnos entiendan que en lugar de una fuerza hacia arriba que sustente al avión, los alerones generan una fuerza hacia abajo, la famosa "carga aerodinámica" que muchas veces se escucha durante las retransmisiones de una carrera de Fórmula 1. Esta fuerza hace que los monoplazas permanezcan bien adheridos al suelo, lo que contribuye a su estabilidad, permitiéndoles tomar curvas a muy alta velocidad sin perder el control de los mismos.

[1] T. López-Arias, G. Zendri, L. M. Gratton, S. Oss, *Revista Española de Física* **28**, 14 (2014).
[2] Holger Babinsky, *Physics Education* **38**(6), 497 (2003).

Collisions in the Macroscopic World: Billiard Balls

S. Pinto, **L. Santos***, J. Couto, F. Leal, G. Barbosa

Colégio Casa Mãe, Portugal.

*e-mail: l_f_santos@hotmail.com

Background: A collision is an interaction by means of forces between two particles within a short period of time, which occurs when they move towards one another and contact takes place between them [1,2]. The coefficient of restitution, however, is a parameter associated with the behaviour of two bodies during a collision and, according to Newton's Law of Restitution, is defined as the reason between the withdrawal velocity ($\vec{v}_{A_{final}} - \vec{v}_{B_{final}}$) and the approach velocity ($\vec{v}_{A_{initial}} - \vec{v}_{B_{initial}}$) [2].

Theoretically, elastic collisions occur only when a system's kinetic energy is conserved, which means that there isn't any loss nor transformation of kinetic energy into other type of energy within the system [1]. Moreover, in an elastic collision, since there is conservation of kinetic energy, the withdrawal velocity equals the approach velocity of the particles, therefore the coefficient of restitution is total [2].
Taking this into account, we questioned ourselves: "Can collisions in the macroscopic world be classified as elastic?".

Methodology: In order to obtain the answer to our previously stated question, we resorted to an experimental study with a deductive approach primarily based on mathematical physics, in which we filmed two billiard balls colliding and then analyzed our video trials using the *Tracker Video Analysis and Modeling Tool*.

Results: In all of the trials, the curves described in the velocity as a function of time and kinetic energy as a function of time graphs were quite similar, both between the same variable graph of each ball as well as when in comparison with the other ball.

In general, by analysing the velocity as a function of time graphs, we noticed that the collisions took place within the 0,2 second mark and the 0,3 second mark, in which we observe an abrupt variation of the magnitude values of the velocity of each ball, which tend to increase during the approach and decrease during the withdrawal of the balls.

Furthermore, when we examined the kinetic energy as a function of time graphs, we perceived that within the time period in which the collision occurs, these curves also describe sudden variations and then the values drop down almost in a consistent way.

Conclusions: In response to the question we proposed at the beginning of this study – "Can collisions in the macroscopic world be classified as elastic?" – the results we obtained were enough for us to state with certainty that collisions in the macroscopic world can never be classified as elastic, only as inelastic (or perfectly inelastic, for that matter).

This happens because there will always be some deformation, loss and/or transformation of kinetic energy as the systems aren't truly isolated and varying forces will constantly be acting on it. In fact, you can hear a billiard ball collision, which means that some of the system's kinetic energy is being transferred away from it by sound. Besides, the billiard balls eventually come to a stop due to the force of friction caused by the contact that takes place between them and the billiard table, that is, the withdrawal velocity does not equal the approach velocity of the particles, hence the coefficient of restitution being far from total.

[1] R. A. Serway, J. W. Jewett, *Physics for Scientists and Engineers* (9th ed.), Cengage Learning (2013).
[2] R. Earl, J. Nicholson, *The Concise Oxford Dictionary of Mathematics* (6th ed.), Oxford University Press (2021).

Teaching/Learning experiences in Physics: engineering degrees

J. Daza, L. Escoda, M. Soler, J. Planella, **J. J. Suñol***

GID-Physics, Department of Physics, Campus Montilivi s/n, University of Girona, 17003 Girona, Spain.

*e-mail: joanjosep.sunyol@udg.edu

The educational innovation group in Physics (https://www.udg.edu/en/ice/Innovacio-docent/Grups-dinnovacio-docent/GID-en-Fisica) is linked to the Institute of Educational Sciences (ICE) of the University of Girona. The most recent activities of this group have focused on diverse experiences: a) flipped classroom, b) learning physics with peer mentoring, c) teamwork and d) blended learning [1,2]. The perception of the students has been collected in surveys and questionnaires specifically designed. In recent years, the influence of the pandemic has been confirmed as the same activities have been carried out one year in person and another virtually. Thus, due to the pandemic some specific adaptations (from face-to-face to on-line) have been performed.

Regarding our experience in flipped classroom, the assessment of the students in general is positive. This methodology has been applied also to problems solving and laboratory sessions. The analysis of the assessment marks indicates a slight increase if compared to those obtained in previous academic years. A detected problem is the wrong time management of some students. A positive remark is that the interaction between professors and learners has been improved. Furthermore, the face-to-face sessions are recorded. Thus, students have access to a professor edited version of the session and to a large variety of content materials (free access, adaptation to learning needs).

Regarding peer mentoring, the mentors are expert students of higher courses who act in the classroom when the students have some doubt when trying to solve (usually in a group) one of the practical cases raised by the professor. The students who act as mentors have been trained in previous sessions with the support of an academic tutor. Likewise, the analysis of the academic results is being carried out during these last years and it is verified that the dropout rate has decreased significantly, and that the percentage of students who end up passing the subject that same academic year is around 50% higher than before.

Regarding the experiences of teamwork, it has been found that students with a more favorable opinion on this learning procedure are those who already have previous experience in this methodology. In addition, students often agree with the grade obtained and accept peer criticism constructively. Rubrics have also been shown to be a good teaching tool for co-assessment teamwork.

Blended learning is an efficient combination of different teaching-learning methods, teaching-learning models and learning styles. The overall level of satisfaction with this methodology is high. Likewise, the score of laboratory sessions (face-to-face) is higher than those of problems (face-to-face) and theory sessions (on line). Blended learning favours the interaction with professors by two pathways (direct contact and virtual environment). Furthermore, statistical analysis of surveys show that blended learning also favours academic interaction with the peers. Likewise, the students' perception is that blended learning is associated to an increase of the working time.

[1] J. J. Suñol, *Proceedings Edulearn* **21**, 10927 (2021).
[2] M. Soler, L. Escoda, J. J. Suñol, J. Planella, *Proceedings Edulearn* **21**, 10915 (2021).

Acknowledgements: GID-Physics agrees the support of the ICE of the University of Girona.

Laboratorio virtual para estudiar la caracterización de lentes multifocales

Diego Montagud-Martínez[1,2,*], Vicente Ferrando[1], Laura Remón[3], Anabel Martínez-Espert[4], Walter D. Furlan[2] y Juan A. Monsoriu[1]

[1]*Centro de Tecnologías Físicas, Universitat Politécnica de València, 46022 Valencia, España.* [2]*Departamento de Óptica y Optometría y Ciencias de la Visión, Universitat de València, 46100 Valencia, España.* [3]*Departamento de Óptica, Universidad de Zaragoza, 50009 Zaragoza, España.* [4]*Clínica Aiken, Fundación Aiken, 46004 Valencia, España.*

*e-mail: diemonma@upvnet.upv.es

El uso de lentes multifocales está cada día más extendido, por lo que el estudio preliminar de su comportamiento bajo diferentes parámetros de diseño es interesante desde un punto de vista docente. En este trabajo presentamos un nuevo laboratorio virtual desarrollado en lenguaje de código abierto python que permite obtener, de forma sencilla, la caracterización óptica de lentes multifocales a partir de un conjunto de métricas [1]. Mediante esta aplicación el estudiante puede seleccionar entre lentes estándar (monofocal, bifocal y trifocal) y algunas lentes comerciales, con perfiles difractivos predefinidos, y una serie de parámetros de configuración tales como esfera, cilindro, eje, aberración esférica y diámetro de la pupila. El programa muestra una previsualización del mapa de fase y la irradiancia axial en el rango de vergencias de -1 a 4 D. Para realizar la caracterización de la lente con la configuración seleccionada se dispone de diferentes métricas como la *Modulation Transfer Function* (MTF) en las direcciones X e Y, la *Point Spread Function* (PSF) y la simulación de imágenes a partir de una lista de objetos seleccionables. Mediante el cálculo de estas métricas en una vergencia seleccionada por el estudiante se puede analizar la calidad óptica de los diferentes focos, así como los efectos de diferentes aberraciones, como la división de los focos que provoca el astigmatismo o la extensión de foco producida por la aberración esférica.

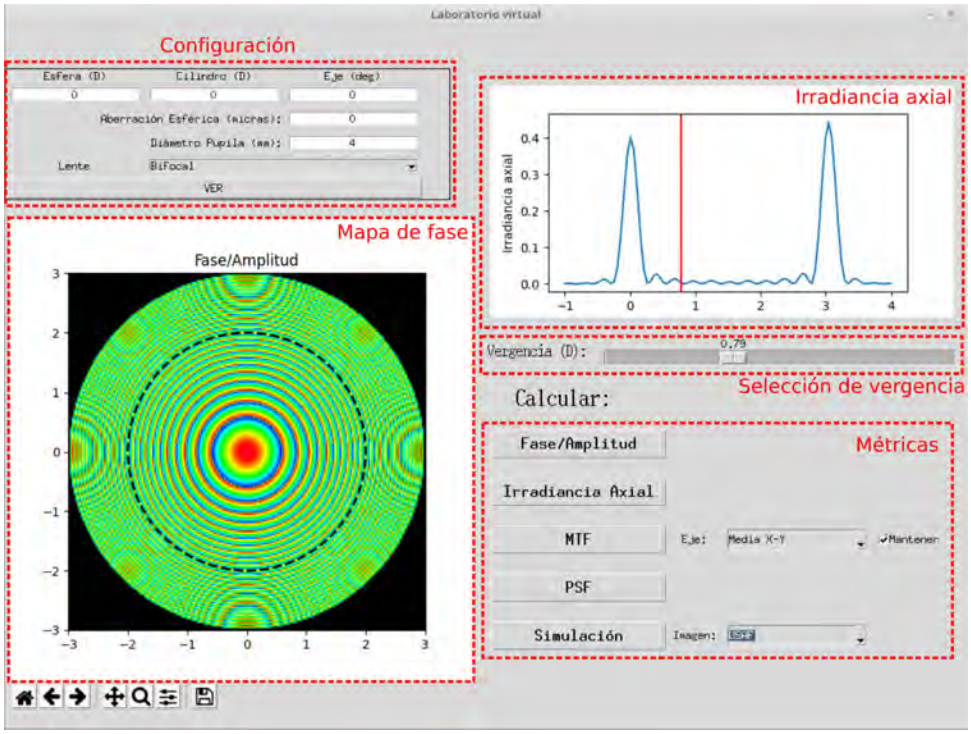

Figura 1. Interfaz gráfica del laboratorio virtual desarrollado en lenguaje python.

[1] P. Artal, *Handbook of visual optics: Fundamentals and eye optics*, CRC Press (2007).

Agradecimientos: Diego Montagud-Martínez agradece la financiación otorgada por la beca Margarita Salas del Ministerio de Universidades de España financiado por the European Union-Next Generation EU.

On teaching thermodynamics in 21st century

J. Güémez*, J. A. Mier

Applied Physics Department, University of Cantabria, Spain.
*e-mail: julio.guemez@unican.es

The application of Einstein's special relativity postulates – with their physical requirements and demands –, allows to obtain a relativistic Minkowski's 4-vector equation (generalising the first law of thermodynamics: $\mathrm{d}K_{\mathrm{cm}} + \mathrm{d}U = \Sigma_{\mathrm{k}}\delta W_{\mathrm{k}} + \delta Q$ [1, pp. 101-2]), given by [2]:

$$\mathrm{d}E^{\mu} \;=\; \Sigma_{\mathrm{k}}\delta W^{\mu}_{\mathrm{k}} + \delta Q^{\mu} \;\longrightarrow\; E^{\mu}_{\mathrm{f}} - E^{\mu}_{\mathrm{I}} = \Sigma_{\mathrm{k}} W^{\mu}_{\mathrm{k}} + Q^{\mu}\,. \tag{1}$$

This 4-vector equation transforms between inertial reference frames, in the standard configuration with speed V, by the Lorentz transformation $\mathcal{L}^{\mu}_{\nu}(V)$, according to the principle of relativity. Equation (1) is applied both to problems in pure mechanics (mechanical energy conservation processes) and in thermodynamics (mechanical energy dissipation, or mechanical energy production processes [2]). By inspecting the spatial and temporal components in Eq. (1), two different equations are yielded: (i) [spatial components] the linear-impulse–linear-momentum variation equation (relativistic Newton's second law) and (ii) [temporal components] the energy–work–heat equation (relativistic first law of thermodynamics).

Example. A block, with inertia $\mathcal{M}$, accelerates under the action of an external force $\mathbf{F} = (F\sin\alpha, F\cos\alpha, 0)$, and against a friction force (Amontons-Coulomb type) $f_{\mathrm{R}} = \mu_{\mathrm{d}}N$, on a horizontal surface. As the process' 4-vector fundamental equation we have:

$$E^{\mu}_{\mathrm{f}} - E^{\mu}_{\mathrm{I}} = W^{\mu}_{\mathrm{F}} + W^{\mu}_{\mathrm{R}} + W^{\mu}_{\mathrm{G}} + W^{\mu}_{\mathrm{N}} + Q^{\mu}\,, \tag{2}$$

where subscripts F, R, G and N stand for external, kinetic friction, gravitational and normal forces, respectively.

As a 4-vector fundamental equation we have:

$$\begin{pmatrix} c\gamma_v\mathcal{M}v \\ 0 \\ 0 \\ \gamma_v\mathcal{M}c^2 \end{pmatrix} - \begin{pmatrix} 0 \\ 0 \\ 0 \\ \mathcal{M}c^2 \end{pmatrix} = \begin{pmatrix} cF\sin\alpha\, t_0 \\ cF\cos\alpha\, t_0 \\ 0 \\ \mathbf{F}\cdot\mathbf{x}_0 \end{pmatrix} + \begin{pmatrix} cf_{\mathrm{R}}t_0 \\ 0 \\ 0 \\ 0 \end{pmatrix} + \begin{pmatrix} 0 \\ -c\mathcal{M}gt_0 \\ 0 \\ 0 \end{pmatrix} + \begin{pmatrix} 0 \\ cNt_0 \\ 0 \\ 0 \end{pmatrix} + \begin{pmatrix} 0 \\ 0 \\ 0 \\ Q \end{pmatrix}, \tag{3}$$

where $\gamma_v = (1 - v^2/c^2)^{-1/2}$ is the Lorentz factor, $\mathbf{x}_0 = (x_0, 0, 0)$ is the displacement and $\mathbf{F}\cdot\mathbf{x}_0 = F\sin\alpha\, x_0$ is the work done by the external force. From matrix Eq. (3) one obtains:

Normal force. For the normal force one has: $N = \mathcal{M}g - F\cos\alpha$. Thus, $f_{\mathrm{R}} = \mu_{\mathrm{d}}(\mathcal{M}g - F\cos\alpha)$.

Newton's second law. Linear-impulse–linear-momentum variation equations are (speed v_0 at time t_0):

$$\mathcal{M}\mathrm{d}(\gamma_v v) \;=\; [F\sin\alpha - \mu_{\mathrm{d}}(\mathcal{M}g - F\cos\alpha)]\mathrm{d}t\,, \tag{4}$$

$$\gamma_{v_0}\mathcal{M}v_0 \;=\; [F\sin\alpha - \mu_{\mathrm{d}}(\mathcal{M}g - F\cos\alpha)]t_0\,. \tag{5}$$

Complementary dynamical relationship. Using relationship $v\mathrm{d}(\gamma_v v) = \mathrm{d}(\gamma_v c^2)$, from Eq. (4) one obtains the kinetic-energy–pseudo-work equation for the process [2]:

$$\mathcal{M}\mathrm{d}(\gamma_v c^2) \;=\; [F\sin\alpha - \mu_{\mathrm{d}}(\mathcal{M}g - F\cos\alpha)]\mathrm{d}x\,, \tag{6}$$

$$(\gamma_{v_0} - 1)\mathcal{M}c^2 \;=\; [F\sin\alpha - \mu_{\mathrm{d}}(\mathcal{M}g - F\cos\alpha)]x_0\,, \tag{7}$$

where $\mathrm{d}x = v\mathrm{d}t$, x_0 is the block's displacement at t_0 and $K(t_0) = (\gamma_{v_0} - 1)\mathcal{M}c^2$ its kinetic energy.

First law of thermodynamics. From temporal components in Eq. (3), the energy–work–heat equation reads:

$$\mathcal{M}\mathrm{d}(\gamma_v c^2) = \mathbf{F}\cdot\mathrm{d}\mathbf{x} + \delta Q\ ;\ (\gamma_{v_0} - 1)\mathcal{M}c^2 = F\sin\alpha\, x_0 + Q\,. \tag{8}$$

Thermal effects equation. By comparing Eqs. (7) and (8), energy dissipated as heat at t_0 is:

$$Q(t_0) \;=\; -\mu_{\mathrm{d}}(\mathcal{M}g - F\cos\alpha)x_0\,;\, T\Delta S_{\mathrm{U}} = \mu_{\mathrm{d}}(\mathcal{M}g - F\cos\alpha)x_0 > 0\,. \tag{9}$$

As the entropy of the universe is increased, $\Delta S_{\mathrm{U}} > 0$, the process is irreversible.

In the low-speed limit, $\lim_{v_0/c\to 0}(\gamma_{v_0} - 1)c^2 = \frac{1}{2}v_0^2$, the classical equations are recovered.

For translation with rotation processes, the 4-vector Eq. (1) is generalised (by means of the cross-product between 4-vectors, represented here as $\otimes$) to a 4-tensor-moment equation [3] as:

$$r^{\mu}\otimes\mathrm{d}E^{\mu} \;=\; \Sigma_{\mathrm{k}} r^{\mu}\otimes\delta W^{\mu}_{\mathrm{k}} + r^{\mu}\otimes\delta Q^{\mu}\ ;\ \mathrm{d}J^{\mu\nu} = \Sigma_{\mathrm{k}} M^{\mu\nu}_{\mathrm{k}}\mathrm{d}t + M^{\mu\nu}_{\mathrm{ph}}\mathrm{d}t\,, \tag{10}$$

providing, in addition, the angular-impulse–angular-momentum variation equation.

[1] C. Fernández Pineda, S. Velasco Maíllo, *Introducción a la Termodinámica*, Ed. Síntesis, Madrid (2009).

[2] J. Güémez, Relativistic mechanics and thermodynamics: part I. A linear-translation four-vector formalism, *Eur. J. Phys.* **41** 065805 (2020)

[3] J. Güémez, J. A. Mier, submitted to *Eur. J. Phys.* (2022).

The challenge of teaching Physics to unmotivated undergraduate students: a case study of Health and Food Sciences degrees at the University of Valencia

M. J. Hernández Lucas*, J. C. Jiménez Muñoz

Department of Earth Physics and Thermodynamics, Faculty of Physics, University of Valencia.

*e-mail: m.jesus.hernandez@uv.es

Physics is a semester first-year core subject included in all the Degrees Programmes managed by the UVEG's Faculty of Pharmacy: Food Science and Technology, Gastronomic Sciences, Human Nutrition and Dietetics and Pharmacy. The main objective of the subject is to initiate students in physical concepts and phenomena of interest in health and food sciences, showing different applications in these fields (related to fluids mechanics, thermodynamics and wave phenomena), both in classroom as in laboratory sessions.

Teachers involved in these degrees must face an important challenge: to teach Physics to highly unmotivated students with low skills in Physics. In the case of the Pharmacy degree (survey results collected during the first class), approximately 60-70% of students coursed Physics during the first course of Baccalaureate, and only 20-25% coursed Physics during the second course of Baccalaureate. Moreover, around 70-80% of students admitted ignoring any application of Physics in Pharmacy, and therefore they were not convinced of the usefulness of Physics in their degree. Percentages are even worse in the other degrees, since, for example, in Nutrition Degree the number of students coursing Physics in the previous year is about 6%, and most of the students manifest a lack of interest for the subject which is considered to be very difficult. It is important to remark that these problems were aggravated during the last two courses because of the impact of virtual and/or hybrid teaching due to the COVID-19 pandemic [1,2].

With the intention of overcoming these barriers, a group of Physics teachers involved in Health and Food Sciences degrees at the University of Valencia participated in two Teaching Innovation Projects supported by the University of Valencia during the courses 2020-21 and 2021-22. Different teaching materials and activities were collaboratively designed in order to increase interest and motivation.

- Multimedia activities to be performed on line:
  - Videos showing some of the physical phenomena in an attractive way
  - Videos explaining laboratory experiments to be carried out in lab sessions
  - Videos with a detailed resolution of exercises
  - Questionaries to reinforce and review the different topics, which contribute to ongoing assessment
- Gamification activities:
  - Kahoot quizzes: Winners are rewarded with an insignia in the virtual classroom and UVEG corporative gifts or extra score for the final rating of the subject,
  - "Journalist role": Students must write a short text in a newspaper format or web page news section about invited talks given by graduated students about their final degree thesis and their CV. The best works receive a "Pulitzer prize"
  - Team works in multidisciplinary topics leading to presentation as posters or oral communications in front of the class (students discuss about the role of Physics to achieve the SDGs, Physics involved in household appliances, ways of cooking food, astronauts' food, molecular gastronomy, etc.).

All these activities are managed through the virtual classroom environment under the Moodle platform and the *Edumedia* (video creation and visualization).

A satisfaction survey was elaborated for students of Degree in Pharmacy and Degree in Human Nutrition and Dietetics (courses 2020/21 and 2021/22) to obtain information about students' assessment of the different activities (using a scale from 1 to 5). Overall, the activities received a score higher than 4, with most of the activities surpassing 4.5. The students also concluded that these activities significantly favored their interest in Physics and contributed to improve their understanding of the subject and made the course friendlier and more affordable.

[1] T. Feder, *Physics Today* **73**(6), 22 (2020).
[2] K. Gamage, D. Wijesuriya, S. Ekanayake, A. Rennie, C. Lambert, N. Gunawardhana, *Education Sciences* **10**(10), 291 (2020).

Acknowledgements: We thank the Servei de Formació Permanent i Innnovació Educativa (SPIE) of Universitat de València (Teaching Innovation Projects UV-SFPIE_PID-1355545 and UV-SFPIE_PID-1640695).

Hacia una propuesta de enseñanza de las condiciones de frontera para los campos electromagnéticos

E. Baradit*, I. Sánchez, R. Aedo

Departamento de Física, Universidad del Bío-Bío, Avenida Collao 1202, Concepción, Chile.

*e-mail: ebaradit@ubiobio.cl

Entre los temas de electromagnetismo que parecen sencillos se encuentran las condiciones de frontera para los campos eléctricos y magnéticos en la separación de dos medios. Sin embargo, la exposición de éstos en diferentes libros de textos no es univoca y conlleva a dificultades en su comprensión. En particular, para el campo electrostático esto ocurre tanto con la asignación de los medios, como con la presentación gráfica de los vectores de campo e incluidos los vectores unitarios normales a la frontera de separación de dichos medios.

La presentación de este tema es realizada de diferente forma cuando se desea obtener las condiciones para las componentes tangenciales y normales del campo en la superficie de separación de dos materiales dieléctricos. A modo de ejemplo, en las figuras 1 y 2 se observa la diferencia en la representación de los campos y los medios en dos de los textos bases para la enseñanza del electromagnetismo [1,2].

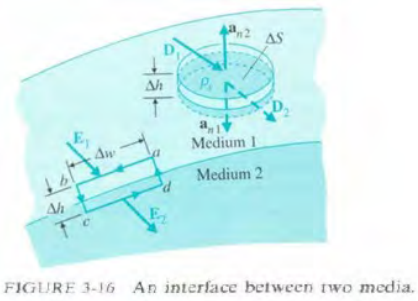

Figura 1. Caso David Cheng.

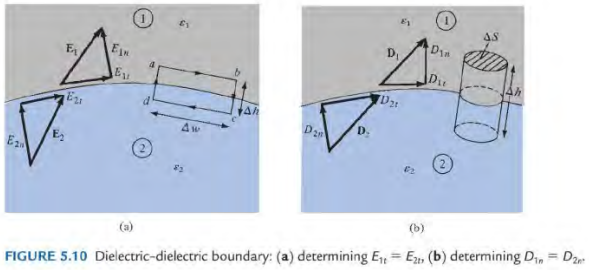

Figura 2. Caso Sadiku.

Como se puede ver de la representación gráfica de Sadiku de los campos, el medio 2 es aquel en que el vector $\vec{E}_2$ se dirije a la superficie de separación de los medios, mientras que en el capítulo correspondiente de Chen este vector se aleja desde ella. El vector $\vec{E}_1$ en Sadiku está dirigido desde la superficie de separación, en Chen hacia dicha superficie. Esta representación se contrasta también con las realizadas por ejemplo por otros autores [3,4,5]. Si bien es cierto esto no genera muchas dificultades para la comprensión y obtención de las componentes tangenciales de los campos $\vec{E}$ y $\vec{D}$, otra cosa ocurre para las componentes normales en presencia de cargas eléctricas superficiales. La diferencia de forma en que se presenta el caso conlleva al estudiante a enfrentarse con una incertidumbre.

Algunos textos obtienen por diferentes caminos las siguientes condiciones

$$D_{1n} - D_{2n} = \sigma_s \,, \qquad D_{2n} - D_{1n} = \sigma_s$$

En este trabajo se propone un único método para analizar las condiciones de frontera para los campos electromagnéticos y encontrar la expresión matemática a utilizar en cada tipo de ejercicio o problema tratado. Esto con el fin de evitar el uso indiscriminado de formas de análisis que puedan inducir al error y de esta manera mejorar la estabilidad del aprendizaje, favoreciendo los procesos de diferenciación progresiva y la reconciliación integradora de los contenidos al descartar análisis diferentes para cada tipo de problema.

[1] David Cheng, *Fundamentos de Electromagnetismo para Ingeniería*, Addison WesleyIberoamericana (1998).
[2] M. Sadiku, *Elementos de Electromagnetismo*, Compañia Editorial Continental (1999).
[3] J. Reitz, F. Milford, *Foundations of Electromagnetic Theory*, Addison Wesley (1960).
[4] J. Edminister. *Electromagnetismo*, Mc Graw Hill (1992).
[5] D. Griffiths, *Introduction to Electrodynamics*, Prentice Hall (2017).

Online examination procedure with a tool developed in Visual .NET

T. P. Iglesias*, J. L. Legido, M. A. Rivas

Departamento de Física Aplicada, Universidade de Vigo, Campus As Lagoas Marcosende s/n, 36310 Vigo, Spain.

*e-mail: tpigles@uvigo.es

During the first wave of the Covid-19 pandemic, the confinement of the population in Spain, as in many other countries, seriously affected university teaching in the second half of the 2019-2020 academic year. This work describes how we adapted to the situation in the subject of Physics II of the Chemical Sciences degree at the University of Vigo. We discuss how teaching and knowledge assessment were adjusted, as well as the dedicated tool that we developed in order to carry out online exams in a reliable way.

Acknowledgements: We thankful to 'Xunta de Galicia' of Spain the financial support provided by the project ED431C 2020/06 V055. This project is co-financed with FEDER funds.

Uso de CalcMe (Wiris) como recurso didáctico en la enseñanza y evaluación de matemáticas y física

Miguel Villaplana Pérez*, Santiago González de la Hoz, Facundo Ballester

Departamento de Física Atómica, Molecular y Nuclear, Universidad de Valencia, España.

*e-mail: Miguel.Villaplana@uv.es

En los actuales planes docentes de la educación universitaria, el profesor es, además de un transmisor de conocimientos, un orientador/guía de los estudiantes en su proceso de aprendizaje. En este nuevo modelo es imprescindible introducir actividades complementarias a los exámenes que permitan a los estudiantes, por un lado, poner a prueba su nivel de conocimientos en tiempo real y a los profesores, por otro lado, detectar posibles deficiencias en la docencia y corregirlas a tiempo.

El uso de herramientas basadas en las nuevas tecnologías de la información facilita la gestión de este tipo de actividades. En esta línea, la Universidad de Valencia (UV) dispone de un entorno virtual de aprendizaje basado en Moodle [1] que permite al profesor plantear tareas individualizadas durante el curso que facilitan la evaluación continua.

La integración en el entorno virtual de la UV de la herramienta CalcMe de Wiris [2] simplifica enormemente la creación de un banco de preguntas para el aprendizaje y la evaluación de los alumnos. CalcMe ofrece un entorno de programación interactivo con una serie de utilidades que incluyen la generación de números aleatorios, el cálculo vectorial y matricial, cálculo diferencial, etc. En este entorno hemos elaborado problemas y programado tareas específicas para la asignatura de Métodos Estadísticos y Numéricos (MEN) del Grado en Física de la UV. Especialmente útil es la capacidad de CalcMe de generar números aleatorios, que permite que un mismo problema se formule y se asigne a diferentes alumnos variando datos, funciones y parámetros aleatoriamente, haciendo que los ejercicios sean diferentes para cada estudiante y reduciendo el tamaño del banco de preguntas. Un ejemplo de ello aparece en la Figura 1.

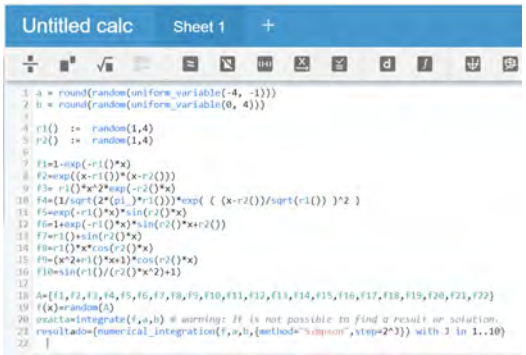

Figura 1: Programación en CalcMe de una integral por Simpson, asignando aleatoriamente la función (entre 10) y los límites de integración, y cómo aparece el enunciado en Moodle para el caso de la regla trapezoidal. El alumno puede comprobar los resultados numéricos sin penalización.

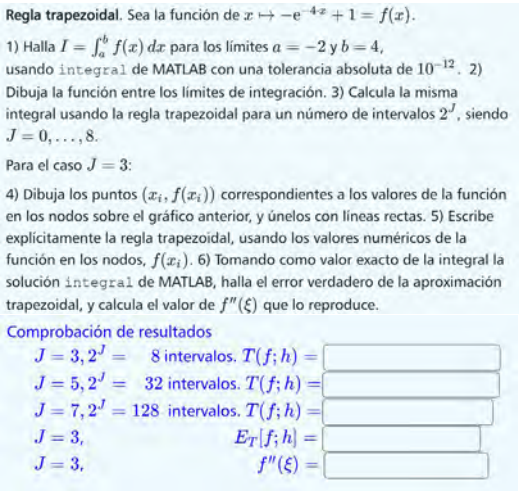

Con este sistema, hemos creado **boletines de problemas online** donde cada alumno se enfrenta a ejercicios distintos y puede comprobar sus cálculos tantas veces como desee, sin penalización. Además, el alumno ha de subir a Moodle la solución manuscrita de los problemas asignados junto con los cálculos en MATLAB [3] para evaluar aquellos aspectos no numéricos de la resolución, como figuras, razonamientos y conclusiones. Este sistema de enseñanza, aprendizaje y evaluación continua se ha utilizado en la asignatura MEN del curso 2021/22. Vamos a exportar nuestra experiencia a otras asignaturas como Iniciación a la Física Experimental y Física Nuclear y de Partículas.

[1] Moodle docs: http://docs.moodle.org/es/Acerca_de_Moodle
[2] Documentación de CalcMe de Wiris: https://docs.wiris.com/calcme/index.html
[3] Documentación de MATLAB: https://es.mathworks.com/help/matlab

Agradecimientos: Agradecemos el apoyo del MICINN y del Programa GenT de la Generalitat Valenciana.

Experiencia de aula invertida y gamificación en la docencia de un laboratorio de física de primer curso

P. Palacios [1], J. C. Jiménez-Sáez[1], F.J. Sánchez[1], J. Gaite[1], S. Muñoz[2]

[1]*Dpto. de Física Aplicada en Ingeniería Aeronáutica y Naval, ETSIAE, Universidad Politécnica de Madrid (UPM), 28040 Madrid, España.*

[2]*Dpto. de Estructura de la Materia, Física Térmica y Electrónica, Facultad de Ciencias Físicas, Universidad Complutense de Madrid (UCM), 28040 Madrid, España.*

*e-mail: pablo.palacios@upm.es

Este trabajo expone cómo mejorar la enseñanza de un laboratorio experimental, en nuestro caso, el laboratorio de Física. Las técnicas tradicionales de realización de prácticas de laboratorio no hacen énfasis en la adquisición y dominio por parte del alumno de una serie de competencias transversales. Dada la premura de tiempo con que se realizan dichas prácticas, únicamente se centran en la adquisición de un conjunto de conocimientos específicos. El alumno llega al laboratorio desconociendo tanto instrumental como procedimientos, de forma que la primera parte de una práctica de laboratorio debe dedicarse a subsanar este defecto. Esto obliga al profesor a dedicar parte del tiempo de práctica a corregir este problema. En este sentido, el modelo pedagógico del aula invertida encaja a la perfección en la parte experimental de enseñanza de una asignatura como la Física.

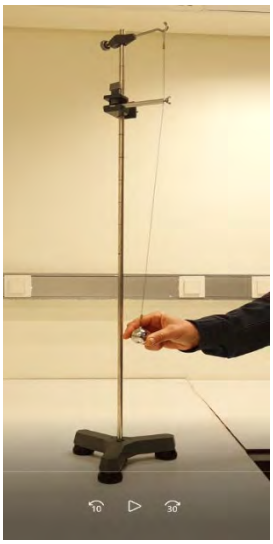

El alumno debe preparar y estudiar mínimamente y de una forma amena la práctica fuera de casa. El vídeo educativo es una herramienta básica para llevar a cabo esta tarea. Con el vídeo pretendemos que el alumno aprenda, por un lado, los principios básicos que subyacen en cada práctica, y por otro, a manejar el instrumental de laboratorio que deberá manejar viendo ejemplos en tiempo real.

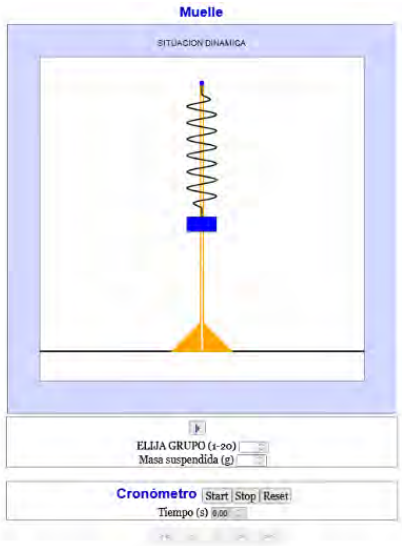

El objetivo fundamental que pretende alcanzar este proyecto es mejorar la calidad de la enseñanza impartida en la enseñanza del laboratorio de una asignatura experimental. El alumno, antes de ir al laboratorio, puede ver y repetir las veces que desee la visualización de un vídeo sobre la práctica, mejorando así su preparación a la hora de realizar la práctica. Al llegar al laboratorio, puede poner en práctica de inmediato lo que ha visto. No es necesario que reciba una formación in situ tan extensa como normalmente se hace o que se tenga que leer un manual que explique el funcionamiento del instrumental y que deberá entender sobre la marcha en un muy breve espacio de tiempo. Acabada la práctica, realizará una simulación en la cual podrá "jugar" con el instrumental que ha manejado. De esta forma podrá repetir la práctica o parte de ella tantas veces como desee. Además de entregar un informe relativo a la práctica, el alumno deberá contestar un cuestionario que rellene usando los resultados de la simulación y que permitirá al profesor medir el grado de aprendizaje del alumno sobre los principios y habilidades asociados a la práctica. Las simulaciones son una técnica esencial en cualquier asignatura para reforzar la enseñanza porque el alumno las ve como un elemento lúdico y no como trabajo. Esto permite el uso de la Gamificación, una metodología de enseñanza que utiliza este tipo de estrategias formativas. Operando de esta forma esperamos obtener una mejora en la enseñanza. En definitiva, el uso de estas dos metodologías aumenta la motivación de los alumnos y mejora su formación.

Agradecimientos: P.P., J.C. J y F.J. S. agradecen el soporte de la Universidad Politécnica de Madrid a través del proyecto de innovación educativa "Aula invertida y gamificación en la impartición del laboratorio de Física".

Elaboration of calculated questions using Moodle and Wolfram language

Juan José Miralles Canals

Departamento de Física Aplicada, Universidad de Castilla-La Mancha, España.

*e-mail:juan.miralles@uclm.es

In this contribution a methodology for solving Moodle calculated questions using a computer algebra system (CAS) is proposed. In particular, a CAS tool is used, the Wolfram Language (Mathematica). It is described how to link symbolic expressions in Wolfram Language with the own mathematical language used in Moodle.

A code has been developed, in Wolfram language, that allows us to convert symbolic solutions of physics problems, solved from Mathematica, in Wolfram language, to Moodle language.

Then given a function of several variables, solution of a physical problem solved in Mathematica, and expressed in Wolfram language, the developed code allows us to translate the solution function to a function of several variables expressed in Moodle language, to later be able to build a calculated question in Moodle.

In addition, some examples, in order to illustrate this methodology, are given. The examples are solutions to proposed problems, and they are shown, graded from lowest to highest degree of difficulty, about topics from physics and mathematics.

[1] J. J. Miralles Canals, M. Cañas Carretón, G. Vergara Pla, *EDULEARN16 Proceedings 8th International Conference on Education and New Learning Technologies*, 6701 (2016).
[2] Moodle (open-source): https://docs.moodle.org/28/en/Calculated_question_type. [29/01/2016]
[3] J.J. Miralles Canals, *Mathematica y Moodle: Elaboración de preguntas calculadas* [Webinar], Wolfram Events Europe. [26/11/2020].

La óptica en la historia militar

David González, **Julia Gil***

Departamento de Física, Universidad de Extremadura, España.

*e-mail: juliagil@unex.es

Desde sus orígenes, la especie humana, cuya hostilidad parece estar conectada con su inteligencia, ha conocido el estrecho e inquebrantable vínculo entre la guerra y la tecnología. Ejemplos como el "Proyecto Manhattan" prueban que, mientras la primera optimiza el desarrollo de la segunda, la segunda estimula y determina cómo concluye la primera. Y es que la historia es una revelación de cuán decisiva ha sido la ciencia para el devenir de las civilizaciones, condicionando cuáles sobrevivían y cuales colapsaban.

Durante las últimas décadas, las armas nucleares y los misiles guiados han caracterizado las estrategias defensivas de los países desarrollados. Pero, hoy en día, es la óptica el campo que, junto con la electrónica, constituye la base de cualquier sistema militar moderno (Figura 1). El objetivo de este artículo es, precisamente, analizar sus múltiples aplicaciones bélicas.

Durante la Antigüedad y el Medievo, la naturaleza de la luz era todavía desconocida, pero no algunos de sus fenómenos asociados. Ilustrativos ejemplos a considerar son las técnicas de iluminación del campo de batalla, la invención del catalejo por Lippershey y el posible uso del espejo ustorio por Arquímedes en Siracusa [1].

Respecto a su actual y vasta selección de aplicaciones en la guerra, la óptica interviene, por ejemplo, en labores de vigilancia satelital, comunicaciones (fibras ópticas), dispositivos de visión térmica y nocturna (Figura 2) y en armas y contramedidas láser (basadas en las Leyes de Snell [2].

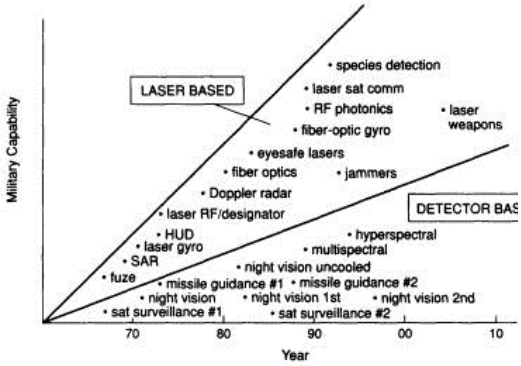

Figura 1. Relación directa entre el desarrollo de la óptica y las capacidades militares.

Con todo lo hasta ahora expuesto y sin lugar a dudas, la óptica continuará su desarrollo en el futuro, habiéndose de generalizar por completo su uso en el seno militar. De entre la gran lista de proyectos en los que los científicos ya trabajan, destacan la propulsión láser y el uniforme invisible (del que "*Hyperstealth Biotechnology*" ha obtenido un prototipo haciendo uso de las propiedades refractivas).

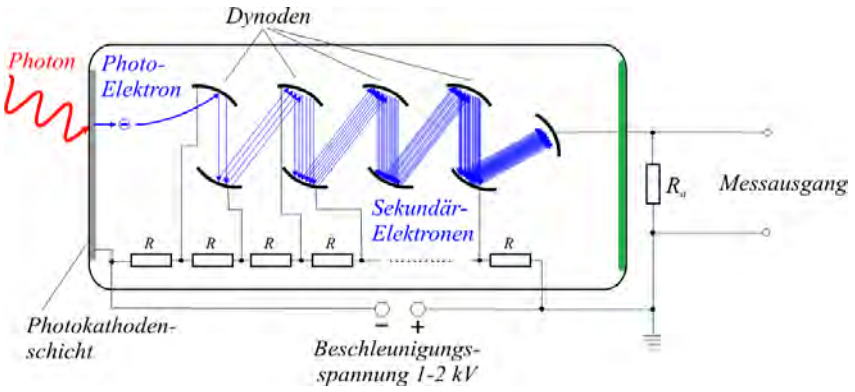

Figura 2. Constitución interna de un dínodo, pequeño dispositivo que transforma la radiación infrarroja en luz visible y que se emplea en los visores nocturnos.

[1] Simms, D. L., *Technology and Culture* **18**, 1 (1977).
[2] https://nap.nationalacademies.org/read/5954/chapter/7

The use of discussion boards in undergraduate physics courses in experimental science degrees

E. Yubero*, A. Clemente, A. López-Caravaca, N. Galindo, J. F. Nicolás

Applied Physics Department, Miguel Hernandez University, Elche, Spain.

*e-mail: eyubero@umh.es

The aim of this paper is to investigate the use of a discussion board such as *Piazza* among students of the first year Physics course of the Biotechnology degree. This discussion board has been used during the last 7 years in the subject and some conclusions have been obtained about its use and how it influences the student's performance.

Online tools and software for learning outside the classroom have become more prevalent and accessible for use. A primary example of these tools are online discussion boards like *Piazza*. This type of tool has become particularly relevant due to the increase in the number of online courses, especially during the recent pandemic.

Discussion forums are by nature asynchronous; contributions occur at different instants allowing the user a sense of timeless availability [1].

Several students can be online at the same time, allowing each student's messages to even mimic the behaviour of real-time conversations. The user can decide the degree of involvement at any given moment. Participants can indicate their contributions to problem solving without worrying about being overlooked or not being heard due to shyness or reluctance to speak in public [2].

Piazza is a free discussion board (www.piazza.com) with a relatively high-functionality. This platform combines a traditional discussion board with wiki functionalities and was developed with the aim of increasing participation in the classroom. Additionally, Piazza has been integrated into flipped classrooms. Piazza also provides information on student's use that can be employed by instructors to find out if and how students are using it. Some of the variables that can be obtained are: course enrolment; percent of enrolled students who made a contribution; total number of posts; total contributions; number of instructor/students' responses; percentage of questions receiving instructor/student responses; percentage of students' responses endorsed by the instructor; number of students' questions and average response time.

The following table shows the main indicators of the use of the platform over the last 7 years. As can be seen, the number of users of the platform ranges between 89 and 106. It should be noted that there are 75 new students each year, so the rest are students who are re-enrolling in the course. The number of different Posts inserted during the course varies between 430 and 670, with a maximum (825) in the year when teaching was online due to the pandemic. The total number of contributions, including students' and teacher's contributions, is very high, in some cases exceeding 5000 inputs. This means an average of 50 contributions per student and course. Finally, it is noted that the response time is very short, around one, indicating a quick response to the questions asked.

Year	Enrolment	Total Post	Total Contributions	Avg. Respond Time
2021	98	591	5455	1.2
2020	106	825	5347	1.02
2019	93	692	5480	0.6
2018	106	631	4032	1.01
2017	92	568	3574	1.8
2016	89	437	2538	0.9
2015	89	574	5489	0.9

Table 1. Evolution of the main parameters related to student participation in the forum. The average time is measured in hours.

The inclusion of specific requirements of Piazza participation being considered in the grading structure was identified as an important potential contributing factor in the rate of Piazza participation. On the other hand, the presence of students repeating the course means that there is a higher response rate to the questions proposed in the forum.

[1] Andresen, M. A. *Journal of Educational Technology & Society* **12**, 249 (2009).
[2] Washington T. et al., *The Online Journal of New Horizons in Education* **9**, 219 (2019).

Acknowledgements: This work has been supported by the Vice-rectorate of Studies of the Miguel Hernandez University through the University Teaching Innovation Programme (PIEU), specifically under the project PIEU-B/2021/33.

Improving the Teaching of Physics with Space Projects

Marília Peres[1,2,*], Inês Bruno[3], Vera Silva[4]

[1,3,4]*Escola Secundária José Saramago-Mafra, Portugal.*
[2]*Sociedade Portuguesa de Física.*

*e-mail: mariliaperes@esjs-mafra.net

The main aim of this presentation is to describe the role of non-formal contexts in the learning of Physics. The projects conducted by the European Space Agency (ESA), like Astro PI [1] and CanSat [2], using an inquiry-based approach, enhance school pupils' literacy and competence in STEM-related subjects, such as Physics, Programming, Robotics and Mathematics.

In the Astro PI challenge, students conduct scientific investigation in space by writing computer programs that run on Raspberry Pi computers aboard the International Space Station (ISS). In the CanSat, students also have to plan a scientific mission, but in this case to be performed by a mini satellite, approximately the size of a soda can, that is designed, built and tested by them, and launched from an altitude of approximately 1000 m.

Both projects have been integrated in our school's science club "Clube de Ciência Viva" and require from participating teams the application of some contents taught as part of the Physics' course syllabus in secondary education. but also the acquisition of further knowledge and competences that go beyond this curriculum, through their own investigation, teamwork and, occasionally, collaboration with experienced researchers.

During the last two years, these projects allowed students to explore concepts such as magnetism, irradiance, pressure, temperature, angular acceleration, and movements with appreciable air drag. Through the use of low-cost sensors, experiments were conducted to measure physical magnitudes. However, the validity of the obtained results depends on the correct calibration of measuring devices. This process was carefully planned and executed by students (Figure 1), allowing them to understand different aspects involved in experimental work, namely the necessity of studying uncertainties and measurement errors.

As these projects went along, students were likewise provided with the opportunity to develop some other competences, specifically problem solving and critical thinking. The feedback given by students and their performance throughout the projects suggest that participating in non-formal and experiential learning activities fostered their motivation, improved their understanding of the Physics' syllabus and the nature of science.

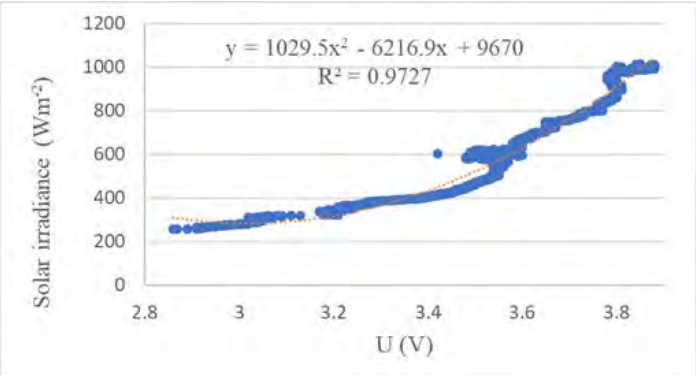

Figure 1. LDR calibration with a pyranometer at the National Laboratory of Engineering and Geology (LNEG)

[1] Honess, D., Quinlan, O., *Acta Astronautica* **138**, 43 (2017).
https://www.sciencedirect.com/science/article/abs/pii/S0094576516313807
[2] ESA CanSat guidelines 2021-2022, ESA (2021).
https://cansat.esa.int/wp-content/uploads/2021/11/CanSat_guidelines_2021-22.pdf

Acknowledgements: Sociedade Portuguesa de Física, Ciência Viva: Portugal.

Los teléfonos inteligentes: un laboratorio de bolsillo

Camila F. Marín Sepúlveda*, Juan C. Castro-Palacio, Juan A. Monsoriu

Centro de Tecnologías Físicas: Acústica, Materiales y Astrofísica, Universitat Politècnica de València, Camino de Vera, s/n, 46022 València, Spain.

*e-mail: cmarin@doctor.upv.es

Los sensores de los teléfonos inteligentes (smartphones) ofrecen grandes oportunidades para la enseñanza de la Física experimental en todos los niveles de enseñanza donde se imparte esta asignatura [1-8].

En un mismo teléfono se integran múltiples sensores que pueden ser utilizados, a través de aplicaciones gratuitas para móviles, en demostraciones y laboratorios docentes de física (figura 1).

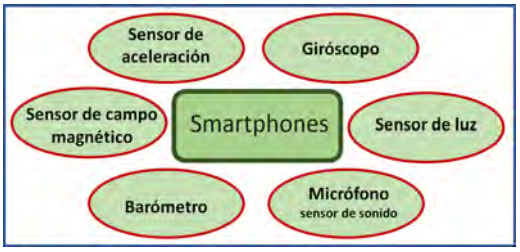

Figura 1. Los teléfonos inteligentes incorporan un conjunto amplio de sensores que pueden ser utilizados para la enseñanza y divulgación de la Física.

Los smartphones constituyen una herramienta sencilla, atractiva, motivadora y de bajo coste para que, no solo los alumnos, sino también el público en general pueda tener un acercamiento a la física.

En el presente cartel se muestra un conjunto de ejemplos de utilización de los teléfonos inteligentes en la enseñanza de la Física [9]. Así mismo, a partir del estudio de las experiencias puestas en práctica desde los proyectos didácticos desarrollados en la ETSID, Universitat Politècnica de València, se ilustran diferentes estrategias en relación con el uso de los teléfonos inteligentes como herramienta de divulgación de la Física.

[1] P. Vogt, J. Kuhn, Experiments using cell phones in physics classroom education: The computer-aided *g* determination, *Phys. Teach.* **49**, 383 (Sept. 2011).
[2] P. Vogt, J. Kuhn, Analyzing simple pendulum phenomena with a smartphone acceleration sensor, *Phys. Teach.* **50**, 439 (Oct. 2012).
[3] J. C. Castro-Palacio, L. Velazquez-Abad, M. H. Gimenez, J. A. Monsoriu, Using a mobile phone acceleration sensor in physics experiments on free and damped harmonic oscillations, *Am. J. Phys.* **81**, 472 (2013).
[4] J. C. Castro-Palacio, L. Velazquez-Abad, F. Gimenez, J. A. Monsoriu, A quantitative analysis of coupled oscillations using mobile accelerometer sensors, *Eur. J. Phys.* **10**, 737 (2013).
[5] J. C. Castro-Palacio, L. Velázquez-Abad, J.A. Gómez-Tejedor, F. J. Manjón, J. A. Monsoriu, Using a smartphone acceleration sensor to study uniform and uniformly accelerated circular motions, *Rev. Bras. Ens. Fis.* **36**(2), 2315 (2014).
[6] M. H. Giménez, J. C. Castro-Palacio, J. A. Monsoriu, Direct visualization of mechanical beats by means of an oscillating smartphone, *Phys. Teach.* **55**, 424 (2017).
[7] S. O. Parolin, G. Pezzi, Smartphone-aided measurements of the speed of sound in different gaseous mixtures, *Phys. Teach.* **51**, 508 (Nov. 2013).
[8] I. Salinas, M. H. Giménez, J. A. Monsoriu, C. Castro-Palacio, Characterization of linear light sources with the smartphone's ambient light sensor, *Phys. Teach.* **56**, 562 (2018).
[9] Web del Proyecto Smartphysics: https://smartphysics.webs.upv.es/

The Smartphone as a Variable Voltage Supply: Cases of the *RC*, *RL* and *RLC* Series Circuits

Ives Torriente García, Juan C. Castro-Palacio*, Juan A. Monsoriu

Centro de Tecnologías Físicas: Acústica, Materiales y Astrofísica, Universitat Politècnica de València, Camino de Vera, s/n, 46022 València, Spain.

*e-mail: juancas@upvnet.upv.es

The smartphone sensors offer good opportunities for physics teaching laboratories within introductory and first-year university courses [1-8]. The published work covers a wide range of topics such as linear and circular motions, oscillations, hydrostatics, waves, acoustics, optics, and magnetism. However, not much has been published in relation to the use of smartphones sensors to study the basic electric circuits commonly included in general physics courses for engineering [9-12].

In this work, we will use the smartphone as a variable voltage generator to the study *RC*, *RL* and *RLC* series circuits (see *RC* circuit in figure 1) in first-year physics courses for engineering. For this purpose, the tone generator function within the free Android "Physics Toolbox Suite" app. has been used. Simultaneously, the sound oscilloscope included in the same app. has been used to visualise the voltage signals at the different components.

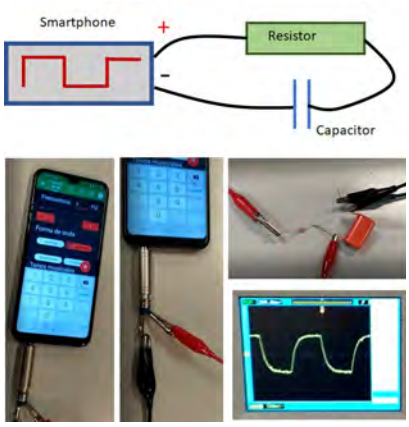

Figure 1. Study of the *RL* circuit using the smartphone as a function generator. The schematic representation of the circuit (upper panel) and pictures of the actual components (lower panel).

[1] P. Vogt, J. Kuhn, Experiments using cell phones in physics classroom education: The computer-aided g determination, *Phys. Teach.* **49**, 383 (2011).
[2] P. Vogt, J. Kuhn, Analyzing simple pendulum phenomena with a smartphone acceleration sensor, *Phys. Teach.* **50**, 439 (2012).
[3] J. C. Castro-Palacio, L. Velazquez-Abad, M. H. Gimenez, J. A. Monsoriu, Using a mobile phone acceleration sensor in physics experiments on free and damped harmonic oscillations, *Am. J. Phys.* **81**, 472 (2013).
[4] J. C. Castro-Palacio, L. Velazquez-Abad, F. Gimenez, J. A. Monsoriu, A quantitative analysis of coupled oscillations using mobile accelerometer sensors, *Eur. J. Phys.* **10**, 737 (2013).
[5] J. C. Castro-Palacio, L. Velázquez-Abad, J.A. Gómez-Tejedor, F. J. Manjón, J. A. Monsoriu, Using a smartphone acceleration sensor to study uniform and uniformly accelerated circular motions, *Revista Brasileira de Ensino de Fisica* **36**(2), 2315 (2014).
[6] M. H. Giménez, J. C. Castro-Palacio, J. A. Monsoriu, Direct visualization of mechanical beats by means of an oscillating smartphone, *Phys. Teach.* **55**, 424 (2017).
[7] S. O. Parolin, G. Pezzi, Smartphone-aided measurements of the speed of sound in different gaseous mixtures, *Phys. Teach.* **51**, 508 (2013).
[8] I. Salinas, M. H. Giménez, J. A. Monsoriu, J. C. Castro-Palacio, Characterization of linear light sources with the smartphone's ambient light sensor, *Phys. Teach.* **56**, 562 (2018).
[9] K. Forinash, Smartphones as portable oscilloscopes for physics labs, *Phys. Teach.* **50**, 242 (2012).
[10] J. R. Groff, Estimating RC Time Constants Using Sound, *Phys. Teach.* **57**, 393 (2019).
[11] S. R. Pathare, M. K. Raghavendra, S. Huli, Low-Cost Alternative for Signal Generators in the Physics Laboratory, *Phys. Teach.* **55**, 301 (2017).
[12] K. Forinash, Smartphones—Experiments with an External Thermistor Circuit, *Phys. Teach.* **50**, 566 (2012).

Acoustic Determination of the Gravitational Acceleration

Camila F. Marín Sepúlveda*, Juan C. Castro-Palacio, Juan A. Monsoriu

Centro de Tecnologías Físicas: Acústica, Materiales y Astrofísica, Universitat Politècnica de València, Camino de Vera, s/n, 46022 València, Spain.

*e-mail: cmarin@doctor.upv.es

In recent years, a wide range of physics teaching experiments using smartphone sensors has been published. Many topics within introductory and first-year university courses are covered [1-8], such as linear and circular motions, oscillations, beats, acoustics, optics, and magnetism. These experiments have proved to increase the motivation and independence of engineering students as the smartphone is a very familiar device to them.

In this work, we will use sound wave resonance in an air column to study the free fall of a body inside an aluminium pipe (figure 1). The multiple resonances of a sound wave in the pipe allow to construct the curve of the distance *versus* time in a constant acceleration motion from where the gravitational constant can be obtained by means of a fitting.

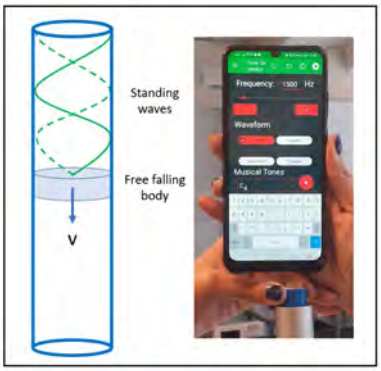

Figure 1. Experimental setup used to determine the gravitational constant.

Apart from putting together two topics of general physics, namely, kinematics and acoustics, another contribution of this work is to use a smartphone to generate and analyse the sound waves simultaneously, all in one device. The single-tone sound wave is generated by the free mobile app. Physics Toolbox Suite for Android. At the same time the sound wave is generated, another Android app., the Voice Recorder, is active and recording the standing sound wave established inside the pipe while the body falls. The result of this work for the gravitational constant is compared with the published value in the literature yielding a percentage difference of less than 8 %.

[1] P. Vogt, J. Kuhn, Experiments using cell phones in physics classroom education: The computer-aided *g* determination, *Phys. Teach.* **49**, 383 (2011).
[2] P. Vogt, J. Kuhn, Analyzing simple pendulum phenomena with a smartphone acceleration sensor, *Phys. Teach.* **50**, 439 (2012).
[3] J. C. Castro-Palacio, L. Velazquez-Abad, M. H. Gimenez, J. A. Monsoriu, Using a mobile phone acceleration sensor in physics experiments on free and damped harmonic oscillations, *Am. J. Phys.* **81**, 472 (2013).
[4] J. C. Castro-Palacio, L. Velazquez-Abad, F. Gimenez, J. A. Monsoriu, A quantitative analysis of coupled oscillations using mobile accelerometer sensors, *Eur. J. Phys.* **10**, 737 (2013).
[5] J. C. Castro-Palacio, L. Velázquez-Abad, J. A. Gómez-Tejedor, F. J. Manjón, J. A. Monsoriu, Using a smartphone acceleration sensor to study uniform and uniformly accelerated circular motions *Revista Brasileira de Ensino de Fisica* **36**(2), 2315 (2014).
[6] M. H. Giménez, J. C. Castro-Palacio, J. A. Monsoriu, Direct visualization of mechanical beats by means of an oscillating smartphone, *Phys. Teach.* **55**, 424 (2017).
[7] S. O. Parolin, G. Pezzi, Smartphone-aided measurements of the speed of sound in different gaseous mixtures, *Phys. Teach.* **51**, 508 (2013).
[8] I. Salinas, M. H. Giménez, J. A. Monsoriu, J. C. Castro-Palacio, Characterization of linear light sources with the smartphone's ambient light sensor, *Phys. Teach.* **56**, 562 (2018).

Social-emotional learning: a case study in academic institutions of Portuguese speaking countries

K. Kristiani[1], L. Sirqueira[2], M. G. Silva[1], S. Francisco[3,4], M. A. Salgueiro da Silva[3,5], **T. M. Seixas**[3,5,*]

[1]*Faculty of Education, Arts and Humanities, National University of East Timor, Liceu Dr. Francisco Machado, Dili, East Timor.* [2]*Escola Estadual Raimundo Pinheiro da Silva, Av Fernando Corrêa da Costa, 3610 - Jardim Shangri-lá, Cuiaba-MT, CEP 78070-001, Brasil.* [3]*Department of Physics and Astronomy, Faculty of Sciences, University of Porto, Rua do Campo Alegre, 687, 4169-007 Porto, Portugal.* [4]*Escola Superior Pedagógica da Lunda Norte (ESPLN) da Universidade Lueji A'Nkonde, Angola.* [5]*Centre for Earth and Space Research of the University of Coimbra (CITEUC), Portugal.*

*e-mail: tmseixas@fc.up.pt

Students differ in their behavioural, emotional and social skills and their successful performance entails not only cognitive skills, but also social–emotional learning competencies, the also known conceptualized noncognitive skills. Literature [1] refers to these competencies as the "capacity to maintain social relationships, regulate emotions", usually linked with positive outcomes, that could influence students' chance to manage goals and learning behaviours to achieve success in their academic life.

Despite the lack of consensus in the research on these skills, sometimes fragmented by complexity and diversity disciplinary differences [2], there is a revisited increased attention from high school and college educationalists about the relationship between social–emotional skills and students' performance outcomes.

To investigate social–emotional competencies, the present research addresses twenty-five key questions about the social–emotional learning [3, 4], with four scales, measuring regulation (n = 9 items), growth mindset (n = 4 items), self-efficacy (n = 4 items), and social awareness (n = 8 items), which are administered as part of a larger survey [4]. Participants could find the survey through links from a questionnaire on the University of Porto website. Exploratory analyses are conducted on data of samples restricted to high school and college Portuguese speaking institutions in Angola, East Timor, Brazil and Portugal. Students' responses are analysed in a five-points Likert scale. Mean, standard deviations and Cronbach's alpha internal reliability are reported for each of the survey scales.

We discuss the educational implications of the social–emotional learning competences assessed by the survey and explore several possible interventions. Social–emotional learning measures are suggested to be used in future as an indicator of student performance.

As future work, the authors are planning to extend the current survey to additional institutions in the participating countries.

[1] C. J. Soto, C. M. Napolitano, M. N. Sewell, H. J. Yoon, B. Roberts, W. *Journal of Personality and Social Psychology*. Advance online publication. http://dx.doi.org/10.1037/pspp0000401 (2022).
[2] R. Neumann, *Studies in Higher Education* **26**(2), 135 (2001).
[3] C. C. Vriesema, H. Gehlbach, *Educational Researcher* **50**(9), 618 (2021).
[4] M. R. West, K. Buckley, S. B. Krachman, N. Bookman, *Journal of Applied Developmental Psychology* **55**, 119. https://doi.org/10.1016/j.appdev.2017.06.001 (2017).

Acknowledgements: This work was carried out under project UID/Multi/00611/2020, funded by FCT/MEC (PIDDAC) and FEDER — European Regional Development Fund through COMPETE 2020 — Operational Programme Competitiveness and Internationalization (project: POCI-01-0145-FEDER-006922).

Diseñando un átomo. Un ejemplo de ABProblemas

Arcadio Sotto, Jesús M. Arsuaga, Pablo Melón

Departamento de Ciencias de la Educación, Universidad Rey Juan Carlos, Madrid, España.

*e-mail: arcadio.sotto@urjc.es

En el presente trabajo se muestra un ejemplo de la aplicación del Aprendizaje Basado en Problemas como método activo de enseñanza dentro de la metodología global que encierra el proceso de enseñanza-aprendizaje de una asignatura de Didáctica de las Ciencias Naturales diseñada para estudiantes del Grado en Educación Primaria. Persiguiendo el afán de "enseñar a enseñar" se muestra el desarrollo de cada una de las partes que engloba el método didáctico elegido y su posible combinación con otras metodología o métodos de enseñanza como la Clase Invertida o la Gamificación. El diseño mostrado fue puesto en práctica en un aula de Educación Primaria mostrado resultados satisfactorios en lo concerniente a la asimilación de estos contenidos y métodos por parte de los estudiantes.

Acknowledgements: The authors express thanks for the funding support from the European Community Project, MiniOpenLab-Open community, and Hands-on approach to Sustainable Development and STEM Education Project, Erasmus +. (2020/00157/001) and the National Investigation Agency of Spain, STEMind for Education Project. AEI (EIN 2020-112313).

La situación de la Física en los nuevos currículos de ESO y Bachillerato

Arcadio Sotto, **Jesús María Arsuaga***, Pablo Melón

Grupo de Investigación en Educación STEM (GIE-STEM).
Departamento de Ciencias de la Educación. Universidad Rey Juan Carlos.
C/ Tulipán, s/n. 28933 – Móstoles, Madrid, España.

*e-mail: jesusmaria.arsuaga@urjc.es

En marzo y abril de 2022 se han publicado los decretos que establecen la ordenación y las enseñanzas mínimas de la Educación Secundaria Obligatoria y del Bachillerato [1,2]. Estos decretos están vinculados a la nueva Ley Orgánica 3/2020, de 29 de diciembre, más conocida como LOMLOE o "*Ley Celaá*" que fue impulsada por Dña. María Isabel Celáa Diéguez, entonces al frente del Ministerio de Educación y Formación Profesional, aunque siete meses después de su aprobación fue relevada de sus funciones ministeriales [3]. Por tanto, el posterior desarrollo normativo, que se ha producido con un cierto retraso, posiblemente originado por el relevo ministerial, ya no ha tenido lugar bajo su responsabilidad, sino que ha correspondido la titularidad a la nueva ministra, Dña. María del Pilar Alegre Continente. Quien ha dado continuidad a todo el proceso ha sido el Secretario de estado de Educación, D. Alejandro Tiana Ferrer, un veterano experto en la materia que ya fue Secretario de estado de Educación en el pasado (2004-2008) y rector de la UNED (2013-2018).

No se puede saber con seguridad cuál será el futuro de toda esta legislación ya que, como sucede en nuestro país en temas educativos, la nueva ley obtuvo el respaldo mínimo para salir adelante (177 votos a favor, siendo necesarios para su aprobación 176 debido a su condición de ley orgánica) y está actualmente recurrida ante el Tribunal Constitucional.

Tanto el decreto de la ESO como el del Bachillerato insisten en la importancia de las competencias clave, aunque estas ya existían en la anterior ley educativa LOMCE. Las competencias clave han sido definidas a partir de la "*recomendación del Consejo de la Unión Europea relativa a las competencias clave para el aprendizaje permanente*", teniendo en cuenta también los "*Objetivos de Desarrollo Sostenible*" [4,5]. En la Tabla 1, se especifican las ocho competencias clave de la LOMLOE.

1.	**En comunicación lingüística.**
2.	**Plurilingüe.**
3.	**Matemática y en ciencia y tecnología (STEM).**
4.	**Digital.**
5.	**Personal, social y de aprender a aprender.**
6.	**Ciudadana.**
7.	**Emprendedora.**
8.	**Conciencia y expresión culturales**

Tabla 1. Competencias clave de la LOMLOE.

En esta comunicación se presenta un análisis de la nueva ley de educación y de los decretos de enseñanzas mínimas en relación con las etapas ESO y Bachillerato. Se lleva a cabo una comparación con las anteriores leyes educativas desde una perspectiva STEM y específicamente en relación con la Física.

[1] https://www.boe.es/buscar/act.php?id=BOE-A-2022-4975
[2] https://www.boe.es/buscar/doc.php?id=BOE-A-2022-5521
[3] https://www.boe.es/diario_boe/txt.php?id=BOE-A-2020-17264
[4] https://eur-lex.europa.eu/legal-content/ES/TXT/PDF/?uri=CELEX:32018H0604%2801%29
[5] https://www.un.org/sustainabledevelopment/es/objetivos-de-desarrollo-sostenible

Agradecimientos: Los autores agradecen el apoyo, colaboración y soporte económico que el grupo especializado en investigación educativa GIE-STEM ha recibido de la Universidad Rey Juan Carlos, de la Agencia Estatal de Investigación (Proyecto STEMIND for Education, EIN2020, 112313) y de la UE (Proyecto MiniOpenLabs, Erasmus+ 2020-1-ES01-KA201-082706).

Propuesta práctica para la enseñanza-aprendizaje de los espectros atómicos en el último curso de secundaria

María Consolación Rodríguez-Palazón[1,*], Rafael Garcia-Molina[2]

[1]*Departamento de Química Analítica, Facultad de Química, Campus Regional de Excelencia Internacional "Campus Mare Nostrum", Universidad de Murcia, E-30100 Murcia, España.*
[2]*Departamento de Física, Facultad de Química, Universidad de Murcia, E-30100 Murcia, España.*

*email: mconsolacion.rodriguez@um.es

El aprendizaje de las ciencias, especialmente de la física y la química, presenta en la actualidad una serie de problemas, como la falta de base matemática, su carácter abstracto o la complejidad y extensión de los contenidos. Dentro del currículo oficial de física y química para el nivel de cuarto de la ESO, el aprendizaje de las transiciones electrónicas y los espectros atómicos supone un reto, dado su carácter esencialmente abstracto y teórico [1].

En este trabajo se propone el diseño, desarrollo, aplicación y evaluación de tres trabajos prácticos de carácter cualitativo para la mejora de la enseñanza-aprendizaje de los contenidos relacionados con la estructura de la materia. En función de su naturaleza [2], las actividades propuestas se clasifican en experimento ilustrativo (actividad 1, encender bombillas en un microondas), trabajo práctico (actividad 2, llama de colores) e investigación (actividad 3, construcción de un espectroscopio). En la secuencia propuesta, se aumenta progresivamente la participación activa del alumnado, pasando de una primera actividad en la que tiene un papel de mero receptor de información, a una última, en la que su participación es totalmente activa y autónoma. En el estudio participan dos grupos de cuarto de la ESO, uno de ellos (grupo experimental) realizó las actividades propuestas, así como los cuestionarios de evaluación mientras que el otro grupo (grupo control) solo realizó los cuestionarios.

El grado de aprendizaje se evalúa teniendo en cuenta el porcentaje de acierto de cada alumno tras la realización del pretest y postest de cada actividad. Para cada grupo se evaluó la ganancia normalizada de aprendizaje (GN) y, a excepción del grupo control en la segunda actividad, la GN supera el 30 %, situándose en una ganancia de aprendizaje media, según el método propuesto por Hake [3] (fig. 1). Los resultados estadísticos muestran, en base al valor *p* obtenido, que no hay diferencias significativas entre los dos grupos, por lo que no se pueden establecer resultados del todo concluyentes. Son muchos los factores que influyen en el aprendizaje del alumnado, por lo que la realización de trabajos prácticos, es necesaria pero no la única forma de mejorar su aprendizaje.

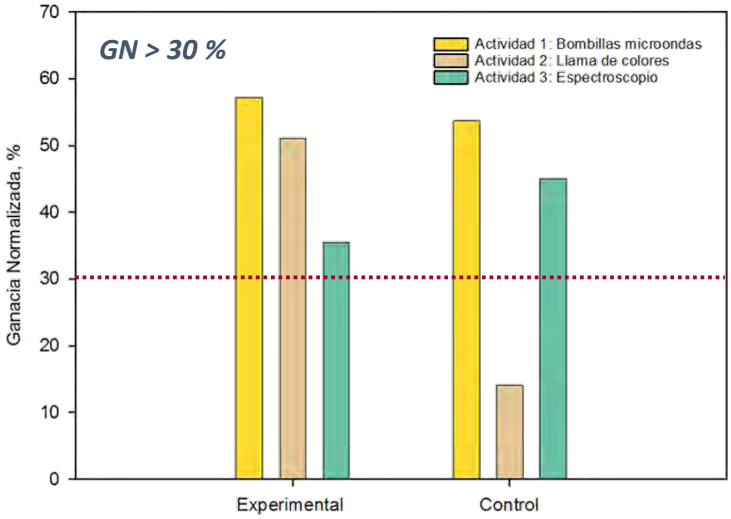

Figura 1. Comparación de la ganancia normalizada obtenida por ambos grupos en cada una de las actividades.

[1] Aragón, S., Soliveres, A. Maturano, I., *Revista FCEFyN* **7**, 83 (2020).
[2] Caamaño, A., *Alambique* **39**, 8 (2004).
[3] Hake, R., *American Journal of Physics* **66**, 64 (1998).

Physical analysis of a literary work: E. A. Poe's *The Pit and the Pendulum*

Irene Carrión[1,*], Ana Teresa Gea[1], Mercedes Contreras[1], Gema María Muñoz[1], Rafael Garcia-Molina[2]

[1]*Grado en Física, Universidad de Murcia, España.* [2]*Departamento de Física, Universidad de Murcia, España.*

*e-mail: irene.carrionl@um.es

Literature and science are two ways of exploring reality. We bring these two paths together through the famous short story *The Pit and the Pendulum* by the well-known American writer Edgar Allan Poe [1]. We have studied the oscillatory movement of the scythe that descends with constant speed and whose purpose is to end our protagonist's life, who is tied face up on the ground.

The text says: "It might have been half an hour, perhaps even an hour […]. What I then saw confounded and amazed me. The sweep of the pendulum had increased in extent by nearly a yard. As a natural consequence its velocity was also much greater. But what mainly disturbed me was the idea that it had perceptibly descended".

We have, then, the case of a pendulum whose length varies with time. The equation in partial derivatives that describes the evolution with time of the angle θ that the pendulum makes with the vertical, as well as its length r, is the following:

$$r(t)\ddot{\theta} + 2\dot{r}(t)\,\dot{\theta} + g\sin\theta = 0,$$

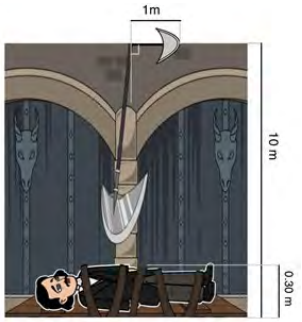

Figure 1: Diagram of initial conditions.

We have used the scarce information provided in the text (the pendulum height is 30-40 feet and it takes a lapse of several days to reach the prisoner) and have assumed reasonable values for the initial angle and the length of the pendulum (as depicted in figure 1). A program has been written to solve the differential equation using the fourth-order Runge Kutta method. The main results we obtained are summarised in what follows.

On the one hand, assuming that the pendulum increases its length at a rate of 5 mm/s, the scythe reaches the ground after approximately 32 minutes. However, if we assume that the scythe takes several days to approach the doomed man, as it can be deduced from the prisoner's account, the pendulum would have to descend with a speed smaller than 0.115 mm/s (an absurdly low speed) to take more than a day to reach him.

On the other hand, we observe how the increase in the amplitude of the oscillations made by scythe is not linear (figure 2), but growths at a low rate and does not add up to the large amplitude implied in the story.

The story goes that the condemned man escapes because the rats gnaw at his bonds when the pendulum has about 12 swings left to reach him. The period of the pendulum's swings in that stretch is around 6 seconds, so the rats have over one minute to do so. In addition, to escape from the pendulum when it moves away just after touching him, the prisoner has only around 3 seconds to get up and do so.

Therefore, from this analysis we can conclude that, although Edgar Allan Poe's story is a brilliant tale of terror, it does not capture the reality that physics show us of such a scene.

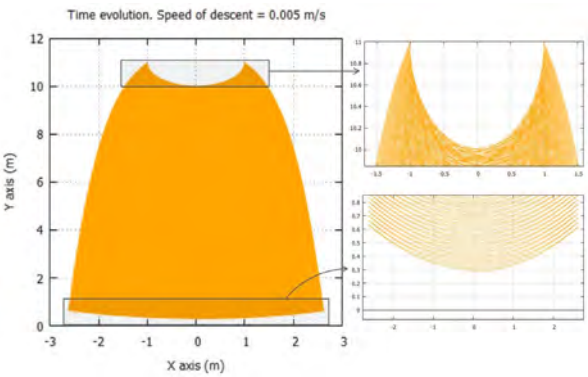

Figure 2: Time evolution of the pendulum from the time it starts its descent until it reaches the ground.

[1] Edgar Allan Poe, *The Pit and the Pendulum* (1842).

Estudio acústico de campanas de Alcoy mediante software de audio de uso libre

José Jorge Llopis Juan[1,*], Rafael Garcia-Molina[2]

[1]*Grado en Física, Universidad de Murcia, España.* [2]*Departamento de Física, Universidad de Murcia, España.*

*e-mail: jjorge.llopis@um.es

Se han estudiado algunas propiedades acústicas de varias campanas de la ciudad de Alcoy (Alicante). Primeramente, se ha descrito la campana desde el punto de vista histórico, musical y físico-acústico dando importancia a los modos de vibración.

En cuanto a las propiedades a analizar, se ha estudiado una relación utilizada por los aficionados a las campanas para obtener su masa a partir de su diámetro. Por otro lado, se han efectuado grabaciones del sonido de 12 campanas, con el objetivo de obtener sus principales frecuencias o parciales. A partir de los parciales se comprueba si existen relaciones de proporcionalidad entre ellos [1], si se guarda relación entre el radio de la campana y sus frecuencias y cómo varía la señal acústica cuando se golpea la campana a distintas alturas [2].

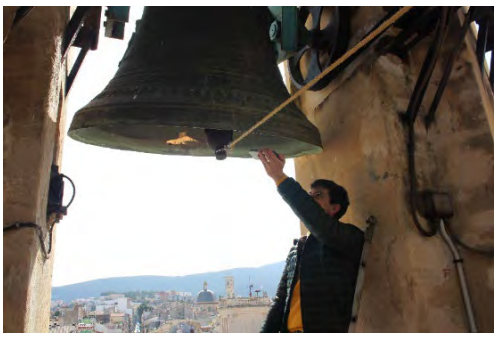

Figura 1. Toma de datos con el teléfono móvil.

Para poder verificar estas relaciones se ha subido a los campanarios para poder medir con fiabilidad los diámetros y captar los sonidos mitigando ruidos. Para registrar los sonidos se ha utilizado la grabadora del teléfono móvil (figura 1) y los archivos se han estudiado desde la aplicación Wavanal, que es un programa diseñado para conocer e identificar las frecuencias principales (figura 2) con sus amplitudes, entre otras propiedades.

Este estudio permite obtener unos resultados orientativos mediante un dispositivo experimental que está al alcance de los estudiosos de las campanas y sin coste económico alguno. Todo esto se ha analizado en un entorno donde la contaminación acústica de la calle, propio de las ubicaciones de los campanarios en el núcleo urbano de una ciudad, puede influir en las mediciones. También puede influir en el resultado obtenido la existencia de inscripciones y muescas de desgaste que alejan a las campanas estudiadas de una campana ideal.

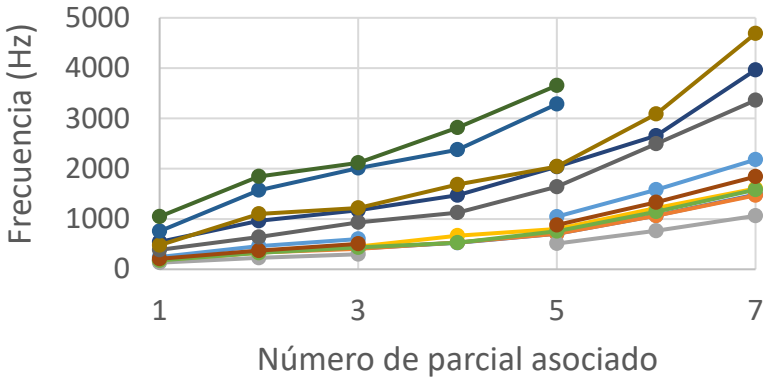

Figura 2. Parciales obtenidos en las campanas estudiadas.

[1] T. D. Rossing, The Acoustics of Bells: Studying the vibrations of large and small bells helps us, *American Scientist* 72, 440 (1984).
[2] E. Wiegman, *Acoustical Measurements on Church-bells and Carillons* [Tesis doctoral, Escuela Técnica de Delft]. Delft, Países Bajos (1949).

Agradecimientos: Campaneros de la catedral de Valencia, Grupo de campaneros de Alcoy.

Multidisciplinary collaborative learning. Application to the analysis of citrus cultivation in the Vega Baja del Segura against rising energy prices

J. M. Cámara-Zapata*, H. Puerto, A. Conesa, J. M. Brotons

Centro de Investigación e Innovación Agroalimentaria y Agroambiental (CIAGRO), Universidad Miguel Hernández

*e-mail: jm.camara@umh.es

The current rise in energy prices is hindering the economic viability of agricultural production, specifically lemon production in the Vega Baja del Segura. The analysis of the problem constitutes a paradigmatic case of searching for solutions through multidisciplinary analysis. Therefore, an activity has been proposed to students of different subjects and degrees (Law and business administration, Electronic and automatic industrial engineering, Agro-food and agri-environmental engineering and Master's degree in agronomic engineering) consisting of the analysis of the situation and the proposal of solutions aimed at improving the resilience of the sector. Collaborative work enhances student motivation and contributes to the development of important skills that are difficult to acquire. From the teaching point of view, the interaction has allowed i) developing learning strategies aimed at transferring knowledge from the classroom to the agricultural sector in relation to energy efficiency, ii) promoting the design of blended learning experiences by developing online audiovisual material to disseminate basic concepts of each area of knowledge, iii) design tools aimed at improving the creative process (Design Thinking) and finally, iv) encourage the creation of interactive learning environments to collaborate with students from different degrees.

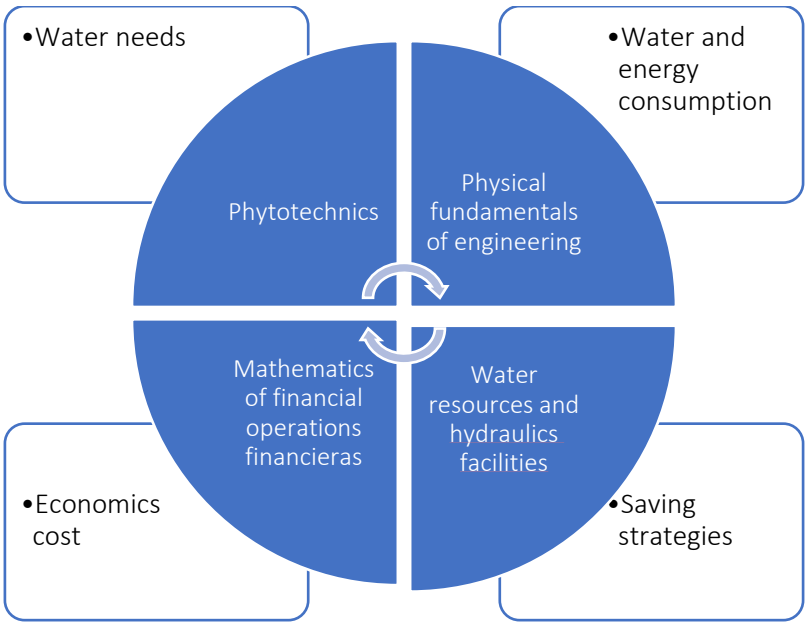

Figure 1. Collaborative work with indication of subjects and objectives

Mujeres en Física

Presentaciones orales

Jueves 14/07:

15:30-16:00 (Charla Invitada) Maite Paramio (Universitat Autònoma Barcelona). *Asociación de Mujeres Investigadoras y Tecnólogas (AMIT)*

16:00-16:15 Chantal Ferrer-Roca (Universitat de Valencia). *Mujeres en STEM con la Feria Experimenta de Valencia*

16:15-16:30 Anabel I. Morales (Instituto de Física Corpuscular (IFIC, CSIC & University of Valencia)). *Proyecto Meitner*

16:30-16:45 Alba de las Heras (Universidad de Salamanca). *The future researchers in Optics and Photonics: gender bias in the PhD theses defended in Spain in 2015-2020*

16:45-17:00 Elisabet Pérez-Cabré (Universitat Politècnica de Catalunya). *20/21 Spanish Central IDL Event in Terrassa: promoting a balanced participation in gender*

17:00-18:00 **Café**.

18:00-18:15 Ana Jesús López Díaz (Universidad de A Coruña). *Una actividad para reflexionar, con perspectiva de género, sobre los procesos de transferencia del conocimiento universitario*

18:15-18:30 Màriam Tòrtola (Instituto de Física Corpuscular (IFIC, CSIC & University of Valencia)). *An initiative to invert gender statistics at nuclear and particle physics workshops: @FlipPhysics*

18:30-18:45 Mª Teresa Ceballos (Instituto de Física de Cantabria (CSIC-Universidad de Cantabria)). *Más allá de Madame Curie: iniciativas IFCA para todos los públicos por la visibilización de científicas*

18:45-19:00 María S. Millán (Universitat Politècnica de Catalunya). *Women in Physics trending topic in a MSc course. Pilot experience*

19:00-19:15 Pas García Martínez (Universitat de València). *I Encuentro Virtual de Alumnas de Física*

19:15-19:30 Isabel Saura (Universidad de Murcia). *Visibilidad de la mujer en la ciencia desde la actividad cotidiana: concursos, encuestas y otras propuestas sencillas*

Mujeres en STEM con la Feria Experimenta de Valencia

Chantal Ferrer-Roca, Amparo Pons-Martí, Jordi Vidal, Miguel V. Andrés

Facultad de Física, Universidad de Valencia, España.

*e-mail: Chantal.Ferrer@uv.es

La Feria-Concurso Experimenta (enlace uv.es/experimenta) es una iniciativa organizada por la Facultat de Física de la Universitat de València que se propone interesar al alumnado de enseñanza secundaria (ESO, Bachillerato y ciclos formativos de grado medio) en la ciencia y la tecnología, transmitiendo el interés por comprender el mundo que nos rodea. Los grupos participantes (más del 50 % mujeres) desarrollan proyectos experimentales STEM que exponen y explican al público visitante, incidiendo de forma especial en los principios físicos que los fundamentan y en las relaciones entre la física y la tecnología y otras ciencias [1].

Son conocidos los bajos porcentajes de participación de mujeres en estudios y profesiones relacionados con la física y algunas ingenierías. Como estudiantes, constituyen aproximadamente el 25 % del alumnado universitario en nuestras facultades de física. Los porcentajes de profesionales, en particular en ámbito académico, son inferiores. Se ha demostrado que las acciones de visibilización y el incremento de referentes tienen efectos decisivos para atraer el talento de las mujeres hacia estas áreas.

Desde 2005, año en que se celebró la primera convocatoria de esta feria, junto al estrechamiento de lazos entre la universidad y la enseñanza secundaria, ha sido una prioridad apoyar el trabajo de las mujeres en el ámbito STEM, visibilizando e incrementando su presencia. Las acciones concretas emprendidas incluyen un reconocimiento a mujeres científicas y tecnólogas que han contribuído de forma significativa a la física y la tecnología (sección "Tu también puedes ser…" de las bases de participación [2]: Donna Strickland, Ursula Franklin, Jane Feynman, etc.). Pero las acciones quizá de mayor calado tienen que ver con un trabajo constante, año tras año, para conseguir que el 50 % de los miembros de la organización, jurados y alumnado colaborador sean mujeres; y para visibilizar de forma sistemática en fotografías, videos y plan de comunicación la participación real de más del 50 % de mujeres que presentan y explican sus proyectos STEM en la feria, que se celebra en el Museo de la Ciencia de Valencia desde hace años [3].

Tras 17 convocatorias, con alrededor de 1000 proyectos presentados y 4500 participantes, unos 40000 visitantes han vivido una experiencia fuera de lo común: cientos de mujeres, al mismo tiempo divulgando sus experimentos STEM a jurados paritarios y ayudadas por decenas de estudiantes colaboradoras.

Figura 1. Participante explicando su proyecto al público en 2019.

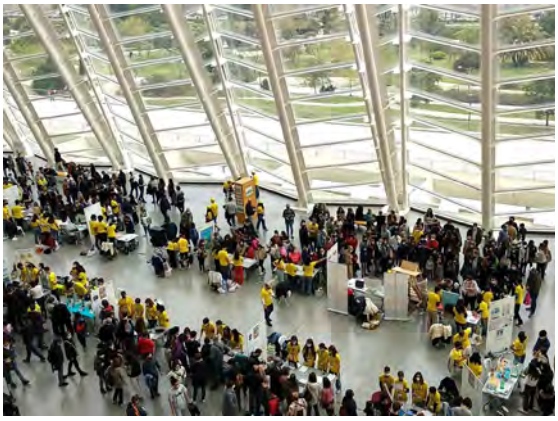

Figura 2. Vista de la Feria Experimenta de 2022 en el Museo de la Ciencia de Valencia.

[1] Chantal Ferrer-Roca, M.-V. Andrés, A. Pons-Martí, J. Vidal, A. Marco, A. Cros, G. Saavedra, J. C. Barreiro, La Feria-concurso "Experimenta" de Valencia cumple diez años: 2005-2015, ponencia invitada en 25º Encuentro Ibérico de Enseñanza de la Física, XXXV Bienal de Física de la RSEF, Gijón (2015).
[2] enlace https://go.uv.es/experimenta/mujeres (23/4/2022).
[3] como, por ejemplo, el enlace https://go.uv.es/experimenta/11febrero (23/4/2022) o la nota de comunicación https://go.uv.es/experimenta/notaprensa (23/4/2022).

Reconocimientos: Proyectos FCT-20-15571 y FCT-21-16582 de la Fundación Española para la Ciencia y la Tecnología del Ministerio de Ciencia e Innovación y otras entidades colaboradoras, que incluyen la RSEF y la DEDF.

Proyecto Meitner

A. I. Morales[1], A. Molina[1], B. Rubio[1], A. Aparici[1], J.R. Bertomeu[2], C. Escobar[1], I. Ladarescu[1], O. Mena[1], R. Molina[1], M. Moreno-Llácer[1], E. Nácher[1], S. Orrigo[1], J. Palacios[1], S. Pastor[1], D. Rodríguez[1], S. Rubio[3], J. Simon[2], J. L. Tain[1], M. Tórtola[1], M. Villaplana[1]

[1]*Instituto de Física Corpuscular (IFIC, CSIC & University of Valencia), Spain.*
[2]*Instituto Interuniversitario López Piñero. University of Valencia, Spain.*
[3]*Unidad de Cultura Científica y de la Innovación. University of Valencia, Spain.*

*Presentadora a definir

En esta contribución presentamos "Proyecto Meitner" [1], una acción de divulgación científica con la que el Instituto de Física Corpuscular (IFIC, CSIC-Universitat de València) recupera y revaloriza la contribución de las grandes pioneras de la Física Nuclear, de Partículas y Astropartículas a través de la figura de Lise Meitner. Durante 2021 contamos con tres actividades principales: la puesta en escena, por parte de CRIT Companyia de Teatre [2], de *Proyecto Meitner. Una historia de ciencia y traición*, obra escrita por el profesor de Historia de la Ciencia y dramaturgo Robert M. Friedman [3], las jornadas de Ciencia y Género "Mujeres pioneras en Física Nuclear y de Partículas", y el concurso para centros de secundaria "Express-Arte ConCiencia". La versión española de la obra arranca con un innovador *videomapping* protagonizado por el equipo científico de Proyecto Meitner y finaliza con un coloquio entre artistas, personal científico y público asistente. En 2021, se realizaron 18 representaciones en teatros de la Comunidad Valenciana, entre los que destacan el Teatro Rialto [4] y el Teatre Talia [5], llegando a unas 2300 personas de todas las edades. Las jornadas, dirigidas principalmente a profesorado de ciencias, incluyeron ponencias, mesas redondas, entrevistas y monólogos, y contaron con la colaboración del autor de la obra y la famosa escritora Rosa Montero [6]. En cuanto al concurso, recibimos cerca de 80 trabajos artísticos sobre mujeres pioneras de la Física Nuclear, de Partículas y Astropartículas de todo el territorio español. Un jurado especializado en ciencia, arte y género seleccionó 20 obras para una exposición digital que está disponible en nuestra página web. Finalmente, se discutirá el impacto y las perspectivas futuras del proyecto, ya que planeamos ampliarlo con nuevas actividades.

[1] https://recordandoalise.es/en/
[2] https://teatrecrit.com/
[3] R. M. Friedman, *Proyecto Meitner. Una historia de ciencia y traición*. Algar Editorial (ISBN: 9788491425311) & Bromera (ISBN: 9788413582153). 2021.
[4] https://ivc.gva.es/es/ivc/agenda-ivc/proyecto-meitner-recordando-a-lise-meitner
[5] https://www.teatretalia.es/proyecto-meitner
[6] https://www.rosamontero.es/novela-ridicula-idea-no-verte.html

The future researchers in Optics and Photonics: gender bias in the PhD theses defended in Spain in 2015-2020

Rosa Ana Pérez-Herrera[1], **Alba de las Heras**[2,*], María-Baralida Tomás[3], Beatriz Santamaría[4], Clara Benedí-García[5], Ana I. Gómez-Varela[6], Verónica González-Fernández[7], Martina Delgado-Pinar[8]

[1]*Dept. of Electric, Electronic and Communication Engineering, Universidad Pública de Navarra, Spain.* [2]*Dpto. de Física Aplicada, Universidad de Salamanca, Spain.* [3]*Instituto Universitario de Física Aplicada a las Ciencias y las Tecnologías, Universidad de Alicante, Spain.* [4]*Dpto. Ing. Química, Mecánica y Diseño Industrial, Universidad Politécnica de Madrid, Spain.* [5]*Indizen Optical Technologies S.A., Spain.* [6]*Dpto. de Física Aplicada, Universidade de Santiago de Compostela, Spain.* [7]*Dpto. de Óptica, Universidad Complutense de Madrid.* [8]*Dpto de Física Aplicada, Universitat de València, Spain.*

*e-mail: albadelasheras@usal.es

The lack of diversity in STEM areas (science, technology, engineering and mathematics) and, in particular, gender stereotypes, lead in the worst cases to inequality and discrimination. This issue, which has become a hot topic in the last years since inclusive science means a better science, must be solved because it is a matter of social justice. Also, the problem is shifting to earlier stages of the scientific career: the Equality Committee of the National Council for Research in Spain (CSIC) shows in its last survey (2020) that women do not even begin a PhD [1]. The scientific system does not seem to overcome the problem but the contrary, and thus, positive policies should be put in action as soon as possible.

In this work, we perform a quantitative analysis about the underrepresentation of young female researchers in Optics and Photonics. In particular, we have analysed the systematic gender bias in the theses defended in Spain between 2015-2020 in this field. To do so, we used the repository TESEO from the Spanish Ministry of Education [2], where all the theses defended in Spain are compiled. We classified the theses attending to their UNESCO codes, which is an international standard for identifying different research topics. We analysed 80 UNESCO codes and a total of 4200 theses, and identified the gender of the theses authors according to their first name, the accessible information from this repository.

Figure 1 shows the data disaggregated by gender, attending to the main blocks of the UNESCO codes where the theses with descriptors related to Optics and Photonics can be found, that is: 21 (Astronomy and Astrophysics, 5 descriptors); 22 (Physics, 45 descriptors), 23 (Chemistry, 11 descriptors), 24 (Life Science, 2 descriptors), 25 (Earth and Space Science, 3 descriptors), 32 (Medical Sciences, 3 descriptors), and 33 (Technological Sciences, 11 descriptors). As an example of the gender bias, only 7 of the 45 descriptors belonging to 22-Physics show a balanced composition between male and female PhD candidates, while there are fields where the imbalance from the parity is higher than 30%, favouring male researchers. There are also some other implicit biases that we are currently studying, that involve the nature of the scientific topic. Our data shows that even within the same area of research, male and female researchers choose different topics of study attending to the fundamental vs. applied nature of the field. This is a work in progress for the workgroup of Women in Optics and Photonics from SEDOPTICA, and it will be presented soon.

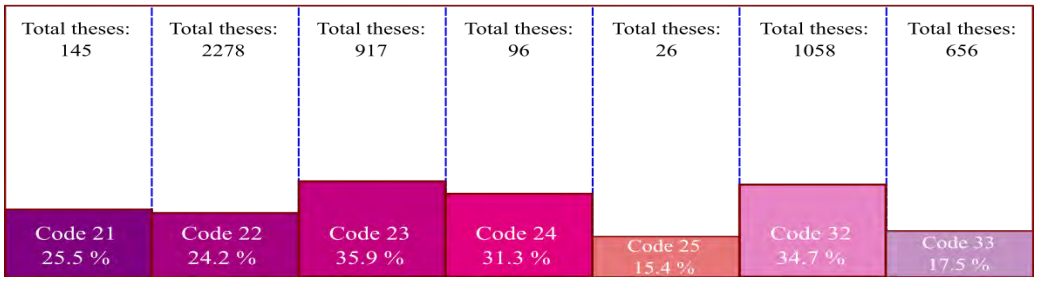

Figure 1. Percentage of female authors of doctoral theses in Optics and Photonics, 2015-2020, Spain.

[1] Consejo Superior de Investigaciones Científicas, "Informe anual 2020." 2020. [Online]. https://www.csic.es/es/el-csic/ciencia-enigualdad/ (accessed Apr. 1st, 2022).
[2] Ministerio de Educación, Cultura y Deporte. Gobierno de España., "Teseo." [Online]. https://www.educacion.gob.es/teseo/irGestionarConsulta.do (accessed Apr. 1st, 2022).

Acknowledgements: To SEDOPTICA for its constant support, and Alcon for sponsoring the Women in Optics and Photonics Committee. We also thank the Spanish Ministry of Education for the TESEO database.

20/21 Spanish Central IDL Event in Terrassa: promoting a balanced participation in gender

Elisabet Pérez-Cabré*, María Sagrario Millán, Jesús Armengol

Terrassa School Optics & Optometry, Universitat Politècnica Catalunya, Violinista Vellsolà 37, 08222 Terrassa, Spain.

*e-mail: elisabet.perez@upc.edu

The School of Optics and Optometry of Terrassa (FOOT) of the Universitat Politècnica of Catalunya (UPC), organized the third edition of the central event of the International Day of Light (IDL) in Spain. The FOOT, in its proposal and motivation, set out to give special emphasis to Light, Vision and Visual Health and considered four main aspects during the programming of the activities for the IDL celebration:

- To actively promote balanced participation of women and men from the constitution of the organising committee itself to the design of all the activities.
- To remark the transversal impact of light and increase people's awareness of its relevant role in everyday life.
- To reach a wide and heterogeneous audience (people of various ages, backgrounds and motivations).
- To achieve both local engagement and widespread dissemination.

The local organising committee included representatives of the FOOT and its board of trustees, the UPC, the Spanish Society of Optics (SEDOPTICA) and the Terrassa City Council. The Terrassa IDL event covered over a week and was planned to occupy different locations and allow simultaneous activities. Briefly, the program included outreach conferences, debates and round tables, exhibitions (among them, one highlighting the role of women in light science and related technologies), free eye examinations, leisure and cultural activities and more. A detailed description of the activities can be found in the program of the event [1] and a summary video is also provided [2]. This work will highlight the active promotion of balanced gender participation and will analyse the figures of the event.

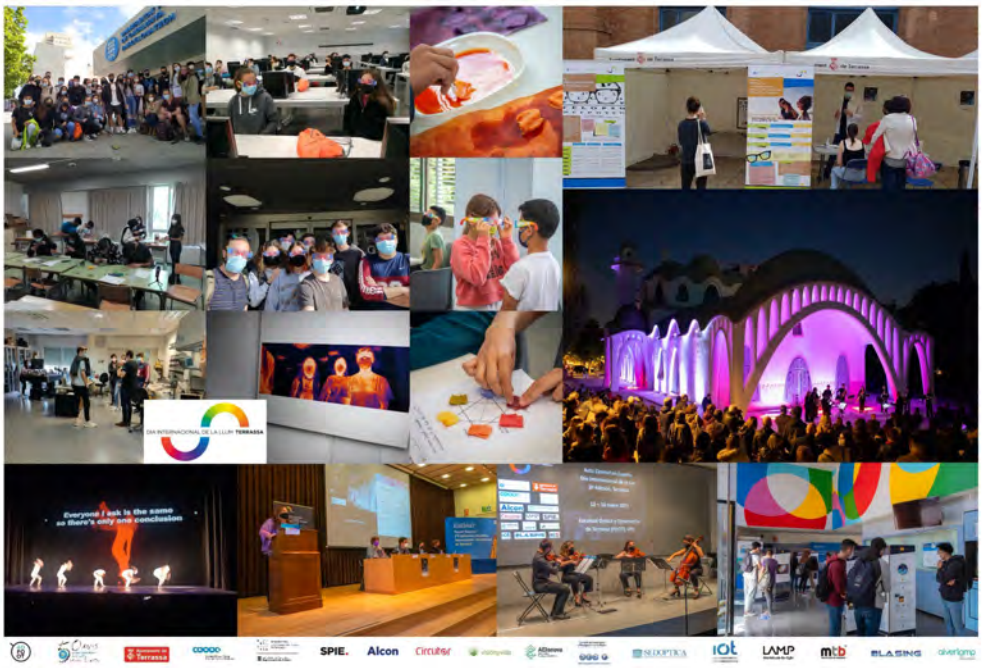

Figure 1. A photographic mosaic of activities in the 3rd edition of the Central IDL event in Spain (12-16 May 2021).

[1] Complete event program: https://diadelaluz.es/storage/files/DIL_2021_Programa_Oficial.pdf (in Spanish) (2021).
[2] Summary video 3rd ed. Central IDL event in Spain: https://www.youtube.com/watch?v=IBhCGNJvVUs (2021).

Acknowledgements: The authors thank the Spanish Committee of the IDL and all the organizations and companies that contributed to the realization of the 3rd edition of the Spanish central IDL event held in Terrassa in 2020-2021.

Una actividad para reflexionar, con perspectiva de género, sobre los procesos de transferencia del conocimiento universitario

Ana Jesús López Díaz

EPEF, Campus Industrial de Ferrol, Universidad de A Coruña, 15471, Ferrol, A Coruña, España.

e-mail: ana.xesus.lopez@udc.es

A las dos misiones clásicas de la Universidad, investigación y docencia, hay que sumar hoy en día una tercera; la transferencia del conocimiento. La Academia debe explotar su potencial intelectual, científico y tecnológico y promover la transmisión de su saber a la sociedad para contribuir a la mejora del bienestar de la ciudadanía. Los resultados de la prueba piloto lanzada por la ANECA en 2018 para evaluar e incentivar la actividad de transferencia, el denominado "sexenio de transferencia", han evidenciado una importante brecha de género. Conscientes de la necesidad de reflexionar sobre el proceso de transferencia del conocimiento; los factores causantes de esta brecha, las iniciativas que las universidades y organismos públicos han de llevar a cabo para reducirla; así como las estrategias de empoderamiento de las investigadoras para afrontar con éxito estos nuevos retos, en septiembre de 2021 se desarrollaron en línea desde la Universidade da Coruña las jornadas *Transferencia del conocimiento universitario desde una perspectiva de género* https://www.transferenciaexenero.gal/es/inicio-es/ subvencionadas por el Instituto de las Mujeres y cofinanciadas por el Proyecto Erasmus +, MATES (Maritime Alliance for Fostering the European Blue Economy through a Marine Technology Skilling Strategy). En ellas se analizaron, con perspectiva de género, los procesos de generación, difusión y transferencia del conocimiento a través de ponencias, mesas redondas y talleres articulados en tres áreas temáticas: *Género, transferencia del conocimiento y excelencia universitaria*, *Transferencia con perspectiva de género: el papel de las OTRI* y *Mujeres en investigación e innovación: situación y retos*. El interés por este tema y por tanto el éxito de estas jornadas, se puso de manifiesto en el elevado número de asistentes de distintas universidades y centros de investigación, la alta participación en las distintas actividades del programa y en los resultados de una encuesta de satisfacción. En esta comunicación se presenta una descripción de la actividad, los resultados obtenidos y las conclusiones más relevantes para integrar la dimensión de género en el ciclo completo de generación, difusión y transferencia del conocimiento universitario.

Agradecimientos: Actividad subvencionada por el Instituto de las Mujeres, convocatoria PAC 2020, proyecto 24/4ACT/20 y por el proyecto Erasmus + MATES (Maritime Alliance for Fostering the European Blue Economy through a Marine Technology Skilling Strategy).

An initiative to invert gender statistics at nuclear and particle physics workshops: @FlipPhysics

Raquel Molina Peralta[1,2,*], Gabriela A. Barenboim[1,2], Valentina De Romeri[1,2], Olga Mena Requejo[1], Ana Isabel Morales López[1], María Moreno Llácer[1,3], Sonja E. A. Orrigo[1], Emma Torró Pastor[1], Mariam Tórtola Baixauli[1,2]

[1]*Instituto de Física Corpuscular (CSIC/Universitat de València), Parc Científic UV, C/ Catedrático José Beltrán, 2, 46980 Paterna, Spain.* [2]*Departament de Física Teòrica, Universitat de València, 46100 Burjassot, Spain.* [3]*Departamento de Física Atòmica, Molecular i Nuclear, Universitat de València, 46100 Burjassot, Spain.*

*e-mail: Raquel.Molina@ific.uv.es

The lack of referents of female researchers and professors in nuclear and particle physics has motivated the birth of the @FlipPhysics workshop series [1]. The initiative seeks to fill this gap, making visible those talented female physicists working in these areas while giving the opportunity to young female students who are starting a research career to present their work. The workshop is held in an in-person format and supportive environment with the aim also of enlarging the female's research network. The first workshop took place from the 21st to 25th of March 2022 at IFIC, Valencia. The participants had the opportunity to be introduced by mostly female scientists to more than 10 different topics such as nuclear physics, particle physics, neutrinos, dark matter, cosmology, gravitational waves, machine learning, medical physics or quantum computing. We also organized several special sessions as the gender equality session with talks given by experts, round tables in gender equality and maternity in physics, the communication skills session, with writing and public speaking activities, and the student session with experts working also outside academia. The statistics were successfully inverted with around 75 % women of the 200 participants, being about 85 % of the speakers also female. The workshop is expected to be repeated in 2024.

[1] https://indico.ific.uv.es/event/6372/

Más allá de Madame Curie: iniciativas IFCA para todos los públicos por la visibilización de científicas

M. T. Ceballos* R. García, C. E. Graafland, D. Herranz,
S. Martínez-Núñez, J. Piedra, M. Seror, R. Vilar

Instituto de Física de Cantabria (CSIC-Universidad de Cantabria)

*e-mail: ceballos@ifca.unican.es

Es una situación en la que seguro que muchos/as nos hemos encontrado alguna vez... en una charla pública preguntamos por el nombre de científicas importantes y el único nombre que surge es el de Marie Curie. Pero las personas que hacemos ciencia cada día sabemos que ella solo fue la punta del iceberg.

El Instituto de Física de Cantabria a través de su comisión de igualdad y diversidad en colaboración con el departamento de difusión cuenta con una larga trayectoria de actividades enfocadas a dar visibilidad a las científicas tanto del presente como del pasado, en los campos relacionados con la ciencia de las diferentes líneas de investigación del centro. El público al que esta labor va destinada incluye desde escolares en la etapa de infantil hasta estudiantes de universidad, pasando por todas las etapas educativas, además del público general.

El objetivo de esta labor es conseguir transmitir que no solo Madame Curie tuvo un papel relevante en la Física (en la ciencia en general) sino que el nombre y el trabajo de otras muchas científicas esté presente en la cultura científica de la sociedad.

Desde la divulgación y como primer campo de actuación, abordamos el papel de las científicas en nuestro programa "Expandiendo la ciencia: investigadores/as en la escuela", de charlas en los centros educativos. La visibilización tiene una doble vertiente, ciencia contada por científicas del IFCA y charlas específicas visibilizando las "gigantas" del pasado en cuyos hombros nos apoyamos las personas en ciencia del presente.

Con este objetivo en mente, anualmente participamos también en la celebración del "Día internacional de las mujeres y las niñas en la ciencia" con dos iniciativas concretas: el *concurso de cómics* sobre mujeres científicas (que ha celebrado en 2022 su V edición) y el *ciclo de conferencias científicas "Ateneas"* en colaboración con el Ateneo de Santander.

Finalmente, en el aspecto formativo, la comisión se focaliza en dos actividades principales: la educación superior y el personal del propio centro. Con el punto de mira en las enseñanzas universitarias, impartimos un bloque de Igualdad en Ciencia en la asignatura transversal "Habilidades, valores y competencias transversales" del grado de Física, del grado de Matemáticas, del doble grado de Física y Matemáticas y del grado de Ingeniería Informática de la Universidad de Cantabria. A través de este bloque pretendemos hacer visible entre el futuro personal científico y técnico aún en formación, la situación actual de las mujeres en ciencia, las dificultades a las que se enfrentan por razón de su género, abordando iniciativas legales y sociales para avanzar en la eliminación de la brecha de género en la ciencia. Por otro lado, organizamos charlas formativas en igualdad y diversidad dirigidas al personal del centro con el objetivo de mejorar sus conocimientos y de proporcionar herramientas útiles para aplicar la perspectiva de género en su labor diaria.

El balance a lo largo de los años en que llevamos realizando estas actividades es realmente positivo. Aunque somos conscientes de que son pequeños granitos de arena, hemos podido constatar que cuando ahora preguntamos en los colegios o en charlas públicas por nombres de científicas importantes, no solo aparece el nombre de Madame Curie... ¿será que algo está(mos) realmente cambiando?

"*Women in Physics*" trending topic in a MSc course. Pilot experience

María S. Millán[1,*], Verónica González[2], Martina Delgado-Pinar[3]

[1]*Dept. Optics and Optometry, Universitat Politècnica de Catalunya BarcelonaTech, Spain.*
[2]*Dpto. De Óptica, Universidad Complutense de Madrid, Av. Arcos del Jalon 118, Madrid, Spain.*
[3]*Departamento de Física Aplicada – ICMUV, Universitat de València, Spain.*

*e-mail: m.millan@upc.edu

Over the last decade, one of the authors (M.S. Millán) has included the theme "Women in Physics" as a trending topic in the content and syllabus of Managing light with devices, an elective course in the Optical Engineering teaching unit of the 60 ECTS Master in Photonics' degree [1] offered by three universities (Universitat Politècnica de Catalunya, Universitat de Barcelona, Universitat Autònoma de Barcelona) and a photonics research institute (Institut de Ciències Fotòniques) in the Barcelona (Spain) area. It participates in the EUROPHOTONICS Erasmus Mundus Joint Master Degree, which involves four more European university partners (Marseille-France, Karlsruhe-Germany, Tampere-Finland, Vilnius-Lithuania). The Master in Photonics aims to educate future researchers in the field of science and technology of light and promote entrepreneurial activity in photonics amongst its students.

The activities of the Women in Physics topic are revised every year for updates and better coverage of the issue. A stage pattern has proved to be useful to motivate and get the involvement of the participants:

- Announcement in the educational virtual platform. Inclusion in the syllabus.
- A 2-hour class is scheduled close to a special day for women across the world, for instance, the International Day of Women & Girls in Science (11th Feb) or Women's Day (8th March).
- Proposal of a few short readings on the topic from science news magazines.
- Invited talk (female researcher) about a theme related with the course content.
- Time for a snack break and relaxed discussion with the participation of the lecturer.
- Invitation to share opinions and experiences. Tips and guidance for future career.

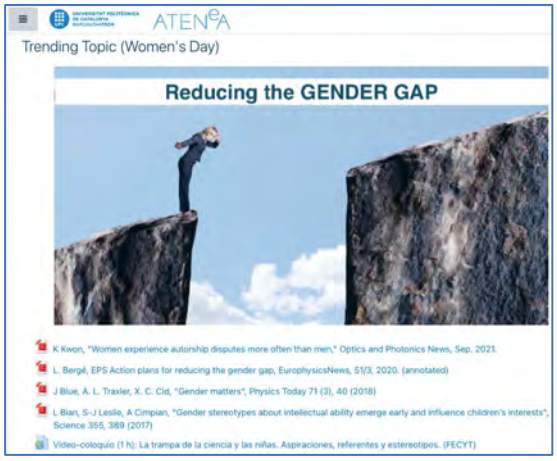

Figure 1. Screenshot of the educational platform. Picture from *EuroPhysics News* (L. Bergé [2]).

In 2022, two board members of the Women in Optics and Photonics Committee of the Spanish Society of Optics (SEDOPTICA-MOF) [3] participated in the activity. Verónica González presented the initiative "Cuenta con ellas" (count on women), which aims to create a database of female researchers in Optics and Photonics. This initiative will help organizing committees of conferences and workshops to get in touch with female experts, promote the equality in such events, and prevent all-men-panels. As an example of the work of female researchers, Martina Delgado lectured on "In-fibre acousto-optic devices", a topic included in the course syllabus. A break around a small optical gift, some drinks, biscuits and chocolates gave way to a relaxed discussion. The comments received later showed that all participants echoed the session.

The low rates of women in the area of physics require awareness-raising activities. Our pilot experience shows a simple way to penetrate in a physics-related course contents and gain visibility. Most importantly, it is a positive action to reduce gender stereotypes in STEM, addressed to both male and female students who are starting their professional career in physics and life-style personal project.

[1] https://photonics.masters.upc.edu/en (last accessed on 22th April, 2022).
[2] L. Bergé, *Europhysics News* **51**, 28 (2020). https://doi.org/10.1051/epn/2020306
[3] https://areamujersedoptica.wordpress.com/

Acknowledgement: Agencia Estatal de Investigación (PID2020-114582RB-I00/AEI/10.13039/501100011033).

I Encuentro Virtual de Alumnas de Física

Pascuala García-Martínez[1,*], Anabel Morales[2], Bárbara Álvarez[3], Màriam Tòrtola[2], Núria Garro[1], Irene Abril[4], Julia Hernández[4], Mariela Menghini[5], Lucía Alballe[6], Arantxa Fraile[7], Teresa Ripollés[8], Ana Gayol[9], Milagros Morcillo[10], Sònia Estradé[7], Pilar López Sancho[11], Marta Bueno[12], Teresa Samper[1]

[1]*Universitat de València.* [2]*Instituto de Física Corpuscular (IFIC).* [3]*Universidad de Oviedo.* [4]*Universidad Complutense de Madrid.* [5]*IMDEA Nanociencia.* [6]*Sincrotrón ALBA.* [7]*Universitat de Barcelona.* [8]*Universidad Rey Juan Carlos.* [9]*Universidad de Vigo.* [10]*Universidad de Córdoba.* [11]*Instituto de Ciencia de Materiales de Madrid CSIC.* [12]*Universidad de Salamanca.*

*e-mail: pascuala.garcia@uv.es

El pasado 12 de julio de 2021 se celebró virtualmente el I Encuentro de Alumnas de Física a nivel estatal organizado por la Comisión de Igualtat de la Facultat de Física de la Universitat de València y por el Grupo Especializado de Mujeres en Física de la RSEF, con la participación de unas 40 personas y con la motivación de **mejorar** sus conocimientos de física, **generar** una red de sororidad alrededor del interés por la física, **visibilizar** el papel de las físicas, **recibir formación** en género y **tejer redes** de cooperación y colaboración para ayudar a eliminar barreras y obstáculos que encuentren las alumnas en su trayectoria profesional futura.

Después de la inauguración por parte de la vicerrectora de Igualdad, Diversidad y Sostenibilidad de la Universitat de València, Dra. Dña. Elena Martínez, seguida de la conferencia de Milagros Morcillo Arencibia, titulada “El camino de la(s) Física(s): cómo ser física y no morir en el intento”. A continuación, varias estudiantes predoctorales contaron sus áreas de investigación en física. La tarde se dedicó exclusivamente a temas de género con la conferencia de Sònia Estradé titulada "Cultura de la no cultura y dimensión de género en la física", un debate en grupos de trabajo con la temática “Tejiendo Redes Físicas” y finalizando con una Mesa Redonda titulada “La carrera de una física, ¿pasa la prueba de la luz ultravioleta? Con Pilar López Sancho, Marta Bueno, moderada por Teresa Samper.

Figura 1. Algunos instantes e imágenes del encuentro.

También pudimos escuchar interesantes consejos y experiencias de profesionales que trabajan en física en pequeñas píldoras grabadas, algunos de los fotogramas se muestran en la figura 1. También pudimos recoger ilustrativos testimonios que fueron surgiendo surgieron en la sesión de grupo de trabajo con alumnas. Algunas de las frases destacables fueron las siguientes: “Los familiares y amigos no ven el perfil femenino adecuado para carreras científicas y nos desaniman”, “Hay que confiar en nosotras mismas y también busca alternativas en las aulas para que las alumnas participen”, “Los profesores tratan con más respeto a alumnos que a alumnas y toman más en cuenta sus preguntas ellas lo perciben así y lo denuncian, organizándose para apoyarse”, “Existe el sesgo de no asociar chicas a carreras de ciencias duras familiares y amigos incluso de docentes”.

La jornada se puede encontrar en:
https://www.youtube.com/channel/UCTWVpSC0TqzxJfPOBsDYKgw/videos.

Agradecimientos: El Encuentro fue financiado por la Unitat d’Igualtat de la Universitat de València en su convocatoria de ayudas 2021 para impulsar la igualdad entre mujeres y hombres.

Visibilidad de la mujer en la ciencia desde la actividad cotidiana: concursos, encuestas y otras propuestas sencillas

Ana María Bravo Martín[1], José Juan Fernández Melgarejo[2], Ángel Ferrández Izquierdo[3], Pascual Lucas Saorín[3], **Isabel M. Saura Llamas**[4,*], Rafael Garcia-Molina[5]

[1]*Departamento de Lengua Española y Lingüística General, Universidad de Murcia, España.* [2]*Departamento de Electromagnetismo y Electrónica, Universidad de Murcia, España.* [3]*Departamento de Matemáticas, Universidad de Murcia, España.* [4]*Departamento de Química Inorgánica, Universidad de Murcia, España.* [5]*Departamento de Física, Universidad de Murcia, España.*

*e-mail: ims@um.es

Los estereotipos comunes asocian las capacidades intelectuales de alto rendimiento (genialidad, excelencia y brillantez) más con los hombres que con las mujeres. Como consecuencia, muchas mujeres dejan de percibir determinadas carreras como adecuadas a sus capacidades, lo que conlleva que las mujeres se encuentran infrarrepresentadas en aquellos campos científicos donde se persigue y se valora especialmente la brillantez intelectual como la Física, las Matemáticas o la Filosofía [1]. Se han propuesto numerosas medidas para aumentar la vocación femenina en las carreras STEM (Science, Technology, Engineering, and Mathematics), pero una de las más efectivas y sencilla de llevar a cabo es proporcionar a las niñas, en una etapa temprana de su educación, modelos femeninos de éxito que representen toda la potencialidad de lo que ellas pueden alcanzar [2].

El Grupo de Transferencia de Conocimiento de la Universidad de Murcia *PaCienciaLaNuestra* ha desarrollado algunas actividades sencillas para aumentar la visibilidad de las mujeres en la Ciencia. Básicamente nos hemos centrado en la realización de un concurso de preguntas/respuestas sobre algunas figuras femeninas representativas de las disciplinas STEM, en el diseño de encuestas dirigidas al alumnado de nuestros respectivos campos científicos y en la publicidad de algunas fechas significativas.

Concursos. En enero de 2022 se puso en marcha el concurso "Mujeres y Ciencia. Doce cuestiones de género". El concurso estaba destinado a toda la comunidad universitaria (estudiantes, PDI y PAS) y su objetivo esencialmente ha sido contribuir a visibilizar el papel de la mujer en la Ciencia, recuperando referentes femeninos de la historia. En los primeros días de cada mes se ha formulado una pregunta sobre una científica famosa en una página web *ad hoc* (https://www.um.es/paciencialanuestra/concurso.php). La respuesta a esta pregunta es relativamente sencilla, de manera que puede encontrarse con facilidad en internet (aunque no de forma directa). Se intenta que la dificultad sea baja para que concursar sea sencillo, esto es, se pretende fomentar la curiosidad de la persona que participa más que evaluar su conocimiento profundo de la historia científica. El/La participante completa el formulario que hay insertado en la página web que se envía por correo electrónico a la organización. Cada mes se sortea un premio entre los/as acertantes. Para premiar la fidelidad, también se sorteará un premio entre los/as participantes que hayan respondido correctamente los doce meses.

Encuestas. Con motivo del Día Internacional de la Mujer y la Niña en la Ciencia, se ha propuesto a las estudiantes de algunas asignaturas que compartieran sus motivaciones para elegir la carrera, las dificultades que se han encontrado, sus intereses, el desarrollo de sus estudios, sus aspiraciones y sus reivindicaciones. Con los testimonios recibidos, se ha confeccionado un documento-resumen al que se le ha dado publicidad a través de la plataforma de docencia on-line de la Universidad (el Aula Virtual en la Universidad de Murcia). El resultado de estas opiniones es francamente significativo.

Publicidad de fechas. A través de la lista de distribución de correos electrónicos de la Universidad de Murcia (anuncios@listas.um.es), se han destacado todas las fechas significativas relacionadas con la Mujer y la Ciencia. Entre estas fechas sobresalen el Día de la Mujer y la Niña en la Ciencia (11 de febrero), el Día Internacional de la Mujer Matemática (12 de mayo) y el Día Internacional de la Mujer en la Ingeniería (23 de junio).

[1] Bian, L.; Leslie, S.-J.; Cimpian; A. *Science* **355**, 389–391 (2017).
[2] Dasgupta, N.; Stout, J. G. *Policy Insights from the Behavioral and Brain Sciences* **1**, 21–29 (2014).

Agradecimientos: Vicerrectorado de Transferencia y Divulgación Científica de la Universidad de Murcia.

Didáctica e Historia de la Física

Presentaciones orales

Jueves 14/07:

15:30-16:00 José Benito Vázquez Dorrío, Miguel Ángel Queiruga-Dios. *Algunas herramientas práctico-mentales para el aprendizaje de la Física*

16:00-16:15 Javier Pulgar, Diego Ramírez, Cristian Candia. *Fostering between-group collaboration in physics education through random group assignment*

16:15-16:30 Javier Pulgar. *A Teacher Ed. Initiative for Effective Collaboration via Classroom Network Analysis in Physics Education*

16:30-16:45 Gabriel Pinto. *Enfriamiento del agua en recipientes cerámicos como el botijo: Un recurso para la formación STEAM*

16:45-17:00 Luis Moreno Martínez. *"¿Eso para qué sirve?". Una experiencia de recreación de un gabinete histórico de física en las aulas de ESO*

17:00-18:00 **Pósteres y café**.

18:00-18:30 Arcadio Sotto, Jesús M. Arsuaga, Pablo Melón. *Diseño de laboratorios STEM sostenibles*

18:30-18:45 Jesús María Arsuaga Ferreras, Arcadio Sotto Díaz, Pablo Melón Jiménez. *La Física en el nuevo currículo de Primaria*

18:45-19:00 Cabrera, Bastián Carnero, Carlos Damián Rodríguez-Fernández, Damián Insua-Costa, Irene Romo-Díez, Javier Prada-Rodrigo, Javier Varela-Carballo, José Paz-Martín, Sabela Fernández-Rodicio, Verónica Villa-Ortega, Víctor W. Segundo Staels. *I NW MYRO: How students from different universities managed to organize a face-to-face congress after two long pandemic years*

19:00-19:15 Pablo De Ruyt, Javier Pulgar. *Lectura de libros de divulgación para estimular la reflexión conceptual en física moderna escolar*

Algunas herramientas práctico-mentales para el aprendizaje de la Física

José Benito Vázquez Dorrío[1,*], Miguel Ángel Queiruga-Dios[2]

[1]*Departamento de Física Aplicada, Universidade de Vigo, España.*
[2]*Departamento de Didácticas Específicas, Universidad de Burgos, España.*

*e-mail: bvazquez@uvigo.es

Existen evidencias que relacionan la utilización de metodologías activas por parte del profesorado de Física con un mayor rendimiento académico del alumnado si las condiciones necesarias se ponen en juego [1]. Metodologías que, como mínimo actualmente, deben generar motivación intrínseca, inducir al uso de las tecnologías y promover un trabajo experimental colaborativo que suponga trabajar en equipo para aprender [2]. Hay una gran cantidad de investigaciones que indican que, en general, se propicia una actitud más positiva hacia la Física con un enfoque de enseñanza más práctico, basado en actividades manipulativas que hagan dudar al mismo tiempo al alumnado de sus intuiciones al enfrentarles a situaciones experimentales reales (Fig. 1). Pero para alcanzar un resultado positivo de activación mental los agentes implicados deben tener suficiente preparación básica en niveles guiados de instrucción basada en la indagación para acceder a estas metodologías, sin la cual no tiene, en el mejor de los casos, una incidencia significativa positiva sobre el aprendizaje en comparación con estrategias docentes tradicionales [3]. Las actividades práctico-mentales requieren que el alumnado realice tareas guiadas de investigación experimental dentro y/o fuera del aula, usando sus conocimientos y sentidos para observar, e instrumentos de diferente índole para potenciar estos, aumentando al mismo tiempo el interés la atención y la motivación por los contenidos.

En este trabajo se presenta una fundamentación, revisión y utilidad en el aula de estas bien conocidas herramientas práctico-mentales [4-5] que permiten relacionar, mediante actividades experimentales sencillas en el aula o fuera de ella, los conceptos, principios y leyes de la Física con sus aplicaciones e implicaciones, su relevancia para la vida cotidiana, su naturaleza investigadora, su evolución histórica y su proyección social [6]. Se muestran los resultados de su empleo tanto en los primeros cursos de Física de Grados en Ingeniería [7-9] como en cursos de profesorado en formación de secundaria y universidad [10-11].

Figura 1. Actividades relacionadas con el Electromagnetismo [7].

[1] Hake, R. R, *American Journal of Physics* **66**, 64 (1998).
[2] Cairns, D., *International Journal of Science Education* **41**, 2113 (2019).
[3] Gil, M., Cordero, J. M., y Cristóbal, V, *Revista de Educación* **379**, 32 (2018).
[4] Vázquez-Dorrío, B., García-Parada, E., González-Fernández, P. M, *Enseñanza de las Ciencias: Revista de Investigación y Experiencias Didácticas* **12**, 63 (1994).
[5] Vázquez-Dorrío, B., Rúa-Vieites A., *Revista Iberoamericana de Educación* **42/7**, 1 (2007).
[6] Costa, M. F. M., Vázquez-Dorrío, B, *Revista Eureka sobre Enseñanza y Divulgación de las Ciencias* **7**, 462 (2010).
[7] http://www.clickonphysics.es/cms/
[8] Vázquez-Dorrío, B., *Revista de Formación e Innovación Educativa Universitaria* **5**, 12 (2012).
[9] Vázquez-Dorrío, B., Vijande J., *Revista Española de Física* **32**, 22 (2018).
[10] Vázquez-Dorrío, B., en *Innovar na universidade: experiencias do profesorado*, *Andavira Editora* 85 (2012).
[11] Vázquez-Dorrío, B., en *Nuevos escenarios en la docencia universitaria*, *Educación Editora*, 457 (2016).

Fostering between-group collaboration in physics education through random group assignment

J. Pulgar[1,2,*], D. Ramírez,[2,3] C. Candia[4]

[1]*Physics Department, Universidad del Bío Bío, Concepción 4051381, Chile.* [2]*Grupo de Investigación en Didáctica de las Ciencias y Matemática (GIDICMA), UBB, Chile.* [3]*C. Investigación en Complejidad Social, Universidad del Desarrollo, Las Condes, 7610658, Chile.* [4]*Data Science Institute, Fac. Ingeniería, Universidad del Desarrollo, Las Condes, 7610658, Chile.*

*e-mail: jpulgar@ubiobio.cl

Classroom collaboration is critical for human development across disciplines and activities. Nonetheless, we are far from fully comprehend the ways in which individuals collaborate, as well as the drivers for seeking out help and advice from others for learning physics. Outside-group social interactions are rarely a point of attention in physics education studies, whereas in other disciplines, such as the sociology of innovations, between-group interactions are critical for the emergence of good ideas and collective learning [1]. Social relationships are rooted in similarity and affinity (i.e., homophily), and thus classroom collaboration is more likely to happen among those who are friends and display familiar behaviours [2]. The effects of student collaboration are well documented in PER, yet such academic gains depend on the set of norms and expectations defined by the nature of the tasks, teachers' roles, and the investment onto one's group [3].

The study was conducted in a sample of high school physics students (N = 90) from four courses in Southern Chile. To address the group activities designed, the teacher defined two alternative grouping mechanisms, namely: random assignment (experimental, n_e = 44); and friendship-based groups (control n_c = 44). Two courses were selected for each condition. We gather information onto students' group membership, and the following social networks: friendship; academic prestige (i.e., Who is a good physics student?); and physics collaboration. We to determine two brokerage variables linked with information flow: gatekeeper (i.e., source actor from other group) and representative (i.e., destination actor from another group).

Figure 1 depicts OLS multiple regression models fitted for Outside-group collaboration, representative and gatekeeper brokerage using outside-group friendship, good student nomination, inside-group collaboration, and the experimental conditions and gender as factors. As shown, outside-group collaboration is associated with having friends outside the group. External collaborative ties also are linked with higher rates of gatekeeper and representative brokerage, yet these roles are engaged by students in opposite sides of the academic hierarchy (see good student nomination coefficients). Further, the experimental group shows higher rates of representative brokerage compared to the control group. Students with more friends distributed throughout the classroom are more likely to engage in outside-group collaboration and brokerage, evidence that could inform grouping mechanisms and instructional strategies to guide group-level processes in the face of physics activities.

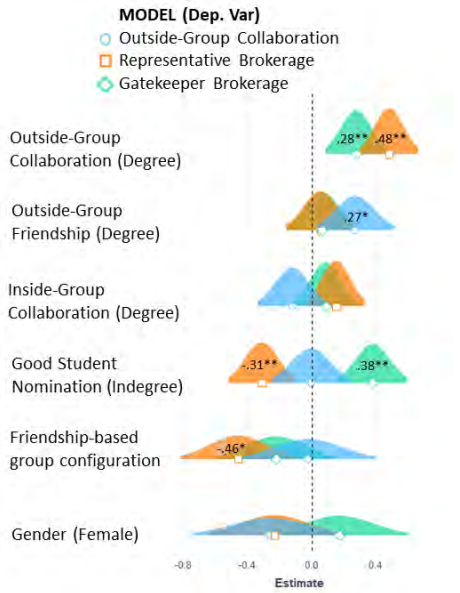

Figure 1. Graphic visualization of OLS multiple regression models for Outside-group collaboration (blue), Representative brokerage (orange), and Gatekeeper brokerage (green). Note: *p < .05; **p < .01.

[1] J. Pulgar, *Thinking Skills & Creativity* **42**, 100942 (2021).
[2] H. Weber, M. Schwenzer, S. Hillmert, *Network Science* **8**, 469 (2020).
[3] J. Pulgar, C. Candia & Leonardi, P. *Physical Review Physics Education* **16**, 010137 (2020).

Acknowledgements: This material is supported by project FONDECYT 11220385, ANID, Chile; and project 2020217 IF/F, Vicerrectoria de Investigacion y Postgrado, Universidad del Bio Bio, Concepcion, Chile.

A Teacher Ed. Initiative for Effective Collaboration via Classroom Network Analysis in Physics Education

J. Pulgar[1,2]

[1]*Physics Department, Universidad del Bío Bío, Concepción 4051381, Chile.* [2]*Grupo de Investigación en Didáctica de las Ciencias y Matemática (GIDICMA), UBB, Chile.*

e-mail: jpulgar@ubiobio.cl

In the constant pursuit of learning outcomes, researchers have recommended a teacher education oriented to collaborative approaches [1]. Both students and teachers experience obstacles when participating and implementing collaborative activities in the classroom. For instance, students across all levels of education display poor social and communication skills for effective collaboration [2]. These limitations have rarely been addressed by teachers in their daily practice, as they have shown to implement collaborative learning activities by emphasizing the cognitive gains of group work yet avoiding the importance of collaborative skills [2]. Pre-service and in-service teachers have shown to display lack of attention to collaborative skills and guidance for students to effectively engage in social processes [3]. Furthermore, the ways in which student collaborate and its effectiveness are sensitive to the nature of the learning activity and social norms embedded in the classroom [4], and the dedication to group-level processes [5].

This work attempts to tackle some of these limitations by offering tools to comprehend the complexities of student interactions in the classroom through social network analysis (SNA), and its relationship with teaching methodologies in physics education. This classroom network initiative is part of an ongoing research project funded by Chile's National Association of Research and Development (ANID). The program begins with and introduction of SNA's basic principles (e.g., cohesion, centrality) and visualizations, all contextualized in real data from social dimensions typically observed in physics education classrooms (e.g., friendship, academic prestige, and collaboration networks). Further, teacher participants are asked to observe maps of students' social relationships in a classroom (e.g., see Fig. 1), and to inform the teaching strategies and activities they consider the most appropriate for such group of students. Analysis of these responses should inform the different set of variables that teacher weight in when designing learning activities in physics classrooms.

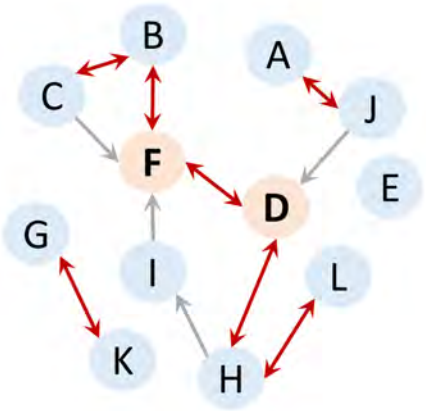

Figure 1. Classroom collaboration network in physics. Red arrows are collaboration between friends; grey arrows are collaboration with no friendship; orange nodes are perceived as high achieving students.

The content of the classroom network analysis initiative has been validated by groups of experts in science education and network science. Here I share the steps for developing the program, its activities and instruments for data collection, and information related to its validation. I further show preliminary results from a pilot study conducted in a sample of in-service teachers in physics and mathematics education.

[1] L. Kyei-Blankson, *Int. Journal of Science and Math. Ed.* **12**, 1047 (2014).
[2] H. Le, & T. Wubbels, *Cambridge Journal of Education* **48**(1), 103 (2018).
[3] I. Ruys, H. Van Keer, & A. Aelterman, *Journal of Curriculum Studies* **44**, 349 (2012).
[4] J. Pulgar, *Thinking Skills & Creativity* **42**, 100942 (2021)
[5] J. Pulgar et al., arXiv:2203.05638 (2022).

Acknowledgements: This material is supported by project FONDECYT 11220385, ANID, Chile.

Enfriamiento del agua en recipientes cerámicos como el botijo: Un recurso para la formación STEAM

Gabriel Pinto[1,2]

[1]*Grupo Especializado de Didáctica e Historia de la Física y la Química (GEDH), Reales Sociedades Españolas de Física y de Química, Plaza de las Ciencias, Ciudad Universitaria, 28040 Madrid.* [2]*E.T.S. de Ingenieros Industriales, Universidad Politécnica de Madrid (UPM), José Gutiérrez Abascal 2, 28006 Madrid.*

e-mail: gabriel.pinto@upm.es

Los objetivos del trabajo son: fomentar la cultura y la educación científica, promover la curiosidad y la indagación, aprender conceptos de varias disciplinas (física, química, matemáticas, geología, tecnología, biología, geografía…), mostrar la necesidad de experimentar para aprender ciencia, usar objetos cotidianos en actividades educativas, y promover enfoques CTS (*ciencia, tecnología y sociedad*). Lo tratado, mostrado para conocimiento e inspiración del profesorado, se articula sobre un tema central: el enfriamiento del agua contenida en recipientes cerámicos porosos, al evaporarse. El fenómeno, conocido desde hace siglos, se usa en distintos países, siendo emblemático el botijo español. Se muestra así que la *sabiduría popular* ha encontrado soluciones ingeniosas para resolver problemas y mejorar la vida, con los medios disponibles.

El enfriamiento del agua y la cantidad que se evapora con el tiempo son fáciles de medir. Hace años, analizamos un caso concreto; con los principios de transferencia de masa y calor, planteamos las ecuaciones diferenciales que describen los fenómenos producidos (Fig. 1). Considerando los parámetros involucrados y el cálculo simultáneo de algunas magnitudes, se resolvieron las ecuaciones por métodos numéricos [1]. Se obtuvieron valores de masa de agua evaporada y temperatura próximos a los experimentales. Todo este planteamiento es abordable en asignaturas de últimos cursos de titulaciones de Grado pero también, con distintas orientaciones, en todas las etapas educativas. Por ejemplo, puede servir para introducir la estructura, propiedades y procesado de arcillas (silicatos laminares). O puede estudiarse la influencia de la humedad del ambiente con el '*pájaro bebedor*', un juguete científico popular, encerrado o no en una campana transparente. Con una maceta introducida en otra mayor, y disponiendo arena humedecida entre ambas, se pueden fabricar los dispositivos ideados por el nigeriano Mohammed Bah Abba, conocidos como *pot-in-pot*, que conservan mejor los alimentos (al disminuir su velocidad de degradación al descender la temperatura). Esta aplicación permitió a niñas de ciertos poblados acudir a la escuela, pues dependían de la recolección y venta rápida de ciertas verduras [2].

La aparición de estos planteamientos en diversos medios de comunicación, durante los pasados años, ha servido para popularizar y divulgar conceptos científicos. Otros autores han enfocado el estudio en la influencia del clima [3] y en la geometría del recipiente [4], por citar algunos ejemplos. Se considera que el conjunto de lo tratado abre vías para abordar, en las aulas, enfoques de lo que se conoce como STEAM (por las siglas en inglés de *ciencia, tecnología, ingeniería, artes y matemáticas*).

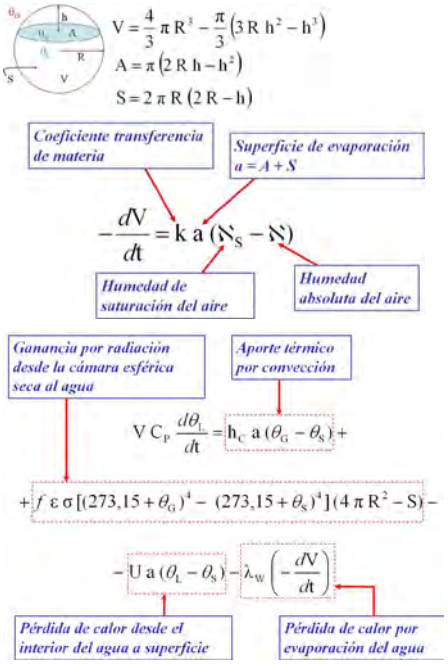

Figura 1. Modelo de botijo, con parámetros geométricos, y ecuaciones de velocidad de evaporación del agua y su variación térmica.

[1] J. I. Zubizarreta, G. Pinto, *Chemical Engineering Education* **29**, 96 (1995).
[2] G. Pinto *et al.*, *IV Congreso de Docentes de Ciencias de la Naturaleza*, pp. 413-422, Santillana (2017).
[3] A. Martínez de Azagra, J. del Río, *Journal of Maps* **11**, 240 (2015).
[4] J. Ortega-Casanova *et al.*, *Case Studies in Thermal Engineering* **26**, 101022 (2021).

Agradecimientos: Se agradecen las ayudas prestadas por la UPM (Proyecto de innovación educativa IE22.0506), la Obra Social «la Caixa» (Proyecto divulgativo «Ciencia y tecnología al alcance de tod@s»), y la Comunidad de Madrid, a través del Convenio Plurianual con la UPM en su línea de actuación Programa de Excelencia para el Profesorado Universitario, en el marco del V PRICIT (V Plan Regional de Investigación Científica e Innovación Tecnológica).

«¿Eso para qué sirve?». Una experiencia de recreación de un gabinete histórico de física en las aulas de ESO

Luis Moreno Martínez[1,2]

[1]*Departamento de Física y Química, CEIPSO Vicente Aleixandre, Miraflores de la Sierra, Comunidad de Madrid.* [2]*Grupo Especializado de Didáctica e Historia de la Física y la Química, Reales Sociedades Españolas de Física y de Química.*

e-mail: luis.morenomartinez@educa.madrid.org

El estudio histórico de las prácticas y materiales de la enseñanza de las ciencias constituye una perspectiva de gran actualidad en la investigación en historia y didáctica de las ciencias. Se trata de una línea de investigación que ha experimentado una notable expansión en las últimas décadas a través de la publicación de múltiples trabajos académicos sobre las prácticas pedagógicas, la cultura material, los manuales, los espacios y las biografías del profesorado [1]. En el contexto español, uno de los docentes de tiempos pretéritos cuya obra ha sido recientemente recuperada y analizada es el profesor Modesto Bargalló Ardévol (1894-1981). Bargalló fue una figura clave en la renovación de la enseñanza de las ciencias físicas, químicas y naturales del primer tercio del siglo XX que se vio obligado al exilio en México en 1939. Antes de exiliarse, desarrolló una prolífica actividad enseñando ciencias a los futuros maestros de la Escuela Normal de Maestros de Guadalajara y publicando diversos libros, manuales, traducciones, artículos, boletines y revistas sobre didáctica e historia de las ciencias. Entre esta amplia producción impresa se incluyen varios textos de enseñanza de la física, como *El gabinete de Física* (1924), obra en la que Bargalló detalló la construcción de cerca de cuarenta aparatos de física a partir de objetos cotidianos y útiles sencillos. Si bien los aparatos construidos por Bargalló y sus estudiantes perecieron con el paso del tiempo, el abundante uso de ilustraciones de este profesor para difundir sus prácticas pedagógicas ha hecho posible conocer y recuperar su gabinete de física [2].

La presente comunicación analiza una experiencia de recreación del gabinete histórico de física del profesor Bargalló realizada con alumnado de la materia de Física y Química de segundo y tercer curso de Educación Secundaria Obligatoria durante el curso escolar 2021-2022. Se trata de una experiencia didáctica que, lejos de buscar la reproducción fidedigna de los artefactos que conformaron el histórico gabinete, ha pretendido inspirar y motivar al alumnado en el diseño de aparatos análogos, identificando y aplicando los principios físicos que operan en su funcionamiento. Para la construcción de estos artefactos el alumnado, además de trabajar en equipo, hizo uso de residuos y productos cotidianos, potenciando la reutilización de los mismos. La experiencia ha permitido así identificar dificultades conceptuales y concepciones alternativas del alumnado sobre aprendizajes básicos de la física escolar (mecánica, electrostática, conducción del calor…), fomentar el aprendizaje experimental y manipulativo de la ciencia, concienciar al alumnado sobre la importancia del reciclaje y la reutilización de materiales y explorar las múltiples utilidades didácticas de la historia de la ciencia.

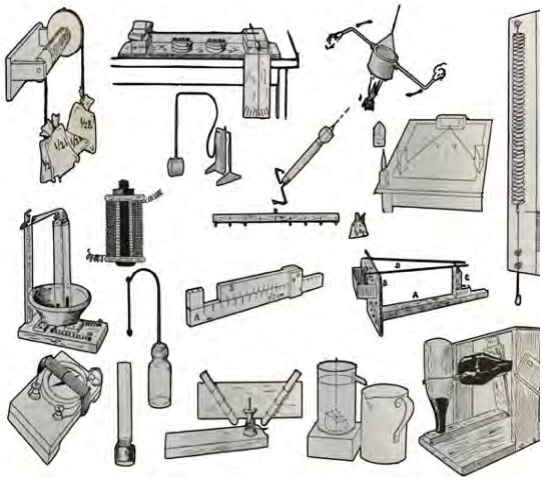

Figura 1. Algunos aparatos del gabinete de física del profesor Modesto Bargalló.

[1] John Rudolph, *How we teach science? What's changed and why it matters*, Harvard University Press (2019).
[2] Luis Moreno Martínez, *Revista Española de Física* **36**(1), 11 (2022).

Diseño de laboratorios STEM sostenibles

Arcadio Sotto*, Jesús M. Arsuaga, Pablo Melón

Departamento de Ciencias de la Educación, Universidad Rey Juan Carlos, Madrid, España.

*e-mail: arcadio.sotto@urjc.es

Con el fin de fomentar la motivación y el acercamiento al mundo de las ciencias naturales y en especial a la Física, se ha diseñado un conjunto de prácticas de laboratorio dirigidos a abordar el temario de Ciencias de la Naturaleza en los últimos cursos de la enseñanza Primaria y primeros de la ESO. Los experimentos diseñados se consideran asequibles económicamente para cualquier centro docente d nuestro territorio como garantía de la sostenibilidad de los mismos. Se propone una metodología de Aprendizaje Basado en Experimentos/Laboratorio que pretende despertar el interés y la curiosidad de los estudiantes hacia estas materias y de esta forma conseguir las condiciones necesarias para que se logre un aprendizaje significativo. Los laboratorios engloban muchos contenidos básicos como los Ciclos del Agua y las Rocas desde una perspectiva STEAM que persigue crear sinergias conducentes a un proceso de enseñanza-aprendizaje holístico desde el diseño y significativo como resultado.

Acknowledgements: The authors express thanks for the funding support from the European Community Project, MiniOpenLab-Open community, and Hands-on approach to Sustainable Development and STEM Education Project, Erasmus +. (2020/00157/001) and the National Investigation Agency of Spain, STEMind for Education Project. AEI (EIN 2020-112313).

La Física en el nuevo currículo de Primaria

Arcadio Sotto, **Jesús María Arsuaga***, Pablo Melón

Grupo de Investigación en Educación STEM (GIE-STEM),
Departamento de Ciencias de la Educación. Universidad Rey Juan Carlos.
C/ Tulipán, s/n. 28933 – Móstoles (Madrid), España.

*e-mail: jesusmaria.arsuaga@urjc.es

La ley Orgánica 3/2020, de 29 de diciembre, más conocida como LOMLOE o "*Ley Celaá*" fue impulsada por la ministra María Isabel Celáa Diéguez siete meses antes de ser relevada como responsable del Ministerio de Educación [1]. Como desgraciadamente sucede en España de forma reiterada, la nueva ley no fue consensuada con los partidos de la oposición y se aprobó exclusivamente con los votos de los partidos que conforman el Gobierno y algunos de sus socios de legislatura (obtuvo 177 votos a favor, siendo necesarios para su aprobación 176 debido a su condición de ley orgánica). Está actualmente recurrida ante el Tribunal Constitucional y su vigencia dependerá de la permanencia del actual bloque de gobierno en las próximas elecciones generales.

Como desarrollo natural de la LOMLOE, se ha publicado recientemente en el B.O.E. (2 de marzo de 2022) el nuevo diseño que el Ministerio de Educación y Formación Profesional ha elaborado para la etapa Primaria explicitando la ordenación general de la etapa y la concreción de las enseñanzas mínimas [2]. Como es bien conocido, posteriormente, cada comunidad autónoma deberá elaborar su currículo específico.

A diferencia de otros países más avanzados en la potenciación del ámbito STEM en el diseño del sistema educativo, los especialistas en formación del profesorado y los profesionales de la docencia, tanto en secundaria/bachillerato como en la universidad del ámbito científico, prestamos una atención insuficiente a las etapas Infantil y Primaria que percibimos como un territorio ajeno a nuestra actividad académica.

Figura 1. Isabel Celaá (izda.), Ministra de Educación hasta julio de 2021 y Alejandro Tiana (dcha.), Secretario de Estado de Educación cuando se aprobó la LOMLOE y que permanece en el puesto en la actualidad.

Por eso, habitualmente, el conocimiento que tenemos de las competencias en el ámbito STEM que las leyes educativas prestan a los estudiantes de las etapas anteriores a la ESO, y más específicamente a la Física, es borroso y deficiente.

El objeto de esta comunicación es la presentación de un análisis de la nueva ley de educación y del decreto de enseñanzas mínimas en relación principalmente con la etapa Primaria, comparándolos con las anteriores leyes educativas. Todo ello enfocado desde una perspectiva vinculada de forma global al ámbito STEM y concretando con más detalle los contenidos y referencias que competen al campo de la enseñanza de la Física. Como primera circunstancia, llama la atención que de nuevo se cree en la etapa Primaria el área de Conocimiento del Medio Natural, Social y Cultural, tradicionalmente conocido como "*Cono*", aunque la norma matiza que podrá desdoblarse en Ciencias de la Naturaleza y Ciencias Sociales.

Igualmente, se hará referencia en esta comunicación a las posibles consecuencias que la nueva normativa debería tener en el diseño de los estudios universitarios conducentes a la obtención de los títulos de grado que habilitan para la actividad profesional en la etapa Primaria en lo referente la formación científica de los futuros maestros y más específicamente en el campo de la Física [3].

[1] https://www.boe.es/diario_boe/txt.php?id=BOE-A-2020-17264
[2] https://www.boe.es/buscar/doc.php?id=BOE-A-2022-3296
[3] https://www.boe.es/diario_boe/txt.php?id=BOE-A-2007-22449

Agradecimientos: Los autores agradecen el apoyo, colaboración y soporte económico que el grupo especializado en investigación educativa GIE-STEM ha recibido de la Universidad Rey Juan Carlos, de la Agencia Estatal de Investigación (Proyecto STEMIND for Education, EIN2020, 112313) y de la UE (Proyecto MiniOpenLabs, Erasmus+ 2020-1-ES01-KA201-082706).

I NW MYRO: How students from different universities managed to organize a face-to-face congress after two long pandemic years

Alba de las Heras[1], Alejandro Doval[2], Alicia Muñoz-Ramos[2], Ana García-Cabrera[1], Bastián Carnero[2], **Carlos Damián Rodríguez-Fernández**[2,*], Damián Insua-Costa[2], Irene Romo-Díez[2], Javier Prada-Rodrigo[1], Javier Varela-Carballo[2], José Paz-Martín[2], Sabela Fernández-Rodicio[2], Verónica Villa-Ortega[2], Víctor W. Segundo Staels[1]

[1]*OSAL Student Chapter, Universidad de Salamanca, E-37008 Salamanca, Spain.* [2]*Asociación de Estudiantes y Grupo de Divulgación LUZADA, Santiago USC Young Minds Section y USCOPTICA Student Chapter, Universidade de Santiago de Compostela, E-15782 Santiago de Compostela, Spain.*

*e-mail: damian.rodriguez@usc.es

When we talk about scientific meetings in the field of physics, we usually think about an event organized by senior researchers and university professors gathering the most relevant experts in the topics of interest. This contribution tells a different story, that of the I Northwest Meeting of Young Researchers in Optics (I NW MYRO), an ongoing self-organized event exclusively driven by physics students from different universities and academic stages, from undergraduates to PhD candidates, with the support of the Real Sociedad Española de Física (RSEF) and other international scientific societies, such as the European Physical Society (EPS) via Young Minds (YM) and Optica.

Figure 1. I Northwest Meeting of Young Researchers in Optics logo.

The objective of this contribution is to explain how two outreach-oriented groups of physics students managed to organize a face-to-face event in Santiago de Compostela to celebrate the International Day of Light 2022 by gathering an important number of experts in optics and photonics representing different universities, research institutes and companies from the northwest of Spain and the north of Portugal.

The birth of the idea of a meeting exclusively driven by young researchers is tightly related to the existence of different outreach-oriented student associations in the universities of Santiago de Compostela (USC) and Salamanca (USAL). These young groups are USCOPTICA, YM Santiago USC and LUZADA from the USC and OSAL, from the USAL, being all of them organizers of this meeting. These organizations favour the scientific networking among students within their own universities, but also facilitate the creation of strong bonds with students from other universities, which is why both groups met some time ago. Once the decision of organizing the I NW MYRO was taken and the scope established, the search for funding and speakers took place. This stage was hard, however, we accomplished it thanks to soft skills developed during the day-to-day work of the student associations, such as teamworking, leadership, time-management or creative problem-solving. Special mention is required for the financial and organizational support that scientific societies such as RSEF (but also Optica, SEDOPTICA and Young Minds EPS) provided us.

The I NW MYRO will be held from May 5th to 7th in Santiago de Compostela with a long and gender-egalitarian list of excellent researchers in Optics and Photonics as speakers, industrial and women in science round-tables, and outreach activities in two different science museums. This would not be possible without the hard work that students do in groups supported by scientific associations such as Delegaciones de Estudiantes from RSEF, Optica Student Chapters or EPS Young Minds Sections, which are the seeds of the leading scientists of tomorrow.

Acknowledgements: We thank the Real Sociedad Española de Física (RSEF) for their economical support to the I NW MYRO and the RSEF Galicia and Salamanca local sections and Grupos Especializados de Mujeres en Física (GEMF) and Óptica Cuántica y Óptica No Lineal (GEOCONL) for their support. We also thank our other sponsors Universidade de Santiago de Compostela (USC) and its Facultade de Física, Optica and EPS Young Minds for their economical support and our partners SEDOPTICA, Menlo Systems GmbH., Aimen, BFlow SL and, specially, Facultade de Óptica e Optometría from USC for providing the venue for the I NW MYRO.

Lectura de libros de divulgación para estimular la reflexión conceptual en física moderna escolar

P. De Ruyt[1,2,3,*], J. Pulgar[3,4]

[1]*Ciencias Básicas, Universidad del Bío Bío, Chillán, Chile.* [2]*Colegio San Agustín, Quirihue, Chile.*
[3]*Grupo de Investigación en Ciencias y Matemática (GIDICMA), Universidad del Bío Bío, Chile.*
[4]*Departamento Física, Universidad del Bío Bío, Concepción, Chile.*

*e-mail: pderuytm@gmail.com

Estudios de investigación en enseñanza de la física han permitido diferenciar entre estudiantes expertos y aprendices, de acuerdo con sus estrategias de resolución de problemas y motivaciones [1]. La evidencia sugiere que incluso resolver un gran número de problemas algebraicos en física no asegura el desarrollo de aprendizajes, sino que este objetivo depende de las estrategias de resolución de problemas puestas en práctica [2]. Aquí se han identificado dos tipos fundamentales: Knowledge-Development o Desarrollo de Aprendizaje; y Means-End [1]. La primera se observa en quienes buscan aprender profundamente mediante la reflexión de conceptos al resolver problemas en física, mientras que la segunda se traduce en una estrategia superficial que busca encontrar la ecuación y variables adecuadas con el objetivo de terminar la actividad, estrategia también conocida como *plug and chug*. [3]

Con el objetivo de estimular una mayor atención a la dimensión conceptual de los contenidos en física, este proyecto, en actual desarrollo, explora el efecto de una innovación didáctica basada en el uso de textos de física divulgativos en la enseñanza escolar, y su efecto sobre las estrategias de aprendizaje. En esta primera parte, el estudio de diseño cuasi-experimental con pre y post test se realizó en dos cursos paralelos de física escolar en Chile, durante dos meses en modalidad de educación híbrida. El grupo control (GC) (nc = 20) y experimental (GE) (ne = 21) trabajaron los mismos contenidos de física moderna, pero mediante tratamientos distintos. La condición experimental incluyó la integración de textos de divulgación científica. El GC destinó sesiones de resolución de problemas, mientras el GE reemplazó las guías de problemas por pautas de reflexión grupal de las lecturas. Se administró el Inventario de Estrategias de Aprendizaje de R. Shmeck [4], que mide cuatro orientaciones hacia el procesamiento de información: Procesamiento Profundo (PP); Procesamiento Elaborativo (PE); Estudio Metódico (EM); y Retención de Hechos (RH). De acuerdo con la literatura, el procesamiento profundo y elaborativo de la información se relacionan con aprendizajes significativos [5].

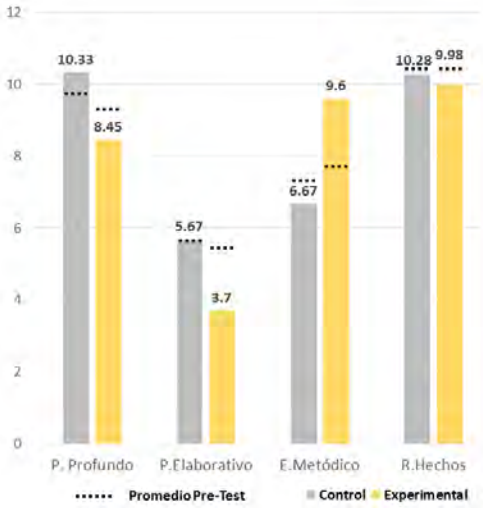

Figura 1. Promedio post test dimensiones de Estrategias de Aprendizaje grupos Control y Experimental.

Resultados preliminares de este estudio muestran que, mediante pruebas T de student se evidencia diferencias significativas en la Estudio Metódico (EM) entre los GC (M=6.67; D=2.07) y GE (M=9.6; D=1.69), $T_{(38)}$ 4.09, $p < .001$, $d = 1.5$ (ver Fig. 1). Sin embargo, el GC aumentó significativamente las dimensiones de Procesamiento Elaborativo (PE) y Profundo (PP), mientras el GE no evidenció cambios en estas variables. Además, no se encontraron diferencias en Retención de Hechos (RH). Se discutirán las posibles causas de estos resultados, junto a nuevas evidencias de la implementación de la metodología basada en libros científicos en cursos de ciencia escolar.

[1] T. Byun, G. Lee, *American Journal of Physics* **82**, 906 (2014).
[2] P. B. Khol, N. D. Finklestein, *Phys. Rev. ST Phys. Educ. Res.* **4**, 010111 (2008).
[3] E. Kim, S. Park, *American Journal of Physics* **70**, 759 (2002).
[4] R. Schmeck, *Individual differences and learning strategies in learning and study strategies*, Plenum Press (1988).
[5] J. Pulgar, I. Sanchez, *Formación Universitaria* **7**, 3 (2014).

Física Médica

Presentaciones orales

Lunes 11/07:

15:30-16:00 Emilio Soria. *Inteligencia artificial en física médica*

16:00-16:15 Joaquin López Herraiz. *Harmonization of Medical Images is Key for Robust and Generalizable Artificial Intelligence Models*

16:15-16:30 Clara Freijo Escudero. *Deep learning-based scatter correction of chest X-Rays*

16:30-16:45 Javier Pérez Curbelo. *Event selection with Neural Networks for Compton camera imaging of multi-energy radioactive sources*

16:45-17:00 Alberto Corbi Bellot. *Sensores inerciales, cronofiduciales, sueño y Alzheimer*

17:00-18:00 **Coffee Break**.

18:00-18:30 Alfonso López. *Radiofísica, una especialidad con futuro*

18:30-18:45 Rafael Garcia-Molina. *Simple yet reasonably accurate simulations of dose point kernels in liquid water by iodine radionuclides*

18:45-19:00 Alicia Reija Vecino. *Radiobiology experiments with laser induced radiation sources: exploring the UHDR regime*

19:00-19:30 Networking.

Martes 12/07:

15:30-16:00 M. C. Jimenez Ramos (USevilla/CNA). *Medical Applications with Ion Beams at Centro Nacional de Aceleradores*

16:00-16:15 Consuelo Guardiola (IMB-CNM-CSIC). *Experimental microdosimetry maps in proton therapy*

16:15-16:30 Isabel Abril Sánchez (UA). *Interaction of swift-ions and secondary electrons in liquid water: Bragg peaks and radial deposited dose*

16:30-16:45 Michael Seimetz (i3M-CSIC-UPV). *Scintillating fibre proton beam monitor for biomedical applications*

16:45-17:00 Nerea Encina Baranda (UCM). *Prompt-Gamma Correction in 124I PET Imaging*

17:00-17:30 **Café**.

17:30-17:45 Juan Peñas (USC). *A laser-driven proton source for medical radioisotope production*

17:45-18:00 Gabriela Llosá Llácer (IFIC, CSIC-U. Valencia). *MACACO Compton camera for medical applications*

18:00-18:15 Teresa Rodríguez (USevilla/CNA). *Experimental study of proton-induced cross sections of β^+ isotopes for PET range verification in particle therapy*

18:15-18:30 Francisco Camarena. *Aplicaciones neurológicas de los ultrasonidos*

Miércoles 13/07:

15:30-15:45 Jose Borreguero Morata. *Prepolarized Magnetic Resonance Imaging of soft and hard biological tissues in a low field scanner*

15:45–16:00 Teresa Guallart Naval. *Portable magnetic resonance imaging indoors, outdoors and at home*

16:00-16:15 Diana Andrés Bautista. *Thermal patterns generated by ultrasound holograms*

16:15-16:30 Irene Pi Martín. *Evaluation of lateral and axial resolution in photoacoustic tomography with linear US probe and pixel-based beamformers*

16:30-16:45 Mailyn Pérez-Liva. *Ultrafast-Ultrasound for PET radiotracer Arterial Input Function Quantification in the Rat Carotid Artery*

16:45-17:00 Andrew Coathup. *Phase-contrast x-ray imaging with a laser-driven x-ray source in air*

17:00-18:00 **Café**.

18:00-18:15 Rosa Maria Cibrian Ortiz de Anda. *Self organizing maps aplicados al análisis de los datos obtenidos mediante termografía infrarroja para el diagnóstico y seguimiento de la diabetes*

18:15-19:00 Asamblea.

Pósteres

- Miguel Martinez Albaladejo. *Commissioning and quality assurance of 192-Ir high-dose-rate brachytherapy sources based on micro-ionization chamber dosimetry*
- Vicente Puchades Puchades. *Método rápido de verificación de la estabilidad de un conjunto cámara pozo-electrómetro de uso clínico*
- Fernando Illescas Martinez. *Statistical analysis of the pre-treatment quality assurance results from a new TrueBeam linac*

Harmonization of Medical Images is Key for Robust and Generalizable Artificial Intelligence Models

Joaquin L. Herraiz[1,2,*], Nerea Encina-Baranda[1,2], Sara Gómez[2], Angel Nava[2], Juan Arrazola[2]

[1]*Nuclear Physics Groups and IPARCOS, Complutense University of Madrid, Spain.*
[2]*Health Research Institute of the Hospital Clinico San Carlos (IdISSC), Madrid, Spain.*

*e-mail: jlopezhe@ucm.es

Medical image analysis using artificial intelligence (AI) has the potential to improve the diagnosis, and prognosis of multiple diseases. However, in order to get the large number of cases required to train the AI tools, acquisitions from multiple sites obtained with a variety of devices and acquisitions protocols are needed. In this work, we studied the importance of considering the origin and characteristics of the medical images used for training AI models, and how mixing images from multiple sources may introduce important biases. For example, if not all pathologies considered in the model were acquired with the same equipment, the AI tool may learn to distinguish the type of scanner rather than the pathologies themselves. This has been clearly seen in the case of AI analysis of X-rays from COVID-19 patients, where many published results have been proved to be heavily biased.

There is a growing effort to harmonize acquisitions and medical imaging databases to reduce the dependence of the results of the AI models on the imaging devices and acquisition protocols. Many harmonization techniques have been proposed [1], such as the adaptation of the histogram of values, Cycle-GAN Neural Networks, and harmonization of the features extracted from the images (for instance with the COMBAT method initially proposed in genomic analysis [2]).

In this work, we evaluated the performance of these approaches, as well as additional ones based on information available in the DICOM header of the medical images, to make heterogeneous medical images more compatible, so that AI models trained with one device work better when applied to other ones (domain adaptation). 1430 Chest X-rays (CXR) of patients with pneumonia and healthy patients in DICOM format acquired in posteroanterior orientation with different scanners extracted from the anonymized Physionet database [3] were used. Large differences in image quality depending on the scanner were found (Fig 1A)

The AI model trained with one single scanner to classify CXR cases as healthy/pneumonia, failed when applied directly to cases of another scanner (50% success rate). After harmonization techniques were applied, a success rate of 73% was achieved.

In conclusion, AI methods are still not being widely used in clinical practice, in part due to their inability to generalize across a variety of imaging devices and acquisition protocols. Proper harmonization of medical images is therefore key for robust and generalizable artificial intelligence models.

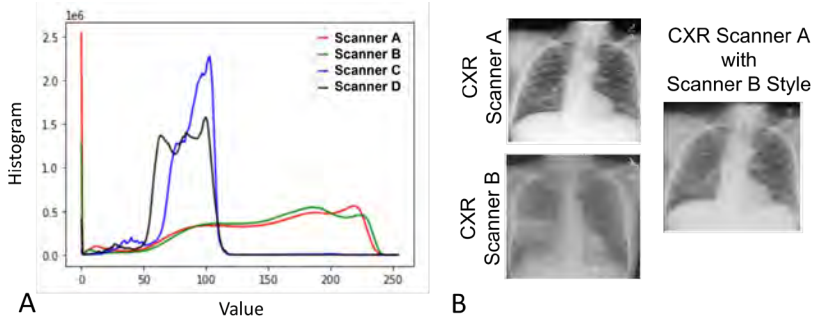

Figure 1. (A) Histogram of the initial values of CXRs from different scanners showing the large differences in the image properties. (B) Example of the use of a Cycle-GAN Neural Network to transfer the style of a CXR into another one.

[1] Yang Nan et al., Data harmonisation for information fusion in digital healthcare: A state-of-the-art systematic review, meta-analysis, and future research directions. *Information Fusion* **82**, 99-122 (2022).
[2] R. Da-Ano et al., Performance comparison of modified ComBat for monization of radiomic features for multicenter studies. *Scientific Reports* **10**, 10248 (2020).
[3] Physionet MIMIC-CXR Database, *https://physionet.org/content/mimic-cxr/2.0.0*

Acknowledgements: IdISSC Research grant 2021.

Deep Learning-Based Scatter Correction of Chest X-Rays

Clara Freijo[1,*], Joaquín L. Herraiz[1,2], Fernando Arias-Valcayo[1] ,Paula Ibáñez[1,2], Gabriela Moreno[1], Amaia Villa-Abaunza[1], José Manuel Udías[1,2]

[1]*Nuclear Physics Group, EMFTEL and IPARCOS, Faculty of Physical Sciences, University Complutense of Madrid, CEI Moncloa, 28040 Madrid, Spain.* [2]*Health Research Institute of the Hospital Clinico San Carlos (IdISSC), 28040 Madrid, Spain.*

*e-mail: cfreijo@ucm.es

Chest X-Ray image (CXR) is the first tool globally employed to detect cardiopulmonary diseases [1]. These acquisitions are affected by scattered photons, which reduce the image quality. The use of anti-scatter grids is the standard method to reduce the scatter contribution, but it is difficult to use with patients who cannot stand upright for the image acquisition. On the other hand, scatter can be estimated and corrected using Monte Carlo (MC) simulations, but it requires long computational times.

In this work, we propose two deep learning-based models to estimate and correct the scatter present in CXRs: a single-energy model, in which a U-Net-like neural network (NN) [2] is trained with pairs of scatter uncorrected (input) and scatter fraction (output) images; and a dual-energy model, in which an uncorrected scatter image acquired with a low-energy spectrum is also used as an additional input channel. The final scatter-corrected images are calculated by subtracting the scatter estimations from the uncorrected images. Input and output images for training, validation and testing are obtained from chest CTs affected by COVID-19 using MC simulations [3].

We compared the accuracy of both models for the scatter correction using several metrics: mean absolute percentage error (MAPE), structural similarity index measure (SSIM) and relative error. Besides, we studied how scatter correction improves the contrast in lung regions affected by COVID-19 calculating the percentage contrast improvement factor (PCIF).

Both models yield very accurate results in scatter correction (Figure 1), with a MAPE of 4.1 and 3.8%, a relative error of 2.0 and 1.9%, and SSIM of 0.9966 and 0.9970 for the single and dual-energy models, respectively. The dual-energy model shows a slightly better accuracy. However, the difference between the methods is not statistically significant. Additionally, results show that scatter correction improves the contrast value in 15 out of 17 cases by 5% on average. Again, the two proposed deep learning-based models reproduce accurately the expected results, being the average relative difference with respect to the ground truth 0.8% and 0.61%, respectively (Figure 2). Further studies are needed to determine if the same precision in scatter correction can be achieved when applying the models to real acquisitions.

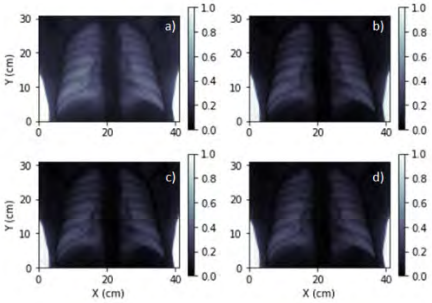

Figure 1: a) Uncorrected scatter image (input of the NN); b) scatter-corrected ground truth image; c) scatter correction estimation with the single energy model; d) scatter correction estimation with the dual energy model.

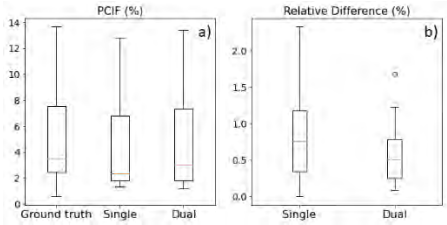

Figure 2: a) Percentage contrast improvement factor for ground truth images and single and dual model estimations; b) Relative difference in the percentage contrast improvement factor between ground truth and deep-learning-based estimations.

[1] E. Çalli et al., *Medical Image Analysis* **72**, 102 (2021).
[2] N. Ibtehaz and MS. Rahman, *Neural Networks* **121**, 74 (2020).
[3] P. Ibáñez et al., *Medical Physics* **48(12)**, 8089 (2021).

Física Médica
Oral

Event selection with Neural Networks for Compton camera imaging of multi-energy radioactive sources

J. Pérez Curbelo*, L. Barrientos, E. Muñoz, J. Roser, V. Sanz, G. Llosá

Instituto de Física Corpuscular (IFIC- CSIC/UV). C/ Catedrático Beltrán, 2. E-46980, Paterna, Valencia, Spain.

*e-mail: japercur@ific.uv.es

The interest in the application of Compton camera imaging to medical physics is increasing worldwide. The IRIS group at IFIC-Valencia (http://ific.uv.es/iris) has developed a Compton camera prototype consisting of three detector planes of $LaBr_3$ crystals coupled to silicon photomultiplier arrays, which has been tested under several irradiation conditions [1,2]. The selection of signal events and background reduction is one of the main issues in order to obtain high quality images. Research has been conducted in this sense employing neural networks (NNs) for event classification [3]. In this work, images were obtained employing experimental data from an array of 37 ^{22}Na sources taken with the second prototype, MACACO II [4], and NNs were used to select useful events prior to image reconstruction.

The NNs were trained with simulated data, and then applied both to simulated and experimental data. The experimental setup consisted in a two-layer system, with 50 mm distance between the planes. The ^{22}Na array was placed at 70 mm from the first plane. The system was simulated using GATE v8.2, reproducing the detector geometry and distances, but considering a squared array of 9x9 ^{22}Na sources. The simulation output data were divided into three classes according to the event type: Type 0 was set to good coincidence events generated by 1275 keV photons interacting in the two detectors, Type 1 was set to those generated by 511 keV and Type 2 was set to random, backscattering and background events. The image in ideal conditions can be obtained using only events from Type 0. The three files were used to train two NNs for event classification. One NN was trained using events with deposited energy higher than 511 keV (NN1) and the other one with deposited energy lower than 511 keV (NN2). NN1 and NN2 had 8 and 3 fully connected layers, respectively. In both NNs ReLu activation function was used for entrance and hidden layers, while sofmax was used in the output layer. Hyperparameters such as optimizer, learning rate, number of epochs and batch size, were selected from a tuning performed by using the platform Weights & Biases. The NNs were successful in eliminating randoms and backscattering events on simulation data, and in selecting events up to the maximun energy deposition allowed for Compton scattered 1275 keV photons in the first plane (760 keV).

The trained NN was applied to real data taken with the ^{22}Na array and the output data classified as good events (1275 keV photons) were used to reconstruct the position of the 37 sources in the array by using a Maximum Likelihood Expectation Maximization algorithm [5]. This method was compared to event selection with an energy cut on 600 keV to reject 511 keV photons. As shown in Fig 1., the use of NNs for event classification improves the image quality, allowing a larger number of sources to be identified.

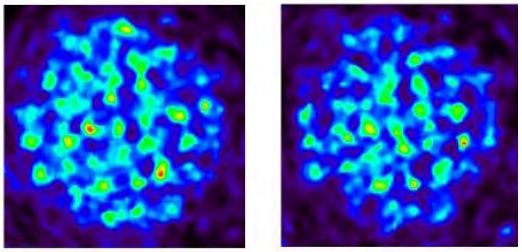

a b

Figure 1. Images of experimental data: (a) NNs output data and (b) data with 600 keV energy cut.

[1] G. Llosá et al., *Therapy. Front. Oncol.* **6**, 14 (2016).
[2] A. Ros et al., *Phys. Med. Biol.* **65**, 245027 (2020).
[3] E. Muñoz et al., *Scientific Reports* **11**, 9325 (2021).
[4] L. Barrientos et al., *Nuclear Inst. and Methods in Physics Research A* **1014**, 165702 (2021).
[5] J. Roser et al., *Phys. Med. Biol.* **65**, 145005 (2020).

Acknowledgements: This work has received funding from the Ministerio de Ciencia e Innovación (FPA2017-85611-R, PID2019-110657RB-I00).

Sensores inerciales, cronofiduciales, sueño y Alzheimer

Alberto Corbi*, Daniel Burgos
Instituto de Investigación, Innovación y Tecnología Educativas (UNIR iTED), Universidad Internacional de La Rioja (UNIR), Av. de la Paz, 137, Logroño, España.
*e-mail: alberto.corbi@unir.net

La enfermedad de Alzheimer (AD) es un proceso neurodegenerativo causado por la acumulación de β-amiloides y proteínas-τ en el cerebro. En un individuo sano, estas sustancias son producidas durante el día de manera natural por el propio organismo como mecanismo de defensa, pero son recicladas durante el sueño profundo, restaurando el equilibrio. Sin embargo, en un enfermo de AD, el *tándem* $\beta + \tau$ acaba formando condensados de manera inadvertida, colapsando eventualmente las sinapsis.

Sin embargo, la ejecución de ensayos clínicos con (potenciales) pacientes de AD es complicada por la naturaleza agresiva asociada a los individuos afectados por esta enfermedad. Las razones de tipo ético y de respeto a la intimidad son también un factor limitante en este campo de investigación. Por esta razón, en [1] se ha diseñado un sistema que permite monitorizar el sueño de personas con AD de manera no intrusiva. La implementación está basada en el uso de sensores inerciales para el seguimiento de los movimientos del enfermo durante la noche. El hardware subyacente tiene forma de cómoda pulsera, la cual registra aceleraciones de manera continua (durante casi un mes) y los datos se almacenan (valores *empaquetados* de 32-bit) en un SSD a una frecuencia de 50 Hz. La monitorización se realiza sin necesidad de conexión a la red eléctrica o a Internet (reforzando la premisa de respeto a la privacidad). Seguidamente, se estiman los periodos de sueño mediante el algoritmo descrito en [2].

En el transcurso de la investigación se ha supervisado el sueño de 3 grupos de participantes según su estado clínico de avance de la enfermedad (sano, AD-leve y severo) durante varias noches. A continuación, aplicando un método de máxima verosimilitud, ha sido posible clasificar con gran precisión el estado de deterioro cognitivo de estos pacientes de manera no supervisada. Para destilar los periodos de sueño de los de vigilia, se usa un filtro de paso bajo consistente en una ventana deslizante (con umbral k) que identifica eventos t de quietud $QS(t)$ de un 1 s y los etiqueta mediante la expresión:

$$QS(t) = 1 \qquad \forall \quad k \quad \longrightarrow \quad k^2 > (f-1)^{-1} \times \sum_{i=1}^{f} (a_{x,y,z} - \overline{a_{x,y,z}})^2 \ , \quad \text{de lo contrario, } QS(t) = 0 \ .$$

Posteriormente se suman todos los sucesos con $QS(t) = 1$. Sólo los bloques i con duración superior a 10 min son etiquetados como segmentos de *sueño profundo* mediante $DS_i = [\text{len}(QS(t) = 1) > 600 \text{ s}]$, la cual se corresponde con la fórmula de Iverson (1 o 0 si es verdadera o falsa). A continuación, se calcula la *transformada wavelet* a partir del agregado de todos los DS_i. Este paso devuelve varios *escalogramas*, las cuales representan una suerte de sistema de *fiduciales temporales* (*cronofiduciales*). Por último, cada escalograma pasa por una red neuronal convolucional pre-entrenada y es clasificado según el estado de avance de la enfermedad. Los resultados reportan una tasa de éxito del 85 %.

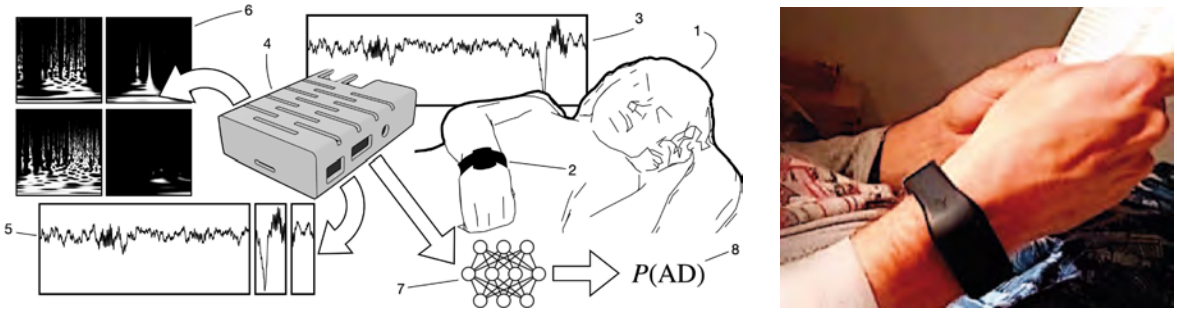

Figure 2. Participante (1) con sensor inercial (2) que mide aceleraciones de manera continua (3). El flujo es analizado por una micro-computadora (4) que destila periodos de sueño de vigilia (5) y a continuación deriva escalogramas. Por último, una red neuronal pre-entrenada (7) es aplicada y se obtiene probabilidad de AD severo, leve o de salud (8).

[1] A. Corbi and D. Burgos, Connection between sleeping patterns and cognitive deterioration in women with Alzheimer's disease, *Sleep & Breathing* **26**, 361 (2022).
[2] M. Borazio, E. Berlin, N. Kücükyildiz, P. M. Scholl and K. van Laerhoven, *Towards a Benchmark for Wearable Sleep Analysis with Inertial Wrist-worn Sensing Units*, ICHI, Verona, Italy, IEEE Press (2014).

Agradecimientos: Los autores desean hacer llegar su agradecimientos a todos los participantes en este estudio, sus familias y centros asistenciales colaboradores (La Molineta, Lares, DomusVi y La Saleta).

Simple yet reasonably accurate simulations of dose point kernels in liquid water by iodine radionuclides

Mario Mompean-Herrero, Pablo de Vera, **Rafael Garcia-Molina***

Departamento de Física, Universidad de Murcia, Murcia, Spain.

*e-mail: rgm@um.es

Nowadays, many advances in medicine come hand in hand with new developments in physics. Nuclear medicine is responsible for trying to diagnose and cure diseases using radioactive isotopes, unstable atomic nuclei that emit energy due to various processes, such as β^- decays or discrete Auger electron emissions. These ejected electrons carry the excess energy of the excited nucleus and deliver energy to matter as they travel through it interacting with its atoms and molecules, so that in the end a given spatial distribution of dose is produced around the emission point. Depending on the type of process that triggers the electron release, determined by the nature of each radioisotope, the energy emitted and its distribution around the emission point may change. If we know how the energy spreads in the medium, depending on each isotope, we can choose which one will be more convenient to use in a particular clinical situation.

For example, some techniques such as radio-immunotherapy introduce different radioactive isotopes bound to antibodies selectively into the nuclei of cancer cells to cause their death due to the emission of low energy electrons, which may confine the dose within the nuclei of the ill cells. The problem here is that it is not trivial to accurately know how the dose is distributed, especially at the small nanometer scales of the sensitive biomolecules such as DNA.

In this work we have developed a Monte Carlo simulation code that follows in detail the motion through liquid water of the electrons emitted by radioactive iodine nuclides (either ^{131}I or ^{125}I, which emit through different deexcitation mechanisms). The elastic collisions of the electrons are taken into account by a screened Rutherford cross section [1,2], whereas the inelastic collisions, leading to the energy loss of the electrons, is accounted for by empirical approximate stopping power formulas for high and low energy electrons [1,3]. The extension of such approach to take into account the ejection of secondary electrons is explored, trying to keep the simplicity and speed of the simulation code by appropriate parametrisation of more detailed energy-loss models [4].

Despite the simplicity of the simulation code, the obtained dose point kernels for electrons emitted by radioactive iodine isotopes show promising agreement with available experimental data [5], as well as other simulations [6] and theoretical calculations [7].

[1] D. C. Joy, *Scanning Microscopy* **5**, 329 (1991).
[2] M. Dapor, *Transport of Energetic Electrons in Solids* 3rd ed., Springer Tracts in Modern Physics vol. 271, Cham-Switzerland (2020).
[3] T. Nguyen-Truong, *Ultramicroscopy* **149**, 26 (2015).
[4] P. de Vera, I. Abril, R. Garcia-Molina, *Physical Chemistry Chemical Physics* **23**, 5079 (2021).
[5] S. Okigaki, A. Ito, I. Uchida, T. Tomaru (1994). Calculation of dose point kernels for five radionuclides used in radio-immunotherapy. National Laboratory for high energy physics, 94, 34 (1994).
[6] C. Bousis, D. Emfietzoglou, P. Hadjidoukas, H. Nikjoo,A. Pathak, *Nuclear Instruments and Methods in Physics Research, Section B: Beam Interactions with Materials and Atoms* **269**, 1650 (2011).
[7] N. Falzone, Q. Lee, J. M. Fernández-Varea, C. Kartsonaki, A. E. Stuchbery, T. Kibédi, K. A. Vallis, *Physics in Medicine and Biology* **62**, 2239 (2017).

Acknowledgements: We acknowledge financial support by the European Union's Horizon 2020 Research and Innovation programme under the Marie Sklodowska-Curie grant agreement no. 840752 *NanoEnHanCeMent*, the Spanish Ministerio de Economía y Competitividad and the European Regional Development Fund (Projects no. PGC2018-096788-B-I00), the Fundación Séneca (Project no. 19907/GERM/15) and the Conselleria d'Educació, Investigació, Cultura i Esport de la Generalitat Valenciana (Project no. AICO/2019/070).

Radiobiology experiments with laser induced radiation sources: exploring the UHDR regime

A. Reija[1,2*], R. Contreras-Martinez[2,4], A. Coathup[2], A. Alejo[2], A. Bembibre[2], J. Benlliure[2], J. Peñas[2], M.E. Aguado-Barrera[3], A. Vega-Gliemmo[3], C. Ruiz[4], M. Seimetz[1]

[1]*Instituto de Instrumentación para Imagen Molecular (I3M), CSIC - Universitat Politècnica de València, Spain.* [2]*Instituto Galego de Física de Altas Enerxías (IGFAE), Universidade de Santiago de Compostela, Spain.* [3] *Fundacion Pública Galega de Medicina Xenómica, Instituto de Investigación Sanitaria de Santiago de Compostela, Spain.* [4]*Instituto de Física Fundamental y Matemáticas, Universidad de Salamanca, Spain.*

*e-mail: alicia.reija@rai.usc.es

Since the development of the Chirped Pulse Amplification (CPA) technique, the generation of ultra-short and ultra-intense laser pulses and its applications in particle acceleration has become a very active field of research. When a laser pulse of these characteristics impinges on a solid target, different particle acceleration mechanisms can take place depending on several parameters such as the laser intensity on focus, its angle of incidence or the target thickness [1]. This results in the possibility of generating pulsed radiation sources such as x-rays or polyenergetic proton beams for preclinical research. In addition, the particle acceleration occurs due to the generation of electric fields of the order of TV/m within a few microns, so laser-driven acceleration gives rise to compact alternatives to conventional radiofrequency accelerators. These laser-induced radiation sources are capable of producing relevant doses in short periods of time, which makes them suitable for radiobiological research related to Ultra High Dose Rate therapy techniques (UHDR/FLASH) [2].

The Laser Laboratory for Acceleration and Applications (L2A2) of the University of Santiago de Compostela (USC) is equipped with two beamlines, both of them delivering 35 fs laser pulses. With the low energy line (1 mJ per pulse, 1 kHz repetition rate) impinging on a copper target, we have developed a stabilized, table-top x-ray source for *in vitro* irradiation in radiobiological experiments. The dose deposition has been measured with radiochromic films, and we report a peak dose rate of 10^9 Gy/s. To test its suitability for systematic experiments, we have irradiated a human alveolar basal epithelial adenocarcinoma cell line at several exposure times and dose values. DNA double-strand breaks (γ-H2AX *foci*) and DNA damage response (53BP1 *foci*) were evaluated by immunofluorescence, as shown in Fig. 1. Both the preparation of cell cultures and the analysis of post-irradiation effects were performed at the FPGMX and the Instituto De Investigación Sanitaria of Santiago de Compostela.

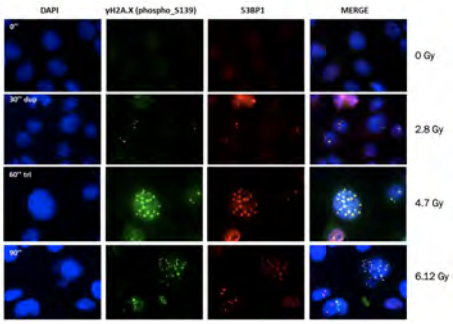

Figure 1. 24h post-irradiation DNA double-strand breaks analysed under microscope, at four dose and exposure time values.

At the same time, we have set up a proton source using the high energy output of the laser beamline, which delivers 1.2 J pulses at a 10 Hz repetition rate. Several detectors have been developed and installed to fully characterize the proton spectrum. In the Institute for Instrumentation in Molecular Imaging (I3M), we have designed and built an experimental setup for the irradiation of *in vitro* cell cultures, which comprises a magnetic energy selector that allows for the separation of the broad energy proton spectrum into monoenergetic beamlets with energies up to a few MeV [3]. We expect a proton fluence of 10^6 cm^{-2} over the surface of the cell culture dish, and a dose deposition ranging from 18 to 65 mGy per shot, depending on the chosen proton energy beamlet.

[1] A. Macchi, *A superintense laser-plasma interaction theory primer*, Springer (2012).
[2] P. Chaudhary *et al*, *Frontiers in Physics* **9** (2022).
[3] A. Torralba *et al*, *Quantum Beam Science* **6**(1), 10 (2022).

Acknowledgements: Project RTI-2018-101578-B-C22 financed by MCIN/AEI /10.13039/501100011033 and FEDER "Una manera de hacer Europa". Project AICO/2020/207 financed by Generalitat Valenciana.

Medical Applications with Ion Beams at Centro Nacional de Aceleradores

M. C. Jiménez Ramos[1,2]

[1]*CNA (U. Sevilla, J. Andalucía, CSIC), Av. Thomas A. Edison 7, 41092 Sevilla, Spain.*
[2]*Departamento de Física Aplicada II, Universidad de Sevilla, E-41012 Sevilla, Spain.*

e-mail: mcyjr@us.es

The National Accelerator Centre (CNA) is a Singular Scientific and Technical Facility in which there are currently 4 particle accelerators, a Co-60 irradiator, a Positron Emission Tomography (PET) system combined with Computerised Axial Tomography (TAC) for humans and a micro-PET for animals. This talk will show examples of some of the research in the field of Medical Physics carried out in two of the Centre's accelerators, specifically the Pelletron 3MV Tandem accelerator, model 9SDH-2, from National Electrostatics Corporation (NEC) and the Cyclone 18/9 cyclotron manufactured by Ion Beam Applications (IBA, Belgium), capable of accelerating protons and deuterons to 18 and 9 MeV, respectively. The latter has eight irradiation ports, seven of which are dedicated to the production of the positron-emitting radioisotopes most used in the medical imaging modality PET. The other output of this cyclotron is an external line that transports the beam to an adjacent bunker, where physics experiments in several areas can be performed.

Some of the noteworthy research in the field of Medical Physics in these two facilities are:

- Preparation of a radiobiology beam line at the 18 MeV proton cyclotron facility at CNA [1], which has given rise to the PhD Thesis of Anna Baratto-Roldán in 2021. Collaboration with the Andalusian Centre for Molecular Biology and Regenerative Medicine (CABIMER).
- Measurement of the reaction cross sections of β+ emitters of interest in proton therapy with the 18 MeV cyclotron [2], which is part of the Thesis work of Teresa Rodríguez-González.
- Test and calibration of a Compton camera for treatment monitoring in proton therapy with high energy photons [3]. Collaboration with the Image Reconstruction, Instrumentation and Simulations for Medical Imaging Applications (IRIS) Group of the Institute of Corpuscular Physics (IFIC).
- Testing and calibration of detectors for the characterisation of proton beams accelerating by ultra-intense laser pulses, aimed at the study of radiobiological effects of ultra-short pulses on living cells [4]. Collaboration with the Laser Acceleration of Ions and Applications Group of the Institute of Instrumentation for Molecular Imaging (I3M).
- Development of real-time dosimeter based on micro-opto-electromechanical systems [5] (PCT application number PCT/EP2022/054706). Collaboration with the National Microelectronics Centre of Barcelona (CNM-IMB) and the French National Centre for Scientific Research (CNRS).
- Feasibility of iTED detectors for PET range verification with the 18 MeV cyclotron [6]. Collaboration with the IFIC Gamma and Neutron Spectroscopy Group.
- Characterisation of new 3D-detectors for microdosimetry in hadrontherapy [7,8]. Collaboration with the CNM-IMB and the University of Santiago de Compostela.

[1] A. Baratto-Roldán et al., *Physica Medica* **74**, 19 (2020).
[2] T. Rodríguez-González et al., *Radiation Physics and Chemistry* **190**, 109759 (2022).
[3] A. Ros García et al., *Radiation Physics and Chemistry* **190**, 109759 (2022).
[4] M. Seimetz et al., *IEEE Transactions on Nuclear Science* **62**, 3216 (2015).
[5] C. Guardiola et al., *Scientific Reports* **11**, 10414 (2021).
[6] J. Balibrea-Correa et al., *submitted to EPJ-Plus*.
[7] D. Bachiller-Perea et al., *IEEE Transactions on Instrumentation and Measurement* **6**, 9339896 (2021).
[8] C. Guardiola et al., *Physics in Medicine and Biology* **66**, 114001 (2021).

Acknowledgements: M. C. Jiménez-Ramos acknowledges the support to this work through a VI PPIT-US contract.

Experimental microdosimetry maps in proton therapy

C. Guardiola[1,*], Diana Bachiller-Perea[2], Celeste Fleta[1], Ludovic De Marzi[3,4], Faustino Gómez[5]

[1]*Centro Nacional de Microelectrónica (IMB-CNM, CSIC), Bellaterra, 08193, Spain.* [2]*UIJCLab, CNRS/IN2P3, Université Paris Cité, Université Paris-Saclay, 91405 Orsay, France.* [3]*Institut Curie, PSL Research University, Centre de protonthérapie d'Orsay, Orsay 91898, France.* [4]*Institut Curie, University Paris Saclay, PSL Research University, Inserm U 1021-CNRS UMR 3347, Orsay, France.* [5]*Dep. de Física de Partículas, Universidad de Santiago de Compostela, 15782, Spain.*

*e-mail: consuelo.guardiola@imb-cnm.csic.es

Proton therapy achieves very high dose conformity around the target, allowing a better protection of the organs at risk [1]. The determination of the relative biological effectiveness (RBE) depends, i.a., on the lineal energy transfer (LET). Besides, there is a rising interest in the medical-physics community in placing the enhanced LET of the beam within the tumour or removing it from the most sensitive normal structures around [2]. To face this challenge, we customized an array of silicon 3D-cylindrical microdetectors specifically designed for this purpose [3-5]. The sensor consists of 11×11 independent microdetectors (covering 2.2 mm × 2.2 mm) that are based on a new diode architecture with 3D-cylindrical electrodes (25 µm diameter, 20 µm depth, and 200 µm pitch).

A pristine peak of 100 MeV protons was used in the Orsay Proton Therapy Centre (CPO, France) with clinical fluence rates (~ 10^8 $cm^{-2}\cdot s^{-1}$). The microdosimetry spectra were obtained at different positions of the Bragg curve by using a water-equivalent phantom (Figure 1). Microdosimetry maps showing the variation of the lineal energy with depth in two dimensions were obtained in situ during irradiation at clinical fluence rates for the first time with a spatial resolution of 200 µm, the highest achieved so far (Figure 2). The experimental results were crosschecked with Monte Carlo simulations and also compared to literature results. We present here the first 2D microdosimetry maps obtained at clinical fluence rates. The clinical implementation of these measurements would allow for the RBE optimization of proton therapy treatments. This work consolidates the capability of the new 3D-cylindrical architecture as microdosimeters as well as commissioning under clinical conditions.

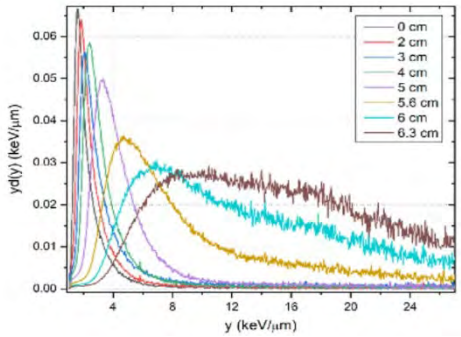

Figure 1. Experimental microdosimetric spectra obtained with the microdetectors at the different solid-water depths.

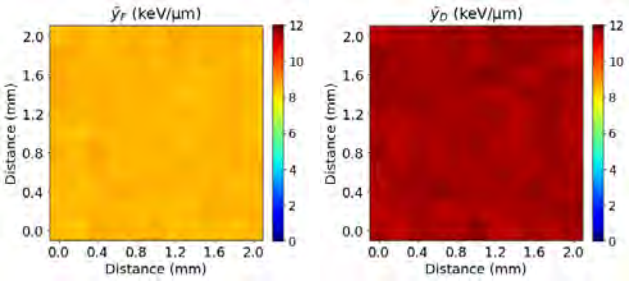

(8.6 ± 0.1) keV·µm^{-1} (11.60 ± 0.13) keV·µm^{-1}

Figure 2. Experimental frequency-mean lineal energy (left), and dose-averaged lineal energy (right) for each of the 11×11 microdetectors for a representative SP34 solid-water thickness, namely 6.3 cm. Average values of both and for each array are depicted at the bottom of each figure.

[1] Schardt D., Elsässer T., Schulz-Ertner, D., *Reviews of Modern Physics* **82**, 383 (2010).
[2] Bassler N. et al., *Acta Oncol.* **49**(7), 1170 (2010).
[3] Guardiola C. et al., *Applied Physics Letters* **107**, 023505 (2015).
[4] Prieto-Pena J. et al., *IEEE Transactions on Nuclear Science* **66**(7), 1840 (2019).

Interaction of swift-ions and secondary electrons in liquid water: Bragg peaks and radial deposited dose

Isabel Abril[1,*], Pablo de Vera[2], Maurizio Dapor[3], Simone Taioli[3], Paolo E. Trevisanutto[4], Stefano Simonucci[5], Rafael Garcia-Molina[2]

[1]*Departament de Física Aplicada, Universitat d'Alacant, E-03080 Alacant, Spain.* [2]*Departamento de Física, Universidad de Murcia, E-30100 Murcia, Spain.* [3]*European Centre for Theoretical Studies in Nuclear Physics and Related Areas (ECT*), Bruno Kessler Foundation, Trento, Italy.* [4]*Dipartimento di Ingegneria, Unità di Ricerca di Fisica non lineare e Modelli matematici, Università Campus Bio-Medico, Via Alvaro del Portillo 21, Roma, 00154 Italy.*
[5]*Division of Physics, School of Science and Technology, Università di Camerino and INFN Sezione di Perugia, Italy.*

*e-mail: ias@ua.es

A current advanced technique to treat cancer is hadrontherapy, based on the interaction of swift ion beams with living tissue, whose purpose is the destruction of the malignant tumour cells producing minimal effects on the surrounding healthy tissue [1]. To improve the precision of this technique it is necessary to realistically determine the physical processes behind this therapy, which take place at very different space, energy and time scales [2]. Liquid water makes up around 75–80% of the mass of soft human tissues, therefore it represents an appropriate surrogate of living tissue in the study of radiation dosimetry [3].

Ion beams present a very well-defined penetration range in matter, with a characteristic depth-dose curve, the Bragg peak, where a large fraction of their energy is deposited towards the end of their trajectories. Due to this feature, deep-seated tumours close to sensitive organs can be treated without inflicting much damage to the healthy surrounding areas. However, the precise location of the Bragg peak for beams of different energies is very sensitive to the average energy loss per unit path length of ions in tissue. The spatial distribution of energy deposition is evaluated by the simulation code SEICS [4], which includes the main interaction phenomena between the projectile and the target constituents, such as the electronic stopping force due to energy loss to target electronic excitations and ionisations, the elastic scattering with the target nuclei, the dynamical changes in projectile charge-state due to electronic capture and loss processes, and the nuclear fragmentation reactions, providing depth-dose curves in excellent agreement with available experimental data [5].

In order to quantify the biodamage produced in the target, it is essential to know the spatial and energy distribution of the secondary electrons generated by the projectile [6,7], as well as the subsequent low-energy electron cascade, which can propagate appreciable amounts of energy relatively far away from the ion's path. For this purpose, we use the event-by-event Monte Carlo code SEED [8], which provides a detailed description of the elastic and inelastic processes of low-energy electrons in liquid water. The electron elastic cross-sections are calculated from first principles methods based on the solution of the Dirac equation [9]. Concerning electronic interactions, the dielectric formalism together with a realistic model to describe the excitation spectrum of liquid water [9] allows to calculate the electron energy and angular cross-sections [6,7]. As a result of this simulation the radial dose of the deposited energy in liquid water can be obtained around the ion path, and it is possible to evaluate the influence of different physical events [9].

[1] D. Schardt, T. Elsasser, D. Schulz-Ertner, *Rev. Mod. Phys.* **82**, 383 (2010).
[2] A. V. Solov'yov(ed.), *Nanoscale Insights into Ion-Beam Cancer Therapy*, Springer Int. (2017).
[3] H. Nikjoo, S. Uehara, D. Emfietzoglou, *Interaction of Radiation with Matter*, CRC Press (2012).
[4] R. Garcia-Molina, I. Abril, S. Heredia-Avalos, I. Kyriakou, D. Emfietzoglou, *Phys. Med. Biol.* **56**, 6475 (2011).
[5] P. de Vera, I. Abril, R. Garcia-Molina, *Radiat. Res.* **190**, 282 (2018).
[6] P. de Vera, R. Garcia-Molina, I. Abril, A.V. Solov'yov, *Phys. Rev. Lett.* **110**, 148104 (2013).
[7] P. de Vera, R. Garcia-Molina, I. Abril, *Phys. Rev. Lett.* **114**, 018101 (2015).
[8] M. Dapor, I. Abril, P. de Vera, R. Garcia-Molina, *Phys. Rev. B* **96**, 064113(2017).
[9] S. Taioli, P. E. Trevisanutto, P. de Vera, S. Simonucci, I. Abril, R. Garcia-Molina, M. Dapor, *J. Phys. Chem. Lett.* **12**, 487 (2021)

Acknowledgements: We acknowledge funding from the European Union's Horizon 2020 Research and Innovation programme (Marie Sklodowska-Curie grant agreement no. 840752), the Spanish Ministerio de Economía y Competitividad and the European Regional Development Fund (Project no. PGC2018- 096788-B-I00), the Fundación Séneca (Project no. 19907/GERM/15) and the Conselleria d'Educació, Investigació, Cultura i Esport de la Generalitat Valenciana (Project no. AICO/ 2019/070).

Scintillating fibre proton beam monitor for biomedical applications

A. Sánchez Paños[1], J. Juan[1], M.C. Jiménez-Ramos[2,3], J. García López[2,4], **M. Seimetz**[1,*]

[1]*Instituto de Instrumentación para Imagen Molecular (i3M), CSIC-Universitat Politècnica de València, Valencia, Spain.*
[2]*Centro Nacional de Aceleradores (CNA), Universidad de Sevilla-CSIC-Junta de Andalucía, Sevilla, Spain.*
[3]*Departamento de Física Aplicada II, Universidad de Sevilla, Sevilla, Spain.*
[4]*Departamento de Física Atómica, Molecular y Nuclear, Universidad de Sevilla, Sevilla, Spain.*

*e-mail: mseimetz@i3m.upv.es

The importance of proton therapy for cancer treatment is rapidly increasing. At the same time, preclinical research on the effects of high-LET radiation in living cells and organisms is carried out at many accelerator facilities. A precise measurement of the particle flux is a basic requirement for such applications. This is ideally provided in real-time, at high spatial and timing resolution, and with negligible interference with the proton beam.

We report on a design study and laboratory tests for a multi-channel proton (or ion) beam monitor based on scintillating fibres. A previous model developed by our group using fibres with 500 µm square cross section coupled to photomultipliers showed high detection efficiencies, high-rate capacity, and a timing resolution below 1 ns in beam tests at the Heidelberg Ion Therapy Center (HIT) [1]. At present, our aim is to expand the sensitive area up to 200×200 mm^2 in combination with an intrinsic, spatial resolution of 250-500 µm according to the lateral size of the fibres. Each fibre is coupled to a SiPM. We are currently testing various models of photosensors to find an optimum combination of the sensitive area (about 1 mm^2) and micropixel dimensions for a wide dynamic range. Single-particle pulses from α and β sources have been visualized on a fast oscilloscope. For the digital readout of multiple channels a solution based on ASICs is envisaged; experiments with a TOFPET2 system are ongoing.

Another central aspect of the detector design is the mechanical support and mounting of tens to hundreds of fibres forming a detection plane. All the fibres must be precisely aligned to avoid gaps which would compromise the detection efficiency. We are exploring free-standing options without introducing additional material in the particle path. The lateral scattering caused by such a monolayer is particularly relevant for clinical applications with pencil beams. Some of the components used in our tests are shown in Figure 1.

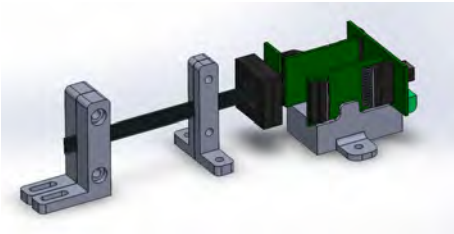

Figure 1. Set of 0.5 mm fibres connected to a 8×8 array of 1.3 mm SiPMs with ASIC readout (schematic view).

We envisage two fields of application with somewhat different configurations of such a SciFi detector. On the one hand, the beam monitor may allow for precise timing with therapeutic proton and ion beams of several tens or hundreds of MeV when used in coincidence with secondary detectors, *e.g.*, for background suppression in particle range measurements based on prompt-gamma emission [2]. On the other hand, fast scintillators can be calibrated for short, ultra-intense particle bunches with an overall light output resulting from numerous scintillation events [3]. This option is potentially interesting for laser-ion acceleration and novel radiotherapy modalities at ultra-high dose rates.

[1] P. Magalhaes Martins, R. Dal Bello, M. Seimetz, G. Hermann, Th. Kihm and J. Seco, *Frontiers in Physics* **8**, 169 (2020).
[2] R. Dal Bello, P. Magalhaes Martins, St. Brons, G. Hermann, Th. Kihm, M. Seimetz and J. Seco, *Phys. Med. Biol.* **65**, 095010 (2020).
[3] M. Seimetz *et al.*, *Trans. Nucl. Sci.* **62**, 3216 (2015).

Acknowledgements: Project LINKA20351 financed by CSIC within the i-LINK+2020 program. Research co-financed by the European Union through Programa Operativo del Fondo Europeo de Desarrollo Regional (FEDER) of the Comunitat Valenciana, IDIFEDER/2021/004.

Prompt-Gamma Correction in ^{124}I PET Imaging

Nerea Encina-Baranda[1], Alejandro Lopez-Montes[1,2], Joaquin L. Herraiz[1,3]

[1] *Nuclear Physics Groups and IPARCOS, Complutense University of Madrid, Spain.*
[2] *Department of Biomedical Engineering, Johns Hopkins University, Baltimore, MD, USA.*
[3] *Health Research Institute of the Hospital Clinico San Carlos (IdISSC), Madrid, Spain.*

*e-mail: nencina@ucm.es

Positron Emission Tomography (PET) is a biomedical imaging technique that provides quantitative information of the biodistribution of a radiolabeled molecule administered to an animal or patient. One of the most promising new cancer treatment approaches is radioimmunotherapy that combines target-specific agents such as monoclonal antibodies (mAb) with radionuclides for enhanced therapeutic effects and imaging. The slow pharmacokinetics [1] of mAb require the use of radionuclides with long half-lives for PET imaging. However, most of these radionuclides such as ^{124}I, ^{52}Mn, ^{76}Br are non-pure positron emitters, and they may emit additional prompt-gammas in each β^+ decay. If the energy of these additional gammas is within or close to the PET energy window (centered at 511keV), they can be detected and create spurious coincidences. These coincidences produce a significant background which reduces the contrast of the reconstructed images.

In this work, we propose using a fast Monte Carlo Method to estimate and correct the spurious background due to the prompt gammas when using non-pure positron emitters in PET, more specifically ^{124}I. Scatter and the spurious background were estimated using MC-GPU PET (fast Monte Carlo simulator for PET based on GPU) using the workflow shown in Figure 2.b. The iterative process can be repeated until convergence. Typically 2 or 3 iterations are enough.

We used a OSEM-3D algorithm implemented in CUDA using 60 updates for the reconstructions. Randoms correction were performed using delayed coincidences. The attenuation correction was performed based on a 511 keV μ-map obtained from a CT with the PET, acquired with the Inveon PET/CT scanner. Four mice were injected with an average activity of 270 μCi of ^{124}I bound to a monoclonal antibody and 167 μCi of ^{68}Ga-PSMA, with branching ratios of 0.23 and 0.89, respectively, with 350 - 650 keV energy window.

The results in Figure 2.c shows the feasibility of this method to correct the scatter and the spurious background with MC-GPU PET estimation. The proposed approach is being extended to other non-pure beta emitters radionuclides.

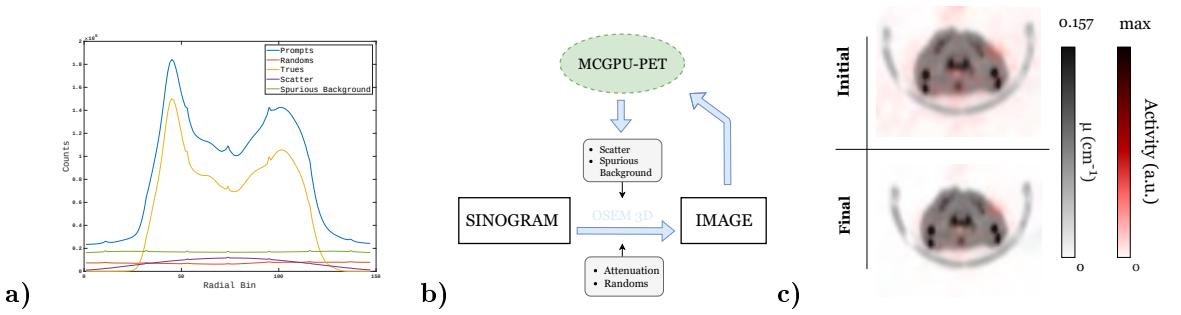

Figure 1: **a)** Radial Profiles obtained from a ^{124}I acquisition. The tails of the profile show the presence of a background due to scatter, randoms and prompt gammas (spurious background), **b)** *Workflow*, **c)** Initial image (corrected by attenuation and randoms) and final corrected image by scatter and spurious coincidences with MCGPU-PET with 2 iterations.

[1] Conti, M., Eriksson, L., *EJNMMI Physics* **3**, 8 (2016).

Acknowledgements: MICINN Proyecto Retos RTI2018-095800-A-I00, Siemens Healthineers (Proyecto Art.83 UCM)

Física Médica
Oral

A laser-driven proton source for medical radioisotope production

J. Peñas[1,*], A. Alejo[1], A. Bembibre[1], D. Cortina-Gil[1], C. Ruiz[2], M. Seimetz[3], J. Benlliure[1]

[1]*Instituto Galego de Física das Altas Enerxías (IGFAE), Universidade de Santiago de Compostela, Santiago de Compostela, Spain.* [2]*Instituto Universitario de Física Fundamental y Matemáticas, Universidad de Salamanca, Salamanca, Spain.* [3]*Instituto de Instrumentación para Imagen Molecular (I3M), CSIC-Universitat Politècnica de València, Valencia, Spain.*

*e-mail: juan.penas@usc.es

At present, radioisotope production for medical imaging and therapy is mainly done at conventional accelerators. Over the last decades, the use of ultraintense lasers for this purpose has been proposed and studied [1], as alternative in terms of availability and footprint. These compact systems can accelerate, via laser-plasma interaction, charged particles such as protons, ions or electrons [2,3], as well as neutrons and x-ray generation [4], which can induce radioisotope production through nuclear reactions [1].

At the Laser Laboratory for Acceleration and Applications (L2A2) of the Universidade de Santiago de Compostela a high repetition rate femtosecond laser of 45 TW is used for ion acceleration. It can deliver pulses of 1.2 J and 35 fs at 10 Hz, which are focussed on a few micron spotsize area, achieving intensities of more than 10^{19} W/cm^2. The high repetition rate of the laser requires a positioning mechanical assembly that maintains the same focal incidence conditions while refreshing the target material at each shot. This is important in order to guarantee a sufficient and stable pulse intensity on target during the whole irradiation. A multi-target wheel holding plain target foils of few micron thickness is mounted on a set of three high-precision mechanical stages to perform the positioning. A map of the target surface is generated by measuring the deformation of each shot point with a laser-position sensor, and is then programmed into the stages which automatically correct the laser focal position on the target shot-by-shot with micron resolution. This procedure allows for series of tens to hundreds of shots in a row in the same focal conditions.

Ion pulses of few MeV have been measured using a time-of-flight detector at the L2A2, showing typical maxwellian-like exponential energy spectra and high stability both in maximum energy and spectral temperature. By placing a secondary target along the flight path of the accelerated ions, nuclear reactions can be induced in order to produce certain radioisotopes of interest. Activity levels of ^{11}C via the ^{11}B(p,n)^{11}C reaction, of about several MBq, can be estimated for one hour of irradiation at a laser repetition rate of 10 Hz, which are in the range of doses required for preclinical Positron Emission Tomography (PET) imaging. An experimental device, consisting of two CsI(Tl) detectors and a moving boron disk target has been designed for the characterization of the laser-induced production of ^{11}C at the L2A2.

[1] Z. Sun, *AIP Advances* **11**, 040701 (2021).
[2] H. Daido et al., *Rep. Prog. Phys.* **75**, 056401 (2012).
[3] M. Roth & M. Schollmeier, *CERN Yellow Reports* **1**, 231 (2016).
[4] H. A. Sumeruk et al., *Phys. of Plasmas* **14**, 062704 (2007).

Acknowledgements: This work was supported by the Spanish Ministerio de Ciencia, Innovación y Universidades under grants RTI2018-101578-B-C21, RTI2018-101578-B-C22, FPI predoctoral BES-2017-08917, and Unidad de Excelencia María de Maetzu under project MdM-2016-0692-17-2, the Xunta de Galicia grant GRC ED431C 2017/54 and a grant by Generalitat Valenciana of the program Grupos de Investigación Consolidables (AICO/2020/207). Action co-financed by the European Union through the Programa Operativo del Fondo Europeo de Desarrollo Regional (FEDER) of the Comunitat Valenciana 2014-2020 (IDIFEDER/2018/022).

MACACO Compton camera for medical applications

L. Barrientos, M. Borja-Lloret, J. V. Casaña, F. Hueso-González, J. Pérez Curbelo, A. Ros, J. Roser, C. Senra, R. Viegas, **G. Llosá***

Instituto de Física Corpuscular (IFIC- CSIC/UV). C/ Catedrático Beltrán, 2. E-46980, Paterna, Valencia, Spain.

*e-mail: gabriela.llosa@ific.uv.es

The IRIS group of IFIC (http://ific.uv.es/iris) is developing a Compton camera for medical applications. The system consists of three planes of $LaBr_3$ crystals of size 25.8 x 25.8 x 5 mm^3 coupled to silicon photomultiplier arrays. Its main application is treatment monitoring in hadron therapy and it is also being evaluated for radiotracer imaging. In the former application, the aim is to determine the irradiation position of the therapeutic protons by imaging the distribution of photons (*prompt* gammas) emitted by the tissue upon irradiation [1].

After the successful results obtained with the second prototype [2,3], system improvements have been implemented both in instrumentation and in data analysis. The system features a spectral image reconstruction code that allows determining both the spatial and the energy distribution of the photons [4,5], and also combining coincidence events generated by the interaction of the photons in any two or in all three planes [6]. Neural Networks are being employed for event selection [3]. In the instrumentation aspect, two new prototypes have been developed. One of them, MACACO III, employs the same readout ASIC as the previous prototype, the VATA64HDR16 from IDEAS, but the readout board has been replaced by the AliVATA DAQ system that allows the three detector planes to be operated with a single board. In addition, the photodetectors previously employed with 8 x 8 elements of 3 x 3 mm^2 size and 50 x 50 μm^2 microcell size, have been replaced by a model with 25 x 25 μm^2 microcell size to reduce electronics saturation, which has led to an improved energy resolution and a lower dependence of the detector response with temperature variations [7]. The second prototype, MACACOp, employs TOFPET2 ASIC from PETsys, with a significant improvement in timing resolution and dynamic range [8].

The two systems have been fully characterized in the laboratory and in beam tests. Tests at the Spanish National Accelerator Center (CNA) in Sevilla have been performed with an 18 MeV proton beam. Protons impinge a graphite target to produce 4.4 MeV photons, and the target is moved in 1 mm steps. Both systems have been able to reconstruct the images at each position and detect such small variations in the photon emission distribution. In addition, tests have also been carried out at the clinical gantry of the Protontherapy centre in Cracow, with a proton beam at different energies impinging a solid water (RW3) phantom (Fig. 1). Preliminary results allow detection of 2 mm variations in the proton range.

[1] J. Krimmer et al., *Nucl. Inst. Meth.* **818** (2017).
[2] A. Ros et al., *Phys. Med. Biol.* **65**, 245027 (2020).
[3] E. Muñoz et al., *Scientific Reports* **11**, 9325 (2021).
[4] E. Muñoz et al., *Phys. Med. Biol.* **65**, 025011 (2020).
[5] J. Roser et al., *Phys. Med. Biol.* **65**, 145005 (2020).
[6] J. Roser et al., submitted to *Phys. Med. Biol.* (2022).
[7] L. Barrientos et al., in preparation for *Phys. Med. Biol.* (2022).
[8] R. Viegas et al., in preparation for *Phys. Med. Biol*. (2022).

Acknowledgements: This work has received funding from the Ministerio de Ciencia e Innovación (FPA2017-85611-R, PID2019-110657RB-I00).

Figure 1. Experimental setup with the two prototypes in Cracow protontherapy centre.

Prepolarized Magnetic Resonance Imaging of soft and hard biological tissues in a low field scanner

J. Borreguero[1,2,*], J.M. González[1], E. Pallás[2], J.P. Rigla[1], F. Galve[2], J.M. Benlloch[2], J. Alonso[2]

[1]*Tesoro Imaging S.L. Valencia (Spain).* [2]*MRILab, Institute for Molecular Imaging and Instrumentation (i3M), Spanish National Research Council (CSIC) and Universitat Politècnica de València (UPV), Valencia, Spain.*

*pepe.morata@tesoroimaging.com

Low-Field Magnetic Resonance Imaging (LF-MRI) is gaining momentum as an affordable low-cost alternative to clinical MRI, which is extremely expensive and inaccessible. The main cost driver in an MRI scanner is the superconducting magnet required to generate the strong, homogeneous static field (B_0). By lowering B_0, the need for superconducting magnets is removed, resulting in a drastic cost reduction. Unfortunately, the signal-to-noise ratio (SNR) of the images is also thereby compromised. Prepolarization is a technique designed to compensate for the SNR loss in LF-MRI, where sample magnetization is boosted by an intense, not necessarily homogeneous, magnetic pulse of amplitude B_p before the start of the imaging pulse sequence, which is then executed at a lower but highly homogeneous B_0.

Here we present a 0.5 T prepolarizer module (Fig. 1a, [1]) for a B_0 = 0.26 T LF-MRI scanner. This module costs only 7.5 k€ and has allowed us to demonstrate the world-first prepolarization images of hard biological tissues [2]. The SNR gain due to prepolarization has been characterized for different B_p strengths (Fig. 1b). Experimental deviations found at high B_p are consequence of mechanical vibrations due to magnetic forces, Eddy currents and off-resonance effects. Fig. 2 compares equivalent imaging protocols with (PMRI, bottom row) and without (MRI, upper row) a prepolarization pulse. In all cases, B_0 = 0.26 T and B_p = 0.49 T, so $|\overrightarrow{B_0} + \overrightarrow{B_p}|$ = 0.56 T. The theoretical (experimental) SNR boosts for a mouse brain, a human tooth and a cattle bone are 1.72 (1.75), 1.94 (2.02) and 1.97 (2.00) respectively. Note than a SNR enhancement ×2 shortens the acquisition by a factor of 4 for the upper row images in Fig. 2.

All in all, we have designed, built and characterized a prepolarization module that can be easily incorporated into a LF-MRI scanner. Our results show it as a valid addition to LF-MRI systems, opening a new low-cost scenario that could make this option attractive for numerous applications. Specifically, PMRI may become a useful tool for non-invasive dental or bone imaging, both of which make heavy use of potentially harmful X-ray technologies.

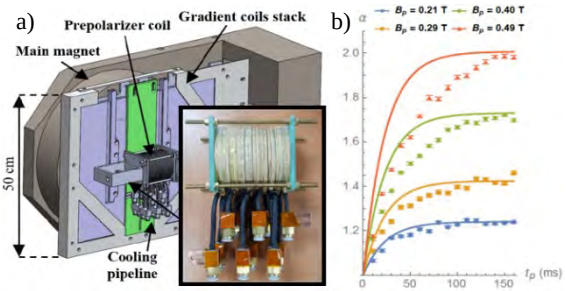

Figure 1. a) Setup CAD. b) Experimental (dots) and simulated (lines) SNR gain (α) as a function of prepolarizer pulse length.

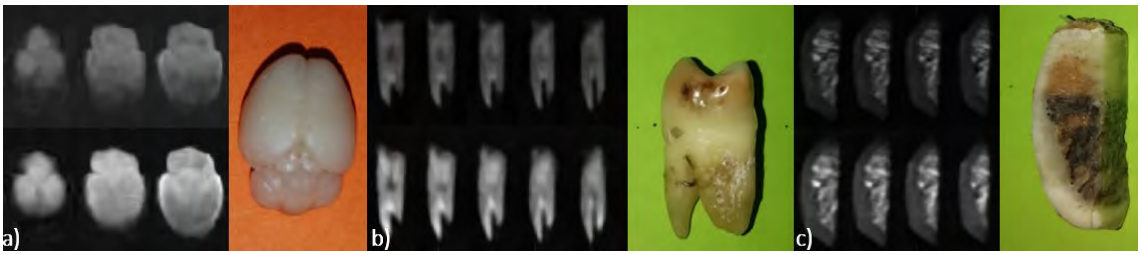

Figure 2. Comparative between MRI (upper row) and PMRI (bottom row) images obtained in same scanning time with identical protocols and parameters in different biological samples: a) mice brain. b) human tooth. c) cattle femur.

[1] Rigla *et al*., A Fast 0.5 T Prepolarizer Module for Preclinical Magnetic Resonance Imaging, *IEEE Transactions on Magnetics* **58**(2), 5100208 (2022).
[2] Borreguero *et al*., Prepolarized MRI of Hard Tissues and Solid-State Matter, *NMR in Biomedicine* e4737 (2022) doi: 10.1002/nbm.4737.

Portable magnetic resonance imaging indoors, outdoors and at home

Teresa Guallart-Naval[1,*], José M. Algarín[2], Rubén Pellicer-Guridi[3,4], Fernando Galve[2], Yolanda Vives[4,5], Rubén Bosch[1], Eduardo Pallás[2], José M. González[1], Juan P. Rigla[1], Pablo Martínez[1], Francisco J. Lloris[3], Jose Borreguero[1], Alfonso Ríos[1], José M. Benlloch[2], Joseba Alonso[2]

[1]*Tesoro Imaging S.L., Valencia, 46022, Spain.* [2]*Institute for Molecular Imaging and Instrumentation, Spanish National Research Council and Universitat Politècnica de València, Valencia, 46022, Spain.* [3]*PhysioMRI Tech S.L., Valencia, 46022, Spain.* [4]*Asociación de investigación MPC, San Sebastián, 20018, Spain.* [5]*Department of Electronic Engineering, Universitat de València, Burjassot, 46100, Spain.*

*e-mail: teresa.guallart@tesoroimaging.com

Magnetic resonance imaging (MRI) is an essential tool for the diagnosis and treatment of numerous health conditions. However, its use is limited to a small fraction of potential patients due to its high cost and lack of portability. Low-field (< 0.3T) cheap and light MRI systems are starting to become a valuable complement to standard MRI [1]. The main penalty to pay for operating in this regime is a significant loss in signal to noise ratio (SNR) and spatial resolution. Nevertheless, the diagnostic value of the resulting reconstructions is not necessarily compromised; for example, contrast-to-noise ratio (CNR) is less strongly dependent on field strength, and it is a more relevant metric for diagnosis than SNR [2].

At the MRILab, we have developed a 70 mT extremity MRI scanner inspired on a previous system [3]. The control electronics are based on MaRCoS, an open-source, high-performance Magnetic Resonance Control System [4]. We have mounted the system on a wheeled structure, with an overall weight ≈ 250 kg and component cost < 50 k€, and demonstrated the true portability with the world-first MRI images of patients inside their house [1].

To benchmark the scanner performance in various scenarios, we have acquired systematic images of a volunteer's knee in different locations (Fig. 1), including a) an MRI physics laboratory; b) in open air, powered from a small fuel-based generator; and c) at the volunteer's home. These images were all acquired with the same parameters (T1-weighted 3D-TSE with a total scan time ≈ 12 min) on the right knee of the same volunteer. To compare image quality, we estimate the SNR of each image (Fig. 1 right) calculating the signal strength as the average voxel brightness in a region of the femur (red boxes), and the noise as the average voxel brightness in the background (white boxes). Despite small differences in SNR values, the main anatomical features and different tissues remain clearly identifiable in all scenarios. Furthermore, the volunteer carries a fixation metallic implant screwed to the femur, which leads to strong artifacts in standard clinical systems but appears sharp in our low-field acquisitions (Fig. 2).

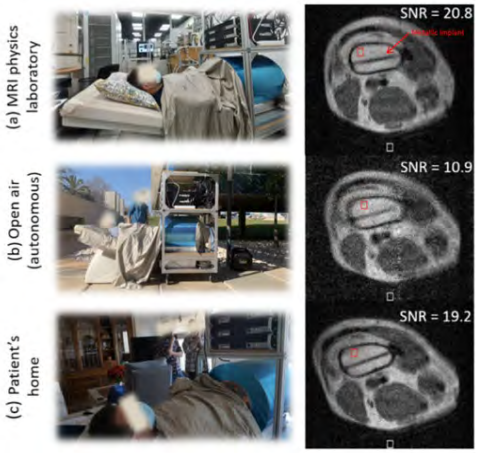

Figure 1. Photographs during acquisitions (left) and axial slice from 3D-TSE reconstructions (right, no post-processing) at different locations.

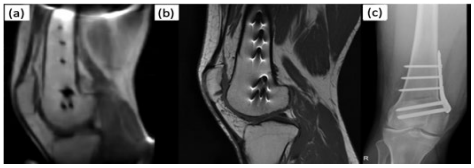

Figure 2. Images of volunteer's fixation metallic implant attached to the femur: (a) sagittal view acquired with our scanner; (b) sagittal view acquired with a 3T system; and (c) lateral X-ray computed radiography.

In conclusion, we have demonstrated that it is possible to have a truly portable, low-cost and easy to maintain and install MRI scanner. These devices open the door to expanding MRI applications to home and hospice care, small clinics, rural areas, field hospitals, NGO camps, etc., making MRI available to a large fraction of the world's population with no or insufficient access.

[1] T. Guallart-Naval, J. M. Algarín, *et al.* (2022). arXiv:2203.03455.
[2] S. Ghazinoor *et al.* JMRI (2007). https: //doi.org/10.1002/jmri.20854.
[3] T. O'Reilly *et al.* MRM (2020). https:// doi.org/10.1002/mrm.28396.
[4] T. Guallart-Naval *et al.* (2022). arXiv:2203.11314, 2022.

Thermal patterns generated by ultrasound holograms

Diana Andrés[1,*], Jonathan Vappou[2], Noé Jiménez[1], Francisco Camarena[1]

[1]*Instituto de Instrumentación para Imagen Molecular (UPV-CSIC), Valencia, Spain.*
[2]*Université de Strasbourg, Centre National de la Recherche Scientifique (CNRS), ICube, Strasbourg, France.*

*e-mail: dandres@i3m.upv.es

In this work, we use 3D-printed acoustic holographic lenses coupled to a low-cost magnetic resonance imaging (MRI) compatible transducer to create thermal holographic patterns in an absorbing medium. First, acoustic holograms are designed with time-reversal methods, considering the time invariance of the acoustic wave equation, by setting virtual sources along the shape of the desired acoustic image. The wavefront produced by these point sources is numerically computed and captured in a plane parallel to the transducer surface. The corresponding holographic lens is designed with the complex conjugated phase information of the wavefront at the transducer working frequency, considering each column of the lens vibrates as an elastic Fabry-Pérot resonator [1]. To evaluate the acoustic field generated in the medium, numerical simulations were performed with a k-space pseudo-spectral method [2]. With the maximum pressure of the resulting field in stationary state we calculate the tissue heating by solving the Penne's bio-heat equation [3], retrieving the desired holographic thermal pattern.

Two thermal patterns were designed: one with the shape of the number '2' designed for a flat transducer and other designed to enlarge the natural focus of an elliptical focused transducer for therapeutical applications. To characterize the holographic acoustic field generated by the transducer-lens system, measurements were done with a piezoelectric hydrophone in degassed water. Thermal pattern was experimentally generated in liver tissue and measured with two different instrumentals: and infrared (IR) camera recording the temperature field at the surface of the tissue and MR-thermometry.

Simulation and measurement of the '2'-shaped acoustic-hologram are in good agreement, with a relative error of 31%. Thermal holographic patterns measured with IR-camera and MR-thermometry matched with thermal simulations (Figs. 1b and 1c). For this image, peak temperature raised 4.5 °C after 12 s at 20 W acoustic power. For the focused transducer hologram, an ellipsoidal thermal pattern of 7 × 30 mm^2 size was obtained, modifying its natural focus of 11 × 16 mm^2, and raising the focal spot temperature up to 6 °C after 30 s.

In conclusion, with the use of 3D-printed holographic lenses, thermal holographic patterns can be generated in absorbing media. With acoustic holograms, heating region can be adapted to very specific therapeutical targets in any part of the body. This technology is proposed as a low-cost alternative to phased-array systems used in clinical applications for hyperthermia treatments.

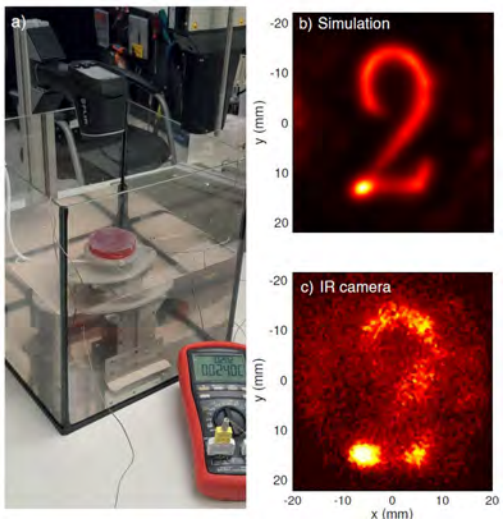

Figure 1. a) Experimental setup. b) Simulated and c) experimental thermal pattern.

[1] Jiménez-Gambín, S., Jiménez, N., Benlloch, J. M., Camarena, F., *Physical Review Applied* **12**(1), 014016 (2019).
[2] Treeby, B. E., Jaros, J., Rendell, A. P., Cox, B. T., *The Journal of the Acoustical Society of America* **131**(6), 4324 (2012).
[3] Pennes, H. H., *Journal of Applied Physiology* **1**(2), 93 (1948).
[4] Andrés, D., Vappou, J., Jiménez, N., Camarena, F., *Applied Physics Letters* **120**(8), 084102 (2022).

Acknowledgements: This research has been supported by the Spanish Ministry of Science, Innovation, and Universities through Grants IJC2018-037897-I, FPU19/00601, and PID2019-111436RBC22, by the Agència Valenciana de la Innovació through Grants INNCON/2021/8 and INNVA1/2020/92, and by Generalitat Valenciana through Grant AICO/2020/268. Action co-financed by the European Union through the Programa Operativo del Fondo Europeo de Desarrollo Regional (FEDER) of the Comunitat Valenciana 2014–2020 (Nos. IDIFEDER/2018/022 and IDIFEDER/ 2021/004). Action co-financed by BPI France, Région Grand Est and FEDER (UFOGUIDE project).

Evaluation of lateral and axial resolution in photoacoustic tomography with linear US probe and pixel-based beamformers

I. Pi-Martín*, A. Cebrecos, J.J García-Garrigós, N. Jiménez, F. Camarena

Instituto de Instrumentación para Imagen Molecular (i3M), Consejo Superior de Investigaciones Científicas (CSIC), Universitat Politècnica de València (UPV), Camino de Vera s/n, 46022, Valencia, Spain.

*e-mail: irpimar@upv.es

Photoacoustic (PA) imaging techniques use the ability of some materials (chromophores) to emit sound after being excited by a pulsed light [1]. These materials, after absorbing the laser energy, become acoustic sources whose signals can be recorded with a typical ultrasonic (US) acquisition system and conform molecular images [1]. This technique allows to differentiate the chromophores of tissues, for example oxyhemoglobin and deoxyhemoglobin, since each chromophore has a characteristic absorption spectrum, which makes it a promising medical imaging technique with molecular contrast, better resolution than pure ultrasound imaging and greater tissue penetration than optical techniques [1]. Classical ultrasonic linear phased arrays, often employed in ultrasound imaging systems, have been adapted for their use in photoacoustic imaging systems. However, the use of these receptors reduces the quality of the obtained PA images, since the laser-generated acoustic signals are travelling in all directions in the 3D-space, which makes it necessary to use more complex reconstruction algorithms that take advantage of the properties of the recorded ultrasonic signals, obtaining images with improved resolution and contrast.

The main objective of this work is to compare the resolution of a PA tomography system using a laser beam excitation, a linear ultrasound probe and using pixel-based beamformers: Delay And Sum (DAS) [2], Delay Multiply And Sum (DMAS) [3], Minimum-Variance (MV) [4] and MV-DMAS [5]. To achieve this, both experiments and simulations have been carried out with two point-like absorbers initially overlapped and are separated until we are able to identify them as two independent sources in the reconstructed image using pixel-based beamformers. We use the criterium of 6 dB in the amplitude difference between the peaks and the valley in the reconstructed image to determine whether they have been resolved or not. The experiments and the simulations showed a good agreement as shown in Figure 1. The obtained results ease a proper choice of the most suitable beamformer depending on the limitations of the linear probe tomography system.

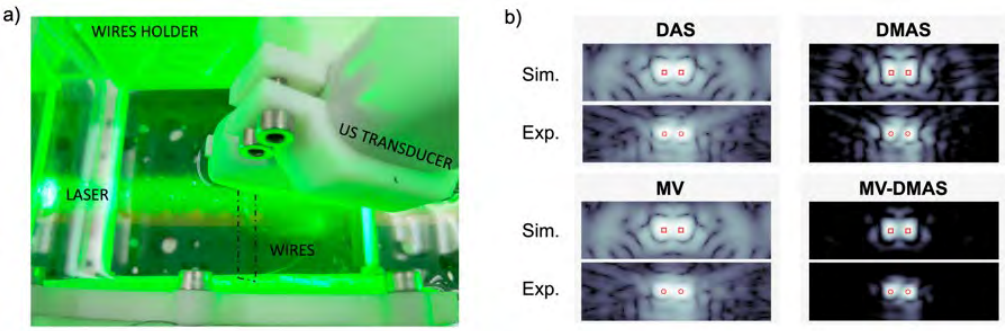

Figure 1. a) Experimental set-up. b) Beamformed simulated and experimental data from lateral resolution study, all reconstructions are shown with a dynamic range of 60 dB. The original sources have been marked in red.

[1] P. Beard, Biomedical photoacoustic imaging, *Interface Focus*, vol. 1, no. 4, pp. 602-631 (2011).
[2] V. Perrot, M. Polichetti, F. Varray, and D. Garcia, So you think you can DAS? A viewpoint on delay- and-sum beamforming, *Ultrasonics*, vol. 11, no. May 2020, p. 106309 (2021).
[3] G. Matrone, A. S. Savoia, G. Caliano, and G. Magenes, The delay multiply and sum beamforming algorithm in ultrasound B-mode medical imaging, *IEEE Trans. Med. Imaging*, vol. 34, no. 4, pp. 940– 949 (2015).
[4] N. Q. Nguyen and R. W. Prager, Minimum Variance Approaches to Ultrasound Pixel-Based Beamforming, *IEEE Trans. Med. Imaging* vol. 36, no. 2, pp. 374–384 (2017).
[5] M. Mozaffarzadeh, A. Mahloojifar, M. Orooji, K. Kratkiewicz, S. Adabi, and M. Nasiriavanaki, Linear-array photoacoustic imaging using mínimum variance- based delay multiply and sum adaptative beamforming algorithm, *J. Biomed. Opt.*, vol. 23 (2018).

Ultrafast-Ultrasound for PET radiotracer Arterial Input Function Quantification in the Rat Carotid Artery

M. Perez-Liva[1,2,*], T. Yoganathan[2], J. Cal-Gonzalez[3], J.M. Udias[1], J.L. Herraiz[1], T. Viel[2], B. Tavitian[2]

[1]*Nuclear Physics Group and IPARCOS, Complutense University of Madrid, 28040 Madrid, Spain.* [2]*Université Paris Cité, Paris-Cardiovascular Research Center, INSERM U970, France.* [3]*Ion Beam Applications Spain, PT Center Madrid, Spain.*

*e-mail: mailyn01@ucm.es

Accurate assessment of the arterial input function (AIF) in the carotid artery would be ideal for radiotracer modelling of cerebral PET. This is highly challenging in rodents as the internal diameter of the carotid artery is smaller than the spatial resolution of preclinical PET scanners [1] and it is also blurred by the effect of the respiratory motion. Here, we used co-registration of Ultrafast Ultrasound Doppler of the rat carotid artery with PET dynamic acquisition to enable segmentation-based correction of motion (MoCo) and partial volume correction (PVC) for improved radiotracer quantification.

Animal experiments were performed under the French ethical committee approval N°18-146. Measurements were performed using our hybrid imaging system PETRUS, that combines an Ultrafast Ultrasound Imaging (UUI) scanner with a small animal PET/CT (nanoScan, Mediso) [2,3] (Fig. 1A). PET and UUI volumes were acquired simultaneously and precisely registered in the same spatial coordinates [2]. Adult male rats (n=6) were injected IV with 55 MBq of [^{18}F]FDG and imaged during 60 minutes. Radioactivity concentration counted in serial blood samples drawn from the left common carotid were compared with image-derived AIF of the right common carotid, segmented from the Doppler volume using isodata unsupervised classification [4] (Fig. 1 B). A modification of the local projection method [5] with motion deconvolution to account for PVC and MoCo was applied to the dynamic PET sequences.

The maximum longitudinal and axial displacements of the carotid artery estimated with ultrasound were 2.1 and 0.7 mm, respectively. The differences in mean area under the curve (AUC) between ground-truth AIFs (i.e., obtained from blood sampling) and uncorrected ones were 29%. After PVC, mean differences in AUC were reduced to 9 %, and after MoCo and PVC, they were reduced to 3 % (Fig. 1 C). Maximal differences at individual time points between ground-truth and, uncorrected, after PVC, and after PVC and MoCo, were 72%, 16 %, and 8 %, respectively.

Ultrafast Doppler co-registration with dynamic PET can be used for motion and PVE correction of small moving structures in preclinical PET. This allows for increased accuracy of image-derived AIF quantification in the rat carotid artery. Better quantification of the AIF should benefit PET radiotracer quantification in rodent brain.

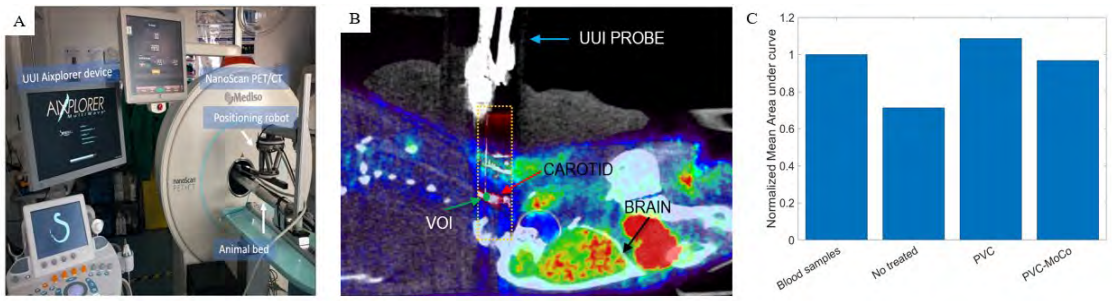

Figure 1. A-PETRUS setup for the simultaneous and co-registered acquisition of PET/CT and Ultrafast Ultrasound Image (UUI). B- Fusion of PET/CT/ UUDI to record the carotid artery motion and anatomy, used in this study to improve the quantification of the Arterial Input Function. C-Comparison of normalized mean area under AIF curves for Blood samples and Input functions without correction, PVC and PVC-MoCo.

[1] Moses, W. *Nucl. Inst. Meth. Phys. R.S. A* **648**, S236 (2011).
[2] Provost J., *et al*., *Nature Biomed. Eng.* **2**(2), 85 (2018).
[3] Pérez-Liva M, *et al.*, *Phys. Med. Biol.* **63**(19), 19NT01 (2018).
[4] Magid, A., *et al.*, *IEEE Trans. Syst. Man. and Cyb.* **20**(5), 1238 (1990).
[5] Cal-González, *et al.*, *Phys. Med. Biol*., **63**(1), 015005 (2017).

Acknowledgements: Plan Cancer (ASC16026HSA-C16026HS), ANR-10-IDEX-0001-02, Plateforme Imageries du Vivant - PIV), (ANR-11-INBS-0006) and Infrast. Biologie-Santé (IBISA). CARPEM Siric grant (BT), CARPEM Postdoc (MPL).

Phase-contrast x-ray imaging with a laser-driven x-ray source in air

A. Coathup[1], R. Contreras-Martinez[1,2], C. Ruiz[2], A. Reija[1,3], M. Seimetz[3], J. Benlliure[1]

[1]*Instituto Galego de Física de Altas Enerxías (IGFAE), Universidade de Santiago de Compostela, Spain.* [2]*Instituto de Física Fundamental y Matemáticas, Universidad de Salamanca, Spain.* [3]*Instituto de Instrumentación para Imagen Molecular (I3M), CSIC - Universitat Politècnica de València, Spain.*

*e-mail: andrew.coathup@usc.es

A laser-driven x-ray source in air has been set-up and stabilized at the Laser Laboratory for Acceleration and Applications (L2A2) at the Instituto Galego de Física de Altas Enerxías (IGFAE) in the Universidade de Santiago de Compostela (USC). High-energy ultrashort laser pulses are focused onto the surface of a target material, reaching intensities greater than 10^{17} W/cm^2 and ionizing the target material, producing x-ray radiation. The x-ray source has a very small source size (15µm) and a high fluence (10^9 photons/s) making it an attractive option for phase-contrast x-ray imaging.

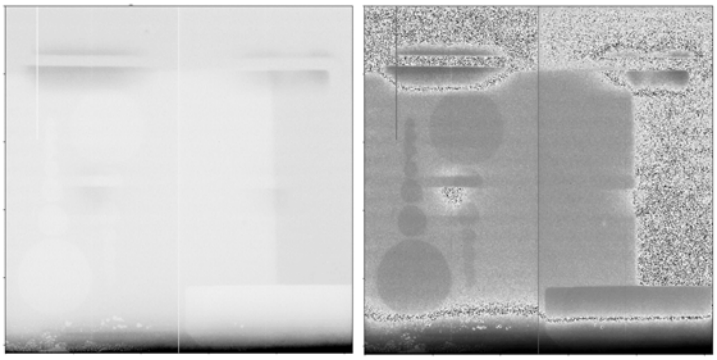

Figure 1. (Left) Raw x-ray image of the PLA contrast-detail phantom. (Right) Phase contrast enhanced image of the same phantom.

Here we present the first phase-contrast images from the laser-driven x-ray source (Figure 1). An in-house 3D printed contrast-detail phantom made of Polylactic acid (PLA) plastic (Figure 2) was irradiated for 60s. PLA plastic has optical properties that are conducive to phase-contrast imaging due to its large ratio of the real to the imaginary part of the index of refraction and has been used previously in phase-contrast studies [1]. The phantom was placed at a distance of 8.7cm from the source. The detector was placed at a distance of 30cm from the source. These distances were chosen taking into account the propagation distance required for phase contrast to manifest itself, the physical sizes of the object and detector, the magnification of the object, and the dose requirements to produce an image.

The phase image (figure 1 – right) was retrieved from the original x-ray image (figure 1 – left) using the Paganin algorithm [2]. The phase extracted image shows increased contrast both qualitatively, as can be seen in figure 1, and quantitatively through calculation of the mean object grayscale values with respect to the mean value of the background.

This first phase-contrast x-ray image produced by the laser-driven x-ray source in air at the L2A2 is the first step in the exploration of the capabilities of this source as a phase-contrast imaging modality.

Figure 2. Picture of the PLA plastic contrast-detail phantom.

[1] Esposito, G. et al. *Physics in Medicine and Biology* **64** (2019).
[2] Paganin, D. et al. *Journal of microscopy* **206.1**, 33-40 (2002).

Self organizing maps aplicados al análisis de los datos obtenidos mediante termografía infrarroja para el diagnóstico y seguimiento de la diabetes

L. Carbonell[1], **R. Cibrián**[2,*], M. Ibáñez[3], A. J. Serrano-López[3], J. I. Priego[4], C. Macian[1], R. Salvador-Palmer[2]

[1]*Clínica Universitaria Podológica. Facultat d'Infermeria i Podologia.* [2]*Biofísica y Física Médica. Facultat de Medicina i Odontologia.* [3]*Ciencia de Datos, Escuela Técnica Superior Ingeniería. Universitat de València. España.*

*e-mail: rosa.m.cibrian@uv.es

La termografía infrarroja es una tecnología no invasiva, sin contacto y de bajo coste que permite registrar la energía radiante emitida por un cuerpo, proporcionando una imagen de su temperatura superficial. Esta técnica está siendo ampliamente utilizada tanto para evaluar la actividad física y deportiva, como en el campo biomédico para monitorizar la temperatura de la piel en diferentes patologías que afectan la vascularización periférica. En este sentido, la termografía puede ser una técnica prometedora para el seguimiento de la diabetes mellitus, una enfermedad con una gran incidencia en países industrializados, que produce como efecto más pernicioso una afectación vascular, que puede ser cuantificada con esta técnica y por tanto controlar que se puedan producir complicaciones asociadas, como el pie diabético que puede acabar en la necesidad de amputaciones.

En estudios previos [1, 2] hemos establecido un protocolo centrado en 9 regiones de interés (ROIs) en la planta del pie de los pacientes, para estudiar: la variación de la temperatura de dichas ROIs ante un estrés mecánico (caminar 100 m) y la recuperación de la temperatura basal tras un estrés térmico por enfriamiento.

En este trabajo presentamos los resultados correspondientes al estudio de 60 pacientes diabéticos y 60 controles a los que se les ha aplicado el protocolo indicado. La Fig. 1 muestra las diferencias entre controles y diabéticos en las distintas ROIs, y la figura 2 muestra el mapa autoorganizado (SOM) correspondiente a las características termográficas analizadas en los dos grupos estudiados para la caracterización del patrón del paciente diabético.

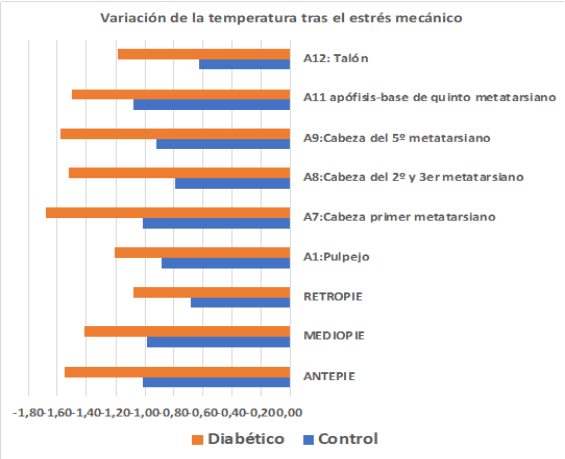

Figura 1. Variación de temperatura de las ROIs analizadas tras el estrés mecánico, tanto en los pacientes diabéticos como en los controles.

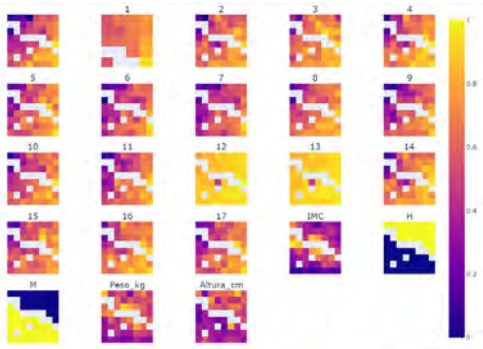

Figura 2. SOM correspondiente a la distribución de las variables analizadas en pacientes diabéticos y controles, en función de la variación de temperatura, determinada mediante termografía infrarroja

[1] Priego Quesada J. I. et al. (2018) **DOI:** https://doi.org/10.1007/978-3-319-68195-5_112
[2] Lucía Carbonell et al. (2018) **DOI:** 10.1080/21681163.2018.1542349

Acknowledgements: A todos los pacientes y controles que han participado en el estudio.

Commissioning and quality assurance of ^{192}Ir high-dose-rate brachytherapy sources based on micro-ionization chamber dosimetry

M. Martinez-Albaladejo[1,*], I. Seedhouse[2], V. Puchades Puchades[1], J. Suarez Arteaga[1], D. Ramos Amores[1], A. Serna Berna[1]

[1]*Medical Physics and Radiation Protection Department, Complejo Hospitalario Universitario de Cartagena, Servicio Murciano de Salud, Calle Minarete, s/n, 30202, Región de Murcia, Spain.*
[2]*Radiotherapy Physics Department, University Hospitals of North Midlands NHS, Stoke-on-Trent ST4 6QG, UK.*

*e-mail: mma52b@ad.sms.carm.es

Introduction: The purpose of this work is to establish an end-to-end test to check that a high-dose-rate (HDR) afterloader delivers the planned dose through the correct dwell time scaling, correct source positioning and correct source calibration of a ^{192}Ir brachytherapy (BT) source based on the absolute dose measurement performed by a PinPoint 3D ionization chamber.

Material and methods: The absorbed dose to water in water medium can be determined from the detector reading (M) in a phantom material using the formalism [1]: $D_w = M \cdot ACF \cdot DCF$, where ACF and DCF are the atmospherical and dose correction factors, respectively.

Annual cross-calibrations have been performed between 2 field instruments (PTW31016 PinPoint) and a NPL secondary standard (NE2611) as reference detector, in a Gulmay kV unit [2]. Single line plans are delivered by a GammaMed afterloader with the normalization of 1Gy in the effective point of the chamber (at 4.8cm from the closest source position). A CT scan of the slab phantom is used, with a rectangular insert which hosts consistently the chamber and catheter (Fig. 1).

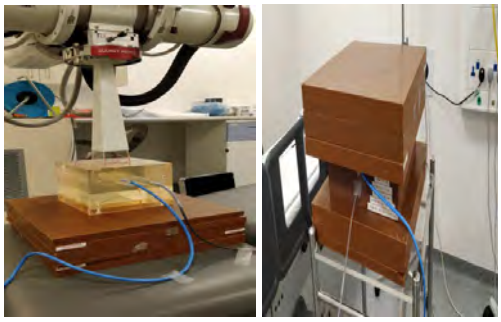

Figure 1. XR cross-calibration procedure (left side) and setup for the BT measurements (right), where a 6F catheter is connected to the afterloader and the micro-chamber is inserted into the phantom.

Results: The data are recorded in an in-house program coded in Visual Studio and compared with the expected values estimated by Eclipse Treatment Planning System (TPS) and MC code Geant4. On average after two years, the measured absorbed dose has been: 102.2 ±1.0 cGy (k=1) as shown in Fig.2. The expected point doses by the TPS and Geant4 (diff.) are 100.0 (-2.2%) and 100.3 (-1.9%) cGy, respectively. The expanded uncertainty has been 4.4% (k=1) estimated by quadratic propagation of the variance, slightly lower to the estimations found in the literature within In-Vivo Dosimetry in BT.

Conclusion: This study provides a practical check of the source calibration entered in the TPS and subsequent dwell time scaling and source positioning, based on the absolute dose determination of HDR sources, embedded efficiently in the unit post-exchange quality assurance and sensitive to alleged errors.

This dose formalism is novel and was not found elsewhere in literature. The usage of the slab phantom has the advantage that no additional material is required other than those used for external beam RT dosimetry at IPEM centres. Therefore, it seems useful for interdepartmental BT audits.

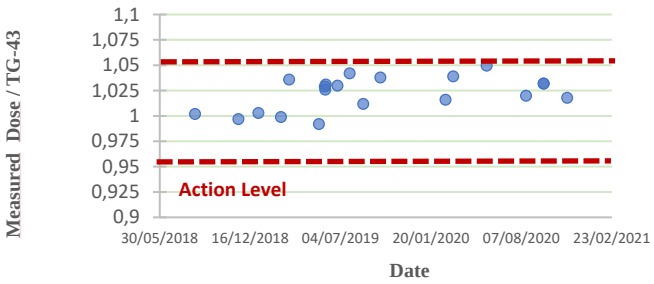

Figure 2. Trend in the measurements wrt. expected doses after 2 years.

[1] D. Baltas, L. Sakelliou, N. Zamboglou. *The Physics of Modern Brachytherapy for Oncology*. Taylor & Francis (2009).
[2] The IPEMB code of practice for the determination of absorbed dose for x-rays below 300 kV generating potential. *Phys. Med. Biol*. **41** (1996).

Método rápido de verificación de la estabilidad de un conjunto cámara pozo-electrómetro de uso clínico

V. Puchades Puchades*, M. Martinez-Albadalejo, D. Ramos Amores, J. Suarez Arteaga, A. Serna Berna

Servicio de Radiofísica y Protección Radiológica, Hospital General Universitario Santa Lucía. Servicio Murciano de Salud.

*e-mail: vicente.puchades2@carm.es

Introducción: En cada cambio de fuente de braquiterapia o en cada medida mensual de la estabilidad de la fuente hay que usar un instrumental que nos permita medir el TKRA de la fuente. La medida del TKRA se realiza de forma usual mediante el uso de cámaras pozo+electrómetro. Sin embargo no hay soluciones comerciales económicas y que estén extendidas en el uso clínico para la verificación de la estabilidad de las cámaras pozo. En este trabajo proponemos una forma de verificar la estabilidad de la cámara pozo antes de su uso.

Material y métodos: Hemos verificado la estabilidad del conjunto Cámara Pozo (HDR 1000PLUS de Standar Imaging) Electrómetro (CDX2000B de Standar Imaging) de nuestro servicio. Para ello se ha irradiado la cámara pozo con un campo de 10x10cm^2 y energía 6MV y DFS 100cm con 100UM(Tasa 100UM/min), corrigiendo el valor de la lectura electrométrica por el factor de presión y temperatura. Antes de cada medida se irradió el electrómetro con 500UM de calentamiento. Un total de 12 adquisiciones (media de 3 medidas) se han recopilado a lo largo de un año.

Resultados: En la Tabla 1 se muestra los datos recogidos durante un año. Se observa un buen comportamiento de nuestra cámara pozo al ser irradiada. No hemos encontrado discrepancias de más de 1% en la estabilidad mediante este método. EL uso de estas medidas previas nos permite acotar un posible problema en la medida del TKRA y descartar que sea por mal funcionamiento del electrómetro o de la cámara pozo. Este sistema de verificación de la estabilidad del conjunto cámara electrómetro cobra importancia en los cambios de fuente a la hora de verificar que el certificado de calibración de la fuente proporcionado por el fabricante sea el adecuado según la actual legislación española.

E(MV)	DFD	UM	Valor M de referencia	Valor UM/Dosis Quick check	kpt	M1 (nC)	M2 (nC)	M3 (nC)	M*	Desviación respecto a referencia
6	100,00	100	8206,1	0,994	1,011	8145,0	8139,3	8143,9	8184,1	0,27%
6	100,00	100	8206,1	0,997	1,020	8135,5	8142,3	8139,9	8277,1	-0,87%
6	100,00	100	8206,1	0,999	1,015	8125,0	8120,0	8122,4	8236,1	-0,36%
6	100,00	100	8206,1	0,995	1,008	8135,0	8133,3	8135,6	8158,7	0,58%
6	100,00	100	8206,1	1,001	1,004	8148,8	8152,2	8153,4	8192,3	0,17%
6	100,00	100	8206,1	1,003	1,008	8145,6	8144,2	8142,1	8233,7	-0,34%
6	100,00	100	8206,1	0,999	1,015	8147,3	8141,3	8142,2	8257,5	-0,63%
6	100,00	100	8206,1	1,000	1,004	8145,0	8139,3	8143,9	8175,3	0,38%
6	100,00	100	8206,1	0,995	1,006	8147,1	8142,8	8146,1	8153,2	0,64%
6	100,00	100	8206,1	1,003	1,005	8135,4	8139,0	8137,5	8202,5	0,04%
6	100,00	100	8206,1	0,999	1,012	8136,7	8139,9	8135,0	8226,6	-0,25%
6	100,00	100	8206,1	0,997	1,014	8143,7	8144,1	8147,1	8234,2	-0,34%

Tabla 1: Datos de un año de medidas de la estabilidad. M* es el valor de la media de la lectura ionométrica corregida.

Conclusiones: Se ha descrito una forma rápida, accesible y económica de verificar la estabilidad de un conjunto cámara pozo-electrómetro para la medida del TKRA de fuentes radioactivas de uso clínico.

Statistical analysis of the pre-treatment quality assurance results from a new TrueBeam linac

F. Illescas Martinez[1,*], M. Martinez-Albaladejo[2], J. Suarez Arteaga[2], V. Puchades Puchades[2], D. Ramos Amores[2], A. Serna Berna[2]

[1] *Faculty of Mathematics, Universidad de Murcia. C.Campus Universitario, 9, 30100, Murcia, Spain.*
[2] *Medical Physics and Radiation Protection Department at Complejo Hospitalario Universitario de Cartagena, Servicio Murciano de Salud, C. Minarete, s/n, 30202, Cartagena, Spain.*

*e-mail: fernando.illescasm@um.es, radiofisicayprchuc@gmail.com

Introduction: This work is based on the study of the different procedures for the quality control (QA) of VMAT (Volumetric Modulated Arc Therapy) plans of the new state-of-the-art linear accelerator at Hospital General Universitario Santa María del Rosell, TrueBeam, developed by Varian Medical System. For this purpose, we have a clinical database of patients with different types of dysplasia and different dosimetry systems such as PTW-Octavius 4D (O4D), Portal Dosimetry (PD) and Quasar; database that we are updating as more patients are treated.

Methodology: The data is evaluated using different comparative methods, either to find significant differences or to find high linear correlations between the various parameters available to us. Methods such as the Wilcoxon test for related samples that do not follow a normal distribution, the Student's t-test or the Pearson's correlation coefficient value are used. All of them are implemented in MATLAB, and then entered in the SPSS software to be more certained about the process.

Results: The analysis includes 142 patients. The items are divided into 2 groups depending on the type of energy used: 6X (17) and 6FFF (125). We make comparisons between the different dosimetry systems abovementioned, adding that we have different gamma indices (3 %/1mm and 3 %/2mm) for O4D and PD (Table 1). The study of the Pearson correlation between the monitor units and the different quantitative variables corresponding to the dosimetry systems is also carried out.

Hypothesis summary			
Comparisons		FFF	6X
Oct 4D 3 %/2mm	PD 3 %/2mm	0.677	0.549
Oct 4D 3 %/1mm	PD 3 %/1mm	0.738	0.033
Oct 4D 3 %/2mm	Oct 4D 3 %/1mm	0.001	0.001
PD 3 %/2mm	PD 3 %/1mm	0.001	0.012

Table 1. p-values as results of the Wilcoxon signed rank test for related samples with null hypothesis: the median of the differences between the different variables is equal to 0.

We obtain interesting results, some of which are highly anticipated, such as the finding of significant differences when comparing the same dosimetry system with its different gamma indices, for example the comparison between O4D 3 %/2mm and O4D 3 %/1mm with a probability of $p < 0.001$, and others not as expected, such as the finding of a significant difference between O4D and PD with gamma indices 3 %/1mm with a p-value of $p < 0.033$, a result only achieved in the 6X (Fig.1 and Fig.2). In this last group, we also see that there is a high linear correlation with a value of -0.732 between the monitor units and PD in both gamma indices.

		Octavius 4D 3%/2mm	Octavius 4D 3%/1mm	Porta Dosimetry 3%/2mm	Portal Dosimetry 3%/1mm
Total Monitor Units	Pearson correlation	-,062	,074	-,432	-,397
	Sig. (bilateral)	,492	,410	,000	,000
	N	125	125	125	125

Figure 1. Correlation table for the FFF energy between the total monitor units and the dosimetry systems O4D and PD.

		Octavius 4D 3%/2mm	Octavius 4D 3%/1mm	Portal Dosimetry 3%/2mm	Portal Dosimetry 3%/1mm
Total Monitor Units	Pearson correlation	,214	,408	-,681	-,732
	Sig. (bilateral)	,409	,104	,003	,001
	N	17	17	17	17

Figure 2. Correlation table for the 6X energy between the total monitor units and the dosimetry systems O4D and PD.

Conclusion: A first statistical analysis of the pre-treatment QA results under different dosimetry systems for a new linac is performed. Future work may be needed to consolidate and extend this study.

Termodinámica y Análisis Térmico

Presentaciones orales

Lunes 11/07:

15:30-15:45 Josefa Salgado Carballo. *Thermophysical characterization of a Firefighting Foam based on eco-friendly soap compounds and bentonite clay. Effectiveness laboratory testing*

15:45-16:00 Pablo Vallet Moreno. *Doped Lithium Ionic Liquids as potential electrolites*

16:00-16:15 Angel Manuel Fernandez Fernandez. *Análisis de cristalización de hidrato de metano en un poro de sílice empleando Dinámica Molecular*

16:15-16:30 J.J. Suñol Martínez. *Thermal analysis of magnetic materials*

16:30-16:45 Juan José Parajó Vieito. *Calorimetric and electrochemical studies of lithium salt dissolved in pure ethylammonium nitrate ionic liquid*

16:45-17:00 José Francisco Martinez López. *Calorimetría de mezclas binarias de L-carvona con alcoholes de cadena corta C2-C3*

17:00-17:15 Consolación Sánchez Sánchez. *Development of real-time polymerase chain reaction methods for the quantification of Methanoculleus, Methanosarcina and Methanobacterium in anaerobic digestion*

Pósteres

- José Ramón Solana Quirós. *Effective two-body potentials for fluid argon including three-body interactions*
- José Luis Legido Soto. *Thermophysical characterization of peloids enriched with microalgae*
- José Luis Legido Soto. *Study of the thermal properties of mixtures of clays and thermal waters of Latin America*
- Ângela Queirós. *Density of alumina nanofluids (15 nm) in water at different temperatures*
- Fátima Muiño Blanco. *Thermal analysis of Eco-Friendly Soap-Based Firefighting Foam. Effect of the bentonite addition*
- Pablo Vallet Moreno. *Broad Band Dielectric Spectroscopy of nanofluids*
- Antía Santiago Alonso. *Experimental characterisation of ionic gels for energy storage applications*

Thermophysical characterization of a Firefighting Foam based on eco-friendly soap compounds and bentonite clay. Effectiveness laboratory testing

J. Salgado[1,*], F. Muiño[1,2], J.J. Parajó[1], A. Amigo[2], M. Villanueva[1], C. Trasar-Cepeda[3], Á. Prieto-Fernández[3] and S. González-Prieto[3]

[1]*Grupo NaFoMAT. Departamento de Física Aplicada, Facultad de Física, Universidad de Santiago de Compostela. 15782 Santiago de Compostela. A Coruña. Spain.*
[2]Grupo Propiedades Termofísicas y Superficiales de Líquidos. Departamento de Física Aplicada. *Facultad de Física, Universidad de Santiago de Compostela. 15782 Santiago de Compostela. A Coruña. Spain*
[3]*Misión Biológica de Galicia. Sede de Santiago de Compostela. CSIC. 15706 Santiago. A Coruña. Spain.*

*e-mail: j.salgado.carballo@usc.es

The use of firefighting foams and of other natural or synthetic additives for improving the extinguishing effect of water in forest fires has been increasing in the last decades and is nowadays a widespread practice. However, due to the negative and sometimes long lasting environmental impact of several of the most used firefighting agents there is growing interest on the development of alternative "eco-friendly" formulations [1,2].

Kawahara *et al*. [2] developed a novel firefighting foam, with significantly lower environmental risk and suitable for its application in forest fires, consisting of natural soaps, methylglycinediacetic acid (MGDA) as chelating agent, propylene glycol; hexylene glycol and water.

The present work proposes an improvement of the flame retardant formulated by these researchers, based on the addition of bentonite clay. To determine the most efficient concentration of bentonite, thermophysical properties of the retardant precursors as well as of mixtures containing different clay amounts (1%, 2%, 3%, 4% and 8%) were determined. The stability of the clay into the liquid mixtures was analysed from the behaviour of the refraction index against time, while differential scanning calorimetry and thermogravimetry were used to study the thermal behaviour of these samples. Additionally, transport properties as density and viscosity against clay concentration and temperature were also determined.

Finally, the effect of the modified formulations of the retardant were tested in a soil with high organic matter content applying thermal shocks at different temperatures and exposure times and carrying out the thermal analysis of heated and unheated soils.

[1] T. Kawano, K. Otsuka, T. Kadono, R. Inokuchi, Y. Ishizaki, B. Dewancker, K. Uezu, *Advanced Materials Research* **875-877**, 699 (2014).
[2] T. Kawahara, S Hatae, T. Kanyama, Y. Ishizaki K. Uezu. *Environ. Control Biol.* **54** (1), 75 (2016).

Acknowledgements: This work was supported by Fundación Humanismo y Ciencia through the project 2021-PO025. J. J. Parajó thanks funding support of I2C postdoctoral Program of Xunta de Galicia. Authors also acknowledge M. Gómez (RIAIDT-USC) for the technical support in thermal analysis measurements.

Doped Lithium Ionic Liquids as potential electrolites

Pablo Vallet[1,*], Juan José Parajó[1], Antía Santiago[1], María Villanueva[1], Jean LeBideau[2], Josefa Salgado[1], Luis Miguel Varela[1]

[1]*NaFoMat group, departments of Física de Partículas and Física Aplicada, Rúa de José María Suárez Núñez, s/n, 15782 Santiago de Compostela, A Coruña, Spain.*
[2]*Institut des Matériaux Jean Rouxel (IMN) Université de Nantes - CNRS (UMR 6502) 2 rue de la Houssinière B.P.32229, 44322 Nantes cedex 3 – France.*

*e-mail: Pablo.vallet.moreno@usc.es

Current electrolytes in Li-ion batteries are composed, mainly, by a mixture of carbonates and lithium salt, and, as it was widely reported, they have significant security and efficiency issues such as high flammability and high vapour pressure [1]. Additionally, and from an industrially point of view, liquid electrolytes present implementation problems in mass production on the assembly line due to the possibility of spillage.

To solve these industrial questions, the implementation of solid (or semi-solid) electrolytes with similar, or, if possible, better electrochemical properties than currently used is one of the objectives of 4th generation of Li-ion batteries.

As it is well known, Ionic liquids (ILs) are characterized by amazing features like high thermal stability, negligible vapor pressure, high ionic conductivity, non-flammability, low toxicity and high electrochemical window among others [2-5] and then, they have been studied as smart electrolytes during the last decade. Furthermore, ILs and its mixtures with inorganic salts of electrochemistry interest, as lithium salts, can be encapsulated in rigid scaffolds (silica scaffolds, for example) without important changes on the main properties of the electrolytic mixture to conform a semisolid electrolyte, although before the industrial implementation further and deeper studies must be performed.

Figure 1.- Semisolid nano-encapsulated IL electrolyte in a silica scaffold.

In this work, the effect of the addition of Lithium nitrate salt to ammonium and imidazolium nitrate based ILs is studied by means of different experimental techniques such as broad band dielectric spectroscopy (BBDS), ionic conductivity, cyclic voltammetry (CV), nuclear magnetic resonance (NMR), Fourier Transform Infrared (FT-IR), density and viscosity, differential scanning calorimetry (DSC) and thermogravimetric analysis (TGA). Additionally, the nanoencapsulation of these mixtures in silica scaffolds was preformed and samples were analysed with the same experimental techniques and procedures and results were compared with the obtained for the bulk liquid samples.

[1] T. Vogl, S. Menne, A. Balducci, Phys. Chem. Chem. Phys. 16, 25014–25023 (2014).
[2] O. Russina, R. Caminiti, T. Méndez-Morales, J. Carrete, O. Cabeza, L.J. Gallego, L.M. Varela, A. Triolo, *J. Mol. Liq.* **205**, 16 (2015).
[3] H. Porthault, C. Calberg, J. Amiran, S. Martin, C. Páez, N. Job, B. Heinrichs, D. Liquet, R. Salot, *J. Power Sources* **482**, 229055 (2021).
[4] J.J. Parajó, P. Vallet, L.M. Varela, M. Villanueva, J. Salgado, *Environ. Sci. Pollut. Res.* **29**, 24983 (2022).
[5] P. Vallet, S. Bouzón-Capelo, T. Méndez-Morales, V. Gómez-González, Y. Arosa, R. de la Fuente, E. López-Lago, J.R. Rodríguez, L.J. Gallego, J.J. Parajó, J. Salgado, M. Turmine, L. Segade, O. Cabeza, L.M. Varela, *J. Mol. Liq.* **350**, 118483 (2022).

Acknowledgements: This work was supported by Spanish Ministry of Economy and Competitiveness and FEDER Program through the projects, MAT2017-89239-C2-1-P as well as by Xunta de Galicia through GRC ED431C 2020/10 project and the Galician Network of Ionic Liquids (ReGaLIs) ED431D 2017/06. P. Vallet and J. J. Parajó thank funding support of FPI Program from Spanish Ministry of Science, Education and Universities and I2C postdoctoral Program of Xunta de Galicia, respectively.

Análisis de cristalización de hidrato de metano en un poro de sílice empleando Dinámica Molecular

Angel Manuel Fernández Fernández[1], **María M. Conde**[2], **Germán Pérez Sánchez**[3] **Martín Pérez Rodríguez**[1], Manuel Martínez Piñeiro[1*]

[1]*CINBIO, Departamento de Física Aplicada, Universidade de Vigo, España.*, [2]*Dpto. de Ingeniería Química Industrial y Medio Ambiente, Escuela Técnica Superior de Ingenieros Industriales, Universidad Politécnica de Madrid, 28006, España,* [3]*Departamento de Química, CICECO, Universidade de Aveiro, Portugal*
*e-mail: mmpineiro@uvigo.es

Los hidratos de gas son compuestos cristalinos de inclusión no estequiométricos formados por moléculas de agua y pequeños gases como CO_2, H_2S, N_2, gases nobles o pequeños hidrocarburos, como el CH_4, C_2H_6 o C_3H_8. Los hidratos de gas se obtienen a presiones moderadas y temperaturas en torno a 0ºC siendo el hidrato de metano el más abundante en la naturaleza y del que se estima que hay enormes cantidades en fondos marinos y bajo el permafrost continental. Estos depósitos podrían suponer una estratégica fuente de energía [1]. El metano se obtiene por descomposición de la materia orgánica que fluye verticalmente hasta encontrarse con el permafrost o el fondo oceánico, saturando el agua que se encuentra empapando los espacios intergranulares de las rocas sedimentarias. En este ambiente confinado de alta presión y baja temperatura, el gas queda atrapado en forma de hidrato.

En este trabajo se estudia el crecimiento del hidrato de metano confinado en un poro de silice empleando Dinámica Molecular (DM). Se emplean campos de fuerzas atomísticos OPLS-AA para la sílice (α-cuarzo) y el metano y el rígido no polarizable TIP4P/Ice [2] para el agua. Se diseñó un poro plano α-cuarzo de $4.022 \times 4.022 \times 9.26$ nm dejando un espacio hueco de 7nm. Se eliminaron los silicios terminales y los oxígenos se saturan con hidrógeno para obtener la neutralidad del sistema. El poro quedó formado por 1536 átomos de oxígeno, 704 de silicio y 256 de hidrógeno. En el centro del poro se situó una semilla de hidrato formada por 8 celdas unidad de la esturtura sI, que hacen un total de 368 moléculas de agua y 64 de metano. Ésta se rodeó por 2272 moléculas de agua, dejando un pequeño espacio a ambos lados del poro que se llenó con 256 moléculas de metano.

Se aplicaron condiciones periódicas de contorno, radio de corte 1.5nm y se el método de las sumas de Ewald para las correcciones electrostáticas de largo alcance. Se realizaron simulaciones NVT a 260 y 270K y en el colectivo NpT a 260K y 100bar, para lo cual se empleó el termostato de Nosé-Hoover y el barostato de Parrinello-Raman. Todas las simulaciones se llevaron a cabo con el software GROMACS/2021.1.

Las simulaciones fueron del orden de 500ns, hasta que se alcanzó el equilibrio y después se estableció un periodo de producción de 200ns más. Al final de la simulación, las celdas del hidrato se observan desplazadas y ligeramente deformadas con respecto a la posición inicial de la semilla, por lo que para caracterizar la estructura obtenida se obtuvieron los perfiles de densidad y se calcularon los parámetros de orden F_3 [3] y F_4 [4] así como el ángulo del enlace de hidrógeno promediados durante el periodo de producción y a lo largo del eje Z. Todos ellos muestran como el metano, inicialmente situado junto a las paredes de sílice, es sustituido por moléculas de agua que quedan fuertemente adsorbidas por puentes de hidrógeno. Los parámetros de orden muestran que esta capa adsorbida se trata de un fluido y que el metano queda atrapado como hidrato en el interior del poro. Las deformaciones que se observan en el cristal se deben posiblemente a la imposición del confinamiento al que se ve sometido el cristal que no puede crecer con total libertad en las tres direcciones.

[1] E. D. Sloan and C. Koh, *Clathrate Hydrates of Natural Gases 3rd Edition*, CRC Press, (2007).
[2] J. L. F. Abascal, E. Sanz, R. García-Fernández, C. Vega, *J.Chem.Phys.* **23** 234511 (2005).
[3] L. Baez, P. Clancy, *Ann. N. Y. Acad. Sci.* **1** 177-186 (1994).
[4] P. Rodger, T. Forester, W. Smith, *Fluid Ph. Equilibria* **116** 326-332 (1996).

Agradecimientos: Ministerio de Economía y Competitividad [grant No. FIS2015-68910-P] proyecto cofinanciado por el Fondo Europeo Desarrollo Regional, FEDER, Sudoe EU Program KET4F-Gas [grant No. SOE2/P1/P0823]; Consellería de Educación Universidade y Formación Profesional, Xunta de Galicia [FSE-GALICIA 2014-2020]; CICECO-Aveiro Institute of Materials, UIDB/50011/2020, UIDP/50011/2020 & LA/P/0006/2020, financiado por los fondos nacionales FCT/MEC (PIDDAC) y FCT – Fundação para a Ciência e a Tecnologia, I.P.; MICINN (Grant No. PID2019-105898GA-C22), CAM and UPM (Project No. APOYO - JOVENES - 01HQ1S-129-B5E4MM) Universidad Politécnica de Madrid (www.upm.es, Magerit Supercomputer) y Centro de Supercomputación de Galicia (CESGA, www.cesga.es).

Thermal analysis of magnetic materials

J. Daza, **J. J. Suñol***, W. Ben Mbarek, J. Saurina, L. Escoda

Department of Physics. University of Girona, Campus Montilivi s/n, 17003 Girona, Spain.

*e-mail: joanjosep.sunyol@udg.edu

Microstructural changes in soft and hard magnetic materials can provoke the loss or the improvement of the desired magnetic behaviour. Thermal analysis techniques are useful to provide information about the characteristic temperatures at which these structural transformations (as well as the magnetic transformations: Curie or Néel) occurs. Likewise, thermodynamic parameters as the enthalpy and entropy changes and, the specific heat can also be obtained from calorimetry.

In this work, we analyse some soft magnetic Fe, Ni, Fe-Co and Fe-Mn rich alloys produced by mechanical alloying (powdered particles). At low temperatures, differential scanning calorimetry (DSC) scans show broad exothermic processes linked to the release of the mechanically induced microstrain. At higher temperatures (> 600 K), exothermic peaks linked to the grain growth of the nanocrystalline alloys are found. The activation energy of the crystallization process can be determined by analysing (Kissinger linear method) the DSC scans at different heating rates. Fig. 1. Show the linear fitting of the main crystallization process of some Fe-rich alloys. Higher transition temperature and activation energy indicate higher thermal stability.

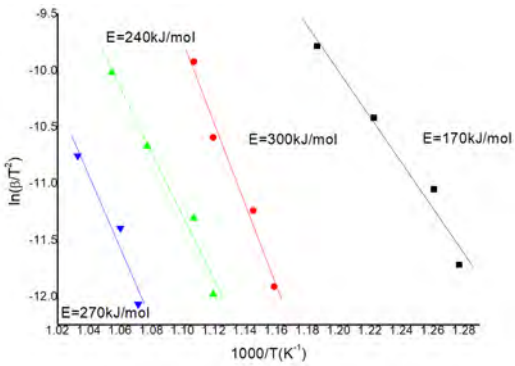

Figure 1. Activation energy of the main crystallization processes of some Fe rich alloys (Kissinger linear fitting method).

The optimized design of annealing temperature-time conditions favour the development of alloys with improved soft magnetic behaviour: high magnetization of saturation, high remanence and low coercivity [1]. Furthermore, the controlled addition of magnetic and non-magnetic elements shifts the functional magnetic response and the working temperature interval. The production of these magnetic materials with the desired nanocrystalline microstructure is a field of continuous research [2]. Temperature diagrams can be obtained. Fig. 2. shows the transformation temperatures of Ni rich (Heusler) alloys with a martensitic transformation.

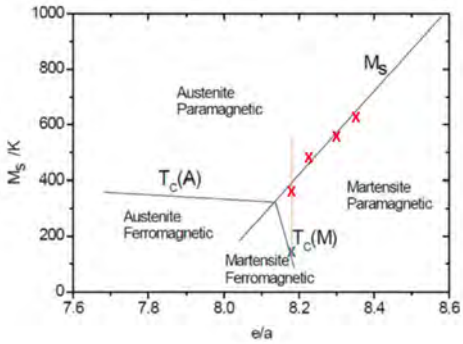

Figure 2. Transformation temperatures diagram: some Heusler alloys with martensitic transformation.

The enthalpy and entropy changes are determined by the integration of the DSC signal. Furthermore, in multi-component alloys the mixing enthalpy is a key parameter. Mechanical alloying favour the extension of the solubility limits and a minor effect of the mixing enthalpy constraints.

[1] A. Carrillo, J. Daza, J. Saurina, L. Escoda, J.J. Suñol, *Materials* **14**, 4542 (2021).
[2] J. Daza, W. Ben Mbarek, L. Escoda, J.J. Suñol, *Metals* **11**, 1896 (2021),

Acknowledgements: Financial support from the PID2020-115215RB-C22 project.

Calorimetric and electrochemical studies of lithium salt dissolved in pure ethylammonium nitrate ionic liquid

J. J. Parajó[1,2,*], P. Vallet[1], J. Salgado[1], M. Villanueva[1], O. Cabeza[3], L.M. Varela[1], A.T.S.C. Brandao[2], C.M. Pereira[2], R. Costa[2]

[1]*Grupo NaFoMAT. Departamentos de Física Aplicada y Física de Partículas. Facultade de Física. Instituto de Materiales (iMATUS). Universidade de Santiago de Compostela.* [2]*CIQUP, Institute of Molecular Sciences (IMS) - Departamento de Química e Bioquímica, Faculdade de Ciências da Universidade do Porto.* [3]*Grupo Mesturas. Departamento de Física y Ciencias de la Tierra. Universidade de A Coruña.*

*e-mail: juanjose.parajo@usc.es

The most relevant properties of Ionic Liquids (ILs) are their wide electrochemical windows, high thermal stabilities, non-flammability, and the possibility of tuning their conductivities by adding stable inorganic salts. The interfacial phenomena associated to electrochemical processes will depend not only on the properties of the two phases involved as well as the interfacial properties, which are distinct from the bulk adjacent phase.

The importance of calorimetric studies and the inexistence of a model that allows the systematic prediction of the effect of adding salts on the electric double layer (EDL) structure, imposes complex challenges for the formulation of the IL + inorganic salt electrolyte mixtures. The addition of lithium salts is highly reported due to their importance for energy storage applications and the need to work at high concentration levels (0.5 or 1 M lithium salts concentrations are commonly used) [1].

Differential scanning calorimetry (DSC) and termogravimetry (TGA) were used in this work to determine the liquid window, which is essential to get a useful operation temperature range for a selected electrolyte. The lowest limit of liquid range of the fluids, associated to melting or glass transition temperatures, was determined using differential scanning calorimetry (DSC), whereas the upper limit, which is given by degradation or boiling temperatures, was stablished by means of thermogravimetric analysis (TGA). The main conclusion of this study was that salt addition induces melting-point depressions, but no boiling point elevations were detected. [2]

The electrochemical properties of the Hg/ethylammonium nitrate interface were followed through the interpretation of differential capacity curves and potential of zero charge values based on an acceptable model that accurately describes the effect of chemical nature of ions in the EDL thickness [3]. The selection of non-structured mercury electrode allowed to decouple the template effect of the surface in defining the anatomy of the double layer structure. The model followed to estimate the thickness of the charge plane of the adjacent layer to the electrode by the EAN was based on a simple Helmholtz model and its applicability was validated with the ions size obtained independently using informatic tools. After the method validation, the EAN was mixed with different molalities of $LiNO_3$, focussing on concentrations below 0.1 m and extending the study to the saturation range (2 m).

The correlation between differential capacitance, pzc and charge density curves vs. the mixture composition was obtained. The asymmetric U-shaped of the C(E) curves measured at the Hg/pure EAN are not affected by the presence of the inorganic ions from the salt, however, the values of thickness of the double layer estimated from the integral capacities' present non-monotonic behaviour (e.g., the thickness of the charge plane at rational negative potentials increase for a specific range of lithium molalities).

[1] A. Martinelli, A. Matic, P. Jacobsson, L. Börjesson, A. Fernicola, and B. Scrosati, *J. Phys. Chem. B* **113**, 11247 (2009).
[2] J. Salgado, J.J. Parajó, M. Villanueva, J.R. Rodríguez, O. Cabeza, L.M. Varela, *J. Chem Thermodyn.* **13**, 164 (2019).
[3] R. Costa, C. M. Pereira and F. Silva, *Phys. Chem. Chem. Phys.* **12**, 11125 (2010).

Acknowledgements: The authors thank: Fundaçao para a Ciência e Tecnologia (FCT), for financial support (funded by national funds through the FCT/MCTES (PIDDAC)) to CIQUP, Faculty of Sciences, University of Porto (Project UIDB/00081/2020) and IMS- Institute of Molecular Sciences", LA/P/0056/2020; to Spanish Ministry of Economy and Competitiveness and FEDER Program through the projects, MAT2017-89239-C2-1-P as well as by Xunta de Galicia through GRC ED431C 2020/10 project and the Galician Network of Ionic Liquids (ReGaLIs) ED431D 2017/06. J. J. Parajó and P. Vallet thank funding support of I2C postdoctoral Program of Xunta de Galicia and FPI Program from Spanish Ministry of Science, Education and Universities, respectively. R. Costa thank FCT for funding through program DL 57/2016 – Norma transitória (SFRH/BPD/89752/2012).

Calorimetría de mezclas binarias de L-carvona con alcoholes de cadena corta C_2-C_3

José F. Martínez López[1,*], Ana Mª Jiménez Morales[2], Juan I. Pardo Fernández[2], José S. Urieta Navarro[2], Alejandro Bautista Avis[2], Ana Mª Mainar Fernández[2]

[1]*Instituto de Investigación Mixto Agroalimentario de Aragón (IA2), Universidad de Zaragoza, 50013 Zaragoza.*
[2]*Instituto de Investigación en Ingeniería de Aragón(I3A), Universidad de Zaragoza, 50018 Zaragoza.*

*e-mail: jfmarti@unizar.es

La determinación experimental de propiedades termofísicas de mezclas de compuestos presentes en aceites esenciales de plantas con alcoholes es importante de cara al diseño de instalaciones y procesos de extracción. El compuesto R-carvona o L-carvona, designado según IUPAQ) como (5R)-5-Isopropenil-2-metil-2-ciclohexen-1-ona, (Figura1), es una cetona quiral, terpenoide monocíclico, que está presente en los aceites volátiles de la hierbabuena (*Mentha spicata*). Usado en la industria alimentaria y en productos ambientadores y aromaterapia, su importante bioactividad y propiedades ha sido recientemente revisada [1].

Figura 1. L-carvona.

En este trabajo se presenta un estudio de las capacidades caloríficas molares a presión atmosférica ($C_{P,m}$) para mezclas binarias formadas por L-carvona con etanol y con propanol. Las capacidades caloríficas de estas mezclas se han medido entre 298.15 y 328.15 K, cada 10 grados, en todo el rango de composición. Las medidas se han realizado mediante un calorímetro de tipo Calvet de la firma Setaram, modelo C80. El procedimiento experimental y los cálculos implicados han sido descritos en un trabajo previo [2].

Las capacidades caloríficas molares de exceso, $C^E_{P,m}$ obtenidas de los datos experimentales se han comparado con las calculadas mediante el método *COSMO-RS* y mediante *UNIFAQ*. En todas las mezclas los resultados obtenidos mediante *COSMO-RS* presentan mejores resultados que los obtenidos mediante *UNIFAQ*.

En la figura 2, se muestran los resultados obtenidos para las mezclas de L-carvona (1) + etanol (2).

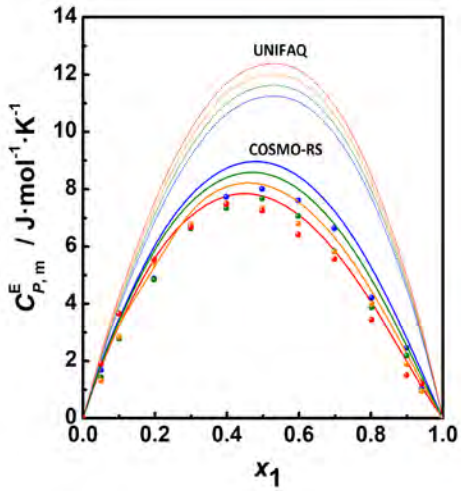

Figura 2. Capacidades caloríficas molares de exceso para las mezclas: L-carvona(1) + etanol(2) a las temperaturas de 298,15 K (●); 308,15 (■); 318,15 K (■) y 328,15 (●)

[1] Pina, L.; Serafini, M.; Oliveira, M.; Sampaio, L. *Phytochemistry*, **196**, 113080 (2022).
[2] Martínez, J.F.; Schneider, S.; Salavera, D.; Mainar, A.M.; Urieta J.S.; Pardo, J.I. *J. Chem. Thermodynamics* **92**, 146 **(**2016).

Agradecimientos: Los autores agradecen el apoyo financiero proporcionado por el Gobierno de Aragón: Departamento de Ciencia, Universidad y Sociedad del Conocimiento (Grupo E39_20R).

Development of real-time polymerase chain reaction methods for the quantification of Methanoculleus, Methanosarcina and Methanobacterium in anaerobic digestion

Consolación Sánchez-Sánchez[1,*], Mercedes Aranda-Medina[2], Alicia Rodríguez[3], Alejandro Hernández[3], María G. Córdoba[3], Francisco Cuadros-Blázquez[1], Santiago Ruiz-Moyano[3]

[1]*Departamento de Física Aplicada, Escuela de Ingenierías Agrarias, Universidad de Extremadura, Avda. de Adolfo Suárez S/n, 06007, Badajoz, Spain.* [2]*Expresión Gráfica, Escuela de Ingenierías Industriales, Campus Universitario, Av de Elvas sn 06006, Badajoz, Spain.* [3]*Instituto Universitario de Investigación de Recursos Agrarios (INURA), Escuela de Ingenierías Agrarias, Universidad de Extremadura, Avda. Adolfo Suarez, s/n, 06071, Badajoz, Spain.*

*e-mail: consolis@unex.es

Due to the great environmental impacts generated by the processes of obtaining conventional energy, in recent years, more and more companies are betting on other sources of renewable energy such as Anaerobic Digestion (AD) technology. To promote this technology, it is essential to know at the molecular level the dynamics of microbial communities, the correlations between environmental variables and methanogenic community structure.

In the present study, three primer pairs were selected from seven primer pairs which were designed and tested with different concentrations and conditions to detect Methanosarcina, Methanoculleus and Methanobacterium by real-time polymerase chain reaction (PCR) based on the SYBR Green System.

The functionality of the developed methods was demonstrated by the high linear relationship of the standard curves, and the specificity of each primer was empirically verified by testing DNA isolated from methane-producing and non-producing strains. These assays also exhibited good repeatability and reproducibility, which indicates the robustness of the methods.

The described primers were successfully used to investigate the methanogenic communities of 10 samples from an anaerobic co-digestion of tomato industry. Ct values below 28 were obtained for each of the primer pairs designed. The genus Methanosarcina was the dominant methanogenic group.

Acknowledgements: Funding: This study was supported by the Junta de Extremadura and the European Social Fund for the financial support received through the aid destined to the training of predoctoral personnel PD18050 (Consolación Sánchez-Sánchez), by the Junta de Extremadura and the European Union (FEDER funds) through the projects with Ref.: GR21012.

Effective two-body potentials for fluid argon including three-body interactions

J. R. Solana
Department of Applied Physics, University of Cantabria, Spain.
e-mail: solanajr@unican.es

Sadus et al. [1,2] proposed the following simple relationship between the three-body E_3 and two-body E_2 contributions to the configurational energy of Ar, Kr and Xe

$$\frac{E_3}{E_2} = \lambda \frac{\nu\rho}{\varepsilon\sigma^6},$$

where $\rho = N/V$ is the number density, ν is the nonadditive parameter, ε is the potential depth and σ the distance at which the pair potential $u(r) = 0$. This relationship, which was derived on the basis of computer simulations in the liquid phase at subcritical temperatures considering the Barker-Fisher-Watts (BFW) potential for the two-body (2B) interactions and the Axilrod-Teller (AT) approximation for thre three-body (3B) interactions, allows to incorporate the 3B interactions into an effective 2B potential, which simplifies the calculations either from theory or from computer simulations. A value $\lambda = -2/3$ was reported in [1], but from further simulations a value $\lambda = -0.85$ was recommended [2].

The aim of this work is twofold. On the one hand, to analyze whether a similar relationship holds for the Lennard-Jones potential. On the other hand, to see whether the relationship still holds for spercritical temperatures and wider density ranges.

To this end, first we have carried out Monte Carlo NVT computer simulations to obtain the 2B and 3B contributions to the configurational energy for Ar with the LJ and BFW potentials at tempertature $T = 140\,\mathrm{K}$, that corresponds to reduced temperatures $T^* = kT/\varepsilon = 0.9853$ and $T^* = 1.1686$ for BFW and LJ potentials, respectively, and reduced densities in the liquid range $0.5 \leq \rho^* \leq 0.7$, with $\rho^* = \rho\sigma^3$. The results, shown in Fig. 1, are consitent with the roughly constant value of λ reported in [1,2]. Our results provide $\lambda = -0.77$ for LJ and $\lambda = -0.88$ for BFW.

Next, we have carried out simulations for wide ranges of temperatures and densities, including supercritical temperatures. The results are shown in Fig. 2, from which it is clear that the parameter λ must have a more complex dependence on temperature and density than reported in refs. [1,2].

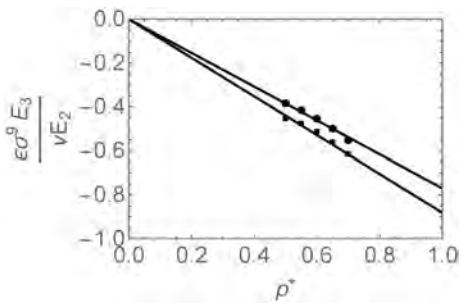

Figure 1: Ratio of the three-body to two-body energies for argon at $T = 140\,\mathrm{K}$ with the LJ (circles) and BFW (squares) potentials as a function of the reduced density ρ^*. The solid lines are linear fittings.

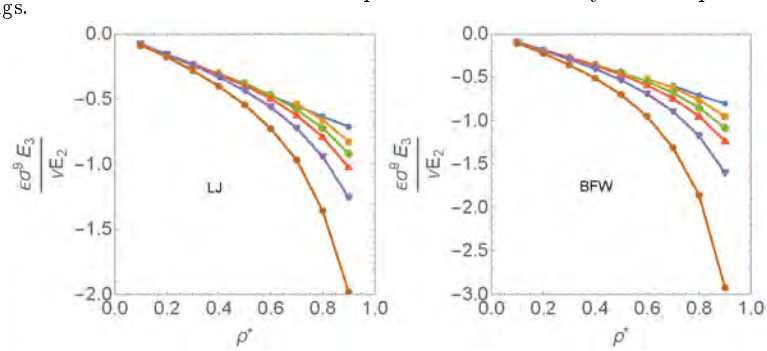

Figure 2: Ratio of the 3B to 2B energies for argon with the LJ (left) and BFW (right) potentials as a function of the reduced density ρ^* for reduced temperatures $T^* = 0.7, 1.0, 1.5, 2.0, 3.0$, and 5.0, respectively, from top down. (Note that the reduced temperatures are not equivalent for both potentials because the values of ε are different). The curves are guides for the eye.

[1] G. Marcelli, R. J. Sadus, *J. Chem. Phys.* **112**, 6382 (2000).
[2] L. Wang, R. J. Sadus, *J. Chem. Phys.* **125**, 074503 (2006).

Thermophysical characterization of peloids enriched with microalgae

C. P. Gómez, A. Kashyap, M. M. Mato, T. P. Iglesias, M. L. Mourelle, **J. L. Legido***

Department of Applied Physics, University of Vigo, Campus As Lagoas Marcosende s/n, 36310 Vigo, Spain.

*e-mail: xllegido@uvigo.es

In this work, the thermophysical properties of mixtures of a clay, mineral water and the microalgae are presented. These types of mixtures are called peloids [1]. Peloids are thermotherapeutic agents that are used in numerous spas and thermal centres, their behaviour depends on their physical properties and these properties will determine its form of application.

The properties studied are density, specific heat, thermal conductivity, and thermal diffusivity as a function of the concentration of the water, at atmospheric pressure and a temperature of 308.15 K.

The specific heat has been determined using a CALVET microcalorimeter [2]. The density of the mixtures was carried out by a pycnometric method [3]. A Decagon KD2 Pro conductivity meter was used to measure thermal conductivity [4]. Thermal diffusivity was calculated from the data obtained on thermal conductivity, density and specific heat [5].

The properties studied will help in choosing the most suitable type of application for each mixture for the different applications in the field of cosmetics, thermalism and wellness [6,7].

[1] C. Gomes, M.I. Carretero, M. Pozo, F. Maraver, P. Cantista, F. Armijo, J.L. Legido, F. Teixeira, M. Rautureau, R. Delgado. *Applied Clay Science* **75–76**, 28 (2013).
[2] M.M. Mato, L.M. Casás, J.L. Legido, C.P. Gómez, L.M. Mourelle, D. Bessières, F. Plantier. *J. Therm. Anal. Calorim*. **130**, 479 (2017).
[3] N. Glavas, M.L. Mourelle, C.P. Gómez, J.L. Legido, N.R. Smuc, M. Dolenec, N. Kovac. *Appl. Clay Sci.* **135**, 119 (2017).
[4] V. Caridad, J.M. Ortiz de Zárate, M. Khayet, J.L. Legido, *Appl. Clay Sci*. **93-94**, 23 (2014).
[5] L.M. Casás, M. Pozo, C.P. Gómez, E. Pozo, D. Bessières, F. Plantier, J. L. Legido, *Appl. Clay Sci.* **72**, 18 (2013).
[6] L. Mourelle, C.P. Gómez, J.L. Legido, *Cosmetics* **4**, 46 (2017).
[7] L. Mourelle, C.P. Gómez, J.L. Legido, *Mar. Drugs* **19**, 666 (2021).

Acknowledgements: We thank María Perfecta Salgado González for her collaboration with the technical measurements. We are also thankful for the financial support provided by the project ED431C 2020/06 V055 by ‘‘Xunta de Galicia’’ of Spain. This project is co-financed with FEDER funds.

Study of the thermal properties of mixtures of clays and thermal waters of Latin America

D. Fernández-Marcos, C. P. Gómez, M. M. Mato, T. P. Iglesias, M. L. Mourelle, **J. L. Legido***

Department of Applied Physics, University of Vigo, Campus As Lagoas Marcosende s/n, 36310 Vigo, Spain.

*e-mail: xllegido@uvigo.es

In most Latin American countries there are places where mixtures of clay and thermal water are used for therapeutic and cosmetic purposes. In Argentina, in the Copahue thermal complex in the state of Neuquén, a peloid is used therapeutically [1]. In Brazil, the so-called Peruíbe Black Mud is well known [2]. Other mixtures are the Chilca salt mines in Peru [3], the San Vicente Hot Springs in Ecuador [4], Cubagua in the Margarita Islands in Venezuela [5], and in Colombia in the Totumo volcano in Cartagena [6].

In Central America we can also find different types of peloids, such as in the Arenal volcano in the area of Fortuna in Costa Rica [7], and in the Caribbean islands, the mixtures of Cuba stand out in the Baños de San Diego and Pinar del Rio [8].

In this work, the thermal properties (specific heat, thermal conductivity, density and thermal diffusivity) of mixtures of clays with thermal waters from Latin America are studied.

The thermal conductivity has been measured with the Decagon KD2 Pro probe [9], the specific heat has been determined using a CALVET microcalorimeter [10], the density of the mixtures was determined by a pycnometric method [11]. Thermal diffusivity was calculated from the data obtained on thermal conductivity, specific heat and density [12].

[1] M. Baschini, G. Pettinari, J. Vallés, C. Aguzzi, P. Cerezo, A. López-Galindo, M. Setti, C. Viseras. *Appl. Clay Sci.* **49**, 205-212 (2010).
[2] P. Gouvêa, Z. Britschka, C. Gomes, N. Queiroz, P. Salvador, P. Silva. *Int. J. Environ. Res. Public Health* **18**, 1666 (2021).
[3] M. L. Cerón Loayza, N. Raysa Furet, J. Bravo Cabrejos, A. Bustamante Dominguez, J. Quispe Marcatoma, A. Trujillo Quinde, *Revista de Investigación de Física* 8 (2), (2005).
[4] J.E. Parrales Villamar, Tesis, Universidad de Guayaquil. Ecuador. 2015.
[5] Hernández A.C., Sánchez-Espejo R., Meléndez W., González G., López-Galindo A., Viseras C., *Appl. Clay Sci*, **175**, 30-39 (2019).
[6] D. Luccio, I. Banda Guerra, L.E. Correa Valero, D. F. Morales Giraldo, S. Maggi, M. Palmisano, *Science of the Total Environment* **759**, 144225, (2021).
[7] G.L. Madrigal Redondo, R. Vargas Zúñiga, G. Carazo Berrocal, N. Ramírez Arguedas. *Int. J. of Pharmacy and Analytical Research* **4**(4), 418 (2015).
[8] M. Suarez Munoz, C. Melian Rodriguez, A. Gelen Rudnikas, et al. *Appl. Clay Sci*. **36-47**, 104 (2015).
[9] M.M. Mato, L.M. Casás, J.L. Legido, C.P. Gómez, L.M. Mourelle, D. Bessières, F. Plantier. *J. Therm. Anal. Calorim.* **130**, 479-484 (2017).
[10] N. Glavas, M.L. Mourelle, C.P. Gómez, J.L. Legido, N.R. Smuc, M. Dolenec, N. Kovac. *Appl. Clay Sci.* **135**, 119 (2017).
[11] V. Caridad, J.M. Ortiz de Zárate, M. Khayet, J.L. Legido, *Appl. Clay Sci.* **93-94**, 23 (2014).
[12] L.M. Casás, M. Pozo, C.P. Gómez, E. Pozo, D. Bessières, F. Plantier, J. L. Legido. *Appl. Clay Sci.* **72**, 18 (2013).

Acknowledgements: We thank María Perfecta Salgado González for her collaboration with the technical measurements. We are also thankful for the financial support provided by the project ED431C 2020/06 V055 by ‘‘Xunta de Galicia’’ of Spain. This project is co-financed with FEDER funds.

Density of alumina nanofluids (15 nm) in water at different temperatures

Â. Queirós[1, 2], M. F. Coelho[1, 2], M. A. Rivas[2], J. L. Legido[2], T. P. Iglesias[2]

[1]*CIETI-Centro de Inovação em Engenharia e Tecnologia Industrial, ISEP, Porto, Portugal.*
[2]*Departamento de Física Aplicada, Universidade de Vigo, Campus As Lagoas Marcosende s/n, 36310 Vigo, Spain.*

*e-mail: apoqu@isep.ipp.pt

Following our study about thermophysical properties of nanofluid [1-5] in this work the density of alumina (15 nm) nanoparticles in water is presented. The density of the mixtures was carried out by a pycnometric method. The measurements were carried out at various concentrations (up to 2% in volume) at atmospheric pressure and at twelve temperatures (from 288.15 K to 343.15 K).

The study shows the influence of the volume fraction and temperature on this quantity showing a linear increment as the volume fraction increases. This linear behaviour is described empirically by Pak and Cho [6] equation.

The enhancement of density, defined as the ratio of the nanofluid density and that of the base fluid, was calculated and its behaviour was analysed. It is discussed whether their positive values can be considered greater than what would be expected. The contributions to density of these nanofluids from water and nanoparticles are separated.

[1] T. P. Iglesias, M. A. Rivas, R. Iglesias, J. C. R. Reis, F. Coelho, *J. Chem. Thermodyn.* **66**, 123 (2013).
[2] R. Iglesias, M. A. Rivas, J. C. R. Reis, T. P. Iglesias, *J. Chem. Thermodyn.* **89**, 189 (2015).
[3] M. F. Coelho, M. A. Rivas, E. M. Nogueira, T. P. Iglesias, *J. Chem. Thermodynamics* **158**, 106423 (2021).
[4] M. F. Coelho, M. A. Rivas, G. Vilão, E. M. Nogueira, T. P. Iglesias, *J. Chem. Thermodynamics* **132**, 164 (2019).
[5] T. P. Iglesias, G. Vilão, J. C. R. Reis, *Journal of Applied Physics* **122**, 074102 (2017).
[6] B. C. Pak and Y. I. Cho, *Experimental Heat Transfer an International Journal* **11**, 151 (1998).

Acknowledgements: We thankful to 'Xunta de Galicia' of Spain the financial support provided by the project ED431C 2020/06 V055. This project is co-financed with FEDER funds.

Thermal analysis of Eco-Friendly Soap-Based Firefighting Foam. Effect of the bentonite addition

F. Muiño-Blanco[1,2,*], J. J. Parajó[1], M. Villanueva[1], S. González-Prieto[2], J. Salgado[1]

[1]*Grupo NaFoMAT. Departamento de Física Aplicada, Facultad de Física, Universidad de Santiago de Compostela. 15782 Santiago de Compostela. A Coruña. Spain.*
[2]*Misión Biológica de Galicia. Sede de Santiago de Compostela. CSIC. 15706 Santiago. A Coruña. Spain.*

*e-mail: fatima.muino@mbg.csic.es

Flame retardant agents are natural or synthetics additives used for improving the effectiveness of water in extinction fire. Their effectiveness mainly depends on its ability to increase water retention and prolong the isolation time of the fuel from the source of ignition and/or oxygen by including foaming agents, moisturizers and/or superabsorbents in its composition. However, currently the most used fire extinguishing agent is still water, essentially because of the side-effects of phosphorous, nitrogen, sulphur, fluorine and aluminium contents of extinguishing agents that can cause the pollution into rivers and forest surroundings after their application.

The concern about the environmental effects of these flame retardant agents has led to the search for alternative formulations with less impact or "eco-friendly" increased during the last years [1]. Thus, firefighting foams involving naturally derived fatty acid salts (soap) as the main component have recently been developed. In particular, Kawahara and collaborators [2] proposed a mixture of potassium laurate, potassium oleate and sodium oleate, as the soap components, with methylglycinediacetic acid (MGDA), propylene glycol, hexylene glycol and water. So far, these efforts on searching short-term firefighting foams have been focussed on their toxicity towards aquatic and/or semiaquatic environments, although their effect on terrestrial ecosystems is still unknown [3].

In the present work, an optimization of the flame retardant of Kawahara *et al*. [2] is proposed by the addition of bentonite clay (with weight concentrations of 1%, 2%, 3%, 4% and 8%), which can retain water longer during exposure to the heat source. Thermal behaviour of these samples by means of differential scanning calorimetry and thermogravimetry was studied obtaining that the evaporation peak of water showed a shift towards higher temperatures with the intermediate concentrations (2% and 3%) of bentonite.

Finally, the effect of the retardant was checked, in laboratory, in a soil exposed to thermal shocks at different temperatures in terms of carbon content reduction.

[1] H. Mizuki, K. Uezu, T. Kawano, T. Kadono, M. Kobayashi, S. Hatae, Y. Oba, S. Iwamoto, S. Mitumune, Y. Nagatomo, Y. Owari, H. Umeki, Y. Ymagaga, *Journal of Environmental Engineering and Management* **16**, 403 (2007).
[2] T. Kawahara, S Hatae, T. Kanyama, Y. Ishizaki K. Uezu. *Environ. Control Biol.* **54** (1), 75 (2016).
[3] T. Kawano, K. Otsuka, T. Kadono, R. Inokuchi, Y. Ishizaki, B. Dewancker, K. Uezu, *Advanced Materials Research* **875-877**, 699 (2014).

Acknowledgements: This work was supported by Fundación Humanismo y Ciencia through the project 2021-PO025. J. J. Parajó thank funding support of I2C postdoctoral Program of Xunta de Galicia. Authors also acknowledge M. Gómez (RIAIDT-USC) for the technical support in thermal analysis measurements.

Broad Band Dielectric Spectroscopy of nanofluids

Pablo Vallet[1,*], Noelia Freire[2], Juan José Parajó[1], Josefa Salgado[1], Alfredo Amigo[2]

[1]*Grupo NaFoMat, Departamento de Física Aplicada, Universidade de Santiago de Compostela, Campus Vida s/n, 15782, Santiago de Compostela, Spain.*
[2]*Propiedades Termofísicas e Superficiais de Líquidos. Departamento de Física Aplicada, Universidade de Santiago de Compostela, Campus Vida s/n, 15782, Santiago de Compostela, Spain.*

*e-mail: pablo.vallet.moreno@usc.es

Nanofluids are composed by a mixture of, at least, a base lubricant and dispersed nano additives particles, as Choi defined in 1995 [1]. Usually, nanofluids are studied with the aim to obtain the best equilibrium between increase in thermal conductivity (positive effect) and viscosity (negative effect) and many bibliographic studies can be found in this field.

Since the global economy is moving to a decarbonized system of production to reduce the CO_2 emissions, electric vehicles (EVs) are increasing rapidly in manufacturing and attention [2]. Hence, the lubricants need to comply new safety requirements, since many EVs are built alternating permanent magnet synchronous motor and current induction motors [3]. Here, the dielectric constant and the electrical conductivity, obtained by electrochemical impedance spectroscopy (EIS), are critical parameters to ensure the proper operation inside the electrical motor (EM). As the last authors pointed out [3], the electrical conductivity should be in the specific range between 10^{-6} and 10^{-12} $S \cdot cm^{-1}$. An electrical shock, compromising user safety, due to current leaks can appears if the conductivity is higher than 10^{-6} $S \cdot cm^{-1}$. On the other hand, if the lubricant is a complete insulator (conductivity below 10^{-12} $S \cdot m^{-1}$), a static current may appear and may lead to a damage to the EV. Furthermore, and obviously, electronic conductivity and short circuit should be completely avoided.

In this work, nanolubricants based on Matic VI transmission fluid (supplied by Repsol), dopped with different nano additive particles (graphene nanoplaquets, graphene oxide and titanate oxide) at different concentrations (0.5% and 1% in weight proportions) are analysed to obtain the electrical conductivity. To ensure that this property is correctly determined, dielectric spectroscopy is measured. To ensure that the Ohmic regime is achieved, he electrical conductivity is evaluated analysing the imaginary part of the electrical permittivity following the well-known criterion that the slope in a logarithm base of $log\varepsilon''$ vs $\log \omega$ should be -1.00 ± 0.02 [4].

[1] S.U.S. Choi, *Am. Soc. Mech. Eng. Fluids Eng. Div. FED* (1995): pp. 99–105. (accessed April 18, 2022).
[2] K. Holmberg, A. Erdemir, *Tribol. Int.* **135** (2019) 389–396.
[3] E. Rodríguez, N. Rivera, A. Fernández-González, T. Pérez, R. González, A.H. Battez, *Tribol. Int.* **171** (2022) 107544.
[4] J. Leys, M. Wübbenhorst, C. Preethy Menon, R. Rajesh, J. Thoen, C. Glorieux, P. Nockemann, B. Thijs, K. Binnemans, S. Longuemart, *J. Chem. Phys.* **128** (2008).

Acknowledgements: This work was supported by Spanish Ministry of Economy and Competitiveness and FEDER Program and the State Research Agency (AEI) of Spain and the European Regional Development Fund through the projects, MAT2017-89239-C2-1-P and PID2020-112846RB-C22 as well as by Xunta de Galicia through GRC ED431C 2020/10 project and the Galician Network of Ionic Liquids (ReGaLIs) ED431D 2017/06. P. Vallet and J. J. Parajó thank funding support of FPI Program from Spanish Ministry of Science, Education and Universities and I2C postdoctoral Program of Xunta de Galicia, respectively.

Experimental characterisation of ionic gels for energy storage applications

A. Santiago[1,*], J. J. Parajó[1], P. Vallet[1], M. Villanueva[1], J. Le Bideau[2], L.M. Varela[1], J. Salgado[1]

[1] *Grupo NaFoMAT. Departamentos de Física Aplicada y Física de Partículas. Facultade de Física. Instituto de Materiales (iMATUS). Universidade de Santiago de Compostela. 15782 Santiago de Compostela, Spain.*
[2] *Institut des Matériaux Jean Rouxel (IMN) Université de Nantes - CNRS (UMR 6502) 2 rue de la Houssinière B.P.32229, 44322 Nantes cedex 3 – France.*

*e-mail: antia.santiago@rai.usc.es

In recent years, the fast growth of the technology market created the need to develop better energy storage systems. Current batteries still have shortcomings in terms of efficiency and safety, especially at high temperatures. In addition, electrolytes that make up the batteries are based on flammable and volatile mixtures that can put the safety of the operator at risk [1]. Ionic liquids (ILs) appear as an alternative to conventional electrolytes in the development of new batteries trying to solve these disadvantages.

ILs are organic salts consisting of a cation and an anion whose melting point is below than 100 ºC [2]. Among their main characteristics, it is important to highlight the (practically) unlimited combinations that can be formed; the large number of cations and anions with different properties (i.e., alkyl chain length, functional group present in the alkyl chain length, functional group present in the compound) make it possible to obtain the most suitable compound for each application [3].

Figure 1. Ionogel formed by [Chol][TFSI] in PVDF matrix.

For the optimisation of ILs as electrolytes, mixtures of these fluids are made with inorganic salts of a common cation, lithium in the most cases [4,5] (but also multivalent salts) [6]. However, these ILs and mixtures with inorganic salts must be immobilised in a matrix for use in electrochemical devices such as batteries (superconductors or fuel cells) [7,8]. The resulting material from this confinement of IL (or mixtures with inorganic salts) in a matrix (silica, polymeric, etc.) are known as ionogels or ionic gels (Fig- 1), that have electrical conductivities similar (or even higher) to those at the liquid state and are mechanically stable, so they are very easily manipulated.

In this work we study the physicochemical and electric properties of ionogels formed by dissolutions of ILs and [Li][TFSI] in silica and polymeric matrix (PVDF) by experimental characterisation techniques such as differential scanning calorimetry (DSC), thermogravimetry (TGA), nuclear magnetic resonance (NMR) and dielectric relaxation spectroscopy (BBDS). The selected ILs are [Chol][TFSI] and [BMPyrr][TFSI].

[1] P. Vallet, J.J. Parajó, L.Fernández-Míguez, F. Sotuela, A. Morcillo, M. Villanueva, O. Cabeza, V.V. Matveev, A.V. Ievlev, K. Tutukin, L.M. Varela, J. Salgado, J., *Chemistry Proceedings* **3**(1), 115 (2020).
[2] G. A. O. Tiago, I. A. S. Matias, A. P. C Ribeiro & L. M. D. R. S. Martins, *Molecules* **25**(24), 5812 (2020).
[3] M. Galiski, A.Lewandowski, I. Stpniak, *Electrochimica Acta* **51**(26), 55675580 (2006).
[4] C.-W. Liew, S. Ramesh, K. Ramesh, A.K. Arof, *J. Solid State Electrochem* **16**, 1869 (2012).
[5] O. Russina, R. Caminiti, T. Méndez-Morales, J. Carrete, O. Cabeza, L.J. Gallego, L.M. Varela, A. Triolo, *J. Mol. Liq.* **205**, 16 (2015).
[6] J. Salgado, J.J. Parajó, M. Villanueva, J.R. Rodríguez, O. Cabeza, L.M. Varela, *J. Chem. Thermodyn.* **134**, 164 (2019).
[7] J.J. Parajó, P. Vallet, L. Fernández-Miguez, M. Villanueva, O. Cabeza, L.M. Varela, J. Salgado, *Chem. Proc.*, MDPI, 131 (2020).
[8] J. Le Bideau, L. Viau, A. Vioux, *Chem. Soc. Rev.* **40**, 907 (2011).

Acknowledgements: This work was supported by Spanish Ministry of Economy and Competitiveness and FEDER Program through the projects, MAT2017-89239-C2-1-P as well as by Xunta de Galicia through GRC ED431C 2020/10 project and the Galician Network of Ionic Liquids (ReGaLIs) ED431D 2017/06. P. Vallet and J. J. Parajó thank funding support of FPI Program from Spanish Ministry of Science, Education and Universities and I2C postdoctoral Program of Xunta de Galicia, respectively.

Física de la atmósfera y el océano

Presentaciones orales

Martes 12/07:

15:30-15:40 José Manuel Vaquero (U de Extremadura). *The meteorological observations of Jovellanos in the castle of Bellver*

15:40-15:50 I. Tovar (U Extremadura). *Recovering meteorological information from the "Extremadura" newspaper (1924-1927)*

15:50-16:00 Albenis Pérez-Alarcón (U Vigo). *Overview of moisture sources for the precipitation of tropical cyclones through a Lagrangian approach*

16:00-16:10 José Carlos Fernández-Alvarez (U Vigo). *Atmospheric Rivers moisture sources projections landfalling the Iberian Peninsula*

16:10-16:20 Eloisa Raluy (U Murcia). *Impact of aerosols on atmospheric rivers in regional climate simulations: development of an identification algorithm and a climatological analysis*

16:20-16:30 Roger Sori (U Vigo). *The oceanic and terrestrial origin of precipitation in the great world river basins: their role in drought severity*

16:30-16:40 Gleisis Alvarez-Socorro (U Vigo). *Global climatology of nocturnal low-level jets with the ERA5 reanalysis*

16:40-16:50 David Barriopedro (IGEO-CSIC-UCM). *A multiparametric perspective of the North Atlantic eddy-driven jet*

16:50-17:00 Marie Drouard (IGEO-CSIC-UCM). *Contrasting dynamics of short and long atmospheric blocks in the Northern Hemisphere*

17:00-18:00 **Pósteres y café**.

18:00-18:10 J. Manuel Garrido Pérez (U Complutense). *Storyline description of the summer air stagnation response to anthropogenic warming forcing in Europe and the contiguous United States*

18:10:18:20 Juan A. Añel (U Vigo). *Stratospheric contraction caused by greenhouse gas emissions*

18:20-18:30 Samuel Benito Barca (U Complutense). *Driving mechanisms for boreal winter stratospheric ozone response to ENSO*

18:30-18:40 Gines Garnés (U Murcia). *On the role of Aerosols on Atmospheric Circulation in Regional Climate Experiments*

18:40-18:50 Leandro Cristian Segado-Moreno (U Murcia). *Spatial and temporal variability of surface ozone in a climate simulation over Europe and its relationship with climate parameters*

18:50-19:00 Susana Bayo.Besteiro (U Vigo). *The impact of climate change on photovoltaic power generation for solar installations in the Atacama desert*

Pósteres

- Jose M. Garrido-Perez, D. Barriopedro, R. García-Herrera and C. Ordóñez. *How climate change is affecting the patterns of electricity demand in Spain?*
- C. Ordóñez, Jose M. Garrido-Perez, R. García-Herrera. *Did the meteorology affect the near-surface ozone concentrations over Europe during the COVID-19 lockdown of early spring 2020?*
- A. Bernáldez, J.M. Vaquero, M. Antón, A. Sánchez-Lorenz. *Preliminary results about long-term trends in downward surface shortwave radiation over Spain (1985–2021)*
- Xavier Navarro, Ricard Kirchner, Raúl Rodríguez-Solà, M. Carmen Casas-Castillo. *Análisis de escala simple de veinticinco años de registros de la red pluviométrica de Barcelona*
- Jesús Rodríguez-Camacho, Sergio Toledo-Redondo, Jorge Portí, Jesús Fornieles, David Blanco, Juan Francisco Gómez-Lopera, Alfonso Salinas, María del Carmen Carrión. *Long-term analysis of Schumann Resonance measured at the Sierra Nevada ELF station*

The meteorological observations of Jovellanos in the castle of Bellver

José Manuel Vaquero

Departamento de Física, Universidad de Extremadura, Spain.

e-mail: jvaquero@unex.es

The development of meteorology in Spain began in the 18th century, just as it occurred in other European countries. Anduaga [1] has shown that there were three communities that led to the first systematic meteorological observations [2]. In the first place, the astronomical observatories of Cádiz and Madrid encouraged this kind of observations. In addition, the medical community also made a notable effort in this regard and, finally, the "Sociedades Económicas de Amigos del País" promoted meteorological studies related to agricultural activities.

Until now, no one has revealed the interest of Gaspar Melchor de Jovellanos (1744–1811) in atmospheric sciences, despite his evident connexion with the Economic Societies and agricultural sciences. I began to read his correspondence (Obras Completas, volumes II-IV [3]) expecting to find numerous references to weather or climate, and the first results were quite discouraging. However, I continued to consult his diary (*Obras Completas*, volumes VI-VIII) and there I found an enormous collection of comments of a meteorological nature.

But the surprise was capital when I saw in the last notebook of his diary, the twelfth, a complete set of systematic meteorological observations made during his imprisonment in the Bellver castle in Mallorca for almost a year (which practically coincides with the year of 1806). For all these reasons, the objective of this work is twofold: (i) I am going to show the enormous interest in meteorology by Jovellanos and (ii) I am going to describe in detail the barometric record obtained by Jovellanos at Bellver castle.

[1] A. Anduaga Egaña, *Meteorología, ideología y sociedad en la España contemporánea*, Madrid: CSIC (2012).
[2] F. Domínguez-Castro et al., "Early Spanish meteorological records (1750-1850)", *International Journal of Climatology* **34**, 593 (2014).
[3] G.M. Jovellanos, *Obras Completas*, 14 tomos, Gijón: KRK Ediciones (1984-2010).

Acknowledgements: This research was supported by the Economy and Infrastructure Counselling of the Junta of Extremadura through project IB20080 and grant GR18097 (co-financed by the European Regional Development Fund).

Recovering meteorological information from the "Extremadura" newspaper (1924-1927)

I. Tovar, **M. C. Gallego***, V. M. S. Carrasco, N. Bravo-Paredes, J. M. Vaquero

Departamento de Física, Universidad de Extremadura, Spain.

*e-mail: maricruz@unex.es

Preliminary results of the analysis of meteorological, geophysical and space phenomena found in the review of the Extremadura regional press during the years 1923-1927 are presented. We are developing a database of news of interest for Earth and Space sciences from the Extremadura regional press. It will be very useful to know and study the different geophysical and space events that have taken place in Extremadura and, in particular, to know details of the past climate that help us to understand the effects of global warming.

Some recent studies have shown us the interest of using newspapers in rural areas, relatively sparsely populated and little studied by researchers, as the region of Extremadura. Bravo-Paredes et al. (2020) [1] located various rogations for rain in the press at the end of the 19th century and the beginning of the 20th century. This information helped establish a clear relationship between the celebration of rogations for rain in Extremadura and the well-known NAO index. Another interesting example is the article by García-Garrido et al. (2020) [2]. They studied a landslide event that took place on January 1831 at the Pedregoso Mountains, Cabeza del Buey, SW Spain. This landslide had not been documented to date and was only described in the local press. This event involved an estimated amount of dislodged material in the order of 10^4 m^3 being one of the largest landslides reported in Extremadura.

We are presenting here a review of the newspaper "Extremadura" from April 1923 to December 1927. A total of 332 episodes of interest for Earth and Space sciences have been found, which indicates how profitable this kind of press reviews are.

Among the most interesting episodes that have been located, the following stand out: (i) strong thunderstorms during the month of June 1925, which caused considerable damage in many towns in Extremadura, (ii) an exceptional fireball in Don Benito on December 27, 1926, and (iii) two railway accidents caused by landslides (February 10, 1924; February 18, 1927) probably caused by rain.

[1] N. Bravo-Paredes, M.C. Gallego, F. Domínguez-Castro, J.A. García, J.M. Vaquero, Pro-pluvia Rogation Ceremonies in Extremadura (Spain): Are They a Good Proxy of Winter NAO?, *Atmosphere* **11**, 282 (2020); https://doi.org/10.3390/atmos11030282

[2] J.P. García-Garrido, M.C. Gallego, T. Palacios, R.M. Trigo, J.M. Vaquero, Heavy rainfall and landslides in January 1831 at Pedregoso Mountains (Cabeza del Buey, SW Spain), *Atmosphere* **11**, 544 (2020); https://doi.org/10.3390/atmos11050544

Acknowledgements: This research was supported by the Economy and Infrastructure Counselling of the Junta of Extremadura through project IB20080 and grant GR18097 (co-financed by the European Regional Development Fund).

Overview of moisture sources for the precipitation of tropical cyclones through a Lagrangian approach

Albenis Pérez-Alarcón[1,2,*], José C. Fernández-Alvarez[1,2], Raquel Nieto[1], Luis Gimeno[1]

[1]*Centro de Investigación Mariña, Universidade de Vigo, Environmental Physics Laboratory (EPhysLab), Ourense, Spain.*
[2]*Departamento de Meteorología, Instituto Superior de Tecnologías y Ciencias Aplicadas, Universidad de La Habana, La Habana, Cuba.*

*e-mail: albenis.perez.alarcon@uvigo.es

Tropical cyclones (TCs) not only produce heavy rainfall in tropical latitudes but also in mid-latitudes. In this work, we investigated the moisture sources for the precipitation of TCs in each basin, namely the North Atlantic Ocean (NATL), Central and East Pacific Ocean (NEPAC), Western North Pacific Ocean (WNP), South Pacific Ocean (SPO), North Indian Ocean (NIO) and South Indian Ocean (SIO). To do this, we applied the Lagrangian moisture source diagnostic method developed by Sodeman et al. [1] and implemented in the TRansport Of water VApor (TROVA) tool to the trajectories of all air parcels that precipitated over the TCs location. The pathways of atmospheric parcels were from the global outputs of the FLEXPART model [2]. Meanwhile, the National Hurricane Center and the Joint Typhoon Warning Center provided the 6-hourly information of all TCs through the best track archives.

Our results revealed that the moisture often came from ocean sources. Nevertheless, the Central America and Indian Peninsula terrestrial sources played an important role in supplying moisture for TCs over the NEPAC and NIO basins, respectively. In summary, the contributions from the western NATL, the Caribbean Sea and the Gulf of Mexico accounted for ~91% of moisture in the NATL basin. In NEPAC, the eastern tropical Pacific Ocean and Central America mainland supplied ~92% of total moisture, while the western North Pacific Ocean, the Philippine Sea and the South China Sea contributed ~90% in WNP. The Arabian Sea, the Bay of Bengal and the Indian Peninsula supported approximately 95% of moisture in the NIO basin. Most of the moisture (~91) that precipitated over the TCs location in the SIO basin was supplied from the tropical Indian Ocean, while the Coral Sea and the western SPO provided substantial moisture (~91%) for the precipitation of TCs in the SPO basin

[1] Sodemann, H., Schwierz, C., & Wernli, H. *Journal of Geophysical Research* **113**, D03107 (2008).
[2] Stohl, A., Forster, C., Frank, A., Seibert, P., & Wotawa, G. *Atmospheric Chemistry and Physics* **5**, 2461 (2005).

Acknowledgements: A.P-A. acknowledges support from the UVigo PhD grant. J.C.F-A. acknowledge support from the Xunta de Galicia. This study received support from the LAGRIMA project (grant no. RTI2018-095772-B-I00) and partial support from the Xunta de Galicia under the Project ED431C2021/44. This work has also been supported by the computing resources and technical support provided by the Centro de Supercomputación de Galicia (CESGA).

Moisture sources projections under climate change for Atmospheric Rivers landfalling the Iberian Peninsula

José C. Fernández-Alvarez[1,2,*], Albenis Pérez-Alarcón[1,2], Jorge Eiras-Barca[1,3], Alexander M. Ramos[4], Raquel Nieto[1], Luis Gimeno[1]

[1]*Centro de Investigación Mariña, Universidade de Vigo, Environmental Physics Laboratory (EPhysLab), Campus As Lagoas s/n, Ourense, 32004, Spain.* [2]*Departamento de Meteorología, Instituto Superior de Tecnologías y Ciencias Aplicadas, Universidad de la Habana, La Habana 10400, Cuba.* [3]*Defense University Center, The Spanish Naval Academy, Marín, Spain.* [4]*Instituto Dom Luiz (IDL), Facultade de Ciências, Universidade de Lisboa, Lisbon, Portugal.*

*e-mail: jose.carlos.fernandez.alvarez@uvigo.es

In the field of moisture transport, Atmospheric Rivers (ARs) are known as narrow corridors of water vapor, generally 2000 km or more in length. These account for more than 90% of the meridional moisture transport and latent heat associated with storm tracks in the extratropical atmosphere [1]. The ARs are associated with extreme precipitation events, floods, landslides, extensive property damage, and losses of life [2, 3]. In the context of climate change, it is projected that the water-holding capacity of the atmosphere increases about 7 % K^{-1} at lower troposphere and for the column integrated moisture [4], however the future changes in moisture sources contribute to moisture transported by ARs to higher latitudes by the end-century are not known. To determine these changes simulations of the Weather Research and Forecasting (WRF-ARW) model forced with Community Earth System Model (CESM2) and the FLEXPART-WRF model forced with the WRF-ARW outputs are used. The analysis was carried out mainly by determining the anomaly moisture uptake for the mid-century (MC, 2049-2053) and end-century (EC, 2096-2100) periods, considering the annual and seasonal changes of the variable. It was obtained that the moisture uptake anomaly increased with maximum values, ~ 7-8 % K^{-1}, in winter for MC and EC. In addition, a latitudinal increase in the anomalous moisture uptake pattern is projected over the central Atlantic and a longitudinal expansion towards the Gulf of Mexico.

[1] Zhu, Y., Newell, R. E. A proposed algorithm for moisture fluxes from atmospheric rivers, *Monthly Weather Review* **126**, 725 (1998).
[2] Ramos, A. M., Trigo, R. M., Liberato, M. L., Tomé, R. Daily precipitation extreme events in the Iberian Peninsula and its association with atmospheric rivers, *Journal of Hydrometeorology* **16**, 579 (2015).
[3] Gimeno, L. et al., Major mechanisms of atmospheric moisture transport and their role in extreme precipitation events, *Annual Review of Environment and Resources* **41**, 117 (2016).
[4] Gershunov, A. et al., Precipitation regime change in Western North America: the role of atmospheric rivers, *Scientific Reports* **9**, 1 (2019).

Acknowledgements: José C. Fernández-Alvarez acknowledge the support from the Xunta de Galicia under the grant no. ED481A-2020/193. Albenis Pérez-Alarcón acknowledges a PhD grant from the University of Vigo. The authors thank the Defense University Center at the Spanish Naval Academy (CUD-ENM) for all the support provided for this research. In addition, this work has been possible thanks to the computing resources and technical support provided by CESGA (Centro de Supercomputación de Galicia). This work is supported by the LAGRIMA project (grant no. RTI2018-095772-B-I00) funded by the Ministerio de Ciencia, Innovación y Universidades, Spain. Partial support was also obtained from the Xunta de Galicia under the Project ED431C 2021/44 (Programa de Consolidación e Estructuración de Unidades de Investigación Competitivas (Grupos de Referencia Competitiva) and Consellería de Cultura, Educación e Universidade).

Impact of aerosols on atmospheric rivers in regional climate simulations: development of an identification algorithm and a climatological analysis

Eloisa Raluy*, Juan Pedro Montávez, Amar Halifa, Pedro Jiménez-Guerrero

Department of Physics, University of Murcia, Murcia, Spain.

*eloisa.raluyl@um.es

Atmospheric rivers (ARs) play an essential role in extreme precipitation phenomena. To predict such events, a correct simulation of ARs becomes indispensable. Since most of the regional climate models do not take aerosols into account in an interactive way, the main objective pursued in this project is to analyse the role of aerosols in the intensity and location of ARs.

The identification of ARs has always been carried out in global climate simulations with algorithms developped for those models. However, these algorithms may not be valid in regional climate models, due to the presence of boundaries in the simulation domain. In this project, a new identification algorithm of ARs in regional climate models (AIRA) is presented. The implemented algorithm has been proved to be able to properly identify the vapor structures associated with ARs.

AIRA was applied to a set of hourly data from three regional simulations (BASE, ARI and ARCI), covering a period of 20 years. In BASE, aerosols are prescribed, while in both ARI and ARCI the model incorporates aerosols dynamically. In ARI, aerosols are only taken into account in radiation and in ARCI they are taken into account in radiation and in the processes associated with cloud formation and precipitation.

AIRA has identified a similar number of ARs in the three simulations (about 250 ARs), with a mean duration between one and two days and with a mean direction of 40° from the East. These ARs explain up to a 30% of the total precipitation in the Iberian Peninsula. The differences between the three simulations are significant in the spatial distribution of the precipitation and in the trajectory of some ARs. Although the number of detected ARs is similar, the temporal steps with ARs common to the three simulations are only a 37% of the total BASE steps with ARs.

The behavior of ARs in the different simulations is modified depending on the present aerosols and the meteorological situation. A preliminary analysis of the physical causes that explain the different behavior of the ARs in the three experiments shows that both the displacement and the intensification of ARs are due to a change in the thickness gradient. This is caused by changes in the temperature field, mainly due to processes related to the microphysics of the clouds (indirect effects), while radiative effects have turned out to be less significant on this aspect.

The oceanic and terrestrial origin of precipitation in the great world river basins: their role in drought severity

Rogert Sorí [1,*], Luis Gimeno-Sotelo[1], Milica Stojanovic[1,2], José Carlos Fernández-Alvarez[1,3], Albenis Pérez-Alarcón[1,3], Raquel Nieto[1], Luis Gimeno[1]

[1]*Centro de Investigación Mariña, Environmental Physics Laboratory (EPhysLab), Universidade de Vigo, Campus As Lagoas s/n, Ourense 32004, Spain.* [2]*Department Meteorology and Geophysics, Sofia University St. Kliment Ohridski, 1164 Sofia, Bulgaria.* [3]*Departamento de Meteorología, Instituto Superior de Tecnologías y Ciencias Aplicadas, Universidad de La Habana, La Habana 10400, Cuba.*

*e-mail: rogert.sori@uvigo.es

In this study, we initially investigated the origin of the precipitation over 50 major world river basins. For this aim, the global monthly outputs from the Lagrangian Particle Dispersion Model (FLEXPART), considering a forward in time experiment from the entire oceans and continents were used. The horizontal resolution was 0.25º and the period of study is from 1980 to 2018. These outputs permitted to estimate a "Lagrangian precipitation" from the oceanic (PLO) and terrestrial (PLT) origin, which sum is close to the precipitation over the basins. Following this approach, the percentage of precipitation from oceanic and terrestrial origin was determined for each river basin, and compared with the precipitation from the Multi-Source Weighted-Ensemble Precipitation (P_{MSWEP}) (Beck et al., 2019). The results show a great amount of PLT over the major number of river basins, confirming the importance of terrestrial recycling and moisture export across the continents. However, the influence of PLO seems to be dominant over a great part of the western North American river basins, and some basins located in western Eurasia and Southeast Asia. The multivariate Standardised Precipitation Index (SPI) (McKee et al., 1993) was utilised to assess the temporal evolution of dry/wet conditions in the river basins. It was calculated at 1- and 3-months temporal scales using the P_{MSWEP} as well as PLO and PLT series, resulting in the series of SPI_{MSWEP}, SPI_{PLO}, and SPI_{PLT}. Afterwards, was calculated the number of drought episodes that affected each river basin. The results showed that at the 1-month temporal scale the number of drought episodes is larger than at 3-month, due to the greater variability of the SPI_{MSWEP}, which result in a major number of flash droughts. Those basins more (less) affected by drought episodes according to the SPI_{MSWEP} at a 1-month temporal scale are located in northern Eurasia and North America (tropical South America and Africa). In addition, we present the relationship between the severity of drought episodes and the correspondent severity computed with the SPI_{PLO}, and SPI_{PLT}. Finally, a copula analysis revealed the conditional probability of occurrence of drought, severe and extreme drought, and extreme drought conditions according to the SPI_{MSWEP} with the SPI_{PLO} and SPI_{PLT}, confirming the crucial role of PLO (PLT) deficit in North America (Eurasian) river basins.

[1] Beck, H. E., Wood, E. F., Pan, M., Fisher, C. K., Miralles, D. M., van Dijk, A. I. J. M., McVicar, T. R., and Adler, R. F. MSWEP V2 global 3-hourly 0.1° precipitation: methodology and quantitative assessment. *Bulletin of the American Meteorological Society* **100(3)**, 473 (2019).
[2] McKee, T.B., Doesken, N.J., Kleist, J. The relationship of drought frequency and duration to time scales. In Proceedings of the Eighth Conference on Applied Climatology, Boston, MA, USA, 179–184 (17–22 January 1993).

Acknowledgements: This work is supported by the LAGRIMA project (Grant RTI2018-095772-B-I00) funded by the Ministerio de Ciencia, Innovación y Universidades, Spain.

Global climatology of nocturnal low-level jets with the ERA5 reanalysis

Gleisis Alvarez-Socorro[1,*], José C. Fernández-Alvarez[1,2], Raquel Nieto[2], Luis Gimeno[2]

[1]*Departamento de Meteorología, Instituto Superior de Tecnologías y Ciencias Aplicadas, Universidad de la Habana, La Habana 10400, Cuba.* [2]*Centro de Investigación Mariña, Universidade de Vigo, Environmental Physics Laboratory (EPhysLab), Campus As Lagoas s/n, Ourense, 32004, Spain.*

*e-mail: gleisis1998@gmail.com

Nocturnal low-level jets (NLLJs) can be defined as filamentary regions or corridors of anomalously high wind speeds found within 1 km of the troposphere [1]. They are common global meteorological phenomena and are considered an important global mechanism of moisture transport, since their changes in frequency will lead to modifications in local and even global hydrological cycles [2], hence the importance of knowing their behavior. For this study, reanalysis data from ERA5 (~0.25°) [3] from 2014 to 2018 were used to find global NLLJs. The methodology applied to calculate the NLLJs index (INLLJs) is based on the temporal evolution of the vertical wind structure and the diurnal-nighttime variation of the wind fields at the surface and at ~4 km height [1]. It was analyzed for July and January in the Northern (HN) and Southern Hemispheres (HS) respectively, because of its main association with the warm season [1]. The results show similarity with previous investigations, but greater detail was observed in geographycal distribution of the NLLJs due to the higher spatial resolution of ERA5. For the HN, the maximum INLLJs values were observed in the Great Plains region, southern Asia and in a large part of the African continent. Frequencies of days with NLLJs ranging from 60-100 % were determined for HN. However, for HS, the areas with the highest INLLJs and frequency of NLLJs days (~ 45-80%) correspond to Australia, central and southern Africa and South America.

[1] Rife, D.L., Pinto, J.O., Monaghan, A.J., Davis, C.A., Hannan, J.R. Global distribution and characteristics of diurnally varying low-level jets, *Journal of Climate* **23**, 5041 (2010).
[2] Gimeno, L., Dominguez, F., Nieto, R., Trigo, R., Drumond, A., Reason, C.J.C., Taschetto, A.S., Ramos, A.M., Kumar, R., Marengo, J. Major Mechanisms of Atmospheric Moisture Transport and their Role in Extreme Precipitation events, *Annual Review of Environment and Resources* **41,** 117 (2016).
[3] Hersbach, H et al. The ERA5 global reanalysis, *Quarterly Journal of the Royal Meteorological Society* **146**, 1999 (2020).

Acknowledgements: This work is supported by the LAGRIMA project (grant no. RTI2018-095772-B-I00) funded by the Ministerio de Ciencia, Innovación y Universidades, Spain. Partial support was also obtained from the Xunta de Galicia under the Project ED431C 2021/44 (Programa de Consolidación e Estructuración de Unidades de Investigación Competitivas (Grupos de Referencia Competitiva) and Consellería de Cultura, Educación e Universidade). José C. Fernández-Alvarez acknowledge the support from the Xunta de Galicia under the grant no. ED481A-2020/193.

A multiparametric perspective of the North Atlantic eddy-driven jet

David Barriopedro[1,*], Blanca Ayarzagüena[2], Marina García-Burgos[1,2], Ricardo García-Herrera[1,2]

[1]*Instituto de Geociencias (IGEO), CSIC-UCM, Spain.*
[2]*Dpto. Física de la Tierra y Astrofísica, Universidad Complutense de Madrid, Spain.*

*e-mail: david.barriopedro@csic.es

The North Atlantic eddy-driven jet (EDJ) is an essential component of the Euro-Atlantic atmospheric circulation. It has been typically described in terms of latitude and intensity, but this is not enough to fully characterize its variability and complex EDJ configurations. Here, we present a set of daily parameters of the EDJ based on low-tropospheric zonal wind data for the 1948-2020 period. They describe the intensity, sharpness, location, edges, tilt and other zonal asymmetries of the EDJ, therefore dissecting its structure beyond the latitudinal regimes. This allows for assessments of specific EDJ aspects and a multi-parametric treatment of EDJ configurations in a manageable way.

Overall, variations in EDJ parameters reflect distinctive patterns of eddy forcing and wave breaking, with anticyclonic eddies playing a major role in shaping the EDJ structure. A multimodal behavior of the EDJ is only detected in latitude, which largely influences the longitudinal position of the EDJ. Other aspects of the EDJ are less constrained by the latitude and display a variety of configurations. Four multi-parametric states (northern, central, tilted and split EDJs) provide a satisfactory description of recurrent patterns of the EDJ. They participate in meridional migrations of the EDJ, but yield less dramatic transitions than viewed from the latitudinal perspective. Finally, the EDJ parameters help to better understand the EDJ influence on European climate. In many regions, latitude and intensity contain limited information on near-surface anomalies, and their signals can be masked by the additional effect of other EDJ parameters (Figure 1).

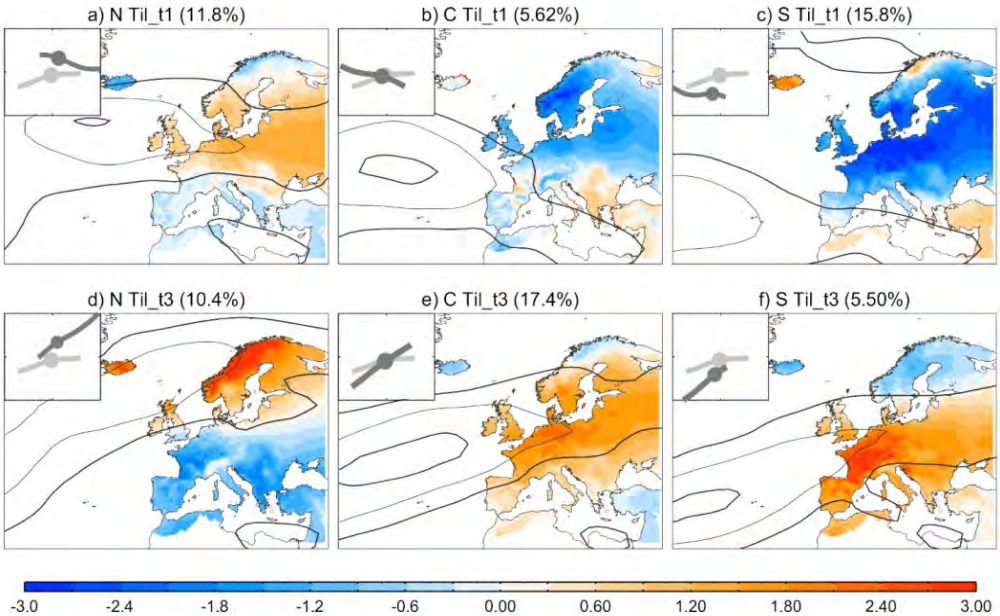

Figure 1. Composites of zonal wind at 850-700 hPa (contours, with contour interval of 5 m s^{-1} starting at 5 m s^{-1}) and 2 m temperature anomalies (shading, ºC) for EDJs of the three latitudinal regimes with: a-c) low (lower tercile, t1); d-f) high (upper tercile, t3) tilts. Panel columns represent the northern (N, a, d), central (C, b, e) and southern (c, f) EDJ regimes. The inset of each panel represents snake-plots of the EDJ for the climatology (light grey) and the composite (dark grey). The percentage of winter days included in the composite is shown in the title

Acknowledgements: This research is part of the CSIC Interdisciplinary Thematic Platform (PTI) Clima y Servicios Climáticos (PTI-CLIMA) and POLARCSIC (PTI-POLAR) activities. This work was supported by the Spanish Ministerio de Ciencia, Innovación y Universidades through the JeDiS (RTI2018-096402-B-I00) project. MGB was also supported by the Spanish Ministerio de Ciencia e Innovación (Grant PRE2019-090618).

Contrasting dynamics of short and long atmospheric blocks in the Northern Hemisphere

Marie Drouard[1,2,*], Tim Woollings[1], David Sexton[3], Carol McSweeney[3]

[1]*University of Oxford, Department of Physics, Oxford, UK.* [2]*Instituto de Geociencias (CSIC-UCM), Madrid, Spain.*
[3]*Met Office Hadley Centre, Exeter, UK.*

*e-mail: m.drouard@igeo.ucm-csic.es

Atmospheric blocking is a phenomenon of major importance for daily weather due to its long persistence (up to 4–5 weeks). It corresponds to a localized large-scale reversal of the atmospheric circulation that, as its name indicates, blocks the westerly zonal flow. In winter, blocks are associated with cold spells and in summer with hot days and sometimes heatwaves.

The aim of this work is to better understand why some blocks last only five days (short blocks in the following) and other more than ten days (long blocks), to better characterise long blocks.

We show that long blocks often involve cyclonic Rossby wave breaking, while short blocks are equally associated with both cyclonic and anticyclonic wave breakings. This main result is reproduced in several coupled climate models. Three mechanisms might explain the lower number of long anticyclonic blocks: 1/ a downstream reinforcement of the anticyclone during anticyclonic blocks might be associated with a stronger downstream advection of the block; 2/ the mean zonal wind is reinforced by synoptic eddies towards a more northward position during anticyclonic blocks, whereas synoptic eddies force the mean zonal wind to the south of the block during cyclonic blocks, which has been previously shown to be associated with more persistent weather patterns; 3/ strong and/or sustained eddy feedback is needed to maintain long anticyclonic blocks. A combination of these three mechanisms might explain why some blocks last longer and why anticyclonic blocks are less present at extreme durations.

Storyline description of the summer air stagnation response to anthropogenic warming forcing in Europe and the contiguous United States

Jose M. Garrido-Perez[1,*], C. Ordóñez[1], D. Barriopedro[1,2], R. García-Herrera[1,2], Jordan L. Schnell[3], Daniel E. Horton[4]

[1]*Departamento de Física de la Tierra y Astrofísica, Facultad de Ciencias Físicas, UCM, 28040, Madrid, Spain.*
[2]*Instituto de Geociencias (IGEO, CSIC-UCM), 28040, Madrid, Spain.*
[3]*Cooperative Institute for Research in Environmental Sciences, NOAA/Global Systems Laboratory, Boulder, CO, USA*
[4]*Department of Earth and Planetary Sciences, Northwestern University, Evanston, IL, USA.*

*e-mail: josgarri@ucm.es

Air stagnation situations are characterized by stable weather, weak winds within the lower troposphere and lack of rainfall. These conditions minimize the horizontal dispersion and vertical mixing of air masses as well as the scavenging of pollutants, favouring their accumulation in the lower atmospheric layers and the occurrence of poor air quality events. Climate model projections suggest that air stagnation will increase north of the Mediterranean and in large areas of the contiguous United States in the future (Figure 1), but these projections are subject to large uncertainties. Storylines of atmospheric circulation change, or physically self-consistent narratives of plausible future events, have recently been proposed as a non-probabilistic means to represent uncertainties in climate change projections. This work [1] applies the storyline approach to 21st century projections of summer air stagnation over Europe and the United States. For that purpose, we use a Climate Model Intercomparison Project Phase 6 (CMIP6) ensemble to generate stagnation storylines based on the forced response of three remote drivers of the Northern Hemisphere mid-latitude atmospheric circulation: North Atlantic warming, North Pacific warming, and tropical versus Arctic warming.

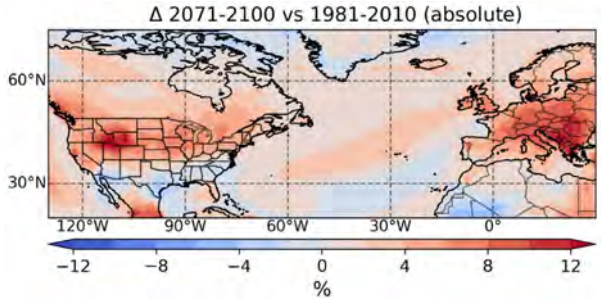

Figure 1. Absolute change in stagnation occurrence (%) from 1981–2010 to 2071–2100 for a high radiative forcing scenario.

Under a high radiative forcing scenario (SSP5-8.5), strong tropical warming relative to Arctic warming is associated with a strengthening and poleward shift of the upper westerlies, which in turn would lead to decreases in stagnation over the northern regions of North America and Europe, as well as increases in some southern regions, as compared to the multi-model mean. On the other hand, North Pacific warming tends to increase the frequency of stagnation over some regions of the U.S. by enhancing the frequency of stagnant winds, while reduced North Atlantic warming does the same over Europe by promoting the frequency of dry days.

Given the response of stagnation to these remote drivers, their evolution in future projections will substantially determine the magnitude of the stagnation increases. This is especially true in Europe, where differences of ∼2 summer stagnant days per degree of global warming are found amongst the different storyline combinations. For example, the greatest projected increase in stagnation for most European regions leads to the smallest increase in stagnation for southwestern Europe; i.e. limited North Atlantic warming combined with near-equitable tropical and Arctic warming. In the U.S., only the atmosphere over the northern Rocky Mountain states demonstrates comparable stagnation projection uncertainty, due to opposite influences of remote drivers on the meteorological conditions that lead to stagnation.

[1] Jose M. Garrido-Perez, C. Ordóñez, D. Barriopedro, R. García-Herrera, Jordan L. Schnell and Daniel E. Horton, A storyline view of the projected role of remote drivers on summer air stagnation in Europe and the United States, *Environmental Research Letters* **17**, 014026 (2022).

Stratospheric contraction caused by greenhouse gas emissions

Juan A. Añel[1,*], Petr Pisoft[2], Petr Sacha[2,3], Ales Kuchar[4], Laura de la Torre[1]

[1]*EPhysLab, CIM-UVigo, Univ. de Vigo, Campus As Lagoas, 32004, Ourense, Spain.* [2]*Department of Atmospheric Physics, Faculty of Mathematics and Physics, Charles University, Prague, Czech Republic.* [3]*Institute of Meteorology and Climatology, University of Natural Resources and Life Sciences, Vienna, Austria.* [4]*Institute for Meteorology, Leipzig University, Leipzig, Germany.*

*e-mail: j.anhel@uvigo.es

Rising emissions of anthropogenic greenhouse gases (GHG) have led to tropospheric warming and stratospheric cooling over recent decades. Consequently, the troposphere has expanded, and the rise of the tropopause has been suggested as one of the most robust fingerprints of anthropogenic climate change. Conversely, at altitudes above ~ 55 km (in the mesosphere and thermosphere) observational and modelling evidence indicates a downward shift in the height of pressure levels or decreasing density at fixed altitudes. Here we show that the stratosphere has contracted substantially over the last decades and that the main driver for this are increasing concentrations of GHG. Also, we show that this trend will continue, and the mean climatological thickness of the stratosphere will decrease by 1.3 km following RCP 6.0 by 2080. The short emergence time of this trend (less than 15 years) makes it a novel and independent indicator of GHG induced climate change. Also, we present the ability of the different state-of-the-art reanalyses to monitor this phenomenon and how sulfate aerosol injection in the stratosphere can affect it.

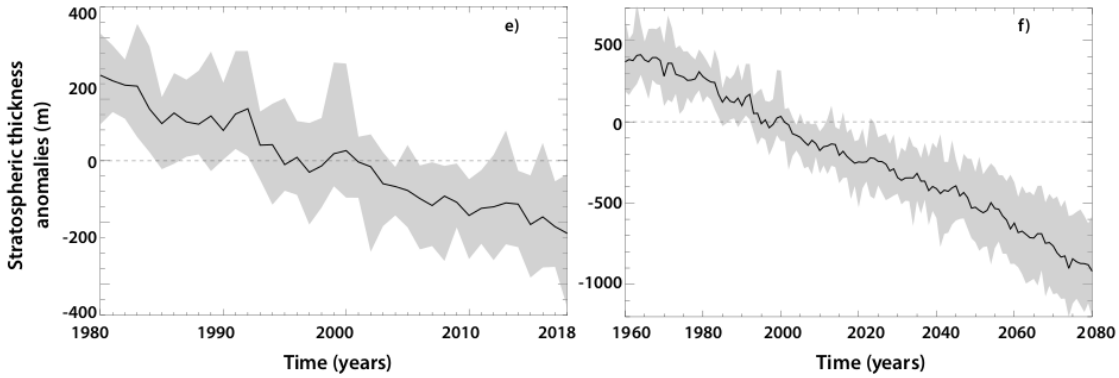

Figure 1. Anomalies of stratospheric thickness for the period 1960-2080 from CCMI models. Solid line: mean. All the simulations correspond to the AllForcings experiment. The grey areas cover the maximum and minimum of the CCMI models used.

[1] Pisoft et al., *Env. Res. Lett.* **16**, 064038 (2021).
[2] Añel J. A., *Contemp. Phys.*, **57**, 230 (2016).

Driving mechanisms for boreal winter stratospheric ozone response to ENSO

Samuel Benito-Barca*, Natalia Calvo, Marta Abalos, Blanca Ayarzagüena

Departamento de Física de la Tierra y Astrofísica, Universidad Complutense de Madrid, Madrid, España.

*e-mail: samubeni@ucm.es

Stratospheric ozone is an important component in the climate system. It plays a key role in the radiative budget and protecting Earth from harmful solar ultraviolet (UV) radiation and can exert a significant influence on the Northern Hemisphere (NH) surface climate. Previous studies have shown that El Niño-Southern Oscillation (ENSO), which is the main source of interannual variability in the global climate, has impacts on stratospheric circulation, but its effects on stratospheric ozone have been less investigated. The present study constitutes the first comprehensive analysis of the NH stratospheric ozone signal and its driving mechanisms in response to different El Niño flavors (Eastern Pacific and Central Pacific El Niño) and La Niña in boreal winter. The use of simulations from the Whole Atmosphere Community Climate Model (WACCM), a chemistry-climate model with a well resolved stratosphere, allows us to evaluate the contributions of the advection by the residual circulation of the Brewer Dobson Circulation (BDC), the isentropic mixing and the chemical processes to ENSO-related ozone variations.

The examination of total column ozone (TCO) reports a reduction in the tropics and an increase at middle and high latitudes from December to March during EP El Niño events and the opposite behavior during La Niña. Interestingly, no significant impact on extratropical TCO has been found during CP El Niño. The analysis of the continuity equation for zonal-mean ozone concentration reveals that tropical ozone variations in the lower stratosphere are mainly driven by advection through changes in tropical upwelling, with a contribution from changes in chemical process above 30 hPa. In the extratropical stratosphere, ENSO ozone variations result from a combination of changes in advection by downwelling in the shallow and deep branches of the residual circulation and also changes in horizontal mixing linked to Rossby wave breaking and polar vortex anomalies. In contrast with the large impact of EP-El Niño and La Niña on the residual circulation, the effect of CP El Niño on the shallow branch is small, and no significant impact is found on the deep branch. This results in the lack of extratropical signal in TCO during CP El Niño events.

On the role of Aerosols on Atmospheric Circulation in Regional Climate Experiments

Ginés Garnés*, **Juan Pedro Montávez**, Pedro Jiménez-Guerrero, Amar Halifa

Department of Physics, University of Murcia, Murcia, Spain.

*e-mail: gines.g.m@um.es

Nowadays, the regional climate models used to generate the necessary synoptic information in order to describe the atmospheric circulation do not take into account aerosols interactions with radiation nor clouds. The purpose of this work is to determinate whether the inclusion of interactive aerosols (aerosol-radiation interactions, ARI, and aerosol-cloud interactions, ACI) in the model leads to significant changes in the circulation by means of circulation types (CTs).

This study covered Europe for winter (DJF). A principal component analysis (PCA) and the K-means clustering method were employed to classify CTs using the sea level pressure (SLP).

The results reflected significant differences in winter SLP patterns. Focusing on the two most important CTs, in BASE scenario (with no interactive aerosols), CT1 is characterised by a western zonal flux, whereas CT2 is mainly depicted by a low-pressure area centered in Italy and a light pressure gradient. Both interactive-aerosols simulations (ACI and ARI) produce a SLP reduction in the Center-East of Europe, what entails an inclination southwards of the flux direction. The effects on the second weather type is an increase of SLP, also in the Central-East part of the continent, what means a weakness of the Mediterranean low and a intensification of pressure field in Scandinavia. Even though both ACI and ARI simulations lead to variations of equal sign, those of ARI's are stronger. In other words, the inclusion of aerosol interactions with cloud microphysics makes that ARI effects diminish.

Regarding the differences in CTs frequency, CT1 and CT2 decrease in both ACI and ARI simulations, although they are not quite remarkable.

Moreover, an analysis of the aerosol optical depth (AOD) anomaly in ARI and ACI scenarios and its relation to SLP was carried out. According to AOD anomalies, negative SLP differences in CT1 correspond with a decrease of black aerosols (radiation absorbent aerosols) and an increase of white aerosols (radiation reflective aerosols). This causes a minor storage of energy in the atmosphere, reducing temperature and therefore the thickness of atmospheric layers. On the contrary, positive differences of SLP observed in CT2 match with an increase of black aerosols and a decrease of white ones. As a result, temperature in atmospheric layers and thickness rise. Therefore, aerosols modifies the energy balance, thickness driving changes in the atmospheric circulation patterns.

Spatial and temporal variability of surface ozone in a climate simulation over Europe and its relationship with climate parameters

Leandro Cristian Segado Moreno*, Juan Pedro Montávez, Pedro Jiménez-Guerrero

Department of Physics, University of Murcia, Murcia, Spain.

*e-mail: leandrocristian.segadom@um.es

Ozone (O_3) is one of the atmospheric pollutants of greatest concern due to its adverse effects on human health, as well as on other animals and plants. However, despite the fact that the causes of tropospheric ozone formation are known in detail, the variables that control its concentrations in areas near the surface are not entirely clear. Although initially the emission of nitrous oxides (NOx), together with temperature and surface radiation are the main factors which determine the formation and concentration of tropospheric ozone, observations over Europe show large concentrations of ozone in regions in which emissions of NO_x are very limited. This leads us to think that pollutants transport must play a main role in the concentrations obtained in many locations.

In this work, data on tropospheric ozone concentrations between 1991 and 2010 in the European area is analyzed, along with its relationship with climatic variables, both in space and time. Specifically, the relationships of tropospheric ozone with temperature, surface solar radiation (rsds) and nitrogen dioxide concentration (NO_2) are analyzed. Likewise, the relationship between tropospheric ozone concentration and surface atmospheric circulation is studied in detail, by means of composites and analysis of the Empirical Orthogonal Functions (EOFs), in order to determine the degree of relevance of the atmospheric circulation in those situations in which anomalous concentrations of ozone on the surface occur. The results obtained show that the relationships of ozone with temperature and radiation depend to a great extent on the studied site, being especially notable the area of North Africa, in which extreme ozone events are associated with a decrease in temperature, opposite to the expected result, being the main causes related to transport from polluted European regions.

The impact of climate change on photovoltaic power generation for solar installations in the Atacama desert

S. Bayo-Besteiro*, L. de la Torre, X. Costoya, A. Pérez-Alarcón, M. Gómez-Gesteira, M. de Castro, Juan A. Añel

EPhysLab, CIM-UVigo, Universidade de Vigo, Ourense, Galicia, Spain.

*e-mail: sbayo@uvigo.es

The solar power installed capacity has experienced significant development in the last years worldwide. The irradiance is the essential variable to produce solar power, although the temperature plays an essential role too in the efficiency of a solar installation. The Atacama desert in South America is one of the regions on our planet with some of the greatest irradiance levels; thus, its solar power installed capacity has experienced a significant boost in the last ten years. One of the keys to improving the profitability and the efficiency of a solar installation is to know the future power generation. For example, such knowledge lets to make appropriate geographical choices of the areas to be exploited.

In this work, we analysed variations in photovoltaic (PV) generation in the Atacama desert during the period 2021-2060 by means of an ensemble of three regional climate models from the CORDEX project. We validated the accuracy of these simulations by comparing them with data from the ERA5 reanalysis. The results show that for 2021-2060 the number of days with high-temperature values will increase compared to 1980-2005. For the case of irradiance, the number of days with high values will decrease; meanwhile, low irradiance days will increase, especially for the period 2041-2060. Overall, a decrease in PV generation is projected along the period studied (higher for (2041-2060)). The changes in the distribution of temperatures are expected to be the main responsible for reducing PV generation.

How climate change is affecting the patterns of electricity demand in Spain?

Jose M. Garrido-Perez[1,*], D. Barriopedro[1,2], R. García-Herrera[1,2], C. Ordóñez[1]

[1]*Departamento de Física de la Tierra y Astrofísica, Facultad de Ciencias Físicas, UCM, 28040, Madrid, Spain.*
[2]*Instituto de Geociencias (IGEO, CSIC-UCM), 28040, Madrid, Spain.*

*e-mail: josgarri@ucm.es

Climate change is one of the main concerns worldwide due to its environmental and socio-political implications. It impacts many sectors of our society, such as health, tourism, agriculture or energy. In particular, the need to balance electricity supply and demand has become an important international policy concern in a context of growing world energy consumption. On the one hand, the supply has received considerable attention. The market is tending to move away from fossil fuels to renewable energies in order to decarbonize the energy system and decrease greenhouse gas emissions. However, there has been little quantitative analysis about how the regional patterns of electricity demand will change under global warming.

Temperature is the main meteorological driver of the day-to-day variability of electricity demand. Both cold and warm days are associated with high electricity demand due to the use of electricity heating appliances and cooling systems, respectively. Consequently, the Spanish energy system is characterized by a seasonal cycle of electricity demand with two relative maxima in winter and summer. Nowadays, the occurrence of extreme electricity demand days is higher in winter than in summer, but this may change with the projected increase in temperatures over the twenty-first century. This work [1] evaluates the influence that climate change could exert on electricity demand patterns in Spain conditioned on the level of global warming, with special attention to the seasonal occurrence of extreme demand days. For this purpose, assuming the currently observed electricity demand–temperature relationship holds in the future, we have generated daily time series of pseudo-electricity demand from the recent past until the late twenty-first century by using simulated temperatures from statistical downscaling of global climate model experiments.

We have found that, despite the minor warming effects on the median values of daily electricity demand, the mean values as well as the frequency and severity of extreme electricity demand days are expected to increase significantly in Spain, even for low levels of regional warming. Moreover, the occurrence of these extremes will experience a seasonal shift from winter to summer due to the projected temperature increases in both seasons. Under a high radiative forcing scenario of greenhouse gas emissions (RCP8.5), the extended summer season (June–September) will concentrate more than 50% of extreme electricity demand days by mid-century, increasing to 90% before the end of the century (Figure 1).

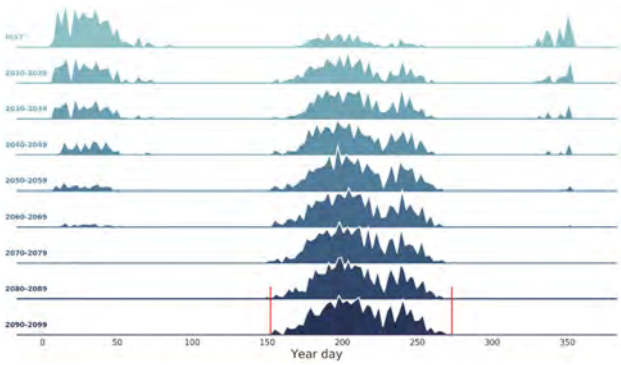

Figure 1. Probability density function of extreme electricity demand days for the 1961–2000 historical period (HIST) and for each decade from 2020 to 2099.

Finally, we have shown that future changes in electricity demand could have considerable spatial heterogeneity over the country, which has strong implications for the management of the electricity system. While Spain is warming up faster than the global mean, there are some regions that will be exposed to lower warming than others. In particular, northwestern Spain will experience the seasonal shift later than the rest of the country due to the relatively mild summer temperatures and lower projected warming there.

[1] Jose M. Garrido-Perez, D. Barriopedro, R. García-Herrera and C. Ordóñez, Impact of climate change on Spanish electricity demand, *Climatic Change* **165**, 50 (2021).

Did the meteorology affect the near-surface ozone concentrations over Europe during the COVID-19 lockdown of early spring 2020?

C. Ordóñez[1,*], Jose M. Garrido-Perez[1], R. García-Herrera[1,2]

[1]*Departamento de Física de la Tierra y Astrofísica, Facultad de Ciencias Físicas, UCM, 28040, Madrid, Spain.*
[2]*Instituto de Geociencias (IGEO, CSIC-UCM), 28040, Madrid, Spain.*

*e-mail: carlordo@ucm.es

Over the last two years non-pharmaceutical intervention measures in the form of social distancing and lockdowns have been applied to reduce the transmission of SARS-CoV-2. At the beginning of the pandemic, from mid-March to late April 2020, most European countries were under strict lockdowns. This caused unprecedented falls in industrial activity and vehicle use, two of the main sources of air pollution.

This work [1] focuses on the impact of that lockdown on the near-surface ozone concentrations in Europe. For that purpose, we have analysed 1-h daily maximum nitrogen dioxide (NO_2) and maximum daily 8-h running average ozone (MDA8 O_3) observations at ~1300 background sites of the European Environment Agency's air quality database (AirBase) as well as daily meteorological fields form a reanalysis.

As expected, NO_2 concentrations decreased considerably, with relative reductions ranging from 5% to 55% with respect to the same period in 2015–2019 for 80% of the sites. However, surface O_3 decreased in the Iberian Peninsula and increased over northwestern and central Europe. In some countries like Germany, O_3 concentrations were typical of the summer season. Atmospheric conditions were also unusual, with anomalously stable, dry, and warm weather over large parts of the continent and meteorological anomalies of opposite sign in the southwest. This could have raised the O_3 concentrations over most of Europe except in Iberia.

As the meteorology seemed to play a substantial role, we have built statistical models to separate the effect of meteorology and emissions, and to estimate the expected O_3 concentrations during that period in the absence of a lockdown. The results indicate that a considerable fraction of the observed O_3 enhancements in northwestern and central Europe can be explained by elevated temperatures, low atmospheric humidity and high solar radiation (Figure 1). On the other hand, the O_3 reduction in Iberia is attributable to low solar radiation and high specific humidity, and to a lesser extent low temperatures, while weak zonal winds partly compensated those effects.

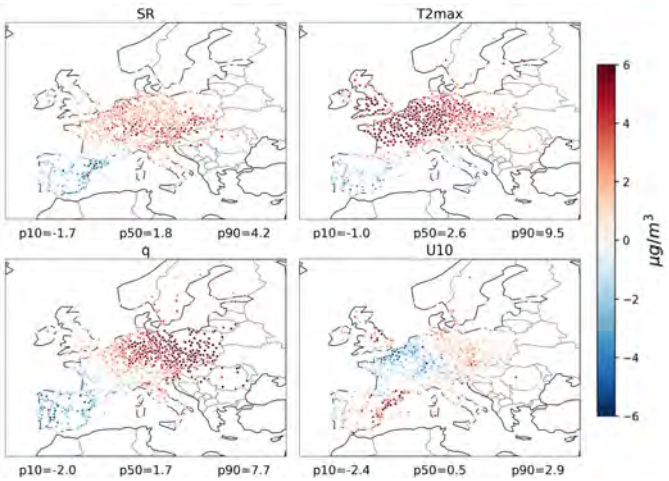

Figure 1. Average differences between predicted MDA8 O_3 using daily meteorology of 15 March – 30 April 2020 and after replacing the daily values of a meteorological field (incoming solar radiation at surface, SR; 2-m daily maximum temperature, T2max; 2-m specific humidity, q; 10-m zonal wind, U10) by the climatological values in 2015–2019.

While this analysis shows a dominant role of the meteorology during the early-spring lockdown, it is well known that other factors (e.g. sharper decreases in emissions of nitrogen oxides than those of volatile organic compounds) have yielded regional ozone enhancements over some regions during the pandemic.

[1] Ordóñez C., Garrido-Perez J.M., García-Herrera R, Early spring near-surface ozone in Europe during the COVID-19 shutdown: Meteorological effects outweigh emission changes, *Science of The Total Environment* **747**, 141322 (2020).

Preliminary results about long-term trends in downward surface shortwave radiation over Spain (1985–2021)

A. Bernaldez[1], **J.M. Vaquero**[2,*], M. Anton[1], A. Sanchez-Lorenzo[1]

[1] *Departamento de Física, Facultad de Ciencias, Universidad de Extremadura, Badajoz, España.*
[2] *Departamento de Física, Centro Universitario de Mérida, Universidad de Extremadura, Mérida, España.*

*e-mail: jvaquero@unex.es

The downward surface shortwave radiation (SSR) is a component of the solar radiation that plays an important role in our planet life by driving the main processes that occur in the atmosphere and oceans. Not only is the study of solar radiation important because it modulates the global energy balance but it has also important impacts in different socio-economic sectors such as agriculture and solar energy production [1].

There has been a growing interest in the study of solar radiation tendencies in the last decades since there is strong evidence showing that this variable has not remained constant over the years but instead significant decadal changes have been reported [1]. A widespread reduction in SSR has been proved to have occurred from the 1950s to the 1980s, a phenomenom that has been called *global dimming*. In contrast, a recovery and subsequent increase in SSR since the 1980s have been reported (*brightening period*).

Although previous studies have focused on SSR trends in Spain [2], no one has done an update up to the present days. Thus, the main objective of this study is to examine SSR temporal changes for a long period (+30 years, from the 1980s up to the present time) over different stations.

The radiation dataset was obtained from the Spanish Agencia Estatal de Meteorología (AEMET). SSR measurements were permofed using Kipp & Zonem pyranometers, which were periodically calibrated against international standards in order to ensure the reliability and traceability of the measurements.

Daily radiation data (measured in kJ m^{-2}) of 70 stations are available, but for this study only the series starting at least in the early 1980s were considered. Taking into account this constrain, the number of series available is reduced to 13, from which Bilbao, Oviedo and Valladolid are discarded as several temporal inhomogeneities have been detected, which results in a final dataset consisting of 10 stations (Albacete, Cáceres, La Coruña, Logroño, Madrid, Málaga, Murcia, Palma de Mallorca, San Sebastián and Santander).

Daily radiation data was averaged to obtain monthly values for each station and monthly anomalies were calculated as differences to the 1985-2021 mean. Individual annual anomalies have been calculated by averaging the monthly anomalies and individual seasonal annomalies have been computed in a similar way. The seasons were defined as: winter (DJF), spring (MAM), summer (JJA) and autumn (SON). Both annual and seasonal mean series for Spain have been computed by the arithmetic mean of the individual annual and seasonsal series of the 10 stations, respectively. An analysis of the trends in SSR have been performed, both for individual stations and the average of Spain.

The results show a significant positive trend of +3.85 Wm^{-2} per decade for the annual series of SSR during the 1985-2021 period. The seasonal series also exhibited an increase with the strongest and significant ($p < 0.05$) rates in summer (+6.94 Wm^{-2} per decade) and autumn (+3.72 Wm^{-2} per decade). These results are in agreement with those obtained in previous studies but there are small differences in some values due to corrections in the dataset and homogenization methods applied, as well as the longest period considered in this study.

[1] A. Sanchez-Lorenzo, M. Wild, M. Brunetti, J. A. Guijarro, M. Z. Hakuba , J. Calbó, S. Mystakidis, and B. Bartok, *Journal of Geophysical Research: Atmospheres* **120**, 9555-9569 (2015).
[2] A. Sanchez-Lorenzo, J. Calvó, and M. Wild, *Global and Planetary Change* **100**, 343-352 (2013).

Análisis de escala simple de veinticinco años de registros de la red pluviométrica de Barcelona

Xavier Navarro[1], **Ricard Kirchner**[2,*], Raúl Rodríguez-Solà[3], M. Carmen Casas-Castillo[2]

[1]*Dept. de Física, EPSEVG, Universitat Politècnica de Catalunya, Víctor Balaguer s/n, 08800 Vilanova i La Geltrú.*
[2]*Departmento de Física, ESEIAAT, Universitat Politècnica de Catalunya, Colom 1, 08222 Terrassa.*
[3]*Departmento de Física, ETSEIB, Universitat Politècnica de Catalunya, Avda. Diagonal 647, 08028 Barcelona.*

*e-mail: ricard.kirchner@upc.edu

El área metropolitana de Barcelona, de aproximadamente 100 km^2 de extensión, dispone de una red densa de pluviómetros de balancín que se empezó a instalar en 1983, y ha ido siendo gestionada desde entonces por diferentes empresas (CLABSA, Aqualogy, y actualmente BCASA). Se dispone de los registros 5-minutales de lluvia de una veintena de pluviómetros, a lo largo de 25 años de funcionamiento desde 1994 hasta 2019. A partir de estos registros de lluvia ha sido posible realizar un análisis de escala simple específico para cada pluviómetro, con el fin de poner de manifiesto las características, ligeramente diferentes, de la precipitación recogida en cada una de las zonas del área urbana.

Las series de máximos anuales de intensidad cumplen relaciones de escala del tipo $I_t \overset{dist}{=} \lambda^{K(q)} I_{\lambda t}$, expresión que indica que la intensidad I_t para una cierta duración t se puede describir por la misma distribución estadística que el segundo miembro de la ecuación, en el cual $I_{\lambda t}$ es la intensidad de lluvia para una duración diferente λt, siendo λ la relación de escala entre ellas. El exponente $K(q)$ es una función de escala del orden q de los momentos estadísticos: cuando puede aproximarse por una expresión lineal como βq se dice que la distribución está describiendo una magnitud monofractal o de escala simple; si no es así lo que se tiene es un multifractal. Existen varios estudios [1, 2] que muestran como el exponente de escala β suele ser un buen indicador del tipo de régimen pluviométrico, de su irregularidad. Así, cuando este exponente se calcula a partir de la agregación de registros diarios de lluvia, en los lugares en los cuáles estos registros son más regulares se obtienen valores más altos (sobre -0.5) que en donde es más frecuente tener máximos aislados de lluvia intensa y registros irregulares (más cercanos al valor límite -1). Para el Observatori Fabra, a 411 m de altura, se obtuvo [2] un valor del exponente β de -0.78, tanto para los registros del pluviómetro totalizador Hellmann como para los del pluviógrafo Jardí operando al unísono entre 1927 y 1992.

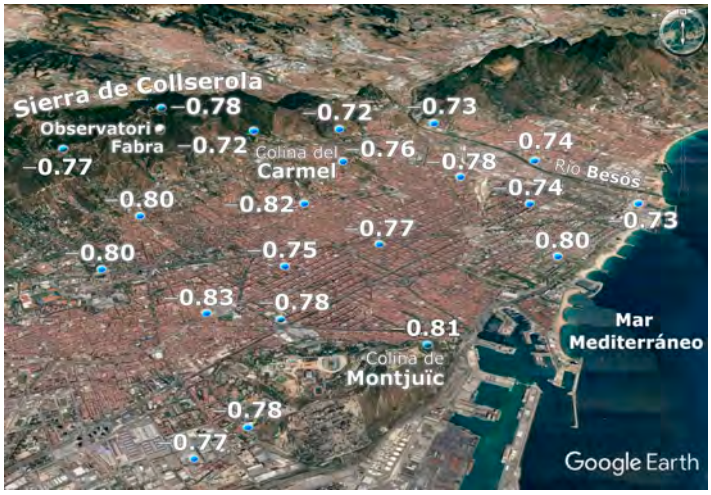

Figura 1. Valores de β en cada pluviómetro de la red de Barcelona.

El estudio detecta pequeñas diferencias pluviométricas entre las diferentes zonas urbanas mediante el análisis de escala simple. Se han obtenido valores de β para los diferentes pluviómetros entre -0.72 y -0.83 (Fig. 1). La distribución espacial de β muestra relación con características topográficas como la altura o la distancia al mar. A excepción de la zona central, en el llano de la ciudad se obtienen valores alrededor de -0.80 que van aumentando hacia las afueras, en especial en la cuenca del río Besós, con valores de -0.73 y -0.74.

[1] Casas-Castillo MC, Rodríguez-Solà R, Llabrés- Brustenga A, García-Marín AP, Estévez J, Navarro X. A Simple Scaling Analysis of Rainfall in Andalusia (Spain) under Different Precipitation Regimes. *Water* **14**, 1303 (2022). https://doi.org/10.3390/w14081303
[2] Rodríguez-Solà R, Casas-Castillo MC, Navarro X, Redaño Á. A study of the scaling properties of rainfall in Spain and its appropriateness to generate intensity-duration-frequency curves from daily records. *Int. J. Climatol.* **37**,770 (2017). https://doi.org/10.1002/joc.4738

Long-term analysis of Schumann Resonance measured at the Sierra Nevada ELF station

J. Rodríguez-Camacho[1], S. Toledo-Redondo[2], J. Portí[1], J. Fornieles[3], D. Blanco[1], J. F. Gómez-Lopera[1], A. Salinas[3], **M. C. Carrión**[1,*]

[1]*Departamento de Física Aplicada, Universidad de Granada, Spain.*
[2]*Departamento de Electromagnetismo y Electrónica, Universidad de Murcia, Spain.*
[3]*Departamento de Electromagnetismo y Física de la Materia, Universidad de Granada, Spain.*

*e-mail: mcarrion@ugr.es

Schumann Resonance (SR) is a natural electromagnetic phenomenon that consists of the resonance of the EM field propagating within the cavity delimited by the surface of the Earth and the lower ionosphere, mainly excited by lightning activity. The SR appears in the Extremely Low Frequency (ELF) band of the electromagnetic spectrum, and the approximate values for the first three resonance modes are 8, 14 and 20 Hz. An ELF station was designed and deployed by the authors of this work at Sierra Nevada, Granada, Spain, which comprises two ground based magnetometers, oriented in the North-South (NS) and East-West (EW) directions, respectively. More details can be found in [1].

A methodology to process the time domain magnetic field recorded at this station has been proposed by the authors in [2]. The first part of the scheme is based on the Welch method to obtain the amplitude spectrum of the recordings. For this purpose, the data are split into 10-min long intervals, and each one of these intervals is also split into 10-sec long windows with a 5-sec overlap. After applying a Hann window, we obtain its FFT. We average the FFT of all the 10-sec long windows and the output of this first part of the scheme is the amplitude spectrum of each 10-min long interval of recordings. A second part of the process consists of the removal of the anthropogenic noise that may appear due to electrical machinery, transport systems or other sources near the ELF station. In a third step, a fitting curve made up of three lorentzian functions and a linear part is fitted to the amplitude spectrum, thus obtaining a value for each amplitude, central frequency and width of each one of the three first SR mode for each 10-min interval.

Finally, the analysis of the long term variations of the parameters of the resonances -amplitude, central frequency and width- gives information on the global lightning activity and other parameters concerning the state of the Earth's atmosphere. The authors have performed a study of the SR measured at the Sierra Nevada ELF station. In order to perform this study, a set of programs based on the Pandas package has been implemented. The code 'Variations.py' includes a wide range of functions which allow to analize the SR variations using different time-scales -seasonal, monthly and daily- and also spectrograms, analysis of the rate of saturations of the magnetometers and statistical studies. A masking process of anomalous intervals is applied to the recordings. Some python notebooks have been created to easily visualize the study of the SR and will be shared to the scientific comunity together with the experimental data.

The results have been compared to previous works. The general diurnal evolution of the three main storm centers on Earth -Africa, Asia, and America- is similar to that observed in previous works, and the results also corroborate an intesification of the SR during the transition months that precede the super El Niño episode that happened at the end of 2015 and the beginning of 2016. More detail of this study can be found in [3].

[1] Fornieles-Callejón, J., Salinas, A., Toledo-Redondo, S., Portí, J., Méndez, A., Navarro, E. A., et al., *Radio Science* **50**, 191 (2015).

[2] Rodríguez-Camacho, J., Fornieles, J., Carrión, M. C., Portí, J., Toledo-Redondo, S. and Salinas, A., *Journal of Geophysical Research: Atmospheres* **123**(23), 13277 (2018).

[3] Rodríguez-Camacho, J., Salinas, A., Carrión, M. C., Portí, J., Fornieles, J. and Toledo-Redondo, S., *Journal of Geophysical Research: Atmospheres* **127** (2022).

Acknowledgements: This work has been supported by the investigation research projects FIS2017- 90102-R, of the Ministry of Economy and Competitiveness (MINECO) of Spain, cofinanced by the Fund European Regional Development (FEDER), and PID2020-112805GA-I00, of the Ministry of Science and Innovation of Spain, and the Ministry of Education, Science and Sport of Spain through the FPUgrants for PhD studentship (reference: FPU15/04291).

Información y Computación Cuánticas

Presentaciones orales

Martes 12/07:

15:30-15:45 Alejandro Pozas-Kerstjens, Nicolas Gisin, Marc-Olivier Renou. *Proofs of network quantum nonlocality aided by machine learning*

15:45-16:00 María Hita-Pérez, Pedro Orellana, Manuel Pino, Juan José García Ripoll. *Quasi Bound-State in the continuum in a heavy fluxonium qutrit*

16:00-16:15 Paula García-Molina, Javier Rodríguez-Mediavilla, and Juan José García-Ripoll. *Quantum Fourier analysis for multivariate functions and applications to a class of Schrödinger-type partial differential equations*

16:15-16:30 Pablo Díez Valle. *Understanding single-layer QAOA advantage*

16:30-16:45 Emanuel-Cristian Boghiu, Flavien Hirsch, Pei-Sheng Lin, Marco Túlio Quintino, Joseph Bowles. *Device-independent and semi-device-independent entanglement certification in broadcast Bell scenarios*

16:45-17:00 Javier Cerrillo. *Transfer-Tensor Method: Analysis and Propagation Tool for Open Quantum Systems*

17:00-18:00 **Café**.

18:00-18:15 Javier Argüello-Luengo, Alejandro González-Tudela, Daniel González-Cuadra. *Tunable long-range fermion-mediated interactions in cold-atom quantum simulators*

18:15-18:30 S. C. Wein, J. C. Loredo, M. Maffei, P. Hilaire, A. Harouri, N. Somaschi, A. Lemaître, I. Sagnes, L. Lanco, O. Krebs, A. Auffèves, C. Simon, P. Senellart, C. Anton-Solanas. *On demand time-entanglement in the Fock basis generated by sequential excitation of a two-level atom*

18:30-18:45 David Fernández Fernández, Yue Ban, Gloria Platero Coello. *Quantum control of two qubits spin hole gates*

18:45-19:00 Alberto Castro, Adrián García Carrizo, David Zueco, Fernando Luis. *Optimal control of molecular spin qudits*

19:00-19:15 Jordi Picó-Cortés, Gloria Platero. *Applications of Floquet engineering in ac-driven spin qubits*

Proofs of network quantum nonlocality aided by machine learning

Alejandro Pozas-Kerstjens[1,2,*], Nicolas Gisin[3,4], Marc-Olivier Renou[5]

[1]*Instituto de Ciencias Matemáticas (CSIC-UAM-UC3M-UCM), 28049 Madrid, Spain.* [2]*Departamento de Análisis Matemático, Universidad Complutense de Madrid, 28040 Madrid, Spain.* [3]*Group of Applied Physics, University of Geneva, 1211 Geneva 4, Switzerland.* [4]*Schaffhausen Institute of Technology – SIT, Geneva, Switzerland.* [5]*ICFO – Institut de Ciències Fotòniques, The Barcelona Institute of Science and Technology, 08860 Castelldefels (Barcelona), Spain.*

*e-mail: physics@alexpozas.com

We formally prove a conjecture initially formulated by using machine learning techniques to identify quantum nonlocality in networks. Quantum nonlocality is a consequence of Bell's theorem, which implies that nature cannot be modeled using only local variables. Both, theoretical advances and experimental improvements, are allowing to move the focus from bipartite settings to scenarios where many independent sources distribute physical systems among different parties in a network.

Nonlocality in networks is defined in a way analogous to the standard notion, namely by opposition to admitting a network-local model. Network-local correlations are those that can be generated by assuming that the sources in the network distribute independent classical shared randomness, and the parties process the randomness they receive to generate an outcome. For example, in the triangle scenario of Fig. 1, local correlations admit models of the form

$$P(a,b,c) = \int \mathrm{d}\alpha \mathrm{d}\beta \mathrm{d}\gamma\, \mu_{BC}(\alpha)\mu_{AC}(\beta)\mu_{AB}(\gamma) \times P_A(a|\beta,\gamma)P_B(b|\gamma,\alpha)P_C(c|\alpha,\beta), \qquad (1)$$

where α, β and γ denote sources of classical shared randomness distributed with densities $\mu_{BC}(\alpha)$, $\mu_{AC}(\beta)$ and $\mu_{AB}(\gamma)$, respectively, and P_A, P_B and P_C represent local operations on the variables received by each party.

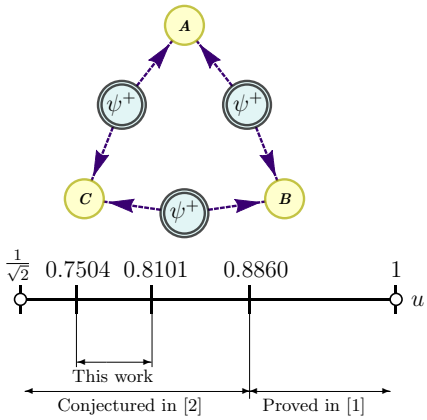

Figure 1. (Top) The triangle scenario, where we look for classical realizations of the quantum probability distributions described in Ref. [1], which are parameterized by $1/\sqrt{2} \leq u \leq 1$. (Bottom) The current standing of proofs of nonlocality for the family of distributions.

Recently, an interesting family of quantum distributions in the triangle scenario was proven not to admit triangle-local models for a certain range of its defining parameter [1]. Due to its interest in the field, Ref. [2] analyzed triangle nonlocality in the family by means of deep learning techniques. Surprisingly, this approach lead the authors to conjecture that the family of distributions of Ref. [1] did not admit models of the form of Eq. (1) well beyond the limits established by the original proof (see Fig. 1). However, the inherent features of the formalism of deep learning prevent this conjecture to become a rigorous demonstration.

In this work [3], we prove the conjecture formulated in Ref. [2] for a certain range of the parameter characterizing the family of distributions. We do so by reducing the original four-outcome distributions to families of two-outcome ones, and analyzing if these admit local models using the inflation technique [4]. Our construction provides a large family of network Bell inequalities that can contribute in deciding another long-standing open question, namely whether the binary-outcome triangle scenario without inputs supports network nonlocality. More broadly, our results can be framed in the context of artificial intelligence augmentation, which views machine learning as an enabling tool, rather than an automated solver. In this picture, the machine learning approach of Ref. [2] pointed to an interesting question, which in turn has produced results that have increased our understanding of triangle nonlocality, and provided paths for advancing other problems in the field.

[1] M.-O. Renou *et al.*, *Phys. Rev. Lett.* **123**, 140401 (2019).
[2] T. Kriváchy *et al.*, *npj Quantum Inf.* **6**, 70 (2020).
[3] A. Pozas-Kerstjens, N. Gisin, and M.-O. Renou, arXiv:2203.16543 (2022).
[4] E. Wolfe, R. W. Spekkens, and T. Fritz, *J. Causal Inference* **7**, 20170020 (2019).

Quasi Bound-State in the continuum in a heavy fluxonium qutrit

María Hita-Pérez[1,*], Pedro Orellana[2], Juan José García-Ripoll[1], Manuel Pino[3]

[1]*Institute of Fundamental Physics IFF-CSIC, Calle Serrano 113b, Madrid 28006, Spain.*
[2]*Physics Department, Universidad Técnica Federico Santa María, Casilla 110 V, Valparaiso, Chile.*
[3]*Nanotechnology Group, USAL-Nanolab, Universidad de Salamanca, E-37008 Salamanca, Spain.*

*e-mail: hitaperezmaria@gmail.com

Quantum excitations generally decay when coupled to a band of states with a continuous spectrum, however, there are some exceptions to those decay processes where a confined state lying at the continuum part of the spectrum lives forever. Those bound states in the continuum (BIC) were predicted long ago and have appeared on several platforms as solid-state devices or photonic devices. Some recent works have found BICs modes in typical quantum-information set-ups, such as superconducting circuits, and argue their usefulness for quantum information applications. In this case, BICs correspond to plasma excitations spatially localized in a superconducting waveguide, while a qubit is used to enforce the necessary boundary conditions.

In this talk, we show how to construct a BIC state [1], more precisely a quasi-BIC state, localized within a fluxonium device when it is capacitively coupled to a waveguide [2]. First, we introduce an effective model for the Hamiltonian, flux, and charge operators of the fluxonium qutrit, obtained via an analytical approach based on Gram-Schmidt orthogonalization and with numerical methods. Then, we analyze the capacitive coupling to a waveguide, finding that the second excited state only decays to the first excited, which is a transition that can be strongly suppressed using a large shunting capacitance for the fluxonium.

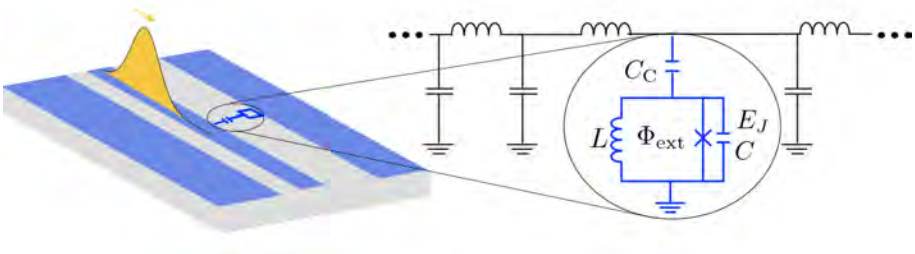

Figure 1. Fluxonium qubit capacitively coupled to a superconducting waveguide.

[1] M. Hita-Pérez, P. Orellana, J.J. García-Ripoll, and M. Pino "Quasi Bound-State in the continuum in a heavy fluxonium qutrit", *in preparation.*
[2] V.E. Manucharyan, J. Koch, L.I. Glazman, and M.H. Devoret, *Science* **326**, 113 (2009).

Acknowledgements: This work has been supported by European Commission FET-Open project AVaQus GA 899561 and CSIC Quantum Technologies Platform PTI-001.

Quantum Fourier analysis for multivariate functions and applications to a class of Schrödinger-type partial differential equations

Paula García-Molina*, Javier Rodríguez-Mediavilla, Juan José García-Ripoll

Instituto de Física Fundamental, IFF-CSIC, Calle Serrano 113b, 28006 Madrid, Spain

*e-mail: paula.garcia@iff.csic.es

In quantum numerical analysis quantum computers assist in the resolution of numerical analysis problems, among which partial differential equations (PDEs) stand out. Although highly-efficient methods to solve them have been proposed [1], they are not adequate for current noise intermediate-scale (NISQ) devices. Variational quantum algorithms [2] arise as an suitable alternative due to their lower hardware requirements and noise resilience. In this paradigm, a variational quantum circuit encodes the solution to a complex problem (a PDE in our case) and the parameters of the circuit are tuned through a learning process that optimizes a loss function. Both fault-tolerant and NISQ algorithms for quantum numerical analysis need an efficient representation of functions and differential operators. In this work [3], we propose a Fourier encoding to map functions and differential operators to the states of an n-qubit quantum register, whose representation can be extended with quantum Fourier interpolation [4]. Combined, both tools provide an efficient representation, with errors that can decrease doubly exponentially in the number of qubits. This favorable scaling motivates the application of these ideas on NISQ hardware, transforming the PDE into a variational principle that can be optimized using both existing and novel space-efficient variational *Ansätze* [5, 6], that take into account a problem's symmetries, and global and gradient-based optimizers.

We consider PDEs of the form $[D(-i\nabla) + V(\mathbf{x})]\, f(\mathbf{x}) = E f(\mathbf{x})$, defined over a regular domain, with periodic boundary conditions and real functions $D(\mathbf{p}), V(\mathbf{x}) \in \mathbb{R}$. We assume that the PDE is a lower-bounded Hamiltonian operator $H = D(-i\nabla) + V(\mathbf{x}) \geqslant E_{\min}$, and we seek the ground state $E_{\min}$ using a variational quantum algorithm suitable for solving static PDEs with a Hamiltonian nature. We test our method for the PDE of the one-dimensional quantum harmonic oscillator, reaching low infidelities of order 10^{-4}–10^{-5} using only 3 to 4 qubits (Fig. 1(a)), demonstrating the high compression of information in a quantum computer. Practical fidelities are limited by the noise and the errors of the evaluation of the cost function in real computers, but they can also be improved through error mitigation techniques, recovering the ideal energy with an error ε of $O(10^{-2})$ (Fig. 1(b)).

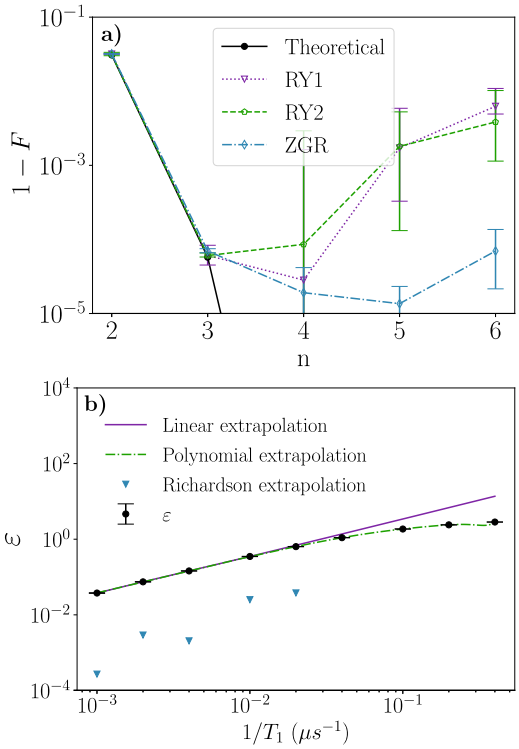

Figure 1. Harmonic oscillator results. (a) Lowest infidelity $1-F$ for $n = 2, 3, 4, 5, 6$ qubits using the ZGR [5,6] and the R_Y *Ansätze* with depths 1 (RY1) and 2 (RY2). (b) Zero-noise extrapolation for the energy error ε (RY1 with thermal relaxation and 3 qubits).

[1] D. W. Berry, *J. of Phys. A* **47**, 105301 (2014).
[2] A. Peruzzo et al., *Nat. Commun.* **5**, 4213 (2014).
[3] P. García-Molina et al., *Phys. Rev. A* **105**, 012433 (2022).
[4] J. J. García-Ripoll, *Quantum* **5**, 431 (2021).
[5] C. Zalka, *Proc. R. Soc. A* **454**, 313 (1998).
[6] L. Grover, and T. Rudolph, arXiv:quant-ph/0208112.

Acknowledgements: Work funded by: MCIN/AEI/10.13039/501100011033, "FSE invierte en tu futuro", FPU19/03590, Spanish Project No. PGC2018-094792- B-I00 (MCIU/AEI/FEDER, UE), CAM/FEDER Project No. S2018/TCS-4342 (QUITEMAD-CM), Comunidad de Madrid Sinergicos 2020 project NanoQuCo-CM (Y2020/TCS6545) and CSIC Quantum Technology Platform PT-001.

Understanding single-layer QAOA advantage

Pablo Díez-Valle*, Diego Porras, Juan José García-Ripoll

Instituto de Física Fundamental IFF-CSIC, Calle Serrano 113b, Madrid 28006, Spain.

*e-mail: pablo.diez@csic.es

The Quantum Approximate Optimization Algorithm (QAOA) was originally proposed as a hybrid variational algorithm suitable for solving combinatorial optimization problems on NISQ devices [1]. Even though it has been shown, from reasonable theoretic assumptions, that the shallowest version of the algorithm already engineers a quantum probability distribution that is classically hard to sample [2], this formal sampling advantage may or may not translate into a practical advantage in the optimization scenario. In our work [3], we study a simple, single-layer generalization of the QAOA ansatz, and we analize its performance both from the optimization point of view—i.e. the probability to find the ground state— and also by understanding the types of states it prepares—i.e. the probability distributions that are hard to sample, according to [2].

With a new theoretical approach, our study reveals that the shallowest QAOA on universal Ising spin models creates pure, but thermal-like states with Gaussian perturbations (see Fig.1a). The sampling advantage manifests itself in the fact that these states resemble Boltzmann distributions with a temperature lower than can be efficiently simulated classically according to state-of-art techniques, such as Markov Chain Monte Carlo algorithms (see Fig.1b). Moreover, we connect the sampling advantage and the optimization properties, presenting that this low temperature also implies an advantage with respect to optimization, because there is an algebraic (Grover-like) enhancement of the ground state probability.

We believe that, in addition to opening new avenues for proving quantum advantages, the tools in this manuscript may shed light on more complex circuits, as well as offer new methods to understand the behavior of adiabatic quantum computers and quantum simulators.

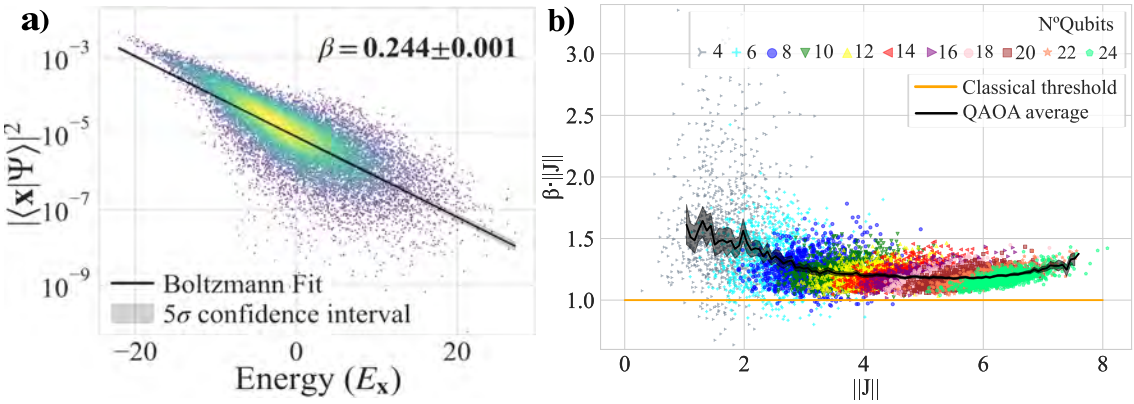

Figure 1: (a) Eigenstate probabilities (dots) and fitted Boltzmann distribution (line) for single-layer QAOA ansatz with optimal angles. (b) Effective temperatures β as a function of the interaction matrix J norm for Sherrington-Kirkpatrick problems. We show the average of these results (black line) and the threshold given by Monte Carlo methods (orange line) which demonstrates that the distributions obtained with one-layer QAOA are hard to sample classically.

[1] E. Farhi et al., *arxiv:1411.4028* (2014).
[2] E. Farhi et al., *arxiv:1602:07674* (2019).
[3] P. Díez-Valle et al., *arxiv: 2201.03358* (2022).

Acknowledgements: This work has been supported by European Commission FET Open project AVaQus Grant Agreement 899561, PGC2018-094792- BI00 (MCIU / AEI / FEDER, UE),Comunidad de Madrid Sinergicos 2020 project NanoQuCo-CM (Y2020/TCS6545), CSIC Quantum Technologies Platform PTI001, and CAM/FEDER project No. S2018/TCS-4342 (QUITEMAD-CM).

Device-independent and semi-device-independent entanglement certification in broadcast Bell scenarios

Emanuel-Cristian Boghiu[1,*], **Flavien Hirsch**[2], Pei-Sheng Lin[3], Marco Túlio Quintino[2,4], Joseph Bowles[1]

[1]*ICFO – Institut de Ciencies Fotoniques, 08860, Castelldefels, Spain.* [2]*Institute for Quantum Optics and Quantum Information (IQOQI), Boltzmanngasse 3, 1090 Vienna, Austria.* [3]*Department of Physics and QFort, National Cheng Kung University, Tainan 701, Taiwan.* [4]*Faculty of Physics, University of Vienna, Boltzmanngasse 5, 1090 Vienna, Austria*

*e-mail: Cristian.Boghiu@icfo.eu, link: arXiv:2111.06358

One of the most fascinating aspects of quantum theory is that it does not obey the same commonsense form of causality that is observed at the macroscopic level. Consider an entangled quantum system that is prepared and shared between several spatially separated laboratories and then measured. Remarkably, the correlations between measurement outcomes defy explanation via shared classical resources alone: a phenomenon called Bell nonlocality. Aside from foundational implications, Bell nonlocality plays a key role in quantum information technologies: it serves as fuel for device-independent protocols. The most basic of these protocols is that of entanglement certification: since Bell nonlocality requires the use of entangled states, its observation implies a certificate of entanglement in the underlying physics. Device-independent entanglement certification is highly desirable as it allows us to ensure entanglement even when the measurements performed by parties are untrusted and uncharacterised.

It is known that entanglement alone is not sufficient to observe Bell nonlocality, since some mixed entangled states are known to admit so-called local hidden-variable models. For example, the isotropic state (local unitary equivalent to the two-qubit Werner state),

$$\rho(\alpha) = \alpha|\Phi^+\rangle\langle\Phi^+| + (1-\alpha)1/4,$$

is entangled for $\alpha > \frac{1}{3}$, however, it cannot violate any Bell inequality for $\alpha \lessapprox 0.683$. An important discovery in this respect was that of activation. The basic message is as follows: some quantum states that show only classical behaviour in the orthodox "standard scenario" can have their non-classicality activated, or revealed, by subjecting the state to a more complex measurement scenario. This both expands the set of entangled states that exhibit non-classical behaviour, and rekindles the hope of proving Bell nonlocality of all entangled states. There are a number of different techniques that have been shown to activate quantum states.

In this work we focus on a technique called broadcasting (Figure 1) and show through semidefinite programming techniques that device-independent entanglement certification is possible for the two-qubit Werner state in essentially the entire range of entanglement ($\alpha > 0.338$). To get the same results with other techniques one needs at least 2515 copies of the quantum state and to perform entangling measurements, while with broadcasting we only need 1 copy of the state, local measurements and 2 quantum channels. This makes it much more experimentally friendly. In this work we also construct Bell inequalities tailored to the broadcast scenario, and show how broadcasting can lead to stronger notions of Bell nonlocality activation. In particular, we exploit these ideas to show that bipartite states admitting a local hidden-variable model for general (POVM) measurements can lead to genuine tripartite nonlocal correlations. Finally, we extend the concept of EPR steering to the broadcast scenario, and present novel examples of EPR steering activation of the two-qubit isotropic state.

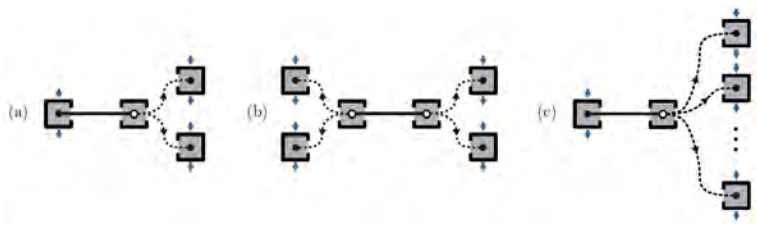

Figure 1. The broadcasting scenario. One (or more) of the local systems is broadcast via the application of a quantum channel, resulting in a multipartite state, sent to distant parties. Local measurements are performed on this state, and the resulting statistics are used to rule out a local hidden variable description for the original bipartite state.

Non-Markovian Dynamical Maps: Analysis Tool for Open Quantum Systems

Javier Cerrillo*

Área de Física Aplicada, Universidad Politécnica de Cartagena, España.

*e-mail: javier.cerrillo@upct.es

The effect of an environment on an open quantum system is fully described by the memory kernel in the terms presented in the Nakajima-Zwanzig formalism. It contains the key information of its interaction with the environment and, together with the Hamiltonian, it is sufficient to predict the trajectory at later stages. Its computation in realistic settings is nevertheless impractical and it has historically remained a formal result.

We proposed [1] a general approach based on non-Markovian dynamical maps to extract full information from the initial trajectories of a system and compress it into non-Markovian transfer tensors. The non-Markovian transfer tensor method (TTM) is equivalent to solving the Nakajima-Zwanzig equation and, therefore, can be used to reconstruct the dynamical operators (the system Hamiltonian and memory kernel) from quantum trajectories obtained in simulations or experiments and also to accurately and efficiently propagate the state of the system to arbitrarily long time scales.

The concept underlying the approach can be generalized to physical observables such as absorption [2] and emission spectra [3] with the goal of learning and manipulating the trajectories of an open quantum system. From this perspective, it is possible to relate engineered control and steering mechanisms to its corresponding memory kernel so as to determine the architecture of their physical implementations.

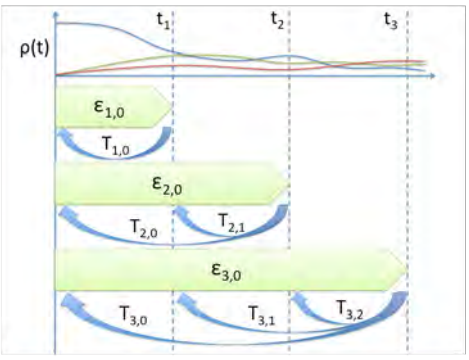

[1] Javier Cerrillo and Jianshu Cao, *Phys. Rev. Lett.* **112**, 1104401 (2014).
[2] R. Rosenbach, J Cerrillo, S.F. Huelga, J. Cao, M.B. Plenio, *New Journal of Physics* **18**, 23035 (2016).
[3] M. Buser, J. Cerrillo, G. Schaller, J. Cao, *Physical Review A* **96**, 062122 (2017).

Tunable long-range fermion-mediated interactions in cold-atom quantum simulators

Javier Argüello-Luengo[1,*], Alejandro González-Tudela[2], Daniel González-Cuadra[3]

[1]*ICFO - Institut de Ciències Fotòniques, The Barcelona Institute of Science and Technology, Av. Carl Friedrich Gauss 3, 08860 Castelldefels (Barcelona), Spain.* [2] *Institute of Fundamental Physics IFF-CSIC, Calle Serrano 113b, 28006 Madrid, Spain.* [3]*Institute for Quantum Optics and Quantum Information of the Austrian Academy of Sciences, 6020 Innsbruck, Austria.*

*e-mail: javier.arguello@icfo.eu

Engineering and controlling long-range interactions between ultra-cold atoms would allows to obtain unprecedented many-body phases, such as supersolid [1], magnetic [2,3] and topological ones [4,5], as well as enabling the simulation of quantum chemistry [6] and high-energy problems [7]. Unfortunately, this constitutes an outstanding challenge since atoms generally interact locally via collisions. A way of going beyond this limitation is by using Fermi-Bose mixtures, where fermionic atoms can act as mediators, giving rise to long-range RKKY-type interactions characterized by the dimensionality and density of the fermionic gas. Such interactions have very recently been realized experimentally [8,9] confirming the feasibility of that approach. Here, we propose several tuning knobs, accessible in current experimental platforms, that allow to further control the range and shape of the mediated interactions, extending the existing quantum simulation toolbox. In particular, we include an additional optical lattice for the fermionic mediator, as well as anisotropic traps to change its dimensionality in a continuous manner (see Figure 1). This allows us to interpolate between power-law and exponential decays, introducing an effective cutoff for the interaction range, as well as to tune the relative interaction strengths at different distances. Finally, we show how our approach allows to investigate frustrated regimes that were not previously accessible, where symmetry-protected topological phases as well as chiral spin liquids emerge [10].

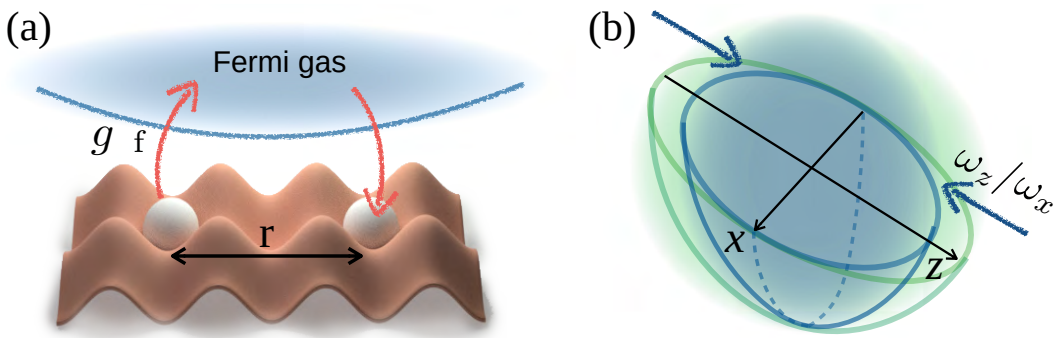

Figure 1. (a) Two bosonic atoms (white) separated by distance r and trapped in an optical lattice (red) experience an effective long-range interaction mediated by a Fermi gas trapped in an harmonic potential (blue). The contact Bose-Fermi interactions ($g_{\rm bf}$) virtually populates the conduction band of the Fermi gas. (b) By controlling the strength of the trapping potential in an orthogonal direction, ω_z/ω_x, one can continuously tune the dimension of the Fermi gas from 1D to 2D, introducing additional modulating frequencies.

[1] J. Léonard, A. Morales, P. Zupancic, T. Esslinger, and T. Donner, *Nature* 543, 87 (2017).
[2] A. V. Gorshkov, et al., *Phys. Rev. Lett.* 107, 115301 (2011).
[3] R. M. W. van Bijnen and T. Pohl, *Phys. Rev. Lett.* 114, 243002 (2015).
[4] S. de Léséleuc, V. Lienhard, P. Scholl, D. Barredo, S. Weber, N. Lang, H. P. Büchler, T. Lahaye, and A. Browaeys, *Science* 365, 775 (2019).
[5] N. Y. Yao, et al., *Phys. Rev. Lett.* 110, 185302 (2013).
[6] J. Argüello-Luengo, A. González-Tudela, T. Shi, P. Zoller, and J. Cirac, *Nature* 574, 215 (2019).
[7] E. Zohar, J. I. Cirac, and B. Reznik, *Rep. Prog. Phys.* 79, 014401 (2015).
[8] B. J. DeSalvo, K. Patel, G. Cai, and C. Chin, *Nature* 568, 61 (2019).
[9] H. Edri, B. Raz, N. Matzliah, N. Davidson, and R. Ozeri, *Phys. Rev. Lett.* 124, 163401 (2020).
[10] J. Argüello-Luengo, A. González-Tudela, and D. González-Cuadra, *arXiv*:2203.17022 (2022).

On demand time-entanglement in the Fock basis generated by sequential excitation of a two-level atom

S. C. Wein[1, 2], J. C. Loredo[3], M. Maffei[2], P. Hilaire[3], A. Harouri[3], N. Somaschi[4], A. Lemaître[3], I. Sagnes[3], L. Lanco[3,5], O. Krebs[3], A. Auffèves[2], C. Simon[1], P. Senellart[3], **C. Anton-Solanas**[3,6,*]

[1]*University of Calgary, Calgary, Canada T2N 1N4.*
[2]*Université Grenoble Alpes, CNRS, Grenoble INP, Institut Nèel, 38000 Grenoble, France.*
[3]*C2N, CNRS, Université Paris-Saclay, UMR 9001, 10 Boulevard Thomas Gobert, 91120 Palaiseau, France.*
[4]*Quandela SAS, 10 Boulevard Thomas Gobert, 91120 Palaiseau, France.*
[5]*Université Paris Diderot, Paris 7, 75205 Paris CEDEX 13, France.*
[6]*Institute of Physics, Carl von Ossietzky University, 26129 Oldenburg, Germany.*

*e-mail: c.anton.so@gmail.com

During the spontaneous emission of light from an excited two-level atom, the atom briefly becomes entangled with the photonic field, producing the entangled state $\alpha|e,0\rangle + \beta|g,1\rangle$, where g and e are the ground and excited states of the atom, and 0 and 1 are the vacuum and single photon states [1].

With a very simple protocol, we experimentally show that the spontaneous emission can be used to deliver on demand photon-number entanglement encoded in time. By exciting a charged quantum dot (an artificial two-level atom) with two delayed π pulses, we generate a photon-number Bell state $\alpha|00\rangle + \beta|11\rangle$, see a sketch of the protocol and the emitted wavepacket in Fig. 1. We characterise the quantum properties of this state using time-resolved photon-correlation measurements [2].

We theoretically show that applying longer sequences of π pulses to a two-level atom produces multipartite entangled states with properties linked to the *Fibonacci* sequence. We believe that these new photonic states could have applications in quantum technology. Additionally, our excitation protocol could be applied on other energy level systems, such as the biexciton-exciton cascade, to produce high-dimensional entanglement.

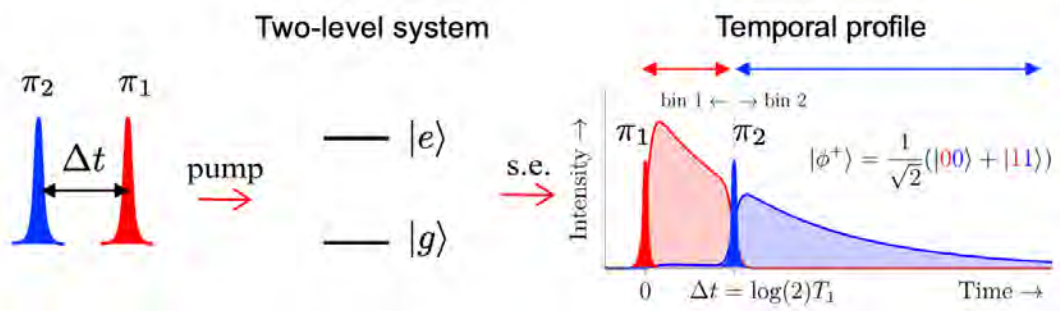

Figure 1. Schematic representation of the double π pulse excitation on a two-level system. The first [second] π-pulse excites the two-level atom at $t = 0$ [$t = log(2)T_1$], the emitted photonic wavepacket is a time-entangled Bell state: the first [second] temporal bin is encoded in a red [blue] color. The vacuum and single photon states are distributed in these time bins generating the Bell state $|\phi^+\rangle = (|00\rangle + |11\rangle)/\sqrt{2}$.

[1] V. Weisskopf, E. Wigner, Berechnung der natürlichen linienbreite auf grund der diracschen lichttheorie, *Zeitschrift für Physik* **63**, 54 (1930)
[2] S. C. Wein, *et al.* arXiv:2106.02049 [quant-ph] (2021). (Accepted in Nature Photonics)

Quantum control of two qubits spin hole gates

David Fernández Fernández[1,*], Yue Ban[2,3], Gloria Platero Coello[1]

[1] *Instituto de Ciencia de Materiales de Madrid (ICMM-CSIC), Madrid, Spain.*
[2] *Department of Physical Chemistry, University of the Basque Country UPV/EHU, Bilbao, Spain*
[3] *EHU Quantum Center, University of the Basque Country UPV/EHU, Biscay, Spain*

*e-mail: david.fernandez@csic.es

Hole spins in semiconductor quantum dots (QDs) are attracting significant attention as candidates for fast, highly coherent, spin qubits [1-4]. They have long coherence time due to the weak hyperfine coupling to nuclear spins and have demonstrated to have rapid operation times due to the inherently strong spin–orbit coupling (SOC).

In this work we investigate how to control a two-hole spin qubit consisting of a triplet and a singlet hole states. For that purpose, we implement a driving protocol based on Shortcuts to Adiabaticity (STA), minimizing noise effects while enhancing robustness [5, 6]. We consider the fast quasi-adiabatic (FAQUAD) approach and analyze its feasibility to manipulate hole spin qubits and compare with other alternative protocols. We can initialize the qubit in an arbitrary state and perform a NOT gate by changing the detuning between dots. In addition, we achieve a SWAP-like two-qubits gate with a fidelity beyond error correction threshold. We study the robustness of the protocol regarding systematic errors in the detuning, as well as charge noise [7].

Furthermore, we study the direct transfer of entangled holes in QD arrays between edge sites by using inverse engineering techniques. We demonstrate that spin-conserving and spin-flipping direct transfer between edges can be achieved in a controlled way with all-electrical protocols by dynamically tuning the tunnelling rates between dots [8].

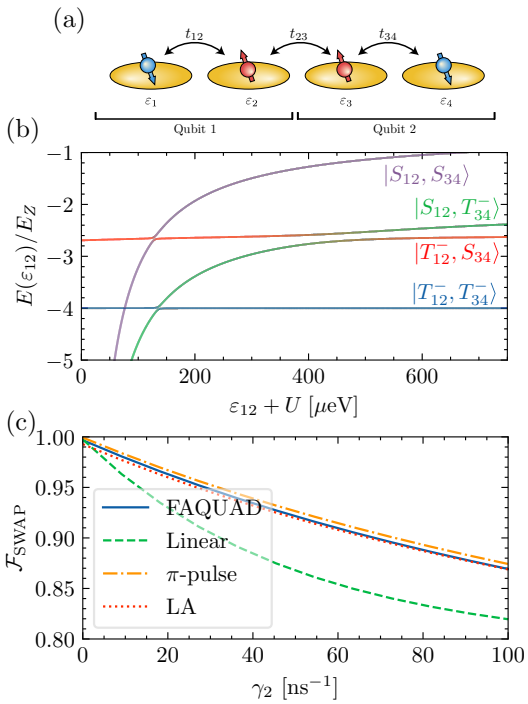

Figure 1. (a) Schematic picture of a quadruple quantum dot encoding two S-T qubits. (b) Energy level diagram of the system. (c) Fidelity of a SWAP gate against charge noise for different protocols.

[1] D. Jirovec, et al, *Nat. Mat.* **20**, 1106-1112 (2021).
[2] N. W. Hendrickx et al., *Nat. Commun.* **11**, 3478 (2020).
[3] A. Bogan, et al., *PRL* **118**, 167701 (2017).
[4] A. Bogan, et al., *PRL* **120**, 207701 (2018).
[5] Y. Ban, et al., *Nanotech.* **29**, 505201 (2018).
[6] Y. Ban, et al., *Adv. Quantum Technol.* **2**, 1900048 (2018).
[7] D. Fernández-Fernández, et al., arXiv 2204.07453 (2022)
[8] D. Fernández-Fernández, et al., *submited.*

Optimal control of molecular spin qudits

Alberto Castro[1,2*], Adrián García Carrizo[2], Daviz Zueco[3,4], Fernando Luis[3,4]

[1]*ARAID Foundation, Avenida de Ranillas 1, 50018 Zaragoza, Spain.* [2]*Institute for Biocomputation and Physics of Complex Systems (BIFI) of the University of Zaragoza, Edificio de Institutos Universitarios de Investigación, Calle Mariano Esquillor, 50018 Zaragoza, Spain.* [3]*Instituto de Nanociencia y Materiales de Aragón (INMA), CSIC-Universidad de Zaragoza, Pedro Cerbuna 12, 50009 Zaragoza, Spain.*
[4]*Departamento de Física de la Materia Condensada, Universidad de Zaragoza, 50009 Zaragoza, Spain.*

*e-mail: acastro@bifi.es

We demonstrate, numerically, the possibility of manipulating the spin states of molecular nanomagnets with shaped microwave pulses designed with quantum optimal control theory techniques. The state-to-state or full gate transformations can be performed in this way in shorter times than using simple monochromatic resonant pulses. This enhancement in the operation rates can therefore mitigate the effect of decoherence. The optimization protocols and their potential for practical implementations are illustrated by simulations performed for a simple molecular cluster hosting a single Gd^{3+} ion. Its eight accessible levels (corresponding to a total spin $S = 7/2$) allow encoding an 8-level qudit or a system of three coupled qubits. All necessary gates required for universal operation can be obtained with optimal pulses using the intrinsic couplings present in this system. The application of optimal control techniques can facilitate the implementation of quantum technologies based on molecular spin qudits.

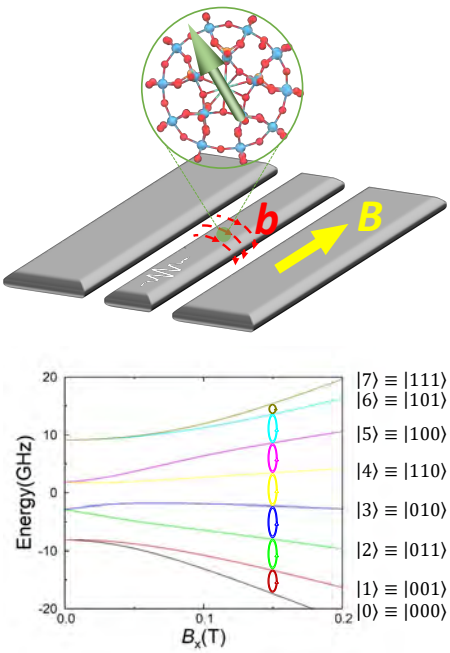

Top: Schematic image of a molecular spin subject to a static magnetic field $\vec{B}$ and to an arbitrarily shaped microwave magnetic field $\vec{b}$, here generated by a transmission line. *Bottom*: spin energy levels of the GdW_{30} polyoxometalate cluster, whose structure is shown in the top. The 8 spin states, associated with the $S = 7/2$ spin of the central Gd^{3+} ion, enable encoding a $d = 8$ qudit or three qubits. The coloured circular arrows mark the seven transitions that can be implemented by means of resonant monochromatic pulses.

[1] Castro, A. *et al.*, `https://arxiv.org/abs/2111.15313`

Applications of Floquet engineering in ac-driven spin qubits

Jordi Picó-Cortés[1,2,*], Gloria Platero[2]

[1] *Theoretische Physik, Universität Regensburg, 93040 Regensburg, Germany.*
[2] *Instituto de Ciencia de Materiales de Madrid (CSIC) E-28049, Spain.*

*e-mail: Jordi.Pico-Cortes@physik.uni-regensburg.de

Quantum dots (QDs) offer a powerful platform for quantum computation due to the possibility of employing well known solid-state architectures inherited from semiconductor electronics. In recent years, experiments on QD arrays have showcased the possibility of increasingly complex protocols for manipulation of QD-based qubits, but decoherence due to a noisy environment has remained a key issue. One promising venue for improvement is the use of ac gates in order to tune the properties of the QD arrays, in what is often called Floquet engineering. Here, we discuss two recently developed applications of ac gates for the manipulation and distribution of QD-based qubits. First, we show the possibility of employing the interference between the different photoassisted paths in ac driven QDs to suppress unintended processes. This allows us to develop a protocol to transfer entangled electron pairs between distant quantum dots [1]. Second, we describe a method for increasing the resistance of two-electron qubits to electric noise by inducing a second-order sweetspot in which the dephasing time due to electric noise is zero up to third order in the coupling between the electrons and the environment [2]. These applications showcase the possibilities of ac-based techniques in quantum technologies.

[1] Jordi Picó-Cortés, Fernando Gallego-Marcos, Gloria Platero, *Physical Review B* **99**, 155421 (2019).
[2] Jordi Picó-Cortés, Gloria Platero, *Quantum* **5**, 607 (2021).

Tecnologías Cuánticas

Presentaciones orales

Miércoles 13/07:

15:30-16:15 Carlos Navarrete Benlloch. *Time-crystalline order in lone and coupled quantum self-sustained oscillators*

16:15-16:30 Xi Chen. *Variational Approach to Coherent Matter-Wave Splitting*

16:30-16:45 Yan Chen, Yue Ban, Ran He, Jin-Ming Cui, Yun-Feng Huang, Chuan-Feng Li, Guang-Can Guo, and Jorge Casanova. *A Neural Network Assisted* $^{171}Yb^{+}$ *Quantum Magnetometer*

16:45-17:00 Nilo Mata, Isabel Gonzalo, Miguel A. Porras. *Promoting quantum tunneling via Zeno Dynamics*

17:00-18:00 **Café**.

18:00-18:15 Miguel Varga, Jon Lasa-Alonso, Carlos Maciel-Escudero, Martín Molezuelas-Ferreras, Iker Gomez-Viloria, Garbriel Molina-Terriza. *Understanding the normal modes of optical fibers for quantum communications*

18:15-18:30 Álvaro Navarrete, Marcos Curty. *Decoy-State Quantum Key Distribution Secure Against Trojan-Horse Attacks*

18:30-18:45 Víctor Zapatero, Marcos Curty. *Simple and passive quantum key distribution*

18:45-19:00 Xoel Sixto, Víctor Zapatero, Álvaro Navarrete, Marcos Curty. *Quantum cryptography with intensity correlations*

19:00-19:15 Cristian Tabares and Alejandro González-Tudela. *Tunable photon-mediated interactions between spin 1 atoms*

19:15-19:30 Santiago Oviedo Casado. *Power-law scaling of correlations in statistically polarized nano-NMR*

Time-crystalline order in lone and coupled quantum self-sustained oscillators

Ming Li[1], Danyang Chen[1,2], Germán J. de Valcárcel[3], **Carlos Navarrete-Benlloch**[1,*]

[1]*Wilczek Quantum Center, School of Physics and Astronomy, Shanghai Jiao Tong University, 200240, China.*
[2]*Department of Physics and Astronomy, Northwestern University, Evanston, Illinois 60208, USA.*
[3]*Dep. d'Òptica i Optometria i Ciencies de la Visió, Universitat de València, Dr. Moliner 50, 46100 Burjassot, Spain.*

*e-mail: derekkorg@gmail.com

The possibility of observing systems in a state of spontaneous robust temporal oscillations insensitive to the effect of any source of noise (including the unavoidable quantum fluctuations) has sparked a lot of debate in the last decade. Originally introduced as potential exotic equilibrium states of matter [1], these were dubbed *time crystals* by analogy with regular crystals, whose periodic spatial pattern shows the same type of robustness. While nowadays we know that time-crystalline order cannot exist in generic systems at equilibrium, several non-equilibrium workarounds have been suggested to circumvent their limitations. In particular, it has been suggested that the long-term (asymptotic) state of driven-dissipative systems might spontaneously break time-translational symmetry, given the right conditions.

In this work we consider the quantum version of an incoherently-pumped oscillator subject to nonlinear loss (so-called, *quantum Van der Pol oscillator* [2]), which in the classical regime serves as the paradigm of a self-sustained oscillator. We use this generic driven-dissipative model to analyze how robust the classical oscillatory states are to quantum noise, arriving to the conclusion that quantum fluctuations always tend to restore (through phase diffusion) the time-translational symmetry broken at the classical level. In this sense, we argue that such systems are not true time crystals, since their oscillations are not robust. We prove this both through a Floquet-based linearization technique that we developed recently [2,3], as well as first-principles numerical simulations based on phase-space stochastic techniques.

In an attempt to halt the phase diffusion responsible for destroying time-crystalline order, we consider a feedback mechanism by which the oscillator's state at some time t acts as a driving mechanism at a later time $t+\tau$. Denoting by g the feedback rate strength, we show that in this case the phase diffusion rate receives a $(1+g\tau)^{-2}$ contribution, which indeed makes the oscillations more robust, but still not fully insensitive to quantum fluctuations except in the unphysical $g\tau \to \infty$ limit.

On the other hand, we also study the possibility of halting phase diffusion and stabilize the self-sustained oscillatory states by coupling several oscillators in a lattice, entering the many-body realm. Let us denote by L the number of oscillators (system size), which we arrange in 1D, 2D, or 3D square geometries, but consider as well all-to-all connections, that is, the so-called mean-field or ∞D limit. Our analysis shows that the phase diffusion rate receives now a $1/L$ contribution at long times for all geometries, and hence one of the conditions for the existence of time-crystalline order is indeed satisfied: many-body effects in the thermodynamic $L \to \infty$ limit halt phase diffusion asymptotically. However, we also show that by the time phase diffusion is halted, the phase variance has reached an asymptotic value that scales as L^{β}, where $\beta=0$ for ∞D, $1>\beta>0$ for 2D and 3D, and $\beta>1$ for 1D. This is a consequence of the Lieb-Robinson bound, which limits the speed at which correlations can propagate in the many-body system, and which applied to our case says that time-crystalline order is clearly achieved for ∞D and might be achieved in practice for large-but-finite systems in 2D and 3D, but possibly not at all in 1D. To our knowledge, it is the first time that this strong conclusion is unequivocally reached by considering full quantum dynamics of a driven-dissipative many-body lattice model.

We propose concrete implementations based on modern quantum platforms such as superconducting circuits where our findings can be experimentally explored.

[1] F. Wilczek, *Phys. Rev. Lett.* **109**, 160401 (2012).
[2] C. Navarrete-Benlloch, T. Weiss, S. Walter, and G. J. de Valcárcel, *Phys. Rev. Lett.* **119**, 133601 (2017).
[3] C. Navarrete-Benlloch, R. Garcés, N. Mohseni, and G. J. de Valcárcel, *Phys. Rev. A* **103**, 023713 (2021).

Acknowledgements: This work was funded by the Spanish Ministerio de Ciencia, Innovación y Universidades, Agencia Estatal de Investigación, and the European Union Fondo Europeo de Desarrollo Regional (FEDER) through Projects No. FIS2014- 60715-P, No. FIS2017-89988-P, and No. PID2020-120056GB-C22. C.N.-B. thanks sponsorship from the Yangyang Development Fund, as well as support from a Shanghai talent program and from the Shanghai Municipal Science and Technology Major Project (Grant No. 2019SHZDZX01).

Variational Approach to Coherent Matter-Wave Splitting

Xi Chen[1,2]

[1]*Department of Physical Chemistry, University of the Basque Country UPV/EHU, Apartado 644, 48080 Bilbao, Spain.*
[2]*EHU Quantum Center, University of the Basque Country UPV/EHU, Barrio Sarriena, s/n, 48940 Leioa, Biscay, Spain.*

e-mail: xi.chen@ehu.eus

We report an efficient protocol for coherent matter-wave splitting in Bose-Einstein condensates. Following the variational principle [1], we inversely engineer the quantum dynamics in the mean-field approximation, which is indeed the shortcuts to adiabaticity [2] for the system. We evaluate the shortcuts by numerical simulations with the multi-configurational time-dependent Hartree method for bosons, see Fig. 1. We also introduce atom interferometry as one of the most straightforward applications of our protocol. Further extensions of the work will pave the way for developing quantum technologies for metrology.

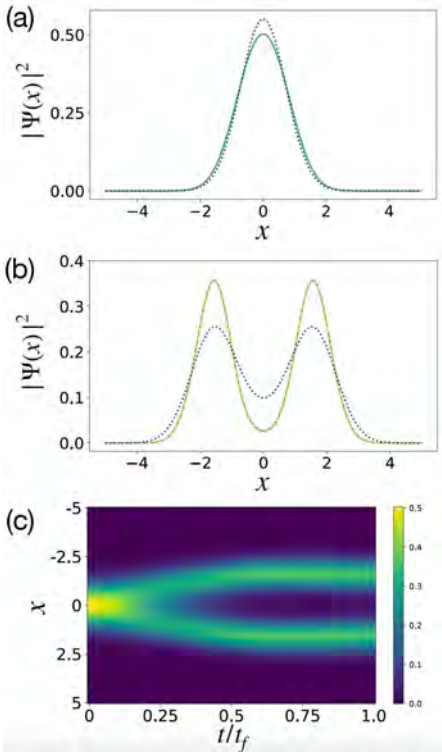

Figure 1. (a) The initial ground state of the BEC with nonlinearity gN=1 (curve) and the variational ansatz (dotted curve). The fidelity between them is F=0.99755, where the optimal parameter a=1.05. (b) The wave packets after coherent splitting, the target ground state (dashed curve), and the variational ansatz (dotted curve). We simulate the many-body dynamics by MCTDHB of M=3 with N=1000 bosons. The fidelity between the final state and the target state is F=0.99996. (c) The wave packet dynamics during the STA of operation time t_f=7.60. We plot the heatmap of $|\Psi(x,t)|^2$. The BECs population on the three natural orbits are 999.59, 0.40704, and 0.0013845, respectively.

[1] V. M. Pérez-García, H. Michinel, J. I. Cirac, M. Lewenstein, and P. Zoller, *Phys. Rev. A* **56**, 1424 (1997).
[2] D. Guéry-Odelin, A. Ruschhaupt, A. Kiely, E. Torrontegui, S. Martínez-Garaot, and J. G. Muga, *Rev. Mod. Phys.* **91**, 045001 (2019).

Acknowledgements: X. C. acknowledges Ramón y Cajal program (RYC-2017-22482).

A Neural Network Assisted $^{171}Yb^{+}$ Quantum Magnetometer

Yan Chen[1,2], **Yue Ban**[3,*], Ran He[1,2], Jin-Ming Cui[1,2], Yun-Feng Huang[1,2], Chuan-Feng Li[1,2], Guang-Can Guo[1,2], and Jorge Casanova[3,4]

[1]*CAS Key Laboratory of Quantum Information, University of Science and Technology of China, Hefei 230026, China.*
[2]*CAS Center for Excellence in Quantum Information and Quantum Physics, University of Science and Technology of China, Hefei 230026, China.*
[3]*Department of Physical Chemistry, University of the Basque Country UPV/EHU, Apartado 644, 48080 Bilbao, Spain.*
[4]*IKERBASQUE, Basque Foundation for Science, Plaza Euskadi 5, 48009 Bilbao, Spain.*

*e-mail: ybanxc@gmail.com

A versatile magnetometer must deliver a readable response when exposed to targets fields in a wide range of parameters. In this work, we experimentally demonstrate that the combination of a $^{171}Yb^{+}$ atomic sensor with adequately trained neural networks [1] enables the characterisation of target fields in distinct challenging scenarios, schematically shown in Fig. 1. In particular, we estimate parameters of radio frequency drivings with large shot noise, including the limiting case of continuous data acquisition with single-shot measurements, and in regimes where the magnetometer delivers a response that significantly departs from the standard harmonic behavior [2].

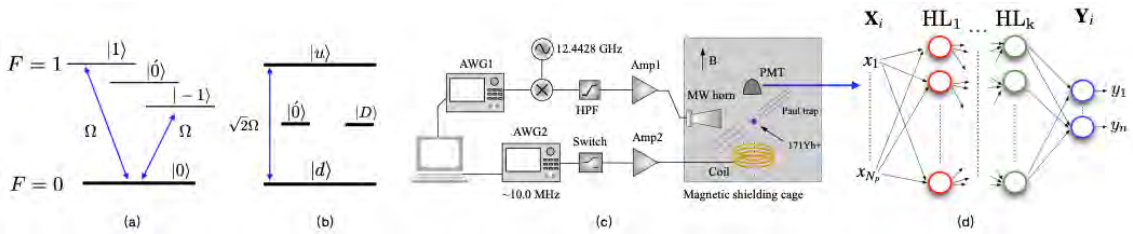

Figure 1. (a) Energy scheme of the $^{171}Yb^{+}$ atomic sensor and the corresponding transitions. This leads to the level configuration in (b) which is defined in the dressed state basis. (c) Schematic configuration of the experimental setup. (d) Scheme of the neural network. The response from PMT, i.e. **X**, is processed by a number of hidden layers and the NN gives the outputs **Y**.

[1] Y. Ban, J. Echanobe, Y. Ding, R. Puebla and J. Casanova, *Quantum Sci. Technol.* **6**, 045012 (2021).
[2] Y. Chen, Y. Ban, R. He, J.-M. Cui, Y.-F. Huang, C.-F. Li, G.-C. Guo, and J. Casanova, arXiv: 2203.05849 (2022).

Promoting quantum tunneling via Zeno Dynamics

Nilo Mata[1,*], Isabel Gonzalo[2], Miguel A. Porras[3]

[1] *Universidad Politécnica de Madrid, Spain.*
[2] *Departamento de Óptica, Facultad de Ciencias Físicas, Universidad Complutense de Madrid, Ciudad Universitaria s/n, 28040 Madrid, Spain.*
[3] *Grupo de Sistemas Complejos, ETSIME, Universidad Politécnica de Madrid, Rios Rosas 21, 28003 Madrid, Spain.*
*e-mail: n.mata@alumnos.upm.es

Quantum tunneling (QT) is one of the most fundamental phenomena in quantum physics. It plays a crucial role in many physical processes such as nuclear fusion, high-energy particle collisions, reaction kinetics, and is at the core of recent quantum technologies [1]. On the other hand, and unlike classical objects, a quantum system is perturbed under the action of measurements. In particular, it is known that frequently checking whether a quantum system is in its initial state slows down the evolution [2, 3], which is called quantum Zeno effect, and more generally quantum Zeno dynamics (QZD). The higher the frecuency of measurements, the lower the probability of evolution, which is impossible with continuous measurements [2, 3].

Mixing QT and QZD, we study the dynamics of a tunneling particle while it is frequently observed [4]. Unlike previous works, ours involves momentum measurements. These are performed to ascertain if the momentum direction is the same as initially, say, positive. Thus, we prevent the natural evolution of the particle (reflection changing its momentum sign), as in Fig. 1(a), forcing the particle to mantain its initial positive sign, as in Fig. 1(b), and causing the particle to traverse the barrier easier. Tunneling probability P_N increases with the number N of measurements within the tunneling time interval, as seen in Fig. 1(c), and tends to unity when N goes to infinity. Measurements are less effective as the particle becomes classical (higher action), as illustrated in Fig. 1(d).

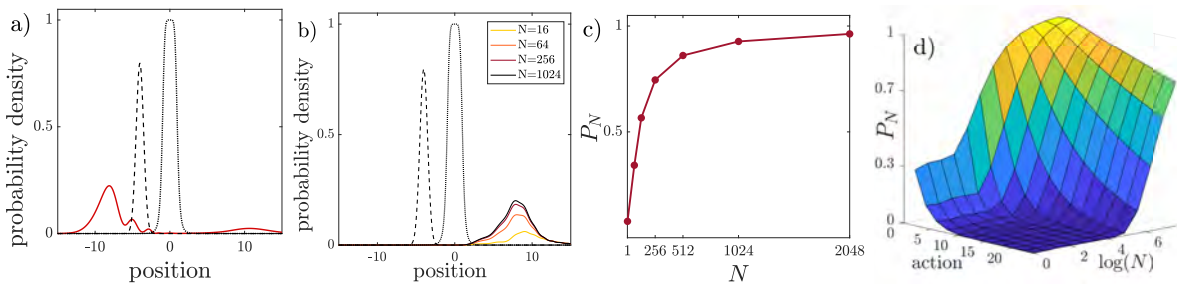

Figure 1. a) Initial (dashed), partially reflected and transmitted (red) probability densities through a potential barrier (dotted). Position is in units of the initial wavepacket width Δx. b) The same but with N measurements. c) Tunneling probability versus number of measurements. d) Tunneling probability versus number of measurements and normalized action $p_0\Delta x/\hbar$, where p_0 is the initial mean momentum of the particle.

We model the measurements as von Neumann projections into the positive-momentum subspace (selective), and also as short interactions with probe particles (nonselective) that acquire information on the sign of momentum. With both models of measurements QZD enhances QT, nonselective measurements being more effective.

The implementation of this QZD control of QT would have an impact on the quantum technologies where QT is a key ingredient.

[1] A. Knothe, L. Glazman and V. I Fal'ko, *New J. Phys.* in press (2022) https://doi.org/10.1088/1367-2630/ac5d00
[2] P. Facchi, V. Gorini, G. Marmo, S. Pascazio, and E.C.G. Sudarshan, *Phys. Lett. A* **275**, 12-19 (2000).
[3] M.A. Porras, A. Luis, and I. Gonzalo, *Phys. Rev. A* **90**, 062131 (2014).
[4] M.A. Porras, N. Mata, I. Gonzalo, arXiv:2202.10150v2 (2022) (submitted to Phys. Rev. Lett.).

Acknowledgements: M.A.P. acknowledges support from Project No. PGC2018-093854-B-I00, and M.A.P. and I.G. from project No. FIS2017-87360-P of the Spanish Ministerio de Ciencia, Innovación y Universidades. N.M. acknowledges support from grant No. D480 (Beca de colaboración de formación) of the Universidad Politécnica de Madrid.

Understanding the normal modes of optical fibers for quantum communications

Miguel Varga[1,*], Jon Lasa-Alonso[1,2], Carlos Maciel-Escudero[1,3], Martín Molezuelas-Ferreras[1], Iker Gomez-Viloria[1], Gabriel Molina-Terriza[1,2,4]

[1]*Centro de Física de Materiales, Paseo Manuel de Lardizabal 5, 20018, Donostia - San Sebastián, Spain.* [2]*Donostia International Physics Center, Paseo Manuel de Lardizabal 4, 20018, Donostia - San Sebastián, Spain.* [3]*CIC NanoGUNE BRTA and Department of Electricity and Electronics, UPV/EHU, 20018, Donostia - San Sebastián, Spain.* [4]*IKERBASQUE, Basque Foundation for Science, María Díaz de Haro 3, 48013, Bilbao, Spain.*

*e-mail: miguel.varga@ehu.eus

Here I will talk about a work-in-progress we are realizing in the Quantum Nanophotonics Laboratory, located at the Materials Physics Center, in Donostia. Our aim is to generate a real-world quantum communication system by using commercial telecom optical fibers.

Recently there was reported several communication protocols by using single-mode optical fibers and photons discretized in the polarization [1] or time-bin [2] degrees of freedom. In both cases the length of the alphabet was 2.

Our proposal is to use a more versatile degree of freedom for the photons as the angular momentum. That is, using photons that are cylindrically and mirror symmetric [3]. This kind of light as proved to be resilient against external noise [4] and, moreover, entangled states that are eigenstates of angular momentum are protected against cylindrically symmetric scatterers [5].

This kind of states are the natural choice for quantum communications through few-modes fibers. The first step is to understand how are the natural modes of the fibers. For this purpose, we have set up an optical arrangement as depicted in Fig. 1. With a continuous laser we generate states of well defined orbital angular momentum and helicity incident on an optical fiber. After passing through the optical fiber, the light states are measured by means of a complete polarization tomography. This allows us to determine which states are preserved and how the incident states are splitted in the normal states of the fiber. The idea that arises is to understand the problem as an input-output system and obtain the transmission matrix for the fiber an, thus, finding the normal modes.

Understanding the normal modes is a first step for achieving the implementation of a quantum communications protocol. This will allows us to enhance the actual communications by means of sending data that will be more stable and efficient than actual protocols.

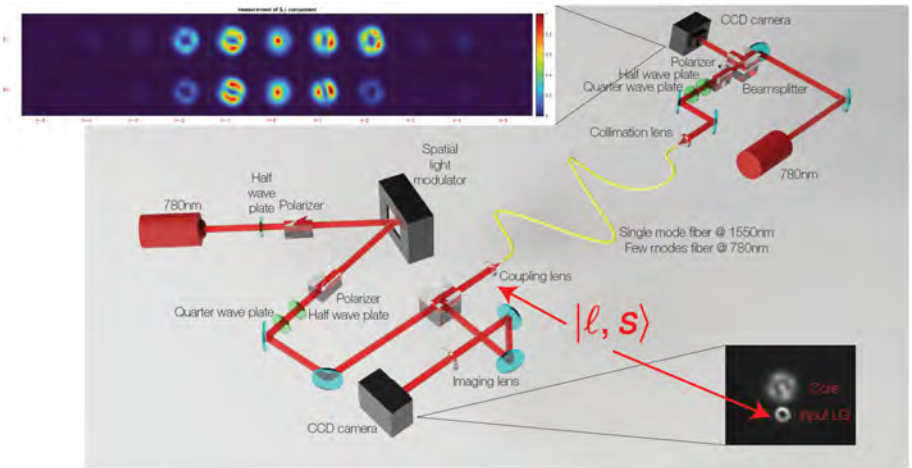

Figure 1. Experimental setup for determining the normal modes of a few-modes optical fiber.

[1] Raju Valivarthi *et al.*, *Nature Photonics* **10**, 676–680 (2016).
[2] Sören Wengerowsky *et al.*, *Proc. Natl. Acad.* **116**, 6684 (2019).
[3] Jon Lasa-Alonso *et al.*, *New J. Phys.* **22**, 123010 (2020).
[4] Osvaldo Jiménez-Farías *et al.*, *Sci. Rep.* **5**, 8424 (2015).
[5] Alexander Büse *et al.*, *Phys. Rev. Lett.* **121**, 173901 (2018).

Decoy-State Quantum Key Distribution Secure Against Trojan-Horse Attacks

Álvaro Navarrete*, Marcos Curty

EI Telecomunicación, Dept. of Signal Theory and Communications, University of Vigo, E-36310 Vigo, Spain.
atlanTTic Research Center, University of Vigo, E-36310 Vigo, Spain.

*e-mail: anavarrete@com.uvigo.es

Most security proofs of quantum key distribution (QKD) disregard the effect of information leakage from the users' devices, and, thus, do not protect against Trojan-horse attacks (THAs). In a THA, the eavesdropper injects strong light into the QKD apparatuses, and then analyzes the back-reflected light to learn information about their internal setting choices. Only a few recent works consider this security threat, but predict a rather poor performance of QKD unless the devices are strongly isolated from the channel.

We present an improved finite-key security analysis for decoy-state-based QKD schemes in the presence of THAs, which significantly outperform previous analyses [1]. For this, we take advantage of the reference technique [2] equipped with a Cauchy-Schwarz-based constraint to incorporate the information leakage from the bit/basis and intensity encoding setups in the security analysis. This requires the users to bound a single parameter that encapsulates all the imperfections, which in practice can be directly related to the amount of isolation of Alice's transmitter. Besides, we use novel concentration bounds to deal with the finite-key effects.

For illustration purposes, we evaluate the performance of the standard decoy-state BB84 protocol and the decoy-state loss-tolerant protocol in the presence of THAs. The results demonstrate the feasibility of both schemes over long distances given that the information leakage is small enough, which could be achieved by increasing the isolation of the devices. Besides, for the decoy-state BB84 case, we compare the secret-key rate attainable with our security proof with that obtained in previous works [1]. The improvement in terms of performance is clear, as shown in Fig. 1, in which our analysis basically allows to double the maximum achievable distance attained by previous works in some realistic scenarios.

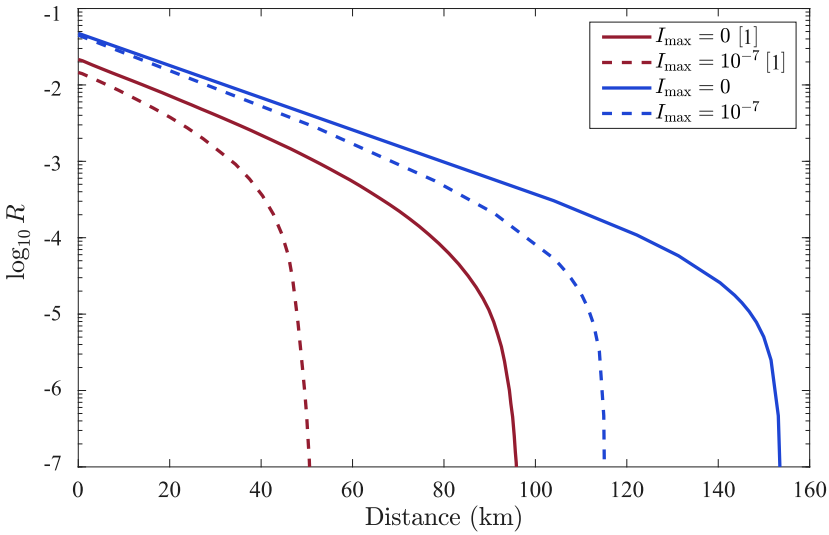

Figure 1. Comparison between the secret-key rates R obtained in the presence of a THA for the case of $N = 10^{12}$ transmitted signals. Our results correspond to the blue lines, while those from [1] correspond to the red lines.

[1] Wang, W., Tamaki, K., & Curty, M., *New Journal of Physic* **20**, 083027 (2018).
[2] Pereira, M., Kato, G., Mizutani, A., Curty, M. & Tamaki, Kiyoshi, *Science Advances* **6**, eaaz4487 (2020).

Simple and passive quantum key distribution

Víctor Zapatero*, Marcos Curty

Escuela de Ingeniería de Telecomunicación, Departamento de Teoría de la Señal y Comunicaciones, Universidad de Vigo, Vigo E-36310, España.

*e-mail: vzapatero@com.uvigo.es

Quantum key distribution (QKD) exploits fundamental properties of quantum-mechanical systems to securely distribute cryptographic keys between remote parties through an insecure channel. This task is known to be impossible using classical cryptography alone, which makes QKD a promising candidate for long-term communication security. Nowadays, QKD has become a mature and prolific industry within the field of quantum information science, thanks to the combined efforts of theorists and experimentalists. Notwithstanding, the security of real QKD implementations is not fully established yet, due to the difficulty of experimentally guaranteeing that the QKD devices stick to the assumptions and models presumed in the security proofs.

A particularly controversial assumption present in QKD security analyses is that no information leakage takes place through the boundaries of Alice's and Bob's labs. This premise opens the door for the so-called Trojan horse attacks (THAs), where an adversary injects bright light pulses into a QKD transmitter and then measures the back-reflected light, aiming to extract information about the internal setting choices of the transmitter. A possible solution to avoid this problem is to consider a passive (rather than active) QKD transmitter, where the protocol settings are set at random using inherent quantum randomness of the device, in so circumventing THAs. What is more, hardware-wise, passive transmission typically allows simpler architectures than active transmission. Notably though, these advantages come at the price of decreasing the key generation rate. This is so because, in a passive transmitter, additional post-selection is required to discard those rounds where the randomly generated settings do not lie in certain acceptance intervals.

In this work, we propose a simple and passive QKD transmitter tailored for the decoy-state BB84 protocol [1,2,3], the most popular practical QKD protocol to the date. Essentially, our scheme carefully combines two previously-known ideas: a proposal to passively generate random photon-polarizations in a plane (suitable for the BB84) [4], and a proposal to passively generate random intensity laser pulses for the application of the decoy-state method [5]. On top of it, we elaborate a custom-made security analysis to evaluate the secret-key-rate performance of our passive QKD transmitter.

[1] Hwang, W. Y. *Physical Review Letters* **91**, 057901 (2003).
[2] Lo, H.-K., Ma, X. & Chen, K. *Physical Review Letters* **94**, 230504 (2005).
[3] Wang, X. B. *Physical Review Letters* **94**, 230503 (2005).
[4] Curty, M., Ma, X., Lo, H. K., & Lütkenhaus, N. *Physical Review A* **82**, 052325 (2010).
[5] Curty, M., Ma, X., Qi, B., & Moroder, T. *Physical Review A* **81**, 022310 (2010).

Acknowledgements: Víctor Zapatero acknowledges support from an FPU predoctoral scholarship granted by the Spanish Ministry of Universities (former Ministry of Education), under which the proposed research project was partly carried out.

Quantum cryptography with intensity correlations

Xoel Sixto*, Víctor Zapatero, Álvaro Navarrete, Marcos Curty

Escuela de Ingeniería de Telecomunicación, Departamento de Teoría de la Señal y Comunicaciones, Universidad de Vigo, Vigo E-36310, España.

*e-mail: xsixto@com.uvigo.es

Quantum key distribution (QKD) enables information-theoretically secure delivery of cryptographic keys between distant parties through an insecure channel. This possibility (which is inaccessible from the point of view of classical communications) makes QKD a promising candidate for private communications secure in the long-term. For this reason, QKD has experienced a tremendous development both in theory and in practice, in so becoming the most mature application of quantum information science. Nevertheless, despite this progress, various challenges must be addressed in order to achieve the widespread adoption of QKD.

In particular, aiming to enhance the key generation performance of QKD implementations, it is very desirable to boost the repetition rate of the laser sources in QKD transmitters. Nevertheless, for clock rates of the order of GHz, intensity correlations between succeeding pulses appear [1,2], possibly opening a security loophole. To be precise, in the absence of ideal single-photon sources, most QKD protocols use attenuated lasers that operate emitting phase-randomised weak coherent pulses. These sources allow QKD users to implement the so-called decoy-state method [3,4,5], a standard procedure that enables a tight estimation of the secret key length of a QKD session by means of using multiple intensities for QKD transmission. Unfortunately though, the presence of intensity correlations invalidates the central assumption of the decoy-state method, namely, that the photon-number detection statistics do not depend on the intensity of the laser. This being the case, the question arises of how to account for arbitrary intensity correlations in the security analyses of QKD, a question for which existing results are notably restricted [1,6,7].

In two consecutive works [8,9], we solve this pressing problem by developing the missing security analysis for decoy-state QKD with arbitrary intensity correlations. The central ideal is to pose a restriction on the maximum bias that an adversary may induce between the photon-number detection statistics associated to different intensity settings. Particularly, this is accomplished by using a fundamental result presented in [10], which constraints how much the measurement statistics of non-orthogonal quantum states can differ. We refer to this result as the Cauchy-Schwarz constraint, because it is a consequence of the Cauchy-Schwarz inequality in complex Hilbert spaces. Notably, our analysis relies on a very general and experimental-friendly characterization of the intensity correlations. Moreover, it may be combined with detailed correlation models, which are expected to be pointed out by ultrafast QKD experiments in the near future. Putting it all together, our results provide a fundamental step towards foolproof security of high-speed QKD systems, with their imperfections.

[1] Yoshino, K. I. et al. *npj Quantum Information* **4**, 1-8 (2018).
[2] Grunenfelder, F., Boaron, A., Rusca, D., Martin, A. & Zbinden, H. *Applied Physics Letters* **117**, 144003 (2020).
[3] Hwang, W. Y. *Physical Review Letters* **91**, 057901 (2003).
[4] Lo, H.-K., Ma, X. & Chen, K. *Physical Review Letters* **94**, 230504 (2005).
[5] Wang, X. B. *Physical Review Letters* **94**, 230503 (2005).
[6] Nagamatsu Y., Mizutani, A., Ikuta, R., Yamamoto, T., Imoto, N., & Tamaki, K. *Physical Review A* **93**, 042325 (2016).
[7] Mizutani, A. et al. *npj Quantum Information* **5**, 8 (2019).
[8] Zapatero, V., Navarrete, Á., Tamaki, K., & Curty, M. *Quantum* **5**, 602 (2021).
[9] Sixto, X., Zapatero, V., Curty, M. (In preparation).
[10] Pereira, M., Kato, G., Mizutani, A., Curty, M. & Tamaki, K. *Science Advances* **6**, eaaz4487 (2020).

Acknowledgements: Víctor Zapatero acknowledges support from an FPU predoctoral scholarship granted by the Spanish Ministry of Universities (former Ministry of Education), under which the proposed research project was carried out.

Tunable photon-mediated interactions between spin 1 atoms

Alejandro González-Tudela, **Cristian Tabares***

Institute of Fundamental Physics IFF-CSIC, Calle Serrano 113b,28006 Madrid, Spain.

*e-mail: cristian.tabares@csic.es

Quantum simulators are highly controllable devices that exploit quantum effects to answer questions about another system. They can be built using different platforms, such as ultracold atoms in optical lattices, superconducting circuits or atoms interacting with nanophotonic structures [1]. This last system is particularly interesting because the nanophotonic environment can be tailored to generate exotic photon-mediated interactions between atoms [2], with both dissipative and coherent evolutions, opening the door for the exploration of a wide range of physical models. However, these atoms have been typically considered as two-level systems, which limits the type of models that can be explored [3,4]. Our work considers the full hyperfine structure of the atoms to go beyond this and study effective spin-1 interactions between the quantum emitters, where Raman-assisted transitions allow a mapping to well known models such as the Ising or the XX spin-1 interactions. In this context new complications appear, such as the different rates of each transition according to the corresponding Clebsch-Gordan coefficients, and we also propose different ways to solve them. These results could be interesting both in quantum simulation (where they could be applied to study spin chains or even simulating some lattice gauge theories [5,6], and also be the base for digital-analog schemes) and quantum computation (as a way to obtain quantum gates between qutrits [7]).

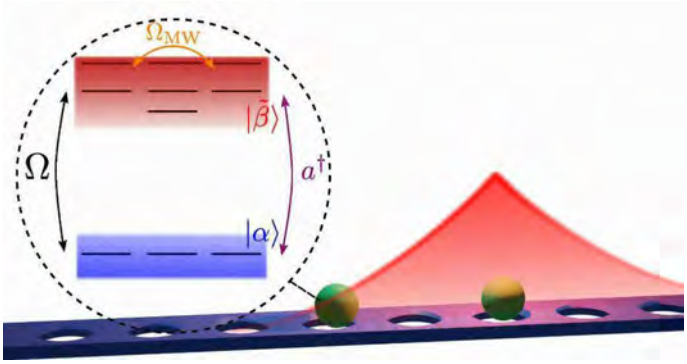

Figure 1. Main panel: Schematic representation of two atoms trapped near a 1D photonic crystal waveguide, showing the atom-photon bound state that allows the tunable interactions. Inset: Full multilevel structure of a real atom, including the excited states that are adiabatically eliminated to obtain the effective spin-1 interactions between the quantum emitters.

[1] E. Altman et al., *PRX Quantum* **2**, 017003 (2021).
[2] D.E. Chang, J.S. Douglas, A. González-Tudela, C.-L. Hung, and H.J. Kimble, *Rev. Mod. Phys.* **90**, 031002 (2018).
[3] A. González-Tudela, C.-L. Hung, D. E. Chang, J. I. Cirac, and H. J. Kimble, *Nature Photonics* **9**, 320 (2015).
[4] J. S. Douglas, H. Habibian, C.-L. Hung, A. V. Gorshkov, H. J. Kimble, and D. E. Chang, *Nature Photonics* **9**, 326 (2015).
[5] E. Zohar, A. Farace, B. Reznik, and J. I. Cirac, *Phys. Rev. A* **95**, 023604 (2017).
[6] T. Armon, S. Ashkenazi, G. García-Moreno, A. González-Tudela and E. Zohar, *Phys. Rev. Lett.* **127**, 250501 (2021).
[7] Y. Wang, Z. Hu, B. C. Sanders, and S. Kais, *Front. Phys.* **10** (2020).

Power-law scaling of correlations in statistically polarized nano-NMR

Santiago Oviedo-Casado

Racah Institute of Physics, The Hebrew University of Jerusalem, 91904 Givat Ram, Jerusalem, Israel.

e-mail: oviedo.cs@mail.huji.ac.il

Nuclear magnetic resonance is ubiquitous, with applications ranging from determining protein structure to medical imaging. While tremendously successful, there are significant challenges as it requires: (1) huge spatially homogeneous magnetic fields over the whole sample volume, (2) sufficiently concentrated sample due to low sensitivity.

Alternatives rely on tiny samples where nuclei can statistically orient themselves in the same direction, creating a magnetic signal that is detected with quantum sensors. The main challenge in this approach is molecular diffusion, which causes signal decay. The latter has typically being considered exponential, which severely limits resolution. However, this model misses out key features of diffusion signal correlations. We use three independent state-of-the-art experiments to show that a recent hypothesis of long-lived signals due to power-law decay of correlations at long times is feasible.

To elucidate the conundrum we performed several NV-center based experiments that probed the long decay tail of the signal autocorrelation. We analyzed these results combining statistical tools and numerical simulations, showing convincingly that the magnetic signal survives for longer times than those expected with the exponential model, confirming the theoretical hypothesis and allowing for significant improvements in spectral resolution.

Our work opens the door for future experiments that target J-couplings in organic compounds, which have remained elusive due to the assumed resolution limitations. They also allow for improved measurements of the diffusion coefficients by using the more precise autocorrelation power-law model.

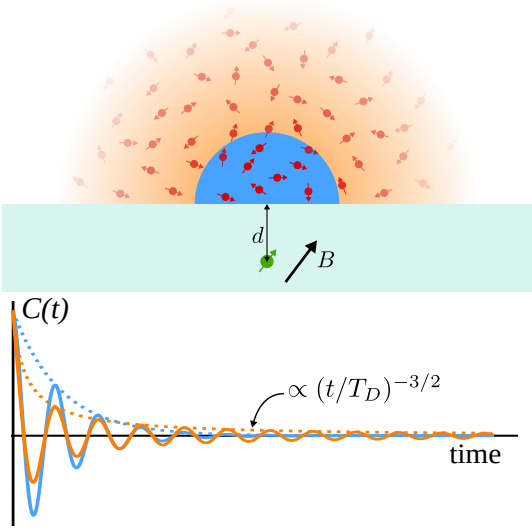

The NV center is located at a depth d below the diamond surface. In the standard diffusion model a hemisphere sensing volume (blue) of radius $\sim d$ is considered, in which the nuclei interact with the NV center. Alternatively, we accurately take into account the $1/r^3$ dependence of the dipole-dipole interaction. The color intensity of the orange hemisphere indicates the interaction strength of the nuclear spins (red) with the NV center. (c) Decay of the auto-correlation according to the exponential and the power-law decay model. With the accurate dipole-dipole model, decay is (nearly) exponential for short times ($t \ll T_D$) and a power-law for $t \gg T_D$.

Óptica Cuántica y Óptica No Lineal

Presentaciones orales

Miércoles 13/07:

15:30-15:45 Laura Rodríguez Suñé (Univ. Politecnica Catalunya). *Combined experimental-theoretical study of harmonic generation in silicon at nanoscale*

15:45-16:00 Carlos Rodríguez Fernández Pousa (Univ. Miguel Hernández). *Incoherent self-loss-modulated Q-switch in Frequency Shifting Loops*

16:00-16:15 Shroddha Mukhopadhyay (Univ. Politecnica Catalunya). *Nonlinear conversion efficiency enhancement in gold grating nanostructure*

16:15-16:30 Antonio García Blázquez (Univ. Autónoma de Madrid). *Symmetry indicators of second order photocurrent with application to monolayer GaSe from first principles*

16:30-16:45 Adolfo Esteban Martín (Univ. de Valencia). *Interferometric Phase Retrieval via Nonlinear Transient Detection Imaging*

16:45-17:00 Elena Pinilla Cienfuegos (Univ. Politecnica Valencia). *Optical bistability based on the integration of a molecular nanomaterial in silicon photonics*

17:00-18:00 **Pósteres y café**.

18:00-18:15 David Novoa Fernandez (UPV/EHU). *High-quality compression of ultrafast near-UV light in hollow anti-resonant fibres*

18:15-18:30 Miguel López Ripa (Univ. Salamanca). *In-line and ultraestable spatiotemporal characterization of constant and time-varying optical vortices*

18:30-18:45 Abraham Loredo Trejo (Univ. de Valencia). *Simultaneous tuning of four-wave mixing and polarization modulation instability in microstructured optical fiber*

18:45-19:00 Víctor Wilfried Segundo Staels (Univ. Salamanca). *Use of gas-filled multipass cells to generate clean supercontinuum spectra*

19:00-19:15 Carlos Damián Rodríguez Fernández (U. Santiago Compostela). *Ionic Liquids as tunable nonlinear optical materials*

19:15-19:30 Luis Sánchez-Tejerina San José (Univ. Salamanca). *"Non-linear, purely magnetic magnetization response to femtosecond structured laser pulses*

Jueves 14/07:

15:30-15:45 Alberto Muñoz de las Heras (IFF CSIC - Univ. Trento). *Anyonic Molecules in Atomic Fractional Quantum Hall Liquids: A Quantitative Probe of Fractional Charge and Anyonic Statistics*

15:45-16:00 Ivan Morera Navarro (Univ. Barcelona). *Superexchange liquefaction of strongly correlated lattice dipolar bosons*

16:00-16:15 Eduardo Zubizarreta Casalengua (UAM - U. Wolverhampton). *Emitting single and squeezed photons*

16:15-16:30 "Miguel Cornelles Soriano (IFISC, Illes Balears)". *Photonic reservoir computing using quantum resources*

16:30-16:45 Sergi Terradas Briansó (CSIC- Univ. Zaragoza). *Ultrastrong Waveguide QED with Giant Atoms*

16:45-17:00 Abel Rojo Francàs (Univ. Barcelona). *Exact diagonalization correction method for a few-particles trapped in a harmonic potential*

17:00-18:00 **Pósteres y café**.

18:00-18:15 Rodrigo Martín Hernández (Univ. Salamanca). *Magnetically-pumped High Harmonic Generation with circularly polarized driving fields*

18:15-18:30 Juan Jose Esteve Paredes (Univ. Autónoma de Madrid). *Light-matter interaction from density functional theory with application to attosecond electron dynamics*

18:30-18:45 Ana García Cabrera (Univ. Salamanca). *Multi-vortex high-harmonic beams from graphene's anisotropy*

18:45-19:00 Raúl García Álvarez (Univ. Politécnica de Madrid). *The shortest focused X-Waves with Orbital Angular Momentum*

19:00-19:15 Alba de las Heras (Univ. Salamanca). *Extreme-ultraviolet scalar and vectorial vortices with very high topological charge*

19:15-19:30 Iker Gomez Viloria (CFM Donostia). *Prohibited optical trapping regimens unlocked by focused OAM beams*

Pósteres

- Luis Alberto Sánchez Domínguez (Univ. de Valencia). *Novel Methods for the Characterization of Forward Brillouin Scattering in Optical Fibers and its Applications*
- Ignacio López Quintás (Univ. Salamanca). *Collinear optical vortices with tailored topological charge generated by angular momentum transfer*
- Juan Lizarraga Lallana (Univ. Autónoma de Madrid). *Light polarisation under evanescent coupling in exciton-polariton couplers*
- Francisco Javier Serrano Rodríguez (Univ. Salamanca). *High-performance simulations of high-order harmonic generation based on artificial intelligence*
- José Ramón Salgueiro Piñeiro (Univ. Vigo). *Efficient computation of azimuthal perturbation eigenpairs of vortex solitons*
- Manuel Eduardo Barredo Alamilla (Uiv. Nacional Autónoma de Mexico). *Cherenkov radiation in chiral matter*
- Manuel Valiente (Univ. de La Laguna). *Quantum liquids and droplets with low-energy interactions in one dimension*
- Inmaculada Pérez Pérez (University of Jena). *Fiber-based biphoton spectroscopy*

Combined experimental-theoretical study of harmonic generation in silicon at nanoscale

L. Rodríguez-Suné[1,*], M. Scalora[2], C. Cojocaru[1], N. Akozbek[3], R. Vilaseca[1], J. Trull[1]

[1]*Universitat Politècnica de Catalunya, Physics Department, Rambla Sant Nebridi 22, 08222 Terrassa, Spain.* [2]*Aviation and Missile Center, US Army CCDC, Redstone Arsenal, Huntsville, Al, United States.*
[3]*US Army Space & Missile Defense Command, Tech Center, Redstone Arsenal, AL 35898, United States.*

*e-mail: laura.rodriguez.sune@upc.edu

Second and third harmonic generation (SHG and THG) are two nonlinear processes in which when light interacts with a nonlinear material, new frequencies are generated. These processes are typically studied in thick materials with high nonlinearities and under phase matching conditions and low material absorption with the aim of achieving high conversion efficiencies. They are described through the nonlinear polarization, which is usually approximated to the electric dipole contribution described by the second and third order susceptibilities $\chi^{(2)}$ and $\chi^{(3)}$. This approximation starts to fail when the nanoscale is reached: SHG and THG conversion efficiencies are drastically reduced and phase matching conditions and absorption no longer play a significant role. In this case, other nonlinear contributions to the nonlinear polarization, such as magnetic dipole and electric quadrupole interactions, must be taken into account.

The development of functional nonlinear silicon photonic devices has advanced significantly in recent years thanks to the progress in nano-fabrication techniques. These devises can emit light, modulate signals electro-optically and process data at speeds higher that electronic chips. Most of the interest in nonlinear silicon photonics is due to its high compatibility with CMOS technology, offering structure sizes down to 10nm at low cost. For this reason, it is crucial to understand how light interacts with semiconductors, such as silicon, at the nanoscale. That is why in this work we present a combined experimental and theoretical study of light matter interaction with nanolayers of silicon with the objective of understanding the intrinsic, nonlinear optical properties of this material at nanoscale. This knowledge can then be used to design structures with more complex topologies.

In Fig.1 we show the experimental set-up we have developed, with which we are capable of measuring harmonic signals from different samples as a function of incident angle, polarization and pump wavelength, and in transmission and reflection. The measurements are compared with numerical results based on a microscopic hydrodynamic model which accounts for different possible contributions to the nonlinear polarization [1,2]. This comparative experimental-theoretical study identifies, distinguishes and explains the different contributions to the harmonics generated by silicon at nanoscale. We measure and estimate the efficiency of the harmonic signal using no assumptions about effective surface or volume nonlinearities other that effective electron masses and densities.

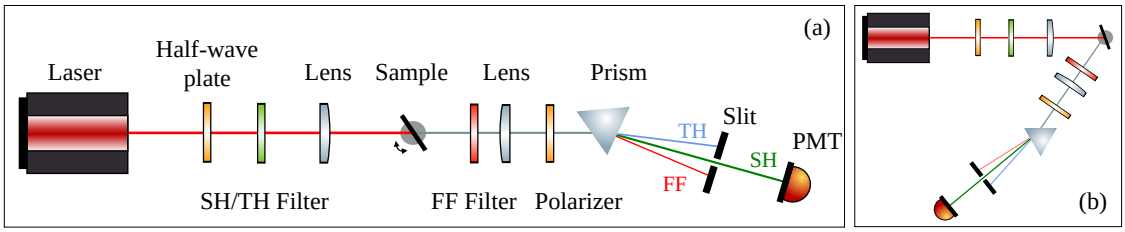

Figure 1. Experimental set-up developed to measure second and third harmonic signals from different samples as a function of pump wavelength, incident angle, polarization and in (a) transmission and (b) reflection.

[1] M. Scalora, M. A. Vincenti, D. de Ceglia, V. Roppo, M. Centini, N. Akozbek and M. J. Bloemer, *Second- and third-harmonic generation in metal-based structures*, Phys. Rev. A 82, 043828 (2010).
[2] L. Rodríguez-Suné, J. Trull, M. Scalora, R. Vilaseca, and C. Cojocaru, *Harmonic generation in the opaque region of GaAs: the role of the surface and magnetic nonlinearities*, Opt. Express 27, 26120-26130 (2019).

Acknowledgements: LRS, JT and CC acknowledge to US Army Research Laboratory Cooperative Agreement Nº W911NF1920279 issued by US ARMY ACC-APG-RTP and Spanish Agencia Estatal de Investigación (project no. PID2019-105089GB-I00/AEI/10.13039750110001103 3).

Incoherent self-loss-modulated Q-switch in Frequency Shifting Loops

M. Cuenca, H. Maestre, G. Torregrosa, **C. R. Fernández-Pousa***

Dept. Ingeniería de Comunicaciones, Centro de Investigación en Ingeniería de Elche (I3E), Universidad Miguel Hernández, 03202 Elche, Spain.

*e-mail: c.pousa@umh.es

Generation of broadband light with distinctive temporal and spectral characteristics represents a recurrent demand for a variety of practical scenarios, including ranging, reflectometry, and optical sensors systems [1]. We here report on the incoherent Q-switched emission of all-fiber Frequency Shifting Loops (FSL), where pulses are chirped and inherently tagged by seed ASE events.

An FSL, schematically shown in Fig. 1(a), is a loop where an acousto-optic frequency shifter (FS) translates the optical frequency and an EDFA compensates for losses, enabling hundreds or even thousands of recirculations. An apodized fiber Bragg grating (FBG) with an approximately Gaussian spectral profile and a FWHM of 1.63 nm is placed after the EDFA to restrict ASE growth upon recirculation. When driven solely by its ASE, FSLs show a rich dynamics that depends on the product between the recirculation round-trip time τ_c and the imparted frequency shift f_s. If the product $f_c\tau_c$ is not a rational number, the optical output is modeless and, under suitable conditions, comprises Q-switched pulses. The analysis of this regime has been restricted so far to numerical simulations [2].

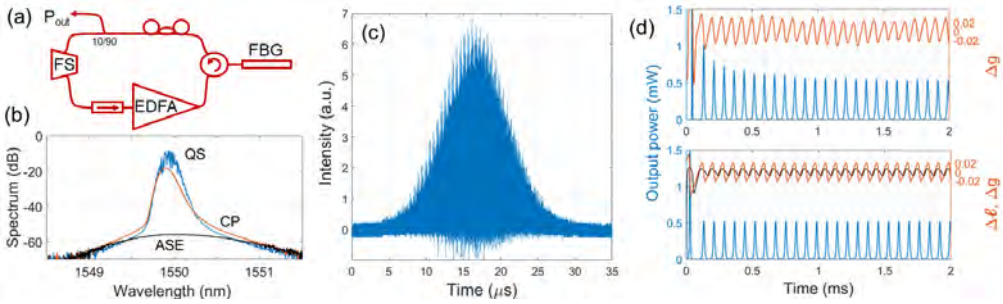

Figure 1. (a) Scheme of the FSL. (b) Spectra of ASE, CP and QS emissions. (c) QS pulse intensity. (d) Intensity (blue), gain (orange) and loss (black) in a build-up transient: above, experiment; below, simulation.

The loop's round-trip time, $\tau_c = 108$ ns, is much larger than the inverse of the spectral width (∼20 GHz), so the emission is incoherent and the FSL acts as a regenerative amplifier. By increasing the FS driving power, gain can exceed loss at the FBG reflection peak. The FSL outputs, subsequently, light of constant power (CP) or Q-switched (QS) pulses at ∼10 kHz rates. In both cases, the +78-MHz frequency shift forces ASE to leave the FBG. The emission central wavelength is therefore shifted with respect to the FBG center due to the action of the FS, as shown in Fig. 1(b). Q-switching is initiated spontaneously by ASE, leading to pulses that fade when the recirculating frequency exits the filter's passband. Incoherent Q-switched pulses are thus generated by loss modulation induced by frequency translation. Their intensity reflects the underlying recirculation process as spikes at multiples of the loop's round-trip time, see Fig. 1(c). These spikes represent seed ASE events whose amplitude follows the gain's spectral distribution as their frequency is progressively shifted.

The Q-switching mechanism also shows interesting dynamical aspects. Loop loss, and thus EDFA gain, are high (>15 dB), and so the gain section is to be modeled as a discrete component with its specific gain recovery time (620 μs). The EDFA operates in saturation, with an average gain clamped to compensate for the losses undergone by pulses during its frequency translation. Pulses are chirped, and built from the standard balance between small variations of loss $\Delta\ell$ and gain Δg that results in symmetric sech^2 intensity profiles. This process has been modeled as an incoherent recirculation system and compared, as show in Fig. 1(d), with synchronous measurements of gain and compression.

[1] J.I. Kim, V.V. Ogurtsov, G. Bonnet, L.P. Yatsenko, and K. Bergmann, *Appl. Phys. B* **122**, 295 (2016).
[2] J.-N. Maran, P. Besnard, and S. LaRochelle, *J. Opt. Soc. Am. B* **23**, 1302 (2006).

Acknowledgements: Grant PID2020-120404GB-I00, Ministerio de Ciencia e Innovación and Agencia Estatal de Investigación (MCIN/AEI/10.13039/501100011033).

Nonlinear conversion efficiency enhancement in gold grating nanostructure

S. Mukhopadhyay[1,*], J. Trull[1], L. Rodríguez-Suné[1], M. Scalora[2], M. A. Vincenti[3], G. Leo[4], C. Cojocaru[1]

[1]*Universitat Politècnica de Catalunya, Physics Department, Rambla Sant Nebridi 22, 08222 Terrassa, Spain.* [2]*Aviation and Missile Center, US Army CCDC, Redstone Arsenal, Huntsville, AL, United States.* [3]*Deparment of Information Engineering, University of Brescia, Via Branze 38, 25123 Brescia, Italy.* [4]*Laboratoire Matériaux et Phénomènes Quantiques, Université de Paris & CNRS, 10 rue Alice Domon et Léonie Duquet, 75013 Paris, France.*

*e-mail: shroddha.mukhopadhyay@upc.edu

Metal nanostructures are known to exhibit light-matter interaction enhancement under a broad range of irradiation wavelengths by means of plasmonic resonances and have large-scale applications in imaging, sensing, solar cells, surface enhanced spectroscopy etc. Despite their high absorption in the visible and near infrared range, metals are highly nonlinear materials. Resonant metal nanostructures (nanolayers, gratings, nanoantennas or nanoparticles), can largely improve efficiencies of nonlinear optical processes like second and third harmonic generation (SHG and THG) from metal surfaces. At the nanoscale, the conventional approximations used in most of the theoretical models describing the light-matter interactions are not always applicable, so the surface and volume contribution to the nonlinear signal has to be revised [1].

Here we investigate the second and third harmonic generation and enhancement in the opaque region of a gold nano-grating designed to have a resonance at the fundamental wavelength around 800 nm. We present a combined experimental and theoretical approach based on a detailed microscopic hydrodynamic model that relies on temporal and spatial derivatives and accounts for competing surface, magnetic, and bulk nonlinearities arising from both free (conduction) and bound (valence) electrons [2].

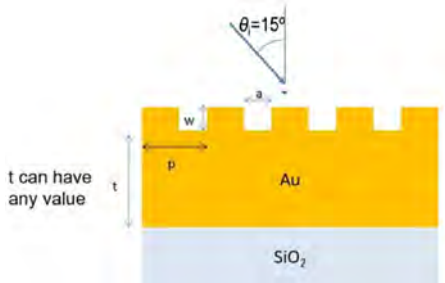

Figure 1. Gold Grating structure; p = 620 nm.

We measure the TM and TE components of the SH signal at 400 nm as a function of the fundamental beam polarization, tuning the fundamental wavelength around the resonance and compared with the predictions of out theoretical model. Experimental value of the relative enhancement induced by the grating with respect to SHG from a planar gold nanolayer gives an enhancement factor of 1000 at the central resonant wavelength, perfectly in agreement with the predictions of our model. The same model predicts a 500-enhancement factor for the THG with respect to the plain gold layer.

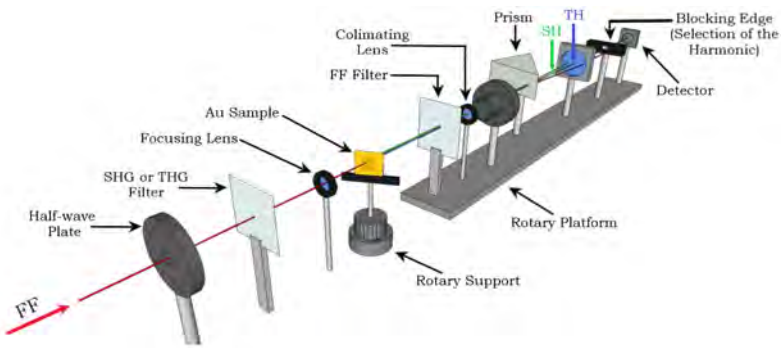

Figure 2. Experimental setup for measurements in transmission.

[1] L. Rodriguez-Suñé, J. Trull, C. Cojocaru, et al, *Optics Express* **29**, 8581 (2021).
[2] M. Scalora, M. A. Vincenti, D. de Ceglia, C. Cojocaru, *J. Opt. Soc. Am.* **B 32**, 2129 (2015).

Acknowledgements: SH, LRS, JT and CC acknowledge to US Army Research Laboratory Cooperative Agreement Nº W911NF1920279 issued by US ARMY ACC-APG-RTP and Spanish Agencia Estatal de Investigación (project no. PID2019-105089GB-I00/ AEI/10.13039750110001103 3).

Symmetry indicators of second order photocurrent & application to monolayer GaSe from first principles

M. A. García-Blázquez[1,*], J. J. Esteve-Paredes[1], J. J. Palacios[1,2]

[1]*Departamento de Física de la Materia Condensada, Universidad Autónoma de Madrid, E-28049 Madrid, Spain.* [2] *Instituto Nicolás Cabrera (INC) and Condensed Matter Physics Center (IFIMAC), Universidad Autónoma de Madrid, E-28049 Madrid, Spain.*

*e-mail: manuelantonio.garcia@uam.es

We present a general analysis of the implications of spatial symmetries on the photogalvanic effect in a crystalline solid, based on its space group and the band representations at the relevant points in the Brillouin zone. This second order photocurrent has a strong dependence on the atomic details of the material [1], which enhances the importance of employing selection rules to provide some sort of guidance in the search of candidate solids to exhibit this effect. Apart from the well-known need to break inversion symmetry, we focus on the role of rotational and mirror symmetries in 2D materials, where bands can be divided into two non-interacting sets according to their parity under a horizontal reflection, whenever that symmetry is present in the system. We find that some of these symmetry requirements can situationally be restrictive at frequencies near the band edge, specially in 2D materials, which points to the introduction of symmetry-perturbing strains as a catalyst for stronger second order photocurrents.

These results are particularized for a crystalline single-layer of GaSe, which is a promising non-linear optical semiconductor. We compute the first and second order conductivity tensors via DFT calculations, which are qualitatively described in terms of band representations, and compare the results at low-energy with the analytical results provided by the ***kp***-formalism [2]. Furthermore, we show explicitly how the sums over the Brillouin zone which are required to compute the conductivity tensors can be reduced to sums over the irreducible Brillouin zone, thereby reducing computation time by a factor of the order of the crystallographic point group of the material.

[1] Ibañez-Azpiroz, J., Tsirkin, S. S., Souza, I. *Physical Review B*, **97(24)**, 245143 (2018).
[2] Cook, A. M., M Fregoso, B., De Juan, F., Coh, S., Moore, J. E. *Nature communications*, **8**(1), 1-9 (2017).

Interferometric Phase Retrieval via Nonlinear Transient Detection Imaging

A. Esteban-Martín*, J. García-Monreal, E. Roldán, F. Silva, G. J. de Valcárcel

Departament d'Òptica i Optometria i Ciències de la Visió, Universitat de València, Dr. Moliner 50, 46100-Burjassot, Spain.

*e-mail: adolfo.esteban@uv.es

A transient detection imaging system (TDI), also known as optical novelty filter, is an adaptive interferometric device that detects temporal changes in a scene while suppressing its static parts. Removal of background improves contrast and helps visualizing and measuring intensity and phase. Following the first TDI proposal by Cudney et al. [1], most TDI systems are based on photorefractive two-wave mixing [2]. Previous works rely on conventional intensity measurements, where partial information about input signal phase changes are obtained by previous calibration.

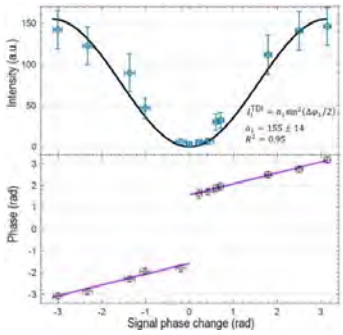

Figure 1. Transient output intensity(top) and phase (bottom) depending on the applied signal-phase change. Intensity is fitted whereas phase follows the linear theoretical Equation.

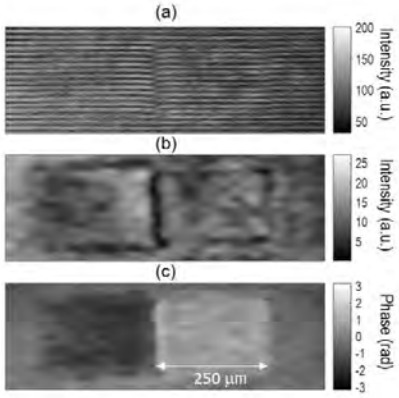

Figure 2. Example of transient interferogram (a), intensity (b) and retrieved differential phase (c) of a squared-shape phase moving object from left to right.

In this work, we report our results on the TDI output complex-field and its relation with the input signal phase changes. The experimental setup is based on a single-frequency laser emitting at 532nm and SBN and BaTiO3 crystals. The laser beam is split into a signal beam, a pump beam, and a reference beam for interferometry. Signal and pump beams intersect at the nonlinear crystal, which has its c^+-axis oriented to get strong energy transfer from signal to pump under steady-state operation. Therefore, the output beam contains images only when the input signal beam changes. The input signal beam is reflected onto a piezo-mirror which allows fine control of phase changes. Output signal phase is retrieved from off-axis holographic Fourier technique which, compared to conventional intensity-based TDI, provides important additional features such as directionality of the phase change, higher resolution, and differential-phase measurement for enhanced sensitivity without calibration.

We have evidenced the linear relation between input and output phases for the entire range from $-\pi$ to π (see Figure 1) in excellent agreement with our theory [3], where the output-signal transient phase, is given by:

$$\frac{\Delta\varphi_1}{2} + \frac{\pi}{2}\operatorname{sign}\Delta\varphi_1$$

and just depends on the input signal phase change $\Delta\varphi_1$, and predicts a π jump "amplification" around zero.

The results indicate that interferometric transient phase measurements improves inference from intensity, reaching $\lambda/30$ resolution (see Figure 1), and provides differential-phase detection. Moreover, we report new results on interferometric transient phase retrieval microscopy of moving objects (see Figure 2).

We believe that this work takes advantage of background suppression with high phase-sign sensitivity, especially important for low-power small-phase change signals sensors, and opens up new possibilities.

[1] R. S. Cudney, R. M. Pierce, and J. Feinberg, *Nature* **332**(6163), 424 (1988).
[2] M. Woerdemann, F. Holtmann, and C. Denz, *Appl. Phys. Lett.* **93**, 021108 (2008).
[3] A. Esteban-Martín, J. García-Monreal, F. Silva, and G. J. de Valcárcel, *Optics Express* **28**, 28782 (2020).

Acknowledgements: We acknowledge financial support from the Spanish Government and EU-FEDER through project PID2020-120056GB-C22.

Optical bistability based on the integration of a molecular nanomaterial in silicon photonics

Elena Pinilla-Cienfuegos[1,*], Alba Vicente[1], Jorge Parra[1], Juan Navarro Arenas[1], Pablo Sanchis-Kilders[1], Roger Sanchis-Gual[2], Ramon Torres-Cavanillas[2], Mónica Giménez-Marqués[2], Eugenio Coronado[2]

[1]*Nanophotonics Technology Center (NTC), Universidad Politécnica de Valencia, Valencia, Spain.*
[2]*Instituto de Ciencia Molecular (ICMol), Universitat de València, Valencia, Spain.*

*e-mail: epinilla@ntc.upv.es

Electro-optical bistability is a functionality which can be crucial for a wide range of applications as it can enable non-volatile and ultra-low power switching performance [1]. In this work an advance in Nanophotonics is presented with a new approach for the development of low-power on-chip optical switching devices. This new approach is based on the integration of an encapsulated molecular nanomaterial that presents bistable Spin Crossover (SCO) phenomenon at room temperature (RT) in the Si platform [2].

SCO is a spin-state switching phenomenon present in some molecular compounds such as the coordination complexes of transition-metal ions in which, under certain external stimulus (variation of temperature, pressure, electric field, or light irradiation), the electronic configuration can be switched between two molecular spin states, Low Spin (LS) and High Spin (HS) states [3]. Furthermore, the spin state change is accompanied by a change in the structural, magnetic, and optical properties, as well as in the electrical conductivity and color. These properties vary as a function of the external stimulus following a hysteretic response, recognized as one of the most promising aspects of the system since hysteresis confers bistability and thus a memory effect (Figure 1a).

Finally, the SCO material can be synthetized as nanoparticles so that it can be easily integrated in the silicon platform and have the potential to allow optical switching at room temperature (Figure 1b).

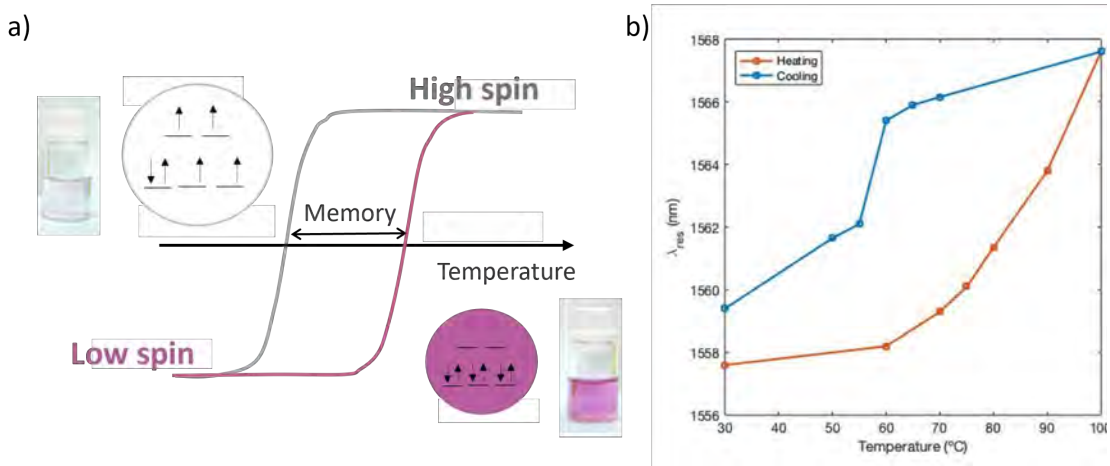

Figure 1. (a) Schematic of the spin configurations and typical spin transition curve with abrupt hysteresis. In the low spin state (LS), electrons are paired, the color of the complex is purple/pink, and the volume is smaller. In the high spin state (HS), the electrons are unpaired, the complex gets a transparent color and the volume increases. (b) Measurement of the optical signal (λ_{res}, resonance frequency) as a function of the temperature where the expected hysterical response is clearly observed. Patent pending (P202130999).

[1] A. H. Atabaki *et al.*, *Nature* **556** (no. 7701), 349 (2018).
[2] M. Giménez-Marqués *et al. J. Mater. Chem. C* **3** (no. 30) 7946 (2015).
[3] O. Kahn and C. Jay Martinez, *Science* **279** (no. 5347) 44 (1998).

Acknowledgements: E.P.-C. gratefully acknowledges support from Generalitat Valenciana (Grant No. SEJIGENT/2021/039).

High-quality compression of ultrafast near-UV light in hollow anti-resonant fibres

David Novoa[1,2,3,*], Jie Luan[3], Philip St. J. Russell[3]

[1]*Department of Communications Engineering, University of the Basque Country (UPV/EHU), Torres Quevedo 1, 48013 Bilbao, Spain.* [2]*IKERBASQUE, Basque Foundation for Science, Plaza Euskadi 5, 48009 Bilbao, Spain.*
[3]*Max-Planck Institute for the Science of Light, Staudtstrasse 2, 91058 Erlangen, Germany.*

*e-mail: david.novoa@ehu.eus

Coherent ultrafast light sources emitting in the ultraviolet (UV) are important in many fields such as time-resolved spectroscopy [1]. Among the different approaches available for generating ultrashort UV pulses with durations ≲10 fs, broadband-guiding anti-resonant fibres (ARFs) filled with gases stand out owing to their excellent UV transparency and pressure-tunable dispersion [2]. This has permitted, for instance, the compression of near-UV pulses in ambient air-filled ARF [3], but at the expense of spectral red-shifting and limited energy because of the Raman effect originated in the molecular air constituents.

Here we report the generation and direct characterization of μJ-level, ~8.5 fs near-UV pulses centered at 400 nm in an argon-filled ARF. The quality of the pulses *Q*, defined as the ratio between the pulse energy contained within the main temporal lobe of the pulse to the whole pulse energy (given in percentage), reaches extremely high values up to 98%. This is possible by a judicious choice of fibre parameters (namely length, core size, core-wall thickness, and filling gas pressure) and post-compensation of the spectral phase distortion introduced by the output window of the gas cell and the air path using a combination of dispersive mirrors and glass wedges.

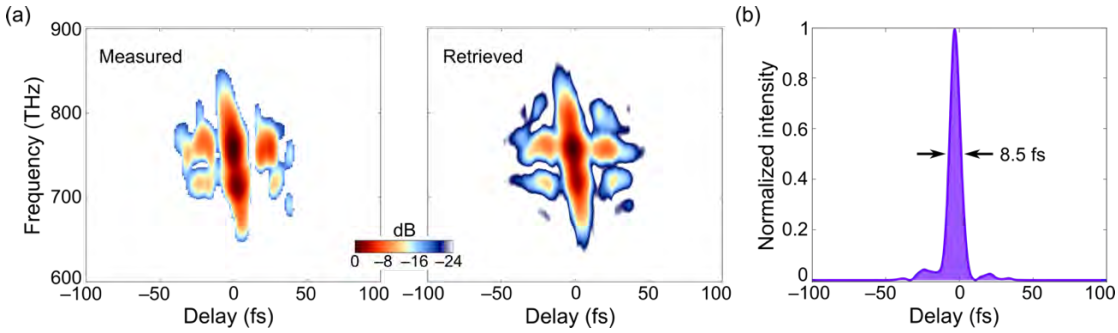

Figure 1. (a) Measured and retrieved spectrograms obtained by self-diffraction frequency-resolved optical gating. Both traces contain the same main features, namely they are composed of a central stripe surrounded by several satellite lobes. (b) Retrieved near-UV pulse with ~8.5 fs duration and *Q* ~ 98%.

In this study we launched ~60 fs near-UV pulses of 4.4 μJ energy in a 1.15 m-long kagomé-style ARF with ~22 μm-core diameter and ~90 nm core-wall thickness [3]. Upon propagation in the ARF filled with argon at 250 mbar, the pump pulses underwent soliton-effect temporal self-compression, enabled by the interplay of nonlinear self-phase modulation with the negative group-velocity dispersion of the fibre [2]. The outcoupled near-UV pulses were severely distorted in the time domain due to propagation through the MgF_2 window of the output gas cell and the air path to the diagnostics. Following compensation of this excessive positive dispersion using a set of negatively-chirped mirrors and silica wedges, the self-compressed near-UV pulses with μJ-level energy were then characterized using self-diffraction frequency-resolved optical gating. Both measured and retrieved spectrograms (see Fig. 1a) are in very good agreement, yielding a clean pulse of ~8.5 fs duration and extremely high quality as quantified by a *Q* parameter reaching 98% (Fig. 1b). Interestingly, the near-UV pulses were measured at the point of use, i.e. without need for numerical back-propagation to infer the actual pulse structure at the fibre endface, and therefore may readily find applications in fields such as pump-probe spectroscopy or femtochemistry.

[1] R. Borrego-Varillas *et al*., *Chem. Sci.* **10**, 9907 (2019).
[2] P. St.J. Russell, P. Hölzer, W. Chang, A. Abdolvand and J. C. Travers, *Nat. Photonics* **8**, 278 (2014).
[3] J. Luan, P. St.J. Russell and D. Novoa, *Opt. Express* **29**, 13787 (2021).

In-line and ultraestable spatiotemporal characterization of constant and time-varying optical vortices

Miguel López-Ripa*, Íñigo J. Sola, Benjamín Alonso

Departamento Física Aplicada, Universidad de Salamanca, Plaza de la Merced s/n 37008 Salamanca, Spain.

*e-mail: miguellr@usal.es

During the last decades, the generation and study of optical vortices has gained great interest due to their multiple applications such as optical tweezers or optical machining among others [1]. However, the complex set-ups and the high dependency to external perturbations of conventional spatiotemporal characterization techniques [2] complicates their study.

In this contribution, we present the study of constant and time-varying optical vortices using an in-line, robust and ultraestable spatiotemporal characterization technique [3]. The spatiotemporal technique is based on the properties of birefringent uniaxial crystals in order to obtain a bulk lateral shearing interferometer which combines spectral and lateral interferometry. Furthermore, the temporal reference required by our technique is obtained using amplitude swing [4], making the whole system robust against external perturbations. We have taken advantage of the high stability of the whole system, associated with its compact configuration, to characterize temporally and spectrally the wavefronts of optical vortices with constant and time-varying orbital angular momentum (OAM).

The optical vortices were generated using a Ti:Sapphire pulsed laser (central wavelength around 800 nm) and nanostructured plates commonly known as s-waveplates. As explained in [3], depending on the incident beam properties after the s-waveplates we can either generate constant optical vortices or two delayed vortices with an average time-varying OAM. On one hand, in the left part of Fig.1 (Exp. 1) it is shown a snapshot of the spatiospectral characterization of a constant OAM vortex of ℓ=+4, which corresponds to the second harmonic of an optical vortex of ℓ=+2. On the other hand, in the right part of Fig.1 (Exp. 2) they are shown three temporal snapshots of the spatiotemporal characterization of the average structure of two delayed optical vortices with different OAM (ℓ=+2 and ℓ=0). In t_1 and t_3, the individual vortices of ℓ=+2 and ℓ=0 are observed, respectively, whereas t_2 corresponds to its superposition. These results were found to be in good agreement with theoretical simulations [3].

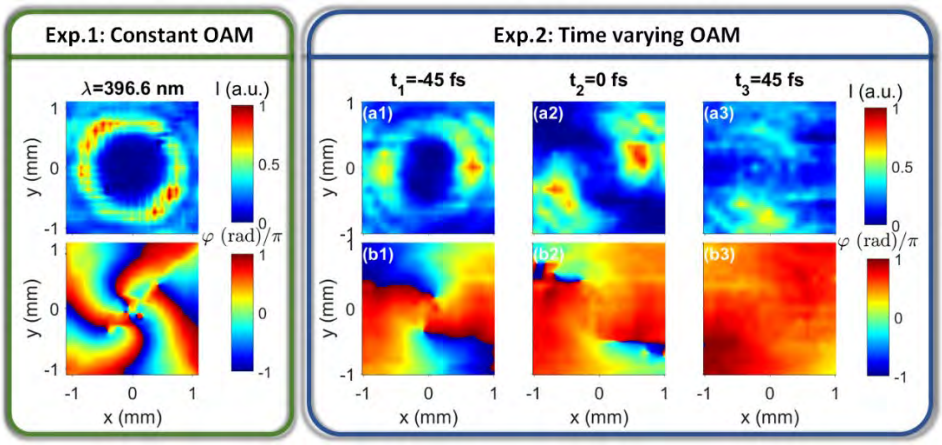

Fig. 1. Green box [Exp. 1]: spatiospectral characterization of a pulsed optical vortex of ℓ=+4. Blue box [Exp. 2]: spatiotemporal characterization of two delayed optical vortices of ℓ=+2 and ℓ=0 for three different times of the pulse.

In conclusion the compact and ultraestable set-up of our spatiotemporal technique enables to easily characterize temporally or spectrally the wavefronts of complex spatiotemporal pulsed beams such as optical vortices. Moreover, the spatiotemporal technique can be used in all the transparency range of the birefringent crystals, so we believe it could be a key tool to ease the characterization of ultrafast phenomena.

[1] Y. Shen, X. Wang, Z. Xie, C. Min, X. Fu, Q. Liu, M. Gong, X. Yuan, *Light Sci. Appl.* **8**, 90 (2019).
[2] S. W. Jolly, O. Gobert, F. Quéré, *J. Opt.* **22**, 103501 (2020).
[3] M. López-Ripa, I. J. Sola, B. Alonso, *Photon. Res.* **10**, 922-931 (2022).
[4] B. Alonso, W. Holgado, I. J. Sola, *Opt. Express* **28**, 15625-15640 (2020).

Simultaneous tuning of four-wave mixing and polarization modulation instability in microstructured optical fiber

A. Loredo-Trejo[1,2,*], A. Díez[1,2], E. Silvestre[1,3], M. V. Andrés[1,2]
[1]*Laboratory of Fiber Optics, ICMUV, Universidad de Valencia, 46100 Valencia, Spain.* [2]*Departamento de Física Aplicada y Electromagnetismo, Universidad de Valencia, 46100 Valencia, Spain.* [3]*Departamento de Óptica, Universidad de Valencia, 46100 Valencia, Spain.*

*e-mail: abraham.loredo@uv.es

In this communication, we report simple methods to simultaneously generate and tune widely spaced spectral sidebands generated through scalar four-wave mixing (FWM) and polarization modulation instability (PMI) produced in weakly-birefringent microstructured optical fibers (MOFs). In this experimental study, we show that proper control of the fiber properties, in particular, chromatic dispersion and phase birefringence can lead the simultaneous generation and tuning of both nonlinear effects. Changing the refractive index (RI) in the holes surrounding the core of a MOF affects both, chromatic dispersion and birefringence. Thus, tunability of PMI/FWM bands can be attained by fine-tuning the RI in the holes [1, 2]. Here, we used two practical methods. First, a set of solutions of different ethanol-water (EtOH-H_2O) concentrations were prepared and were infiltrated into the fiber. Then, the RI of holes can be adjusted in a wide range by changing the solution concentration. The second method is based on the thermo-optic properties of the liquid infiltrated into the MOFs. In the case of EtOH-H_2O solutions, the thermo-optic coefficient is negative and can be remarkably large for high EtOH concentrations. This second technique enables continuous and dynamic tuning of the RI around an initial value.

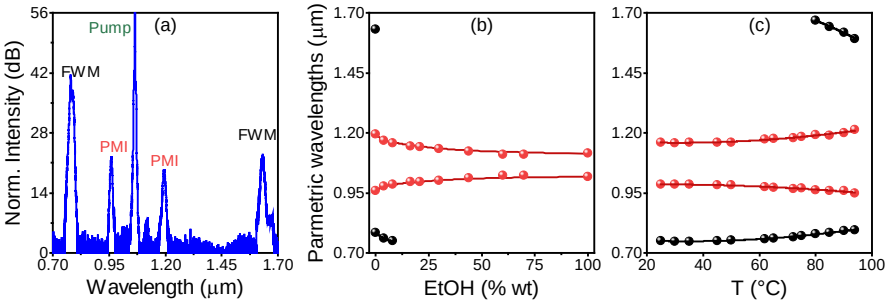

Figure 1. (a) Light spectrum transmitted through the fiber when the fiber holes were filled with a solution at 0 %wt of EtOH. Parametric wavelengths as a function of (b) EtOH concentration and (c) temperature. Pump polarization adjusted to excite the slow-axis eigenmode. PMI and FWM wavelengths are depicted by red and black dots, respectively. Dots are experimental data and lines are a guide to the eye.

We performed the experiments in a liquid-filled, triangular lattice solid-core MOF with hole diameter and pitch of d = 1.8 μm and Λ = 2.9 μm, respectively. We investigate experimentally the simultaneous generation and tuning of PMI/FWM sidebands employing the methods mentioned above. A Nd: YAG microchip laser emitting at 1064 nm was used as the pump. Figure 1(a) shows the light spectrum exiting one fiber, where two pairs of sidebands generated through PMI and FWM can be observed.

Increasing the ethanol concentration of the filling solution causes the FWM sidebands to move away from the pump wavelength, indicating an increase in the frequency shift between the pump and the FWM. The opposite was observed for PMI sidebands, which are shifted towards the pump wavelength, which indicates a decrease of the frequency shift with EtOH concentration. Experiments of PMI/FWM tuning with temperature were performed with the fiber infiltrated with a solution at 8 %wt. Increasing the fiber temperature causes the FWM bands to shift toward the pump wavelength, indicating that the FWM frequency shift decreases with temperature; again, the opposite was observed with the PMI sidebands. We were able to simultaneously tune the PMI and FWM sidebands in the temperature range of the experiments, from 20 °C to 95 °C. Figure 1 (b)-(c) summarizes the parametric wavelengths as a function of EtOH concentrations and temperature.

[1] L. Velázquez-Ibarra, A. Díez, E. Silvestre, and M. V. Andrés, *Optics Letters* **41**, 2600 (2016).
[2] A. Loredo-Trejo, A. Díez, E. Silvestre, and M. V. Andrés, *Optics Letters* **45**, 4891 (2020).

Use of gas-filled multipass cells to generate clean supercontinuum spectra

V. W. Segundo Staels*, E. Conejero Jarque, J. San Roman

[1]*Grupo de Investigación en Aplicaciones del Láser y Fotónica, Departamento de Física Aplicada, Universidad de Salamanca, E-37008, Salamanca, Spain.*

*e-mail: vwsstaels@usal.es

One of the most efficient nonlinear effects used to achieve ultrashort laser pulses is the self-phase modulation (SPM) [1]. Among the new post-compression setups which have been devised to generate large spectral broadening, multipass cells (MPC) are gaining relevance [2,3]. Multipass cells consist of a cavity formed by two mirrors and usually filled with gas, where a laser pulse travels during multiple roundtrips. To obtain short and clean pulses, one can let the pulse propagate in the enhanced frequency chirp regime, a regime introduced in optical fibers in the 1980s [4]. In this region, the spectrum is broadened with a clean spectral shape and phase because the dynamics is dominated by the nonlinearity, specially by SPM, but with the dispersion being non-negligible.

In order to study if this regime can be achieved in MPCs, we use a 3D numerical to simulate the propagation of a 177 fs full width half maximum (FWHM) Yb laser pulse with a central wavelength of 1030 nm. The propagation occurs along 20 roundtrips in a 40 cm confocal cavity filled with argon. The model calculates the evolution of the envelope of the pulse field affected by diffraction, dispersion, SPM and self-steepening.

We can delimit the enhanced frequency chirp regime by imposing the following three conditions: $L_{NL} < L < L_D$ and $1 < N = \sqrt{L_D/L_{NL}} < 20$, where L is the propagation length, L_{NL} is the nonlinear length and L_D is the dispersion length [5]. The third condition imposes that the maximum peak power reached during the propagation must be below its critical value. In these circumstances, we perform a scan in gas pressure and pulse energy looking for the best conditions of spectrum broadening while conserving a smooth shape.

An optimal region can be found for 10 bar and 100 μJ and its surroundings. In figure 1 we show the result obtained for this particular case. The spectrum obtained (Fig. 1(a)) presents a smooth spectral phase and a clean shape, far from the characteristic SPM oscillations. This shape assures a Fourier Limit compression factor of more than 12, with sidelobes less than 0.4 % of its peak intensity, entering in the few-cycle regime without showing any temporal secondary structure (Fig. 1(b)). This new regime opens a way to obtain clean ultrashort optical pulses using the multipass post-compression scheme

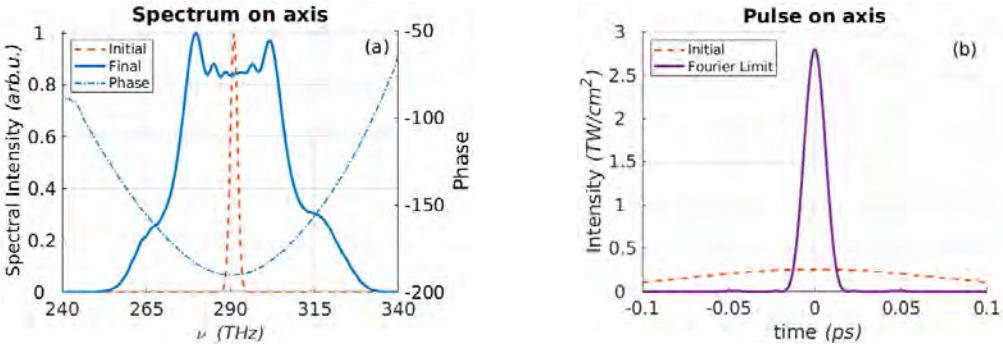

Figure 1. On axis spectral (a) and temporal (b) intensity profiles of a 100 μJ, 177 fs FWHM pulse in confocal cavity filled with 10 bar of argon. Temporal profile is plotted together with the Fourier Limit, reaching a compression factor of more than 12.

[1] T. Nagy, P. Simon, and L. Veisz, *Adv. Phys. X* **6**, 1845795 (2021).
[2] M. Hanna *et al.*, *Laser Photonics Rev.* **15**, 2100220 (2021).
[3] A.-L. Viotti *et al.*, *Optica* **9**, 197 (2022).
[4] W. J. Tomlinson, R. H. Stolen, and C. V. Shank, *JOSA B* **1**, 139 (1984).
[5] A. Couairon and A. Mysyrowicz, *Phys. Rep.* **441**, 47 (2007).

Acknowledgments: Ministerio de Economía y Competitividad (PRE2020-092181); Ministerio de Ciencia e Innovación (PID2019-106910GB-I00).

Ionic Liquids as tunable nonlinear optical materials

Carlos Damián Rodríguez-Fernández[1,*], Luis M. Varela[1], Christian Schröder[2], Raúl de la Fuente, Elena López Lago[1]

[1]*NaFoMat group, Departamento de Física Aplicada and Departamento de Física de Partículas, Universidade de Santiago de Compostela, E-15782 Santiago de Compostela, Spain.* [2]*University of Vienna, Department of Computational Biological Chemistry, Währingerstr. 17, A-1090 Vienna, Austria.*

*e-mail: damian.rodriguez@usc.es

Ionic Liquids (ILs) are a family of ionic materials that are found in the liquid state at temperatures below 100 °C, and, even, at room temperature. Their high thermal and electrochemical stability, negligible vapour pressure and tunability, makes them promising smart materials in different fields. In the case of photonics, ILs exhibit relevant optical properties such as luminescence [1], liquid crystal character [2] or material dispersion [3] that can be task-specifically tuned. In this contribution, we explore, by means of DFT calculations at the B3LYP/6-31++G(d,p) level of theory, the possibility of tailoring the Electro-Optical Kerr Effect (EOKE) susceptibility in ILs throughout designing the extent of charge delocalization in their composing ions. Specifically, we considered the widespread 1-alkyl-3-methylimidazolium cation with alkyl side chains (-CH_2-) of length from one to five units and functionalized derivatives incorporating fluorine atoms (-CF_2-), oxygen atoms (-CH_2-O-CH_2-) or conjugated character (-CH=CH-).

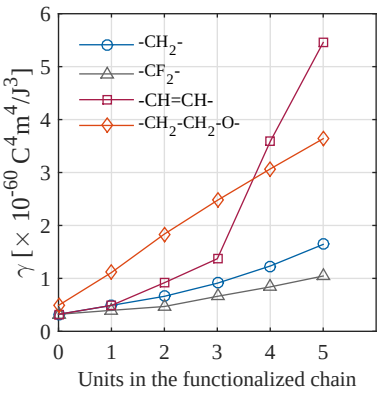

Figure 1. Second hyperpolarizability for the EOKE nonlinear process of different 1-alkyl-3-methylimidazolium based cations differing in the functionalization and length of their side chain.

Our results show that the presence of charge delocalization in the ions has a large impact in their second order hyperpolarizability, γ, and, in general, in their nonlinear optical (NLO) response. Increasing the length of those chains functionalized with saturated units (only σ bonds), produces a moderate increase of the second order hyperpolarizability while, increasing the length of the conjugated chain (that with resonant π bonds), leads to a much higher enhancement of the NLO response. In fact, ILs based on this family of imidazolium cations are able to exhibit EOKE susceptibilities one order of magnitude higher than those of standard KDP, DKDP or BBO nonlinear crystals, suggesting that some ILs could be used as efficient NLO materials.

In conclusion, EOKE susceptibility can be tailored in ILs by means of the smart design of the charge delocalization in their structure and, specially, in the side chains of cationic heterocycles. Our simulations suggest that proper tailoring of the charge delocalization regions can be used to obtain ILs with nonlinear susceptibilities above those of standard nonlinear crystals such as KDP, DKDP or BBO.

[1] K. Tanabe, Y. Suzui, M. Hasegawa, T. Kato, *J. Am. Chem. Soc.* **134**, 5652(2012).
[2] C. Hardacre, J.D. Holbrey, P.B. McCormac, S.E.J. McMath, M. Nieuwenhuyzen, K.R. Seddon, *J. Mater. Chem.* **11**, 346(2001).
[3] C.D. Rodríguez Fernández, Y. Arosa, B. Algnamat, E. López Lago, R. de la Fuente, *Phys. Chem. Chem. Phys.* **22**, 14061(2020).

Acknowledgements: This work was supported by Ministerio de Economia y Competitividad (MINECO) and FEDER 17 Program through the projects (MAT2017-89239-C2-1-P); Xunta de Galicia and FEDER (GRC ED431C 2016/001, ED431D 2017/06, ED431E2018/08). C. D. R. F. thanks the support of Xunta de Galicia through the grant ED481A-2018/032. We also thank the Centro de Supercomputacion de Galicia (CESGA) facility, Santiago de Compostela, Galicia, Spain, for providing the computational resources employed in this work.

Non-linear, purely magnetic magnetization response to femtosecond structured laser pulses

Luis Sánchez-Tejerina[1,*], Rodrigo Martín-Hernández[1], Rocío Yanes[2], Luis Plaja[1], Luis López-Díaz[2], Carlos Hernández-García[1]

[1]*Grupo de Investigación en Aplicaciones del Láser y Fotónica, Dpto. Física Aplicada, Universidad de Salamanca, E-37008, Salamanca, Spain.*
[2]*Dpto. Física Aplicada, Universidad de Salamanca, E-37008, Salamanca, Spain.*

*e-mail: luis.stsj@usal.es

Since the pioneering work on ultrafast laser induced demagnetization [1], femtosecond (fs) laser pulses have attracted a lot of interest as a unique path to achieve sub-ps control of magnetic states. Most of the phenomena involved in these studies are related with non-linear effects of the electric field on the magnetization of the sample [2]. Nonetheless, the recent technological advances in the development of structured laser pulses have opened the possibility to study non-linear effects induced solely by the magnetic field. In particular, the use of azimuthally polarized ultrafast laser pulses. allows for the generation of Tesla-scale fs magnetic fields, isolated from the electric field [3]. Such novel isolation of the magnetic field poses the question of the effect of the magnetic field alone on this ultrashort and ultraintense scale.

In this contribution we show analytically and numerically that isolated circularly polarized magnetic fields promote a non-linear slow cumulative effect on the magnetization of a magnetic sample. Remarkably, such effect scales quadratically with the amplitude of the magnetic field. Our work shows that this effect can be understood as a drift field acting perpendicularly to the plane defined by the circular polarization state, evolving with the envelope of the laser pulse. This effect can be used to obtain purely precessional sub-ps switching with hundreds of Tesla on ferromagnets [4] or even to excite self-sustain oscillations in antiferromagnets with only several tens of Tesla. Our work introduces the possibility to perform ultrafast magnetization from non-linear magnetic effects in which undesirable effects that typically appear from the use intense electric fields, such as heating of the sample, can be avoided.

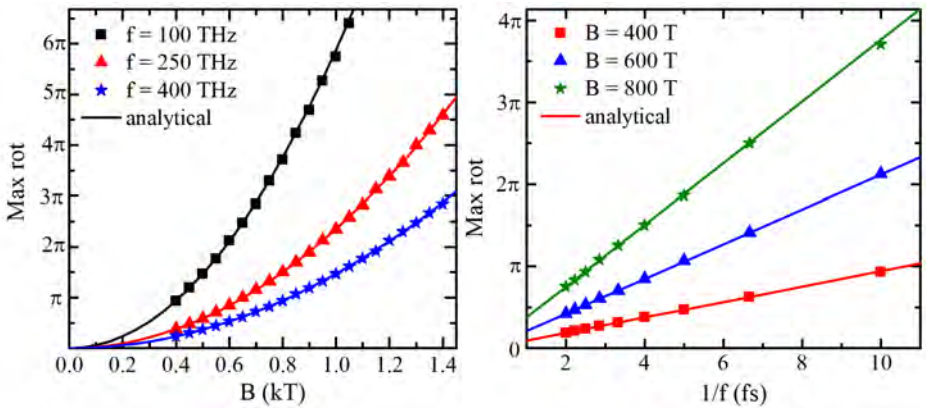

Figure 1. (a) Total rotation of a ferromagnetic sample after the application of a laser pulse of width $t_p = 750$ fs as a function of the magnetic field amplitude. (b) Total rotation of a ferromagnetic sample after the application of a laser pulse of width $t_p = 750$ fs as a function of main frequency.

[1] E. Beaurepaire, J.-C. Merle, A. Daunois, and J.-Y. Bigot, *Phys. Rev. Lett.* **76**, 4250 (1996).
[2] C. Wang, Y. Liu, *Nano Convergence* **7** (2020).
[3] M. Blanco, F. Cambronero, M. T. Flores-Arias, E. Conejero Jarque, L. Plaja, and C. Hernández-García *ACS Photonics* **6** (2019).
[4] L. Sánchez-Tejerina, R. Yanes, R. Martín-Hernández, L. Plaja, L. López-Díaz, C. Hernández-García, *in preparation*.

Acknowledgements: This work has been funded by the ERC Starting Grant ATTOSTRUCTURA, grant agreement No. 851201; Ministerio de Ciencia de Innovación y Universidades (PID2019-106910GB-I00, RYC-2017-22745); Junta de Castilla y León FEDER (SA287P18).

Anyonic Molecules in Atomic Fractional Quantum Hall Liquids: A Quantitative Probe of Fractional Charge and Anyonic Statistics

Alberto Muñoz de las Heras[1,2,*], Elia Macaluso[2], Iacopo Carusotto[2]

[1]*Institute of Fundamental Physics IFF-CSIC, Calle Serrano 113b, 28006 Madrid, Spain.*
[2]*INO-CNR BEC Center and Università di Trento, via Sommarive 14, 38123 Trento, Italy.*

*e-mail: a.munozdelasheras@gmail.com

Fractional quantum Hall (FQH) liquids are strongly correlated phases of matter arising in strongly interacting two-dimensional systems subjected to an external magnetic field. Such systems host quasihole and quasiparticle excitations known as anyons that feature fractional charge and intermediate statistics that fall outside the traditional distinction between bosons and fermions. Notwithstanding its exotic nature and the promising perspectives that anyons open up for topological quantum computing, a conclusive signature of anyonic statistics has long remained elusive [1]. Here we studied the quantum dynamics of massive impurities embedded in a strongly interacting, two-dimensional atomic gas driven into the FQH regime under the effect of a synthetic magnetic field. For suitable values of the atom-impurity interaction strength, each impurity can capture one or more quasihole excitations of the FQH liquid, forming a bound molecular state with novel physical properties [2,3]. An effective Hamiltonian for such anyonic molecules is derived within the Born-Oppenheimer approximation, which provides renormalized values for their effective mass, charge, and statistics by combining the finite mass of the impurity with the fractional charge and statistics of the quasiholes. The renormalized mass and charge of a single molecule can be extracted from the cyclotron orbit that it describes as a free particle in a magnetic field. The anyonic statistics introduces a statistical phase between the direct and exchange scattering channels of a pair of indistinguishable colliding molecules and can be measured from the angular position of the interference fringes in the differential scattering cross section. Implementations of such schemes beyond cold atomic gases are highlighted, in particular, in photonic systems. Our results were published in [4].

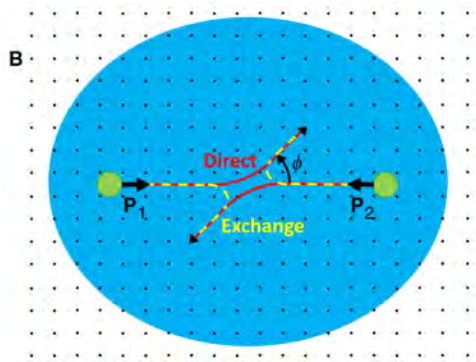

Figure 1. Scattering of two anyonic molecules (green circles) formed by the binding of the same number of quasiholes to a pair of identical impurities in the bulk of a FQH fluid (blue region). The two molecules are given momentum kicks against each other (P1 and P2, respectively). Because of their indistinguishability, two scattering channels contribute to the differential scattering cross section at an angle ϕ: The two channels are labeled as "direct" (red, solid trajectories) and "exchange" (yellow, dashed ones) and involve a relative phase determined by the anyonic statistics. As one can guess from textbook two-slit interference, information about the statistics can be extracted from the global position of the interference fringe pattern.

[1] David Tong, *Lectures on the Quantum Hall effect*, arXiv:1606.06687 (2016)
[2] Zhang et al., *Physical Review Letters* **113**, 160404 (2014)
[3] Lundholm and Rougerie, *Physical Review Letters* **116**, 170401 (2016)
[4] Alberto Muñoz de las Heras, Elia Macaluso, and Iacopo Carusotto, *Phyical Review X* **10**, 041058 (2020)

Acknowledgements: European Union H2020-FETFLAG-2018-2020 project "PhoQuS" (No. 820392), Provincia Autonoma di Trento, Q@TN initiative, and Google via the quantum NISQ award.

Superexchange liquefaction of strongly correlated lattice dipolar bosons

Ivan Morera[1,2,3*], Rafał Ołdziejewski[4,5], Grigori E. Astrakharchik[6], Bruno Juliá-Díaz[1,2]

[1] *Departament de Física Quàntica i Astrofísica, Facultat de Física, Universitat de Barcelona, E-08028 Barcelona, Spain.* [2] *Institut de Ciències del Cosmos, Universitat de Barcelona, ICCUB, Martí i Franquès 1, E-08028 Barcelona, Spain.* [3] *Institute for Theoretical Physics, ETH Zurich, 8093 Zurich, Switzerland.* [4] *Max Planck Institute of Quantum Optics, 85748 Garching, Germany.* [5] *Munich Center for Quantum Science and Technology, Schellingstrasse 4, 80799 Munich, Germany.* [6] *Departament de Física, Universitat Politècnica de Catalunya, Campus Nord B4-B5, E-08034 Barcelona, Spain*

*e-mail: imorera@icc.ub.edu

Recently, a new class of ultradilute quantum droplets has been produced in ultracold atomic systems, both in bosonic dipolar systems and in bosonic mixtures. Such quantum droplets are characterized by being self-bound objects similar to the case of water droplets. The main difference is that the equilibrium density can be eight orders of magnitude smaller than in liquid water. Furthermore, the stability of these quantum droplets can be understood from a compensation between mean-field interactions and quantum fluctuations.

In this talk I will present a new type of quantum liquids and droplets which appear in dipolar bosonic systems loaded in one-dimensional optical lattices [1]. These appear in the strongly interacting regime and I will show how their formation can be understood from the appearance of superexchange processes. These processes liquefy the system when being close to the self-bound insulating state (Fig. 1). I will discuss how such lattice quantum liquids can be produced in dipolar bosonic systems which could already be realized in current ultracold atomic laboratories by adding a one-dimensional optical lattice.

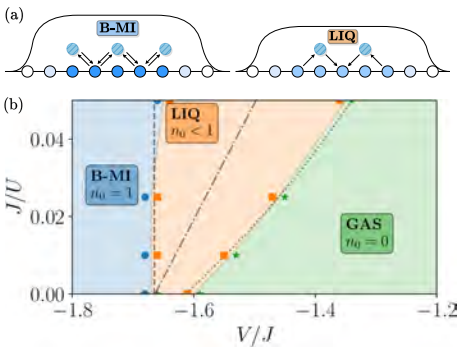

Figure 1. Panel (a): Schematic representation of a density profile in self-bound Mott insulator (B-MI) having unit filling and liquid drop (LIQ) in which particles are bound but holes are present. Arrows indicate the different superexchange processes through doublon formation. Panel (b): Phase diagram for dipolar bosons in a one-dimensional optical lattice. Different phases can be characterized by their respective equilibrium densities n_0. We encounter a gaseous phase (GAS), a liquid one, and a self-bound Mott-insulator. Dashed and dotted-dashed lines denote respectively LIQ-to-B-MI and GAS-to-LIQ transitions obtained in perturbation theory. Dotted line indicates the formation of a bound state (dimer) in the two-body problem.

[1] I. Morera, R. Ołdziejewski, G. E. Astrakharchik, and B. Juliá-Díaz, *arXiv:2204.03906v1* (2022).

Acknowledgements: This work has been funded by Grant No. PID2020-114626GB-I00 from the MICIN/AEI/10.13039 /501100011033 and by the Ministerio de Economia, Industria y Competitividad (MINECO, Spain) under grants No. FIS2017-84114-C2-1-P and No. FIS2017- 87534-P. We acknowledge financial support from Secretaria d'Universitats i Recerca del Departament d'Empresa i Coneixement de la Generalitat de Catalunya, co-funded by the European Union Regional Development Fund within the ERDF Operational Program of Catalunya (project QuantumCat, ref. 001-P001644). R. O. acknowledges support by the Max Planck Society and the Deutsche Forschungsgemeinschaft (DFG, German Research Foundation) under Germany's Excellence Strategy – EXC-2111 – 390814868.

Emitting single and squeezed photons

E. Zubizarreta Casalengua[1,2,*], F. P. Laussy[2,3], E. del Valle[1]

[1] *Departamento de Física Teórica de la Materia Condensada, Universidad Autónoma de Madrid, 28049 Madrid, Spain.* [2] *Faculty of Science and Engineering, University of Wolverhampton, Wulfruna St, Wolverhampton WV1 1LY, UK.* [3] *Russian Quantum Center, Novaya 100, 143025 Skolkovo, Moscow Region, Russia.*

*e-mail: eduardo.zubizarreta@estudiante.uam.es

Many applications of quantum light require the study of photon correlations, which play a central role in Quantum Optics. We show that the statistics of the photons emitted by many light-matter systems, when resonantly excited using coherent sources, can be controlled and optimized at the N-photon level by purposely tuning the excitation, modulating the emission from Sub- to Super-Poissonian due to both external and self-homodyne interferences [1,2]. Particularly, the well-known photon/polariton blockade is investigated in detail, providing a vast and rich landscape of photon correlations and paving the way to subsequent optimization. These works highlight the close relationship between two relevant quantum attributes of light, photon antibunching and quadrature squeezing, which were so far studied as unrelated topics [3]. This interference mechanism can be implemented in photon spectroscopy, where the theory displays interesting results as well. When the laser-qubit detuning is large, a perfect circle of antibunching between photons with different frequencies arises due to quantum interferences, revealing exotic multi-mode squeezing properties of great potential for applications such as quantum spectroscopy and the generation of highly entangled states of light.

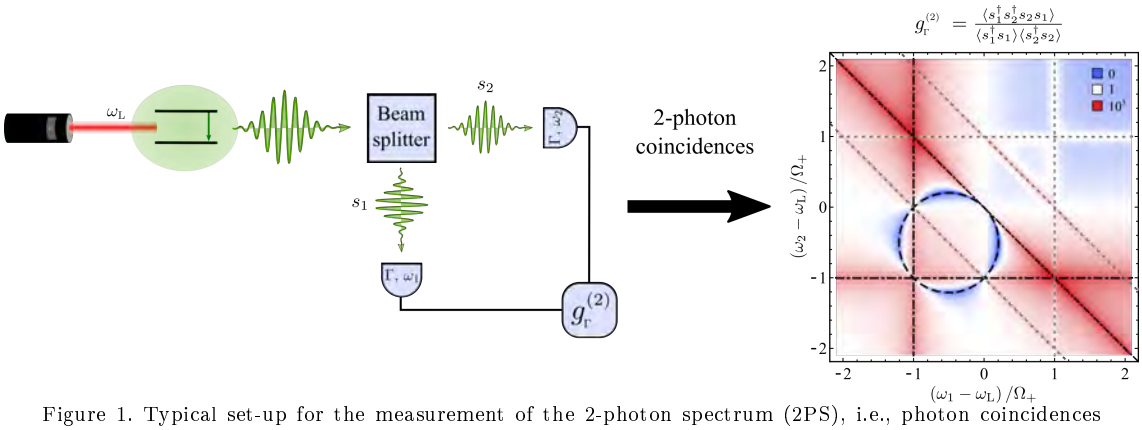

Figure 1. Typical set-up for the measurement of the 2-photon spectrum (2PS), i.e., photon coincidences detected at different frequencies, for a qubit driven by a laser. The 2PS, on the right-hand side, shows a characteristic circle of anticorrelation (in blue), which we have identified as rooted in two-mode squeezing

[1] Conventional and Unconventional Photon Statistics, Zubizarreta Casalengua *et al.*, *Laser & Photonics Reviews* **14**, 1900279 (2020).

[2] Tuning photon statistics with coherent fields, Zubizarreta Casalengua *et al.*, *Phys. Rev. A* **101**, 063824 (2020).

[3] Origin of Antibunching in Resonance Fluorescence, Hanschke *et al.*, *Phys. Rev. Lett.* **125**, 170402 (2020).

Photonic reservoir computing using quantum resources

Jorge García-Beni, Gian Luca Giorgi, **Miguel C. Soriano***, Roberta Zambrini

Instituto de Física Interdisciplinar y Sistemas Complejos (IFISC, UIB-CSIC), Campus Universitat de les Illes Balears E-07122, Palma de Mallorca, Spain.

*e-mail: miguel@ifisc.uib-csic.es

Photonic implementations of brain-inspired computing concepts have achieved state-of-the-art performance in tasks ranging from speech recognition to chaotic time-series prediction. Here, optical feedback is exploited for photonic reservoir computing using quantum resources.

Reservoir Computing is a paradigm of Machine Learning that harnesses the information processing potential of complex dynamical systems [1]. Recently, quantum systems have been suggested as promising candidates for reservoir computing due to the significant growth in phase space degrees of freedom [2]. In this contribution, we propose a photonic platform for reservoir computing and on-line data processing, in the realm of continuous variable quantum optics. A performing reservoir computing scheme requires the availability of a high-dimensionality phase space, a non-linear input-output transformation and a short-term memory, which can be readily available in physical systems [3].

Figure 1 shows a schematic representation of the photonic platform, which includes a feedback loop, nonlinear crystals, an optical beamsplitter and a photodetector. The external input information to be processed is injected in the form of modulated optical pulses. An optical beamsplitter effectively mixes the input pulses with previous pulses that propagate along the feedback loop, providing a mechanism to retain memory into the system. The beamsplitter also allows to send part of the optical pulses to the output photodetector, with the reflectivity of the beamsplitter controlling the memory of the reservoir. The non-linear crystals provide the needed interaction between different optical modes that are contained in the optical pulses. For reservoir computing purposes, we extract the information from the quantum correlations of the optical modes within the pulses, expressed in terms of their covariance matrix.

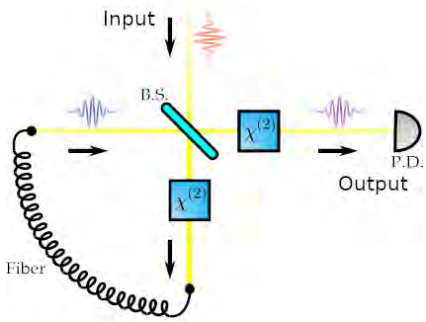

Figure 1. Schematic representation of the proposed photonic platform. The external input to be processed is injected in the form of modulated optical pulses. BS stands for beamsplitter and PD for photodiode. The feedback fiber loop contains a non-linear crystal ($\chi^{(2)}$). The output signal is measured using a homodyne detection scheme.

We tackle the challenge of quantum measurements and back-action in the context of sequential information processing. The performance of the photonic platform, characterized by the information processing capacity [4], is numerically tested for each of the main parameters that can be externally tuned. The role of quantum effects, i.e. squeezing, is addressed in connection with the computational capacity of the system.

Our analytical and numerical results show that, in spite of the dissipative nature of quantum measurements, quantum optical systems can be used for sequential information processing in an experimentally feasible manner and that they may provide advantages over classical dynamical systems.

[1] M. Lukoševičius, and H. Jaeger, *Computer Science Review* **3**, 127–149 (2009).
[2] P. Mujal, R. Martínez-Peña, J. Nokkala, J. García-Beni, G. L. Giorgi, M. C. Soriano, and R. Zambrini, *Advanced Quantum Technologies* **4**, 2100027 (2021).
[3] G. Tanaka, et al., *Neural Networks* **115**, 100–123 (2019).
[4] J. Dambre, D. Verstraeten, B. Schrauwen, and S. Massar, *Scientific Reports* **2**, 514 (2012).

Acknowledgements: We acknowledge the Spanish State Research Agency through the QUARESC project (PID2019-109094GB-C21 and -C22/ AEI / 10.13039/501100011033). We also acknowledge funding by CAIB through the QUAREC project (PRD2018/47).

Ultrastrong waveguide QED with giant atoms

Sergi Terradas-Briansó[1,*],Carlos A. González-Gutiérrez[1],Franco Nori[2,3,4],Luis Martín-Moreno[1], David Zueco[1]

[1]*Instituto de Nanociencia y Materiales de Aragón (INMA), CSIC-Universidad de Zaragoza, Zaragoza 50009, Spain.* [2]*Department of Physics, The University of Michigan, Ann Arbor, Michigan 48109-1040, USA.* [3]*Theoretical Quantum Physics Laboratory, RIKEN Cluster for Pioneering Research, Wako-shi, Saitama 351-0198, Japan.*[4]*RIKEN Center for Quantum Computing (RQC), 2-1 Hirosawa, Wako-shi, Saitama 351-0198, Japan.*

*e-mail: sterradas@unizar.es

The field of waveguide quantum electrodynamics studies the interaction between quantum emitters and propagating one-dimensional electromagnetic fields. One of the more widely used approximations in this field is the dipole approximation, which assumes the emitters can be approximated as point-like particles when compared to the wavelength of the electromagnetic field. In recent years single emitters that break this assumption by coupling to a single electromagnetic mode at different points have been realized experimentally and are known in the literature as giant atoms. These giant atoms have many properties such as tunable decay rates and Lamb shifts, non-Markovian spontaneous emission and bound states due to the interference between the emission from different coupling points and others. See [1] for a recent review.

In the presented work, we extend the theory of giant atoms, previously restricted to perturbative light-matter couplings, to deal with the ultrastrong coupling regime (USC).

Using static and dynamical polaron methods we address the low energy subspace of a giant atom coupled to an ohmic waveguide beyond the standard rotating wave approximation.

We analyze the equilibrium properties of the system by computing the atomic frequency renormalization as a function of the coupling, characterizing the localization-delocalization quantum phase transition for a giant atom, which depends on the spacing between coupling points. We show that virtual photons dressing the ground state are non-exponentially localized around the contact points but instead decay as a power-law as shown in Fig 1.

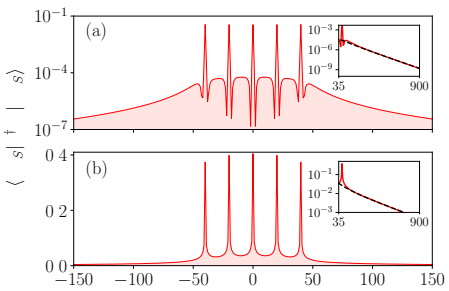

Figure 1. Ground state photons of a giant atom with five equidistant connection points for two coupling strengths α. (a) Illustrates the case is in the delocalized phase, ($\alpha = 1$). (b) Shows a photonic profile in the localized phase ($\alpha = 2$). A power-law fitting is plotted in the insets of both cases.

The spontaneous emission dynamics of an initially excited giant atom are also studied, pointing out the effects of ultrastrong coupling on the Lamb shift and the decay rate, as well as the intrinsic non-Markovianity of the giant atoms. Finally we comment on the existence of the so-called oscillating bound states, for which the emitted radiation is trapped while oscillating between the coupling points of the emitter [2], beyond the rotating wave approximation.

[1] Anton Frisk Kockum, *Quantum Optics with Giant Atoms—the First Five Years. In: International Symposium on Mathematics, Quantum Theory, and Cryptography. Mathematics for Industry, vol 33.*, Springer, Singapore (2021).

[2] Lingzhen Guo, Anton Frisk Kockum, Florian Marquardt and Göran Johansson, *Physical Review Research* **2**, 043014 (2020).

Exact diagonalization correction method for a few-particles trapped in a harmonic potential

Abel Rojo-Francàs[1,2,*], Felipe Isaule[3], Bruno Juliá-Díaz[1,2]

[1] *Departament de Física Quàntica i Astrofísica, Facultat de Física, Universitat de Barcelona, E-08028 Barcelona, Spain.* [2] *Institut de Ciències del Cosmos, Universitat de Barcelona, ICCUB, Martí i Franquès 1, E-08028 Barcelona, Spain.* [3] *School of Physics and Astronomy, University of Glasgow, Glasgow G12 8QQ, United Kingdom.*

*e-mail: abel.rojo@fqa.ub.edu

The study of ultracold atoms is of great interest nowadays due to the great control in laboratories of traps, interactions, number of particles, etc. There are several studies focused on this field [1]. It is frequent to study systems of few particles trapped in a harmonic potential [2] and to consider a contact interaction [3]. One technique used to study this systems is the exact diagonalization [4], whose consists of constructing the Hamiltonian and diagonalizing it exactly. Although, for the harmonic oscillator it is necessary to truncate the basis and as a consequence, the energies obtained are an upper bound of the exact ones.

In our work, we use the fact that the two-particle case has an analytical solution [5] to develop a method to correct the effect of the basis truncation. Solving the two-particle case and introducing a truncation on the basis, we obtain for a given energy, a relation between the value of the exact interaction strength g and the one used in the truncated calculation g' as

$$\frac{1}{g} = \frac{1}{g'} - \frac{1}{g_c}\,, \tag{1}$$

where $1/g_c$ is a correction term with an analytical expression [6]. This value of this correction depends on the state energy and the number of the modes used in the calculation. This correction is exact for the two-particle case even for a small number of modes.

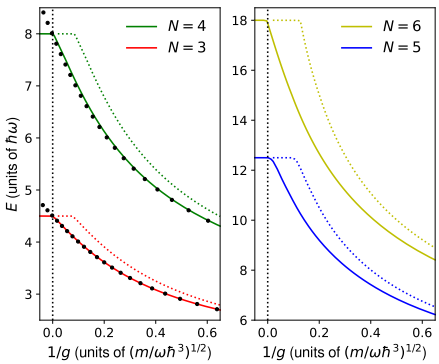

Figura 1: Ground-state energies for $N = 3$ to $N = 6$ distinguishable particles computed using 20 single-particle modes. The dotted lines correspond to the truncated calculations, whereas the solid lines correspond to the corrected energies obtained using Eq. (1). The black circles correspond to the exact values for $N = 3$ and $N = 4$ [3].

We use (1) to correct the energy spectrum for systems with more than two particles. In Fig 1 we show the ground state energy for $N > 2$ as a function of $1/g$. We appreciate the big effect of the correction, especially in the large interacting regime. In addition, for three and four particles, we benchmark our results, with excellent results. For five and six particles, due to the correction, we recover the theoretical energy in the infinite interacting limit.

This method allows a less resource-intensive and more accurate calculation of the energy spectrum using exact diagonalization with a simple additional calculation. Although this method is based on the energy correction, it is also useful for correcting other properties, such as the density profile. In this work, we only consider systems with symmetric interactions: with all interactions equal. Although we suspect that for systems with each interaction different, all of them can be corrected with this procedure for each of their values.

[1] T. Sowiński and M. Á. García-March, *Reports on Progress in Physics* **82**, 104401 (2019).
[2] A. Rojo-Francàs, A. Polls, and B. Juliá-Díaz, *Mathematics* **8**, 1196 (2020).
[3] E. K. Laird, Z.-Y. Shi, M. M. Parish, and J. Levinsen, *Phys. Rev. A* **96**, 032701 (2017).
[4] D. Raventós, T. Graß, M. Lewenstein, and B. Juliá- Díaz, *Journal of Physics B: Atomic, Molecular and Optical Physics* **50**, 113001 (2017).
[5] T. Busch, B.-G. Englert, K. Rzażewski, and M. Wilkens,*Foundations of Physics* **28**, 549 (1998).
[6] A. Rojo-Francàs, F. Isaule, B. Juliá-Díaz arXiv:2202.12749

Acknowledgements: We thank Prof. Joan Martorell for his support in all aspects reported in this work. We also thank Emma Laird for sending us her results for SU(N) fermions from Ref. [3].

Magnetically-pumped High Harmonic Generation with circularly polarized driving fields

Rodrigo Martín-Hernández*, Luis Plaja, Carlos Hernández-García

[1]*Grupo de Investigación en Aplicaciones del Láser y Fotónica, Departamento de Física Aplicada, Universidad de Salamanca, E-37008, Salamanca, Spain.*

*e-mail: rodrigomh@usal.es

High Harmonic Generation (HHG) is well-stablished as a standard tool to obtain coherent high-frequency light emission and attosecond pulses [1]. In the most common scheme, a linear-polarized electric field interacts with an atomic gas jet generating a fast-oscillating dipole. The process results in the emission of high-order harmonics whose spectrum is characterized by a broad plateau that extends towards a cut-off frequency. On the other side, the simultaneous development of ultrafast structured light beams is opening new scenarios to control strong light-matter interactions. In particular, it has been recently proposed that isolated Tesla-scale femtosecond magnetic fields can arise from azimuthally polarized vector beams [2], enabling alternative perspectives in ultrafast magnetism, spintronics [3], and, why not, in ultrafast, nonlinear, and quantum optics.

In this work, we pioneer a new mechanism in HHG through the use of a circularly polarized electric field simultaneously pumped by a strong, isolated linearly polarized magnetic field. We numerically solve the three-dimensional time-dependent Schrödinger equation in the hydrogen atom. While in the standard HHG scheme the efficient generation of high order harmonics is not feasible with circularly polarized drivers [4], we show that the combined use of intense linearly polarized PHz oscillating magnetic fields not only allows the generation of high-order harmonics, but extends the cut-off frequency by hundreds of harmonic orders (Fig. 1 a). Remarkably, the attosecond pulse associated with the extended spectrum exhibits elliptical polarization with a temporal width of ~80 attoseconds (Fig. 1 b). In this proposal, linearly polarized isolated magnetic fields over 10^4 T are considered, which can be obtained from the use of a stationary wave generated by two counter-propagating laser beams (Fig. 1 c) with intensities around 10^{18} W/cm^2. Such laser beams are easily achieved nowadays in petawatt laser facilities. The stationary wave generates a slab grating in the gas target where the HHG process takes place, therefore diffracting at different angles the generated harmonics. Our work introduces novel HHG schemes aided by petawatt lasers, allowing exotic configurations and the generation of extremely broad high harmonic spectra towards the X-rays.

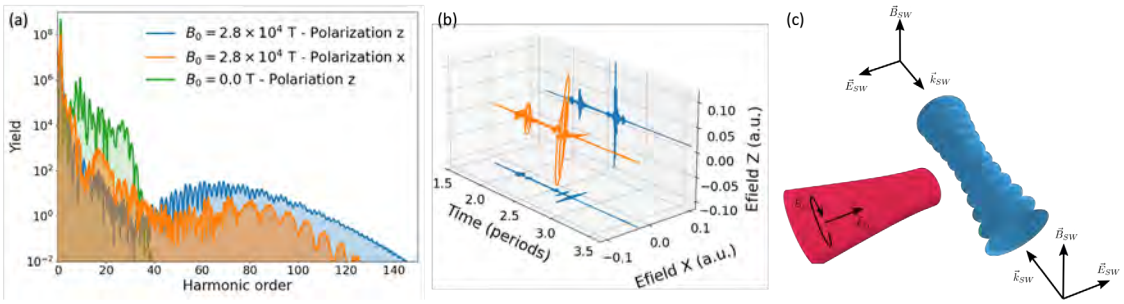

Figure1. (a) HHG spectrum for the standard scheme (linearly polarized driving beam along the z direction) in green, compared with the generated spectrum using the circularly polarized driving beam (in the x-z plane, four-period 800 nm pulse with a peak intensity of $1.6 10^{14}$ W/cm^2) simultaneously pumped with a 800 nm linearly polarized magnetic field of $2.8 10^4$ T (blue and orange stand for the z and x components. (b) Attosecond pulse obtained after filtering the HHG spectrum in (a) above the 60th harmonic order. (c) Scheme of the stationary wave configuration, where the circularly polarized Gaussian driving beam ($\vec{E}_D$) simultaneously pumps HHG with the slabs of magnetic field (blue) arising from the vertically polarized stationary wave ($\vec{B}_{SW}$).

[1] Jeffrey L. Krause, Kenneth J. Schafer, and Kenneth C. Kulander, *Phys. Rev. Lett.*, **68**, 3535 (1992).
[2] M. Blanco, F. Cambronero, M. Teresa Flores-Arias, et al., *ACS Photonics*, **6,** 38 (2019).
[3] Jakob Walowski and Markus Münzenberg; *Journal of Applied Physics*, **120**, 140901 (2016).
[4] K. S. Budil, P. Salières, Anne L'Huillier, T. Ditmire, and M. D. Perry, *Phys. Rev. Lett.*, **48**, 3437 (1993).

Acknowledgements: European Research Council (851201); Ministerio de Ciencia de Innovación y Universidades (PID2019-106910GB-I00, RYC-2017-22745); Junta de Castilla y León FEDER (SA287P18).

Light-matter interaction from density functional theory with application to attosecond electron dynamics

M. Malakhov[1], A. Picón[1], G. Cistaro[1], **J. J. Esteve-Paredes**[2,*], A.J. Uría-Alvarez [2], J.J. Palacios[2,3]

[1] *Departamento de Química, Universidad Autónoma de Madrid, E-28049 Madrid, Spain.*
[2] *Departamento de Física de la Materia Condensada, Universidad Autónoma de Madrid, E-28049 Madrid, Spain.*
[3] *Instituto Nicolás Cabrera (INC) and Condensed Matter Physics Center (IFIMAC), Universidad Autónoma de Madrid, E-28049 Madrid, Spain.*

*e-mail: juan.esteve@uam.es

We present a methodology to address light-matter interaction with focus on attosecond electron dynamics in 2D materials starting from density functional theory calculations. We combine an accurate DFT-based evaluation of optical matrix elements and Berry connections with the time-resolved Schrödinger equation including several laser pulses, both at the infrared and the x-ray regimes. In the end, carrier dynamics and light absorption can be obtained and readily compared with available experiments without the aid of any phenomenological parameters. Our methodology is particularly suited for DFT calculations based on Gaussian basis sets as those used in codes such as GAUSSIAN or CRYSTAL as a post-selfconsistent procedure. The use of Gaussian basis sets saves computational effort, as all coordinate space integrations become analytical. Our procedure also entails a proper quantification of several approximations for optical matrix elements widely used in the literature and its effect in reproducing experimental curves.

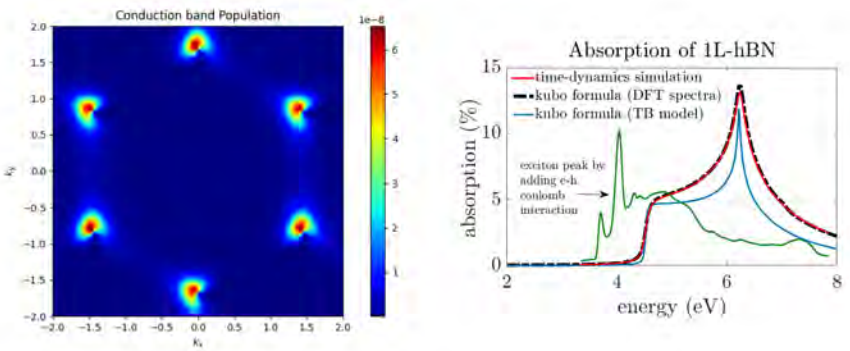

Figure 2. Simulations in monolayer hBN. (Left) Excitation of carriers resolved in reciprocal space. (Right) Light absorption from simulations compared with linear response theory.

[1] G. Cistaro *et al.*, *Phys. Rev. Research* **3**, 013144 (2021).
[2] J.J Esteve *et al.*, arXiv:2201.12290 (2022, submitted).

Multi-vortex high-harmonic beams from graphene's anisotropy

Ana García-Cabrera*, Roberto Boyero-García, Óscar Zurrón Cifuentes, Julio San Román, Carlos Hernández-García, Luis Plaja

Departamento de Física Aplicada, Universidad de Salamanca, Plaza de la Merced s/n, E-37008, Salamanca, Spain.

*e-mail: anagarciacabrera@usal.es

High-order harmonic generation (HHG) is a unique tool to produce ultrafast structured laser beams in the extreme ultraviolet (EUV) spectral regime. The deep understanding of this process in gaseous media has triggered the emergence of a wide variety of interaction schemes to control the spatiotemporal properties of the emitted beams, resulting from both spin and orbital angular momentum conservation (SAM and OAM, respectively) [1]. By contrast, HHG in solids has begun to attract the interest of the community more recently. Crystals offer rich scenarios in HHG, where the coupling of the electromagnetic field with the target's structure introduces new phenomena, such as the matter-Talbot effect [2], or the recently observed anisotropic HHG from single-layer graphene [3].

Here, we study HHG in single-layer graphene driven by a mid-infrared vector beam (VB) at normal incidence (see Fig. 1, left panel). The exploration of the coupling of graphene's symmetries with the SAM and OAM of the driving beam requires a macroscopic picture of the interaction. In unstructured media, like gases, HHG preserves the geometry of a cylindrical VB driver [4], which is composed by two OAM modes, $l = \pm 1$. In such case, the simultaneous conservation of SAM and parity leads to the photon composition rules for the qth-order harmonic: $q = n_1 + n_2$ odd and $|n_2 - n_1| = 1$, where $n_1$and n_2 are the number of photons of the two modes. Hence, the OAM of the harmonic beam is restricted to $l = \pm 1$, constituting the cylindrical harmonic VB. In contrast, our theoretical simulations show that graphene's anisotropy [5] imprints two distinct properties into the generated harmonics: (1) a spin-dependent angular diffraction pattern and, (2) high OAM components. Strikingly, the fundamental symmetry associated with the simultaneous spin-orbit conservation forces the splitting of the harmonic beam into a set of EUV vortices with $|l| = 1$ and well-defined helicity. The right panel of Fig. 1 shows the intensity and phase distributions of the multi-vortex formation for the 9th harmonic, for the left circular (a and b) and right circular (c and d) components. Our study highlights the non-trivial interplay between the structural symmetries of the target and the driving beam in HHG, as well as its understanding in terms of both spin-dependent diffraction and the fundamental law of simultaneous conservation of SAM and parity. This opens exciting new routes for the generation of spatially complex EUV structured beams and for a deeper understanding of the ultrafast electron dynamics in solid systems.

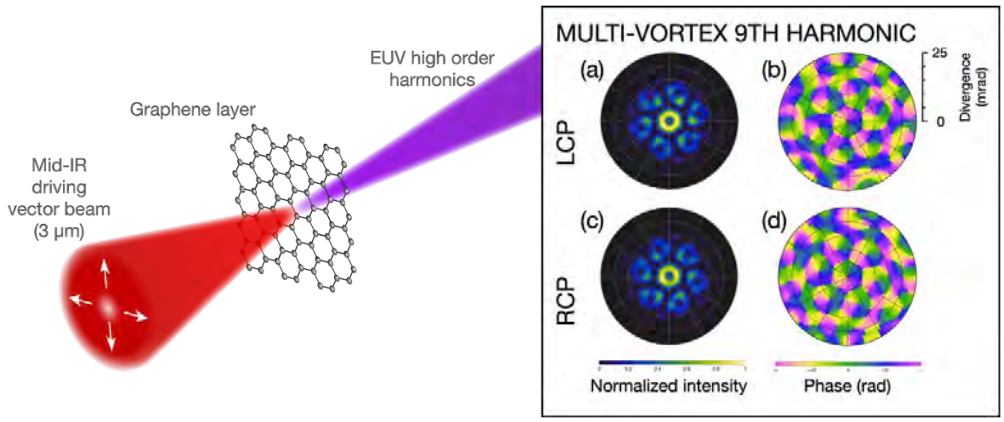

Figure 1. Multi-vortex high-order harmonics in single-layer graphene from a mid-infrared vector beam. The right panel shows the intensity and phase distribution of the 9th harmonic (33 nm).

[1] K. Dorney et al., *Nat. Photonics*, **13**, 123 (2019).
[2] A. García-Cabrera, C. Hernández-García, L. Plaja, *New J. Phys.* **23**, 093011 (2021).
[3] N. Yoshikawa, T. Tamaya, K. Tanaka, *Science* **356**, 736 (2017).
[4] C. Hernández-García et al., I. J. Sola, *Optica* **4**, 520 (2017).
[5] Ó. Zurrón-Cifuentes et al., *Opt. Express* **27**, 7776 (2019).

The shortest focused X-Waves with Orbital Angular Momentum

Raúl García-Álvarez*, Miguel A. Porras

Grupo de Sistemas Complejos, ETSIME, Universidad Politécnica de Madrid, Ríos Rosas 21, 28003 Madrid, España

*e-mail: raul.galvarez@upm.es

In recent years there has been growing interest in ultrashort light pulses with orbital angular momentum (OAM). The first pulses developed with OAM were of Laguerre-Gauss (LG) type. However, these pulsed beams experience diffraction, by which their focus is limited. Therefore, we investigate diffraction-free and dispersion-free wavepackets, the so-called focused X-waves (FX-waves), which also can have OAM. The use of diffraction-free ultrashort pulsed beams would allow for a longer interaction with matter, or long-range transmission of information through OAM channels. In contrast to the more familiar X-waves, FX-waves have recently been synthesized [1] under paraxial and quasi-monochromatic conditions (hundreds of femtoseconds). The future goal would be to shrink these pulses to a few femtoseconds and a nonparaxial, ideally infinitely long focus on the wavelength scale for ultrafast and high-resolution applications.

Here we show the existence of a lower bound to the number of optical cycles for FX-waves carrying OAM similar to that found for X-waves and LG pulses [2,3]. To study the shortest FX-waves with OAM, we have used an ultra-wide spectrum $f(\omega) = e^{-\epsilon\omega}$, with $\epsilon \ll 1$. Given a topological charge m of the vortex carried by the FX-wave, the number of oscillations of the electric field is always larger than $|m|/2$.

The spatiotemporal structure of FX-waves is rather complex. As seen in Fig. 1(a), the different frequencies in the ultra-wide spectrum are spatially distributed at different radii, with the redder frequencies at larger radii, and the whole FX-wave is increasingly blue shifted with m. As a result, the frequency ω_f at the the most intense ring surrounding the vortex, of radius r_M [vertical lines in Fig. 1(a)] is independent of m.

FX-waves containing frequencies from 0 to ∞ are not completely realistic. Therefore, we have studied the effect of truncating the spectrum at a cut-off frequency ω_h, as in Figs. 1 (b) and (c). Since according to Fig. 1(a), higher frequencies are located at smaller radii, truncation would only modify the inner part of the FX-wave. Indeed the radial profiles of fluences, with and without truncation, are almost identical except in the vicinity of the vortex [Fig. 1(b)], and the temporal shapes at the maximum of fluence, r_M [Fig. 1(c)] are identical except for the sidelobes arising from truncation.

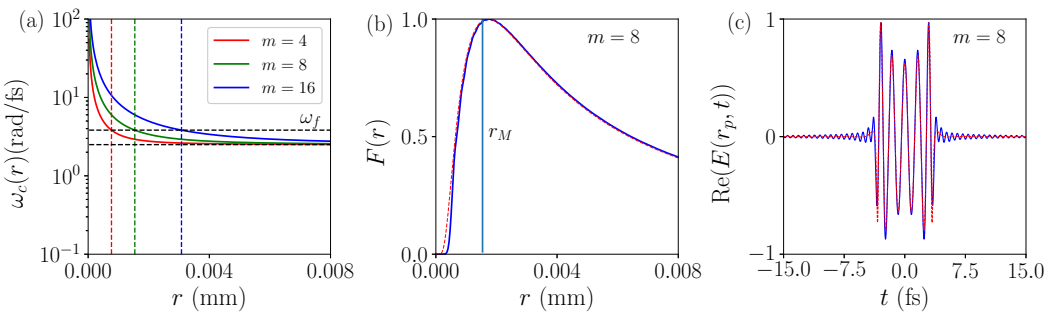

(a) Radial distribution of the central or mean frequency, $\omega_c(r)$, of a FX-wave with superluminal group velocity $v_g = 0.0004$ mm/fs, $\epsilon = 0.2$ fs and $m = 4, 8$, and 16. The vertical lines represent the radii of the most intense ring around the vortex. (b) Radial profile of energy density of a FX-wave with $|m| = 8$ (red dashed line) and with the ultra-wide spectrum upper limited by $\omega_h = 0.7$ rad/fs (solid line). (c) Real electric field at $r = r_M$ of the untruncated and truncated FX-waves in Fig. 1(b). All fields are normalized to their peak values.

[1] Murat Yessenov, Layton A. Hall, et al., arXiv:2201.08297 (2022).
[2] M. A. Porras, *Phys. Rev. Lett.* **122**, 123904 (2019).
[3] M. A. Porras and R. García-Álvarez, *Phys. Rev. A* **105**, 013509 (2022).

Extreme-ultraviolet scalar and vectorial vortices with very high topological charge

Alba de las Heras[1,*], Alok Kumar Pandey[2], Julio San Román[1], Javier Serrano[1], Luis Plaja[1], Sophie Kazamias[2], Olivier Guilbaud[2], and Carlos Hernández-García[1]

[1]*Grupo de Investigación en Aplicaciones del Láser y Fotónica, Departamento de Física Aplicada, Universidad de Salamanca, Pl. La Merced s/n, Salamanca E-37008, Spain.* [2]*Laboratoire Irène Joliot-Curie, Université Paris-Saclay, UMR CNRS, Rue Ampère, Bâtiment 200, Orsay Cedex F-91898, France.*

*e-mail: albadelasheras@usal.es

Scalar and vectorial vortices are two paradigmatic beam structures carrying orbital angular momentum. On the one hand, a scalar vortex presents a twisted wavefront and homogenous polarization. On the other hand, a vectorial vortex combines a twisted phase and a spatially varying polarization. The topological charge in both scalar and vectorial vortices is the parameter characterizing the number of wavefront twists in one wavelength.

We demonstrate the up-conversion of scalar and vectorial vortices from the infrared (IR) to the extreme-ultraviolet (XUV) regime, by means of the conservation laws in high harmonic generation (HHG). For a scalar vortex, the topological charge in HHG scales linearly with the harmonic order i.e., $\ell_q = q\ell_1$ [1,2]. The analogous conservation law applies for a vector-vortex in terms of the Pancharatnam charge, ie. $\ell_{P,q} = q\ell_{P,1}$ [3]. In Fig. 1, we show the characterization of the 25th harmonic beam resulting from a vortex driver of $\ell_1 = 4$ (left) or from a vector-vortex driver of $\ell_{P,1} = 2$ (right). The experimental XUV beam (top row) is characterized using wavefront sensing metrology, which enables a full measurement of intensity and phase [2]. The theoretical beam (bottom row) is computed in the full quantum strong-field approximation and considers propagation effects in the transverse plane [2,3]. Our results demonstrate the up-conversion of scalar and vectorial phase singularities leading to very high topological charges in the XUV, up to $\ell_{25} = 100$. Such structured XUV beams may encourage advances in high-resolution imaging, attochemistry, or the fundamentals of intense laser-matter interactions.

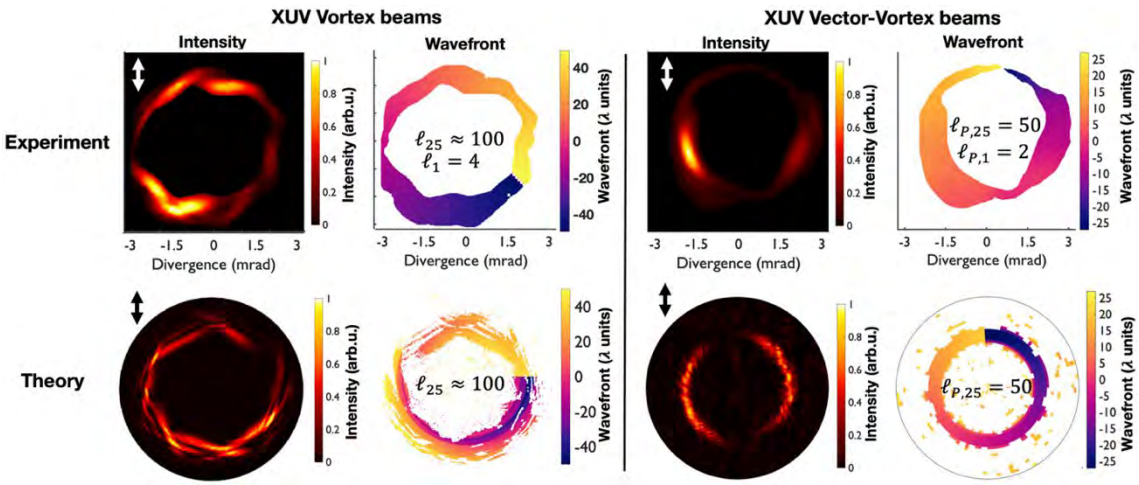

Figure 1. Characterization of XUV vortex and vector-vortex beams. We show the experimental (top row) and theoretical (bottom row) intensity of the vertical polarization projection and wavefront of the 25th harmonic beam. In the left panel, the HHG driver is a vortex of $\ell_1 = 4$, whereas in the right panel the driver is a vectorial vortex of $\ell_{P,1} = 2$.

[1] C. Hernández-García, A. Picón, J. San Román, and L. Plaja, *Phys. Rev. Lett.* **111**, 083602 (2013).
[2] A. K. Pandey, A. de las Heras, T. Larrieu, J. San Román, J. Serrano, L. Plaja, E. Baynard, M. Pittman, G. Dovillaire, S. Kazamias, C. Hernández-García, and O. Guilbaud, *ACS Photonics* **9**, 944 (2022).
[3] A. de las Heras, A. K. Pandey, J. San Román, J. Serrano, E. Baynard, G. Dovillaire, M. Pittman, C. G. Durfee, L. Plaja, S. Kazamias, O. Guilbaud, and C. Hernández-García, *Optica* **9**, 71 (2022).

Acknowledgements: European Research Council (ATTOSTRUCTURA - 851201).

Prohibited optical trapping regimens unlocked by focused OAM beams

I. Gomez-Viloria[1,*], Á. Nodar[1], M. Molezuelas-Ferreras[1], J. J. M. Varga[1], G. Molina-Terriza[1,2,3]

[1]*Centro de Física de Materiales, Paseo Manuel de Lardizabal 5, 20018 Donostia-San Sebastian, Spain.*
[2]*Donostia International Physics Center, Paseo de Manuel Lardizabal 4, 20018 Donostia-San Sebastián, Spain.*
[3]*IKERBASQUE, Basque Foundation for Science, Maria Diaz de Haro 3, 48013 Bilbao, Spain.*

*e-mail: iker_gomez@hotmail.com

In this work, we present a novel optical trapping method which extends the known trapping regime provided by common focused Gaussian beams, making use of Laguerre-Gaussian (LG) beams with orbital angular momentum (OAM). This new possibility of trapping was discovered thanks to an efficient and general optical forces calculation procedure, formed by a fully analytical formula [1] in terms of well-defined helicity multipoles [2] and which enables displaced laser beams calculations [3,4]. The fields interacting with the sphere were derived by the application of Generalized Lorentz-Mie theory, which gives an analytical description of our system and extends the validity of the calculated expressions to particles of any size. Apart from that, the chosen decomposition provides us some computational tools for increasing the efficiency of the calculated simulations, which at the end of the day, has been crucial in the discovering of the mentioned behaviour. The most remarkable computational technique is the use of "master displacement matrices", which basically multiply chains of these pre-calculated matrices in order to represent any arbitrary displacement of the incident field.

One of our proposals was obtained by the calculation of the stability maps for the Z axis (beam propagation direction) shown in figures 1 and 2. Here is possible to recognize the new zones in the trapping regime unlocked by the use of LG beams with OAM. The totality of the results was fulfilled with stability maps for the X/Y axes, which just confirmed the desired trapping regime.

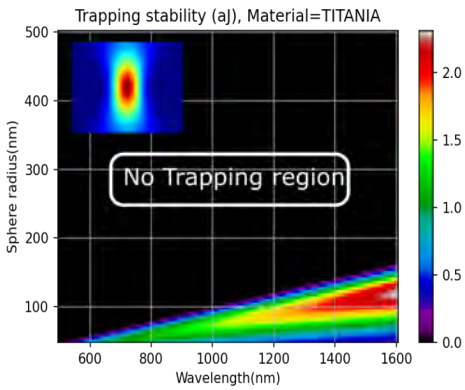

Figure 1. Trapping stability measured as the trapping potential height (aJ). The map has been created for a water suspended Titania (TiO_2) sphere, trapped by Gaussian beam focused with an objective lens of NA=1.20.

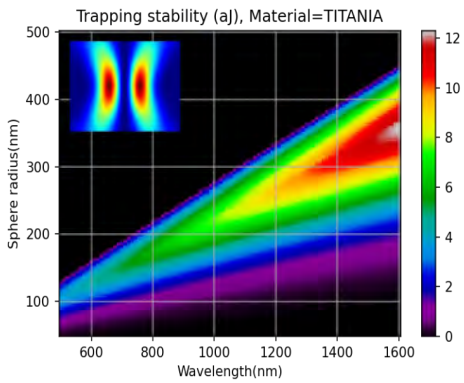

Figure 2. Trapping stability measured as the trapping potential height (aJ). The map has been created for a water suspended Titania (TiO_2) sphere, trapped by LG OAM beam focused with an objective lens of NA=1.20.

On the other hand, due to the well-defined helicity multipole decomposition, our formula naturally distinguish which force terms corresponds to each helicity contained in the incident light beam. In addition, although for the case with spherical particles the calculations are the simplest, it also enables to implement particles with different shapes. This study gives a very useful tool for exploring the relation between optical forces and the angular momentum of light.

[1] A. A. Ranha-Neves and C. Lenz-Cesar, *J. Opt. Soc. Am.* B **36**, 1525 (2019).
[2] M. E. Rose, *Multipole Fields*, Wiley, New York (1955).
[3] X. Zambrana-Puyalto, D. D'Ambrosio, G. Gagliardi, *Laser & Photonics Reviews* **15**, 2000528 (2021).
[4] W.-K. Tung, *Group Theory in Physics*, World Scientific, Singapore (1985).

Novel Methods for the Characterization of Forward Brillouin Scattering in Optical Fibers and its Applications

L. A. Sánchez[1,*], A. Díez[1,2], J. L. Cruz[1,2], M. V. Andrés[1,2]

[1]*Laboratory of Fiber Optics, ICMUV, Universidad de Valencia, Dr. Moliner 50, 46100, Burjassot, Spain.*
[2]*Dpto. de Física Aplicada y Electromagnetismo, Universidad de Valencia, Dr. Moliner 50, 46100, Burjassot, Spain.*

*e-mail: luis.sanchez@uv.es

Forward scattering of light by transverse acoustic waves in an optical fiber is an optomechanical phenomenon known as forward Brillouin scattering (FBS). This phenomenon generates frequency shifts in the scattered wave from 30 MHz to 1 GHz in conventional optical fibers. The transverse acoustic mode resonances (TAMRs) behind this phenomenon are the radial $R_{0,m}$ modes and the torsional-radial $TR_{2,m}$ modes, and they can be easily excited in an optical fiber by electrostriction using an optical pump wave [1]. Lately, there has been a growing interest in the development of applications based on FBS such as fiber sensing and also in the use of FBS for fiber characterization.

The detection of the modulation induced by TAMRs in optical fibers is not simple and usually requires hundreds of meters of fiber and using interferometric techniques. Recently, we reported a novel detection technique based on a long-period fiber grating (LPG). The LPG acts as the transducer for the effective index modulation generated by the acoustic wave, converting it into variations in optical transmittance of a probe signal. The LPG allows the detection of the TAMRs with just a few cm of fiber, which reduces the linewidth broadening of the TAMRs due to structural inhomogeneities, obtaining quality factors of up to 5×10^3.

The sensitivity of TAMRs resonance frequency to physical magnitudes as temperature and strain, in conjunction with the LPG interrogation method, allow the development of point sensing schemes based on FBS. In particular, we have demonstrated the combined use of $R_{0,m}$ modes and a subgroup of $TR_{2,m}$ to simultaneously and discriminately measure temperature and strain, thanks to the different response of those acoustic modes to these magnitudes (Figure 1(a)). The accuracies obtained were ± 0.2 °C in the case of temperature and ± 25 με for the strain [2]. The different properties of radial and torsional-radial modes can also be used to characterize the elastic properties of the optical fiber, such as Poisson's ratio. $R_{0,m}$ mode frequencies depend on the longitudinal acoustic velocity of silica, while $TR_{2,m}$ modes depend on the shear acoustic velocity. From an asymptotic fit of the experimental measurements of both types of modes, the ratio between both velocities can be obtained, from which the Poisson's ratio can be calculated [3]. In our experiment we obtained Poisson's ratio of the optical fiber in a temperature range of 100 ºC with a relative error lower than 1 ‰ (Figure 1(b)).

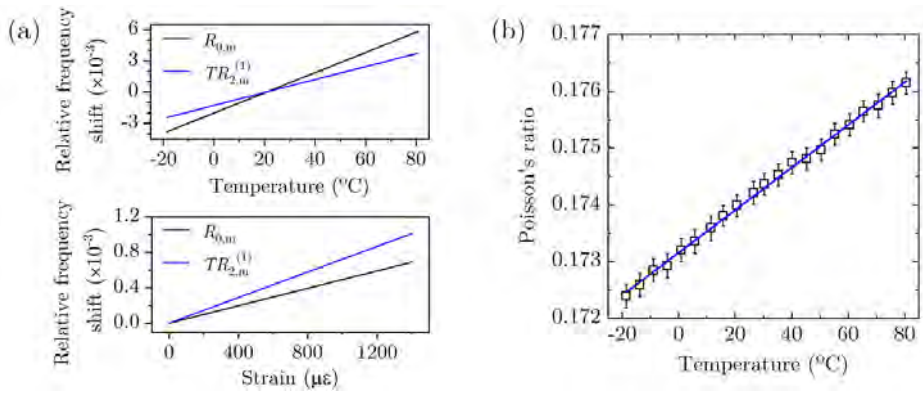

Figure 1. (a) Temperature and strain dependence of $R_{0,m}$ modes and $TR_{2,m}$ modes in an optical fiber. (b). Poisson's ratio of the optical fiber at different temperatures.

[1] A. S. Biryukov, M. E. Sukharev, and E. M. Dianov, *Quantum Electronics* **32**, 765 (2002).
[2] L. A. Sánchez, A. Díez, J. L. Cruz, and M. V. Andrés, *Optics Express* **30**, 14384 (2022).
[3] L. A. Sánchez, A. Díez, J. L. Cruz, and M. V. Andrés, *Optics Express* **30**, 42 (2022).

Acknowledgements: This work was supported by European Regional Development Fund (PDI2019-104276RB-I00); European Commission (H2020-MSCARISE-2019-872049); Generalitat Valenciana (IDIFEDER/2020/064, PROMETEO/2019/048); Ministerio de Ciencia, Innovación y Universidades (PDI2019-104276RB-I00).

Collinear optical vortices with tailored topological charge generated by angular momentum transfer

Ignacio Lopez-Quintas[1,*], Warein Holgado[1], Rokas Drevinskas[2], Peter G. Kazansky[2], Íñigo J. Sola[1], Benjamín Alonso[1]

[1]*Grupo de Aplicaciones del Láser y Fotónica (ALF). Deparatmento de Física Aplicada, Universidad de Salamanca, Spain.*
[2]*Optoelectronics Research Centre, University of Southampton, United Kingdom.*

*e-mail: ilopezquintas@usal.es

Special light beams exhibiting a structured field and carrying orbital angular momentum (OAM) appear as interesting tools in different fields such as particle manipulation, telecommunications or in several areas of light-matter interaction, including materials processing and nonlinear optics, among others. The coupling of spatially varying linear polarization fields (*i.e.*, radial or azimuthal) with spin and orbital angular momenta can be exploited to obtain optical vortices exhibiting different topological charges [1]. We propose a versatile in-line method suitable to obtain collinear optical vortices from focused or collimated beams, being continuous wave or pulsed. We consider a radial input mode of the form $R_m^{l_0}$ where l_0 and m denote the corresponding OAM and polarization azimuthal index respectively (m defined as the number of times that the orientation of the local linear polarization distribution is rotating 2π radians for a variation of 2π radians in the azimuthal coordinate) and demonstrate theoretically that there is a different OAM transfer to the final vortices depending on the m value of the input beam. Numerical simulations of the output vortices agree with the theoretical predictions, which are further confirmed by experimental measurements (see Fig. 1).

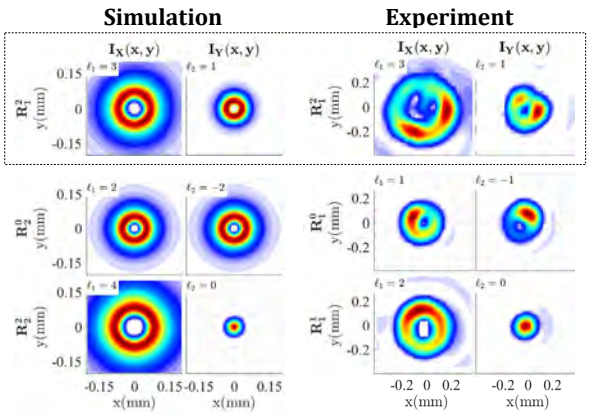

Figure 1. Representation of the x and y components of the spatial intensity profiles in focused beams for several simulated and experimental vortices [1]. For the R_1^2 case (top panels) a direct comparison between the simulated and experimental results can be made, illustrating the good agreement.

For the experiments, we used femtosecond laser pulses and combinations of special structured waveplates (s-waveplates) with standard retarders to generate radial modes with different additional OAMs that were used as input to produce the final optical vortices. Characterization of the obtained vortices was performed by a combination of the STARFISH technique and in-line interferometry [2-4]. Due to the perpendicular linear polarization of the obtained vortices, these can be separated and individually manipulated in potential applications. Thanks to its simplicity, the proposed method has been successfully applied for the generation of time varying optical vortices characterized by a novel technique [5].

[1] I. Lopez-Quintas, W. Holgado, R. Drevinskas, P. G. Kazansky, I. J. Sola, B. Alonso, *Journal of Optics* **22**, 095402 (2020).
[2] B. Alonso, I. J. Sola, O. Varela, J. Hernandez-Toro, C. Mendez, J. San Roman, A. Zaïr, L. Roso, *Journal of the Optical Society of America* **27**, 933 (2010).
[3] B. Alonso, I. J. Sola, *IEEE Journal of Selected Topics in Quantum Electronics* **25**, 8900307 (2019).
[4] B. Alonso, I. Lopez-Quintas, W. Holgado, R. Drevinskas, P. G. Kazansky, C. Hernández-García, I. J. Sola, *Communication Physics* **3**, 151 (2020).
[5] M. López-Ripa, Í. J. Sola, B. Alonso, *Photonics Research* **10**, 922 (2022).

Light polarisation under evanescent coupling in exciton-polariton couplers

Juan Lizarraga[1,*], A. Yulin[2], J. Beierlein[3], S. Klembt[3], S. Höfling[3], C. Antón-Solanas[1], M. D. Martín[1], L. Viña[1,4]

[1]*Dept. Física de Materiales & Inst. N. Cabrera, Univ. Autónoma, Madrid 28049, Spain.* [2]*Faculty of Physics and Engineering ITMO University St. Petersburg 197101, Russia.* [3]*Technische Physik, Universität Würzburg, Am Hubland, D-97074 Würzburg, Germany.* [4]*Instituto de Física de la Materia Condensada, Universidad Autónoma, Madrid 28049, Spain*

*e-mail: juan.lizarraga@estudiante.uam.es

Exciton polaritons are solid-state quasi-particles resulting from the strong interaction of light and matter. They constitute a quantum fluid possessing properties that bridge the best characteristics of light (low effective mass, extended spatial and temporal coherence) and matter (Coulomb interactions, magnetic response). A lateral patterning in semiconductor microcavities (via controlled dry etching) allows to arrange polaritons in versatile geometries, providing fundamental and application-oriented results, from topological simulators [1], to one-dimensional waveguides with a large list of functionalities [2].

Pushing forward our research on waveguided polaritons, our recent studies have focused on a polariton device consisting of two coupled one-dimensional waveguides (see sample image in Fig. 1a), where polaritons, injected in one of the input terminals (Fig. 1a-[I]), display Josephson-like oscillations between the two coupled waveguides (Fig. 1a-[II]) [3]. The resulting polariton splitting ratio in the output terminals (Fig. 1a-[III]) can be controlled via different parameters (e.g. laser pump power, and length of coupling region), and interestingly, our results show that the polariton population in each output waveguide is polarisation dependent and display polarisation beatings [4].

In this work, we study the degree of linear polarisation (DLP) and its propagation characteristics at the output terminals, after experiencing Josephson-like interactions through a long (50 μm) coupling region (see Fig. 1b where the DLP is evaluated in the vertical (*V*) and horizontal (*H*) polarisation basis). The DLP map shows orthogonally polarised polaritons in the up/down output terminals (blue/red color, respectively). We extend our analysis to quantitatively compare the polariton populations in the up/down output terminals as a function of the linear polarisation orientation of the polariton emission, see Fig. 1c. We find that the polariton populations in both terminals reach their maxima around the diagonal polarisations (*D*= diagonal, *A* = antidiagonal), since these constitute the polarisation eigenstates for polariton propagation. Furthermore, we also observe a small phase difference between these maxima and the exact D/A azimuths, which is probably related to certain experimental parameters such as Josephson-like coupling strength, pumping power or length of the coupling region.

This polariton coupler constitutes a fundamental example of an all-optical solid-state device that controllably splits information (propagating polariton condensates) encoded in the polarisation degree of freedom. Further experiments under resonant excitation would allow to increase the degree of polariton coherence and, probably, harness more functionalities in such a device via interference.

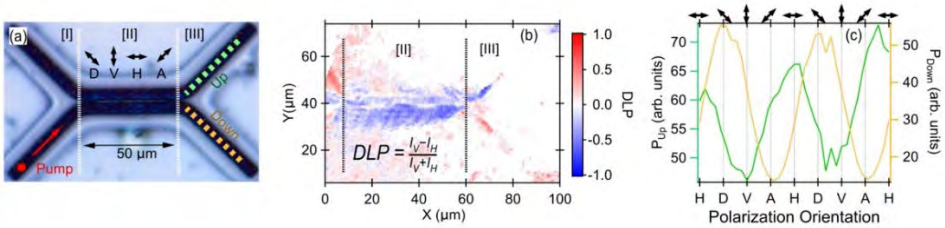

Figure 1. (a) Optical microscope image of a polariton coupler: [I] input terminals, (red circle indicates the pump laser), [II] coupling region, [III] output terminals (green/orange dotted lines: regions where the polariton populations are studied). Linear polarisations are labelled as A (anti-diagonal), V (vertical), H (horizontal) and D (diagonal). (b) Real space map of the DLP in the regions [II, III]. (c) Polariton populations in the up (green) and down (orange) output terminals as a function of the linear polarisation orientation. $P_{up/down}$ are obtained integrating the emission intensities in panel (a).

[1] P. St-Jean *et al.*, *Nature Photon* **11**, 651 (2017).
[2] M. Klaas *et al.*, *Appl. Phys. Lett.* **114**, 061102 (2019).
[3] J. Beierlein *et al.*, *Phys. Rev. Lett.* **126**, 075302 (2021).
[4] E. Rozas *et al.*, *ACS Photonics* **8**, 2489 (2021).

High-performance simulations of high-order harmonic generation based on artificial intelligence

Javier Serrano*, Carlos Hernández-García

Grupo de Investigación en Aplicaciones del Láser y Fotónica, Departamento de Física Aplicada, Universidad de Salamanca, Pl. La Merced s/n, Salamanca E-37008, Spain.

*e-mail: fjaviersr@usal.es

Artificial intelligence is an emerging field that is being successfully used in a broad set of fields and applications, including physics. Thanks to the growing computing power provided by modern GPUs —and software libraries that allows to easily use these technologies—, artificial intelligence (and particularly deep learning) is becoming a powerful tool in ultrafast and nonlinear optics. For example, machine learning algorithms can predict the X-ray pulse properties of free electron lasers [1].

One of the fields in which artificial intelligence may provide powerful computing capabilities is in the simulation of high-order harmonic generation (HHG). HHG is a nonperturbative process in which high-order harmonics— extending up to the X-rays— result from the highly nonlinear interaction of an intense, infrared femtosecond laser pulse, with an atomic, molecular or solid target. The exact simulation of HHG requires a detailed evolution of the electronic wavepacket dynamics in the vicinity of each atom or molecule of the target, which is obtained through the resolution of the time-dependent Schrödinger equation (TDSE). Solving TDSE for single-atom HHG simulations using modern hardware is quite time consuming. However, a simulation that can be compared to experiments requires its macroscopic description, i.e. to account for the harmonic emission in all the atoms in the target. Thus, the macroscopic simulation would require to solve the TDSE 10^3 to 10^6 times, which makes the macroscopic simulation prohibitive. Our group has expertise in the development of microscopic and macroscopic approaches to simulate HHG in the most stringent situations [2, and citations therein]. Interestingly, it has been recently proposed to use deep neural networks to speed-up the microscopic TDSE calculation in HHG [3].

In this work we propose to apply artificial intelligence to macroscopic simulations of HHG. We create and train a neural network to infer single-atom HHG calculated through the TDSE (see Fig. 1), so macroscopic calculations can take advantage of this trained network to obtain experimentally comparable results of TDSE. This improvement will allow us not only to accelerate the macroscopic simulations of HHG, but to obtain for the first time TDSE-based macroscopic simulations of HHG, without the need of resorting to approximations like the Strong Field Approximation. As a consequence, studies of the macroscopic signature of effects that are not well reproduced in such approximations, like electronic correlations or the properties of low-order, perturbative harmonics, can be theoretically studied. In addition, we belive that artificial intelligence can set the path towards in-situ simulations that can guide future HHG experiments.

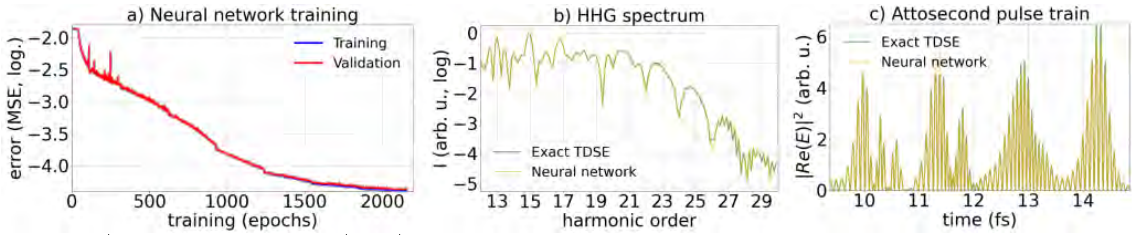

Figure 1. a) Evolution of the error (MSE) of the neural network during training with the TDSE. Sample single-atom results in the frequency (b) and time (c) domain using TDSE (green) and the neural network (orange).

[1] Sanchez-Gonzalez, A., Micaelli, P., et al. Accurate prediction of X-ray pulse properties from a free-electron laser using machine learning. *Nat Commun* **8**, 15461 (2017)

[2] Hernández-García, C., A. Pérez-Hernández, J., et al. High order harmonic propagation in gases within the Discrete Dipole Approximation, *Physical Review A* **82**, 033432 (2010)

[3] Lytova, M., Spanner, M. et al. Deep learning and high harmonic generation, *arXiv:2012.10328v2* (2021)

Acknowledgements: This work has been funded by the ERC Starting Grant ATTOSTRUCTURA, grant agreement No. 851201; Ministerio de Ciencia de Innovación y Universidades (PID2019-106910GB-I00, RYC-2017-22745); Junta de Castilla y León FEDER (SA287P18).

Efficient computation of azimuthal perturbation eigenpairs of vortex solitons

José R. Salgueiro*, Ángel Paredes, Humberto Michinel
Universidade de Vigo, E.E. Aeronáutica e do Espazo, Ourense 32004.
*e-mail: jrs@uvigo.es

Calculation of the perturbation eigenstates of non linear systems with angular momentum, i.e. those supporting vortex solitons, has proved to be problematic in the past. Although the eigenvalue problem is well defined and actually has been already solved for some different systems, its solution often requires from a big computational effort and long computation times, obtaining even sometimes erroneous results if the problem is not managed with care. Here we present a systematic method to get fast solutions which allow to know about the stability of the different stationary states of this kind of systems. We apply it to a system described by the cubic-quintic nonlinear Schrödinger equation for the sake of comparison, but it is applicable to other systems of the like.

The z-direction propagating vortex-like stationary states of such media come described by a function $\Psi(r,\phi,z) = \psi(r)\exp(il\phi)\exp(i\beta z)$, where $l = 1, 2, \ldots$ is the angular momentum, β is the propagation constant and $\psi(r)$ the r-dependent field envelope. This function fulfills the nonlinear Schödinger equation,

$$i\frac{\partial\Psi}{\partial z} = -\nabla^2\Psi - (|\Psi|^2 - |\Psi|^4)\Psi. \tag{1}$$

The stability of solutions can be studied by azimuthally perturbing them with small functions $F(r,z) = f(r,z)\exp[i(l+p)\phi]\exp[(\delta+i\beta)z]$ and $G(r,z) = g(r)\exp[i(l-p)\phi]\exp[(\delta^*+i\beta)z]$, where p is the order of the perturbation and δ the growth rate (real part). Replacing the perturbed state into the system equation (1) yields, after linearization, a pair of evolution equations for the perturbations F and G. These functions, together with the rate δ, were traditionally obtained by propagating these perturbed linearized equations until the perturbation fields F and G no longer change its shape and the growth rate stabilizes [1,2]. This is actually a version of the direct power method. Convergence is usually slow requiring from a long propagation distance and a long computation time, specially in cases for which the growth rate is close to zero (weak instability). In this case it is also necessary to increase the number of sampling points to get enough accuracy.

In order to improve the efficiency we chose to solve the problem changing the strategy. First, from replacement of the perturbed field into Eq. (1) it is obtained a generalized eigenvalue problem $\mathcal{A}(f|g^*)^T = (i\delta)\mathcal{B}(f|g^*)^T$, where $(i\delta)$ is the eigenvalue and matrices $\mathcal{A}$ and $\mathcal{B}$ are,

$$\mathcal{A} = \begin{pmatrix} \nabla_r^2 - \frac{(l+p)^2}{r^2} + Q & R \\ R & \nabla_r^2 - \frac{(l-p)^2}{r^2} + Q \end{pmatrix} \Bigg\| \; \mathcal{B} = \begin{pmatrix} -I & 0 \\ 0 & I \end{pmatrix}$$

being I a identity subblock matrix, $\nabla_r^2 \equiv \partial_r^2 + (1/r)\partial_r$, $Q = -\beta + (2n_2 - 3n_4\psi^2)\psi^2$ and $R = (n_2 - 2n_4\psi^2)\psi^2$. Matrix $\mathcal{A}$ is real but non-symmetric and so it may contain complex eigenvalues. Actually, those in the form of complex conjugate pairs are the interesting ones as the imaginary part accounts for the real part of δ which is the growth rate of the perturbation. Finding no complex eigenvalues is then an indication of the system stability.

The eigenvalue problem is solved using a combined method to improve efficiency. First, a direct eigenvalue solver (as for instance the QZ algorithm) is used with a coarse number of points (few hundreds of samples) in order to estimate the eigenvalues and select the interesting ones (complex conjugate pairs if any). Then, this estimation is refined to a much finer sampling using the inverse power method. Following this strategy we were able to compute solutions with 5×10^4 samples without too much effort. This technique allowed to reproduce the results for the stability of bright vortex solitons [2] as well as to determine the stability of the dark solitons supported by a cubic quintic model. The method is, however, useful for more general nonlinear systems supporting vortex solitons.

[1] Soto-Crespo, J. M., Heatley, D. R., Wright, E. M., Akhmediev, N. N., *Phys. Rev. A* **44**, 636 (1991).
[2] Michinel, H., Salgueiro, J. R., Paz-Alonso, M. J.,*Phys. Rev. E* **70**, 066605 (2004).

Acknowledgements: We thank the support of MCIN of Spain through the project PID2020-118613GB-I00, as well as Xunta de Galicia (grant ED431B 2021/22).

Cherenkov radiation in chiral matter

Manuel Eduardo Barredo Alamilla*, Luis F. Urrutia Ríos

Instituto de Ciencias Nucleares, Universidad Nacional Autónoma de México, 04510 México, CDMX, México.

*e-mail: eduardobarredo@correo.nucleares.unam.mx

In unconventional materials like anisotropic media, metamaterials, and topological insulators the Cherenkov radiation can manifest some richer properties, for instance, the reverse Cherenkov radiation and the Dyakonov-Cherenkov radiation. In chiral matter the research of Cherenkov radiation is of recent interest. Kirill Tuchin, using the Lorentz-violating CPT-odd, calculates the dispersion relation for the left- and right-handed photon polarisations and calculate the radiation gauge fields for an anisotropic dispersive medium. He computes the scattering matrix element and, with that, the spectrum of photons radiated in a solid angle, proving the existence of the Cherenkov radiation in chiral media such as Weyl semimetals, quark gluon plasma (QGP) and axionic dark matter.

We study the modifications of electromagnetic radiation within chiral media in presence of time-dependent sources in general. In order to describe the electromagnetic response of these materials we use the electrodynamics developed by Carroll, Field and Jackiw [1] based on the addition of a Lorentz-violating Chern-Simons term in the Lagrangian density in the photonic sector of the form,

$$\mathcal{L}_{LV} = \frac{1}{8\pi}\tilde{b}_\mu \tilde{F}^{\mu\nu} A_\nu, \tag{1}$$

where the violating coefficients $\tilde{b}_\mu = (b_0, \vec{b})$ correspond to precise physical terms in chiral matter, with b_0 and $\vec{b}$ are the separation of the energy and momentum space between the Weyl nodes, respectively.

We implement a Green's function approach [2], considering only the spatial components of the violating coupling constant, $b_0 = 0$, in the Chern-Simons Lagrangian. After fixation of the vector $\vec{b}$ in the z axis, we take advantage of the cylindrical symmetry to construct the Green's function in the far-field regime taking some approximations. Furthermore, we use this result to analyze the emitted radiation of a fast moving particle travelling parallel to the vector $\vec{b}$. From the spectral distribution we find out that chiral matter produces an splitting of the Cherenkov radiation with each cone corresponding to the two different phase velocities of the two polarisations of the light. In addition it allows the phenomenon of Cherenkov radiation for a chiral medium with index refraction $n = 1$.

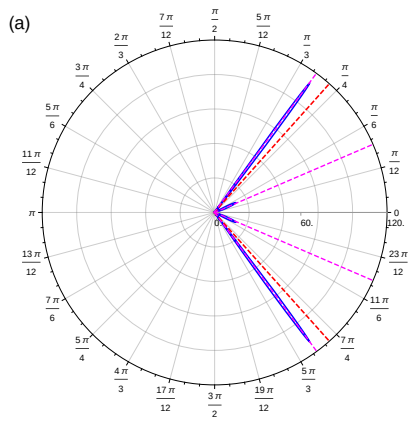

Figure 1. Angular distribution for the radiated energy per unit frequency in a chiral dielectric medium with $b/\omega = 0.5$, $n = 2$, $\omega/c = 13.96\ \mu\mathrm{m}^{-1}$ for the solid blue line.

The splitting of the Cherenkov radiation in chiral medium is a consequence of the effective birrefringence in chiral matter. Figure 1 shows the spectral distribution of energy in a chiral medium with a refraction index $n = 2$. The charge moves from left to right with a speed of 3/4 the speed of light. The red dashed line corresponds to the standard Cherenkov radiation with $\vec{b} = 0$. We conclude that the Green's function approach using suitable approximations allows us to obtain analytical forms to study modifications to electromagnetic radiation in chiral matter.

[1] S. M. Carroll, G. B. Field, and R. Jackiw, *Phys. Rev. D* **41**, 1231 (1990).
[2] A. Martín-Ruiz, M. Cambiaso, and L. F. Urrutia, *Phys. Rev. D* **92**, 125015 (2015).

Quantum liquids and droplets with low-energy interactions in one dimension

I. Morera[1], B. Juliá-Díaz[1], **M. Valiente**[2,*]

[1]*Departament de Física Quàntica i Astrofísica, Facultat de Física, Universitat de Barcelona, Barcelona, Spain.* [2]*Departamento de Física, Universidad de La Laguna, Tenerife, Spain.*

*e-mail: mvalient@ull.edu.es

We consider interacting one-dimensional bosons in the universal low-energy regime. The interactions consist of a combination of attractive and repulsive parts that can stabilize quantum gases, droplets and liquids. In particular, we study the role of effective three-body repulsion, in systems with weak attractive pairwise interactions. Its low-energy description is often argued to be equivalent to a model including only two-body interactions with non-zero range. Here, we show that, at zero temperature, the equations of state in both theories agree quantitatively at low densities for overall repulsion, in the gas phase, as can be inferred from the S-matrix formulation of statistical mechanics. However, this agreement is absent in the attractive regime, where universality only occurs in the long-distance properties of quantum droplets. We develop analytical tools to investigate the properties of the theory, and obtain astounding agreement with exact numerical calculations using the density-matrix renormalization group [1].

[1] I. Morera, B. Juliá-Díaz and M. Valiente, arXiv:2103.16499 (2021).

Fiber-based biphoton spectroscopy

I. Pérez Pérez[1,*], M. Afsharnia[1], M. Weißflog[1], S. Saravi[1], T. Pertsch[1,2], F. Setzpfandt[1,2]

[1]*Institute of Applied Physics, Abbe Center of Photonics, Friedrich-Schiller-University Jena, Albert-Einstein-Str. 15, 07745 Jena, Germany.*
[2]*Fraunhofer Institute for Applied Optics and Precision Engineering, Albert-Einstein-Str. 15, 07745 Jena, Germany.*

*e-mail: inmaculada.perez.perez@uni-jena.de

Entangled photon pair sources are of great interest thanks to their many potential applications in quantum technologies. Due to their potential, big efforts are put into developing sources with specific characteristics. One of the challenges faced in this context is the characterization of the resulting photon pairs.

In this project, we implement a simple method to estimate the wavelengths of spectrally correlated photon pairs by means of a dispersive medium. This can be especially useful for setups where direct spectroscopy measurements are not possible.

This method has been tested for photon pairs produced with different sources: one generated by Spontaneous Parametric Down Conversion (SPDC) and the other by Spontaneous Four Wave Mixing (SFWM). The photons are each coupled into a long single-mode optical fiber and eventually reach a Single Photon Detector (SPD). The difference between their times of arrival is measured and used to determine their wavelengths based on the corresponding energy conservation law and the dispersive nature of the fibers, which act as a delay line.

The calculated wavelengths show a good agreement with our reference values, with percent errors under 5%. This study was performed assuming steady conditions where potential disturbances such as vibrations or temperature gradients were not considered. Additionally, we observed a high sensitivity to the length of the dispersive elements. Solutions to this problem are discussed in the poster.

Despite these limitations, our results suggest that this method can be implemented for future spectroscopy measurements of correlated photon pairs as long as the corresponding energy conservation law and the dispersion character of the fibers are known.

Inteligencia Artificial en Física de la Materia Condensada

Presentaciones orales

Miércoles 13/07:

15:30-16:20 Eliska Greplova (TU Delft). *A data-driven perspective on quantum matter*

16:20-16:40 Sergio G. Rodrigo (Universidad de Zaragoza). *Design of plasmonic superconducting transition-edge-sensors with neural networks*

16:40-17:00 Daniel del Pozo (Universitat de Barcelona). *Transition metals oxidation state determination through Electron Energy-Loss Spectra and Support Vector Machines*

17:00-18:00 **Pósteres y café**.

18:00-18:20 Borja Requena (ICFO). *Certificates of quantum many-body properties assisted by machine learning*

18:20-18:40 Pablo Serna (Universidad de Murcia). *Machine learning and displacement transformations to locate the many body localization transition*

18:40-19:00 Alejandro Jose Uria-Alvarez (Universidad Autonónoma de Madrid). *Deep learning for disordered topological insulators through their entanglement spectrum*

19:00-19:20 Juan José García (Universidad Autonónoma de Madrid). *Deep Learning for the modeling and inverse design of radiative heat transfer*

Pósteres

- Pedro Moronta (CSIC). *Can random laser networks learn?*
- Miguel Dalmau (Universidad Autónoma de Madrid & CSIC). *Graph convolutional neural networks for accelerating property predictions of small organic molecules*

Design of plasmonic superconducting transition-edge-sensors with neural networks

Sergio G. Rodrigo[1,2,*], Carlos Pobes[2,3], Luis Martín-Moreno[2,3], and Agustín Camón Lasheras[2,3]

[1]*Departamento de Física Aplicada, Facultad de Ciencias, Universidad de Zaragoza, 50009 Zaragoza, Spain.*
[2]*Instituto de Nanociencia y Materiales de Aragón (INMA), CSIC-Universidad de Zaragoza, 50009 Zaragoza, Spain.*
[3]*Departamento de Física de la Materia Condensada, Universidad de Zaragoza, Zaragoza 50009, Spain.*

*e-mail: sergut@unizar.es

We demonstrate the use of neural networks (NN) to improve the design of plasmonic nanostructures. The scattering properties of a plasmonic nanostructure calculated by a slow numerical method is subrogated by a trained NN. The NN results are almost indistinguishable from those calculated with the numerical solver (FDTD method), but up to 10^6 times faster. We illustrate the capabilities of this approach by optimizing a Transition Edge Sensor (TES) to efficiently absorb infrared light. TES are extremely sensitive thermometers made of superconducting metals operating at their transition temperature, where small variations in temperature give rise to a measurable increase in electrical resistance. Coupled to suitable absorbers, they are used as radiation detectors with very good energy resolution in several experiments. TES has been thoroughly investigated for the detection of radiation in the X-ray range. Recently, we purposed a plasmonic TES to work at telecom wavelengths [1]. We designed a high absorbing TES (98% at λ = 1550 nm) by nanostructuring directly its metal surface, avoiding the use of an extra absorber to reduce the total heat capacity and to simplify the fabrication.

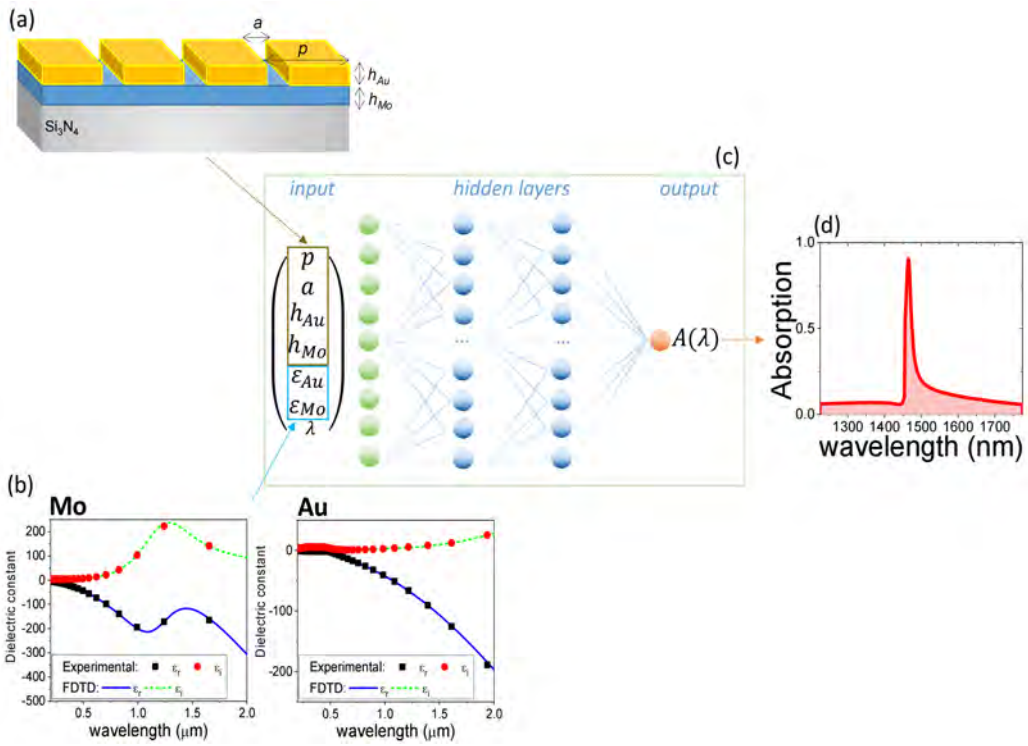

Figure 1. The NN model takes as input: the geometrical parameters of the nanostructure, the dielectric constants of the materials, and the wavelength of light λ. The output layer predicts the absorption at λ.

[1] Sergio G. Rodrigo, Carlos Pobes, Marta Sánchez Casi, Luis Martín-Moreno, and Agustín Camón Lasheras, *Opt. Express* **30**, 12368-12377 (2022)

Acknowledgements: All authors acknowledge also the Aragón government project Q-MAD.

Transition metals oxidation state determination through Electron Energy-Loss Spectra and Support Vector Machines

Daniel del Pozo Bueno[1,2,*], Francesca Peiró[1,2], Sònia Estradé[1,2]

[1]*LENS-MIND, Dept. Enginyeries Electrónica i Biomèdica, Universitat de Barcelona, C/ Martí i Franquès, 1-11 08028 Barcelona, Spain.* [2]*Institute of Nanoscience and Nanotechnology (IN^{2}UB), Universitat de Barcelona, C/ Martí i Franquès, 1-11 08028 Barcelona, Spain.*

*e-mail: ddelpozo@ub.edu

Electron Energy-Loss Spectroscopy (EELS) is a powerful spectroscopic technique to study locally the composition and properties of materials at the nanoscale, which is carried out in the Scanning and Transmission Electron Microscopes (S/TEM). The recent technological advances in S/TEM devices are leading to higher spatial and energy resolution resulting in an enormous increase of the total amount of data acquired in EELS measurements. Thus, currently this technique offers better energy and spatial resolutions making possible a better nanometric characterization, at the cost of producing large spectral datasets.

The machine learning methods provide a large variety of tools to properly deal with these large amounts of spectral data in an automated manner, at the same time that allow for extracting valuable physical information. A promising machine learning strategy for identifying EELS data is the Support Vector Machine (SVM) [1], in particular the soft-margin SVM, which is a supervised machine learning algorithm allowing the multiclass classification, even with non-linear data, and that can be used as a probabilistic classifier.

The soft-margin SVM has shown promising results identifying the oxidation state in transition metal (TM) oxides, manganese and iron oxides, through the study of their EELS spectra, namely, their white lines (L_3 and L_2) as shown in Figure 1 [2]. The algorithm has been implemented in Python from the library Scikit-learn [3], in particular, the LIBSVM library [4]. It has presented a performance, above 90% classifying the TM oxidation state, even if considering the usual level of noise and additional instrumental energy shifts.

In conclusion, the SVM applied to EEL spectra makes the most of its simplicity (few parameters to optimize) and short computation times to correctly and automatically identify the oxidation state of the transition metals. Furthermore, for large spectral datasets the computing times can even be reduced by implementing the Stochastic Gradient Descend (SDG), which is an iterative method that optimizes, and so, accelerates model training enabling also faster parameter optimization.

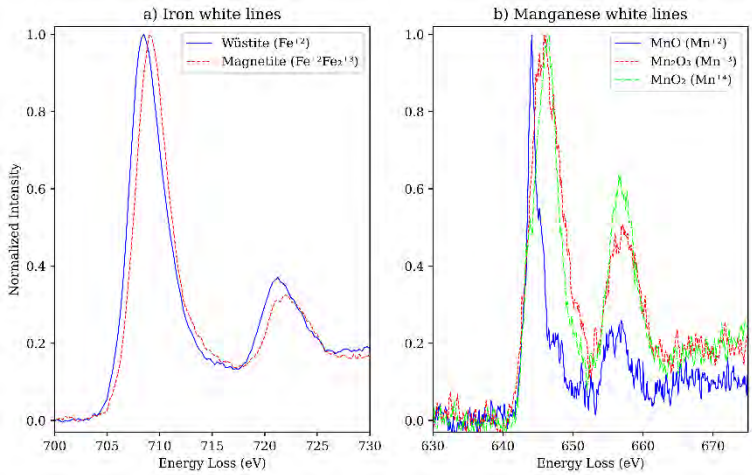

Figure 1. Iron oxides Electron Energy-Loss Spectra: a) Iron white lines for the magnetite (Fe3O4) and wüstite (FeO) oxides, b) Manganese white lines for three manganese oxides.

[1] C. Cortes and V. Vapnik, *Machine Learning* **20**, 273 (1995).
[2] D. del-Pozo-Bueno, F. Peiró and S. Estradé, *Ultramicroscopy* **221**, 113190 (2021).
[3] F. Pedregosa et al., *Journal of Machine Learning Research* **12**, 2825 (2011).
[4] C. C. Chang and C. J. Lin, *ACM Trans. Intell. Syst. Technol.* **2**, 1-39 (2011).

Certificates of quantum many-body properties assisted by machine learning

Borja Requena[1,*], Gorka Muñoz-Gil[1,2], Maciej Lewenstein[1,3], Vedran Dunjko[4], Jordi Tura[5,6]

[1]*ICFO - Institut de Ciencies Fotoniques, The Barcelona Institute of Science and Technology, Av. Carl Friedrich Gauss 3, 08860 Castelldefels (Barcelona), Spain.*
[2]*Institute for Theoretical Physics, University of Innsbruck, Technikerstr. 21a, A-6020 Innsbruck, Austria.*
[3]*ICREA, Pg. Lluís Companys 23, 08010 Barcelona, Spain.*
[4]*LIACS, Leiden University, Niels Bohrweg 1, 2333 CA Leiden, Netherlands.*
[5] *Instituut-Lorentz, Universiteit Leiden, P.O. Box 9506, 2300 RA Leiden, The Netherlands.*
[6]*Max-Planck-Institut für Quantenoptik, Hans-Kopfermann-Str. 1, 85748 Garching, Germany.*

*e-mail: borja.requena@icfo.eu

The Computationally intractable tasks are often encountered in physics and optimization. Such tasks usually comprise a cost function to be optimized over a so-called feasible set, which is specified by a set of constraints. This may yield, in general, to difficult and non-convex optimization tasks. A number of standard methods are used to tackle such problems: variational approaches focus on parameterizing a subclass of solutions within the feasible set. In contrast, relaxation techniques have been proposed to approximate it from outside, thus complementing the variational approach to provide ultimate bounds to the global optimal solution.

In this work [1], we propose a novel approach combining the power of relaxation techniques with deep reinforcement learning in order to find the best possible bounds within a limited computational budget. We illustrate the viability of the method in the context of finding the ground state energy of many-body quantum systems, a paradigmatic problem in quantum physics. We benchmark our approach against other classical optimization algorithms such as breadth-first search or Monte-Carlo, and we characterize the effect of transfer learning. We find the latter may be indicative of phase transitions, implementing a completely autonomous approach. Finally, we provide tools to generalize the method to other common applications in the field of quantum information processing.

[1] B. Requena, G. Muñoz-Gil, M. Lewenstein, V. Dunjko, J. Tura, arXiv:2103.03830 (2021).

Acknowledgements: ICFO group acknowledges support from: ERC AdG NOQIA, Agencia Estatal de Investigación (the R&D project CEX2019-000910-S, funded by MCIN/ AEI/10.13039/501100011033, Plan National FIDEUA PID2019-106901GB-I00, FPI), Fundació Privada Cellex, Fundació Mir-Puig, and from Generalitat de Catalunya (AGAUR Grant No. 2017 SGR 1341, CERCA program). G.M.-G. acknowledges funding from Fundació Obra Social "la Caixa" (LCF-ICFO grant). J. T. thanks the Alexander von Humboldt foundation for support. This project has received funding from the Deutsche Forschungsgemeinschaft (DFG, German Research Foundation) – Project number 414325145 in the framework of the Austrian Science Fund (FWF): SFB F7104. This project has received funding from the European Union's Horizon 2020 research and innovation programme under grant agreement No 899354. This work was supported by the Dutch Research Council (NWO/OCW), as part of the Quantum Software Consortium programme (project number 024.003.037).

Machine Learning and Displacement transformations to locate the Many Body Localization transition

Pablo Serna*, Miguel Ortuño, Andrés M. Somoza

Departamento de Física — CIOyN, Universidad de Murcia, Murcia 30071, Spain.

*e-mail: pablo.sernamtnez@um.es

The Many-Body localization (MBL) transition [1] is one of the simplest interacting quantum problems, and yet even its precise location in relatively simple models is disputed. The main hurdle is the exponential increase of the size of the Hilbert space with the system size. It imposes constraints to memory and computational time that are very hard to overcome.

Recently, several techniques have been developed to deal with this issue. In particular, the use of unitary displacement transformations [2,3] to obtain eigenstates provides a way to control the approximations that are necessarily made to access large system sizes. With this technique the memory constraint can be overcome but it is compensated with a longer computational time to fully diagonalize the Hamiltonian [4].

We will show how using Machine Learning techniques, namely gradient boosting and deep neural networks, we can exploit the data obtained during the process of diagonalization with displacement transformations to speed up the proccess. The insight from this techniques allow us to classify localized and extended states up to system sizes much larger than what is reported in the literature $L \gg 32$.

[1] Basko DM, Aleiner IL, Altshuler BL. *Ann Phys* (2006) 321:1126–205. doi:10.1016/j.aop.2005.11.014
[2] Rademaker L, Ortuño M. *Phys. Rev. Lett.* 116 (2016) 010404. doi:10.1103/PhysRevLett.116.010404
[3] Rademaker L, Ortuño M, Somoza AM. *Annalen der Physik* 529 (2017), 1600322. doi:10.1002/andp.201600322
[4] Serna P, Ortuño M, Somoza AM. *Frontiers in Physics* (2021) 664. doi:10.3389/fphy.2021.767001

Acknowledgements: We acknowledge support by AEI (Spain) grant PID2019-104272RB-C52 and Fundacion Seneca grant 19907/GERM/15.

Deep learning for disordered topological insulators through their entanglement spectrum

Alejandro José Uría-Álvarez*, Daniel Molpeceres-Mingo, Juan José Palacios

Departamento de Física de la Materia Condensada, Condensed Matter Physics Center (IFIMAC), and Instituto Nicolás Cabrera (INC), Universidad Autónoma de Madrid, Cantoblanco 28049, Spain

*e-mail: alejandro.uria@uam.es

Calculation of topological invariants for crystalline systems is well understood in reciprocal space, allowing for the topological classification of a wide spectrum of materials [1, 2]. While working in the reciprocal space may still be possible for disordered materials, computations will become too expensive due to the mandatory increase in cell size. On top of that, the most popular techniques such as the Wilson loop [3] are only well-defined in insulating materials, generally defined as systems with fully occupied bands or partially occupied ones, but separated from the rest by a gap across the whole Brillouin zone.

In this work [4], we present a technique based on the entanglement spectrum, which can be used to identify the hidden topology of systems [5] without translational invariance. By training a neural network to distinguish between trivial and topological phases using the entanglement spectrum obtained from crystalline or weakly disordered phases, we can predict the topological phase diagram for generic disordered systems. This approach becomes particularly useful for gapless systems, while providing a computational speed-up compared to the commonly used Wilson loop technique for gapful situations. Our methodology is illustrated in two-dimensional models based on the Wilson-Dirac lattice Hamiltonian.

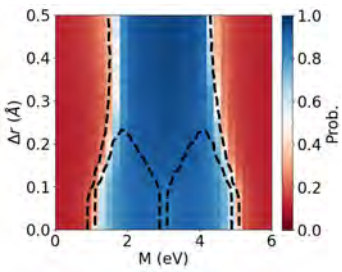

Figure 1. Topological phase diagram as predicted by the neural network. Black lines correspond to gap contour lines for 0.1 eV.

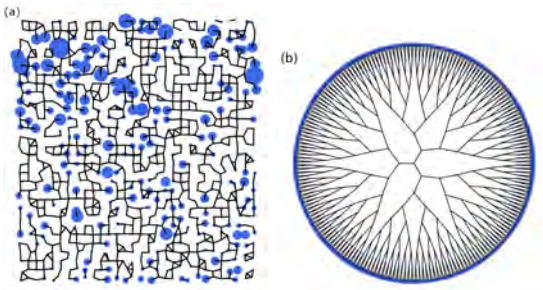

Figure 2. Edge state in (a) an amorphous lattice and (b) in the Bethe lattice.

[1] M. G. Vergniory, L. Elcoro, C. Felser, N. Regnault, B. A. Bernevig, and Z. Wang, *Nature* **566**, 480 (2019).
[2] T. Olsen, E. Andersen, T. Okugawa, D. Torelli, T. Deilmann, and K. S. Thygesen, *Phys. Rev. Materials* **3**, 024005(2019).
[3] Dominik Gresch, Gabriel Autes, Oleg V. Yazyev, Matthias Troyer, David Vanderbilt, B. Andrei Bernevig, and Alexey A. Soluyanov, *Phys. Rev. B*, **95**, 075146 (2017)
[4] A. J. Uría-Álvarez, D. Molpeceres-Mingo, J. J. Palacios *Phys. Rev. B* **105**, 155128 (2022).
[5] L. Fidkowski, *Phys. Rev. Lett.* **104**, 130502 (2010)

Deep Learning for the modeling and inverse design of radiative heat transfer

J. J. García-Esteban*, J. Bravo-Abad, J. C. Cuevas

Departamento de Física Teórica de la Materia Condensada and Condensed Matter Physics Center (IFIMAC), Universidad Autónoma de Madrid, E-28049 Madrid, Spain.

*e-mail: juanjose.garciae@uam.es

Deep learning is having a tremendous impact in many areas of computer science and engineering. Motivated by this success, deep neural networks are attracting an increasing attention in many other disciplines, including physical sciences. In this work [1], we show that artificial neural networks can be successfully used in the theoretical modeling and analysis of a variety of radiative heat transfer phenomena and devices. By using a set of custom-designed numerical methods able to efficiently generate the required training datasets, we demonstrate this approach in the context of three very different problems, namely, *(i)* near-field radiative heat transfer between multilayer systems that form hyperbolic metamaterials (figure 1), *(ii)* passive radiate cooling in photonic-crystal slab structures (figure 2), and *(iii)* thermal emission of subwavelength objects. Despite their fundamental differences in nature, in all three cases we show that simple neural network architectures trained with datasets of moderate size can be used as fast and accurate surrogates for doing numerical simulations, as well as engines for solving inverse design and optimization in the context of radiative heat transfer. Overall, our work shows that deep learning and artificial neural networks provide a valuable and versatile toolkit for advancing the field of thermal radiation.

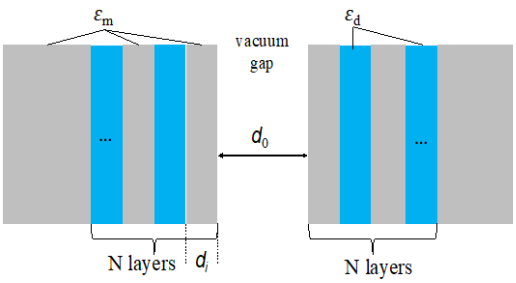

Figure 1. Sketch of two identical multilayer systems separated by vacuum and composed of layers of width d_i alternating between a Drude metal (grey) with permittivity ε_m and a dielectric (blue) with permittivity ε_d. Inspired by the design from [2].

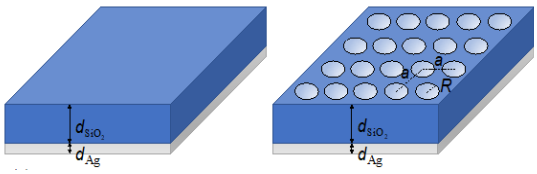

Figure 2. Left: Schematics of a silica mirror used in [3] as a passive radiative cooler, consisting of a SiO_2 slab of thickness d_{SiO2} and a silver thin film of thickness d_{Ag}. Right: same mirror, but with a periodic array of holes in the silica layer, with radius R and lattice parameter a.

[1] J. J. García-Esteban, J. Bravo-Abad and J. C. Cuevas, *Phys. Rev. Appl.* **6**, 064006 (2021).
[2] H. Iizuka and S. Fan, *Phys. Rev. Lett.* **120**, 063901 (2018).
[3] J. Kou, Z. Jurado, Z. Chen, S. Fan and A. J. Minnich, *ACS Photonics* **4**, 626 (2017).

Acknowledgements: J.J.G.E. was supported by the Spanish Ministry of Science and Innovation through a FPU grant (FPU19/05281). J.B.A. acknowledges financial support from Ministerio de Ciencia, Innovación y Universidades (RTI2018-098452-B-I00). J.C.C. acknowledges funding from the Spanish Ministry of Science and Innovation (PID2020-114880GB-I00).

Can random laser networks learn?

Pedro Moronta[1,*], Antonio Consoli[1,2], Jorge Bravo-Abad[3], Ceferino López[1]

[1]*Instituto de Ciencia de Materiales de Madrid (ICMM), Consejo Superior de Investigaciones Científicas (CSIC), Spain.*
[2]*ETSI de Telecomunicación, Universidad Rey Juan Carlos, Spain.*
[3]*Departamento de Física Teórica de la Materia Condensada and Condensed Matter Physics Center (IFIMAC), Universidad Autónoma de Madrid, Spain.*

*e-mail: p.moronta@csic.es

The ever-increasing energy demand of conventional Artificial Intelligence (AI) hardware calls for disruptive approaches in which the training process can be less power-hungry and less environmentally harmful. Reservoir computing and extreme machine learning are two particularly appealing approaches that, by exploiting the natural dynamics of input-driven randomly connected neural networks, feature minimal energy requirements. Remarkably, photonics is emerging as a natural testbed to implement both reservoir computing and extreme machine learning that can represent realistic alternatives to the ubiquitous von Neumann architecture [1].

In this preliminary work, we discuss how a network of coupled random lasers (RLs) can be tailored to realize a novel platform for reservoir computing and extreme machine learning. We generalize to complex networks our recent experimental and numerical work investigating the coupling of few RLs based on a pumped gain-medium strip connecting two rough mirrors [2]. We particularly focus on a system based on three-resonator arranged in a Z-shaped configuration and show how the coupling of lasers modes between non-neighbouring resonators via a linking resonator can indeed provide the basis for a whole new paradigm in reservoir computing.

[1] Shen, Y., Harris, N., Skirlo, S. et al., *Nat. Photon.* **11**, 441 (2017).
[2] N. Caselli, A. Consoli, Á. Mateos Sánchez, and C. López, *Optica* **8**, 193(2021).

Graph convolutional neural networks for accelerating property predictions of small organic molecules

Miguel Dalmau[1,2,*], Jorge Bravo-Abad[2], Eduardo Hernández[1]

[1]*Instituto de Ciencia de Materiales de Madrid, CSIC.*
[2]*Departamento de Física Teórica de la Materia Condensada and IFIMAC, UAM.*

*e-mail: Eduardo.Hernandez@csic.es

In recent years graph neural networks (GNNs), a branch of deep learning exploiting graph structures, have found a very wide range of applications across industry and science [1]. GNNs offer significant potential in the context of property prediction of solids [2] and molecules [3], for which graph features (nodes and edges) allow for a natural self-contained and accurate description of the system.

In this work, we demonstrate an efficient implementation of graph convolutional neural networks for accelerating the property predictions of small molecules made up of C, H, O, N, F (of up to nine atoms not counting H). Using an existing database containing quantum chemical calculations of 134,000 molecules [4], we show how a GNN architecture consisting of a small number of GNN convolutional layers, followed by a densely connected neural network enables an efficient prediction of the internal energy of the considered class of molecules (see Fig. 1). In our approach, each graph node represents an atom, and the corresponding edges include information about atom distances, bond angles and, optionally, dihedral angles.

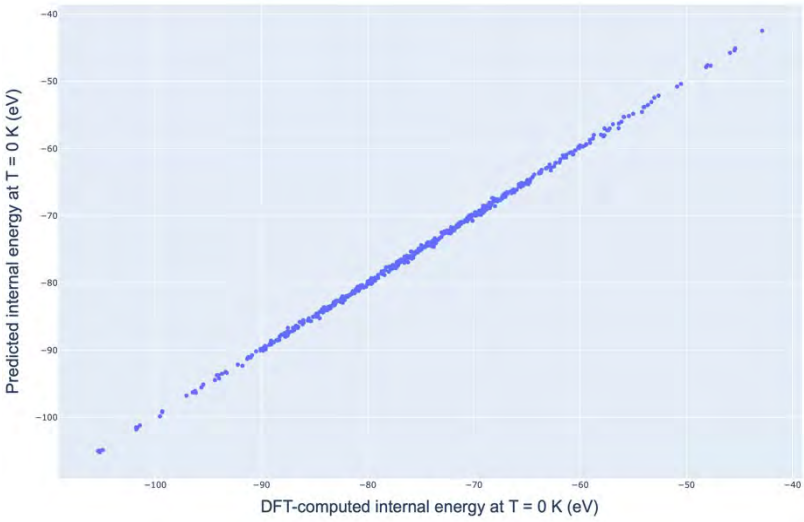

Figure 1. Comparison between the predicted internal energy at T=0K predicted by the proposed GCNN implementation and that calculated with a density-functional-theory approach. Each blue circle in the figure represents the results of one of the molecules included in a test set not included in the training process of the proposed algorithm.

[1] J. Zhou *et al.*, Graph neural networks: A review of methods and applications, *AI Open* **1**, 57 (2020).
[2] T. Xie and J. C. Grossman, Crystal Graph Convolutional Neural Networks for an Accurate and Interpretable Prediction of Material Properties, *Phys. Rev. Lett.* **120**, 145301 (2018).
[3] K. Choudhary, and B. DeCost, Atomistic Line Graph Neural Network for improved materials property predictions, *NPJ Computational Materials* **7**, 185 (2021).
[4] R. Ramakrishnan, P.O. Dral, M. Rupp, and O. A. von Lilienfeld, Quantum chemistry structures and properties of 134 kilo molecules, *Scientific Data* **1**, 140022 (2014).

Fronteras en Materia Blanda Condensada

Presentaciones orales

Miércoles 13/07:

15:30-16:00 Pietro Tierno. *Topological Boundary Constraints in Artificial Colloidal Ice*

16:00-16:15 Alejandro Cuetos Menéndez. *Estudio mediante simulación de propiedades emergentes en colonias celulares*

16:15-16:30 Alvaro Domínguez Alvarez. *Beyond classic phoresis: new insights into self-phoresis*

16:30-16:45 Alexis de la Cotte. *Orientational correlations of active defects in flat and curved space*

16:45-17:00 Pablo Maynar Blanco. *Understanding an instability in vibrated granular monolayers*

17:00-17:12 Flash talks of the posters.

17:12-18:00 **Pósteres y café**.

18:00-18:15 Ramon Planet Latorre. *The uncanny weight of granular columns*

18:15-18:30 Carlos Miguel Barriuso Gutiérrez. *Discovering dynamic laws from observations: the case of self-propelled, interacting colloids*

18:30-18:45 Miguel Ángel Ramos Ruiz. *Ultrastable glasses: going very deep into the energy landscape of glasses*

18:45-19:00 José Manuel Romero Enrique. *Casimir contribution to the interfacial Hamiltonian for 3D wetting*

19:00-19:15 José Martín Roca. *Magnetic colloids adsorbed at fluid interfaces acting as interfacial swimmers and colloid adsorption probes*

Jueves 14/07:

15:30-16:00 Chantal Valeriani. *Trapping active particles up to the limiting case: bacteria enclosed in a biofilm*

16:00-16:15 Caleb Anderson. *MIPS and Activity Cycles in Fire Ants*

16:15-16:30 Raúl Rica Alarcón. *Collapse of magnetite-decorated pNIPAM microgels trapped with optical tweezers*

16:30-16:45 Alessandro Patti. *Phase behaviour and dynamics of colloidal cuboids: paving the path to biaxial nematic liquid crystals*

16:45-17:00 Javier Rojo González. *Nematics in 3-tori: Doubly twisted structures and defect-populated configurations*

17:00-18:00 **Café**.

Pósteres

- Juan Pablo Miranda López. *Collective behaviour of energy depot repulsive particles*
- María Isabel García de Soria Lucena. *Dynamics of hard particles confined by an isotropic harmonic potential*
- Jose Martin Roca. *Discovering dynamic laws from observations: the case of self-propelled, interacting colloids*
- Carlos Miguel Barriuso Gutiérrez. *Simulating active agents with Dissipative Particle (hydro)Dynamics*

Topological Boundary Constraints in Artificial Colloidal Ice

Carolina Rodríguez-Gallo[1,2], Antonio Ortiz-Ambriz[1,2,3] **Pietro Tierno**[1,2,3,*]

[1] *Departament de Física de la Matèria Condensada, Universitat de Barcelona, 08028 'Barcelona, Spain.*
[2] *Universitat de Barcelona Institute of Complex Systems (UBICS), Universitat de Barcelona, 08028 Spain.*
[3] *Institut de Nanociència i Nanotecnologia, Universitat de Barcelona, 08028 Barcelona Spain.*

*e-mail: ptierno@ub.edu

The effect of boundaries and how these can be used to influence the bulk behavior in geometrically frustrated systems are both long-standing puzzles, often relegated to a secondary role. In this talk, I will investigate boundary effects in a geometrically frustrated system, namely an artificial colloidal ice (ACI). The ACI recently emerge as a microscale soft matter analog of a frustrated nanoscale spin ice system. The artificial colloidal ice is realized by confining interacting paramagnetic colloids to a lattice of gravitational double wells [2]. With this system, both via numerical simulations and "proof of concept" experiments, I will demonstrate that boundaries can be engineered to control the bulk behavior in a colloidal artificial ice [3]. I will also show that an antiferromagnetic frontier forces the system to rapidly reach the ground state (GS), as opposed to the commonly implemented open or periodic boundary conditions. Further, strategically placing defects at the corners may be used to generate novel bistable states, or topological strings, which result from competing GS regions in the bulk. The presented results could be generalized to other frustrated micro- and nanostructures where boundary conditions may be engineered with lithographic techniques.

[1] A. Ortiz-Ambriz and P. Tierno, *Nature Comm.* **7**, 10575 (2016).
[2] Ortiz-Ambriz, C. Nisoli, C. Reichhardt, C. J. O. Reichhardt, and P. Tierno, *Rev. Mod. Phys.* **91**, 041003 (2019).
[3] Carolina Rodríguez-Gallo, Antonio Ortiz-Ambriz, and Pietro Tierno, *Phys. Rev. Lett.* **126**, 188001 (2021).

Acknowledgements: This project has received funding from the European Research Council (ERC) under the European Union's Horizon 2020 research and innovation programme (grant agreement no. 811234). P. T. acknowledge support the Generalitat de Catalunya under Program ÏCREA Acadèmia".

Estudio mediante simulación de propiedades emergentes en colonias celulares

Alejandro Cuetos

Departamento de Sistemas Físicos, Químicos y Naturales. Universidad Pablo Olavide. Sevilla, España.

*e-mail: acuemen@upo.es

Las colonias celulares (biofilms en el caso de procariotas, pero también órganos o tumores en el caso de eucariotas) son agregados de células que presentan muchas similitudes con fluidos coloidales. Como diferencia fundamental, las colonias celulares son sistemas activos que de forma intrínseca suelen encontrarse fuera del equilibrio. Así, es habitual que las células tengan mecanismos propios (flagelos, cilios, etc ...) que provocan un movimiento autónomo por parte de las células. En otros casos, el carácter de sistema activo y la situación de fuera del equilibrio surge del propio proceso de alargamiento y reproducción celular, que en bacterias suele venir dado por el mecanismo conocido como fisión binaria.

Centrándonos en la situación en que las células no tienen capacidad de movimiento autónomo, pero crecen y se dividen por fisión binaria, las colonias celulares son agregados compactos, pudiendo ser en función del número de células bi o tridimensionales. En función de las características de las células y de las condiciones ambientales pueden presentar distintos niveles de orden parcial, asemejándose a tactoides nemáticos, y una variedad de propiedades mecánicas y estructurales.

En los últimos años se han comenzado a utilizar para el estudio de estas comunidades celulares técnicas de simulación ampliamente utilizadas en la ciencia coloidal. Presentamos en este trabajo algunos ejemplos del uso de estas técnicas, explorando las propiedades físicas que se pueden deducir de estos estudios, presentando resultados experimentales que al menos cualitativamente confirman los resultados obtenidos por simulación. De esta forma, en primer lugar se presentará el modelo que se ha desarrollado para la realización de estos estudios. Nuestro modelo se basa en la descripción de grano grueso de propiedades de las células individuales, como son forma, tamaño, velocidad de crecimiento y coeficiente de difusión, obteniendo con él propiedades emergentes colectivas de toda la colonia. Con este modelo se ha explorado como condiciona la competición entre difusión pasiva de las células y el proceso de elongación/división a las propiedades estructurales globales de la colonia celular [1].

También hemos estudiado el crecimiento de una colonia bacteriana en un entorno rico en polímeros. En este caso hemos comprobado la existencia de distintos escenarios. En estos escenarios, que dependen del tamaño y concentración de partículas poliméricas, las propiedades de la colonia celular pueden venir condicionadas bien por un aumento efectivo de la viscosidad del medio, o bien por la actuación de fuerzas de depleción [2].

Finalmente, mostraremos resultados sobre las propiedades micromecánicas de las colonias celulares. Aquí mostraremos como el crecimiento de la colonia provoca un aumento continuo de las tensiones mecánicas en el interior de la colonia, sugiriendo la existencia de mecanismos biológicos para limitar este aumento de las tensiones internas.

[1] R. D. Acemel, F. Govantes y A. Cuetos, *Scientific Reports* **8**, 5340 (2018).
[2] F. J. Lobo-Cabrera, A. Patti, F. Govantes, and A. Cuetos, *Phys. Rev. E* **103**, 052407 (2021).

Beyond classic phoresis: new insights into self-phoresis

Alvaro Domínguez

Departamento de Física Atómica, Molecular y Nuclear, Universidad de Sevilla, Apdo. 1065, 41080 Spain.

e-mail: dominguez@us.es

The notion of chemophoresis describes the displacement of a particle in an ambient fluid due to an externally imposed gradient in chemical composition, *and in the absence of a net external force and torque*: therefore, the particle's momentum is balanced by the momentum of the ambient flow, and the particle is not dragged, but instead it *swims*. The phenomenon of classic phoresis can be understood in the context of linear–response theory: the phoretic velocity $\mathbf{V}$ of the particle in a fluid solution can be obtained as

$$\mathbf{V} = \mathcal{L}_{\rm lin}\ (\nabla n)_{\rm ext}\,,$$

for a sufficiently small gradient $(\nabla n)_{\rm ext}$ in solute concentration over the scale of the particle size, in terms of the phoretic coefficient $\mathcal{L}_{\rm lin}$ given by a Green–Kubo expression.

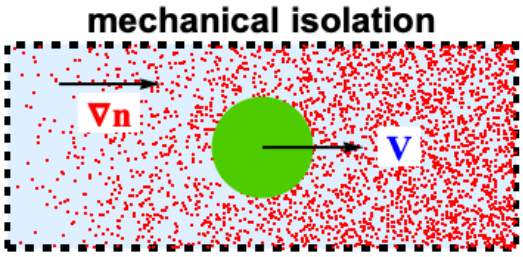

A closely related phenomenology is observed for self-phoretic particles, which have attracted much attention in the last years as a physical realization of artificial swimmers. In this case, the particle's surface is catalytically active, so that it induces a composition gradient $(\nabla n)_{\rm act}$. The experimental observations involving self-phoretic particles are then customarily addressed as another instance of classic phoresis but in a self-generated gradient,

$$\mathbf{V} = \mathcal{L}_{\rm lin}\ (\nabla n)_{\rm act}\,.$$

However, an additional role of the particle's chemical activity has been recently identified [1,2], namely, as responsible for a specific *activity–induced response*, so that one has to write

$$\mathbf{V} = (\mathcal{L}_{\rm lin} + \mathcal{L}_{\rm act})\ [(\nabla n)_{\rm ext} + (\nabla n)_{\rm act}]\,,$$

in the more general scenario, where $\mathcal{L}_{\rm act}$ is the activity–induced contribution to the phoretic coefficient. We will describe the theoretical framework behind this result and possible observational consequences. In particular, we argue that the piece $\mathcal{L}_{\rm act}$ of the response could actually be as large as $\mathcal{L}_{\rm lin}$ in realistic configurations: this would mean a change in paradigm as it disproves the claim that "self-phoresis is phoresis in a self-induced gradient".

[1] A. Domínguez, M. Popescu, C. Rohwer, S. Dietrich, *Physical Review Letters*, **125**, 268002 (2020).
[2] A. Domínguez, M. Popescu, *Current Opinion in Colloid & Interface Science*, submitted (2022).

Orientational correlations of active defects in flat and curved space

J. Nambisan[1], **A. de la Cotte**[2,*], D. Pearce[3], L. Giomi[4], A. Fernandez-Nieves[2,5]

[1]*School of Physics, Georgia Institute of Technology, Atlanta, Georgia, USA.*
[2]*Department of Condensed Matter Physics, University of Barcelona, Barcelona, Spain.*
[3]*Departments of Biochemistry and Theoretical Physics, Université de Genève, Genève, Switzerland.*
[4]*Instituut-Lorentz, Universiteit Leiden, Leiden, The Netherlands.*
[5]*ICREA-Institucio Catalana de Recerca i Estudis Avançats, 08010 Barcelona, Spain.*

*e-mail: alexis.delacotte@gmail.com

Topological defects are salient signatures of active nematics, which are partially-ordered systems intrinsically out of equilibrium. We experimentally study the dynamics of microtubule-kinesin active nematics constrained to both flat space and toroidal 2D space and inquire whether the defects develop any form of order. In flat space, +1/2 defects develop short range ferromagnetic order (mediated by -1/2 defects) and antiferromagnetic order at length scales comparable to the mean defect spacing. Both these effects and the corresponding correlations are seen to persist independent of the total defect density, and without any global orientational order [1]. In contrast, on curved space, we find that defect orientations strongly couple to the surface they live in, resulting in both +1/2 and -1/2 defects developing orientational order in regions of non-zero Gaussian curvature.

[1] D. Pearce *et al.*, *Phys. Rev. Lett.* **127**, 197801 (2021).

Understanding an instability in vibrated granular monolayers

P. Maynar[1,2,*], M. I. García de Soria[1,2], J. J. Brey[1,2]

[1]*Área de Física Teórica, Universidad de Sevilla, Spain.* [2] *Institute for Theoretical and Computational Physics, Universidad de Granada, Spain.*

*e-mail: maynar@us.es

We investigate the dynamics of an ensemble of smooth inelastic hard spheres confined between two horizontal plates separated a distance smaller than twice the diameter of the particles, in such a way that the system is quasi-two-dimensional. The bottom wall is vibrating and, therefore, it injects energy into the system in the vertical direction and a stationary state is reached. It is found that, if the size of the plates is small enough, the stationary state is homogeneous. Otherwise, a cluster of particles is developed. The instability is understood by using some effective hydrodynamic equations in the horizontal plane. Moreover, the theoretical prediction for the size of the system above which it becomes unstable agrees very well with Molecular Dynamics simulation results without any fitting parameter [1].

[1] P. Maynar, M. I. García de Soria, and J. J. Brey, *Phys. Rev. E* **99**, 032903 (2019).

The uncanny weight of granular columns

R. Planet[1,*], C. Anderson[1], I. Zamorano[1], A. Fernandez-Nieves[1,2]

[1] *Departament de Física de la Matèria Condensada, Universitat de Barcelona, Martí i Franquès 1, 08028, Barcelona, Spain.* [2] *ICREA-Institució Catalana de Recerca i Estudis Avançats, 08010 Barcelona, Spain.*

*e-mail: rplanet@ub.edu

Granular matter exhibits unusual mechanical properties. For example, when filling a cylindrical column with grains, the weight measured at the bottom of the column does not scale linearly with added mass, but asymptotically saturates towards a constant value. This observation is well-known in the granular matter community; it is referred to as the "Janssen's effect". The weight is partially supported by the lateral walls through frictional interactions with the grains. However, it has been recently observed that the weight measured at the bottom can become larger than the total added mass when the columns are sufficiently small compared to the diameter of the grains [1]. In this talk, we will review this "reverse" Janssen effect, and present new results using grains with different geometry. We find that columns filled with non-spherical particles also display the overshoot in weight observed with spherical grains, but now the compressive forces responsible for the reverse Janssen behavior are restricted to a narrower range in depth; we argue that packing effects are behind the quantitative differences between spherical to non-spherical grains.

[1] S. Mahajan, M. Tennenbaum, S.N. Pathak, D. Baxter, X. Fan, P. Padilla, C. Anderson, A. Fernandez-Nieves, and M.P. Ciamarra *Phys. Rev. Lett.* **124**, 128002 (2020).

Discovering dynamic laws from observations: the case of self-propelled, interacting colloids

Miguel Ruiz-Garcia[1], **C. Miguel Barriuso Gutierrez**[2,*], Lachlan C. Alexander[3], Dirk G. A. L. Aarts[3], Luca Ghiringhelli[4], Chantal Valeriani[2]

[1] *Department of Mathematics, Universidad Carlos III de Madrid, Avenida de la Universidad 30, 28911 Leganés, Spain.* [2] *Departamento de Estructura de la Materia, Física Térmica y Electrónica, Universidad Complutense de Madrid, 28040 Madrid, Spain.* [3] *Department of Chemistry, Physical and Theoretical Chemistry Laboratory, University of Oxford, South Parks Road, Oxford OX1 3QZ, United Kingdom.* [4] *IRIS Adlershof, Humboldt-Universität zu Berlin, Zum Großen Windkanal 6, 12489 Berlin, Germany.*

*e-mail: carbarri@ucm.es

Active matter spans a wide range of time and length scales, from groups of cells and synthetic self-propelled particles to schools of fish, flocks of birds, or even human crowds. The theoretical framework describing these systems has shown tremendous success at finding universal phenomenology. However, further progress is often burdened by the difficulty of determining the forces that control the dynamics of the individual elements within each system. Accessing this local information is key to understanding the physics dominating the system and to create the models that can explain the observed collective phenomena. In this work, we present a machine-learning model, a graph neural network based on [1], that uses the collective movement of the system to learn the active and two-body forces controlling the individual dynamics of the particles. We verify our approach using numerical simulations of active brownian particles, considering different interaction potentials and levels of activity. Finally, we apply our model to experiments of electrophoretic Janus particles, extracting the active and two-body forces that control the dynamics of the colloids. Due to this, we can uncover the physics dominating the behavior of the system. We extract an active force that depends on the electric field and also area fraction. We also discover a dependence of the two-body interaction with the electric field that leads us to propose that the dominant force between these colloids is a screened electrostatic interaction with a constant length scale. We expect that this methodology can open a new avenue for the study and modeling of experimental systems of active particles.

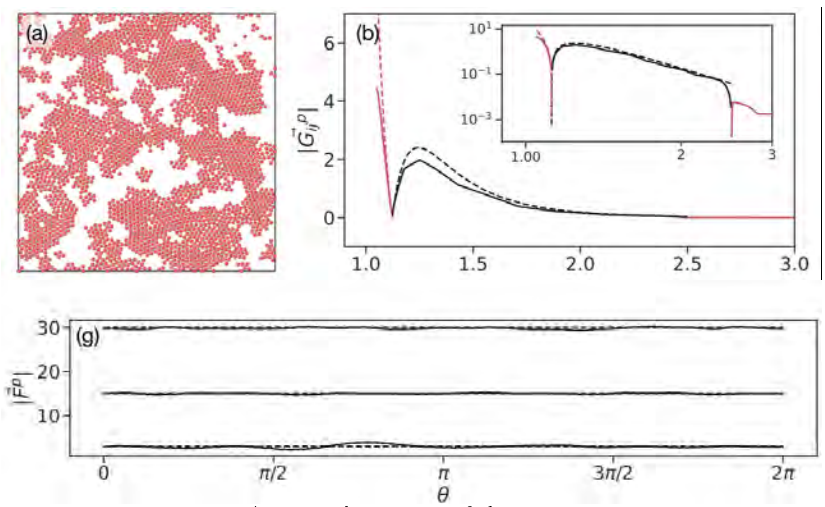

Figure 2. Average cluster size of damaging events in liquid water as a function of the distance from the ion track for different values of the carbon-ion energy.

[1] M. Cranmer, A. Sanchez Gonzalez, P. Battaglia, R. Xu, K. Cranmer, D. Spergel, and S. Ho, *Advances in Neural Information Processing Systems* **33**, 17429 (2020).

Ultrastable glasses: going very deep into the energy landscape of glasses

Manuel Moratalla[1], Marta Rodríguez-López[2], Cristian Rodríguez-Tinoco[2], Javier Rodríguez-Viejo[2], Rafael Jiménez-Riobóo[3], **Miguel A. Ramos**[1,4,*]

[1]*Departamento de Física de la Materia Condensada, Instituto "Nicolás Cabrera", Universidad Autónoma de Madrid, 28049 Madrid, Spain.* [2]*Departamento de Física, Facultat de Ciències, Universitat Autònoma de Barcelona, and Catalan Institute of Nanoscience and Nanotechnology (ICN2), 08193 Bellaterra, Spain.* [3]*Instituto de Ciencia de Materiales, Consejo Superior de Investigaciones Científicas (CSIC), 28049 Madrid, Spain.* [4]*Condensed Matter Physics Center (IFIMAC), Universidad Autónoma de Madrid, 28049 Madrid, Spain.*

*e-mail: miguel.ramos@uam.es

Already in 1948 Kauzmann pointed out [1] that the configurational entropy of many supercooled liquids, obtained from their specific heat, extrapolated to negative values below a critical "Kauzmann temperature" T_K. This entropy crisis or "Kauzmann paradox" has led many authors to speculate on the possible existence of an "ideal glass" which should correspond to the best and most stable glass achievable, associated with the lowest relative minimum within the potential energy landscape of the substance (see Fig. 1). This ideal glass would have zero configurational entropy, equal to that of crystals, and has been associated to the possible existence of an underlying thermodynamic glass transition occurring at T_K.

In the last years, the existence of glasses with very high thermodynamic and kinetic stability has been realized experimentally. So-called *ultrastable glasses*, usually prepared through physical vapor deposition (PVD) under optimized deposition rates and temperatures, represent a unique class of materials with low enthalpies and high kinetic stabilities [2]. These glasses show remarkable physico-chemical properties, such as high thermal stability or improved mechanical and thermodynamic behavior, offering unprecedented opportunities for practical applications, as well as to understand many aspects of the glassy state.

Specifically, it is well known that glasses exhibit thermal, vibrational and acoustic properties at low temperatures anomalously different from those found in crystalline solids, and with a striking degree of universality. The question has naturally arisen as whether these peculiar low-temperature "glassy anomalies" persist or vanish in these highly-stable glasses. Interestingly, our earlier low-temperature specific-heat measurements on (highly anisotropic) ultrastable glasses of indomethacin [3] prepared by PVD showed the suppression of the ubiquitous linear term below 1–2 K traditionally ascribed to the existence of tunneling two-level systems (TLS) in glasses. This finding apparently challenged the opposite behaviour found in hyperaged glasses of geological amber [4]. To shed more light on this controversial issue, we will present very recent, unpublished results of low-temperature specific heat on a different ultrastable glass, TPD, whose degrees of anisotropy and stability can be controlled.

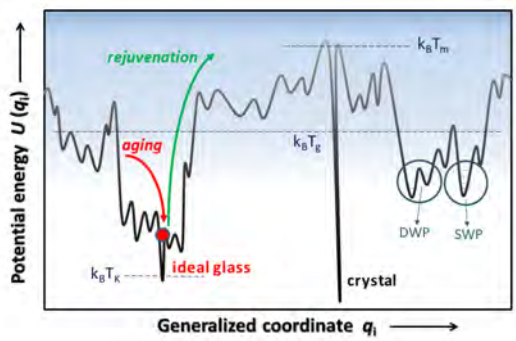

Figure 1. Schematic projection of the potential energy landscape of a substance, ranging from the supercooled liquid state below the melting temperature T_m, through the glass transition temperature T_g, down to the solid states at lower temperatures. Possible aging or rejuvenation processes are depicted. DWP and SWP refer to expected double or single well potentials, respectively, which are relevant for the low-temperature properties of glasses.

[1] W. Kauzmann, *Chem. Rev.* **43**, 219 (1948).
[2] C. Rodríguez-Tinoco, M. González-Silveira, M. A. Ramos, J. Rodríguez-Viejo, *Riv. Nuovo Cim.* (2022). https://doi.org/10.1007/s40766-022-00029-y
[3] T. Pérez-Castañeda, C. Rodríguez-Tinoco, J. Rodríguez-Viejo, M. A. Ramos, *Proc. Natl. Acad. Sci.* **111**, 11275 (2014).
[4] T. Pérez-Castañeda, R. J. Jiménez-Riobóo, M. A. Ramos, *Phys. Rev. Lett.* **112**, 165901 (2014).

Casimir contribution to the interfacial Hamiltonian for 3D wetting

Alessio Squarcini[1], **José M. Romero-Enrique**[2,*], Andrew O Parry[3]

[1]*Institut für Theoretische Physik, Universität Innsbruk, Innrain 52, 6020 Innsbruck , Austria.* [2]*Departmento de Física Atómica, Molecular y Nuclear, Universidad de Sevilla, Avenida Reina Mercedes s/n, 41012 Sevilla (España),* [3]*Department of Mathematics, Imperial College London, South Kensington Campus, London SW7 2AZ.*

*e-mail: enrome@us.es

Previous treatments of three-dimensional (3D) short-ranged wetting transitions [1-6] have missed an entropic or low temperature Casimir contribution to the binding potential describing the interaction between the unbinding interface and wall. This we determine by exactly deriving the interfacial model for 3D wetting from a more microscopic Landau-Ginzburg-Wilson Hamiltonian [7]. The Casimir term changes the interpretation of fluctuation effects occurring at wetting transitions so that, for example, mean-field predictions are no longer obtained when interfacial fluctuations are ignored. While the Casimir contribution does not alter the surface phase diagram [1], it significantly increases the adsorption near a first-order wetting transition and changes completely the predicted critical singularities of tricritical wetting [8], including the non-universality occurring in 3D arising from interfacial fluctuations. Using the numerical nonlinear renormalization group [8] we show that, for critical wetting, the asymptotic regime is extremely narrow with the growth of the parallel correlation length characterised by an effective exponent in quantitative agreement with Ising model simulations, resolving a longstanding controversy.

[1] H. Nakanishi and M. E. Fisher, *Phys. Rev. Lett.* **49**, 1565 (1982).
[2] F. P. Buff, R. A. Lovett, and F. H. Stillinger, *Phys. Rev. Lett.* **15**, 621 (1965).
[3] A. O. Parry, J. M. Romero-Enrique, and A. Lazarides, *Phys. Rev. Lett.* **93**, 086104 (2004).
[4] A. O. Parry, C. Rascón, N.R.Bernardino, and J.M. Romero-Enrique, *Phys. Rev. Lett.* **100**, 136105 (2008). Erratum: *Phys. Rev. Lett.* **100**, 259902 (2008).
[5] A. O. Parry,C. Rascón, N. R. Bernardino, and J. M. Romero-Enrique, *J. Phys.: Condens. Matter* **18**, 6433 (2006).
[6] J. M. Romero-Enrique, A. Squarcini, A. O. Parry, and P. M. Goldbart, *Phys. Rev. E* **97**, 062804 (2018).
[7] A. Squarcini, J. M. Romero-Enrique, and A. O. Parry, accepted in *Phys. Rev. Lett.* (2022).
[8] C. J. Boulter and F. Clarysse, *EPJE* **5**, 465 (2001).
[9] R. Lipowsky and M. E. Fisher, *Phys. Rev. B* **36**, 2126 (1987).

Magnetic colloids adsorbed at fluid interfaces acting as interfacial swimmers and colloid adsorption probes

F. Martínez-Pedrero[1], José Martín-Roca[2], Francisco Ortega[1,3], Chantal Valeriani[2], Carles Calero[4], Ramón G. Rubio[1,3]

[1]*Departamento de Química Física, Facultad de Ciencias Químicas, Universidad Complutense de Madrid, Spain.*
[2]*Departamento de Estructura. de la Materia, Física Térmica y Electrónica, Universidad Complutense de Madrid, Spain.*
[3]*Instituto Multidisciplinar, Universidad Complutense de Madrid.* [4]*Departament de Física de la Matèria Condensada, Universitat de Barcelona, Spain.*

*e-mail: fernandm@ucm.es

Due to the large surface energy reduction linked to the adsorption of colloids at a fluid interface, these nano- microparticles are often used as stabilizing units in the formation of highly stable complex interfacial fluids, Pickering emulsions, foams and colloidosomes [1]. In addition, they act as probes in the characterization of interfacial microrheological properties or as model systems in the study of different phenomena, ranging from the study of 2D phase transitions to transport in the low Reynolds number regime under confined geometries [2, 3]. In this presentation, we will show how magnetic microparticles suspended in aqueous solutions can be accurately transported at the fluid interface by developing Stokesian and non-Stokesian strategies. In Stokesian designs, magnetic particles are dynamically assembled on interfacial micromotors or conveyor belts, which are driven by remotely controlled generation of local hydrodynamic flows [4, 5], while in non-Stokesian counterparts, adsorbed and non-adsorbed particles are driven by itinerant magnetic potentials generated by lattices or rails of adsorbed colloids [4, 6]. In the last part of this talk, we will show how tracking the rotational-translational mechanism undergone by these particles, when under the influence of a rotating field, yields information on the kinetics and dynamics of particle adsorption in the presence of electrolytes or anionic and cationic surfactants [7].

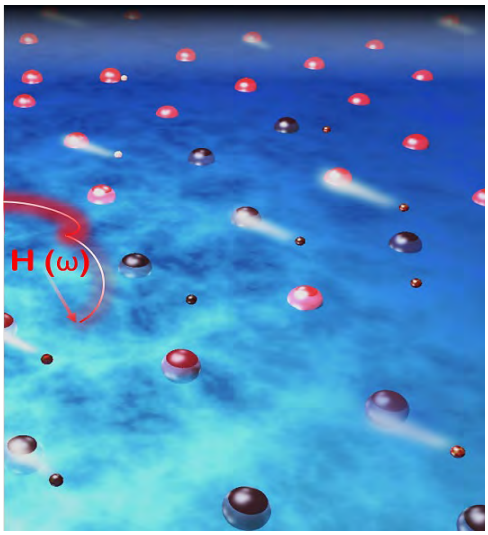

Figure 1. Small microparticles adsorbed at a fluid interface are transported through a lattice of larger spheres, in a practically deterministic motion, by periodically inverting the vertical component of a precessing field.

[1] E. Guzmán, F. Martínez-Pedrero, C. Calero, A. Maestro, F. Ortega, R.G. Rubio *Advances in Colloid and Interface Science*, **302**, 102620 (2022).
[2] S. Q. Choi, S. Steltenkamp, J. A. Zasadzinski, T. M. Squires, *Nature Communications* **2**, 312 (2011).
[3] K. Zahn, R. Lenke, G. Maret, *Physical review letters* **82**, 2721 (1999).
[4] A: Mateos-Maroto, F. Ortega, R.G. Rubio, C. Calero, F. Martínez-Pedrero, *Physical Review Applied* **16**, 064045 (2021).
[5] F. Martínez-Pedrero, A. González-Banciella, A. Camino, A. Mateos-Maroto, F. Ortega, R.G. Rubio, I. Pagonabarraga, C. Calero. *Small* **17**, 2101188 (2021).
[6] F. Martínez-Pedrero, F. Ortega, R.G. Rubio, C. Calero *Advanced Functional Materials* **30**, 2070333 (2020).
[7] J. Martín-Roca, M. Jiménez, F. Ortega, C. Calero, Ch. Valeriani, R.G. Rubio, F. Martínez-Pedrero, *Journal of Colloid and Interface Science*, 614, 378 (2022).

Trapping active particles up to the limiting case: bacteria enclosed in a biofilm

Chantal Valeriani

Departamento de Estructura de la Materia, Fisica termica y Electronica, Universidad Complutense de Madrid, Spain.

e-mail: cvaleriani@ucm.es

Active matter systems are composed of constituents, each one in nonequilibrium, that consume energy in order to move [1]. A characteristic feature of active matter is collective motion leading to nonequilibrium phase transitions or large scale directed motion [2]. A number of recent works have featured active particles interacting with obstacles, either moving or fixed [3,4,5]. When an active particle encounters an asymmetric obstacle, different behaviours are detected depending on the nature of its active motion. On the one side, rectification effects arise in a suspension of run-and-tumble particles interacting with a wall of funnelled-shaped openings, caused by particles persistence length [6]. The same trapping mechanism could be responsible for the intake of microorganisms in the underground leaves [7] of Carnivorous plants [8]. On the other side, for aligning particles [9] interacting with a wall of funnelled-shaped openings, trapping happens on the (opposite) wider opening side of the funnels [10,11]. Interestingly, a cylindrical confinement considerably modulates the swimming features of an active colloidal swimmer [12], with respect to the colloid in bulk.

Active particles can be synthetic (such as synthetic active colloids) or alive (such as living bacteria). A prototypical model to study living microswimmers is P. fluorescens, a rod shaped and biofilm forming bacterium. Biofilms are microbial communities self-assembled onto external interfaces. Biofilms can be described within the Soft Matter physics framework [13] as a viscoelastic material consisting of colloids (bacterial cells) embedded in a cross-linked polymer gel (polysaccharides cross-linked via proteins/multivalent cations), whose water content vary depending on the environmental conditions. Bacteria embedded in the polymeric matrix control biofilm structure and mechanical properties by regulating its matrix composition. We have recently monitored structural features of Pseudomonas fluorescens biofilms grown with and without hydrodynamic stress [14,15]. Bacteria are capable of self-adapting to hostile hydrodynamic stress by tailoring the biofilm chemical composition, thus affecting both the mesoscale structure of the matrix and its viscoelastic properties that ultimately regulate the bacteria-polymer interactions [16].

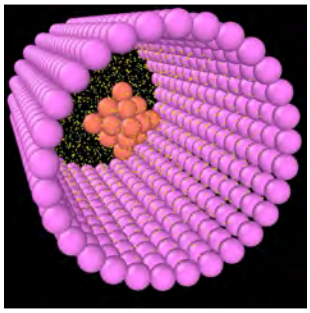

Figure 1. Active colloid in a cylindrical confinement.

[1] C. Bechinger et al., *Rev. Mod. Phys.* **88**, 045006 (2016).
[2] T. Vicsek, A. Zafeiris, *Phys. Rep.* **517**, 71 (2012).
[3] C. Bechinger et al., *Reviews of Modern Physics* **88**, 045006 (2016)
[4] R Martinez, F Alarcon, DR Rodriguez, JL Aragones, C Valeriani, *EPJ E* **41** 1 (2018).
[5] DR Rodriguez, F Alarcon, R Martinez, J Ramírez, C Valeriani, *Soft matter* **16**, 1162 (2020).
[6] C. O. Reichhardt and C. Reichhardt, *Annual Review of Condensed Matter Physics* **8**, 51 (2017).
[7] W Barthlott, S Porembski, E Fischer, B Gemmel, *Nature* **392**, 447 (1998).
[8] C B. Giuliano, R Zhang, R.Martinez Fernandez, C.Valeriani and L.Wilson (in preparation, 2022).
[9] R Martinez, F Alarcon, JL Aragones, C Valeriani, *Soft matter* **16**, 4739 (2020).
[10] P. Galajada, J. Keymer, P. Chaikin and R.Austin, *Journal of Bacteriology* **189**, 8704 (2007).
[11] M. Wan, C.O. Reichhardt, Z. Nussinov, and C. Reichhardt, *Physical Review Letters* **101**, 018102 (2008).
[12] C Miguel Barriuso Gutierrez, J Martin-Roca, V Bianco, I Pagonabarraga, C Valeriani, *arxiv* (2022).
[13] J N. Wilking , T E. Angelini , A Seminara , M P. Brenner , and D A. Weitz *MRS Bulletin* **36** 385 (2011).
[14]J Jara, F Alarcón, A K Monnappa, J Ignacio Santos, V Bianco, P Nie, M Pica Ciamarra, A Canales, L Dinis, I López-Montero, C Valeriani, B Orgaz, *Frontiers in Microbiology* **11**, 3460 (2021).
[15] P Nie, F Alarcon, I López-Montero, B Orgaz, C Valeriani, M Pica Ciamarra, *Soft Material* **0 1**, (2021).
[16] J Martin Roca, V Bianco, F Alarcon, A K. Monnappa, P Natale, F Monroy, B Orgaz, I Lopez-Montero, C Valeriani, *arxiv* (2022).

MIPS and Activity Cycles in Fire Ants

Caleb Anderson[1,2,*], Alberto Fernandez-Nieves[2,3]

[1]*Department of Physics, Georgia Institute of Technology, USA.*
[2]*Department of Condensed Matter Physics, University of Barcelona, Spain.*
[3]*ICREA-Institució Catalana de Recerca i Estudis Avançats, Spain.*

*e-mail: caleb91.13@gmail.com

Since its origin in the studies of bird flocks in the 1990's [1], active matter theory has sought to understand the behaviours of a broad class of systems that have energy added and dissipated at the single particle level [2]. In fact, most biological systems can be considered active systems, from schools of fish to intercellular fluids. Great strides have been made in understanding and predicting common features of these systems, such as collective motion, which is the tendency of local alignment interactions to lead to system-wide symmetry breaking, even in 2D [3], and motility induced attraction and phase separation, which is the tendency for motility effects to lead to the formation of dense stationary clusters in the absence of local alignment [4]. As the field has evolved, more and more remarkable predictions of active matter theory have been tested and proven in synthetic systems, which have the advantage of simpler interactions compared to the biological systems that originally launched the field. However, active matter theory's broadest impact likely remains in the study of biological systems. Here we seek to understand the crowd dynamics of *Solenopsis Invicta*, fire ants, which are social insects with complex interactions, within the framework of active matter.

We begin by studying the nature of interactions between pairs of ants, and show that one of the dominant effects in low-density groups of ants is motility-induced attraction. When the density of ants is increased, attraction can eventually lead to phase separation, such that the ants form dense, long-lasting clusters of stationary ants surrounded by a background of moving ants.

As we continue to increase the density of ants in our cells, the ants begin to exhibit spontaneous bursts of high activity, called activity cycles. While in an activity cycle, motility effects become less important in the crowd dynamics.

We show that the result of the suppression of motility effects is that the ants can now exhibit collective motion, which in large vertical columns, leads to the formation of spontaneous waves (Figure 2). The ants in the wave exhibit collective motion that is switched on and off not via density or rotational noise, as it has been in theory and experiments so far. Instead, local changes in the activity of the ants necessarily leads to alignment and propagates an "activity wave".

[1] Vicsek, T., et al., Novel Type of Phase Transition in a System of Self-Driven Particles, *Physical Review Letters* **75**, 1226 (1995).
[2] Marchetti, M. C., et al. Hydrodynamics of Soft Active Matter, *Reviews of Modern Physics* **85**, 1143 (2013).
[3] Toner, J. & Tu, Y. Long-Range Order in a Two-Dimensional Dynamical XY-Model: How Birds Fly Together, *Physical Review Letters* **75**, 4326 (1995).
[4] Cates, M. E. and Tailleur, J., Motility-Induced Phase Separation, *Annual Reviews of Condensed Matter Physics* **6**, 219 (2015).

Collapse of magnetite-decorated pNIPAM microgels trapped with optical tweezers

Sergio Orozco-Barrera[1], Miguel Ángel Fernández-Rodríguez[1,2], **Raúl A. Rica**[1,*]

[1] *Nanoparticles Trapping Laboratory, Department of Applied Physics, Universidad de Granada, Av. Fuentenueva s.n., 18071 Granada, Spain.*

[2] *Laboratory of Surface and Interface Physics, Department of Applied Physics, Universidad de Granada, Av. Fuentenueva s.n., 18071 Granada, Spain.*

*e-mail: rul@ugr.es

Microgels are versatile nanoparticles composed of crosslinked hydrogels which typically exhibit thermo-responsiveness. They are extensively used in applications that make use of their softness and ability to be swollen in an aqueous phase, e.g. as drug carriers or Pickering emulsion stabilizers [1]. In these applications, the systems inherit the thermo-responsiveness of the microgels [1,2]. Therefore, it is critical to understand the way in which the microgels collapse upon heating above their lower critical solution temperature (around 32 °C for pNIPAM and pVCL microgels). There is an open debate around the way in which this collapse happens, whether it is a first order transition. In fact, the usual diameter vs temperature plots produced by dynamic light scattering seem to hint to more complex transition phenomena [3,4]. In the present study, we use optical tweezers [5] to trap single microgels and measure this collapse upon self-heating in pure water and in the presence of conductive salts. The self-heating is achieved decorating the microgels with magnetite nanocubes that absorb radiation from the trapping laser (see Fig. 1). We find interesting features, such as partial collapses which produce bistable trapping dynamics, and collapses that seem to hint to a first order transition.

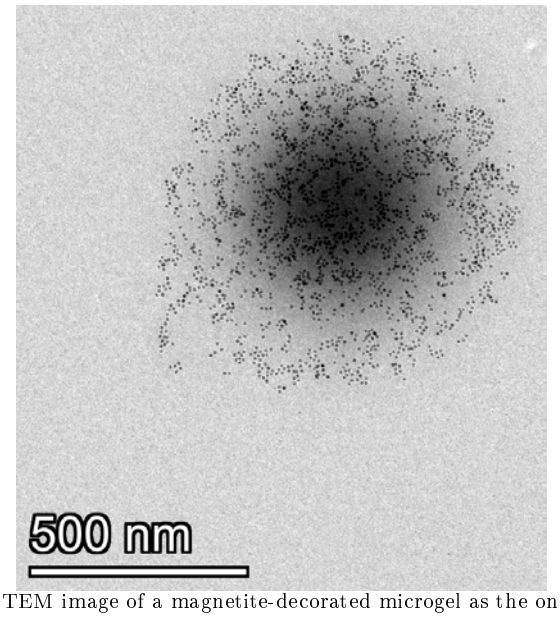

Figure 1. TEM image of a magnetite-decorated microgel as the ones we trap with optical tweezers.

[1] M.A. Fernandez-Rodriguez, A. Martin-Molina, & J. Maldonado-Valderrama, *Advances in Colloid and Interface Science* **288**, 102350 (2021).

[2] I. Navarro Arrebola, L. Billon, & G. Aguirre, *Advances in Colloid and Interface Science* **287**, 102333 (2021).

[3] R. Keidel *et al.*, *Science Advances* **4**, eaao7086 (2018).

[4] S. Bocheneck *et al.*, *Langmuir* **35**, 16780–16792 (2019).

[5] J. Gieseler *et al.*, *Advances in Optics and Photonics* **13**, 74–241 (2021).

Acknowledgements: The Authors acknowledge financial support from FEDER/Junta de Andalucía-Consejería de Transformación Económica, Industria, Conocimiento y Universidades/ Proyecto P18-FR-3583. MAFR acknowledges financial support from the project PID2020-116615RA-I00 and grant IJC2018-035946-I funded by MCIN/AEI/10.13039/501100011033.

Phase behaviour and dynamics of colloidal cuboids: paving the path to biaxial nematic liquid crystals

E. M. Rafael[1], L. Tonti[1], D. Corbett[1], A. Cuetos[2], **A. Patti**[1,3,*]

[1] *Department of Chemical Engineering, The University of Manchester, Manchester M13 9PL, UK.*
[2] *Department of Physical, Chemical and Natural Systems, Pablo Olavide University, 41013 Seville, Spain.*
[3] *Department of Applied Physics, University of Granada, 18071 Granada, Spain.*

*e-mail: apatti@ugr.es

Colloidal cuboids have an especially rich phase behaviour [1, 2] and the potential to self-assemble into biaxial nematic (N_B) liquid crystals [3]. Over the last few decades, several theoretical works have predicted the existence of a wide region of the phase diagram where biaxial nematics would be stable, but imposed rather strong constraints on the particle rotational degrees of freedom, which artificially enhance the stability of the N_B phase [4, 5, 6].

In this contribution, we present molecular simulation results that clarify the relevance of fully unfreezing the rotational degrees of freedom to accurately determine the range of stability of the N_B phase. Our results show that only a large size dispersity or the presence of an external field can induce the formation of thermodynamically stable biaxial nematics [7, 8]. In particular, surprisingly weak field strengths are able to spark a uniaxial-to-biaxial phase transition at the self-dual shape, where prolate and oblate geometries fuse into one, suggesting a path to exploit low-energy uniaxial-to-biaxial order switching.

Motivated by this scenario, we have also simulated the unsteady-state reorientation dynamics when a field is applied (uniaxial-to-biaxial switching) and then removed (biaxial-to-uniaxial switching) [9]. We detected a strong correlation between the response time, being the time taken for the system to reorient, and particle anisotropy, which spans from rod-like to plate-like geometries. Interestingly, self-dual shaped cuboids, theoretically considered as the most suitable to promote phase biaxiality for being exactly in between prolate and oblate particles, exhibit surprisingly slow response times.

[1] A. Cuetos, M. Dennison, A. Masters, A. Patti, *Soft Matter* **13**, 4720 (2017).
[2] A. Patti and A. Cuetos, *Mol. Simul.* **44**, 516 (2018).
[3] E. van den Pol, A. Petukhov, D. Thies-Weesie, D. Byelov, G. Vroege, *Phys. Rev. Lett.* **103**, 258301 (2009).
[4] M. P. Taylor and J. Herzfeld, *Phys. Rev. A* **44**, 3742 (1991).
[5] S. Belli, A. Patti, M. Dijkstra, R. van Roij, *Phys. Rev. Lett.* **107**, 148303 (2011).
[6] Y. Martínez-Ratón, S. Varga, E. Velasco, *Phys. Chem. Chem. Phys.* **13**, 13247 (2011).
[7] A. Cuetos, E. M. Rafael, D. Corbett, A. Patti, *Soft Matter* **15**, 1922 (2019).
[8] E. M. Rafael, A. Cuetos, D. Corbett, A. Patti, *Soft Matter* **16**, 5565 (2020).
[9] E. M. Rafael, L. Tonti, D. Corbett, A. Cuetos, A. Patti, *Phys. Fluids* **33**, 067115 (2021).

Acknowledgements: E.M.R. acknowledges the Malaysian Government Agency *Majlis Amanah Rakyat* for funding his Ph.D. at the University of Manchester. A.P. and L.T. acknowledge the Leverhulme Trust Research Project Grant RPG-2018-415, the assistance given by Research IT and the use of the Computational Shared Facility at The University of Manchester. A.C. acknowledges the Spanish Ministerio de Ciencia, Innovación y Universidades and FEDER for funding (Project No. PGC2018–097151-B-I00) and C3UPO for the HPC facilities provided. A.P. is supported by a "Maria Zambrano Senior" distinguished researcher fellowship, financed by the European Union within the NextGenerationEU program.

Nematics in 3-tori: Doubly twisted structures and defect-populated configurations

Javier Rojo-González[1,*], Alexis de La Cotte[1], Alberto Fernández-Nieves[1,2]

[1]*Departament de Física de la matèria condensada, Universitat de Barcelona, 08028, Barcelona, España.*
[2]*ICREA-Institució Catalana de Recerca i Estudis Avançats, 08010, Barcelona, España.*

*e-mail: j.rojo@ub.edu

Nematic liquid crystals are partially ordered fluids characterized by an apolar vector field, called director, that represents the average orientation of its anisotropic building blocks. Confining a nematic liquid crystal can frustrate its order, leading necessarily to the presence of topological defects which are regions where the alignment is not defined. Each topological defect can be characterized by a quantity called topological charge. Mathematically, the Poincaré-Hopf index theorem relates the total topological charge to the confining topology [1]. For instance, a 2-sphere must have a total topological charge of +2, so that the presence of defects is mathematically required.

In the case of the 2-torus, the total topological charge must be equal to 0, and thus defect free configurations of the material are allowed. In prior experimental work in our group, we filled a 3-torus with a nematic liquid crystal and found spontaneous chiral symmetry breaking without defects [2]. In this talk, we will report on alternative configurations populated by defects. Those appear as s=±1 pairs, with the s=+1 and s=-1 defects most often located in regions of positive and negative Gaussian curvature respectively. There are, however, other defect structures we observe.

[1] H. Hopf, *Math. Ann.* **96**, 209 (1926).
[2] E. Pairam et al, *Proceedings of the national academy of sciences* **110**, 9295 (2013).

Collective behaviour of energy depot repulsive particles

Juan Pablo Miranda[1,2,*], Demian Levis[1,3], Chantal Valeriani[2,4]

[1] *Departament de Física de la Matèria Condensada, Universitat de Barcelona, Martí Franquès 1, 08028 Barcelona, Spain.* [2] *Departamento de Estructura de la Materia, Física Térmica y Electrónica, Universidad Complutense de Madrid, 28040 Madrid, Spain.* [3] *UBICS University of Barcelona Institute of Complex Systems, Martí Franquès 1, 08028 Barcelona, Spain.* [4] *GISC-Grupo Interdisciplinar de Sistemas Complejos, 28040 Madrid, Spain*

*e-mail: juanpami@ucm.es

In this work we consider an active particle model, that reproduces the motion of microscopic biological objects, such as cells or bacteria, that is described with Langevin dynamics. The particles are able to take energy from their environment, store it into an internal energy depot and convert it into kinetic energy [1]. This model uses a velocity dependant friction function [2]. We have studied a two dimensional suspension of repulsive particles, where the interaction between the particles is implemented with a WCA potential.

$$\dot{\mathbf{v}} = -\gamma(\mathbf{v})\mathbf{v} - \frac{1}{m}\boldsymbol{\nabla} U(\mathbf{r}) + \mathcal{F}(t)\ , \quad \gamma(\mathbf{v}) = \gamma_0 - \frac{q_0 d_2}{c + d_2 \mathbf{v}^2}.$$

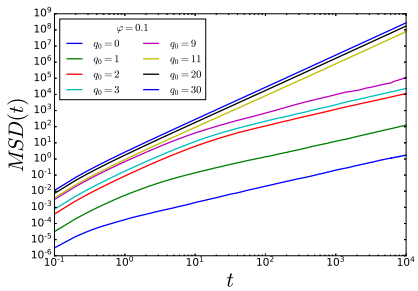

Figure 1. Mean squared displacement over time for different systems of $\varphi = 0.1$ and different values of q_0.

The parameters q_0, d_2 and c express the properties of the energy depot. We have studied both dynamical and structural features of the system. The pump rate of energy from the environment into the internal depot is q_0. d_2 is The rate of conversion of the internal depot energy to the particles kinetic energy, this implies that the particle is self propelling. c represents the internal dissipation, which takes into account the energy loss due to intern dissipative processes. In our study we fix the parameters d_2, and c, and we study the effect of different q_0 values.

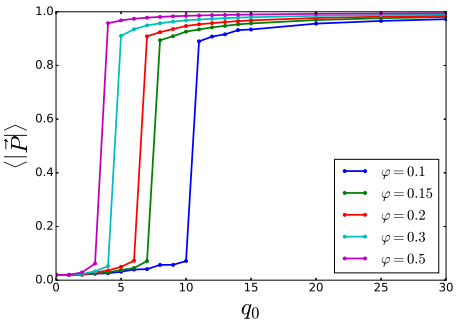

Figure 2. a) Mean polar order parameter as a function of q_0 parameter for the studied volume fractions φ.

The friction function will cancel at some velocity v_0, $\mathbf{v}_0^2 = \frac{q_0}{\gamma_0} - \frac{c}{d_2}$, this imposes two regimes onto the system; when $\mathbf{v} > \mathbf{v}_0$ the friction will be positive and the motion is damped. When $\mathbf{v} < \mathbf{v}_0$ we have negative friction, meaning that the motion of the slow particles is pumped as if the particles had an additional source of energy.

So far we have studied the diffusion through the mean squared displacement, finding different regimes as we increase q_0 (Fig.1). The main studied structural feature is a phase transition between an ordered an a disordered state for different volume fractions φ and values of q_0 (Fig.2).

The interest of this model comes from the fact that its able to mimic several properties of the biological microscopic matter, as self propulsion, collective motion or out of equilibrium phase transitions.

The interest in the model comes from the difference from other models such as Vicsek's or Active Brownian Particles, that address self-propulsion as a random process, while here the friction is the cause of this phenomenon.

[1] Schweitzer, F., Ebeling, W., & Tilch, B., *Physical Review Letters* **80(23)**, 5044 (1998).
[2] Erdmann, U., Ebeling, W., Schimansky-Geier, L., & Schweitzer, F., *The European Physical Journal B-Condensed Matter and Complex Systems* **15(1)**, 105-113 (2000).

Dynamics of hard particles confined by an isotropic harmonic potential

M. I. García de Soria[1,2,*], P. Maynar[1,2], E. Trizac[3], and D. Guéry-Odelin[4]

[1]*Área de Física Teórica, Universidad de Sevilla, Spain.* [2] *Institute for Theoretical and Computational Physics, Universidad de Granada, Spain.* [3] *LPTMS, Université Paris-Saclay, France.* [4] *Laboratoire Collisions, Agrégats, Réactivité, Université de Toulouse, France.*

*e-mail: gsoria@us.es

The dynamics of a system composed of elastic hard particles confined by an isotropic harmonic potential is studied. In the low-density limit, the dynamics is described by the Boltzmann equation and the system does not reach equilibrium except for some particular class of initial conditions. On the contrary, the system reaches a periodic in time state in which the velocity distribution function is Gaussian, but with the hydrodynamic fields oscillating in time with some specific profiles. It is shown that this so-called *breather* state is completely specified by the constants of the motion, the mean square displacement, $\langle r^2 \rangle$, at the initial time and its derivative with respect to time also at the initial time. This is due to the fact that, at this level of description, $\langle r^2 \rangle$ verifies a closed second order differential equation. For low but finite densities, the dynamics of the system is analyzed by taking into account the finite size of the particles. Under well-controlled approximations, a closed evolution equation for $\langle r^2 \rangle$ is derived, obtaining that it decays to its equilibrium value, oscillating with a frequency slightly modified with respect to the Boltzmann values. The time average of the oscillations is also renormalized. An excellent agreement is found between Molecular Dynamics simulation results and the theoretical predictions for the frequency and the time average of the oscillations. For the relaxation time, the agreement is not as good as for the two previous quantities and the origin of the discrepancies is discussed.

Simulating active agents under confinement with Dissipative Particles (hydro)Dynamics

C. Miguel Barriuso Gutierrez[1], **José Martín-Roca**[1,3], Valentino Bianco[3], Ignacio Pagonabarraga[4] and Chantal Valeriani[1,2]

[1]*Dpto. de Estructura de la Materia, Física Térmica y Electrónica, Universidad Complutense de Madrid, 28040 Madrid, Spain.* [2]*GISC - Grupo Interdisciplinar de Sistemas Complejos 28040 Madrid, Spain.* [3]*Dpto. de Química Física, Facultad de Química - Universidad Complutense de Madrid, 28040 Madrid, Spain.* [4]*Departament de Física de la Matèria Condesada, Facultat de Física - Universitat de Barcelona, Carrer de Martí i Franquès, 1, 11, 08028 Barcelona, Spain*

In this ongoing work we are developing a framework to simulate active agents taking into account both hydrodynamics and thermal fluctuations. Currently we are limiting our study to colloids and polymers although the framework will be applicable to agents with a wide range of structures. To achieve this we propose an extension of the widely known simulation software LAMMPS [1] that allows the implementation of hydrodynamic self-propulsion via force redistribution among solvent particles, this extension, in combination with the Dissipative Particle Dynamics (DPD) package [2], enables these kind of simulations. Similar approaches using lattice Boltzmann (LB) methods [3] and Multi-Particle Collision dynamics (MPC) [4] have been already well studied. With DPD and MPC dynamics we can easily simulate agents with more complex shapes taking into account thermal fluctuations, both of which are harder to implement using LB methods. Our approach takes advantage of the versatility of the LAMMPS code, being MPI-parallelizable and allowing the combination of our implementation with the wide range of features LAMMPS offers.

We are interested in the subsets of active matter systems known as active colloids and active polymers, which have very useful and broad applications. Their collective behaviour is rich and complex, and in many cases cannot be ascribed solely to the agents motion: hydrodynamic interactions need to be taken into account . This is the case, for example, of many self-propelled microorganisms, or *microswimmers*, whose movement is an essential aspect of life. A successful model for this systems is the so-called *squirmer*, in their simplest form these are hard spheres that take into account the propulsion induced by the beating cilia and flagella as a prescribed steady velocity of the solvent particles tangential to the surface of the sphere. This model serves as inspiration for our project.

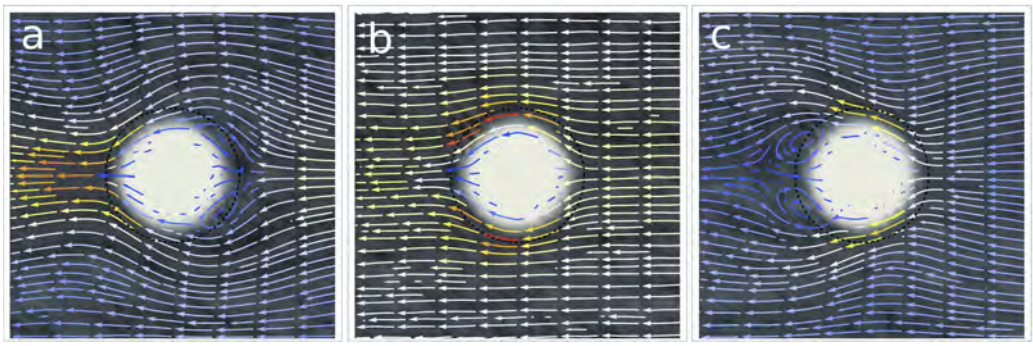

Figura 1: Solvent velocity field around a squirmer self-propelling in the positive x-axis in the colloid (left) and laboratory (right) reference frame, for $\beta = -5$ (*pusher*, left) and $\beta = 5$ (*puller*, right).

Referencias

[1] A. P. Thompson et al, Comp Phys Comm, **271** (2022) 10817.
[2] Groot and Warren, J Chem Phys, **107**, 4423-35 (1997)
[3] F. Alarcon, E. Navarro-Argemí, C. Valeriani, and I. Pagonabarraga, Phys. Rev. E **99**, 062602
[4] Zöttl, A., Stark, H. 2018, Simulating squirmers with multi-particle collision dynamics, *Eur. Phys. J. E* **41** 61

Nuevos retos en superconductividad

Presentaciones orales

Lunes 11/07:

15:30-16:00 José Lado (Aalto University). *Topological and nodal superconductivity in artificial van der Waals materials*

16:00-16:15 Miguel M. Ugeda (Donostia International Physics Center, Centro de Física de Materiales (CSIC-UPV-EHU) and Ikerbasque). *Observation of superconducting Leggett modes from competing pairing instabilities in single-layer NbSe2*

16:15-16:30 Edwin Herrera (Universidad Autónoma de Madrid). *Quantum-well states at the surface of the heavy fermion URu2Si2*

16:30-17:00 Flash Talks (Pósteres 1-9).

17:00-18:00 **Pósteres y café**.

18:00-18:15 Rosa López (Instituto de Física Interdisciplinar y Sistemas Complejos IFISC (CSIC-UIB)). *Surpassing the uncertainty thermodynamic relation in normal-superconductor quantum dots*

18:15-18:30 María José Calderón (Instituto de Ciencia de Materiales de Madrid, ICMM-CSIC). *Mott Correlations in Moiré Heterostructures*

18:30-18:45 Wen Wan (Donostia International Physics Center). *Nontrivial doping evolution of electronic properties in Ising-superconducting alloys*

18:45-19:00 Ramón Aguado (Instituto de Ciencia de Materiales de Madrid, ICMM-CSIC). *Quantum dot Josephson junction in a transmon circuit: a novel design for Andreev qubits*

19:00-19:15 Francisco Jesús Matute-Cañadas (Universidad Autónoma de Madrid). *Signatures of interactions in the Andreev spectrum of nanowire Josephson junctions*

19:15-19:30 Ángel Ibabe (Universidad Autónoma de Madrid). *Joule heating effects in hybrid superconductor-semiconductor nanowire devices*

Martes 12/07:

15:30-16:00 Anna Palau (Institut de Ciència de Materials de Barcelona, ICMAB-CSIC). *Nano-engineered high-temperature superconductors and hybrid systems for energy-efficient functional devices*

16:00-16:15 Akashdeep Kamra (Universidad Autónoma de Madrid). *Interfacial control of vortex-limited critical current in type II superconductor films*

16:15-16:30 Emma Campillo (Lund University). *Modelling of vortex core magnetization and Pauli paramagnetic effects*

16:30-17:00 Flash Talks (Pósteres 10-18).

17:00-18:00 **Pósteres y café**.

18:00-18:15 Antonella Meninno (Centro de Física de Materiales (CSIC-UPV/EHU) and University of the Basque Country). *Ab initio study of possible metastable occupation of tetrahedral sites in Palladium Hydride compounds*

18:15-18:30 Fabián A. Cuellar (Universidad Complutense de Madrid). *Extremely long range, high-temperature Josephson coupling across a half metalllic ferromagnet*

18:30-18:45 Jordi Picó-Cortés (Universität Regensburg and nstituto de Ciencia de Materiales de Madrid, ICMM-CSIC). *Non-equilibrium transport in Josephson junctions through interacting nanostructures*

18:45-19:00 Antonio Badía (Instituto de Nanociencia y Materiales de Aragón (INMA), CSIC-Universidad de Zaragoza). *Electromagnetic modelling in macroscopic superconductivity. Fundamentals and applications*

19:00-19:15 Enrique Villa Benito (Centro de Astrobiología CSIC-INTA). *Ti/Al bi-layer Kinetic Inductance Detector (BiKID) configuration for CMB experiments*

19:15-19:30 Fabian Sigloch (Instituto de Nanociencia y Materiales de Aragón (INMA), CSIC-Universidad de Zaragoza). *Large output voltage to magnetic flux change in nanoSQUIDs based on direct-write Focused Ion Beam Induced Deposition technique*

Pósteres

- Carlos Uriarte González (Universidad Rey Juan Carlos). *Design of a levitating system for the study of the superfluidity at ultra low temperatures*
- Rishav Harsh (Donostia International Physics Center, DIPC). *Superconducting dome by tuning through a van Hove singularity in a two-dimensional metal*
- César González-Ruano (Universidad Autónoma de Madrid). *Tuning magnetic anisotropies with superconductivity and spin-orbit interaction in epitaxial ferromagnet-superconductor hybrids*
- Aiswarya Kethamkuzhi (Institut de Ciència de Materials de Barcelona, ICMAB-CSIC). *Study of the overdoped state in TLAG grown YBCO thin films oxygenated with ozone*
- Marta Fernández-Lomana (Universidad Autónoma de Madrid). *Tunneling spectroscopy at very high magnetic fields in the iron based superconductor KFe2As2*
- Celia González Sánchez (Universidad Autñonoma de Madrid). *Towards hybrid van der Waals Josephson Junctions based on NbSe2*
- Jordi Alcalà (Institut de Ciència de Materials de Barcelona, ICMAB-CSIC). *Local modulation of the superconducting order parameter for energy-efficient functional devices based on fluxonic effects*
- Miguel Águeda (Universidad Autónoma de Madrid). *Superconducting gap and magnetoresistance of layered AuSn4*
- Gabriel Caballero (IMDEA Nanociencia). *Magneto-transport properties and anomalous Hall effect of superconductor/ferromagnetic heterostructures*
- Ignacio Figueruelo Campanero (IMDEA Nanociencia and Universidad Complutense). *Fabrication and characterization of the high-temperature superconductor* $Bi_2Sr_2CaCu_2O_8^+$ *for van der Waals heterostructures*
- Ana Parente (Universidad Complutense). *Low dimensional effects in superconducting nanostructures*
- Aleix Barrera (Institut de Ciència de Materials de Barcelona, ICMAB-CSIC). *Hybrid superconducting-ferromagnetic structures for sustainable functional devices*
- Mario Gómez (Universidad Autónoma de Madrid). *The Little-Parks effect in full-shell Al-InAs hybrid superconductor-semiconductor nanowire devices*
- Pablo García (Universidad Autónoma de Madrid). *Reduced size STM in high magnetic fields*
- David Rodríguez (Centro de Astrobiología CSIC-INTA). *High-quality factor NbTiN superconducting resonators for quantum technologies*
- Cristina García-Pérez (IMDEA Nanociencia). *Hybrid Superconducting Nanowire Single-Photon Detectors*
- Thomas Günkel (Institut de Ciència de Materials de Barcelona, ICMAB-CSIC). *Tuning the electronic structure of High-Temperature Superconducting films by field-induced oxygen diffusion*
- Raquel Sánchez-Barquilla (Universidad Autónoma de Madrid). *STM at high magnetic fields in the superconducting series FeSe1-xSx*

Topological and nodal superconductivity in artificial van der Waals materials

Viliam Vaňo, Somesh Chandra Ganguli, Mohammad Amini, Md N. Huda, Markus Aapro, Linghao Yan, Maryam Khosravian, Guangze Chen, Shawulienu Kezilebieke, **Jose L. Lado***, Peter Liljeroth

Department of Applied Physics, Aalto University, Espoo, Finland.

*e-mail: jose.lado@aalto.fi

Van der Waals materials have allowed realizing a variety of emergent quantum states, including magnetic, correlated, and superconducting states. Interestingly, the tunability of these materials provides an outstanding playground to engineer elusive states of matter typical of complex correlated quantum materials. Here we show that van der Waals materials provide a natural materials platform realizing topological moire superconductors [1] and nodal superconductivity [2]. First, we will discuss how CrBr3/NbSe2 heterostructures provide a platform for engineering moire topological superconductivity [1]. We demonstrate the twist between the two materials gives rise to a moire Yu-Shiba-Rusinov electronic structure. The moire pattern further allows to open up topological states in regions of the phase space that would otherwise be topologically trivial, leading to a topological superconducting state whose topological edge states inherit the moire length. Furthermore, we will show how ultraclean 1H-TaS2 monolayers realize a nodal topological superconductor with f-wave symmetry [2]. We demonstrate that in the presence of disorder, the nodal superconductor is driven to a conventional superconducting state as a direct consequence of the pair breaking effect of impurities in the nodal state. Furthermore, we show that, associated with the superconducting gap, strongly fluctuating many-body correlations emerge and discuss their potential role as the underlying pairing mechanism of the nodal state. Our results demonstrate the potential of van der Waals materials for realizing unconventional superconducting states, providing highly tunable platforms to explore exotic coherent states in quantum materials.

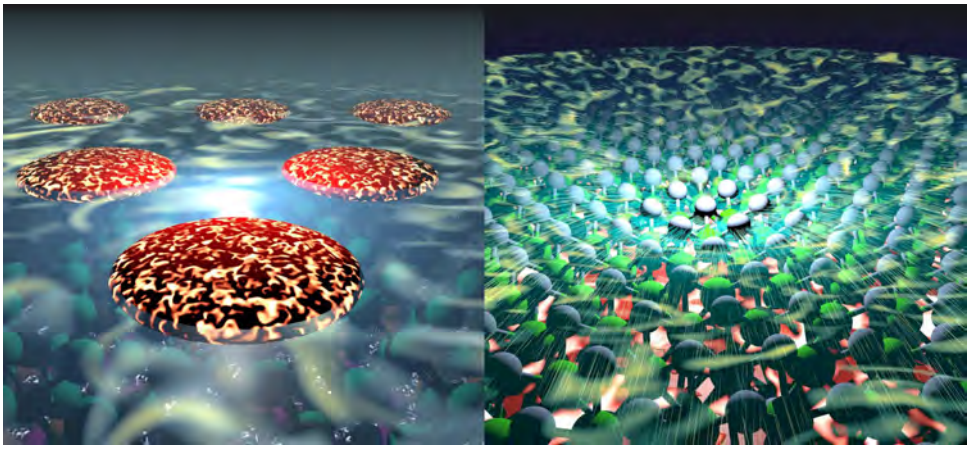

[1] Shawulienu Kezilebieke, Viliam Vaňo, Md N. Huda, Markus Aapro, Somesh C. Ganguli, Peter Liljeroth, and Jose L. Lado, *Nano Lett.* **22**(1) 328 (2022)
[2] Viliam Vaňo, Somesh Chandra Ganguli, Mohammad Amini, Linghao Yan, Maryam Khosravian, Guangze Chen, Shawulienu Kezilebieke, Jose L. Lado, Peter Liljeroth, arXiv:2112.07316 (2021).

Acknowledgements: We acknowledge financial support from Academy of Finland and from the Jane and Aatos Erkko Foundation.

Observation of superconducting Leggett modes from competing pairing instabilities in single-layer $NbSe_2$

Wen Wan[1], Paul Dreher[1], Daniel Muñoz-Segovia[1], Rishav Harsh[1], Francisco Guinea[1,2], Fernando de Juan[1,4], **Miguel M. Ugeda**[1,3,4,*]

[1]*Donostia International Physics Center (DIPC), Paseo Manuel de Lardizábal 4, 20018 San Sebastián, Spain.*
[2]*IMDEA Nanoscience, C/Faraday 9, 28049 Madrid, Spain.*
[3]*Centro de Física de Materiales (CSIC-UPV-EHU), Paseo Manuel de Lardizábal 5, 20018 San Sebastián, Spain.*
[4]*Ikerbasque, Basque Foundation for Science, 48013 Bilbao, Spain.*

*e-mail: mmugeda@dipc.org

In certain unconventional superconductors with sizable electronic correlations, the availability of closely competing pairing channels leads to characteristic soft collective fluctuations of the order parameters, which leave fingerprints in many observables and allow to scrutinize the phase competition. Superconducting layered materials, where electron-electron interactions are enhanced with decreasing thickness, are promising candidates to display these correlation effects. For example, while bulk $NbSe_2$ is essentially a conventional superconductor, recent experiments in the thin-film regime have shown evidence of competing unconventional nematic pairing. In this work, we report the existence of a soft collective mode in single-layer $NbSe_2$, observed as a characteristic resonance excitation in high resolution tunneling spectra. This resonance is observed along with higher harmonics, its frequency $\Omega/2\Delta$ is anticorrelated with the local superconducting gap Δ, and its amplitude gradually vanishes by increasing the temperature and upon applying a magnetic field up to the critical values (T_C and H_{C2}), which sets an unambiguous link to the superconducting state. Aided by a microscopic model, we interpret this resonance as a collective Leggett mode that represents the fluctuation towards a proximate *f*-wave triplet state, due to subleading attraction in the triplet channel. Our findings demonstrate the fundamental role of correlations in superconducting 2D transition metal dichalcogenides, opening a path towards unconventional superconductivity in simple, scalable and transferable 2D superconductors.

[1] W.Wan, P. Dreher et al., *arXiv:2101.04050v2* (2021).

Quantum-well states at the surface of the heavy fermion URu_2Si_2

Edwin Herrera[1,2,3,*], Isabel Guillamón[1], Víctor Barrena[1], William Herrera[3], Jose Augusto Galvis[2], Alfredo Levy Yeyati[4], Jan Rusz[5], Peter M. Oppeneer[5], Georg Knebel[6], Jean Pascal Brison[6], Jacques Flouquet[6], Dai Aoki[7], Hermann Suderow[1]

[1]*Laboratorio de Bajas Temperaturas, Unidad Asociada UAM/CSIC. Dep. de Física de la Materia Condensada. Instituto Nicolás Cabrera and Condensed Matter Physics Center (IFIMAC). Universidad Autónoma de Madrid, E-28049 Madrid, Spain.*
[2]*Facultad de Ingeniería y Ciencias Básicas Universidad Central, 111321 Bogotá, Colombia.*
[3]*Departamento de Física. Universidad Nacional de Colombia, 111321 Bogotá, Colombia.*
[4]*Departamento de Física Teórica de la Materia Condensada. Instituto Nicolás Cabrera and Condensed Matter Physics Center (IFIMAC). Universidad Autónoma de Madrid, E-28049 Madrid, Spain.*
[5]*Department of Physics and Astronomy, Uppsala University, Box 516, S-75210 Uppsala, Sweden.*
[6]*University Grenoble Alpes, CEA, IRIG-PHELIQS, F-38000 Grenoble, France.*
[7]*IMR, Tohoku University, Oarai, Ibaraki 311 - 1313, Japan.*

*e-mail: edwin.herrera@uam.es

Electrons can form a two-dimensional electron gas at metal surfaces. Lateral confination, for example between surface steps, then leads to quantum well states. Electronic correlations considerably modify the band structure of some metals, leading to heavy fermions, unconventional superconductivity, and other new ordered phases. However, it remains open if correlated quantum well states can be formed at their surface. The heavy fermion metal URu2Si2 shows a bulk electronic band structure with correlated heavy electron bands that become superconducting below 1.5 K. Here we study atomically flat terraces on surfaces of URu2Si2 using millikelvin scanning tunneling spectroscopy. We find two-dimensional heavy fermions (2DHF) that obey the electron-in-a-box quantization with an effective mass 17 times the free electron mass. The lifetimes of the quantum well states are tens of picoseconds for energies of few meV, showing their correlated nature. We model the connection between surface and bulk states and show that the surface superconducting density of states is strongly affected by the 2DHF. Our results provide a route to realize quantized correlated electrons.

Surpassing the uncertainty thermodynamic relation in normal-superconductor quantum dots

Gonzalo Manzano[1], **Rosa Lopez**[1,*], Kun Woo Kim[2]

[1]*Instituto de Física Interdisciplinar y Sistemas Complejos IFISC (CSIC-UIB), E-07122 Palma de Mallorca, Spain.* [2]*Center for Theoretical Physics of Complex Systems, Institute for Basic Science (IBS), Daejeon 34126, Republic of Korea.*

*e-mail: rosa.lopez-gonzalo

With rapid advances toward miniaturization at the nanoscale, thermal machines are critical. Optimizing their performance will help develop devices that consume less energy and put less strain on our energy resources. Our work addresses this goal. To this purpose we need to fulfil some constraints. For example, the second law of thermodynamics dictates that entropy production always increases under non-equilibrium conditions, which places an upper bound on the efficiency of a thermal machine. A more restrictive limit on entropy has been formulated for classical systems, a new non-equilibrium principle that relates entropy, current, and current fluctuations. This principle was christened the *thermodynamic uncertainty relation*. It expresses a trade-off between power fluctuations and the entropy production rate normalized to the current average square. To overcome this relation, we use a quantum system, a quantum dot coupled to ferromagnetic contacts, and a superconductor as a source of coherent states. We show that such a device can function like a thermal machine when a temperature gradient or electrical bias is applied between the contacts. Due to the proximity effect in the quantum dot, transport occurs while maintaining coherence through Andreev reflection. This action provides the necessary ingredient to overcome the uncertainty relation. Here we discuss the different modes of operation of this thermal engine that show the best performance, i.e., an optimal regime with high efficiency and suppression of current fluctuations.

Mott Correlations in Moiré Heterostructures

María José Calderón[1,*], A. Camjayi[2], E. Bascones[1]

[1]*Instituto de Ciencia de Materiales de Madrid, ICMM-CSIC, Sor Juana Inés de la Cruz 3, 28049 Madrid, Spain.*
[2]*Departamento de Física, FCEyN, UBA and IFIBA, Conicet, Pabellón 1, Ciudad Universitaria. Buenos Aires 1428 CABA, Argentina.*

*e-mail: mariaj.calderon@csic.es

The discovery of insulating states and superconductivity [1] in magic angle twisted bilayer graphene has marked a new era in the research of quantum materials. Many other moiré heterostructures have since showed a large variety of electronic states in complex phase diagrams which resemble those of correlated materials such as high-Tc superconductors or heavy fermions. Some of the moiré heterostructures show exotic superconductivity whose origin is under debate. In this talk, I will discuss the role of electronic correlations in moiré heterostructures, where narrow bands can lead to an increased importance of interactions in the determination of their electronic properties. Using dynamical mean field theory, we explore the emergence of Mott physics in these materials. In particular, I will discuss the case of ABC graphene trilayer on hBN [2], where we find a significant reorganization of the electronic spectral weight even in the metallic state and antiferromagnetic order close to the metal insulator Mott transition. Our picture is supported by recent photocurrent experiments that have found a broad absorption peak consistent with a direct optical excitation across a Mott gap [3]. Our results are not only relevant for ABC trilayer graphene on hBN but also for other graphene moiré heterostructures and other quantum materials in which the nature of correlations is also under debate.

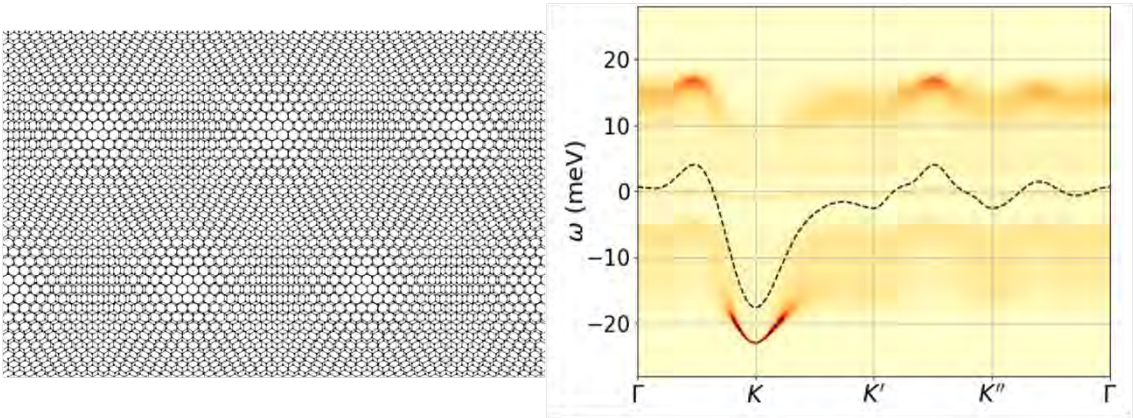

Figure 1. Left: Moiré pattern created by the lattice mismatch between two honeycomb layers. Right: Effect of electronic interactions in the band structure of the moiré heterostructure formed when rhombohedral trilayer graphene is aligned with a boron nitride substrate. The dashed line marks the non-interacting band.

[1] Y. Cao et al., *Nature* **556**, 43 (2018); 80 (2018).
[2] M.J. Calderón, A. Camjayi, E. Bascones, arXiv:2202.13857.
[3] J. Yang et al., *Science* **375**, 1295 (2022).

Acknowledgements: M.J.C and E.B. acknowledge funding from PGC2018-097018-B-I00 (MCIN/AEI/FEDER, EU). A.C. acknowledges support from UBACyT and PICT-2018-04536.

Nontrivial doping evolution of electronic properties in Ising-superconducting alloys

Wen Wan[1,*], Darshana Wickramaratne[2], Paul Dreher[1], Rishav Harsh[1], I. I. Mazin[3], Miguel M. Ugeda[1,4,5]

[1]*Donostia International Physics Center (DIPC), Paseo Manuel de Lardizábal 4, 20018 San Sebastián, Spain.*
[2]*Center for Computational Materials Science, U.S. Naval Research Laboratory,Washington, DC 20375, USA.*
[3]*Department of Physics and Astronomy, George Mason University, Fairfax, VA 22030, USA.*
[4]*Centro de Física de Materiales (CSIC-UPV-EHU), Paseo Manuel de Lardizábal 5, 20018 San Sebastián, Spain.*
[5]*Ikerbasque, Basque Foundation for Science, 48013 Bilbao, Spain.*

*e-mail: wwan@dipc.org

Transition metal dichalcogenides offer unprecedented versatility to engineer 2D materials with tailored properties to explore novel structural and electronic phase transitions. In this work, we present the atomic-scale evolution of the electronic ground state of a monolayer of $Nb_{1-\delta}Mo_{\delta}Se_2$ across the entire alloy composition range ($0 < \delta < 1$) using low-temperature (300 mK) scanning tunneling microscopy and spectroscopy (STM/STS). In particular, we investigate the atomic and electronic structure of this 2D alloy throughout the metal to semiconductor transition (monolayer $NbSe_2$ to $MoSe_2$). Our measurements let us extract the effective doping of Mo atoms, the bandgap evolution and the band shifts, which are monotonic with δ. Furthermore, we demonstrate that collective electronic phases (charge density wave and superconductivity) are remarkably robust against disorder. We further show that the superconducting T_C changes non-monotonically with doping. This contrasting behavior in the normal and superconducting state is explained using first-principles calculations. We show that Mo doping decreases the density of states at the Fermi level and the magnitude of pair-breaking spin fluctuations as a function of Mo content. Our results paint a detailed picture of the electronic structure evolution in 2D TMD alloys, which is of utmost relevance for future 2D materials design.

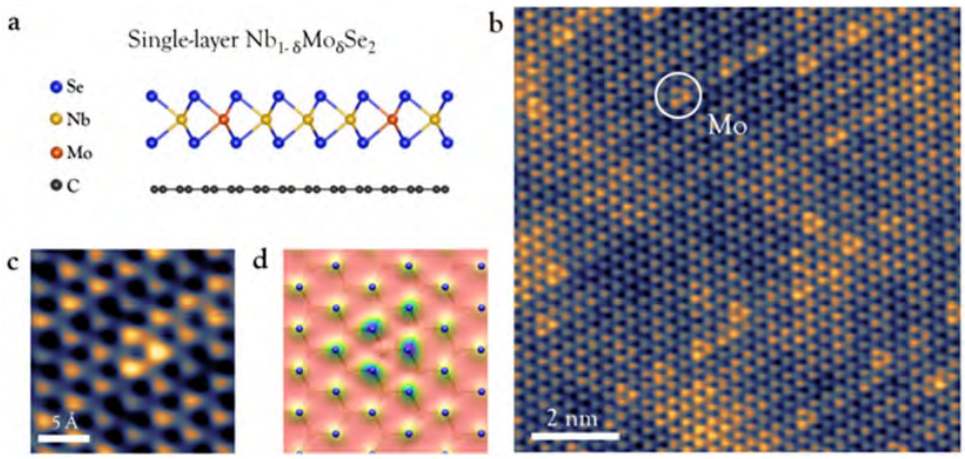

Figure 1. Atomic structure of the monolayer $Nb_{1-\delta}Mo_{\delta}Se_2$ alloy. a) Side view sketch of $Nb_{1-\delta}Mo_{\delta}Se_2$, including the graphene substrate. b) High-resolution STM image of $Nb_{0.02}Mo_{0.98}Se_2$ (Vs = - 0.5 V, It = 0.059 nA, T = 0.34 K). c) STM image of an individual substitutional Mo atom embedded in the $NbSe_2$ atomic lattice (V_s = - 0.55 V, I_t = 0.1 nA, T = 0.34 K). d) Charge density isosurface of the occupied Mo states for Mo substituting on the Nb site.

[1] Wen Wan, Darshana Wickramaratne, Paul Dreher, Rishav Harsh, I. I. Mazin, Miguel M. Ugeda, *Advanced Materials* doi:10.1002/adma.202200492 (2022).
[2] Wen Wan, Rishav Harsh, Paul Dreher, Fernando de Juan, Miguel M. Ugeda, arXiv:2203.05650 (2022).

Singlet-doublet transitions of a quantum dot Josephson junction detected in a transmon circuit

Ramón Aguado

Instituto de Ciencia de Materiales de Madrid (ICMM), Consejo Superior de Investigaciones Científicas (CSIC), Sor Juana Inés de la Cruz 3, 28049 Madrid, Spain.

*e-mail: ramon.aguado@csic.es

Recent efforts have focused on replacing the weak link in the Josephson Junction (JJ) of a superconducting qubit by electrostatically-gateable technologies compatible with high magnetic fields [1]. Such alternatives are crucial in order to reach a regime relevant for readout of topological qubits based on Majorana zero modes [2]. In this talk, I will focus on JJs based on semiconducting nanowires that contain quantum dots. Similar to the problem of a quantum impurity in a superconductor, the physics of such system is governed by the fermionic parity and spin of the two possible ground states, doublet or singlet, and their corresponding Yu-Shiba-Rusinov (YSR) subgap excitations. Changes in the fermionic parity of the ground state occur as a quantum phase transition where the energy of the subgap excitations crosses zero energy. After an introduction about such excitations in hybrid superconductor/semiconductor nanowires, I will explain how microwave spectroscopy in a transmon circuit allows to probe the ground state parity of the quantum dot Josephson junction as a function of gate voltages, external magnetic flux, and magnetic field [3]. The measured parity phase diagram is in very good agreement with that predicted by the superconducting single-impurity Anderson model. Furthermore, continuous time monitoring of the circuit allows to resolve the quasiparticle dynamics of the quantum dot Josephson junction across the phase boundaries. Away from the transition, in either the singlet or doublet phase, the lifetime in the ground state sector is of the order of several milliseconds, exceeding that of the excited state by more than an order of magnitude. These results hold promise towards realizing Andreev qubits in the YSR regime, which benefit from long parity lifetimes.

[1] R. Aguado, A perspective on semiconductor-based superconducting qubits, *Applied Physics Letters* **117**, 240501 (2020).
[2] R. Aguado and Leo Kouwenhoven, Majorana qubits for topological quantum computing, *Physics Today* **73**(6), 44 (2020).
[3] Arno Bargerbos, Marta Pita-Vidal, Rok Žitko, Jesús Ávila, Lukas J Splitthoff, Lukas Grünhaupt, Jaap J Wesdorp, Christian K Andersen, Yu Liu, Leo P Kouwenhoven, Ramón Aguado, Angela Kou, Bernard van Heck, *arXiv:2202.12754*

Acknowledgements: Support from the Spanish Ministry of Science and Innovation through Grant PGC2018-097018-BI00 and from the CSIC Research Platform on Quantum Technologies PTI-001is acknowledged.

Signatures of interactions in the Andreev spectrum of nanowire Josephson junctions

F. J. Matute-Cañadas[1,*], C. Metzger[2], Sunghun Park[1], L. Tosi[3], P. Krogstrup[4], J. Nygård[4], M. F. Goffman[2], C. Urbina[2], H. Pothier[2], A. Levy Yeyati[1]

[1]*Departamento de Física Teórica de la Materia Condensada, Condensed Matter Physics Center (IFIMAC) and Instituto Nicolás Cabrera, Universidad Autónoma de Madrid, 28049 Spain.*
[2]*Quantronics group, Service de Physique de l'État Condensé (CNRS, UMR 3680), IRAMIS, CEA-Saclay, Université Paris-Saclay, 91191 Gif-sur-Yvette, France.*
[3]*Centro Atómico Bariloche and Instituto Balseiro, CNEA, CONICET, 8400 San Carlos de Bariloche, Río Negro, Argentina.*
[4]*Center for Quantum Devices, Niels Bohr Institute, University of Copenhaguen, Universitetsparken 5, 2100 Copenhagen, Denmark.*

*e-mail: francisco.matute@uam.es

Hybrid semiconducting/superconducting nanostructures combined with circuit-QED techniques are allowing to explore superconducting proximity effects with an unprecedented degree of detail. For instance, these techniques have permitted to reveal the fine structure, due to spin-orbit coupling, of Andreev states in semiconducting nanowire Josephson junctions [1]. While some of the observed transition lines of the microwave spectrum could be explained in terms of non-interacting models with a few conducting channels [1-3], other expected transition lines from these models could not be clearly identified and some other experimental features remained unexplained.

In this work [4] we show that the inclusion of electron-electron interactions in the normal region of the junction is necessary to account for these unexplained features, which consist in the splitting of certain degeneracies expected in the non-interacting models. This allows to identify the corresponding transition lines in the experimental spectra.

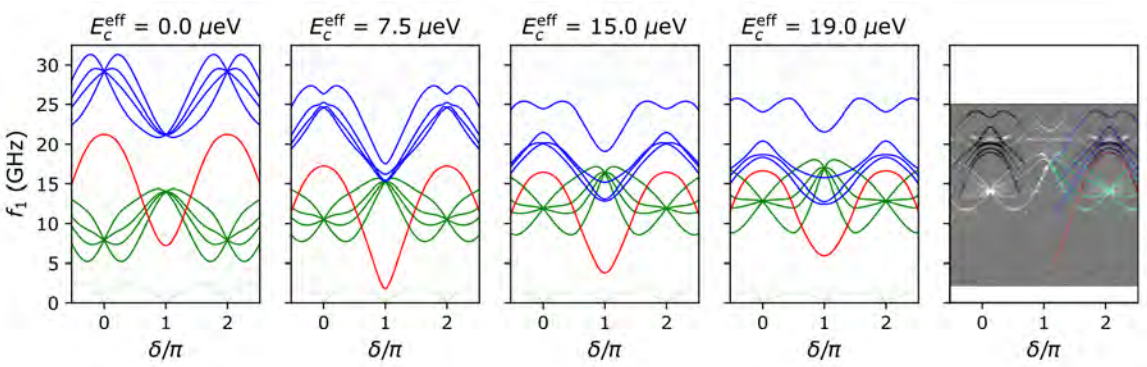

Figure 1. Evolution of the transition lines with the effective charging energy E_C^{eff} of the normal region of the junction, calculated with the model described in [4]. The lines are shown in function of the phase difference δ between the superconducting leads and the parameters are chosen so that the results reasonably reproduce the experimental spectrum shown in the rightmost panel. Green lines correspond to transitions between odd parity states where one trapped quasiparticle is excited from one Andreev level to another. Their degeneracies at $\delta = 0, \pi$ are protected by time reversal symmetry. Red and blue lines correspond to transitions between even parity states where two quasiparticles are excited from the ground state to the same spin split Andreev doublet (red) or to different doublets (blue). The latter we call *mixed pair transitions* and their degeneracies at $\delta = 0, \pi$ are those which are broken by the interaction.

[1] L. Tosi, C. Metzger, M. F. Goffman, C. Urbina, H. Pothier, Sunghun Park, A. Levy Yeyati, J. Nygård, and P. Krogstrup, *Phys. Rev. X* **9**, 011010 (2019).
[2] Sunghun Park, C. Metzger, L. Tosi, M. F. Goffman, C. Urbina, H. Pothier, and A. Levy Yeyati, *Phys. Rev. Lett.* **125**, 077701 (2020).
[3] C. Metzger, Sunghun Park, L. Tosi, C. Janvier, A. A. Reynoso, M. F. Goffman, C. Urbina, A. Levy Yeyati, and H. Pothier, *Phys. Rev. Research* **3**, 013036 (2021).
[4] F.J. Matute-Cañadas, C. Metzger, Sunghun Park, L. Tosi, P. Krogstrup, J. Nygård, M. F. Goffman, C. Urbina, H. Pothier and A. Levy Yeyati, arXiv:2112.05625, to be published in Phys. Rev. Lett.

Joule heating effects in hybrid superconductor-semiconductor nanowire devices

A. Ibabe[1,*], M. Gómez[1], G. Steffensen[1], J. Nygard[2], A. Levy Yeyati[1], E. J. H. Lee[1]

[1]*Department of Condensed Matter Physics, Universidad Autónoma de Madrid, Spain, Ciudad Universitaria de Cantoblanco, Spain.*
[2]*Center for Quantum Devices and Station Q Copenhagen, Niels Bohr Institute, Univ of Copenhagen, Copenhagen, Denmark.*

*e-mail: angel.ibabe@uam.es

Hybrid superconductor-semiconductor nanowires have attracted a great deal of interest in the past decade. In a large part, this owes to their potential as a platform for the realization of a topological superconductor and of Majorana zero modes, as first outlined by the pioneering theory works of Oreg at al. [1] and Lutchyn et al. [2] which were followed by intensive experimental efforts towards this goal [3-5]. More recently, interest in such a material system has also been directed at the development of novel types of hybrid superconducting qubits [6]. A key element for the above research directions relies on having high-quality nanowires with reproducible properties. However, despite the impressive improvements related to hybrid nanowire growth in the past years [7], experiments still show a great deal of variability in the behavior of fabricated devices, which consequently makes their interpretation more difficult. To gain a better understanding of each individual device, it is crucial to perform a thorough characterization of its properties, which is typically accomplished by performing low bias quantum transport measurements.

Here, we show that Joule heating effects can also provide rich information related to the superconductivity in such devices, thereby constituting a complimentary characterization tool for this type of system. In this work, we study two different device geometries based on InAs nanowires with epitaxial Al shells: single nanowire junctions and mesoscopic superconducting islands. We show that Joule heating can drive a superconductor-to-normal metal transition of the epitaxial shell, manifested as a suppression of the Andreev excess current [8]. We investigate signatures of this transition in our transport measurements aimed at obtaining information regarding heat dissipation, as well as of the superconductivity in different parts of our devices.

[1] Y. Oreg et al., *Phys. Rev. Lett.* **105**,177002 (2010).
[2] R. M. Lutchyn et al. *Phys. Rev. Lett.* **105**, 077001 (2010).
[3] V. Mourik et al., *Science* **336**, 1003 (2012).
[4] S. M. Albrecht et al., *Nature* **531**, 206 (2016).
[5] E. Prada et al., *Nature Rev. Phys.* **2**, 575 (2020)
[6] L. Tosi, *Phys. Rev. X* **9**, 011010 (2019); M. Hays, *Science* **373**, 430 (2021).
[7] P. Krogstrup et al., *Nature Mater.* **14**, 400 (2015); Chang et al., *Nature Nanotechnol.* **10**, 232 (2015).
[8] M. Tomi et al., *Phys. Rev. B* **104,** 134513 (2021).

Nano-engineered high-temperature superconductors and hybrid systems for energy-efficient functional devices

A. Palau[1,*], J. Alcalà[1], A. Barrera[1], A. Fernández-Rodríguez[1], T. Günkel[1], S. Marinkovic[2], A. V. Silhanek[2], LL. Balcells[1], N. Mestres[1]

[1]*Institut de Ciència de Materials de Barcelona, ICMAB-CSIC, Campus UAB, Bellaterra, Spain.*
[2]*Experimental Physics of Nanostructured Materials, Q-MAT, CESAM, Université de Lieġe, B-4000 Lieġe, Belgium.*

*e-mail: palau@icmab.es

Today advances to store and analyse massive information offer huge opportunities and unprecedented benefits in business, healthcare, security, and society. The emergence of Internet of Things and Big-Data analysis offer major advantages but require to explore novel technologies for information storage and processing in a sustainable way. Multifunctional materials based on complex oxides offer unique opportunities to tune their magnetic or electric properties with multiple external inputs, thus providing the basis for realizing energy-efficient electronic devices. Among numerous outstanding properties of strongly correlated functional oxides, superconducting cuprates are of special interest due to their inherent energy efficiency. In spite of great technological advancements in the recent years, electronic devices based on High Temperature Superconductors (HTS) are still in the early stage with respect to those based on conventional low-temperature superconductors. An important drawback is their complexity and high sensitivity on doping which imposes extreme demands on the micro-, nano-fabrication. In this talk, I will introduce different types of structures and hybrid systems based on superconducting films, specially designed to obtain novel functional properties which can be tuned with temperature, magnetic or electrical fields, or geometry constrains [1,2,3]. On one hand, field-induced oxygen vacancy modulations provide a viable mechanism to reversibly tune the superconducting parameter (Fig. 1 (a)) opening comprehensive prospects for gate-modulated electronic quantum devices - superconducting transistors, reversible patterning of weak-links or other nanostructures to create vortex pinning landscapes on demand (Fig. 1 (b)) [1]. The combination of HTS with other functional materials in hybrid systems can be exploited to create and manipulate non-trivial spin textures though loss-less supercurrents (Fig. 1 (c)) [3] or magnetic-superconductor metasurfaces for unprecedented control of magnetic fields at micro-, nano-scale.

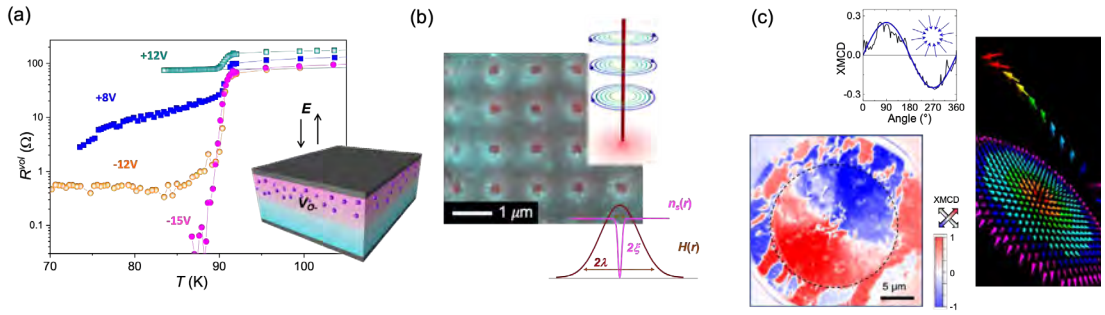

Figure 1. (a) Reversible critical temperature modulation of HTS through field induced oxygen diffusion. (b) Nanoscale spatial modulation of T_c for reversible pinning landscapes. (c) Singular magnetic domains such as monopolar-like configurations obtained in hybrid superconductor-ferromagnetic systems.

[1] Palau et al., *ACS Appl. Mater. Interfaces* **10**, 30531(2018); Marinkovíc et al., *ACS Nano* **14**, 11765 (2020).
[2] Rouco et al., *Nano Letters* **19**, 4174 (2019).
[3] Palau et al., *Advanced Science* **3**, 1600207 (2016); Alcalà et al., *Springer Nature Book* **6**, 167 (2021).

Interfacial control of vortex-limited critical current in type II superconductor films

Marius K. Hope[1], Morten Amundsen[2], Dhavala Suri[3], Jagadeesh S. Moodera[3,4], **Akashdeep Kamra**[5,1,*]

[1]*Center for Quantum Spintronics, Department of Physics, Norwegian University of Science and Technology, Trondheim NO-7491, Norway.* [2]*Nordita, KTH Royal Institute of Technology and Stockholm University, SE-106 91 Stockholm, Sweden.* [3]*Francis Bitter Magnet Laboratory & Plasma Science and Fusion Center, Massachusetts Institute of Technology, Cambridge, Massachusetts 02139, USA.* [4]*Department of Physics, Massachusetts Institute of Technology, Cambridge, Massachusetts 02139, USA.* [5]*Condensed Matter Physics Center (IFIMAC) and Departamento de Física Teórica de la Materia Condensada, Universidad Autónoma de Madrid, Madrid E-28049, Spain.*

*e-mail: akashdeep.kamra@uam.es

In a small subset of type II superconductor films, the critical current is determined by a weakened Bean-Livingston barrier posed by the film surfaces to vortex penetration into the sample. A film property thus depends sensitively on the surface or interface to an adjacent material. We theoretically investigate the dependence of vortex barrier and critical current in such films on the Rashba spin-orbit coupling at their interfaces with adjacent materials. Considering an interface with a magnetic insulator, we find the spontaneous supercurrent resulting from the exchange field and interfacial spin-orbit coupling to substantially modify the vortex surface barrier, consistent with a previous prediction. Thus, we show that the critical currents in superconductor-magnet heterostructures can be controlled, and even enhanced, via the interfacial spin-orbit coupling. Since the latter can be controlled via a gate voltage, our analysis predicts a class of heterostructures amenable to gate-voltage modulation of superconducting critical currents. It also sheds light on the recently observed gate-voltage enhancement of critical current in NbN superconducting films.

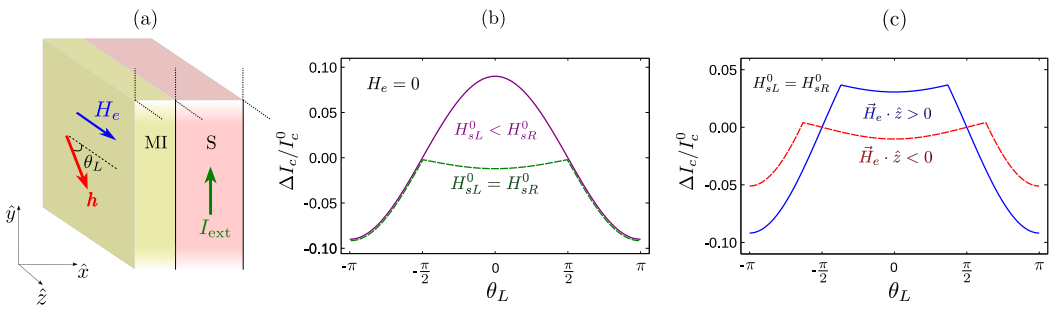

[1] M. K. Hope, M. Amundsen, D. Suri, J. S. Moodera, and A. Kamra, *Phys. Rev. B* **104**, 184512 (2021).
[2] M. Rocci, D. Suri, A. Kamra, G. Vilela, Y. Takamura, N. M. Nemes, J. L. Martinez, M. G. Hernandez, and J. S. Moodera, *Nano Letters* **21**, 216 (2021).

Acknowledgements: We acknowledge financial support from the Spanish Ministry for Science and Innovation – AEI Grant CEX2018-000805-M (through the "Maria de Maeztu" Programme for Units of Excellence in R&D), and the Research Council of Norway through its Centers of Excellence funding scheme, project 262633, "QuSpin". Work at MIT is supported by ARO (W911NF-20-2-0061), NSF (DMR 1700137 and C-Accel Track C Grant No. 2040620), ONR (Nos. N00014-16-1-2657 and N00014-20-1-2306), and CIQM-NSF DMR-1231319.

Modelling of vortex core magnetization and Pauli paramagnetic effects

E. Campillo[1,*], E. M. Forgan[2], Elizabeth Blackburn[1]

[1]*Division of Synchrotron Radiation Research, Lund University, SE-22100 Lund, Sweden.*
[2]*School of Physics and Astronomy, University of Birmingham, Birmingham B15 2TT, United Kingdom.*

*e-mail: emma.campillo@sljus.lu.se

To better understand the behaviour of $CeCu_2Si_2$ and other Pauli limited superconductors, we present a physically-based expression for the size and magnetisation of the vortex cores in Pauli-limited superconductors, based on the results of first-principles computations [1].

Unconventional superconductors, with pairing mechanisms and properties that are not accounted for BCS theory are a subject of continuing interest.

We have studied the vortex lattice (VL) that develops inside $CeCu_2Si_2$ [2] when a magnetic field is applied. The magnetic field in the VL may be expressed as a sum of Fourier components in momentum-space and the magnitude of each Fourier component as a function of field or temperature, often called the 'form factor' (FF). This can be extracted from the measured integrated neutron scattering (SANS) intensity [3] and contains information about the magnetic field distribution inside and outside the vortex cores.

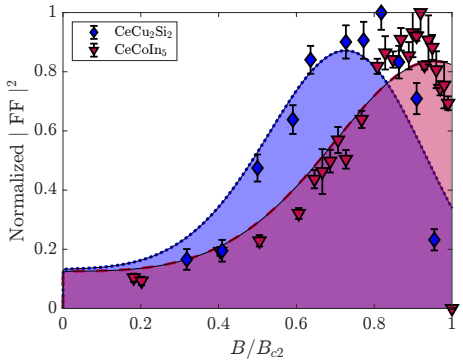

Figure 1. Comparison between the normalized squared form factor of $CeCu_2Si_2$ at 40 mK and $CeCoIn_5$ at 50 mK [11]. The lines are the results of fits using the model developed for PPE.

We find that $CeCu_2Si_2$ shows a strong increase of SANS intensity from the flux lines as the applied field is increased towards the edge of the superconducting phase [4]. This has previously been observed in $CeCoIn_5$ [5] (Figure 1) and indicates that the superconductivity in this material is not destroyed by the same mechanism as in almost all other superconductors but instead by Pauli paramagnetic effects (PPE) [6]. It is thought to be responsible for weaker anomalies in the form factor seen in $TmNi_2B_2C$ [7] and $YBa_2Cu_3O_7$ [8,9].

Relying on the results of first-principles numerical calculations, we have obtained algebraic expressions which indicate how the size and magnetisation of the vortex cores varies with field and hence obtain general results for the variation of the SANS intensity / VL form factor as a function of field and temperature for superconductors exhibiting PPE.

Furthermore, in our work on YBCO and Ca-doped YBCO [9,10], there are deviations from the London model at the highest fields measured (Figure 2), which may suggest speculated that Pauli paramagnetic effects are responsible, and the next step would be to apply our model to this data.

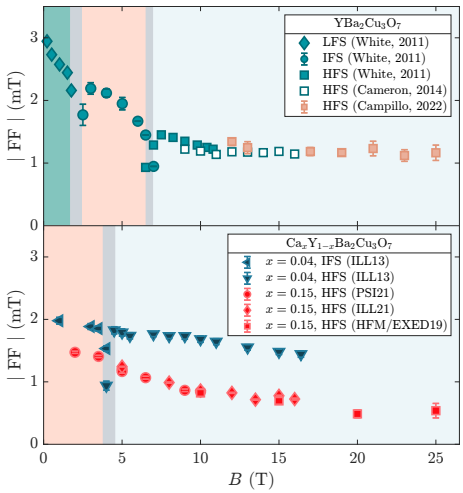

Figure 2. Evolution of the form factor with magnetic field at base temperature for (top) $YBa_2Cu_3O_7$ [9] and (bottom) $Ca_xY_{1-x}Ba_2Cu_3O_7$ [10].

[1] Ichioka, M. & Machida, *Phys. Rev. B* **76**, 064502 (2007).
[2] Steglich, F. *et al.*, *Phys. Rev. Lett.*, **43**, 1892 (1979).
[3] Christen H. D. *et al.*, *Phys. Rev. B*, **15**, 4506 (1977).
[4] Campillo, E. *et al.*, *Phys. Rev. B*, **104**, 184508 (2021).
[5] Bianchi, A. D. *et al.*, *Science*, **319**, 177–180 (2008).
[6] Clogston, A. M., *Phys. Rev. Lett.*, **9**, 266 (1962).
[7] DeBeer-Schmitt, L. *et al.*, *Phys. Rev. Lett.*, **99**, 167001 (2007).
[8] Cameron, A. *et al.*, *Phys. Rev. B*, **90**, 054502 (2014).
[9] Campillo, E. *et al.*, *arXiv preprint arXiv:2203.01705* (2022).
[10] Cameron, A. & Campillo, E. *et al.*, *In preparation.*
[11] White, J. S. *et al.*, *Journal of Physics*, **12**, 023026 (2010).

Ab initio study of possible metastable occupation of tetrahedral sites in Palladium Hydride compounds

Antonella Meninno[1,2,*], Ion Errea[1,2,3]

[1]*Centro de Física de Materiales (CSIC-UPV/EHU), Donostia, Basque Country, Spain.*
[2]*Fisika Aplikatua 1 Saila, University of the Basque Country (UPV/EHU), Donostia, Basque Country, Spain.*
[3]*Donostia International Physics Center (DIPC), Donsotia, Basque Country, Spain.*

*e-mail: ameninno001@ikasle.ehu.eus

Palladium hydrides are one of the rare examples of superconducting hydrides at ambient pressure. Even if their critical temperature is around 10 K, they are fascinating superconductors because of their inverse isotope effect: the palladium compound has a larger critical temperature than the hydrogen compound, in clear contradiction with standard electron-phonon superconductors. As shown by Errea et al. [1], this anomalous behavior is induced by the large anharmonicity of the hydrogen vibrations in the octahedral sites they occupy.

In recent times, in a controversial paper [2], high temperature superconductivity was observed in PdH compounds. The authors of the paper measure traces of superconductivity as high as at 54K for PdH if this compound is obtained through fast cooling in the synthesis. If the compound is obtained with slow cooling no superconductivity is observed. Their conclusion is that superconductivity depends strongly on the sites occupied by hydrogen atoms.

In this work we present first principles calculations including anharmonic effects within the stochastic self-consistent harmonic approximation (SSCHA) [3] in order to unveil the possible existence of dynamically stable structures with full or partial occupation of tetrahedral sites, which may be metastable. We discuss the implications of these possible structures in superconductivity.

[1] I. Errea, M. Calandra, F. Mauri, *Physical Review B* **89**(6), 064302 (2014).
[2] H. M. Syed, T. J. Gould, C. J. Webb, E. Gray, arXiv:1608.01774.g
[3] I. Errea, M. Calandra, F. Mauri, *Physical Review Letters* **111**(17), 177002 (2013).

Acknowledgements: We have received funding from the European Research Council (ERC) under the European Unions Horizon 2020 research and innovation programme (grant agreement No 802533).

Extremely long range, high-temperature Josephson coupling across a half metallic ferromagnet

D. Sanchez-Manzano[1], S. Mesoraca[2], **F. A. Cuellar**[1,*], M. Cabero[3,4], V. Rouco[1], G. Orfila[1], X. Palermo[2], A. Balan[2], L. Marcano[5], A. Sander[2], M. Rocci[1], J. Garcia-Barriocanal [6], F. Gallego[1], J. Tornos[1], A. Rivera[1], F. Mompean[7,8], M. Garcia-Hernandez [7,8], J. M. Gonzalez-Calbet[4,9], C. Leon[1], S. Valencia[5], C. Feuillet-Palma[10], N. Bergeal[10], A. Buzdin[11,12], J. Lesueur[10], Javier E. Villegas[2], J. Santamaria[1,8]

[1]*GFMC. Dept. Fisica de Materiales. Facultad de Fisica. Universidad Complutense. 28040 Madrid.*
[2]*Unité Mixte de Physique, CNRS, Thales, Université Paris-Saclay, 91767 Palaiseau. France.*
[3]*IMDEA Nanoscience Campus Universidad Autonoma 28049 Cantoblanco Spain.*
[4]*Centro Nacional de Microscopia Electronica. Universidad Complutense 28040 Madrid.*
[5]*Helmholtz-Zentrum Berlin für Materialien und Energie, Albert-Einstein-Strasse 15, D-12489, Berlin, Germany.*
[6]*Characterization Facility, University of Minnesota, 100 Union St. S.E., Minneapolis, MN 55455, USA.*
[7]*Instituto de Ciencia de Materiales de Madrid ICMM-CSIC 28049 Cantoblanco. Spain.*
[8]*Unidad Asociada UCM/CSIC, "Laboratorio de Heteroestructuras con aplicación en spintrónica"*
[9]*Dept. Quimica Inorganica. Facultad de Quimica. Universidad Complutense, 28040 Madrid.*
[10]*Laboratoire de Physique et d'Etude des Matériaux, CNRS, ESPCI Paris, PSL Research University, UPMC, 75005, Paris, France.*
[11]*Université Bordeaux, CNRS, LOMA, UMR 5798, F-33405 Talence, France.*
[12]*Sechenov First Moscow State Medical University, Moscow 119991, Russia.*

*e-mail: f.cuellar@ucm.es

Two superconductors coupled through a weak link or spacer yield a phase coherent quantum state: that is the Josephson effect. Singlet (opposite-spin) Cooper pairs decay over very short distances in ferromagnetic materials, and thus the Josephson coupling can only occur with a nanometer-size separation. It is possible however, to generate triplet (equal-spin) Cooper pairs, allowing superconductor coupling across magnetic barriers with considerably large distances. We demonstrate extremely-long-range, high-temperature Josephson coupling across the half-metallic manganite $La_{0.7}Sr_{0.3}MnO_3$ with superconducting $YBa_2Cu_3O_7$[1]. Observed in planar junctions displaying the hallmarks of Josephson physics: an interference pattern in the critical current (Fraunhofer pattern) and quantum phase locking under microwave excitation (Shapiro steps). The conjunction of quantum coherent transport and full spin polarization can bring unique opportunities for the practical realization of superconducting spintronics, and novel strategies in quantum computing.

[1] D. Sanchez-Manzano *et al.*, Extremely long-range, high-temperature Josephson coupling across a half-metallic ferromagnet, *Nat. Mater.* **21**(2), 188 (2022).

Non-equilibrium transport in Josephson junctions through interacting nanostructures

Jordi Picó-Cortés[1,2,*], Andrea Donarini[1], Gloria Platero[2], Milena Grifoni[2]

[1] *Theoretische Physik, Universität Regensburg, 93040 Regensburg, Germany.*
[2] *Instituto de Ciencia de Materiales de Madrid (CSIC) E-28049, Spain.*

*e-mail: Jordi.Pico-Cortes@physik.uni-regensburg.de

Studying transport through interacting nanostructures is challenging due to the interplay between strong interactions and the coupling to large thermalized leads. In the case of superconducting leads, this is further complicated by a number of features particular to Josephson junctions, chiefly the effect of Cooper pairs and the resulting anomalous transport. In this work, we develop a diagrammatic approach to transport through weakly coupled Josephson junctions [1,2] which treats the interaction inside the dot exactly and employ it to describe the conventional, Josephson, and Andreev currents. The dynamics of Cooper pairs out of equilibrium are described in a particle-conserving formalism, which avoids issues arising from the usual BCS treatment, allowing us to extend the description of electron pairing and the $0-\pi$ transition beyond the usual equilibrium treatment.

[1] S. Pfaller, A. Donarini, and M. Grifoni, *Physical Review B* **87**, 155439 (2013).
[2] M. Governale, M.G. Pala and J. König, *Physical Review B* **77**, 134513 (2008).

Electromagnetic modelling in macroscopic superconductivity. Fundamentals and applications

Antonio Badía-Majós

Instituto de Nanociencia y Materiales de Aragón (INMA), CSIC-Universidad de Zaragoza, Departamento de Física de la Materia Condensada (EINA), 50018-Zaragoza, Spain
*e-mail: anabadia@unizar.es

Macroscopically, the properties of superconducting materials are customarily described through the quasistationary Maxwell equations for the fields $\mathbf{E}, \mathbf{B}$ and a phenomenological material law for the current density $\mathbf{J}$. In its simplest form, the material law reduces to the condition $\|\mathbf{J}\| = \{J_c, 0\}$ ($J_x = \{\pm J_c, 0\}$ in 1D problems). This is the central idea of the so-called *critical state theory* [1], that has been successfully applied over decades for the analysis of magnetic flux penetration in type-II superconductors.

The big accomplishment of the theory relies both on its mathematical simplicity and on the straightforward physical interpretation. Related to this, a wealthy variety of upgrades have appeared in the literature so as to allow the description of a wider and wider class of experimental situations. The efforts have been focused (i) on the search of a fundamental justification for the initially *heuristic* approximation and, (ii) on the generalisation of the model, allowing us to deal with more and more complex configurations. Based on thermodynamic arguments applied to the physics of vortices in superconductors, we proposed a model [2], that provides the conceptual support for the soundness of the theory, as well as a specific statement to be used in macroscopic superconductivity. The main ingredient is the so-called *dissipation function* in terms of the components of the current density vector, either parallel or perpendicular to the local magnetic field, i.e.: $\mathcal{F}(J_\parallel, J_\perp)$ (Fig. 1).

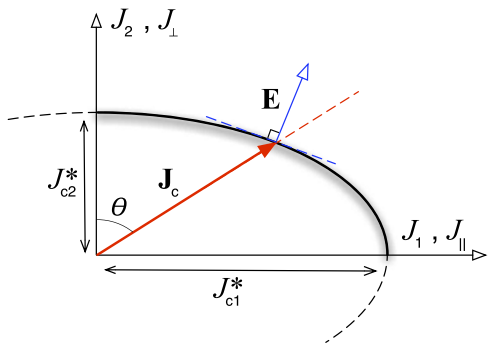

Figure 1. Geometrical interpretation of the dissipation law in a practical superconductor.

We will show that, by inserting $\mathcal{F}(\mathbf{J})$ in a dedicated minimisation principle, one may solve a variety of problems in applied superconductivity [3], such as those related to the engineering of superconducting magnets, electric current transport and magnetic levitation devices (Fig. 2).

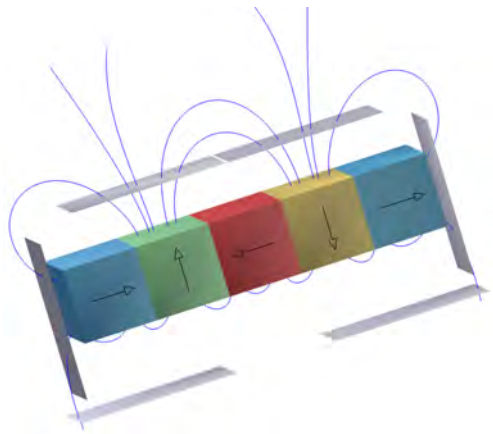

Figure 2. Simulation of a multiscale levitation system with a Hallbach magnet array and 6 wrapping superconducting plates.

[1] C P Bean, *Rev. Mod. Phys.* **36**, 31 (1964).
[2] A Badía-Majós and C López, *Supercond. Sci. Technol.*, **28**, 024003 (2015).
[3] A Badía-Majós *Macroscopic Superconductig Phenomena: An Interactive Guide*, IOP Publishing (2021).

Acknowledgements: Dr. C López is gratefully acknowledged for valuable and essential discussions. Financial support from project PID2020-113034RB-I00 (Agencia Estatal de Investigación) is acknowledged.

Ti/Al bi-layer Kinetic Inductance Detector (BiKID) configuration for CMB experiments

M. C. de Ory[1], D. Rodriguez[1], B. Aja[2], L. de la Fuente[2], E. Villa[1], Juan P. Pascual[2], E. Artal[2], D. Granados[3], J. Martin-Pintado[1], A. Gomez[1,*]

[1.] *Centro de Astrobiología CSIC-INTA, 28850 Torrejón de Ardoz, Spain.*
[2.] *Dpt. Ing. Comunicaciones, Universidad de Cantabria 39005 Santander, Spain.*
[3.] *IMDEA Nanociencia, Calle Faraday 9, Campus de Cantoblanco, 28049 Madrid, Spain.*

* e-mail: mcalero@cab.inta-csic.es

Superconducting kinetic inductance detectors (KIDs) are promising for mm/sub-mm/fir range astronomical experiments, particularly those requiring large format cameras with extremely high detection and polarization sensitivity. They are optimal for studying the Cosmic Microwave Background (CMB) or dark matter experiments. KIDs are LC resonators that exploit the changes in the superconducting kinetic inductance with incoming radiation. The core advantage of KIDs over other types of detectors is that passive frequency-domain multiplexing is enabled, making it possible to integrate and read out thousands of resonators in a single transmission line. KIDs based on bi-layer combinations of Titanium (Ti) / Aluminium (Al) have demonstrated outstanding sensitivity down to 80 GHz [1]. However, for the frequency range below 110 GHz, only single-polarization detectors have been reported so far.

In this work, we present the development of an on-chip dual-polarization detector optimized for the W-band (75-110 GHz). The device is based on a BiKID structure. It consists of two Lumped Element KIDs (LEKIDs) arrays placed in an orthogonal configuration on both sides of a high resistivity silicon wafer [2]. Microwave simulations have been performed to optimize the absorption in the desired frequency range, KIDs resonant frequencies and quality factors. Cryogenic optical characterization in low background, using a cryogenic blackbody and bandpass filters, confirms absorption at 90 GHz. Also, the Noise Equivalent Power (NEP) has been measured, showing the high sensitivity provided by the detector [3].

[1] A. Catalano et al., *A&A* **580**, 1-6, (2015).
[2] B. Aja et al., *IEEE Trans. Microw. Theory Tech.* **69**, 1 (2021).
[3] R. Markus, **Vol. 12**. KIT Scientific Publishing (2014).

Acknowledgements: The Spanish Ministry of Science and Innovation supported this work under Grant PID2019-105552RB, Grant SEV-2016- 0686, PID2019-110610RB-C22 and ONR-Global through Grant DEFROST N62909-19-1-2053. We also acknowledge support from CSIC Research Platform PTI-001.

Large output voltage to magnetic flux change in nanoSQUIDs based on direct-write Focused Ion Beam Induced Deposition technique

Fabian Sigloch[1,*], Soraya Sangiao[1,2], Pablo Orús[1], José María de Teresa[1,2]

[1]*Instituto de Nanociencia y Materiales de Aragon (INMA), Universidad de Zaragoza-CSIC, 50009 Zaragoza, Spain.* [2]*Laboratorio de Microscopías Avanzadas (LMA), Universidad de Zaragoza, 50018 Zaragoza, Spain.*

*e-mail: fsigloch@unizar.es

Direct write techniques such as Focused Electron/Ion Beam Induced (FEBID/FIBID) deposition constitute versatile, resist-free approaches for the fabrication of nanostructures, offering an alternative to conventional methods such as Optical or Electron Beam Lithography. In FEBID/FIBID a gaseous precursor containing the element of interest is delivered into the chamber of a Scanning Electron Microscope (SEM) or a Focused Ion Beam (FIB) microscope. The beam is scanned over a substrate following a predefined pattern, locally irradiating and decomposing the precursor gas into its volatile and non-volatile constituents. The volatile component is pumped away whereas the non-volatile part remains on the substrate resulting in the bottom-up growth of the wanted structure upon repeated irradiation of the desired area.

The irradiation of the commercially available precursor gas $W(CO)_6$ with Ga^+ ions results in a W-C based material with well-established superconducting properties. Planar deposits exhibit a critical temperature of $T_c = 4\,K - 5\,K$, an upper critical magnetic field of $B_{c,2} = 7\,T - 8.5\,T$ and a critical current density of $J_c = 0.01\,MA/cm^2 - 0.1\,MA/cm^2$ [1]. The London penetration depth is reported to be $\lambda_L = 850\,nm$ and the superconducting coherence length as $\xi = 6\,nm - 9\,nm$ [1]. Ga^+ FIBID of the $W(CO)_6$ precursor enables the fabrication of superconducting nanostructures with line widths of 50 nm with high precision and reproducibility.

In this work we present the fabrication of nanoscale Superconducting Quantum Interference Devices (nanoSQUIDs) of W-C by Ga^+ FIBID. The SQUID loop is formed by a 50 nm-thick and 200 nm-wide film with a rectangular inner loop of $(300 \times 700)nm^2$. The Josephson Junctions (JJs) are formed by 300 nm-long constrictions with a cross-sectional area of down to $(50 \times 50)nm^2$.

The SQUIDs show a critical temperature of up to $T_c = 4.29\,K$ and a critical current of up to $I_c = 8.51\,\mu A$. The normal-state resistance of the JJs is $R_N = 496\,\Omega$. Upon variation of the external magnetic field we observe periodic oscillations in the critical current, I_c, and upon injection of a constant bias current $I_b \sim I_c$ the voltage drop across the structure exhibits a sinusoidal dependence with the external magnetic field. The transfer coefficient is remarkably high with up to $V_\Phi = 1301\,\mu A/\Phi_0$ due to the comparably high normal-state resistance of the JJs.

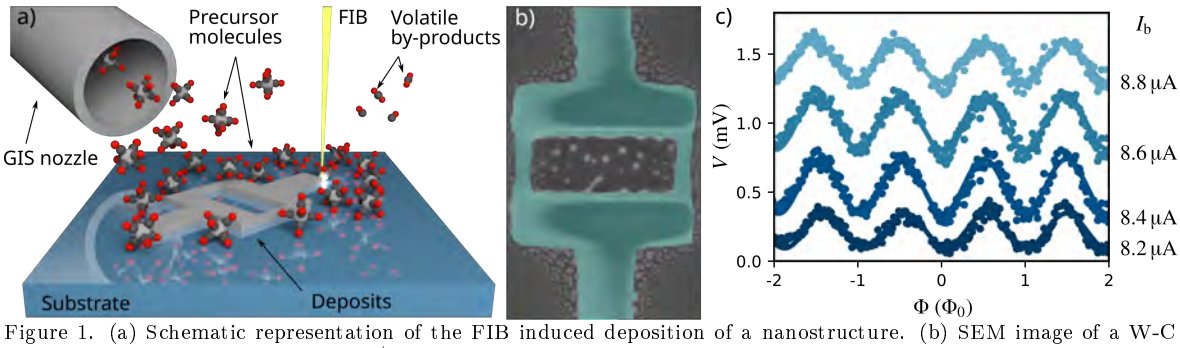

Figure 1. (a) Schematic representation of the FIB induced deposition of a nanostructure. (b) SEM image of a W-C (blue) nanoSQUID fabricated by Ga^+ FIBID and (c) the corresponding periodic modulation of the voltage, V, in dependence of the magnetic flux threading the SQUID loop, Φ. The different lines correspond to different bias currents $I_b \sim I_c$. Reproduced from [2].

[1] Pablo Orús *et al.*, *Nanomaterials* **12(8)**, 1367 (2022).
[2] Fabian Sigloch *et al.*, *arXiv [Preprint]*, arXiv:2203.05278 [cond-mat.supr-con] (2022).

Acknowledgements: The *FET-Open FIBSuperProbes* project is funded by H2020 through the grant 892427.

Design of a levitating system for the study of the superfluidity at ultra low temperatures

Manuel Arrayás Chazeta, **Carlos Uriarte González***, José Luis Trueba Santander

Matemática Aplicada, Ciencia e Ingeniería de los Materiales y Tecnología Electrónica, Universidad Rey Juan Carlos, Spain.

*e-mail: carlos.ugonzalez@urjc.es

A mechanical design of a magnetic trap for the study of superfluidity in He^4 and He^3 up to temperatures of 100mk is presented. The design consists of a set of coils that allow levitating a superconducting sphere of type I superconductor (Indium) immersed in a superfluid (Fig. 1).

The novelty of this design is the posibility to control the movement of the superconducting sphere in a horizontal plane, allowing a wide variety of movements to be established in the bulk of the superfluid. This feature appears to be promising in the study of various characteristics of superfluids. The finite element studies carried out in conjunction with the analytical models developed to study the stability of the magnetic field show the possibility of establishing oscillatory movements of the sphere, which will allow expanding the experiments previously carried out in superfluidity [1, 2]. Most importantly, the studies developed evidence the possibility to establish both rectilinear and circular uniform movements, which in turn opens up a whole new multitude of studies, including quantum turbulence [3] and dynamics of Andreev-bound states in the topological superfluid 3He-B [4].

The system has been built and inserted into an optical cryostat at Lancaster University and is ready to start comparing experimental evidence with developed models. The complete results of this study are published in [5].

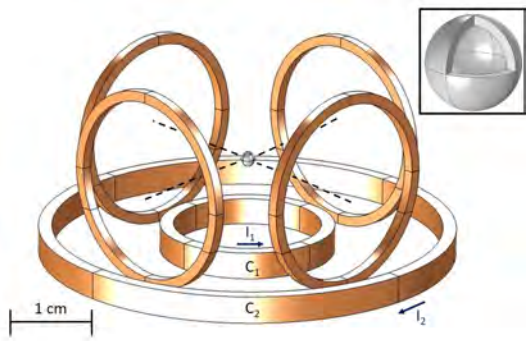

Figure 1. Device configuration. The two coils placed in the horizontal plane produce the stable levitation of the sphere and the four vertical coils drive the sphere in the different control movements. Inset: Hollow In sphere. The sphere has a hollow inside to reduce its overall density.

[1] J. Jäger B.Schuderer and W.Schoepe, *Phys. Rev.Lett.* **74**, (1995).
[2] S. Liu,G.Labbe and G.G.Ihas, *J. LowTemp.Phys.* **148**, (2007).
[3] R. Hanninen and W.Schoepe, *J. LowTemp.Phys.* **11**, (2010).
[4] L. Chuan et. al., *Nat. Mater* **17**, (2010).
[5] M. Arrayás J.L. Trueba C. Uriarte D. Zmeev, *Scientific Reports* **11**, (2021).

Acknowledgements: These results were obtained under the predoctoral founds URJC C1PREDOC2020.

Superconducting dome by tuning through a van Hove singularity in a two-dimensional metal

Wen Wan[1], **Rishav Harsh**[1,*], Paul Dreher[1], Fernando de Juan[1], Miguel M.Ugeda[1,2,3]

[1]*Donostia International Physics Center (DIPC), Paseo Manuel de Lardizábal 4, 20018 San Sebastián, Spain.* [2]*Centro de Física de Materiales (CSIC-UPV-EHU), Paseo Manuel de Lardizábal 5, 20018 San Sebastián, Spain.*
[3]*Ikerbasque, Basque Foundation for Science, 48013 Bilbao, Spain.*

*e-mail: rishav.harsh@gmail.com

Chemical substitution is a promising route for the exploration of a rich variety of doping- and/or disorder-dependent collective phenomena in low-dimensional quantum materials. Two dimensional (2D) crystals such as single layer transition metal dichalcogenides (TMDs) enable to explore a wealth of exotic electronic phenomena in presence of strong spin-orbit coupling and lack of inversion symmetry. Here we show that TMD alloys are ideal platforms to explore the effects of chemical substitution. In particular, we demonstrate the emergence of superconductivity in the otherwise metallic single-layer $TaSe_2$ by minute electron doping provided by substitutional W atoms at the Ta lattice sites. We investigate the temperature- and magnetic field-dependence of the superconducting state of $Ta_{1-\delta}W_{\delta}Se_2$ with electron doping (δ) using variable temperature (0.34–4.2 K) scanning tunneling spectroscopy (STS). We unveil the emergence of a superconducting dome spanning $0.003 < \delta < 0.03$ with a maximized critical temperature of 0.85 K, a significant increase from that of bulk $TaSe_2$ ($T_C = 0.14$ K). Superconductivity emerges from an increase of the density of states (DOS) as the Fermi surface approaches a van Hove singularity due to doping. Once the singularity is reached, however, the DOS decreases with δ, which gradually weakens the superconducting state, thus shaping the superconducting dome. Lastly, our doping-dependent measurements allow us to unambiguously track the development of a Coulomb glass phase triggered by disorder due to W dopants.

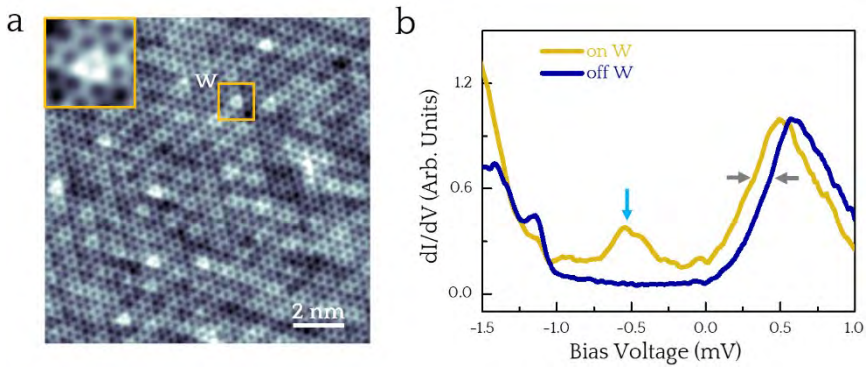

Figure: (a) Atomically resolved STM image of $Ta_{0.994}W_{0.006}Se_2$ ($V_t = -1$ V, I = 0.8 nA, T = 4.2 K). The inset show a zoom-in of the W atom boxed in the main image. (b) Large-scale dI/dV curves on pristine $TaSe_2$ (blue) and on one of the W atoms (yellow).

[1] Wen Wan et.al., arXiv:2203.05650 (2022).

Acknowledgements: M.M.U. acknowledges support by ERC Starting grant LINKSPM and the Spanish MINECO under grant no. PID2020-116619GB-C21. F.J R.H. acknowledges support from Marie Skołodowska-Curie Actions Individual Fellowships under HORIZON 2020 program for project MAGTMD.

Tuning magnetic anisotropies with superconductivity and spin-orbit interaction in epitaxial ferromagnet-superconductor hybrids

César González-Ruano[1,*], Diego Caso[1], Lina G. Johnsen[2], Coriolan Tiusan[3,4], Michel Hehn[4], Niladri Banerjee[5], Jacob Linder[2], Farkhad G. Aliev[1]

[1]*Departamento Física de la Materia Condensada C-III, Instituto Nicolás Cabrera (INC) and Condensed Matter Physics Institute (IFIMAC), Universidad Autónoma de Madrid, Madrid 28049, Spain.*
[2]*Department of Physics, Center for Quantum Spintronics, Norwegian University of Science and Technology, 7491 Trondheim, Norway.*
[3]*Department of Physics and Chemistry, Center of Superconductivity Spintronics and Surface Science C4S, Technical University of Cluj-Napoca, Cluj-Napoca 400114, Romania.*
[4]*Institut Jean Lamour, Nancy Universitè, 54506 Vandoeuvre-les-Nancy Cedex, France.*
[5]*Department of Physics, Loughborough University, Epinal Way, Loughborough LE11 3TU, UK.*

*e-mail: cesar.gonzalez-ruano@uam.es

Generation and control over long-range triplet (LRT) Cooper pairs is a key milestone for applications in superconducting spintronics. It has been commonly expected that these proximity effects require complex ferromagnetic multilayers, non-collinear magnetization or half-metals. With our work, we propose a new platform compatible with commercial spintronics.

We have studied all-epitaxial V/MgO/Fe junctions with competing in-plane and out-of-plane (OOP) magnetic anisotropies, and spin-orbit coupling (SOC) at the MgO interface. First, we experimentally demonstrated a thousand-fold increase in tunneling anisotropic magnetoresistance below the vanadium critical temperature (T_C), which supports LRT formation depending on the mangetic configuration of the Fe layer [1]. Then we studied the converse effect: the transformation of the in-plane and out-of-plane magnetocrystalline anisotropies of the Fe layer driven by the superconductivity of vanadium through the SOC-bearing MgO interface. Under an in-plane rotation of an external magnetic field, new easy axes for the magnetization appear below T_C, resulting in new stable in-plane magnetic configurations [2]. The effective perpendicular magnetic anisotropy (PMA) is also enhanced, inducing a partial OOP magnetization reorientation without any applied field, and a reduction of the field required to induce a complete OOP transition [3]. We modelled our results in terms of an additional contribution to the free energy of the ferromagnet arising from the controlled generation of triplet Cooper pairs, which depends on the relative angle between the exchange field of the ferromagnet and the spin-orbit field.

Our findings, supported by theoretical and numerical modelling of the ferromagnet-superconductor interaction, offer the ability to tune magnetic anisotropies using superconductivity - a key step in designing future cryogenic magnetic memories.

[1] I. Martínez et al., *Phys. Rev. Appl.* **13**, 014030 (2020).
[2] C. González-Ruano et al., *Phys. Rev. B* **102**, 020405(R) (2020).
[3] C. González-Ruano et al., *Sci. Rep.* **11**, 19041 (2021).

Study of the overdoped state in TLAG grown YBCO thin films oxygenated with ozone

Aiswarya Kethamkuzhi*, Lavinia Saltarelli, Kapil Gupta, Albert Queraltó, Joffre Gutierrez, Xavier Obradors, Teresa Puig

Institut de Ciència de Materials de Barcelona, ICMAB-CSIC, Campus de la UAB, 08193 Bellaterra, Catalonia, Spain.

*e-mail: akethamkuzhi@icmab.es

High temperature superconductors (HTS) are one of the most ambitious achievements since the discovery of superconductivity and they have the potential to revolutionize large-scale applications in the form of coated conductors (CC). $REBa_2Cu_3O_{7-d}$ (REBCO, RE = Rare Earth) coated conductors which belong to the class of HTS called cuprates are one of the highly studied materials due to their exceptional superconducting properties. Although there are many material science and engineering challenges set forth in the fabrication of high performance CC. The novel growth method developed at ICMAB for the fabrication of REBCO thin films is an ultrafast (100-1000 nm/s) and cost effective technique which combines Chemical Solution Deposition (CSD) with a non-equilibrium Transient Liquid Assisted Growth (TLAG) method [1].

The final step in the fabrication of REBCO coated conductors is called oxygenation and it determines the doping state which highly governs the superconducting properties of REBCO. Going to the overdoped state in REBCO films increases the condensation energy and therefore it is a very robust and homogeneous technique to increase current density J_c. The increase in current density in the overdoped state is already demonstrated in TFA-CSD and PLD grown YBCO films oxygenated at lower temperatures [2]. However, to attain the overoped state is quite challenging since the oxygen diffusion is very slow at lower temperatures. In this work we want to overcome this challenge using ozone assisted oxygenation to study the overdoped state of YBCO grown via TLAG-CSD because ozone can enhance the process of oxygen diffusion. The YBCO is oxygenated with a mixture of ozone/oxygen and the doping state is characterized by transport measurements, charge carrier density measurement and c-axis parameter. The primary investigation of the doping state shows that ozone treated YBCO films falls beyond the optimally doped region. Therefore ozone assisted oxygenation is a very promising method to go to the overdoped state and improve the performance of REBCO coated conductors. Results on different ozone treatments at different ozone concentrations, temperature and dwell times, together with their consequences to the charge carrier density and superconducting properties will be presented.

[1] Soler, L., Jareño, J., Banchewski, J. et al. Ultrafast transient liquid assisted growth of high current density superconducting films, *Nat. Commun.* **11**, 344 (2020)
[2] Stangl, A., Palau, A., Deutscher, G. *et al.*, Ultra-high critical current densities of superconducting $YBa_2Cu_3O_{7-\delta}$ thin films in the overdoped state, *Sci. Rep.* **11,** 8176 (2021).

Tunneling spectroscopy at very high magnetic fields in the iron based superconductor KFe_2As_2

M. Fernández-Lomana[1,*], B. Wu[1], E. Herrera[1], A. A. Haghighirad[2], H. Suderow[1,3], A. E. Böhmer[2,4] I. Guillamón[1,3]

[1]*Laboratorio de Bajas Temperaturas, Departamento de Física de la Materia Condensada, Instituto de ciencia de Materiales Nicolás Cabrera, Condensed Matter Physics Center (IFIMAC), Universidad Autónoma de Madrid, E-28049 Madrid, Spain.* [2]*Institute for Quantum Materials and Technologies (IQMT), Karlsruhe Institute of Technology, 76021 Karlsruhe, Germany.* [3]*Unidad Asociada de Bajas Temperaturas y Altos Campos Magnéticos, UAM, CSIC, Cantoblanco, E-28049 Madrid, Spain.* [4]*Institut für Experimentalphysik IV, Ruhr-Universität Bochum, 44801 Bochum, Germany.*

*e-mail: marta.fernandez-lomana@uam.es

After the discovery of high-temperature superconductivity in iron pnictide compounds, a large amount of experimental and theoretical effort has been made on the study of magnetic, superconducting and normal state properties. In the 122 system, superconductivity, with a $T_c \simeq 38$K, was first reported on $BaFe_2As_2$. Subsequently the $(Ba_{1-x}K_x)Fe_2As_2$ was studied in detail [1]. We present scanning tunneling spectroscopy measurements in KFe_2As_2. It has been proposed to be a nodal superconductor. The electronic effective mass is strongly enhanced due to the proximity to an orbital-selective Mott transition [1]. Here we make first STM measurements at very low temperatures and high magnetic fields [2]. At zero field, we identify a strong anisotropy of the superconducting gap. In the mixed state, we observe the vortex lattice at very large values of the magnetic field. We finally present measurements of the bandstructure in superconducting and normal phases, obtained at zero magnetic field and at a magnetic field of 20 T from quasiparticle interference scattering.

[1] F. Hardy et al., *Phys. Rev. Lett.* **111**, 027002 (2013).
[2] M. Fernández-Lomana et al., *Rev. Sci. Instrum.* **92**, 093701 (2021).

Towards hybrid van der Waals Josephson Junctions based on $NbSe_2$

C. González Sánchez[1,*], J. Cuadra[1], V. Barrena[1], A. Spuri[2], E. Scheer[2], H. Suderow[1], A. di Bernardo[2], E. J. H. Lee[1]

[1]*Department of Condensed Matter Physics, Universidad Autónoma de Madrid, Ciudad Universitaria de Cantoblanco, Spain.*
[2]*Department of Physics, Universität Konstanz, Universitätsstraße 10, Konstanz, Germany.*

*e-mail: celia.gonzalezs@uam.es

The emergence of van der Waals heterostructures has paved the way for a "designer" approach, in which novel devices and new physics can be obtained by combining the properties of distinct two-dimensional materials. Among the many possibilities in this context, heterostructures based on superconducting few-layer $NbSe_2$ attract great interest for studying Josephson effects and the superconducting proximity effect in 2D systems [1]. Interestingly, recent work has reported on signatures of a topological superconducting phase in heterostructures based on $NbSe_2$ and 2D ferromagnets [2]. Moreover, first demonstrations of magnetic vdW Josephson junctions have been very recently reported using a similar material combination [3, 4, 5, 6]. Motivated by the above developments, we present here our first steps towards the fabrication of nanodevices based on $NbSe_2$, including our first attempts to fabricate Josephson junctions with ferromagnetic and antiferromagnetic tunnel barriers.

[1] N. Yabuki et al., *Nat. Commun.* **7,** 10616 (2016).
[2] S. Kezilebieke et al, *Nat.* **588,** 424 (2020).
[3] H. Idzuchi et al., *Nat. Commun.* **12,** 5332 (2021).
[4] K. Kang et al., *arXiv:2101.01327*
[5] L. Ai et al., *Nat. Commun.* **12,** 6580 (2021).
[6] K. Kang et al., *arXiv: 2201.09185*

Local modulation of the superconducting order parameter for energy-efficient functional devices based on fluxonic effects

Jordi Alcalà*, Alejandro Fernández-Rodriguez, Aleix Barrera, Thomas Günkel, Lluís Balcells, Narcís Mestres, Anna Palau

Institut de Ciència de Materials de Barcelona (ICMAB-CSIC), Campus UAB 08193, Bellaterra, Barcelona, Spain.

*e-mail: jalcala@icmab.es

The expanding use and increasingly complex nature of Information and Communication Technologies (ICT) goes hand in hand with an increase in its energy demands and will heavily impact on the future climate change. Up to now, expansion of storage capabilities and ICT performance is based on improvements and innovations in the semiconductor technology. However, the scalability and power consumption of current devices based on silicon oxide semiconductors is reaching their physical limits. Superconducting technologies, with intrinsic energy efficiency associated to dissipationless supercurrents, may bring revolutionary ideas to design functional devices for sustainable ICT.

Our goal is focused on the exploration of new strategies for the design of energy-efficient functional devices based on high-temperature superconductors. In particular, we use field-induced oxygen vacancy modulations, combined with high resolution lithography techniques, to locally and reversibly tune the superconducting parameter, opening comprehensive prospects for gate-modulated electronic devices. With a proper device design, we have been able to homogenously and reversibly tune a superconducting channel or part of it, ON and OFF, by means of an electric field as external control parameter. Moreover, by using of micro-metric arrays of metallic contacts with different sizes and shapes we have been able to locally and reversibly deoxygenate the material and create gate-modulated insulating regions within the superconducting device, acting as reversible pinning landscapes with controlled motion of flux quanta (vortices) [1, 2]. The normal state resistance, the superconducting critical temperature and the critical current density can be reversibly manipulated in confined active volumes of the film by gate-tunable oxygen vacancy diffusion. The geometry of specific patterns as triangle dots or lines in our YBCO tracks done by photolithography process can modify the behavior of the vortex dynamics and the corresponding magnetic trapped fields, improving our superconducting properties. Lateral oxygen mobility may be finely modulated, at the micro-and nano-scale, by tuning the applied bias voltage and operating temperature thus providing the basis for the design of homogeneous and flexible transistor-like devices with loss-less superconducting drain-source channels.

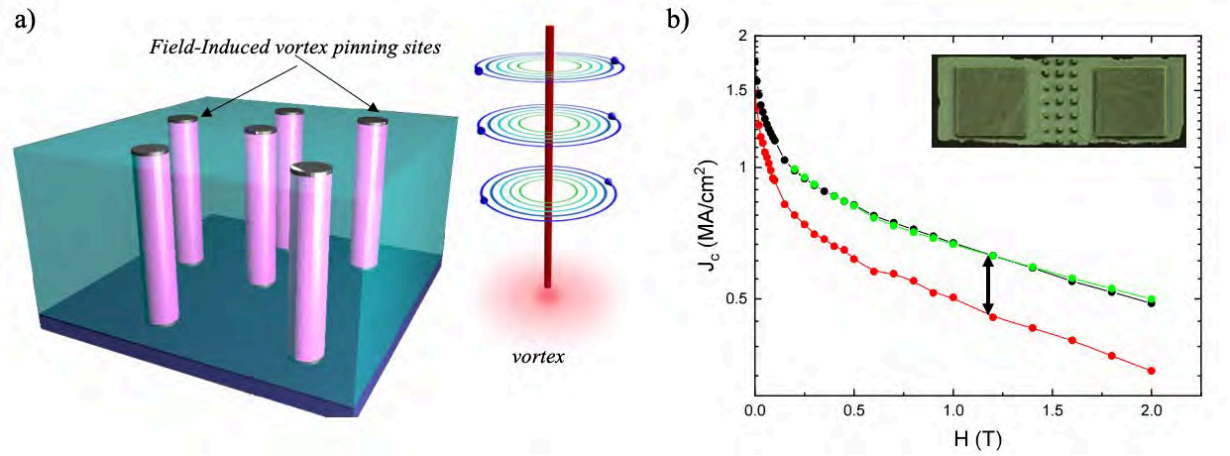

Figure 1. a) Schematic representation of field-induced vortex pinning landscape. b) Critical current density modulation of a superconducting track with engineered pinning sites.

[1] Alcalà et al. *Surfaces and Interfaces of Metal Oxide Thin Films, Multilayers, Nanoparticles and Nano-composites*, Springer, Book Chapter, 167(2021).
[2] Palau et al., *ACS Appl Mater. Interfaces* **10,** 30522 (2018).

Superconducting gap and magnetoresistance of layered $AuSn_4$

Edwin Herrera[1], Beilun Wu[1], Evan O'Leary[2], Alberto M. Ruiz[3], **Miguel Águeda**[1,*], Pablo García Talavera[1], Víctor Barrena[1], Jon Azpeitia[4], Carmen Munuera[4], Mar García-Hernández[4], Linlin Wang[2], Adam Kaminski[2], Paul C. Canfield[2], José J. Baldoví[3], I. Guillamón[1], H. Suderow[1]

[1]*Laboratorio de Bajas Temperaturas y Altos Campos Magnéticos, Departamento de Física de la Materia Condensada, Instituto Nicolás Cabrera and Condensed Matter Physics Center (IFIMAC), Unidad Asociada UAM-CSIC, Universidad Autónoma de Madrid, E-28049 Madrid, Spain.*
[2]*Ames Laboratory, Ames and Department of Physics & Astronomy, Iowa State University, Ames, IA 50011, USA.*
[3]*Instituto de Ciencia Molecular (ICMol), Universidad de Valencia, Catedrático José Beltrán 2, 46980 Paterna, Spain.*
[4]*Instituto de Ciencia de Materiales de Madrid, Consejo Superior de Investigaciones Científicas (ICMM-CSIC), Sor Juana Inés de la Cruz 3, 28049 Madrid, Spain.*

*e-mail: miguel.agueda@estudiante.uam.es

$PtSn_4$ and $PdSn_4$ are nonsuperconducting semimetals showing a huge magnetoresistance which has been related to a possibly topologically non-trivial bandstructure. Here we synthesize and characterize single crystals of the related superconducting compound $AuSn_4$. We obtain a residual resistance ratio above 120 and a critical temperature of T_c = 2.35 K. We measure the magnetoresistance (MR) up to 14 T and find an approximately linear and large MR at low temperatures, with a field induced increase of the resistance by about 500%. We measure the band structure using angular resolved photoemission spectroscopy (ARPES) and compare with Density Functional Theory (DFT) calculations. We measure the superconducting density of states and its temperature dependence using Scanning Tunneling Microscopy (STM) and find a superconducting gap value compatible with BCS theory. The shape of the density of states suggests a large distribution of values of the superconducting gap over the multiple Fermi surface sheets. STM furthermore provides a critical temperature T_c which is larger than Tc observed using bulk techniques. We suggest that this might be due to localized modifications of T_c due to stacking faults.

Magneto-transport properties and anomalous Hall effect of superconductor/ferromagnetic heterostructures

Gabriel Caballero[1], Ana Parente[2], Eugenia Sebastiani[2], Andrés Taborda[2], Manuel Osorio[1], Ignacio Figueruelo[1,2], Álvaro Muñoz-Noval[1,2], Elvira Gonzalez[1,2], Mariela Menghini[1]

[1]*IMDEA Nanociencia, C/Faraday 9, Madrid, Spain.*
[2]*Facultad Ciencias Físicas, Universidad Complutense de Madrid, Plaza de Ciencias 1, Madrid, Spain.*

*e-mail: gabriel.caballero@imdea.org

Ferromagnetism and superconductivity are of high interest not only from the point of view of fundamental condensed matter physics but also due to their potential applications in quantum computing, memories, sensors, etc. Although these states of matter can be considered antagonist, the interplay between a ferromagnet (FM) in contact with a superconductor (SC) can lead to a wide variety of exotic phenomena. For example, it has been predicted that the screening currents in the SC can nucleate skyrmions in the FM [1] or that magnetic skyrmions can induce superconducting vortices in the absence of an external magnetic field [2].

We have fabricated Hall bars of ferromagnetic multilayers [Pd (6 Å)/ Co (3 Å)]$_{20}$ by magnetron sputtering and optical lithography. These multilayers present perpendicular magnetic anisotropy (PMA). Anti-dot nanostructures of superconducting Nb were fabricated on top of the ferromagnetic multilayer. We have characterized the magneto-electric properties and the anomalous Hall effect of the fabricated SC/FM heterostructures above and below the SC critical temperature (T_C).

[1] V. L. Vadimov et al., *Appl. Phys. Lett.* **113**, 032402 (2018).
[2] J. Baumard et al., *Phys. Rev. B* **99**, 014511 (2019).

Fabrication and characterization of the high-temperature superconductor $Bi_2Sr_2CaCu_2O_{8+\delta}$ for van der Waals heterostructures

Ignacio Figueruelo[1,2,*], Julia García[1], Aída Serrano[3], Elvira M. Gonzalez[1,2], Mariela Menghini[1]

[1]*IMDEA-Nanociencia, Cantoblanco, 28049 Madrid, Spain.*
[2]*Departamento Física de Materiales, Facultad Ciencias Físicas, Universidad Complutense, 28040 Madrid, Spain.*
[3]*Departamento de Electrocerámica, Instituto de Cerámica y Vidrio (CSIC), 28049 Madrid, Spain.*

*e-mail: Ignacio.figueruelo@imdea.org

2D layered van der Waals materials have been one of the most interesting and richest topics in condensed matter physics in the last decade due to their fascinating properties, including emergent phenomena which can arise from stacking materials with different properties. $Bi_2Sr_2CaCu_2O_{8+\delta}$ (BSCCO-2212) is one of the most studied high Tc superconductors in which, depending on the hole doping, different quantum phases appear such as Mott insulator associated with an antiferromagnetic order, non-conventional superconductivity, strange metal or pseudo-gap phase.

In this work, we have characterized the structural and superconducting properties of BSCCO-2212 exfoliated flakes with the final aim of fabricating van der Waals heterostructures based on high-Tc superconductors. The exfoliated flakes have thicknesses between 20-100 nm and have been characterized by different techniques such as Raman spectroscopy, AFM and transport measurements at low temperatures and high magnetic fields.

Low dimensional effects in superconducting nanostructures

A. Parente[1,*], M. Abuin[2], José. L. Prieto[2], M. Menghini[3], E. M. González[1,3], A. Muñoz-Noval[1]

[1]*Departmento de Física de Materiales, Facultad de Ciencias Físicas, Universidad Complutense, 28040 Madrid, Spain.*
[2]*Instituto de Sistemas Optoelectrónicos y Microelectrónica, Universidad Politécnica, 28040 Madrid, Spain.*
[3]*IMDEA Nanociencia, Cantoblanco, 28049 Madrid, Spain.*

*e-mail: aparente@ucm.es

Due to the miniaturization of electronic devices, quantum mechanical effects become important. A fundamental question is how the collective properties of these devices, such as superconductivity, are affected when the systems dimensions are reduced. In this context, low dimensional effects in superconducting nanostructures have been studied.

In this work, superconducting nanostructures have been fabricated combining nanolithography techniques with DC magnetron sputtering. Morphological characterization has been done using different microscopy techniques such as AFM and SEM. Transport measurements al low temperature allows the distinction of two different regimes due to lateral confinement: nanowire regime and thin film regime. The main goal of this work is to study how the fabrication process influences the superconducting properties of these nanostructures.

Hybrid superconducting-ferromagnetic structures for sustainable functional devices

A. Barrera*, J. Alcalà, T. Gunkel, L. Balcells, N. Mestres, A. Palau

Institut de Ciència de Materials de Barcelona (ICMAB-CSIC), Campus de la UAB 08193 Bellaterra, Spain.

*e-mail: abarrera@icmab.es

Technology of Internet of Things (IoT) aims to implant a huge amount of wireless sensor networks (WSN) to enhance people comfortability and society control [1]. However, the desire of apply the Internet of Things in all possible objects and places, requires the development of new processing technologies that work in nano and micro scale in an efficient and sustainable way. Regarding to this field, multifunctional oxides have attracted special attention for their capacity to modify their magnetic or electric properties by applying an adequate stimulus. In specific, superconducting cuprates mixed with ferromagnetic materials (FM-SC hybrids) have presented novel and unique magnetic tunability.

The combination of YBCO (SC) and permalloy (FM) materials in hybrid devices (Figure 1 (a)), one can manipulate magnetic textures, through loss-less superconducting stray fields or transport super-currents. Multiple magnetic states with different magnetoresistance signal can be stabilized at remanence and modified by applying small magnetic fields or currents (Figure 1 (b)) [2].

Furthermore, these two antagonist materials (FM with aligned spins and SC with cooper pairs of opposite spins) can be combined to induce complex interactions that may be used for several applications. In particular, hybrid FM-SC metamaterials open new venues for energy-efficient information storage and manipulation and magnetic field control and guidance [3].

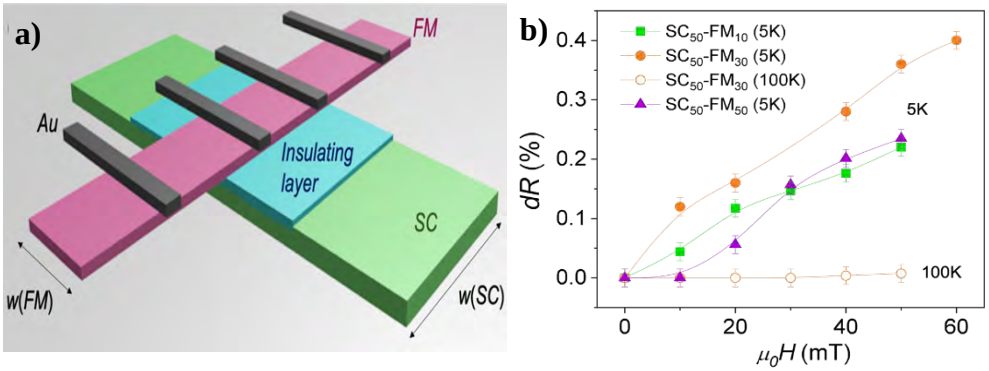

Figure 1. (a) Schematic of SC-FM devices. (b) Remanent magnetoresistance ratio as a function of the magnetic field.

[1]L. Atzori, A. Iera, et al., *Comput. Networks* **54**, 2787 (2010).
[2] J. Alcalà, A. Barrera, A. Palau, et al., *Surfaces and Interfaces of Metal Oxide Thin Films*, ***Chapt 6***, Springer (2021).
[3] J. Prat-Camps, N. Carles, et al., *Appl. Phys. Lett.* **105**, 234101 (2014).

Acknowledgements: We acknowledge financial support from Spanish Ministry of Science, Innovation and Universities (MICIU) through SUMATE project (RTI2018-095853-B-C21), co-financed by the European Regional Development Fund, and the METAMAG project (FUNMAT-FIP-2020), and Severo Ochoa FUNFUTURE (CEX2019-000917-S). We also thank support from the European Union for NANOCOHYBRI project (Cost Action CA 16218) and MetaMagIC EU CHIST-ERA project (PCI2021-122028-2A), co-financed by the AEI, and from the Catalan Government with 2017-SGR-1519 and Xarmae.

The Little-Parks effect in full-shell Al-InAs hybrid superconductor-semiconductor nanowire devices

M. Gómez[1,*], Á. Ibabe[1], I. Casal[1], G. O. Steffensen[2], J. Nygard[3], A. Levy Yeyati[2], E. J. H. Lee[1]

[1]*Departmet of Condensed Matter Physics, Universidad Autónoma de Madrid, Spain.*
[2] *Department of Theoretical Condensed Matter Physics, Universidad Autónoma de Madrid, Spain.*
[3]*Center of Quantum Devices, Niels Bohr Institute, University of Copenhagen, Denmark.*

*e-mail: mario.gomezg@uam.es

The experimental realization of a topological superconductor and Majorana zero modes (MZMs) has been a hot topic in Condensed Matter Physics during the last decade. One of the most promising proposed routes towards this goal is based on semiconducting nanowires with strong spin-orbit coupling, induced superconductivity, and an external magnetic field [1, 2]. Despite the remarkable improvements in the experiments over the past years, a fully conclusive demonstration of such an exotic phase is however still lacking.

More recently, a proposal to realize the elusive Majorana quasiparticles using lower magnetic fields has been put forward. In this case, the topological phase transition results from the application of an odd number of magnetic fluxes in full-shell proximitized nanowires [3, 4]. This system has been studied in the tunnel regime, whereby zero-bias peaks were interpreted in favor of a topological origin [4]. A detailed study of the Josephson effect in this type of hybrid nanowires is however still missing.

In this work, we measured different superconducting devices based on hybrid InAs nanowires with a full epitaxial Al shell. We first studied the superconductivity of the Al shell with an external magnetic field applied parallel to the nanowire axis, observing characteristic Little-Parks oscillations of the critical current (Figure 1). Unexpectedly, we also observed the onset of a finite, small resistance in the superconducting shell in the Little-Parks regime. In parallel, we explored Josephson junctions fabricated by partially removing the Al shell in a nanowire segment to create a semiconducting weak link. Here, we studied the Little-Parks oscillations of the superconducting gap and of the excess and switching currents of our junctions (Figure 2). We anticipate that the exploration of the Josephson effect in this hybrid system will contribute to shedding further light onto the physics of full-shell superconductor-semiconductor nanowires.

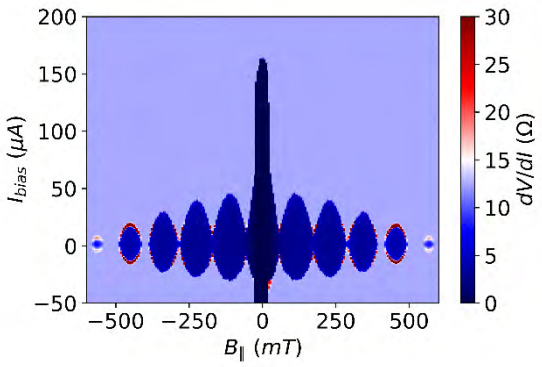

Figure 1. Current biased measurement of the differential resistance as a function of parallel magnetic field in the epitaxial Al shell.

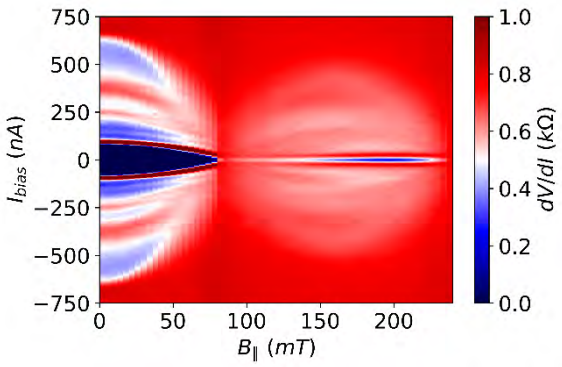

Figure 2. Current biased measurement of the differential resistance as a function of parallel magnetic field in the Al/InAs-NW/Al Josephson Junction.

[1] R. M. Lutchyn et al., *Phys. Rev. Lett.*, **105**, 077001 (2010).
[2] Y. Oreg et al., *Phys. Rev. Lett.* **105**, 177002 (2010).
[3] R. M. Lutchyn et al., *arXiv:1809.05512* (2018).
[4] S. Vaitiekenas et al., *Science* **367**, eaav3392 (2020).

Reduced size STM in high magnetic fields

Pablo García[1,*], Rafael Álvarez-Montoya[1], Raquel Sanchez-Barquilla[1], Beilun Wu[1], Edwin Herrera[1], Juan Ramón Marijuan[2], Hermann Suderow[1,3], Isabel Guillamón[1,3]

[1]*Laboratorio de Bajas Temperaturas, Departamento de Física de la Materia Condensada, Instituto de Ciencia de Materiales Nicolás Cabrera, Condensed Matter Physics Center (IFIMAC), Universidad Autónoma de Madrid, E-28049, Spain.* [2]*Segainvex, Universidad Autónoma de Madrid, 28049 Madrid, Spain.* [3]*Unidad Asociada de Bajas Temperaturas y Altos Campos Magnéticos, UAM, CSIC, Cantoblanco, E-28049 Madrid, Spain.*

*e-mail: pablo.garciat@estudiante.uam.es

Cryogenic Scanning Tunneling Microscopy (STM) has been instrumental in the development of scanning probe microscopies. Actually, the first observation of the work function, which established vacuum tunneling, could only be confirmed after knowing the cryogenic properties of piezoelectric materials, with measurements performed at ETH and at UAM [1]. The reduction of thermal activation and smearing is unavoidable to obtain surfaces with a spatial and energy resolution that allows sufficiently accurate comparison to calculations [2]. The addition of a magnetic field opens new prospects, such as the observation of vortex lattices in superconductors or of Landau quantization [3,4,5]. For the latter, it is of particular importance to decrease as far as possible the size of the STM. Although efforts made during past years have led to some improvements [6,7,8], the size is still far above the typical sizes available for instruments used in high magnetic fields. Here we discuss efforts to further reduce the size of the STM, with the aim to be able to work at extremely high magnetic fields and to build a system allowing for rotation of the STM in a magnetic field. Both the head and the base of the main body of the STM have been manufactured through 3D printing in grade 3 Titanium, which could turn out to be a good method to optimize the weight without modifying too much the stiffness of the microscope. Finite element calculations of the 3D printed system support the latter aspect. The STM has a diameter of 16 mm and a height of 23 mm. We discuss a new design of the approach motor and the piezotube support system, as well as results of the first tests.

[1] G. Binning and H. Rohrer, *Nobel Lecture, Physics* (1986).
[2] I. Guillamón et al., *Physical Review Letters* **101**, 166407 (2008).
[3] H. Suderow, I. Guillamón, J. G. Rodrigo and S. Vieira, *Superconductor Science and Technology* **27**, 063001 (2014).
[4] I. Guillamón et al., *Nature Physics* **10**, 851 (2014).
[5] F. Martín Vega et al., Tunneling spectroscopy of WTe_2: bandstructure and high magnetic field Landau quantization, in preparation.
[6] H. Suderow, I. Guillamón, and S. Vieira, *Review of Scientific Instruments* **82**, 033711 (2011).
[7] M. Fernández-Lomana et al., *Review of Scientific Instruments* **92**, 093701 (2021).
[8] Y. Jae Song et al., *Review of Scientific Instruments* **81**, 121101 (2010).

High-quality factor NbTiN superconducting resonators for quantum technologies

D. Rodriguez[1,*], M. C. de Ory[1], M. T. Magaz[1], D. Granados[2], A. Gomez[1]

[1]*Centro de Astrobiología CSIC-INTA, 28850 Torrejón de Ardoz, Spain.*
[2]*IMDEA Nanociencia, Calle Faraday 9, Campus de Cantoblanco, 28049 Madrid, Spain.*

* e-mail: drodriguez@cab.inta-csic.es

NbTiN thin films have recently demonstrated advantageous properties over traditional superconductors such as Nb and Al for superconducting quantum applications. For instance, it has higher Tc and a very high upper critical field [1,2], allowing maintaining high internal quality factors even in presence of high magnetic fields.

We present our work on developing NbTiN superconducting lumped element resonators (LERs). Each LER consists of a series inductance-capacitance circuit coupled in parallel to a single transmission line. Contrary to coplanar wave resonators, LERs allow large freedom in the geometry design, which enables to control of key parameters such as the quality factor and the induced field volume. In addition, LERs are intrinsically multiplexable on-chip, which allows the simultaneous readout of several qubits at different frequencies. These types of resonators are crucial elements in many quantum applications [3] such as quantum electrodynamics circuitry, quantum sensing, and astronomy detectors. The work presented here includes the nanofabrication process of high-quality superconducting NbTiN films and the cryogenic set-up developed for its calibration including a proper IQ cryogenic calibration process.

A complete analysis of the NbTiN resonators performance as a function of thickness has been performed which includes the thickness dependence of critical parameters such as sheet resistance, kinetic inductance, critical temperature, upper critical field, and BCS parameter. The quality factors of over 1 million obtained in this work and the noise traces prove the good performance of these devices and open the possibility of their application in quantum technologies as highly sensitive detectors for quantum communications or as basic building blocks for molecular spin qubits or gatemon qubits.

[1] Zaytseva, I., Abaloszew, A., Camargo, B.C. et al., *Sci. Rep.* **10,** 19062 (2020).
[2] Swails, N. S. Depairing current density in NbTiN superconducting films (Doctoral dissertation). (2018).
[3] Stefan Weichselbaumer et al., *Phys. Rev. Applied* **12**, 024021 (2019).

Acknowledgments: This work was supported by Spanish Ministry of Science and Innovation under Grant PID2019-105552RB, Grant SEV-2016- 0686, and ONR-Global through Grant DEFROST N62909-19-1-2053. This project has also received funding from the European Union's Horizon 2020 research and innovation program under grant agreement No 862893 (FATMOLs). We also acknowledge support from CSIC Research Platform PTI-001.

Hybrid Superconducting Nanowire Single-Photon Detectors

Cristina García-Pérez[1,*], Julia García-Pérez[1,], Marina C. De Ory[1], María Acebrón[1], María Teresa Magaz[1,2], Ramón Bernardo-Gavito[1], Alicia Gómez[2], Daniel Granados[1]

[1]*IMDEA Nanociencia, Calle Faraday, 9, 28049 Madrid, Spain.*
[2]*Centro de Astrobiología (CAB) INTA-CSIC, Ctra. Torrejón-Ajalvir km.4, 28850 Madrid, Spain*

*e-mail: cristina.garcia@imdea.org

Superconducting nanowire single-photon detectors (SNSPDs) exhibit extremely high timing performance and sensitivity [1]. Nevertheless, their operating temperature is restricted to low temperatures (T<10K), increasing the cost and operation complexity [2]. In an SNSPD, a short voltage pulse is obtained when a photon hits the nanowire, and it breaks Cooper pairs, generating a hotspot with a finite resistance. These detectors exhibit a shallow dark count rate (DCR), low jitter, high detection efficiency, fast time response and polarization sensitivity. However, they have limitations related to the latching and reset dead time,and some frequency bands are not accessible due to constraints imposed by the superconducting bandgap.

To enhance the performance of SNSPDs, most groups have focused their efforts on fabricating the devices on top of photonic structures or optimizing the nanowire geometry [3]. Our objective is to manufacture hybrid systems based on traditional superconductors (Nb, NbTi, NbTiN) and 2D materials (Graphene, TMDs) maintaining good performance but reducing latching, reset time[2], and expanding the detection limit. Graphene would quickly release the thermal energy of the hotspot and lessen the latching effects due to its high thermal conductivity and sizeable kinetic inductance. TMDs would act as absorbers, expanding the detection limit.

SNSPDs have been manufactured by a bottom-up scheme.The Nb nanowires are produced via electron-beam lithography (EBL) with PMMA resist onto SiOx/Si followed by metal evaporation of an Nb layer with a thickness of <50 nm. Graphene is fabricated by chemical vapour deposition (CVD) and transferred on top of the nanowires. They were characterized by scanning electron microscopy (SEM), atomic force microscopy (AFM), optical microscopy and micro-Raman spectroscopy. The voltage pulse response has been investigated under different bias current conditions, different operation temperatures below de T_c and different illumination conditions. All measurements have been performed in a close circuit cryostat setup, with optical access and scanning capabilities. Preliminary results show $T_c \approx 5.8$K and $I_c(T=4.48K) \approx 58\mu A$ (Figure 1 (a)). We have investigated how the photoresponse varies locally within the area of the superconducting meander by scanning the SNSPS under a 488nm focused laser spot with several illumination powers. We are currently studying the dynamic response to pulsed light (488 nm) for meanders of different width with and without graphene layers on top. Nb meanders with graphene exhibit a four-fold increase in their response when compared to nanowires without (Figure 1 (b)).

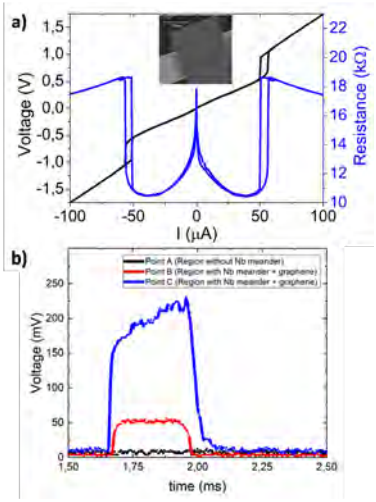

Figure 1. (a) I-V curve obtained at T=4.48 K. Inset: SEM image of a ~ 1 mm-long and 315 nm-wide Nb meander. (b)Voltage pulses measured when illuminating the hybrid system (2 µm width Nb meander with graphene) with 488 nm laser light at 333 Hz in several regions.

[1] Rogalski A., and Sizov F., *Opt. Elect. Rev*. **19**(3), 346 (2011).
[2] Hadfield R. *Nature Photon* **3,** 696 (2009).
[3] Zhang, W., You, L., Li, H. et al., *Sci. China Phys. Mech. Astron*. **60**, 120314 (2017).

Acknowledgements: This work is partially supported through Grants DETECTA ESP2017-86582-C4-3-R and EQC2018-005134-P (MICIN-AEI), P2018/NMT-4291 TEC2-SPACE-CMand G#2019-T2/IND-13367 (C.Madrid). A.G. and D.G. acknowledge the Office of Naval Research Global for the financial support through Grant ONR-G #N62909-19-1-2053 (DEFROST). IMDEA Nanociencia acknowledges support from the "Severo Ochoa" programme for Centres of Excellence in R&D (MINECO, Grant SEV-2016-0686).

Tuning the electronic structure of High-Temperature Superconducting films by field-induced oxygen diffusion

T. Günkel[1,*], A. Fernandez-Rodríguez[1], J. Alcalà[1], N. Mestres[1], J. Suñe[2], A. Palau[1]

[1]*Institut de Ciència de Materials de Barcelona, ICMAB-CSIC, Campus UAB, 08193 Bellaterra, Spain.*
[2]*Dept. d'Enginyeria Electrònica, Universitat Autònoma de Barcelona, 08193 Bellaterra, Spain.*

*e-mail: tgunkel@icmab.es

A unique feature of high-temperature superconductors is that their properties strongly depend on their carrier concentration. In cuprates, reversible modulation of the carrier density can be produced using electric field pulses, inducing a "Resistive Switching (RS) effect" to eventually achieve a metal-insulating transition (MIT) [1]. The mechanism underlying the RS effect in these materials is still unclear, although oxygen vacancies certainly play a key role. Oxygen ex-corporation/incorporation in the system implies a variation of the charge carriers and accordingly a valence change in the transition metal 3d band.
We present studies on the bipolar RS effect in $YBa_2Cu_3O_{7-\delta}$ superconducting thin films evaluated by hysteretic $I(V)$ curves measured on micrometric metal electrodes. Temperature-dependent transport and resistance measurements together with micro-Raman experiments were performed to evaluate the local oxygen diffusion through the material in different electrode configurations. In particular, the implication of the intrinsic anisotropic oxygen diffusion in cuprates has been studied experimentally and corroborated with simulations. We demonstrate that non-volatile volume phase transitions can be induced to generate transistor-like devices with free-resistance channels in which the electric field magnitude and direction, temperature, and anisotropic oxygen mobility determine their characteristics. Furthermore the controlled oxygen diffusion is exploited to demonstrate its possible applications as memristive devices for neuromorphic computing [2].

[1] Palau, Anna, et al., *ACS applied materials & interfaces* **10**, 30522–30531 (2018).
[2] Fernández-Rodríguez, Alejandro, et al., *Materials* **13**, 281 (2020).

STM at high magnetic fields in the superconducting series $FeSe_{1-x}S_x$

Raquel Sánchez-Barquilla[1,2,*], Pablo García[1,2], Francisco Martín-Vega[1,2], Beilun Wu[1,2], Edwin Herrera[1,2], Juan Schmidt[3,4], Mingyu Xu[3,4], Sergey Bud'ko[3,4], P.C. Canfield[3,4], Hermann Suderow[1,2], Isabel Guillamón[1,2]

[1]*Laboratorio de Bajas Temperaturas y Altos Campos Magnéticos, Departamento de Física de la Materia Condensada, Instituto Nicolás Cabrera and Condensed Matter Physics Center (IFIMAC), Universidad Autónoma de Madrid, Cantoblanco, E-28049 Madrid, Spain.* [2]*Unidad Asociada de Bajas Temperaturas y Altos Campos Magnéticos, UAM/CSIC, Cantoblanco, E-28049 Madrid, Spain.* [3]*Ames Laboratory, U.S. DOE, Iowa State University, Ames, Iowa 5011, USA.* [4]*Department of Physics and Astronomy, Iowa State University, Ames, Iowa 50011, USA.*

*e-mail: raquel.sanchezb@uam.es

$FeSe_{1-x}S_x$ is the simplest Fe-based superconductor. Without doping, bulk single crystals undergo a tetragonal to orthorhombic transition at T_{nem} = 90 K and a superconducting transition at T_c = 8.5 K [1]. When doping, Tc changes, reaching the maximum value around x = 0.09. At x = 0.17, the structural transition disappears, and the material remains in the tetragonal phase. At x = 0.29, the material is well above the nematic transition with T_c = 5 K [1]. FeSe has a peculiar band structure with small Fermi surface pockets and Fermi energies. Tight-binding models show that the Fermi surface consists of two electron bands ε and δ and one hole band α [2, 3], although recent studies suggest that the single hole pocket around Γ splits into two pockets at the surface [4].

Here, we present STM measurements at very low temperatures (0.1 K) and at high magnetic fields (up to 15 T) in two compounds of the series: FeSe (x=0) and $FeSe_{0.71}S_{0.29}$ (x=0.29). First, we compare the superconducting gap in the nematic (x = 0) and the tetragonal phases (x = 0.29) at zero magnetic field. We have performed quasi-particle interference (QPI) measurements, where we can resolve different bands and find a change from two-fold to four-fold symmetry at energies below the superconducting gap. Finally, we have observed the vortex lattice under very large magnetic fields and discuss the changes in the vortex core shape induced by doping.

[1] P. Wiecki et al., *Phys. Rev B* **98**, 020507(R) (2018).
[2] S. Mukherjee et al., *Phys. Rev. Lett.* **115**, 026402 (2015).
[3] A. Kreisel et al., *Phys. Rev. B* **92**, 224515 (2015).
[4] C. Li et al., *Phys. Rev. X* **10**, 031033 (2020).

Sistemas interactuantes de baja dimensionalidad fuertemente correlacionados

Presentaciones orales

Miércoles 13/07:

15:30-15:50 Michael Pepper (University College London). *Non-Magnetic Fractionally Quantized Conductance in Quasi-One Dimensional Semiconductor Structures*

15:50-16:10 Dragana Popovic (National High Magnetic Field Laboratory, Florida State University). *Quench dynamics in two-dimensional electron systems: Long-range vs short-range Coulomb interactions*

16:10-16:30 Yuval Gefen (Weizmann Institute of Technology). *The Role of Neutral Modes at the Edge of Quantum Hall Phases: The Emergence of Superconductivity*

16:30-16:50 Vladimir Kravtsov (ICTP). *Sensitivity of (multi)fractal eigenstates to perturbation of the Hamiltonian*

16:50-17:05 Manuel Pino (Universidad de Salamanca). *Scaling up the Anderson transition in random-regular graphs*

17:05-18:00 **Pósteres y café**.

18:00-18:20 Vladimir Dobrosavljevic (Florida State University, Tallahassee, Florida, USA). *Disorder-dominated quantum criticality in moiré bilayers*

18:20-18:40 Javier E. Villegas (Unité mixte de Physique CNRS/Thales). *Tunnel electroresistance and photomemristive effects in strongly-correlated oxide/metal junctions*

18:40-19:00 C. Anton-Solanas (Universidad Autónoma de Madrid). *Exciton-polaritons with 2D materials, from cryogenic to ambient conditions*

19:00-19:15 J. Molina-Vilaplana (Universidad Politécnica de Cartagena). *A Non-Gaussian Variational Approach to Interacting Bosons in One Dimensional Lattices*

19:15-19:30 Alberto Rodríguez (Universidad de Salamanca). *Chaos for Interacting Bosons and Random Two-Body Hamiltonians*

Jueves 14/07:

15:30-15:50 I V Yurkevich (Aston University). *Superconducting edge states in a topological insulator*

15:50-16:10 Victor Kagalovsky (Shamoon College of Engineering). *The emergence of the non-interacting channel in the strongly interacting 1D system*

16:10-16:30 Vincent Humbert (Unité mixte de Physique CNRS/Thales). *Overactivated transport in the localized phase of the Superconductor-Insulator transition*

16:30-16:45 Shamashis Sengupta (IJCLab Paris-Saclay). *Superconductor-Insulator transition in YSi thin films*

16:45-17:05 Aviad Frydman (Bar Ilan University). *The Superconducting Dirac Point in Proximitized Graphene*

17:05-17:45 **Café**.

17:45-18:05 Claire Marrache-Kikuchi (Université Paris-Saclay). *Crossover from impurity-controlled superconductivity to granular superconductivity in (TMTSF)2ClO4*

18:05-18:25 Mariela Menghini (IMDEA Nanociencia). *Room temperature Mott metal-insulator transition in V2O3 compounds*

18:25-18:40 María Tenorio Tuñas (Instituto Catalán de Nanociencia y Nanotecnología). *Doped Nanoporous graphene as a new material for ultrasharp superlattice heterojunctions*

18:40-18:55 Enrique Abad (Universidad de Extremadura). *Ping-pong balls in motion: peculiarities of diffusive transport and structure formation*

18:55-19:10 Vladimir Gasparian (California State University, Bakersfield). *Anomalous Faraday effect in a PT -symmetric dielectric slab*

Pósteres

- Jose Antonio Moreno (Universidad Autónoma de Madrid). *Electronic band structure inside the superconducting gap from Yu-Shiba-Rusinov states in quasi two-dimensional 2H-NbSe2-xSx*
- Pablo de Vera Gomis (Universidad de Murcia). *Ab-initio electronic excitation spectra of ceria: input data for surface-science radiation-transport simulations*
- Miguel Águeda Velasco (Universidad Autónoma de Madrid). *Thin films of superconducting Au proximitized with Nb under magnetic fields*
- Arin Escobar Ortiz (Universidad Autónoma de Madrid). *Coexistence of superconductivity and excitonic condensates in two-dimensional crystals*

Electron Interactions in Quasi-1D Semiconductor Nanostructures

M. Pepper

University College London, UK.

e-mail: michael.pepper@ucl.ac.uk

Lateral confinement of electrons in a 2D electron gas results in the establishment of size quantized quantum levels and a quantization of the conductance. The levels appear at values of conductance of $2ne^2/h$, where n is the subband index and the factor of 2 arises from the spin degeneracy. However, as the width of the conducting channel increases but transport is still quasi-1D the energy levels become determined by the mutual interactions between the electrons. As the ground state changes with increasing interaction the carriers will tend to adopt a zig-zag configuration to decrease the electron-electron repulsion.

We describe our recent work in which the behaviour of the levels and the conductance values have been measured in wide channels at very low values of carrier concentration, just prior to the transition to 2D transport. Using holes in Ge and electrons in GaAs evidence is presented for the splitting of the line of electrons comprising the ground state into two. Following this ground state splitting we observed non-magnetic fractionally quantized conductance plateaus which for holes in Ge may correspond to fractional charges of $e/2$ and $e/4$. Electrons in GaAs showed a strong $(2/5)\,e^2/h$ plateau which can be theoretically explained on the basis of interaction enhanced backscattering, however we have observed even fractions at values of 1/2 and 1/6 which are difficult to explain on this basis.

Y. Gul, S. N. Holmes, M. Myronov, S. Kumar, M. Pepper, *Journal of Physics. Condensed Matter* **30**, 09LT01 (2018).
S. Kumar, M. Pepper, S. N. Holmes, H., Montagu, Y. Gul, D. A. Ritchie, I. Farrer, *Physical Review Letters* **122**, 086803 (2019).
S. Kumar, M. Pepper, D. Ritchie, I. Farrer, H. Montagu, *Applied Physics Letters* **115** (12), 123104 (2019).
S-C. Ho, H-J. Chang, C-H. Chang, S-T. Lo, G. Creeth, S. Kumar, I. Farrer, D. Ritchie, J. Griffiths, G. Jones, M. Pepper, T-M. Chen, *Physical Review Letters* **121**, 106801 (2018).
S. Kumar, M. Pepper, *Applied Physics Letters* **119**, 110502 (2021).
G. Shavit, Y.Oreg, *Physical Review Letters* **123**, 036803 (2019).

Quench dynamics in two-dimensional electron systems: Long-range vs short-range Coulomb interactions

Dragana Popović

National High Magnetic Field Laboratory, Florida State University, Tallahassee, FL 32310, USA.

e-mail: dragana@magnet.fsu.edu

Understanding the dynamics of isolated disordered systems and its dependence on the range of interactions has been attracting a lot of research attention, but many questions remain open, especially in two spatial dimensions. At the same time, experiments have been limited mostly to those on synthetic quantum matter, such as ultracold atoms. This talk will describe experiments on strongly disordered, two-dimensional electron systems (2DESs) in Si metal-oxide-semiconductor field-effect transistors (MOSFETs) with a very weak thermal coupling of the 2DES to the environment. Two sets of practically identical devices have been studied, the only difference being the thickness of the oxide that separates the 2DES from the metallic gate. In thin-oxide MOSFETs, the metallic gate screens the long-range Coulomb interaction, reducing it to a short-range, dipolelike form.

We find that there is practically no difference in the dc transport, including the critical behavior near the metal-insulator transition, between the two sets of devices [1]. In contrast, there is a striking difference in their dynamics, measured after taking the 2DES far from equilibrium by a rapid change of carrier density. In the long-range case, the dynamics is glassy, and the thermalization time diverges as temperature $T \rightarrow 0$ [2]. In the short-range case, on the other hand, there is no evidence of glassy behavior, but the thermalization is anomalously slow and strongly sensitive to thermal coupling to the environment, suggesting the proximity to a many-body-localized (MBL) phase [3]. Our results demonstrate that the MBL phase in a 2D electron system can be approached by tuning the interaction range, thus paving the way to further studies of the breakdown of thermalization and MBL in real materials. These findings provide qualitatively new insights into the problems of dynamics and thermalization in strongly disordered, interacting systems.

[1] P. V. Lin and D. Popović, *Phys. Rev. Lett.* **114**, 166401 (2015).
[2] D. Popović, book chapter in *Strongly Correlated Electrons in Two Dimensions*, edited by S. V. Kravchenko, Pan Stanford Publishing Pte. Ltd, Singapore (2017), and references therein.
[3] L. J. Stanley, P. V. Lin, J. Jaroszynski, and D. Popović, arXiv:2110.11473; submitted (2021).

Acknowledgements: This work was supported by NSF Grants Nos. DMR-1307075, DMR-1707785, DMR-2104193 and the National High Magnetic Field Laboratory (NHMFL) through the NSF Cooperative Agreements Nos. DMR-1157490, DMR-1644779, and the State of Florida.

The Role of Neutral Modes at the Edge of Quantum Hall Phases: The Emergence of Superconductivity

Jukka I. Vayrynen[1], Moshe Goldstein[2], **Yuval Gefen**[3,*]

[1]*Department of Physics and Astronomy, Purdue University, West Lafayette, Indiana 47907 USA.*
[2]*Raymond and Beverly Sackler School of Physics and Astronomy, Tel Aviv University, Tel Aviv 6997801, Israel.*
[3]*Department of Condensed Matter Physics, Weizmann Institute of Science, Rehovot 76100, Israel.*

*e-mail: yuval.gefen@weizmann.ac.il

We consider a fractional quantum Hall bilayer system with an interface between quantum Hall states of unequal filling fractions, motivated by a recent approach to engineering artificial edges. We show that random tunneling and strong repulsive interactions within one of the layers will drive the system to a stable fixed point with two counterpropagating charge modes which have attractive interactions. As a result, slowly decaying correlations on the edge become predominantly superconducting. We discuss the resulting observable effects, and derive general requirements for electron attraction in Abelian quantum Hall states. Next we address the physics of neutral modes, which emerge ubiquitously at the edge of fractional quantum Hall phases. In the limit of strongly interacting neutralons we show that neutralon superconductivity emerges, where pairing is replaced by a quarteting mechanism. We discuss several manifestations of this effect, realizable in existing experimental platforms. Furthermore, this superconducting gapping mechanism may be exploited to facilitate the observation of interference of the accompanying charged anyons.

Sensitivity of (multi)fractal eigenstates to perturbation of the Hamiltonian

M. A. Skvortsov[1], **V. E. Kravtsov**[2,*], M. Amini[3]

[1]*Landau Inst. for Theoretical Physics, Chernogolovka, Russia.* [2]*Abdus Salam ICTP, Trieste, Italy.*
[3]*Department of Physics, University of Isfahan, Isfahan, Iran.*

*e-mail: kravtsov@ictp.it

We study the response of an isolated quantum system governed by the Hamiltonian drawn from the Gaussian Rosenzweig-Porter random matrix ensemble to a perturbation controlled by a small parameter. We focus on the density of states, local density of states and the eigenfunction amplitude overlap correlation functions which are calculated exactly using the mapping to the supersymmetric nonlinear sigma model. We show that the susceptibility of eigenfunction fidelity to the parameter of perturbation can be expressed in terms of these correlation functions and is strongly peaked at the localization transition: It is independent of the effective disorder strength in the ergodic phase, grows exponentially with increasing disorder in the fractal phase and decreases exponentially in the localized phase. As a function of the matrix size, the fidelity susceptibility remains constant in the ergodic phase and increases in the fractal and in the localized phases at modestly strong disorder. We show that there is a critical disorder strength inside the insulating phase such that for disorder stronger than the critical the fidelity susceptibility decreases with increasing the system size. The overall behavior is very similar to the one observed numerically in a recent work by Sels and Polovnikov [*Phys. Rev. E* **104**, 054105 (2021)] for the normalized fidelity susceptibility in a disordered XXZ spin chain.

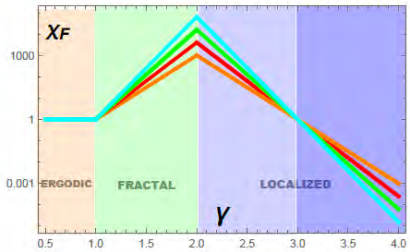

Figure 1. Sketch of the fidelity susceptibility for the Gaussian RP ensemble as a function of disorder for different system sizes (in increasing order from orange to cyan).

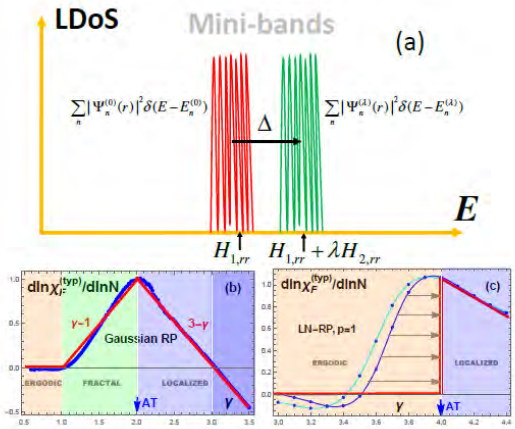

Figure 2. Mini bands in the local spectrum shifted flowing the diagonal matrix element (a); Logarithmic derivative of the typical fidelity susceptibility as a function of disorder for the Gaussian RP ensemble (b) and for the log-normal RP ensemble (c). Two localized phases with increasing and decreasing fidelity susceptibility as function of the system size are shown in light and dark blue, while the regions of multifractal and ergodic phases are shown by green and yellow, respectively.

[1] M. A. Skvortsov, M. Amini and V. E. K Kravtsov, *arXiv cond-mat: 2205.10297* (2022).

Acknowledgements: Google Quantum Research Award ‘Ergodicity breaking in quantum many-body systems’ (VEK).

Scaling up Anderson transition in random-regular graphs

M. Pino

Nanotechnology Group, USAL-Nanolab, Universidad de Salamanca, E-37008 Salamanca, Spain.

e-mail: manuelpino@usal.es

We study the Anderson model in lattices with the connectivity of a random-regular graph. Despite previous analysis of its metallic phase, it is still under debate the actual nature of this metal. We will briefly summarizes those previous results and explain our analysis based on the multifractal ansatz [1]. Our results show that fractal dimensions are continuous across the Anderson transition, but a discontinuity occurs on their derivatives, implying the existence of a nonergodic metallic phase with multifractal eigenstates [2]. The scaling analysis for the first fractal dimensions gives critical exponent $\nu = 0.94 \pm 0.08$ and critical disorder $W_C = 18.17 \pm 0.02$. Thus, our analysis strongly indicate that ergodicity is only recovered at zero disorder.

[1] M. Pino, J. Tabanera, P. Serna, *Journal of Physics A: Mathematical and Theoretical* **52**, 475101 (2019).
[2] M. Pino, *Physical Review Research*, **2**, 042031 (2021).

Disorder-dominated quantum criticality in moiré bilayers

Vladimir Dobrosavljević

[1]*Department of Physics and National High Magnetic Field Laboratorym,*
Florida State University, Tallahassee, Florida 32306, USA.

e-mail: vlad@magnet.fsu.edu

Moiré bilayer materials have recently attracted much attention following the discovery of various correlated insulating states at specific band fillings. Here we discuss the metal-insulator transitions (MITs) that have been observed in the same devices, but at fillings far from the strongly correlated regime dominated by Mott-like physics, displaying many similarities to other examples of disorder-dominated MITs. We propose [1] a minimal theoretical model describing the interplay of interactions and disorder, which able to capture most experimental trends observed on several devices.

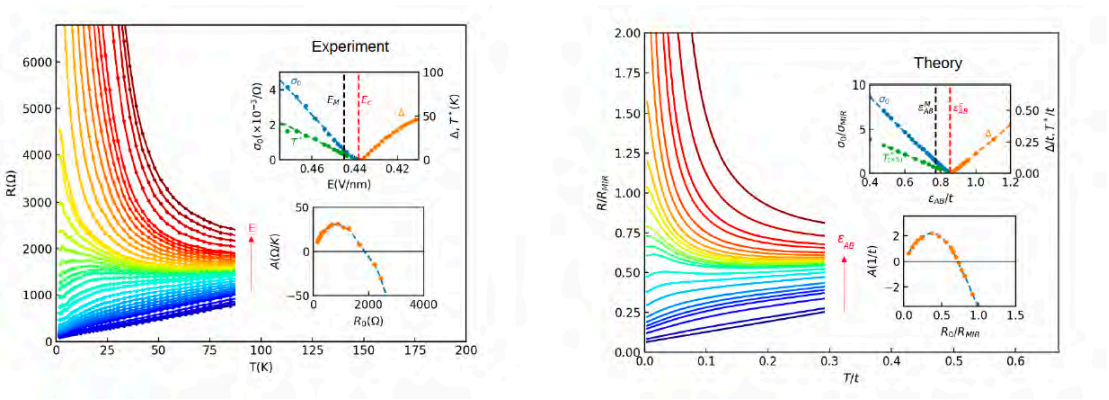

Figure 1. Resistivity curves: Experiment vs. Theory

[1] Yuting Tan, Pak Ki Henry Tsang, V. Dobrosavljević, preprint arXiv:2203.16498

Tunnel electroresistance and photomemristive effects in strongly-correlated oxide/metal junctions

R. El Hage[1], V. Humbert[1], V. Rouco[1], G. Krieger[2], A. Sander[1], J. Charliac[3], J. Grandal[4], M. Varela[4], K. Seurre[1], S. Collin[1], J. Briatico[1], C. Leon[4], S, Mesoraca[1], J. Trastoy[1], D. Preziosi[2], J. Santamaría[4], **Javier E. Villegas**[1,*]

[1]*Unité Mixte de Physique, CNRS, Thales, Université Paris-Saclay, Palaiseau, France.*
[2]*Uniiversité de Strasbourg, CNRS, IPCMS UMR 7504, 67034 Strasbourg, France.*
[3]*Ecole Polytechnique, Laboratoire de Physique des Interfaces et Couches Minces, Palaiseau, France.*
[4]*GFMC, Departamento de Física de Materiales, Facultad de Física, Universidad Complutense de Madrid, Spain.*

*e-mail: Javier.villegas@cnrs-thales.fr

Memristive circuit elements constitute a cornerstone for novel electronic applications, such as neuromorphic computing, called to revolutionize information technologies. By definition, memristors are sensitive to the history of electrical stimuli, to which they respond by varying their electrical resistance across a continuum of non-volatile states. Here we demonstrate memristive effects produced by redox-driven oxygen exchange in tunnel junctions composed of a complex-oxide (either the superconducting cuprate $YBa_2Cu_3O_7$ or the strongly correlated nickelate $NdNiO_3$) in direct contact with a metal. Despite their ultimate simplicity –a single interface between two dissimilar electrodes– these junctions show a very rich behaviour. On the one hand, a switching of the of tunnelling conductance qualitatively and quantitatively similar to the acclaimed tunnel electroresistance (TER) generally observed in ferroelectric tunnel junctions. Interestingly, the use of superconducting electrodes allow us to extend this concept to tunnelling of superconducting quasiparticles, for which the switching effects are much stronger than for normal electrons[1]. On the other hand, the use of nickelate electrodes allowed us to uncover another unexpected effect: the metal-to-insulator (MIT) transition characteristic of those materials has a strong effect on the oxygen ion mobility, and thus interplays with the redox mechanism. This modifies the MIT itself, and radically affects the tunnel resistance switching as well as the lifetime of the memristive resistance states[2]. Finally, and strikingly, we have found that the oxygen exchange across the junctions interfaces can be controlled via illumination, by exploiting a competition between electrochemistry, photovoltaic effects and photo-assisted ion migration. This leads to a unique photo-memristive effect, in which both electrical and optical stimuli can trigger the switching across resistance states in a way determined by the dual optical-electrical history[3]. In addition to their fundamental interest, the unveiled effects have considerable technological potential.

[1] Rouco, V. *et al.* Quasiparticle tunnel electroresistance in superconducting junctions. *Nat. Commun.* **11**, 1–9 (2020).
[2] Humbert, V. *et al.* An oxygen vacancy memristor ruled by electron correlations. *Under Rev.* (2022).
[3] Hage, R. El *et al.* Superconducting bimodal ionic photo-memristor. (2022) doi:10.48550/arxiv.2204.09255.

Acknowledgements: Work supported by ERC grant N° 647100 “SUSPINTRONICS”, ERC grant Nº 966735 “SUPERMEM”, French ANR grant ANR-17-CE30-0018-04 “OPTOFLUXONICS”, COST action “Nanocohybri” and Spanish AEI PID2020-118078RB-I00. JS thanks a the D’Alembert program funded by the IDEX Paris-Saclay, ANR-11-IDEX-0003-02, for financing a stay at Unité Mixte CNRS/Thales. We (JS, J-E V) acknowledge funding from Flag ERA ERA-NET To2Dox project.

Exciton-polaritons with 2D materials, from cryogenic to ambient conditions

C. Anton-Solanas[1,2,3,*], M. Waldherr[2], H. Shan[1], L. Lackner[1], B. Han[1], E. Sedov[4], C. Rupprecht[2], H. Knopf[5], F. Eilenberger[5], T. H. Harder[2], S. Tongay[6], K. Watanabe[7], T. Taniguchi[7], S. Klembt[2], A. V. Kavokin[4], S. Höfling[2], C. Schneider[1]

[1]*Institute of Physics, Carl von Ossietzky University, 26129 Oldenburg, Germany.*
[2]*Technische Physik, Universität Würzburg, D-97074 Würzburg, Am Hubland, Germany.*
[3]*Dept. Física de Materiales & Inst. N. Cabrera, Univ. Autónoma, Madrid 28049, Spain.*
[4]*Westlake University, 18 Shilongshan Road, Hangzhou 310024 Zhejiang Province, China.*
[5]*Fraunhofer-Institute for Applied Optics and Precision Engineering IOF, 07745 Jena, Germany.*
[6]*Arizona State University, Tempe, Arizona 85287, USA.*
[7]*National Institute for Materials Science, 1-1 Namiki, Tsukuba 305-0044, Japan.*

*e-mail: c.anton.so@gmail.com

Atomically thin crystals of transition metal dichalcogenides (TMDCs) have emerged as a new platform to study tightly bound excitons and many-body excitations in ultimately thin materials. Their giant dipole coupling to light makes them prime materials for (nano-)photonic and electronic devices, and for fundamental research on cavity quantum electrodynamics. Additionally, TMDC excitons can emit at room temperature, and they offer unique, tailorable interactions based on van-der-Waals engineering.

The strong coupling between excitons and confined photons yields the formation of exciton-polaritons; these are solid-state quasiparticles with properties linked to matter (Coulomb interactions, magnetic response) and light (extended spatial and temporal coherence). The bosonic character of exciton-polaritons enables their capability to condense into a macroscopic coherent state [1], like the laser emission, with additional features such as controllable nonlinear interactions.

In first place, I will discuss our recent results on the condensation of TMDC exciton-polaritons at cryogenic temperatures [2], created in a sample embedding a monolayer of $MoSe_2$ in a hybrid optical microcavity composed by AlGaAs mirrors and a dielectric top mirror. Secondly, in a different sample composed by a monolayer of WSe_2 embedded in a fully dielectric mirror, I will show recent results on condensation signatures of room-temperature TMDC exciton-polaritons (extended first-order coherence in time and space) [3].

Our future experiments will explore open-cavity configurations containing optical lattices (see recent related work [4]) coupled to TMDC interlayer excitons [5]. We believe that this platform offers a powerful approach to study complex systems, such as the Bose-Hubbard model.

[1] J. Kasprzak, et al. Nature **443**, 409 (2006).
[2] C. Anton-Solanas, et al. Nature Materials **20**, 1233 (2021).
[3] H. Shan, et al. Nature Communications **12**, 6406 (2021).
[4] L. Lackner, et al. Nat Commun **12**, 4933 (2021).
[5] J. Michl, et al. arXiv:2105.09948 (2021).

Oral

codes of the symposium and of this communication

A Non-Gaussian Variational Approach to Interacting Bosons in One Dimensional Lattices

T. Quian[1], J.J. Fernandez-Melgarejo[2], D. Zueco[3], **J. Molina-Vilaplana**[4,*]

[1]*College of Physics and Optoelectronic Engineering, Ocean University, China.* [2]*Departmento de Electromagnetismo y Electronica, Universidad de Murcia, Spain.* [3] *Instituto de Nanociencia y Materiales de Aragon (INMA), CSIC-Universidad de Zaragoza, Spain.*[4]*Department de Automatica, Tecnologia Electronica e Ingenieria Electrica, Universidad Politecnica de Cartagena, Spain*

*e-mail: javi.molina@upct.es

We present a variational method for studying the ground state of strongly interacting quantum many-body bosonic systems. Our approach constructs a class of variational non-Gaussian wavefunctions which extend Gaussian states by means of nonlinear canonical transformations (NLCT) on the fields of the theory under consideration. Different choices of NLCT are related with different variational manifolds. The key advantage of such states over simple Gaussian states is that they support the presence of non-factorizable correlations thus making possible to describe systems with strong interactions between particles. The presented scheme is self-consistent and requires no other assumptions than the choice of a NLCT-variational manifold.

We illustrate this method with the Bose-Hubbard model, which provides a theoretical description of interacting cold atoms in optical lattices. Our ansatz provides a family of non-symmetric approximate ground states for the Bose-Hubbard at finite lattices at and at arbitrarily large values of the interaction strength. Indeed, we compute the approximate ground state energy of the system at different locations in the phase diagram. We find that for different values of the interaction, the NLCT-trial states, sensibly improve the ground state energy estimation when the system is in the Mott phase while in the superfluid phase, the prediction is similar to Gaussian state. The method can be extended to investigate systems at finite temperature and out-of -equilibrium.

Chaos for Interacting Bosons and Random Two-Body Hamiltonians

Lukas Pausch[1], Edoardo G. Carnio[1,2], Andreas Buchleitner[1,2], **Alberto Rodríguez**[3,*]

[1]*Physikalisches Institut, Albert-Ludwigs-Universität-Freiburg, Hermann-Herder-Straße 3, D-79104, Freiburg, Germany.* [2]*EUCOR Centre for Quantum Science and Quantum Computing, Albert-Ludwigs-Universität Freiburg, Hermann-Herder-Straße 3, D-79104, Freiburg, Germany.* [3]*Departamento de Física Fundamental, Universidad de Salamanca, E-37008 Salamanca, Spain.*

*e-mail: argon@usal.es

We identify the chaotic phase of the Bose-Hubbard Hamiltonian by the energy-resolved correlation between spectral features and structural changes of the associated eigenstates as exposed by their generalized fractal dimensions (Fig. 1). The eigenvectors are shown to become ergodic in the thermodynamic limit, in the configuration space Fock basis, and we demonstrate that the fluctuation of the generalized fractal dimensions among near-in-energy eigenstates is a rather sensitive probe of quantum chaos that exhibits a qualitative basis-independent behaviour [1].

We scrutinize the chaotic phase of the model in relation to the bosonic embedded random matrix ensemble, which mirrors the dominant few-body nature of many-particle interactions, and hence the Fock space sparsity of quantum many-body systems. The energy dependence of the chaotic regime is well described by the bosonic embedded ensemble, which also reproduces the Bose-Hubbard chaotic eigenvector features [2]. Despite this agreement, in terms of the fractal dimension distribution, these two models depart from each other and from the Gaussian orthogonal ensemble as Hilbert space grows [1,2]. These results provide further evidence of a way to discriminate among different many-body Hamiltonians in the chaotic regime.

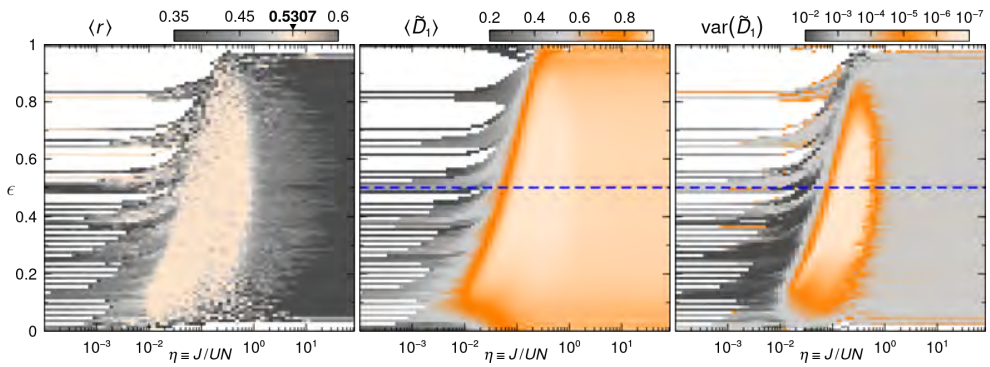

Figure 1. Chaotic phase of the Bose-Hubbard Hamiltonian exposed by spectral statistics (left), and eigenvector features characterized by generalized fractal dimensions (middle and right), for an irreducible Hilbert subspace of a system of 12 bosons in 12 spatial modes.

[1] L. Pausch. E. G. Carnio. A. Rodríguez, A. Buchleitner, *Phys. Rev. Lett.* **126**, 150601 (2021).
[2] L. Pausch, E. G. Carnio, A. Buchleitner, A. Rodríguez. *New J. Phys.* **23**, 123036 (2021).

Acknowledgements: The authors acknowledge support by the state of Baden-Württemberg through bwHPC and the German Research Foundation (DFG) through Grants No. INST 40/467-1 FUGG (JUSTUS cluster), No. INST 40/575-1 FUGG (JUSTUS 2 cluster), and No. 402552777. E.G.C. acknowledges support from the Georg H. Endress foundation. A.R. acknowledges support by Universidad de Salamanca through a Grant USAL-C1 (No. 18K145) and by Spanish MCIN/AEI through Grant No. PID2020-114830GB-I00.

Superconducting edge states in a topological insulator

I. V. Yurkevich[1,*], V. Kagalovsky[2]

[1]*School of Informatics and Digital Engineering, Aston University, Birmingham B4 7ET, UK.* [2]*Shamoon College of Engineering, Bialik/Basel St., 84100 Beer-Sheva, Israel.*

*e-mail: i.yurkevich@aston.ac.uk

We study the stability of multiple conducting edge states in a topological insulator against perturbations allowed by the time-reversal symmetry. A system is modelled as a multi-channel Luttinger liquid, with the number of channels equal to the number of Kramers' doublets at the edge. Assuming strong interactions and weak disorder, we first formulate a low-energy effective theory for a clean translation invariant system and then include the disorder terms allowed by the time-reversal symmetry. In a clean system with N Kramers' doublets, N − 1 edge states are gapped by Josephson couplings and the single remaining gapless mode describes collective motion of Cooper pairs synchronous across the channels. Disorder perturbation in this regime, allowed by the time reversal symmetry is a simultaneous backscattering of particles in all N channels. Its relevance depends strongly on the parity if the number of channel N is not very large. Our main result is that disorder becomes irrelevant with the increase of the number of edge modes leading to the stability of the edge states superconducting regime even for repulsive interactions.

We account for the most relevant, in the renormalisation group sense, inter-mode interactions in a clean system. Assuming that interactions are strong and disorder is weak, we first consider a translation-invariant system, imposing the restriction of momentum conservation, and work out the low-energy Hamiltonian keeping only gapless modes, and only then add the disorder terms allowed by symmetries.

The main feature of the topological multi-mode insulator is the absence of single-particle inter-channel scattering terms amongst translation invariant contributions. All single-particle processes are taken into account at the level of derivation of multi-channel Luttinger liquid where channels are eigenmodes of a single-particle two-dimensional Hamiltonian. These modes are orthogonal to each other and localised in a narrow region in the boundary layer of the two-dimensional sheet so that we may assume that density-density interactions are long-ranged on the scale of the mode's separation.

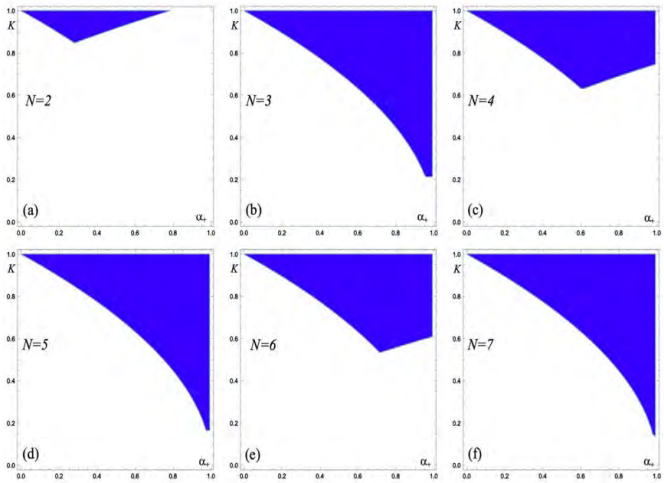

Figure 1. The phase diagram for a set of N Kramers' doublets under repulsive density–density interaction. The blue regions represent stable SC regime.

Studying the effect of disorder on the remaining conducting channel, we must add terms breaking momentum conservation allowed by the symmetry. There is another constraint on the type of terms that we are allowed to add, they must be compatible with the condition that (N − 1) modes have been frozen, i.e. the new added terms must commute with those we used to decide which modes are gapped. This criterion was formulated by Haldane. The emerging phase diagram is presented in Fig. 1 above.

[1] I. V. Yurkevich and V. Kagalovsky, *Scientific Reports* **11** (1), 1-7 (2021).

Acknowledgements: This work was supported by the Leverhulme Trust Grant No. RPG-2019-317.

The emergence of the non-interacting channel in the strongly interacting 1D system

V. Kagalovsky

Shamoon College of Engineering, Beer-Sheva, 8410802 Israel.

e-mail: victork@sce.ac.il

We consider a strongly interacting one-dimensional (1D) system with two channels. When single-electron inter-channel backscattering processes $L_2^\dagger R_1$ (right-moving electron in the first channel backscatters into the left-moving state in the second channel) and $R_1^\dagger L_2$ (left-moving electron in the second channel backscatters into the right-moving state in the first channel) become relevant, we define two new fields. One field $\phi_g = \frac{1}{2}(\phi_1 + \phi_2 + \theta_1 - \theta_2)$ is frozen (gapped) by these relevant perturbations, whereas the second one $\phi_f = \frac{1}{2}(\phi_1 + \phi_2 - \theta_1 + \theta_2)$ remains free. We solve the problem exactly for arbitrary intra- and inter-channel interactions and find effective Luttinger parameter and velocity for the free field.

The free field contributes unity $\frac{e^2}{h}$ to the conductance of the system in agreement with previous studies [1,2], but in addition, it turns out that the parameters of the free field are independent of the interactions between right- and left-moving electrons in the same channel and between electrons moving in the same direction in different channels. Finally, if the inter-channel interactions are weak, the free field becomes non-interacting (effective Luttinger parameter $K = 1$) independently of how strong intra-channel interactions are!

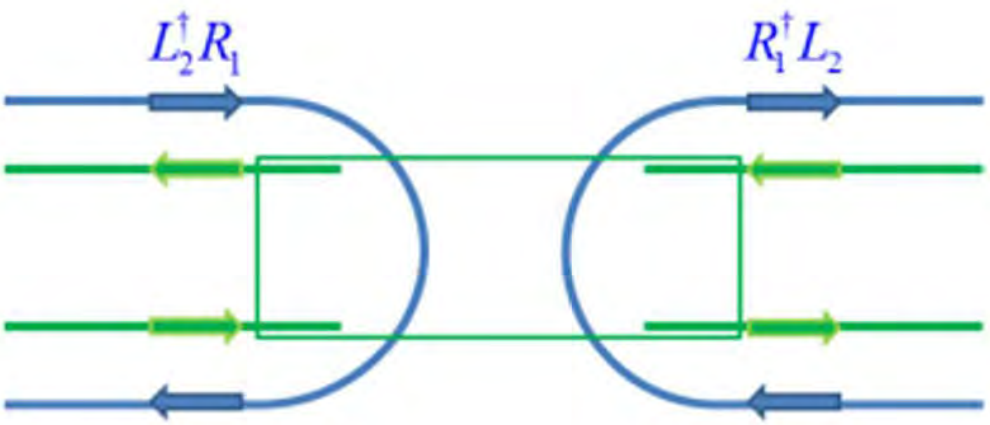

Figure 1. The blue field $\phi_g = \frac{1}{2}(\phi_1 + \phi_2 + \theta_1 - \theta_2)$ is frozen (gapped) by the relevant inter-channel perturbations and the green field $\phi_f = \frac{1}{2}(\phi_1 + \phi_2 - \theta_1 + \theta_2)$, orthogonal to the blue one, remains open and becomes non-interacting.

[1] D. L. Maslov, M. Stone, *Phys. Rev. B* **52**, R5539 (1995).
[2] G. Shavit, Y. Oreg, *Phys. Rev. Lett.* **52**, 036803 (2019).

Overactivated transport in the localized phase of the Superconductor-Insulator transition

Vincent Humbert[1,3,*], Miguel Ortuño[2], Andres M. Somoza[2], Laurent Bergé[3], Louis Dumoulin[3], C. A. Marrache-Kikuchi[3]

[1]*Unité Mixte de Physique, CNRS, Thales, Université Paris-Saclay, 91767, Palaiseau, France.*
[2]*Departamento de Fısica - CIOyN, Universidad de Murcia, Murcia 30071, Spain.*
[3]*Université Paris-Saclay, CNRS/IN2P3, IJCLab, 91405 Orsay, France.*

*e-mail: vincent.humbert@cnrs-thales.fr

Quantum phase transition is occurring following a violent rearrangement of the charge carriers by tuning an external parameter. This is well shown in the Superconductor-Insulator Transition (SIT): beyond a critical disorder, two-dimensional superconducting films become insulating. While studied for decades, the universal SIT picture came under scrutiny as conventional theories fails to describe many phenomena [1-5], and in particular the insulating state of many systems which show unusual behaviors at low temperatures.

In this talk, I will present experimental and theoretical investigation of these insulating features found in many different systems. We experimentally measured and analyzed over 100 insulating Nb_xSi_{1-x} films in the vicinity of the SIT. This allowed us to realize a systematic study of the two observed regimes at low temperatures [6]. At intermediate temperatures, electronic transport is activated. We show it is dominated by charging energies between superconducting grains and that the sample thickness variation results in a large spread of activation temperatures, which can be fine-tune via a change in disorder. At the lowest temperature an apparently more insulating, or over-activated, behavior is measured.

We show that the transition between these two regimes is governed by the apparition of superconducting grains, inducing an increased gap that the carriers have to overcome. We theoretically found that the relation between the characteristic energies of these regimes is described by a simple law, which is confirmed both experimentally on many other systems [6-14] and numerically.

[1] V.M. Vinokur et al., *Nature* **452**, 613 (2008).
[2] A. Kapitulnik et al., *Rev. Mod. Phys*. **91**, 011002 (2019).
[3] M.V. Feigel'man et al., *Ann. Phys.* **325**, 1390 (2010).
[4] B. Sacépé et al., *Nat. Phys*. **7**, 239 (2011).
[5] K. Bouadim et al., *Nat. Phys*. **7**, 884 (2011).
[6] V. Humbert et al., *Nature Comm*. **12**, 6733 (2021).
[7] R. Dynes et al., *Phys. Rev. Lett*. **40**, 479 (1978).
[8] K.A. Parendo et al., *Phys. Rev. B* **76**, 100508 (2007).
[9] J.J. Kim et al., *Phys. Rev. B* **46**, 11709 (1992).
[10] G. Sambandamurthy et al., *Phys. Rev. Lett.* **94**, 01703 (2005).
[11] T.Y.I. Baturina et al., *JETP Lett.* **88**, 752 (2008).
[12] T.I. Baturina et al., *Phys. Rev. Lett.* **99**, 257003 (2007).
[13] C.J. Adkins et al., *J. Phys. C: Solid State Phys.* **13**, 3427 (1980).
[14] N. Tajima et al., *Europhys. Lett.* **83**, 27008 (2008).

Superconductor-Insulator transition in Y_xSi_{1-x} thin films

L-H-H. To, **S. Sengupta***, F. Pallier, C. Baumier, L. Bergé, L. Dumoulin, S. Marnieros, C. Marrache-Kikuchi

IJCLab, CNRS, University Paris-Saclay, 91405, Orsay, France.

*e-mail: sengupta@ijclab.in2p3.fr

We have studied low temperature transport properties of a-Y_xSi_{1-x} disordered thin films. The electronic properties are governed by the interplay between localization, Coulomb interactions, and superconductivity. As a function of the stoichiometry, these films can either be superconducting or insulating at low temperatures.

Amorphous Y_xSi_{1-x} films (thickness varying from 300 to 600 Å) were synthetized by electron-beam co-deposition from two separate sources under ultrahigh vacuum. As shown by AFM, SEM and EDX measurements, these films are quite homogeneous both in composition and thickness with a film roughness of about 3 – 4 Å.

In the case of superconducting thin films, the critical temperature T_c evolves from 200 mK to 990 mK when the composition is varied from 22% to 32% of Y. a-Y_xSi_{1-x} therefore belongs to the class of disordered superconductors that are of interest both for understanding the fundamental mechanisms of superconductor-insulator transition [1] and to engineer high kinetic inductance devices that can be used in quantum circuits [2,3]. In the case of insulating thin films, our preliminary results indicate a strong electron-phonon decoupling, which could be the signature of many-body localized states in this system (Fig. 1). a-Y_xSi_{1-x} is an interesting material to probe this theoretically predicted new state and possible signatures of a finite-temperature insulator [4].

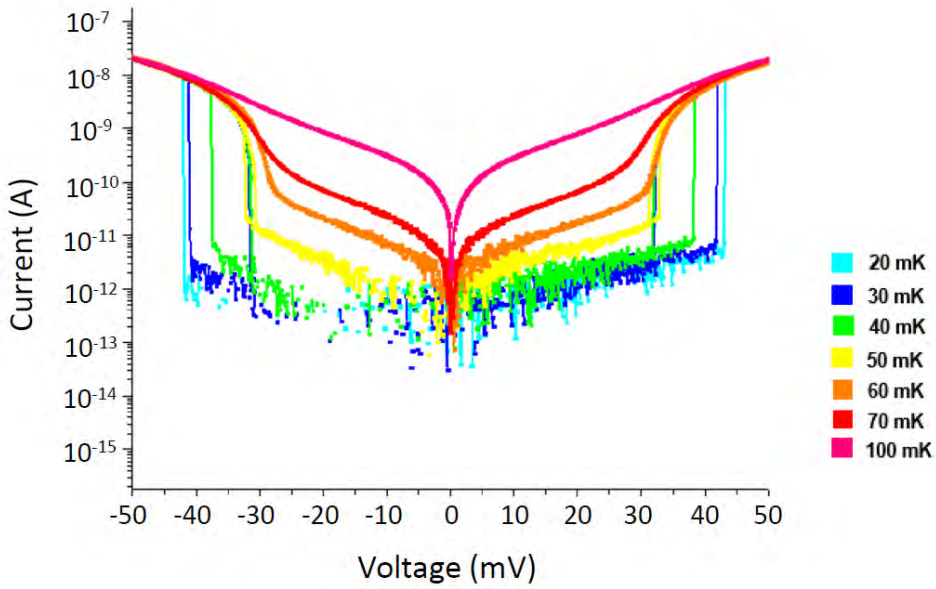

Fig. 1: Hysteretic jumps in current-voltage characteristics at different temperatures.

[1] B. Sacépé, M. Feigel'man, and T. M. Klapwijk, *Nature Physics* **16**, 734 (2020).
[2] B. Douçot, and L. B. Ioffe, *Reports on Progress in Physics* **75**, 072001 (2012).
[3] B. A. Mazin, *AIP Conference Proceedings* **1185**, 135 (2009).
[4] D. M. Basko, I. L. Aleiner, and B. L. Altshuler, *Physical Review B* **76**, 052203 (2007).

The Superconducting Dirac Point in Proximitized Graphene

Gopi Nath Daptary, Udit Khanna, Eyal Walach, Efrat Shimshoni, **Aviad Frydman***

Department of Physics, Bar Ilan University, Ramat Gan, 52900, Israel.

*e-mail: aviad.frydman@gmail.com

Two-dimensional (2D) materials, composed of single atomic layers, have attracted vast research interest since the breakthrough discovery of graphene. One major benefit of such systems is the simple ability to tune the Fermi level through the charge neutrality point between electron and hole doping. For 2D Superconductors, this means that one may potentially achieve the regime described by Bose Einstein Condensation (BEC) physics of small bosonic tightly bound electron pairs.

In my talk I will describe an experiment showing that single layer graphene (SLG), in which superconducting pairing is induced by proximity to a low-density superconductor, amorphous indium oxide, can be tuned from hole to electron superconductivity through an ultra-law carrier density regime. This leads to the presence of an additional Dirac point as seen in Fig. 1.

We have studied, both experimentally and theoretically, the vicinity of this "Superconducting Dirac point" and found an unusual situation where reflections at interfaces between normal and superconducting regions within the graphene, suppress the conductance and, at the same time, Andreev reflections maintain a large phase breaking length. In addition, the Fermi level can be adjusted so that the momentum in the normal and superconducting regimes perfectly match giving rise to ideal Andreev reflection processes and enhanced superconductivity. This leads to the surprising finding that the critical temperature of the SLG/indium oxide bilayer is maximal at the charge neutrality point, in contrast to previous experimental and theoretical results.

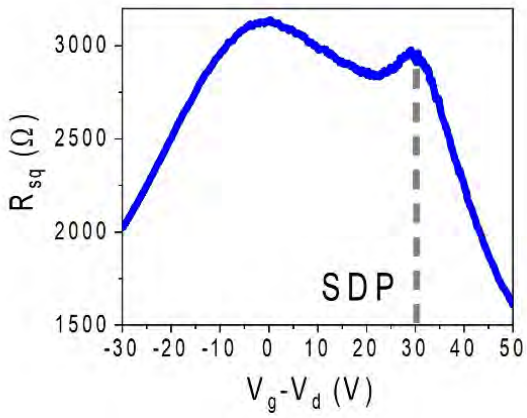

Figure 1. Resistance versus gate voltage of a single layer graphene/indium oxide bilayer showing the presence of an additional superconducting Dirac Point.

Crossover from impurity-controlled superconductivity to granular superconductivity in (TMTSF)2ClO4

S. Yonezawa[1], Y. Maneo[1], K. Bechgaard[2], **C. A. Marrache-Kikuchi**[3,*], D. Jérome[4]

[1]*Department of Physics, Kyoto University, Japan.* [2]*Department of Chemistry, Oersted Institute, University of Copenhagen, Denmark.* [3]*IJCLab, Univ. Paris-Saclay, France.* [4]*Laboratoire de Physique des Solides, Univ. Paris-Saclay, France.*

*e-mail: claire.marrache@universite-paris-saclay.fr

The organic superconductor $(TMTSF)_2ClO_4$ is an archetypal quasi-1D non-s-wave superconductor [1,2]. It also exhibits an order-disorder transition, due to ClO_4 tetrahedral anions orientation at T_{AO} = 24 K, that can be controlled by the cooling rate across T_{AO} [2]. Thus, this compound provides a rare opportunity to precisely study how non-s-wave superconductivity evolves with disorder.

We will first review some specific heat measurements which provide more evidence for the exotic nature of the superconducting order parameter, and show that superconductivity corresponds to the strong scattering limit in this quasi-1D compound.

Moreover, we performed simultaneous measurements of the c-axis resistivity and AC susceptibility of $(TMTSF)_2ClO_4$ single crystals, under precise control of the cooling rate across T_{AO}. The measurements were performed below 1 K, using a dedicated compact susceptometer [3]. Higher cooling rates increase the residual resistance and reduce T_c (Fig. 1), as expected for the destruction of non-s-wave superconductivity by non-magnetic impurities [2]. However, when the disordered volume fraction increases, the critical temperatures derived from resistivity and from susceptibility deviate from each other, while superconducting shielding is incomplete and dissipation finite. All these features indicate that superconductivity becomes inhomogeneous at high disorder.

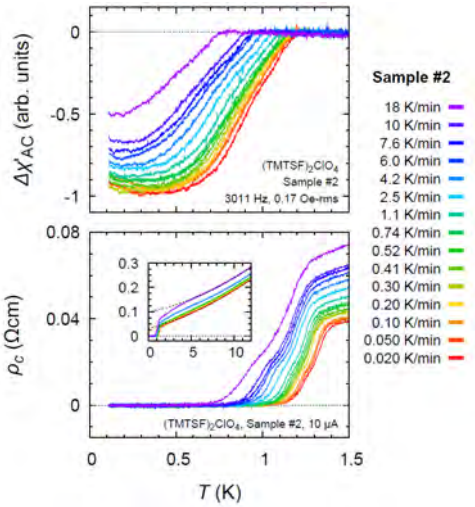

Figure 1. Real part of the AC susceptibility and c-axis resistivity as a function of the temperature for a $(TMTSF)_2ClO_4$ single crystal, cooled with various cooling rates across the anion-order temperature T_{AO} = 24 K.

[1] For recent reviews, see: S. E. Brown, *Physica C* **514**, 279 (2015); D. Jérome and S. Yonezawa, *C. R. Physique* **17**, 357 (2016).
[2] S. Yonezawa et al., *Phys. Rev. B.* **85**, 140502R (2012).
[3] S. Yonezawa et al., *Rev. Sci. Instrum.* **86**, 093903 (2015).

Room temperature Mott metal-insulator transition in V_2O_3 compounds

Mariela Menghini[1,2,*], Pía Homm[2], Wei-Fan Hsu[2], Simon Mellaerts[2], Jin Won Seo[3], Jean-Pierre Locquet[2]

[1]*IMDEA Nanociencia, Madrid, Spain.*
[2]*Department of Physics and Astronomy, KU Leuven, Leuven, Belgium.*
[3]*Department of Materials Engineering, KU Leuven, Leuven, Belgium.*

*e-mail: mariela.menghini@imdea.org

Vanadium sesquioxide (V_2O_3) is an archetypal Mott insulator in which the atomic positions in the unit cell and the electron correlations change as temperature, pressure or doping are varied, paving the way for different structural, electronic and magnetic phase transitions to occur. One example is the purely electronic isostructural Mott transition around room temperature in bulk Cr-doped V_2O_3 between corundum paramagnetic metallic (PM) and insulating (PI) phases. Remarkably, this phase transition has been elusive in thin film compounds so far [1]. We will present results of a room temperature Mott metal-insulator transition (MIT) in 1.5% Cr-doped and pure V_2O_3 thin films achieved via continuous lattice deformations induced by heteroepitaxy [2]. This MIT is characterized by a colossal change ($\Delta R/R$ up to 100,000 %) in room temperature resistivity and a broad range of optical constants values as a consequence of a strain-modulated bandgap. Moreover, the controlled epitaxial strain allows to stabilize the structural, electronic and optical properties of the films at different intermediate states, between the PM and PI phases, inaccessible in bulk materials. Controlling phase transitions in correlated systems by epitaxial strain can offer a radical new approach to create the next generation of Mott devices.

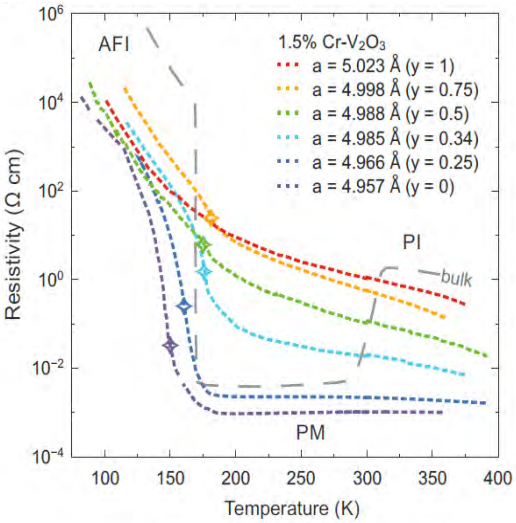

Figure 1. Resistivity curves R(T) of 1.5% Cr-doped V2O3 films with different in-plane lattice parameters engineered by heteroepitaxy. T_{MIT} is indicated with a star symbol. The gray dashed line corresponds to a 1% Cr-doped V2O3 single crystal from Ref. [3].

[1] P. Homm et al., *Appl. Phys. Lett.* **107**, 111904 (2015).
[2] P. Homm et al., *APL Materials* **9**, 021116 (2021).
[3] H. Kuwamoto et al., *Phys. Rev. B* **22**, 2626 (1980).

Doped Nanoporous graphene as a new material for ultrasharp superlattice heterojunctions

M. Tenorio[1,*], C. Moreno[1,2], P. Febrer[1], J. Castro-Esteban3, P. Ordejón[1], D. Peña[3], M. Pruneda[1], A. Mugarza[1,4]

[1] *Catalan Institute of Nanoscience and Nanotechnology (ICN2), CSIC and The Barcelona Institute of Science and Technology, Campus UAB, Bellaterra, 08193 Barcelona, Spain.*
[2]*Departamento de Ciencias de la Tierra y Fisica de la Materia Condensada, Universidad de Cantabria, 39005, Santander, Spain.*
[3]*Centro de Investigación en Química Biolóxica e Materiais Moleculares (CiQUS), Departamento de Química Orgánica, Universidade de Santiago de Compostela. Santiago de Compostela 15782, Spain.*
[4]*ICREA Institució Catalana de Recerca i Estudis Avançats, Lluis Companys 23, 08010 Barcelona, Spain.*

*e-mail: maria.tenorio@icn2.cat

Bottom-up synthesis has shown to be a very efficient method to build graphene nanoarchitectures with atomic precision. The most illustrative example is the plethora of graphene nanoribbons (GNR) that have been created practically *à la carte*. Despite such impressive advances in 1D homostructures, going beyond in structural complexity has turned to be a tough challenge. In particular, the synthesis of heterostructures has been limited to 1D, with no control on size and distribution of fusing components [1]. Here we report a novel synthetic strategy to fabricate atomically precise, lateral superlattice heterojunctions built in a Nitrogen-doped nanoporous graphene structure. For that we harness our ability to create parallely-aligned graphene nanoribbons superlattices [2] in order to guide the synthesis of a second GNR component, in this case an N-doped isostructural counterpart, within the empty channels of the superlattice. The final step consists on fusing laterally [3] the components alternatively into a hybrid nanoporous graphene (h-NPG). The electronic structure is that of a superlattice of type-II heterojunctions whose atomically sharp stepped potential, at the ultimate limit of a single carbon-carbon bond unveils the presence of in-gap tunnelling states and interface quantum dipoles. We envision that our fabrication scheme will facilitate a new class of atomically precise hybrid nanomaterials with high flexibility on structural composition and functionality, unfolding their impact in the fields of (opto)electronics, catalysis, and bio-chemistry.

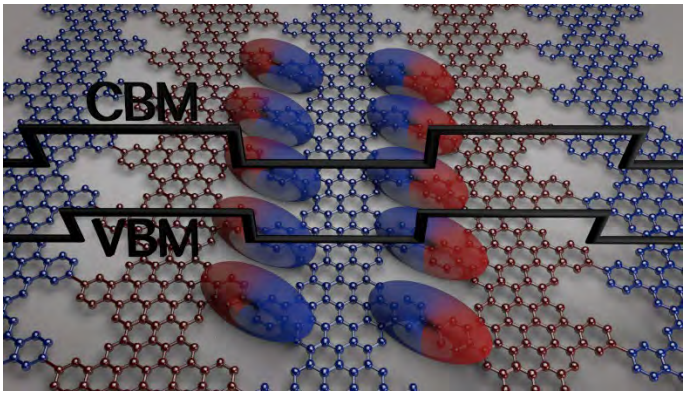

Figure 1. Illustrative representation of the nitrogen doped nanoporous graphene, a superlattice of atomically sharp lateral heterojunctions.

[1] J. Cai, C.A. Pignedoli, L. Talirz, P. Ruffieux, H. Söde, L. Liang, V. Meunier, R. Berger, R. Li, X. Feng, K. Müllen, R. Fasel, *Nat. Nano*. **9**, 896 (2014).
[2] C. Moreno, M. Paradinas, M. Vilas-Varela, M. Panighel, G. Ceballos, D. Peña, A. Mugarza, *Chem. Comm*. **54**, 9402 (2018).
[3] C. Moreno, M.Vilas-Varela, B. Kretz, A. Garcia-Lekue, M. V. Costache, M. Paradinas, M. Panighel, G.Ceballos, S. O. Valenzuela, D. Peña, A. Mugarza, *Science* **360**, 199 (2018).

Ping-pong balls in motion: peculiarities of diffusive transport and structure formation

M. A. López-Castaño[1], J. F. González-Saavedra[1], A. Rodríguez Rivas[2], **E. Abad**[3,*], S. B. Yuste[4], F. Vega Reyes[4]

[1] *Department of Physics, University of Extremadura, Badajoz, Spain.*
[2] *Department of Physical, Chemical, and Natural Systems, Pablo de Olavide University, Seville, Spain.*
[3] *Department of Applied Physics and ICCAEx, University of Extremadura, Mérida, Spain.*
[4] *Department of Physics and ICCAEx, University of Extremadura, Badajoz, Spain.*

*e-mail: eabad@unex.es

We consider a collection of fluidized identical hollow spheres (ping-pong balls) resting on a horizontal metallic grid [1]. Fluidization is achieved by means of a turbulent air current coming from below (see Fig. 1, left). The upflow is adjusted so that the particles do not levitate over the grid, resulting in quasi-two-dimensional dynamics. The intricate diffusive behaviour displayed by this granular system (see Fig. 1, right) is related to the effective potential characterizing the hydrodynamic interactions between the constituents. Changes in the effective potential can be induced by tuning the granular temperature T and the packing fraction Φ, which results in a rich variety of spatial structures. We discuss the error sources characterizing the experimental trajectories of the spheres and provide realistic estimates for the total localization error (see Supplemental Material in [1]).

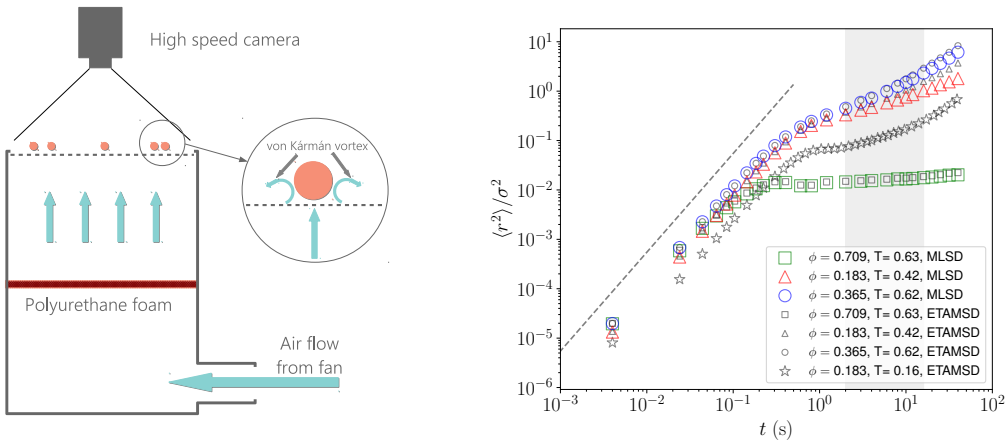

Figure 1: Left: Experimental setup. Right: Time dependence of the mean logarithmic square displacement (MLSD) and of the ensemble average of the time averaged mean square displacement (ETAMSD) in units of sphere diameter σ for different T and Φ.

[1] Miguel Ángel López-Castaño, Juan Francisco González-Saavedra, Álvaro Rodríguez-Rivas, Enrique Abad, Santos Bravo Yuste and Francisco Vega Reyes, *Pseudo-two-dimensional dynamics in a system of macroscopic rolling spheres*, *Phys. Rev. E* **103**, 042903 (2021).

Acknowledgements: We acknowledge funding from the Government of Spain through Project No. FIS2016-76359-P and from the regional Extremadura Government through Projects No. GR18079 and No. IB16087, both partially funded by the ERDF.

Anomalous Faraday effect in a *PT*-symmetric dielectric slab

Vladimir Gasparian[1,2,*], Peng Guo[1], Esther Jódar[2]

[1]*California State University, Bakersfield, USA.* [2]*Universidad Politécnica de Cartagena, Murcia, Spain.*

*e-mail: vgasparyan@csub.edu

We discuss the anomalous behavior of the Faraday (transmission) and Kerr (reflection) rotation angles of the propagating light, in a simple parity-time (*PT*) symmetric model with two complex δ-potentials placed on both boundaries of the ordinary dielectric slab. It is shown that, for a given set of parameters describing the system, a phase transition can take place. In the anomalous phase the value of one of the Faraday and Kerr rotation angles can become negative, and both angles suffer from spectral singularities and give a strong enhancement near the singularities.

Electronic band structure inside the superconducting gap from Yu-Shiba-Rusinov states in quasi two-dimensional 2H-$NbSe_{2-x}S_x$

Jose A. Moreno[1,*], Edwin Herrera[1,2,3], Víctor Barrena[1], Anita Smeets[1], Samuel Mañas[4], Eugenio Coronado[4], José J. Baldoví[4,5], Isabel Guillamón[1], Hermann Suderow[1]

[1]*Laboratorio de Bajas Temperaturas y Altos Campos Magnéticos, Departamento de Física de la Materia Condensada, Instituto Nicolás Cabrera and Condensed Matter Physics Center (IFIMAC), Unidad Asociada UAM-CSIC, Universidad Autónoma de Madrid, E-28049 Madrid, Spain.*
[2]*Departamento de Física, Universidad Nacional de Colombia, Bogotá, Colombia.*
[3]*Facultad de Ingeniería y Ciencias Básicas, Universidad Central, Bogotá, Colombia.*
[4]*Instituto de Ciencia Molecular (ICMol), Universidad de Valencia, Catedrático José Beltrán 2, 46980 Paterna, Spain.*
[5]*Max Planck Institute for the Structure and Dynamics of Matter, Luruper Chaussee 149, D-22761 Hamburg, Germany.*

*e-mail: josea.moreno@uam.es

Yu-Shiba-Rusinov (YSR) states in s-wave superconductors due to magnetic impurities provide features in the subgap density of states whose spatial dependence pictures the electronic anisotropy. When YSR states extend over large distances, they provide subgap electronic excitations whose band structure contains an intrinsic electron hole anisotropy which is absent in the normal phase. This is particularly interesting in presence of multiple bands and a large anisotropy. However, viewing the full band structure requires YSR impurities with extremely well defined YSR peaks inside the small energy range of the superconducting gap. Here we show a considerable enhancement of the spatial extension of YSR states in superconducting 2H-$NbSe_{2-x}S_x$ and identify features coming from the whole Fermi surface, including Se and Nb derived bands. These features are absent around Fe impurities in pure 2H-$NbSe_2$. Density Functional calculations suggest that the two-dimensional electronic properties of S doped 2H-$NbSe_2$ enhance the YSR pattern over the whole Fermi surface. By investigating nanometric fields of view via Scanning Tunneling Microscopy (STM) with different Fe impurity density and different S dopings, we furthermore demonstrate that the cross-over between isolated YSR states and gapless Abrikosov-Gorkov superconductivity occurs at a very small Fe impurity concentration.

Ab-initio electronic excitation spectra of ceria: input data for surface-science radiation-transport simulations

Pablo de Vera[1,*], Andrea Pedrielli[2], Maurizio Dapor[2], Paolo E. Trevisanutto[3], Nicola Pugno[4], Isabel Abril[5], Simone Taioli[2], Rafael Garcia-Molina[1]

[1]*Departamento de Física – Centro de Investigación en Óptica y Nanofísica, Universidad de Murcia, E-30100, Murcia, Spain.* [2]*European Centre for Theoretical Studies in Nuclear Physics and Related Areas (ECT*), Bruno Kessler Foundation, Trento, Italy.* [3]*Dipartimento di Ingegneria, Unità di Ricerca di Fisica non lineare e Modelli matematici, Università Campus Bio-Medico, Via Alvaro del Portillo 21, Roma, 00154 Italy.*
[4]*Laboratory of Bio-Inspired, Bionic, Nano, Meta Materials & Mechanics, Department of Civil, Environmental and Mechanical Engineering, University of Trento, Italy.*
[5]*Departament de Física Aplicada, Universitat d'Alacant, E-03080 Alacant, Spain.*

*e-mail: pablo.vera@um.es

Cerium oxides (CeO_2 and Ce_2O_3) are transition metal oxides presenting many applications, which range from nanoparticle-based radioenhancers in hadrotherapy for cancer treatment [1] to fuel cells and catalysis for hydrogen production and water splitting. The interaction of radiation (and in particular of energetic electrons) with these materials underlies some of these applications, as well as powerful surface analysis techniques, such as reflection electron energy loss spectroscopy (REELS), of great relevance to get electronic information of these materials.

The study of cerium-based oxides is also of fundamental interest to understand the electronic properties of strongly correlated materials affected by the presence of highly-localized 4f states. In fact, while both oxides experimentally show insulator behaviours, density functional theory (DFT) predicts correctly an insulator state for CeO_2, while wrongly a metallic one for Ce_2O_3 [2]. A phenomenological way to correct this failure is to use the DFT+U method, in which the addition of a Hubbard correction increases the effective Coulomb repulsion by the sum of the strong on-site Coulomb interaction of localized electrons and the strength of the exchange interaction.

In this contribution we report DFT+U and linear-response time-dependent density functional theory (LR-TDDFT) calculations of the dielectric response of bulk CeO_2 and Ce_2O_3, showing that the inclusion of local field effects overcomes the discrepancy between calculations and experiments (Fig. 1). In particular, the macroscopic dielectric function or the closely related energy los function (ELF) are key quantities to calculate the electron inelastic scattering cross-sections, which are then used within Monte Carlo simulations to model the transport of electrons and to predict the REELS spectrum [3]. The agreement between the simulated and measured REELS is used to validate the TDDFT-calculated electronic excitation spectra of cerium oxides in a broad energy and momentum transfers region.

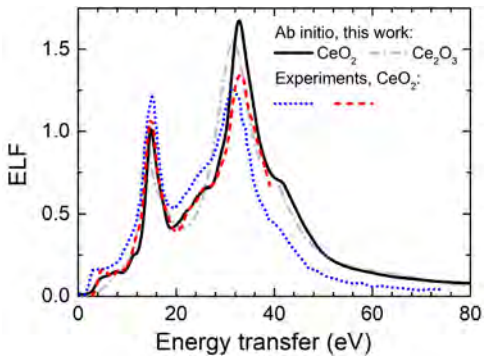

Figure 1. Calculated energy-loss functions in the optical limit of CeO_2 and Ce_2O_3, compared to the experimental data available for CeO_2 [3].

[1] S. McKinnon, S. Guatelli, S. Incerti, V. Ivanchenko, K. Konstantinov, S. Corde, M. Lerch, M. Tehei, A. Rosenfeld, *Physic in Medicine and Biology* **32**, 1584 (2016).
[2] N. V. Skorodumova, R. Ahuja, S. I. Simak, I. A. Abrikosov, B. Johansson, B. I. Lundqvist, *Physical Review B* **64**, 115108 (2001).
[3] A. Pedrielli, P. de Vera, P. E. Trevisanutto, N. M. Pugno, R. Garcia-Molina, I. Abril, S. Taioli, M. Dapor, *Physical Chemistry Chemical Physics* **21**, 19173 (2021).

Acknowledgements: We acknowledge financial support by the CARITRO project *High-Z ceramic oxide nanosystems for mediated proton cancer therapy*, the European Union's Horizon 2020 Research and Innovation programme under the Marie Sklodowska-Curie grant agreement no. 840752 *NanoEnHanCeMent*, the Spanish Ministerio de Economía y Competitividad and the European Regional Development Fund (Projects no. PGC2018-096788-B-I00, the Fundación Séneca (Project no. 19907/GERM/15) and the Conselleria d'Educació, Investigació, Cultura i Esport de la Generalitat Valenciana (Project no. AICO/2019/070).

Thin films of superconducting Au proximitized with Nb under magnetic fields

Miguel Águeda[1,*], Edwin Herrera[1], Beilun Wu[1], Hisa Matsuki[2], Jason Robinson[2], Isabel Guillamón[1], H. Suderow[1]

[1]*Laboratorio de Bajas Temperaturas y Altos Campos Magnéticos, Departamento de Física de la Materia Condensada, Instituto Nicolás Cabrera and Condensed Matter Physics Center (IFIMAC), Unidad Asociada UAM-CSIC, Universidad Autónoma de Madrid, E-28049 Madrid, Spain.*
[2]*Quantum Materials and Devices Group, Department of Materials Science & Metallurgy, University of Cambridge, 27 Charles Babbage Road, CB3 0FS Cambridge, United Kingdom.*

*e-mail: miguel.agueda@estudiante.uam.es

We study a nanometer thin Au film on top of a Nb film using millikelvin Scanning Tunneling Microscopy (STM). We observe a superconducting gap in Au induced by proximity. The Au film thickness has a spatial variation which we characterize by making STM images in the usual topography mode. At zero magnetic field we observe that the superconducting density of states at the Fermi level in Au is very small and does not vary significantly over large areas whole surface. However, there is a sizeable variation of the tunneling conductance at the quasiparticle peaks, suggesting that the gap size slightly changes with the film thickness. This shows that the proximity induced superconductivity in the Au film is intrinsically inhomogeneous. When applying a magnetic field we observe a very strong spatial dependence of the superconducting density of states, suggesting a disordered distribution of normal and superconducting areas. We discuss the implications of our results for the vortex lattice in the Au proximitized superconductor and possible future developments of tunneling experiments on proximitized Au films.

Coexistence of spin-triplet superconductivity and excitonic condensates in two-dimensional crystals

José Vicente Álvarez Carrera[1], **Fernando Escobar Ortiz**[2,*]

[1] *Departamento de Física de la Materia Condensada, Facultad de Ciencias, Universidad Autónoma de Madrid, Spain.* [2] *Departamento de Física de la Materia Condensada, Facultad de Ciencias, Universidad Autónoma de Madrid, Spain.*

*e-mail: fernando.escobar@estudiante.uam.es

The coexistence of superconductivity and other fermionic phases has been studied widely ([1], [2], among many). However, this study has been centered mostly on magnetic phases and charge density wave phases. With the recent discovery of superconductivity and excitonic condensate phases in monolayer WTe_2 [3], [4], it is important to determine whether these two phases can coexist. We perform a mean-field study of a simple two-band model which allows for the formation of excitons, intra- and inter-band Cooper pairs in the spin-triplet state. We find out that the coexistence between these two apparently competing phases at $T = 0$ is possible because of the superconducting order parameter vanishing on certain regions of the Brillouin zone. We show that the appearance of superconductivity is robust to variations of the pairing potentials.

[1] Leroux, Maxime and Mishra, Vivek and Opagiste, Christine and Rodière, Pierre and Kayani, Asghar and Kwok, Wai-Kwong and Welp, Ulrich, *Phys. Rev. B* **102**, 094519 (2020).
[2] Metlitski, Max A. and Sachdev, Subir, *Phys. Rev. B* **82**, 075127 (2010).
[3] Valla Fatemi, Sanfeng Wu, Yuan Cao, Landry Bretheau, Quinn D. Gibson, Kenji Watanabe, Takashi Taniguchi, Robert J. Cava and Pablo Jarillo-Herrero, *Science* **362**, 926-929 (2018).
[4] Jia, Y., Wang, P., Chiu, CL. et al., *Nat. Phys.* **18**, 87-93 (2022).

Avances en la caracterización de nanomateriales mediante Microscopía de Fuerzas Atómicas

Presentaciones orales

Martes 12/07:

15:00-15:05 The Organizers. *Welcome*

15:05-15:40 Agustina Asenjo Barahona. *Dissipative Magnetic Force Microscopy*

15:40-15:55 Guillermo López-Polín. *High efficiency devised based on the anomalous Nernst effect of Co/Pt magnetic multilayers with perpendicular magnetic anisotropy*

15:55-16:10 Jorge Marqués Marchán. *Nucleation and current-induced bubble structures motion in PMA multilayers*

16:10-16:35 Daniel Martín Jimenez. *Chemical bond imaging using torsional and flexural higher eigenmodes of qPlus sensors*

16:35-17:00 Cesar Gonzalez Pascual. *Detecting molecules in defective MoS2 with SPM techniques*

17:00-17:30 **Café**.

17:30-18:05 M. Teresa Cuberes Montserrat. *Visualization of nanostructural arrangements at organic-inorganic hybrid matrices by Ultrasonic Force Microscopy*

18:05-18:20 Sergio Molina-Prados. *Co-localized scanning probe microscopy/Raman scattering studies of hybrid plasmonic substrates*

18:20-18:35 Francisco Miguel Espinosa Barea. *Sub-10 nm patterning of few-layer MoS2 and MoSe2 nanoelectronic devices by oxidation scanning probe lithography*

18:35-19:00 Eider Berganza Eguiarte. *Writing bioactive nanostructures with Scanning Probe Lithography techniques*

Miércoles 13/07:

15:00-15:55 Thilo Glatzel. *Kelvin Probe Force Microscopy and Spectroscopy*

15:55-16:30 Mónica Luna Estévez. *Unraveling the Charge Transfer and Trapping on Single Gold Metal Nanoparticles on TiO2 during photo(electro) catalytic H2 production*

16:30-16:45 Ignasi Fina. *On the origin of extrinsic charging effects in piezoelectric force microscopy experiments*

16:45-17:00 Horacio Vargas Guzman. *Quantitative electrostatic force tomography for virus capsids in interaction with an approaching nanoscale probe*

17:00-18:00 **Pósteres y café**.

18:00-18:35 Cristina Gomez-Navarro. *Mechanics of Defective 2D Materials*

18:35-18:50 Aitor Zambudio Sepúlveda. *Fine Defect Engineering of 2D Monolayers Friction*

18:50-19:05 Yolanda Manzanares Negro. *Controlling fracture properties of MoS2 by introducing atomic vacancies*

Jueves 14/07:

15:00-15:35 Nuria Gavara Casas. *Bio-AFM is the new black in biomedical sciences*

15:35-15:50 Marina Pilar López Yubero. *Effects of energy metabolism on the mechanical properties of breast cancer cells*

15:50-16:05 Juan García Sánchez. *The viscoelasticity of adherent cells follows a single power-law with distinct local variations within a single cell and across cell lines*

16:05-16:30 Andra C. Dumitru. *Decoding mechanical fingerprints of cellular components in pathological conditions: a multiscale perspective*

16:30-16:33 Alejandro Martin-Gonzalez. *Condensin-driven loop extrusion on supercoiled DNA*

16:55-17:45 **Café**.

17:45-18:00 Victor Gisbert. *High-Speed Bimodal AFM nanomechanical mapping of collagen self-assembly*

18:00-18:15 Giovanni Sáenz-Arce. *Nanomechanical properties of trophozoites and extracellular vesicles of the free-living amoeba Naegleria fowleri*

18:15-18:40 Mercedes Hernando Pérez. *Physical principles of protein nanocages: AFM, a single molecule approach*

18:40-18:45 The Organizers. *Closing remarks*

Pósteres

- Mª Dolores Samper Madrigal. *Study of the effect of reactive/non-reactive additives on the microstructure of biopolymer blends by means of AFM-QNM*
- Juan López Martinez. *AFM Surface deterioration evaluation to monitor thermoplastic starch films degradation under composting conditions*
- Diana Méndez Arvelo. *Visualization of interfacial layers of organic molecules on graphite by Three-Dimensional Atomic Force Microscopy*
- Daniel Gallego Fuente. *Development of a technological AFM microscope for operation in UHV*
- Diego Alonso Aldave Valle. *Deterministic transfer of gold nanowires in scanning probe assisted nanowire circuitries*
- Eva Osuna Bris. *Nano-scale conductivity of Hi3(HITP)2 Metal-Organic Framework*
- Miriam Jaafar Ruiz - Castellanos. *Unraveling Dissipation-Related Features in Magnetic Imaging by Bimodal Magnetic Force Microscopy*
- Mario Navarro Rodríguez. *Charge injection and conductivity measurements on highly insulating materials*
- Ana Cros. *Ultraviolet light assisted Kelvin probe force microscopy of dislocations in GaN structures for power applications*
- Pablo Ares. *Isolation of Highly Stable Antimonene under Ambient Conditions*
- J.G. Vilhena. *All-Atom Single-Protein AFM Nanomechanical Spectroscopy Mapping*
- Emilio Rayón Encinas. *A microstructural study by stiffness mapping using the QNM-AFM technique. A case study: Improvement of the miscibility of a PHB-PCL blend*

Dissipative Magnetic Force Microscopy

Jorge Marqués-Marchán[1], Alvaro Gallo-Cordova[1], Miriam Jaafar[2], M. del Puerto Morales[1], **Agustina Asenjo**[1,*]

[1]*Instituto de Ciencia de Materiales de Madrid, CSIC, 28049 Madrid, Spain.*
[2]*Dpto. Física de la Materia Condensada and IFIMAC, UAM, 28049 Madrid, Spain.*

*e-mail: aasenjo@icmm.csic.es

The usefulness of the scanning probe microscopies (SPM) in the characterization of biomaterials is beyond question. The SPM has been extensively used in the evaluation of the morphology and mechanical properties of individual molecules, viruses or cells and its manipulation [1]. In the field of nanomagnetic materials for life science, the magnetic nanoparticles are the most extended elements with a broad range of applications. One of the challenges is this field is the characterization of individual elements. The Magnetic Force Microscopy (MFM) arises a unique technique not only to obtain information about the magnetic configuration of different nanostructures, but also to determine the magnetic anisotropy of individual nanoparticles [2]. However, other important question, the evaluation of the heating capacity of the magnetic nanoparticles used in hyperthermia treatment is still an open question.

Measuring dissipation in scanning force microscopy relies on extracting physical information from either tip or sample by recording variations in the cantilever oscillation as some energy is transferred in every oscillation cycle into dissipative processes [3]. The dissipative maps in Magnetic Dissipation Force Microscopy (MDFM) have been used to distinguish between Néel and Bloch domain walls [4], detect magnetic nanoparticles [5] or to obtain 2D maps of the sample stray field [6]. In addition, the MDFM mode allows to improve the lateral resolution [7] or to distinguish artefacts [8].

In this work, we have used MDFM mode to evaluate the dissipation of energy at the nanoscale in flowers-like magnetic nanoparticles [9]. The flower-like nanoparticles present a magnetic behaviour close to superparamagnetic state at room temperature. Thus, the magnetic moment can be reoriented due to the stray field of the MFM tip. The loss of energy depends on the cluster size, the tip stray field and the measurements conditions. We have also analysed the correlation between the maximum dissipation and the morphology of the clusters.

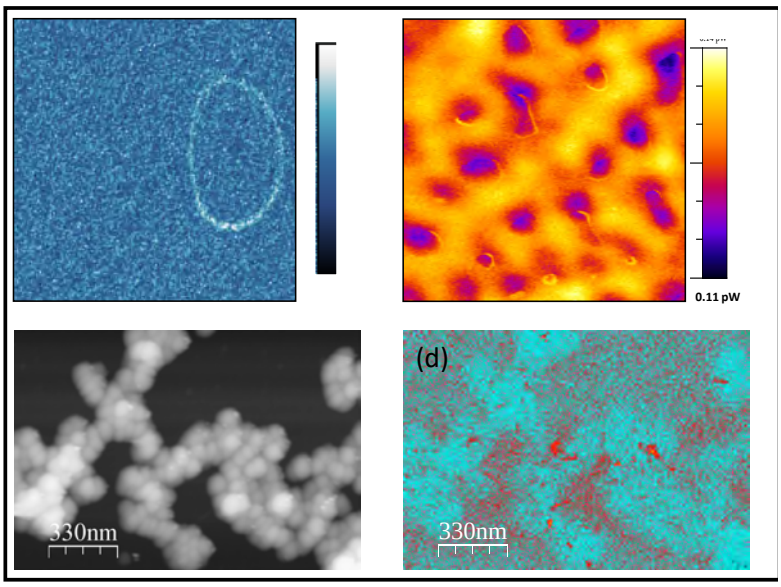

Figure: Dissipation images corresponding to (a) Saturated Co disc [6], (b) CoPt multilayer [7] and (d) flower-like nanoparticles. (c) is the corresponding topographic image of the flower-like nanoparticles

[1] C. Gómez-Navarro, F. Moreno-Herrero, P. J. de Pablo, J. Colchero, J. Gómez-Herrero, A. M. Baró, *Proc. Natl. Acad. Sci.* **99**, 8484 (2002).
[2] C. Moya, Ó. Iglesias-Freire, N. Pérez, X. Batlle, A. Labarta, A. Asenjo, *Nanoscale* **7**, 8110 (2015).
[3] W. Denk and D. W. Pohl, *Appl. Phys. Lett.* **59**, 2171 (1991).
[4] P. Grütter, Y. Liu, P. LeBlanc and U. Dürig, *Appl. Phys. Lett.* **71**, 279 (1997).
[5] B. Torre, G.Bertoni, D. Fragouli, A. Falqui, M. Salerno, A. Diaspro, R. Cingolani and A. Athanassiou,. *Scientific Reports* **1**(1), 1–8 (2011).
[6] Ó. Iglesias-Freire, J. R. Bates, Y. Miyahara, A. Asenjo and P. H. Grütter, *Appl. Phys. Lett.* **102**, 022417 (2013).
[7] M. Jaafar, Ó. Iglesias-Freire, P. García-Mochales, J. J. Sáenz and A. Asenjo, *Nanoscale* **8**(38), 16989 (2016).
[8] M. Jaafar and A. Asenjo, *Appl. Sci.* **11**(22), 10507 (2021).
[9] H. Gavilán, Veintemillas-Verdaguer, C. Johansson, M.P. Morales, *Part. Part. Syst. Charact.* **34** (2017).

High efficiency devised based on the anomalous Nernst effect of Co/Pt magnetic multilayers with perpendicular magnetic anisotropy

Guillermo Lopez-Polin[1,*], Hugo Aramberri[2], Jorge Marques-Marchan[1], Benjamin I. Weintrub Weintrub[3], Kirill I. Bolotin[3], Jorge Iribas Cerda[1], Agustina Asenjo[1]

[1]*Instituto de Ciencia de Materiales de Madrid (ICMM-CSIC), 28049, Madrid, Spain.*
[2]*Materials Research and Technology Department, Luxembourg Inst. of Science and Tech. (LIST), L-4362, Luxembourg.*
[3]*Department of Physics, Freie University Berlin 14195 Berlin, Germany.*

*e-mail: guillermo.lopez-polin@uam.es

The anomalous Nernst effect (ANE) is a thermomagnetic effect that can be exploited for energy harvesting to make use of wasted thermal energy from natural sources or from different electronic devices[1]. The effect depends on the direction of the magnetization of the sample with respect to the direction of a thermal gradient. Thus, in order to maximize the ANE without applying any external field, it is very convenient to have the remanence of the system in a well-defined direction. Here we report on the ANE response of microscopic devices based on multilayers of Co/Pt with high perpendicular magnetic anisotropy[2]. We fabricated micrometre sized devices to enhance the thermal gradient and achieve high efficiency thermoelectric devices. Consequently, the thermal decay occurs across a very small space, giving thermal gradients three orders of magnitude higher than the achieved in macroscopic devices. We extracted the magnetization of the microscopic structures from magnetic force microscopy (MFM) images. We also measured the maximum current and power provided by the device. We obtained record voltages of approximately 30 mV/cm and power densities of around 14 W/cm^3. This work tries to emphasize the importance of evaluating the resistance or the maximum current admitted by materials with high ANE for energy harvesting purposes.

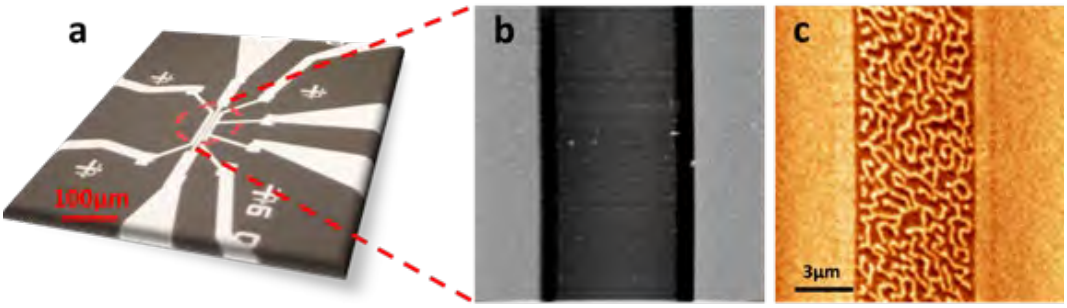

Figure 1. a) Picture of the device used to measure the ANE thermopower of microscopic multilayers. b) Atomic Force microscopy and c) MFM images of the magnetic multilayer without remanent magnetization, showing the worm-like structure of the magnetic domains.

[1] Sakai, A.; Minami, S.; Koretsune, T.; Chen, T.; Higo, T.; Wang, Y.; Nomoto, T.; Hirayama, M.; Miwa, S.; Nishio-Hamane, D. *Nature* **581** (7806), 53 (2020).
[2] Hashimoto, S.; Ochiai, Y.; Aso, K. *Journal of Applied Physics* **66** (10), 4909 (1989).

Nucleation and current-induced bubble structures motion in PMA multilayers

J. Marqués-Marchán[1,*], R. Guedas[2], M. C. Pérez Carmona[1], J. L. Prieto[2], A. Asenjo[1]

[1]*Instituto de Ciencia de Materiales de Madrid, CSIC, C\Sor Juana Inés de la Cruz 3, 28049, Spain.*
[2]*Instituto de Sistemas Optoelectrónicos y Microtecnología (ISOM), Universidad Politécnica de Madrid, Avda. Complutense 30, Madrid, E-28040, Spain*

*e-mail: jorge.marques@csic.es

Perpendicular Magnetic Anisotropy (PMA) multilayers have been intensely studied in the past due to their applications in magnetic recording [1]. More recently, this kind of materials has renewed its interest due to the discovery of the DMI (Dzyaloshinskii-Moriya Interaction) that appears in the interfaces of ferromagnetic and heavy metals multilayers [2]. DMI interaction promotes the development of exotic configurations so called “skyrmions” and bubbles of great interest in spintronics [3].

In this work, CoPt nanostructures with different shapes and sizes are fabricated by electron beam lithography. The CoPt multilayers are grown by sputtering over Si/SiO2 substrates. Apart from the macroscopic characterization of the CoPt thin films, the nanostructures have been studied by AFM (Atomic Force Microscopy) and MFM (Magnetic Force Microscopy). The goal of this work is to control the nucleation, motion and annihilation of the magnetic bubbles by applying external magnetic fields and current. Nanometer size magnetic bubbles are created in these PMA multilayer nanostructures as demonstrated by the MFM imaging experiments. Besides the MFM imaging in remanent state, a Variable Field MFM system has been used to obtain images under in-plane or out of plane magnetic fields [4]. By applying an in-situ out of plane magnetic field in the VF-MFM system, we are able to control the density of bubbles due to their annihilation. The shape and the size of the bubbles is also analyzed as well as the dependence with the geometry of the nanostructures.

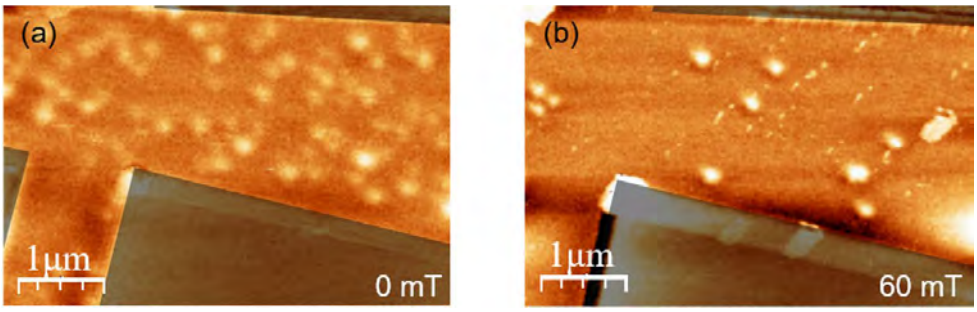

Figure 1. MFM images in remanence of a selected area of a nanostructure (a) after the nucleation of the bubbles and (b) after applying a perpendicular field of 0 mT antiparallel to the bubble magnetic moment.

[1] A. Kirilyuk et al., *Journal of Magnetism and Magnetic Materials* **171**, 45 (1997).
[2] T. Moriya, *Physical Review* **120**(1), 91 (1960).
[3] J. Sampaio et al., *Nature Nanotechnology* **8**, 839 (2013).
[4] M. Jaafar et al., *Ultramicroscopy* **109**(6), 693 (2009).

Chemical bond imaging using torsional and flexural higher eigenmodes of qPlus sensors

Daniel Martin-Jimenez[1,4,*], Michael G. Ruppert[2], Alexander Ihle[1,4], Sebastian Ahles[3,4], Hermann A. Wegner[3,4], André Schirmeisen[1,4] , Daniel Ebeling[1,4]

[1]*Institute of Applied Physics (IAP), Justus Liebig University Giessen, Heinrich-Buff-Ring 16, 35392 Giessen, Germany.*
[2]*University of Newcastle, Callaghan, NSW, 2308 Australia.*
[3]*Institute of Organic Chemistry, Justus Liebig University Giessen, Heinrich-Buff-Ring 17, 35392 Giessen, Germany.*
[4]*Center for Materials Research (LaMa), Justus Liebig University Giessen, Heinrich-Buff-Ring 16, 35392 Giessen Germany.*

*e-mail: Daniel.martin-jimenez@ap.physik.uni-giessen.de

Non-contact atomic force microscopy (AFM) with CO-functionalized tips allows to visualize the chemical structure of adsorbed molecules and identify individual inter- and intramolecular bonds. This technique enables in-depth studies of on-surface reactions and self-assembly processes. Herein, we analyze the suitability of qPlus sensors, which are commonly used for such studies, for the application of modern multifrequency AFM techniques. Two different qPlus sensors were tested for submolecular resolution imaging via actuating torsional and flexural higher eigenmodes and via bimodal AFM. The torsional eigenmode of one of our sensors is perfectly suited for performing lateral force microscopy (LFM) with single bond resolution. The obtained LFM images agree well with images from the literature, which were scanned with customized qPlus sensors that were specifically designed for LFM [1]. The advantage of using a torsional eigenmode is that the same molecule can be imaged either with a vertically or laterally oscillating tip without replacing the sensor simply by actuating a different eigenmode. Submolecular resolution is also achieved by actuating the 2nd flexural eigenmode of our second sensor. In this case, we observe particular contrast features that only appear in the AFM images of the 2nd flexural eigenmode but not for the fundamental eigenmode. With complementary laser Doppler vibrometry measurements and AFM simulations we can rationalize that these contrast features are caused by a diagonal (i.e. in-phase vertical and lateral) oscillation of the AFM tip [2].

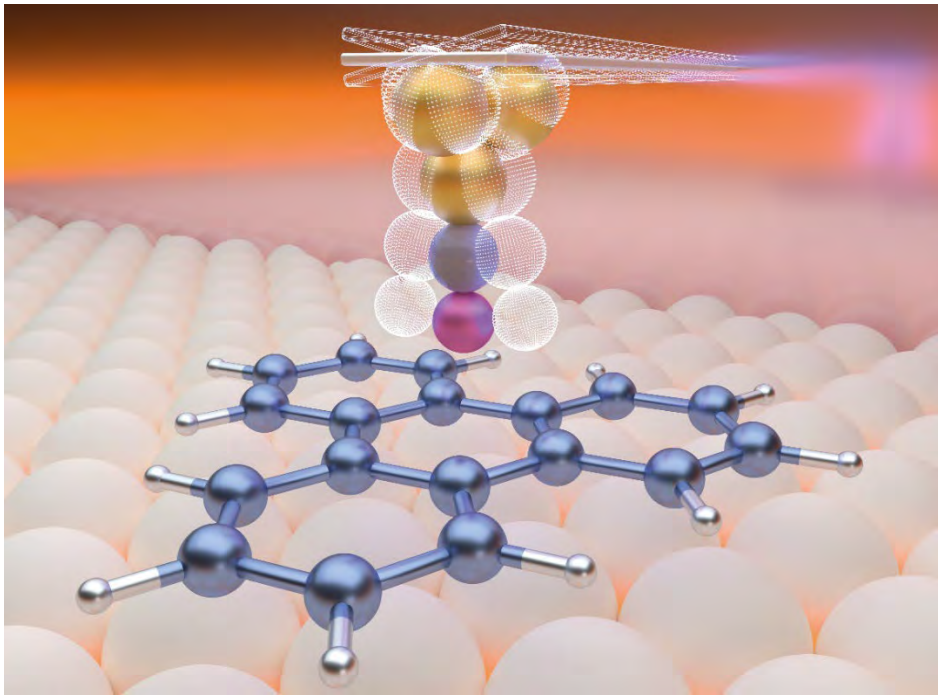

[1] A. J. Weymouth, E. Riegel, O. Gretz and F. J. Giessibl, *Phys. Rev. Lett.*, **124**, 196101 (2020).
[2] D. Martin-Jimenez, M. G. Ruppert, A. Ihle, S. Ahles, H. A. Wegner, A. Schirmeisen and D. Ebeling, *Nanoscale* **14**, 5329 (2022).

Detecting molecules in defective MoS2 with SPM techniques

César González[1,2]

[1]*Dpto Física de Materiales, Universidad Autónoma de Madrid 28040 Madrid, Spain.*
[2]*Instituto de Magnetismo Aplicado UCM-ADIF, Vía de Servicio A-6, 900, E-28232 Las Rozas de Madrid, Spain.*

e-mail: cesar.gonzalez@ucm.es

Since graphene was discovered some years ago [1], the interest in two dimensional (2D) materials has grown exponentially. The so-called transition-metal di-chalcogenides have recently attracted great attention due to their promising properties. One of the most studied compounds is MoS2 due to its potential nanoelectronic, optoelectronic and spintronic applications [2]. Very recently, this material has been proposed as a fundamental part in gas sensors [3]. In those cases, the molecules, weakly bonded to the poorly reactive MoS2 substrate, changed the electric current measured in the sensor.

In this work, we have performed density functional theory (DFT) simulations using the VASP code [4] in order to find the most stable structures of small inorganic molecules (such as H2O, N2, O2, CO, NO and CO2) adsorbed on different point defects of the MoS2 monolayer [5]. Our results show that the molecules can be bonded to the Mo atoms in the substitutional defects. In our analysis, the Sulphur divacancy occupied by two Mo atoms has been selected as the most interesting defect. Once the molecules are bonded to this point, they can be identified using the Scanning Probe Microscopies (SPM). Following the original idea of chemical identification proposed some years ago [6], each molecule will lead to a different force curve when an atomic force microscope (AFM) tip is approached. In figure 1, the forces of CO, NO, CO2, H2O and O2 molecules are represented. The resulting value and position of the minimum force characterize the kind of molecule that has been scanned by the AFM. At the same time, the use of a metallic tip allows the calculation of the conductance as a second fingerprint of each molecule. This second parameter will help to elucidate the molecule adsorbed in cases with comparable force (see in Figure 1 the similar values obtained for O2 and NO). Using these parameters, the molecules can be identified in future experimental measurements.

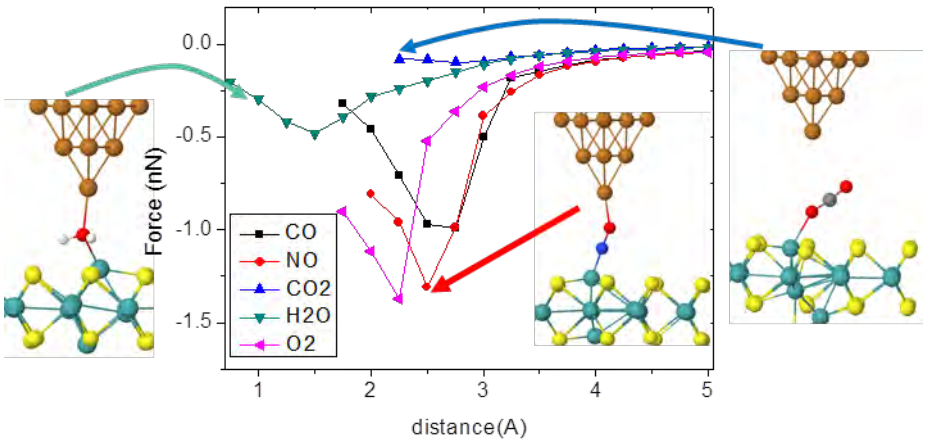

Figure 1. Force curves of a Cu tip contacting to different molecules adsorbed on a defect formed by the substitution of two S by two Mo atoms in the MoS2 monolayer. The ball and stick models of the contact point (minimum force) are shown for: a H2O/CO2 molecule, on the left/right side, and on the inset a NO molecule.

[1] K. S. Novoselov et al., *Science* **306**, 666 (2004).
[2] B. Radisavljevic et al., *Nat. Nanotechnol.* **6**, 147(2011); J. Yoon et al., *Small* **9**, 3295 (2013).
[3] H. Li, et al., *Small* **8**, 63 (2012); Q. Y. He, et al., *Small* **8**, 2994 (2012).
[4] G. Kresse and J. Hafner, *Phys. Rev. B* **47**, R558 (1993).
[5] C. González, et al., *Phys. Chem. Chem. Phys.* **19**, 9485 (2017); C. González and Y. J. Dappe, *Physical Review B* **95**, 214105 (2017).
[6] Y. Sugimoto et al., *Nature* **446**, 64 (2007).

Acknowledgements: Red Española de Supercomputación for the computer resources and the technical support provided different computational projects funded in the recent years as QCM-2016-1-0024 or FI-2022-1-0020.

Visualization of nanostructural arrangements at organic-inorganic hybrid matrices by Ultrasonic Force Microscopy

M. Teresa Cuberes

Department of Applied Mechanics and Project Engineering, Mining and Industrial Engineering School of Almadén, University of Castilla-La Mancha, Plaza Manuel Meca 1, 13400 Almadén, Spain.

e-mail: teresa.cuberes@uclm.es

Ultrasonic Force Microscopy (UFM) is a relatively new extremely Atomic Force Microscopy (AFM)-based technique, extremely powerful for mapping surface and subsurface stiffness inhomogeneities [1]. We have applied UFM/AFM, X-ray Diffraction (XRD), Small Angle X-ray Scattering (SAXS), Fourier Transform - Infrared Spectroscopy (FT-IR), and performed Contact-Angle measurements, and Drug Release experiments [2], to gain insight into the nanostructural organization and surface morphology of organic-inorganic ureasil-polyether hybrid films intended for drug delivery. These films are known to consist of highly correlated siloxane nodes, separated ~2,5 nm, linked by polyether chains [3].

The UFM images reveal a new nanoscale structure in ureasil-poly(propylene oxide)400 films (u-PPO400) (Fig. 1 (a)) that can be understood if clusters of the correlated siloxane nodes form beads, which align into strands, which in turn gather into hybrid polymer ropes, imaged by AFM on the film surface. The described structure impacts the behaviour of the film matrix as host. On u-PPO400 films loaded with Dexamethasone Acetate (DMA), AFM/UFM indicates that the DMA drug molecules form aggregates aligned along the direction defined by the polymer ropes in the unloaded matrix (Fig. 1(c)), presumably in locations depleted from ureasil nodes.

In this contribution, the interpretation of the UFM images will be discussed in view of the data obtained by the aforementioned different techniques. The results illustrate the potential of AFM-based procedures, in combination with additional physico-chemical techniques to picture the nanostructural arrangements in polymer matrices intended for drug delivery.

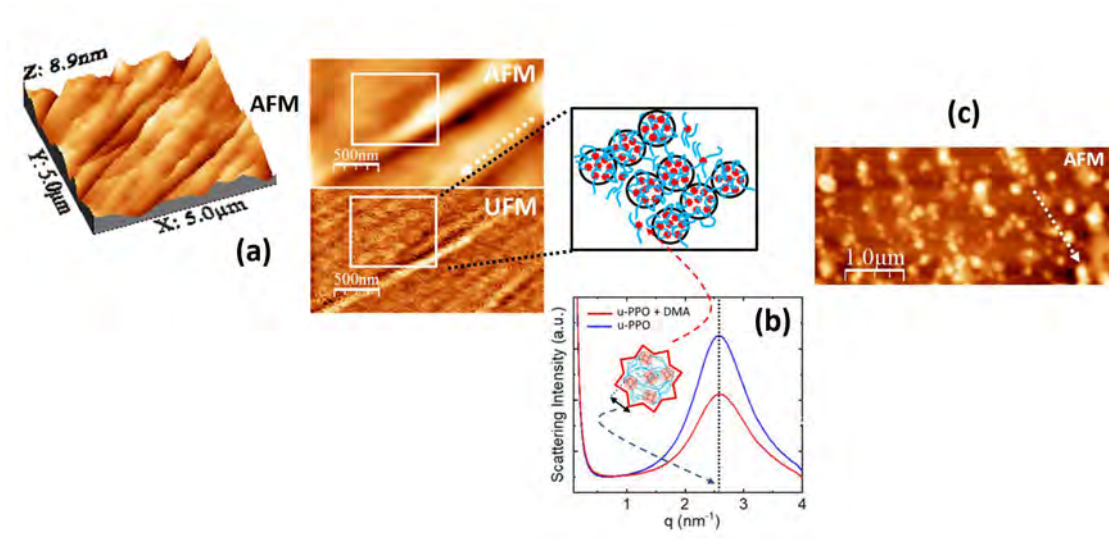

Figure 2. (a) AFM and UFM on ureasil-Polyethylene Oxide (u-PPO400). (b) SAXS on u-PPO, unloaded and loaded with DMA. (c) AFM on DMA-loaded u-PPO400

[1] C. V. Santilli, L. A. Chiavacci, L. Lopes, S. H. Pulcinelli, and A. G. Oliveira, *Chemistry of Materials* **21**, 463 (2009).
[2] M. T. Cuberes, Mechanical Diode-Based Ultrasonic Atomic Force Microscopies. In *Applied Scanning Probe Methods XI: Scanning Probe Microscopy Techniques*, Bhushan, B., Fuchs, H., Eds.; Springer; pp. 39-71 (2009).
[3] J. A. Oshiro, A. Lusuardi, E. M. Beamud, L. A. Chiavacci, and M. T. Cuberes, *Nanomaterials* **11** (2021).

Co-localized scanning probe microscopy/Raman scattering studies of hybrid plasmonic substrates

Sergio Molina-Prados[1,*], Ana Cros[2], Gladys Mínguez[1], Núria Garro[2]

[1]*GROC-UJI, Institut de Noves Tecnologies de la Imatge (INIT), Universitat Jamue I, Spain.*
[2]*Institut de Ciència dels Materials (ICMUV), Universitat de València, Spain.*

*e-mail: molinapr@uji.es

Surface enhanced Raman scattering (SERS) has demonstrated its potential as an ultrasensitive sensing probe in a wide variety of fields. While there are reports of out-standing enhancement factor (EF) values, the background of the technique is far from being well understood. Intensive research efforts are still directed toward describing the electromagnetic and chemical processes leading to SERS effect. In this context, scanning probe microscopies (SPM) can be used for the thorough characterization of SERS substrates. Furthermore, if SPM can be combined with Raman scattering in a single microscope system, a detailed characterization of the most active SERS regions (often referred to as hot spots) could throw light on the fundamental SERS mechanisms.

We have prepared different hybrid plasmonic substrates mixing graphene oxide (GO) sheets with colloidal Au nanoparticles (NPs) synthesized by laser ablation and drop-casting the solution on Pt-coated flat surfaces. We observe the SERS EF of a probe molecule (methylene blue) reaching values greater than 10^3 and showing a remarkable improvement in the reproducibility over large areas of the GO-Au NP substrates, in comparison with conventional plasmonic NPs substrates. The morphology and electro-optical coupling of the GO-Au NP nanohybrids have been investigated using SPM, including Kelvin probe, and correlated with the local SERS EF performing co-localized confocal Raman spectroscopy. There are two different configurations of these SERS substrates with Au NPs located either under or on top of the GO flakes. While it is not possible to distinguish them in the topography maps due to the veil-like coverage of GO, contact potential difference changes larger than 50 mV are observed between both configurations, revealing electron transfer from GO towards the NPs. The comparison with the co-localized SERS maps allows to associate SERS hot spot sites with Au NPs located on top of GO.

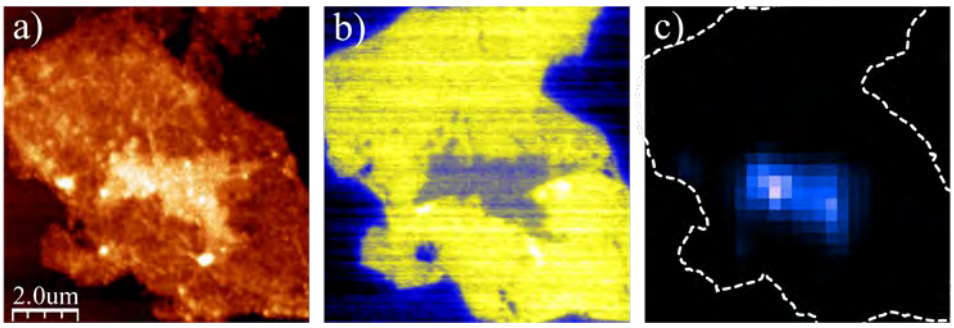

Figure 1. The co-localized maps of a hybrid GO-AuNP flake showing a) surface topography (0 to 60 nm); b) contact potential difference (10 to 60 mV); c) SERS intensity (0 to 1000).

Sub-10 nm patterning of few-layer MoS2 and MoSe2 nanoelectronic devices by oxidation scanning probe lithography

Y. K. Ryu[1], A. I. Dago[1], Y. He[2,3], **F. M. Espinosa**[1,*], C. Munuera[1], E. López- Elvira[1], R. Garcia[1]

[1]*Instituto de Ciencia de Materiales de Madrid, CSIC. Sor Juana Inés de la Cruz 3, 28049 Madrid, Spain.*
[2]*The State Key Laboratory of Robotics and Systems, Robotics Institute, Harbin Institute of Technology, Harbin, Heilongjiang 150080, PR China.*
[3]*Center for Precision Engineering, Harbin Institute of Technology, Harbin, Heilongjiang 150001, PR China.*

*e-mail: francisco.espinosa@csic.es

The properties of 2D materials devices are very sensitive to the physical, chemical and structural interactions that might happen during processing. Low-invasive patterning methods are required to fabricate devices at the nanoscale [1-3]. Here we developed a process that combines oxidation scanning probe lithography (o-SPL) and oxygen plasma to fabricate nanoribbon field-effect transistors and nano-constrictions on few-layer MoS_2 and $MoSe_2$ [4]. The oxygen plasma has a double role in this process. First, it forms a thin, uniform oxide layer on top of the flake surface to enable o-SPL nanopatterning with full control of shape and size. Second, the oxide layer thins down the flake. Both plasma-based and o-SPL oxides are soluble in deionized H_2O, which enabled etching and the definition of electrically isolated nano-constrictions and nanoribbons. The accuracy and robustness of the process was applied to pattern sub-10 nm wide constrictions and nanoribbon transistors.

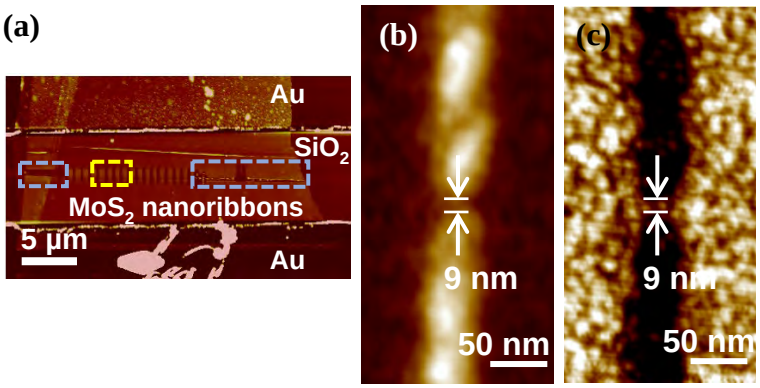

Figure 1. a) AFM topographic image of MoS2 nanoribbons FET. The channel consists of an array of 17 nanoribbons of 300 nm half-pitch and 5 nm of thickness. b) AFM topographic image of a sub-10 nm constriction fabricated by o-SPL on an oxygen plasma treated MoS2 flake. c) AFM topographic image of the constriction shown in (b) after water etching.

[1] F. M. Espinosa, Y.K. Ryu, K. Marinov, D. Dumenco, A.Kis, R.Garcia, *Appl. Phys. Lett.* **106**, 103503 (2015).
[2] A.I. Dago, Y.K. Ryu, R.Garcia, *ACS Appl. Mater. Interfaces* **10**, 40054 (2018).
[3] Y. K. Ryu and R. Garcia, *Nanotechnology* **28**, 142003 (2017).
[4] Y. K. Ryu, A. I. Dago, Y. He, F. M. Espinosa, C. Munuera, E. López- Elvira and R. Garcia, *Appl. Surface Science* **539**, 148231 (2021).

Writing bioactive nanostructures with Scanning Probe Lithography techniques

Eider Berganza[1,2,*], Srivatsan K. Vasatham[1], Mirsana Ebrahimkutty[3], Gurunath Apte[4], Chunting Zhong[1], Milos Galic[3], Thi-Huong Nguyen[4], Michael Hirtz[1]

[1]*Institute of Nanotechnology (INT) and Karlsruhe Nano Micro Facility (KNMF), Karlsruhe Institute of Technology (KIT), Hermann-von-Helmholtz-Platz 1, 76344 Eggenstein-Leopoldshafen, German.y*
[2]*Instituto de Ciencia de Materiales de Madrid, CSIC, 28049, Madrid, Spain.*
[3]*University of Münster, Robert-Koch-Straße 31, Münster, Germany.*
[4]*Institute for Bioprocessing and Analytical Measurement Techniques (IBA), 37308 Heilbad Heiligenstadt, Germany.*

*e-mail: eider.eguiarte@gmail.com

The creation of biologically inspired artificial membranes on substrates with custom size and in close proximity to each other provides a platform to study complex biological processes in a simplified manner. Additionally, artificial membranes can also be used as building blocks for chemical or biological sensors integrated in microfluidic devices [1,2].

In this regard, Scanning Probe Lithography tools have opened a new paradigm, as they enable direct writing of lipid membranes with spatial resolution down to 100 nm. We have used Dip-Pen Nanolithography with Phospholipids (l-DPN), which deposits nanosized elements, by transferring absorbed molecules on the AFM tip through a water meniscus onto the substrate, to create an in-vitro platform for the study of lipid membrane curvature driven effects. Curvature represents a key parameter, which is synergized with the lipid composition and mediates many relevant biological processes, such as membrane trafficking, viral interactions or membrane fusion. By anchoring nanoparticles to the substrate prior to lithography and direct writing lipids on top, we are able to impose the desired curvature, circumventing complex nanofabrication processes through a simple and low-cost method [3].

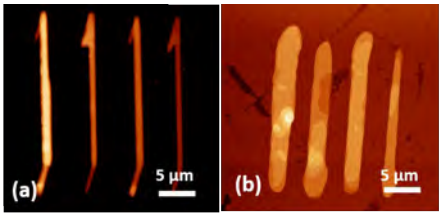

Figure 1. Phospholipid ink lines direct-written with Dip-Pen Nanolithograpy on (a) chemically-modified Silicon and on (b) bare Silicon substrate.

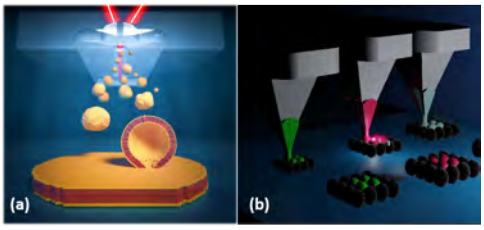

Figure 2. (a) FluidFM technology vs. (b) Dip-Pen Nanolithography.

Although l-DPN has generally being conceived as a 2D lithography technique, by tuning the substrate properties that hamper the spread of phospholipids, we have recently achieved to perform 3D writing (see Figure 1), which can be later metalized to extend the use of this structures beyond the field of biophysics [4].

On the other hand, we have proposed the use of the fluid force microscopy (FluidFM) technology to overcome some inherent limitations of L-DPN (Figure 2). FluidFM features a hollow AFM cantilever with submicron sized aperture that locally disperses a chosen solution [5], combines the accuracy of force control positioning and the versatility of microfluidics. Unlike in l-DPN where the operation is necessarily performed in air environment, direct writing of a single bilayer is achieved in liquid, where by adjusting the working pressure and dwell time, the size of the patches can be tuned [6].

[1] Castellana, E.T.; Cremer, P.S., *Surf. Sci. Rep.* **61** (10), 429 (2006).
[2] Liu, H. Y.; Kumar, R.; Zhong, C.; Gorji, S.; Paniushkina, L.; Masood, R.; Wittel, U. A.; Fuchs, H.; Nazarenko, I.; Hirtz, M., *Adv. Mater*. **33**, 2008493 (2021).
[3] Berganza, E.; Ebrahimkutty, M. P.; Vasantham, S. K.; Zhong, C.; Wunsch, A.; Navarrete, A.; Galic, M.; Hirtz, M., *Nanoscale* **13**, 12642 (2021).
[4] Berganza, E. et al. in preparation.
[5] Berganza, E.; Apte, G.; Vasantham, S. K.; Nguyen, T-H.; Hirtz, M., *Polymers* **14**(**7**) 1327 (2022).
[6] Berganza, E.; Hirtz, M., *ACS Appl. Mat. Int.* **13**(43), 50774 (2021).

Kelvin Probe Force Microscopy and Spectroscopy

Th. Glatzel*, U. Gysin, A. Hinaut, R. Pawlak, E. Meyer

Department of Physics, University of Basel, Klingelbergstr. 82, 4056 Basel, Switzerland

*e-mail: thilo.glatzel@unibas.ch

Scanning probe microscopy is one of the most important surface science methods for characterizing a variety of different surface and subsurface properties at the nanoscale. Atomic force microscopy, and in particular Kelvin probe force microscopy (KPFM)[1,2], allows the detection of atomic scale forces and separation into their different components, namely Van der Waals, magnetic, electric and chemical bonding forces. KPFM allows the electrostatic forces to be separated from these components and the work function, surface band bending, and electric dipole strength to be determined at the nanometer scale. In the presentation, I will discuss the different techniques used to perform these measurements using various examples and present the advantages and disadvantages of these techniques. Finally, I will also highlight the spectroscopy mode and the determination of the local work function differences at molecular and atomic scales and will give an overview on recent achievements.

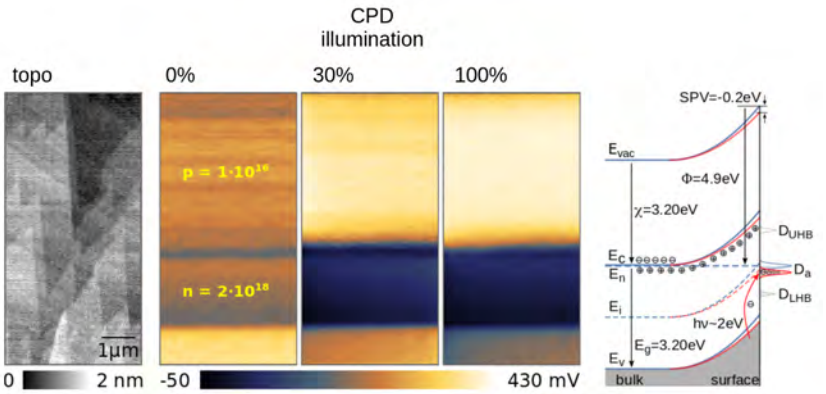

Figure 1. a) Topography, b) dark KPFM and c) 30 % laser-power illuminated (470–480 nm and a maximum power of 50 mW) KPFM images of a SiC p/n-junction. The scan size is 4×8 μm^2. d) 100 % laser- power illuminated KPFM image. e) shows a schematic band diagram of the surface band bending as well as the characteristic energies for the n-doped SiC sample including known defect states in dark (blue) and under illumination (red). Under illumination electrons are excited to the acceptor-type defects D_a and the band-bending is reduced [3].

[1] S. Sadewasser and Th. Glatzel (Eds.), *Kelvin Probe Force Microscopy Measuring and Compensating Electrostatic Forces*, Springer (2011).
[2] S. Sadewasser and Th. Glatzel (Eds.), *Kelvin Probe Force Microscopy - From Single Charge Detection to Device Characterization*, Springer (2018).
[3] U. Gysin et al., *Beilstein Journal of Nanotechnology* **6**, 2485 (2015).

Unraveling the Charge Transfer and Trapping on Single Gold Metal Nanoparticles on TiO_2 during photo(electro) catalytic H_2 production

Monica Luna[1,*], Mariam Barawi[2], Sacha Gómez-Moñivas[3], Jaime Colchero[4], Yi-Hsien Lu[5,6], Ravi Chintala[5], Patricia Reñones[2], Virginia Altoe[5], Lidia Martínez[7], Yves Huttel[7], Seiji Kawasaki[5,6], Alexander Weber-Bargioni[5], Victor A. de la Peña O´Shea[2], Peidong Yang[6,8], Paul D. Ashby[5], Miquel Salmeron[6,9]

[1]*IMN-Instituto de Micro y Nanotecnología (CNM-CSIC), 28760 Tres Cantos, Spain.*
[2]*IMDEA-ENERGIA, 28935, Móstoles, Spain.*
[3]*Dept. Ingeniería Informática, Escuela Politécnica Superior, UAM, Campus de Cantoblanco, Madrid 28049, Spain.*
[4]*Departamento de Física, Universidad de Murcia, Campus de Espinardo, Murcia, Spain.*
[5]*Molecular Foundry, Lawrence Berkeley National Laboratory, California, 94720 United States.*
[6]*Materials Sciences Division, Lawrence Berkeley National Laboratory, California, 94720 United States.*
[7]*Instituto de Ciencia de Materiales de Madrid (ICMM-CSIC), 28049 Madrid, Spain.*
[8]*Department of Chemistry, University of California, Berkeley, California 94720, United States.*
[9]*Materials Science and Engineering Dept. University of California Berkeley, California 94720, United States.*

*e-mail: monica.luna@csic.es

We present a study of the effect of gold nanoparticles (Au NPs) on TiO_2 on charge generation and trapping during illumination with photons of energy larger than the substrate band gap. We used a novel characterization technique, photoassisted Kelvin probe force microscopy (PA-KPFM), to study the process at the single Au NP level. We found that the photoinduced electron transfer from TiO_2 to the Au NP increases logarithmically with light intensity due to the combined contribution of electron−hole pair generation in the space charge region in the TiO_2−air interface and in the metal−semiconductor junction. Our measurements on single particles provide direct evidence for electron trapping that hinders electron−hole recombination, a key factor in the enhancement of photo(electro)catalytic [1].

[1] M. Luna, M. Barawi, S. Gómez-Moñivas, J. Colchero, Y.-H. Lu, R. Chintala, P. Reñones, V. Altoe, L. Martínez, Y. Huttel, S. Kawasaki, A. Weber-Bargioni, V. A. de la Peña O´Shea, P. Yang, P. D. Ashby, M. Salmeron, *ACS Appl. Mater. Interfaces*,**13**, 50531 (2021).

Acknowledgements: The authors thank Prof. Eran Edri, María U. González, and Judit Meseguer-Oliver for fruitful discussions and Asylum customer support.

On the origin of extrinsic charging effects in piezoelectric force microscopy experiments

Huan Tan, Jike Lyu, Yunwei Sheng, Pamela Machado, Tingfeng Song, Akash Bhatnagar, Mariona Coll, Florencio Sánchez, Josep Fontcuberta, **Ignasi Fina***

[1]*Institut de Ciència de Materials de Barcelona (ICMAB-CSIC), Campus UAB, Bellaterra 08193, Spain.* [2]*Zentrum für Innovationskompetenz SiLi-nano, Martin-Luther-Universität Halle-Wittenberg, 06120 Halle, Germany.* [3]*Institute of Physics, Martin-Luther-Universität Halle-Wittenberg, 06120 Halle, Germany.*

*e-mail: ifina@icmab.es

Piezoelectric force microscopy has demonstrated to be a powerful technique to characterize ferroelectricity at the nanoscale. Piezoresponse in any material has several contributions. The intrinsic contribution resulting from the intrinsic piezoelectric nature of the characterized material shows clear signatures, usually allowing its identification. In addition to this intrinsic response, several contributions might appear. The most important one is that resulting from charging effects. Non-compensated surface charge induces a deformation with a quadratic dependence on the applied electric field. One usually compensates these surface charges by the application of subsidiary external DC voltage. However, the selection of this external DC voltage is usually done as a guesswork and its relation with the properties of the material has not been identified so far.

Here, we show piezoelectric force microscopy characterization of films of different materials, these are $BaTiO_3$, $BiFeO_3$, $LuFeO_3$ and $Hf_{0.5}Zr_{0.5}O_2$. We observe that depending on the material the extrinsic charging contribution is very different. In addition, we observe that the sign and magnitude of the required DC voltage to compensate surface charges also depends on the material. To disclose its origin, we have performed complementary transport characterization. It is found that materials showing rectifying I-V characteristics for positive polarity require negative compensating voltage ($BaTiO_3$, $BiFeO_3$) and vice versa ($LuFeO_3$). Interestingly, $Hf_{0.5}Zr_{0.5}O_2$ shows symmetric I-V characteristics in agreement with the negligible presence of charging effects. Therefore, there is a direct connection between charge compensation and transport properties and I will discuss the origin of this. Finally, we demonstrate that the found correlation can be used to predict compensating voltage in non-ferroelectric materials, allowing to easily disclose possible artefacts.

[1] H. Tan et al., to be submitted.

Acknowledgements: This project was supported by a 2020 Leonardo Grant for Researchers and Cultural Creators, BBVA Foundation.

Quantitative electrostatic force tomography for virus capsids in interaction with an approaching nanoscale probe

Christopher D. Cooper[1], Ian Addison-Smith[1], **Horacio V. Guzman**[2,3,*]

[1] *Department of Mechanical Engineering, Universidad Técnica Federico Santa María, 2390123 Valparaíso, Chile.* [2] *Department of Theoretical Physics, Jožef Stefan Institute, Jamova 39, 1000 Ljubljana, Slovenia.* [3] *Departamento de Física Teórica de la Materia Condensada, Universidad Autónoma de Madrid, E-28049 Madrid, Spain.*

*e-mail: horacio.guzman@ijs.si

Electrostatic interactions are crucial for the assembly, disassembly and stability of proteinaceous viral capsids. Yet at the molecular scale elucidating the organization and structure of the capsid proteins in response to an approaching nanoprobe is a major challenge in biomacromolecular research. Here, we report on novel analytical models and simulations that allow the quantification of localized subnanometric electrostatic interactions between an AFM tip and proteinaceous capsid. We have validated our results in terms of total electrostatic forces with previous semi-empirical generalized models available length scales (l_s>1nm). The theoretical results provide a new route in the interpretation of the localized interactions arising between virus capsids and an AFM nanoprobe, which describe the contributions of specific amino acid and atoms to the detected forces. While the localized understanding of electrostatic interactions can be directly employed for the quantitative interpretation of force microscopy experiments in basic virological characterizations and in diverse nanomedicine applications, where specific regions of the protein cages are aimed to electrostatically interact with molecular sized functionalized inhibitors, or tailoring protein-cage functional properties for nucleic acid delivery.

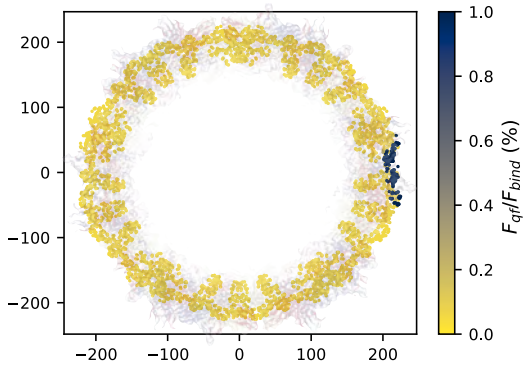

Figure. Normalized electrostatic interactions between a Zika virus capsid and an AFM Tip located at 2 Å from the x-axis.

Acknowledgements: H.V.G thanks the financial support by the Slovenian Research Agency (Funding No. P1-0055).

Mechanics of defective 2D materials

Cristina Gomez-Navarro[1,2,*], G. Lopez-Polin[1,2], Y. Manzanares-Negro[1,2], A. Zambudio[1,2], J. Gomez-Herrero[1,2]

[1]*Condensed Matter Physics Dept., Universidad Autónoma de Madrid, Madrid, E-28049, Spain.*
[2]*Condensed Matter Department, Universidad Autónoma de Madrid, Madrid, E-28049, Spain.*

*e-mail: cristina.gomez@uam.es

The mechanical behaviour of 2D materials is governed by an extremely low bending rigidity and high in plane stiffness and strength. This unique combination makes these materials appealing for fundamental research as the thinnest membranes ever known but also in applications where flexibility and strength are desirable.

In this talk I will give an overview of the mechanical properties of 2D materials to provide a framework to our recent studies on mechanical response of graphene and MoS_2 with induced atomic defects.

I will show that controlled induction of diluted atomic vacancies in these 2D materials substantially modify their elastic response including elastic modulus [1], thermal expansion coefficient [2], and friction coefficient [3]. In addition, it constitutes an effective approach to avoid their catastrophic failure upon fracture [4,5].

[1] G. López-Polín *et al*., *Nature Physics* **11**, 26 (2015).
[2] G. López-Polín, *et al*., *Carbon* **116**, 670 (2017).
[3] A. Zambudio *et al*., *Carbon* **182**,735 (2021).
[4] Yolanda Manzanares-Negro *et al*., *ACS nano* **15**, 1210 (2021).
[5] G. López-Polín *et al*., *Nanoletters* **15** 3, 2050 (2015).

Fine Defect Engineering of 2D Monolayers Friction

A. Zambudio[1,2,*], E. Gnecco[3], J. Colchero[1], R. Pérez[4,5],
J. Gómez-Herrero[2,5], C. Gómez-Navarro[2,5]

[1]*Optics and Nanophysics Research Center, Universidad de Murcia, E-30100, Murcia, Spain.*
[2]*Condensed Matter Physics Dept., Universidad Autónoma de Madrid, Madrid, E-28049, Spain.*
[3]*Otto Schott Institute of Materials Research, Friedrich Schiller University of Jena, D-07743, Jena, Germany.*
[4]*Theory Condensed Matter Physics Dept., Universidad Autónoma de Madrid, Madrid, E-28049, Spain.*
[5]*Condensed Matter Physics Center, Universidad Autónoma de Madrid, Madrid, E-28049, Spain.*

*e-mail: aitor.zambudio@uam.es

Two-dimensional (2D) materials display low friction coefficient and good wear properties. However, the emergence of atomic-scale defects, inherent to any large-scale production method, strongly influence its friction and other mechanical properties. Up to date tribological studies on 2D materials with defects involve the presence of coexistent substitution and vacancy-like defects with different sizes[1]. This leads to a difficult interpretation and comparison between results, and prevents from a fundamental understanding of the role of defects in the friction of atomically thin materials.

In this work, we quantify the influence of controlled-induced monoatomic vacancies in the tribology of single-layers of graphene and molybdenum disulfide (MoS_2) using Atomic Force Microscopy (AFM) in air and High Vacuum (HV) conditions. The global friction coefficient is compared for several defect densities. At the atomic-scale, we are able to resolve single-atom vacancies in Lateral Force (LF) images, and to quantify the friction behaviour at the nanoscale.

Our fine post-process method provides the means for a thorough analysis of the real-space distribution of friction with nanometer resolution, thus enabling the discrimination between the influence on the global friction of the area very localized at the vacancy site and the altered surrounded region around the defect [3]. The relevance of both contributions is quantified and compared for graphene and MoS_2, and the underlying mechanisms are explained. These results elucidate the subtle connection between friction, reactivity and mechanical properties of two-dimensional materials.

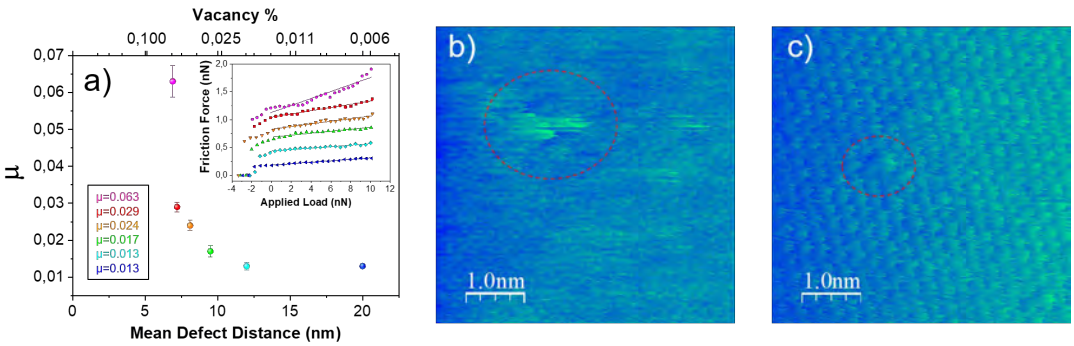

Figure 1. a) Friction coefficient *vs* mean defect distance for graphene monolayer. Inset: Friction force *vs* applied load curves from where friction coefficients are extracted. b) and c) Lateral Force image showing the friction of a monovacancy within graphene (b) and MoS2 (c) lattices with nanometric resolution.

[1] S. Kwon, J-H. Ko, K-J. Jeon, Y-H. Kim, J. Y. Park, *Nano Lett.* **12**, 6043 (2012).
[2] A. Zambudio, E. Gnecco, J. Colchero, R. Pérez, J. Gómez-Herrero, C. Gómez-Navarro, *Carbon* **182**, 735 (2021).
[3] G. López-Polín, M. Ortega, G. Vilhena, I. Alda, J. Gómez-Herrero, P. A. Serena, C. Gómez-Navarro, R. Pérez, *Carbon* **116**, 670 (2017).

Controlling fracture properties of MoS_2 by introducing atomic vacancies

Y. Manzanares-Negro[1,*], G. López-Polin[1,2], K. Fujisawa[3], T. Zhang[3], F. Zhang[3], E. Kahn[3], N. Perea-López[3], M. Terrones[3], J. Gómez-Herrero[1,4], C. Gómez-Navarro[1,4]

[1]*Departamento de Física de la Materia Condensada, Universidad Autónoma de Madrid, Madrid E-28049, Spain.* [2]*ICMM, Campus de Cantoblanco, Madrid E-28049, Spain.* [3]*Center for 2-Dimensional and Layered Materials, The Pennsylvania State University, University Park, PA 16802, USA.* [4]*IFIMAC Condensed Matter Physics Center (IFIMAC). Universidad Autónoma de Madrid, Madrid E-28049, Spain.*

*e-mail: yolanda.manzanares@uam.es

Transition metal dichalcogenides (TMDs) are very appealing materials due to their mechanical properties such as flexibility, bendability and breaking strength. However, their high crystallinity leads to a very high brittleness, thus restricting their mechanical reliability. In this work, we explore the effects that small densities of vacancies produce on the fracture properties of MoS_2 single layers.

Microdrums of MoS2 were subsequently irradiated with different doses of Ar^+ and Ga^+ ions and indented with an AFM tip until fracture.

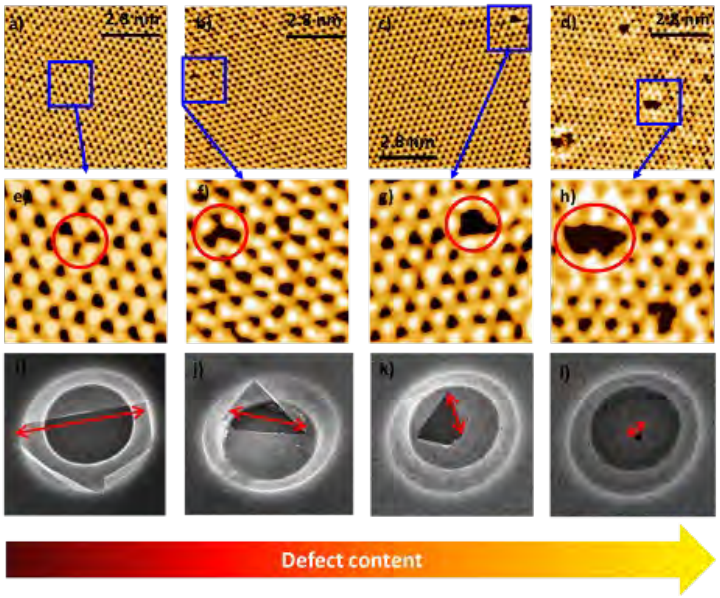

Figure 2. a-d) Representative HR-STEM images of MoS_2 single layers with different doses of ion irradiations. e-h) HR-STEM images of a sulphur single vacancy, sulfur double vacancy, Mo vacancy and the surrounding crystal deformation and a defect created by several missing atoms, respectively. i-l) SEM images of broken samples with different defect densities showing the size of the crack produced.

SEM images of the broken samples provided the length of the cracks created in indentation experiments. In these images we observe that the presence of vacancies highly restricts the expansion of the fracture. An analysis of the measurements tells us that while the breaking strength is reduced by a 40% due to the presence of atomic vacancies, the fracture toughness increases.

To sum up, here we show an effective manner to tune the fracture properties of MoS_2 for different purposes by adjusting the density and size of defects of the material to obtain the desired toughness/breaking strength relation.

[1] Yolanda Manzanares-Negro et al., *ACS nano* **15**, 1210 (2021).

Bio-AFM is the new black in biomedical sciences

Núria Gavara

Serra Húnter programme, Unitat de Biofísica i Bioenginyeria, Facultat de Medicina i Ciències de la Salut, Universitat de Barcelona.

e-mail: ngavara@ub.edu

In the last years it has been acknowledged that cellular fate and behaviour are greatly influenced by the mechanical properties of the cells, as well as their environment. The mechanical characterisation of cells and tissues using AFM is no longer a niche technique by those working on biophysical sciences. Instead, it is slowly becoming another method within the toolkit of techniques typically boasted in high-impact papers on basic cell biology or biomedical sciences. While this constitutes a fantastic opportunity for those long working on the field, it has also posed exciting challenges, which i will convey during the talk. From an instrumental side, a massive push has been aimed at building AFMs in combination with advanced light microscopy and super-resolution setups, and to increase the overall user-friendliness of AFM operation. From an experimental and modelling side, new protocols acknowledge the complexity of cellular mechanics, moving beyond the simplest hertzian models at quasi-static regimes. In addition, AFM is morphing into a high-throughput method, thus stressing the need for fully-automated but reliable pipelines to extract mechanical parameters from the thousands of acquired force-distance curves. Finally, the advent of big data and machine learning approaches for disease diagnostic opens new avenues, but raises questions on how we can turn AFM into a more 'multiplex' technique to further its impact in life sciences and biomedicine research.

Effects of energy metabolism on the mechanical properties of breast cancer cells

Marina L. Yubero[1,*], Priscila M. Kosaka[1], Álvaro San Paulo[1], Marcos Malumbres[2], Montserrat Calleja[1], Javier Tamayo[1]

[1]*Bionanomechanics Lab, Instituto de Micro y Nanotecnología, IMN-CNM (CSIC), Isaac Newton 8 (PTM), E-28760, Tres Cantos, Madrid, Spain.* [2]*Cell Division and Cancer Group, Centro Nacional de Investigaciones Oncológicas (CNIO), C/Melchor Fernández Almagro, 3, E-28029, Madrid, Spain.*

*e-mail: marinap.lopez@csic.es

Tumorigenesis induces actin cortex remodelling, which makes cancerous cells softer [1]. Cell deformability is chiefly determined by cortical tension driven by myosin-II activity and by actin fiber network architecture at the cell cortex [2]. However, it is still unclear what the weight of each contribution is, and how these contributions change during cancer development. The effect of energy metabolism on this phenomenon and its reprogramming in cancer has been little studied, even though cells anomalous metabolism is an essential cancer hallmark.

Here, we perform precise two-dimensional mechanical phenotyping based on Atomic Force Microscopy (AFM). Power-law rheology parameters E_0 and β are obtained from force-distance curves [3], to unveil the contributions of myosin II, actin fiber architecture and energy metabolism to the deformability of healthy (MCF-10A), non-invasive cancerous (MCF-7), and metastatic (MDA-MB-231) human breast epithelial cells.

The results show marked differences in the nature of the active processes that build up cell stiffness, namely that healthy cells use ATP-driven actin polymerization whereas metastatic cells use myosin II activity. Non-invasive cancer cells exhibit an anomalous behaviour, as their stiffness is not as affected by the lack of nutrients and ATP, suggesting that energy metabolism reprogramming is used to sustain active processes at the actin cortex.

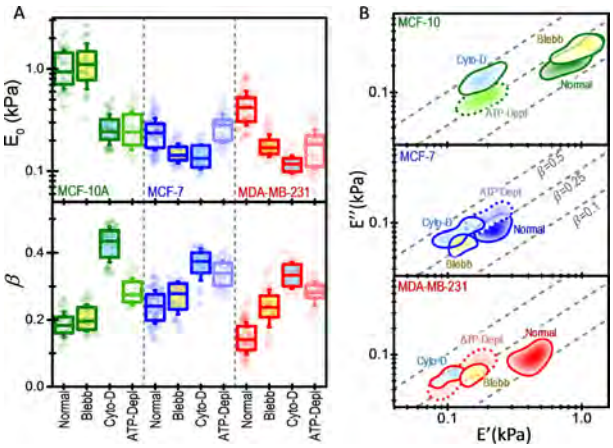

Figure 1. Power-law rheology parameters of the studied breast cell lines in normal conditions, treated with cytoskeletal drugs and in ATP-depletion conditions.

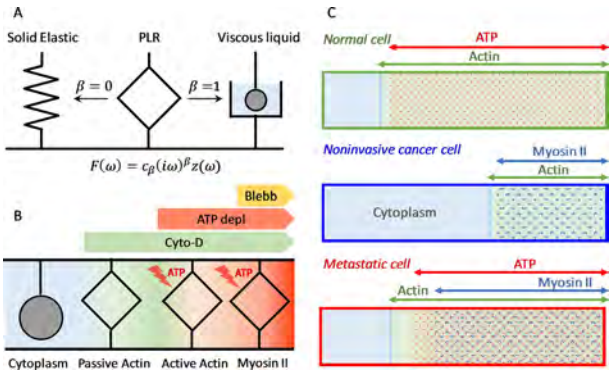

Figure 2. Sketch of uncoupling the effects of actin network, myosin II-driven contractility, and ATP hydrolysis on the cell stiffness.

[1] Salbreux, G., Charras, G. & Paluch, E., *Trends Cell Biol.* **22**, 536 (2012).
[2] Calzado-Martín, A., Encinar, M., Tamayo, J., Calleja, M. & San Paulo, A., *ACS Nano.* **10**, 3365 (2016).
[3] Efremov, Y. M., Wang, W. H., Hardy, S. D., Geahlen, R. L., & Raman, A. *Scientific Reports* **7(1)**, 1-14 (2017).

Acknowledgements: European Research Council Grant 681275-LIQUIDMASS-ERC-CoG-2015, under Grant Agreement No. 731868 – VIRUSCAN. Spanish Science, Innovation and Universities Ministry through project CELLTANGLE reference RTI2018-099369-B-I00. Comunidad de Madrid (iLUNG B2017/BMD-3884). Ramón y Cajal grant RYC-2017-21640 to P.M.K. MCIU (CSIC13-4E-1794) and EU (FEDER, FSE).

The viscoelasticity of adherent cells follows a single power-law with distinct local variations within a single cell and across cell lines

Juan G. Sánchez*, Francisco M. Espinosa, Ruben Miguez, Ricardo García

Departamento de Nanoestructuras y Superficies, Instituto de Ciencia de Materiales de Madrid, CSIC, c/Sor Juana Inés de la Cruz 3, 28049 Madrid, Spain.

*e-mail: juan.g.s@csic.es

AFM-based force–distance curves are commonly used to characterize the nanomechanical properties of live cells [1]. The transformation of these curves into nanomechanical properties requires the development of contact mechanics models [2]. Spatially–resolved force–distance curves involving 1 to 2 µm deformations were obtained on HeLa and NIH 3T3 (fibroblast) cells. An elastic and two viscoelastic models were used to describe the experimental force–distance curves (FDCs). The best agreement was obtained by applying a contact mechanics model that accounts for the geometry of the contact and the finite–thickness of the cell and assumes a single power–law dependence with time. Our findings show the shortcomings of elastic and semi–infinite viscoelastic models to characterize the mechanical response of a mammalian cell under micrometer–scale deformations. The parameters of the 3D power–law viscoelastic model, compressive modulus and fluidity exponent showed local variations within a single cell and across the two cell lines. The corresponding nanomechanical maps revealed structures that were not visible in the AFM topographic maps [3,4].

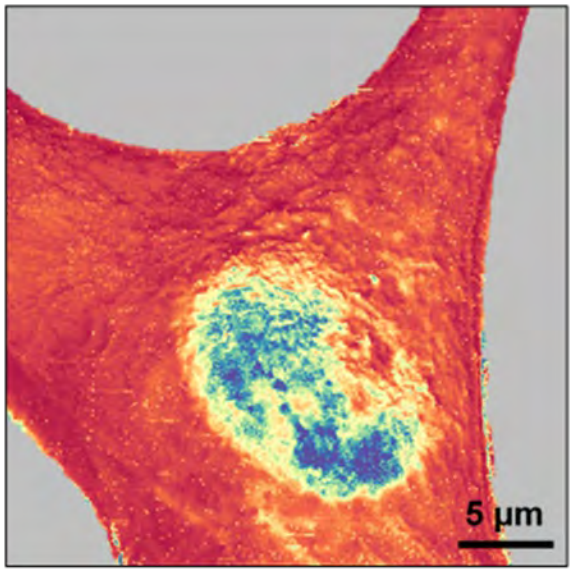

Figure 1. Compressive modulus map of a fixed NIH 3T3 cells, clearly differentiating between the cytoplasm and the nuclear regions. FDCs taken at $F_{peak} = 3\ nN, v = 150\ \mu m/s$, map of 512 x 512 pixels.

[1] R. Garcia, *Chem. Soc. Rev.* **49,** 5850 (2020).
[2] P. D. Garcia and R. Garcia, *Nanoscale* **10**, 19799 (2018).
[3] C. R. Guerrero, P. D. Garcia..., *ACS Nano* **13**, 9629 (2019).
[4] J. G. Sanchez, F. M. Espinosa…, *Nanoscale* **13**, 16339 (2021).

Acknowledgements: This project was supported by the Ministerio de Ciencia e Innovación (PID2019-106801GB-I00) and the Comunidad de Madrid S2018/NMT-4443 (Tec4Bio-CM).

Decoding mechanical fingerprints of cellular components in pathological conditions: a multiscale perspective

Andra C. Dumitru

Centro Nacional de Investigaciones Cardiovasculares Carlos III (CNIC), Madrid, Spain.

e-mail: acdumitru@cnic.es

Defective molecular, cellular and tissue mechanics are emerging hallmarks for several pathologies like cancer, fibrosis or blood disorders [1-3]. Clinical studies associate diabetes mellitus (DM), a chronic disease characterized by hyperglycemia, to global stiffening in several tissues, among them the myocardium. At molecular level, high glucose and its by-products determine the time-dependent accumulation of advanced glycation end products (AGEs), which cause irreversible damage to extracellular matrix (ECM) proteins. However, the modification by glycation of ECM proteins fails to explain the observed altered mechanical properties of cardiomyocytes from diabetic heart tissue. Despite the current use of AGEs as clinical biomarkers of DM and their correlation with increased heart failure risk, the mechanism of action bridging alterations at molecular and tissue level remains elusive.

In this talk, I will show how methylglyoxal, a glucose by-product and major contributor to protein glycation in diabetes, induces cardiomyocyte stiffening through AGE modifications of the giant protein titin, the main responsible of cardiomyocyte stiffness. We further discovered titin is heavily glycated in functionally compromised hearts of diabetic mice. An in-depth multiscale characterization of the DM mechanical landscape in vitro using atomic force microscopy (AFM)-based methods provides the missing mechanistic link between titin glycation and cardiomyocyte stiffening. Our single-molecule AFM data shows that methylglyoxal induces substantial formation of intramolecular crosslinks in titin domains, which become remarkably stiffer as a result of reduced contour length, and, unexpectedly, enhanced mechanical folding.

We speculate that intramolecular crosslinks in mechanical proteins can contribute to altered mechanical properties of diabetic tissues beyond the myocardium, which could open new windows of opportunity to develop therapies that revert stiffening intramolecular crosslinks in AGEs.

[1] P. Romani, L. Valcarcel-Jimenez, C. Frezza, S. Dupont, *Nat. Rev. Mol. Cell Biol.* **22**, 22 (2021).
[2] A.C. Dumitru, M. Poncin, L. Conrard, Y. Dufrêne, D. Tyteca, D. Alsteens, *Nanoscale Horiz.* **3**, 293 (2018).
[3] A.C. Dumitru, D. Mohammed, M. Maja, J. Yang, S. Verstraeten, A. del Campo, M-P. Mingeot-Leclercq, D. Tyteca, D. Alsteens, *Adv. Sci.* **7**, 2002643 (2020).

Condensin-driven loop extrusion on supercoiled DNA

E. Kim[1], **A. Martin-Gonzalez**[2,*], B.Pradahn[1], J. Van der Torre[2], C. Dekker[2]

[1]*Max Planck Institute for Byophysics, Max Planck, Frankfurt, Germany.* [2]*Bio-nanoscience department, Faculty of Applied Sciences, Technical University of Delft, Delft, Netherlands.*

*e-mail: a.martingonzalez@tudelft.nl

Condensin, a structural maintenance of chromosomes (SMC) complex, has been shown to be a molecular motor that organizes chromosomes by extruding loops of DNA. In cells, such loop extrusion is challenged by many potential conflicts, e.g., due to the torsional stresses that are generated by DNA-processing enzymes. It has so far remained unclear how DNA supercoiling affects loop extrusion. Here, we use Atomic Force Microscopy to image the process of loop extrusion and its effects on DNA supercoiling in the presence of ATP. Our findings provide insight into the topology-regulated loading and formation of supercoiled loops by SMC complexes and clarify the interplay of loop extrusion and supercoiling.

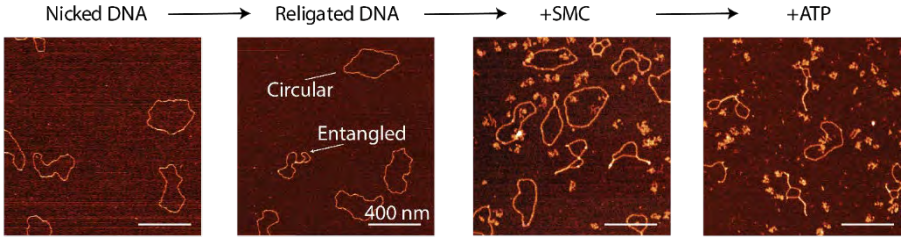

[1] Yatskevich, S., Rhodes, J. & Nasmyth, K. Organization of Chromosomal DNA by SMC Complexes, *Annu. Rev. Genet.* **53**, 445 (2019).
[2] Sun, M., Nishino, T. & Marko, J. F. The SMC1-SMC3 cohesin heterodimer structures DNA through supercoiling-dependent loop formation, *Nucleic Acids Res.* **41**, 6149 (2013).

High-Speed Bimodal AFM nanomechanical mapping of collagen self-assembly

Victor G. Gisbert[1], Simone Benaglia[1], Manuel Uhlig[1], Roger Proksch[2], Ricardo Garcia[1,*]

[1]*Instituto de Ciencia de Materiales de Madrid, CSIC, c/ Sor Juana Ines de la Cruz 3, 28049 Madrid, Spain.*
[2]*Asylum Research-Oxford Instruments, Santa Barbara, USA.*

*e-mail: r.garcia@csic.es

Collagen is the most abundant structural protein of the extracellular matrix. The assembly of collagen fibrils play relevant roles in a variety biological processes. The formation fibrils during the self-assembly process of collagen I have been studied by AFM [1,2]. Those studies lacked the time and mechanical properties resolution to clarify the mechanism of the earlier stages of collagen assembly and fibril structure formation.

We have developed a high-speed bimodal AFM [3,4] that combines the *ms* time resolution of high-speed AFM [5] with the nanomechanical force sensitivity of bimodal AFM [6,7]. High-speed bimodal AFM characterizes the earliest stages of the self-assembly of the collagen fibrils by proving time-resolved and high-spatial resolution maps of the evolution of the elasticity of the fibrils during the growth.

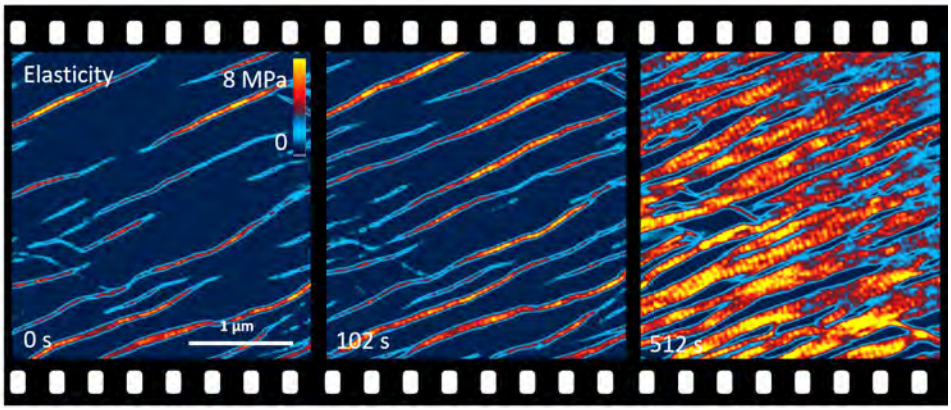

Figure 1. High-speed bimodal AFM map of elastic modulus. The sequence captures the merging of and the alignment of the D-bands of several microribbons.

[1] F. Jiang, H. Hörber, J. Howard, D.J. Müller., *J. Struct. Biol*. **148**, 268 (2004).
[2] D. R. Stamov, E. Stock, C. M. Franz, T. Jähnke, H. Haschke, *Ultramicroscopy* **149**, 86 (2015).
[3] Victor G. Gisbert, Simone Benaglia, Manuel R. Uhlig, Roger Proksch, Ricardo Garcia, *ACS Nano* **15**, 1850 (2021).
[4] Victor G. Gisbert, Ricardo Garcia, *ACS Nano* **15**, 20574 (2021).
[5] T. Ando, *Nanotechnology* **23**, 062001 (2012).
[6] S. Benaglia, V.G. Gisbert, A.P. Perrino, C.A. Amo, R. Garcia, *Nat. Protoc.* **13**, 2890 (2018).
[7] E. T. Herruzo, A. P. Perrino, R. Garcia, *Nat. Commun.* **5**, 3126 (2014).

Nanomechanical properties of trophozoites and extracellular vesicles of the free-living amoeba *Naegleria fowleri*

Lissette Retana-Moreira[1,2], María Fernanda Steller-Espinoza[1], Natalia Chacón-Camacho[1], Desire Daniela Arrieta-Murillo[3], Jocelyn Cortés-Espínola[3], Alberto Cornet-Gómez[4,5], **Giovanni Sáenz-Arce**[3,*], Oscar Rojas-Carrillo[6], Antonio Osuna[4,5], Elizabeth Abrahams-Sandí[1,2]

[1]*Departamento de Parasitología, Facultad de Microbiología, Universidad de Costa Rica, Costa Rica.* [2]*Centro de Investigación en Enfermedades Tropicales (CIET).* [3]*Departamento de Física, Universidad Nacional, Heredia, Costa Rica.* [4]*Departamento de Parasitología, Grupo de Bioquímica y Parasitología Molecular CTS-183, Universidad de Granada, Granada, Spain.* [5]*Instituto de Biotecnología, Universidad de Granada, Granada, Spain.* [6]*Laboratorio de Investigación y Tecnología de Polímeros, Escuela de Química, Universidad Nacional, Heredia, Costa Rica.*

*e-mail: gsaenz@una.ac.cr

Naegleria fowleri is a thermophilic free-living amoeba that produces primary amoebic meningoencephalitis (PAM), a severe and fulminant infection of the central nervous system, fatal in more than 95% of cases. Until 2019, more than 440 cases of PAM were reported worldwide[1]; however, the true incidence of the disease is unknown[2]. Due to the characteristics of PAM, rapid and accurate diagnosis and early treatment are key to fight this infection. In this sense, a reliable diagnosis panel using the pathogen-specific extracellular vesicles (EVs) could probably improve on-time intervention and prognosis. In recent years, extracellular vesicles (EVs) have become subject of intensive research due to their proven participation in intercellular communication, modulation of the immune response, pathogenesis, metastasis, drug delivery and diagnosis.

To our knowledge, the secretion of EVs by trophozoites of *N. fowleri* has not been reported yet. In this study, we present a topographic characterization and determination of nanomechanical properties of a clinic isolate of *Naegleria fowleri*[3] and the extracellular vesicles (EVs) secreted by trophozoites of this isolate using atomic force microscopy (AFM). For thi purpose, properties like adhesion, modulus and stiffness of trophozoites and EVs were achieved using PinPoint mode in a NX-10 (Park System, Korea) AFM.

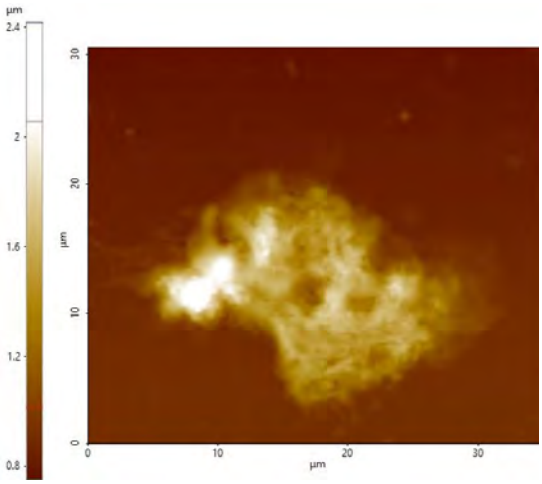

Figure 1. Topography image of trophozoites of *Naegleria fowleri* (A) and extracellular vesicles (B).

[1] Jahangeer M, Mahmood Z, Munir N, Waraich, U, Mahmood Tahir I, Muhammad A, Muhammad Ali Shah S, Zulfqar A, Zainab, R. *Naegleria fowleri*: sources of infection, pathophysiology, diagnosis and management; a review, *Clinical and Experimental Pharmacology and Physiology* **47**, 199 (2019).
[2] Matanock A, Mehal JM, Liu L, Blau DM, Cope JR. Estimation of undiagnosed *Naegleria fowleri* primary amebic meningoencephalitis, United States, *Emerging Infectious Diseases* **24**, 162 (2018).
[3] Retana Moreira L, Zamora Rojas L, Grijalba Murillo M, Molina Castro SE, Abrahams Sandí E. Primary amebic meningoencephalitis related to groundwater in Costa Rica: diagnostic confirmation of three cases and environmental investigation, *Pathogens* **9**, 629 (2020); doi:10.3390/pathogens9080629.

Acknowledgements: This work was funded by research projects: C-1061: "Caracterización de antígenos de excreción/secreción y antígenos somáticos en amebas de vida libre mediante empleo de anticuerpos policlonales producidos en roedores" and C-2600: "Secreción de vesículas extracelulares por *Naegleria fowleri* y evaluación de su potencial rol inmunomodulador en un modelo *in vitro*" of the Vicerrectoría de Investigación of the Universidad de Costa Rica and SIA 0287-17 “Programa de Investigación en Física Aplicada: Interacción Materia-Energía (IFA)” of the Universidad Nacional.

Physical principles of protein nanocages: AFM, a single molecule approach

Mercedes Hernando Pérez

Departamento de Fisica de Materiales, Universidad Autónoma de Madrid, C/ Francisco Tomás y Valiente, nº 7, Cantoblanco, E-28049 Madrid. Spain.

e-mail: mercedes.hernando@uam.es

Viruses are nanosized, genome-filled, protein containers with remarkable thermodynamic and interesting physical properties. Virus capsid must meet conflicting stability requirements. Viral Capsids must be stable enough to withstand harmful environmental conditions to protect the viral genome [1-3]. Also, they must be able to disassemble, in a controlled manner, to release their genome into the host cell, at the right time and place to give rise to a productive infection [4]. To adapt to these conditions and complete their cycle, viruses have evolved by modifying their capsid to achieve greater stability and protect the genetic material. These changes are manifested in physical properties (elastic constant, surface charge density, electromechanical properties, etc.) [5-8].

Here I will present the physical characterization of viruses with Atomic Force Microscopy (AFM) in liquid media to understand the relationship between mechanical properties, structure, and biological function. Physical properties characterization of viral capsids provides crucial information, not only for gaining insights into their biological cycle, but also designing nano-containers for applications in bionanotechnology and nanomedicine.

[1] Carrasco. C *et al*., *PNAS* **106**, 5475 (2009).
[2] Hernando. E *et al*., *Virology*, **267**, 299 (2000).
[3] Moody. M.F, *Journal of Molecular Biology* **293**, 401 (1999).
[4] Mateu, M. G., *Archives of Biochemistry and Biophysics* **531**, 65 (2013).
[5] Hernando-Pérez. M *et al*., *Small* **8**, 2366 (2012).
[6] Cartagena. A, *Nanoscale* **5**, 4729 (2013).
[7] Hernando-Pérez. M *et al*., *Nanoscale* **7**, 17289 (2015).
[8] Hernando-Pérez. M *et al*., *ACS Nano* **13**, 7842 (2019).

Study of the effect of reactive/non-reactive additives on the microstructure of biopolymer blends by means of AFM-QNM

Harrison de la Rosa-Ramírez, Daniel García-García, Jaume Sempere, María Dolores Samper

Instituto de Tecnología de Materiales (ITM), Universitat Politècnica de València (UPV), 03801 Alcoy, Spain.

Biopolymers such as PLA need to be loaded to improve their poor mechanical properties. In this study, a blend of PLA with PE of natural origin (bio-PE) is formulated. However, these two biopolymers are incompatible due to their different polarities. To improve the compatibility of the two biopolymers by avoiding the use of petroleum-derived substances, two types of additives were tested, a PVA and EVA (non-reactive compatibilization) and DCP (for reactive compatibilization).

Using AFM in contact mode under Quantitave Nanomechanical Measurement mode, the effect of compatibilisers on the microstructure of the blend was analysed. This study, which identifies the type of microstructure as well as the cohesion, miscibility and nanomechanical properties of the individual phases, is of great importance for modelling the behaviour of the material under mechanical stress.

Figure shows the microstructure of the formulations analysed in this study by AFM-QNM. It was found that the use of additives increased the compatibility of bioPE, which appears as a finer dispersed phase in the PLA matrix. In addition, it was possible to determine the elastic modulus of each phase, which by the rule of mixtures contributes to the average stiffness obtained for the whole material. From the study of this work it was possible to establish that:

(i) the Increase in interfacial adhesion was higher when using the EVA compatibiliser, showing a droplet size reduction microstructure of the bioPE

(ii) The 50% decrease in crystallinity observed by DSC and other techniques, may affect the resulting nanomechanical properties determined by AFM-QNM.

(iii) There was a plasticization effect of both PLA and bioPE caused by the effect of compatibilizers.

Figure. QNM-AFM elastic modulus maps acquired on PLA-bioPE blends (a) and PLA-bioPE+EVA additive (b). Stiffness profile measurement (c).

[1] M. Aldas, E. Rayón, J. López-Martínez, M.P. Arrieta, *Polymers* **12**, 226 (2020).
[2] J.M. Ferri, D. García-García, E. Rayón, M.D. Samper, R. Balart, *Polymers* **12**, 1344 (2020).

Acknowledgements: (PID2020-116496RB-C22). Investigación competitiva proyectos. Agencia Estatal de Investigación.

AFM Surface deterioration evaluation to monitor thermoplastic starch films degradation under composting conditions

Cristina Pavon[1,*], Miguel Aldas[2], Franciszek Pawlak[1], **Juan López-Martínez**[1]

[1]*Instituto de Tecnología de Materiales (ITM), Universitat Politècnica de València (UPV), 03801 Alcoy, España.*
[2]*Departamento de Ciencia de Alimentos y Biotecnología, Facultad de Ingeniería Química y Agroindustria, Escuela Politécnica Nacional, Quito 170525, Ecuador.*

*e-mail: jlopezm@mcm.upv.es

The potential of bioplastics to produce sustainable materials and reduce dependence on fossil fuels has allowed their introduction into the plastics industry, which is currently seeking a more sustainable orientation of plastics toward a circular economy. As consequence, the production of biodegradable polymers has increased in the last years, particularly for short-term applications, such as bags, cutlery, and packaging materials [1].

Biodegradable plastics are produced from renewable materials such as starch or cellulose and can be biodegraded by composting or anaerobic digestion [2]. Composting of a biodegradable polymer allows safe disposal of the materials and facilitates closing the loop of the circular economy. For a plastic to be considered compostable, it must degrade by biological processes in a standardized environment at a rate consistent with other compostable materials and under specific conditions (e.g. temperature, humidity) [3]. To achieve complete biodegradation, a polymer must first biodeteriorate. Biodeterioration is a superficial degradation that modifies the mechanical, physical, and chemical properties of the material [4].

In this work, the biodeterioration of Mater-Bi®NF866 films was followed through its degradation under composting conditions by Atomic Force Microscopy (AFM). The obtained peak force error images showed a correlation of the reduction in the roughness of the films with the increase in the composting time. The results showed that biodegradation occurs hydrolytically, and that direct and indirect damage is produced in the films due to microbiological attacks [4]. As well, the results suggest that Mater-Bi®NF866 films have low biodeterioration protection, as high differences in the roughness of the surface were found in just 7 days of composting. Moreover, the material surface present significant differences during the thermophilic phase of the composting process (until day 90).

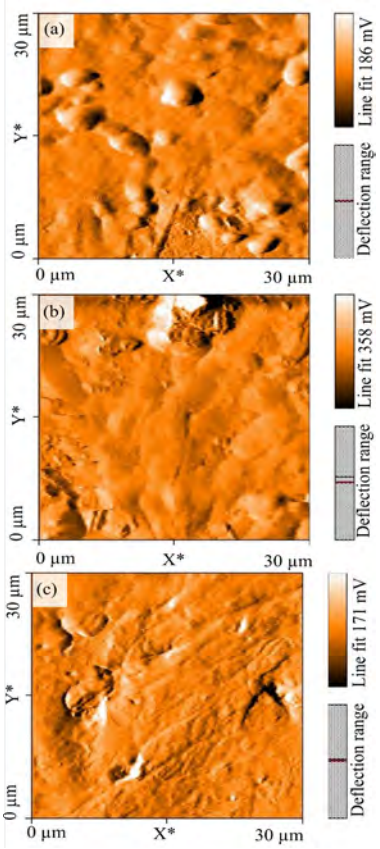

Figure 1. Peak force error images of the surface of thermoplastic starch films at (a) 0 days, (b) 7 days and (c) 21 days under composting conditions.

[1] M. Aldas, C. Pavon, J. M. Ferri, M. P. Arrieta, and J. López-Martínez, *Polymers* **13**, 1506 (2021).
[2] J. H. Song, R. J. Murphy, R. Narayan, and G. B. H. Davies, *Philosophical Transactions of the Royal Society B: Biological Sciences* **364**, 2127 (2009).
[3] International Standards Organization, *ISO 20200 Plastics — Determination of the degree of disintegration of plastic materials under simulated composting conditions in a laboratory-scale test*, 2016.
[4] K. N. Fotopoulou and H. K. Karapanagioti, *Handbook of Environmental Chemistry* **78**, 71 (2019).

Acknowledgements: The authors thank (PID2020-116496RB-C22). Investigación competitiva proyectos. Agencia estatal de Investigación. C.P. thanks Santiago Grisolía fellowship (GRISOLIAP/2019/113) from Generalitat Valenciana.

Visualization of interfacial layers of organic molecules on graphite by Three-Dimensional Atomic Force Microscopy

Diana Méndez*, Ricardo García

Instituto de Ciencia de Materiales de Madrid, CSIC, c/ Sor Juana Ines de la Cruz 3, 28049 Madrid, Spain.

*e-mail: diana.mendez@csic.es

The aging of 2D materials happens through the adsorption of hydrocarbon molecules that are present in ambient air and purified water. It has been observed that these molecules show strong interactions with graphene and other hydrophobic surfaces that result into ordered solvation layers [1]. Polycyclic aromatic hydrocarbons (PAHs) are also present as trace contaminants in air, water and soil [2] and π-π interactions have shown to lead to a strong adsorption onto graphene materials [3].

Three dimensional AFM (3D AFM) is an advanced Atomic Force Microscopy technique which allows to image the organization of liquid molecules above a solid surface with sub-nm resolution [4-5]. In this work, 3D AFM is used to study the solid-liquid interface formed by a 1-hydroxypyrene solution in hexane and the graphite (HOPG) surface. The results are compared to the already studied hexane-HOPG interface, allowing to observe the interfacial structure that will be determined by the interactions of the involved molecules.

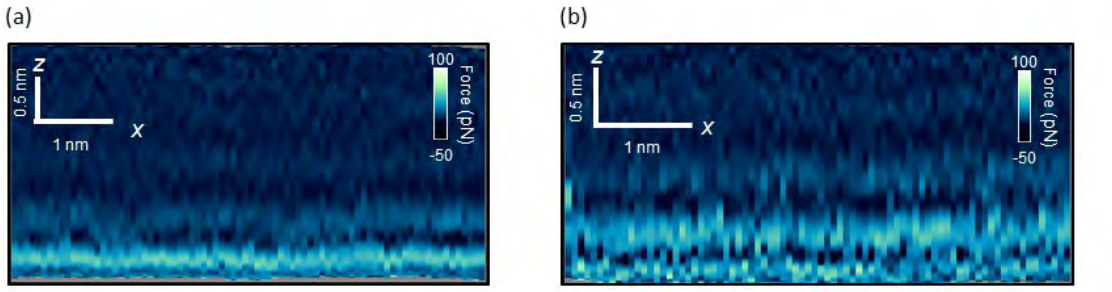

Figure 1. 3D AFM images of (a) solvation layers of hexane over a HOPG surface and (b) solvation layers of a 0.01 mM 1-hydroxypyrene in hexane solution over a HOPG surface.

[1] M. R. Uhlig, S. Benaglia, R. Thakkar, J. Comer and R. Garcia, *Nanoscale* **13**, 527 (2021).
[2] Anna M. Fan, *Chapter 64 - Biomarkers in toxicology, risk assessment, and environmental chemical regulations*, Academic Press (2014).
[3] Jun Wang, Zaiming Chen, and Baoliang Chen, *Environmental Science & Technology* **48**, 4817 (2014).
[4] T. Fukuma and R. Garcia, *ACS Nano* **12**, 11785 (2018).
[5] M. R. Uhlig, D. Martin-Jimenez, and R. Garcia, *Nat. Commun.* **10**, 2606 (2019).

Development of a technological AFM microscope for operation in UHV

D. Gallego-Fuente[1,*], P. Ares[1,2], J. Gomez-Herrero[1,2]

[1]*Departamento de Física de la Materia Condensada, Universidad Autónoma de Madrid, Spain.*
[2]*Condensed Matter Physics Center (IFIMAC), Universidad Autónoma de Madrid, Spain.*

*e-mail: daniel.gallego@uam.es

Atomic Force Microscopy (AFM) is a key tool for the study of nanoscopic systems. Since its invention in 1986[1], AFM research and development has been continuously in progress, including new measurement methods, new features and adapting to different environments in which to operate.

The majority of AFMs that operate in Ultra High Vacuum environments (UHV) are focused on the study of atomically resolved systems. However, they lack the versatility of more standard AFMs under ambient conditions. Here, we are tackling the development of a technological AFM operating in UHV but based on the same operation principles of standard AFMs, combining all their capabilities with those of standard UHV technology. Our setup will include advanced measuring modes, sample manipulation and lithography, as well as optical sample location.

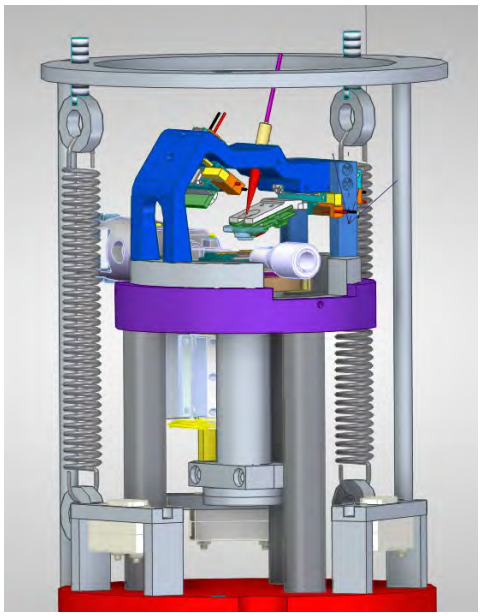

Figure 1. Technological AFM design with spring damping, including a long-range piezotube XYZ scanner, laser focuser and photodiode.

To perform lithography, indentations, and general sample manipulation, a long-range XYZ scanner will be employed along with the beam deflection method for the force detection. Ultra-clean electrical nano-circuits will be fabricated by deposition and manipulation of gold nanowires under UHV conditions. Furthermore, the electrical characterization of such circuits will be possible under different contact schemes. On top of that, the combination with optical characterization approaches will allow the precise multidisciplinary study of nanoscopic defects in 2D materials.

In conclusion, this instrument will be a complementary and useful tool in relation with the existing systems, as well as being a stepping stone in the development of UHV-compatible SPM microscopy. Its simplicity in use and broad range of applicability will help to bridge the gap in the understanding of electrical, mechanical and optical properties at the nanoscale.

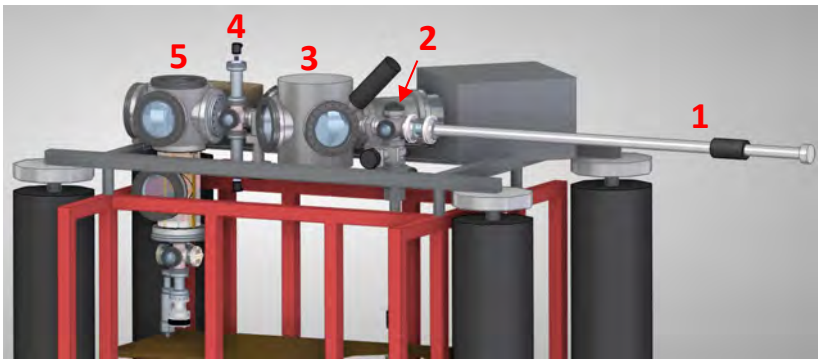

Figure 2. UHV system consisting (from right to left) of a transfer stage (1), insertion (2), preparation (3), multi tip and sample storage (4) and AFM (5) chambers.

[1] Binnig, G., Quate, C. F., Gerber, C., *Physical Review Letters* **56**, 930 (1986).

Deterministic transfer of gold nanowires in scanning probe assisted nanowire circuitries

Diego A. Aldave[1,*], Guillermo López-Polín[1], Pablo Ares[1,2], Julio Gomez-Herrero[1,2]

[1]*Departamento de Física de la Materia Condensada, Universidad Autónoma de Madrid, España.*
[2]*Condensed Matter Physics Center (IFIMAC), Universidad Autónoma de Madrid, España.*

*e-mail: diego.aldave@uam.es

The study of the properties and application of low-dimensional materials requires the fabrication of electronic circuits in the micro- and nanoscale with different geometries. For this purpose, top-down fabrication approaches are used for their capability to fabricate complex circuitries in short period of time. Among these approaches, electron beam lithography (EBL) is a widely used technique to fabricate such devices for its good spatial resolution and the possibility of fabricating complex devices. However, complications may arise during the fabrication process of the circuitry structures due to the limitations of this technique and the desired complexity of the device. Moreover, we must consider the possible damages to the sample caused by the chemical products used to remove the resists.

In other to avoid these limitations, a recent work introduced the scanning probe assisted nanowire circuitry (SPANC) [1]. This technique consists in the nanomanipulation of gold nanowires deposited by drop casting on the sample substrate, using a tip of an atomic force microscope (AFM). The great advantages of this technique are the high precision with which the nanowires can be placed to contact the sample and the possibility of working with different electrodes configurations in the same sample without damaging it, which is a remarkable advantage over other approaches. In the present work, we introduce an improvement of the SPANC technique by substituting the drop casting for a deterministic transfer of the gold nanowires on the sample substrate using polydimethylsiloxane (PDMS). This method allows us to select the suitable nanowires and transfer them to the work area, positioning them close to the desired place and orientation using an optical microscope. Thus, the time required to build up the circuitry is reduced significantly. Furthermore, we achieve cleaner sample surfaces applying short-time oxygen plasma baths to the PDMS before and after the gold nanowires drop casting. We applied this method to contact electrically graphene flakes in four-terminal configuration (figure 1) and study their electrical properties. The surfaces of these samples are remarkable clean and were prepared in lesser time than using a drop casting deposition. We also demonstrate the possibility of using this method to repair electrical contacts, transferring just the precise number of nanowires needed and positioning them with good precision.

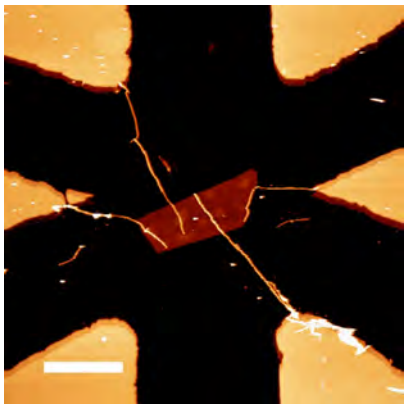

Figure 1. AFM topographic image of a graphene device fabricated combining a deterministic transfer of gold nanowires with the SPANC technique. The gold electrodes are made thermal evaporation using a stencil mask. Scale bar: 5 µm

[1] M. Moreno-Moreno, P. Ares, C. Moreno, F. Zamora, C. Gómez-Navarro, J. Gómez-Herrero, *Nano Lett.* **19**, 5459 (2019).

Nano-scale conductivity of $Hi_3(HITP)_2$ Metal-Organic Framework

E. Osuna[1,2,*], A. Zambudio[3], D. Rodríguez San-Miguel[4], Y. Belce[4], J. Gómez-Herrero[1,2], C. Gómez-Navarro[1,2], J. Puigmartí-Luis[4,5]

[1]*Condensed Matter Physics Dept., Universidad Autónoma de Madrid, Madrid, E-28049, Spain.*
[2]*Condensed Matter Physics Center, Universidad Autónoma de Madrid, Madrid, E-28049, Spain.*
[3]*Optics and Nanophysics Research Center, Universidad de Murcia, E-30100, Murcia, Spain*
[4]*Departament de Ciència dels Materials i Química Física, Institut de Química Teòrica i Computacional, University of Barcelona (UB), 08028 Barcelona, Spain.*
[5]*Institució Catalana de Recerca i Estudis Avançats (ICREA), Pg. Lluís Companys 23, 08010 Barcelona, Spain.*

*e-mail: eva.osunab@estudiante.uam.es

Metal-Organic Frameworks (MOFs) are compounds formed by metallic ions or clusters linked together by organic molecules forming one-dimensional, two-dimensional or three-dimensional structures. MOFs have attracted researchers' attention in recent years because they present the rare combination of being crystalline, electrically conductive and porous materials [1].

However, usual MOF preparation methods have poor control over the orientation, compactness, roughness profile and morphology of the MOF crystals, which can greatly impact their function and performance. Very recently, it has been shown that sample preparation using microfluidics to simulate microgravity conditions allows the control over these parameters and generates crack-free two-dimensional MOFs [2].

Here, we study the transport properties of 2D films of nanometric thickness of $Hi_3(HITP)_2$ grown in simulated microgravity conditions. $Hi_3(HITP)_2$ is a MOF which is considered the "analogue of graphene" in MOFs compounds and serves as a prototype material.

By using conductive atomic force microscopy, we study the in-plane and out-of-plane electrical conductivity of these MOF films at the nanoscale. We compare our results at the nanometric scale with those reported at the microscale [1, 2] with special emphasis on the realization of electrical contacts by varying the electrode materials and the pressure applied to the contact.

[1] R.W. Day, D. K. Bediako, M. Rezaee et al., *ACS Cent. Sci.* **5 12**, 1954 (2019).
[2] N. Contreras-Pereda, D. Rodríguez San-Miguel et al., *Adv. Mater.* **33** (2021).

Unraveling Dissipation-Related Features in Magnetic Imaging by Bimodal Magnetic Force Microscopy

Miriam Jaafar[1,2,*], Agustina Asenjo[3]

[1]*Departamento de Física de la Materia Condensada and Condensed Matter Physics Center (IFIMAC), Universidad Autónoma de Madrid, Avda. Francisco Tomás y Valiente 7, 28049 Madrid, Spain.*
[2]*Instituto Nicolás Cabrera, Universidad Autónoma de Madrid, Avda. Francisco Tomás y Valiente 7, 28049 Madrid, Spain.*
[3]*Instituto de Ciencia de Materiales de Madrid (ICMM), Consejo Superior de Investigaciones Cientificas (CSIC), C/Sor Juana Inés de la Cruz, 3, 28049 Madrid, Spain.*

*e-mail: miriam.jaafar@uam.es

Magnetic Force Microscopy (MFM) [1] is the principal characterization technique for the study of low-dimensional magnetic materials. Advantages of MFM include relatively high spatial resolution, simplicity in operation as well as sample preparation. Nonetheless, during years, the samples under study were limited to samples in the field of data storage, such as longitudinal hard disk, thin films, or patterned nanostructures. Nowadays, thanks to the advances and developments in the MFM modes and instrumentation, other fields are emerging like skyrmionic structures, 2D materials or biological samples. However, in these experiments artifacts in the magnetic images can have strong impact and need to be carefully verified for a correct interpretation of the results. In general, when imaging magnetic materials with MFM the most typical artifact is the crosstalk between the topography and the magnetic signal. In addition, in some cases electrostatic signal could be also misinterpreted as magnetic information. With MFM we detect the magnetic force gradient between the tip and sample. However, during MFM imaging the tip stray field (sample stray field) can modify the sample (tip moment) configuration. These reversible or irreversible changes can be significant if the sample (tip) is magnetically soft.

For that reason, in this work we will explore new ideas combining the multifrequency modes with the information obtained from the experimental dissipation of energy associated to tip-sample interactions [2].

Bimodal Scanning Force Microscopy (SFM) is based on the simultaneous excitation and detection of two cantilever vibration modes, usually, the 1st and the 2nd modes. The multifrequency concept in SFM and its applications has been developed in the last ten years [3] for the characterization at the nanoscale of mechanical or electrical properties in samples with heterogeneous behaviour. In addition, bimodal MFM has recently been used for quantitative imaging with high-spatial resolution [4].

The evaluation of the dissipation of energy during the MFM operation by measuring variations in the cantilever oscillation corresponds to the so-called Magnetic Dissipation Force Microscopy (MDFM) mode. The dissipative maps in MDFM have been used to distinguish between Néel and Bloch domain walls, to detect magnetic nanoparticles or to obtain a 3D map of the sample stray field.

Bimodal- MDFM could be a promising technique for increase the possibilities of low dimensional systems characterization. We demonstrated that it is possible to distinguish between tilt of spins at the tip apex and changes in the magnetic state of the sample [5]. Using an amplitude of the second mode A_2 much smaller than the one of the first mode A_1 ($A_1/A_2 >> 1$) the phase shift of the second mode is free of these undesirable effects. These results display a clear advantage of bimodal MFM.

[1] Kazakova, O.; Puttock, R.; Barton, C.; Corte-León, H.; Jaafar, M.; Neu, V.; Asenjo, A. Frontiers of magnetic force microscopy. *J. Appl. Phys.* **125**, 060901 (2019).
[2] Jaafar M. and Asenjo A., *Appl. Sci.* **11**(22), 10507 (2021).
[3] Garcia, R.; Herruzo, E.T., *Nat. Nanotechnol.* **7,** 217 (2012).
[4] Gisbert, V.G.; Amo, C.A.; Jaafar, M.; Asenjo, A.; Garcia, R., *Nanoscale* **13**, 2026 (2021).
[5] Jaafar, M.; Iglesias-Freire, Ó.; García-Mochales, P.; Sáenz, J.J.; Asenjo, A., *Nanoscale* **8**, 16989 (2016).

Charge injection and conductivity measurements on highly insulating materials

Mario Navarro*, Andrés M. Somoza, Elisa Palacios-Lidón

Departamento de física, University of Murcia, Edificio CIOyN (Campus Espinardo), E-30100 Murcia, Spain.

*e-mail: mario.navarror@um.es

The access to the electrostatic properties and charge dynamics of highly insulating materials has been shown to be a difficult task. With the help of Kelvin Probe Force Microscopy (KPFM) we can gain access to these otherwise inaccessible charge dynamics in the nanoscale. By coupling this technique with appropriate theoretical models we can gain insight about the conductivity of a given material.

In this work we explore the process of charge relaxation in the surface of a material, considering both surface and bulk conduction. In order to study this process, the scanning probe is used both to inject charge into the material (Fig. 1) and to monitor the evolution of the deposited charge over time (Figs. 2, 3). We establish the equations that describe the charge relaxation process and show that both 3-d bulk conductivity and 2-d surface conductivity can be easily extracted from the KPFM measurements.

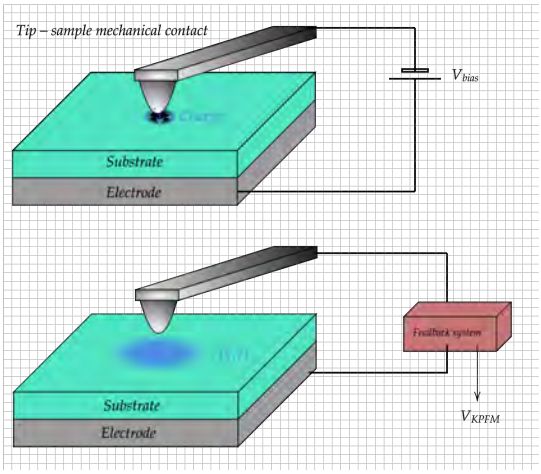

Figure 1. Diagram for the charge injection process.

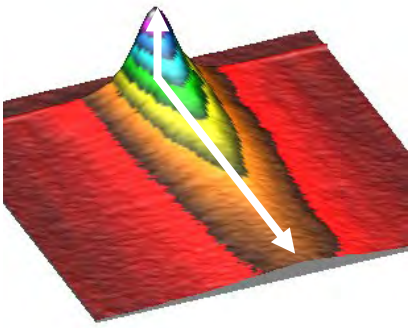

Figure 2. Time evolution of charge injected in a SiO_2 surface. The vertical axis represents the magnitude of the potential while the horizontal axis represents time.

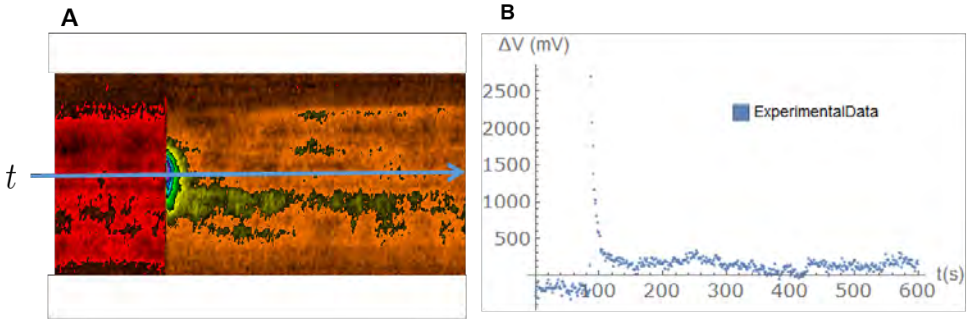

Figure 3. A) Time evolution of the surface potential at a given scan line, B) Profile along the blue line in A).

Acknowledgements: This research was funded by the Ministerio de Ciencia e Innovación and the Agencia Estatal de Investigación and associated Funds of the European Union through the projects "Nano and Meso Scales: Modelling, Structure and Characterization" (PID2019- 104272RB-C52/AEI/10.13039/501100011033) and the Fundación Seneca through the project 20860/PI/18.

Ultraviolet light assisted Kelvin probe force microscopy of dislocations in GaN structures for power applications

Jesús Ortiga-Fibla[1], Núria Garro[1], Frank Brunner[2], Eldad Bahat Treidel[2], **Ana Cros**[1,*]

[1]*Institute of Materials Science (ICMUV), University of Valencia, Spain.*
[2]*Ferdinand-Braun-Institut (FBH), Gustav-Kirchhoff-Strasse 4, 12489 Berlin, Germany.*

*e-mail: Ana.Cros@uv.es

Failure analysis and optimization of electronic devices can benefit greatly from a detailed knowledge of their electrical properties, both at the micro and nanometer scales. Atomic force microscopy (AFM) techniques and, in particular, Kelvin probe force microscopy (KPFM) are adequate to study local electrical properties in correlation to surface topography. In KPFM, electrostatic forces are detected and cancelled for the determination of the contact potential difference (CPD) of the sample with respect to the tip. When combined with above band gap illumination, surface photovoltage (SPV) provides information about carrier dynamics at point and extended defects.

GaN, with outstanding material properties, is highly suitable for high-power electronic applications. Two GaN structures grown on sapphire by MOCVD (Metal Organic Chemical Vapor Deposition) have been studied. The epitaxial layers were grown by metalorganic vapor phase epitaxy (MOVPE) on 100 mm diameter *c*-plane sapphire substrates. Sample S1 is an epitaxial stack consisting of a 2 µm un-intentionally doped GaN buffer layer, a 2.4 µm n^+-GaN:Si ($N_D = 3.0 \times 10^{18}$ cm^{-3}) highly conductive layer, and a 5 µm n^--GaN:Si drift layer with doping concentration of $N_D = 4 \times 10^{16}$ cm^{-3}. S2 has a similar structure the main difference being the variation of coalescence time, the thickness of the undoped GaN buffer (1.5 µm for S2), and a thin 50 nm n^+-GaN:Si ($N_D = 10^{19}$ cm^{-3}) cap layer.

The AFM topography shows two monolayer high terraces characteristic of MOCVD growth (RMS ~ 0.5 nm). We observe three features related to defects: Deep (~10 nm) and shallow (~1 nm) pits, ascribed to open core and pure screw dislocations, respectively, and mixed dislocations. In CPD and SPV images, the defects present specific characteristics when compared with the surrounding material: (i) open core dislocations show higher CPD, related to the trapping of positive charge. Under ultraviolet illumination (325 nm, i. e. above bandgap) the charge is screened by the photogenerated electron-hole pairs, and the CPD contrast disappears. (ii) Pure screw dislocations do not show any special CPD or SPV features. (iii) Mixed dislocations show no specific CPD features prior to illumination. However, upon illumination their CPD is ~ 100 mV smaller than the surrounding material, indicating an excess of negative charge. After light is switched off, CPD of these defects remains low for several hours. Pure and mixed dislocations have been mainly observed in S1, while open core dislocations are present in S2.

Figure 1 shows the AFM topography (a), light assisted KPFM (b) and SPV (c) images characteristic of S1. Features marked as #1 and #2 are identified as mixed and pure screw dislocations, respectively. They present similar SPV and charge dynamics.

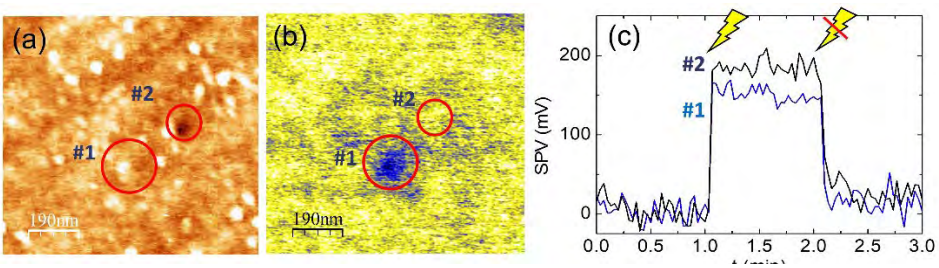

Figure 1. (a) Topography (colour scale from 0 to 2 nm, RMS 0.3 nm). (b) Light assisted KPFM (CPD colour scale from 710 to 910 mV). (c) SPV vs. time when light is turned on and off (time resolution 2 s).

Acknowledgments: This project has received funding from the ECSEL Joint Undertaking (JU) under grant agreement No 101007229. The JU receives support from the European Union's Horizon 2020 research and innovation programme and Germany, France, Belgium, Austria, Sweden, Spain, Italy. Also financed by the European Union-NextGeneratonEU, PCI2021-121970/ AEI / 10.13039/501100011033.

Isolation of Highly Stable Antimonene under Ambient Conditions

P. Ares[1,2,*], F. Aguilar-Galindo[3], D. Rodríguez-San-Miguel[4], D. A. Aldave[1,2], S. Díaz-Tendero[3,5], M. Alcamí[3,6], F. Martín[2,3,5], J. Gómez-Herrero[1,2], Félix Zamora[2,4,5]

[1]*Department of Condensed Matter Physics, Universidad Autónoma de Madrid, Spain.* [2]*Condensed Matter Physics Center (IFIMAC), Universidad Autónoma de Madrid, Spain.* [3]*Department of Chemistry, Universidad Autónoma de Madrid, Spain.* [4]*Department of Inorganic Chemistry, Universidad Autónoma de Madrid, Spain.* [5]*Instituto Madrileño de Estudios Avanzados en Nanociencia (IMDEA-Nanociencia), Cantoblanco, Spain.*

*e-mail: pablo.ares@uam.es

The extraordinary success of graphene and its tremendous potential applications paved the way for the rising of a completely new family of 2D materials. Graphene is a semimetal with zero-gap, which limits its use in the electronics technology. Transition metal dichalcogenides present a band gap in the range of 1.5 - 2.5 eV [1], which makes them inappropriate for some optoelectronics applications where band gaps in the 0.1 - 1 eV range are commonly preferred. Black phosphorous (BP) [2], a layered allotrope of phosphorous, presents an energy gap in this range and hence it is now intensely studied to better understand its electronics properties in the few-layer conformation. However, it shows a relatively large reactivity; exfoliated flakes of BP are highly hygroscopic and tend to uptake moisture from air. The long term contact with water condensed on the surface seems to degrade BP in hours [3]. Phosphorus belongs to the nitrogen group (group 15 in the periodic table of elements). In this same group, we also find antimony, a silvery lustrous, non-hygroscopic, gray metal with a layered structure similar to that of BP. Theoretical calculations [4] point out towards an electronic structure with a band gap suitable for optoelectronics applications. In this work, we report both micromechanical exfoliation of antimony down to the single-layer regime and experimental evidence of its stability [5]. Our experiments demonstrate that single/few-layer antimony flakes are highly stable in ambient conditions showing mechanical stability upon origami nanomanipulation and no degradation over month periods.

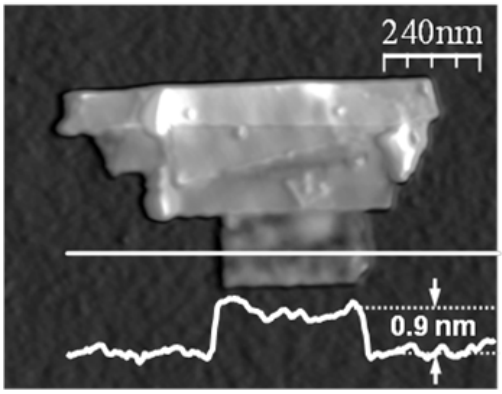

Figure 1. AFM topography image of an antimonene flake with a monolayer terrace at its bottom.

[1] Wang Q. H., Kalantar-Zadeh K., Kis A., Coleman J. N. & Strano M. S. *Nature Nanotechnology* **7**, 699 (2012).
[2] Castellanos-Gomez A. *Journal of Physical Chemistry Letters* **6**, 4873 (2015).
[3] Island J. O., Steele G. A., v. d. Zant H. S. J. & Castellanos-Gomez A. *2D Materials* **2**, 011002 (2015).
[4] Aktürk O. Ü., Özçelik V. O. & Ciraci S. *Physical Review B* **91**, 235446 (2015).
[5] Ares P., Aguilar-Galindo F., Rodríguez-San-Miguel D., Aldave D. A., Díaz-Tendero S., Alcamí M., Martín F., Gómez-Herrero J. & Zamora F. *Advanced Materials* **28**, 6332 (2016).

All-Atom Single-Protein AFM Nanomechanical Spectroscopy Mapping

J. G. Vilhena*, Maria Ortega, Rubén Peréz

Departamento de Física Teórica de la Materia Condensada, Universidad Autónoma de Madrid, E-28049 Madrid, Spain.

*e-mail: guilherme.vilhena@uam.es

Atomic force microscopy is an invaluable characterization tool in almost every biophysics laboratory. However, obtaining atomic/sub-nanometer resolution on single proteins has thus far remained elusive—a feat long achieved on hard substrates. In this regard, nanomechanical spectroscopy mapping may provide a viable approach to overcome this limitation. By complementing topography with mechanical properties measured locally, one may thus enhance spatial resolution at the single-protein level. In this work, we perform all-atom molecular dynamics simulations of the indentation process on a single immunoglobulin G (IgG) adsorbed on a graphene slab. Our simulations reveal three different stages as a function of strain: a noncontact regime—where the mechanical response is linked to the presence of the water environment—followed by an elastic response and a final plastic deformation regime. In the noncontact regime, we are able to identify hydrophobic/hydrophilic patches over the protein. This regime provides the most local mechanical information that allows one to discern different regions with similar height/topography and leads to the best spatial resolution. In the elastic regime, we conclude that the Young modulus is a well-defined property only within mechanically decoupled domains. This is caused by the fact that the elastic deformation is associated with a global reorganization of the domain. Differences in the mechanical response are large enough to clearly resolve domains within a single protein, such as the three subunits forming the IgG. Two events, unfolding or protein slipping, are observed in the plastic regime. Our simulations allow us to characterize these two processes and to provide a strategy to identify them in the force curves. Finally, we elaborate on possible challenges that could hamper the interpretation of such experiments/simulations and how to overcome them. All in all, our simulations provide a detailed picture of nanomechanical spectroscopy mapping on single proteins, showing its potential and the challenges that need to be overcome to unlock its full potential.

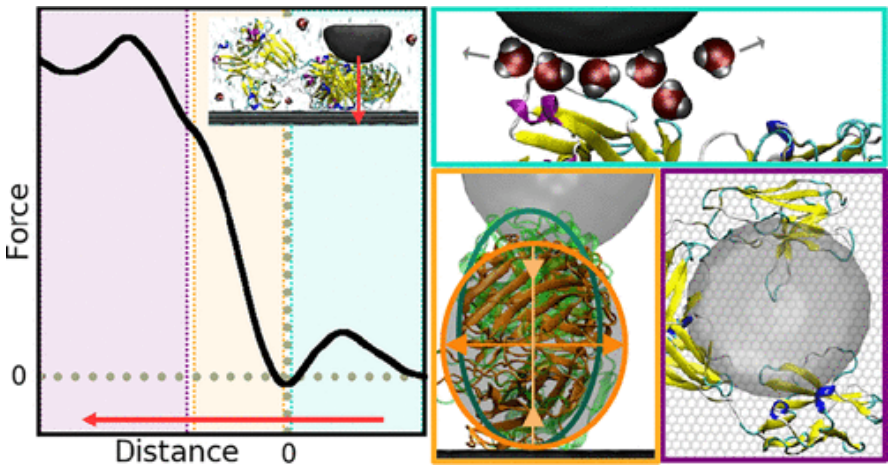

J. G. Vilhena et al., *ACS Sensors* **6**(2), 553 (2021).

A microstructural study by stiffness mapping using the QNM-AFM technique. A case study: Improvement of the miscibility of a PHB-PCL blend

Antonio Cascales[1], Joaquín Hernández-Fernández[2], José Miguel Ferri[1], Santiago Ferrándiz[1], **Emilio Rayón**[1]

[1]*Instituto de Tecnología de Materiales (ITM), Universitat Politècnica de València (UPV), 03801 Alcoy, España.*
[2]*Departamento de Ciencias Naturales y Exactas, Universidad de la Costa, Barranquilla, Colombia.*

*e-mail: emraen@upvnet.upv.es

In formulating polymer blends, it is desirable to achieve good cohesion and miscibility between the different phases. Low miscibility between the components often leads to a decrease in the mechanical and strength properties of the material. The miscibility can be improved by the use of additives, which generate free radicals. For this type of study, an analysis of the microstructure resulting from the blend is required. The microstructural study can be performed topographically by AFM or electron microscopy, but it is not always useful because the fracture surface does not adequately reveal the different phases.

In these cases, where the chemical composition and topography are homogeneous, the AFM-Quantitative Nanomechanical Measurement (QNM) mode has proven to be very useful for its ability to reveal the phases and their interfaces according to their resulting stiffness by picoindentation. This mode acquires stiffness imaging based on force-distance curves, at a high speed and high resolution indentation measurements [1] (2KHz).

In this study, an AFM under QNM mode was used to obtain mechanical stiffness maps of Poly(3-hydroxybutyrate)/Poly(caprolactone), PHB-PCL blends formulations [2]. A Veeco AFM was used in Peak Force tapping mode.

The results of this study were displayed as stiffness maps, Figure 1a. These images revealed the microstructure of the PHB-PCL phases, displaying a low miscibility between them. In addition, the elastic modulus value at each scanned point could be quantified, which was useful to identify each phase. On the other hand, the additive dicumyl peroxide (DCP) was tested at different amounts (0, 0.25, 0.50, 0.75 and 1 wt%). By means of stiffness micrographs, the effect of increased miscibility could be seen in the form of a refining and mixing of the microstructure and the average stiffness of the sample, Figure 1b.

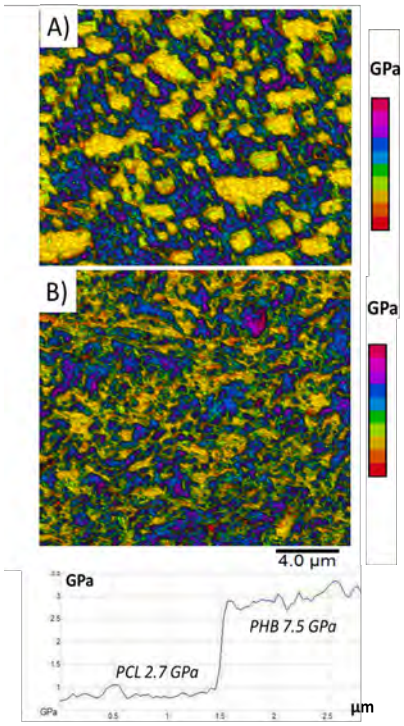

Figure 1. QNM-AFM elastic modulus maps acquired on PHB-PCL (a) and PHB-PCL+DCP additive (b). Stiffness profile

Therefore, AFM in QNM mode was effective and useful to resolve the microstructure of an immiscible blend while quantifying its dimensions and nanomechanical properties of single phases.

[1] M. Aldas, E. Rayón, J. López-Martínez, M.P. Arrieta, *Polymers* **12**, 226 (2020).
[2] J.M. Ferri, D. García-García, E. Rayón, M.D. Samper, R. Balart, *Polymers* **12**, 1344 (2020).

Acknowledgements: (PID2020-116496RB-C22). Investigación competitiva proyectos. Agencia Estatal de Investigación.

Nuevas fronteras y retos en magnetismo

Presentaciones orales

Lunes 11/07:

15:00-15:05 Organisers. *Presentation*

15:05-15:50 Aurelien MANCHON (Aix-Marseille Université (AMU)). *Exploring the Potentials of Spin-Orbitronics*

15:50-16:10 Elvira Paz (INL). *Spintronic devices based on Magnetic Tunnel Junctions*

16:10-16:20 Jorge Marqués Marchán (CSIC). *Distinguishing local demagnetization contribution to the magnetization process in multisegmented nanowires*

16:20-16:30 Santiago Osorio (CNEA). *Creation of single chiral soliton states in monoaxial helimagnets*

16:30-16:40 Luis Sánchez-Tejerina San José (USAL). *Magnetic order excitation by magnetic fields from sub-picosecond structured laser pulses*

16:40-16:50 Akashdeep Kamra (UAM). *Employing magnons for generating multi-qubit entangled states for quantum error correction*

16:50-17:00 María Vélez Fraga (UNIOVI). *Bloch singularities and topological magnetic dipoles in a ferromagnetic microstructure*

17:00-18:00 **Pósteres (IEEE Networking) y café**.

17:45-18:05 Saul Velez (UAM). *Chiral spintronics with magnetic insulators*

18:05-18:15 Arantxa Fraile Rodríguez (UB). *Insights into the structural and magnetic texture of maghemite nanoflowers for biomedicine and environmental remediation*

18:15-18:25 Rodrigo Martín Hernández (USAL). *Spatial isolation of femtosecond magnetic needles driven by azimuthally-polarized laser beams*

18:25-18:35 Alonso José Campos Hernández (IMDEA Nanociencia). *FORC and coercivity angular measurements analysis of the magnetic interactions in arrays of FeNi nanowires*

18:35-18:45 Aun Nawaz Khan (US). *Magnetocaloric effect in doped all-d-metal Ni-(Co)-Mn(X)-Ti (X = Fe and Cr) Heusler alloys*

18:45-18:55 Ana Parente Campos (UCM). *Magnetic nanostructures with different spin textures and topological protection*

18:55-19:05 Alejandro Sánchez Miñarro (ICMAB). *Spin-orbit mixed states in an electromagnetic field*

19:05-19:15 Sebastian Bustingorry (CNEA). *Universal critical exponents of the magnetic domain wall depinning transition*

Pósteres

- José Miguel García-Martín (CSIC). *Novel magnetic nanostructures: nanopillars and patterned antidots*
- Diego Caso Parajón (UAM). *Edge spin wave transmission through a vertex domain wall in triangular dots*
- Zaida Curbelo Cano (IMDEA Nanociencia). *Synthesizing MnAlC / hydrogel composites for 3D-printing of alternative permanent magnets*
- Jose Angel Fernandez Roldan (HZDR). *Current- and Oersted-field- dynamics of a Bloch Point in cylindrical Ni nanowires*
- Ester M. Palmero (IMDEA Nanociencia). *Role of the particle size in the development of customized permanent magnet composites and flexible filaments for additive manufacturing*
- Antonio David Subires Santana (DIPC). *Electronic band structure of the Co pnictide Ca(CoAs)2 probed by ARPES*
- Luis Moreno-Ramírez (US). *Temperature First Order Reversal Curves (TFORC) distributions of magnetocaloric materials*
- Miriam Jaafar (UAM). *Magnetic Force Microscopy for biomedical applications*

Exploring the potentials of spin-orbitronics

Aurélien Manchon

Centre Interdisciplinaire de Nanoscience de Marseille (CINaM), Aix-Marseille University, France.

e-mail: aurelien.manchon@univ-amu.fr

The ever-increasing demand of information technology for power-efficient components has led to the search for alternative solutions to mainstream microelectronics. In this context, spintronics devices stand out as competitive candidates, especially for memory and logic applications. A promising route harvests unconventional transport properties arising from spin-orbit coupling in magnetic heterostructures lacking inversion symmetry.

In these systems, typically multilayers of transition-metal ferromagnets and heavy materials (e.g., W, Pt, Ta, Bi_2Se_3, WTe_2), interfacial spin-orbit coupling promotes a wealth of remarkable physical phenomena: the generation of spin-orbit torques, the interconversion between spin and charge currents, and the stabilization of topological magnetic skyrmions. These effects have gathered extraordinary interest and have led to remarkable experimental breakthroughs, including extremely fast magnetic reversal, terahertz emission, and current-driven skyrmion motion. The recent synthesis of novel classes of materials, including all-oxide heterostructures, noncollinear antiferromagnets, and van der Waals heterostructures, has profoundly enriched this vivid field of research by unlocking unforeseen forms of torques and magnetic interactions, thereby enhancing the functionalities of spin-orbitronic devices.

This lecture will provide a theoretical perspective of the advancement of the fascinating field of spin-orbitronics, focusing on two emblematic mechanisms: the spin-orbit torque and the Dzyaloshinskii-Moriya interaction. I will examine what theory and materials modeling can tell us about these two effects, and what future research directions they open. I will first introduce key concepts in spintronics, such as spin currents and spin-transfer torque, and show how spin-orbit coupling enables new physical effects of high interest for potential applications. I will present standard phenomenological descriptions of these two effects, spin-orbit torque and Dzyaloshinskii-Moriya interaction, determine the symmetry rules that govern them, and give a broad overview of the current state-of-the-art of the field from experimental and theoretical standpoints. Finally, I will explore how spin-orbitronics takes a completely new form in materials possessing low crystalline symmetries, such as Fe_3GeTe_2, CuPt/CoPt bilayers, and noncollinear antiferromagnets (e.g., Mn_3Sn).

I hope this seminar will not only encourage electrical engineers to engage in this beguiling field of research and explore the device implications of this new technology, but also reach out to scientists working in adjacent fields (terahertz science, for instance) who could bring inspiring new ideas to spintronics [1-5].

[1] A. Manchon, J. Železný, I. M. Miron, T. Jungwirth, J. Sinova, A. Thiaville, K. Garello, and P. Gambardella, Current-induced spin-orbit torques in ferromagnetic and antiferromagnetic systems, *Rev. Mod. Phys.* **91**, 035004 (2019).

[2] A. Belabbes, G. Bihlmayer, F. Bechstedt, S. Blügel, and A. Manchon, Hund's rule-driven Dzyaloshinskii-Moriya interaction at 3*d*-5*d* interfaces, *Phys. Rev. Lett.* **117**, 247202 (2016).

[3] E. Jué, C. K. Safeer, M. Drouard, A. Lopez, P. Balint, L. Buda-Prejbeanu, O. Boulle, S. Auffret, A. Schuhl, A. Manchon, I. M. Miron, and G. Gaudin, Chiral damping of magnetic domain walls, *Nature Mater.* **15**, 272 (2016).

[4] S. Laref, K.-W. Kim, and A. Manchon, Elusive Dzyaloshinskii-Moriya interaction in monolayer Fe_3GeTe_2, *Phys. Rev. B* **102**, 060402 (2020).

[5] L. Liu et al., Symmetry-dependent field-free switching of perpendicular magnetization, *Nat. Nanotech.* **16**, 277 (2021).

Acknowledgements: This work was supported by the King Abdullah University of Science and Technology (KAUST, Thuwal, Saudi Arabia) and by the Excellence Initiative of Aix-Marseille Université - A*Midex, a French "Investissements d'Avenir" program.

Spintronic devices based on Magnetic Tunnel Junctions

Elvira Paz*, L. Benetti, T. Böhnert, A. Jenkins, A. Schulman, A. Talantsev, R. Ferreira

INL – International Iberian Nanotechnology Laboratory, Av. Mestre José Veiga s/n 4715-330 Braga, Portugal.

*e-mail: elvira.paz@inl.int

Magnetic Tunnel Junction (MTJ) is a complex stack of different materials with a lot of different layers, where it is mandatory to have two ferromagnetic layers separated by a thin dielectric barrier and a mechanism to pin the polarization of one of the magnetic layers in a fixed direction, i.e., pinned layer. By tunning the thicknesses and materials of the different layers devices can be fabricated for a lot of different applications, in this presentation we are going to focus on magnetic sensors and spin-torque nano-oscillators (STNO).

Magnetic sensors have attracted significant interest having due to important applications in the automotive industry as rotation sensors and for the medical industry to measure the magnetic signals produced by our body. To achieve a large signal to noise ratio the sensing area should be as large as possible as the noise is inversely proportional to the area. To increase the area a lot of sensors can be connected in series, or the area of each sensor can be large. To have a linear variation of the resistance with the field the polarization of the pinned layer must be perpendicular to the easy axis of the other ferromagnetic layer, the free layer. The easy axis of the free layer can be set perpendicular by the shape anisotropy, by soft pinning the free layer [1,2] or by having an out of plane free layer.

With a soft pinned MTJ where 1102 pillars of 100x100 μm^2 are connected in series it is possible to detect down to 115 $pT/Hz^{0.5}$ at 196 Hz without amplification. These sensors were successfully integrated into commercial strain gauge devices, as a competitive alternative of extension-meters. Instead of direct measurement of extensions associated with a force, applied to a strain gauge, the MTJ sensor detects variations of magnetic field, associated with displacements of the magnet, mounted on the strain gauge platform. A resolution of positioning down to 100 nm is obtained without amplification.

When the dimensions of the MTJ pillars are reduced to the range of 100-400nm, new physical phenomena become noticeable, in particular spin transfer torque, that can be used to explore dynamic properties of the magnetization. Vortex nano-oscillators are a particular type of STNO which explore dynamics of free layers with a non-trivial and non-uniform micromagnetic configuration. These devices can generate RF currents, typically in the range of 100-1000MHz when excited with DC currents [3], and conversely, they can generate a DC output when excited with RF currents with frequencies matching the resonant states [4]. These devices have recently attracted a lot of attention due to their potential application in neuromorphic computation and the ongoing efforts will be reported.

The CMOS integration of these devices is very important for very dense devices, for example, sensors to perform magnetic imaging, an interesting application that these very sensitive sensors make possible, as shown in figure 1. I addition CMOS integration is essential for performing large scale computation with these devices (i.e., neuromorphic computing) where a lot of MTJs or a lot of connections are needed.

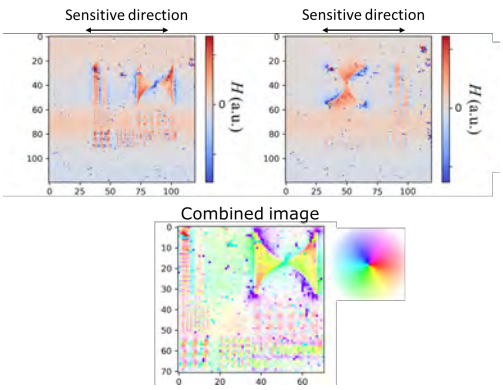

Figure 1. Magnetic image of a patterned multilayer [5nm Ta / 8nm NiFe]x20

[1] E. Paz, S. Serrano-Guisan, R. Ferreira and P. P. Freitas, *Journal of Applied Physics* **115**, 17E501 (2014).
[2] E. Paz, R. Ferreira and P. P. Freitas, *IEEE Transactions on Magnetics* **52**, 4002104 (2016).
[3] J. D. Costa, S. Serrano-Guisan, B. Lacoste, A. S. Jenkins, T. Böhnert, M. Tarequzzaman, J. Borme, F. L. Deepak, E. Paz, J. Ventura, R. Ferreira and P. P. Freitas, *Scientific Reports* **7**, 7237 (2017).
[4] A. Jenkins, L. San Emeterio Alvarez, S. Memshawy, P. Bortolotti, V. Cros, P. P Freitas, R. Ferreira, *Communications Physics* **4**, 1-7 (2021).

Acknowledgements: FET-OPEN SpinAge, FET-Open RadioSpin, PT2020 Newest.

Distinguishing local demagnetization contribution to the magnetization process in multisegmented nanowires

J. Marqués-Marchán[1,*], J.A. Fernandez-Roldan[2], C. Bran[1], R. Puttock[3,4], C. Barton[3], J.A. Moreno[5], J. Kösel[6,7], M. Vazquez[1], O. Kazakova[3], O. Chubykalo-Fesenko[1], A. Asenjo[1]

[1]*Instituto de Ciencia de Materiales de Madrid, CSIC, 28049 Madrid, Spain.*
[2]*Helmholtz-Zentrum Dresden-Rossendorf e.V., Institute of Ion Beam Physics and Materials Research, 01328 Dresden, Germany.*
[3]*National Physical Laboratory, Hampton Road, Teddington TW11 0LW, United Kingdom.*
[4]*Department of Physics, Royal Holloway University of London, Egham TW20 0EX, United Kingdom.*
[5]*Physical Science and Engineering Division, King Abdullah University of Science and Technology, Thuwal 239556900, Saudi Arabia.*
[6]*Computer Electrical and Mathematical Science and Engineering Division, King Abdullah University of Science and Technology, Thuwal 23955-6900, Saudi Arabia.*
[7]*Research Unit Sensor Applications, Sensor Systems Division, Silicon Austria Labs, A-9524 Villach, Austria.*

*e-mail: jorge.marques@csic.es

The excellent response of cylindrical magnetic nanowires (NWs) to external stimuli (magnetic, electrical or mechanical), as well as their interesting magnetic properties raising form their high aspect-ratio and curved geometry, position the NWs as promising materials for their use in different fields, ranging from biomedical to spintronics applications [1]. The versatility of these nanostructures is based on the tunability of their magnetic properties by the appropriate selection of the composition and morphology. For instance, the controlled reversal magnetization in cylindrical nanowires have proposed recently as an alternative to the three-dimensional (3D) racetrack memory devices [2]. Besides, the stochastic magnetization switching behaviour is attracting attention for the development of neuromorphic devices [3].

In this work, we present a study of the magnetization reversal process in multilayered CoNi/Cu nanowires. The non-standard MFM images obtained under in-plane magnetic field, so called 3D images [4], are correlated with the magnetoresistance measurements and micromagnetic simulations. Figure 1 shows an MFM 3D image of the NW. Thanks to this combined studied, the contribution of the individual segments to the demagnetization process can be distinguished. Results show that the magnetization reversal process in these nanowires does not occur through a single Barkhausen jump, but by several switching corresponding to the magnetization reversal processes of individual CoNi segments in the NW. Moreover, the existence of vortex states is confirmed by their footprint in the magnetoresistance measurements as well as in the magnetic imaging measurements. In addition, the either deterministic or stochastic character of the magnetization process is analysed. We observe different switching fields among the segments due to a slightly variation in geometrical parameters or magnetic anisotropy.

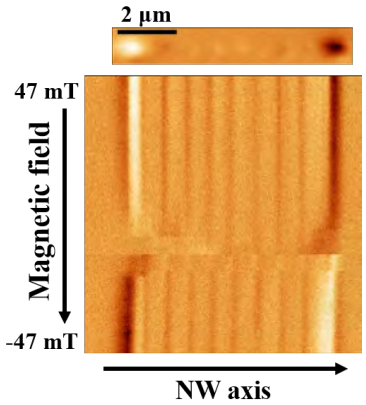

Figure 1. Standard MFM image (up) and 3D image (below) of a CoNi/Cu NW.

[1] Moreno, J.A.; Bran, C.; Vazquez, M.; Kosel, J., *IEEE Transactions on Magnetics* **57** (2021).
[2] Rial, J.; Proenca, M.P., *Nanomaterials* **10**, 1-14 (2020).
[3] Azam, M.A. et al., *Nanotechnology* **31**(14), 145201 (2020).
[4] Jaafar, M. et al., *Nanoscale Res. Lett.* **6**(1), 407 (2011).

Creation of single chiral soliton states in monoaxial helimagnets

Santiago A. Osorio[1,*], Victor Laliena[2], Javier Campo[3], Sebastian Bustingorry[1]

[1]*Instituto de Nanociencia y Nanotecnología, CNEA-CONICET, Centro Atómico Bariloche, (R8402AGP) S. C. de Bariloche, Río Negro, Argentina.* [2]*Department of Applied Mathematics, University of Zaragoza, C/María de Luna, 3, 50018 Zaragoza, Spain.* [3]*Aragon Nanoscience and Materials Institute (CSIC-University of Zaragoza) and Condensed Matter Physics Department, University of Zaragoza, C/Pedro Cerbuna 12, 50009 Zaragoza, Spain.*

*e-mail: santiago.osorio@cab.cnea.gov.ar

In monoaxial chiral helimagnets the Dzyaloshinskii-Moriya interaction favors inhomogeneous distributions of the magnetization with chiral modulations termed chiral solitons. These localized magnetization textures crystallize at low magnetic field leading to the emergence of a chiral soliton lattice [1]. In a magnetic field perpendicular to the chiral axis the system undergoes a phase transition to the uniform state at a critical field B_c [2]. Above this critical field value, a single chiral soliton comprises the lowest level excitation over the stable uniform state, surviving as a metastable configuration [3]. We study theoretically, using micromagnetic simulations, the metastability of a single chiral soliton and propose a strategy to obtain such a state from the chiral soliton lattice [4]. We show that using spin-polarized currents chiral solitons in the chiral soliton lattice can be pushed against each other and it is possible to destroy the solitons one-by-one in a controlled way. A state with one chiral soliton can be obtained by these means for a suitable choice of the external field and the current density (Fig. 1). An important feature of our proposal is that it exhibits a strong robustness against the magnetization distribution in the initial state, even if the initial state is metastable. Our proposal could be relevant in the study of metastable solitons from both the experimental and technological applications.

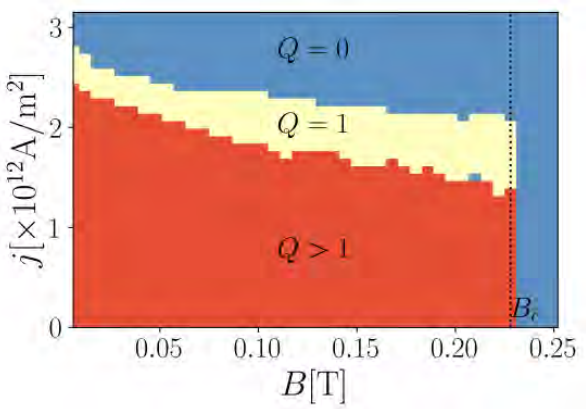

Figure 1. Phase diagram in the $j-B$ space, with j the applied current density and B the external magnetic field, indicating the final number of chiral solitons Q after applying a pulse of current. In the yellow region a metastable single chiral soliton is obtained ($Q = 1$).

[1] Y. Togawa, Y. Kousaka, K. Inoue and J. Kishine, *J. Phys. Soc. Jpn.* **85**, 112001 (2016).
[2] V. Laliena *et al*, *Phys. Rev. B* **93**, 134424 (2016).
[3] V. Laliena, S. Bustingorry, and J. Campo, *Sci. Rep.* **10**, 20430 (2020).
[4] S. A. Osorio, V. Laliena, J. Campo and S. Bustingorry, *Appl. Phys. Lett.* **119**, 222405 (2021).

Acknowledgements: This work was supported by Grant No. PGC2018099024B100 funded by MCIN/AEI/10.13039/501100011033. Grants OTR02223 from CSIC/MICIN and DGA-M4 from Diputación General de Aragón, Spain, are also acknowledged. This work was also supported by the Grant No.PICT 2017-0906 from the Agencia Nacional de Promoción Científica y Tecnológica, Argentina.

Magnetic order excitation by magnetic fields from sub-picosecond structured laser pulses

Luis Sánchez-Tejerina[1,*], Rodrigo Martín-Hernández[1], Rocío Yanes[2], Luis Plaja[1], Luis López-Díaz[2], Carlos Hernández-García[1]

[1]*Grupo de Investigación en Aplicaciones del Láser y Fotónica, Dpto. Física Aplicada, Universidad de Salamanca, E-37008, Salamanca, Spain.* [2]*Dpto. Física Aplicada, Universidad de Salamanca, E-37008, Salamanca, Spain.*

*e-mail: luis.stsj@usal.es

The manipulation of magnetic properties can be exploited in a wide range of applications, such as detectors, actuators, memories, etc. Ultrafast, yet efficient, ways of manipulating magnetic textures could widen even more the use of magnetically ordered systems. The pioneering work on ultrafast laser induced demagnetization in Ni [1], demonstrated that ultrafast laser sources can promote femtosecond (fs) ferromagnetic switching, opening the door to a large number of theoretical and experimental studies on femtomagnetism. Recent technological advances in structured laser sources are opening the door to novel magnetic manipulation schemes. In particular, it has been recently proposed that Tesla-scale fs magnetic fields, isolated from the electric field, can be obtained through the use of ultrafast azimuthally polarized laser beams [2]. Such configuration offers the opportunity to perform pure magnetic interactions with an intense fs B field.

In the present work [3] we show that non-linear magnetic field effects driven by structured laser pulses provide a way to manipulate the magnetic order of ferro- and antiferromagnetic materials. We introduce a novel ferromagnetic switching scheme on sub-ps time-scales by purely magnetic precession of the magnetization with field amplitudes of hundreds of Tesla. We provide an analytical expression that relates the magnetic field amplitude, frequency and pulse duration to achieve switching. Interestingly, lower magnetic fields are enough to excite self-oscillations in AFM materials even after the laser pulse. In this case, the effect can be enhanced or inhibited by the application of a train of laser pulses by properly choosing the polarization and time delay between the pulses. In this sense, it could be possible to construct an artificial neuron excited by this mechanism. The isolation of the magnetic field avoids the heating due to the electric field which may drive stochastic processes or even damage the sample. Our work opens a promising scenario for the manipulation of magnetic states on fs time scales through the use of structured laser beams.

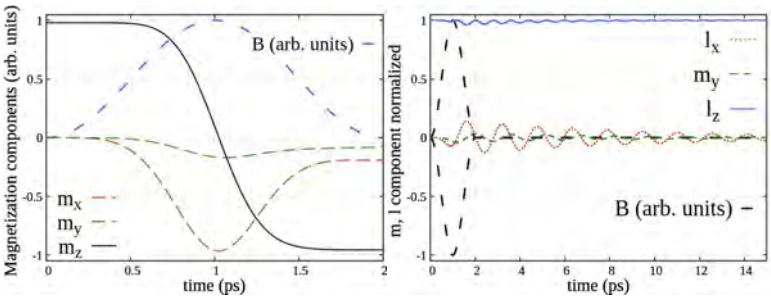

Figure 1. (a) Ferromagnetic switching due to a laser pulse with amplitude $B = 400$ T, main frequency $f = 100$ THz and pulse width $t_p = 750$ fs. (b) Antiferromagnetic oscillations after a laser pulse with amplitude $B = 200$ T, main frequency $f = 125$ THz and pulse width $t_p = 637.5$ fs. (c) Antiferromagnetic oscillations after four laser pulses with amplitude $B = 120$ T, main frequency $f = 125$ THz and pulse width $t_p = 637.5$ fs. The amplitude of the oscillations is the same as in (b).

[1] E. Beaurepaire, J.-C. Merle, A. Daunois, and J.-Y. Bigot, *Phys. Rev. Lett.* **76**, 4250 (1996).
[2] M. Blanco, F. Cambronero, M. T. Flores-Arias, E. Conejero Jarque, L. Plaja, and C. Hernández-García *ACS Photonics* **6** (2019).
[3] L. Sánchez-Tejerina, R. Yanes, R. Martín-Hernández, L. Plaja, L. López-Díaz, C. Hernández-García, in preparation.

Acknowledgements: This work has been funded by the ERC Starting Grant ATTOSTRUCTURA, grant agreement No. 851201; Ministerio de Ciencia de Innovación y Universidades (PID2019-106910GB-I00, RYC-2017-22745); Junta de Castilla y León FEDER (SA287P18).

Employing magnons for generating multi-qubit entangled states for quantum error correction

Ida C. Skogvoll[1], Jonas Lidal[1], Jeroen Danon[1], and **Akashdeep Kamra**[2,1,*]

[1] *Center for Quantum Spintronics, Department of Physics, Norwegian University of Science and Technology, Trondheim NO-7491, Norway.* [2] *Condensed Matter Physics Center (IFIMAC) and Departamento de Física Teórica de la Materia Condensada, Universidad Autónoma de Madrid, Madrid E-28049, Spain.*

*e-mail: akashdeep.kamra@uam.es

The ongoing rapid progress towards quantum technologies relies on and strives for new hybrid platforms optimized for specific quantum computation and communication tasks. We theoretically study a spin qubit exchange-coupled to an anisotropic ferromagnet that hosts magnons with a controllable degree of intrinsic squeezing. We find this system to physically realize the quantum Rabi model from isotropic to the Jaynes-Cummings limit with coupling strengths that can foray into the deep-strong regime. We demonstrate that the composite nature of the squeezed-magnon enables concurrent excitation of 3 spin qubits coupled to the same magnet. Thus, 3-qubit Greenberger-Horne-Zeilinger and related states needed for implementing Shor's quantum error correction code can be robustly generated. Our analysis highlights some unique advantages offered by this hybrid platform and hopes to motivate corresponding experimental efforts.

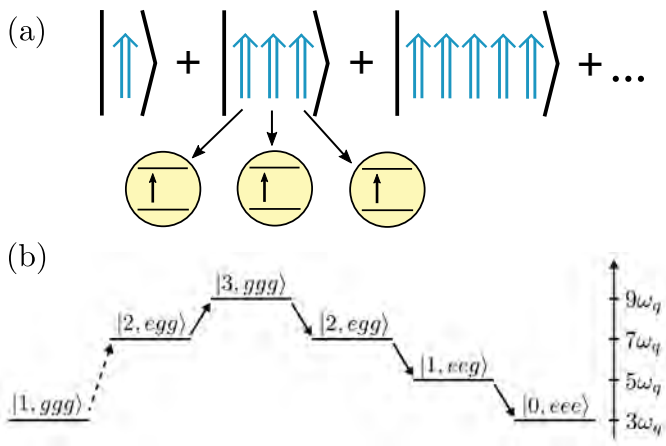

[1] I. C. Skogvoll, J. Lidal, J. Danon, and A. Kamra, *Phys. Rev. Applied* **16**, 064008 (2021).

Acknowledgements: We acknowledge financial support from the Research Council of Norway through its Centers of Excellence funding scheme, project 262633, "QuSpin", and the Spanish Ministry for Science and Innovation – AEI Grant CEX2018-000805-M (through the "Maria de Maeztu" Programme for Units of Excellence in R&D).

Bloch singularities and topological magnetic dipoles in a ferromagnetic microstructure

Javier Hermosa[1,2], Aurelio Hierro-Rodríguez[1,2], Carlos Quirós[1,2], José I. Martín[1,2], Andrea Sorrentino[3], Lucía Aballe[3], Eva Pereiro[3], **María Vélez**[1,2,*], Salvador Ferrer[3]

[1]*Depto. Física, Universidad de Oviedo, 33007 Oviedo, Spain.* [2]*CINN (CSIC – Universidad de Oviedo), 33940 El Entrego, Spain.* [3]*ALBA Synchrotron, 08290 Cerdanyola del Vallès, Spain.*

*e-mail: mvelez@uniovi.es

Bloch points are magnetic singularities defined by the condition of zero magnetization ($m_x = m_y = m_z = 0$). They are essential for the understanding of magnetization reversal in many different systems such as stripe domain patterns, skyrmion lattices or magnetic nanowires. The singular character of Bloch points is associated with a topological charge defined by the flux of an emergent field $\mathbf{B^e}$ across a closed surface $Q = \frac{1}{4\pi\hbar}\oiint \mathbf{B^e} \cdot d\boldsymbol{S}$ [1] with $B_i^e = \frac{\hbar}{2} \in_{ijk} \boldsymbol{m} \cdot \partial_j \boldsymbol{m} \times \partial_k \boldsymbol{m}$. The quantitative analysis of these singularities requires experimental vector magnetization maps $\boldsymbol{m}(\boldsymbol{r})$ with high spatial resolution, which is possible by means of X-ray vector magnetic tomography [2].

We present high resolution vector magnetic tomograms of 140 nm thick permalloy microstructures fabricated by e-beam lithography on a Si-N membrane [3], obtained at the Mistral Beamline of the ALBA Synchrotron. Among the magnetic singularities found are the Bloch point topological dipole shown in Figure 1: Two closely spaced Bloch points are identified consisting of a CW vortex and either a head-to-head domain wall (at BP(-Q)) or a tail-to-tail domain wall (at BP(+Q)). The Bloch points mediate the chirality transitions that occur at the kinks of the central domain wall in the microstructure. The calculated emergent field lines tend to aggregate into bundles carrying a fractional amount of the emergent field flux of each individual Bloch point, which can be used to generalize the concept of magnetic vortex in low symmetry configurations without a well-defined polarity and chirality.

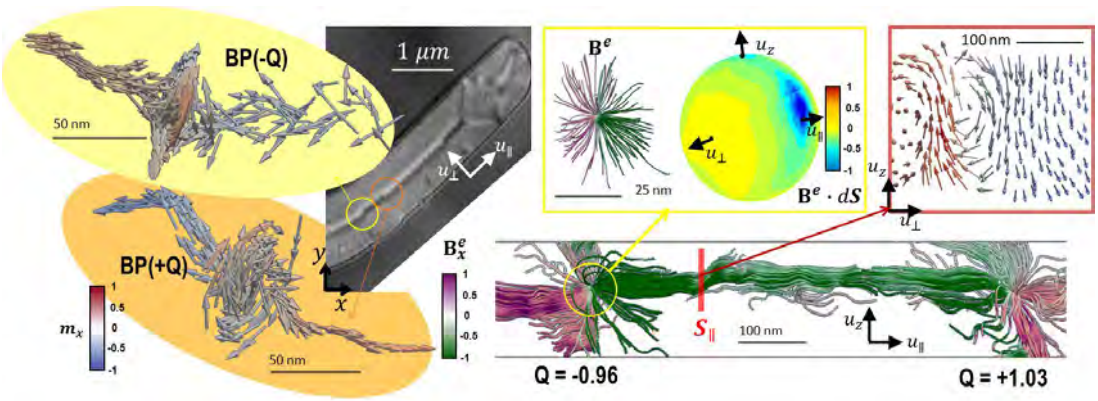

Figure 1. Magnetization configuration $\boldsymbol{m}(\boldsymbol{r})$ at a Bloch point dipole with opposite topological charges reconstructed by X-ray vector magnetic tomography. Bloch points decorate the kinks of the central domain wall of the permalloy microstructure (yellow and orange circles in the X-ray magnetic transmission microscopy image at normal incidence). The emergent field lines B^e (calculated from the experimental $\boldsymbol{m}(\boldsymbol{r})$) deviate strongly from the spherical symmetry of an isolated monopole, as shown by the hot spots of emergent field flux $\mathbf{B}^e \cdot d\boldsymbol{S}$ on a spherical shell surrounding BP(-Q). A cross section of the magnetic configuration at a bundle of B^e lines shows that it corresponds to an asymmetric vortex across the sample thickness.

[1] B. Göbel, I. Mertig, O. A. Tretiakov, *Physics Reports* **895**, 1-28 (2021)
[2] A. Hierro-Rodriguez, C. Quirós, A. Sorrentino, L. M. Alvarez-Prado, J. I. Martín, J. M. Alameda, S. McVitie, E. Pereiro, M. Vélez & S. Ferrer, *Nature Comm.* **11**, 6382 (2020).
[3] J. Hermosa, A. Hierro-Rodríguez, C. Quirós, M. Vélez, A. Sorrentino, L. Aballe, E. Pereiro, S. Ferrer and J. I. Martín, *Micromachines* **13**, 204 (2022).

Acknowledgements: Work supported by Spanish MICINN grant PID2019-104604RB/AEI/10.13039/501100011033 and by Asturias FICYT, grant AYUD/2021/51185 with the support of FEDER funds.

Chiral spintronics with magnetic insulators

Saül Vélez

Departamento de Física de la Materia Condensada & IFIMAC, Universidad Autónoma de Madrid, Spain.

e-mail: saul.velez@uam.es

The use of the spin of the electrons in devices is having a tremendous impact on our electronics and computing technologies. Tell-tale examples are found in the electric switching and reading of magnetic tunnel junctions as well as in the controlled displacement of magnetic domain walls in magnetic thin films. Despite the enormous progress that has been made, current devices are restricted to the use of metallic ferromagnets, which typically suffer from high losses and are limited in frequency.

Magnetic insulators (MIs), such as rare earth garnets ($R_3Fe_5O_{12}$; R=Y, Tm, ...), have attracted a lot of interest because of their low Gilbert damping and high-frequency dynamics. Although being electrically insulating, MIs can couple to spin currents, making thus possible to employ these materials as active elements in electronic devices.

In this talk, we will show how we can stabilize chiral domain walls and skyrmions in $Tm_3Fe_5O_{12}$ (TmIG) coupled to Pt and manipulate them by proximity electric currents (Fig. 1) [1,2]. We will demonstrate the chiral nature of the domain walls and skyrmions via nitrogen-vacancy magnetometry and investigate their dynamics driven by current pulses. Our results reveal that the domain walls in TmIG exhibit mobilities comparable to those achieved with metallic ferromagnets and show that the dynamics of the skyrmions are governed by the ferrimagnetic order of the crystal and pinning, resulting in a large skyrmion Hall effect characterized by a negative deflection angle and hopping motion. Further, we will show that the mobility of the walls and skyrmions can be modified by coupling TmIG to an in-plane magnetized $Y_3Fe_5O_{12}$ (YIG) layer, which distorts the spin texture of the domain walls and skyrmions leading to a directional-dependent rectification of their dynamics. This effect, which is equivalent to a magnetic ratchet, is exploited to control the flow of domain walls and skyrmions in devices. Finally, we will demonstrate that chiral interactions in YIG leads to a magnetic-field dependent directional propagation of spin waves, an effect analogous to drift currents driven by electric fields in conductors [3].

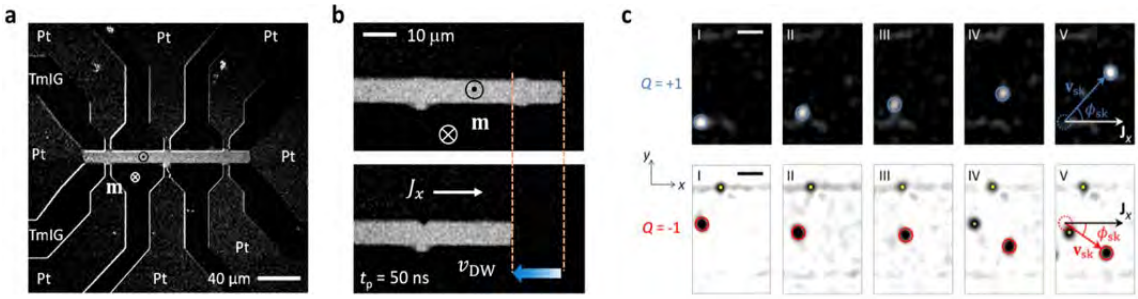

Figure 1. (a) Magneto-optical Kerr effect (MOKE) image of a TmIG/Pt device showing current-induced switching of TmIG (bright region). (b) Demonstration of current-driven wall motion. A current pulse $J_x \sim 10^{12}$ A m^{-2} in Pt drives the walls in TmIG at velocities v_{DW} of 300 m/s. (c) MOKE images showing the displacement of skyrmions in YIG/TmIG/Pt following a sequence of current pulses. The topological charge of the skyrmions (Q), which can be controlled by the orientation of the skyrmion core (bright/dark), results in a transverse deflection of the skyrmions.

[1] S. Vélez et al., *Nat. Comm.* **10**, 4750 (2019).
[2] S. Vélez et al., *Nat. Nanotech.* (2022).
[3] R. Schlitz et al., *Phys. Rev. Lett.* **126**, 257201 (2021).

Insights into the structural and magnetic texture of maghemite nanoflowers for biomedicine and environmental remediation

M. Escoda-Torroella[1,2,*], C. Moya[1-3], **A. Fraile Rodríguez**[1,2,*], A. Gallo-Cordova[4], M.P. Morales[4], A. Labarta[1,2], X. Batlle[1,2]

[1]*Departament de Física de la Matèria Condensada, Martí i Franquès 1, 08028 Barcelona, Spain.* [2]*Institut de Nanociència i Nanotecnologia (IN2UB), Universitat de Barcelona, 08028 Barcelona, Spain.*
[3]*Université libre de Bruxelles, Engineering of Molecular Nanosystems, 1050 Bruxelles, Belgium.* [4]*Instituto de Ciencia de Materiales de Madrid, ICMM/CSIC, 28049 Madrid, Spain.*

*e-mail: arantxa.fraile@ub.edu

Single-core magnetite/maghemite nanoparticles have been extensively studied because of their outstanding properties for biomedical and environmental applications [1,2]. Recently, great interest has focused on multicore nanoparticles, such as aggregates of cores arranged as nanoflower (NF)-like structures. Nevertheless, there is still a lot to understand about both the structure and magnetic properties of the NF to achieve good control over their performance in applications. In particular, the origin of the nearly demagnetized remanent state has still to be interpreted. In this work, three different samples synthesized by the polyol method were studied [3,4]. The size of the NFs (i.e., the overall size of the aggregate) was determined by transmission electron microscopy (TEM), obtaining values of 38 ± 10 nm, 122 ± 14 nm, and 379 ± 135 nm for NF40, NF100, and NF400 samples, respectively. All the samples showed an individual core size of ca. 5 nm, which was determined by TEM. Nevertheless, the crystalline size obtained by X-ray diffraction was about twice the size of the individual cores measured by TEM, showing a crystallographic correlation length that extended well beyond the individual cores. In addition, selected area electron diffraction patterns were not the ones expected for a polycrystalline sample as they showed a high degree of texture associated with preferential orientations of the cores within the NF. This complex crystalline structure led to hysteresis loops showing high values of both saturation magnetization (ca. 80 emu/g) and initial susceptibility, but with almost zero remanent magnetization and coercive field at 300 K. Therefore, a deeper understanding of the internal magnetic structure of the NF and the corresponding magnetic properties are key to optimize their performance in applications.

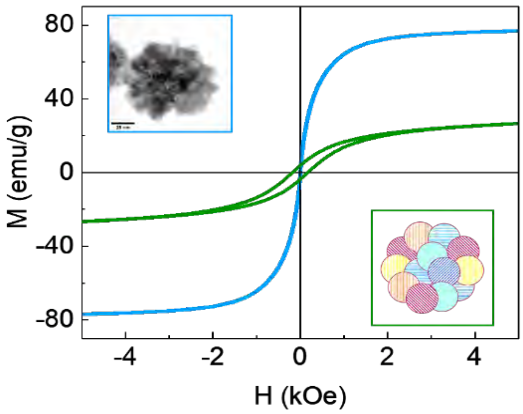

Figure 1. Comparison of the hysteresis cycles of a polycrystalline nanoparticle (green) and a NF (blue).

[1] X. Batlle and A. Labarta, *J. Phys. D. Appl. Phys.* **35**, R152 (2002).
[2] X. Batlle. *et al.*, *J. Magn. Magn. Mater.* **543**, 168594 (2022).
[3] Gavilán, H. *et al.*, *Part. Part. Syst. Charact.* **34**, 1–12 (2017).
[4] M. Escoda-Torroella, 2022, Tuning the performance of magnetic, semiconductor, and multifunctional hybrid nanostructures, Doctoral Thesis, Universitat de Barcelona, Barcelona.

Acknowledgements: The work was supported by Spanish MCIU and AEI (MAT2015-68772-P; PGC2018-097789-B-I00) and European Union FEDER funds. M.E-T. acknowledges Spanish MCIU for BES-2016-077527.

Spatial isolation of femtosecond magnetic needles driven by azimuthally-polarized laser beams

Rodrigo Martín-Hernández*, Luis Sánchez-Tejerina, Enrique Conejero Jarque, Luis Plaja, Carlos Hernández-García

Grupo de Investigación en Aplicaciones del Láser y Fotónica, Departamento de Física Aplicada, Universidad de Salamanca, E-37008, Salamanca, Spain.

*e-mail: rodrigomh@usal.es

Femtosecond laser sources have great potential to trigger, control, and observe ultrafast magnetic phenomena. Since the pioneering work on ultrafast laser-induced demagnetization by Beaurepaire et al. [1], the interest on the potential applications of ultrafast laser pulses in magnetism has boosted. In particular, the development of ultrafast structured light beams has opened new perspectives in the field. Recently, it has been shown how Tesla-scale femtosecond magnetic fields, isolated from the electric field in a spatial volume, can be obtained from the interaction between azimuthally polarized vector beams and metallic nanoantennas [2]. These ultrafast isolated magnetic sources have opened a new perspective in ultrafast magnetism to study pure magnetic interactions where the key role is played by the magnetic, like magnetic switching in ferromagnetic materials [3] or oscillations in the Néel vector in antiferromagnetic materials.

In this work, we study the effect of different antenna geometries to optimize the efficiency and isolation of ultrafast magnetic fields. We have performed simulations using the Particle-In-Cell code OSIRIS [4], where circular apertured antennas generate isolated magnetic nanoprobes (fig. 1 a). However, a significant magnetic-to-electric field ratio is limited to distanced of few nanometers. Our simulations demonstrate how novel geometries enhance this contrast, allowing to keep the electric field below the sample damage threshold. As an example, the use of a double apertured antenna (Fig. 1 b), enhances the contrast ratio by a factor of three (Fig. 1 c). Further optimization of the antenna geometry could boost this contrast enhancement. Our work paves the route to employ polarization structured laser beams along metallic nanoantennas to achieve pure magnetic interactions with matter at ultrafast scales.

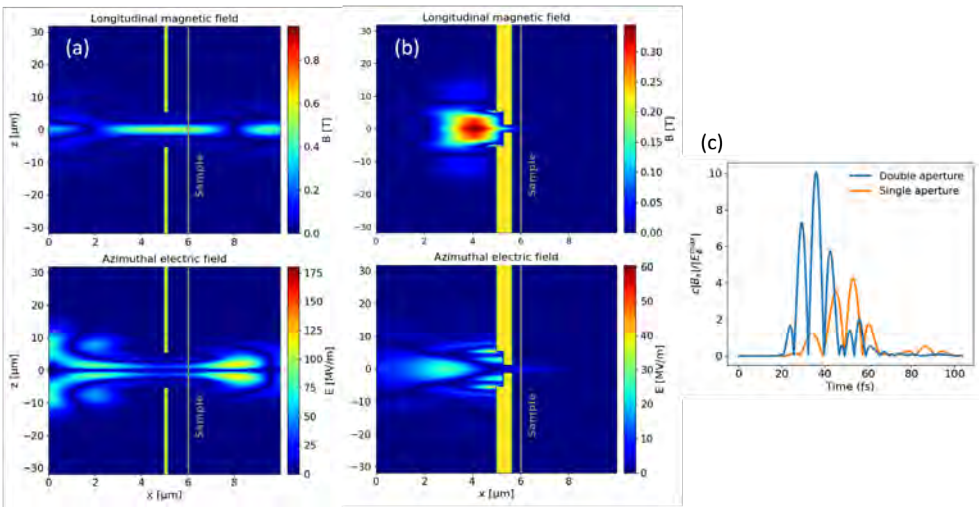

Figure 1: Spatial distribution, at *y=0,* of the longitudinal magnetic and azimuthal electric fields using (a) a single apertured antenna, as proposed in [2], and (b), a double apertured antenna. (c) Temporal evolution of the contrast at the sample for both antennas. The driving laser is a two-period 5 μm pulse, with a peak amplitude of 151 MV/m.

[1] E. Beaurepaire, J.-C. Merle, et al., *Phys. Rev. Lett.* **76**, 4250 (1996).
[2] M. Blanco, F. Cambronero, M. T. Flores-Arias, E. Conejero Jarque, et al., *ACS Photonics* **6**, 38 (2019).
[3] L. Sánchez-Tejerina, R. Yanes, R. Martín-Hernández, L. Plaja, L. López-Díaz, C. Hernández-García, *in preparation.*
[4] R. A. Fonseca, L. O. Silva, F. S. Tung, et al., *Lecture Notes in Computer Science* **2331**, 342 (2002).

Acknowledgements: European Research Council (851201); Ministerio de Ciencia de Innovación y Universidades (PID2019-106910GB-I00, RYC-2017-22745); Junta de Castilla y León FEDER (SA287P18).

FORC and coercivity angular measurements analysis of the magnetic interactions in arrays of FeNi nanowires

Alonso J. Campos-Hernandez*, Ester M. Palmero, Alberto Bollero

Group of Permanent Magnets and Applications, IMDEA Nanociencia, 28049, Madrid, Spain.

*e-mail: alonsojose.campos@imdea.org

Compositional variation in magnetic nanowires (NWs) permits the tailoring of the magnetic properties under controlled synthesis conditions [1]. In this study arrays of FeNi NWs have been electrodeposited into anodized aluminum oxide (AAO) membranes (Fig. 1a). Chemical composition analysis of the samples showed anomalous co-deposition, where Fe deposits in ratios higher than its electrolyte molar fraction under different trends. The trends observed within this behaviour were explained within a modified Bocris-Drazic-Despic (BDD) model [2].

Coercivities (H_c) ranging from 0.2 kOe to 1.0 kOe were obtained (Fig. 1b), observing an increase in H_c for a diminished Fe concentration. The angular study of the magnetization reversal mechanisms (dominated by a transverse domain wall mechanism) hinted at the decrease in the magnetostatic interactions between NWs as the source of the rise in H_c. First-order reversal curve (FORC) analysis indicated a reduced value of the magnetic interactions in the arrays, except for the $Fe_{0.80}Ni_{0.20}$ NWs which showed a FORC diagram corresponding to magnetically interacting NWs (Fig. 1c). All the diagrams showed a high-intensity spot at around H_c = 1 kOe, with weakening intensity for an increased Fe content due to the higher interactions.

This work shows the possibility of tailoring the magnetic properties of FeNi NWs by tuning the electrochemical parameters and, thus, their composition and crystallographic structure. This approach is of interest in developing NW-based applications such as magnetic recording and sensing devices, and opens the path to explore the possibility of forming ordered phases with outstanding permanent magnet properties (e.g., the $L1_0$-ordered FeNi phase [3]).

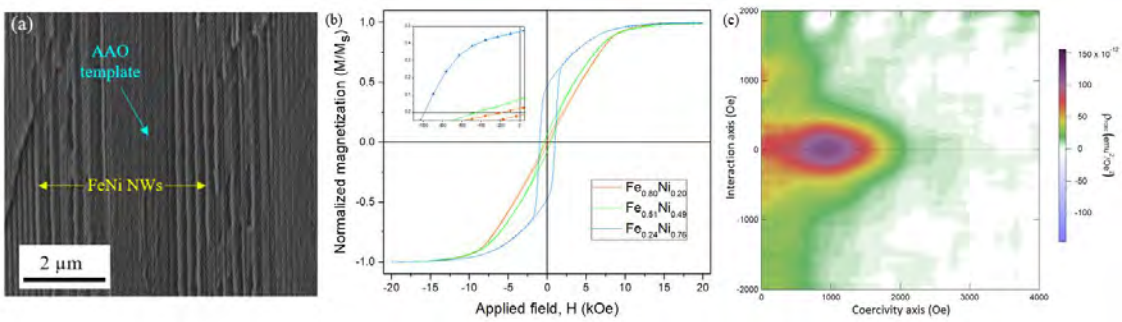

Figure 1. (a) SEM image of an array of FeNi NWs into an AAO membrane; (b) room temperature hysteresis loops measured for arrays of FeNi NWs with different compositions; and (c) FORC diagram for $Fe_{0.80}Ni_{0.20}$ NWs.

[1] Palmero, E. M. *et al.*, *J. Appl. Phys.* **116**, 033908 (2014).
[2] Dragos O. *et al.*, *J. Electrochem. Soc.* **163**, 83-94 (2015).
[3] Lewis, L. H. *et al.*, *J. Phys.: Condens. Matter* **26**, 064213 (2014).

Acknowledgements: Authors acknowledge financial support from EU M-ERA.NET and MICINN through the projects *COSMAG* (PCI2020-112143) and *NEXUS* (PID2020-11521RB-C21). A.J.C.-H. acknowledges support from "La Caixa" Foundation (ID 100010434) through the Doctoral INPhINIT Incoming program (LCF/BQ/DI20/1178002). E.M.P. acknowledges support from AEI through the Juan de la Cierva – Incorporación program (IJC2020-043011-I/MCIN/AEI/10.13039/501100011033) and EU by NextGenerationEU/PRTR.

Magnetocaloric effect in doped all-d-metal Ni-(Co)-Mn(X)-Ti (X = Fe and Cr) Heusler alloys

Aun N. Khan*, Luis M. Moreno-Ramírez, Álvaro Díaz-García, Jia Yan Law, Victorino Franco

Dpto. Física de la Materia Condensada. ICMS-CSIC. Universidad de Sevilla, P.O. Box 1065, Sevilla 41080, Spain.

*e-mail: akhan@us.es

All-d-metal Heusler alloys show elevate magnetocaloric/barocaloric effects ascribed to the undergoing martensitic transformation while retaining excellent mechanical properties in contrast to other well studied Heusler alloys [1,2]. However, for magnetocaloric applications of this system, high magnetic fields are still needed (much larger than those expected in real applications around 1-2 T) to obtain significant values and to overcome the hysteresis ascribed to the transformation and, therefore, for being considered as a potential candidate for magnetic refrigeration systems. In this work, we synthesized by arc melting a series of doped all-d-metal Ni-(Co)-Mn(X)-Ti (X = Fe and Cr) Heusler alloys (with parent composition of $Ni_{36}Co_{14}Mn_{35}Ti_{15}$) and investigate its martensitic transformations and magnetocaloric properties. On the one hand, doping the alloy with Cr (1 and 3 at.%) increases latent heat due to the increase of the martensite cell distortion but also leads to the overlapping of the martensitic and Curie transitions (increases the martensitic transition temperature and reduces the Curie temperature) which significantly reduces the magnetization difference between austenite and martensite and, therefore, reducing significantly the isothermal entropy change with respect the parent alloy. Both combined effects drastically reduce the magnetocaloric performance even for small Cr doping amounts. On the other hand, Fe doping (from 3 to 7 at.%) reduces latent heat due to the reduction of the martensite cell distortion and leads to separation of martensitic and Curie transitions (reduces the martensitic transition temperature while does not significantly affects to the Curie temperature), improving the magnetization difference among both phases. This magnetization change increment together with the latent heat reduction reduces the magnetic field needed for driving completely the martensitic transformation. This effect also leads to higher isothermal entropy change values at moderate magnetic field changes of 1-2 T (30% enhancement) and to improve the sweeping rate of the martensitic transition with the magnetic field (which is directly related to the adiabatic temperature change). These features probes the applicability improvement for the Ni(Co)-Mn(Fe)-Ti alloys.

[1] Vinicius G. de Paula, Mario S. Reis, *Chemistry of Materials* **33**(14), 5483 (2021).
[2] A. Taubel *et al.*, *Acta Materialia* **201**, 425 (2020).

Acknowledgements: Work supported by AEI/FEDER-UE, Spain (grant PID2019-105720RB-I00), US/JUNTA/FEDER-UE, Spain (grant US-1260179), Consejería de Economía, Conocimiento, Empresas y Universidad de la Junta de Andalucía, Spain (grant P18-RT-746) and Sevilla University under VI PPIT-US program. Aun N. Khan acknowledges a FPI fellowship from the Spanish MICINN. LMMR acknowledges a postdoctoral fellowship from Junta de Andalucía and European Social Fund (ESF).

Magnetic nanostructures with different spin textures and topological protection

A. Parente[1,*], M. Abuin[2], José. L. Prieto[2], M. Menghini[3], E. M. González[1,3], A. Muñoz-Noval[1,3]

[1]*Departmento de Física de Materiales, Facultad de Ciencias Físicas, Universidad Complutense, 28040 Madrid, Spain.*
[2]*Instituto de Sistemas Optoelectrónicos y Microelectrónica, Universidad Politécnica, 28040 Madrid, Spain.*
[3]*IMDEA Nanociencia, Cantoblanco, 28049 Madrid, Spain.*

*e-mail: aparente@ucm.es

New emergent phenomena due to topological effects have become a very active research frontier in condensed matter physics. Artificial magnetic nanostructures have opened a way to study topological phenomena such as frustration, emergent magnetic monopoles, synthetic antiferromagnetism or magnetic phase transitions.

In this work, different magnetic nanostructures with topological protection have been fabricated combining nanolithography techniques with DC magnetron sputtering. Morphological characterization using different microscopy techniques (AFM and SEM) and magnetic (magnetic force microscopy MFM) have been complemented with micromagnetic simulations in MuMax3 and transport measurements al low temperature.

The sensitivity of the textures and robustness of the topological protection in some of the structures under external magnetic fields have been investigated. The main goal of this work is to study the magnetic properties, spin textures and frustration in systems with different geometry and the influence of the geometry in the formation and ordering of magnetic defects.

Spin-orbit mixed states in an electromagnetic field

A. S. Miñarro*, Gervasi Herranz

Institut de Ciència de Materials de Barcelona (ICMAB-CSIC), Campus UAB, 08193 Bellaterra, Catalonia, Spain.

*e-mail: asanchez3@icmab.es

Spin-orbit mixing is an important problem in condensed matter. For instance, spin-orbit entanglement in the t2g manifold may play an important role in exotic phenomena, like quantum spin liquids in 4d and 5d systems. An interesting question is how these states interact with electromagnetic fields, which may hold potential to tune their properties and reveal interesting physics. Motivated by our recent discovery of large gyrotropic signals in some Jahn-Teller manganites [1], here we explore the interaction of light with spin-mixed t2g − eg states in 3d metals. We show that spin-orbit mixing enables electronic transitions that are sensitive to circularly polarized light, giving rise to a gyrotropic response. Such interactions offer the opportunity to use electromagnetic waves at optical wavelengths to entangle orbital and spin degrees of freedom. Interestingly, we find that, in addition to spin-orbit coupling, orthorhombic Jahn-Teller interactions are relevant to enhance the observed optical gyrotropy in solid-state 3d systems with octahedral symmetry. Our approach, which includes a group-theoretic treatment of spin-orbit coupling, has wide applicability and provides a versatile tool to explore the interaction of electromagnetic fields with electronic states in transition metals with arbitrary spin-orbit coupling strength and point-group symmetries.

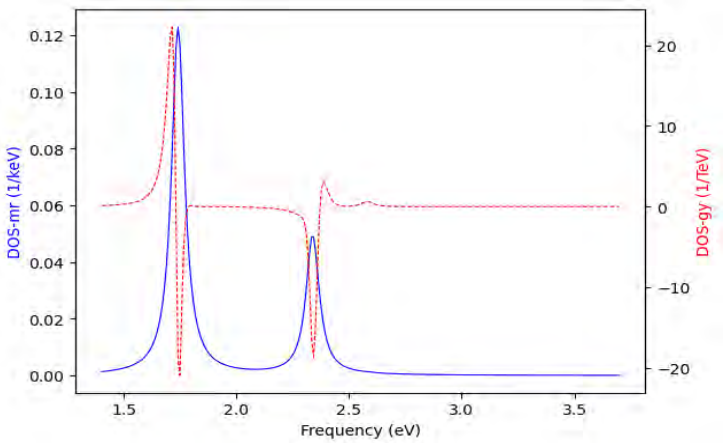

Figure 1. Non-gyrotropic (blue line) and gyrotropic (red line) signals taken from numerical calculations of the density of states of the non-perturbed ground states for the system perturbed with left-handed or right-handed circularly polarized light being the sum (left plus right) and the difference (left minus right) respectively.

[1] B. Casals et al., *Phys. Rev. Lett.* **117**, 026401 (2016).

Acknowledgements: This work is supported by the PID2020-118479RB-I00 and Severo Ochoa FUNFUTURE (CEX2019-000917-S) projects of the Spanish Ministry of Science and Innovation (MCIN/AEI/10.13039/501100011033).

Universal critical exponents of the magnetic domain wall depinning transition

Lucas Albornoz[1,2,3], Ezequiel Ferrero[1], Alejandro Kolton[3,4], Vincent Jeudy[2], **Sebastian Bustingorry**[1,*], Javier Curiale[1,3]

[1]*Instituto de Nanociencia y Nanotecnología, CNEA-CONICET, Centro Atómico Bariloche, (R8402AGP) S. C. de Bariloche, Río Negro, Argentina.* [2]*Université Paris-Saclay, CNRS, Laboratoire de Physique des Solides, 91405 Orsay, France.* [3]*Instituto Balseiro, Universidad Nacional de Cuyo-CNEA, Centro Atómico Bariloche, Avenida E. Bustillo 9500 (R8402AGP), San Carlos de Bariloche, Río Negro, Argentina.* [4]*Centro Atómico Bariloche, Comisión Nacional de Energía Atómica (CNEA), Consejo Nacional de Investigaciones Científicas y Técnicas (CONICET), Avenida E. Bustillo 9500 (R8402AGP), San Carlos de Bariloche, Río Negro, Argentina.*

*e-mail: sbusting@cab.cnea.gov.ar

The depinning transition rules the low velocity response of domain walls in magnetic thin films. Understanding the depinning transition is key to unveil the role of disorder in magnetic systems. We presente here results of magnetic-field-driven domain wall dynamics in a ferrimagnetic GdFeCo thin film with perpendicular magnetic anisotropy using low-temperature magneto-optical Kerr microscopy. Measurements performed in a practically athermal condition allow for the direct experimental determination of the velocity ($\beta = 0.30 \pm 0.03$) and correlation length ($\nu = 1.3 \pm 0.3$) exponents of the depinning transition [1]. The whole family of exponents characterizing the transition is deduced, providing evidence that the depinning of magnetic domain walls is better described by the quenched Edwards-Wilkinson universality class.

[1] L. A. Albornoz, E. E. Ferrero, A. B. Kolton, V. Jeudy, S. Bustingorry and J. Curiale, *Phys. Rev. B* **104**, L060404 (2021).

Acknowledgements: This work was supported by Grants No.PICT 2016-0069, No.PICT 2017-0906 and No.PICT 2017-1202 from the Agencia Nacional de Promoción Científica y Tecnológica, Argentina.

Novel magnetic nanostructures: nanopillars and patterned antidots

Elena Navarro[1], María Ujué González[2], Fanny Béron[3], Felipe Tejo[4], Juan Escrig[5], Andreas Kaidatzis[6], Rafael P. del Real[4], Raquel Álvaro[2], Dimitrios Niarchos[6], Manuel Vázquez[4], **José Miguel García-Martín**[2,*]

[1]*Dpto. de Física de Materiales, Universidad Complutense de Madrid, Madrid, Spain.*
[2]*Instituto de Micro y Nanotecnología, CSIC, Tres Cantos, Spain.*
[3]*Instituto de Física Gleb Wataghin, UNICAMP, Campinas, Brazil.*
[4]*Instituto de Ciencia de Materiales de Madrid, CSIC, Madrid, Spain.*
[5]*Departamento de Física, USACH, Santiago, Chile.*
[6]*Institute of Nanoscience and Nanotechnology, NCSR Demokritos, Athens, Greece.*

*e-mail: josemiguel.garcia.martin@csic.es

Two different nanostructures are studied in this contribution: large-area nanopillar arrays fabricated by glancing angle deposition with magnetron sputtering (MS-GLAD) and magnetic thin films perforated with long-range order arrays of nanoholes prepared by focused ion beam (patterned antidots).

MS-GLAD is an easy and versatile route to fabricate arrays of nanostructures in large areas in a single processing step. In our work, nanostructured films with vertical or tilted nanopillars composed by polycrystalline Fe and Fe_2O_3 have been fabricated depending on whether the substrate is kept rotating azimuthally during deposition or not, respectively [1]. The magnetic properties of these films can be tuned with the specific morphology. In particular, the growth performed through a collimator mask mounted onto a not rotating azimuthally substrate produces almost isolated well-defined tilted nanopillars that exhibit a magnetic hardening. The first-order reversal curves diagrams and micromagnetic simulations revealed that a growth-induced uniaxial anisotropy, associated with an anisotropic surface morphology produced by the GLAD in the direction perpendicular to the atomic flux, plays an important role in the observed magnetic signatures.

Magnetic antidots are being studied for different applications, such as magnonic crystals for microwave devices, magnetically-active plasmonic media, magnetic biosensing, and magneto-resistance sensors. In our work, a top-down approach using focused ion beam has been employed to fabricate Co/Permalloy hard-soft bilayer antidot arrays [2]. The antidots have a 40 nm diameter and two symmetries are studied: square and hexagonal. A dependence of magnetic coercivity on the relative thicknesses of the magnetically hard (Co) and soft (Permalloy) layers is found; increasing Permalloy thickness results in lower magnetic coercivity. Furthermore, the long-range periodicity of these antidots results in higher magnetic coercivity and a stronger magnetic domain-wall pinning, compared to identical hard/soft bilayers of short-range order deposited on porous anodic alumina. Finally, magnetic force microscopy (MFM) imaging of the antidot arrays shows striking qualitative differences between the two symmetries: square symmetry arrays have inhomogeneous magnetic state and a high density of immobile super-domain walls, whereas hexagonal symmetry arrays show a homogeneous magnetic configuration.

[1] E. Navarro *et al*., *Nanomaterials* **12**, 1186 (2022).
[2] A. Kaidatzis *et al*., *J. Magn. Magn. Mat.* **498**, 166142 (2020).

Acknowledgements: The service from the MiNa Laboratory at IMN. Funding from MINECO, Comunidad de Madrid, European Union, Fondecyt, Dicyt-Usach, São Paulo Research Foundation, Brazilian National Council for S., NSRF Greece-EU, NATO.

Edge spin wave transmission through a vertex domain wall in triangular dots

Diego Caso[1,*], Farkhad Aliev[1,2]

[1]*Departamento de Física de la Materia Condensada C03, Universidad Autónoma de Madrid, Cantoblanco, Madrid 28049, Spain.* [2]*Instituto Nicolás Cabrera (INC) and Condensed Matter Physics Institute (IFIMAC), Universidad Autónoma de Madrid, Cantoblanco, Madrid 28049, Spain.*

*e-mail: diego.caso@uam.es

Spin waves (SWs), being usually reflected by domain walls (DWs), could also be channeled along them. Recent studies allowed observation of spin waves along domain walls in rectangular, circular [1] and triangular dots in the ground or metastable states. Triangular dots could also present edge pinned inhomogeneous magnetic states, depending on the direction of the external magnetic field. These edge domain walls yield the interesting, and potentially applicable to real devices property of broadband spin wave confinement to the edges of the structure [2,3], with capabilities to be redirected at angles exceeding 100 degrees. It has been previously shown how these waves could be generalized for arbitrary shapes and propose few devices (such as edge spin wave interferometers, controllers or splitters) where edge spin waves could be implemented [3].

Here we present simulation results obtained on amorphous YIG ($Y_3Fe_5O_{12}$) based triangles where edge spin waves (ESW) were propagated over the corner in 2 micron sized triangles with a fixed thickness of 85 nm. The superior vertex angle, studied in the range of 40º-75º, has been optimized in order to obtain a higher transmission coefficient over the vertex of the edge spin waves. Our simulations showed resonance increase of the ESW transmission for the angles close to 50 degrees. A slight excess of the transmission above one could be due to a positive interference with SWs propagating directly from the microwave field source to the opposite edge. A generated upper vertex domain wall's topology seems to be key in understanding the efficiency of the ESW propagation. We have investigated the phase shift of the SWs at the DW, which drops to $\pi/2$ at the high transmission range of angle apertures. We have also optimized the applied bias field to maximize the effectiveness of the exchange energy channels that behave as propagation routes for the spin wave.

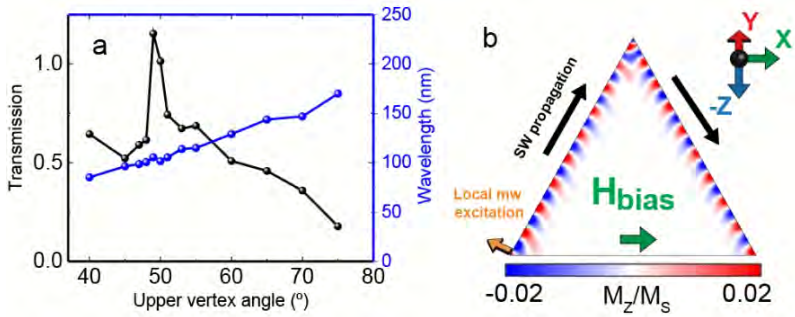

Figure 1. Wavelength of the signal and transmission coefficient of the ESW propagation through the upper vertex topology, showing a distinct increment for upper vertex angles in the 49-50 degree range. b) Snapshot of an edge spin wave propagated through both sides on a 2 micron side YIG triangle with a local microwave sinusoidal excitation perpendicular to the left side.

[1] F. G. Aliev, et al., *Phys. Rev. B* **84**, 144406 (2011).
[2] A. Lara, V. Metlushko, F. G. Aliev, *J. Appl. Phys.* **114**, 213905 (2013).
[3] A. Lara, J. Robledo, K.Y. Guslienko, F. G. Aliev, *Scientific Reports* **7**, 5597 (2017).

Acknowledgements: Authors acknowledge support by Spanish Ministerio de Ciencia (RTI2018-095303-B-C55, CEX2018-000805-M) and Consejería de Educación e Investigación de la Comunidad de Madrid (NANOMAGCOST-CM Ref. P2018/NMT-4321) Grants. D.C. has been supported by Comunidad de Madrid by contract through Consejería de Ciencia, Universidades e Investigación y Fondo Social Europeo (PEJ-2018-AI/IND-10364).

Synthesizing MnAlC / hydrogel composites for 3D-printing of alternative permanent magnets

Zaida Curbelo*, Ester M. Palmero, Cristina M. Montero, and Alberto Bollero
Group of Permanent Magnets and Applications, IMDEA Nanociencia, 28049 Madrid, Spain

*e-mail: zaida.curbelo@imdea.org

3D-printing technologies attract much interest in high-tech sectors due to the possibility of fabricating complex and high-performance objects with tailored properties and a minimal waste generation [1]. In the permanent magnets (PMs) sector, the manufacturing of magnets by 3D-printing requires a high filling factor and no deterioration of the magnetic properties. Many works on additive manufacturing (AM) of PMs focus on NdFeB, however the present challenge is finding alternative rare earth-free PMs to address the criticality of rare-earths. MnAl-based alloys are promising candidates thanks to its high availability and diminished environmental impact [2]. A recent technology known as Fused Filament Fabrication (FFF) [3] has proved the potential that MnAlC alloy shows to be used for the development of alternative PMs by AM.

This work is focused on developing magnetic composites, using a hydrogel as matrix material and gas-atomized MnAlC particles of ferromagnetic τ-phase were used as filler. Different amounts of MnAlC particles were considered to end with composites with several filler loading. The quasi-spherical MnAlC particles showed a mean particle size of 50 µm. Firstly, hydrogels were chemically synthesized using alginate (ALG) as precursor material, and methylcellulose (MC) that was incorporated as additive for thickening the resulting mixture [4]. Afterwards, the MnAlC particles were added and stirred for obtaining homogeneous composites. Different ALG:MC ratios were analysed (2.5:1 and 1:1), and it was found that 2.5:1 is a suitable proportion for AM as it allows an adequate viscosity of the resulting composite to be loaded in syringes (Fig. 1a) and used in the direct ink writing (DIW) 3D-printing technology.

Figures 1b and 1c show the Scanning Electron Microscopy (SEM) images of the resulting cured composites (PM particles / hydrogel), which manifest a smooth surface with the MnAlC particles well dispersed along the hydrogel matrix. The hysteresis loops of the cured composites with different MnAlC load were measured by Vibrating Sample Magnetometry (VSM). The magnetization curves in Fig. 1d reveal that the magnetization scales with the MnAlC content in the composite, while the coercive field remains constant. Magnetometry measurements show that the magnetic properties of the MnAlC particles are not deteriorated along the composite synthesis process. The synthesized composites based on MnAlC particles and hydrogel present suitable and promising properties for their application in the development of a new generation of alternative PMs by additive and bonding manufacturing technologies.

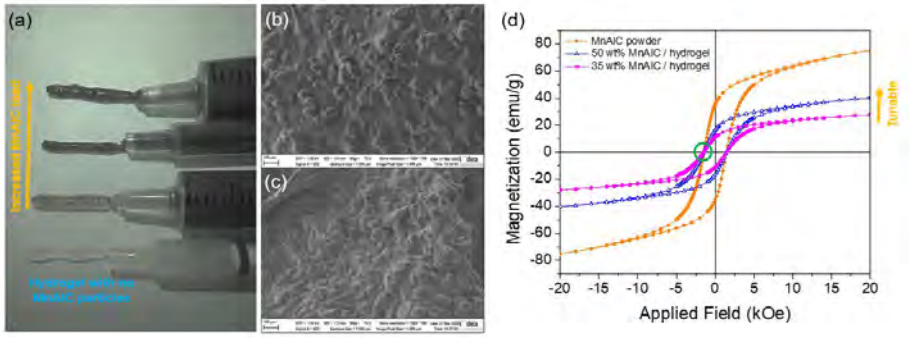

Figure 1. (a) Syringes loaded with hydrogel and composites with different MnAlC particles load; SEM images of the composites with (b) 35 wt% and (c) 50 wt% content of MnAlC particles [scale bar: 100 µm]; (d) Hysteresis loops for the composites with 35 wt% and 50 wt% MnAlC content, measured at room temperature.

[1] L.E. Murr, *J. Mater. Sci. Technol.* **32**, 987 (2016).
[2] J. Rial et al., *Acta Mater.* **157**, 42 (2018); C. Muñoz-Rodríguez et al., *J. Alloys Compd*. **847**, 156361 (2020).
[3] E.M. Palmero et al., *Sci. Technol. Adv. Mater.* **19**, 465 (2018); *Addit. Manuf.* **33**, 101179 (2020).
[4] D. Podstawczyk et al., *Addit. Manuf.* **34**, 101275 (2020).

Acknowledgements: Authors acknowledge Höganäs AB (Sweden) for providing the gas-atomized MnAlC particles through an industrial IMDEA-Höganäs collaboration and the financial support from MICINN by *NEXUS* (PID2020-115215RB-C21). E.M.P. acknowledges support from AEI through the Juan de la Cierva – Incorporación program (IJC2020-043011-I/MCIN/AEI/10.13039/501100011033) and EU by NextGenerationEU/PRTR.

Current- and Oersted-field- dynamics of a Bloch Point in cylindrical Ni nanowires

Jose A. Fernandez-Roldan[1,2,*], Cristina Bran[2], Manuel Vazquez[2], Oksana Chubykalo-Fesenko[2]

[1]*Department of physics, University of Oviedo, Oviedo, Spain.* [2]*Helmholtz-Zentrum Dresden - Rossendorf e.V., Institute of Ion Beam Physics and Materials Research, 01328 Dresden, Germany.*
[3]*Instituto de Ciencia de Materiales de Madrid, ICMM-CSIC, Madrid, Spain.*

*e-mail: j.fernandez-roldan@hzdr.de

As three-dimensional nanomagnetism evolves, novel non-trivial magnetic textures emerge as appealing information carriers for spintronics based on curved nanosystems and particularly Cylindrical Nanowires (NWs) [1,2]. One of the most fascinating candidates that is likely to reach the high velocities required for fast recording technologies is the Bloch Point (BP) domain wall (DW). Recently, theoretical evidence indicated that BPs in NWs could reach high velocities close to 2 km/s in the magnonic regime [2]. While the observation of the BP DW in cylindrical NWs is no longer recent [2], scarce numerical studies that combine both spin-polarized current and Oersted field have been published in NWs [4,5], despite first attempts to measure DW velocities are in progress [6].

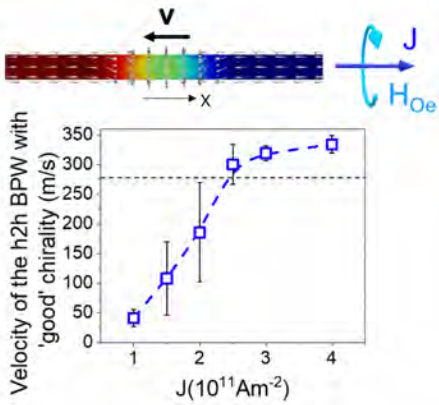

Figure 1. The mean velocity of a head-to-head Bloch Point DW driven by a spin-polarized current in a Ni nanowire as a function of the current density

In this work we evaluate the dynamics of the BP DW under both current directions in a Ni NW with 100 nm in diameter. We investigate two cases: i) pre-nucleated BP DW, and ii) the BP DW formed from the transformation of a Vortex-Antivortex DW. Here the effects of both spin-polarized current and Oersted field are considered. We discuss in detail the role of the chirality of the BP in relation to the Oersted field, also reported previously in precursors of BPs [4].

Here we show that while the pre-nucleated DW with the same chirality as that of the Oersted field propagates always against the current direction, the BP originated either from the transformation of the BP with the opposite chirality or from the vortex-antivortex DW can either stop the propagation or propagate parallel to the current. Finally, we provide values of the velocities achieved by the BP in the NW as a function of applied current in Fig. 1.

We conclude that BPs with vanishing momentum propagate opposite to the current with velocities that may be suppressed by the Oersted field. Importantly for spintronic applications, momentum plays a major role in the dynamics of BPs that has not been envisaged up to know.

[1] A. Fernandez-Pacheco et al., Three-dimensional nanomagnetism. *Nat Commun* **8**, 15756 (2017).
[2] S. Da Col et al., Observation of Bloch-point domain walls in cylindrical magnetic nanowires, *Phys. Rev. B*, **89**, 180405 (2014).
[3] X.-P. Ma et al., Cherenkov-type three-dimensional breakdown behavior of the Bloch-point domain wall motion in the cylindrical nanowire, *Appl. Phys. Lett.* **117**, 062402 (2020).
[4] J.A. Fernandez-Roldan et al., Electric current and field control of vortex structures in cylindrical magnetic nanowires, *Phys. Rev. B* **102**, 024421 (2020).
[5] C. Bran et al, Magnetic Configurations in Modulated Cylindrical Nanowires, *Nanomaterials* **11**, 600 (2021). DOI: 10.3390/nano11030600
[6] M. Schöbitz et al., Fast Domain Wall Motion Governed by Topology and Oersted Fields in Cylindrical Magnetic Nanowires. *Phys. Rev. Lett.* **123**, 217201 (2019).

Role of the particle size in the development of customized permanent magnet composites and flexible filaments for additive manufacturing

Ester M. Palmero*, Daniel Casaleiz, Javier de Vicente, Alberto Bollero

Group of Permanent Magnets and Applications, IMDEA Nanociencia, 28049 Madrid, Spain.

*e-mail: ester.palmero@imdea.org

Multi-material additive manufacturing (AM) is nowadays of large interest in high-technology sectors for fabricating complex high-performance objects with tailored properties [1]. For permanent magnets (PMs), the challenge is to develop magnets by AM with no geometrical restrictions, high loading (i.e., high filling factor, FF), and non-deteriorated PM properties [2], together with finding alternatives (e.g., improved ferrites and the promising MnAlC-based alloys) to rare earth-based magnets [3].

Highly loaded composites (PM particles/polymer) were synthesized by solution casting, followed by extrusion of filaments for 3D-printing by Fused Filament Fabrication (FFF) technology, being reported recently for the very first time (Fig. 1a) [4]. Several alternative PM materials were studied (gas-atomized τ-MnAlC, Sr-ferrite and hybrids -Sr-ferrite/NdFeB). Particle size and fine-to-coarse particles ratio (FP/CP) play a key role on the flexibility and powder loading of MnAlC filaments (length>10 m), reaching FF>80% and non-deteriorated PMs properties [4]. These results will be compared to the obtained for filaments based on Sr-ferrite (coercivity, H_c~3 kOe, FF=92%), NdFeB (H_c=10.2 kOe, FF=83%) and hybrid composites (H_c=8 kOe, FF=90%). MnAlC-based objects were 3D-printed under controlled temperature (Fig. 1a), proving, through magnetic flux density measurements, that alternative PM materials can be efficiently synthesized and processed to develop novel PMs by AM (Fig. 1b) [4].

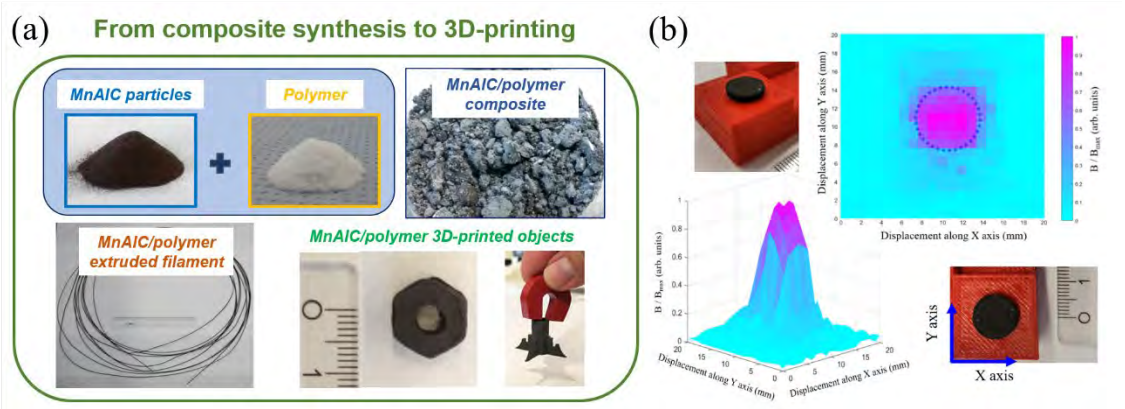

Figure 1. (a) Images of gas-atomized MnAlC particles, polymer, MnAlC/polymer composite, filament and 3D-printed objects; and (b) 3D-printed MnAlC-based disc together with the 3D plot and 2D maps of the magnetic flux density measured at the disc surface.

[1] L.E. Murr, *J. Mater. Sci. Technol.* **32**, 987 (2016).
[2] C. Huber et al., *Appl. Phys. Lett.* **109**, 162401 (2016); J. Jaćimović et al., *Adv. Eng. Mater.* **19**, 1700098 (2017).
[3] A. Bollero et al., *ACS Sustainable Chem. Eng.* **5**, 3243 (2017); J. Rial et al., *Acta Mater.* 157, **42** (2018); J. Rial et al., *Engineering*, **6**, 173 (2020); C. Muñoz-Rodríguez et al., *J. Alloys Compd.* **847**, 156361 (2020).
[4] E.M. Palmero et al., *Sci. Technol. Adv. Mater.* **19**, 465 (2018); *IEEE Trans. Magn.* **55**, 2101004 (2019); *Addit. Manuf.* **33**, 101179 (2020).

Acknowledgements: Authors acknowledge collaborations with B. Skårman, H. Vidarsson and P.-O. Larsson (Höganäs, Sweden) by the industrial contract *GAMMA*, and A. Nieto and R. Altimira (IMA, Spain), and financial support from: MICINN by *NEXUS* project (PID2020-115215RB-C21); EU M-ERA.NET by *COSMAG* project (PCI2020-112143); and CM by *NanoMagCOST* project (P2018/NMT-4321). E.M.P. acknowledges support from AEI through the Juan de la Cierva – Incorporación program (IJC2020-043011-I/MCIN/AEI/10.13039/501100011033) and EU by NextGenerationEU/PRTR.

Electronic band structure of the Co pnictide $Ca(CoAs)_2$ probed by ARPES

David Subires[1,*], L. Sánchez[1], J. Dai[2], M. Tallarida[2], T. Yilmaz[3], E. Vescovo[3], M.Shatruk[4], S. Blanco-Canosa[1,5]

[1]*Donostia International Physics Center (DIPC), E-20018 San Sebastián, Spain.*
[2]*ALBA Synchrotron Light Source, Cerdanyola del Vallès 08290, Catalonia, Spain.*
[3]*NSLS II, Brookhaven National Laboratory, Upton, New York, 11973,USA.*
[4]*Department of Chemistry and Biochemistry, Florida State University, Tallahassee, Florida 32306, USA.*
[5]*IKERBASQUE, Basque Foundation for Science, 48013 Bilbao, Spain.*

*e-mail: david.subires@dipc.org

Topological quantum materials represent an ideal scenario where to study the interplay between different interactions that can manifest interesting micro and macroscopic properties. One of this type of materials are the Weyl semimetals whose low-energy excitations are Weyl fermions. By the bulk-surface correspondence, these materials have topological protected Fermi arcs surface states. The experimental observation of these surface states gives an unequivocal proof that a particular compound is a Weyl semimetal [1]. Here, we report the experimental band structure of the recently predicted magnetic Weyl semimetal [2] Co-pnictide ACo_2X_2 (A = Ca, Ce and X = P, As). We present the angle-resolved photoemission spectroscopy (ARPES) measurements and density functional theory calculations to describe the electronic band structure and the possible existence of Weyl fermions in $Ca\,(CoAs)_2$.

[1] Su-Yang Xu et al., *Science*, **349**, 613-617 (2015).
[2] Yuanfeng, Xu et al., *Nature*, **586**, 702-707 (2020).

Temperature First Order Reversal Curves (TFORC) distributions of magnetocaloric materials

Luis M. Moreno-Ramírez*, Victorino Franco

Dpto. Física de la Materia Condensada, ICMS-CSIC Universidad de Sevilla, Spain.

*e-mail: lmoreno6@us.es

Magnetocaloric (MC) materials, those that experience a significant temperature change when submitted to magnetic field variations in adiabatic conditions, deserve the attention of the magnetic research community due to their implementation on a new energy efficient solid-state cooling technology. The effect is associated to significant magnetization changes driven by temperature and magnetic field, classifying the MC materials according to the order of their thermomagnetic phase transition: first- and second-order type. Typically, the materials undergoing first-order transitions present higher MC response than those with second order ones, although they have associated undesired thermal and magnetic hysteresis, which significantly reduce their response in cyclic conditions, limiting their applicability in refrigeration devices. Therefore, the understanding of the different sources and mechanism of hysteresis is a relevant topic in current research.

First Order Reversal Curve (FORC) distributions of magnetic materials is a well-recognized tool to extract information about magnetic interactions or to fingerprint magnetic materials. Recently, the possibility to use this technique to analyze the thermal hysteresis associated to the first-order magnetocaloric materials has been shown [1]. This so called TFORC technique is based on the analysis of the minor loops of the magnetization (M) in the hysteretic region, defining a certain set of reversal curves. These distributions represent the content of hysterons, which are defined as the elemental thermal hysteresis loop.

In this work, we set the basis for the interpretation of TFORC diagrams by performing a systematic study based on modelling of first-order phase transitions using a phenomenological transformation mechanism and correlating the obtained diagrams with the characteristics of the transition. The use of skewed normal distributions for modelling the transformation process between different phases allows us to calculate reversal magnetization curves. The transformation characteristics explored are: transition temperatures, temperature ranges of the transformations, symmetry/asymmetry between cooling and heating processes and existence of secondary phases. Each of them produces different shapes in the distributions, such as circular, ellipsoidal, semicircular or triangular [2]. In addition, we systematically modified the different distribution parameters to analyze the influence on the reversible magnetocaloric response and to link it to the different obtained TFORC distributions. The simulated results are compared to those of experimental data for a NiMnIn alloy, which allow us to separate the effects on the TFORC distributions of the structural transformation and the temperature dependence of magnetization of the martensitic and austenitic phases [3].

[1] V. Franco et al., *IEEE Magnetics Letters* **7**, 6602904 (2016).
[2] L. M. Moreno-Ramírez et al., *Metals* **10**, 1039 (2020).
[3] Á. Díaz-García et al., *Journal of Alloys and Compounds* **867**, 159184 (2021).

Acknowledgements: Work supported by AEI/FEDER-UE, Spain (grant PID2019-105720RB-I00), US/JUNTA/FEDER-UE, Spain (grant US-1260179), Consejería de Economía, Conocimiento, Empresas y Universidad de la Junta de Andalucía, Spain (grant P18-RT-746) and Sevilla University under VI PPIT-US program. LMMR acknowledges a postdoctoral fellowship from Junta de Andalucía and European Social Fund (ESF).

Magnetic Force Microscopy for biomedical applications

Miriam Jaafar[1,2*], Agustina Asenjo[3]

[1]*Departamento de Física de la Materia Condensada and Condensed Matter Physics Center (IFIMAC), Universidad Autónoma de Madrid, Avda. Francisco Tomás y Valiente 7, 28049 Madrid, Spain.*
[2]*Instituto Nicolás Cabrera, Universidad Autónoma de Madrid, Avda. Francisco Tomás y Valiente 7, 28049 Madrid, Spain.*
[3]*Instituto de Ciencia de Materiales de Madrid (ICMM), Consejo Superior de Investigaciones Cientificas (CSIC), C/Sor Juana Inés de la Cruz, 3, 28049 Madrid, Spain.*

*e-mail: miriam.jaafar@uam.es

Atomic Force Microscopy (AFM) is a powerful technique in biophysics and nanomedicine since it allows imaging and manipulating nanostructures in physiological conditions on a single molecule level [1]. Magnetic Force Microscopy (MFM) [2] is an AFM-based technique where a nanometric magnetic probe is scanned in close proximity to a surface detecting the local magnetic fields gradients near it. MFM has been applied to the study of a variety of magnetic systems, including magnetic nanoparticles. Advantages of MFM include relatively high spatial resolution, simplicity in operation as well as sample preparation. However, artifacts in the magnetic images can have strong impact and need to be carefully verified for a correct interpretation of the results. In general, when imaging magnetic materials with MFM the most typical artifact is the crosstalk between the topography and the magnetic signal. In addition, in some cases electrostatic signal could be also misinterpreted as magnetic information. With MFM we detect the magnetic force gradient between the tip and sample. However, during MFM imaging the tip stray field (sample stray field) can modify the sample (tip moment) configuration. These reversible or irreversible changes can be significant if the sample (tip) is magnetically soft.

Despite the importance of studying magnetic nanostructures with biological applications in physiological conditions, the applicability of MFM to these systems was limited up to now because of the difficulty in developing MFM for detecting magnetic interactions in liquids [3]. This is a consequence of the higher damping forces acting on the cantilever when working in liquid environment, as compared to air, which results in a significant loss of sensitivity of the MFM signal.

In the work presented here, we will explore new ideas combining non-standard MFM operation modes such as Bimodal MFM [4] with the information obtained from the experimental dissipation of energy associated to tip-sample interactions [5,6]. In addition, we will analyse the influence of the chosen cantilever on the obtained MFM signal-to-noise ratio. We will demonstrate that further improvement on the performance can be gained [7] by using magnetic probes fabricated by Focused Electron Beam Induced Deposition (FEBID) growth onto specially designed cantilevers for liquid medium.

[1] Dufrêne Y. F. et al., *Nature Nanotechnology* **12**, 295 (2017).
[2] Kazakova, O.; Puttock, R.; Barton, C.; Corte-León, H.; Jaafar, M.; Neu, V.; Asenjo, A., *J. Appl. Phys*. **125**, 060901 (2019).
[3] P. Ares, M. Jaafar, A. Gil, J. Gómez–Herrero and A. Asenjo, *Small* **11**(36), 4731 (2015).
[4] Gisbert, V.G.; Amo, C.A.; Jaafar, M.; Asenjo, A.; Garcia, R., *Nanoscale* **13**, 2026 (2021).
[5] Jaafar M. and Asenjo A., *Appl. Sci*. **11**(22), 10507 (2021).
[6] Jaafar, M.; Iglesias-Freire, Ó.; García-Mochales, P.; Sáenz, J.J.; Asenjo, A., *Nanoscale* **8**, 16989 (2016).
[7] Jaafar M. et al., *Nanoscale* **12**, 10090(2020).

Energía y Sostenibilidad

Presentaciones orales

Martes 12/07:

15:30-16:10 Víctor A. de la Peña O'Shea (Instituto IMDEA Energia). *Solar fuels by artificial photosynthesis: from inorganic to hybrid multifunctional materials*

16:10-16:30 Judit García Ferrero (Universidad de Salamanca). *Brayton cycle coupled to CSP plants: comparative analysis of central tower and parabolic dish farms*

16:30-16:50 Francisco Cuadros Blázquez (Universidad de Extremadura). *Secuestro de Carbono en una Planta Híbrida Biogás-Fotovoltaica Seguida de un Proceso de Compostaje*

17:00-18:00 **Pósteres y café**.

18:00-18:40 Mercedes Ballesteros Perdices (CIEMAT). *Aportaciones desde el sector energético a la lucha contra el cambio climático*

18:40:19:00 Alberto Sánchez González (Universidad Carlos III). *Flux mapping in heliostat fields: Analytic function with astigmatism and defocus*

19:00-19:20 Youssouf Doumbia (Universitat Politécnica de València). *Investigation of the stability and efficiency of MA-doped FAPbBr3 thin film for solar cells*

Miércoles 13/07:

15:30-16:10 Carlos del Cañizo Nadal (Instituto de Energía Solar, Universidad Politécnica de Madrid). *Improving the quality of solar grade silicon through defect engineering*

16:10-16:30 Joeluis Cerutti Torres (Universidad Politécnica de Madrid). *Into an accurate and low computational cost prediction of bandgaps in Copper based delafossite oxides: a DFT and ML study with experimental comparison*

16:30-16:50 Klègayéré Emmanuel Koné (Universitat Politécnica de València). *Insight of ZnO/CuO and ZnO/Cu2O solar cells efficiency with SCAPS simulator*

17:00-18:00 **Café**.

18:00-18:20 Amal Bouich (Universitat Politécnica de València). *Opportunities and Challenges of Lead-Free Perovskite for high efficiency and stable solar cells with a low-cost technique*

18:20-18:40 Armel Ignace N'Guessan (Universitat Politécnica de València). *Enhanced the CIGS solar cell efficiency through structural engineering at the buffer/CIGS interface*

18:40-19:00 Pablo Sanchez Palencia Vallejo (Instituto de Energia Solar, Universidad Politécnica de Madrid). *The compositional and configurational space of spinel nitride solid solutions: accelerated exploration of electronic properties through machine learning*

19:00-19-20 Roberto Gómez-Calvet (Universidad Europea de Valencia). *The 2030 power sector transition in Spain: advantages and drawbacks of massive deployment of solar photovoltaic sources*

Pósteres

- Pablo Palacios Clemente (Universidad Politécnica de Madrid, Instituto de Energía Solar). *Assessing composition engineering as mechanism to deal with stability and toxicity problems of inorganic halide perovskites with improved absorption features for photovoltaic applications*
- Antonio Angel Moya Molina (Universidad de Jaen). *Charge and energy stored in electric double layer capacitors from potentiostatic discharge*
- Victoria Beltran (Universidad Politécnica de Cartagena). *Artificial Intelligence Applied to the Prediction of Module Temperature for Building-Integrated Photovoltaic*

Solar fuels by artificial photosynthesis: from inorganic to hybrid multifunctional materials

Víctor A. de la Peña O'Shea

[1]*Photoactivated Processes Unit IMDEA Energy Institute, Technological Park of Móstoles, Av. Ramón de la Sagra 3, 28935 Móstoles, Madrid, Spain.*

e-mail: *victor.delapenya@imdea.org*

The continuing rise in atmospheric CO_2 levels has become one of the most enduring problems faced by humankind. Finding sustainable ways to turn CO_2 into valuable products is imperative to mitigate global warming and to provide a long-term solution to the growing energy demand. Solar energy is the largest exploitable renewable energy source. By mimicking nature, the scientific community has devoted great efforts to develop different technologies such as artificial photosynthesis (AP), where solar energy and natural resources can be directly converted into renewable and carbon-neutral fuels and chemicals.

Photocatalytic materials have focused on the use of inorganic semiconductors such as metal oxides and chalcogenides. In this work, different strategies to modulate the light response and improve the charge separation and transport such as: (i) The modification of optoelectronic properties of through the use of band gap engineering strategies, allow controlling the absorption of incident photons, redox capabilities and subsequently the photocatalytic performance; (ii) the use of co-catalysts play an important role in the selectivity; (iii) the design of multijuntions materials such as hybrid composed by a mixture of inorganic and organic semiconductors. In the case of organic one, the development of conjugated porous polymers have recently attracted significant attention as promising photocatalysts for solar fuel generation. The synergy between organic and inorganic semiconductors results in an extended light absorption range, improved textural properties and higher stability to photo-corrosion. Interestingly, these hybrid heterostructures can effectively facilitate the charge transfer and reduce the recombination of photogenerated electrons and holes, resulting in enhanced photocatalytic performances.

A deeper understanding of the reaction mechanism is crucial to achieve real progress in the development of the AP process, directly impacting on the advance of solar fuels technologies and multitude of light-driven reactions. However, this is a complex issue that involves multielectronic reactions occurring at different timescales (i.e. fs-s). In order to clarify the effect of different parallel and competitive reactions in the activity and products distribution, advanced in-situ characterization and theoretical calculations were performed to clarify the reaction mechanism of these systems.

[1] Collado L., Reñones P., Fermoso J., Fresno F., Garrido L., Pérez-Dieste V., Escudero C., Hernández-Alonso M. D, Coronado J. M, Serrano D.P, de la Peña O'Shea V. A. *Appl. Catal. B: Environ.* 120931 (2022).
[2] L. Collado, A. Reynal, F. Fresno, M. Barawi, V. Perez Dieste, C. Escudero, J. M. Coronado, D. Serrano, J. Durrant, V. A. de la Peña O'Shea. *Nat. Commun.* **9**, 4986 (2018).
[3] Barawi M., Collado Laura, Gomez-Mendoza M., Oropeza F. E, Liras M., de la Peña O'Shea V. A. *Adv. Energy Mater*. **11**(43), 2101530 (2021).
[4] García-Sánchez A., Gomez-Mendoza M., Barawi M., Villar-Garcia IJ., Liras M., Gándara F., de la Peña O'Shea V. A. *J. Am. Chem. Soc.* **142**(1), 318 (2020).
[5] Liras, M Barawi, V. A. de la Peña O'Shea, *Chem. Soc. Rev*. **48**, 5454 (2019).
[6] Collado L., Naranjo T., Gomez-Mendoza M., López-Calixto C. G, Oropeza F. E, Liras M., Marugán J., de la Peña O'Shea *V. Adv. Funct. Mater.* **31**(51), 2170376 (2021).
[7] Fresno F.; Villar-García, I.; Collado, L.; Alfonso-Gonzalez, E.; Reñones, P.; Barawi, M.; de la Peña O'Shea, V. A *J. Phys. Chem. Lett.* **9**, 7319 (2018).

Acknowledgements: This work has also received funding from the European Research Council (ERC) under the European Union's Horizon 2020 research and innovation program (HyMAP project, grant agreement No. 648319) and FET-PROACT HYSOLCHEM project, Agreement number PR00312). Financial support has also been received from AEI-MINECO/FEDER, UE through the Nympha Project (PID2019-106315RB-I00), and Lineas Estrategicas programme (SOLFTURE).

Brayton cycle coupled to CSP plants: comparative analysis of central tower and parabolic dish farms

Judit García-Ferrero[1], Rosa P. Merchán[1], M.J. Santos[1], A. Medina[1], A. Calvo Hernández[1]

[1]*Departmento de Física Aplicada e Instituto de Física Fundamental y Matemáticas (IUFFYM), Universidad de Salamanca, 37008, Salamanca, España.*

*e-mail: jgferrero@usal.es

Solar energy is one of the most promising alternative energy sources. Particularly, Concentrated Solar Power (CSP) technology has the potential to provide not only electrical but also thermal energy. CSP systems are highly flexible to be configurated in multiple ways: hybridized with fuel (conventional or renewable) for dispatchable generation, coupled with thermal energy storage or even hybridized with other renewable energy systems as PV.

Two different Concentrated Solar Power (CSP) technologies are analyzed from a thermodynamic and thermo-economic perspective. A Central Solar Tower (ST) plant and an array of Parabolic Dishes (PD) performing a single-stage recuperative Brayton cycle are compared for two power outputs (4.6 MW and 20 MW) and different locations placed approximately at the same longitude and quite different latitudes in a south-north line: Ouarzazate (Morocco), Seville and Salamanca (both in Spain). While the ST counts with a Brayton cycle turbine in the range of MW, each PD that compounds the farm integrates a micro-gas turbine in other to achieve the power outputs mentioned above. The power block is hybridized with a combustion chamber aiming to supply energy under lack of solar irradiance conditions. The thermodynamic model for each system is further developed in previous works [1], including all the subsystem efficiencies and losses. Aiming to compare the two CSP systems from the thermo-economic viewpoint, a set of economic indicators such as the Levelized Cost of Electricity (LCoE), Net Present Value, Benefit to Cost Ratio and Internal Rate of Return are surveyed.

In regard of thermodynamics, some results should be pointed out. Among the locations studied, Ouarzazate presents the maximum solar records, yielding to the highest annual solar share, specially for 20 MW scale (0.54 for ST and 0.76 for PD). But it is important to note that overall plant thermal efficiency is greatly influenced by ambient temperatures. Thus, northern locations as Salamanca, with relatively poorer solar conditions, but with lower ambient temperatures, allow good overall efficiencies. For ST, overall and heat engine efficiencies overpass PD results by 35% for all the locations and power scales. Regarding thermo-economic indicators, Fig. 1 depicts the LCoE outputs obtained for all cases studied. The best LCoE is achieved by ST at 20 MW power scale in Ouarzazate (135 USD/MWh) and the worst result is presented by PD, 4.6 MW, in Salamanca (203.5 USD/ MWh). These values are in the range of other CSP projects including stand-alone PD and thermal storage ST geometries [2].

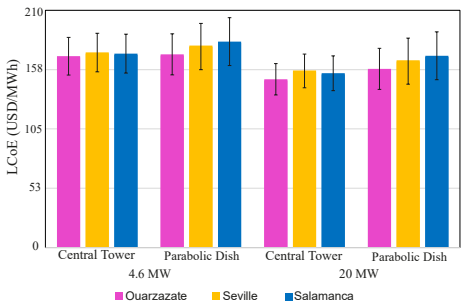

Figure 1: Levelized Cost of Electricity (LCoE) results for ST and PD technologies, three locations and two power scales (4.6 MW and 20 MW).

Although this study proves that this kind of technology is feasible and bankable, more research is needed in order to lower costs, reach economic indicators comparable to other renewable technologies, and promote a solid integration of CSP systems into the market.

[1] J. García-Ferrero, I. Heras, M. J. Santos, R. P. Merchán, A. Medina, A. González, A. Calvo Hernández, Thermodynamic and Cost Analysis of a Solar Dish Power Plant in Spain Hybridized with a Micro-Gas Turbine, *Energies* **13**, 5178 (2020).

[2] R. P. Merchán, M. J. Santos, A. Medina, A. Calvo Hernández. High temperature central tower plants for concentrated solar power: 2021 overview, *Renewable and Sustainable Energy Reviews* **155**, 111828 (2022).

Acknowledgements: Rosa P. Merchán acknowledges financial support from University of Salamanca and Banco Santander.

Secuestro de Carbono en una Planta Híbrida Biogás-Fotovoltaica Seguida de un Proceso de Compostaje

Francisco Cuadros Blázquez[1,*], Consolación Sánchez Sánchez[1], Almudena González González[2], Francisco Cuadros Salcedo[2]

[1]*Departamento de Física Aplicada, Escuela de Ingenierías Agrarias, Universidad de Extremadura, Avda. de Elvas s/n, 06006 Badajoz.*
[2]*Metanogenia S.L. Avda. de Elvas, s/n, 06006. Badajoz.*

*e-mail: cuadros1@unex.es

Actualmente, en España el destino mayoritario de todos los residuos sólidos urbanos e industriales es el vertedero. Las otras vías de gestión posibles, mucho más recomendables desde el punto de vista energético y medioambiental, como son el reciclaje o la valorización material o energética, si bien han ido aumentando su implantación en los últimos años, representan aún unos niveles muy por debajo de la media de la Unión Europea. Concretamente, el 24,32% en España frente al 36% de media en Europa [1], [2].

En regiones como Extremadura, donde el peso del sector agroindustial es muy importante, es necesaria la implantación de tecnologías biológicas de tratamiento de los residuos que generan, ya que contienen un alto poder contaminante. En efecto, varios estudios realizados previamente por el Grupo de Investigación DTERMA de la Universidad de Extremadura (al cual pertenecen dos de los autores de la presente comunicación) indican que la contaminación anual producida solo por las industrias almazarera, vitivinícola, tomatera y de matadero de cerdos es equivalente a la generada anualmente por la población residente en nuestra región.

Dicho Grupo de Investigación ha publicado varios trabajos sobre la viabilidad energética, económica y medioambiental de la Biometanización (o Digestión Anaerobia, DA) de los residuos agroindustriales en Extremadura, cuantificando el secuestro de carbono provocado en dicho proceso (ver, por ejemplo, [3]) Sin embargo, el contenido de carbono del residuo tratado mediante DA no se acaba aquí, es necesario enlazar a continuación con un proceso de compostaje del digestato (fracción sólida del efluente obtenido tras la DA), de modo que se cierre el ciclo ecológico completo del carbono “desde la cuna hasta la tumba”.

En este trabajo se presentan los resultados obtenidos sobre el secuestro de carbono obtenido en la codigestión de un 90 % de residuos de la industria láctea (lactosuero) y de un 10% de estiércol de oveja llevada a cabo en una planta piloto de unos 2 m^3 de capacidad del biodigestor, alimentada eléctricamente con una instalación fotovoltaica de unos 0,5 kWp. Después de la DA se ha continuado con el compostaje de la fracción sólida del efluente digerido (40% del total), hasta obtener un enmendante agrícola de gran calidad. La fracción líquida (el 60% restante) se ha analizado y se ha comprobado que es apta para su uso en riego de frutales cuyo fruto no entre en contacto con ella o en riego de forrajes para alimentación animal, cerrando así el ciclo de vida del residuo inicial.

[1] España Circular 2030. Estrategia Española de Economía Circular (2018). Ministerio de Agricultura y Pesca, Alimentación y Medio Ambiente. Ministerio de Economía, Industria y Competitividad.
[2] IDAE (2011). Situación y Potencial de Valorización Energética Directa de Residuos. https://www.idae.es/uploads/documentos/documentos_11227_e15_residuos_c3ead071.pdf.
[3] Cuadros Blázquez, F., González González, A., Sánchez Sánchez, C., Díaz Rodríguez, V., Cuadros Salcedo, F. *Journal of Cleaner Production* **181**, 136 (2018).

Agradecimientos: Los autores agradecen a la Junta de Extremadura y a la Unión Europea (Fondos FEDER) la ayuda concedida para la realización de este trabajo. Ref. Proyecto: GR21012.
Consolación Sánchez Sánchez agradece a la Junta de Extremadura y al Fondo Social Europeo (FSE) por el apoyo financiero recibido a través de la ayuda destinada a la formación de personal predoctoral PD18050.

Aportaciones desde el sector energético a la lucha contra el cambio climático

Mercedes Ballesteros

Departamento de Energía- CIEMAT Avda. Complutense, 40 29040 Madrid, España.

e-mail: m.ballesteros@ciemat.es

Los esfuerzos mundiales realizados, hasta la fecha, para mitigar el cambio climático culminaron en el Acuerdo de París de 2015, en virtud del cual 195 países adoptaron el primer acuerdo, universal y vinculante jurídicamente, para mantener el incremento de la temperatura media mundial por debajo de 2 °C y seguir esforzándose por limitar el aumento a 1,5 °C. Este objetivo climático es tremendamente ambicioso y, teniendo en cuenta que la producción de electricidad y el transporte son responsables del 70% de las emisiones de gases de efecto invernadero [1], no podrá alcanzarse sin una reforma importante de los sistemas de producción y consumo de energía a escala mundial.

Existe consenso a nivel mundial en considerar que el modelo energético actual, basado en el crecimiento del consumo y en el uso de recursos fósiles, es insostenible, tanto por los riesgos relativos a la seguridad de suministro como por su contribución al cambio climático. La UE, comprometida con los Acuerdos de París, ha considerado que la descarbonización del sector de la energía constituye un paso crucial para la neutralidad climática de la UE y por ello, a finales del 2018 el Consejo europeo aprobó el denominado Paquete de Energía Limpia para todos los europeos (también conocido como "paquete de invierno") [2], orientado a alcanzar los objetivos climáticos europeos a 2030 (al menos 55% de reducción), manteniendo la seguridad de suministro y la competitividad de los precios de la energía.

Para cumplir estos objetivos, el reglamento de gobernanza establece que todos los Estados miembros deben elaborar su Plan Nacional Integrado de Energía y Clima (PNIEC) para el período de 2021 a 2030. Los PNIECs, además de fijar los objetivos de reducción de emisiones de gases de efecto invernadero y de penetración de renovables y eficiencia y ahorro energético, incluyen objetivos nacionales de financiación, así como objetivos para implementar tecnologías bajas en carbono en 2050.

El PNIEC español fue aprobado por el Consejo de Ministros el 16 de marzo de 2021 y publicado en el BOE de marzo del mismo año [3]. El PNIEC identifica objetivos y adopta medidas en las cinco dimensiones de la Unión de la Energía: la descarbonización, incluidas las energías renovables; la eficiencia energética; la seguridad energética; el mercado interior de la energía y la investigación, innovación y competitividad. Entre otras medidas, se prevé el impulso de la instalación de potencia de producción de origen renovable, cuya distribución concreta por tecnologías renovables dependerá de la evolución de los costes relativos de cada una de ellas; el cese total de la actividad de centrales de carbón como máximo en 2030; el impulso de las tecnologías de almacenamiento, así como del coche eléctrico y del uso de biocarburantes

En esta ponencia se presentará el conjunto de objetivos y compromisos de la Unión Europea para la descarbonización del sector energético y se analizan las principales características del PNIEC español.

[1] IEA. *Greenhouse Gas Emissions from Energy: Overview, Statistics report*, August 2021
[2] Directorate-General for Energy (European Commission). *Clean energy for all Europeans*. July 2019. https://data.europa.eu/doi/10.2833/21366.
[3] BOE-A-2021-5106. 31 de marzo de 2021. https://www.boe.es/diario_boe/txt.php?id=BOE-A-2021-5106.

Flux mapping in heliostat fields: Analytic function with astigmatism and defocus

Alberto Sánchez-González

Department of Thermal and Fluids Engineering, Universidad Carlos III de Madrid, Spain.

e-mail: asgonzal@ing.uc3m.es

Thousands of mirrors, called heliostats, track the sun and concentrate solar energy into a central receiver atop a tower in Solar Power Tower (SPT) plants. Sunray incidence on the mirror is not normal, leading to off-axis aberrations or astigmatism, that distort the flux distribution on the target [1]. This work presents a flux mapping model that reproduces the aberrations due to heliostat defocus and astigmatism.

There are two flux mapping approaches: Monte Carlo Ray-Tracing (MCRT) and convolution. The convolution method, faster than MCRT, produces analytic functions from the superposition of error cones (concentration, sunshape, and optical errors). However, the existing analytic functions disregard the effect of astigmatism, which is relevant in actual plants.

Depending on the defocus distance from the circle of least confusion (δ), Igel and Hughes [2] stated the geometric relationships between tangential and sagittal planes. These correlations have been introduced in UNIZAR analytic function [3], which is valid for unusual, focused heliostats ($\delta = 0$).

The following proposed analytic function computes the concentration ratio of flux density (C) as a function of ξ and ζ, heliostat coordinates on the image plane, where *erf* stand for the Gaussian error function and *aw* and *ah* are the integration limits.

$$C = \frac{\cos\omega}{J} \cdot 0.25 \cdot [erf\,(\xi + aw) - erf\,(\xi - aw)] \cdot [erf\,(\zeta + ah) - erf\,(\zeta - ah)]$$

The proposed analytic function is validated against MCRT simulations. For instance, for incidence angle $\omega = 60°$, Figure 1 compares both flux maps for several δ defocus planes.

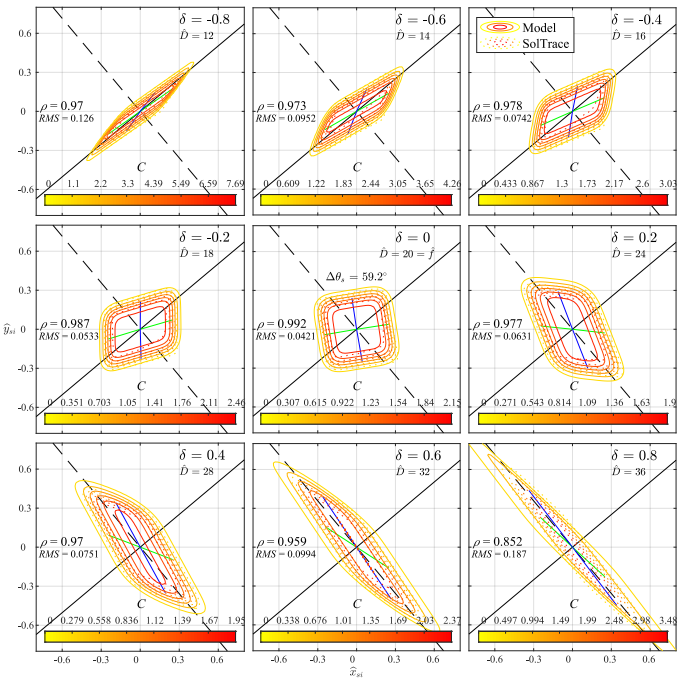

Figure 1. Concentration maps by the model (solid lines) and MCRT (dotted) for several δ defocus distances.

For Gemasolar plant, consisting of 2650 heliostat and a 18-panel cylindrical receiver, the following Figure 2 shows the flux map at 8:30 solar time in the Equinox.

In comparison with MCRT Cross-correlation coefficients above 90% are achieved with the proposed analytic function.

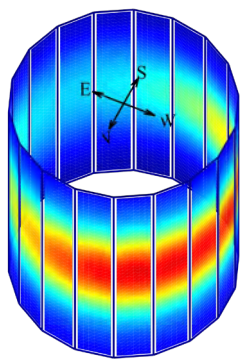

Figure 2. Flux map on receiver by Gemasolar heliostat field.

[1] F. Henault, *Solar Energy* **112**, 183 (2015).
[2] E. Igel, R. Hughes, *Solar Energy* **22**, 283 (1979).
[3] F.J. Collado et al., *Solar Energy* **37**, 215 (1986).

Investigation of the stability and efficiency of MA-doped $FAPbBr_3$ thin film for solar cells

Youssouf Doumbia[1,*], Amal Bouich[2], Donafologo Soro[3], Bernabé Mari[4]

[1,3,4]*Institut de Disseny per a la Fabricació i Producció Automatitzada, Universitat Politècnica de València.*
[2]*Département des Sciences et Technologie,Ecole Normale Supérieure (ENS) d'Abidjan Côte d'Ivoire.*

*e-mail: doumbiayoussouf59@yahoo.fr

Organometal halide perovskite solar cells are becoming one of the most competitive emerging technologies. They have achieved a power conversion efficiency (PCE) of 22.7% in 10 years. They generally have excellent efficiency but low stability. This degradation of perovskite devices has been associated with mobile ion migration. The $MAPbBr_3$ perovskite materials are significantly more stable under ambient conditions but have a more significant bandgap (2.3 eV) than the $FAPbBr_3$ perovskite materials, which are interesting bandgap. This work uses a mixture of these two materials with a high proportion of $FAPbBr_3$ to obtain a stable active layer with a suitable bandgap by the one-step spin-coating method. We used a ratio of 6% of MA in the mixture to prepare the layer. In addition, the prepared layer was annealed for 30 min at 100°C.

We found intermediate properties as expected, notably the stability and the bandgap, whose value is 1.93 eV. Indeed, the degradation process of the prepared thin film is slower than that of pure $FAPbBr_3$. The absorption of the mixture is suitable for use in photovoltaics.

Improving the quality of solar grade silicon through defect engineering

Carlos del Cañizo

[1]*Instituto de Energía Solar – Universidad Politécnica de Madrid. ETSI Telecomunicación, Avenida Complutese, 30. 28040 Madrid – Spain.*

e-mail: carlos.canizo@upm.es

A large fraction of the carbon footprint of a PV module comes from the silicon ultrapurification step. It takes 99% pure metallurgical silicon and ultrapurifies it to 99,9999999% or more, resulting in a product referred to as polysilicon, which is used to feed the crystal growers. The conventional purification process converts the metallurgical silicon to trichlorosilane, which is distilled and converted back to silicon in a Siemens-type reactor. A huge investment in electricity and cooling is needed, with energy demand in the range of 50-75 kWh/kg. Alternative purification routes that avoid the transformation to chlorosilanes by applying metallurgical-like methods are under research. The silicon feedstock produced this way, the so-called Upgraded Metallurgical Grade Silicon (UMG), besides being cheaper, requires less energy for its manufacture, in the range of 30 kWh/kg, resulting in a clear environmental benefit.

The challenge for UMG is to demonstrate that the electronic quality of the material is not ultimately limited by its purity, so that the beneficial impact "per kg" is also maintained as "per watt". In this respect, the presence of foreign elements and impurities in UMG-silicon in larger amounts than in standard polysilicon is at first sight a major handicap. However, a careful and precise mitigation of their eventual detrimental effects by means of impurity compensation and defect engineering carried out during the manufacturing process and the cell fabrication stage has demonstrated comparable levels of electronic quality between polysilicon and a novel UMG-Si developed by a Spanish company [1].

In this work, the quality of UMG-Si is characterized with a number of advanced techniques, including Photoconductance-based lifetime measurements. As an example, figure 1 shows carrier lifetime values after an optimized phosphorus diffusion gettering (PDG) process, reaching values higher than 200 µs for wafers coming from different ingots, bricks and heights in the brick. The possibility of implementing a second PDG process has also been studied, concluding that it is generally beneficial over a relatively wide range of experimental parameters, and that it allows to obtain a record value of 645 µs.

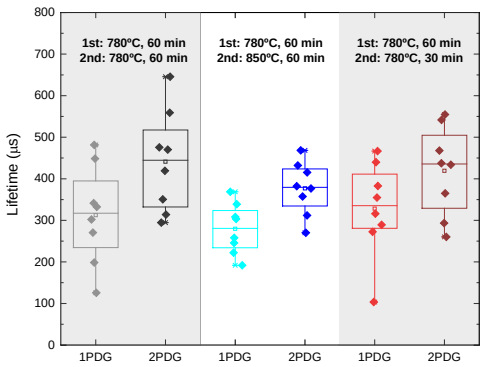

Figure 1. Lifetime values at 10^{15} cm^{-3} injection level obtained from UMG-Si wafers after PDG processes under the specified conditions.

These values are above the threshold value required to achieve >21% efficiency in state-of-the-art PERC solar cell structures [2].

In this work we will also explore a fabrication route for UMG-Si advanced solar cells, with the purpose of obtaining high-efficiency, low cost and more environmentally-friendly devices.

[1] E. Forniés *et al.*, *Solar Energy* **220**, 354 (2021).
[2] A Hofstetter *et al.*, *Prog. Photovolt. Res. Appl.* **24**, 122 (2016).

Acknowledgements: MCIN/ AEI /10.13039/501100011033 is acknowledged for funding the Project PID2020-113533RB-C31. This work is also part of the Project MADRID-PV2 (S2018/EMT-4308) funded by the Regional Government of Madrid with the support from FEDER Funds.

Into an accurate and low computational cost prediction of bandgaps in Copper based delafossite oxides: a DFT and ML study with experimental comparison

J. Cerutti Torres[1,*], P.Sanchez-Palencia[2,3], A. Bouich[1,4], B. Marí[4], P. Palacios[1,3]

[1] *Departamento de Física Aplicada a las Ingenierías Aeronáutica y Naval. ETSI Aeronáutica y del Espacio, Universidad Politécnica de Madrid, Pz. Cardenal Cisneros, 3, 28040 Madrid, Spain.* [2] *Departamento de Tecnología Fotónica y Bioingeniería, ETSI Telecomunicación, Universidad Politécnica de Madrid, Ciudad Universitaria, s/n, 28040 Madrid, Spain.* [3] *Instituto de Energía Solar, ETSI Telecomunicación, Universidad Politécnica de Madrid, Ciudad Universitaria, s/n, 28040, Madrid, Spain.* [4] *Institut de Disseny I Fabricació, Universitat Politècnica de València, València, Spain.*

*e-mail:j.ctorres@upm.es

Copper based delafossite oxides of the form $CuMO_2$ have been reported as promising candidates for transparent conducting oxides (TCOs) materials in the construction of solar cell devices, among other applications based on their optical and electronical properties [1]. We report density functional theory simulations on the compounds of the form $CuMO_2$ with $M = Al, Ga, Fe, Cr, Ni, Co$, and compare them with experimental results. For the calculations GGA, GGA+U and HSE schemes were tested, and their results compared. The use of hybrid functionals in HSE approximation improves considerably the bandgaps when compared with the experimental results but takes considerable time to converge. Therefore, using the projected DOS for the different elements in HSE simulations, different GGA+U were performed to obtain the parameter U that more accurately placed the d orbitals of the transition metals in the valence band. Having the bands accurately described in a GGA+U scheme, other optical calculations with a reasonable computational cost and an acceptable accuracy can be performed. Lastly, machine learning is used to estimate the bandgaps of mixed delafossite compounds of the form $\mathrm{CuM}_x\mathrm{N}_{1-x}\mathrm{O}_2$ being M, N the same metals previously mentioned.

[1] H. Shaili *et al*, *RSC Adv.* **11**, 25686 (2021).

Insight of ZnO/CuO and ZnO/Cu_2O solar cells efficiency with SCAPS simulator

Klègayéré Emmanuel Koné[1,*], Amal Bouich[1], Donafologo Soro[2], Bernabé Mari Soucasse[1]

[1]*Departament de Física Aplicada, Instituto de diseño y Fabricación (IDF)-Universitat Politécnica de València (UPV), Camí Vera, Spain.*

[2]*Département des Sciences et Technologie, Ecole Normale Supérieure (ENS) d'Abidjan, Cocody, Côte d'Ivoire.*

*e-mail: koneemmanuel277@gmail.com

Despite the low power conversion efficiency of ZnO/CuO and ZnO/Cu_2O solar cells, these cells are promising devices for photovoltaic applications. In order to optimize their yields, we used the SCAPS-1D program to perform simulations of n- ZnO/p-CuO and n-ZnO/p-Cu_2O thin-film solar cells (Figure 1) by varying certain parameters [1,2,3]. Its parameters which were thickness, bandgap, electron affinity, relative dielectric permitivity, shallow uniform donor density ND, shallow uniform acceptor density NA etc. The short circuit current and efficiency were 28.39 mA.cm^{-2}, 10.44 mA.cm^{-2} and 28.42 %, 16.38 % respectively for cells n- ZnO/p-CuO and n-ZnO/p-Cu_2O (Figure 2). Our results reveal that the n- ZnO/p-CuO solar cell is more efficient than the n-ZnO/p-Cu_2O solar cell and can be used to convert solar energy into electricity.

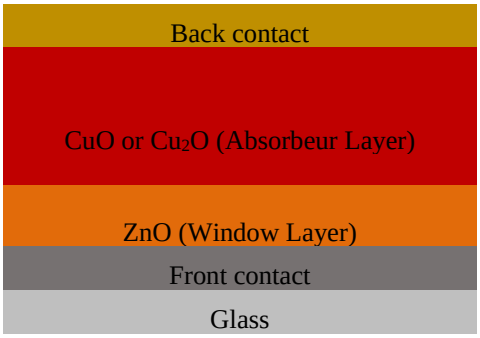

Figure 1. Structure of the solar cell.

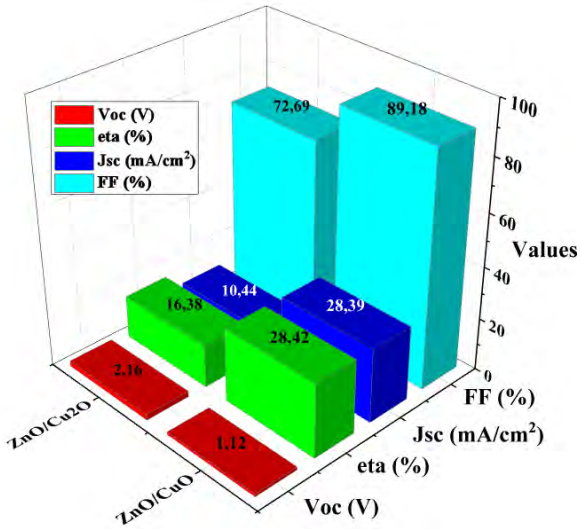

Figure 2. Characteristics parameters of solar cell.

[1] Nguyen Dinh Lam, Modelling and numerical analysis of ZnO/CuO/Cu_2O heterojunction solar cell using SCAPS, *Eng. Res. Express* **2**, 025033 (2020).

[2] Hussain S, Cao C, Usman Z, Chen Z, Nabi G, Khan WS and Mahmood T, Fabrication and photovoltaic characteristics of Cu_2O/TiO_2 thin film heterojunction solar cell, *Thin Solid Films* (2012)

[3] Sawicka-Chudy P, Sibiński M, Wisz G, Rybak-Wilusz E and Cholewa M, Numerical analysis and optimization of Cu_2O/TiO_2, CuO/TiO_2, heterojunction solar cells using SCAPS, *Journal of Physics* (2018).

Opportunities and Challenges of Lead-Free Perovskite for high efficiency and stable solar cells with a low-cost technique

Amal Bouich[1,*], Julia Mari Guaita[2], Bernabé Mari[1], Pablo Palacios

[1]*Instituto de Diseño y Fabricación (IDF), Universitat Politècnica de València (UPV), Spain.* [2]*Física Aplicada a las Ingenierías Aeronáutica y Naval & Instituto de Energía Solar, Universidad Politécnica de Madrid, Madrid, Spain.*

*e-mail: bouich.amal@gmail.com

Lead-Free Perovskite is n-type semiconductor material considered a potential candidate with a tunable bandgap used as absorber layer solar cells. The MASn1-xPbxI3 samples were successfully prepared by the solution mixed spin coating technique. The XRD analysis revealed the polycrystalline nature of the films. It observed from the morphology that the homogeneity of the films very corresponds to replace Pb with Sn. The AFM analysis showed the big grain and the rough surface of the films. The optical absorption indicates a remarkable shift to the lower wavelength and the optical band gap was found to vary from 1.82 to 1.8 eV with V- doped contents. The measured intensity of the PL peak in MAPbSn3 films is about 30% higher than in MAPbI3 films. We manufacture the Device Manufacture Spiro- OmeTAD/MASnI3/TiO2/FTO where Voc=0.887 V, Jsc=14.02 mA/cm2, FF=83.72% and eta=10.42%. In perovskite-based devices using MASnI3 as an absorber, it was found to be more stable despite of its lower efficiency, which could be improved by enhancing the bandgap alignment of MaSnI3. The results also allow the development of a new, reliable production system for PSCs.

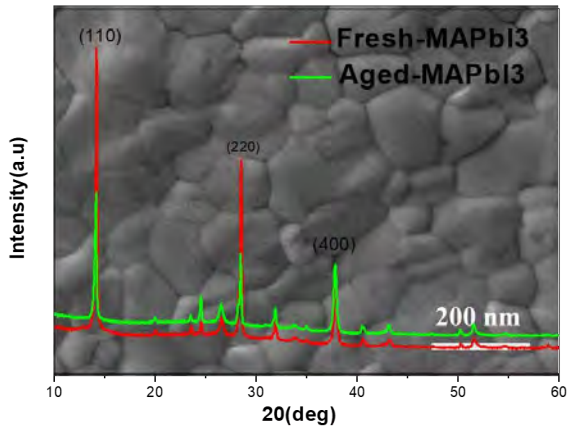

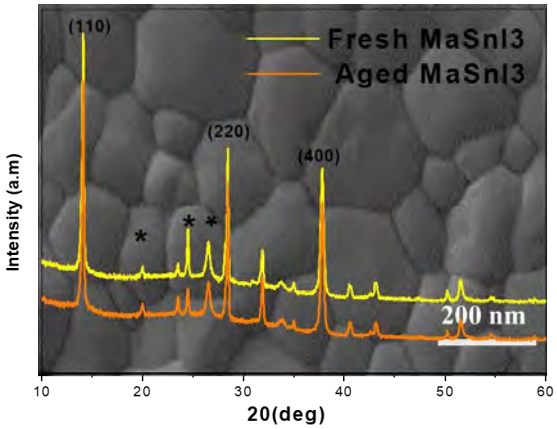

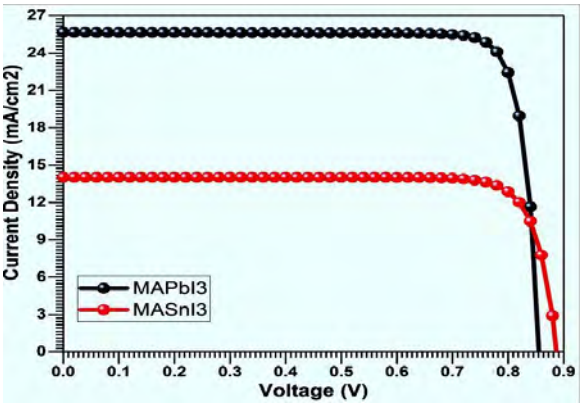

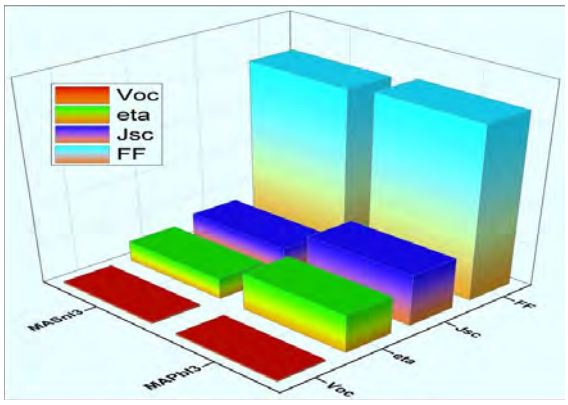

CIGS solar cell efficiency enhanced by structural engineering at buffer/CIGS interface

Armel Ignace N'guessan[1,*], Amal Bouich[1], Donafologo Soro [2], Bernabé Mari[1]

[1]*Instituto de Diseño y Fabricación (IDF), Universitat Politécnica de València (UPV), Spain.*
[2]*Département des Sciences et Technologie, Ecole Normale Supérieure (ENS) d'Abidjan, Côte d'Ivoire.*

*e-mail: amosphysique07@gmail.com

For CIGS-based solar cells with the following structure (ZnO/buffer/p-CIGS/back contact) the most influential interfaces are the (buffer/CIGS) and (CIGS/back contact) interfaces.

In this study we present the results of the numerical simulation of our heterojunction thin film solar cell based on CIGS with two buffer layers less toxic than CdS: $ZnO_{1-x}S_x$ and SnS_2. The SnS_2 in addition to being non-toxic has electrical properties close to CdS such as gap and electronic affinity. $ZnO_{1-x}S_x$ has the advantage of having a variable gap, which allows the discontinuity of the band structure at the buffer/CIGS interface to be modified.

From the optimized Zn(O,S) layer parameters by varying the sulphur content in $ZnO_{1-x}S_x$, we vary the thickness, the carrier concentration of both absorber and buffer layers and propose an structure of our solar cell. The calculations are performed keeping the other parameters constant and considering a p-CIGS/p+-$MoSe_2$/Mo back contact with a work function of the metal Mo = 5.49 eV and a forward reflection R = 5%, using the SCAPS software.

The optimization of the Zn(O,S) buffer layer leads to a sulfur composition S/(O+S) ratio of 0.79 with more enhanced performance for the $Zn(O_{0.30}S_{0.79})$/GIGS contact. Above 0.79 the performance of the solar cell is affected depending on its thickness and carrier concentration. The results after stimulation show that the performance of CIGS-based solar cells with $Zn(O_{0.30}S_{0.79})$ and SnS_2 as the buffer layers are slightly different in terms of efficiency with 23.54% and 23.44% respectively. In addition, there is a difference in the open circuit voltage (Voc) and short current (Jsc) due to the reduction of interface recombination at the $Zn(O_{0.30}S_{0.79})$/CIGS interface and the type of band structure at the buffer/CIGS interface.

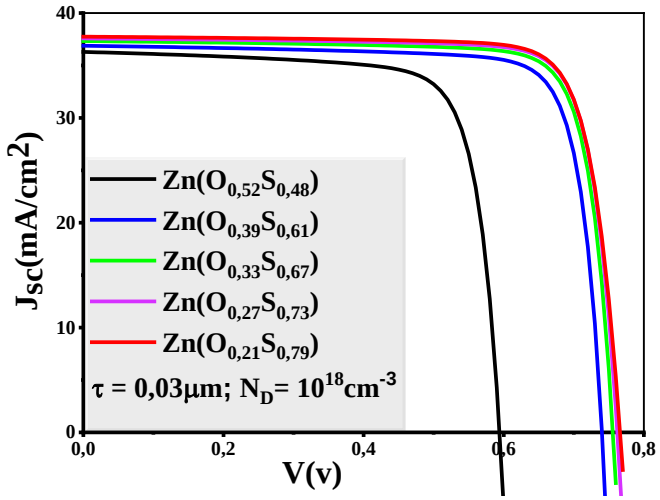

Figure 1. *J -V* curve of S/(S+O) composition ratio.

The compositional and configurational space of spinel nitride solid solutions: accelerated exploration of electronic properties through machine learning

Pablo Sánchez-Palencia[1,2,*], Said Hamad[3], Pablo Palacios[1,4], Ricardo Grau-Crespo[5], Keith T. Butler[6]

[1]*Instituto de Energía Solar, ETSI Telecomunicación, Universidad Politécnica de Madrid, Ciudad Universitaria, s/n, 28040, Madrid, Spain.*
[2]*Departamento de Tecnología Fotónica y Bioingeniería, ETSI Telecomunicación, Universidad Politécnica de Madrid, Ciudad Universitaria, s/n, 28040 Madrid, Spain.*
[3]*Department of Physical, Chemical and Natural Systems, Universidad Pablo de Olavide, 41013 Sevilla, Spain.*
[4]*Departamento de Física aplicada a las Ingenierías Aeronáutica y Naval. ETSI Aeronáutica y del Espacio, Universidad Politécnica de Madrid, Pz. Cardenal Cisneros, 3, 28040 Madrid, Spain.*
[5]*Department of Chemistry, University of Reading, Reading RG6 6DX, United Kingdom.*
[6]*SciML, Scientific Computing Department, Rutherford Appleton Laboratory, Harwell OX11 0QX, United Kingdom*

*e-mail: p.sanchez-palencia@upm.es

Solid solutions of spinel nitrides with Group IV cations are very suitable materials for optoelectronic applications, thanks to their outstanding properties like a great hardness and oxidation resistance, plus a wide bandgap range when modifying cations partial concentration. Specifically, tin-germanium nitride solid solutions have been previously reported as promising materials for intermediate band solar cells (IBSC), used as host materials where an intermediate band (IB) could be achieved through transition metal hyperdoping of the optimal host [1]. The finding of an operative material like these could contribute to a groundbreaking change in the field of photovoltaics, because of the ideal efficiency limit of up to 63% that could be obtained with just a single layer configuration.

To be able to efficiently explore the vast compositional and configurational space of these materials to find an optimal host, we have performed a thorough study combining density functional theory (DFT) and machine learning (ML) techniques, aiming at a full and accurate description of the electronic properties for all the possible configurations within the space. The implementation of ML and other statistical analysis techniques allows us to reduce the number of DFT calculations required to fulfill that task, accelerating the process by several orders of magnitude [2]. Mixing energies, to give a broad perspective of thermodynamics and intrinsic stability of the different configurations, as well as accurate bandgaps, obtained through correlation of some HSE results and more basic DFT calculations, are successfully reproduced by the ML models. We test several statistical models with different complexity levels and a variety of atomic-level descriptors based on structural information in the process. Our results demonstrate the usefulness of ML for predictions in the configurational space of alloys and show some hints about most suitable methods and descriptors for different target systems and properties.

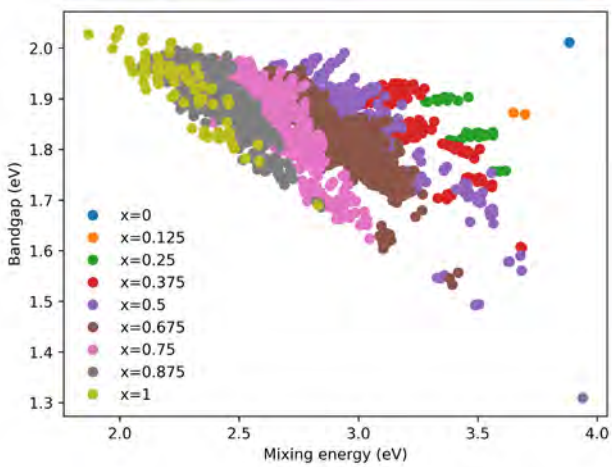

Figure 1. Distribution of predicted mixing energies and bandgaps for all the inequivalent configurations and different inversion.

[1] P. Sánchez-Palencia. G. García, J.C. Conesa, P. Wahnón, P. Palacios, *Acta Materialia* **197**, 316 (2020).
[2] S.D. Midgley, S. Hamad, K.T. Butler, R. Grau-Crespo, *Journal of Physical Chemistry Letters* **12**, 5163 (2021).

Acknowledgements: This work was accomplished thanks to the mobility grants given by Universidad Politécnica de Madrid Programa Propio de I+D+I 2021 and ERASMUS+ european project. P.S-P., as presenting author in this communication, also acknowledges support from Ministerio de Ciencia e Innovación through the project BESTMAT-QC (PID2019-107137RB-C22).

The 2030 power sector transition in Spain: advantages and drawbacks of massive deployment of solar photovoltaic sources

Gómez-Calvet, Roberto[1,*], Martinez-Duart, Jose M.[2], Gómez-Calvet, Ana Rosa[3]

[1]*Business Dept., Universidad Europea de Valencia, Spain.* [2]*Dept. Applied Physics and Materials N. Cabrera Institute, Universidad Autónoma de Madrid, Spain.* [3]*Business Finance Dept., Universidad de Valencia, Spain*

*e-mail: roberto.gomezcalvet@universidadeuropea.es

This work deals with the 2030 power transition in Spain to accomplish with the European Union (EU) target of reaching climate neutrality by 2050. In this line, the EU has realised that if we want to implement the agreements of not increasing the globe temperature in more than 1.5ºC, then the program of eliminating carbon emissions or to reach the Net Zero Emissions has to be accelerated.

Within this context, we analyze in this work the plan established by the Spanish government under the umbrella of the National Plan for Energy and Climate (so-called PNIEC) which fixes very clear objectives for our electricity power system. This Plan is originally based in a very large development of renewable energies which in 2030 will boost the amount of solar photovoltaic (PV) and wind adding up to 73 % of the total mix.

Nonetheless, this large deployment of PV, about 3 times the present value, is not free of controversy due to the massive need of storage capacity and/or backup power plants with very flexible and fast ramping response. Making use of historical data, we present in this work a forecast of the 2030 scenario with some suggestions and recommendations.

To evaluate the impact of high deployment of variables renewable sources, and particularly the effect of large increase of solar photovoltaic we make use of the analysis proposed by [1] based on the *duck curves* presented in Figure 1 and 2.

The relevance of future research opportunities is presented in the last section of this article.

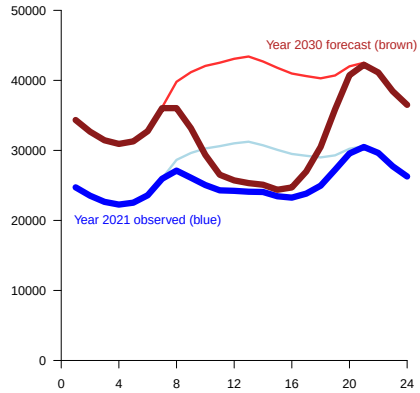

Figure 1. Comparative of present vs 2030 estimated duck curves. Source: Authors

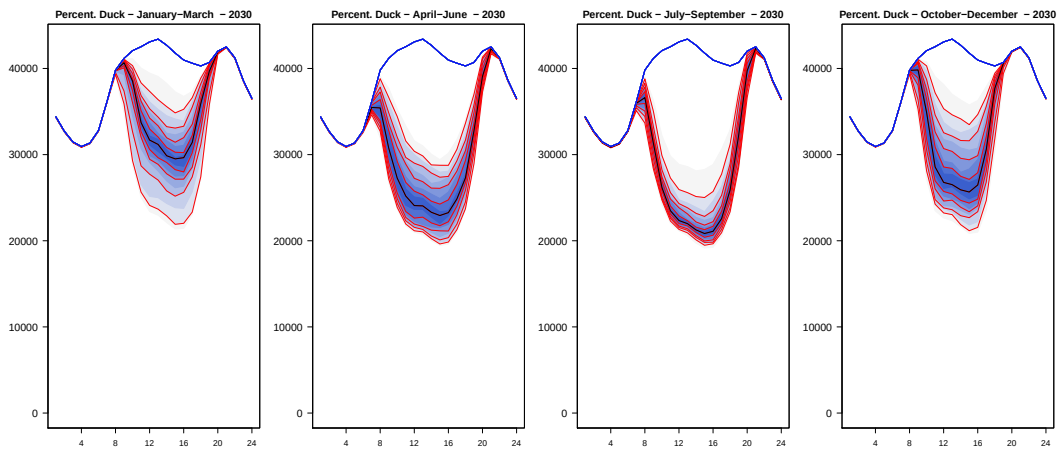

Figure 2. Seasonal percentiles fan-charts of duck curves for the 2030 forecast in Spain. Source: authors.

[1] Denholm, P., O'Connell, M., Brinkman, G., & Jorgenson, J. (2015). Overgeneration from solar energy in California, a field guide to the duck chart. *National Renewable Energy Lab*, Golden, CO (United States).

Acknowledgements: Research suport from Proyectos I+D+i "Retos de Investigación" del Programa Estatal de I+D+i orientada a los retos de la sociedad. Ministry of Science, Innovation and Universities. Ref: RTI2018-100983-B-I00

Assessing composition engineering as mechanism to deal with stability and toxicity problems of inorganic halide perovskites with improved absorption features for photovoltaic applications

P. Sanchez-Palencia[1,2], G. Moreno[1,2], P. Wahnón[1,2], **P. Palacios**[1,3,*]

[1]*Instituto de Energía Solar, ETSI Telecomunicación, Universidad Politécnica de Madrid, Ciudad Universitaria, s/n, 28040, Madrid, Spain.*
[2]*Departamento de Tecnología Fotónica y Bioingeniería, ETSI Telecomunicación, Universidad Politécnica de Madrid, Ciudad Universitaria, s/n, 28040 Madrid, Spain.*
[3]*Departamento de Física aplicada a las Ingenierías Aeronáutica y Naval. ETSI Aeronáutica y del Espacio, Universidad Politécnica de Madrid, Pz. Cardenal Cisneros, 3, 28040 Madrid, Spain.*

*e-mail: pablo.palacios@upm.es

Inorganic perovskites like CsPbI3 are emerging as a family of very promising materials to be used in the photovoltaic field as absorber materials. Nevertheless, besides their remarkable optical absorption properties, these materials have encountered two important bumps in their road towards commercialization, their poor stability and toxicity, being caused the latter by their Pb content. In this work, we explore the possibility of lessening these two problems, as well as obtaining improved photovoltaic efficiencies, through the propitious fine-tuning of the chemical composition. For that purpose, we have performed a systematic DFT study of RbaCs1-aSnbPb1-bI2Br (a = 0 - 0.125, b = 0 -1) perovskites, studying in detail the effects of composition changes and related solid structure distortions on the optoelectronic properties of these materials. Our results provide a complete description on the connections between the chemical composition, crystal structure, intrinsic stability and electronic properties of these materials, which ultimately define their absorption features. Our results suggest that all-inorganic RbaCs1-aSnbPb1-bI2Br (1 > b > 0.5) perovskites meet all the requirements to be highlighted very adequate candidates for photovoltaic applications, thanks to their reduced content in Pb and their improved intrinsic stability and absorption features.

[1] P. Sánchez-Palencia, G. García, P. Wahnón, P. Palacios, *Inorg. Chem. Front.* **9**, 1337 (2022).
[2] P. Sánchez-Palencia, G. García, P. Wahnón, P. Palacios, *Inorg. Chem. Front.* **8**, 3803 (2021).

Acknowledgements: Support from Ministerio de Ciencia e Innovación through the project BESTMAT-QC (PID2019-107137RB-C22.

Charge and energy stored in electric double layer capacitors from potentiostatic discharge

A. A. Moya

Departamento de Física, Universidad de Jaén, Campus Las Lagunillas s/n, 23071 – Jaén, Spain.

e-mail: aamoya@ujaen.es

Electric double layer (EDL) capacitors are electrochemical energy storage devices consisting of two activated carbon porous electrodes separated by liquid electrolyte with a salt dissolved in an aqueous or organic solvent. They store electric charge in the electric double layers at the electrolyte-electrode interfaces without the requirement of redox reactions. These devices show much higher specific energy than conventional capacitors due to high surface area of activated carbon porous electrodes. They, together with rechargeable batteries, store electric charges and therefore renewable energy in a fast, safe and efficient manner so they find application not only in portable electronic devices and electric vehicles, but also as a complement to fluctuating energy sources, such as wind and sunlight. Unlike rechargeable batteries, EDL capacitors present high specific power, rapid charge-discharge capability, and long cycle life.

Electrochemical characterization of EDL capacitors is a classic research topic in the field of the electrochemical power sources [1]. EDL capacitors are usually characterized, by analogy to conventional capacitors, by their differential capacitance. This capacitance can be experimentally determined by using different conventional electrochemical techniques such as cyclic voltammetry, electrochemical impedance spectroscopy, galvanostatic charge-discharge or potentiostatic charge-discharge through a resistor. The experimental data are then interpreted by using a simple electric circuit constituted by the series combination of the equivalent series resistance and the mentioned differential capacitance. In particular, charge and energy are determined from this capacitance by using the usual expressions in conventional capacitors. However, studies on the direct measurement of the electric charge stored in EDL capacitors from the time evolution of the electric current during the discharge through a resistor, have been rare in literature. This can be due to the high values reached by the initial electric current, as well as to the long experimentation time being necessary to obtain precise values of the charge.

In this work, we obtain the electric charge stored in an EDL capacitor from the potentiostatic discharge through a resistor without using an equivalent electric circuit model. Three commercial EDL capacitors with nominal capacitances in the range from 0.1 to 1 F, are selected. The time evolution of the electric current obtained during the potentiostatic discharge through a resistor nominally 10 Ω is gathered by using an Autolab PGSTAT204 potentiostat/galvanostat, and the electric charge is determined by means of coulometric techniques from the area of the current-time curves. Evolution with the initial electric potential of the charge stored in the EDL capacitors, as shown in Figure 1, is analysed and discussed. The capacitance and energy are also studied as a function of the electric potential by means of different statistical parameters.

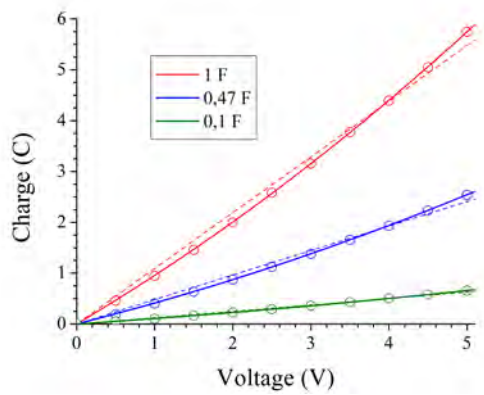

Figure 1. Evolution with potential of the electric charge stored in the EDL capacitors.

[1] A. A. Moya, *J. Power Sources* **397**, 124 (2018).

Artificial Intelligence Applied to the Prediction of Module Temperature for Building-Integrated Photovoltaics

Victoria Beltran[1,*], Carlos Toledo[2], Antonio Urbina[3], Lucía Serrano-Luján[1,4]

[1]*Department of Electronics, Computers Technology and Projects, Technical University of Cartagena (UPCT), Plaza del Hospital 1, 30202 Cartagena (MU), Spain.* [2]*Italian National Agency for New Technologies, Energy and Sustainable Economic Development (ENEA), Centro Ricerche Portici, Largo Enrico Fermi 1 80055, Portici (NA), Italy.* [3]*Department of Sciences and Institute for Advanced Materials and Mathematics (INAMAT2), Public University of Navarra (UPNA), Campus de Arrosadia, 31006 Pamplona (Navarra), Spain.* [4]*Department of Computer Science and Statistics, Rey Juan Carlos University (URJC), Calle Tulipán S/N, 28933 Móstoles (Madrid), Spain.*

*e-mail: victoria.beltran@upct.es

Photovoltaic (PV) systems have been installed worldwide during last decays, reaching 894.2 GWp of installed capacity at the end of 2021 [1]. Building integrated photovoltaics (BIPV) configuration allows for producing electricity at the same place where it is going to be consumed, plus it helps expanding the PV areas for the decarbonization of the energy system [2]. Nevertheless, BIPV exhibits some disadvantages when comparing to ground mounted photovoltaics, such as poor air ventilation which could lead to high working temperatures. Controlling and predicting BIPV temperatures would help to better design the systems, calculate its potential production, as well as predict faults during its performance. Previous works have applied artificial intelligence (AI) techniques to predict module PV temperature, but always applied to ground-mounted PV systems.

The first study using artificial intelligence to model PV module temperature of a BIPV system was recently published [3], and its data is obtained from a deliberately designed set-up, called "PV-cubes" as described by Toledo et al. [4]. Grammatical and Differential evolution, which are classified as Genetic

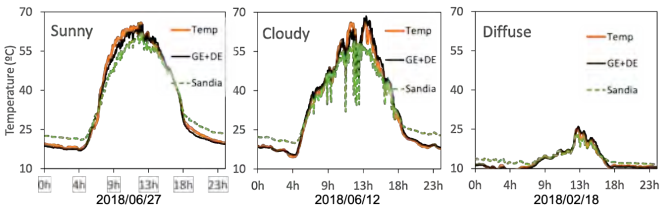

Figure 1. PV module temperature measured vs. modelled in three different types of days using two different approaches: the conventional Sandia model and Genetic Algorithms (Source: [3]).

Algorithms, were applied to 3 days dataset. Datasets were classified into three day-type groups: whether they belong to sunny, cloudy, or diffuse light-types days. The study obtained relative errors of less than 4% when predicting the module temperature. Figure 1 shows an example of the measured and predicted values of PV module temperature, as well as prediction using one of the most common PV module temperature models [5]. Here we present the Artificial Neural Network (ANN) method to predict the module temperature of BIPVs. We compare this method with the GE+DE algorithm and assess which of the two is the most reliable method to obtain a temperature predicting model.

[1] International Renewable Energy Agency (IRENA), Renewable Energy Statistics 2021, available on-line at: https://irena.org/publications/2021/Aug/Renewable-energy-statistics-2021

[2] T. E. Kuhn, C. Erban, M. Heinrich, J. Eisenlohr, F. Ensslen, and D. H. Neuhaus, Review of technological design options for building integrated photovoltaics (BIPV), *Energy and Buildings* **231**, 110381 (2021) doi: 10.1016/j.enbuild.2020.110381.

[3] L. Serrano-Luján, C. Toledo, J. M. Colmenar, J. Abad, and A. Urbina, Accurate thermal prediction model for building-integrated photovoltaics systems using guided artificial intelligence algorithms, *Applied Energy* **315**, 119015 (2022), doi: 10.1016/j.apenergy.2022.119015.

[4] C. Toledo, R. López-Vicente, J. Abad, and A. Urbina, Thermal performance of PV modules as building elements: Analysis under real operating conditions of different technologies, *Energy and Buildings* **223**, 110087 (2020) doi: 10.1016/j.enbuild.2020.110087.

[5] D. L. King, W. E. Boyson, and J. A. Kratochvill, Photovoltaic Array Performance Model, Sandia National Laboratories, SAND2004-3535 (2004).

Física Teórica y de Partículas

Presentaciones orales

Lunes 11/07:

15:30-15:45 Aniol Lobo Salvia. *LHCb Commissioning for run 3 - Milestones in the Trigger System*

15:45-16:00 Diego Mendoza Granada. *Trigger challenges for detecting long-lived particles at LHCb*

16:00-16:15 Carlos García Montoro. *IFIC Contributions to the Computing of the ATLAS Experiment for the Run 3 of the LHC*

16:15-16:30 Ángel Jesús Murcia Gil. *Exact electromagnetic duality with nonminimal couplings*

16:30-16:45 Rafael Delgado López. *quantumfdtd, a computational framework for the Relativistic Schrödinger Equation*

16:45-17:00 Adrián Casado Turrión. *Is gravitational collapse possible in f(R) gravity?*

17:00-18:00 **Pósteres y café**.

18:00-18:15 Shalini Epari. *Search for flavourful 2HDM model in multilepton plus multi-b-jets final states*

18:15-18:30 Mariam Chitishvili. *Measurement of the quadruple-differential angular decay rates of single top quarks produced in the t-channel at ?s=13 TeV*

18:30-18:45 Pablo Martínez-Agulló. *Search for associated production of a Higgs boson and a single-top quark in the 2l+tau final state at 13 TeV in ATLAS*

18:45-19:00 Pablo Martínez-Agulló. *Search for associated production of a Higgs Boson and a single top quark in 3l and 2lSS final states at 13 TeV in ATLAS*

19:00-19:15 Mariia Didenko. *Search for long-lived neutral particles in pp collisions at 13 TeV that decay into displaced hadronic jets in the ATLAS calorimeter*

Martes 12/07:

15:30-15:45 Carlos Solans Sanchez. *Radiation hardness and timing performance of MALTA monolithic Pixel sensors in Tower 180 nm*

15:45-16:00 Rafael Mayo García. *Technological Applications of Extensive Air Showers Simulations*

16:00-16:15 Paula Garcia Moreno. *Commissioning and Monitoring of the Calorimeter sub-detector in LHCb experiment*

16:15-16:30 Rodrigo Alvarez Garrote. *Simulation and reconstruction of scintillation light with X-ARAPUCA photodetectors in SBND*

16:30-16:45 Rafael Delgado López. *Unitarized one-loop graviton-graviton scattering*

16:45-17:00 Álvaro Parra López. *Gravitational particle production in the laboratory*

17:00-18:00 **Café**.

18:00-18:15 Felipe J. Llanes-Estrada. *Some uses of dispersion relations*

18:15-18:30 Miguel Albaladejo Serrano. *On the doubly charmed tetraquark Tcc+ recently discovered at CERN: analysis and predictions*

18:30-18:45 César Jesús Valls. *Analysis and instrumentation developments for the future understanding of neutrino physics with the T2K experiment*

18:45-19:00 Paula Martinez Suarez. *The ATLAS Level-1 Topological Trigger: Run 2 performance and plans for Run 3*

Miércoles 13/07:

15:30-15:45 Naseem Bouchhar. *Data-Driven Calibration of B-Tagged and Large-R Jets for gamma+jet Events in The ATLAS Experiment*

15:45-16:00 Héctor García Cabrera. *Results of the SDHCAL Beam Test data analysis of 2015*

16:00-16:15 Juan Ramón Balaguer Tornel . *IIB orientifold reductions with open strings*

16:15-16:30 Sergio Manthey Corchado. *Light Detection in DUNE's Vertical Drift Module*

16:30-16:45 Laura Pérez Molina. *Photon Detection System in ProtoDUNE phase II*

16:45-17:00 Pablo Barham Alzás. *Core-Collapse Supernova Burst Neutrino detection and trigger in DUNE*

Jueves 14/07:

15:30-16:30 Seminario: Guillelmo Ceballos (MIT). *La medida de la masa del W por el experimento CDF*

16:30-17:00 Entrega de premios de tesis doctorales.

17:00-18:00 **Café**.

18:00-19:30 Junta de Gobierno de la DFTP.

Pósteres

- Laura Remón Martín. *Electromagnetic tensor endowed with polarimetric parameters: application to the vicinity of extremely dense bodies*
- Víctor Montesinos Llácer. *Prediction of symmetric partners of the Zc(3900) and Zb(10610) exotic states using heavy quark spin symmetry and SU(3) flavor symmetry*

LHCb Commissioning for run 3 Milestones in the Trigger System

Aniol Lobo Salvia

ICCUB, Martí i Franquès 1 Barcelona, Spain.

e-mail: aniol.lobo.salvia@cern.ch

This talk aims to provide a brief description of the *Trigger System* of LHCb, its upgrades for run 3 and its particular implantation for the *Radiative Processes Subgrup* as a use case.

The LHCb detector is a single-arm spectrometer designed to provide competitive measurements of CP violation and rare decays of B hadrons [1]. Data taking occurs in campaigns of approximately four years called *runs* separated by *Long Shutdown* periods. The upgrades introduced in the trigger system during the Long Shutdown II will be here discussed.

The trigger system is the responsible of deciding when to store the result of a collision, what we call *event*. From the 30 million collisions that occur per second in the LHCb a large fraction of them are of poor interest. This occurs mainly because they either contain a process already measured with high precision or a collision with low momentum transfer, as opposed to the events containing b quarks which we centre our attention on. The trigger must provide a balance when saving decays interesting for different types of analysis, always keeping a bandwidth acceptable by the data acquisition system [DAQ] and the storage capacity.

The framework update for the trigger system has three main advantages

· Removal of the hardware-based trigger filter [L0]

· Having more information at the stage of the trigger decision

· Offering to possibility to store only the information of the event relevant to the posterior analysis

The first milestone has been achieved via the full optimization of the reconstruction and selection algorithms and via increasing the computing power of the farms, allowing all events to be processed by GPUs and CPUs.

The second milestone was also possible by the optimization of the reconstruction algorithms needed to transform raw detector signal to information relevant to the filtering of events according to physical properties of the reconstructed particles. This was previously done in two stages in the first and second runs due to its high computational cost.

The third major improvement allows for the storage of a larger number of events given a permitted bandwidth, since the weight of the part of the event stored is smaller than the whole event.

[1] LHCb Collaboration, A. A. Alves et al., The LHCb detector at the LHC, *Journal of Instrumentation* **3** (2008).

Trigger challenges for detecting long-lived particles at LHCb

Arantza Oyanguren Campos[1,*], **Diego Mendoza Granada**[1,**], Louis Henry[2,***]

[1]*Experimental unit, Instituto de Física Corpuscular (IFIC). Carrer del Catedràtic José Beltrán Martínez, 2, 46980 Paterna, Valencia. Spain.*
[2]*EP/LBD, CERN. Esplanade des Particules 1, 1217 Meyrin. Switzerland.*

*oyangur@ific.uv.es **diego.mendoza.granada@cern.ch **louis.henry@cern.ch

Collider experiments in high-energy physics (HEP) have sought to test the Standard Model of particle physics (SM), the most successful theory of fundamental interactions. Nonetheless, it is unable of explaining some empirically observed phenomena such as the imbalance of matter and antimatter in the Universe, neutrino masses or the origin of dark matter. This has therefore motivated New Physics (NP) extensions involving beyond the Standard Model (BSM) particles that may be observable in proton-proton collision experiments such as the Large Hadron Collider (LHC) at CERN. The interest in long-lived particles (LLPs) is growing in the HEP community, specially for high-luminosity LHC and B-factory experiments. One of the main challenges for their detection is the behaviour of the trigger algorithm for signals where very displaced vertices are involved. This has an impact on the experiment sensitivity to detect unknown LLPs. Furthermore, the high-luminosity LHC project aims to increase luminosity by a factor of 10 respect to initial LHC's design in order to observe rare new phenomena. In this scope, track reconstruction in real-time will be crucial for LHCb trigger systems when dealing with the large amount of hits in the different subdetectors. Dedicated track reconstruction algorithms have been developed in order to cope with the large data output from proton-proton collision. One example is the *HybridSeeding*, which has been successfully introduced in the LHCb trigger. Great effort is being made to speed up the performance of such algorithm by adopting a GPU-based solution for the first stage of the High Level Trigger. Other strategies take advantage of field-programmable gate array (FPGA) devices, which introduce parallel computational capabilities with a low energy consumption. In this work we evaluate the performance of the current LHCb trigger algorithm for LLP signals and propose new strategies to increase the experiment sensitivity for NP involving LLPs. Moreover, we inspect some features of the *HybridSeeding* algorithm by using FPGA architectures and introducing Artificial Intelligence strategies.

IFIC Contributions to the Computing of the ATLAS Experiment for the Run 3 of the LHC

Carlos García Montoro*, Javier Alberto Aparisi Pozo, Álvaro Fernández Casaní, Esteban Fullana Torregrosa, Santiago González de la Hoz, José Salt Cairols, Javier Sanchez, Miguel Villaplana Perez

Instituto de Física Corpuscular (IFIC), centro mixto CSIC – UV. Catedrático José Beltrán 2, 46980 Paterna, Spain.

*e-mail: carlos.garcia@ific.uv.es

Worldwide LHC Computing Grid (WLCG) sites around the world have been preparing for Run 3, updating their storage and computational resources, as well as their networking. After a budget reduction, the Spanish contribution to the ATLAS Tier2s was lowered from 4% to 3%. Spain has a federated Tier2 (IFIC, IFAE and UAM), where IFIC holds 60% of the resources [1]. IFIC's Tier2 facility is considered a *Nucleus* by the ATLAS Collaboration, i.e. a Tier2 with a large amount of storage and network connectivity that can pass job production on to smaller *Satellite* Tier2s. IFIC provides in-house resources, resources using HPC facilities for simulation, and R&D to the experiment through the ATLAS EventIndex project [3].

Year	2016	2017	2018	2019	2020	2021	2022
CPU (HS06)	14150	20304	27840	33408	31008	27907	45000
Disk (TB)	1800	1872	2112	2430	2592	2235	3480

Table 1. IFIC Pledge 2016 – 2022.

IFIC in-house resources have been increased to yearly satisfy the compromised pledge shown in Table 1. At the end of 2021 IFIC was providing 50,720 HS06 of which around 25% were being provided by servers older than 6 years that are being replaced. Regarding storage, IFIC was providing 3,402 TiB. 2 PiB of them in servers older than 6 years that are being replaced too. The bandwidth has been updated from 2x10 Gbps to a 100 Gbps connection to UV backbone. IFIC is ready for RedIRIS-Nova at 100 Gbps.

IFIC has also provided computing resources to the ATLAS Collaboration through HPC resources of the *Red Española de Supercomputación (RES)*. Between 2018 and 2020 IFIC applied for resources via RES standard calls. At that time IFIC obtained opportunistic resources from Lusitania. Since mid 2020 there has been an agreement with the BSC that grants resources from MareNostrum 4 to the LHC computation community [2]. Thanks to this agreement, around 10 million hours are granted every quarter at BSC for ATLAS. We are able to use these resources for simulation using singularity containers that are pre-placed at MareNostrum.

IFIC has been steadily providing more that 5,000 running job slots since 2019. They can be either single-core or multi-core with 8 cores and they typically use 2 GiB per job slot. Around 2,000 additional job slots are provided by MareNostrum 4 as shown in Figure 1. With all these resources, more than 300 billion events have been processed in the last 5 years.

Figure 1. Slots of Running jobs (IFIC + HPC)

IFIC also plays a key role in ATLAS EventIndex, the catalogue of all ATLAS events. IFIC coordinates the data production and is in charge of the data collection. EventIndex has evolved to cope with the data production rates expected for Run 3[3]. IFIC has designed and developed an architecture that replaces the original HDFS-based storage with a new one based on HBase and Phoenix. Figure 2 shows the cumulative amount of event records processed by EventIndex.

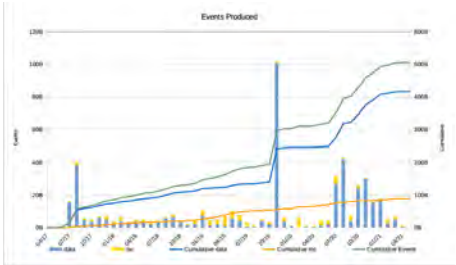

Figure 2. Event records processed by EventIndex.

[1] Santiago González de la Hoz et al., *EPJ Web Conf.* **245**, 07027 (2020).
[2] Carles Acosta-Silva et al., *EPJ Web Conf.* **251**, 02021 (2021).
[3] Dario Barberis et al., The ATLAS EventIndex for LHC Run 3, *EPJ Web Conf.* **245**, 04017 (2020).

Acknowledgements: MICINN in Spain partially supported this work under grant PID2019-104301RB-C21

Exact electromagnetic duality with nonminimal couplings

Pablo A. Cano[1], **Ángel Murcia**[2,*]

[1]*Instituut voor Theoretische Fysica, KU Leuven. Celestijnenlaan 200D, B-3001 Leuven, Belgium.*
[2]*Instituto de Física Teórica UAM/CSIC. C/ Nicolás Cabrera 13-15, C.U. Cantoblanco, E-28049 Madrid, Spain.*

*e-mail: angel.murcia@csic.es

We study nonminimal extensions of Einstein-Maxwell theory with exact electromagnetic duality invariance. Any such theory involves an infinite tower of higher-derivative terms whose computation and summation usually represents a challenging problem. Despite that, we manage to obtain a closed form of the action for all the theories with a quadratic dependence on the vector field strength. In these theories we find that the Maxwell field couples to gravity through a curvature-dependent susceptibility tensor that takes a peculiar form, reminiscent of that of Born-Infeld Lagrangians. We study the static and spherically symmetric black hole solutions of the simplest of these models, showing that the corresponding equations of motion are invariant under rotations of the electric and magnetic charges. We compute the perturbative corrections to the Reissner-Nordström solution in this theory, and in the case of extremal black holes we determine exactly the near-horizon geometry as well as the entropy. Remarkably, the entropy only possesses a constant correction despite the action containing an infinite number of terms. In addition, we find there is a lower bound for the charge and the mass of extremal black holes. When the sign of the coupling is such that the weak gravity conjecture is satisfied, the area and the entropy of extremal black holes vanish at the minimal charge.

quantumfdtd, a computational framework for the Relativistic Schrödinger Equation

Rafael Delgado Lopez[1,*], Sebastian Steinbeißer[2], Michael Strickland[3], Johannes Heinrich Weber[4]

[1]*Matemática Aplicada a las TIC, ETSIS de Telecomunicación (UPM), Campus Sur, 28031 Madrid, Spain.* [2]*Physik-Department, Technische Universität München (TUM), D-85748 Garching b. München, Germany.* [3]*Department of Physics, Kent State University, Kent, OH 44242, USA.* [4]*Institut für Physik & IRIS Adlershof, Humboldt-Universität zu Berlin, Zum Großen Windkanal 6, D-12489 Berlin, Germany*

*e-mail: rafael.delgado@upm.es

We present work [1], in which we extend the publicly available quantumfdtd code. It was originally intended for solving the time-independent three-dimensional Schrödinger equation via finite-difference time-domain (fdtd) method and extracting the ground, first and second excited states. We extend it to (a) include the case of the relativistic Schrödinger equation and (b) add two optimized FFT-based kinetic energy terms for the non-relativistic case. All the three new kinetic terms (the two non-relativistic and the relativistic one) are computed using Fast Fourier Transform (FFT). We release the resulting code as version 3 of quantumfdtd. Finally, the original code now supports arbitrary external file-based potentials and the option to project out distinct parity eigenstates from the solutions.

Most quark models used for phenomenological descriptions of QCD bound states are described by the three-dimensional Schrödinger equation with different potentials. In particular, these models have successfully describe below-threshold charmonium production and bottomonium spectra and have helped to establish confidence in QCD as the first-principles description of hadronic matter [2–4]. Non-relativistic effective field theory methods have been used for a first-principles approach to potential-based non-relativistic QCD (pNRQCD) [5,6]. In order to describe quarkonium evolution in the quark-gluon plasma, these potential models have been extended to finite temperature [7–9] and non-equilibrium [10–14]. In the last case, the potentials are no longer real-valued or spherically symmetric. In the full non-equilibrium case, a full three-dimensional solver, like the one developed in this work, is necessary.

[1] R.L.Delgado, S.Steinbeißer, M.Strickland, J.H.Weber, Comput.Phys.Commun.**272** (2022) 108250
[2] D.Ebert, R.N.Faustov, V.O.Galkin, Phys.Rev.D**67** (2003) 014027
[3] E.Eichten, S.Godfrey, H.Mahlke, J.L.Rosner, Rev.Mod.Phys.**80** (2008) 1161–1193
[4] J.Segovia, P.G.Ortega, D.R.Entem, F.Fernández, Phys.Rev.D**93** (7) (2016) 074027
[5] N.Brambilla, A.Pineda, J.Soto, A.Vairo, Nucl.Phys.B**566** (2000) 275; Phys.Rev. D**60** (1999) 091502
[7] M.Laine, O.Philipsen, P.Romatschke, M.Tassler, J.High Energy Phys.**03** (2007) 054
[8] N.Brambilla, J.Ghiglieri, A.Vairo, P.Petreczky, Phys.Rev.D**78** (2008) 014017; Phys.Rev.D**82** (2010) 074019
[10] A.Dumitru, Y.Guo, M.Strickland, Phys.Lett.B**662** (2008) 37–42
[11] Y.Burnier, M.Laine, M.Vepsalainen, Phys.Lett.B**678** (2009) 86–89
[12] A.Dumitru, Y.Guo, M.Strickland, Phys.Rev.D**79** (2009) 114003
[13] A.Dumitru, Y.Guo, A.Mocsy, M.Strickland, Phys.Rev.D**79** (2009) 054019
[14] Y.Guo, L.Dong, J.Pan, M.R.Moldes, Phys.Rev.D**100** (3) (2019) 036011

Acknowledgements: The code was extensively used and tested in the Computational Physics II online course at the Humboldt-Universität Berlin in winter semester 2020/21 (course by A.Patella and J.H.Weber). R.L.Delgado was supported by the Ramón Areces Foundation post-doctoral fellowship, the INFN post-doctoral fellowship AAOODGF-2019-0000329 and the Spanish grant MICINN: PID2019-108655GB-I00. M.Strickland was supported by the U.S. Department of Energy, Office of Science, Office of Nuclear Physics Award No. DE-SC0013470. J.H.Weber was supported by the U.S. Department of Energy, Office of Science, Office of Nuclear Physics and Office of Advanced Scientific Computing Research within the framework of Scientific Discovery through Advanced Computing (SciDAC) award Computing the Properties of Matter with Leadership Computing Resources. His research was funded by the Deutsche Forschungsgemeinschaft (DFG, German Research Foundation) - Projektnummer 417533893/GRK2575 "Rethinking Quantum Field Theory". We acknowledge the support by the Deutsche Forschungsgemeinschaft (DFG, German Research Foundation) under Germany's Excellence Strategy – EXC-2094 – 390783311 via the Excellence Cluster "ORIGINS". The simulations have been carried out on the computing facilities of the C2PAP and the Leibniz Supercomputing Center (SuperMUC), on the local theory cluster of the Physics Department of TUM, and on the local cluster at the INFN-Firenze.

Is gravitational collapse possible in $f(R)$ gravity?

Adrián Casado-Turrión[1,*], Álvaro de la Cruz-Dombriz[2,3], Antonio Dobado[1]

[1] *Departamento de Física Teórica and Instituto IPARCOS, Universidad Compltense, 28040 Madrid, Spain.* [2] *Departamento de Física Fundamental, Universidad de Salamanca, 37008 Salamanca, Spain.* [3] *Cosmology and Gravity Group, Department of Mathematics and Applied Mathematics, University of Cape Town, Rondebosch 7700, Cape Town, South Africa.*

*e-mail: adricasa@ucm.es

Gravitational collapse is still poorly understood in the context of $f(R)$ theories of gravity. The main reason for this is that junction conditions in these models are different and much more stringent than their counterparts in General Relativity. As a result, the most paradigmatic description of gravitational collapse in Einstein gravity, the Oppenheimer-Snyder model, is known not to be a solution of $f(R)$ theories of gravity, neither in their metric nor Palatini formulations. The smooth matching between the metrics inside and outside the stellar surface (which is possible in General Relativity) is no longer allowed by the junction conditions of $f(R)$ gravity.

For these reasons, we have endeavoured to shed some light on the issue of gravitational collapse in $f(R)$ gravity by means of a systematic treatment of the relevant junction conditions [1]. After thoroughly discussing how the Oppenheimer-Snyder construction should be generalised to fit within $f(R)$ gravity, we shall subsequently proceed to explore the existence of novel exterior solutions compatible with physically viable interiors. We will show that some paradigmatic vacuum metrics cannot represent spacetime outside a collapsing dust star in metric $f(R)$ gravity. In particular, we have found that, in $f(R)$ theories, the exterior solution must be strikingly different from the Schwarzschild metric, which is the only possible exterior spacetime in General Relativity, as per Birkhoff's theorem.

[1] Adrián Casado-Turrión, Álvaro de la Cruz-Dombriz, Antonio Dobado, accepted for publication in *Physical Review D* (2022), arXiv:2202.04439 [gr-qc].

Search for flavourful 2HDM model in multilepton plus multi-b-jets final states

Merve Nazlim Agaras[1], Noemi Cavalli[3], **Shalini Epari**[1,*], Aurelio Juste Rozas[1], Stergios Kazakos[1], Javier Montejo Berlinger[2], Nicola Orlando[1], Tamara Vázquez Schroeder[2]

[1]*IFAE-Barcelona, Spain.*
[2]*CERN, Switzerland.*
[3]*University of Bologna, Italy - TU Dortmund, Germany.*

*e-mail: shalini.epari@cern.ch

A search for flavour violating heavy Higgs bosons decaying to multilepton plus multi-b-jets final states is performed using the full Run-2 dataset collected at $\sqrt{s}$ = 13 TeV with integrated luminosity of 139 fb^{-1}, by the ATLAS experiment at the LHC. The target model is an extension of the Standard Model (SM) with the addition of a second complex Higgs doublet (two-Higgs-doublet model, or 2HDM), giving rise to five Higgs bosons: two CP-even scalar fields (h and H), one CP-odd pseudo-scalar (A) and two charged Higgs ($H^{\pm}$) - without the requirement of a discrete Z_2 symmetry. In the alignment limit, the target model predicts flavour changing neutral currents in the heavy Higgs sector while respecting the SM-like nature of the $h(125)$ particle discovered at the LHC [1].

The analysis considers the production of the heavy scalar (pseudo-scalar) and has four degrees of freedom: the mass of the BSM Higgs $m_H(m_A)$ and ρ_{tq} (the coupling between the top and up/charm or another top quark). The various 2HDM signal types explored lead to final states with same-sign tt, ttq, $tttq$, three top and four top quarks (Figure 1). Benchmark couplings (ρ_{tt} = 0.27 and ρ_{tq}= 0.14) are chosen such that the model explains the excesses seen in previous ATLAS analyses, namely the $t\bar{t}H/t\bar{t}W$ analysis which fits the normalisation of the $t\bar{t}W$ background 60% above the next-to-leading order (NLO) prediction [2], and a dedicated search for that fits a normalisation a factor of two above the NLO prediction [3]. Further, 2HDM models with extra top Yukawa couplings are phenomenologically interesting since they can explain the generation of the baryon asymmetry of the universe [4].

Events are selected with at least two jets and at least one jet tagged as a b-jet. Events are then categorised depending on the multiplicity of light leptons (electron and muon) into channels (same-sign 2l, 3l and 4l channels). A deep neural network (DNN)-based categorisation is used to enhance the purity of each 2HDM signal. The Monte Carlo predictions of the dominant background are corrected and validated using dedicated control and validation regions. Finally, dedicated DNN are trained to discriminate signal from background in each of the signal categories and are used as final discriminants in the fit. A maximum-likelihood fit is performed on all the bins in the control and signal region event categories, to determine the 2HDM signal cross-section (considering all processes together: same-sign tt, ttq, $tttq$, three top and four top) and the normalisation factors for the major irreducible background processes and fake-lepton processes. In absence of an excess above the SM prediction, 95% confidence level limits are derived on model parameters for different benchmark scenarios. This is the first search at the LHC for such flavourful heavy Higgs bosons.

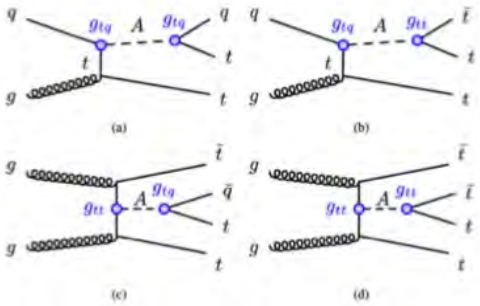

Figure 1. Representative Feynman diagrams for the dominant production and decay modes of the heavy (pseudo-)scalars considered in the analysis.

[1] W.-S, Hou and M. Kikuchi, Approximate Alignment in Two Higgs Doublet Model with Extra Yukawa Couplings, *EPL* **123**, 11001 (2018).
[2] ATLAS Collaboration, Analysis of $t\bar{t}H$ and $t\bar{t}W$ production in multi-lepton final states with the ATLAS detector, ATLAS-CONF-2019-045.
[3] ATLAS Collaboration, Evidence for $t\bar{t}t\bar{t}$ production in the multiple-ton final state in proton-proton collisions at $\sqrt{s}$=13 TeV the ATLAS detector, *Eur. Phys. J. C* **80**, 1085 (2020).
[4] K. Fuyuto, W.-S, Hou and E. Senaha, Electroweak baryogenesis driven by extra top Yukawa couplings, *Phys. Lett. B* **776**, 402 (2018).

Measurement of the quadruple-differential angular decay rates of single top quarks produced in the t-channel at $\sqrt{s}$=13 TeV

Mariam Chitishvili*, Maria Jose Costa Mezquita, Carlos Escobar Ibańez

Instituto de Fisica Corpuscular (IFIC), Centro Mixto Universidad de Valencia - CSIC, Valencia, Spain.
*e-mail: Mariam.Chitishvili@ific.uv.es

The fact that the top-quark lifetime $\mathcal{O}(10^{-25}\text{s})$ is smaller than its hadronisation time scale $\mathcal{O}(10^{-24}\text{s})$ allows this quark to be studied like a free quark. In addition, as its lifetime is also shorter than depolarisation time $\mathcal{O}(10^{-21}\text{s})$ and it decays almost exclusively via on-shell W boson and b quark ($t \to Wb$), the top-quark spin information is directly transferred to its decay products. Because of these exceptional properties, the top-quark production and decay kinematics represent an important probe of physics process beyond the Standard Model (SM).

The tWb vertex structure can be probed using single-top-quark t-channel events. This analysis uses an integrated luminosity of 139 fb^{-1} of proton-proton collision data at centre-of-mass energy of 13 TeV collected by the ATLAS detector during LHC Run 2. This analysis employs a novel model-independent framework proposed in [1] where the quadruple-differential top-quark decay rate, $\frac{1}{\Gamma}\frac{d\Gamma}{d\Omega d\Omega^*}$, is used to simultaneously determine the five generalised helicity fractions and two phases, the polarisation in three orthogonal directions of the produced top quark as well as the t-channel production cross-section.This differential decay (defined from transition amplitudes) can be expressed with orthonormal functions $M^{j_1 j_2}_{m'm}$ and angular coefficients $c^{j_1 j_2}_{m'm}$ that can be measured directly from data:

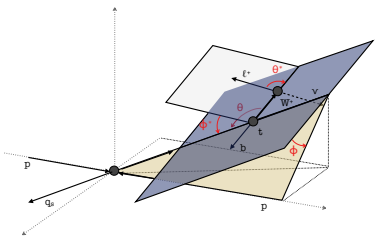

Figure 1. Definition of the four angles $(\phi, \theta, \phi^*, \theta^*)$ used in this analysis.

$$\frac{1}{\Gamma}\frac{d\Gamma}{d\Omega d\Omega^*} = \sum_{j_1 j_2 m' m} c^{j_1 j_2}_{m'm} M^{j_1 j_2}_{m'm}(\phi, \theta, \phi^*, \theta^*)^* \,,$$

where θ and ϕ are the spherical coordinates of the W boson momentum in the top-quark rest frame, θ^* and ϕ^* are the spherical coordinates of the charged-lepton momentum in the W-boson rest frame, and $d\Omega = \sin\theta d\theta d\phi$ and $d\Omega^* = \sin\theta^* d\theta^* d\phi^*$ are the solid angles in the top-quark and W-boson rest frame, respectively.

After measuring the physical quantities previously mentioned, it will be possible to set (the most) stringent limits to the relevant dimension-six Effective Field Theory (EFT) complex operators (C_{tW}, etc) of the tWb vertex [2]. On Fig. 2 one can see the expected sensitivity of the angular coefficients $c^{j_1 j_2}_{m'm}$ for various SM and non-SM predictions given by different generators.

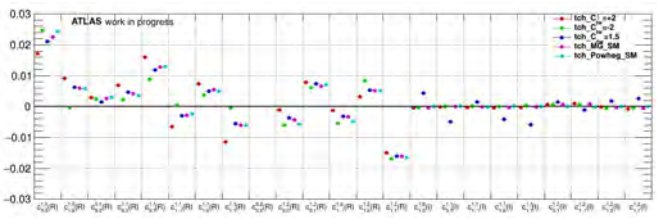

Figure 2. Angular coefficients measured from two SM and three different EFT-varied predictions, provided by different generators, demonstrating which coefficients could be sensitive to the new physics.

Deviations from SM-expected values would provide hints of physics beyond the SM, and furthermore, complex values could imply that the top-quark decay has a CP-violating component.

[1] J. A. Aguilar-Saavedra, J. Boudreau, C. Escobar, and J. Mueller, *Eur. Phys. J. C* **77**, (2017).
[2] M. de Beurs, E. Laenen, M. Vreeswijk, E. Vryonidou, *Eur. Phys. J. C* **78**, (2018).

Search for associated production of a Higgs boson and a single-top quark in the $2\ell+\tau_{had}$ final state at 13 TeV in ATLAS

S. Cabrera, C. Escobar, J. Guerrero, **P. Martínez-Agulló***

Instituto de Física Corpuscular (IFIC), Centro Mixto Universidad de Valencia - CSIC, Valencia, Spain

*e-mail: pablo.martinez.agullo@ific.uv.es

The discovery of a Higgs boson by the ATLAS and CMS experiments in 2012 opened a new field for exploration in the realm of particle physics. In order to better understand the Standard Model (SM) of particle physics, it is of prominent interest to understand the Yukawa coupling of the Higgs boson to the top quark (y_t), being the latter the most massive fundamental particle and, consequently, the one with the largest coupling to the Higgs boson.

The direct measurement of y_t is only possible at the LHC via two associated Higgs productions: with a top-quark-antiquark pair ($t\bar{t}H$) and with a single-top quark (tH). While the $t\bar{t}H$ just permits the determination of the magnitude of y_t, the only way of directly measuring its sign is through the tH production (Fig. 1). This is due to the fact that the two leading order Feynman diagrams for the tH production interfere with each other depending on the y_t sign. Current experimental constrains on y_t favour the SM predictions, but an opposite sign with respect to the expectations of the SM is not completely excluded yet [2].

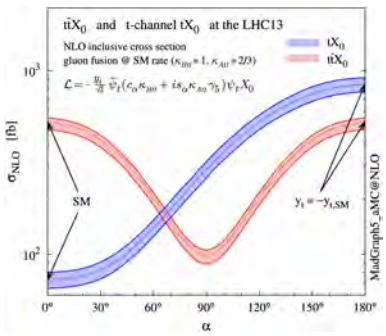

Figure 1. Production cross-section as a function of the CP mixing angle, α, at NLO for tX_0 and $t\bar{t}X_0$, where X_0 represents a Higgs boson [1].

In this work it is presented a search for the tH production in a final state with two light-flavoured-charged leptons (electrons or muons) and one hadronically-decaying tau lepton (named $2\ell+\tau_{had}$ channel). This analysis uses an integrated luminosity of 139 fb^{-1} of proton-proton collision data at centre-of-mass energy of 13 TeV collected by the ATLAS detector during LHC Run 2.

This search is exceptionally challenging due to the extremely small cross-section of the tH process (70 fb), and of the $2\ell+\tau_{had}$ final-state channel, in particular, which only accounts for a 3.5% of the total tH production. Therefore, the separation of the tH signal events from background events is done by means of machine-learning (ML) techniques using boosted-decision trees (BDT) to define both signal (Fig. 2) and control regions to constrain the most important background processes, which are those related to top-quark-antiquark-pair production without and with and additional boson ($t\bar{t}$, $t\bar{t}H$, $t\bar{t}W$ and $t\bar{t}Z$) and Z boson plus jets.

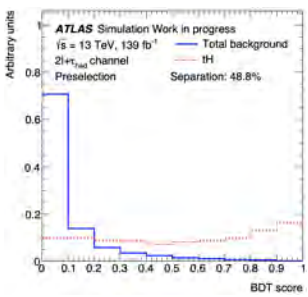

Figure 2. Score of the BDT targeting tH events over all backgrounds, used to define the signal region.

Significant suppression of the background events with jets wrongly selected as leptons or non-prompt leptons originating from heavy-flavour decays is achieved by demanding electrons and muons to pass strict identification and isolation requirements. Simultaneously, hadronic-τ leptons are demanded to pass the requirement of a recurrent-neural-network-based discriminator to reduce misidentifications from jets.

The reconstruction of the events is also enhanced by similar ML methods since in the scenario in which the light-flavour leptons have the same sign, a priori, it is not possible to determine which lepton is originated from the Higgs boson and which from the top quark.

The possible observation of an excess of signal events with respect to the SM prediction, would be an evidence of new physics in terms of CP-violating y_t coupling.

[1] F. Demartin, F. Maltoni, K. Mawatari and M. Zaro, *Eur. Phys. J. C* **75**, 267 (2015).
[2] CMS Collaboration, *Eur. Phys. J. C* **81**, 378 (2021).

Search for associated production of a Higgs boson and a single top quark in 3l and 2lSS final states at 13 TeV in ATLAS

Susana Cabrera Urban, Carlos Escobar, **Jesús Guerrero Rojas***, Pablo Martínez-Agulló

[1]*Instituto de Física Corpuscular (IFIC), Centro mixto Universitat de València – CSIC, Valencia, Spain.*

*e-mail: jguerrero@ific.uv.es

The status of the search to produce a Higgs boson in association with a single top quark (*tH*) in multi-lepton final states is presented. The study uses an integrated luminosity of 139 fb^{-1} of LHC collision data at centre-of-mass-energy of 13 TeV, recorded by the ATLAS experiment. Three final states, targeting Standard Model (SM) Higgs bosons decaying to *WW**, *ZZ** and $\tau\tau$, are examined.

As for today, this is the only analysis sensitive to both the magnitude and the sign of the Yukawa coupling (y_t) of the Higgs boson to the top quark and the first direct search of *tH* production in the ATLAS collaboration. The *tH* process has an extremely low production cross-section (70 fb at $\sqrt{s} =$ 13 TeV), which originates from the destructive interaction of the diagrams where the Higgs couples to the top quark with those where the Higgs couples to the W boson. Other SM processes giving rise to similar final states and conforming the main background of this search, have production cross-sections up to seven times higher than that of *tH*. This is the case for the associated production of a Higgs boson and a pair of top quarks (*ttH*). This fact makes multivariate analysis methods a key tool to distinguish signal events from the diverse large backgrounds. This search is also sensitive to CP-violation since, as shown in Figure 1 (blue line), the cross-section could be up to 10 times higher in the completely inverted hypothesis with respect to the SM prediction (CP mixing angle, α, equal to 180^0) [1]. All these features make this search very challenging and this process exceptionally sensitive to deviations from SM predictions.

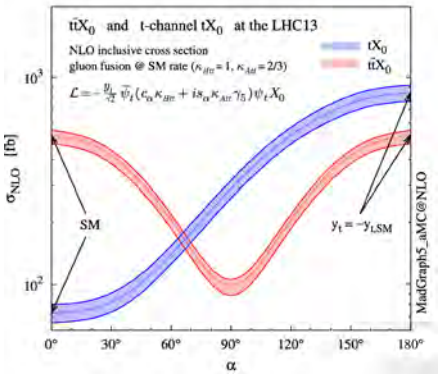

Figure 1. Production cross-section as a function of CP mixing angle α , at NLO for tX_0 and ttX_0 where X_0 represents a Higgs boson [1].

Two final states are studied in this work: three leptons (3l) and two leptons same-sign (2lSS) where only electrons and muons are considered. The hadronically decaying taus are explicitly vetoed. Several enriched regions for the signal and the main backgrounds, as the *tH*-enriched signal region in Figure 2, are defined to estimate the signal strength ($\mu(tH)$) in both channels. The signal strength is defined as the ratio of the measured number of events of a given event sample and the number of events predicted by the SM. Currently, the expected $\mu(tH)$ for each channel are: $\mu(tH) < 8.1$ for the 2lSS final state, and $\mu(tH) < 14.1$ for the 3l final state both at 95% confident level, including all systematics and statistical uncertainties.

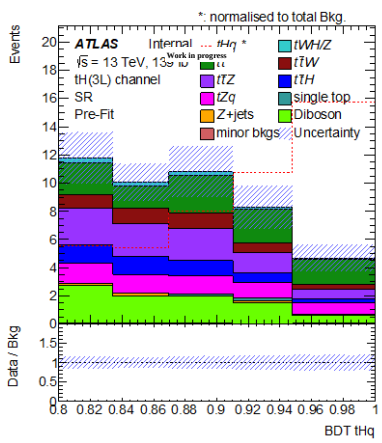

Figure 2. Signal region enriched in *tH*. This region is completely blinded to data.

[1] F. Demartin, F. Maltoni, K. Mawatari, and M. Zaro. *Eur. Phys. J. C* **75**, 267 (2015).

Search for long-lived neutral particles in pp collisions at $\sqrt{s}$ = 13 TeV that decay into displaced hadronic jets in the ATLAS calorimeter

Emma Torró Pastor, **Mariia Didenko***, Victoria Sánchez Sebastián

Instituto de Física Corpuscular (IFIC), Centro Mixto Universidad de Valencia - CSIC, Valencia, Spain.

*e-mail: mariya.didenko@cern.ch

Many Beyond the Standard Model (SM) theories predict the existence of new particles whose lifetimes can be long enough for them to travel a macroscopic distance before decaying. Long-lived particles (LLPs) are allowed in theories such as supersymmetric or neutral naturalness models which feature Hidden Sector (HS) [1] that address the hierarchy problem. The sensitivity of a given search to detect LLPs depends on its nature (neutral or charged) and the decay length (promptly decaying or displaced). The decay of a LLP created in proton-proton collisions in the ATLAS experiment could produce various highly unconventional signatures in the detector.

The analysis presents a search for neutral LLPs decaying hadronically in the ATLAS calorimeters [2]. A benchmark HS model is studied, where neutral long-lived scalar particles with masses ranging from 5 GeV to 475 GeV are produced in pairs from the decay of the mediator with masses between 60 GeV and 1000 GeV. If the scalar decay occurs in the calorimeters, the two resulting quarks are reconstructed as a single jet with unusual features compared to SM jets (see Fig. 1).

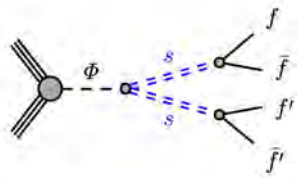

Figure 1: A diagram showing the $\Phi \to ss \to f\bar{f}f'\bar{f}'$ decay used as the benchmark model.

These jets will often have a high ratio of energy deposited in the Hadron Calorimeter (E_H) to energy deposited in the Electromagnetic Calorimeter (E_{EM}), E_H/E_{EM} referred to as the CalRatio. CalRatio jet candidates are first selected by dedicated LLP signature-driven triggers specifically designed for this search. Then, different machine learning techniques such as a neural network (NN) are used to identify displaced jets. In particular, a deep NN is used to predict whether candidate jets are produced by a LLP decay or from the expected sources of background: SM multijets, beam-induced background (BIB) and cosmic rays, and an adversarial training is applied to minimize the impact of Monte Carlo (MC) mismodeling. The use of this NN implies a noticeable improvement in sensitivity compared to the previous version of this search [3]. This is specially the case for low-mass mediators giving rise to low-p_T LLPs, with a challenging discrimination from BIB. MC simulations are not robust in predicting such unconventional signatures. Therefore, the analysis uses data-driven techniques for the background estimation.

The analysis uses the full LHC Run 2 dataset of 13 TeV collisions, corresponding to an integrated luminosity of 139 fb^{-1}. No significant excess of events in the signal region is observed with respect to the data-driven background prediction. The improvements to the analysis and additional data led to an extension of the limits for mediator masses above and below 200 GeV by a factor of around 1.5-2 and 3-5, respectively, compared to the previous version of the analysis [3].

For models with a SM-like Higgs boson mediator, branching fractions to neutral scalars above 10 % are excluded between approximately 2 cm and 12 m in the LLP mean proper lifetime ($c\tau$), depending on the scalar's mass (see Fig. 2).

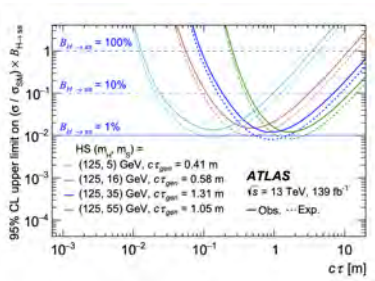

Figure 2: Summary of 95 % CL expected and observed limits on the branching fraction of a Higgs-like mediator to pairs of neutral LLPs considered in this analysis [2]

[1] M. J. Strassler and K. M. Zurek, *Phys. Lett. B* **651**, (2007).
[2] ATLAS Collaboration, arXiv:2203.01009 [hep-ex], Submitted to JHEP (2022).
[3] ATLAS Collaboration, *Phys. Rev. D* **99**, 052005 (2019).

Radiation hardness and timing performance of MALTA monolithic Pixel sensors in Tower 180 nm

Carlos Solans Sánchez

EP Department, CERN, Switzerland.

e-mail: carlos.solans@cern.ch

The MALTA family of depleted monolithic Pixel sensors have been produced in Tower 180 nm CMOS technology with small collection electrode and a novel asynchronous read-out that reduces the front-end power needs that allows to capture 100 MHit/s [1-3]. The challenge is to make this designs radiation hard to the levels of the inner trackers of the experiments at HL-LHC and beyond [4]. Prototypes have been produced with several process modifications to improve the charge collection. Starting from an n- blanket extends the junction to the full pixel size (standard), another one with a gap in the n- blanket (NGAP), and a third one with an extra deep p-well structure at the pixel edges (EDPW) [5]. Prototypes have been produced on high resistivity epitaxial silicon and on Czochralski substrates [6]. MALTA2 (Fig 1.) is the latest demonstrator of this family, and introduces a transistor in series (cascoded) to reduce the RTS noise and increase the gain of the front-end which is relevant for the uniform response of the matrix that does not contain an in-pixel threshold tuning mechanism. This technology is being developed at CERN in the context of the EP R&D and the AIDA innova programmes.

MALTA2 was extensively tested in particle beam tests at SPS CERN in 2021. Results will show its radiation hardness against 150 MRad TID and $2{\times}10^{15}$ 1 MeV n_{eq}/cm^2 NIEL. It will be presented how Czochralski substrates are better than epitaxial substrates for particle tracking at high doses due to the large charge collection that can be quantified by the size of the cluster. Additionally the Timing performance of the pixel will be evaluated with particle beams, where results will be shown on the average time of arrival of a hit to the collection electrode of the pixel. These are in line with the requirements of the bunch-crossing identification of the HL-LHC (25 ns), and not far away from those of the 15 ns bunch structure.

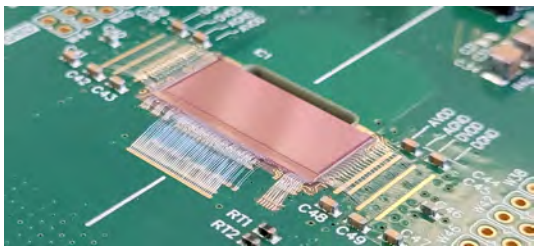

Figure 1. MALTA2 Monolithic Pixel detector.

[1] H. Pernegger et al, NIM A **986**, 164381 (2021).
[2] M. Dyndal et al, JINST **15**, P02005 (2020).
[3] W. Snoeys et al, NIM A **871**, 90 (2017).
[4] E.J. Schioppa et al, NIM A **958**, 162404 (2020).
[5] M. Munker et al, JINST **14**, C05013 (2019).
[6] C. Solans et al, PoS ICHEP2020, 871 (2021).

Acknowledgements: This project has received funding from the European Union's Horizon 2020 Research and Innovation programme under GA no 101004761.

Technological Applications of Extensive Air Showers Simulations

M. Suárez-Durán[1], C. Sarmiento-Cano[2], A.J. Rubio-Montero[3], A. Taboada[2], R. Pagán-Muñoz[3], R. Calderón-Ardila[2], L.A. Núñez[4], I. Sidelnik[5], **R. Mayo-García**[3,*], H. Asorey[2,6]

[1]*Université Libre de Bruxelles, Av. Franklin Roosevelt 50, 1050 Brussels, Belgium.* [2]*Instituto de Tecnologías en Detección y Astropartículas (ITeDA). Centro Atómico Constituyentes (CNEA/CONICET/UNSAM) Av. Gral. Paz 1499, 1450 Villa Maipú, Argentina.* [3]*Centro de Investigaciones Energéticas, Medioambientales y Tecnológicas (CIEMAT), Av. Complutense 40, 28040 Spain.* [4]*Universidad Industrial de Santander, Carrera 27 y Calle 9, 28231 Bucaramanga, Colombia.* [5]*Departamento de Física de Neutrones, Centro Atómico Bariloche (CNEA/CONICET) Av. Bustillo 9500, 8400 San Carlos de Bariloche, Argentina.* [6]*Departamento Física Médica, Centro Atómico Bariloche (CNEA) Av. Bustillo 9500, 8400 San Carlos de Bariloche, Argentina.*

*e-mail: rafael.mayo@ciemat.es

Atmospheric radiation is mainly produced during the interaction of high energy cosmic rays with the atmosphere. After the first interaction of these primary cosmic rays, a series of radiative and decay processes generate a collective process known as Extensive Air Shower (EAS), with up to 10 secondary particles per primary per GeV at the altitude of the maximum development, and continue evolving up to reach the ground level.

Bearing this in mind, to calculate the atmospheric radiation background is a very complex and demanding task. This computation is originated from the integration of all the secondary particles produced by the complete and modulated flux of cosmic rays that impinge on the atmosphere. For doing this we developed ARTI [1], a computational framework that takes advantage of the state-of-the-art radiation propagation and interaction codes, such as CORSIKA [2] and Geant4 [3], to trustworthily estimate the expected flux of radiation at any place in the World under real-time evolving atmospheric and geomagnetic conditions [4]. We are also capable to include the impacts produced during the sudden occurrence of transient astrophysical phenomena. As these calculations require a vast amount of computational resources, several approaches were adopted, such as the recent development of OneDataSim [5], a virtualized application to run ARTI at high-performance computing and cloud-based environments.

In this work, we show some of the implications and technological applications of our research, including results related to the precise calculation of the expected muon flux at underground laboratories, the mining prospecting and volcanoes risk assessment in muography, some new applications for precision agriculture and personal safe ward, and even how we are able to predict the occurrence of silent and non-silent errors at the new exascale supercomputers centres.

In addition, some results will be shown for the future ANDES underground laboratory. Thus, regarding the study of high energetic secondary particles at the tens of TeV scale for this lab background calculations and expected flux of muons for muography geophysical applications, the expected flux over an integration time of 1 year at different altitudes of the ANDES mountain profile will be presented.

In all those cases, the accuracy and statistical significance of previous results have been extended by using these new resources.

[1] C. Sarmiento-Cano *et al*., arXiv:2010.14591 [astro-ph.IM] (2021).
[2] D. Heck *et al*., Forschungszentrum Karlsruhe Report FZKA 6019 (1998).
[3] S. Agostinelli *et al*., *Nucl. Instrum. Meth. A* **506**, 250 (2003).
[4] H. Asorey, L.A. Nuñez, M. Suárez-Durán, *Space Weather* **16**, 461 (2018).
[5] A.J. Rubio-Montero *et al*., in 2021 Winter Simulation Conference Conf. Proc, 1-12 (2021).

Acknowledgements: This work has been partially funded by the Spanish Ministry of Science, Innovation, and Universities CODEC-OSE project (RTI2018-096006-B-I00) and the Comunidad de Madrid CABAHLA project (S2018/TCS-4423), both with European Regional Development Fund (ERDF). It also profited from funding received by the H2020 co-funded project European Open Science Cloud - Expanding Capacities by building Capabilities (EOSC-SYNERGY, No. 857647). Simulations carried out made also use of the computing facilities provided by CETA-CIEMAT and CIEMAT.

Commissioning and Monitoring of the Calorimeter sub-detector of LHCb experiment

Paula Garcia Moreno[1,2]

[1] *Departament de Física Quántica i Astrofísica, Institut de Ciències del Cosmos, Spain.*
[2] *Universitat de Barcelona, Spain.*

e-mail: paula.garcia.moreno@cern.ch

In the upcoming months the LHC will start running again after a three-year shutdown, with the aim of starting a new period of data taking with five times more luminosity (Run 3). Due to that fact, all the LHCb sub-detectors will need to adapt to the new conditions to operate successfully.

The Calorimeter sub-detector is in charge of measuring the energy and position of the electrons, photons and hadrons by reading their energy in the Calorimeter cells [1]. In this talk I will report about the work that has already been performed, the work that is under development and the future steps that are going to be done regarding the Calorimeter sub-detector commissioning and monitoring tasks. Specifically, I will explain in an intuitive way how the Calorimeter software was configured in order to show useful histograms obtained with the firsts runs of the new beams, the problems we faced while working and the solutions we finally encountered.

Finally, I will give a brief report about my work on deciding which mask shape (3x3 cells, 2x2 cells or Swiss Cross cells) is used to perform electromagnetic clusters in the Electromagnetic Calorimeter in the new upgrade conditions [2]. That decision is made taking into account which mask shape is giving a higher resolution in energy and in position.

[1] LHCb collaboration, *Photon and neutral pion reconstruction* **LHCb-2003-091**.
[2] Alexis Vallier, *Photon reconstruction optimisation for the LHCb detector upgrade.*

Acknowledgements: I would want to acknowledge LHCb collaboration and my research group in Institut de Ciències del Cosmos for all the support I received during my work.

Simulation and reconstruction of scintillation light with X-ARAPUCA photodetectors in SBND

Rodrigo Alvarez Garrote*

Departamento de Investigación Básica, CIEMAT, Spain.

e-mail: rodrigo.alvarez@ciemat.es

SBND is a time-projection chamber that collects ionisation electrons and scintillation photons from liquid argon (LArTPC). It will be located 110 m downstream the Booster Neutrino Beam target at Fermilab and it is currently under construction. The SBND physics program is focused on beyond the Standard Model searches (sterile neutrinos, heavy neutral leptons, light dark matter...) and neutrino-argon cross-sections.

The photodetection system (PDS) provides trigger capabilities, cosmic-rays rejection (a large background due to the near-surface detector location), and complementary calorimetry. The PDS includes PMTs and X-ARAPUCAsensors, a novel technology that features single photo-electron resolution at cryogenic temperatures with large area coverage in a cost-effective fashion.

Proper simulation of the light readout and reconstruction is key for a precise determination of the interaction time (t0) and energy reconstruction, thus improving background rejection. In this talk, we present the latest X-ARAPUCA energy and time resolution estimates using a full SBND detector simulation. These results are of great interest because future LArTPC experiments such as DUNE will use X-ARAPUCAs as their PDS.

Unitarized one-loop graviton-graviton scattering

Rafael Delgado Lopez[1,*], Antonio Dobado[2], Domènec Espriu[3]

[1] *Matemática Aplicada a las TIC, ETSIS de Telecomunicación (UPM), Campus Sur, 28031 Madrid, Spain.* [2] *Departamento de Física Teórica and Instituto IPARCOS Universidad Complutense de Madrid, 28040 Madrid, Spain.* [3] *Departament de Física Quàntica i Astrofísica and Institut de Ciències del Cosmos (ICCUB) Universitat de Barcelona, 08028 Barcelona, Catalonia, Spain*

*e-mail: rafael.delgado@upm.es

We analyze [1] the next to leading order (NLO) graviton-graviton scattering amplitude via the Inverse Amplitude Method (IAM), well known to low-energy QCD practitioners [2]. Like the electroweak chiral lagrangian, successfully used for low-energy QCD, the Einstein-Hilbert (EH) lagrangian is a non-linear and non-renormalizable theory whose most relevant operator is a dimension two one containing two derivatives of the dynamical lagrangian. Both lagrangians contain a dimensionful constant in four dimensions: f_π for the pion lagrangian and the Planck mass M_P for the EH lagrangian. However, the EH lagrangian describing gravity is a gauge theory.

We use the tree-level graviton-graviton scattering amplitude given in [3] and the NLO computation done by Dunbar and Norridge [4] using string theory methods. Only counterterms proportional to $\mathcal{R}^2$, $\mathcal{R}_{\mu\nu}\mathcal{R}^{\mu\nu}$ and $\mathcal{R}^{\gamma\delta}_{\alpha\beta}\mathcal{R}^{\alpha\beta}_{\gamma\delta}$ are needed [3]. On-shell (lowest order equations of motion) these counterterms vanish, so that the theory is UV finita at NLO.

Dispersion relation via the inverse amplitude method [2,5] are used to seek for hypothetical graviton-induced resonances similar to those appearing in QCD. We focus on the $++++$ and $----$ helicity channels and analyze the $J = 0$, 2 and 4 partial waves. We look for resonances on the second Riemann sheet as well as for artifacts in the first Riemann sheet. The study of these artifacts is necessary since their appearance can mean that the inverse amplitude method is being applied beyond its validity conditions.

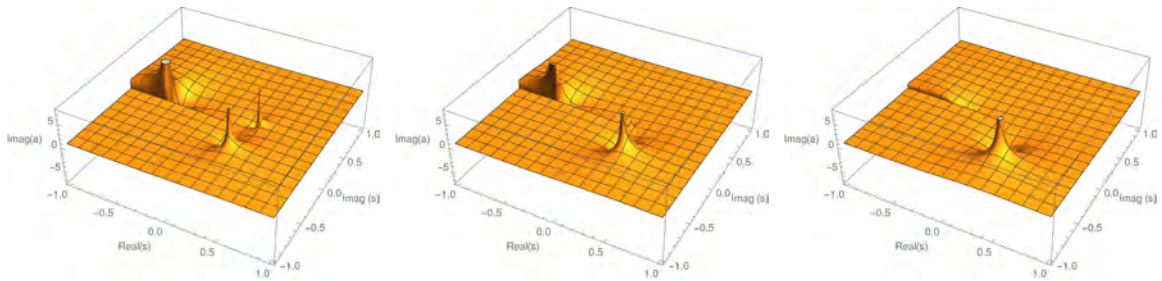

Figure 1: Figure from [1]. From top left, to right: plots of Imag a_0^{IAM} for different values of $\mu/M_p = 0.40$, 0.35, 0.30. μ plays the role of an infrared cutoff [1]. See the dissapearance of the poles on the first Riemann sheet (quadrants I and II).

[1] R.L. Delgado, A. Dobado, D. Espriu, to appear on arXiv.
[2] A. Dobado, J.R. Pelaez, *Phys. Rev. D* **56** (1997) 3057.
[3] G.'t Hooft, M. Veltman, *Ann. Inst. H. Poincaré A* **20** (1974) 69.
[4] D.C. Dunbar, P.S. Norridge, *Nucl. Phys. B* **433** (1995) 181.
[5] Rafael L. Delgado, A. Dobado, F.J. Llanes-Estrada, *Phys. Rev. D* **91** (2015) 7, 075017.

Acknowledgements: R.L.Delgado was supported by the Ramón Areces Foundation post-doctoral fellowship, the INFN post-doctoral fellowship AAOODGF-2019-0000329 and the Spanish grant MICINN: PID2019-108655GB-I00.

Gravitational particle production in the laboratory

Álvaro Parra-López[1,*], Jose A. R. Cembranos[1], Stefan Floerchinger[2], Tobias Haas[2], Natalia Sánchez-Kuntz[2], Mireia Tolosa-Simeón[2]

[1]*Departamento de Física Teórica and IPARCOS, Facultad de Ciencias Físicas, Universidad Complutense de Madrid, Ciudad Universitaria, 28040 Madrid, Spain.*
[2]*Institut für Theoretische Physik, Universität Heidelberg, Philosophenweg 16, 69120 Heidelberg, Germany.*

*e-mail: alvaparr@ucm.es

Considering quantum field theory in a general spacetime results in the appearance of phenomena such as the Unruh effect or Hawking radiation. In particular, the temporal variation of the geometry leads to the production of particles. This mechanism will be present as long as there exist a matter field that feels the time evolution of spacetime, and can explain, for example, the observed abundance of dark matter particles as a result of the heavy expansion carried out during inflation [1]. Since direct detection of such process seems unreachable, the use of *simulators* of these cosmological scenarios has been proposed. This is the main objective of the **analog gravity** field: To reproduce the dynamics of the field in certain geometry using as model a system that can be realized in the laboratory. The most extended analogy makes use of a weakly interacting Bose-Einstein condensate, described by the complex field Φ,

$$\Phi = \text{background} + \text{fluctuations} = \sqrt{n_0} e^{iS_0} + \frac{1}{\sqrt{2}} \left(\phi_1 + i\phi\right). \tag{1}$$

The system can be adjusted such that the imaginary part of the phononic fluctuations ϕ on top of its ground state behave as a massless scalar field in a flat FLRW universe.

Our work generalizes this analogy to FLRW universes with non-zero spatial curvature κ [2]. At the same time, we provide suitable observables in terms of the density contrast that can be used to detect particle production in a real experiment, as seen in [3]. The connection between the known theoretical result for the spectrum of produced particles S_k [4] and the laboratory comes from the proportionality $\delta_c \sim \dot{\phi}$, where $\delta_c(t, \boldsymbol{r}) \propto \sqrt{n_0(r)}\left[n(t, \boldsymbol{r}) - n_0(r)\right]$ is the density contrast and $n(t, \boldsymbol{r}) = |\Phi(t, \boldsymbol{r})|^2$ is the full condensate density.

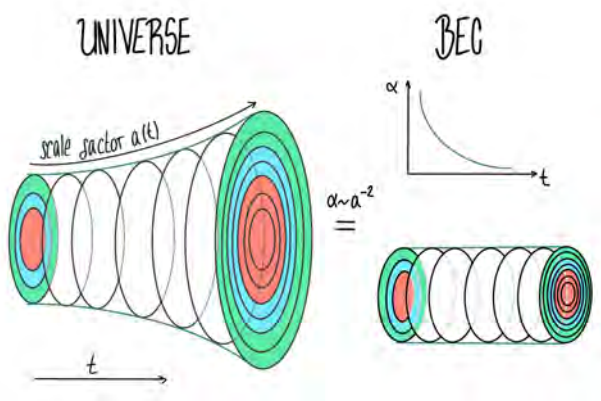

Figure 1. Analogy between BECs and cosmological expansion. Expansion is carried out by decreasing the interaction strength through Feshbach resonance.

This framework can be used to study particle production in the context of inflation through analogs of actions such as

$$S = -\frac{1}{2} \int \mathrm{d}^4 x \sqrt{-g} \left[\partial_\mu \varphi \partial^\mu \varphi + \left(m^2 + \xi R\right) \varphi^2\right], \tag{2}$$

which is of interest in early universe cosmology [1, 5]. In this way, analog models of gravity allow for the exploration of the characteristics of quantum fields in curved spacetime straight from the laboratory.

[1] Jose A. R. Cembranos *et al*, *JHEP* ***2020***, *84 (2020)*..
[2] Mireia Tolosa-Simeón *et al*, *arXiv:2202.10441 (2022)*.
[3] Celia Viermann *et al*, *arXiv:2202.10399 (2022)*.
[4] Natalia Sánchez-Kuntz *et al*, *arXiv:2202.10440 (2022)*.
[5] Álvaro Parra-López and J. A. R. Cembranos, *in preparation* (2022).

Acknowledgements: Spanish MIU (FPU20/05603) and MICINN (PID2019-107394GB-I00).

Some uses of dispersion relations

Felipe J. Llanes-Estrada
Depto. Física Teórica e IPARCOS, Universidad Complutense de Madrid, Spain.
*e-mail: fllanes@fis.ucm.es

Dispersion relations (pioneered by Kramers and Kronig) are integral identities satisfied by scattering amplitudes. They are a consequence of Titchmarsh's and Cauchy's theorems, and thus of analyticity, that follows from causality in scattering. They cannot be directly derived for partial-wave amplitudes [1] of fixed angular momentum t_J on an object extended to distance R because of an exponential factor $T(s,t,u) \propto \exp\left(-2iR\sqrt{(s-4m^2)\sin(\theta(s,t)/2)}\right)$ diverging when s acquires an imaginary part $+is_I$ in the upper complex plane. Because that factor is $exp(2iR\sqrt{|t|})$, there is no obstacle to derive them for fixed-t amplitudes (also allowing partial waves to satisfy them in certain kinematics). They are extensively used in hadron physics, as I will exemplify for Compton scattering [2] that helped limit the possibilities to solve the proton radius puzzle, or by their use to fix the renormalization scale of the real part of an exclusive amplitude once that of the imaginary part has been chosen [3].
Also useful is the Inverse Amplitude Method (IAM) that leans on applying Cauchy's theorem to an appropriately subtracted inverse amplitude $\frac{1}{t_J(s)}$: the exponential factor now appears in a denominator and becomes a convergence factor.
Dispersion relations do not contain by themselves the full dynamical information of the strong interactions: they are best seen as constraints. However, they become very predictive [5] when combined with the momentum expansion of contemporary Effective Field Theories (EFTs) such as Chiral Perturbation Theory or Higgs Effective Field Theory (HEFT). The IAM is especially well suited to this expansion, because the resulting model amplitude satisfies elastic unitarity *exactly* and allows to exploit the validity of EFTs up to their full range $4\pi f$, whereas they fail, even often near threshold, when the amplitude t_J itself is expanded, because of bad unitarity behaviour. An example of the IAM is shown in figure 1, that shows a resonance predicted from supposed near threshold HEFT parameters that could be measured in the accelerator program. Given this potential use to extend the reach of collider measurements in the electroweak sector, we recently completed an investigation of the uncertainties of the IAM [6].

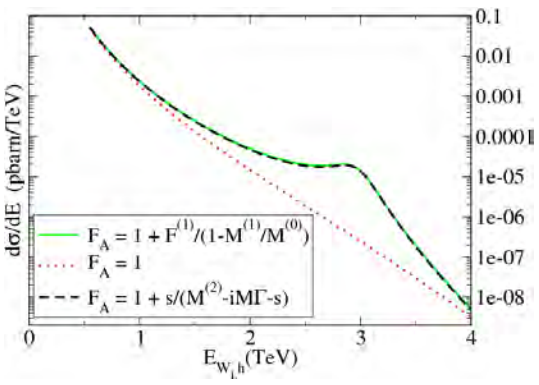

Figura 1: Example $W_L h$ resonance calculated from the IAM as applied to HEFT with coefficients beyond the Standard Model, fed into a form factor parametrization satisfying Watson's final state theorem (thus, having the same pole position as the IAM). (From [4].)

Time permitting, I will describe ongoing work [7] on their use to try to extract the possible slight delay of γ-radiation from astrophysical sources from knowledge of their slight absorption by cosmic electrons (via Compton scattering) or by the Breit-Wheeler process ($\gamma\gamma \to e^-e^+$) on extragalactic background light. Depending on the γ energy, this delay may be measurable by timing events by the arrival of a concurrent gravitational wave and is of interest for multimessenger astrophysics.

[1] F. J. Llanes-Estrada and R. Roldán-González, *SciPost Phys. Core* **5**, 016 (2022).
[2] M. Gorchtein, F. J. Llanes-Estrada and A. P. Szczepaniak, *Phys. Rev. A* **87**, 052501 (2013).
[3] S. J. Brodsky and F. J. Llanes-Estrada, *Eur. Phys. J. C* **46**, 751 (2006).
[4] A. Dobado, F. J. Llanes-Estrada and J. J. Sanz-Cillero, *JHEP* **03**, 159 (2018).
[5] R. L. Delgado, A. Dobado and F. J. Llanes-Estrada, *Phys. Rev. D* **91**, 075017 (2015).
[6] A. Salas-Bernárdez, F. J. Llanes-Estrada, J. Escudero-Pedrosa and J. A. Oller, *SciPost Phys.* **11**, 020 (2021).
[7] D. Beltrán Martínez, F. J. Llanes-Estrada and G. Tejedor García, work in preparation.

Acknowledgements: Supported by grants MICINN: PID2019-108655GB-I00, PID2019-106080GB-C21 (Spain); EU's 824093 (STRONG2020) Univ. Complutense de Madrid under research group 910309 and the IPARCOS institute.

On the doubly charmed tetraquark T_{cc}^{+} recently discovered at CERN: analysis and predictions

Miguel Albaladejo

Instituto de Física Corpuscular (centro mixto CSIC-UV)
Institutos de Investigación de Paterna, C/Catedrático José Beltrán
46980 Paterna, Valencia, Spain.

*e-mail: Miguel.Albaladejo@ific.uv.es

The neutrons and protons composing the matter that usually surrounds us are made up of three quarks (udd and uud, respectively), which are bound by the so-called strong force. They are a type of particles called *baryons*. But nothing in the underlying theory of strong interactions (called *Quantum Chromodynamics*) prevents the existence of other, more exotic forms of baryons, such as the pentaquarks ($qqqq\bar{q}$). Analogously, most known *mesons* are composed of a $q\bar{q}$ pair, but there can exist also tetraquarks ($q\bar{q}q\bar{q}$). In addition, states can be formed including constituent *gluons* (g), which are the carriers of the strong force, such as hybrid mesons ($q\bar{q}g$) or baryons ($qqqg$), glueballs (gg), etc. Finally, to make it even more interesting, quarks come in six *flavors* (u, d, s, c, b, and t), which generates a humongous zoo of possible particles.

The LHCb collaboration at CERN has recently claimed the discovery of the first doubly charmed meson, named T_{cc}^{+} [1,2]. Because of the decay properties of this state, we *know* that it is a $cc\bar{u}\bar{d}$ tetraquark. In this talk we report on our recent work [3], in which we have studied the $DD\pi$ spectrum where a prominent signal from the said state is observed, see Fig. 1. We have performed an analysis of the scattering of the $D^{*+}D^{0}$ and $D^{*0}D^{+}$ systems, in which the T_{cc}^{+} state should appear. A simple model for the scattering amplitude is used, and it is found to describe well the experimental spectrum. Finally, using Heavy-Quark Spin Symmetry, we predict the location of possible heavier $D^{*}D^{*}$ partners.

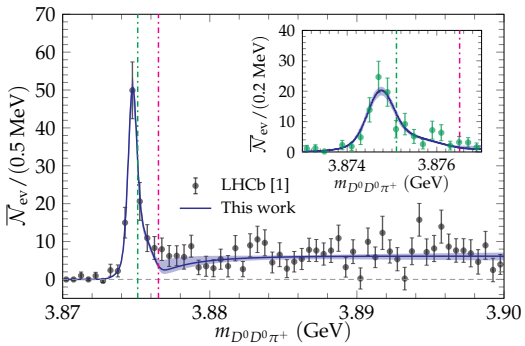

Figura 1: $D^{0}D^{0}\pi^{+}$ spectrum showing the prominent T_{cc}^{+} signal. The data come from the LHCb collaboration [1] and the theoretical curve is our analysis [3]. The green and purple vertical dashed-dotted lines represent the $D^{*+}D^{0}$ and $D^{*0}D^{+}$ thresholds, respectively.

Besides the quark content of the state, it is interesting to learn about *how* these quarks are configured inside the state. For the T_{cc}^{+} two possibilities appear, namely a hadron molecule (a loosely bound state of a D^{*} and a D meson) or a compact tetraquark, in which the four quarks are closely packed and there is no trace of the D^{*} and D mesons. Using Weinberg's compositeness criterion [4], which is in turn based on simple quantum mechanical arguments, we show that the T_{cc}^{+} state has a large molecular component.

[1] R. Aaij et al., LHCb collaboration, Observation of an exotic narrow doubly charmed tetraquark, 2109.01038.
[2] R. Aaij et al., LHCb collaboration, Study of the doubly charmed tetraquark T_{cc}^{+}, 2109.01056.
[3] M. Albaladejo, T_{cc}^{+} coupled channel analysis and predictions, *Phys. Lett. B* **829**, 137052 (2022) [2110.02944].
[4] S. Weinberg, Evidence That the Deuteron Is Not an Elementary Particle, *Phys. Rev.* **137**, B672 (1965).

Analysis and instrumentation developments for the future understanding of neutrino physics with the T2K experiment

C. Jesús-Valls

Institut de Física d'Altes Energies (IFAE) - The Barcelona Institute of Science and Technology (BIST), Campus UAB, 08193 Bellaterra (Barcelona), Spain

*e-mail: cjesus@ifae.es

Nowadays, one of the most active fields of research within high energy physics (HEP) is the study of neutrinos. Despite being theorized in the 1930s and discovered in 1956, neutrinos low interaction probability has slowed down their study notably. It was not until two decades ago that a fundamental property of neutrinos was discovered: neutrino oscillations.
Neutrino oscillations are ruled by six parameters: Three mixing angles ($\theta_{12}, \theta_{13}, \theta_{23}$), two squared neutrino mass differences (Δm^2_{12}, Δm^2_{23}) and one CP-violating phase (δ_{CP}). Concerning their values, three major open questions remain open:

- The θ_{23} octant: Is θ_{23} equal, larger or smaller than 45°?
- The matter-antimatter asymmetry in neutrino oscillations: Is $\delta_{CP} \neq \{0, \pi\}$?
- The mass ordering: Is m_1 larger or smaller than m_3?

A quest has started to answer these questions in what has been named as the era of neutrino precision experiments. Among the existing ones, the Tokai-To-Kamioka (T2K) experiment located in Japan is a leading reference. T2K has been operational since 2010 and has produced some of the most important results in neutrino physics in the last decade: the discovery of a non-null θ_{13}, the best existing constrains for θ_{23} and recently, the first significant hints of a potentially large CP-violation in neutrino oscillations.
Currently, two factors limit further precise measurements in T2K. On one hand, the limited number of collected neutrino events resulting in a significant statistical error. On the other hand, the current systematic errors associated to the event rate predictions. To increase the current statistics, T2K's beam has been recently upgraded and will be upgraded again around 2024, resulting in a 2.6 increase factor of the current neutrino flux. To reduce the systematic errors, two options can be explored:

- Use data to perform dedicated measurements to constrain uncertainties.
- Upgrade the detectors to achieve improved constraints in the future.

My thesis focuses on both of these aspects.
In T2K's oscillation analysis (OA), one of the major nuisances is that of neutrino neutral-current interactions producing a single charged pion in the final state. The current knowledge on this process is very limited, as few tens of events of data have ever been collected in bubble chamber experiments, more than four decades ago. Due to this, constraining this process is crucial in order to alleviate their impact in the OA. In my thesis, using T2K data these interactions are studied in detail for the first time in history.
To measure neutrino interactions, such as the one described above, T2K uses its near detector ND280. ND280 is crucial for the experiment as it constrains the systematic errors associated to the event rate prediction. To push even further the current results of T2K, ND280 is being significantly upgraded with the addition of three new detector technologies: Two new high-angle Time-Projection-Chambers (HATPCs), a novel quasi-3D fully active Super-Fine-Grained-Detector (SuperFGD) and large area plastic scintillator panels which provide very accurate Time-Of-Flight information (ToF panels). In my thesis I have contributed significantly to the development of these new technologies, validating the novel readout of the HATPCs, characterizing and measuring for the first time the PID capabilities of SuperFGD and developing novel Deep Learning reconstruction techniques for SuperFGD and the ToF panels.
With all, T2K is expected to continue to lead the determination of some of the most crucial properties of neutrinos in the next years.

The ATLAS Level-1 Topological Trigger: Run 2 performance and plans for Run 3

Paula Martínez Suárez, on behalf of the ATLAS Collaboration
IFAE-BIST, Universitat Autònoma de Barcelona, Bellaterra (Barcelona), Spain.
e-mail: paula.martinez.suarez@cern.ch

The Large Hadron Collider (LHC) is the world's largest particle accelerator. It consists of a 27 km ring with superconducting magnets capable of accelerating protons currently up to 6.5 TeV, thus producing pp collisions at a centre-of-mass energy of 13 TeV. The ATLAS experiment [1] is one of the two general-purpose detectors installed in the LHC. It consists of an inner tracking detector surrounded by a thin superconducting solenoid providing a 2 T axial magnetic field, electromagnetic and hadronic calorimeters, and a muon spectrometer. During Run 2 (2015-2018), the LHC delivered pp collisions to the ATLAS experiment with an instantaneous luminosity up to 2.1×10^{34} cm^{-2}s^{-1}, at a collision rate of 40 MHz, which is too large to be managed by the detector readout system, storage and offline computing resources. In order to reduce it down to a manageable 1-1.5 kHz while saving as many interesting collisions as possible, the ATLAS detector relies on a two-level trigger system, consisting of a Level-1 trigger (online, hardware) and a High Level trigger (offline, software). The Level-1 trigger is the first rate-reducing step in the ATLAS trigger system with an output rate of up to 100 kHz and a decision latency of less than 2.5 μs, and it provides the input to the High Level trigger.

Since 2017, an important role has been played by the Level-1 Topological Trigger (L1Topo) [2]. This system consists of two AdvancedTCA modules, each of them equipped with two processor FPGAs (Xilinx Virtex7) to run trigger algorithms and one controller FPGA (Kintex7) to communicate with the external trigger systems. Up to 128 algorithms can be implemented to select interesting events by applying kinematic or angular requirements on e/γ and tau clusters, jets, muons and total energy reconstructed in the detector, all of this happening with a latency of 200 ns. This results in a significantly improved background rejection and signal acceptance. The L1Topo system is very important for physics analyses relying on low energy objects, for example Higgs or B-Physics (Fig. 1), where quantities such as the invariant mass or the angular distance between objects are key in order to keep an acceptable trigger rate without the need of raising the energy thresholds.

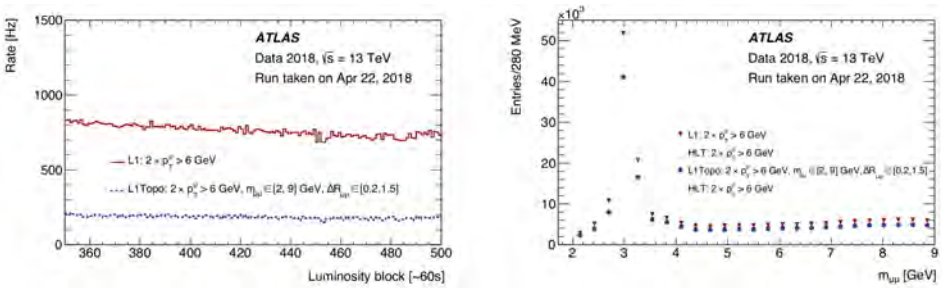

Figure 1. Rate of topological vs. non-topological L1 di-muon triggers w.r.t. time (left) and event acceptance of two HLT triggers seeded by them as a function of the di-muon invariant mass (right). This is an example of how topological requirements can reduce the trigger rates significantly while preserving signal acceptance.

The ATLAS trigger system has undergone several upgrades in preparation for Run 3 (2022-2025), featuring finer granularity in both energy and (η, ϕ) position of the different reconstructed objects, and improved object quality information useful for triggering interesting events. A new L1Topo system with new topological algorithms has been installed and will benefit from all these features. During the beginning of Run 3, the Run 2 L1Topo system will run in parallel for commissioning.

[1] ATLAS Collaboration, *The ATLAS Experiment at the CERN Large Hadron Collider*, JINST 3 (2008) S08003.
[2] ATLAS Collaboration, *Performance of the ATLAS Level-1 topological trigger in Run 2*, CERN-EP-2021-040 (2021).
[3] ATLAS Collaboration,Technical Design Report for the Phase-I Upgrade of the ATLAS TDAQ System, CERN-LHCC-2013-018, ATLAS-TDR-023 (2013).

Data-Driven Calibration of B-Tagged and Large-R Jets for γ+jet Events in The ATLAS Experiment

Naseem Bouchhar*, Miguel Villaplana, Marcel Vos

Instituto de Física Corpuscular (IFIC), Centro Mixto Universidad de Valencia - CSIC, Valencia, Spain.

*e-mail: naseem.bouchhar@ific.uv.es

The ATLAS detector at the Large Hadron Collider (LHC) consists of four components: The inner detector, EM and hadronic calorimeter and muon detector.

Particles in the LHC often decay hadronically, and these decay products may be reconstructed as jets. Jets are the dominant high-p_T processes in the LHC and play a crucial role in understanding the structure of protons, colour interactions and the coupling strength α_s.

Reconstruction of jets are taken from clusters of topologically connected calorimeter cell signals (called topo-clusters), and from tracks (a charged particle hitting the inner detector) [1].

The energy and mass of jets measured in the ATLAS detector are calibrated via a multi-step process shown in figure 1.

The focus here is on data-driven (called in-situ) calibration, in which measurements are made in events where the jet recoils against a well-calibrated reference object shown in figure 2. This is to account for discrepancies in the jet response between data and MC.

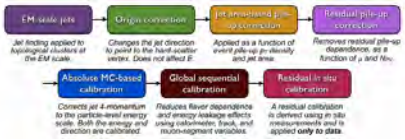

Figure 1. Process for the calibrations of the energy and mass of jets

This talk will be on in-situ calibration results obtained from data-to-MC ratios of the p_T balance between jets and photons for b-tagged jets and large-R jets using the full ATLAS Run2 dataset.

- B-tagged jets: The use of b-tagging is a useful tool in jet analysis that allows one to distinguish from jets originating from the hadronisation of bottom quarks from other quarks. For this talk these jets are small-radius jets (R = 0.4) using Particle Flow Objects (PFOs) [2]. This analysis is using the DL1r tagging algorithm [3].
- Large-R jets: Large-R (R = 1.0) jets clustered with anti-k_t Unified Flow Objects (UFOs), which are a unification of PFOs and TCCs (Track-CaloClusters) [2].

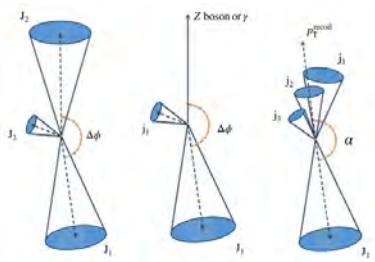

Figure 2. Jet balance against dijet events (left), Z/γ events (middle), multi jet events(right).

[1] The ATLAS Collaboration,Topological cell clustering in the ATLAS calorimeters and its performance in LHC Run 1, *Eur. Phys. J. C* **77**, 490 (2017).
[2] The ATLAS Collaboration, Optimisation of large-radius jet reconstruction for the ATLAS detector in 13 TeV proton-proton collisions, *Eur. Phys. J. C* **81**, 334 (2021).
[3] The ATLAS Collaboration, Optimisation and performance studies of the ATLAS b-tagging algorithms for the 2017-18 LHC Run, *PoS EPS-HEP2017* 733 (2017).

Acknowledgements: We thank CERN for the very successful operation of the LHC, as well as the support staff from our institutions without whom ATLAS could not be operated efficiently. We acknowledge the support of MICINN, Spain and of the GenT Programme Generalitat Valenciana, Spain. And special thanks to Daniel Camarero Muñoz for help in the analysis.

Results of the SDHCAL Beam Test data analysis of 2015

Héctor García Cabrera*, on behalf of the SDHCAL group

Centro de Investigaciones Energéticas, Medioambientales y Tecnológicas.

e-mail: Hector.Garcia2@ciemat.es

The Semi-Digital Hadronic CALorimeter [1] is one of a family of technological prototypes from the CALICE collaboration with the aim to test high granularity technologies for the development of calorimeters in the context of future e^+e^- Higgs Factories. The SDHCAL, built in 2011, is an hadronic calorimeter with Glass Resistive Plate Chambers (GRPC) as active materials and stainless steel as absorber. During the last few years several campaigns of data taking in beam test conditions have been completed, resulting in an analysis of the detector capabilities, energy resolution, development of fine tune corrections and particle identification algorithms.

The data analysis procedures and results are presented. The analysis includes the event building from the raw stream of data into physically meaningful events and algorithms to identify the different particles presen on the beam to create the data sets used for the measurements of efficiency, multiplicity, energy reconstruction and energy resolution. Alongside this measurements, fine tune corrections have been developed to improve and generalize the response of the prototype. These corrections include the study of the incident angle effect and the beam intensity effect.

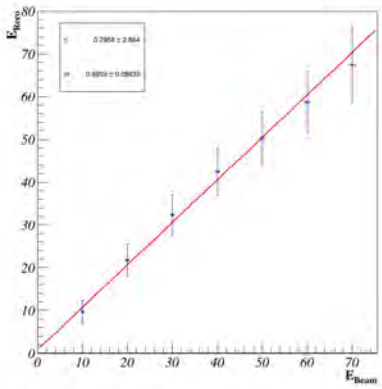

Figure 1. Linearity response of Pions in the SDHCAL.

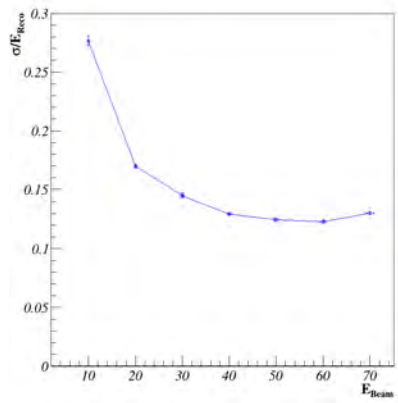

Figure 2. Energy resolution of Pions in the sDHCAL

An efficiency of detection of > 90%, linear response (within +- 10%) and energy resolutions down to 14% have been computed for different angle data sets.

[1] G. Baulieu *et al*., Construction and commissioning of a technological prototype of a high-granularity semi-digital hadronic calorimeter. *JINST* **10**, P10039 (2015). arXiv: 1506.05316 [physics.ins-det].

IIB orientifold reductions with open strings

Juan R. Balaguer[1], Giuseppe Dibitetto[2,3], Jose J. Fernandez-Melgarejo[4], Alejandro Ruipérez[2,3]

[1] *Departamento de Física, Universidad de Murcia,Campus de Espinardo, E-30100 Murcia, Spain.*
[2] *Dipartimento di Fisica e Astronomia, Università di Padova, via Marzolo 8, 35131 Padova, Italy.*
[3] *INFN, Sezione di Padova, via Marzolo 8, 35131 Padova, Italy.*
[4] *Departamento de Electromagnetismo, Universidad de Murcia,Campus de Espinardo, E-30100 Murcia, Spain.*

*e-mail: juanramon.balaguer@um.es

We consider type IIB compactifications on a general 4D group manifold with different types of possible spacetime filling O-planes and the corresponding D-branes parallell to them. Once fluxes allowed by the associated orientifold projection are included, a 6D $\mathcal{N} = (1,1)$ gauged supergravity is obtained. We show how the consistent coupling to dynamical open strings living on the spacetime filling D-branes may be captured by the inclusion of extra vector multiplets and extra embedding tensor deformations on the gauged supergravity side. As a result, the quadratic constraints on the embedding tensor consistently reproduce the (modified) 10D Bianchi identities, and the entire scalar potential of the theory exactly matches the one obtained from reduction of the bulk action plus the DBI contributions.

[1] G. Dibitetto, J. J. Fernández-Melgarejo, and M. Nozawa, "6D (1,1) Gauged Supergravities from Orientifold Compactifications," *JHEP* **05** (2020) 015.
[2] E. Bergshoeff, R. Kallosh, T. Ortin, D. Roest, and A. Van Proeyen, "New formulations of D = 10 supersymmetry and D8 - O8 domain walls," *Class. Quant. Grav.* **18** (2001) 3359–3382.
[3] R. C. Myers, "Dielectric branes," *JHEP* **12** (1999) 022.
[4] L. Martucci, J. Rosseel, D. Van den Bleeken, and A. Van Proeyen, "Dirac actions for D-branes on backgrounds with fluxes," *Class. Quant. Grav.* **22** (2005) 2745–2764.
[5] J. Choi, J. J. Fernández-Melgarejo, and S. Sugimoto, "Deformation of $\mathcal{N} = 4$ SYM with varying couplings via fluxes and intersecting branes," *JHEP* **03** (2018) 128.

Acknowledgements: The work of JRB is supported by Fundación Séneca, Agencia de Ciencia y Tecnología de la Región de Murcia, grant 21472/FPI/20.

Light Detection in DUNE's Vertical Drift Module

Rodrigo Álvarez-Garrote, **Sergio Manthey Corchado***, Laura Pérez-Molina, Andrés de la Torre Rojo

Departamento de Investigación Básica, CIEMAT, Spain.

*e-mail: sergio.manthey@ciemat.es

The Deep Underground Neutrino Experiment (DUNE) is an international project at the Long-Baseline Neutrino Facility (LBNF), in the United States. It is hosted by the U.S. Department of Energy's Fermilab laboratory.

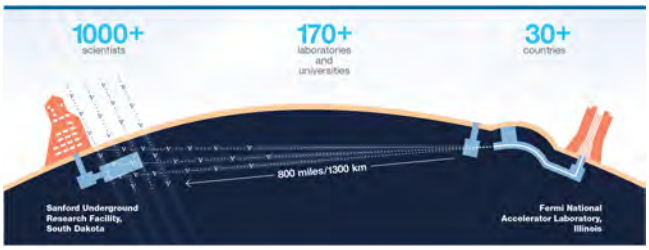

Figure 1. Schematic representation of the DUNE experiment and its different facilities.

DUNE's major goals are to precisely measure the neutrino oscillation parameters, detect neutrinos from supernovas and search for proton decay [1]. It consists of two sets of massive neutrino detectors: Near Detectors (ND) at Fermilab (Illinois) and Far Detectors (FD) 1300 km away at Sanford Underground Research Facility (South Dakota). LBNF produces the world's most intense neutrino beam and provides the infrastructure to study these elusive particles in great detail (Fig. 1).

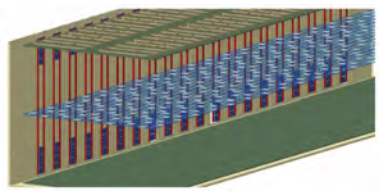

Figure 2. 3D Model of the VD proposal for the 2nd FD module.

DUNE's FD will be composed of four Liquid Argon Time Projection Chambers (LAr-TPCs). The proposed configuration for the 2nd FD module is a Single Phase LAr-TPC with electron Drift along the Vertical axis (VD) with two volumes of (13.5 x 6.5 x 60)m^3 dimensions separated by a cathode plane (Fig. 2). The Photon Detection System (PDS) will make use of large size X-ARAPUCA tiles [2] distributed over three detection planes: one horizontal plane with double sided tiles installed on the high voltage cathode and two vertical planes positioned on the longest cryostat membrane walls. The initial performance of the VD PDS using Monte Carlo simulations [3] is currently being estimated.

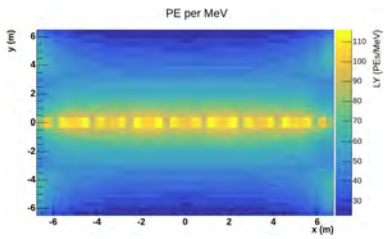

Figure 3. Light-Yield map of the PDS configuration shown in Figure 2.

We present the first studies of the X-ARAPUCA tile distribution over the vertical planes. Different layouts have been simulated in order to optimize the detector's uniformity and maximize the photon collection. Figure 3 shows the number of detected Photo Electrons (PE) per MeV of deposited energy of an example configuration. This information is represented as a Light-Yield 2D map of the central x-y plane (13.5 x 13)m^2 with averaged values over the z axis, being the y axis along the drift direction. These maps have been used to determine which PDS configuration is expected to deliver the best performance.

[1] DUNE Collaboration,*Far Detector Technical Design Report, Volume III*, (2020).
[2] A.A. Machado, E. Segreto, D. Warner, A. Fauth, B. Gelli, R. Máximo, R. A. Pissolatti, L. Paulucci, and F. Marinho, *The X-ARAPUCA: an improvement of the ARAPUCA device*, Journal of Instrumentation, (2018).
[3] L. Paulucci et al, *The DUNE Vertical Drift Photon Detection System*, Journal of Instrumentation, (2021).

Photon Detection System in ProtoDUNE phase II

Rodrigo Álvarez-Garrote, Sergio Manthey Corchado, **Laura Pérez-Molina***, Andrés de la Torre Rojo

Departamento de Investigación Básica, CIEMAT, Spain.
*e-mail: Laura.Perez@ciemat.es

The ProtoDUNE experimental program is designed to test and validate the technologies and design that will be applied to the construction of the Deep Underground Neutrino Experiment (DUNE) Far Detector (FD) at the Sanford Underground Research Facility (SURF). The charge detection system permits both calorimetry and position determination. In addition, the photon-detection system (PDS) enhances the detector capabilities for all DUNE physics goals [1].

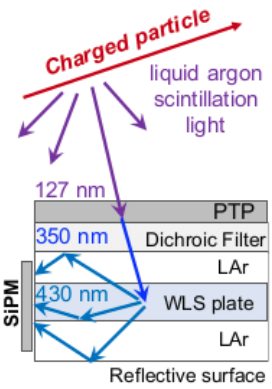

Figure 1. Schematic of the X-Arapuca working principle.

The light collectors, the so-called X-Arapucas [2], are functionally a light trap that captures wavelength-shifted photons inside boxes with highly reflective internal surfaces where they are guided to Silicon Photomultipliers (SiPMs) by wavelength-shifting (WLS) bars.

The two main challenges that the PDS needs to deal with are the difficult detection of the emitted photons ($\lambda \sim 128$ nm) as they are easily absorbed by impurities and the large detection area that is needed.

CIEMAT contribution is focused on the characerization of the X-Arapuca prior to its installation on ProtoDUNE phase II. This final design of the PDS will be installed in DUNE's first FD module.

One of the most important characteristics of the X-Arapuca is its absolute detection efficiency. In order to determine it, we have developed a setup to submerge the X-Arapuca together with reference detectors and an alpha source in Liquid Argon (LAr) at cryogenic temperatures. There are two SiPMs of known efficiency that are used as reference to compute the X-Arapuca one. Also we introduce a Photo-Multiplier Tube (PMT) to monitorize the LAr purity.

The SiPMs and the WLS bar that compose the X-Arapuca are tried in three combinations to see the possible effects on the efficiency. It is computed following two methods so that the results can be cross-checked.

- Baseline method:

$$\epsilon_1(X\text{-}Arapuca) = \frac{PE(X\text{-}Arapuca)}{PE(Ref.\ SiPM)} \cdot \epsilon(Ref.\ SiPM) \cdot f_{corr} \quad . \tag{1}$$

- Simulation method:

$$\epsilon_2(X\text{-}Arapuca) = \frac{PE(X\text{-}Arapuca)}{(LY_{LAr} \cdot En_\alpha \cdot q_\alpha) \cdot f_{sim}} \cdot f'_{corr} \quad . \tag{2}$$

The detected number of Photo Electrons per effective area are indicated as PE. There is a different correction factor depending on the method, but they both correct for the difference in size of the detectors, the SiPMs cross-talk and the fraction of charge not included in the integration range.

The preliminary results obtained with both methods are consistent and so, the X-Arapuca efficiency in LAr is around 2 % for an intermediate SiPM over-voltage. Nevertheless, we are working on improvements for this system, like the the coupling between the bar and the SiPMs, trying to increase the X-Arapuca efficiency for the DUNE FD modules.

[1] DUNE Collaboration, *Deep Underground Neutrino Experiment (DUNE), Far Detector Technical Design Report, Volume III: DUNE Far Detector Technical Coordination*, (2020).
[2] A.A. Machado, E. Segreto, D. Warner, A. Fauth, B. Gelli, R. Máximo, R. A. Pissolatti, L. Paulucci, and F. Marinho, *The X-ARAPUCA: an improvement of the ARAPUCA device*, Journal of Instrumentation, (2018).

Acknowledgements: The work of LPM is supported by the Ministerio de Ciencia e Innovación under FPI contract PRE2020-094863.

Core-Collapse Supernova Burst Neutrino detection and trigger in DUNE

Pablo Barham Alzás* on behalf of the DUNE Collaboration

European Organization for Nuclear Research (CERN), 1211 Geneva 23, Switzerland.

*e-mail: pablo.barham@cern.ch

The Deep Underground Neutrino Experiment (DUNE), a next-generation long-baseline neutrino oscillation experiment, will be a powerful tool to perform low energy physics searches including the detection of supernova neutrinos. DUNE will be uniquely sensitive to the electron neutrino flavour component of the burst of neutrinos expected from the next Galactic core-collapse supernova. The experiment will have four modules of 70-kton liquid argon mass in total, placed 1.5 km underground at the Sanford Underground Research Facility in the USA [1].

Core-collapse supernovae are astrophysical events presenting a large source of neutrinos of all flavours. Measuring the neutrino energy spectra, flavour composition and time distribution will be key in understanding the core-collapse mechanism and can provide insights in neutrino physics topics like neutrino absolute masses, mass ordering and exotics like sterile neutrinos or neutrino magnetic moments [2].

In this work we perform a study of the trigger efficiency using the Photon Detection System (PDS) for different detector technologies. We generate a MC sample of supernova neutrino events using the MARLEY event generator [3] and a sample of the most important radiological backgrounds, which are propagated through a full detector simulation. We use a two-step trigger algorithm:

1. We cluster optical hits with certain time and spatial correlations, scanning over a combination of clustering parameters. We select the combination giving us the highest event detection efficiency for a fixed background rate.

2. We compute the trigger efficiency for a range of burst time windows and minimum cluster multiplicities (the minimum number of reconstructed clusters to activate the trigger).

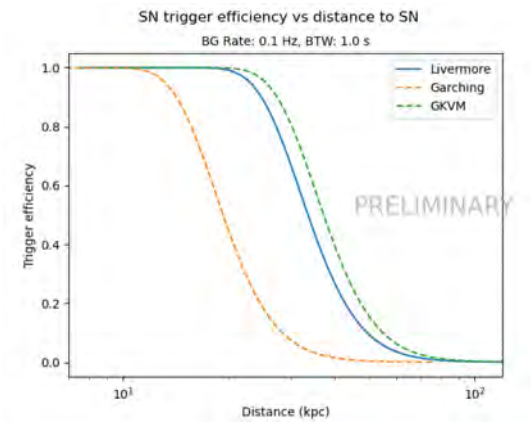

Figure 1. Expected PDS trigger efficiency vs. distance in the Far Detector Vertical Drift module, for three different core-collapse supernova models.

The constraining factor is the tolerated fake trigger rate of 1/month, a DUNE requirement. We find a $\sim$ 100 % trigger efficiency up to a distance of over 20 kpc, the distance to the galaxy edge.

[1] DUNE Collaboration, DUNE Far Detector Technical Design Report, Volume III: DUNE far detector technical coordination (2021).

[2] DUNE Collaboration, Supernova neutrino burst detection with the Deep Underground Neutrino Experiment, *Eur. Phys. J. C* **81**:423 (2021).

[3] Steven Gardiner, Simulating low-energy neutrino interactions with MARLEY, *Computer Physics Communications*, **V 269** (2021).

Electromagnetic tensor endowed with polarimetric parameters: application to the vicinity of extremely dense bodies

J. C. Martin[1], **L. Remón**[1,*], M. Pawlowska[2]

[1]*Departamento de Física Aplicada, Universidad de Zaragoza, C/ Pedro Cerbuna, 12 50009, Zaragoza, España.*
[2]*Department of Theoretical Physics, Wroclaw University of Science and Technology 27 Wybrzeże Wyspiańskiego st., 50-370 Wrocław, Poland.*

*e-mail: lauremar@unizar.es

Electromagnetic flux analysis in the vicinity of mass density singularities constitutes a challenging question. A relativistic treatment based on an adaptation of the Einstein universe equations to an anisotropic Minkowski space has been implemented. The procedure proposed allows one not only to predict the so-called relativistic lens effects, with good agreement with previous formalisms [1] but also to include polarimetric information in the electromagnetic tensor. It is shown that the system quadri-eigenfunction can be approximately assessed by formal analogy to the Navier-Stokes (NS) equations in the case of spherical symmetry. Numerical solutions have also been obtained for different mass density elliptical distributions. In particular, the polarimetric space-time evolution has been analysed, for the first time to our knowledge.

A three-dimensional projection of the solutions can be generated by means of the ray tracing and commercial optical software (ZEMAX, OpticStudio 21.2.1). In order to do so, the complex 3 x 3 n(ξ) refractive index tensor representing the medium properties (ξ being the non-angular oblate spherical coordinate) has been locally adapted by means of an equivalent real, scalar refractive index distribution combined with Jones matrixes formalism, thanks to a procedure specifically developed for this work. Figure 1 shows several trajectories obtained for spherical symmetry, in order to show the agreement between the general method and the NS approximation. Figure 2 shows polarization evolution corresponding to Figure 1 trajectories, where chirality can be appreciated.

The strong influence of the mass gradients in the electromagnetic wave polarimetric behaviour may be a powerful tool for the study of extremely dense matter distributions.

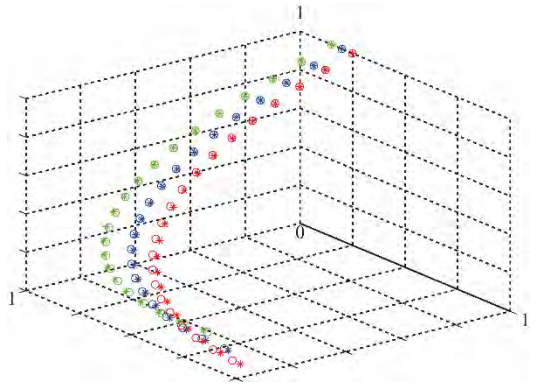

Figure 1. Ray tracing in a medium with mass density distribution $m(r)=\exp(-r^2)$, for three different initial conditions (red, blue and green). Dots: rigorous calculation. Circles: NS approximation.

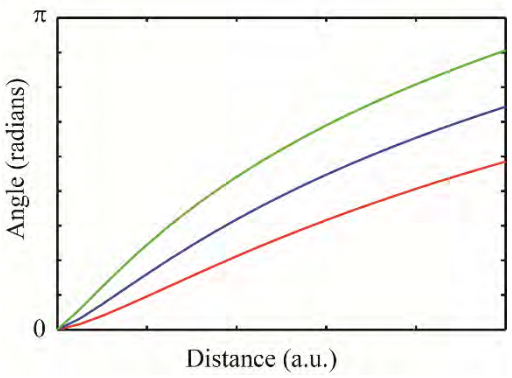

Figure 2. Rotation angle with regard to the initial polarization plane (color correspondence with Fig. 1). Positive angle means dextrogyre rotation.

[1] Sudarshan ECG, Simon R and Mukunda N, *Physical Review A* **28**, 2933 (1983).

Prediction of symmetric partners of the $Z_c(3900)$ and $Z_b(10610)$ exotic states using heavy quark spin symmetry and $SU(3)$ flavor symmetry

Víctor Montesinos*, Miguel Albaladejo, Juan Nieves

Instituto de Física Corpuscular (centro mixto CSIC-UV), Institutos de Investigación de Paterna, C/Catedrático José Beltrán, E-46980 Paterna, Valencia, Spain

*e-mail: vicmonte@ific.uv.es

In the last two decades some states have been found which present difficulties when trying to accommodate them to the conventional quark models, that is, to a three-quark structure in the case of baryons or to a quark-antiquark pair for mesons. Some recent examples in the meson spectrum are:

- **The isovector $J^{PC} = 1^{+-}$ $Z_c(3900)$ state.** It has a charm-anticharm component given that it is observed in the $J/\Psi\ \pi$ and $\bar{D}\ D^*$ spectra, but it is also found to be **charged** (it has isospin equal to one). This state was first seen by the BESIII collaboration in 2013, see Ref. [1].
- **The isovector $J^{PC} = 1^{+-}$ $Z_c(4020)$ state.** Similarly to the $Z_c(3900)$ it has a charm-anticharm component and is charged. First reported by the BESIII collaboration a short time after the $Z_c(3900)$, see Ref. [2].
- **The isovector $J^{PC} = 1^{+-}$ $Z_b(10610)$ and $Z_b(10650)$ states.** They have a bottom-antibottom component and are also charged. First seen by the BELLE collaboration, Ref. [3].
- **The isospin** $1/2$ $J^P = 1^+$ $Z_{cs}(3985)$ **state**. Reported by the BESIII collaboration in 2021 in the $\bar{D}_s D^*$ invariant mass, Ref. [4]. This state has a charm-anticharm component while simultaneously having strangeness.

All the states listed above need to be described by a minimum of four quarks (two quarks and two antiquarks), and are thus known as tetraquarks.

There exist several proposals for the "arrangement" of these four quarks, but among them the meson-antimeson molecule model is prominent given that the masses of these states lie very close to the $\bar{D}^{(*)}D^{(*)}$, $\bar{D}^{(*)}D_s^{(*)}$, $\bar{B}^{(*)}B^{(*)}$ or $\bar{B}_s^{(*)}B^{(*)}$ production energy thresholds. Using a meson-molecular model, we have performed a combined analysis of the $Z_c(3900)$, the $Z_c(4020)$, the $Z_{cs}(3985)$, the $Z_b(10610)$ and the $Z_b(10650)$ states. This combined analysis is made simple due to the existence of some symmetries: *Heavy Quark Spin-Flavor Symmetry* and the more usual $SU(3)$ *light quark flavor symmetry*. With this approach we are able to extend the results in Refs. [5,6] and predict the mass and width of three experimentally unseen states: one Z_{cs} and two Z_{bs} states. The masses of these states lie near the $\bar{D}^*D_s^*$, $\bar{B}_sB^* \simeq \bar{B}_s^*B$ and $\bar{B}_s^*B^*$ energy thresholds, respectively, and we expect these states to couple strongly to these channels.

[1] BESIII collaboration, *Phys. Rev. Lett.* **110**, 252001 (2013).
[2] BESIII collaboration, *Phys. Rev. Lett.* **111**, 242001 (2013).
[3] BELLE collaboration, *Phys. Rev. Lett.* **108**, 122001 (2012).
[4] BESIII collaboration, *Phys. Rev. Lett.* **126**, 102001 (2021).
[5] M. Albaladejo, F.-K. Guo, C. Hidalgo-Duque and J. Nieves, *Phys. Lett. B* **755**, 337 (2016).
[6] Z. Yang, X. Cao, F.-K. Guo, J. Nieves and M.P. Valderrama, *Phys. Rev. D* **103**, 074029 (2021).

Nanociencia y Materiales Moleculares

Presentaciones orales

Martes 12/07:

15:30-16:00 José J. Baldoví Jachán (ICMol-Universidad de Valencia). *Tailoring magnetism in low-dimensional materials*

16:00:16.30 M. José Martínez Pérez (INMA CSIC-Universidad de Zaragoza). *Ultrasensitive magnetic characterization at the nanoscale: from molecules to complex magnetic states*

16:30-16:45 Enrique Burzurí Linares (Universidad Autónoma de Madrid). *Spin-state-dependent electrical conductivity in single-walled carbon nanotubes encapsulating spin-crossover molecules*

16.45-17:00 Giancarlo Franzese (Universidad de Barcelona). *Uniqueness of water compared with other liquids under nano-confinement*

17:00-17:15 Saúl Sánchez González (Universidad de Oviedo). *Relevance of Shockley states on the electrical and thermoelectric response of gold-based single-molecule junctions*

17:15-17:45 **Pósteres y café**.

17:45-18:15 Miguel Anaya Martín (Cambridge University). *Molecular treatment in halide perovskites for next generation optoelectronic device*

18:15-18:30 Arantxa Fraile Rodríguez (Universidad de Barcelona). *Multifunctional Plasmonic Nanostructures with 3-fold Symmetry*

18:30-18:45 Pablo de Vera Gomis (Universidad de Murcia). *Charged-particle electronic cross sections in biomaterials: towards a detailed modelling of nanoscale biodamage*

18.45-19:00 Gabriel Martínez Carracedo. *Accurate exchange constants for bilinear-biquadratic spin models: application to graphene nanostructure*

19:00-19:15 Julia García Pérez (IMDEA). *Electro-optical study of a MoS2 micro-drum resonator*

19:15-19:30 Alberto M. Ruiz (Universidad de Valencia). *Chemical tailoring of the magnetic properties of two-dimensional materials*

Pósteres

- Bruno Cosio Corujo (Universidad de Oviedo). *Study of edge states and topology on 2D flakes of dichalcogenides*
- Gabriel Caballero Catalán (IMDEA). *Electrical properties of mechanically exfoliated MoS2 devices under different ambient conditions*
- Alberto Montoya Ruiz (ICMol-Universidad de Valencia). *Tailoring the magnetic properties of 2D magnetic materials*

Tailoring magnetism in low-dimensional materials

José J. Baldoví*, Dorye L. Esteras, Andrey Rybakov, Alberto M. Ruiz, Gonzalo Rivero

Instituto de Ciencia Molecular (ICMol), Universitat de València, Catedrático Beltrán, 2, ES-46980 Paterna, Spain.

*e-mail: j.jaime.baldovi@uv.es

The recent isolation of two-dimensional (2D) magnets offers tantalizing opportunities for spintronics and magnonics at the limit of miniaturization. [1, 2] One of the key advantages of atomically-thin materials is their outstanding deformation capacity, which provides an exciting avenue to control their properties by strain engineering. Herein, we investigate the magnetic properties, magnon dispersion and spin dynamics of the air-stable 2D magnetic semiconductor CrSBr (T_C = 146 K) [3] under mechanical strain using first-principles calculations. [4] Our results provide a deep microscopic analysis of the competing interactions that stabilize the long-range ferromagnetic order and the orientation of the spin in the monolayer [5]. We showcase that the magnon dynamics of CrSBr can be modified selectively along the two main crystallographic directions as a function of applied strain, probing the potential of this quasi-1D electronic system for magnon straintronics applications. Moreover, we predict a strain-driven enhancement of T_C by ~30%, allowing the propagation of spin waves at higher temperatures.

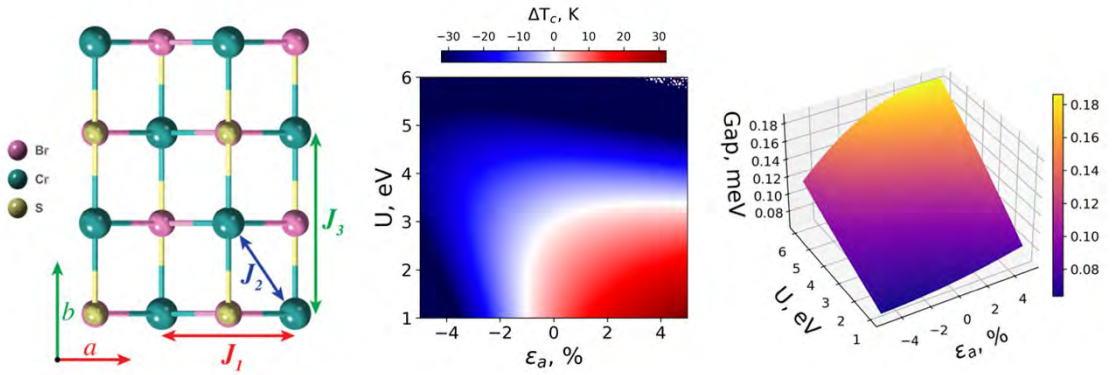

Figure 1. From left to right: (i) chemical structure indicating exchange interactions up to third neighbors, tuning of the (ii) Curie temperature and (iii) gap at Γ-point of the magnon dispersion by uniaxial strain in *a* axis and Coulomb screening.

[1] Huang B.; Clark G.; Navarro-Moratalla E.; Klein D. R.; Cheng R.; Seyler K. L.; Zhong D.; Schmidgall E.; McGuire M. A.; Cobden D. H.; Yao W.; Xiao D.; Jarillo-Herrero P.; Xu X., *Nature* **2017**, *546*, 265-1111.
[2] Gong C.; Li, L., Li, Z., Ji, H., Stern, A., Xia, Y.; Cao T.; Bao W.; Wang C.; Wang Y.; Qiu Z.Q.; Cava R.J.; Louie S.G.; Xia J.; Zhang X., *Nature* **2017**, *546*, 270-1111.
[3] Lee K.; Dismukes A. H.; Telford E. J.; Wiscons R. A.; Wang J.; Xu X.; Nuckolls C.; Dean C. R.; Roy X.; Zhu X., *Nano Lett.* **2021**, *21(8)*, 3511-3517.
[4] Esteras D.L.; Rybakov A.; Ruiz A.M.; Baldoví, J.J., *Nano Letters* **2022**, DOI: 10.1021/acs.nanolett.2c02863.
[5] Boix-Constant C.; Mañas-Valero S.; Ruiz A.M.; Rybakov A.; Konieczny K.A.; Pillet S.; Baldoví J.J.; Coronado E., *Adv. Mater.* **2022**, DOI: 10.1002/adma.202204940.

Spin-state-dependent electrical conductivity in single-walled carbon nanotubes encapsulating spin-crossover molecules

Aysegul Develioglu[1], Julia Villalva[1], Nicolas Montengro-Pohlhammer[2], Rocío Sánchez de Armas[2], Mar García-Hernandez[3], Jose Sánchez-Costa[1], Carmen J. Calzado[2], Emilio M. Pérez[1], **Enrique Burzurí**[4,1,*]

[1]*IMDEA Nanociencia, C/ Faraday 9, 28049 Madrid, Spain.* [2]*Departamento de Química Física, Universidad de Sevilla, Sevilla, Spain.* [3]*Instituto de Ciencia de Materiales de Madrid (ICMM-CSIC), Calle Sor Juana Inés de la Cruz 3, 28049 Madrid, Spain.* [4]*Departamento de Física de la Materia Condensada and Condensed Matter Physics Center (IFIMAC), Universidad Autónoma de Madrid, 28049, Madrid, Spain.*

*e-mail: enrique.burzuri@uam.es

Mixed-dimensional heterostructures [1] combine materials of different dimensionality (0D, 1D, 2D…) to create hybrid materials in which some limitations casted by a specific dimensionality can be overcome.

One of these examples are spin crossover (SCO)-based materials. SCO molecules are promising nanoscale magnetic switches due to their ability to modify their spin state under several stimuli. However, SCO systems face several bottlenecks when downscaling into nanoscale spintronic devices: their instability at the nanoscale, their insulating character and the lack of control when positioning nanocrystals in nanodevices. Here we show the encapsulation of robust Fe-based SCO molecules within the 1D cavities of single-walled carbon nanotubes (SWCNT) [2]. We find that the SCO mechanism endures encapsulation and positioning of individual heterostructures in nanoscale transistors. The SCO switch in the guest molecules triggers a large conductance bistability through individual host SWCNT. Moreover, the SCO transition shifts to higher temperatures and displays hysteresis cycles, and thus memory effect, not present in crystalline samples. Our results demonstrate how encapsulation in SWCNTs provides the backbone for the readout and positioning of SCO molecules into nanodevices, and can also help to tune their magnetic properties at the nanoscale.

Alternatively, we explore additional methods to bond magnetic molecules to 1D SWCNTs [3]. I will introduce the mechanical bond that has allowed us to embrace magnetic porphyrin dimeric rings around carbon nanotubes without disturbing their mutual properties. Spin coherence times of the order of microseconds are found in these mixed-dimensional heterostructures, positioning them for quantum computing.

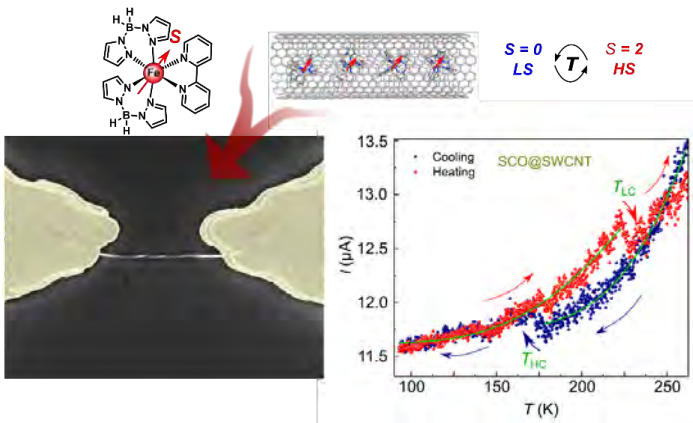

Figure 1. Encapsulation of SCO molecules within 1D SWCNT produces a distinct conductance bistability in the host SWCNT and a modification of the SCO properties in the guest molecule

[1] D. Jariwala, T. J. Marks and M. C. Hersam, *Nature Materials* **16**, 170 (2017).
[2] J. Villalva, A. Develioglu, […], E. Burzurí, *Nature Communications* **12**, 1578 (2021).
[3] S. Moreno-Da Silva, J. I. Martínez […] E. Burzurí, *J. Am. Chem. Soc.* **143**, 21286 (2021).

Uniqueness of water compared with other liquids under nano-confinement

Giancarlo Franzese[1,2]

[1] *Secció de Física Estadística i Interdisciplinària, Departament de Física de la Matèria Condensada, Universitat de Barcelona, 08028 Barcelona, Spain.* [2] *Institut de Nanociència i Nanotecnologia (IN2UB), Universitat de Barcelona, 08028 Barcelona, Spain.*

e-mail: gfranzese@ub.edu

Living organisms, viruses, and technological devices have water layers between their cells or parts and can die or stop working when dehydrated. But why water and not any other fluid? What makes water unique when it is in these tiny pores? We investigate why the water in a pore tinier than one-millionth of a hair moves faster than free water, while other fluids do not. We show that it all depends on the peculiar hydrogen bond interaction of water [1] (Fig. A). The results might be a key factor contributing to the solution of the United Nations Sustainable Development Goals about clean water and sanitation and relate to the switching behavior observed in a hydrated graphene nano-memristor proposed as a memory device that could store the data of 100 trillion flash memories in just 1 cm^3 for quantum computing [2, 3].

On the other hand, water's uniqueness is also essential in cellular membranes. We revise and extend the concept of 'hydration' or 'biological water', i.e., the nanoscopic layer of water covering the surface of biosystems. We find and discuss the existence of a bound/unbound water interface and its effect on dynamics and structure as far as 2.4 nm away from the membrane (Fig. B). The results might be relevant for understanding the role of water in biological activity, e.g., the efficacy of new drugs or vaccines [4, 5, 6].

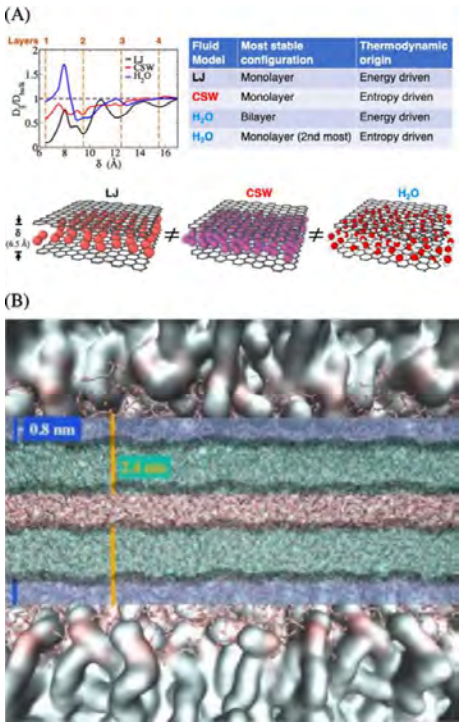

(A) Comparison of the diffusion of a normal fluid (LJ), an anomalous fluid (CSW), and water in a graphene nanopore. Their free energies change differently with the pore size (upper right table), and water is the only one that diffuses faster than bulk under sub-nm confinement (upper left panel). (B) Atomistic simulations of water between two membrane leaflets, Martelli et al. (2021). Away from the lipids (smooth surfaces), we schematically mark three regions: lipid-bound water (blue), unbound water (green), bulk water (red and withe stick molecules), and the interfaces between them (dark regions). Water penetrates between the lipids and persists there even at low hydration.

Referencias

[1] F. Leoni, C. Calero, and G. Franzese, *Nanoconfined Fluids: Uniqueness of Water Compared to Other Liquids*, ACS Nano **15**, 19864 (2021).

[2] H-T. Chin, et al. *Ferroelectric 2D ice under graphene confinement*, Nat. Commun. **12**, 6291 (2021).

[3] G. Franzese, *Supercomputer memories made of water*, https://doi.org/10.32388/9NTVN5.

[4] F. Martelli, J. Crain, and G. Franzese, *Network Topology in Water Nanoconfined between Phospholipid Membranes*, ACS Nano **14**, 8616 (2020).

[5] F. Martelli, C. Calero, and G. Franzese, *Redefining the concept of hydration water near soft interfaces*, Biointerphases **16**, 020801 (2021).

[6] The work has been possible thanks to the financial support of the Spanish MICIN grant PGC2018- 099277-B-C2, the ERDF (A way of making Europe), and the ICREA - Institució Catalana de Recerca i Estudis Avançats.

Relevance of Shockley states on the electrical and thermoelectric response of gold-based single-molecule junctions

Saúl Sánchez-González[1,2,*], Amador García-Fuente[1,2], Jaime Ferrer[1,2]

[1]*Departamento de Física, Universidad de Oviedo, 33007, Oviedo, Spain.*
[2]*Centro de Investigación en Nanomateriales y Nanotecnología, Universidad de Oviedo-CSIC, 33940, El Entrego, Spain.*

*e-mail: sanchezsaul@uniovi.es

Noble metals break preferably exposing (111)-oriented surfaces, that host Shockley type surface states (Sss) [1]. Nevertheless, the relevance of SSs on the electrical properties of gold-based molecular junctions has not been explored in detail. Here, we present ab-initio simulations that show how the gold (111) SS, that lies approximately 0.5 eV below the Fermi energy, is key to determining correctly the electrical and thermoelectric response of the above junctions. We also show that gold's SS appears in our simulations only if d-orbitals are included explicitly in the valence shell. We discuss in detail Benzenediamine (BDA) and Benzenedicarbonitrile (BDCN) gold (111) junctions, where we also include the DFT+Σ correction scheme [2].

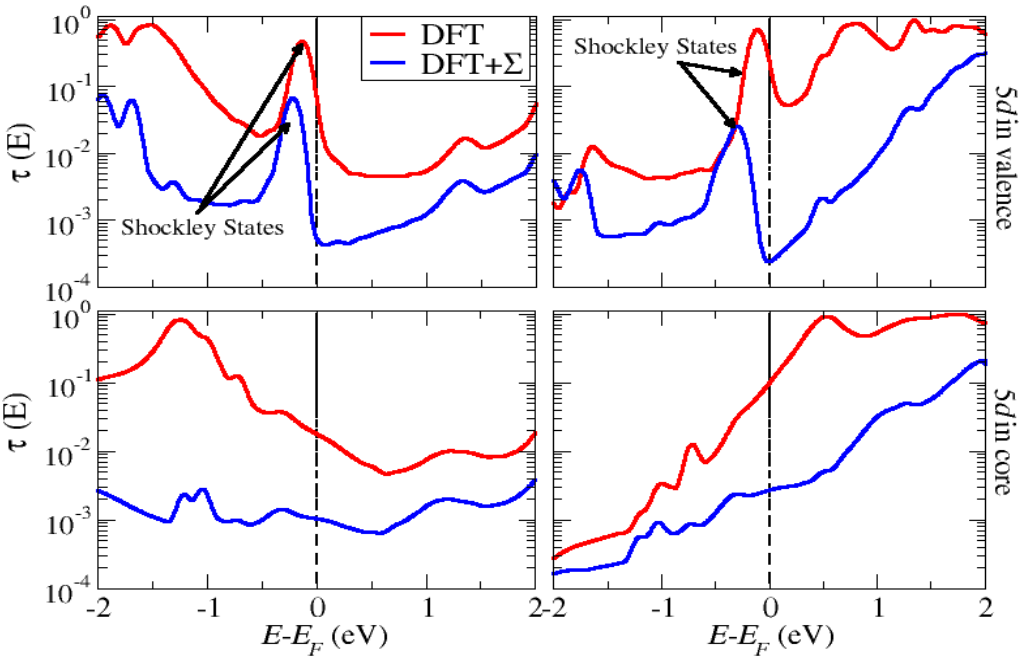

Figure 1. Transmission function of BDA (left panels) and BDCN (right panels). Top (bottom) row corresponds to the junctions where gold's 5d orbitals are explicitly included in the valence (core) shell. The intersection between the graphs and the vertical lines gives the low-voltage conductance. The slope of the transmission function at the Fermi energy is proportional to the thermopower.

[1] B. Yan, B. Stadtmüller, N. Haag, et al., *Nat. Commun*, **6**, 10167 (2015).
[2] J. R. Widawsky, P. Darancet, J. B. Neaton and L. Venkataraman, *Nano Lett.* **12**, 354 (2011).

Multifunctional Plasmonic Nanostructures with 3-fold Symmetry

A. Fraile Rodríguez[1,2,*], J. Rodríguez-Álvarez[1,2], Antonio García-Martín[3], A. Guerrero[4], X. Borrisé[5], F. Pérez-Murano[4], X. Batlle[1,2], A. Labarta[1,2]

[1]*Departament de Física de la Matèria Condensada, Universitat de Barcelona, 08028 Barcelona, Spain.* [2]*Institut de Nanociència i Nanotecnologia (IN2UB), Barcelona, 08028, Spain.* [3]*Instituto de Micro y Nanotecnología IMN-CNM, CSIC, CEI UAM+CSIC, Isaac Newton 8, E28760 Tres Cantos, Madrid, Spain.* [4]*Institut de Microelectrónica de Barcelona (IMB-CNM, CSIC), Bellaterra, 08193, Spain.* [5]*Catalan Institute of Nanoscience and Nanotechnology (ICN2), CSIC and The Barcelona Institute of Science and Technology, Campus UAB, Bellaterra, 08193 Barcelona, Spain.*

*e-mail: arantxa.fraile@ub.edu

In this contribution we present the results of our work with structures that follow 3-fold symmetry designs. These structures present a high degree of geometric frustration due to the fact that plasmonic resonances ultimately rely in the excitation of charge oscillations in the nanostructure and a dipolar excitation cannot be easily accommodated into a 3-fold symmetry. Taking advantage of this feature, several structures exhibiting narrow resonance and the appearance of high energy modes have been studied. We will discuss two of them.

The first is a refractive index sensor based on the excitation of collective excitations in an Au inverted honeycomb plasmonic lattice [1]. Due to its high sensitivity to changes in the surrounding medium, this sensor was able to show sensitivity values ranging from 99 to 395 nm/RIU (RIU stands for refractive index unit) for relatively thin layers of test materials within 50 and 200 nm. The structure was manufactured by a method based on electron beam lithography and the measured optical response agreed with the simulations.

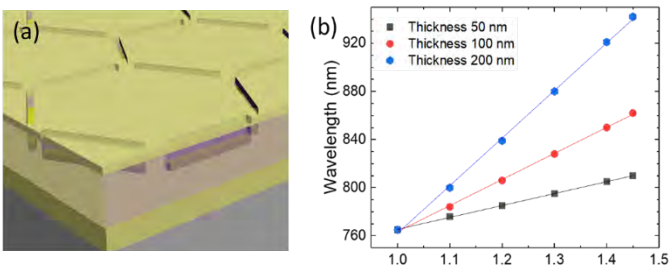

Figure 1. (a) Schematic representation of the structure. (b) Wavelengths of the plasmonic resonance as a function of the refractive index for three values of the test layer thickness.

Our second work is focused on the design and simulation of a simple 3D structure that presents large CD in the near-Infrared (NIR) and optical ranges that can be easily tuned by adjusting its geometrical parameters [2]. Our simulations reveal that the stacked triskelia system present a strong dichroic signal in the extinction. The arising dichroism is mainly due to two extra excitations, not present in the single element case, exhibited by the absorption at wavelengths greater than 0.7 and 1.1 µm, respectively. Furthermore, the position of these two peaks can be shifted by changing either the edge-to- edge distance between the triskelia or their relative angle of rotation. This strongly supports the fact that these additional excitations are caused by the interactions between the two triskelia. Such shifting enables an accurate control of both the wavelength ranges at which the CD appears and its sign, by adjusting the distance between the triskelia and their relative rotation angle, two parameters that can be easily tuned in the manufacturing process.

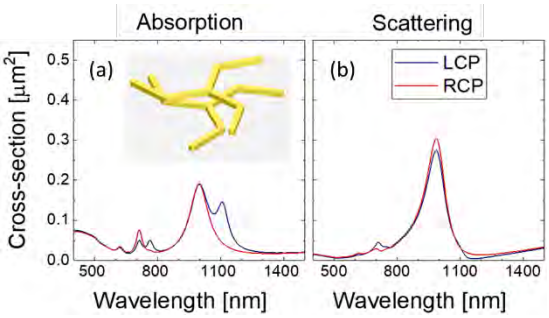

Figure 2. Absorption (a) and scattering (b) cross-section spectra for the stack of two triskelia for right- and left-handed circularly polarised light. The twist angle is 30°.

[1] J. Rodríguez-Álvarez et al., *Nanomaterials* **11**, 5 (2021).
[2] J. Rodríguez-Álvarez et al., *Sci. Rep.* **12**, 26 (2022).

Charged-particle electronic cross sections in biomaterials: towards a detailed modelling of nanoscale biodamage

Pablo de Vera[1,*], Isabel Abril[2], Rafael Garcia-Molina[1]

[1]*Departamento de Física – Centro de Investigación en Óptica y Nanofísica, Universidad de Murcia, E-30100, Murcia, Spain.*
[2]*Departament de Física Aplicada, Universitat d'Alacant, E-03080 Alacant, Spain.*

*e-mail: pablo.vera@um.es

The biological effects of radiation, in terms of cell killing or inactivation, are determined by the damage patterns that the beam particles induce on the nanometre scale. This is particularly true for the swift ions used in the modern ion beam cancer therapy, whose enhanced relative biological effectiveness cannot be explained in terms of macroscopic energy deposits, but it is only understood once the clustering of damaging events on the length scales of the DNA molecules are considered [1]. Swift ions produce numerous very-low energy (<50-100 eV) secondary electrons, which travel distances of a few nanometres around the ion's paths, producing large concentrations of inelastic events in the sensitive biomolecules (Fig. 1).

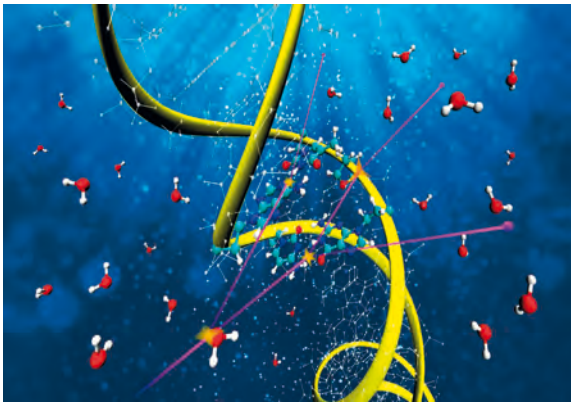

Figure 1. Artistic illustration of the interaction of low energy electrons with DNA in liquid water [7].

The modelling of the energy deposition on the nanoscale is very sensitive to the set of interaction probabilities (cross sections) between charged particles and the relevant biomolecular materials, including liquid water (the main constituent of living tissues) and the building blocks of DNA (bases and backbone), among other biomaterials. The main channel leading to charged-particle energy loss is electronic interactions, and both ionisations (releasing electrons) and electronic excitations (leading to local energy deposits) need to be considered in order to accurately model the nanometric track-structure of ion beams. However, current Monte Carlo simulation codes for radiation transport in biomaterials, such as Geant4-DNA [2], can only describe, up to date, the interaction of charged particles with liquid water, which limits their accuracy.

Over the recent years, in our research group we have exploited the theoretical framework known as the dielectric formalism [3], based on the first Born approximation (FBA), to develop a series of methods to obtain electronic excitation and ionisation cross sections, both integral and differential (in secondary electron ejection energy and angle), for arbitrary biomaterials. These models were first introduced for the impact of ion beams [4,5], to be more recently extended for electron beams by including their particularities in terms of low energy corrections to the FBA and electronic exchange [6,7]. The purpose of this contribution is to review these methods, and to show the general good agreement between theory and experiments got for both ions and electrons in a wide energy range and for a large collection of relevant biomolecular materials. These models and cross sections will be very useful to advance towards a detailed modelling of nanoscale radiation biodamage.

[1] A. V. Solov'yov (ed.), *Nanoscale Insights into Ion-Beam Cancer Therapy*, Springer Int. (2017).
[2] M.A. Bernal *et al.*, *Physica Medica* **31**, 861 (2015).
[3] I. Abril, R. Garcia-Molina, C. D. Denton, F. J. Pérez-Pérez, N. R. Arista, *Physical Review A* **58**, 357 (1998).
[4] P. de Vera, R. Garcia-Molina, I. Abril, A.V. Solov'yov, *Physical Review Letters* **110**, 148104 (2013).
[5] P. de Vera, R. Garcia-Molina, I. Abril, *Physical Review Letters* **114**, 018101 (2015).
[6] P. de Vera, R. Garcia-Molina, *Journal of Physical Chemistry C* **123**, 2075 (2019).
[7] P. de Vera, I. Abril, R. Garcia-Molina, *Physical Chemistry Chemical Physics* **23**, 5079 (2021).

Acknowledgements: We acknowledge financial support by the European Union's Horizon 2020 Research and Innovation programme under the Marie Sklodowska-Curie grant agreement no. 840752 *NanoEnHanCeMent*, the Spanish Ministerio de Economía y Competitividad and the European Regional Development Fund (Projects no. PGC2018-096788-B-I00), the Fundación Séneca (Project no. 19907/GERM/15) and the Conselleria d'Educació, Investigació, Cultura i Esport de la Generalitat Valenciana (Project no. AICO/2019/070).

Accurate exchange constants for bilinear-biquadratic spin models: application to graphene nanostructure

Gabriel Martínez-Carracedo[1,*], László Oroszlány[2,3], Amador García-Fuente[1,4], László Szunyogh[5,6], Jaime Ferrer[1,4]

[1]Departamento de Fisica, Universidad de Oviedo, 33007 Oviedo, Spain. [2]Department of Physics of Complex Systems, ELTE Eötvös Loránd University, 1117 Budapest, Hungary. [3]MTA-BME Lendület Topology and Correlation Research Group, Budapest University of Technology and Economics, 1521 Budapest, Hungary. [4]Centro de Investigación en Nanomateriales y Nanotecnología, Universidad de Oviedo-CSIC, 33940, El Entrego, Spain. [5]Department of Theoretical Physics, Budapest University of Technology and Economics, Budafoki út 8., H-1111 Budapest, Hungary. [6]MTA-BME Condensed Matter Research Group, Budapest University of Technology and Economics, Budafoki út 8., H-1111 Budapest, Hungary.

*e-mail: martinezgabriel@uniovi.es

We propose a new method to determine accuarately the exchange constants of long-range Heisenberg bilinear-biquadratic models (BLBQ). The method uses Hamiltonians and overlap matrices given by DFT calculations within the framework of non-orthogonal basis sets [1,2]. We also compare the results given by this method with the experimental results for triangulene graphene nano-structures making up quantum spin chains (TSCs) [3]. These are S=1 chains and hence exotic phenomena like the Haldane phase arise [4, 5]. We also propose possible experimental settings to change the ground state of finite-length TSCs from a singlet to a triplet. We determine via a combination of exact Diagonalization and DFT calculations (ED) ways to control the above singlet-triplet transition.

[1] László Oroszlány, Jaime Ferrer, András Deák, László Udvardi, and László Szunyoghs, *Phys. Rev. B* **99**, 224412 (2019).
[2] A. I. Liechtenstein, M. I. Katsnelson, V. P. Antropov, V. A. Gubanov. J*ournal of Magnetism and Magnetic Materials*. **67**, (1987).
[3] Mishra, S., Catarina, G., Wu, F. et al., *Nature* **598**, 287 (2021).
[4] F. D. M. Haldane, *Physics Letters A*. **93,** 464 (1983).
[5] Ian Affleck, Tom Kennedy, Elliott H. Lieb, and Hal Tasaki, *Phys. Rev. Lett.* **59**, 799 (1979).

Electro-optical study of a MoS_2 micro-drum resonator

Julia García-Pérez*, Víctor, María Acebrón, Ramón Bernardo-Gavito, Daniel Granados

IMDEA-Nanociencia, Calle Faraday, 9. Madrid28049, Spain.

*e-mail: julia.garcia@imdea.org

Nanoelectromechanical systems (NEMS) are a sort of device capable of transducing an electrical signal to a mechanical motion or in reverse. In particular, drum resonators based on two-dimensional materials have been thoroughly studied in the last few years due to their mechanical properties and potential applications, such as sensors [1]. In this work, we study the electrical and optical properties of micro-drum resonators fabricated with mechanically exfoliated MoS_2.

First, we use maskless optical lithography to deposit Ti/Au electrodes onto a SiOx/Si substrate. These will be used for the electrical actuation of the resonators. To fabricate the NEMS, we mill 5 µm-wide, 500 nm-deep holes between the electrodes with a Focused Ion Beam (FIB) tool. Then, we deterministically transfer a few-layer molybdenum disulfide (MoS_2) flake onto the hole, fully covering it and bridging the two electrodes [2].

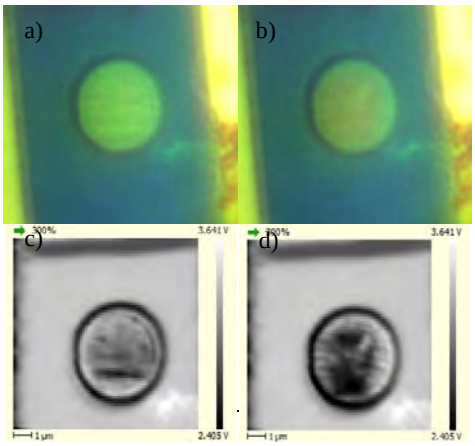

Figure 1. Images of the device at a) V_{DC} = 0V and b) V_{DC}= 40V. Relative reflectance images of the microdrum at c) V_{DC} = 0V and d) V_{DC}= 40V.

By applying DC and RF electric fields between the top electrodes and the bottom of the covered hole we induce mechanical oscillations in the suspended region, studying the resonant membrane's motion at the nanoscale under different tensile strain conditions. Readout of the mechanical movement of the membrane is performed via changes in the system's reflectivity by focusing a laser onto the surface of the suspended region of the flake with a high NA objective. We study the electro-mechanical response of the drum resonator both at atmospheric pressure and in high-vacuum, in this last case, at room temperature and cryogenic conditions. We observe the evolution of the fundamental mode, the first vibrational harmonic and their transition from the linear to the non-linear regime under different excitation conditions [3].

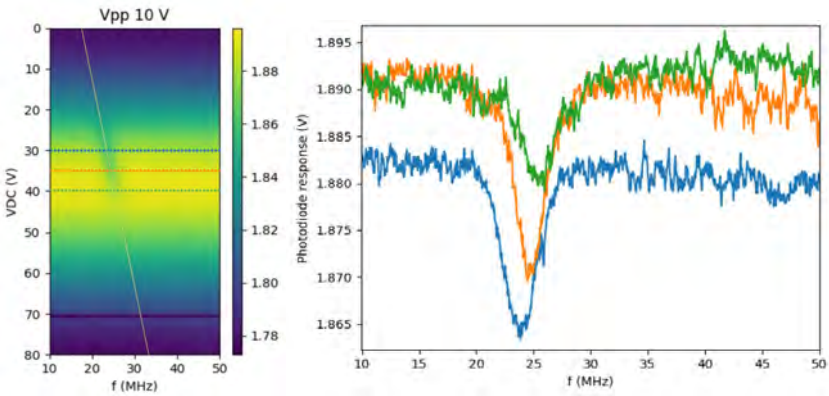

Figure 2. Optical response of a MoS_2 drum resonator at atmospheric pressure subjected to a RF sweep versus different amplitudes of the applied V_{DC}. The frequency of the fundamental mode changes linearly with the applied V_{DC}.

[1] P.G. Steeneken, R.J. Dolleman, D. Davidovikj, F. Alijani and H.S.J. van der Zant, *2D Materials* **8**, 042001 (2021).
[2] A. Castellanos-Gomez, R. van Leeuwen, M. Buscema, H.S.J. van der Zant, G.A. Steele, and W.J. Venstra, *AdvancedMaterials* **25**, 6719 (2013).
[3] D.Davidovikj, F. Alijani, S. J. Cartamil-Bueno, H. Zant, M. Amabili, and P. G. Steeneken, *Nature Communications* **8**, 1253 (2017).

Chemical tailoring of the magnetic properties of two-dimensional materials

Alberto M. Ruiz*, Dorye L. Esteras, Andrey Rybakov, Gonzalo R. Carracedo, José J. Baldoví

[1]*Instituto de Ciencia Molecular (ICMol), Universitat de València, Catedrático Beltrán, 2, ES-46980 Paterna, Spain.*

*e-mail: alberto.montoya@uv.es

The recent discovery of two-dimensional (2D) magnets has provided an unexplored and ideal platform to manipulate and control 2D magnetism and thus having applications in spintronics, magnonics, data storage or quantum computing, among others [1]. CrSBr is a Van der Waals magnetic material, recently isolated to the monolayer limit. It presents a ferromagnetic character with spins pointing in plane, with a curie temperature (T_c) of 145 K [2] and lattice evolution as one cools down below this temperature tends to maximize ferromagnetic interactions along the four different exchange paths [3]. However, a deeper magneto structural study of this material is still lack, relating how magnetic properties change under Coulombic screening and strain modifications.

In this talk we present the theoretical results obtained for the CrSBr monolayer and its structural and electronic properties based on density functional theory (DFT) as implemented in the Quantum Espresso code [3]. By constructing a tight-binding Hamiltonian based on maximally localized Wannier functions (MLWFs), as implemented in the Wannier90 package [4], we could describe the system by choosing *d* orbitals of Cr and *p* orbitals of both S and Br. At this stage, Green functions are used to construct a Heisenberg Hamiltonian to obtain information about the magnetic exchange interactions, as implemented in the TB2J code [5]. Finally, we studied the deposition of organic planar molecules in order to analyse proximity effects between them and CrSBr, through the structural and electronic properties of the resulting heterostructures. This will pave the way for further understanding of the deposition of different molecules that can induce local-strain effects in 2D materials.

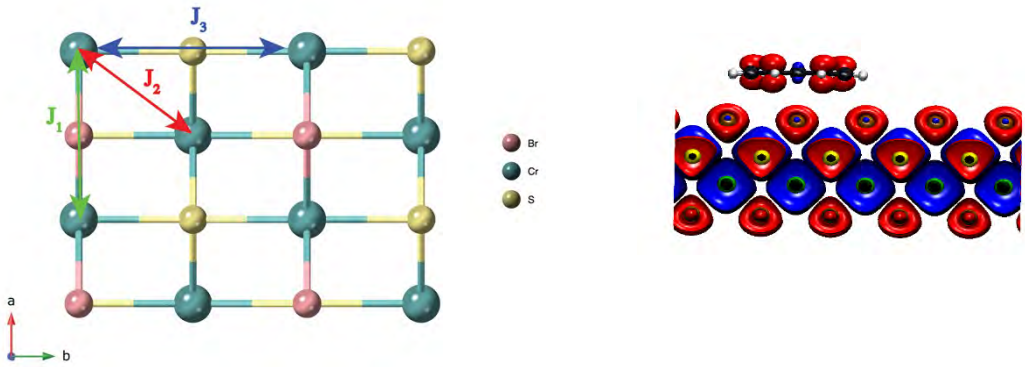

Figure 1. Top view of CrSBr monolayer pointing the J_1, J_2 and J_3 directions (left), spin density of a hybrid heterostructure formed by CrSBr monolayer and an organic molecule (right).

[1] B. Huang, G. Clark, E. Navarro-Moratalla, D. Klein, R. Cheng, K. Seyler, D. Zhong, E. Schmidgall, M. McGuire, D. Cobden, W. Yao, D. Xiao, P. Jarillo-Herrero, X. Xu, *Nature* **546**, 270 (2017).
[2] K. Lee, A. Dismukes, E. Telford, R. Wiscons, J. Wang, X. Xu, C. Nuckolls, C. Dean, X. Roy, X. Zhu, *Nano Lett.* **21**, 3511 (2021).
[3] C. Boix-Constant, S. Mañas-Valero, A. M. Ruiz, A. Rybakov, K. A. Konieczny, S. Pillet, J. J. Baldoví, and E. Coronado, arXiv preprint arXiv:2204.04095 (2022).
[4] A. Mostofi, J. Yates, Y. Lee, I. Souza, D. Vanderbilt, N. Marzari, *Computer Physics Communications* **178**, 685 (2008).
[5] X. He, N. Helbig, M. Verstraete, E. Bousquet, *Computer Physics Communications* **264**, 107938 (2021).

Edge states and topology in dichalcogenides nanostructures

Bruno Cosio-Corujo, Amador García-Fuente, Jonathan Rodríguez-Fernández, Jaime Ferrer

Departamento de Física, Universidad de Oviedo, 33007, Oviedo, Spain.
CINN-CSIC

The study of 2D-materials has been promising since the popularization of graphene. Transition Metal dichalcogenides display a number of interesting electronic and optical properties, where the role of the Spin Orbit interaction is also enhanced.

We show our recent work on diverse nano-structures of the Transition Metal dichalcogenide MoS2 whose electronic structure has been elucidated recently via SPM probes [1,2].

We analyse the emergence and robustness of edge states and look specifically on their possible topological protection via Tight Binding modelling and downfolding. Some of the analysed regular nanostructures have been synthesized already while a few others have not, raising the possibility to identify new types of edge states.

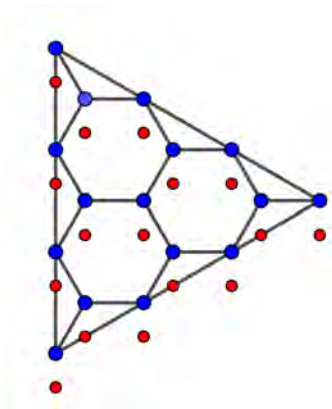

Figure 1. Flake structure of MoS2 with blue dots as the Mo atoms and the red ones as S.

[1] Mark J. Haastrup, Mathias H. R. Mammen, Jonathan Rodríguez-Fernández, and Jeppe V. Lauritsen, Lateral Interfaces between Monolayer MoS2 Edges and Armchair Graphene Nanoribbons on Au(111), *ACS Nano* **15**(4), 6699 **(**2021).

[2] Grønborg, S.S., Salazar, N., Bruix, A. *et al.*, Visualizing hydrogen-induced reshaping and edge activation in MoS2 and Co-promoted MoS2 catalyst clusters, *Nat. Commun.* **9**, 2211 (2018). https://doi.org/10.1038/s41467-018-04615-9.

Electrical properties of mechanically exfoliated MoS_2 devices under different ambient conditions

G. Caballero*, J. Garcia, M. Osorio, V. Marzoa, R. Bernardo-Gavito, M. Menghini, D. Granados

IMDEA-Nanociencia, Cantoblanco,28049, Madrid, Spain.

*e-mail: gabriel.caballero@imdea.org

2D-layered materials such as graphene and transition metal dichacogenides (TMDs) are promising due to their unique electrical, optical and mechanical properties, and their possible applications in electronic, optoelectronic and quantum computation devices.

In this work we focus on the study of 3 terminal field-effect transistor devices, based on mechanical MoS_2 flakes mechanically exfoliated on top of SiO_2/Si substrates. We have characterized the structural properties od MoS_2 devices by means of AFM (Atomic force Microscopy) and Ramana spectroscopy. We will present current-voltage characteristics (I_{SD} vs V_{SD}) and transfer characteristics (I_{SD} vs V_G) performed under ambient and vacuum conditions and at room and low temperature [1,2].

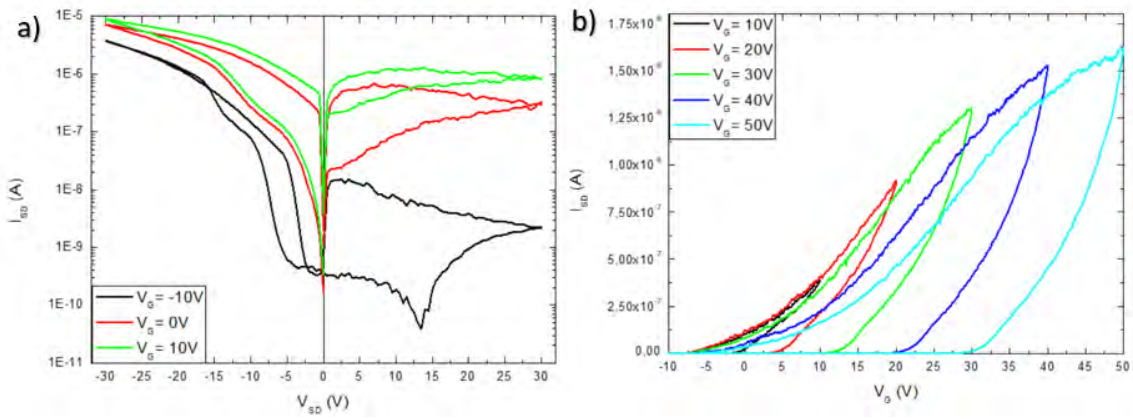

Figure 1. (a) Transfer characteristics (I_{SD} vs V_G) at constant source-drain voltage V_{SD}=1V. (b) Current-voltage characteristics (I_{SD} vs V_{SD}) at different back-gated voltages; V_G= -10 V (black), V_G = 0 V (red) and V_G = 10 V (green).

[1] D. J. Late et al., *ACS Nano* **6**, 5635 (2012).
[2] Y. Shimazu et al., *Scientific Reports* **6**, 30084 (2016).

Física de Plasmas y sus Aplicaciones

Presentaciones orales

Miércoles 13/07:

15:30-16:00 Elena de la Luna (Emilia Solano). *Resultados JET DT Campaign*

16:00-16:15 K. McKay, D.J. Cruz-Zabala, E. Viezzer, R. López-Cansino, R.M. McDermott, R. Dux, and the ASDEX Upgrade Team. *Investigation of the separatrix ion temperature using impurity Charge Exchange Recombination Spectroscopy*

16.15-16.30 E. Sánchez, J. L. Velasco, I. Calvo, S. Mulas. *A quasi-isodynamic configuration with good confinement of fast ions at low beta*

16.30-16.45 Francisco Tabares, Eider Oyarzabal, Daniel Alegre, Macarena Liniers, David Tafalla, Alfonso de Castro, Kieran McCarthy and the OLMAT technical Team. *OLMAT. A new Facility for testing materials under DEMO-relevant Heat Loads*

16.45-17.00 E. Viezzer et al. *Assessment of core-edge integrated ELM-free and small-ELM scenarios for future fusion power plants*

17:00-18:00 **Café**.

18:00-18:15 M. Garcia-Munoz, A. Mancini, J. Segado-Fernandez, E. Viezzer, M. Barragan-Villarejo, J. Ayllon-Guerola, D. Cruz-Zabala, M. Freire-Rosales, J. Garcia-Dominguez, J. Galdon-Quiroga, J. Garcia-Lopez, J. M. Maza, J. F. Rivero-Rodriguez, M. Toscano-Jimenez, L. Velarde-Gallardo and the PSFT team. *High Confinement Regime at Positive versus Negative Triangularity in the SMall Aspect Ratio Tokamak (SMART)*

18:15-18:30 A. de Castro, J. Raukema, D. Alegre, E. Oyarzábal and F. L. Tabarés. *Glow Discharge studies on the direct detection of chemically eroded tin hydride*

Jueves 14/07:

15:30-16:00 L.J Fernandez-Menedez. *Diagnóstico de plasmas inducidos por láser mediante espectroscopía de emisión con resolución especial y temporal*

16:00-16:15 V. Gonzalez-Fernandez, A. Steiger. *Comparison of electric field fall strengths in a hollow cathode discharge in hydrogen and deuterium*

16.15-16.30 Paula Lozano, Antonio Tejero-del-Caz, Rut Morales, Encarnación Muñoz-Serrano. *Numerical simulation of an argon atmospheric pressure plasma jet for biomedical applications*

16.30-16.45 Gonzalo Rodríguez Prieto, Luis Javier Fernández Menéndez, Luis Ernesto Bilbao Dates, Nerea Bordel García. *Excitation temperatures of plasmas at times much larger than current deposition in exploding wires*

16.45-17.00 Aarón Alejo. *Recent developments of high-intensity laser pulse guiding using hydrodynamic optical-field-ionised (HOFI) channels*

17:00-18:00 **Café**.

18:00-18.15 Lozano P, Tejero-del-Caz A, Morales R, Muñoz-Serrano E. *Validity of the Boltzmann relation in electronegative plasmas*

18:15-18:30 C. González-Gago, C. Méndez-López, L.J. Fernández-Menéndez, J. Pisonero, N. Bordel . *Estudio del efecto de la nebulización sobre los parámetros de excitación en plasmas inducidos por láser*

18-30:19:30 All. *General Meeting GEFP*

Experiments with Deuterium/Tritium in JET with a Be/W wall

E. de la Luna* on behalf of JET contributors#

Laboratorio Nacional de Fusión, CIEMAT, Avda. Complutense 40, Madrid, 28040, Spain.

*e-mail: elena.delaluna@ciemat.es

In 2021, high fusion power deuterium-tritium experiments (DTE2) were performed in JET for the first time since the 1997 Deuterium-Tritium (D-T) campaigns in TFTR and JET (DTE1). This represents the culmination of a long-term plan in support of ITER that started in 2011, with the installation of plasma facing components materials similar to those that will be used in ITER (with W in the divertor and Be in the main chamber), and included several enhancements (diagnostics, heating power & new operational scenarios). ITER is a large scale international fusion project, that is currently under construction in France, aimed at demonstrating the scientific and technological feasibility of fusion energy production.

DTE2 delivered fusion energies exceeding the previous record (59 MJ compared to 22 MJ in DTE1) and demonstrated the compatibility of sustained high performance D-T plasmas (up to 5 s) with the ITER-like-wall (ILW). Experiments designed to address specific physics questions provide a unique set of data, with several notable preliminary results. In particular, isotope effects on transport and confinement and the impact of alpha particles on plasmas have been a key aspect addressed. The plasma edge (H-mode pedestal) pressure increases with the ratio of T to D and the core confinement increases in T with respect to D at high input power and high beta [1]. Reduction of turbulent transport and improvement of confinement in the presence of T was anticipated in a strong modelling effort performed before the DTE2 campaign [2,3,4]. The fusion power in the different operational scenarios performed is consistent with predictions made also before DTE2 using an integrated modelling approach [5]. Unambiguous observations of alpha particles and of alpha-driven instabilities were obtained. In particular, thermal confinement does not seem to degrade in the presence of Alfvén activity destabilized by alpha particles or ICRH, which may indicate some interplay between fast particles and main turbulence as found previously for D plasmas. Efficient core heating was demonstrated with a novel Ion Cyclotron Radio Frequency scheme considered for ITER D-T operations: a D-9Be-T three-ion scheme [6], using the Be that is naturally present in the ILW.

This contribution will summarize the motivation for, and the journey towards DTE2, but will focus on the execution of the DTE2 experiments and main results, describing some of the challenges encountered, and highlighting how the unprecedented observations inform the preparation for ITER and other future fusion devices D-T operations.

[1] P. Schneider, AAPPS conference 2021.
[2] J. García et al., *Nuclear Fusion* **57** 014007 (2017).
[3] F.J. Casson et al., *Nuclear Fusion* **60** 066029 (2020).
[4] A. Mariani et al., *Nuclear Fusion* **61** 066032 (2021).
[5] J. Garcia et al., *Nuclear Fusion* **59** 086047 (2019).
[6] Y. Kazakov et al., *Physics of Plasmas* **28** 020501 (2021).

Acknowledgements: This work has been carried out within the framework of the EUROfusion Consortium, funded by the European Union via the Euratom Research and Training Programme (Grant Agreement No 101052200 — EUROfusion). Views and opinions expressed are however those of the author(s) only and do not necessarily reflect those of the European Union or the European Commission. Neither the European Union nor the European Commission can be held responsible for them.

#See the list of authors in the paper "Overview of JET results for optimising ITER operation" by J. Mailloux et al., published in Nuclear Fusion special issue: Overview and Summary Papers from the 28th IAEA Fusion Energy Conference (virtual event, 10-15 May, 2021)

Investigation of the ion temperature in the separatrix and Scrape-Off Layer using impurity Charge Exchange Recombination Spectroscopy

K. McKay[1*], D.J. Cruz-Zabala[1], E. Viezzer[1], R. López-Cansino[1], R.M. McDermott[2], R. Dux[2] and the ASDEX Upgrade Team

[1] *Dept. of Atomic, Molecular and Nucler Physics, University of Seville, 41012 Seville, Spain.*
[2] *Max-Planck-Institut fr Plasmaphysik, 85748 Garching, Germany.*

*e-mail: kiemck1@alum.us.es

In the development of fusion technology it is critical to be able to accurately characterize the ion temperature profile of a plasma. This work determines ion temperature using Charge Exchange Recombination Spectroscopy (CXRS). CXRS consists of injecting neutral particles into the plasma to induce a charge exchange reaction with the ions of the plasma. The photons emitted in these reactions are collected by a spectrometer, producing a light spectrum that can be analyzed to give information about the emitting ions, including temperature. If the injected neutral particles are molecules, then they can potentially contaminate the ion spectral emissions with molecular line emissions, leading to inaccurate temperature measurements.

In this work, a multi-Gaussian fit is designed to identify and subtract the molecular lines from the complex spectra detected by CXRS diagnostics at the ASDEX Upgrade tokamak for discharges in different energy regimes, including H-mode, L-mode, and I-mode. Impurity temperature, rotation, and intensity profiles are determined for the three regimes using measurements at the edge of the plasma and in the Scrape-Off layer, as these regions are most likely to be affected by the injected neutral molecules [1]. The multi-Gaussian fit identified molecular contributions for all three energy confinement modes. Plasma profiles obtained using the multi-Gaussian fit to subtract the molecular contributions showed decreased temperature and intensity in the Scrape-Off layer, indicating molecular lines primarily impact this region of the plasma. The results suggest that the molecules penetrate farther in L-mode and I-mode as compared to H-mode.

1D kinetic simulations are performed to model the neutral density profile and verify where in the plasma neutral molecules are capable of impacting CXRS signals. These simulations show the molecular neutrals penetrating the farthest into the plasma in L-mode, followed by I-mode, with H-mode showing the least penetration, in agreement with the measurements described above. The findings from this work indicate molecular emissions have the potential to impact temperature measurements in the Scrape-Off layer for all three regimes, with the contributions most likely to affect the separatrix ion temperature in the L-mode regime.

[1] D.J. Cruz-Zabala et al., *Plasma Physics and Controlled Fusion* (2022).

A quasi-isodynamic configuration with good confinement of fast ions at low β

E. Sánchez*, J. L. Velasco, I. Calvo, S. Mulas

[1]*Laboratorio Nacional de Fusión-CIEMAT, Avda. Complutense 40, 28040, Madrid, Spain.*

*email: edi.sanchez@ciemat.es

The stellarator possesses some advantages with respect to the tokamak as a fusion reactor concept. Most of the current is externally generated, which reduces the hazard of disruptive current instabilities. Furthermore, the absence of inductive current allows a more straightforward steady-state operation than in tokamaks. However, the lack of axisymmetry of the stellarator implies that good confinement is not guaranteed but requires careful tailoring of the magnetic configuration. The present generation of optimized stellarators, such as HSX and W7-X, are based on magnetic configurations optimized for good neoclassical confinement of thermal species. The optimization of HSX is based on the concept of quasi-symmetry [1], whereas the optimization of W7-X relies on the notion of quasi-isodynamicity [2]. The neoclassical optimization was first demonstrated experimentally in HSX [3], and more recently, in W7-X [4]. However, HSX and W7-X do not confine fast ions (FI) sufficiently well, and further optimization is required. Recently, new vacuum quasi-symmetric configurations optimized for FI confinement have been obtained [5, 6]. In contrast, in quasi-isodynamic devices, FI confinement is known to improve with plasma pressure (β) [7] and so far has been shown to be good enough only in high-β scenarios [8].

This work presents a new four-period stellarator configuration with aspect ratio A=10 and a quasi-isodynamic magnetic field with B=5 T at the magnetic axis. Its most salient property is an excellent confinement of fast ions for moderate values of <β> (~1.5%), which improves further for reactor-scale plasmas with <β>~4%. The new configuration has been obtained using the optimization suite of codes STELLOPT [9], in which the code KNOSOS [10] has recently been included and is used to compute orbit-averaged quantities that are utilized as proxies for the confinement of energetic particles [11]. Monte Carlo full-orbit calculations with ASCOT [12] confirmed the good confinement of energetic ions predicted by the proxies computed with KNOSOS. In this configuration, the effective ripple is smaller than 0.5% in the plasma core and the Mercier MHD stability in all the plasma volume is supported by a significant magnetic well. The ballooning stability up to <β>=4% has been demonstrated using the code COBRA [13]. A preliminary evaluation allows us to foresee a small bootstrap current for <β> values up to 4%. The inclusion of turbulent transport as an additional optimization criterion will be also discussed.

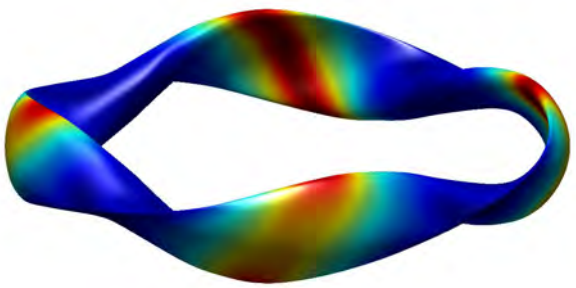

Figure 1. Magnetic field strength on the last closed flux surface of the quasi-isodynamic configuration at b=1.5%.

[1] J Nührenberg, *Phys. Lett.* A **129** (2) (1988).
[2] L. S. Hall et al., *Phys. Fluids* **18** (1995); P. Helander et al., *Plasma Phys. Control. Fusion* **51** (2009).
[3] J. M Canik, *Phys. Rev. Lett.* **98**, 085002 (2007).
[4] C. Beidler et al., *Nature* **598**, E5 (2021).
[5] A. Bader et al., *J. Plasma Phys.* **86** (2020).
[6] S. Henneberg et al., *Nucl. Fusion* **59**(2) (2019).
[7] W. Lotz et al., *Plasma Phys. Control. Fusion* **34**(6) (1992).
[8] A. A. Subbotin et al., *Nucl. Fusion* **46** (2006).
[9] S. A. Lazerson et al., www.osti.gov/biblio/1617636-7pt.
[10] J. L. Velasco et al., *J. Comp. Phys.* **418** (2020).
[11] J. L. Velasco et al., *Nucl. Fusion* **61** (11) (2021).
[12] E. Hirvijoki et al., *Comput. Phys. Commun.* **185** (2014).
[13] R. Sánchez et al., *J. Comp. Physics* **161** (2) (2000).

OLMAT. A new Facility for testing materials under DEMO-relevant Heat Loads

Francisco L. Tabarés[*], Eider Oyarzabal, Macarena Liniers, Daniel Alegre, David Tafalla, Kieran J. McCarthy, Alfonso de Castro and the OLMAT team[#]

Fusion Department. CIEMAT. Madrid. Spain.

[*]e-mail: tabares@ciemat.es

The OLMAT (Optimization of Liquid Metal Advanced Targets, [1]) facility has recently completed the commissioning and start-up phases. Solid and liquid tin (Sn) metallic targets were exposed to a hydrogen neutral beam injector (NBI) particle flux with power densities up to 56±15 MW/m^2, pulse duration up to 150 ms, and repetition rates up to 2 pulses/minute. These beam parameters are well above the estimates based on the typical performance of this NBI system when used for heating plasmas in the TJ-II stellarator. The parameters of the plasma generated through the interaction of the fast (32.5 keV) neutrals and ions with the target were characterized by spectroscopic methods while surface temperature and total absorbed power were followed using pyrometry and infrared (IR) thermography, and calorimetry, respectively. Targets were visually monitored using a fast-frame imaging camera and analyzed ex-situ using TEM/EDX. Electrical isolation of the target permitted recording the floating voltage during irradiation as well as for active biasing tests. In this work, a description of the facility, its operating parameters, plus first results of the exposure of solid (TZM and ITER-grade W) and Liquid Metal (LM) – Capillary porous system (CPS) targets to NBI fluxes, as well as on-going research, are provided. The intrinsic capabilities of OLMAT as a new High Heat Flux (HHF) Facility for testing solid and liquid metal divertor targets under reactor-relevant heat load conditions are assessed and compared with other existing HHF Facilities.

[1] D. Alegre et al., Design and testing of advanced liquid metal targets for DEMO divertor: The OLMAT project, *J. Fus. Energy* https://doi.org/10.1007/s10894-020-00254-5.

[#]The OLMAT Team: Ricardo Carrasco, Fernando Martin, Miguel Navarro, Andres Jimenez-Denche, Francisco Miguel Honrubia, Luis Alberto Bueno, Jose A Sebastian, Emilio Sánchez, Ana Portas, Augusto, Pereira, Angel de la Peña and Jesus Gomez.

Assessment of core-edge integrated ELM-free and small-ELM scenarios for future fusion power plants

E. Viezzer[1,*], M. Austin[2], M. Bernert[3], P. Cano Megias[1], X. Chen[4], D. Cruz Zabala[1], S. Coda[5], E. De la Luna[6], M. Faitsch[3], J. Garcia[7], L. Gil[8], T. Happel[3], G. F. Harrer[9], A. Hubbard[10], J. Hughes[10], A. Kallenbach[3], A. Merle[5], H. Meyer[11], P. Oyola[1], C. Paz-Soldan[12], T. Pütterich[3], O. Sauter[5], M. Siccinio[3], E. R. Solano[6], E. Wolfrum[3], the EUROfusion MST1[#] and ASDEX Upgrade Teams[§]

[1]*University of Seville, Seville, Spain.*
[2]*University of Texas at Austin, Austin, USA.*
[3]*Max Planck Institute for Plasma Physics, Garching, Germany.*
[4]*General Atomics, San Diego, USA.*
[5]*Ecole Polytechnique Fédérale de Lausanne (EPFL), Swiss Plasma Center (SPC), Lausanne, Switzerland.*
[6]*CIEMAT, Madrid, Spain.*
[7]*CEA, Cadarache, France.*
[8]*IST, Lisboa, Portugal.*
[9]*TU Wien, Fusion@ÖAW, Viena, Austria.*
[10]*Plasma Science and Fusion Center, MIT, Boston, USA.*
[11]*UKAEA, Culham, UK.*
[12]*Columbia University, NY, USA.*

*e-mail: eviezzer@us.es

One of our grand challenges towards fusion energy is the achievement of a high-performance plasma core coupled to a boundary solution. The high confinement mode (H-mode) provides such a high-performance fusion core due to the build-up of an edge transport barrier leading to a pedestal. However, it also features type-I edge localized modes (ELMs) which pose a threat for steady-state operation in future fusion devices as they induce large energy fluences onto the plasma facing components, thus damaging the first wall.

For future fusion devices, we need to demonstrate the integration of an ELM-free regime at low q95, low torque with high confinement and compatible with divertor detachment. Several ELM-free and small-ELM regimes have extended their operational space in the past years, with the ultimate goal of providing an alternative core-edge solution to ITER and DEMO. Prominent ELM-free or small-ELM alternatives include the I-mode, QH-mode, EDA H-mode, quasi-continuous exhaust (QCE) and 'grassy' ELM regimes, X-point radiative scenarios and negative triangularity.

Key elements for projecting to future fusion devices include the integration of an ELM-free or small-ELM scenario with high performance, low core collisionality, high density and Greenwald fraction and a power exhaust solution. In nowadays machines, a low pedestal top collisionality and high density separatrix conditions cannot be matched simultaneously. For extrapolation to future fusion machines, compatibility with both needs to be demonstrated.

The state-of-the-art, including access conditions and main signatures, of these alternative regimes is presented. Understanding the underlying physics mechanism of the observed differences in energy and particle transport of these regimes is of paramount importance. The compatibility of these regimes with edge radiative cooling and divertor radiation to achieve detachment will be discussed. Many of these regimes partly match the operational space of ITER and DEMO, however, knowledge gaps remain. Besides compatibility with divertor detachment and a radiative mantle, these include extrapolations to high Q operations, pellet fuelling, impurity transport, energetic particle confinement, amongst others. This talk will discuss these knowledge gaps and possible strategies to close these gaps to show their applicability to ITER and DEMO.

High Confinement Regime at Positive versus Negative Triangularity in the SMall Aspect Ratio Tokamak (SMART)

M. Garcia-Munoz*, A. Mancini, J. Segado-Fernandez, E. Viezzer, M. Barragan-Villarejo, J. Ayllon-Guerola, D. Cruz-Zabala, M. Freire-Rosales, J. Garcia-Dominguez, J. Galdon-Quiroga, J. Garcia-Lopez, J. M. Maza, J. F. Rivero-Rodriguez, M. Toscano-Jimenez, L. Velarde-Gallardo and the PSFT team

University of Seville, Spain.

*e-mail: mgm@us.es

High plasma confinement mode (H-mode) is the reference regime for most future tokamak-based large fusion devices, such as ITER. H-modes are characterized by an edge transport barrier that mitigate the plasma edge turbulence and lead to large plasma pressures and, hence, fusion power throughput. H-mode plasmas presents, however, large edge pressure gradients that develop Edge Localized Modes (ELMs). ELMs are edge localized magnetohydrodynamic (MHD) perturbations that cause large intermittent power loads on the Plasma Facing Components (PFCs) and are thought to be intolerable in future burning devices. Negative Triangularity (NT) shaped plasmas emerge as an attractive baseline scenario for a future tokamak-based fusion power plant as features H-mode-like confinement parameters but without large edge pressure gradients and thus, without ELMs.

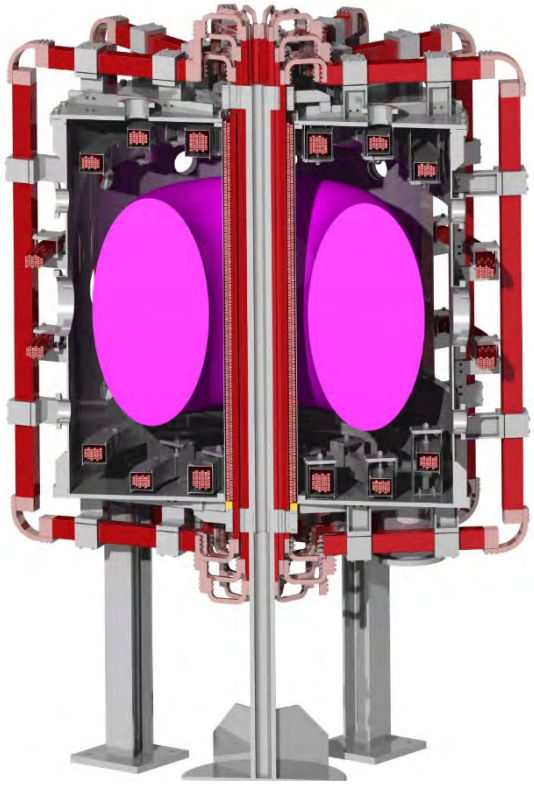

The SMall Aspect Ratio Tokamak (SMART) is a new Spherical Tokamak (ST) under construction at the University of Seville aimed at studying the prospects of Negative Triangularity (NT) shaped plasmas for high confinement plasma regimes (H-mode). SMART has been designed to operate at plasma currents I_P up to 0.5 MA, toroidal magnetic fields B_t up to 1 T and plasma pulse length up to 0.5 sec. A 1 MW Neutral Beam Injection (NBI) shall ensure H-mode access, and a flexible shaping, plasma confinement studies at Positive vs Negative Triangularities.

An overview of the SMART project together with its expected plasma performance, capabilities, and timeline will be presented.

[1] S. Doyle et al., *Fusion Engineering and Design* **171**, 112706 (2021).
[2] A. Mancini et al., *Fusion Engineering and Design* **171**, 112542 (2021).
[3] M. Agredano et al., *Fusion Engineering and Design* **168**, 112683 (2021).
[4] S. Doyle et al., *Plasma Research Express* **3**, 044001 (2021).

Glow Discharge studies on the direct detection of chemically eroded tin hydride

A. de Castro[1,*], J. Raukema[2], D. Alegre[1], E. Oyarzábal[1], F. L. Tabarés[1]

[1]*Laboratorio Nacional de Fusión, Av. Complutense 40, 28040 Madrid, Spain.*
[2]*Eindhoven University of Technology, De Zaale, Eindhoven 5612AZ, The Netherlands.*

*e-mail: alfonsodcc11@gmail.com

Liquid metal divertor configurations, and in particular tin Plasma Facing Components (PFCs), are investigated to ameliorate intrinsic problems (erosion, cracking, melting, embrittlement) of traditional solid tungsten counterparts envisioned for ITER and next step magnetic fusion reactors [1]. Physical/thermal limits of tungsten determine that the handling of the extreme heat flux conditions expected in a fusion reactor divertor (~10 MW/m^2 steady state, up to GW/m^2 range during transient events-ms time scale-) will be a major challenge, especially considering that a non-sufficient lifetime will considerably undermine the technical/economic viability of the reactor. Liquid tin PFCs are aimed to handle power densities beyond the physical limits of tungsten also offering a self-healing plasma interface immune to permanent damage that may enlarge its lifetime. Supported in porous structures, tin has been exposed to different tokamak/linear and laboratory plasmas showing power exhaust capabilities that may overcome the limits of tungsten but revealing intrinsic plasma material interaction problems. In particular, droplet ejection and chemical erosion would increase the tin impurity influx to the confined plasma region (with subsequent plasma contamination and performance degradation) also originating tin re-deposition on undesired in-vessel areas. While liquid droplet ejection has been observed in plasma exposure experiments, the formation of volatile tin hydride (SnH_4) has not been directly detected yet under fusion-like plasma exposure. Volatile tin hydride tends to rapidly decompose even at room temperature conditions, thus complicating its observation and/or diagnosis. Tin hydride generation has been utilized in Extreme UltraViolet (EUV) lithography semiconductor technologies to etch mirror surfaces contaminated with tin debris, using plasmas with low energy ions and significant neutral content [2]. In these conditions, the presence of tin hydride has been indirectly inferred from associated tin deposited layers formed as a consequence of the etching process in which no physical sputtering may be claimed. In fusion related research, the formation of SnH_4 has only been vaguely postulated to explain experimental findings in which potential tin chemical erosion seems to be related to the complex chemistry between it and hydrogen isotopes [3]. In this work, direct current Glow Discharge (GD) H_2 plasma experiments (pressure between 5-35 mTorr, discharge voltage between 250-350 V, plasma current of 50-100 mA and total fluence ~10^{23} m^{-2}) have been conducted in a chamber with walls covered by a tin sheet at a temperature up to 120ºC. Liquid nitrogen cryotrap assisted mass spectrometry (CTAMS [4]) was utilized in the experiments to condense the products of the plasma-surface processes. After plasma operation, the progressive heating of the cryotrap aimed to evaporate the condensed products and a mass spectrometer (SRS 200 Residual Gas Analyzer) placed in the direct line of sight of the cold finger was employed the potential observation of tin hydride traces. During the plasma phase, optical emission spectroscopy was also utilized in an attempt to detect spectroscopic footprints of the compound in real time. Finally, post mortem surface analyses (SEM/EDS as well as profilometry) were employed in witness samples (silicon wafer substrates) and also in parts of the main tin wall exposed to plasma in order to observe and characterize potential tin depositions. The works are completed by a characterization of the neutral and ion fluxes coming from plasma and the estimations of the expected sputtered tin fluxes as well as tentative tin hydride formed ones that are compared to the limits of detection of the mass spectrometry diagnostic. The results of the experimentation are addressed focusing on their global implications and perspectives for a fusion reactor solution based on a liquid tin divertor configuration.

[1] P. Rindt et al., *Fusion Engineering and Design* **173** 112812 (2021).
[2] D. Querimi et al., *Journal of Vacuum Science and Technology B* **38** 052601 (2020).
[3] A. Manhard et al., *Nuclear Fusion* **60**,106007 (2020).
[4] J. Ferreira and F. L. Tabarés, *Journal of Vacuum Science and Technology A* **25,** 246 (2007).

Diagnóstico de plasmas inducidos por láser mediante espectroscopía de emisión con resolución espacial y temporal

Luis Javier Fernández-Menéndez*, Cristina Méndez-López, Cristina González-Gago, Jorge Pisonero, Nerea Bordel

Departamento de Física, Universidad de Oviedo, 33007, Asturias, España.

*e-mail: fernandezmluis@uniovi.es

La espectroscopía de plasmas inducidos por láser, o *Laser-Induced Breakdown Spectroscopy* (LIBS) en inglés, es una técnica basada en el análisis espectral de la emisión de un plasma generado mediante pulsos de radiación láser de alta intensidad y corta duración (ns), que son enfocados sobre la superficie de un determinado material alcanzando altos valores de irradiancia (10^{12} W/cm^2). De esta forma es posible vaporizar y excitar el material, creando un plasma de unos pocos milímetros de tamaño cuya vida media es del orden de cientos de microsegundos [1]. LIBS se emplea habitualmente con fines analíticos ya que proporciona de manera directa y simultánea información de la composición elemental del material irradiado a partir del análisis espectroscópico de la luz emitida por el plasma, permitiendo la determinación de todos los elementos de la tabla periódica, en cualquier tipo de muestra y ambiente. Sin embargo, la determinación de elementos halógenos en LIBS está limitada, ya que presentan señales atómicas de baja intensidad [2]debido fundamentalmente a que tienen energías de excitación e ionización elevadas (>10 eV). La espectroscopía de emisión molecular se ha mostrado como una buena alternativa para la detección indirecta de estos elementos analizando la emisión de moléculas diatómicas formadas por un halógeno y un elemento alcalinotérreo presente en el plasma.

En un estudio previo, nuestro grupo investigó la formación de la molécula de CaF en los plasmas inducidos por láser (LIP), encontrando que su emisión no es homogénea sino que predomina en las regiones más bajas del plasma [3]. Con el objetivo de conocer con mayor detalle las causas de este comportamiento, en este trabajo se presenta un diagnóstico del LIP donde se determinan parámetros fundamentales del mismo como su temperatura de excitación (T_{exc}) y su densidad electrónica (n_e) cuando se utilizan muestras de CaF_2. El cálculo de T_{exc} se realiza mediante diagramas de Boltzmann empleando la radiación atómica del Ca, mientras que el cálculo de n_e se lleva a cabo mediante la determinación del ensanchamiento Stark que sufre la línea H-alpha. Como novedad, se emplea un equipo experimental que permite conocer la distribución espacial y temporal de estos parámetros a medida que el plasma evoluciona. En líneas generales, se ha encontrado que el predominio de la radiación molecular de CaF está ligado a las zonas del plasma en la que se tiene una menor excitación, es decir, donde se registran unos valores más bajos de T_{exc} y n_e.

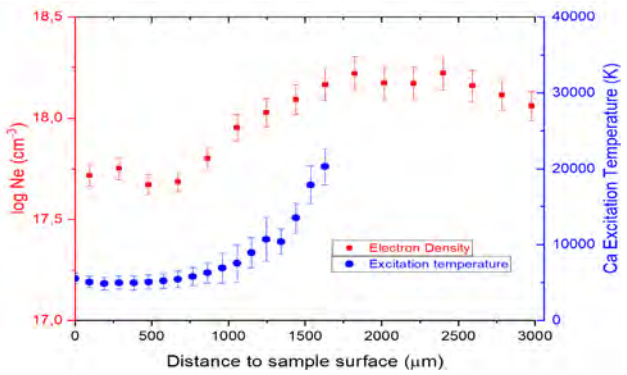

Figura 1. Densidad electrónica (rojo) y temperaturas de excitación (azul) en función de la altura medida sobre el eje vertical de simetría del plasma.

[1] D. W. Hahn and N. Omenetto, *Appl. Spectrosc.* **66**(4) 347, (2012).
[2] C. Alvarez-Llamas, J. Pisonero, and N. Bordel, *J. Anal. At. Spectrom.* **32**(1), 162 (2017).
[3] L. J. Fernández-Menéndez, C. Méndez-López, C. Alvarez-Llamas, C. González-Gago, J. Pisonero, and N. Bordel, *Spectrochim. Acta - Part B At. Spectrosc.* **168**, (2020)

Agradecimientos: Los autores agradecen la financiación del Ministerio de Ciencia e Innovación y del Gobierno del Principado de Asturias mediante el proyecto MCI-21-PID2020-113951GB-100 / AEI / 10.13039/501100011033 y las becas predoctorales MINECO BES-2017-080768 y PA-21-PF-BP20-059.

Comparison of electric field fall strengths in a hollow cathode discharge in hydrogen and deuterium

V. Gonzalez-Fernandez[1,2,*], A. Steiger[3]

[1]*Dpto. de Física Teórica, Atómica y Óptica, Universidad de Valladolid, Paseo Belén 7, E-47011 Valladolid, Spain.*
[2]*Dpto. De Óptica, Universidad Complutense de Madrid, Av. Arcos del Jalon 118, E-28037 Madrid, Spain.*
[3]*Physikalisch-Technische Bundesanstalt, Abbestr. 2-12, D-10587 Berlin, Germany.*

*e-mail: veronicagf@ucm.es

The relevance of the electric field strength (E-field) present in plasmas has involved many efforts to designing innovative strategies to bring reliable measures to the plasma physics community. Namely, atomic hydrogen (H) isotopes are excellent candidates for E-field measurements and the Stark splitting caused by an external E-field is very well known. Nevertheless, studies concerning deuterium (D) are not so common. Undoubtedly, there is an undeniable interest in the comparison between the two isotopes because D atoms are twice as heavy than H atoms.

In this work, we present a detailed comparison of high-resolution E-field strengths falls measurements performed in a hollow-cathode glow discharge operated in 600 Pa pressure. The cathode employed is made of tungsten to guarantee a pure plasma, avoid as maximum the generation of sputtering. The comparison between the D and H measurement are shown in Fig.1. The error bars represent the uncertainties of the determination of the E-field [1].

The E-field measurements are analysed in the frame of two classical discharge models: Rickards [2] and Wronski [3]. Rickards model calculates the energy distribution of ions and neutrals at the cathode of a glow discharge and uses Monte-Carlo simulation to calculate charge exchange collisions. On the other hand, Wronski considers the motion of ions by solving the Boltzmann equation for the ions which are generated in the cathode fall of an abnormal glow discharge. These two models allow to determine important discharge parameters such us the ions energy and their mean free path.

The comparison between deuterium and hydrogen shows very clear trends. In first place, from the Rickards models the conclusion is that the maximum E-field in deuterium is higher than in hydrogen, due to the higher isotope mass. To the contrary, the length of the cathode region is shorter in deuterium than in hydrogen. As a result of this the ion mobility is more restricted in deuterium than in the lighter hydrogen.

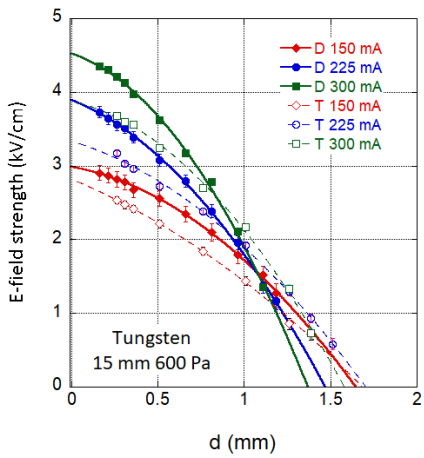

Figure 1. E-field strengths for deuterium (solid lines) and hydrogen (dashed lines); measured in a tungsten cathode of 15 mm of diameter and a pressure of 600 Pa. Figure extracted from [1].

From Wronski model, it is possible to determine the ions energy, leading in higher maximum values for deuterium near the cathode surface, but decreasing faster than hydrogen ones through the cathode region. Nearly identical mean free path is obtained for both isotopes despite their mass difference.

[1] V. Gonzalez-Fernandez, A.Steiger, M. I. de la Rosa, *Spectrochim. Acta B* **180**, 106194 (2021).
[2] J. Rickards, *Vacuum*, **34**, 559-562 (1983).
[3] Z. Wronski, *Vacuum*, **40**, 387-394 (1990).

Acknowledgements: The authors thank DGICYT (Ministerio de Economía y Competitividad) for the project ENE2012-35902, FEDER funds and the grant BES-2013-063248 given to V. Gonzalez-Fernandez. The authors thank C. Pérez for the scientific discussions. V. Gonzalez-Fernandez is especially grateful for the invaluable help and mentoring from M. I. de la Rosa K. Grützmacher.

Numerical simulation of an argon atmospheric pressure plasma jet for biomedical applications

P. Lozano*, A. Tejero-del-Caz, R. Morales, E. Muñoz-Serrano

Departamento de Física, Universidad de Córdoba, Spain.

*e-mail: f72lodup@uco.es

A new research line for the modelling of Cold Atmospheric Plasma (CAP) for biomedical applications is currently being developed in our group. Several studies have shown that CAP-based treatments produce higher degrees of apoptosis when applied to cancer cells, restoring its chemical-resistant sensitivity to specific drugs, and improving its ability to absorb different molecules. All of these suggests that this technology can be used as support in combination with conventional chemotherapy and radiotherapy treatments [1].

We have studied one of the most used plasma devices in practice for biomedical applications called atmospheric pressure plasma jet, APPJ. This technology presents several advantages such as the possibility of controlling the energy distribution of the charged particles and the wide variety of chemical species that can be created in the plasma [2].

We have simulated an APPJ using a multifluid model comprising continuity equations for the species considered in the kinetic model and the electron energy, Poisson´s equation for the electric field and the gas thermal balance equation. After discretizing the equations by considering a control volume formulation combined with an exponential scheme [3], we have developed a Fortran90 code to solve the resulting algebraic system by using a modified implicit procedure for a 5-point formulation based on the Lower-Upper (LU) factorization of the system matrix [4]. Finally, the temporal evolution was implemented using the Gauss-Seidel scheme.

In this communication we present results obtained for an Argon plasma jet with a geometry similar to that used by Greifswald kINPen [5]. A central cathode with 2 mm diameter is surrounded by a quartz tube of 3 mm radius, in contact to a ring anode with a 1mm thickness (see Figure 1). The cathode was grounded, and the anode was polarized to 2 kV pulsed voltage with 1000 ns on-time and 100 ns rise and fall-times.

Figure 2 shows the potential distribution at 200 ns with de plasma successfully created along the tube. We are currently working to include the advection of the Ar flux in the model to describe the plasma jet outside the tube.

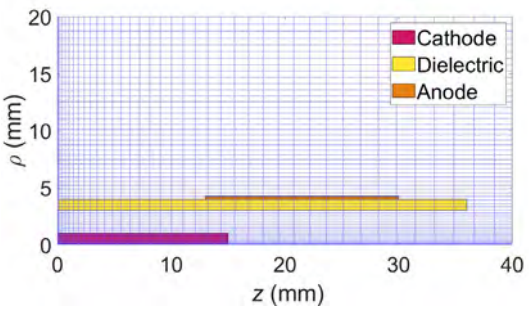

Figure 1. Computational domain (zoom).

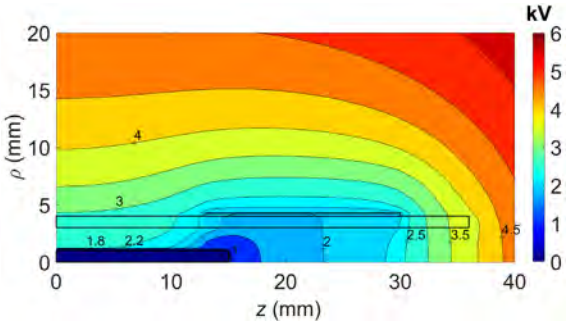

Figure 2. Voltage distribution at 200 ns.

[1] Laroussi, *IEEE Transactions on Plasma Science* **43**, 703 (2015).
[2] Matsusaka, S., *Adv. Power Technol.* **30**, 2851 (2019).
[3] Patankar, *Numerical Heat Transfer and Fluid Flow*, CRC Press (1980).
[4] Scheiner et al., *Numerical Heat Trasnfer* **4**, 1 (1981).
[5] Reuter et al., *J. Phys. D: Appl. Phys.* **51**, 233001 (2018).

Acknowledgements: This work was co-financed by the "Programa Operativo FEDER 2014-2020" and by the Consejería de Economía y Conocimiento de la Junta de Andalucía. The authors also thank the support of the "Programa de Prácticas de Laboratorio, modalidad Curso Académico" of the AECC Foundation, with a grant for a undergraduate student to develop research on cancer thematic.

Excitation temperatures of plasmas at times much larger than current deposition in exploding wires

Gonzalo Rodríguez Prieto[1,*], Luis Javier Fernández Menéndez[2], Luis Ernesto Bilbao Dates[3], Nerea Bordel García[2]

[1]*INEI, ETSII, 13071, C. Real, Spain.* [2]*Department of Physics, University of Oviedo, 33007, Asturias, Spain.* [3]*Departamento de Física, Facultad de Ciencias Exactas, Universidad de Buenos Aires, 1482 Buenos Aires, Argentina.*

*e-mail: gonzalo.rprieto@uclm.es

Exploding wire systems consist on pulsed electrical power devices that force the pass of a large, on the order of kilo-amperes, current through a thin, short metal wire. These exploding wires generate transient plasmas which can be mantained several hundreds of microseconds after the electrical discharge. Using the *AL*ambre *EX*plosivo (ALEX) system located at the INEI research center of C. Real, dependent on the Engineering School of Ciudad Real, University of Castilla-la Mancha, plasmas at times much longer than total electrical energy delivery time had been explored. Exploration was made analyzing the plasma emission spectra at different times after the electrical delivery at wavelengths from 450 to 650 nm, that allow for the calculation of the excitation temperatures of copper atoms from the wire. Together with photos from an image converter and another streak camera, they show that the measured excitation temperature, see fig. 1, are associated with stable plasma structures.

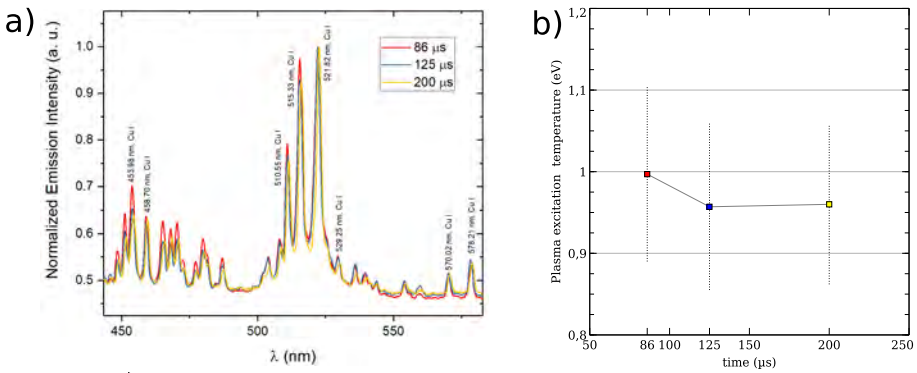

Figure 1. **a)** Spectra taken at times much larger than energy deposition time, 25 μs, at fixed voltage of 25 kV in the capacitors bank. **b)** Electrons excitation temperature after the beginning of the electrical discharge at zero μs.

Acknowledgements: The authors gratefully acknowledge the financial support of the Spanish Government through the project MCI-21-PID2020-113951GB-100 / AEI / 10.13039/501100011033, pre-doctoral grant MINECO BES-2017-080768, and funding by Ministerio de Ciencia, Innovación y Universidades of Spain grant number ENE2016-75703-R, named "MATERIA CON ALTA DENSIDAD DE ENERGIA EN FUSION POR CONFINAMIENTO INERCIAL", and Junta de Comunidades de Castilla-la Mancha grant number SBPLY/17/180501/000264 named "HIDRODINAMICA DE LA MATERIA CON ALTA DENSIDAD DE ENERGIA".

Recent developments of high-intensity laser pulse guiding using hydrodynamic optical-field-ionised (HOFI) channels

A. Alejo[1,2,*], J. Cowley[2], A. Picksley[2], R. Walczak[2], S.M. Hooker[2]

[1]*Instituto Galego de Física de Altas Enerxías (IGFAE), Universidade de Santiago de Compostela, Spain.*
[2]*Department of Physics, University of Oxford, United Kingdom.*
*e-mail: aaron.alejo@usc.es

Laser wakefield electron acceleration has attracted significant attention over the last decades, due to its ability to generate acceleration gradients three orders of magnitude greater than those achieved in conventional accelerators. However, in order to realise a multi-GeV laser-driven plasma accelerator stage, the laser pulse must remain focussed as it propagates through tens of centimetres of low-density ($1 \times 10^{17}\,\mathrm{cm}^{-3}$) plasma. Such propagation lengths are orders of magnitude greater than the Rayleigh range, and hence some form of wave-guiding is required. We recently introduced hydrodynamic optical-field-ionized (HOFI) plasma channels [1], where a plasma channel is formed by the hydrodynamic expansion of a plasma column formed by OFI with elliptically-polarised laser pulses. Since the electron energies generated with OFI are independent of the gas density, channels can be formed with much lower axial densities than is possible with collisional heating, a crucial requirement to build an electron acceleration stage [2].

Here we present several recent experimental developments on HOFI channels. Firstly, we report on the generation of the longest, free-standing waveguide to date, as HOFI plasma channels with lengths of up to 100 mm and on-axis densities as low as $7 \times 10^{16}\,\mathrm{cm}^{-3}$ have been generated and employed to guide laser pulses with intensities greater than $1 \times 10^{17}\,\mathrm{W\,cm}^{-2}$ [3]. These channels were found to exhibit a power attenuation length of 102 mm, in good agreement with numerical calculations considering the measured transverse electron density profiles.

In order to increase the attenuation length, we have also introduced a variant of the HOFI scheme, the conditioned HOFI (CHOFI) channels [4]. In CHOFI, the transverse wings of an intense laser pulse guided by the HOFI channel ionise the collar of neutral gas surrounding the shock front, to form a deep, low-loss plasma channel. We demonstrate through experiments and numerical simulations that the CHOFI channels exhibit power attenuation lengths of $L_{att} = (21 \pm 3)\,\mathrm{m}$, more than two orders of magnitude longer than achieved by regular HOFI channels. We present hydrodynamic and particle-in-cell simulations which demonstrate that meter-scale, low-loss CHOFI waveguides could be generated with a total laser pulse energy of about 1 J per meter of channel.

Finally, future high-repetition rate, multi-GeV plasma accelerator stages will also require waveguides capable of operating at such rates. We present experimental results demonstrating that HOFI channels can be stably generated at kHz-scale pulse repetition rates [5]. Further, we experimentally demonstrate the stable generation of HOFI channels at a mean pulse repetition rate of 0.4 kHz for a period of 6.5 h without degradation of the channel properties due to the effects of heating or damage to the laser optics, and we determine the fluctuations in the key optical parameters of the channels in this period.

[1] Shalloo, R. J., Arran, C., Corner, L., *et al.*, *Physical Review E*, **97**(5), 053203 (2018).
[2] Shalloo, R. J., Arran, C., Picksley, A., *et al.*, *Physical Review Accelerators and Beams*, **22**(4), 041302 (2019).
[3] Picksley, A., Alejo, A., Cowley, J., *et al.*, *Physical Review Accelerators and Beams*, **23**(8), 081303 (2020).
[4] Picksley, A., Alejo, A., Shalloo, R. J., *et al.*, *Physical Review E*, **102**(5), 053201 (2020).
[5] Alejo, A., Cowley, J., Picksley, A., Walczak, R., & Hooker, S. M., *Physical Review Accelerators and Beams*, **25**(1), 011301 (2022).

Acknowledgements: This work was supported by the UK Science and Technology Facilities Council [Grant No. ST/P002048/1, No. ST/R505006/1]; the Engineering and Physical Sciences Research Council [Grant No. EP/ V006797/1]; the Air Force Office of Scientific Research [under Grant No. FA9550-18-1-7005]; the European Union's Horizon 2020 research and innovation programme [Grant No. 653782]; "la Caixa" Foundation (fellowship code LCF/BQ/PI20/11760027); Xunta de Galicia; European Union ERDF; and the "María de Maeztu" Units of Excellence program MDM-2016-0692 and the Spanish Research State Agency.

Validity of the Boltzmann relation in electronegative plasmas

P. Lozano*, A. Tejero-del-Caz, R. Morales, E. Muñoz-Serrano

Departamento de Física, Universidad de Córdoba, Spain.

*e-mail: f72lodup@uco.es

Electronegative plasmas are widely used in industry and medicine processes such as purifying, etching, microelectronic industrial applications, or synthesis of biomaterials. [1] In this context, many authors have developed different models to describe oxygen discharges. In all these models, the plasma-sheath transition plays a key role to understand most of these plasma applications. In order to model this transition, negative ions are normally supposed to follow the Boltzmann relationship with their own temperature. [2]

As pointed out by several authors [3], we show this relationship is inappropriate when different generation-loss processes are considered in the sheath by describing the plasma-sheath transition near a polarized wall using a multifluid model. To this aim, charged particles are described by the continuity equations including the generation-loss processes, the momentum transfer equations keeping the corresponding inertia terms and finally, the Poisson's equation. The electric potential and particle density profiles for an oxygen discharge are obtained. As a result, although electrons always are well described by the Boltzmann relationship due to their negligible mass, negative ions do not fit this relationship when they are generated into the sheath due to the source terms appearing in the continuity equations.

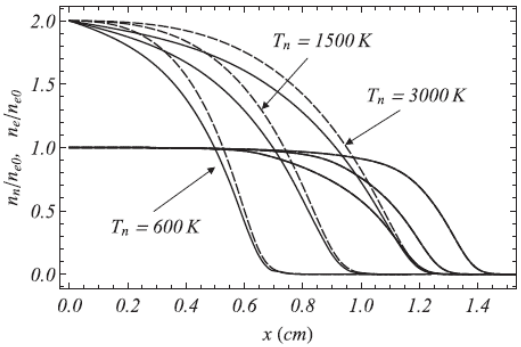

Figure 1. Negative particle density profiles (O^- and e) for different values of T_e obtained from the model (solid lines) and their corresponding Boltzmann relationship (dashed lines) for a negative ion O^- density at the plasma $n_{n0} = 2n_{e0}$.

For this study, we consider a 100 mTorr discharge mainly composed of oxygen molecules O_2, oxygen atoms O, positive ions O_2^+, negative ions O^-, metastables $O_2(a^1\Delta_g)$, and electrons e. The values of the parameters on which the model depends are: the neutral particle density $n_g = 1.61 \times 10^{21}\ m^{-3}$, the neutral temperature $T_g \sim 600 - 3000\ K$, the metastable density $n_* = 0.1n_g$, the oxygen density $n_O = 0.2n_*$, the electron density $n_{e0} = 2.4 \times 10^{15}\ m^{-3}$, the electronegativity $n_{n0}/n_{e0} \sim 0.5 - 4$, and the neutral-ion collision cross section $\sigma_c \sim 0 - 10^{-18} m^2$. The main generation-loss processes present in the discharge are ionization ($O_2 + e \rightarrow O_2^+ + 2e$), dissociative attachment ($O_2 + e \rightarrow O^- + O$), detachment by metastable $(O^- + O_2(a^1\Delta_g) \rightarrow products)$, detachment by atomic oxygen ($O^- + O \rightarrow e + O_2$) and recombination ($O^- + O_2^+ \rightarrow O + O_2$).

Figure 1 illustrates the effect of negative ion temperature on the negative ion density and electron density profiles. Solid lines represent these profiles obtained from the model while dashed lines correspond to the expression of the Boltzmann relationship obtained from the electric potential profile. Electrons always follow the Boltzmann relationship (dashed lines and solid lines overlap) but negative ions differ from this relation. Similar results are obtained for different values of the electron temperature, the mean free path for neutral-ion collisions and electronegativities.

[1] Libermann M A and Lichtenberg, Principles of Plasma Discharges and Materials, Hoboken, NJ: Wiley (2005).
[2] Crespo R M, Palop J I F, Hernández M A, Borrego del Pino S and Ballesteros J, *J. Appl. Phys. D:* **96**, 4777 (2004).
[3] Stoffels E, Stoffels W W and Kroesen G M W, *Plasma Sources Sci. Technol.* **10**, 311 (2001).

Acknowledgements: This work was co-financed by the "Programa Operativo FEDER 2014-2020" and by the Consejería de Economía y Conocimiento de la Junta de Andalucía. The authors also thank the support of the "Programa de Prácticas de Laboratorio, modalidad Curso Académico" of the AECC Foundation with a grant for a undergraduate student to develop a research on cancer thematic.

Estudio de la distribución espacio-temporal de los parámetros de excitación en plasmas inducidos por láser en atmósferas enriquecidas en gases nobles

Luis Javier Fernández-Menéndez, Cristina Méndez-López, **Cristina González-Gago***, Jorge Pisonero, Nerea Bordel

Departamento de Física, Universidad de Oviedo, 33007, Asturias, España.

*e-mail: gonzalezgcristina@uniovi.es

La determinación de halógenos mediante Espectroscopía de Ruptura Inducida por Láser (*Laser Induced Breakdown Spectroscopy*, LIBS) supone un desafío debido a la baja eficiencia de emisión atómica de estos elementos en el rango espectral propio de los sistemas de detección típicamente empleados en LIBS (200-1000 nm). Esto ha motivado la necesidad de llevar a cabo nuevas investigaciones dirigidas a mejorar la sensibilidad de la técnica para estos elementos. En este sentido, la detección de halógenos a partir de la emisión molecular se ha mostrado como una buena alternativa. En el caso particular del F, la recombinación de este elemento con un alcalinotérreo (Ca) se ve favorecida en el plasma inducido por láser (LIP), de modo que la emisión de la molécula de CaF es eficazmente detectada en los sistemas LIBS convencionales. Por otro lado, se ha observado que la generación del LIP en atmósferas constituidas por gases nobles da lugar a un incremento de las señales atómicas [1,2]; sin embargo, los posibles beneficios sobre las señales moleculares todavía no han sido explorados.

En nuestro grupo de investigación se llevó a cabo recientemente un estudio de la dinámica de las emisiones atómica y molecular, mediante medidas con resolución espacial y temporal en distintas atmósferas soplando un flujo continuo de diferentes gases (aire, He o Ar) sobre una muestra de CaF_2 puro. En dicho estudio se observaron diferencias significativas de distribución y evolución temporal entre la emisión atómica (Ca) y la molecular (CaF) (ver Fig. 1), que podrían estar ligadas a las variaciones de temperaturas y densidades electrónicas a lo largo de la pluma del plasma. Es por esto que, en el presente trabajo, se han obtenido las densidades electrónicas (N_e) y las temperaturas de excitación (T_e) analizando sus variaciones espacio-temporales a lo largo de la pluma del plasma para las distintas atmósferas y se ha evaluado su relación con la distribución de la emisión de especies atómicas y moleculares. Las N_e se obtuvieron a partir del ensanchamiento Stark de la línea H-alfa mientras que T_e se calculó a partir de la emisión de Ca I mediante diagramas de Boltzmann. Se ha observado que los parámetros observados muestran una distribución inhomogénea a lo largo de la pluma del plasma y que su distribución varía además en función del gas soplado sobre la muestra.

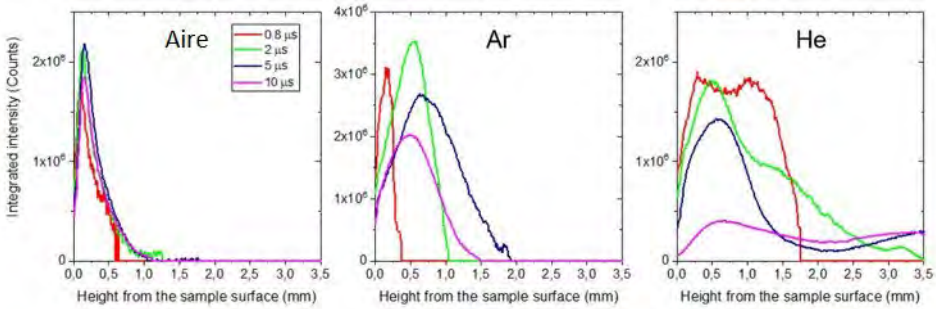

Figura 1. Distribución espacio-temporal de la señal integrada de CaF en diferentes atmósferas (aire, He y Ar).

[1] L. St-Onge, E. Kwong, M. Sabsabi, E. Vadas, *Spectrochim. Acta - Part B At. Spectrosc.* **57**, 1131 (2002).
[2] J. Aguilera, C. Aragón, *Appl. Phys. A*, **69**, 475 (2009).

Agradecimientos: Los autores agradecen la financiación del Ministerio de Ciencia e Innovación y del Gobierno del Principado de Asturias mediante el proyecto MCI-21-PID2020-113951GB-100 / AEI / 10.13039/501100011033 y las becas predoctorales MINECO BES-2017-080768 y PA-21-PF-BP20-059.

Astrofísica y Astropartículas

Presentaciones orales

Jueves 14/07:

15:30-15:45 Victor J. Sánchez Béjar. *Dynamical masses of brown dwarfs and planets*

15:45-16:00 Jun-Yan (Jerry) Zhang. *Chemical Components Analysis of Atmospheres of Ultracool Objects using Laboratorial Spectra*

16:00-16:15 Susana Iglesias. *Evidence for amino acids in the gas of the IC 348 star cluster in Perseus*

16:15-16:30 Javier Olivares Romero. *The dynamical interaction of the Coma Berenices open cluster and Group X*

16:30-16:45 Nicolas Lodieu. *Small-ELF: a propotype for the future ExoLife Finder hybrid optical telescope*

16:45-17:00 Pedro Villalba González. *The Canadian Galactic Emission Mapper (CGEM): An 8-10 GHz Northen Sky Polarization Survey*

17:00-18:00 **Pósteres y café**.

18:00-18:15 Felipe J. Llanes-Estrada. *Galaxy rotation favors prolate dark matter haloes*

18:15-18:30 Oscar del Barco Novillo. *Primordial black hole origin for thermal gamma-ray bursts*

18:30-18:45 Marusa Zerjal. *Nearby young open clusters and their luminosity functions*

18:45-19:00 Ramón Luna Molina. *Structural changes induced by temperature variations in ices of astrophysical interest*

19:00-19:15 Miguel Molero Gonzalez. *Measurement of the Positron, Electron and Proton Anisotropy with AMS-02 on the ISS*

19:15-19:30 Hernán Gonzalo Asorey. *Astroparticle Simulation in Cloud Infrastructures: Applications to Astroparticle Physics*

Pósteres

- Ramón Luna Molina. *Refractive index and density of CO ice*

Dynamical masses of brown dwarfs and planets

V. J. S. Béjar[1,2,*], M. R. Zapatero Osorio[3], R. Rebolo[1,2], N. Lodieu[1,2], E. L. Martín[1,2], B. Gauza[4], and the GTCAO team

[1]*Instituto de Astrofísica de Canarias, E-38205 La Laguna, Tenerife, Spain.*
[2]*Universidad de La Laguna, Dept. Astrofísica, E-38206 La Laguna, Tenerife, Spain.*
[3]*Centro de Astrobiología (CSIC-INTA). Carretera de Ajalvir, km 4, E-28850 Torrejón de Ardoz, Madrid, Spain.*
[4]*Janusz Gil Institute of Astronomy, University of Zielona Góra, Lubuska 2, 65-265 Zielona Góra, Poland.*

*e-mail: vbejar@iac.es

Substellar objects, unlike stars, do not burn hydrogen in their interiors and are no able to reach the main sequence, where the luminosity and effective temperature remain stable, and therefore, they continuously evolve getting fainter and cooler. Since the properties of substellar objects evolve with time, it is difficult to determine their masses without any knowledge of the age and distance. Brown dwarf and planetary mass companions offer a unique opportunity to determine their physical properties and test theoretical evolutionary models. The combination of radial velocity, astrometric and direct imaging techniques allows us to directly measure the dynamical masses of substellar objects.

For these reasons, our group is involved in the development of the Gran Telescopio de Canarias (GTC) Adaptive Optics and Laser Guide Star system (GTCAO-LGS) and the GRANCAIN instrument. The GTCAO system, which is in the last stages of verification and acceptance tests before going to the telescope, together with the GRANCAIN camera is expected to provide nearly diffraction-limited images (resolution of ~50-70 mas) in the near-infrared.

High-resolution images with current ground-based Adaptive Optics (AO) facilities such as GTCAO-LGS system and GRANCAIN at GTC or the EUCLID satellite will identify hundreds of brown dwarf binaries in young clusters and moving groups with separations of few AU and orbital periods of few years. Future instruments such as FRIDA (with GTCAO-LGS) at the GTC, or HARMONY at the ELT will allow us to monitor their orbital motion (both astrometry and radial velocity) and measure their individual masses. With these observations we will be able to determine the mass-luminosity-age relations of substellar objects independently of evolutionary models.

Chemical Components Analysis of Atmospheres of Ultracool Objects using Laboratory Spectra

E. L. Matín[1,2,3], **Jerry Jun-Yan Zhang**[1,2,*], P. Esparza[4], F. Gracia[1], J. L. Rasilla[1], T. Masseron[1,2], A. J. Burgasser[5]

[1]*Instituto de Astrofísica de Canarias (IAC), Calle Vía Láctea s/n, 38200 La Laguna, Tenerife, Spain.* [2]*Departamento de Astrofísica, Universidad de La Laguna (ULL), 38206 La Laguna, Tenerife, Spain.* [3]*Consejo Superior de Investigaciones Científicas (CSIC), 28006 Madrid, Spain.* [4]*Departamento de Química, Universidad de La Laguna (ULL), 38206 La Laguna, Tenerife, Spain.* [5]*Center for Astrophysics and Space Science, University of California San Diego, 9500 Gilman Drive, La Jolla, CA 92092, USA.*

*e-mail: jzhang@iac.es

Substellar objects have ultracool atmospheres where molecules significantly contribute to the complexity of the spectra. To help with spectroscopic analysis, we are building a library of optical to near-infrared molecular absorption spectra using gas cells and a spectrometer at our laboratories. We already have room-temperature spectra of water vapor, ammonia, methane, hydrogen cyanide, hydrogen sulfide, and several other carbohydrates and deuterated molecules as well.

Recently we have investigated ammonia-to-methane ratios from a specific window in H-band near-infrared spectra which minimizes contamination from other chemicals in late-T and Y dwarfs, using laboratory gas spectra and tens of object spectra from Near Infrared Spectrograph (NIRSPEC) on the Keck Telescope and the Hubble Space Telescope (HST) [1,2,3]. The results are concordant with the theoretical abundance model and suggest that all the late-T and Y dwarfs considered in this work have ammonia-to-methane ratios consistent with that of Jupiter within the uncertainties, suggesting that they have similar chemical abundances, and the overall trend also shows ammonia-to-methane ratio increases when spectral type goes from T7 to Y2.

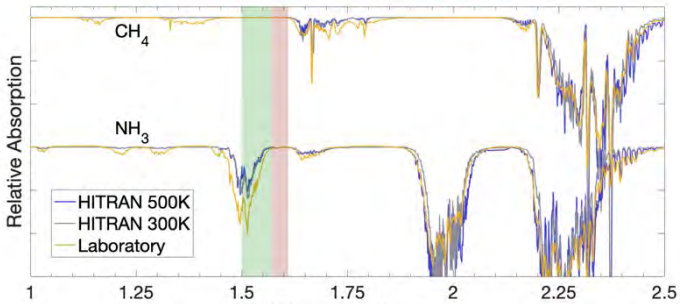

Figure 1. Our laboratory spectrum for ammonia and methane compared to their HITRAN simulated spectra for temperatures of 500 K and 300 K. As an example, a possible wavelength window proposed for NH3-H index is marked with color bands: green for the numerator, red for the denominator.

In the future, we are going to explore more specific spectral window for certain combination of chemicals in our library and we will obtain higher-resolution spectra of objects. Besides, with future deep-sky infrared survey like Euclid, which will be launched into space in 2023. we will have to deal with the spectra of thousands of ultracool objects. Those objects will need to be classified spectroscopically, and our research may provide optimized spectral indices.

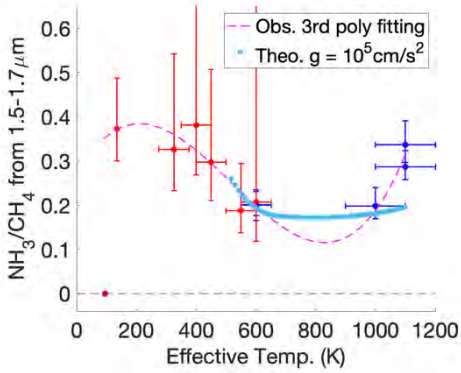

Figure 2. Ammonia-to-methane ratios derived for late-T dwarfs and Y dwarfs with a 95% confidence level from NIRSPEC data (blue) and HST data (red) compared with those of Jupiter and Saturn from IRTF data (red) as a function of Teff. The results are compared with the scaled theoretical ratios of molecular column densities estimated from [4], which are shown in light blue.

[1] Martín, Zhang et al. *Astronomy & Astrophysics* **655**, L3 (2021).
[2] Cushing et al. *Astrophysical Journal* **920**, 20 (2021).
[3] McLean et al. *Astrophysical Journal* **596**, 561 (2003).
[4] Zahnle & Marley, *Astrophysical Journal* **797**, 41 (2014).

Acknowledgements: ELM acknowledges support from the Agencia Estatal de Investigación del Ministerio de Ciencia e Innovación under grant PID2019-109522GB-C53. J.-Y. Zhang acknowledges a summer grant from the Instituto de Astrofisica de Canarias. ELM thanks Mike Cushing for sending the HST infrared spectrum published in [2]. This research has made use of the Simbad database, operated at the centre de Données Astronomiques de Strasbourg, and of NASA's Astrophysics Data System Bibliographic Services.

Evidence for amino acids in the gas of the IC 348 star cluster in Perseus

Susana Iglesias-Grot

Instituto Astrofísica de Canarias.

e-mail: sigroth@iac.es

Amino acids are building-blocks of proteins, basic constituents of all organisms and essential to life on Earth. They are present in carbonaceous chondrite meteorites and comets, but their origin is still unknown. Formation of amino acids in the interstellar medium is posible via specific gas-phase reactions in dark clouds, however sensitive radiosearches at millimeter wavelengths have not revealed their existence yet. The mid-IR vibrational spectra of amino acids provide an alternative path for their identification. We present Spitzer spectroscopic observations in the star-forming region IC 348 of the Perseus Molecular Cloud showing evidence for mid-IR bands of H2, OH, H2O, CO2, C2H2, C4H2, HC5N, C2H6, C6H2, C6H6, PAHs, fullerenes C60 and C70 and emission lines consistent with the most intense laboratory bands of the three aromatic amino acids, tyrosine, phenylalanine and tryptophan and the aliphatic amino acids isoleucine and glycine. Estimates of column densities give values 10-100 times higher for isoleucine and glycine than for the aromatic amino acids as in some meteorites. The strongest bands of each amino acid are also found in the combined spectrum of >30 interstellar locations in diverse star-forming regions supporting the suggestion that amino acids are widely spread in interstellar space. Future mid-IR searches for proteinogenic amino acids in protostars, protoplanetary disks and in the interstellar medium will be key to establish an exogenous origin of meteoritic amino acids and to understand how the prebiotic conditions for life were set in the early Earth.

The dynamical interaction of the Coma Berenices open cluster and Group X

Javier Olivares[1,2,*], Nicolas Lodieu[1,2], Víctor Béjar[1,2], Marusa Zerjal[1,2], Eduardo Martín[1,2]

[1]*Instituto de Astrofísica de Canarias, Calle Vía Láctea s/n, E-38200 La Laguna, Tenerife, Spain.*
[2]*Departamento de Astrofísica, Universidad de La Laguna, E-38206 La Laguna, Tenerife, Spain.*

*e-mail: jolivares@iac.es

Interacting open cluster pairs are fascinating systems whose numbers continue to increase thanks to Gaia data. These pairs pose exciting questions: Were they formed together? Are their populations mixing? What is the rate of these encounters?

Recent studies show that the Coma Berenices (700 Myr, 86 pc) open cluster and the Group X (400 Myr, 98pc) system, despite their unrelated origin, are interacting and will experience a flyby in 13 to 16 Myr. Given their proximity and extension of Coma Berenice's tidal tails (more than 60pc), this pair offers an excellent opportunity to answer the previous questions.

Using Gaia EDR3 we reassess the membership of these two groups extending the search to half of the northern Galactic hemisphere. Our new lists of members are 50 % larger than those from the literature, cover a wider sky region, and reach the Gaia photometric limit at late-M dwarfs with average recovery and contamination rates better than 99 % and 7 %, respectively. Furthermore, with novel Bayesian inference methods, we infer masses, 3D positions and 3D velocities for all members, including the faint M dwarfs. With this exquisite and complete data set, we reexamine the dynamical state of members in the tails and halos and trace forward their present positions to further constrain the time of the flyby. In addition, we estimate the rate of encounters of open clusters in the solar neighbourhood and analyze the role they play in the mixing and enrichment of stellar populations.

Small-ELF: a propotype for the future ExoLife Finder hybrid optical telescope

N. Lodieu[1,2,*], J. Kuhn[3], Y. Zhou[4], G. Moretto[5,6], M. Langlois[5,6], R. Rebolo[1,2,7], K. Lewis[8]

[1]*IAC, Calle Vía Lactea s/n, 38200 La Laguna, Tenerife, Spain.*
[2]*Departamento de Astrofísica, Universidad de La Laguna (ULL), E-38206 La Laguna, Tenerife, Spain.*
[3]*University of Hawaii, Institute for Astronomy, 34 Ohia Ku St, Pukalani, Maui, HI, 96768, USA.*
[4]*Dynamic Intelligent Structures Ltd. 2680 Shell Road, Richmond, BC, V6P3X8, Canada.*
[5]*Centre de Recherche Astrophysique de Lyon - CRAL, Saint-Genis-Laval, France.*
[6]*Centre National de Recherche Scientifique - CNRS, Saint-Genis-Laval, France.*
[7]*Consejo Superior de Investigaciones Científicas, CSIC, Spain.*
[8]*CEO / Creative Entrepreneur Buble Studios, USA.*

*e-mail: nlodieu@iac.es

Technology now exists to enable large optical systems that are capable of resolving and measuring faint sources not accessible with current remote sensing instruments and detectors. The possibility of creating ground-based telescopes at the 50m-scale with sufficient wavefront control to both fully overcome the effects of the atmosphere, but with exquisite coronagraphic capability starting at the telescope entrance pupil, means we may solve some of the most fundamental cross-cutting scientific questions: like, ïs there life outside of the solar system?".

The IAC is part of a consortium with the University of Hawaii and Universities in Lyon to develop the technologies needed for the next generation telescopes aimed at direct imaging of exoplanets around bright stars: the "ExoLife Finder (ELF)" telescope. We have a detailed design for a 3.5-m diameter prototype, nicknamed Small-ELF, to be built and installed at Teide Observatory by 2025. I will present the technological and scientific challenges of such telescope.

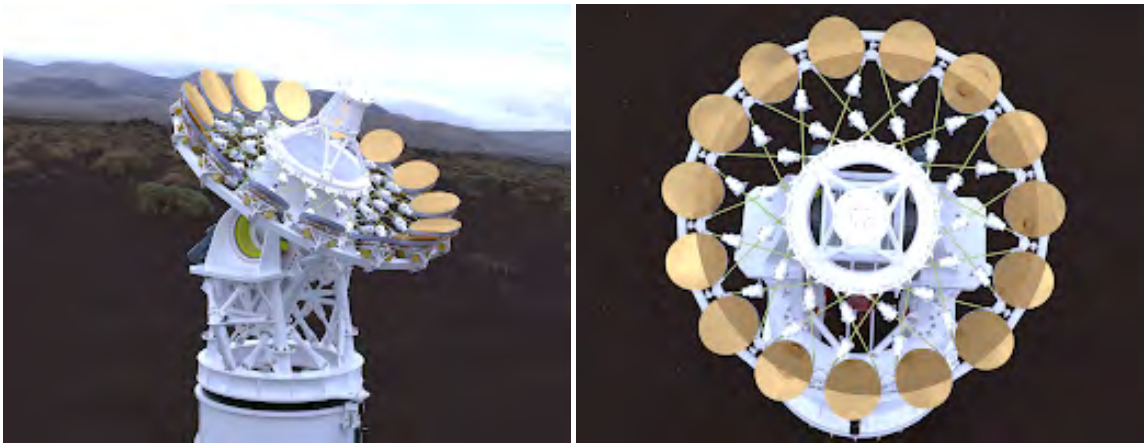

Figure 1. Detailed design of the Small-ELF 3.5-m prototype.

The Canadian Galactic Emission Mapper (CGEM): An 8-10 GHz Northern Sky Polarization Survey

Mandana Amiri[1], Artem Davydov[1], Mark Halpern[1], Gary Hinshaw[1], Joshua MacEachern[1], Tom Landecker[2], Bruce Veidt[2], **Pedro Villalba González**[1,*], Donald V. Wiebe[1], Edward J. Wollack[3], Parham Zarei[1]

[1]*Department of Physics and Astronomy, University of British Columbia, Canada.*
[2]*National Research Council Canada, Dominion Radio Astrophysical Observatory, Canada.*
[3]*NASA Goddard Space Flight Center, United States of America.*

*e-mail: pedrovg@phas.ubc.ca

Inflation is theorized to be a period in the very early universe in which the universe expanded by a factor of at least e^{60} [1]. Since it was first proposed in 1981 [2] it has been confirmed by several observations (see [3], for example), but there is a prediction which has not yet been observed and that would constitute 'smoking-gun' evidence supporting this model, primordial gravitational waves.

Any polarization pattern, and more concretely, the cosmic microwave background (CMB), can be decomposed into two components (E- and B-modes). The ΛCDM model predicts that the CMB polarization is mostly E-mode, with a small B-mode component coming from gravitational lensing. The primordial gravitational waves hypothesized would produce E- and B- modes equally, thus by looking for an excess B-mode signal we would be looking for an imprint of these gravitational waves.

One of the greatest challenges associated with detecting B-modes in the CMB is that CMB B-modes are dominated by polarized Galactic foreground B-modes at all frequencies and angular scales [4]. These foregrounds must therefore be mapped to high precision in order for them to be sufficiently removed from CMB data.

The Canadian Galactic Emission Mapper (CGEM) will be a 4 metre on-axis telescope located at the Dominion Radio Astrophysical Observatory (DRAO) in British Columbia, Canada. It will map the northern sky with ~0.5 degree angular resolution in the band of 8-10 GHz. CGEM will obtain high signal-to-noise Stokes Q and U maps of Galactic synchrotron and spinning dust emission. The main cosmological goal of CGEM is to enable improved foreground models in aid of the CMB B-mode polarization search [5,6]. A secondary goal is to better understand the interstellar medium.

By observing near 10 GHz, CGEM will map these foregrounds at a much higher signal to noise than if they were observed near the CMB window (~100GHz). These maps will then be extrapolated to higher frequency, where they can be used to remove foreground B-modes from CMB data. CGEM will target large angular scales, where the B-mode signal potentially dominates the lensing B-mode signal. In order to aid in the B-mode search, CGEM must have excellent polarization purity. Accordingly, the feed, system geometry, and the shapes of the reflectors are all being carefully optimized to maximize polarization purity.

I will give an overview of CGEM and its science goals. I'll also describe how the experiment is being designed to maximize polarization purity and will outline future plans for the experiment, which we aim to have on sky by the end of 2022.

[1] M. Kamionkowski and E. D. Kovetz, *Annual Review of Astronomy and Astrophysics* **54**, 227 (2016).
[2] A. H. Guth, *Phys. Rev. D* **23**, 347 (1981).
[3] D. N. Spergel and M. Zaldarriaga, *Phys. Rev. Lett.* **79,** 2180 (1997).
[4] L. Page, G. Hinshaw, E. Komatsy et al., *The Astrophysical Journal Supplement Series* **170**, 336 (2007).
[5] The PLANCK Collaboration, *Astronomy & Astrophysics* **641**, A10 (2020).
[6] The BICEP/Keck Collaboration, *Phys. Rev. Lett.* **127**, 151301 (2021).

Acknowledgements: We thank the Dominion Radio Astrophysical Observatory, where CGEM will be located, operated by the National Research Council Canada. DRAO is situated on the traditional, ancestral, and unceded territory of the Syilx Okanagan people.

Galaxy rotation favors prolate dark matter haloes

Adriana Bariego Quintana, **Felipe J. Llanes-Estrada***, Oliver Manzanilla Carretero

Depto. Física Teórica e IPARCOS, Universidad Complutense de Madrid, Spain.

*e-mail: fllanes@fis.ucm.es

The flat rotation velocity $v(r) \to$ constant found by Vera Rubin and collaborators and salient in the SPARC galaxy–rotation data base of 175 galaxies [1] falls off Kepler's law in two dimensions. Thus, it is naturally reproduced by elongated dark matter (DM) distributions [2] with the axis of prolateness perpendicular to the galactic plane (see fig. 1), because the force law external to such distribution, $F(r) = \frac{-2G\lambda}{r}$ naturally leads to $v(r) = \sqrt{2G\lambda}$. We report on recent extensive fits [3] to the rotation data.

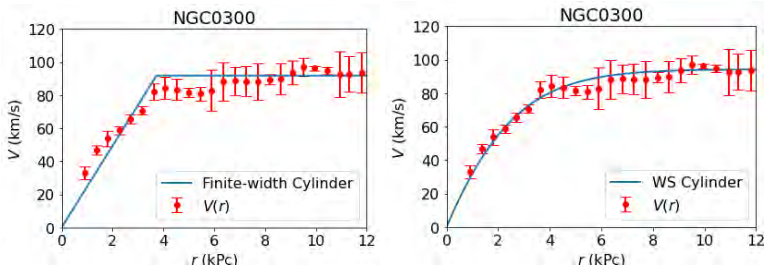

Figura 1: Fits to a typical galactic rotation curve, after discounting the visible matter distribution, with a cylindrical shape. Left: finite width dark matter cylinder with a sharp edge. Right: softened distribution with a Woods-Saxon profile, still cylindrical.

First, contrasting spherical and cylindrical models of DM with different radial profiles, we find that both can work. Spherical DM haloes with $\rho(r) \sim r^{-2}$ (the isothermal exponent) can explain the data; but *essentially any* $\rho(r)$ function with an elongated geometry yields the flattening: for equal dark matter profile except nearly isothermal ones, elongated distributions provide smaller χ^2 than purely spherical ones.

Additionally, we fit ellipsoidal shapes (via models and via a spherical-harmonic expansion) and extract the ratio of the minor to the major semiaxes (figure 2). This is in agreement with cosmological simulations [4], except that we cannot confirm any correlation between ellipticity and galactic mass from the rotation data.

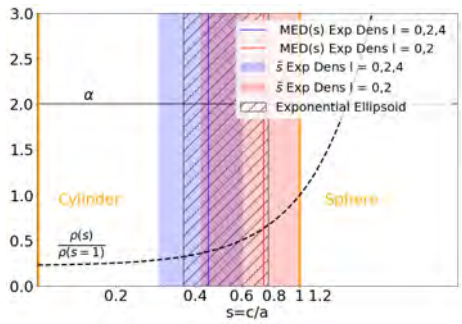

Figura 2: Ratio of the semiaxes of an ellipsoid $s = c/a$ representing a dark matter halo. Our analysis suggests, from empirical rotation curves, that $s < 1$ implying a prolate shape. Shown are the medians and averages with uncertainty with a few terms in a spherical-harmonics expansion, as well as an ellipsoidal model [3] interpolating from pancake to spherical to cylindrical shape.

We find that the geometric mean of the individual halo ellipticities is the adequate measure of deformation because $s = c/a \in (0, \infty)$ corresponds to spherical haloes for $s = 1$, so that the common arithmetic average $\langle s \rangle$ is skewed towards oblateness and fails to reveal that a large majority of galaxy curves suggest prolate haloes.

Several independently coded fitting exercises concur in yielding $s < 1$ for most of the database entries and the oblate exceptions are understood and classified. This likely prolateness (if it would apply to the Milky Way) is of consequence for the estimated dark matter density near Earth, that would be smaller than usually assumed in direct–detection experiments by the factor shown with the dashed line in figure 1.

[1] F. Lelli *et al.*, *Astron. J.* **152**, 157 (2016).
[2] F. J. Llanes-Estrada, *Universe* **7**, 346 (2021).
[3] A. Bariego Quintana, F. J. Llanes-Estrada and O. Manzanilla Carretero, arXiv:2204.06384, under refereeing.
[4] B. Allgood, *et al. Mon. Not. Roy. Astron. Soc.* **367**, 1781 (2006).

Acknowledgements: Financially supported by grant MICINN: PID2019-108655GB-I00 (Spain), and Univ. Complutense de Madrid under research group 910309 and the IPARCOS institute

Primordial black hole origin for thermal gamma-ray bursts

Oscar del Barco

Department of Physics, Campus de Espinardo 30100, University of Murcia, Spain.

e-mail: obn@um.es

The interaction of an atomic-sized primordial black hole (PBH) with a central black hole (CBH) can be described as an intense gamma-ray emission over a certain period of time [1, 2]. Such gamma-ray bursts (GRBs) are of thermal nature, due to the Hawking radiation emitted by the infalling PBH and detectable by modern observatories like FERMILAT or the projected e-ASTROGAM.

Depending on the specific PBH orbit in the CBH Schwarschild spacetime, our numerical calculations for the PBH Hawking temperature show an initial slight heating followed by a dramatic cooling behaviour. This process is consistent with the temperature evolution of already measured thermal-like gamma-ray bursts (GRBs) [3].

Our results might provide an alternative explanation for such thermal-like GRBs based on primordial black hole origin.

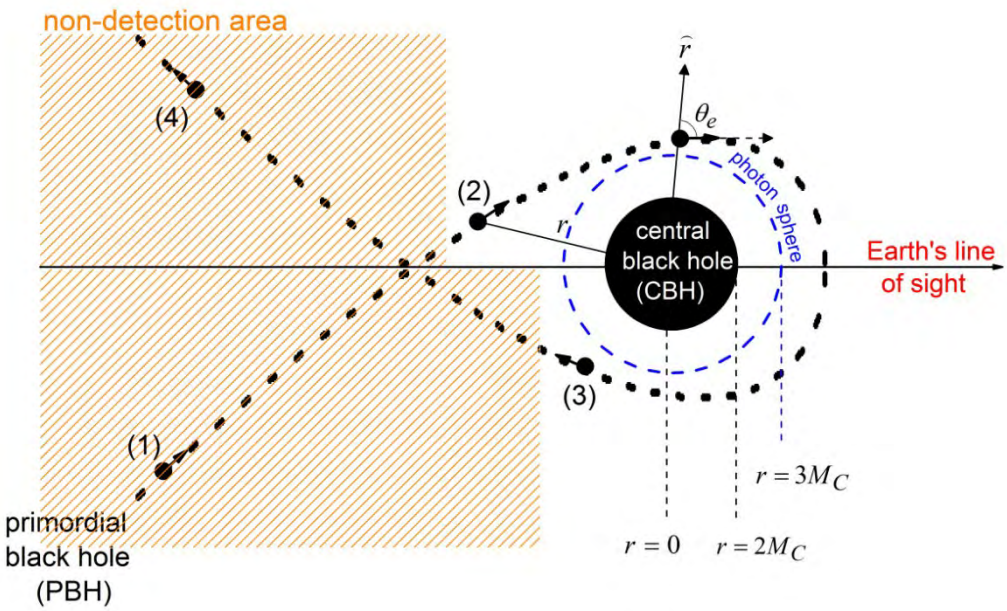

Figure 1. Schematic representation of our binary BH scenario: an atomic-sized PBH approaches a Schwarschild-type CBH describing a typical scattering orbit. The PBH Hawking emission directed toward the Earth might be detected as thermal GRBs.

[1] O. del Barco, *Monthly Notices of the Royal Astronomical Society* **506**, 806 (2021).
[2] O. del Barco, *Monthly Notices of the Royal Astronomical Society* **512**, 2925 (2022).
[3] F. Ryde, *The Astrophysical Journal* **614**, 827 (2004).

Nearby young open clusters and their luminosity functions

Maruša Žerjal[1,2,*], Nicolas Lodieu[1,2], Antonio Pérez Garrido[3], Javier Olivares Romero[1,2], Víctor Sánchez Bejar[1,2], Eduardo Martín Guerrero de Escalante[1,2]

[1]*Instituto de Astrofísica de Canarias, E-38205 La Laguna, Tenerife, Spain.* [2]*Universidad de La Laguna, Dpto. Astrofísica, E-38206 La Laguna, Tenerife, Spain.* [3]*Dpto. Física Aplicada, Universidad Politécnica de Cartagena, 30202 Cartagena, Murcia, Spain.*

*e-mail: mzerjal@iac.es

Nearby open clusters play a benchmark role in the observations related to the fundamental astrophysical processes, such as formation and evolution of stars and their planets. We used Gaia EDR3 catalogue to place stars in the position-velocity space and re-evaluated memberships of young (<1Gyr) open clusters in the vicinity of the Sun (<500 pc). We re-examined their relative ages revealed from their colour-magnitude diagrams and rotation periods from the TESS data. This enables us to study the evolution of the luminosity function over time and speculate about the gradual evaporation and dispersal of their members into the Galactic disk. With the goal to make these results widely available to the professional and amateur communities, we are building a website with our catalogues of cluster members linked to Aladin and CDS virtual observatory tools. An interactive plots of our members offer an opportunity for users to create their personalised 3D plots and colour-colour diagrams.

Acknowledgements: MŽ acknowledges funding from the Consejería de Economía, Conocimiento y Empleo del Gobierno de Canarias and the European Regional Development Fund (ERDF) under grant with reference PROID2020010052.

Structural changes induced by temperature variations in ices of astrophysical interest

Manuel Domingo, Ramón Luna, Carlos Millán, Carmina Santonja, **Miguel Á. Satorre***

Department Applied Physics, EPSA, Centro de Tecnologías Físicas, Universitat Politècnica de València.

*e-mail: msatorre@fis.upv.es

Ices of molecules such as H_2O, CO, CO_2, CH_4, CH_3OH… form part of many astrophysical scenarios. Planets, satellites, comets, trans-Neptunian objects, or grains in the dense interstellar medium present evidence of such ices.

Experiments gather data of astrophysical interest for observations, models, simulations… The results we will present study the structural changes (different amorphous structures, crystallization, and diffusion) of these molecules that suffer when a heat source varies their temperatures.

The experiments consist of depositing pure ices or ice mixtures, warming up the sample, and following possible structural variations by mass spectroscopy and laser interferometry. Double laser interferometry and a quartz crystal microbalance let us study the initial structure of such ices or mixtures.

The presentation also will explore the consequences of such structural changes in different astrophysical contexts to show the potentiality of those results.

Acknowledgements: Funds have been provided for this research by the Spanish MINECO, Project PID2020-118974GB-C22.

Measurement of the Positron, Electron and Proton Anisotropy with AMS-02 on the ISS

J. Casaus[1], **M. Molero**[2,*], M.A. Velasco[1]

[1]*Centro de Investigaciones Energéticas, Medioambientales y Tecnológicas (CIEMAT), Avenida Complutense 40, Madrid, Spain.* [2]*Instituto de Astrofísica de Canarias (IAC), Calle Vía Láctea s/n, Tenerife, Spain.*

*e-mail: mmolerog@iac.es

The Alpha Magnetic Spectrometer (AMS-02) is a multipurpose particle physics detector that was installed onboard the International Space Station (ISS) in May 2011 to carry out a long-term mission of fundamental physics research in space. AMS-02 has operated continuously for more than 10 years and has collected more than 2×10^{11} events. The experiment plans to continue collecting data until the end of the ISS (currently 2030).

As of today, AMS has provided the most precise measurements of the positron [1], electron [2] and proton [3] fluxes in the GeV-TeV energy range. On the one hand, the positron and electron fluxes show an excess at high energies which cannot be explained with the traditional models. On the other hand, the proton flux progressively hardens at high rigidities challenging the traditional acceleration and propagation mechanisms.

The origin of these features remains unclear, and a plethora of models have been proposed. In the case of positrons, the additional contribution cannot be explained by a pure secondary component and the inclusion of nearby primary sources is necessary, whether of astrophysical (pulsars) or a more exotic (dark matter) origin. Pulsars represent the leading candidate as primary sources of positrons due to their capability to inject pairs of $e\pm$ in the medium. Contributions from Geminga and Monogem are commonly used to explain the observed excess and predict anisotropies of amplitude $10^{-2} - 10^{-3}$ [4-7]. In the case of protons, the spectral features could also be explained with the inclusion of local sources of high energy cosmic rays or the modification of the current propagation models [7-8].

In this context, the study of the arrival directions of the individual particle species, e.g. their anisotropy, may help to understand the origin of the observed features and, in particular, allows to explore the impact that nearby sources may imprint in the fluxes.

The AMS results on the positron, electron and proton anisotropy will be presented along with the discussion of the implications of these measurements.

[1] M. Aguilar *et al.* [AMS Collaboration], *Phys. Rev. Lett.* **122**, 041102 (2019).
[2] M. Aguilar *et al.* [AMS Collaboration], *Phys. Rev. Lett.* **122**, 101101 (2019).
[3] M. Aguilar *et al.* [AMS Collaboration], *Phys. Rev. Lett.* **114**, 171103 (2015).
[4] D. Hooper, P. Blasi, and P.D. Serpico., *JCAP* **01,** 25 (2009).
[5] S. Manconi, M. Mauro, and F. Donato, *JCAP* **1701** (2017).
[6] K. Fang, X.-J. Bi, P.-F. Yin, *Monthly Notices of the Royal Astronomical Society* **478**, 4 (2018).
[7] W. Liu, X.-J. Bi, S.-J. Lin, B.-B, Wang, P.-F Yin, *Phys. Rev. D* **96**, 023006 (2017).
[8] G. Bernard, T. Delahaye, Y.-Y. Keum, W. Liu, P. Salati, and R. Taillet, *A&A* **A48**, 555 (2013).

Astroparticle Simulation in Cloud Infrastructures: Applications to Astroparticle Physics

Antonio Juan Rubio-Montero[1], Raúl Pagán-Muñoz[1], Alfonso Pardo-Díaz[2], Iván Sidelnik[3], R. Mayo-García[1], **Hernán Asorey**[4,5,*], for the LAGO Collaboration[6]

[1]*Centro de Investigaciones Energéticas, Medioambientales y Tecnológicas (CIEMAT), Av. Complutense 40, 28040 Madrid, Spain.* [2]*Centro Extremeño de Tecnologías Avanzadas (CETA-CIEMAT), Calle Sola 1, Trujillo, 10200, Spain* [3]*Departamento de Física de Neutrones, Centro Atómico Bariloche (CNEA/CONICET), Av. Bustillo 9500, 8400 San Carlos de Bariloche, Argentina* [4]*Instituto de Tecnologías en Detección y Astropartículas (ITeDA). Centro Atómico Constituyentes (CNEA/CONICET/UNSAM) Av. Gral. Paz 1499, 1450 Villa Maipú, Argentina* [5]*Departamento Física Médica, Centro Atómico Bariloche (CNEA) Av. Bustillo 9500, 8400 San Carlos de Bariloche, Argentina* [6]*The LAGO Collaboration, see the complete list of authors and institutions at http://lagoproject.net/collab.html*

*e-mail: hernan.asorey@iteda.cnea.gov.ar

The Latin American Giant Observatory (LAGO) is an extended astroparticle observatory, consisting of a synchronised network of water Cherenkov detectors operating in Latin America and covering a wide range of altitudes above sea level and geomagnetic rigidity cut-offs[1]. LAGO is operated by the LAGO Collaboration, a highly collaborative organization with 100 members from more than 30 Iberoamerican institutions. LAGO research objectives are focused on studying of high-energy astrophysical and space weather and climate phenomena, by indirectly measuring the temporal evolution of the flux of galactic cosmic rays from ground level[2]. The interaction of such cosmic rays with the atmosphere produces a large number of secondary particles via radiative and decay processes. These true cascades of particles, collectively known as Extensive Air Showers, could reach up to 10^{11} particles at the instant of their maximum development. To accomplish these tasks we have developed several computational tools[3]; that take advantage of the increasing computational capabilities available at high-performance computing facilities and in cloud-based computing environments, such as the European Open Scientific Cloud (EOSC)[4]. With these tools, we can calculate the expected particle flux at any place in the World, including real-time atmospheric and geomagnetic effects, reproducing the expected signals in different types of detectors. We can also calculate the impact in the expected flux due to the occurrence of transient astrophysical phenomena, such as those related to Solar Activity[5] or the high energy component of Gamma-Ray Bursts[6]. In this contribution, we will show how this very complex sequence of simulations is helping us to characterize new sites for our Observatory and the design of improved astroparticle detectors for the LAGO detection network.

[1] I. Sidelnik and H. Asorey, *NIM A* **876**, 173 (2017).
[2] H. Asorey *et al.*, *Space Weather* **16**, 461 (2018).
[3] C. Sarmiento-Cano *et al.*, in *PoS* **358**, 412 (2019).
[4] A.J. Rubio-Montero *et al.*, in *2021 Winter Simulation Conference (WSC)*, 1–12 (2021).
[5] M. Suárez-Durán *et al.*, in *PoS* **236**, 142 (2015).
[6] C. Sarmiento-Cano *et al.*, in *PoS* **395**, 929 (2021).

Acknowledgements: The LAGO Collaboration is thankful to the Pierre Auger Collaboration for their continuous support. It is also acknowledged the support of the LAGO Collaboration members. This work has been partially funded by the H2020 co-funded project European Open Science Cloud - Expanding Capacities by building Capabilities (EOSC-SYNERGY, No. 857647). Simulations carried out made also use of the computing facilities provided by CETA-CIEMAT and CIEMAT.

Refractive index and density of CO ice

Ramón Luna, Manuel Domingo, Carlos Millán, Carmina Santonja, **Miguel Á. Satorre***

Department Applied Physics, EPSA, Centro de Tecnologías Físicas, Universitat Politècnica de València.

*e-mail: msatorre@fis.upv.es

Carbon monoxide is an important frozen component of the Solar System and the interstellar medium grains in molecular clouds. This work shows the experimental results of its density and refractive index in the interval 13 to 28 K. Double laser interferometry lets us obtain the actual real part of the refractive index in a high vacuum chamber. The direct measurement of the mass deposited on a known area by a quartz crystal microbalance determines the average density of the deposited material. Both parameters reflect the same behavior with the deposition temperature.

Additionally, we relate both parameters by the Lorenz-Lorentz (L-L) relationship. We also discuss the implications of considering the possibility of obtaining a linear fit to better represent the experimental behavior of our results or maintain the L-L without the independent term of its linear fit.

Acknowledgements: Funds have been provided for this research by the Spanish MINECO, Project PID2020-118974GB-C22.

Física de Sistemas Complejos

Presentaciones orales

Miércoles 13/07:

15:30-16:00 V. Martín Mayor. *The mystery of rejuvenation and memory in spin-glasses*

16:00-16:15 J. Moreno Gordo. *Temperature Chaos is present in off-equilibrium spin-glass dynamics*

16:15-16:30 J. Cantisán Gómez. *Stochastic Resetting in the Kramers problem*

16:30-16:45 R. Gutiérrez. *Finding generalized optimal paths and unveiling dynamical phase transitions through the large deviations of random walks on graphs*

16:45-17:00 J. Borondo. *Forecasting Fruits and Vegetable Prices: Reservoir computing outperforms traditional methods and neural networks*

17:00-17:15 R. A. Rica. *Brownian dynamics of interacting particles confined in an aqueous Paul trap*

17:15-17:45 **Café**.

17:45-18:15 J. García-Ojalvo. *Temporal oscillations as spatial organizers in multicellular populations*

18:15-18:30 M. Sireci. *A macroecological law of species interactions in microbial ecosystems*

18:30-18:45 J. Fernández-Gracia. *Inferring Generalized Lotka-Volterra parameters from longitudinal microbial data*

18:45-19:00 G. I. Triguero Platero. *From microscopics to macroscopic hydrodynamics of collective cell motion*

19:00-19:15 V. Buendía. *The excitatory-inhibitory branching process: a parsimonious view of cortical asynchronous states, excitability, and criticality*

19:15-19:30 E. Abad. *Normal and anomalous diffusion in evolving domains: a brief overview of some recent results*

Jueves 14/07:

15:30-16:00 M. Castro. *The turning point and end of an expanding epidemic cannot be precisely forecast*

16:00-16:15 P. Carpena. *Contagion effect in exams*

16:15-16:30 P. I. Hurtado. *Building continuous time crystals from rare events*

16:30-16:45 J. C. Losada. *Multipolarity in a Complex Society*

16:45-17:00 M. Grande. *Evolutionary Dynamics of the Ethereum Transaction Network*

17:00-17:15 R. Toral. *Numerical sampling rare of rare trajectories using stochastic bridges*

17:15-17:45 **Pósteres y café**.

17:45-18:15 O. Agam. *"Aging" and slow relaxation in the dynamics of living cells*

18:15-18:30 J. M. Marcos. *Optimal control of bidirectional escape from a symmetric potential well*

18:30-18:45 A. Domínguez. *Colloidal monolayers: bridging the gap between two and three spatial dimensions*

18:45-19:00 P. Maynar. *Kinetic theory of fluids under strong confinement*

19:00-19:15 A. Patrón. *Optimal thermalisation for a generic d-dimensional harmonic oscillator*

19:15-19:30 C. Pérez-Espigares. *Direct evaluation of large deviations in open quantum systems*

Pósteres

- A. V. Coronado. *Nonlinearity test for complex time series*
- S. Martín-Gutiérrez. *Statistical models of social interaction*
- M. I. García de Soria. *Dynamics of hard particles confined by an isotropic harmonic potential*
- B. Skadden. *Variability of spreading rate in forced plumes*
- I. González-Adalid. *Accelerating out-of-equilibrium critical dynamics via magnetic domains*

The mystery of rejuvenation and memory in spin-glasses

Víctor Martín-Mayor

Departamento de Física Teórica, Universidad Complutense, 28040 Madrid, Spain.

e-mail: presenting.authorB@murc.ia

The idea that theoretical physicists could build computers specifically designed to solve their problems, among other examples, has germinated in the Italian/Spanish Janus collaboration. Indeed, the Janus I [1] and Janus II [2] supercomputers deliver since 2008 the highest computing power Worldwide for spin-glasses simulations. The Janus collaboration is formed by researchers from the Universities of Zaragoza, Extremadura-Badajoz, Complutense de Madrid, La Sapienza-Roma and Ferrara, and is very proud to count Giorgio Parisi as a distinguished member.

The main focus of the talk will be describing our recent success in reproducing in a simulation using Janus II the spectacular memory and rejuvenation effects of spin glasses. Although memory and rejuvenation were discovered experimentally more than 20 years ago [3], convincingly reproducing these effects in a simulation seemed hopeless until now, and for very good reasons. Indeed, many pieces of the puzzle had to be gathered. First, we have needed to learn how to quantitatively extract the spin-glass coherence length (i.e. the size of the glassy domains) from simulations of non-equilibrium spin glass dynamics [4]. Second, one needs to reach reasonably large coherence lengths in the simulation, a task that demands the tremendous computing power of Janus II. A third step has been learning how to extrapolate from the numerical time and length scales to the experimental ones [5]. Fourth, Janus II has provided a crucial understanding about how temperature chaos in non-equilibrium dynamics really is [6]. These milestones have made possible undertaking a nice collaboration with the group of Ray Orbach in Texas. The collaboration with the Texan group has taught us how to perform in Janus II true çomputer experiments", in which the very same quantities are computed in the simulation and measured in a CuMn single crystal, and analyzed in a parallel way [7,8]. In fact, the 2022 temperature-chaos experiment by Orbach and Zhai [9] has produced crucial quantitative input to set up a successful simulation of memory and rejuvenation. A big surprise (at least surprising for us) is our finding that no less than three quite distinct length scales control aging dynamics [10].

[1] F. Belleti et al. (Janus Collaboration), *Commm. Phys. Comm.* **178**, 208 (2008).
[2] M. Baity-Jesi et al. (Janus Collaboration), *Commm. Phys. Comm.* **185**, 550 (2014).
[3] J. Jonason, E. Vincent, J. Hammann, J. P. Bouchaud, P. M. and Nordblad *Phys. Rev. Lett.* **81**, 3243 (1998).
[4] F. Belleti et al. (Janus Collaboration), *Phys. Rev. Lett.* **101**, 157201 (2008).
[5] M. Baity-Jesi et al. (Janus Collaboration), *Phys. Rev. Lett.* **120**, 267203 (2018).
[6] M. Baity-Jesi et al. (Janus Collaboration), *Communication Physics* **4**, 74 (2021).
[7] Q. Zhai, et al. (Janus collaboration), *Phys. Rev. Lett.* **125**, 237202 (2020).
[8] I. Paga et al. (Janus collaboration), *JSTAT* **2021**, 033301 (2021).
[9] Q. Zhai and R. Orbach, *Phys. Rev. B* **105**, 014434 (2022).
[10] M. Baity-Jesi et al. (Janus Collaboration), manuscript in preparation (2022).

Temperature chaos is present in off-equilibrium spin-glass dynamics

Marco Baity-Jesi[1], Enrico Calore[2], Andrés Cruz[3,4], Luis Antonio Fernandez[5,4], José Miguel Gil-Narvion[4], Isidoro Gonzalez-Adalid Pemartin[5], Antonio Gordillo-Guerrero[6,7,4], David Iñiguez[4,8,3], Andrea Maiorano[9,10,4], Enzo Marinari[11,10], Víctor Martin-Mayor[5,4], **Javier Moreno-Gordo**[7,4,*], Antonio Muñoz-Sudupe[5,4], Denis Navarro[12], Ilaria Paga[13,5], Giorgio Parisi[11,10], Sergio Perez-Gaviro[14,4,3], Federico Ricci-Tersenghi[11,10], Juan Jesús Ruiz-Lorenzo[15,7,4], Sebastiano Fabio Schifano[16], Beatriz Seoane[5,4], Alfonso Tarancon[3,4], Raffaele Tripiccione[2], David Yllanes[17,4], (Janus Collaboration)

[1]*Eawag, Überlandstrasse 133, CH-8600 Dübendorf, Switzerland.* [2]*Dipartimento di Fisica e Scienze della Terra, Università di Ferrara e INFN, Sezione di Ferrara, I-44122 Ferrara, Italy.* [3]*Departamento de Física Teórica, Universidad de Zaragoza, 50009 Zaragoza, Spain.* [4]*Instituto de Biocomputación y Física de Sistemas Complejos (BIFI), 50018 Zaragoza, Spain.* [5]*Departamento de Física Teórica, Universidad Complutense, 28040 Madrid, Spain.* [6]*Departamento de Ingeniería Eléctrica, Electrónica y Automática, U. de Extremadura, 10003, Cáceres, Spain.* [7]*Instituto de Computación Científica Avanzada (ICCAEx), Universidad de Extremadura, 06006 Badajoz, Spain.* [8]*Fundación ARAID, Diputación General de Aragón, 50018 Zaragoza, Spain.* [9]*Dipartimento di Biotecnologie, Chimica e Farmacia, Università degli studi di Siena, 53100, Siena, Italy.* [10]*INFN, Sezione di Roma 1, I-00185 Rome, Italy.* [11]*Dipartimento di Fisica, Sapienza Università di Roma, and CNR-Nanotec, I-00185 Rome, Italy.* [12]*Departamento de Ingeniería, Electrónica y Comunicaciones and I3A, U. de Zaragoza, 50018 Zaragoza, Spain.* [13]*Dipartimento di Fisica, Sapienza Università di Roma, INFN, Sezione di Roma 1, I-00185 Rome, Italy.* [14]*Centro Universitario de la Defensa, 50090 Zaragoza, Spain.* [15]*Departamento de Física, Universidad de Extremadura, 06006 Badajoz, Spain.* [16]*Dipartimento di Scienze Chimiche e Farmaceutiche, Università di Ferrara e INFN Sezione di Ferrara, I-44122 Ferrara, Italy.* [17]*Chan Zuckerberg Biohub, San Francisco, CA, 94158, United States.*

*e-mail: jmorenogordo@gmail.com

Historically, large responses in a system upon small perturbations in the initial conditions have been regarded as one of the main characteristics of chaotic systems. In fact, spin glasses exhibit a fragile behavior in response to perturbations such as temperature changes. Specifically, arbitrary small changes in the temperature would led to a complete reorganization of the equilibrium configurations of the spin glass. This phenomenon has been called Temperature Chaos [1,2].

This equilibrium definition has focused the research effort on small system sizes that can be equilibrated, which had lead, unfortunately, to a completely separated research line from the experimental works in spin glasses, where the system is always macroscopic and out-of-equilibrium.

In this work [3], we simulate a large system (in the simulation standards) which is always under non-equilibrium conditions. By invoking the static-dynamic equivalence principle we study small regions inside the system and find that the key quantity that is ruling the non-equilibrium Temperature Chaos phenomenon is the coherence length ξ.

Also, a rare-event analysis is needed to deal with the strong spatial heterogeneity (see Fig. 1) of the non-equilibrium Temperature Chaos.

These two ingredients, the identification of the coherence length ξ as a key quantity ruling the phenomenon and the spatial heterogeneity found in the chaoticity of the small studied regions, allow us to quantitatively describe the non-equilibrium Temperature Chaos phenomenon and to extrapolate the behavior of the system for large values of the coherence length.

Moreover, we find a crossover between weak and strong chaos regime controlled by a crossover length $\xi^* \propto (T_2 - T_1)^{-1/\zeta_{\rm NE}}$, whose analysis reveals the close relation with its equilibrium counterpart: the chaotic-length [2].

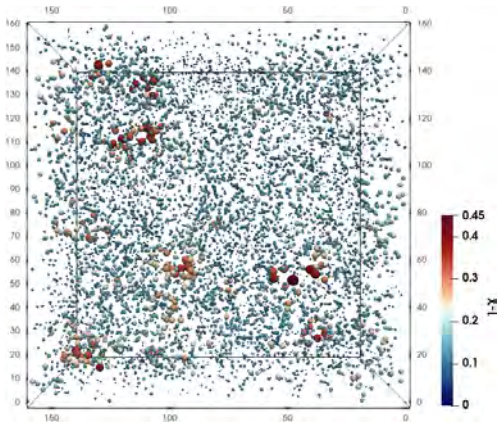

Figure 1. In this figure, we show the spatial heterogeneity of the non-equilibrium Temperature Chaos phenomenon. The cube represents our system and, inside it, we build spherical regions where we perform a measure of the chaotic parameter $1 - X$. We represent the spherical regions with a code of color and with a radius proportional to their chaoticity. We observe how the vast majority of the spherical regions present no chaos and a very small fraction of them present strong chaos.

[1] A. J. Bray, M. A. Moore, *Phys. Rev. Lett.* **58**, 57 (1987).
[2] J. R. Banavar, A. J. Bray, *Phys. Rev. B* **35**, 8888 (1987).
[3] M. Baity-Jesi et al., *Communications Physics* **4**, 74 (2021).

Stochastic resetting in the Kramers problem

Julia Cantisán[1,*], Jesús M.Seoane[1], Miguel A. F. Sanjuán[1,2]

[1] *Nonlinear Dynamics, Chaos and Complex Systems Group, Departamento de Física, Universidad Rey Juan Carlos. Tulipán s/n, 28933 Móstoles, Madrid, Spain*
[2] *Department of Applied Informatics, Kaunas University of Technology Studentu 50-415, Kaunas LT-51368, Lithuania.*

*e-mail: julia.cantisan@urjc.es

The theory of stochastic resetting (SR) asserts that restarting a search process at certain times may accelerate the finding of a target. SR was first studied by Evans and Majumdar [1], who showed that the mean first passage time (MFPT) of a diffusing particle searching for a target in an infinite domain presents a minimum for a certain value of the resetting rate. Some natural processes such as animal foraging or human visual search utilize this mechanism to reduce the search time.

We study stochastic resetting as a strategy to reduce the escape time of a classical diffusing particle trapped in a potential well, which may escape due to thermal fluctuations, i.e., the Kramers problem [2]. This is equivalent to a search process where the target is the top of the energy barrier. We use a Monte Carlo approach, which is necessary for generic complex potentials. We demonstrate that this approach is in agreement with some analytical results and that this technique allows to explore the system in a different way.

We apply two resetting strategies: resetting at deterministic times (see Figure 1) and resetting at exponentially distributed times (treating the resetting events as Poisson events). We find that trajectories whose initial position corresponds to at least a 41% of the height of the potential barrier, show a minimum in the MFPT. For resetting at deterministic times, the best resetting strategy can be predicted in advance as the optimal resetting time interval is related to the wave pattern of first passage times found for the no resetting case.

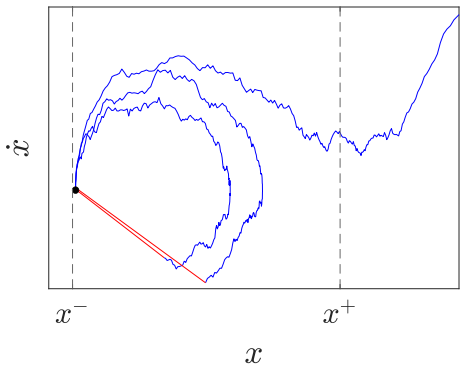

Figure 1. Phase space for a trajectory with deterministic resetting. The vertical dotted lines denote the edges of the potential well. The black point marks the initial condition, which is also the reset position. The trajectory moves around freely diffusing in the potential landscape until at $t = t_r$, the particle is immediately reset. This bit is marked in red. After two resetting events, the particle escapes.

[1] Martin R. Evans and Satya N. Majumdar, *Phys. Rev. Lett.* **106**, 160601 (2011).
[2] Julia Cantisán, Jesús M. Seoane and Miguel A.F. Sanjuán, *Chaos, Solitons and Fractals* **152**, 111342 (2021).

Acknowledgements: This work has been supported by the Spanish State Research Agency (AEI) and the European Regional Development Fund (ERDF, EU) under Projects No. FIS2016-76883-P and No. PID2019-105554GB-I00.

Finding generalized optimal paths and unveiling dynamical phase transitions through the large deviations of random walks on graphs

Ricardo Gutiérrez[1,*], Carlos Pérez-Espigares[2,3]

[1] *Grupo Interdisciplinar de Sistemas Complejos, Departamento de Matemáticas, Universidad Carlos III de Madrid, Spain.* [2] *Departamento de Electromagnetismo y Física de la Materia, Universidad de Granada, Spain.* [3] *Institute Carlos I for Theoretical and Computational Physics, Universidad de Granada, Spain.*

*e-mail: rigutier@math.uc3m.es

In a statistical mechanical formalism of ensembles of trajectories, dynamical large-deviation functions play a role analogous to that of thermodynamic potentials in equilibrium statistical mechanics. This is a powerful approach that has lately illuminated many aspects of non-equilibrium statistical physics. In fact, it can still yield novel perspectives and applications even in the analysis of such a simple process as a random walk on a graph, as we will see.

First we will illustrate how large-deviation functions of random walks can be employed for finding optimal paths and weight distributions in disordered discrete media such as random graphs and complex networks of different kinds, including spatial networks [1]. It is well known that many problems of theoretical and practical interest are related to finding shortest (or otherwise optimal) paths in networks, frequently in the presence of some obstacles or constraints. Another related sets of problems focus on optimal distributions of weights which, for a given connection topology, maximize some kind of flow or minimize a given cost function. In contrast to standard graph-theoretical methods, in our approach the paths are not limited to shortest paths and the weights must not necessarily optimize a given function. They can in fact be tailored to a given statistics of a time-integrated observable, which may be an activity or current, or local functions marking the passing of the random walker through a given node or link. This allows for great flexibility in the definitions of such generalized optimal paths and weight distributions. We illustrate this idea with an exploration of optimal paths in the presence of obstacles, and networks that optimize flows under constraints on local observables.

The study of optimal weight distributions in spatial networks contained in Ref. [1] shows intriguing localized vortex dynamics in random walks, similar to those that have been observed in the presence of exclusion effects [2]. To clarify this behavior, a more detailed study has been performed based on the two-dimensional random walk conditioned on partial currents, which reveals the existence of a dynamical phase transition between delocalized band dynamics and localized vortex dynamics [3]. We present a numerical microscopic characterization of the phases involved, and provide analytical insight based on the macroscopic fluctuation theory. The continuous phase transition is accompanied by spontaneous $\mathbb{Z}_2$-symmetry breaking whereby the stationary solution loses the reflection symmetry of the generator. Dynamical phase transitions similar to this one, which do not rely on exclusion effects or interactions, are expected to be observed in more complex non-equilibrium physics models.

[1] R. Gutiérrez and C. Pérez-Espigares, *Phys. Rev. E* **103**, 022319 (2021).
[2] T. Bodineau, B. Derrida, and J. L. Lebowitz, *J. Stat. Phys.* **131**, 821 (2008).
[3] R. Gutiérrez and C. Pérez-Espigares, *Phys. Rev. E* **104**, 044134 (2021).

Forecasting Fruits and Vegetable Prices: Reservoir computing outperforms traditional methods and neural networks

L.Domingo[1,2,3], M. Grande[3,4], F. Borondo[1,2], J. Borondo[4,5,*]

[1]*Instituto de Ciencias Matemáticas (ICMAT); Campus de Cantoblanco UAM; Nicolás Cabrera, 13-15; 28049 Madrid, Spain.*
[2]*Departamento de Química; Universidad Autónoma de Madrid; CANTOBLANCO - 28049 Madrid, Spain.*
[3]*Grupo de Sistemas Complejos; Universidad Politécnica de Madrid; 28035 Madrid, Spain.*
[4]*AgrowingData; Navarro Rodrigo 2 AT; 04001 Almería, Spain.*
[5]*Departamento de Gestión Empresarial; Universidad Pontificia de Comillas ICADE; Alberto Aguilera 23; 28015 Madrid, Spain.*

*e-mail: jborondo@gmail.com

The main goal of this work is to study the performance of reservoir commuting (RC) [1] based algorithms to predict the evolution of the prices of fruits and vegetables. Anticipating the prices is extremely important as their high volatility makes it difficult for farmers and coops to efficiently market the products. In fact, year in and year out we observe price crises where the commercialization of the product is not profitable, resulting in tons of waste of food. One of the challenges of this time series is that it has few training samples. In addition, the European market is a connected network where prices are influenced by hundreds of factors, such as exports & climate. Thus, we also provide external variables that capture this information to the algorithms to obtain more accurate results. RC is especially useful in this setting, since it uses both the past value of the time series and regressor variables to extrapolate the time series. Moreover, its simple training framework reduces the chances of overfitting the training data. We assess the performance of five RC models and compare the results with two benchmark time series models: a Long-Short Term Memory neural network (LSTM) [2] and a Seasonal Autoregressive Integrated Moving Average (SARIMA) [2].

We have trained the five RC models and the two benchmark models, and evaluated their performance in the test set. Figure 1 shows the prediction of the seven models compared with the true values of the prices' time series. To quantify and compare the performance of the models, we have used several metrics including the mean absolute error (MAE). Our results show clearly that the configurations based on RC outperform both SARIMA and LSTM.

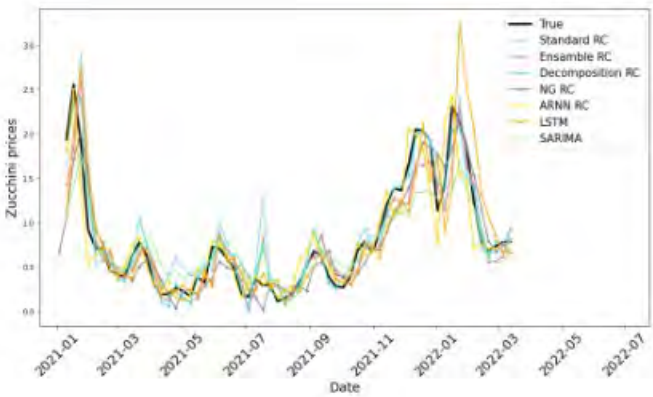

Figure 1. Prediction of the time evolution for the test set of the seven machine learning models studied in this work, together with the real time series.

[1] R. Gao, L. Du, O. Duru, K. F. Yue, Time series forecasting based on echo state network and empirical wavelet transformation, Appl. Soft Comput **102**, 107111 (2021).
[2] S. Hochreiter, J. Schmidhuber, Long short-term memory, *Neural Comput.* **9**, 1735 (1997).
[3] P. Chen, A. Niu, D. Liu, W. Jiang, B. Ma, Time series forecasting of temperatures using sarima: An example from nanjing, *IOP Conference Series: Materials Science and Engineering* **394**, 052024 (2018).

Brownian dynamics of interacting particles confined in an aqueous Paul trap

Carlos D. González-Gómez[1,2], **Raúl A. Rica**[1,*]

[1] *Nanoparticles Trapping Laboratory, Department of Applied Physics, Universidad de Granada, Av. Fuentenueva s.n., 18071 Granada, Spain.*
[2] *Universidad de Málaga, Departamento de Física Aplicada II, Escuela de Ingenierías Industriales, 29071 Málaga, Spain.*

*e-mail: rul@ugr.es

The Brownian dynamics of *individual* microparticles in suspension can be studied in detail with optical tweezers, as it has been demonstrated in multiple situations [1–4]. Optical tweezers can also be used to simultaneously manipulate multiple particles in different potential wells, but the simultaneous trapping of multiple particles in a *single potential well* is not possible with this technique. Paul traps are able to store charged particles in a single potential well, leading to the formation of so-called Coulomb crystals [5]. Typical experiments are performed with ions in vacuum, where the particles interact via Coulomb repulsion. In a liquid, charged microparticles can still be trapped with Paul traps [6], but they have never been tested with multiple particles trapped together.

Here, we present a Paul trap that is able to trap tens of particles in a microfluidic device, which allows us to study the Brownian dynamics of interacting particles. Our Paul trap is composed of two gold microelectrodes deposited on borosilicate glass with ring geometry (see Fig. 1), and implemented together with an optical tweezers setup. This combination creates a hybrid trap [7] that provides us with enhanced manipulation capabilities. First, we characterize the trap by video-tracking the diffusion of a single particle in the potential well under different conditions, and also measuring the electric field within the Paul trap with help of the optical tweezers. Further, we track the trajectory of several particles simultaneously and extract information of their interactions from the analysis of their mean squared displacement using two types of polystyrene particles, one of which strongly polarize in presence of an AC electric field and thus tend to form particle chains. Finally, we discuss the prospects of such a device for fundamental studies of interacting Brownian particles in a potential well.

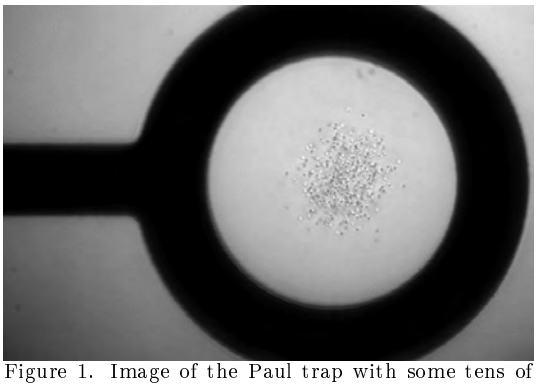

Figure 1. Image of the Paul trap with some tens of 1-μm polystyrene particles trapped together in liquid.

[1] J. Gieseler *et al.*, *Advances in Optics and Photonics* **13**, 74–241 (2021).
[2] I.A. Martínez, É. Roldán, L. Dinis, & R.A. Rica, *Soft Matter*, **13**, 22–36 (2017).
[3] F. Ricci, R.A. Rica *et al.*, *Nature Communications*, **8**, 15141 (2017).
[4] A. Kumar & J. Bechhoefer, *Nature*, **584**, 64?-68 (2020).
[5] R.C. Thompson, *Contemporary Physics*, **56**, 63–79 (2015).
[6] W. Guan, S. Joseph, J.H. Park, P.S. Krstić, & M.A. Reed, *PNAS*, **108**, 9326-9330 (2011).
[7] G.P. Conangla, R.A. Rica & R. Quidant, *Nano Letters*, **20**, 6018-?6023 (2020).

Acknowledgements: The Authors acknowledge financial support from FEDER/Junta de Andalucía-Consejería de Transformación Económica, Industria, Conocimiento y Universidades/ Proyecto P18-FR-3583.

Temporal oscillations as spatial organizers in multicellular populations

Jordi Garcia-Ojalvo

Department of Medicine and Life Sciences, Universitat Pompeu Fabra, Parc de Recerca Biomèdica de Barcelona, Dr. Aiguader 88, 08003 Barcelona, Spain.

*e-mail: jordi.g.ojalvo@upf.edu

Multicellular organisms rely on a careful spatiotemporal orchestration of form and function, covering multiple biological scales that range from molecules to cellular populations. Much current research is being devoted to understanding how space and time are integrated as organisms develop. In this talk I will address this issue in bacterial biofilms, multicellular populations with important clinical and environmental implications. Using a combination of experiments and computational modeling, I will show that oscillations in time, driven by molecular interactions, are transformed into periodicity in space, driven by cellular behavior, not unlike the segmentation clock that underlies somitogenesis in vertebrates. I will discuss the molecular mechanism underlying this phenomenon, and the biological function that this behavior might play in the life cycle of bacterial populations.

A macroecological law of species interactions in microbial ecosystems

M. Sireci[1,*], M.A. Muñoz[1], J.Grilli[3]

[1]*Departamento de Electromagnetismo y Física de la Materia e Instituto Carlos I de Física Teórica y Computacional. Universidad de Granada. E-18071, Granada, Spain* [2]*Quantitative Life Sciences, The Abdus Salam International Centre for Theoretical Physics, 34151 Trieste, Italy*

*e-mail: msireci@onsager.ugr.es

Microbial ecosystems are the archetype of complex systems: their stability, functionality and resilience are "macroscopic"properties emerging from very diverse species "microscopic ïnteractions. These communities are diffused all across the biosphere, from the human gut to glaciers, from soil to activated sludge. Understanding common properties of such diverse communities can pave the way to elucidate the common mechanisms behind the emergence of interactions and coexistence. The question of how coexistence of species is generated and maintained is as old as ecology itself. Many ecological "forces" such as competition, cooperation, demographic fluctuation, environmental fluctuation and filtering, migration, predation etc. are expected to act together in ecosystems. Disentangling the effect and intensity of each of theses forces in natural communities is the focus of present research. Thanks to a recent revolution in the availability of high quality data, natural microbial ecosystems offer an invaluable possibility to tackle this question.Here, we explore if it is possible to discriminate a dominant force at a give resolution of genetic similarity. Indeed, shedding light on how bacteria interact as function of their genetic similarity is extremely relevant both at fundamental and practical level, with consequences on human health. By using both relative-abundances and metagenomic data, we reveal the presence of a new macroecological law relating correlation and phylogenetic similarity. In particular, the average correlation of species abundance fluctuation η_{ij} decays with phylogenetic distance d_{ij} from positive to null values following a stretch exponential function:

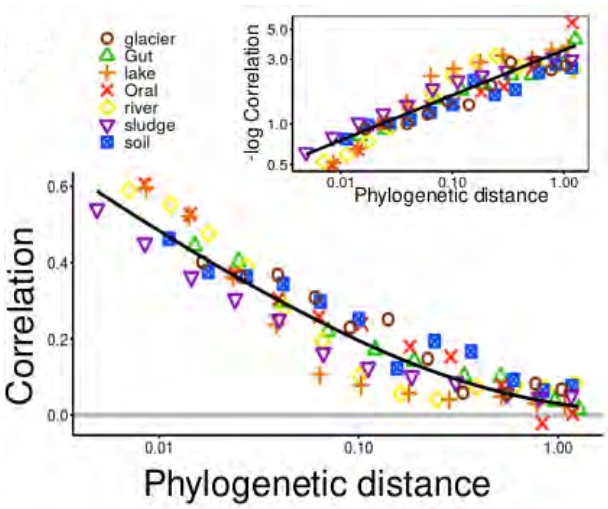

Figure 1. The correlation of abundance fluctuation averaged over all couples within a given discretized distance bin (colored symbols) decays with the phylogenetic distance (log scale). The black line is a stretched-exponential decay, where $\lambda \approx 3.5$. To emphasize the functional dependence, the inset shows the same data but for the log of the correlations and in double logarithmic scale, i.e. a representation in which stretched exponential functions become straight lines; in this case with slope 1/3.

$$\eta_{ij} = e^{-\lambda d_{ij}^{1/3}},$$

consistently in all empirically analyzed biomes both across communities (hosts) and in temporal data for each community, see Fig. 1. By scrutinizing different ecological models, we show that competition cannot reproduce the observed pattern. Instead, the elucidated macroecological law is explained quantitatively by the "correlated stochastic logistic model" (CSLM) pointing to environmental filtering as the dominant ecological force at this resolution level. Finally we show that the macroecological law is valid also for temporal data of a single community, and that the properties of delayed temporal correlation are also reproduced by the CSLM. We conclude by arguing that in order to understand interactions in microbial ecosystems one needs to abandon the concept of species and study the system from different scales, much as done in physics exploiting renormalization group ideas.

Inferring Generalized Lotka-Volterra parameters from longitudinal microbial data

Somaye Sheykhali[1], **Juan Fernández-Gracia**[1,*], Carlos J. Melián[1], Xabier Irigoien[2], Carlos M. Duarte[3], Víctor M. Eguíluz[1]

[1]*Instituto de Física Interdisciplinar y Sistemas Complejos IFISC (CSIC-UIB), Palma, Spain.* [2]*AZTI Tecnalia, Pasaia, Spain.* [3]*Red Sea Research Center (RSRC) and Computational Bioscience Research Center (CBRC), King Abdullah University of Science and Technology, Thuwal, Saudi Arabia*

*e-mail: juanf@ifisc.uib-csic.es

Microbial communities form the largest, more diverse and complex ecosystems on the planet. The interactions among their individuals are diverse, encompassing predation, mutualism, comensalism, amensalism or competition. Measuring these interactions in direction and strength at a large scale is a challenging process that requires a combination of data analysis and modeling. Furthermore, the dynamic nature of the abundances of different species of microorganisms cannot be ignored to present a sound theory on microbial interactions.

Data. We use experimental data that reported the OTU relative abundance – operational taxonomic units, which are quasi-equivalent to a species definition – every day for a period of 20 days in 5 different experiments, with 2 replicates for each. So, for each OTU i we have the relative abundance x_i^t for each $t = 1d, \ldots, 20d$.

Model. We will assume a Generalized Lotka-Volterra model to fit the data. The choice of this model is motivated by the power-law variation in OTU abundances, which suggests a multiplicative process. The model is defined by the following system of non-linear ordinary differential equations

$$\frac{1}{x_i}\frac{d}{dt}x_i = a_i + \sum_{j=1}^{N} \beta_{ij} x_j, \tag{1}$$

where N is the total number of OTUs considered. They consist of a local growth term and an interaction term that encodes the effect of other OTU abundances on the self abundance of one OTU. The particular values of β_{ij} as compared to βji let us define different types of interaction (predation when both have different sign, competition when both are negative, mutualism when both are positive, comensalism when one is positive and the other is 0 and amensalism when one is negative and the other is 0).

Parameter estimation. In order to estimate the best parameters that fit the data we minimize χ^2 assuming the model in Eq. (1). We assume that the fitting is to $\frac{1}{x_i}\frac{dx_i}{dt}$, which is approximated by $W_i^t = \frac{x_i^t - x_i^{t-1}}{x_i^{t-1}}$ from the data. The result of this minimization has the solution

$$a_i = \langle W_i \rangle - \beta_{ij}\langle x_j \rangle \quad \text{and} \quad \beta_{ij} = \Omega_{ik} C_{kj}^{-1}, \tag{2}$$

where $\Omega_{ij} = \langle W_i x_j \rangle - \langle W_i \rangle \langle x_j \rangle$, C_{kj}^{-1} are the elements of the inverse of the covariance matrix ($C_{ij} = \langle x_i x_j \rangle - \langle x_i \rangle \langle x_j \rangle$) and the operator $\langle \cdot \rangle$ denotes the average over all time points. We apply a regularization method to avoid overfitting.

Results. The results of the fitting procedure let us explore the parameters that best fit the data. We find that the fixed points defined by these parameters do not correspond to feasible configurations of the model. We also explore the different types of interactions that are present in the system. Neutral and non-reciproval (commensalist and amensalist) dominate, while reciprocal interactions account for a small percentage of the interactions. These results are statistically significant when compared to randomizations of the interaction matrices.

Discussion. The fitted model reveals thus the intrinsic growth rates and the interaction network among OTUs. The estimated parameters imply fixed points that are not feasible, pointing to the fact that the dynamics might be operating around more complex attractors. The interaction types that dominate the results are non-reciprocated. These type of interactions have been mostly ignored in the modeling literature and deserve more attention for a proper description of microbial ecosystems.

Acknowledgements: We aknowledge funding from grant PID2020-114324GB-C22 funded by MCIN/AEI/10.13039/501100011033.

From microscopics to macroscopic hydrodynamics of collective cell motion

Gloria Irene Triguero Platero[1,*], Luis Bonilla[2], Falko Ziebert[1]

[1] *Institute for Theoretical Physics, Heidelberg University, Germany.* [2] *Department of Mathematics, Universidad Carlos III de Madrid, Spain.*

*e-mail: gloria.triguero_platero@stud.uni-heidelberg.de

Collective cell migration in a cellular monolayer has been studied extensively experimentally, and modelled with many different approaches. In this project, two of the most prominent ones have been developed and critically compared to each other: an Active Vertex Model (AVM) that describes the "microscopic"dynamics of each cell, and a coarse-grained macroscopic description via hydrodynamic variables, in which the monolayer is described as an anisotropic fluid consisting of deformable particles.

As evidenced in reference [1], including effective inertial effects is required in order to match experimental results. Therefore, we here have developed underdamped dynamics for both approaches. Comparing them is expected to shed light on how microscopic changes affect macroscopic behaviour.

The AVM describes the monolayer as a network of polygonal cells [2]. Its dynamics can be captured via the vertices of the polygons or the cell centers. It is possible to go from one description to the other due to the dual nature of the Delaunay triangulation, that connects cell centers, with the Voronoi tesselation, that defines the boundaries. The model is implemented in the *SAMoS* software [2]. The energy function of the system includes terms related to a preferred cell area and perimeter, and a line tension term for the cell-junctions. Then, the forces can be computed as $F_i = -\nabla_{\boldsymbol{r}_i}[E_{VM} + V_{soft}(|\boldsymbol{r}_i - \boldsymbol{r}_j|)]$, where a soft core repulsion has been added to avoid pathologically elongated cells [1]. An example of expanding cell monolayer can be seen in Figure [1].

We then want to obtain a continuum description of the model. In order to do so, we introduce continuum microscopic field variables and then coarse-grain them to get macroscopic variables and their hydrodynamics. We introduce a mass and momentum density $\hat{\rho}(\boldsymbol{x},t)$, $\hat{\boldsymbol{g}}(\boldsymbol{x},t)$, and add a shape tensor field as in reference [3], $\hat{G}^{\alpha}_{ij} = \frac{1}{n}\sum_{\mu=1}^{n} \Delta x_i^{\alpha\mu}\Delta x_j^{\alpha\mu}$.

The macroscopic fields $\phi = \rho$, $\boldsymbol{g}$ and G^{α}_{ij} corresponding to the microscopic fields $\hat{\phi}$ are defined via $\phi(\boldsymbol{x},t) = \int \hat{\phi}\,\mathcal{P}\prod_{\alpha} d\boldsymbol{v}_{\alpha} d\boldsymbol{x}_{\alpha}$ with $\mathcal{P}$ the probability density. The latter satisfies a Fokker-Planck equation, from which we obtain the equations of motion for the macroscopic variables. For long spatial scales compared to the cell size, we then extract the continuum limit of the hydrodynamic equations.

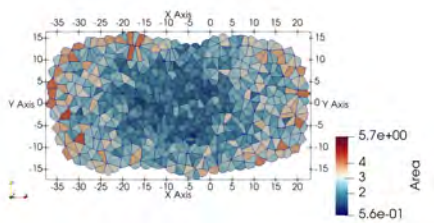

Figure 1. Expanding cell monolayer in which it can be seen that inner cells have smaller area than outer ones, as observed experimentally [1].

This project bears high biophysical relevance, both due to the system studied and to the bridge built between the AVM and its coarse-grained description. It will also allow to compare both models numerically in order to verify their consistency, and their agreement with experimental results.

[1] Luis L. Bonilla, Ana Carpio and Carolina Trenado, *PLOS Computational Biology* **16**, 1–43 (2020).
[2] Daniel L. Barton, Silke Henkes, Cornelis J. Weije, Rastko Sknepnek, *PLOS Computational Biology* **13**, 1005569 (2017).
[3] Arthur Hernandez and M. Cristina Marchetti, *Physical Review E* **103**, 032612 (2021).

The excitatory-inhibitory branching process: a parsimonious view of cortical asynchronous states, excitability, and criticality

Roberto Corral López[1], **Victor Buendía**[2,*], Miguel A. Muñoz[1]

[1] *Dpto. de Electromagnetismo y Física de la Materia e Instituto Carlos I de Física Teórica y Computacional, Universidad de Granada. E-18071, Granada, Spain.* [2] *Dpt. of Computer Science, University of Tübingen, and Max Planck Institute for Biological Cybernetics, Tübingen, 72076, Germany.*

*e-mail: vbuendiar@onsager.ugr.es

The branching process is the minimal model for propagation dynamics, avalanches and criticality, broadly used in neuroscience. In this work we present a simple extension of it, adding inhibitory nodes, which induces a much-richer phenomenology, including a new phase. This novel phase is characterised by features not usually observed in typical active phases, such as constant levels of low activity – independently of the control parameters– and quasioscillations. Remarkably this new phase displays all the key features of "asynchronous states" in cortical networks, and captures a wealth of non-trivial features of spontaneous brain activity, such as collective excitability, hysteresis, tilted avalanche shapes, and partial synchronization, allowing us to rationalize striking empirical findings within a common parsimonious framework.

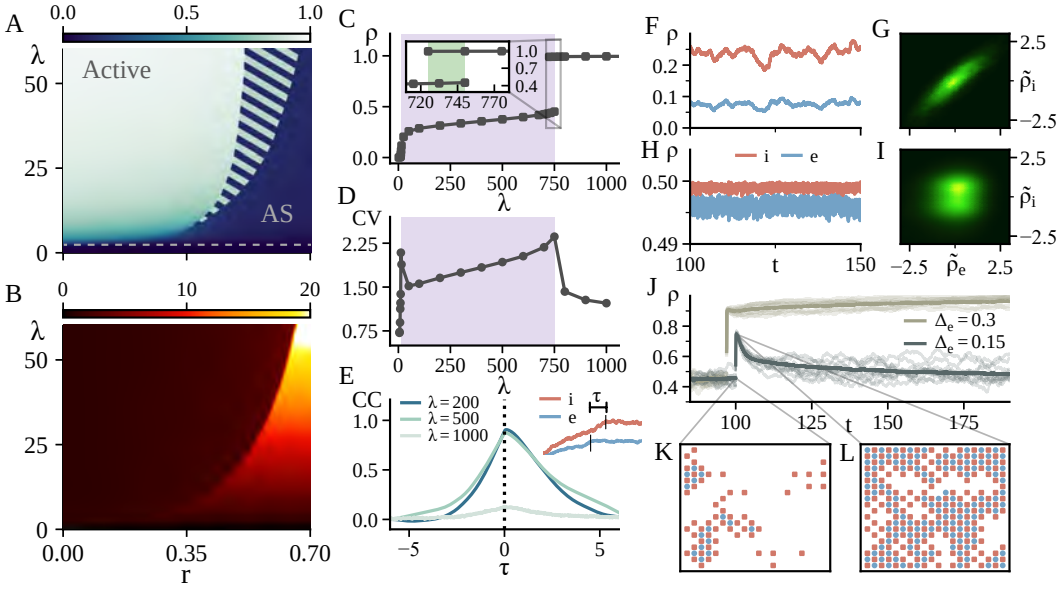

Figure 1. Features of the asynchronous phase. Parameters: λ, infection rate; r, inhibition strength; ρ, average activity (A-B) Analytical results for annealed random networks: (A) Stationary activity. Dashed line indicates the end of the quiescent phase and stripes signal the bistability region between the AI and active phases. (B) Henrici index gauging the level of excitability. (C-L) Results for a 2D lattice with $N = 10^4$. (C) Section of the phase diagram illustrating the discontinuous transition with bistability and (D) coefficient of variation (CV) for different values of λ (E) Lagged cross-correlations (CC) between excitatory and inhibitory time series; total excitatory and inhibitory activity as a function of time is plotted in (F) for the AS phase and in (H) for the standard active phase (G-I) same as in F and H, respectively, plotted normalized activities. (J) Stimulation experiment, where a fraction of excitatory nodes is transiently activated. In the bistability region, this can drive the system from the AS phase to the standard active phase ($N = 20^2$).

[1] Corral, R. Buendía, V., and Muñoz, M.A., The excitatory-inhibitory branching process: a parsimonious view of cortical asynchronous states, excitability, and criticality. *Under review in Phys. Rev. Lett.* Arxiv: https://arxiv.org/abs/2203.16374 (2022).

Acknowledgements: We acknowledge the Spanish Ministry and Agencia Estatal de investigación project PID2020-113681GB-I00, the Consejería de Conocimiento, Investigación Universidad, Junta de Andalucía and European Regional Development Fund, project references A-FQM-175-UGR18 and P20-00173 for financial support. R.C.L. acknoledges funding from grant FPU19/03887. V.B. was supported by a Sofja Kovalevskaja Award from the Alexander von Humboldt Foundation.

Normal and anomalous diffusion in evolving domains: a brief overview of some recent results

F. Le Vot[1] , **E. Abad**[2,*], C. Escudero[3], S. B. Yuste[4]

[1] *Department of Physics, University of Extremadura, Badajoz, Spain.*
[2] *Department of Applied Physics & ICCAEx, University of Extremadura, Mérida, Spain.*
[3] *Department of Fundamental Mathematics, UNED, Madrid, Spain.*
[4] *Department of Physics & ICCAEx, University of Extremadura, Badajoz, Spain.*
*e-mail: eabad@unex.es

Diffusion is usually assumed to occur in a static domain; however, evolving domains are an important paradigm in many situations of interest, as particles can actually be advected by such domains on time scales not much longer than those characteristic of diffusion. In developmental biology, say, the formation of biological structures (e.g. pigmentation or dentition patterns) happens during tissue growth [1]. Another example is the diffusion of cosmic rays in the expanding universe [2].

We will give an overview of some recent results for diffusion in deterministically growing/contracting domains. We will hereby assume that the diffusing particles stick rigidly to the evolving domain and therefore experience a drag as they wait to jump. The jump statistics of these random walkers will be taken to be independent of the parameters governing the domain's evolution.

In the case where the domain growth is controlled by a power-law scale factor, one observes a crossover between a diffusion-controlled regime and another regime where the particles' drift due to the domain evolution becomes the dominant transport mechanism [3]. In this latter scenario, diffusional mixing is strongly hindered, and a strong memory of the initial condition is retained.

Another striking effect takes place in the case of contracting domains. An exponential contraction is able to fully counterbalance diffusive spreading, resulting in the onset of a stationary positional probability density function (pdf). However, as soon as the normal diffusive process is replaced by a subdiffusive Continuous Time Random Walk, strong localization takes place, and the pdf tends to a delta function in the long-time limit (we call this effect the "Big Crunch") [4].

Finally, the effect of the domain evolution has also drastic consequences for first-passage processes and encounter-controlled reactions. These are well illustrated by several examples [5, 6], e.g., the escape of a Brownian walker from a growing hypersphere, "the target problem" in an expanding space, and the kinetics of the $1D$ encounter-controlled coalescence reaction $A + A \to A$, where A denotes a diffusing reactant. In the latter example, the chemical reactions are known to induce self-ordering in a static domain, in the sense that the reactions build up spatial correlations between a set of diffusing particles that are initially scattered at random on the real line. However, such self-ordering processes are strongly slowed down and prematurely brought to an end when the embedding domain expands at a sufficiently fast rate. In addition, a finite number of particles may survive for arbitrarily long times, and the fraction of surviving particles depends on the details of the initial condition. The obtained results highlight the need to extend the existing first-passage theories of chemical kinetics to deal with the interplay between diffusional mixing and advection induced by the evolving domain.

[1] J. D. Murray, *Mathematical Biology. II Spatial Models and Biomedical Applications*, Springer (2003).

[2] V. Berezinsky and A. Z. Gazizov, *Diffusion of Cosmic Rays in the Expanding Universe. I*, The Astrophysical Journal **643**, 8 (2006).

[3] S. B. Yuste, E. Abad and C. Escudero, *Diffusion in an expanding medium: Fokker-Planck equation, Green's function, and first-passage properties*, Phys. Rev. E **94**, 032118 (2016).

[4] F. Le Vot, E. Abad and B. Yuste, Continuous-time random-walk model for anomalous diffusion in expanding media, Phys. Rev. E **96**, 032117 (2017).

[5] F. Le Vot, C. Escudero, E. Abad and S. B. Yuste, *Encounter-controlled coalescence and annihilation on a one-dimensional growing domain*, Phys. Rev. E **98**, 032137 (2018).

[6] E. Abad, C. Escudero, F. Le Vot and S. B. Yuste, *First-Passage Processes and Encounter-Controlled Reactions in Growing Domains, in Chemical Kinetics: Beyond the Textbook*, edited by K. Lindenberg, R. Metzler and G. Oshanin, World Scientific (2019).

Acknowledgements: We acknowledge funding from the Government of Spain through Project No. FIS2016-76359-P and from the regional Extremadura Government through Projects No. GR18079 and No. IB16087, both partially funded by the ERDF.

The turning point and end of an expanding epidemic cannot be precisely forecast

Mario Castro[1,2,*], Saúl Ares[1,3], José A. Cuesta[1,4,5], Susanna Manrubia[1,3]

[1] *Grupo Interdisciplinar de Sistemas Complejos (GISC), Madrid, Spain.*
[2] *Universidad Pontificia Comillas, Madrid, Spain*
[4] *Dept. Biología de Sistemas, Centro Nacional de Biotecnología (CSIC). c/ Darwin 3, 28049 Madrid, Spain*
[4] *Dept. Matemáticas, Universidad Carlos III de Madrid, Leganes, Spain.*
[5] *UC3M-Santander Big Data Institute (IBiDat), c/ Madrid 135, 28903 Getafe, Spain.*
*e-mail: marioc@comillas.edu

Can the turning point and end of an expanding epidemic be precisely forecasted while the epidemic is still spreading? Epidemic spread is characterized by exponentially growing dynamics, which are intrinsically unpredictable. The time at which the growth in the number of infected individuals halts and starts decreasing cannot be calculated with certainty before the turning point is actually attained; neither can the end of the epidemic after the turning point.

An SIR model with confinement (SCIR) illustrates how lockdown measures inhibit infection spread only above a threshold that we calculate. The existence of that threshold has major effects on predictability: A Bayesian fit to the COVID-19 pandemic in Spain shows that a slow-down in the number of newly infected individuals during the expansion phase allows inferring neither the precise position of the maximum nor whether the measures taken will bring the propagation to the inhibition regime. There is a short horizon for reliable prediction, followed by a dispersion of the possible trajectories that grow extremely fast. The impossibility to predict in the midterm is not due to wrong or incomplete data, since it persists in error-free, synthetically produced data sets, and does not necessarily improve by using larger data sets.

Our study [1] warns against precise forecasts of the evolution of epidemics based on mean-field, effective or phenomenological models, and supports that only probabilities of different outcomes can be confidently given.

Also, we suggest that the future of ongoing epidemics is so sensitive to parameter values that predictions are only meaningful within a narrow time window and in probabilistic terms, much as what we are used to in weather forecasts.

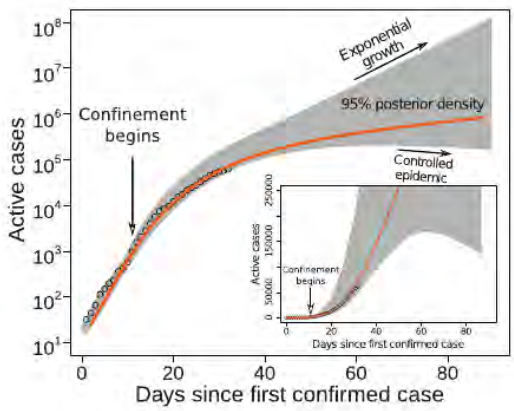

Figure 1. Fit to data obtained in real time for the daily number of active cases in Spain (from March 1st to March 29th) and peak forecast. Despite the reasonable agreement between model and empirical observations in the growing phase, opposite predictions for the future number of active cases can be derived. The solid line represents the expression for I(t) using the median parameters for the posterior distribution.

[1] M. Castro, S. Ares, J. A. Cuesta, S. Manrubia, The turning point and end of an expanding epidemic cannot be precisely forecast, *Proceedings of the National Academy of Sciences* 117(42), 26190 (2020).

Contagion effect in exams

José Javier Arenas[1], **Pedro Carpena**[1,2,*]

[1]*Departamento de Física Aplicada II, Universidad de Málaga, Spain.*
[2]*Instituto Carlos I de Física Teórica y Computacional, Universidad de Málaga, Spain.*

*e-mail: pjcarpena@uma.es

In the last decades the study of collective phenomena has produced a great interest in the field of Statistical Physics within the framework of Complex Systems, being a paradigmatic example flocking, the collective motion of self-propelled organisms [1]. More recently, these studies have been extended to collective human behavior, leading to the field of Sociophysics, in which the collective behavior emerges from the interactions of individuals as elementary units in social structures [2]. In this work we want to introduce a new example of human interaction: the possible existence of a 'social field' in a classroom where a group of students take an exam. We conjecture that the existence of social interactions could lead to a contagion effect among the students, so that a given student who delivers the exam may influence another close student to do the same, and as a result the exams are not spatially delivered at random. Our analysis is carried out by using experimental data registered in 10 high-school classrooms [3], where the students were seated randomly in isolated tables and took an exam (of different subjects). We registered both the spatial location and the exam delivery time for each student in all classrooms. We use the distances between students who finish the exam consecutively (in units of the distance between nearest neighbors) and compare these distances with the random expectation in the corresponding classroom using Monte Carlo simulations. We observe that the experimental distances are significantly (p-value $\sim 10^{-3}$) below the random expectation. This result supports the existence of a short-range spatial interaction between consecutive students (contagion effect). Based on this idea, we propose [3] a distance-driven probabilistic contagion model which works as follows: in a classroom with N students, after j students have delivered their exams and left the classroom, the last one to do so is s_j. This student may influence one of the m students remaining in the classroom located closer to s_j than $d_{\max}$, and does not affect the rest $N-j-m$ students, located further than $d_{\max}$. In this way, the probabilities of being the next one to deliver the exam for one of the affected and one of the not-affected students can be written as:

$$\mathrm{P}_m = \begin{cases} \frac{p}{m} + \frac{1-p}{N-j} & (m \neq 0) \\ 0 & (m = 0) \end{cases}, \quad \mathrm{P}_{N-j-m} = \begin{cases} \frac{1-p}{N-j} & (m \neq 0) \\ \frac{1}{N-j} & (m = 0) \end{cases}$$

Therefore, p quantifies the excess probability shared by the m close students with respect to the random expectation.

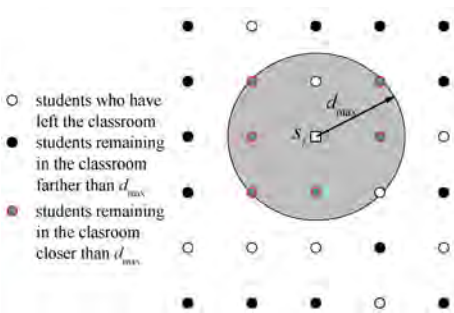

Figure 1. Schematic plot of the contagion model in a classroom with 30 students. The j-th student who delivers the exam, s_j (□) may influence students remaining in the classroom closer than $d_{\max}$ (gray circles).

The model has two input parameters: the contagion probability p and the maximum distance $d_{\max}$ at which the contagion acts (Fig. 1). We can estimate $d_{\max}$ *a priori* by observing which individual distances are clearly over represented in the experimental record as compared to the random expectation, which suggests to use $d_{\max} = 1$ as an appropriate input value. This choice leaves p as the only parameter to be determined. By running the model a large number of times with Monte Carlo simulations and comparing the corresponding results with the experimental data, we obtain a contagion probability $p \simeq 1/6$.

This spatial contagion effect could also appear in other social human activities where the interaction between subjects occurs via single events (similar to an exam delivery), such as for example raised hand votation procedures in assemblies.

[1] J. R. Usherwood, M. Stavrou, J. C. Lowe. K. Roskilly and A. M. Wilson. *Nature* **474**, 494 (2011).
[2] C. Castellano, S. Fortunato, and V. Loreto. *Rev. Mod. Phys.* **81**, 591 (2009).
[3] J. J. Arenas and P. Carpena. Submitted (2022).

Building continuous time crystals from rare events

R. Hurtado-Guiérrez[1,2], F. Carollo[3], C. Pérez-Espigares[1,2], **P.I. Hurtado**[1,2,*]

[1] *Departamento de Electromagnetismo y Física de la Materia, Universidad de Granada, Granada 18071, Spain.* [2] *Institute Carlos I for Theoretical and Computational Physics, Universidad de Granada, Granada 18071, Spain.* [3] *Institut für Theoretische Physik, Universität Tübingen, Auf der Morgenstelle 14, 72076 Tübingen, Germany.*

*e-mail: phurtado@onsager.ugr.es

Symmetry-breaking dynamical phase transitions (DPTs) abound in the fluctuations of nonequilibrium systems. Here we show that the spectral features of a particular class of DPTs exhibit the fingerprints of the recently discovered time-crystal phase of matter. Using Doob's transform as a tool, we provide a mechanism to build classical time-crystal generators from the rare event statistics of some driven diffusive systems. An analysis of the Doob's smart field in terms of the order parameter of the transition then leads to the time-crystal lattice gas (tcLG), a model of driven fluid subject to an external *packing field* which presents a clear-cut steady-state phase transition to a time-crystalline phase characterized by a matter density wave which breaks continuous time-translation symmetry and displays rigidity and long-range spatio-temporal order, as required for a time crystal. A hydrodynamic analysis of the tcLG transition uncovers striking similarities, but also key differences, with the Kuramoto synchronization transition. Possible experimental realizations of the tcLG in colloidal fluids are also discussed.

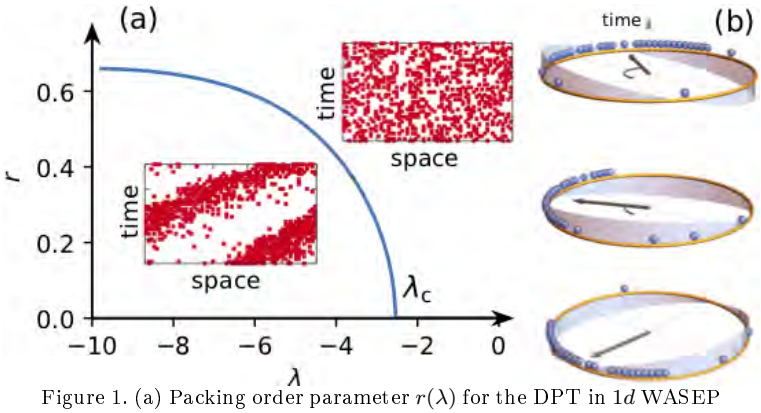

Figure 1. (a) Packing order parameter $r(\lambda)$ for the DPT in $1d$ WASEP as a function of the biasing field λ. Inset: spacetime trajectories for current fluctuations above (top) and below (bottom) the critical point. Note the density wave in the latter case. (b) Time-crystal lattice gas with a packing field (shaded curve) which pushes particles lagging behind the center of mass while restraining those moving ahead, a mechanism that leads to a a rotating condensate. The arrow locates the condensate center of mass, with a magnitude $\propto r_C$.

[1] R. Hurtado-Gutiérrez, F. Carollo, C. Pérez-Espigares and P.I. Hurtado, *Phys. Rev. Lett.* **125**, 160601 (2020).

Multipolarity in a Complex Society

J. Borondo[1,2], R. Caballero[3], J. P. Cárdenas[4], **J. C. Losada**[1,*], G. Olivares[2], J. M. Robles[3]

[1]*Complex System Group, Universidad Politécnica de Madrid. Ciudad Universitaria s/n, Madrid, Spain.*
[2]*ICADE. Dpto. Gestión Empresarial. Universidad Pontificia de Comillas. Alberto Aguilera 23, Madrid. Spain.*
[3]*Data Science and Soft Computing for Social Analytics and Decision Aid. Univ. Complutense de Madrid. Madrid, Spain.*
[4]*Net-Works, Angamos 451, Reñaca, Viña del Mar, Chile.*

*e-mail: juancarlos.losada@upm.es

In today's hyperconnected society, online social networks have become a fundamental tool in public debate. They allow a greater participation of the citizens in the conversations and a better diffusion of their opinions, feelings or affinities. In many cases, the confrontation of ideas occurs in a socially polarized and fragmented way. Online social networks only amplify and increase this polarization, particularly in political contexts. We focus in two types of polarization:

- *Ideological polarization*, in which individuals position themselves around opposing poles of opinion represented by opinion leaders (fundamentally political leaders or parties)
- *Affective polarization*, in which users' opinions are determined by positive sentiments (love) or negative sentiments (hate) towards candidates or parties.

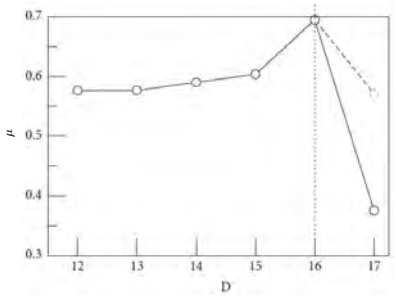

Figure 1. Evolution of the polarization index, μ, since December 11th until December 17th (day of 2017 Chilean Presidential elections). In dotted line, the values corresponding to the electoral campaign period without taking into account the users who only participated on the voting day [3].

In this work we characterize and quantify political polarization and affective polarization, analyzing the different mechanisms of interaction between Twitter users. One can define Twitter as a multilayer social network where each layer represents one of the three interaction mechanisms: following, mentioning, and retweeting. In the mentions layer, users are mainly grouped around politicians, while in the retweets layer, information is spread around the media and other opinion leaders [1]. For this reason, the layer of mentions is the appropriate one to study affective polarization, while ideological polarization is better manifested through the retweets layer.

To analyze the ideological polarization, we infer a continuous opinion distribution by applying a model based on retweet interactions, previously detecting elite users with fixed and antagonist opinions, labeled as +1 and -1 [2].

To analyze the affective polarization, we apply sentiment analysis techniques to the messages mentioning the candidates. Thus, we assign a numerical value to the sentiment of the users towards each candidate, where -1 implies extreme hate, +1 extreme love and 0 indifference [3]. From the distributions of opinions/sentiments, p(x), we compute the polarization index initially described in ref [4]: $\mu = (1 - |\Delta A|)d$, where $|\Delta A|$ is the difference between users in each interval x < 0 and x > 0, and d is half the distance between the gravity centers of the two groups of opinions.

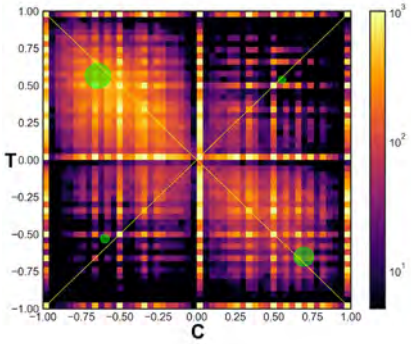

Figure 2. Love-Hate diagram for candidates T and C. The gravity center of each quadrant is shown as green circles with diameters proportional to the number of users in the quadrant [4].

Fig. 1 shows the temporal evolution of the ideological polarization index in the presidential elections in Chile 2017 [2]. Fig 2 shows the love/hate diagram obtained by analyzing affective polarization in the 2016 USA elections towards H. Clinton and D. Trump [3].

[1] J. Borondo, A.J. Morales, R.M. Benito, J.C. Losada. Multiple leaders on a multilayer social media, *Chaos, Solitons & Fractals* **72**, 90 (2015).
[2] G. Olivares, J. P. Cárdenas, J. C. Losada, J. Borondo. Opinion Polarization during a Dichotomous Electoral Process. *Complexity* **2019**, 5854037 (2019)
[3] Losada, J.C., Robles, J.M., Benito, R.M., Caballero, R. Love and Hate During Political Campaigns in Social Networks. *Complex Networks & Their Applications X*, 66-77. Springer, Cham. (2022).
[4] A. J. Morales, J. Borondo, J. C. Losada, and R. M. Benito. Measuring political polarization: Twitter shows the two sides of Venezuela, *Chaos: An Interdisciplinary Journal of Nonlinear Science* **25**, 033114 (2015).

Evolutionary Dynamics of The Ethereum Transaction Network

M. Grande[3,5,*], F. Borondo[1,2], J. Borondo[4,5]

[1]*Instituto de Ciencias Matematicas (ICMAT); Campus de Cantoblanco UAM; Nicolas Cabrera, 13-15; 28049 Madrid (Spain).* [2]*Departamento de Quimica; Universidad Autonoma de Madrid; CANTOBLANCO - 28049 Madrid (Spain).*[3]*Grupo de Sistemas Complejos; Universidad Politecnica de Madrid; 28035 Madrid (Spain).*[4]*Departamento de Gestion Empresarial; Universidad Pontificia de comillas ICADE; Alberto Aguilera 23; 28015 Madrid (Spain).*[5]*AGrowingData; Navarro Rodrigo 2 AT; 04001 Almeria (Spain).*

*e-mail: margrande45@gmail.com

We are witnessing a revolution in the financial system, which is being replaced by the new and innovative Decentralized Finance (DeFi). DeFi projects are tackling long-standing problems and addressing inefficiencies in our current system, improving financial inclusion, increasing liquidity and reducing costs. Unlike the traditional system, where financial applications are difficult to access, rigid, hard to use and expensive, DeFi applications are open and permisionless. Anyone can access them, all they need is an internet connection.

But what really makes this self-organized market of digital currencies attractive for the research community is that all transactions are publicly available, in contrast to the traditional financial system. This represents an unprecedented scenario that allows us to understand and explain the evolution and adoption of a financial system by capturing the complex behavior that emerges from the relationships between users.

In this work we focus on the Ethereum Blockchain, the largest decentralized computing platform in terms of users and usage. We have analyzed the transactions that occur in the network under a complex system perspective, in which nodes are the accounts that operate and links represent the transactions between them. We describe the dynamics and evolution of the system by analyzing its structure and computing its properties over time. Finally, we explore the relationships that exist between these properties and the future price of the network cryptocurrency called Ether (ETH).

Since this system is an evolving system, it is important to define dynamic intervals that capture the evolution of the system. Unlike other works that propose to create networks with an arbitrary time interval, [2], we use the method developed by Darst et al. in [1], that detects evolutionary changes in the configuration of a complex system and generates intervals accordingly. In this method, the size of each interval is determined by maximizing the similarity between the sets of events within consecutive intervals.

We applied the Dynamic time-slicing method [3] on our dataset and found that the activity of the network can be measured by considering regular time intervals of 14 days. We also found a strong correlation between the similarity score obtained from the Dynamic time-slicing method and the Ethereum price.

Next, we analyzed the properties of the resulting networks and found that the degree distribution of the networks are highly heterogeneous, where a small fraction of addresses tend to trade with the vast majority, while most addresses hardly trade with others. We found that the networks are disassortative and present very low clustering.

Finally, we explored the relations between the network properties and the future price of Ethereum and found a strong negative correlation between the exponent of the degree distribution and the price. Hence, our results suggest that the transaction network contains relevant information to explain the evolution and adoption of the system.

[1] A. Darst, R. K., B. Granell, C., C. Arenas, A., D. Gomez, S., E Saramaki, J., and F Fortunato, S., *Detection of timescales in evolving complex systems. Scientific reports* **6**, 39713 (2016).

[2] A. Liang, J., B. Li, L., and C. Zeng, D. *Evolutionary dynamics of cryptocurrency transaction networks: An empirical study. PloS one*, **13(8)** (2018).

[3] `ttps://gitub.com/rkdarst/dynsnap/blob/master/doc/Manual.rst`

Numerical sampling rare of rare trajectories using stochastic bridges

Raul Toral

IFISC (Instituto de Física Interdisciplinar y Sistemas Complejos), Universitat de les Illes Balears-CSIC, Palma de Mallorca

e-mail: raul@ifisc.uib-csic.es

In stochastic systems the most uncommonly occurring events are often the ones that are most consequential. Typical examples beyond the escape of a Brownian particle in a double-well potential include the dynamics of biological switches, the extinction of species in ecology and large fluctuations in chemical reactions. We have recently introduced a numerical method to draw the ensemble of stochastic trajectories that link together any two points (or regions) in phase space [1]. For a given target stochastic process, we construct a stochastic bridge linking initial and final points by defining a new stochastic dynamics that runs reversed in time. This is combined with a recent method to sample events with a very low probability using weighted-ensemble techniques. We show that the statistics of the target process can be recovered by associating a statistical weight with each stochastic bridge. This allows us to dedicate more computational effort to rare trajectories without introducing bias or interdependence. The method is flexible; the target process is fully general, detailed balance is not required, no small-noise approximation is made, and it is not limited to the sampling of trajectories associated to a target macroscopic quantity, nor does it require the introduction of artificial parameters such as temperatures.

We show through several examples that the possibility of sampling the ensemble of trajectories unveils the whole statistical picture of these unlikely-yet-important events, in contrast to the Wentzel-Kramers-Brillouin (WKB) optimal paths, which we verify are only relevant in the limit of small noise. We are able to show that the stochastic bridges produced this way provide the full statistics of the ensemble of transition paths between long-lived states of the target process. This allows one to sample fluctuations around the WKB instanton, and thus to judge if the WKB approximation scheme is accurate at various levels of noise. As an example we show in the figure several (rare) extinction trajectories of an Susceptible-Infected-Susceptible model in the endemic regim and compare them with the predictions of the WKB theory valid in the limit of a large population. Other examples we will analyze in this presentation include the distribution of first-passage times of a biased random walk and the generation of noise-driven transitions from the undifferentiated to either one of the differentiated cell states in a model of cell differentiation.

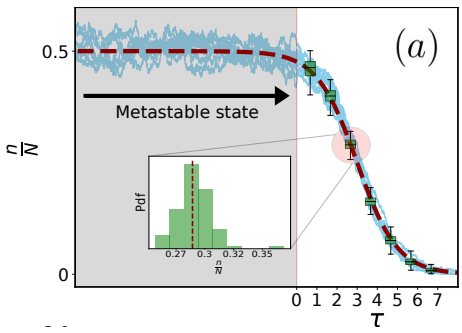

Figure 1. Extinction trajectories for the SIS model compared to the WKB instanton. n is the number of infected individuals in a population of total size N. The inset shows the pdf of n at the given time.

[1] J. Aguilar, J. W. Baron. T. Galla, R. Toral, *arXiv:2112.08252*.

Acknowledgements: Partial financial support has been received from the Agencia Estatal de Investigación (AEI, MCI, Spain) and Fondo Europeo de Desarrollo Regional (FEDER, UE) under Project PACSS (RTI2018-093732-B-C21/C22), and the María de Maeztu Program for units of Excellence in R&D, grant MDM-2017-0711 funded by MCIN/AEI/10.13039/501100011033.

"Aging" and slow relaxation in the dynamics of leaving cells

Oded Agam

The Racah Institute of Physics, The Hebrew University of Jerusalem, Israel.

e-mail: agam@phys.huji.ac.il

Deciphering the cellular metabolic network is, perhaps, the most prominent objective of cell biology. It is a formidable enigma because the metabolic network is a highly complicated system that comprises several thousand different compounds with intricate interactions that are essentially unknown.

Recent experimental data, obtained by Balaban's group, show that the recovery time of *E. coli* cells, after their growth was arrested by acute stress, exhibits distinctive statistical features typical of complex physical systems. These include a memory of the period that the cell was subjected to the stress and slow power-law decay of the distribution of single-cell recovery time. The same features are common to systems that exhibit physical "aging", such as amorphous polymers, stretched DNA, paper crumpling, colloidal solutions, spin glasses, supercooled liquids, and coulomb glasses.

This observation suggests that a relatively simple statistical model can describe the cell in the acute stress regime. Here I present a simple spin model that reproduces the experimental observations in the form of weakly connected cycles. The statistics of the cells' recovery times are obtained from the solution of a crossing problem of a random walker in a potential field which takes into account dynamical correlations.

Optimal control of bidirectional escape from a symmetric potential well

R. Chacón[1,2], P. J. Martínez[3], **J. M. Marcos**[4,*], F. J. Aranda[5], J. A. Martínez[6]

[1] *Departamento de Física Aplicada, Escuela de Ingenierías Industriales, Universidad de Extremadura, Apartado Postal 382, E-06006 Badajoz, Spain* [2] *Instituto de Computación Científica Avanzada (ICCAEx), Universidad de Extremadura, E-06006 Badajoz, Spain* [3] *Departamento de Física Aplicada, E.I.N.A., Universidad de Zaragoza, E-50018 Zaragoza, Spain and Instituto de Nanociencia y Materiales de Aragón (INMA), CSIC-Universidad de Zaragoza, E-50009 Zaragoza, Spain* [4] *Departamento de Física, Facultad de Ciencias, Universidad de Extremadura, E-06006 Badajoz, Spain* [5] *Departamento de Ingeniería Eléctrica, Electrónica y Automática, Facultad de Ciencias, Universidad de Extremadura, E-06006 Badajoz, Spain* [6] *Departamento de Ingeniería Eléctrica, Electrónica y Automática, Escuela de Ingenieros Industriales, Universidad de Castilla-La Mancha, E-02071 Albacete, Spain*

*e-mail: jesusmm@unex.es

We have investigated the effectiveness of zero average periodic forces at yielding directed ratchet escape from a symmetric potential well by considering an asymmetric external periodic force. Optimal enhancement of directed ratchet escape is predicted to occur when the wave form of the zero-average periodic force acting on a damped driven oscillator matches as closely as possible to a biharmonic universal wave form, as predicted by the theory of ratchet universality. Our numerical experiments confirmed those findings, as well as revealed the interplay between heteroclinic instabilities leading to chaotic escape and breaking of a generalized parity symmetry leading to directed ratchet escape to an attractor either at ∞ or at $-\infty$. Specifically, the optimal approximation to the biharmonic universal force triggers the almost complete destruction of the nonescaping basin for driving amplitudes which are systematically lower than those corresponding to a symmetric periodic force having the same period.

[1] R. Chacón, P. J. Martínez, J. M. Marcos, F. J. Aranda and J. A. Martínez, *Phys. Rev. E* **103**, 022203 (2021).

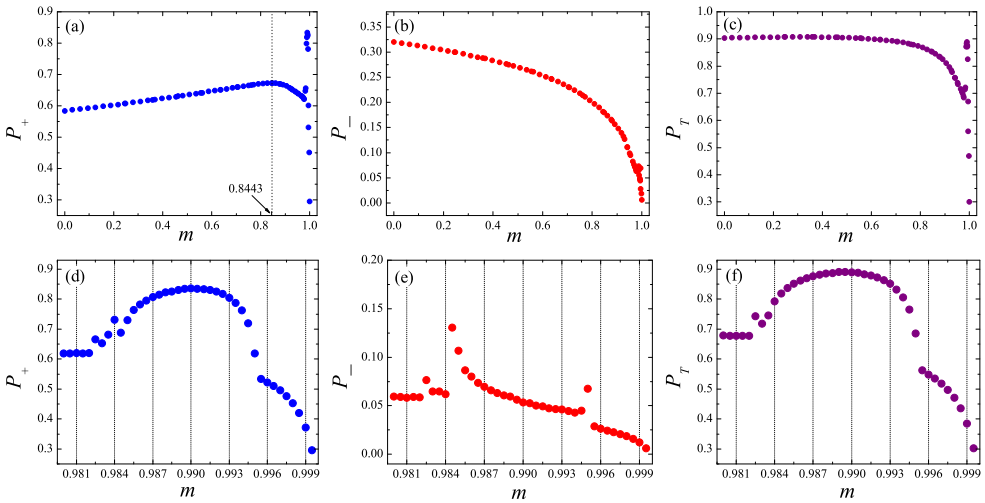

Figure 1. Escape probabilities P_+ (a), P_- (b), $P_T = P_+ + P_-$ (c) of the one-well Duffing oscillator ($\ddot{x} + x - 4x^3 = -\delta\dot{x} + \gamma F(t)$) subjected to the elliptic force $F_{ellip}(t; T, m) \equiv sn(\Omega t; m)cn(\Omega t; m)$ vs the shape parameter m. Versions (d), (e), and (f) show enlargements of the versions (a), (b), and (c) over the range $0.98 < m < 1$, respectively. System parameters: $\delta = 0.2$, $\gamma = 0.28$, $T = 2/0.5268$. The quantities plotted are dimensionless.

Colloidal monolayers: bridging the gap between two and three spatial dimensions

Alvaro Domínguez

Departamento de Física Atómica, Molecular y Nuclear, Universidad de Sevilla, Apdo. 1065, 41080 Spain.

*e-mail: dominguez@us.es

It is well established that, unlike for a three-dimensional fluid, particle interactions prevent the hydrodynamic transport coefficients from being defined for a two-dimensional fluid due to the notorious "long-time tail" feature of the velocity autocorrelation.

A colloidal monolayer formed at a fluid interface builds a bridge between these two limiting cases, and it provides insight on the transition from three down to two spatial dimensions: the positions of the colloidal particles are constrained to a plane and the colloid thus resembles a two-dimensional fluid. But the exchange of particle momentum takes place in three-dimensional space because it is mediated by the ambient fluid in the form of hydrodynamic interactions.

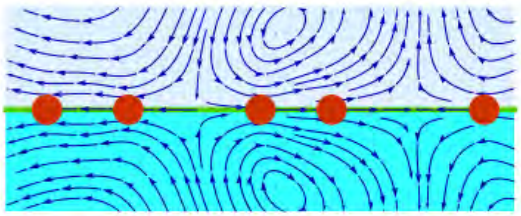

Side view of a colloidal monolayer formed at the interface between two fluids, and sketch of the three-dimensional flows responsible for the hydrodynamic interactions.

Here we study the behavior of the colloidal diffusivity, which is the only hydrodynamic transport coefficient for the two-dimensional colloidal fluid. The starting point is the Smoluchowski equation, i.e., the Fokker-Planck equation for the colloidal particles in the overdamped regime with due account of the hydrodynamic interactions. We then show that the diffusivity exhibits an intermediate behavior between purely two-dimensional and fully three-dimensional fluid: on the one hand, Fick's law, which pertains to *collective diffusion*, breaks down altogether [1-3], as confirmed experimentally [4]. On the other hand, the coefficient of *self-diffusion* (or single–particle diffusion) is finite [5], but the transitional nature of the monolayer shows up in a non-analytic dependence on the colloidal packing fraction [6], at odds with the case of a fully three-dimensional colloid.

[1] J. Bleibel, A. Domínguez, F. Günther, J. Harting, M. Oettel, *Soft Matter*, **10**, 2945 (2014).
[2] S. Panzuela, R. P. Peláez, R. Delgado-Buscalioni, *Physical Review E*, **95**, 012602 (2017).
[3] J. Bleibel, A. Domínguez, M. Oettel, *Physical Review E*, **95**, 032604 (2017).
[4] B. Lin, B. Cui, X. Xu, R. Zangi, H. Diamant, S. A. Rice, *Physical Review E*, **89**, 022303, (2014).
[5] R. P. Peláez, F. Balboa Usabiaga, S. Panzuela, Q. Xiao, R. Delgado-Buscalioni, A. Donev, *Journal of Statistical Mechanics: Theory and Experiment*, 063207 (2018).
[6] A. Domínguez, unpublished (2022).

Kinetic theory of fluids under strong confinement

P. Maynar[1,2,*], M. I. García de Soria[1,2], J. J. Brey[1,2]

[1]*Área de Física Teórica, Universidad de Sevilla, Spain.* [2] *Institute for Theoretical and Computational Physics, Universidad de Granada, Spain.*

*e-mail: maynar@us.es

A kinetic equation for a system of elastic hard spheres or disks confined by a hard wall of arbitrary shape is derived. It is a generalization of the modified Enskog equation in which the effects of the confinement are taken into account and it is supposed to be valid up to moderate densities. A Lyapunov functional, $\mathcal{H}[f]$, is identified. For any solution of the kinetic equation, $\mathcal{H}$ decays monotonically in time until the system reaches the inhomogeneous equilibrium distribution, that is a Maxwellian distribution with a the density field consistent with equilibrium statistical mechanics. From the equation, balance equations for the hydrodynamic fields are derived, identifying the collisional transfer contributions to the pressure tensor and heat flux. This let us to formulate a generalization of the wall theorem to arbitrary non-equilibrium states [1]. The results are generalized to inelastic hard spheres and the extreme case in which the system is confined by two hard walls separated a distance smaller than twice the diameter of the particles is studied in detail [2].

[1] P. Maynar, M. I. García de Soria, and J. J. Brey, *J. Stat. Phys.* **170**, 999 (2018).
[2] P. Maynar, M. I. García de Soria, and J. J. Brey, *Phys. Rev. E* **99**, 032903 (2019).

Optimal thermalisation for a generic d-dimensional harmonic oscillator

Antonio Patrón*, Antonio Prados, Carlos A. Plata

Física Teórica, Universidad de Sevilla, Apartado de Correos 1065, E-41080 Sevilla, Spain.

*e-mail: apatron@us.es

In this work, we study the optimisation problem of minimising the connection time between equilibrium states for an overdamped Brownian particle confined in a d-dimensional harmonic trap, in which the temperature is externally controlled. This system constitutes a paradigmatic model of theoretical interest within the field of stochastic thermodynamics. Moreover, it is also relevant in the experimental context, for it allows to describe accurately the dynamics of realistic systems such as confined colloidal particles in optical traps. The state of the system is fully determined via the variances $z_i \equiv \langle x_i^2 \rangle$, $i = 1, ..., d$, with x_i being the i-th spatial component of the particle. Their time evolution is given via the dynamic equations

$$\frac{dz_i}{dt} = -2k_i z_i + 2T(t), \quad i = 1, ..., d, \tag{1}$$

with k_i being the elastic constant of the harmonic trap in the i-th direction, and $T(t) \in [T_{\min}, T_{\max}]$ being the bath temperature, which is externally controlled at will.

The optimal functional form of $T(t)$ that minimises the connection time between two equilibrium states of the system is sought. Such states are characterised by the initial and final temperatures T_0 and T_f, respectively. Direct application of control theory, specifically Pontryagin's maximum principle, shows that optimal protocols for the temperature are of the *bang-bang* type, that is, the protocol comprises several time windows in which the temperature must take alternatively the minimum ($T_{\min}$) and maximum ($T_{\max}$) values allowed.

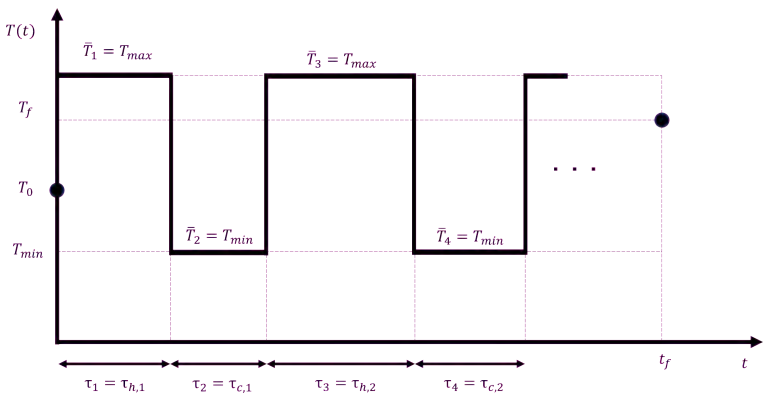

Figure 1. Sketch of the optimal bang-bang control able to connect two equilibrium states of a d-dimensional harmonic oscillator.

For the system of concern, we show that it is possible to explicitly work out the optimal thermal connections. We study their dependence on the limiting values of the temperature, and also on the elastic constants k_i that characterise the confinement in each direction. A rich phenomenology emerges, including striking discontinuities on the minimum connection times when two or more of the elastic constants become equal.

[1] Antonio Patrón, Antonio Prados, and Carlos A. Plata, unpublished.
[2] Carlos A. Plata, David Guéry-Odelin, E. Trizac, and A. Prados, *Phys. Rev. E* **99**, 012140 (2019).
[3] I. A. Martínez, E. Roldán, L. Dinis, D. Petrov and R. A. Rica, *Physical Review Letters* **114**, 120601 (2015).

Acknowledgements: Support from Grant PGC2018-093998-B-I00 funded by MCIN/AEI/10.13039/501100011033/ and by ERDF "A way of making Europe." is acknowledged. C.A.P. acknowledges financial support from Junta de Andalucía and European Social Fund through the program PAIDI-DOCTOR. A. Patrón acknowledges support from the FPU programme through Grant FPU2019-4110.

Direct evaluation of large deviations in open quantum systems

F. Carollo[3], **C. Pérez-Espigares**[1,2,*]

[1]*Departamento de Electromagnetismo y Física de la Materia, Universidad de Granada, Granada 18071, Spain.*
[2]*Institute Carlos I for Theoretical and Computational Physics, Universidad de Granada, Granada 18071, Spain.*
[3]*Institut für Theoretische Physik, Universität Tübingen, Auf der Morgenstelle 14, 72076 Tübingen, Germany.*

*e-mail: carlosperez@ugr.es

Controlling dynamical fluctuations in open quantum systems is essential both for our comprehension of quantum nonequilibrium behavior and for its possible application in near-term quantum technologies. However, understanding these fluctuations is extremely challenging due, to a large extent, to a lack of efficient important sampling methods for quantum systems. In this talk, we present a unified framework—based on population-dynamics methods—for the evaluation of the full probability distribution of generic time-integrated observables in Markovian quantum jump processes. These include quantities carrying information about genuine quantum features, such as quantum superposition or entanglement, not accessible with existing numerical techniques. The algorithm we propose provides dynamical free-energy and entropy functionals which, akin to their equilibrium counterpart, permit one to unveil intriguing phase-transition behavior in quantum trajectories.

[1] F. Carollo, C. Pérez-Espigares, *Physical Review E* **102**, 030104(R) (2020).

Nonlinearity test for complex time series

A. V. Coronado[1], P. A. Bernaola-Galván[1,2], M. Gómez-Extremera[1], P. Carpena[1,2,*]

[1]*Departamento de Física Aplicada II, Universidad de Málaga, Spain.* [2]*Instituto Carlos I de Física Teórica y Computacional, Universidad de Málaga, Spain.*

*e-mail: pjcarpena@uma.es

The nonlinear character of a dynamical system can be studied from the corresponding dynamical equations. Note that the knowledge of the dynamics is essential for both understanding properly the analyzed system and for modeling purposes. However, in the majority of the complex systems of interest, such dynamical equations are not known, and the only available information from the system is typically an output observable time series. Thus, the possible underlying nonlinear dynamics must be assessed from the available time series by applying nonlinearity tests on these data, able to determine if the analyzed time series exhibits or not nonlinear properties.

The canonical reference for linear stochastic time series are stochastic Gaussian time series with only linear correlations. However, the available experimental time series are rarely Gaussian. Therefore, the most widely used nonlinearity test [1] generates surrogate time series with the same marginal (non Gaussian) distribution, and more important, with the same autocorrelation values as the analyzed time series. This property is achieved by calculating the power spectrum of the experimental time series via FFT, and create a signal in the frequency domain with this power spectrum but applying phase randomization to destroy nonlinear correlations. Once the phase-randomized signal in the frequency domain is Fourier-transformed back into real space, a final time series is obtained with the same autocorrelation values as those of the analyzed signal according to the Wiener-Khinchin theorem, but purely linear due to the phase randomization procedure. However, this time series does not present the same marginal distribution as the experimental one, and an iterative process is required [1] to get the same correlations and distributions as the original data. A Monte Carlo set of these surrogate time series is generated, and constitutes the null hypothesis that is statistically tested against the experimental time series to determine its possible nonlinear character.

However, some studies [2] show that the iterative process in [1] needed to create surrogate data introduce correlations in the Fourier phases, therefore producing surrogate time series with nonlinear properties, which are then not adequate to be considered as the reference for linearity. Here, we present a nonlinearity test of general applicability which do not require the generation of surrogate data. Recently [3], we have shown than if a purely linear Gaussian correlated time series is transformed into another time series with different marginal distribution then the autocorrelation C of this time series can be obtained from the correlation C_G of the Gaussian time series by:

$$C = \int_{-\infty}^{\infty}\int_{-\infty}^{\infty} F^{-1}(\Phi(x_G))\, F^{-1}(\Phi(y_G))\, \varphi_2(x_G, y_G, C_G)\, \mathrm{d}x\, \mathrm{d}y$$

where x_G and y_G are Gaussian variables, $\varphi_2()$ is the bivariate Gaussian distribution, $\Phi()$ is the Gaussian cumulative distribution, and $F^{-1}()$ is the inverse cumulative distribution of the final non Gaussian times series. This equation holds if and only if the original Gaussian and the final non Gaussian time series are purely linear. Thus, we can use it to construct a nonlinearity test as follows: a) Given a time series, calculate the autocorrelation function C. b) Use this C value and solve numerically the equation to determine the autocorrelation function C_G, which corresponds to the Gaussian linear time series from where the analyzed time series would have been hypothetically obtained if and only if it is purely linear. c) Transform the analyzed time series to follow a Gaussian distribution and calculate the autocorrelation function C'_G. If the original time series is linear then (statistically) $C_G = C'_G$, but if $C_G \neq C'_G$ then we can conclude that the analyzed time series possess nonlinear character. We have applied this test to a great variety of known linear and nonlinear time series, and have obtained excellent results [4].

[1] T. Schreiber and A. Schmitz. *Phys. Rev. Lett.* **77**, 635 (1996).
[2] C. Räth, M. Gliozzi, I. E. Papadakis and W. Brinkmann. *Phys. Rev. Lett.* **109**, 144101 (2012).
[3] P. Carpena, P. Bernaola-Galván, M. Gómez-Extremera and A. V. Coronado. *Chaos* **30**, 083140 (2020).
[4] P. Carpena, P. Bernaola-Galván, M. Gómez-Extremera and A. V. Coronado (in preparation).

Statistical models of social interaction

Samuel Martin-Gutierrez[1,2,*], Juan C. Losada[1], Rosa M. Benito[1]

[1] *Grupo de Sistemas Complejos, Escuela Técnica Superior de Ingeniería Agronómica, Alimentaria y de Biosistemas, Universidad Politécnica de Madrid, Av. Puerta de Hierro, 2, 28040 Madrid, Spain.*
[2] *Network Inequality group, Complexity Science Hub Vienna, Josefstädter Str. 39, 1080, Wien, Austria*
*e-mail: martin.gutierrez@csh.ac.at

In this work [1] we present three mathematical models to explain how the actions performed by an individual (her activity) influence the collective reaction (or response) of the social system she is embedded in. The models consider different levels of dependence between response and activity. In the first model, we consider activity and response completely independent (Independent Variables model – InV), while in the second and third models individual activity influences collective response. The main difference between these last two models is the distinguishability of the actors. In the Identical Actors (IdA) model, the system is agnostic with respect to the individual that performs the actions, while in the Distinguishable Actors (DiA) model, the dependence between activity and response is determined by the features of the actor that performs the action. In Figure 1 we present a diagram that summarizes the main ideas behind each model.

We use the models to obtain the distribution of the efficiency metric η, defined as the ratio between the number of reactions R triggered by an actor on other members of the system and the number of actions A of the actor:

$$\eta = \frac{R}{A}$$

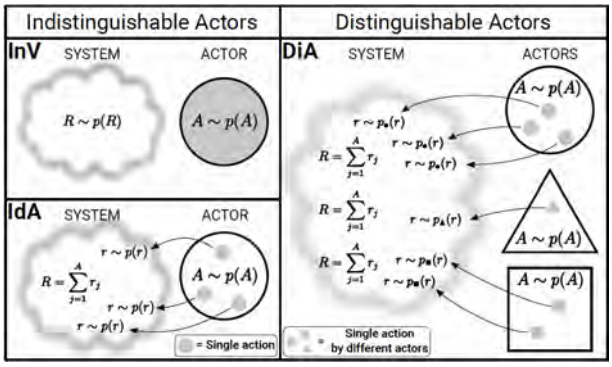

Figure 1. Diagram that summarizes the main characteristics of the three models: Independent Variables (InV), Identical Actors (IdA) and Distinguishable Actors (DiA).

This metric is a generalization of the user efficiency [2]. We tested the models on 29 datasets from three systems of different nature: Twitter conversations, where A and R are tweets and retweets, respectively; the scientific citations network, where A and R are publications and citations; and the Wikipedia collaboration environment, where A is the number of editions and R the number of received messages. In all the systems the efficiency distribution presents a universal shape, illustrated in Figure 2, with small but relevant differences between systems.

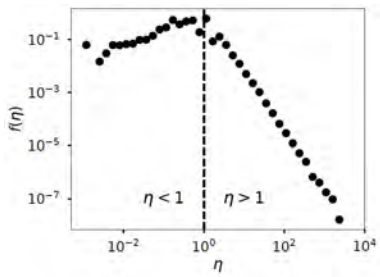

Figure 2. Empirical efficiency distribution corresponding to a Twitter conversation.

The Independent Variables model explains the universal shape of the efficiency distribution and its independence with respect to changes in the activity distribution, two fundamental characteristics for which there was previously only empirical evidence. Additionally, it reproduces the efficiency distribution for the scientific citations network. However, for Twitter and Wikipedia there are small discrepancies with the data caused by $A-R$ correlations. We incorporated these correlations in a parsimonious way in the Identical Actors model and improved the results for both systems. In particular, the IdA model reproduces adequately the right tail ($\eta > 1$) for Twitter and Wikipedia, but not the left tail ($\eta < 1$). To solve these discrepancies, we developed the Distinguishable Actors model, which fits the Twitter data remarkably well.

[1] Martin-Gutierrez, S., Losada, J.C., Benito, R.M., *Sci Rep* **10(1)**, 12126 (2020).
[2] Morales, A.J., Borondo, J., Losada, J.C., Benito, R.M., *Soc Networks* **39**, 1-11 (2014).

Acknowledgements: This work has been supported by the Spanish Ministry of Science, Innovation and Universities (MICIU) under Contract No. PGC2018-093854-B-I00, Spanish Ministry of Education, Culture and Sport (Grant No. FPU15/01461), and by the Austrian research agency (FFG) under project No. 873927.

Dynamics of hard particles confined by an isotropic harmonic potential

M. I. García de Soria[1,2,*], P. Maynar[1,2], E. Trizac[3], D. Guéry-Odelin[4]

[1]*Área de Física Teórica, Universidad de Sevilla, Spain.* [2]*Institute for Theoretical and Computational Physics, Universidad de Granada, Spain.* [3]*LPTMS, Université Paris-Saclay, France.* [4]*Laboratoire Collisions, Agrégats, Réactivité, Université de Toulouse, France.*

*e-mail: gsoria@us.es

The dynamics of a system composed of elastic hard particles confined by an isotropic harmonic potential is studied. In the low-density limit, the dynamics is described by the Boltzmann equation and the system does not reach equilibrium except for some particular class of initial conditions. On the contrary, the system reaches a periodic in time state in which the velocity distribution function is Gaussian, but with the hydrodynamic fields oscillating in time with some specific profiles. It is shown that this so-called *breather* state is completely specified by the constants of the motion, the mean square displacement, $\langle r^2 \rangle$, at the initial time and its derivative with respect to time also at the initial time. This is due to the fact that, at this level of description, $\langle r^2 \rangle$ verifies a closed second order differential equation. For low but finite densities, the dynamics of the system is analyzed by taking into account the finite size of the particles. Under well-controlled approximations, a closed evolution equation for $\langle r^2 \rangle$ is derived, obtaining that it decays to its equilibrium value, oscillating with a frequency slightly modified with respect to the Boltzmann values. The time average of the oscillations is also renormalized. An excellent agreement is found between Molecular Dynamics simulation results and the theoretical predictions for the frequency and the time average of the oscillations. For the relaxation time, the agreement is not as good as for the two previous quantities and the origin of the discrepancies is discussed.

Variability of spreading rate in forced plumes

Pilar López[1], **Benjamín Skadden**[2,3,*], Ania Matulka[4], Ana M. Tarquis[2,3], Juan Carlos Losada[3]

[1]*Department of Biodiversity, Ecology and Evolution, Unit, University Complutense of Madrid, 28040 Madrid, Spain.* [2]*CEIGRAM, ETSIAAB, Universidad Politécnica de Madrid, 28040 Madrid, Spain.* [3]*Grupo de Sistemas Complejos (GSC), Universidad Politécnica de Madrid, 28040 Madrid, Spain.* [4]*Department of Physical Environment Area, Puertos del Estado, 28042 Madrid, Spain.*

*e-mail: benjaskat2@gmail.com

The geophysical importance of forced turbulent plumes is evident as they are a fundamental part of dispersion processes, for example, volcanic plumes. From the earliest investigations, it became clear that one fundamental problem was to determine the value of the entrainment coefficient. In Morton's initial theory, the entrainment coefficient is supposed to be constant. One way to approach the analysis of the entrainment is to study the spreading rate (β). The spreading assumption establishes that the width of a plume increases at a rate proportional to a characteristic spreading velocity. In a quiet environment, there is a simple spreading relationship in which the β represents the linear increase of the dominant eddy dimension with distance from the source. However, several studies have shown that the entrainment coefficient, and therefore β, is not constant (see [1] and references therein).

Forced plumes experiments were set up to be recorded at the height of 2cm (Ho) and two Atwoods (A) [2], using frame-sequencer software (VirtualDubMod). Each image of the sequence was binarised [3]. The recorded plume measurements in all the axial extensions were obtained based on the geometrical information. Its use in a sequence of consecutive images allows the analysis of the vertical and radial measurements' evolution in time (Fig. 1).

We can define the local spreading rate, βlocal, by using the width (wi) corresponding to each depth (zi)

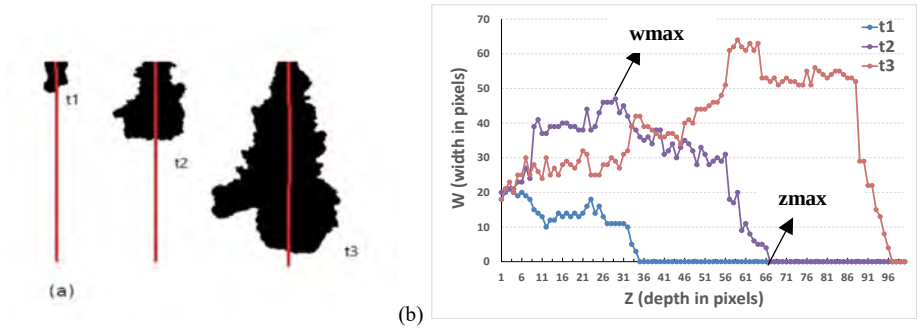

Figure 1. (a) Time development of a plume at different times (t1 = 0.02, t2 = 0.18 and t3 = 0.48 s). (b) Vertical profile of the plume width under conditions Ho = 2 cm and A= 0.01 at each time. The position of maximum width (wmax) and maximum depth (zmax) are pointed at t2.

each time and dividing it by zmax at that time (Fig. 2). When wi is wmax the value obtained is the classical spreading rate (βclassic) [2]. This methodological approach has the advantage of being non-invasive and easily exportable. Further research is in progress to analyse the dependence of the βlocal on Ho and A.

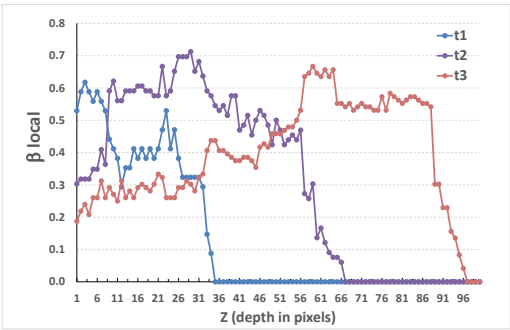

Figure 2. Local spreading rate (βlocal) at different times (t1 = 0.02, t2 = 0.18 and t3 = 0.48 s) under conditions Ho = 2 cm and Atwood= 0.01.

[1] A. Matulka, P. López, J.M. Redondo, A. Tarquis. *Nonlinear Proc Geoph*, **21,** 269, 2014.
[2] P. López, A.M. Tarquis, B. Skadden, A. Matulka, J.M. Redondo. *Eur. J. Mech-B/Fluids*,**92**, 203, 2022.
[3] P. López, A.M. Tarquis, A. Matulka, B. Skadden, J.M. Redondo. *Chaos Solitons Fractals* **105**, 128, 2017.

Acknowledgements: The authors gratefully acknowledge the support of the Instituto Pluridisciplinar (UCM) for its technical support during this experimental work, without which the present study could not have been completed. This study is partially supported by the Fundación Premio Arce (ETSIAAB, UPM) under Grant FPA18PPMAT08

Accelerating out-of-equilibrium critical dynamics via magnetic domains

Isidoro González-Adalid Pemartín[1,*], Emanuel Mompó[2], Antonio Lasanta[3,4], Víctor Martín-Mayor[1,5], Jesús Salas[2,4]

[1]*Departamento de Física Teórica, Universidad Complutense, 28040 Madrid, Spain.* [2]*Departamento de Matemáticas, Universidad Carlos III de Madrid, 28911 Leganés, Spain.* [3]*Departamento de Álgebra, Facultad de Educación, Economía y Tecnología de Ceuta, Universidad de Granada, Cortadura del Valle, s/n, 51001 Ceuta, Spain.* [4]*Grupo de Teorías de Campos y Física Estadística, Instituto Gregorio Millán, Universidad Carlos III de Madrid, Unidad Asociada al Instituto de Estructura de la Materia, CSIC, Spain.* [5]*Instituto de Biocomputación y Física de Sistemas Complejos (BIFI), 50018 Zaragoza, Spain.*

*e-mail: isidorog@ucm.es

Reaching thermal equilibrium fast is an important problem in science and industry. For this reason, the non-equilibrium relaxation has been very studied during the last decades. In fact, the attention received by the counterintuitive Mpemba Effect [1], allowing to cool down faster the hotter of two systems (or heat up faster the cooler system), is reasonable. Indeed, we now understand the general conditions that allow a faster cooling, or faster heating, in a variety of systems like granular matter, spin glasses, or classical and quantum Markovian systems. This knowledge allows to develop better strategies for cooling, or heating, a system. In particular, Amit and Raz have recently designed a faster heating protocol for systems with timescale separation [2].

However, a timescale separation is not present in a second-order phase transition, where critical slowing down evidences a continuum of timescale. In this situation, understanding the mechanism that governs the dynamics is the key to potentially control the evolution. The size of the ordered domains when the system enters the symmetry-broken phase is a natural candidate as a driver for this mechanism.

In our work [3], we focus on the study of the ferromagnetic two-dimensional (2D) Ising spin model. In particular, we study through numerical simulations an unexplored out-of-equilibrium heating protocol, in which the bath temperature starts below the critical temperature, in the ferromagnetic phase (FM), and is later heated above the critical point, in the paramagnetic phase (PM). We show that a faster relaxation can be reached in absence of timescale separation by manipulating the system's internal structure of ordered domains (related with the coherence length ξ) thanks to this excursion in the symmetry-broken phase, see Fig 1.

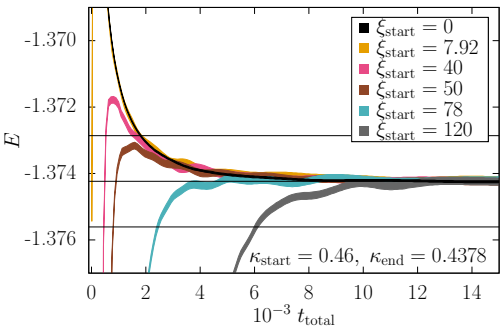

Figure 1. Energy density as a function of the total time $t_{\rm total}$ elapsed since the beginning of our protocol, as computed with the Metropolis dynamics for $\kappa_{\rm start} = 0.46$ (FM), $\kappa_{\rm end} = 0.4378$ (PM), and several values of $\xi_{\rm start}$. Values of $\xi_{\rm start}$ increase from top to bottom. The width of the curves is four times the statistical errors. The three horizontal lines correspond to $E_{\rm eq}$ multiplied by 1.001, 1 and 0.999.

[1] E. B. Mpemba, D. G. Osborne, *Phys. Educ.* **4**, 172 (1969).
[2] A. Gal, O. Raz, *Phys. Rev. Lett.*, **124**, 060602 (2020).
[3] I. González-Adalid Pemartín, E. Mompó, A. Lasanta, V. Martín-Mayor, J. Salas, *Phys. Rev. E*, **104**, 044114 (2021).

Acknowledgements: This work was partially supported by Ministerio de Economía, Industria y Competitividad (MINECO, Spain), Agencia Estatal de Investigación (AEI, Spain), and Fondo Europeo de Desarrollo Regional (FEDER, EU) through Grants No. PGC2018-094684-B-C21, No. FIS2017-84440-C2-2-P, and No. MTM2017-84446-C2-2-R. A.L. and J.S. were also partially supported by Grant No. PID2020-116567GB-C22 AEI/10.13039/501100011033. A.L. was also partly supported by Grant No A-FQM-644-UGR20 Programa operativo FEDER Andalucía 2014–2020. J.S. was also partly supported by the Madrid Government (Comunidad de Madrid-Spain) under the Multiannual Agreement with UC3M in the line of Excellence of University Professors (EPUC3M23), and in the context of the V PRICIT (Regional Programme of Research and Technological Innovation). I.G.-A.P. was supported by the Ministerio de Ciencia, Innovación y Universidades (MCIU, Spain) through FPU Grant No. FPU18/02665.

Tópicos Avanzados en Óptica

Presentaciones orales

Miércoles 13/07:

15:30-15:45 Jesús Armengol Cebrian (Universidad Politécnica de Cataluña). *Optical and visual quality indicators of intraocular lenses measured with an on-bench eye model*

15:45-16:00 Verónica González Fernández (Universidad Complutense de Madrid). *Comparative study of enhanced monofocal lenses for different nominal powers*

16:00-16:15 Sonia Ortiz Peregrina (Universidad de Granada). *Effects of smoking cannabis on visual performance*

16:15-16:30 Miriam Casares López (Universidad de Granada). *The influence of visual function on driving performance under the influence of alcohol*

16:30-16:45 Vahid Pourreza Ghoushchi (Universidad de Murcia). *Periodic blur fluctuations effect on contrast sensitivity*

16:45-17:00 Alberto de Castro Arribas (IO-CSIC, Madrid). *Personalized computational models with OCT. Challenges and opportunities*

17:00-18:00 **Pósteres y café**.

18:00-18:15 Rosa María Martínez Ojeda (Universidad de Murcia). *Enhanced second harmonic imaging of the living human eye using deconvolution*

18:15-18:30 Luis Ordóñez Angamarca (Universidad Jaime I). *Optical sectioning in microscopy with structured illumination and single pixel detection*

18:30-18:45 Manuel Martinez Corral (Universidad de Valencia). *Advances in Fourier Lightfield Microscopy*

18:45-19:00 Víctor Bernardo Puente (Hamamatsu Photonics France). *Quantum imaging with a photon number resolving camera*

19:00-19:15 Jose Manuel Crespo Contiñas (Universidad de Santiago de Compostela). *Computer generated training datasets for deep learning applications to ESPI fringe patterns*

19:15-19:30 Ana Jesús López Díaz (Universidad de La Coruña). *Desarrollo de un sistema de procesado láser 3D asistido por robot para la eliminación de pintura*

Jueves 14/07:

15:30-15:45 Esther Nabadda (Universidad Miguel Hernández). *Synchronous phase detection technique for the evaluation of complex functions displayed on a phase-only modulator*

15:45-16:00 María del Mar Sánchez López ((Universidad Miguel Hernández). *Proof-of-concept depolarization emulator based on a liquid-crystal spatial light modulator*

16:00-16:15 Tomás Lloret López (Universidad de Alicante). *Quality metrics in holographic lenses recorded in a low toxicity photopolymer*

16:15-16:30 José Carlos García Vázquez (Universidad de Alicante). *Reflection gratings stored in a nanoparticle-doped photopolymer*

16:30-16:45 José Carlos Mira Martínez (Universidad de Alicante). *Redes plasmónicas unidimensionales de nanopartículas de oro a partir de redes de relieve fabricadas holográficamente*

16:45-17:00 Víctor Bonal Díaz (Universidad de Alicante). *Latest advances in organic distributed feedback lasers with top-layer resonators*

Pósteres

- E. Josua Fernandez Martinez (Universidad de Murcia). *Manipulating the second order coherence function for super-resolution intensity correlation imaging*
- Laura Clavé Cerezo (Universidad Politécnica de Cataluña). *Visual acuity in phakic and monofocal pseudophakic eyes under red, green, and blue lights*

- Justo Arines Piferrer (Universidad de Santiago de Compostela). *Jacobi Fourier Polynomials: more flexibility for designing ophthalmic solutions*
- Juan Manuel Bueno García (Universidad de Murcia). *Optical coherence tomography in retinitis pigmentosa patients treated with an injection of autologous bone-marrow-derived mononuclear stem cells*
- Diego Montagud-Martínez (Universidad Politécnica de Valencia). *Caracterización cromática de una lente intraocular comercial de foco extendido*
- Anabel Martínez Espert (Universidad de Valencia). *Impacto de la aberración esférica en modelos de ojos teóricos*
- Aina Turull Mallofré (Universidad Politécnica de Cataluña). *Analysis of the accommodation response as a supporting tool during subjective refraction*
- Alba María Paniagua Diaz (Universidad de Murcia). *Visual simulation and correction using economic and compact vertical aligned liquid crystal devices*
- Dulce María Simón Badia (Universidad de Murcia). *Straylight and Optical Memory Effect characterization of ex-vivo cataractous crystalline lenses*
- Pedro Gil (Universidad de Murcia). *Effects of small residual astigmatism on the reading performance of contact lens neophytes*
- Adriana Rosalía Sánchez Montes (Universidad de Alicante). *Numerical analysis of cross-talk phenomena in pixelated PA-LCos devices*
- Joan Josep Sirvent Verdú (Universidad de Alicante). *Precise-Integration Time-Domain for Optical Anisotropic Media*
- Iryna Standret (Universidad de Murcia). *Investigating ergodicity for the determination of optical coherence functions*
- Pien Vinke (Universidad de Murcia). *Impact of the detector response on the temporal second degree of coherence of a chaotic light source*
- Erik Baradit Allendes (Universidad del Bio-Bio). *Characterization of topography hidden under paint by means of algorithms stable to the number of frames under non-uniform illumination*

Optical and visual quality indicators of intraocular lenses measured with an on-bench eye model

Jesús Armengol*, Fidel Vega, María Sagrario Millán

Department of Optics and Optometry, Violinista Vellsolà 37 08222 Terrassa, Spain.

*e-mail: jesus.armengol@upc.edu

Cataract surgery is evolving from a solution to overcome visual impairment to a refractive procedure thanks to the development of intraocular lenses (IOLs) that are better adapted to the visual demands of the patients. Nowadays, there is a myriad of new IOL designs on the market, with associated claims from the manufacturers, that need to be carefully assessed in independent laboratories.

Optical quality indicators of IOL's performance can be measured using an eye model on an optical bench [1] avoiding subject variability. Modern extended range of vision (ERV) IOL designs aim to remedy the loss of the accommodative capacity of the natural lens with either a focal segment or by joining multiple foci (multifocal IOL). In a through-focus analysis of the IOL, the optical imaging quality of the lens is evaluated around the main focus of the eye model (typically corresponding to far vision).

An eye model implemented on a test bench (Figure 1) according to the standard regulation [1] allowed us to assess a variety of commercial IOLs and to extract some optical and visual quality indicators. A more detailed description of the setup is found in Ref. [2].

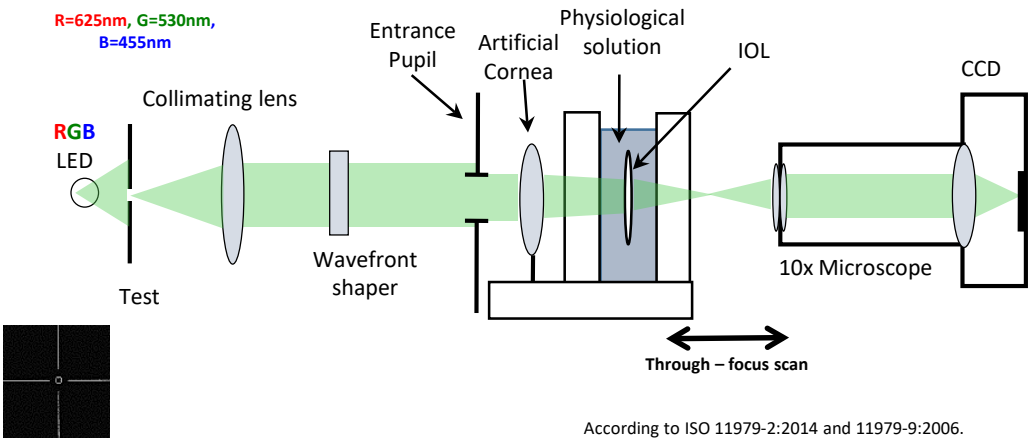

Figure 1. Sketch of the optical setup with an eye model. Test used to obtain the LSF (bottom left).

From the measurement of the line spread function (LSF), the modulation transfer function (MTF) was computed and, further, an optical quality indicator named the Strehl ratio of the radial MTF (SRMTF) (Eq.1) and a visual quality indicator named the visual Strehl ratio (VSMTF) (Eq.2).

$$SRMTF = \frac{\int_0^\infty MTF_r df}{\int_0^\infty MTF_{r_DL} df} \quad (1) \qquad VSMTF = \frac{\int_0^\infty CSF_n * MTF_r \, df}{\int_0^\infty CSF_n * MTF_{r_DL} \, df} \quad (2)$$

In Eq. 1, MTFr stands for radial MTF and subscript DL accounts for diffraction-limited calculation. In Eq. 2, CSFn stands for the neural contrast sensitivity function that represents the neural response of the visual system [3]. In this work we present the through-focus SRMTF and VSMTF results obtained experimentally for a commercial trifocal IOL (Zeiss ATLISA_Tri839MP) and compare between them. The impact of a constant magnification approach along the through-focus range is discussed.

[1] ISO 11979-2:2014 and 11979-9:2006. *"Ophthalmic Implants - Intraocular Lenses" Geneva.*
[2] F. Vega, F. Alba-Bueno, and M. S. Millán, *J. Eur. Opt. Soc. Rapid Publ.* **9**, 14002 (2014).
[3] L. N. Thibos, X. Hong, A. Bradley, and R. A. Applegate, *J. Vis.* **4**(4), 329 (2004).

Funding: Ministerio de Ciencia e Innovación, Agencia Estatal de Investigación (PID2020-114582RB-I00/ AEI / 10.13039/501100011033).

Comparative study of enhanced monofocal lenses for different nominal powers

Verónica González-Fernández[1,*], Nuria Garzón[2], María García-Montero[2], César Albarrán Diego[3], Luis Miguel Sánchez-Brea[1], José Antonio Gómez-Pedrero[1]

[1]*Dpto. de Óptica, Universidad Complutense de Madrid, Av. Arcos del Jalon 118, E-28037 Madrid, Spain.*
[2]*Dpto. de Optometría y Visión, Universidad Complutense de Madrid, Av. Arcos del Jalon 118, E-28037 Madrid, Spain.*
[3]*Dpto. de Óptica, Optometría y Visión, Universitat de València, Doctor Moliner 50 46100 Burjassot, Spain.*

*e-mail: veronicagf@ucm.es

Among the wide range of intraocular lenses (IOLs), monofocal lenses are one of the most common options due to its simplicity. Nevertheless, they present obvious limitations for which different solutions are being designed. One of these solutions, are the called "enhanced" monofocal lenses that improve intermediate vision, without reaching the criteria for extended range lenses. These new designs seek to increases the depth of focus to improve the intermediate vision, without modifying far vision and reducing dysphotopsia.

One of the approaches modifies the spherical aberration in a limited quantity to not compromise the optical quality of the final image. Therefore, the total addition of the lens will be limited. Of course, the different strategies or modifications will lead to different optical performances.

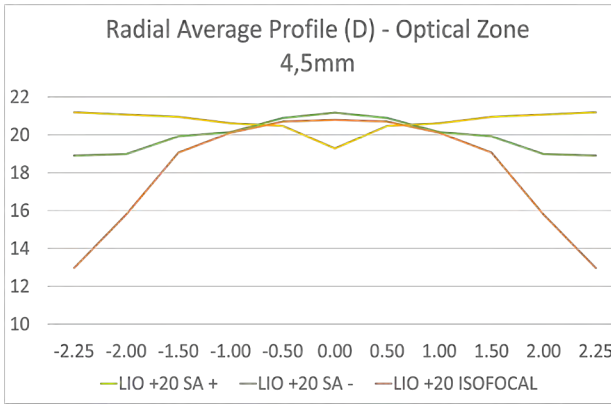

Figure 1. Comparison of the radial average profile for three enhanced monofocal lenses with a nominal power of +20 D: isofocal (orange), with positive spherical aberration (yellow) and negative spherical aberration (green).

In this work, we present the comparative study of three different lenses with the same nominal power: +20.00 D, measured using an optical system based on a quantitative deflectometry technique that measures light deviations through a combination of the Schlieren principle with a phase-shifting method (NIMO TR1504). All lenses were measured in a balanced salt solution at different aperture diameters. The three lenses differ in the sign and amount of spherical aberration induced to enhance intermediate vision. The optical lens power distribution as a function of the aperture radius was described in terms of radial computed colour maps, radial averaged power profiles, spherical aberration, and aberrometric profiles for difference distances from centre.

The power profiles of the lenses analysed showed that the enhanced monofocal lens nominal power did not change from the centre to the periphery, contrary to the enhanced ones that revealed a change toward more positive power values from the centre to the periphery (see Fig. 1). The refractive power of the enhanced monofocal lenses did not reach the value of the nominal distance power (+20.00D) until a radial distance of between -0.5 and +0.50 mm from the centre of the lens.

Acknowledgements: The authors thank Ministerio de Economía y Competitividad for the project PID2019-105918GB-I00.

Effects of smoking cannabis on visual performance

Sonia Ortiz-Peregrina*, Carolina Ortiz, Miriam Casares-López, Pilar Granados-Delgado, José R. Jiménez, Rosario G Anera

Department of Optics, University of Granada, Campus Fuentenueva s/n CP 18071, Granada (Spain)

*e-mail: soniaortiz@ugr.es

Introduction: Cannabis constitute the most widely consumed illicit drug worldwide [1, 2]. Moreover, its consumption is expected to increase due to the legalization in several countries [3]. The main psychoactive compound of cannabis is the so called Δ9-tetrahydrocannabinol (THC) and it is able to bind to the cannabinoid receptors, some of them are present within the visual system [4, 5]. However, visual effects of cannabis consumption remains unknown.

Objective: This study aimed to investigate visual effects of smoking cannabis in several visual functions, and its relationship with visual effects perceived by the user.

Methods: The study was prospectively approved by the University of Granada Human Research Ethics Committee (921/CCEIH/2019). Thirty-one young occasional cannabis users were included in the study. Visual function was evaluated in two different experimental sessions: a baseline session without cannabis use and other session after smoking cannabis. Both sessions were counterbalanced, and visual function was evaluated for visual acuity, contrast sensitivity, stereopsis, accommodative response, straylight and halo perception. Participants completed a questionnaire about self-perceived visual quality under the effects of cannabis. Depending on whether or not they perceived worsening in visual quality after smoking cannabis, they were classified into two groups.

Results: Smoking cannabis significantly deteriorated vision. Visual acuity and contrast sensitivity were significantly reduced ($p<0.001$). Intraocular scattering increased about 9% after cannabis use ($p<0.001$) resulting in greater halo perception ($p=0.016$). Accommodative lag increased after smoking cannabis for 0.4 m ($p=0.006$) and 0.2 m ($p=0.001$). Stereopsis also deteriorated, with an increase of 50.7% for near distance ($p<0.001$) and 213.1% for far distance ($p<0.001$). Despite these results, about one third of the sample indicated that they think their vision is not impaired under cannabis' effect. A binary logistic regression analysis identified contrast sensitivity as the only visual test significantly associated with self-perceived visual quality (Odds ratio: 1.135; 95% CI 1.006, 1.280; $p=0.040$).

Conclusions: Smoking cannabis has negative consequences for visual function. However, some users are not aware of these changes. Contrast sensitivity is associated with the perceived impairment in visual function under cannabis effects.

[1] European Monitoring Centre for Drugs and Drug Addiction (EMCDDA). European Drug Report 2019: Trends and Developments 2019 (Publications Office of the European Union, Luxembourg, 2019).
[2] Spanish Observatory on Drugs and Addictions. Survey on alcohol and drugs in Spain (EDADES), 1995–2017 (Ministerio de Sanidad, Consumo y Bienestar social, Madrid, 2017).
[3] Compton, W. M., Volkow, N. D. & Lopez, M. F. Medical marijuana laws and cannabis use: Intersections of health and policy, *JAMA Psychiatry* **74**, 559 (2017).
[4] Dasilva, M., Grieve, K. L. & Rivadulla, C., Cannabis, endocannabinoid CB1 receptors, and the neuropathology of vision. In Neu-ropathology of Drug Addictions and Substance Misuse (ed. Preedy, V. R.) 738–748 (Elsevier, Amsterdam, 2016).
[5] Yazulla, S. Endocannabinoids in the retina: From marijuana to neuroprotection, *Prog. Retin. Eye Res.* **27**, 501 (2008).
[6] Ortiz-Peregrina, S., Ortiz, C., Casares-López, M., Jiménez J.R., Anera, R.G., Effects of cannabis on visual function and self-perceived visual quality. *Sci Rep.* **11**, 1655.

Acknowledgements: Research Projects PID2020-115184RB-I00, funded by MCIN/ AEI/10.13039/501100011033, and A-FQM-532-UGR20, funded by FEDER/Junta de Andalucía-Consejería de Transformación Económica, Industria, Conocimiento y Universidades.
The authors thank Dräger Iberia (Madrid, Spain) and the local police of Granada City (Granada, Spain) for loan of the Dräger DrugTest 5000 and the Dräger Alcotest 6820 breath analyzer (Dräger Safety AG & Co. KGaA. Lübeck, Germany), and Pago de Almaraes wineries for providing us with the wine used in the study.

The influence of visual function on driving performance under the influence of alcohol

Miriam Casares López*, José Juan Castro Torres, Sonia Ortiz Peregrina, Francesco Martino, Luis Jiménez del Barco

[1]*Department of Optics, Faculty of Sciences, University of Granada, Av. Fuente Nueva s/n, 18071, Granada, Spain.*

*e-mail: clmiriam@ugr.es

Purpose: Driving is a complex task that involves different motor and cognitive abilities. One of these is the visual function, responsible for 83% of the most important driving behaviours [1]. Driving under the influence (DUI) of alcohol is a frequent behaviour among drivers, however this substance deteriorates vision [2,3], which could negatively impact driving. Thus, the aim of this study was to assess the impact of a moderate-high alcohol dose on vision and driving performance, and to analyse the association between visual function and driving under the influence of alcohol.

Methods: a total of 34 participants (17 females), with ages ranging from 20 to 34 years, took part in the experiment. They took two experimental sessions: one in normal conditions (with no alcohol consumption), and a second one after the intake of 450 ml of red wine (approximately 48.6 g of alcohol). Thirty minutes after alcohol intake, the breath alcohol concentration (BrAC) was measured every 20 minutes (mean ± SD; 0.32 ± 0.12 mg/l) with a breath analyzer. In the two sessions, different visual functions were assessed: contrast sensitivity for 6 spatial frequencies (0.75, 1.5, 3, 6, 12, and 18 cpd), the visual discrimination capacity by means of the visual disturbance index (VDI) [4], and the optical quality by means of the MTF-cut off frequency for 4 mm pupil size using a double-pass system, the Optical Quality Analysis System (OQAS II). The driving performance was assessed with the Simax driving simulator v4.0.8 [5]. The scenario was a mountain road of single-lane single carriageway (6 km). The variables analyzed were the standard deviation of lateral position (SDLP, m), the standard deviation (SD) of the angular velocity of the steering wheel (rad/s), and the reaction time (s). An overall visual performance score (OVPS) and an overall driving performance score (ODPS) were calculated from the vision and driving results.

Results: The visual discrimination capacity was significantly impaired under the influence of alcohol on monocular and binocular viewing conditions ($p = 0.004$ and $p < 0.001$ respectively). The mean contrast sensitivity was also reduced in monocular and binocular viewing conditions ($p = 0.001$ and $p < 0.001$ respectively) for all special frequencies ($p \leq 0.001$). The MTF cut-off frequency was significantly reduced following alcohol consumption ($p < 0.001$). Regarding driving performance, an increase of the SDLP was observed, but the change was not significant ($p = 0.080$); the SD of the angular velocity of the steering wheel increased ($p = 0.001$), and the response time was also higher under the effects of alcohol ($p = 0.013$). The ODPS was significantly correlated with the OVPS ($\rho = 0.271$; $p = 0.026$).

Conclusions: Visual function, evaluated by means of the contrast sensitivity, the visual discrimination capacity, and the optical quality, was significantly impaired by the intake of a moderate-high dose of alcohol. Driving performance was impaired as well, and the driving ability was positively correlated with the visual performance under the influence of alcohol. These results highlight the fact that these features of visual function should be taking into consideration to ensure safe driving.

[1] McKnight AJ, Adams BB. *Driver education task analysis. Volume I: task description. Final report.* (1970).
[2] Casares-Lopez M, Castro-Torres JJ, Ortiz-Peregrina S, Martino F, Ortiz C. Changes in Visual Performance under the Effects of Moderate-High Alcohol Consumption: The Influence of Biological Sex. *International Journal of Environmental Research and Public Health* **18**(13), 15 (2021).
[3] Watten RG, Lie I. Visual functions and acute ingestion of alcohol. *Ophthalmic and Physiological Optics* **16**(6), 460 (1996).
[4] Castro JJ, Ortiz C, Pozo AM, Anera RG, Soler M. A visual test based on a freeware software for quantifying and displaying night-vision disturbances: study in subjects after alcohol consumption. *Theoretical Biology and Medical Modelling* **11** (2014).
[5] Ortiz C, Ortiz-Peregrina S, Castro JJ, Casares-Lopez M, Salas C. Driver distraction by smartphone use (WhatsApp) in different age groups. *Accident Analysis and Prevention* **117**, 239 (2018).

Acknowledgements: The authors thank Dräger Iberia (Madrid, Spain) and Local Police of Granada City (Granada, Spain) for lending us the Dräger Alcotest 6820 breath analyzer (Dräger Safety AG & Co. KGaA. Lübeck, Germany) and Pago de Almaraes wineries for providing us with the wine used in the study. This study was supported by Research Projects PID2020-115184RB-I00, funded by MCIN/AEI/10.13039/501100011033, and A-FQM-532-UGR2, funded by FEDER/Junta de Andalucía-Consejería de Transformación Económica, Industria, Conocimiento y Universidades.

Periodic blur fluctuations effect on contrast sensitivity

Vahid Pourreza Ghoushchi*, Juan Mompeán, Pedro M. Prieto, Pablo Artal

Laboratorio de Óptica, Universidad de Murcia, Murcia, Spain.

*e-mail: vahid@um.es

This study investigates the resilience of human vision to the blurring effect induced by defocus oscillations. We applied sinusoidal oscillations in defocus with a range of amplitudes and temporal frequencies and determined the loss in contrast sensitivity. By inducing these defocus oscillations, we could compare them with natural accommodation fluctuations. We measured contrast sensitivity at 12 c/deg monocularly in five young, healthy emmetropic subjects through a tunable lens introducing sinusoidal oscillations of defocus around 0 D at 5, 15, and 25 Hz. Peak-to-peak oscillation amplitude varied from 0.15 D to 3 D. The visual stimulus was a Gabor patch at 3 m, and a two-choice forced-choice protocol was used. Target presentations were randomized through temporal frequency, amplitude, and contrast. The tunable lens was attached to an open-view Hartmann-Shack wavefront sensor [1,2] measuring in real time, thus allowing a) verification of the subject's accommodative state and b) confirmation of the amplitude and frequency of defocus oscillations generated by the lens.

The figure 1 illustrates the average contrast threshold as a function of amplitude for all subjects. Although there was some variability between subjects, contrast sensitivity was fairly constant despite the defocus oscillations introduced. Only for the fastest oscillations (25 Hz) and highest amplitude (+/-1.5 D) contrast sensitivity appears to suffer a relevant degradation.

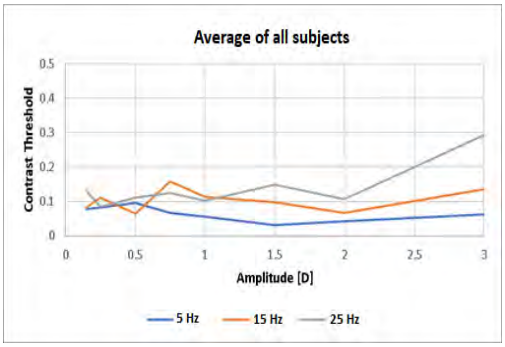

Figure 1. Mean contrast threshold for various defocus oscillations. The contrast sensitivity was fairly constant among the amplitudes introduced.

The data indicate that contrast sensitivity is resilient to induced periodic defocus. The fact that contrast sensitivity only appears to fall for fast and large oscillations in defocus suggests that the eye does not average blur and a short time with the image in or around the focus is enough to detect the target. These results have applications in electronic eyeglasses, visual simulators functioning based on fast periodic oscillations, and have implications in myopia control.

[1] V. P. Ghoushchi, J. Mompeán, P. M. Prieto, and P. Artal, Binocular dynamics of accommodation, convergence, and pupil size in myopes, *Biomed. Opt. Express* **12**, 3282 (2021).
[2] J. Mompeán, J. L. Aragón, P. M. Prieto, and P. Artal, GPU-based processing of Hartmann–Shack images for accurate and high-speed ocular wavefront sensing, *Futur. Gener. Comput. Syst.* **91**, 177 (2019).

Personalized computational models with OCT. Challenges and opportunities

A. de Castro[1, *], E. Martinez-Enriquez[1], P. Urizar[1,2], S. Marcos[1,3]

[1]*Instituto de Óptica, Consejo Superior de Investigaciones Científicas, Calle Serrano 121, Madrid, Spain.*
[2]*2Eyesvision, Plaza de la Encina 10, Tres cantos, Madrid, Spain.*
[3]*Center for Visual Science. The Institute of Optics, University of Rochester, 361 Meliora Hall, NY, USA.*

*e-mail: a.decastro@csic.es

The optics of the human eye can be modelled on a personalized basis with precise knowledge of the geometry of the cornea and crystalline lens surfaces and their index of refraction. While there has been interest in the development of personalized eye models during decades with Purkinje [1,2], Scheimpflug [3,4] or Optical Coherence Tomography images (OCT) [5], these eye models are not being used in clinical settings due to several disadvantages, such as the optical corrections needed to quantify the surfaces of the eye or the uncertainties in the knowledge of the gradient refractive index of the crystalline lens.

With the improvement on image quality and acquisition speed, OCT has become ubiquitous in the eye clinic, where this technique is used to image the retina and the anterior segment of the eye. In our group we have developed algorithms to segment the anterior and posterior surfaces of the cornea and the crystalline lens and to correct the optical distortions present in the image. However, OCT is a point scanning technique and motion can occur during the time a full volumetric scan. We have recently developed a model to simulate the acquisition of data and to study the influence of eye movements that can be used to quantify the precision achieved with different scanning patterns and to design eye motion correction algorithms.

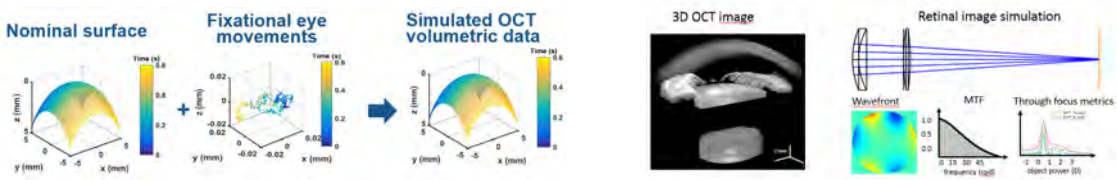

Figure 1. Left: OCT acquisition of the elevation is sequential and takes 0.6 seconds for one of our devices. Our model generates fixational eye movements in that time interval to simulate the OCT data acquired. Right: Volumetric image of the anterior segment and simulation of the retinal image with ray tracing software to study the optics of the post-cataract surgery optical system.

One of the applications of personalized eye models is to predict the outcome of a cataract surgery [6–8]. In this procedure, the crystalline lens is replaced by an intraocular lens (IOL) permanently and current methods to select the optical power of the IOL to implant rely on the outcome of previous surgeries and on assumptions regarding the corneal shape or the estimated lens position. IOL power formulas include empirical constants and need corrections in patients who do not meet the original assumptions of geometric relations in the eye (e.g. post-corneal surgery patients or very short or long axial lengths). In addition, when several IOL designs are possible, the decision of which IOL will be implanted is based on discussions about patient's need and expectations and not in the interactions between the lens design and the expected post-surgical corneal aberrations.

While in the clinical practice the process to select the IOL to be implanted have been improved over the years, computer eye models could be used for simulation of true retinal image quality with a particular IOL design on a personalized basis, allowing more accurate calculations of the optimal IOL power and a more customized IOL selection.

[1] J. Tabernero, P. Piers, A. Benito, M. Redondo, and P. Artal, *Invest Ophthalmol Vis Sci* **47**, 4651 (2006).
[2] P. Rosales and S. Marcos, *Opt Express* **15**, 2204 (2007).
[3] S. Norrby, *Ophthalmic and Physiological Optics* **25**, 153 (2005).
[4]. P. Rosales and S. Marcos, *J Refract Surg* **25**, 421 (2009).
[5] S. Ortiz, P. Perez-Merino, S. Duran, M. Velasco-Ocana, J. Birkenfeld, A. de Castro, I. Jimenez-Alfaro, and S. Marcos, Biomed *Opt Express* **4**, 387 (2013).
[6] C. Canovas and P. Artal, *Biomedical Optics Express* **2**, 1649 (2011).
[7] E. Martinez-Enriquez, P. Pérez-Merino, S. Durán-Poveda, I. Jiménez-Alfaro, and S. Marcos, *Scientific Reports* **8**, 9829 (2018).
[8] S. Marcos, E. Martinez-Enriquez, M. Vinas, A. de Castro, C. Dorronsoro, S. P. Bang, G. Yoon, and P. Artal, *Annual Review of Biomedical Engineering* **23**, 277 (2021).

Acknowledgements: PID2020-115191RB-100, IND2019/BMD-17262, H2020-ICT-2017 779960, NIH NIE P30EY 001319.

Enhanced second harmonic imaging of the living human eye using deconvolution

Rosa M. Martínez-Ojeda[1,*], Laurent M. Mugnier[2], Pablo Artal[1], Juan M. Bueno[1]

[1]*Laboratorio de Óptica, Universidad de Murcia, 30100 Murcia, Spain.*
[2]*ONERA / DOTA, Université Paris Saclay, F-92322 Châtillon, France.*

*e-mail: rosamaria.martinez9@um.es

Second harmonic generation (SHG) imaging is a form of nonlinear (or multiphoton) microscopy providing intrinsic confocality and reduced photodamage, without the use of staining procedures [1]. It is useful to visualize collagen-based tissues, in particular those of the eye [2]. Although broadly used with *ex vivo* samples, its implementation to image living human ocular structures has been successfully reported [3]. However, the presence of aberrations, scattering and non-controlled eye movements limit the imaging performance of this technique. Here, we present a deconvolution procedure to deal with these limitations and improve the quality of *in vivo* SHG images.

The 2nd generation of a compact clinically-adapted SHG microscope was developed to acquire images (0.45s exposure time) from different locations of the cornea and sclera of the living human eye. The whole system was controlled through custom software. The average laser power of the pulse illumination beam was 20 mW, more than 10 times below the maximum permissible exposure (according to ANSI Z136.1-2000). An image processing approach based on a marginal blind deconvolution algorithm [4] was applied to improve contrast and resolution of the recorded SHG images. It is based on a sound statistical framework that avoids the usual degeneracies encountered in blind deconvolution and makes it entirely unsupervised. Original and deconvolved images were compared and evaluated with different quality metrics.

The procedure was able to enhance the quality of the images independently of their location. As an example, Figure 1 compares SHG images before and after deconvolution. This leads to a better visualization of biological details while keeping the total intensity constant (i.e., energy conservation). Although the effectiveness and the increase in quality depended on the metric used, the improvement was readily observable for all imaged areas of the eye.

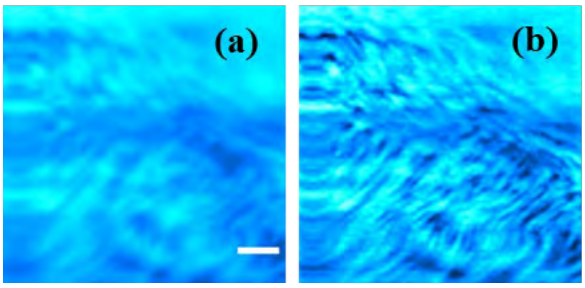

Figure 1. SHG images of the living human eye before (a) and after (b) deconvolution. Bar length: 50 μm.

In conclusion, a blind deconvolution scheme to enhance SHG images of the *in vivo* human eye has been presented. Details on the sample's morphology and structure that couldn't be observed in the original images were visible in the restored ones. Since collagen fibers are better visualized and their spatial distributions accurately assessed, this technique might serve as a clinical tool for early detection of pathologies associated with microscopic changes in tissue organization.

[1] Fine and Hansen, *Appl. Opt.* **10**, 2350 (1971).
[2] Bueno, Gualda and Artal, *Cornea* **30**, 692 (2011).
[3] Ávila, Gambín, Artal and Bueno, *Sci. Rep.* **9**, 10121 (2019).
[4] Blanco and Mugnier, *Opt. Express*, **19**, 23227 (2011).

Acknowledgements: This work was supported by the Agencia Estatal de Investigación, Spain (grants PID2019-105684RB-I00 and PID2020-113919RB-I00).

Optical sectioning in microscopy with structured illumination and single pixel detection

Luis Ordóñez*, Erick Ipus, Armin J. M. Lenz, Jesús Lancis, Enrique Tajahuerce

GROC-UJI, Institute of New Imaging Technologies (INIT), Universitat Jaume I, 12071, Castelló, Spain

*e-mail: lordonez@uji.es

The impact of microscopy has undergone an enormous advance in science. This could not be possible without new technologies that can increase the image resolution, allow us to measure many optical parameters such as the fluorescence emission, optical phase, wavelength, or polarization state, permit high-speed capture rates, and improve the penetration capability in scattering media [1]. In this work we design a new microscope with optical sectioning properties by combining two structured illumination techniques: structured illumination microscopy (SIM) and single-pixel imaging (SPI). As a first application we introduce optical sectioning capability on single-pixel fluorescence microscopy.

SIM techniques increase the image resolution and provides sectioning capability in conventional microscopy methods [2]. By projecting a small number of high frequency periodic fringe patterns with different phase onto the sample and combining the obtained images with the proper phase-shifting algorithm, it is possible to exclude the out of focus areas from the final image.

SPI techniques scan the scene with a set of structured light patterns while the transmitted, reflected, or fluorescence light is detected with a bucket detector [3]. They are advantageous for multidimensional imaging as well as in situations where the amount of light is scarce or a high temporal resolution is required [3]. In our optical configuration we use a DMD to project the light patterns onto the sample, which codify Walsh-Hadamard functions, and a photomultiplier tube (PMT) to detect the fluorescence light emitted by the sample.

Combining SIM and SPI makes optical sectioning possible in imaging with a bucket detector. The key idea is to employ a grating located before the photodetector. This configuration is designed starting from the conventional SIM configuration and exploiting the principle of Helmholtz reciprocity.

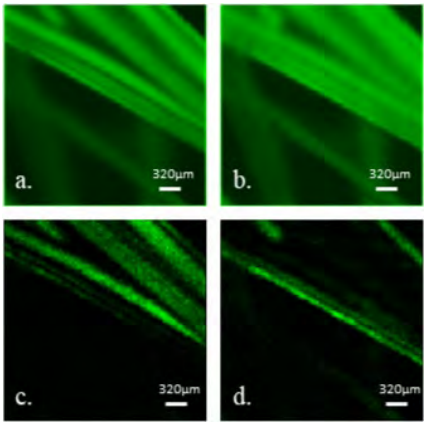

Figure 1. **(a)** and **(b)** are images of cotton fibres obtained with conventional single-pixel microscopy for two different focusing planes located at $z = 0$ and $10\mu m$, respectively. **(c)** and **(d)** are images of the same sample planes obtained with our microscope with optical sectioning.

Preliminary results of the fluorescent SPI and SIM techniques are presented (Fig. 1.) The sample is a set of cotton fibres with green fluorescent ink. Figures 1(a) and (b) show images of the sample focused on different depths, with an axial separation of 10 µm, obtained with a conventional single-pixel microscopy. The two images show cotton fibres located at different distances that appear strongly defocused. Figures 1(c) and (d) show images of the same planes of the sample but obtained with the new single-pixel microscopy technique. Now only the focused cotton fibres in each axial plane are clearly visible. All images have a size of 128x128 pixels.

In summary, we present the principles and implementation of a SPI fluorescence microscope with optical sectioning based on a SIM technique. By combining the high-speed binary modulation of the DMD, a high frequency grating, and the high photosensitivity of the PMT, we are able to image fluorescence samples using structured illumination. Our experimental results show an optical sectioning capability similar to that obtained with conventional SIM techniques with a digital camera.

[1] J. Mertz; *Introduction to Optical Microscopy* (Cambridge University Press, 2019).
[2] D. Dan et al., "DMD-based-LED-illumination super-resolution and optical sectioning microscopy," *Sci. Rep.* **3**, 1116 (2013).
[3] M.P. Edgar et al., "Principles and prospects for single-pixel imaging," *Nat. Photon.* **13**, 13-20 (2019).

Acknowledgements: We acknowledge financial support from Agencia Estatal de Investigación (PID2019-110927RB-I00/AEI/10.13039/501100011033) and Generalitat Valenciana (PROMETEO/2020/029, ACIF/2019/019).

Advances in Fourier Lightfield Microscopy

Manuel Martínez-Corral

3D Imaging and Display Lab., Department of Optics, University of Valencia, 46100 Burjassot, Spain.

e-mail: Manuel.martinez@uv.es

Conventional microscopes have the ability of capturing 2D images of small specimen with high magnification and spatial resolution. This feature is determined by the numerical aperture (NA) of the microscope objective. The main drawback of conventional microscopes is their poor performance for imaging 3D structures. This lack is somehow overcame by capturing stacks of depth images and computing from them the 3D image. The main disadvantage of this procedure is the need of an axial scanning.

In the past few years Lightfield Microscopy (LFM) is showing to be a powerful tool for the recovery of 3D images of samples in a high-speed regime. In few words, an LFM is the result of inserting a microlens array (MLA) at the image plane of a conventional microscope. The images captured by the LFM are composed by a collection of microimages, one per microlens, which store the spatial and de angular information of the light emitted by the sample. Then, a collection of perspective images is computed from the microimages. The main drawback of LFMs is that they provide, after the hybrid (optical plus computational) procedure, images with a spatial resolution that is about 10 times worse that than of the host microscope. Other drawback is the inhomogeneous lateral resolution of computed depth sections. Naturally, much work has been reported aiming to overcome these drawbacks by computational means.

To overcome these drawbacks, Fourier Lightfield Microscopy (FLMic) was proposed. In FLMic the perspective images are captured directly, have a spatial resolution that is about 3 times better than that of LFMs, and have shift invariance. This allows the direct use of deconvolution tools and to avoid the inhomogeneity of depth sections. Other advantage of FLMic is that it can be implemented by inserting an ad-on at one microscope port, and therefore allows to makes use of all the facilities of the microscope.

Along the past few years FLMic has attracted a great interest in the scientific and technological community due to its potential utility in the observation of 3D dynamic processes.

In this contribution we explain the ray-optics theory behind Lightfield concept, and combine it with the wave-optics nature of microscopy applications. We show, also, how to compute these images for obtaining refocused depth images, and also 3D depth maps. Finally, the most recent contributions are reviewed.

[1] B. Javidi et al., Roadmap on 3D integral imaging: Sensing, processing, and display, *Optics Express* **28**, 32266 (2020).

[2] M. Martinez-Corral and B. Javidi, Fundamentals of 3D imaging and displays: a tutorial on integral imaging, light-field, and plenoptic systems, *Advances in Optics and Photonics* **10**, 512 (2018).

Acknowledgements: This research was funded by Grant RTI2018-099041-B-I00, which is cofounded by the Ministerio de Ciencia, Innovacion y Universidades (Spain) and by European Regional Development Fund; by Generalitat Valenciana (Spain) under Grant PROMETEO/2019/048.

Quantum imaging with a photon number resolving camera

Víctor Bernardo Puente

Hamamatsu Photonics France, Spain & Portugal office, C. Argenters 4 edif 2,
Parque Tecnológico del Vallés, 08290 Cerdanyola, Spain.

e-mail: vbernardo@hamamatsu.es

We wish to demonstrate the application of a qCMOS detector, capable of performing quantum enhanced imaging by photon counting. Presenting this work will be beneficial in allowing investigators consider the potential applications of the qCMOS technology in the quantum imaging domain.

Until now, quantum enhanced imaging schemes were realized through correlations between single photons. Due to the limiting readout noise of CCD and CMOS technologies, our ability to count photons was reduced to distinguishing between zero photons and one or more. Acquisition speeds were therefore limited by both the readout rate of the detector array, and the necessity of operating in an extremely sparse regime.

However, the recent development of a qCMOS camera that is capable of photon number resolving due to its low readout noise, has enabled quantum enhanced imaging at higher illumination regimes. Operating in such a way will allow an increased data acquisition rate, accelerating the development of quantum enhanced imaging schemes for their implementation into end-user technologies.

Computer generated training datasets for deep learning applications to ESPI fringe patterns, using true speckle simulation

J. M. Crespo*, V. Moreno

QMatterPhotonics Research Group. Optics Area. Department of Applied Physics. Faculty of Physics / Faculty of Optics and Optometry. University of Santiago de Compostela. E-15782 Santiago de Compostela. Galicia. Spain.

*e-mail: josemanuel.crespo.continas@rai.usc.es

Over the last few years, the ongoing innovation in the field of artificial intelligence (AI) and artificial neural networks (ANN), as well as the development of IT frameworks such as Tensorflow, PyTorch and Keras, have eased the application of these techniques in different fields of scientific research. This simplification in the tools and the reduction of costs of specialized hardware platforms, allows the application of this technology by researchers and students, reducing the workload to develop those AI systems to focus on the problem to solve, and not on the tools supporting that resolution.

Specifically in the field of optical interferometry, these systems have great possibilities for noise removal and image cleaning [1,2], although their great drawback is the need for large datasets of images for training. While for application in biomedical sciences or satellite image processing there are open databases to use in the training phases. In the field of interferometry these training sets are scarce and limited, making necessary generate the training sets using simulation techniques.

Our interferometric use case to apply these AI techniques is the electronic speckle pattern interferometry (ESPI), widely used as optical metrology technique to measure displacement and deformation measurement. Noise, and low visibility are major drawbacks for this technique and the AI has been proved as disruptive technique to enhance and mitigate those major drawbacks.

The ESPI fringe pattern is obtained from a pair of images, I and I', taken from a specimen under study before and after deformation. The fringe pattern is obtained subtracting those images and the resulting intensity pattern is according to the formula [3]

$$|I - I'| = 4\sqrt{I_o I_r}\sin\left(\phi_o - \phi_r + \frac{\varphi}{2}\right)\sin\left(\frac{\varphi}{2}\right)$$

with $I_o, I_r, \phi_o,$ and ϕ_r the amplitude and phase of the object and reference speckle fields, and φ is the optical phase difference induced by the deformation. For the estimation of φ our approach is to use random Zernike polynomials to build the random phase, $\varphi = \sum_0^n c_i Z_i$, where c_i and Z_i are a random coefficient and the i-Zernike polynomial respectively and n is the order of the Zernike expansion. With this approach, any displacement field can be simulated, setting the proper interval for c_i and moreover, selecting the order of the Zernike expansion will control the complexity of the simulated displacement.

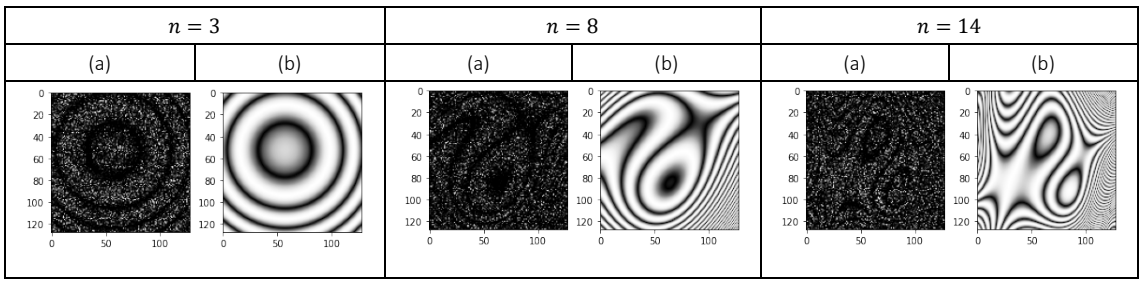

Figure 1. Generated images using Zernike order (n=3, 8, 14) showing increasing complexity. (a) ESPI image using equation (1) and speckle simulation according to the method described by J Goodman [3]. (b) Clean $\sin(\varphi/2)$.

[1] Fungui Hao, Chen Tang, Ming Xu, *Applied Optics* **58**, 3338 (2019).
[2] Crespo J. M., Moreno V., Rabuñal Juan Ramón, Pazos Alejandro, Canabal Carbia Monica. *EOS Annual Meeting (EOSAM 2020)*,115 (2020)
[3] Joseph W. Goodman, *Speckle phenomena in optics*, SPIE (2020).

Desarrollo de un sistema de procesado láser 3D asistido por robot para la eliminación de pintura

Angel Rodríguez, **Ana J. López***, Javier Lamas, Alicia Moreno, Alberto Ramil

Laboratorio de Aplicacións Industriais do Láser, Campus Industrial de Ferrol, Universidade da Coruña. 15471, Ferrol, A Coruña, España.

*e-mail: ana.xesus.lopez@udc.es

La limpieza con láser es una técnica que permite la eliminación controlada de contaminantes superficiales de un material. Desde la década de los 80, se ha aplicado en diferentes campos industriales, como el aeroespacial, automoción, así como en biomedicina, o la conservación del Patrimonio Cultural, entre otros[1,2]. En comparación con los métodos convencionales, la limpieza láser tiene la ventaja de ser una técnica selectiva sin contacto y respetuosa con el medio ambiente. Además, combinada con robots industriales, puede utilizarse para eliminar con precisión los contaminantes en estructuras grandes y complejas, lo que mejora en gran medida la calidad y la eficiencia de la técnica. Sin embargo, el procesado láser automatizado de superficies no planas o superficies 3D no es un tema completamente resuelto y la mayoría de las soluciones propuestas se basan en aproximaciones cuasi 3D o 2.5D[3]. En este trabajo se presenta un sistema de limpieza láser asistido por robot para el procesado de superficies 3D, basado en la integración de un brazo robótico de 6 grados de libertad (6 DOF) con un láser de pulsos ultracortos y un sistema de captura tridimensional de la superficie que permite generar automáticamente las trayectorias del haz láser sobre la superficie asegurando en todo momento la incidencia normal y el control de los distintos parámetros del proceso[4]. El manipulador de 6 GDL permite tanto el desplazamiento como el cambio de orientación del objeto para que el procesado láser se lleve a cabo siguiendo las rutas programadas en una verdadera solución 3D[5]. Tanto el software como el hardware para coordinar el robot y el encendido/apagado del láser fueron desarrollados con enfoque FOSS y, en la medida de lo posible OSHW. Los resultados experimentales muestran la efectividad del sistema propuesto que mejora la eficiencia de la limpieza láser automatizada de objetos 3D y permite su aplicación a otros procesos de ablación láser como el micromecanizado o estructurado de superficies.

[1] Rivas T, Pozo S, Fiorucci MP, López AJ, Ramil A. Nd:YVO4 laser removal of graffiti from granite. Influence of paint and rock properties on cleaning efficacy. *Applied Surface Science* **263**, 563 (2012). https://doi.org/10.1016/j.apsusc.2012.09.110.

[2] Zhang D, Xu J, Li Z, Li K, Wang C, Shan D, et al. Removal mechanism of blue paint on aluminum alloy substrate during surface cleaning using nanosecond pulsed laser. *Optics and Laser Technology* **149** (2022). https://doi.org/10.1016/J.OPTLASTEC.2022.107882.

[3] López AJ, Lamas J, Pozo-Antonio JS, Rivas T, Ramil A. Development of processing strategies for 3D controlled laser ablation: Application to the cleaning of stonework surfaces. *Optics and Lasers in Engineering* **126**, 105897 (2020). https://doi.org/10.1016/J.OPTLASENG.2019.105897.

[4] Lamas J, Ramil A, Yañez A. Smoothing and simplification algorithm for Computer Aided Manufacturing paths with complex curves. *IFAC Proceedings Volumes* (IFAC-PapersOnline), vol. 4, IFAC Secretariat, p. 61 (2009). https://doi.org/10.3182/20091006-3-es-4010.00013.

[5] Rodríguez A, López AJ, Lamas J, Moreno A, Ramil A. Development of a laser cleaning robot system for the processing of 3D surfaces. In: Negahdaripour S, Stella E, Ceglarek D, Möller C, editors. *Multimodal Sensing and Artificial Intelligence: Technologies and Applications II*, SPIE, p. 28 (2021). https://doi.org/10.1117/12.2592111.

Agradecimientos: Este trabajo ha sido parcialmente financiado por el Ministerio de Economía y Competitividad a través del Proyecto BIA2017 8589 R

Synchronous phase detection technique for the evaluation of complex functions displayed on a phase-only modulator

Esther Nabadda[1,*], Pascuala García-Martínez[2], María del Mar Sánchez-López[1,3], Ignacio Moreno[1,4]

[1]*Instituto de Bioingeniería, Universidad Miguel Hernández de Elche, 03202 Elche, Spain.*
[2]*Departamento de Óptica y Optometría y Ciencias de la Visión, Universitat de València, 46100 Burjassot, Spain.*
[3]*Departamento de Física Aplicada, Universidad Miguel Hernández de Elche, 03202 Elche, Spain.*
[4]*Dept. Ciencia de Materiales, Óptica y Tec. Electrónica, Universidad Miguel Hernández de Elche, 03202 Elche, Spain.*

*e-mail:enabadda@umh.es

In this work we combine an encoding method to display complex valued holograms onto a phase-only spatial light modulator (SLM) with a phase-shifting interferometric (PSI) technique for experimentally evaluating the generated complex valued optical fields. Increase in the potential applications of the so-called structured light has drawn great attention to this area of research. One key element is the liquid-crystal (LC) spatial light modulator (SLM) that, under illumination with linearly polarized light parallel to the LC director, produces a phase-only modulation. Using a 2D grating encoding technique [1], the SLM can be used to display complex valued diffractive elements. In most of the cases, the successful generation of the complex hologram is verified by regarding the light intensity distribution in the far field. In cases where the phase distribution is of interest, it is measured typically with a wave-front sensor or through an external interferometer that are added to the system generating the structured light, thus increasing the complexity of the setup.

Here, we demonstrate an efficient common-path polarization interferometer based on the SLM itself, not requiring any external additional element. The same setup can be used to simultaneously display the complex hologram and to apply the phase-shifting values required to retrieve the phase distribution. A simple rotation of a polarizer changes from the intensity configuration to the interferometer configuration. The continuous phase modulation provided by the SLM allows using arbitrary phase bias values, so different classical PSI algorithms [2] can be applied to recover the phase information. The figure shows different examples of the experimental realization of complex light beams based on the coaxial superposition of Laguerre-Gaussian beams. In each case the experimental intensity and phase distributions in the far field reproduce very well the theoretical results, thus confirming the validity of the technique.

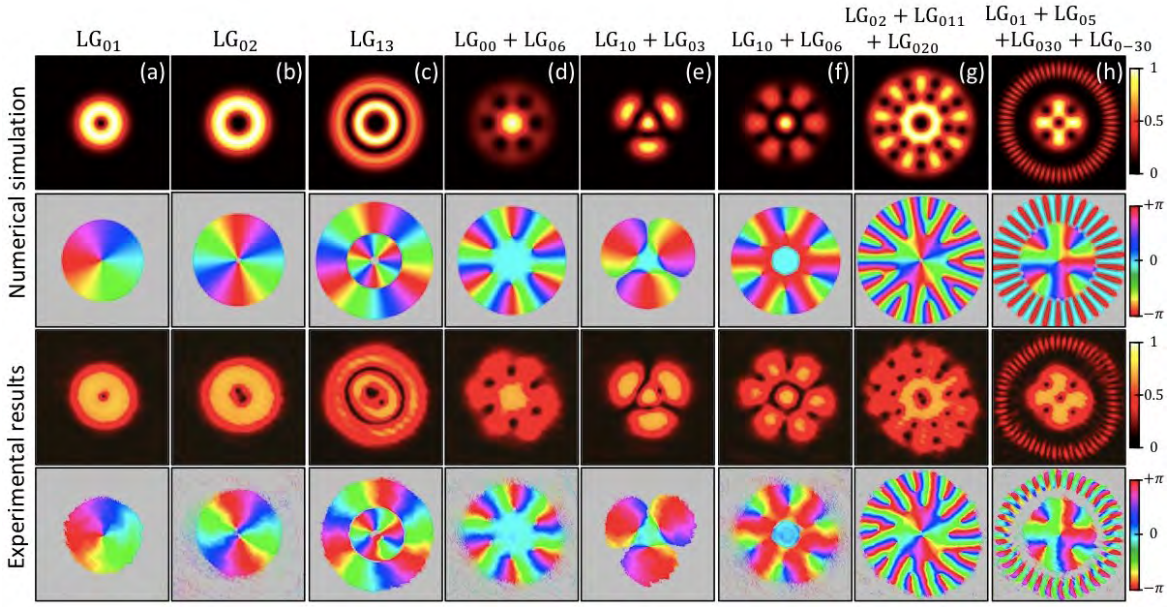

Figure 1. Realization of different superpositions of Laguerre-Gaussian beams. First and second row show simulations of the intensity and phase distributions. Third and fourth rows show the corresponding experimental results.

[1] J. A. Davis, E. D. Wolfe, I. Moreno, D. M. Cottrell, Encoding complex amplitude information onto phase-only diffractive optical elements using binary phase Nyquist gratings, *OSA Continuum* **4**(3), 896 (2021).
[2] K. Creath, Phase-measurement interferometry techniques, *Prog. Optics* **26**, 349 (1988).

Acknowledgements: This work received financial support from MICIN (grant project RTI2018-097107-B-C33). E.N. acknowledges a grant from GV (ref. GRISOLIAP/2020/004).

Proof-of-concept depolarization emulator based on a liquid-crystal spatial light modulator

María del Mar Sánchez-López[1,*], David Marco[1], Guadalupe López-Morales[2], Ángel Lizana[3], Juan Campos[3], Ignacio Moreno[1]

[1]*Instituto de Bioingeniería, Universidad Miguel Hernández de Elche, Spain.*
[2]*Instituto de Investigación en Energías Renovables, Universidad de Ciencias y Artes de Chiapas, México.*
[3]*Departamento de Física, Universitat Autònoma de Barcelona, Spain.*

*e-mail: mar.sanchez@umh.es

There is an increasing interest in studying depolarization indices as channels to improve the image of biological samples [1]. Emulating depolarization effects with controlled precision can help to understand the depolarization mechanisms in these samples. In this work we demonstrate a proof-of-concept depolarization emulator that generates customized spatial patterns of the state of polarization (SoP) and degree of polarization (DoP). The technique is based on sequentially addressing two phase masks to a pixelated liquid-crystal spatial light modulator (SLM), in a time interval that is chosen to be the exposure time of our detector. The polarization properties of the output beam are verified by imaging the SLM screen onto a polarization camera and applying Mueller matrix imaging polarimetry, as shown in Fig. 1. The effective Mueller matrix of the SLM can be regarded as the averaged sum of two linear retarders with spatially-varying retardances $\phi_A(\mathbf{x})$ and $\phi_B(\mathbf{x})$, with $\mathbf{x}$=(x,y) being the spatial coordinates in the SLM. The effective SoP of the output beam is governed by the averaged retardance, while the DoP is governed by the retardance semi-difference $\overline{\delta(\mathbf{x})} = (\phi_A(\mathbf{x}) - \phi_B(\mathbf{x}))/2$. Further details are given in [2].

As an example, Fig.1 illustrates the two phase patterns sequentially addressed to the SLM encoding a word with gradually varying DoP. The phase value in some letters is indicated and the average retardance is $\bar{\phi} = 3\pi$ in all cases. The input state to the SLM is linearly polarized at 45º. Fig.1(c) shows on the Poincaré sphere (PS), and for each letter, the expected output states $\mathbf{S}_A$ (blue dots) and $\mathbf{S}_B$ (purple dots) generated by each pattern, and the theoretical averaged SoP (black dots). The averaged states lie all on the S_2 axis, with an effective DoP that changes gradually from one letter to the next according to $|\cos\bar{\delta}|$. For letters D and N the semi-difference phase is $\bar{\delta} = \pi/4$ and $\bar{\delta} = 3\pi/4$, hence their effective DoP is $\mathrm{DoP}_{\langle \mathbf{S}_e \rangle} = 1/\sqrt{2}$, while for letter R $\bar{\delta} = \pi/2$ and the output becomes fully depolarized. These results are confirmed experimentally by measuring the effective Stokes parameter S_2 and the effective DoP of the output beam, as shown in panels (d,e).

This technique could be useful in testing imaging polarimeters and in biomedical imaging.

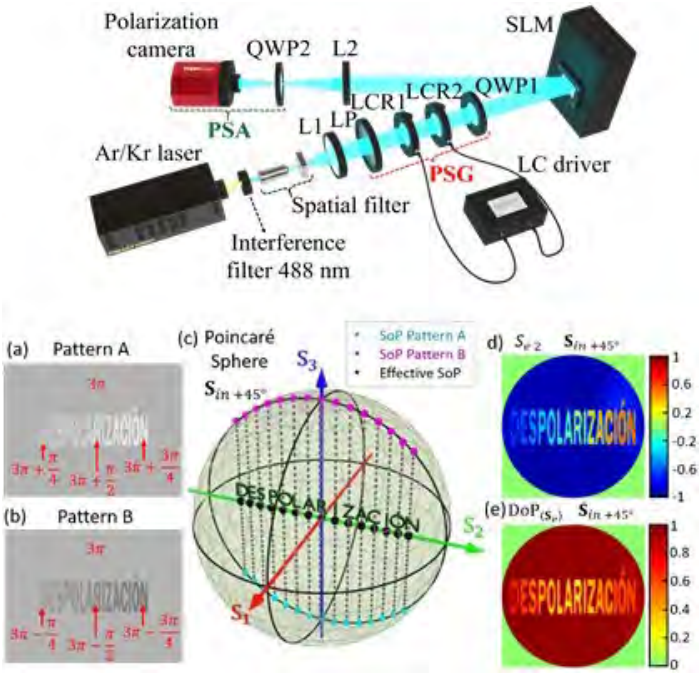

Figure 1. Scheme of the imaging Mueller polarimeter. (a,b) Phase patterns encoding a text, (c) theoretical Stokes parameters on the PS, (d,e) experimental effective Stokes parameter S_2 and DoP of the output beam.

[1] A. Lizana, A. Van Eeckhout, K. Adamczik, C. Rodriguez, J.C. Escalera, E. Garcia-Caurel, I. Moreno and J. Campos, *J. Biomed. Opt.* **22**, 056004 (2017).

[2] D. Marco, G. López-Morales, M.M. Sánchez-López, Á. Lizana, I. Moreno and J. Campos, *Scientific Reports* **11**, 9415 (2021).

Acknowledgements: This work received financial support from MICIN (RTI2018-097107-B-C33 and –C31).

Quality metrics in holographic lenses recorded in a low toxicity photopolymer

Tomás Lloret[1,2,*], Víctor Navarro-Fuster[3], Marta Morales-Vidal[1], Manuel G. Ramírez[1], Kheloud Berramdane[1], José Carlos García-Vázquez[2], Inmaculada Pascual[1,2]

[1]*Instituto Universitario de Física Aplicada a las Ciencias y las Tecnologías, Universidad de Alicante, Carretera San Vicente del Raspeig s/n, 03690 San Vicente del Raspeig, España.*
[2]*Departamento de Óptica, Farmacología y Anatomía, Universidad de Alicante, Carretera San Vicente del Raspeig s/n, 03690 San Vicente del Raspeig, España.*
[3]*Departamento de Física, Ingeniería de Sistemas y Teoría de la Señal, Universidad de Alicante, Carretera San Vicente del Raspeig s/n, 03690 San Vicente del Raspeig, España*

*e-mail: tomas.lloret@ua.es

Holographic Lenses (HLs) are holograms obtained from the interference of an object point (object beam) and a plane beam (reference beam). Unlike conventional refractive lenses (RLs), their physical principle is diffraction, and in addition to spectral dependence, they also exhibit angular dependence [1]. One of the main applications of such HLs is their use in AR optical systems such as head mounted displays (HMD).

HLs also exhibit aberrations [2]. To measure the impact of these aberrations, diffraction efficiency is not a suitable optical parameter. For this purpose, different quality metrics can be used. In this work, the quality of positive symmetrical and negative asymmetrical HLs has been evaluated by studying different metrics: optical quality metrics (Zernike and Seidel coefficients, RMS for Zernike and Seidel aberrations, and critical pupil fraction (PF)); and image quality metrics based on the impulse response of the system (Strehl Ratio (SR), Entropy and cut-off frequency) [3]. The results obtained can be seen in Table 1.

	Positive Symmetrical HLs					Negative Asymmetrical HLs				
Zernike Coef. (μm)	C_4^0	C_2^{-1}	C_3^1	C_2^{-2}	C_2^2	C_4^0	C_2^{-1}	C_3^1	C_2^{-2}	C_2^2
	$-9 \cdot 10^{-3}$	$1.1 \cdot 10^{-1}$	$-2.2 \cdot 10^{-2}$	$-1.8 \cdot 10^{-1}$	0	$-6 \cdot 10^{-3}$	$2.3 \cdot 10^{-2}$	$-6 \cdot 10^{-3}$	$-1.5 \cdot 10^{-6}$	$-7 \cdot 10^{-6}$
Seidel Coef. (μm)	S		C		A	S		C		A
	$8.05 \cdot 10^{-5}$		$2.21 \cdot 10^{-3}$		$6.06 \cdot 10^{-2}$	$-8.05 \cdot 10^{-5}$		$-1.94 \cdot 10^{-5}$		$3.01 \cdot 10^{-7}$
RMS Zernike (μm)	0.209					0.030				
RMS Seidel (μm)	0.011					$1.56 \cdot 10^{-5}$				
PF	0.063					0.25				
SR	0.124 (~12%)					0.856 (~86%)				
Normalized Entropy (10^{-3})	7.7					1.7				
Theoretical Cutoff Freq. (cycles/degree)	68.2					110.7				

Table 1. Optical and image quality metrics for positive symmetrical and negative asymmetrical HLs.

The best results were obtained for negative asymmetrical HLs, therefore their geometry is the most suitable for optical imaging systems.

[1] T. Lloret, V. Navarro-Fuster, M.G. Ramírez, M. Ortuño, C. Neipp, A. Beléndez, and I. Pascual, Holographic Lenses in an Environment-Friendly Photopolymer, *Polymers* **10** (3), 302 (2018).
[3] T. Lloret, V. Navarro-Fuster, M.G. Ramírez, M. Morales-Vidal, A. Beléndez, and I. Pascual, Aberration-Based Quality Metrics in Holographic Lenses, *Polymers* **12** (4), 993 (2020).
[2] P. Artal, *Handbook of Visual Optics* Vol. II (CRC Press, Abingdon UK, 2017).

Acknowledgements: This research was funded by Ministerio de Ciencia, Innovación y Universidades, Spain, under project PID2019-106601RB-I00; Generalitat Valenciana, Spain, under projects CDEIGENT/2018/024, PROMETEO/2021/006, and IDIFEDER/2021/014 (co-funded by European Union through the FEDER Programme); Universidad de Alicante, Spain, under UAFPU20-23.

Reflection gratings stored in a nanoparticle-doped photopolymer

José Carlos García-Vázquez[1,*], Manuel G. Ramírez[2], Kheloud Berramdane[2], José Solla-Gullón[3], Marta Morales-Vidal[2], Tomás Lloret[1], Inmaculada Pascual[1,2]

[1]*Departamento de Óptica, Farmacología y Anatomía, Universidad de Alicante,Carretera San Vicente del Raspeig s/n, 03690 San Vicente del Raspeig, Spain.* [2]*I.U. Física Aplicada a las Ciencias y las Tecnologías Universidad de Alicante, Ap.99, Alicante E-03080.* [3] *Instituto de Electroquímica, Universidad de Alicante, Ap.99, Alicante E-03080, Spain.*

*e-mail: jcgv5@alu.ua.es

Nowadays, the study and optimization of volume holography reflection gratings stored in environmentally compatible photopolymers has a great interest since they can be used as holographic optical elements. One of the main advantages of reflection holograms is that they can be reconstructed using white light. This allows to develop holographic sensors [1]. Unslanted reflection holograms have been stored in an acrylate-poly(vinyl alcohol) based photopolymer development in our research group [2]. With the main objective of increasing the diffraction efficiency of reflection holograms, a series of chemical modifications have been introduced in the same acrylated-based photopolymer. Specifically, this material has been doped with Platinum nanoparticles (Pt-NP), increasing the refractive index modulation in the recorded diffraction gratings. A solid-state laser emitting at 455 nm was employed for stored the unslanted reflection gratings at high spatial frequencies.

Figure 1 shows the transmittance as a function of reconstruction wavelength for doped and undoped photopolymer films. The increase in diffraction effciency is clearly observed when the photopolymer is doped with Pt nanoparticles compared to the value obtained for the undoped photopolymer. A blue-shift wavelength for maximum diffraction effciency is observed in the Pt doped grating. The experimental values are fitted according to Kogelnik's Coupled Wave Theory [3] in order to obtain the optical parameters that described the reflection gratings. Doping with the Pt-NP nanoparticles produces a change in the average refractive index that gives rise to the blue-shift wavelength and an increase in the refractive index modulation that produces a greater diffraction efficiency.

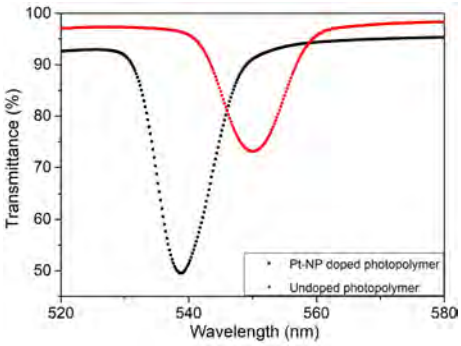

Figure 1: Transmittance as a funtion of reconstruction wavelength for a Pt doped grating (black) and an undoped grating (red).

[1] Yetisen, A. K., Naydenova, I., da Cruz Vasconcellos, F., Blyth, J., & Lowe, C. R. . Holographic Sensors: Three-Dimensional Analyte-Sensitive Nanostructures and Their Applications. Chemical Reviews, 114, 10654-10696 (2014).

[2] Ramírez, M. G., Sirvent, D., Morales-Vidal, M., Ortuño, M., Martínez-Guardiola, F., Francés, J., & Pascual, I. LED-Cured Reflection Gratings Stored in an Acrylate-Based Photopolymer. Polymers, 11, 632 (2019).

[3] Kogelnik, H. Coupled Wave Theory for Thick Hologram Gratings. *The Bell System Technical Journal*, 48, 2909-2948 (1969).

Funding: This research was funded by Ministerio de Ciencia, Innovación y Universidades, Spain, under project PID2019-106601RB-I00; Generalitat Valenciana, Spain, under projects CDEI-GENT/2018/024, PROMETEO/2021/006, and IDIFEDER/2021/014 (co-funded by European Union through the FEDER Programme).

Redes plasmónicas unidimensionales de nanopartículas de oro a partir de redes de relieve fabricadas holográficamente

Jose C. Mira-Martínez[1,*], Víctor Bonal[1], José A. Quintana[2], José M. Villalvilla[1], Pedro G. Boj[2], María A. Díaz-García[1]

[1]*Departamento de Física Aplicada, Universidad de Alicante, 03080 Alicante, España.*
[2]*Departamento de Óptica, Farmacología y Anatomía, Universidad de Alicante, 03080 Alicante, España.*

*e-mail: carlos.mira@ua.es

En los últimos años, las nanopartículas de oro han logrado captar la atención en el campo de la fotónica debido a sus diversas propiedades ópticas. La resonancia del plasmón superficial permite realizar medidas cuantitativas de procesos superficiales, particularmente útil en el desarrollo de sensores de película delgada, de una manera simple y con alta sensibilidad.

Las estructuras fotónicas basadas en nanopartículas metálicas son buenas candidatas en la aplicación de nanodispositivos ópticos debido a su interacción con la luz. Entre sus diversas propiedades, pueden destacarse el guiado de luz a escala nanoscópica o una fuerte amplificación del campo en volúmenes muy pequeños. Existen diferentes estructuras posibles, siendo las redes unidimensionales formadas por nanopartículas metálicas una de las más estudiadas en los últimos años.

En este trabajo se presenta un método novedoso de fabricación de redes plasmónicas unidimensionales de nanopartículas de oro, que pueden tener espaciados de red (periodo) de tan solo 200 nm. El método se basa en un procedimiento desarrollado en nuestro grupo de investigación para la fabricación de redes de relieve en gelatina dicromatada (DCG), consistente en el uso de litografía holográfica y posterior revelado en un plasma de oxígeno [1]. Para la obtención de las nanopartículas de oro se utiliza $HAuCl_4$ como precursor, añadido en una de las etapas del anterior proceso, utilizando además tratamientos térmicos posteriores controlados para favorecer la nucleación.

La formación de nanopartículas fue monitorizada a través de espectroscopia de absorción en diferentes partes del proceso (ver Figura 1). Por otro lado, la distribución de las nanopartículas de Au en función de los parámetros del proceso se estudió mediante imágenes de electrones retrodispersados de microscopía electrónica de barrido (SEM), Figura 2.

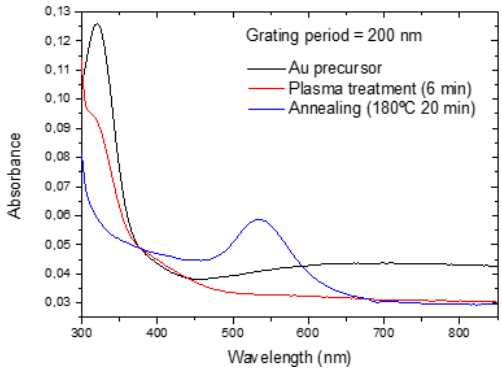

Figura 1. Espectro de absorción de una muestra al introducir el precursor de oro (línea negra), tratamiento de plasma (línea roja) y tratamiento térmico a 180 ºC durante 20 min (línea azul).

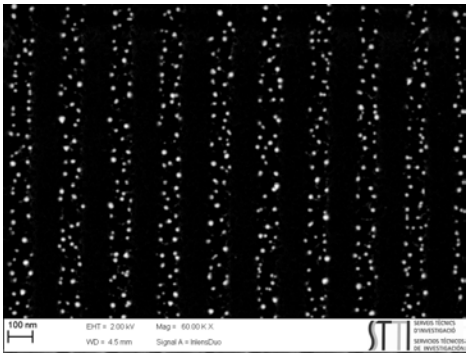

Figure 2. Imagen de BS-FESEM de una red de 200 nm tras un tratamiento en plasma de oxígeno durante 3 min y un tratamiento térmico de 120 ºC durante 8 horas.

[1] J. A. Quintana et al., *Optical Mater* **5**, 1700238 (2017).

Latest advances in organic distributed feedback lasers with top-layer resonators

V. Bonal[1,*], J. A. Quintana[2], J. M. Villalvilla[1], P. G. Boj[2],
R. Muñoz-Mármol[1], J. C. Mira-Martínez[1], M. A. Díaz-García[1]

[1]*Departamento de Física Aplicada, Instituto Universitario de Materiales de Alicante, Universidad de Alicante, 03080 Alicante, Spain.* [2]*Departamento de Óptica, Farmacología y Anatomía, Instituto Universitario de Materiales de Alicante, Universidad de Alicante, 03080 Alicante, Spain.*

*e-mail: victor.bonal@ua.es

Distributed feedback lasers (DFB) are some of the most studied thin film organic lasers, as they are cost-efficient, compact, and easily integrated with other devices. This allows them to be used for a wide range of applications, such as spectroscopy, optical communications, and sensing [1]. DFB lasers typically consist in an active material thin film deposited over a grating engraved in an inorganic substrate. However, DFB lasers can present different architectures depending on the position of the resonator and the materials used for its fabrication.

Here, we study a different DFB architecture with a polymeric resonator deposited on top of the active film [2]. This architecture offers several advantages over the standard one. The device is easier to fabricate, as both films are organic and solution-processable. Additionally, the active film presents a uniform thickness, and the grating period can be easily adjusted for each case as it is fabricated using holographic lithography. In this work, we are going to focus on the influence of the different grating parameters on the final device characteristics, in order to optimize the threshold and efficiency of the devices [3]. Additionally, we are going to explore the capabilities of this architecture to fabricate deep-blue-emitting lasers [4] and we to compare these devices with the standard configuration ones to further explore the advantages of this architecture and the differences between them [5].

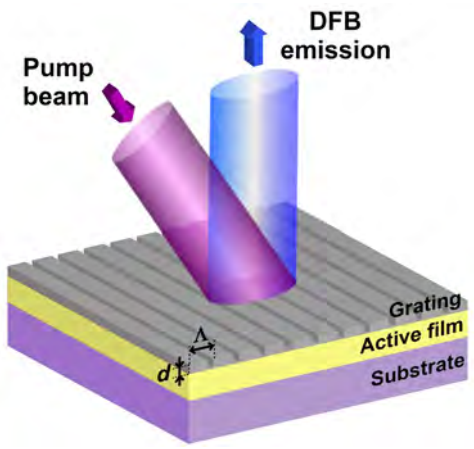

Figure 1. Scheme of the DFB device architecture, including pumping and collection geometry (Λ: grating period; d: grating depth).

[1] Kuehne, A. J. C. & Gather, M. C., *Chem. Rev.* **116**, 12823 (2016).
[2] Quintana, J. A. *et al*., *Adv. Opt. Mater.* **5**, 1700238 (2017).
[3] Bonal, V., Quintana, J. A., Villalvilla, J. M., Boj, P. G. & Díaz-García, M. A., *Sci. Rep.* **9**, 11159 (2019).
[4] Bonal, V. *et al.*, *Adv. Opt. Mater.* **8**, 2001153 (2020).
[5] Bonal, V. *et al.*, *Polymers* **13**, 3843 (2021).

Acknowledgements: Funding from Spanish Ministry of Science and Innovation (grant no. PID2020-119124RB-I00) and Conselleria de Innovación, Universidades, Ciencia y Sociedad Digital de la Comunidad Valenciana (grant no. AICO/2021/093). We also thank V. Esteve and I. Garcés for technical assistance.

Manipulating the second order coherence function for super-resolution intensity correlation imaging

Enrique J. Fernandez*, Iryna Standret, Pien Vinke, Juan M. Bueno

Laboratorio de Óptica, Instituto Universitario de Investigación en Óptica y Nanofísica, Universidad de Murcia, Campus de Espinardo (Edificio 34), E-30100, Murcia, Spain

*e-mail: enriquej@um.es

The Hanbury Brown-Twiss (HB-T) effect evidenced the existence of correlations in the near instantaneous intensities measured at separated space and time points of the light emitted from a thermal light source [1]. The quantum interpretation of the effect was capital for the development and understanding of photon entanglement. Intensity correlation imaging, in both classical and quantum frame, uses second-order or higher coherence of entangled photons, for instance in ghost imaging. In general, two-photon and intensity correlation imaging modalities can be modelled as the convolution of the aperture function of the object with the second order coherence function $G^{(2)}$ [2]:

$$R_{im}(\vec{r}_{im}) = \int_{OBJ} d\vec{r}_{obj} \left| Aper(\vec{r}_{obj}) \right|^2 G^{(2)}(\vec{r}_{obj}, \vec{r}_{im}).$$

In this work we demonstrated a system with a modified second order coherence function $G^{(2)}$ to increase the spatial resolution in intensity correlation imaging modalities. Figure 1 shows a diagram of the experimental set up. By using a paraxial biprism, two virtual images S_1 and S_2 from a thermal light source S_0 were created. A CCD camera was placed in the zone of light intersection from virtual sources after the prism. The second order coherence function $G^{(2)}$ was obtained from sets of images by performing light correlations across pixels in the sensor with short exposure time, preventing the average of the incoming light. The experimental function $G^{(2)}$ obtained with and without the biprism are shown in Figure 2 in the right and left panel, respectively. The comparison of the FWHMs of the functions yielded a near 5.5 factor difference. In addition, this factor could be controlled by changing the effective distance from the source S_0 to the prism. The significant thinning of the $G^{(2)}$ function can boost resolution for intensity correlation imaging modalities, further surpassing the classical limit of diffraction.

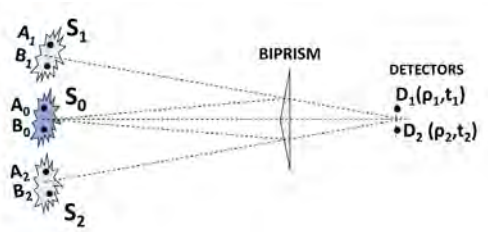

Figure 1. S_0 represents a chaotic light source generated by the rotating diffuser. S_1 and S_2 are the virtual images generated by the paraxial biprism from object S_0. After the biprism the pixels of the CCD camera acted as independent detectors.

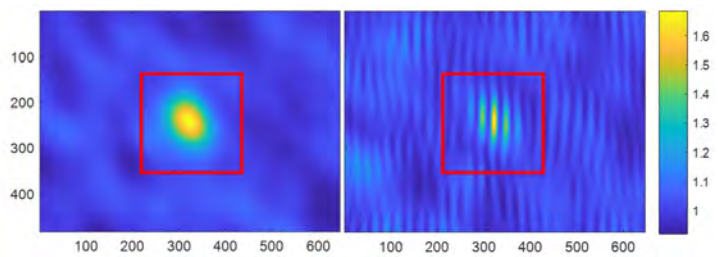

Figure 2. Left: experimental function $G^{(2)}$ obtained from S_0 (i.e. no biprism). Right: $G^{(2)}$ obtained when the biprism generated the virtual images S_1 and S_2. In both cases, axes correspond to pixels on the camera sensor (2 µm/pix).

[1] R. Hanbury Brown and R. Q. Twiss, *Nature* **177**, 27 (1956).
[2] Y. Shih, *An Introduction to Quantum Optics, Photon and Biphoton Physics*, 2nd Edition, CRC Press, (2021).

Acknowledgements: This work was supported by Ministerio de Ciencia e Innovación, Agencia Estatal de Investigación, Spain (PID2020-113919RB-I00).

Visual acuity in phakic and monofocal pseudophakic eyes under red, green, and blue lights

Laura Clavé[1,2,*], Aurora Torrents[2], Miquel Ralló[2], María S. Millán[2]

[1]*Hospital de Mataró, Servicio de Oftalmología, Consorci Sanitari del Maresme, 08304 Mataró, España.*
[2]*Grupo de Óptica Aplicada y Procesado de Imagen, Departamento de Óptica y Optometría, Universitat Politècnica de Catalunya-BARCELONATECH, Terrassa, España.*

*e-mail: lclave@csdm.cat

Introduction: Chromatic aberration of the human eye is caused by the dependence of the refractive index of the ocular media on the wavelength. The replacement of the natural lens of the eye by an intraocular lens might modify the longitudinal chromatic aberration (LCA) of the pseudophakic eye, depending on the chromatic dispersion of the lens material as well as other design features of the implant.[1] Most studies report LCA data as chromatic difference of refraction, but the impact of LCA on the visual acuity (VA) has been scarcely studied, particularly in pseudophakic patients.[2]

Purpose: To assess and compare the impact of quasi-monochromatic illumination on the VA of young phakic and monofocal pseudophakic subjects using red (R), green (G), and blue (B) wavelengths.

Methods: 31 young phakics aged 23.06± 5,11years, with accommodation preserved, and 30 pseudophakics aged 68.64 ± 9.52 years, implanted with a monofocal intraocular lens (Y601075, AJL Ophthalmic, Spain), participated in this study. Distance VA was measured with custom optotype illuminated sequentially with B (455nm), G (530nm), R (625nm), and white (W) LED lights. [2] Near VA was additionally assessed in young phakic eyes under the same illuminations. All VA measurements were taken monocularly and are reported in logMAR scale. Statistical analysis was performed and P-values under 0.05 were considered statistically significant.

Results:

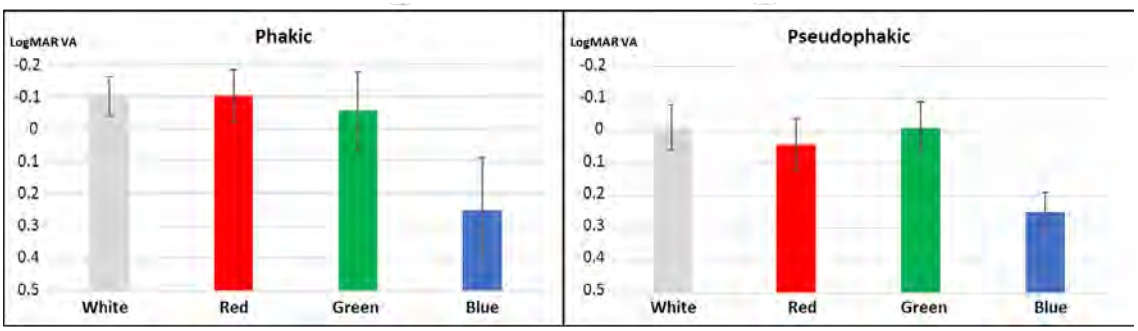

Figure 1: Distance VA under W, R, G, and B lights (mean, SD): (left) phakic group, (right) pseudophakic group.

Discussion: Clinical VA assessment under separated R, G, and B lights allowed the detection of tiny but significant variations in the chromatic difference of refraction existing in phakic and monofocal pseudophakic patients. Pseudophakic patients reached their maximum distance VA under G (used in intraocular power calculation to target postoperative refraction) and W lights. Young phakic subjects, however, reached their maximum distance VA under R illumination (equal to the one obtained with white light) thanks to the combination of LCA and some accommodative effort. Yet for them, the mean near VAs showed balanced results under R, G, and B illuminations, [2] thus adapting their accommodative effort to the chromatic difference of power.

[1] M. Vinas-Pena, A. de Castro, C. Dorronsoro et al., Understanding in vivo chromatic aberrations in pseudophakic eyes using on bench and computational approaches, *Photonics* **9**, 226 (2022).
[2] L. Clavé, A. Torrents, M. Ralló, M.S. Millán, Visual acuity assessment in phakic and pseudophakic eyes under red, green, and blue illumination, *Opt. Pura Apl.* **53**(4), (2020).

Acknowledgements: Agencia Estatal de Investigación (PID2020-114582RB-I00/ AEI / 10.13039/501100011033)

Jacobi Fourier Polynomials: more flexibility for designing ophthalmic solutions

Eva Acosta[1], Enrique Gonzalez-Amador[1, 2], **Justo Arines**[1,*]

[1]*Department of Applied Physics, University of Santiago de Compostela, Faculty of Optics and Optometry.*
[2]*Universidad Politécnica de Tulancingo, Ingenierías No. 100, 43629, Tulancingo, Hidalgo, México.*

e-mail: justo.arines@usc.es

Researchers working in Visual and Ophthalmic Optics are used to work with orthogonal basis to develop optical solutions to improve instrumentation for imaging different structures of the eye or to design lenses to improve people's visual quality. Zernike polynomials (ZP) are the most outstanding basis in this field. Although presenting several advantages in some applications due to their relationship with optical aberrations, the radial dependence of ZP consist in a polynomial of a given integer degree. In this work we add a degree of freedom to the radial dependence by using a subset of Jacobi Polynomials (JP) while keeping the same angular dependence of ZP. We will show the improvement for the correction of refractive errors by numerical simulation of retinal images. We define the Jacobi Fourier Polynomials by [1]:

$$JF(n,p,q,r,\theta) = J_n(p,q,r)\begin{cases}\cos(m\theta)\\ \sin(m\theta)\end{cases} = \sqrt{\frac{w(p,q,r)}{b_n(p,q)}}\,G_n(p,q,r)\begin{cases}\cos(m\theta)\\ \sin(m\theta)\end{cases}$$

where, r and θ are the radial and angular coordinates respectively, $J_n(p,q,r)$ are the Jacobi polynomials, $w(p,q,r)$ is the weighting function, and $b_n(p,q)$ the normalization factor. The parameters p and q must obey $(p-q) > -1$ and $q > 0$. Details on the expression of $w(p,q,r)$, $b_n(p,q)$ and $G_n(p,q,r)$ can be found in [1]. As an example, for the particular case with $p = q = 7$, $n = 0$ and $m = 3$, we get that $JFP(r,\theta) = \sqrt{7}r^3\cos(3\theta)$ is proportional to Zernike $Z_3^3(r,\theta)$ also known as trefoil aberration and commonly used to increase the depth of focus of optical systems [2]. In this work we will keep the azimuthal frequency m=3 and change the radial dependence through *p*, *q* and *n*.

We present our study on the use of a phase in the shape of a JFP added to that of an intra ocular lens, or a contact lens to obtain optical solutions to presbyopia. To study its effect on retinal images, we performed numerical simulations in MATLAB2022a. We used computational Fourier Optics to simulate the images generated by a presbyopic eye and optotypes placed at different vergences within the interval [0,5] D for three different pupil diameters (7,5,3) mm and two different magnitudes of primary spherical aberration (SA) with peak to valley (P-V) values of 0.15 μm and -0.15 μm within a pupil of 5 mm diameter. We compared the performance of the naked eye and that with different JFP with $n = 0$ and $p = q = [7, 8, 9, 10]$ with P-V values of 30 μm and 60 μm at 5 mm pupil diameter. We will also show values for different objective visual criteria: VSOTF, Visual Strehl combined, and image correlation.

Our results show that the extension of the range of clear vision is better with JFP phase with the advantage that it does not depend on the pupil diameter. The centre of the range of clear vision depends on the value of the SA, but it could be adjusted by adding some amount of defocus. Figure 1 shows an example of the images obtained for the naked eye (left) for a JFP phase (right).

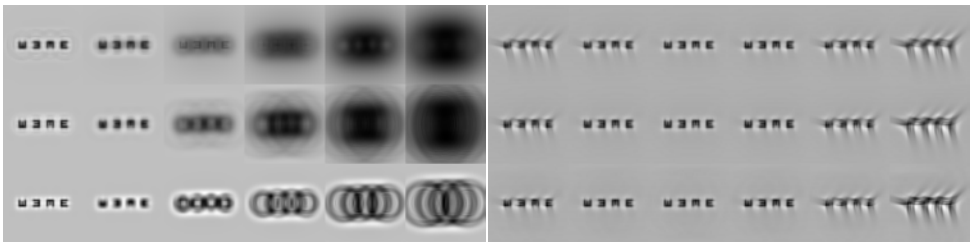

Figure 1. Left: Retinal images for naked eye. Right: Retinal Images obtained with *n=0* and *p=q=8*, P-V = 30μm. In both cases object vergences from 0D to 5D; pupil diameters D= (7,5,3) mm and +0.15 SA.

[1] E. González-Amador, et al., *Optics and Lasers in Engineering* **126**, 105880 (2020).
[2] J. Arines, et al., *Optics Letters* **39**, 3986 (2014).

Acknowledgements: Consellería de Cultura, Educación e Ordenación Universitaria, Xunta de Galicia (ED43B 2020/29), y Ministerio de Ciencia e Innovación PID2020-115909RB-I00.

Optical coherence tomography in retinitis pigmentosa patients treated with an injection of autologous bone-marrow-derived mononuclear stem cells

A. Vanesa García-Navarro[1,2], M. Elena Rodríguez[2], **Juan M. Bueno**[1,*]

[1]*Laboratorio de Óptica, Universidad de Murcia, 30100 Murcia, Spain.*
[2]*Servicio de Oftalmología, Hospital Universitario Virgen de la Arrixaca, 30120 Murcia, Spain.*

*e-mail: bueno@um.es

Retinitis pigmentosa (RP) is a genetic retinal pathology affecting the outer retina [1]. It involves a progressive death of photoreceptors, with loss of central visual acuity and reduction of pigment epithelial functions. Although there's no cure for RP, treatments such as gene therapy and retinal implants are being tested. In particular, a novel treatment based on an intravitreal injection of human bone-marrow-derived mononuclear stem cells (BM-MSCs) is for retinal dystrophy that has been demonstrated promising in both humans and animal models [2,3]. In this study we analyzed the physiological changes at the central macula produced in a set of patients suffering from advanced RP, treated with a single intravitreal injection of autologous BM-MSCs.

The clinical trial was carried out at the Hospital Universitario "Virgen de la Arrixaca" in Murcia (Spain). Eight patients (mean age: 37±11) suffering from advanced RP were involved in the study. Each volunteer received an intravitreal injection of autologous BM-MSCs in one of their eyes. An injection of saline solution (placebo) was injected in the contralateral eye. Patients underwent a complete ophthalmologic test including optical coherence tomography (OCT) imaging (CIRRUS, Carl ZEISS). Evaluation was performed one day before the injection (basal visit) and at different time points during the 12-month follow-up period.

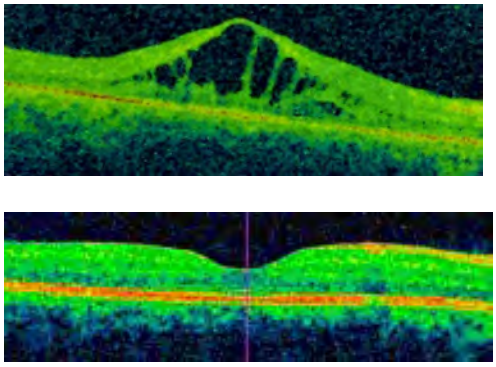

Figure 1. OCT images of a patient suffering from advanced RP (top) and a control subject (bottom). The edema related to the pathological stage is clearly visualized.

At the basal visit (i.e., before injection) measurements in both eyes often showed larger foveal thickness values (>300 μm on average) than those corresponding to normal subjects, what is typically associated to the macular edema present in some RP subjects (see Figure 1). After the injection, the temporal evolution of the retinal thickness was assessed. It is interesting to notice that in patients with thicker edemas there was a reduction in foveal thickness between the basal and the last visit. However, since the initial thickness was different for each patient, the evolution after the treatment with autologous BM-MSCs varies among them. Results show that after 1 year of treatment, most of patients fairly benefit from the therapy, since the central foveal thickness is often reduced or maintained.

In conclusion, this study shows that although the cure of RP has still a challenge, the treatment with a single injection of autologous BM-MSC is reliable, feasible and safe, with possibilities of success. This treatment may have a potential therapeutic effect since it might be useful to reduce the effects of the macular edema and to decrease central macular thickness. Under this perspective, stem cell therapy is an alternative to be developed and merits further investigation.

[1] R. A. Pagon, *Surv. Ophthalmol.* **33**, 137 (1988).
[2] J. B. Jonas, M. Witzens-Harig, L. Arsenievand A. D. Ho, *Acta Ophthalmol.* **86**, 225 (2008).
[3] J. Di Pierdomenico, D. García-Ayuso, M. E. Rodríguez, et al. *Int. J. Mol. Sci.* **21**, 7252 (2020).

Acknowledgements: This work was supported by Ministerio de Ciencia e Innovación, Agencia Estatal de Investigación, Spain (PID2020-113919RB-I00).

Caracterización cromática de una lente intraocular comercial de foco extendido

Diego Montagud-Martínez[1,*], Vicente Ferrando[1], Anabel Martínez-Espert[2, 3], Juan A. Monsoriu[1], Walter D. Furlan[2]

[1]*Centro de Tecnologías Físicas, Universitat Politècnica de València, 46022 Valencia, Spain;* [2]*Departamento de Óptica y Optometría y Ciencias de la Visión, Universitat de València, 46100 Valencia, Spain;* [3]*Clínica Aiken, Fundación Aiken, 46004 Valencia, Spain.*

*e-mail: diemonma@upvnet.upv.es

Gracias a las nuevas tecnologías, como ordenadores, tablets o smartphones, las demandas visuales de los pacientes en distancias intermedias se han incrementado. Debido a esto las lentes intraoculares (IOLs) de foco extendido (EDOF) están en auge ya que presentan un buen rendimiento visual en distancias lejanas e intermedias. Muchas de estas IOLs utilizan óptica difractiva en su diseño [1, 2]. Para caracterizar las propiedades ópticas de estas lentes es importante hacer un estudio policromático con diferentes longitudes de onda.

El objetivo de este trabajo es comprender cual es la estrategia de diseño empleada por la lente comercial EDOF AT LARA 829MP para conseguir la extensión de foco.

Para ello se midieron las propiedades ópticas de la lente para tres longitudes de onda 450 nm, 550 nm, 650 nm y con luz policromática en un banco óptico que cumple la norma ISO 11979-2, 2014 [3] para una pupila de 4.5 mm. Se calcularon las TF-MTFs para 50 líneas por mm y las PSFs y se obtuvieron las imágenes de un test USAF en diferentes vergencias.

Como se puede observar en la Figura 1, la IOL muestra un comportamiento cromático claramente diferente en función de la longitud de onda. Mientras que para el verde presenta un perfil bifocal con ambos focos de altura similar, para el rojo y el azul los perfiles se asemejan más al de una lente monofocal y estos se sitúan entre los dos focos verdes. Por otro lado, la línea negra (luz policromática) muestra el perfil EDOF de la IOL.

La lente EDOF AT LARA 829MP está diseñada para diferentes longitudes de onda, presentando un perfil bifocal para la luz verde, mientras que muestra un perfil monofocal para el rojo y azul. Por tanto, este diseño utiliza las diferentes longitudes de onda para generar un perfil policromático de foco extendido de aproximadamente 2.0 D.

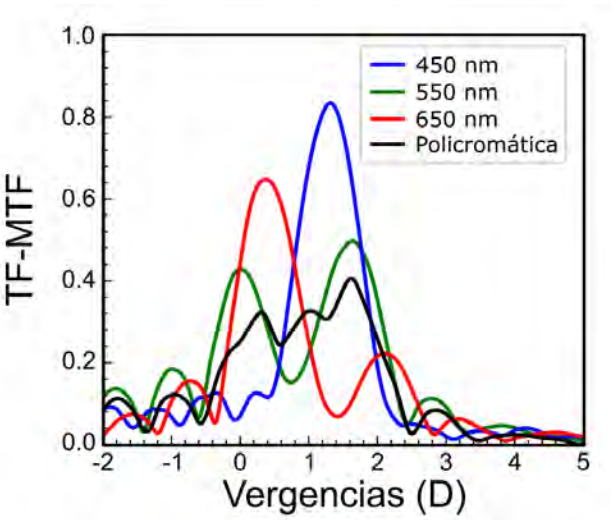

Figura 1. TF-MTF para las tres longitudes de onda y con luz policromática de la IOL AT LARA 829MP en pupila de 4.5 mm

[1] Zvorničanin, J.; Zvorničanin, E.; Premium intraocular lenses: The past, present and future. *J. Curr. Ophthalmol.* **30**, 287 (2018).

[2] Rampat, R.; Gatinel, D. Multifocal and extended depth-of-focus intraocular lenses in 2020. *Ophthalmology* **128**, e164 (2020).

[3] ISO 11979-2. Ophthalmic Implants-Intraocular Lenses-Part 2: Optical Properties and Test Methods. International Organization for Standardization: London, UK, 2014.

Agradecimientos: Diego Montagud-Martínez agradece la financiación otorgada por la beca Margarita Salas del Ministerio de Universidades de España financiado por the European Union-Next Generation EU.

Impacto de la aberración esférica en modelos de ojos teóricos

Anabel Martínez-Espert[1,2,*], Diego Montagud-Martínez[1,3], Vicente Ferrando[3], Juan A. Monsoriu[3], Walter D. Furlan[1]

[1]*Departmento de Óptica y Optometría y Ciencias de la Visión, Universitat de València, 46100 Valencia, España.* [2]*Clínica Aiken, Fundación Aiken, 46004 Valencia, España.* [3]*Centro de Tecnologías Físicas, Universitat Politécnica de València, 46022 Valencia, España.*

*e-mail: amares9@alumni.uv.es

Los modelos de ojo son sistemas utilizados para comprender el funcionamiento de las superficies del ojo [1]. En el área de la óptica fisiológica el uso de modelos de ojos teóricos tiene múltiples aplicaciones, entre ellas, la evaluación teórica de diferentes elementos ópticos, como lentes intraoculares (LIOs). Para realizarla se utilizan programas de trazado de rayos que permiten evaluar la calidad óptica del elemento de estudio. Existen numerosos modelos de ojos teóricos publicados en la literatura científica [1-3]. En ellos, a medida que aumenta la complejidad del sistema los resultados obtenidos se aproximan más a las condiciones clínicas reales. Uno de los modelos más utilizados es el de Liou-Brennan (LB) [2], cuyos parámetros se basan en datos biométricos de pacientes con una media de 45 años. Uno de los parámetros que varía entre los diferentes modelos es la asfericidad (Q), la cual genera aberración esférica (AE) [3]. La norma ISO 11979:2014 [4] especifica los requisitos y métodos de ensayo para determinar las propiedades ópticas de las LIOs. A la hora de evaluarlas de forma teórica LIOs, es posible utilizar los parámetros de dicha norma como un modelo de ojo teórico.

El objetivo del presente estudio es comparar numéricamente el efecto de la AE en tres modelos: El de LB, y dos configuraciones de la norma ISO 11979:2014 [4]. La primera configuración (ISO 1) no presenta AE total (AE= 0.00 µm), mientras que la segunda configuración (ISO 2) tiene una AE total similar a la de LB (AE = 0.28 µm).

Para estudiarlo, se ha utilizado el software de trazado de rayos Zemax (OpticStudio; versión 18.7, LLC, Kirkland, WA, EEUU). Se han programado dos lentes monofocales con diferente Q en la cara posterior y potencia de 20 D. La primera monofocal se programó con una Q = -3.65 que compensa la AE de la configuración ISO 1. Mientras que la segunda monofocal compensa la AE del modelo de LB (Q = -7.85). Se calcularon la *Modulation Transfer Function* (MTF) en el plano focal del modelo, para frecuencias espaciales entre 0 y 60 ciclos/mm (Figura 1). También se realizó una evaluación de los *Spot diagrams* para observar los resultados en el plano focal. La configuración ISO 2 y el modelo de LB presentan un comportamiento similar ya que la Q global de ambos modelos es similar. Sin embargo, hay diferencias entre ambas configuraciones debido a que el ojo teórico de LB es un modelo más complejo que no presenta simetría de revolución. Se observa que al neutralizar la AE en los tres modelos, el comportamiento es similar en los tres casos. Por tanto, la AE es una de las mayores diferencias entre modelos de ojos teóricos.

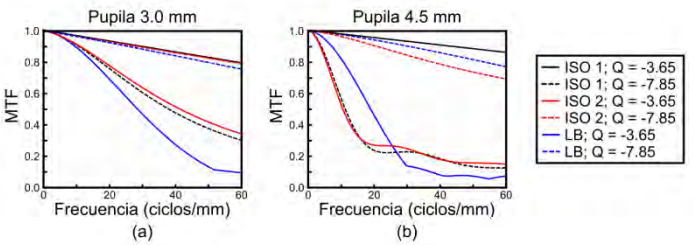

Figura 1. MTFs en el plano focal de los diferentes ojos modelo con (a) 3 mm y (b) 4,5 mm de pupila.

[1] Polans, J.; Jaeken, B.; McNabb, R.P.; Artal, P.; Izatt, J. A. *Optica* **2**, 124 (2015).
[2] Liou, H.L.; Brennan, N.A. *J Opt Soc Am A* **14**, 1684 (1997).
[3] Atchison, D.A. Handbook of Visual Optics, Taylor & Francis Group (2017).
[4] ISO 11979-2:2014. Ophthalmic implants-Intraocular lenses-Part 2: Optical proprieties and test methods.

Agradecimientos: Diego Montagud-Martínez agrade a la beca Margarita Salas del Ministerio de Universidades de España financiado por the European Union-Next Generation EU.

Analysis of the accommodation response as a supporting tool during subjective refraction

Aina Turull-Mallofré*, Carlos E. García-Guerra, Mikel Aldaba, Meritxell Vilaseca, Jaume Pujol

Center for Sensors, Instruments and Systems Development, Universitat Politècnica de Catalunya.
Rambla Sant Nebridi 10, 08222 Terrassa, Spain.

*e-mail: aina.turull@upc.edu

The refraction process aims to find the combination of sphero-cylindrical lenses that maximizes visual acuity with minimum accommodation. The gold standard technique for assessing refraction is subjective refraction, which includes the control of accommodation by means of fogging technique. Despite the importance of accommodation in the refraction process, there is little knowledge on how the accommodative status behaves during the subjective refraction. For this reason, the main purpose of this work was to analyse the accommodation response during subjective refraction in order to obtain the accommodative status when the patient was wearing the subjective refraction. Moreover, we also aimed to find the relationship of the transition point between relaxed and activated accommodation and the subjective refraction, to determine if the information obtained could be used as a supporting tool for the subjective refraction technique.

Thirty healthy young adults between 18 and 30 years old participated in the study. The accommodation response of the right eye was monitored during a sweep of spherical lenses while wearing the subjective refraction. The set-up to monitor the accommodation consisted of a Hartmann-Shack aberrometer coupled to a phoropter that worked as an open-filed instrument and had a monitoring frequency of 10 Hz [1].

A sweep of lenses from +1.50 D to -1.50 D, in steps of 0.25 D relative to the patient's subjective refraction, was presented in front of the corrected eye while monitoring accommodation. The relative accommodation was calculated as the difference between the value of accommodation measured for each induced power of the sweep of lenses (ΔS) and the minimum measured accommodation. For the subjective refraction, the relative accommodation was obtained for ΔS=0. In figure 1, an example of the accommodation as a function of the sweep lenses is shown, where the solid line represents the measured accommodative response. With the aim to obtain the point of transition between the relaxed and activated accommodation two linear fitting were obtained for each ΔS, the first considering the curve between -1.50 D and ΔS, and the second between ΔS and +1.50 D. In figure 1, the curve fitting for ΔS=0 is shown, corresponding to the dashed lines. The induced power ΔS that produced the best cumulative coefficient of determination was chosen as the transition point between relaxed and activated accommodation, as in Figure 1, indicated with the red point.

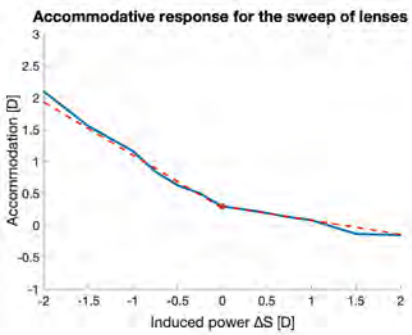

Figure 1. Accommodative response during the sweep of lenses.

The mean relative accommodation ± SD obtained when wearing the subjective refraction was 0.38 ± 0.20 D. The agreement between the value of the traditional subjective and the value of refraction that was in the phoropter in the transition of accommodation obtained by means of the linear fitting was analysed with the Bland-Altmann test. The mean ± SD of the difference between methods and 95% limits of agreement were 0.041 ± 0.41 D (0.84 D, -0.76 D).

We can conclude that there is a tendency of having a residual activated accommodation with the subjective refraction. Moreover, the point of transition between relaxed and activated accommodation may be a significant information to be used during subjective refraction to enhance the procedure and to detect accommodation-related problems during the visual examination.

[1] C. E. García-Guerra, J. Martínez-Roda, M. Aldaba, S. Galera, C. Aransay, F. Díaz-Doutón, J. Pujol, M. Vilaseca; Real-time monitoring of accommodation during subjective refraction, *Invest. Ophthalmol. Vis. Sci.* **61**(7), 1716. (2020).

Acknowledgements: This publication is part of the project PID2020-112527RB-I00, funded by MCIN/AEI/10.13039/501100011033. The first author gratefully acknowledges the Universitat Politècnica de Catalunya and Banco Santander for the financial support of her predoctoral grant FPI-UPC.

Visual simulation and correction using economic and compact vertical aligned liquid crystal devices

Alba M. Paniagua-Diaz[1,*], Juan Mompean[1], Juan L. Aragon[2], Pablo Artal[1]

[1]*Laboratorio de Óptica, Centro de Investigación en Óptica y Nanofísica (CiOyN), Universidad de Murcia, Campus de Espinardo (Ed. 34), 30010 Murcia, Spain.* [2]*Departamento de Ingeniería y Tecnología de Computadores, Universidad de Murcia, Campus de Espinardo, Murcia 30100, Spain.*

*e-mail: a.paniagua-diaz@um.es

In this work we demonstrate the potential of Vertical-Aligned Spatial Light Modulators (SLM) in the simulation and correction of High Order Aberrations (HOA) by testing visual acuity and the contrast sensitivity function in a set of healthy subjects. We perform Visual Acuity (VA) and Contrast Sensitivity function (CS) tests in different subjects, with their vision corrected by the AO system and with the phase map of severe keratoconus (RMS >1 for 5 mm diameter pupil). The applicability of this modulation device for visual adaptive optics correction and simulation is discussed.

Spatial Light Modulators (SLMs) have been responsible for important advances in different applications of Adaptive Optics (AO) such as vision, since they became widely available [1,2]. These devices can essentially modify the amplitude and/or phase of an incident wavefront, although phase-only modulation is the most widely used feature due to its efficiency and versatility. Most widely used SLMs are composed of a Liquid Crystal (LC) device between two linear polarizers. Liquid crystal molecules can be vertically aligned (VA), parallel aligned (PA) or twisted (T), although for simplicity of use and quality, for phase-only applications PA-LCoS are the gold standard. VA-LCoS are typically used as high-contrast amplitude modulators [3], not holding a large depth of phase modulation, barely surpassing π radians. In a recent study it was shown how the use of two VA-LCoS arranged in series (thus allowing phase summation) could develop phase modulation outcomes very similar to those of the gold standard PA-LCoS, with a significant lower cost and improved compactness [4].

Methods: Figure 1 shows the setup used for testing the VA and CS with the phase-only modulation unit consisting of two VA-LCoS devices arranged in series. The optical components of this unit include: the two VA-LCoS modulators (SLM1 and SLM2) with their optical axis at 45º from the horizontal in operating conditions; a linear polarizer P oriented at 45º from the horizontal to achieve phase-only modulation. The plane of SLM1 is optically conjugated with SLM2 to easily implement the phase summation. The optical stimulus is placed at 2.8 meters from the aperture of the system. The aperture has a diameter of 5mm and is conjugated to the surface of the SLMs. The modulated pupil is finally conjugated with the eye's pupil plane. A beam splitter (BS) in front of the eye opens an extra path for a pupil camera, monitoring the centering of the eye in the system.

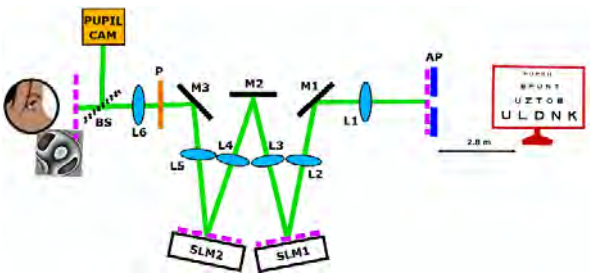

Figure 1. Optical setup for the phase-modulation testing with two VA-LCoS devices arranged in series, whilst evaluating the visual acuity and contrast sensitivity function of different subjects. The conjugated planes are depicted by the pink dashed line.

Results: The results from the VA and CS tests showed a clear difference between the values of VA and CS with the simulated keratoconus, being on average 0.6 points better the corrected VA vs the keratoconus simulated one. In the case of the CS, we found a consistent average drop of 0.35 points in the corrected vs the keratoconus simulated one, in agreement with the expected vision degradation with high-order RMS increase [6].

Conclusions: In this work we demonstrate the capabilities of the VA-LCoS modulation unit for the simulation of HOA and the correction of vision in an open-view configuration. These results pave the way for the use of economic and compact VA-LCoS devices in the correction of vision based on adaptive optics, both for low and high order aberrations.

[1] S. Marcos *et al*., *Vision Research* **132**, 3 (2017).
[2] C. Schwarz *et al.*, *Optics Letters* **36**(24), 4779 (2011).
[3] D. Cuypers *et al.*, *IEEE/OSA Journal of Display Technology* **7**(3), 127(2011).
[4] A. Arias *et al.*, *Optics Express* **28**, 34180 (2020).
[5] A. B. Watson & A. J. Ahumada, *Journal of Vision* **8**(4), 17 (2008).

Straylight and Optical Memory Effect characterization of ex-vivo cataractous crystalline lenses

Dulce Simón[1], Alba M. Paniagua-Díaz[1,*], Carmen Martínez[1], Elena Moreno[1], Alba Rodríguez-Ródenas[1], Inés Yago[2], José María Marín[2], Pablo Artal[1]

[1]*Laboratorio de Óptica, Universidad de Murcia, Campus de Espinardo, 30100 Murcia, Spain.*
[2]*Oftalmología, Hospital Universitario "Virgen de La Arrixaca", El Palmar, Murcia, Spain.*

*e-mail: a.paniagua-diaz@um.es

Cataracts increase the amount of intraocular light scattering in the crystalline lens causing vision impairment by blurring and reducing the contrast in the retinal images. Wavefront shaping techniques in combination with the Optical Memory Effect have been suggested for the optical (non-surgical) correction of scattering in cataractous lenses [1]. In this context, we aim to characterize the scattering properties of excised human lenses by measuring their OME.

Methods: The Optical Memory Effect (OME) is an intrinsic correlation of scattering media that provides the isoplanatic patch of a cataract's correction imaging technique, determining how the transmitted speckle pattern changes with a tilt/shift of the incident beam [2]. We measured this using a 594-nm laser incident on different cataractous lenses by recording the transmitted speckle pattern for different values of tilt/shift and comparing them via cross-correlation. For each cataract stage, we also characterized scattering using the straylight parameter, measured with the Optical Integration Method [3], and the Michelson Contrast of the images obtained. A total of 34 lenses of donors aged between 29 and 67 were measured.

Results: There is a linear relationship between the straylight parameter, image contrast and OME decorrelation (Fig.1d-f), providing a new tool for the prediction of the OME range when only quantitative scattering measurements are taken. In severe cataracts (straylight parameter Log10[s]>2), the OME provides an isoplanatic patch of about 1 degree in tilt and 400 µm in shift, a range that is linearly increased as the optical cataract decreases.

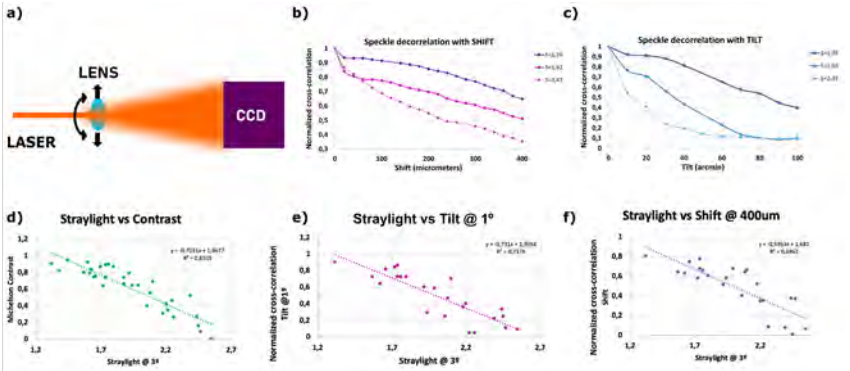

Figure 1. a) Schematic of the experimental configuration for the measurement of the shift and tilt OME. b) Normalized cross-correlation of the transmitted speckle patterns for different values of lateral translation (or shift), in steps of 20 µm. The different curves represent three different crystalline lenses with straylight parameters at 3 degrees of 1,76, 1,92 and 2,47, from quasi transparent to opaque. c) Normalized cross-correlation of the transmitted speckle patterns for different values of tilt, in steps of 10 arcmin, for the different lenses. d-f) Graphs showing the relationship between the Straylight at 3 degrees with the Michelson contrast (d), normalized cross-correlation for a tilt of 1 degree (e) and the normalized cross-correlation for a shift of 400 um (f).

Conclusions: The OME of cataractous excised human lenses has been measured for the first time and is found to be non-negligible for cataracts, being strongly dependent on the scattering strength. This work paves the way to approaches for the non-invasive and real-time correction of cataracts with wearable devices.

[1] Paniagua-Díaz, A. M. *et al.*, *Optics Express* **29**(25), 42208 (2021).
[2] Osnabrugge, G. *et al.*, *Optica* **4**(8), 886 (2017).
[3] Ginis, H. *et al.*, *J. Vis.* **12**(3), 20 (2012).

Effects of small residual astigmatism on the reading performance of contact lens neophytes

Pedro Gil[1,2,*], Alexandra Farcas[2], Celia Hernández[2], Antonio Benito[2], Juan Tabernero[1,2]

[1]*Departmento de Electromagnetismo y Electrónica, Universidad de Murcia, 30100 Murcia, Spain.*
[2]*Laboratorio de Óptica, Universidad de Murcia, 30100 Murcia, Spain.*

*e-mail: pedro.gilf@um.es

The purpose of this work is to compare the effect of toric contact lenses (full corrections of astigmatism) versus spherical soft contact lenses (corrected with the mean spherical equivalent refraction) on the reading performance of novel contact lens (CL) users with low astigmatism.

The reading test consisted of two paragraphs of 92 and 97 words divided into six lines (Arial 10 font) shown on a 23.6" screen at a reading distance of 60 cm and corresponding to a visual acuity (VA) of 0.65. Reading performance parameters (reading time, number and duration of fixations, number of regressions and magnitude of saccades) were recorded using an eye tracking device (GP3 HD, Gazepoint, Vancouver, Canada) at a frequency of 150 Hz. Additionally, contrast sensitivity (CS) at 9 and 15 cpd, respectively, and VA, VA at 40 cm and VA at 60 cm were measured with a Visual Adaptative Optics simulator (VAO; Voptica SL, Murcia, Spain).

Forty contact lens neophytes were recruited. They were divided into two groups, matched by age and refractive error (no statistically significant differences). Subjects in group one (N=21; age 21 ± 4 years; sphere -2.3 ± 0.8 D; cylinder -1.0 ± 0.3 D) were monocularly fitted with a spherical contact lens (Precision1, Alcon Laboratories, Inc, Fort Worth, TX) while subjects in group two (N=19; age 21 ± 4 years; sphere -2.5 ± 1.4 D; cylinder -0.9 ± 0.3 D) were fitted with a toric lens (Precision1 for Astigmatism).

Subjects in the toric group showed a significant improvement ($p < 0.05$) in VA and CS at 9 cpd ($p < 0.05$). Some reading performance magnitudes like the proportion of regressions (Fig. 1) and the mean duration of fixations showed a similar tendency, being slightly worse in the group fitted with spherical lenses, but no significant differences were found.

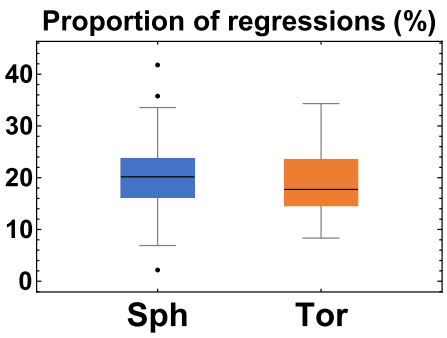

Figure 1. Between-group comparison of the proportion of regressions in reading.

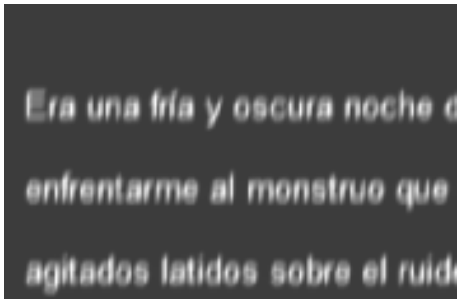

Figure 2. Optical simulation of the reading test for the average subject in the spherical CL group (pupil diameter = 4.5 mm).

In conclusion, subjects with the toric fit showed better VA and CS and tended to perform slightly better in the reading test, but variability was large between subjects. This may be because the text under the conditions previously described is still legible (see optical simulations in Fig. 2) for spherical lens users with low to moderate astigmatism. Rotations and decentrations of the toric lens may explain why the visual perception of the text may look similar between subjects in both groups.

Acknowledgements: Grant PID2019-105639RA-I00 (Ministerio de Ciencia, Innovación y Universidades, Spain) and a predoctoral grant (21602/FPl/21) from Fundación Séneca, Región de Murcia, Spain.

Numerical analysis of cross-talk phenomena in pixelated PA-LCos devices

Adriana R. Sánchez-Montes[1,*], Jorge Francés[1,2], Andrés Márquez[1,2]

[1]*Instituto Universitario de Física Aplicada a las Ciencias y las Tecnologías, Universidad de Alicante, Spain.*
[2]*Departamento de Física, Ingeniería de Sistemas y Teoría de la Señal, Universidad de Alicante, Spain.*

*e-mail: adrianaros.sanchez@gcloud.ua.es

The new technological developments and their impact on both the increase of the resolution and the reduction of the pixel sizes on parallel-aligned liquid crystal on silicon (PA-LCoS) microdisplays have made PA-LCoS a promising candidate for phase-only modulation and spatial light modulators (SLMs) applications. The pixel grid pattern on PA-LCoS induces several phenomena, i.e. the electric field crosstalk in the interpixel region, also known as fringing fields, out-of-plane reorientation of the liquid crystal director, and diffraction effects due to interpixel region. Here, a rigorous numerical methodology has been applied to avoid simplified models that neglect these kinds of phenomena. More specifically, the Frank-Oseen elastic free energy has been minimised to find the optimal LC director distribution [1]. This analysis has been carried on in a three-dimensional domain, taking into account the external field's influence on the pixel. Once the LC director distribution has been estimated, the electrical permittivity tensor is derived and used for a complete three-dimensional Finite-difference time-domain method (FDTD) [2] analysis. The Stokes parameter is determined in reflection from the electromagnetic field computed by FDTD as a function of time and space. Fig. 1 shows the Stokes parameters as a function of the external voltage for the pixel sizes of 5 and 7 μm. The fill factor (FF) is defined as the ratio of the active area of the pixel (i.e., without the interpixel gap area) and the entire area of the pixel in percentage. The interpixel gap sizes considered are 0.2, 0.4 and 0.6 μm dealing with fill-factor of 92%, 85% and 77% for the 5 μm pixel size, and 94%, 89%, and 84% for the 7 μm pixel size. Fig. 1(a)-(b) shows the S_1 parameter for 5 μm and 7 μm pixel sizes, respectively. A reduction of the deviation with respect to the infinite pixel (FF 100%) is considered for the largest pixel size. A similar trend can be perceived for the degree of polarization (DOP). The influence of pixel and interpixel sizes is not clear for S_2 and S_3 parameters. The numerical results here shown are consistent with the experimentation detailed in [3].

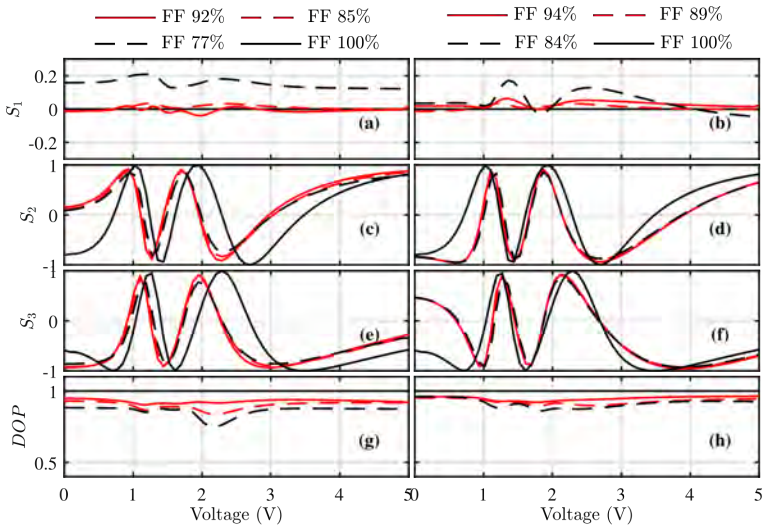

Figure 1. Stokes parameters as a function of external voltage for 5 μm pixel size (a),(c),(e) and (g), and 7 μm pixel size (b),(d),(f) and (h). Three different interpixel gaps are analysed 0.2, 0.4, and 0.6 μm.

[1] S. Moser *et al.*, *Opt. Express*, 27(**18**), 25046 (2019).

[2] J. Francés *et al.*, *Materials*, 13(**17**), (2020).

[3] A. Márquez *et al.*, *Opt. Lett.* 45(**20**), 5732-5735 (2020).

Acknowledgements: This work has been supported by Generalitat Valenciana (projects PROMETEO/2021/006; IDIFEDER/2021/014, cofunded by European Union through the FEDER programme). The corresponding author is grateful to the "Generalitat Valenciana" for the grant (GRISOLIAP/2021/106).

Precise-Integration Time-Domain for Optical Anisotropic Media

Joan Josep Sirvent-Verdú[1], Jorge Francés[1,2,*], Sergi Gallego[1,2], Augusto Beléndez[1,2]

[1] *Instituto Universitario de Física Aplicada a las Ciencias y las Tecnologías, Universidad de Alicante, España.*

[2] *Departamento de Física, Ingeniería de Sistemas y Teoría de la Señal, Universidad de Alicante, España.*

*e-mail: jfmonllor@ua.es

The Precise-Integration Time-Domain (PITD) formulation permits to break through the Courant-Friedrich-Levy (CFL) condition, which limits the accuracy, stability, and indirectly the applicability of the traditional Finite-Difference Time-Domain (FDTD) method. This characteristic permits considering larger time steps than the largest one fixed by the CFL condition. As the conventional FDTD scheme, PI also takes the spatial derivatives through the central finite-difference scheme. This step sets up a set of ordinary differential equations (ODEs) that are solved using the PI Technique [1,2,3]. However, as demonstrated in [4,5], considering larger time steps does not entirely fulfil the hypothesis of the expected reduction of running time simulations. Increasing the time step makes larger some coefficients of the sparse matrix **M**. The memory requirements for storing this matrix dramatically influence the method's performance. Even that, accurate results have been achieved with larger time steps up to six times larger than the upper boundary value fixed by the CFL condition. The results covered in [4,5] focused on validating the method in slits, thin-film filters, binary phase gratings, and twisted-nematic liquid crystal cells (TNLCs) demonstrated the method's accuracy. Here, the technique is applied to different periodic and anisotropic optical media. More precisely, to anisotropic polarization gratings (PG). PG is based on a periodically patterned, uniaxial birefringence in the grating plane that modulates the polarization of light instead of its amplitude [6].

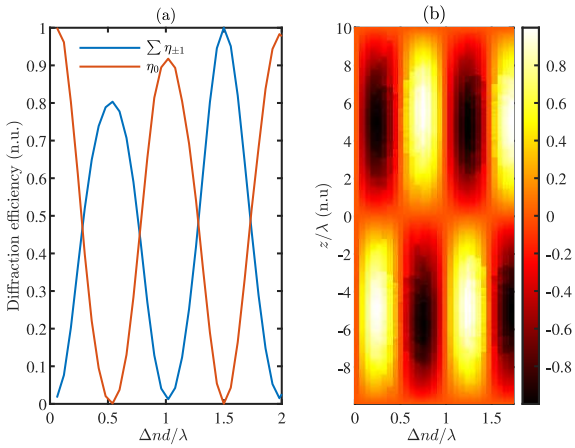

Figure 1. (a) Diffraction efficiency as a function of the normalized retardance. Setup fully defined in [5]. (b) S_4 parameter in the output plane as a function of the normalized retardance.

Fig. 1(a) shows the diffraction efficiency of the 0th- and ±1st-orders as a function of the normalized retardation $\Delta nd/\lambda$, where Δn is the birefringence, d the thickness of the PG, and λ the wavelength. The scheme simulated is fully defined in Fig. 7 in [6]. The results provided by Fig. 1(a) are close to those shown in Fig. 8(a) in [6]. Fig. 1(b) shows the behaviour of the PG when it is illuminated with a plane wave linearly-polarized. More precisely, Fig. 1(b) represents the Stokes parameter S_4 as a function of the normalized output plane (z/λ) and the normalized retardation ($\Delta nd/\lambda$). The results are consistent with those shown in Fig. 9(a) in [6]. Right- and a PG produces left-handed circularly-polarized waves as a function of the normalized retardance parameter.

[1] Wan-Xie, Z., *J. Comput. Appl. Math.* **163**, 59 (2004).
[2] Zhong, W. X and Williams, F. W., *Proc. Inst. Mech. Eng. Part C J. Mech. Eng. Sci.* **208**, 427, (1994).
[3] X. Zhu, X. Ma, J. Shao, *IEEE Microw. Wirel. Compon. Lett.* **1309** (2021)
[4] Sirvent-Verdú, J.J *et al.*, *Materials* **14** (2021).
[5] Sirvent-Verdú, J.J., *Análisis numérico mediante la técnica de integración precisa en diferencias finitas: aplicación a dispositivos ópticos difractivos*, TFG (Universidad de Alicante), (2021).
[6] Oh, C. and Scuti, M., *Opt. Express* 14(**24**), 11870 (2006).

Acknowledgements: The work was supported by Generalitat Valenciana (projects PROMETEO/2021/006; IDIFEDER/2021/014, cofunded by European Union through the FEDER programme).

Investigating ergodicity for the determination of optical coherence functions

Iryna Standret*, Rosa M. Martínez-Ojeda, Juan M. Bueno, Enrique J. Fernandez

Laboratorio de Óptica, Instituto Universitario de Investigación en Óptica y Nanofísica, Universidad de Murcia, Campus de Espinardo (Edificio 34), E-30100, Murcia, Spain.

*e-mail: iryna.standret@um.es

Emission and detection of light are stochastic processes. Ergodicity is one of the most important concepts associated to these stochastic processes. In a stationary process one can assume to be under ergodic condition when the time average of a typical realization $u = {}^{k}x(t)$ of the stochastic process of any deterministic function $F(u)$ is identical to the corresponding ensemble average. Mathematically:

$$\left\langle F\left[{}^{k}x(t)\right]\right\rangle_t = \left\langle F\left[x(t)\right]\right\rangle_E .$$

In this work, we have experimentally determined under which conditions the temporal average is equivalent to a pseudo-ensemble average, populated of realizations of the stochastic process, for the calculation of the second degree of coherence $\gamma^{(2)}$. This function is of capital importance for certain imaging modalities, as ghost imaging. Its mathematical form is:

$$\gamma^{(2)}(r_1, r_2, t_1, t_2) = \frac{\langle I_1(r_1,t_1)\cdot I_2(r_2,t_2)\rangle}{\langle I_1(r_1,t_1)\rangle\cdot\langle I_2(r_2,t_2)\rangle}.$$

Figure 1 depicts the experimental system to measure the function $\gamma^{(2)}$. For the recording of the elements of the ensemble average, sequences of 100 frames each (exposure = 50 µs) were obtained. For the time average version of $\gamma^{(2)}$, sequences of increasing number of frames were retrieved. The function $\gamma^{(2)}$ can be characterized by its FWHM and height over the baseline. Figure 2 summarizes the results, showing both parameters obtained from pseudo-ensemble average and time average (blue and red, respectively).

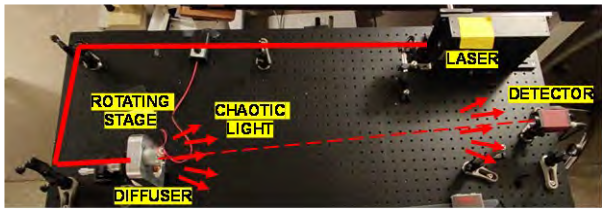

Figure 1. Experimental system compounded by a laser illuminating a rotating diffuser, which created a chaotic light source. A camera was placed in front of the so-generated pseudo-thermal light source.

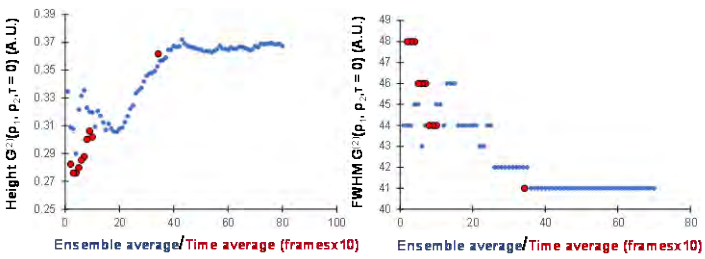

Figure 2. Height and FWHM of $\gamma^{(2)}$. Blue colour stands for ensemble average while red dots indicate time average.

We found that time averages above of 3500 frames reached steady values for the parameters of the $\gamma^{(2)}$. The methods and results are important to optimize the required number of frames in coherence functions, with application in ghost imaging.

[1] E. Wolf, *Introduction to the theory of coherence and polarization of light*, Cambridge University Press (2007).

Acknowledgements: This work was supported by Ministerio de Ciencia e Innovación, Agencia Estatal de Investigación, Spain (PID2020-113919RB-I00).

Impact of the detector response on the temporal second degree of coherence of a chaotic light source

Pien Vinke*, Juan M. Bueno, Enrique J. Fernandez

Laboratorio de Óptica, Instituto Universitario de Investigación en Óptica y Nanofísica, Universidad de Murcia, Campus de Espinardo (Edificio 34), E-30100, Murcia, Spain.

*e-mail: p.vinke@um.es

The Hanbury and Brown-Twiss (HB-T) effect is a form of a non-trivial correlation in both time and space from a thermal or chaotic light source. It was first described in 1954 in the context of radioastronomy, to be soon after demonstrated in the visible range. A new type of interferometer was devised to characterize this effect [1]. This intensity interferometer correlates light signals measured from 2 detectors D_1 and D_2 at time t_1 and t_2, placed at positions ρ_1 and ρ_2. The resulting correlation function obtained in the HB-T interferometer is a version of the second degree of coherence function $\gamma^{(2)}$. The function $\gamma^{(2)}(\rho_1,t_1,\rho_2,t_2)$ allows to characterize the coherence and bunching of incoming photons. Modified versions of HB-T interferometers are used for non-conventional imaging, such as ghost imaging and quantum imaging. Intensity correlations in this context are referred to instantaneous measurements of light intensity, or photon annihilation. In the laboratory, real detectors always exhibit certain integration time t_c, which must be considered to correctly interpret the results of such intensity interferometers, or their counterpart light correlation imaging system [2]. In this work, we studied and experimentally characterized the impact of the detector response t_c on the retrieved temporal $\gamma^{(2)}$. To do so, a fiberized intensity interferometer with 2 avalanche photodiodes, classical version of the HB-T interferometer, was set and calibrated in the laboratory. A pseudothermal (chaotic) light source was generated by rotating a diffuser (48.6 rad/s) with grit index 1500, back illuminated by a 660 nm CW laser. Figure 1 presents two experimental $\gamma^{(2)}(\tau)$ obtained under t_c = 4 µs and t_c = 100 µs, with $\tau = t_1 - t_2$.

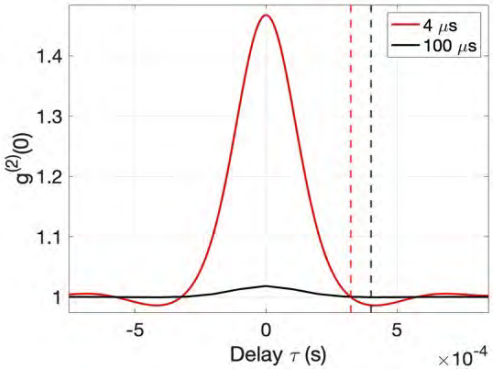

Figure 1. Second order temporal coherence function with t_c = 4 µs (red) and t_c = 100 µs (black). Dashed lines refer to τ_c.

Figure 2 presents $g^{(2)}(0)$ as a function of the ratio t_c/τ_c, with τ_c being the coherence time of the source. It was experimentally determined as:

$$f\left(\frac{t_c}{\tau_c}\right) = 3.03 \cdot 10^{-3} \cdot \frac{t_c}{\tau_c}^{-0.99} + 0.99$$

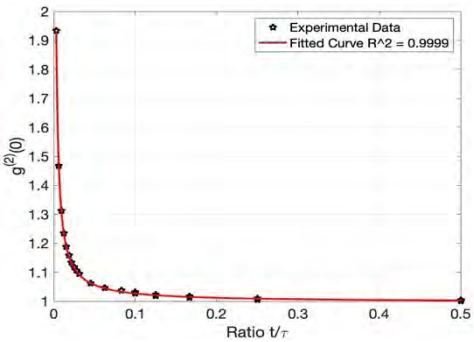

Figure 2. $\gamma^{(2)}(0)$ as a function of ratio t_c/τ_c . Dots represent the experimental data. Red curve represents the best fit function.

This figure indicates that a low ratio t_c/τ_c is necessary to reach the theoretical bunching of 2 for chaotic light sources.

In conclusion, the response time t_c exhibited a major impact on the experimental determination of $g^{(2)}(0)$, preventing the function to reach its theoretical maximum in some cases, and broadening its shape (temporal coherence τ_c). These effects can be modelled and eventually compensated by dedicated signal processing. These results can help to design and process signals more efficiently for ghost imaging, or any other intensity correlation-based imaging modality.

[1] Shapiro, J.H., Boyd, R.W. *Quantum Inf Process* **11**, 949 (2012).
[2] Y. Shih, *An Introduction to Quantum Optics*, CRC Press Taylor & Francis Group (2018).

Acknowledgements: This work was supported by Ministerio de Ciencia e Innovación, Agencia Estatal de Investigación, Spain (PID2020-113919RB-I00).

Characterization of topography hidden under paint by means of algorithms stable to the number of frames under non-uniform illumination

E. Baradit[1,*], M. Avendaño[2], G. Cañas[1], M. Yañez[3], M. Trivi[4], J. Cariñe[5]

[1]*Physics Department, Universidad del Bio-Bio, Av.Collao 1202, Concepción, Chile.*
[2]*Graduate student, Physics Department, Universidad del Bio-Bio, Av.Collao 1202, Concepción, Chile.*
[3]*Department of Statistics, Universidad del Bio-Bio, Av.Collao 1202, Concepción, Chile.*
[4]*Centro de Investigaciones Ópticas de La Plata, PO Box 3, Zip Code 1897, Argentina.*
[5]*Department of Electrical Engineering, Universidad Católica de la Santísima Concepción, Alonso de Ribera 2850, Concepción, Chile.*

*e-mail: ebaradit@ubiobio.cl

The ability to access information about topographies covered under some kind of layer and with a certain activity poses a current and interesting problem for science and technology. This topography is not visible in plain sight.

This study reviews the stability of different qualitative processing algorithms in relation to a processed number of frames N and under non-uniform illumination conditions for a sample covered in fresh paint in the process of drying. The sample consists of an aluminum tube (Fig.1) with perforations of different diameters and depths, illuminated with a 532 nm continuous laser, obtaining dynamic speckle images captured by a CMOS camera which were then processed [1].

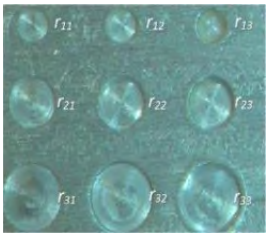

Figure 1: Photography of the sample with cylindrical perforations.

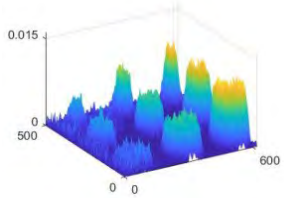

Figure 2: Mobility map obtained using NJDC algorithm.

The algorithms used were separated into non-normalized, including SF, MSF, STD, and DJC, and normalized, including Fujii, NSF, LSI, and NJDC. The NDJC is a modified normalized descriptor [2].

$$NDJC = \frac{1}{< I_k >^2} \sum_{k=1}^{N-1} \frac{(I_k - I_{k+1})^2}{I_k + I_{k+1}}$$

Figure 2 shows an example of mobility images obtained using this descriptor for N=250.

The results show that, under non-uniform illumination, the use of normalized qualitative descriptors to characterize topography hidden under paint reaches a high correlation (>0,98) and is stable to the number of frames (Fig. 3).

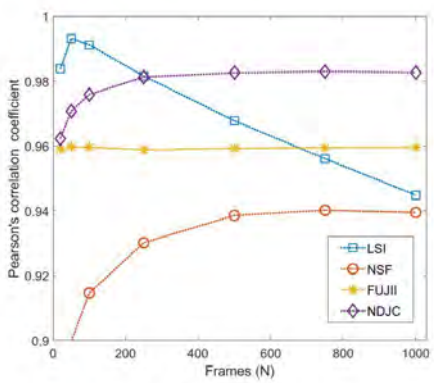

Figure 3: Correlation coefficients versus number of processed frames with normalized algorithms.

[1] Rabal H, Braga R., *Dynamic Laser Speckle and Applications.* CRC Press (2008).
[2] Cariñe J, Guzman R, Torres-Ruiz F., *Optics and Laser in Engineering* **82**, 56 (2016).

Física Nuclear

Presentaciones orales

Martes 12/07:

15:30-16:00 Guillermo Megías (USevilla). *The relevance of Nuclear Physics in neutrino oscillations*

16:00-16:30 Yassid Ayyad (USC). *The relevance of Nuclear Physics in neutrino oscillations*

16:30-16:45 Antía Graña González (USC). *Quasi-free (p,2p) reactions in inverse kinematics for studying the fission yield dependence on temperature and its implication in the stellar nucleosynthesis r-process*

16:45-17:00 Gabriel García Jiménez (USC) and the R3B Collaboration. *Study of (p,2p) events at the CALIFA calorimeter in knockout induced fission of 238U*

17:00-17:30 **Café**.

17:30-17:45 A. Martín Sánchez (UNEX). *Recisión de datos nucleares de 212Po*

17:45-18:00 F. Barranco Blázquez (CSIC-I3M). *Correlation between optical density and particle density in passive PADC (CR-39) detectors for high fluences*

18:00-18:15 M. C. Jiménez-Ramos (USevilla/CNA). *Angular measurements on LGADs to study plasma effects using a Nuclear Microprobe*

18:15-18:30 M. Pallàs (UPC). *Study of decay properties for La to Nd nuclei (A 160) relevant for the formation of the r-process rare-earth peak*

18:30-18:45 Gustavo Alcalá (CSIC-IFIC). *Beta Decay Spectra Measurement for the Study of the Reactor Antineutrino Anomaly*

18:45-19:00 M. A. Millán Callado (USevilla/CNA). *Behaviour of particle detectors in a laser-driven neutron source*

19:00-19:15 A. Perez de la Rada (CIEMAT). *?-delayed neutron spectroscopy of 85As with MONSTER*

19:15-19:30 J. R Murias (UCM). *Investigation of 130Sn populated in the β decay of isomerically-purified 130In isomers*

Miércoles 13/07:

15:30-16:00 M. C. Jimenez Ramos (USevilla/CNA). *Medical Applications with Ion Beams at Centro Nacional de Aceleradores*

16:00-16:15 Consuelo Guardiola (IMB-CNM-CSIC). *Experimental microdosimetry maps in proton therapy*

16:15-16:30 Isabel Abril Sánchezn(UA). *Interaction of swift-ions and secondary electrons in liquid water: Bragg peaks and radial deposited dose*

16:30-16:45 Michael Seimetz (i3M-CSIC-UPV). *Scintillating fibre proton beam monitor for biomedical applications*

16:45-17:00 Nerea Encina Baranda (UCM). *Prompt-Gamma Correction in 124I PET Imaging*

17:00-17:30 **Café**.

17:30-17:45 Juan Peñas (USC). *A laser-driven proton source for medical radioisotope production*

17:45-18:00 Gabriela Llosá Llácer (IFIC, CSIC-U. Valencia). *MACACO Compton camera for medical applications*

18:00-18:15 Teresa Rodríguez (USevilla/CNA). *Experimental study of proton-induced cross sections of β^+ isotopes for PET range verification in particle therapy*

18:15-18:30 D. Godos-Valencia (UNAM-UHU). *46Mn beta-decay experimental studies and its connection with CCSN*

18:30-18:45 J. García-Marcos (UCM). *Quasielastic neutrino-nucleus scattering within realistic nuclear model and Monte Carlo event generator*

18:45-19:00 V. Lérida Toro (CNA). *Unified radiochemical method to determine 129I by AMS in different matrix analysed in oceanographic studies*

19:00-19:15 A. Tarifeño (UPC). *Neutron spectrometry with HENSA: from underground physics to space weather applications*

19:15-19:30 Martina Feijoo Fontán (USC) and R3B collaboration. *Study of multi-nucleon knockout reactions of exotic nuclei in the region of Sn*

Jueves 14/07:

15:30-16:00 Jorge Lerendegui (CSIC-IFIC). *i-TED: Imaging neutron capture sections and applications*

16:00-16:15 N. Mont-Geli (UPC). *Measurement of 27Al(α,n)30P thick target neutron yields at CMAM using the miniBELEN-10A neutron counter*

16:15-16:30 T. Franco Muñoz (UCM). *Realistic treatment of nuclear structure in the neutrino-nucleus interaction*

16:30-16:45 A. Saíz Castillo (USevilla). *Quantum simulation and machine learned analysis of an extended Agassi model*

16:45-17:00 Nerea Encina Baranda (UCM). *Prompt-Gamma Correction in 124I PET Imaging*

17:00-18:00 **Café**.

18:00-18:15 Entrega de Premio GEFN a la mejor tesis doctoral.

18:15-18:30 Charla premio 1.

18:30-18:45 Charla premio 2.

18:45-19:00 Charla premio 3.

19:00-19:30 Reunión GEFN.

Física nuclear
Oral

Quasi-free (p,2p) reactions in inverse kinematics for studying the fission yield dependence on temperature and its implication in the stellar nucleosynthesis r-process

Antía Graña González

Nuclear physics, University of Santiago de compostela, Rúa de Xoaquín Díaz de Rábago, 15705 Santiago de Compostela, A Coruña, Spain.

e-mail: antia1996@gmail.com, antia.grana.gonzalez@usc.es

Although the importance of the fission fragment treatment in stellar nucleosynthesis r-process calculations is well established, an aspect of the phenomenological descriptions of fission that has so far remained relatively unexplored in the r-process is the dependence of the fission yields on the excitation energy or temperature of the compound nuclei [1]. Moreover, the fission yields and fission barrier heights of nuclei far from the stability line are also crucial to correctly describe the r-process cycle as well as the transitions from symmetric to asymmetric fission [2]. To determine all these observables, we have carried out at the GSI facility a new experiment in inverse kinematics and using quasi-free (p,2p) reactions as a novel technique to induce the fission process [3]. These new measurements have been performed with state-of-the art detectors especially designed to measure the fission products with high detection efficiency and acceptance, which were developed by the R3B collaboration [4]. The analysis of this new data will give us for the first time access to the excitation energy of the fissioning system by using the missing mass method and thus it will allow us to investigate the evolution of fission yields with the temperature.

[1] N. Vassh et al., *J. Phys. G: Nucl. Part. Phys.* **46**, 065202 (2019).
[2] T. Kajino et al., *Prog. Part. Nucl. Phys.* **107**, 109 (2019).
[3] J. Benlliure and J. L. Rodríguez-Sánchez, *Eur. Phys. J. Plus* **132**, 120 (2017).
[4] https://www.r3b-nustar.de/

Study of (p,2p) events at the CALIFA calorimeter in knockout induced fission of ^{238}U

Gabriel Garcia Jimenez[1,*], and the R3B Collaboration

[1] *Dpt. de Fisica de Particulas, Universidade de Santiago de Compostela, Santiago de Compostela, Spain.*

*e-mail: gabrielgarcia.jimenez@usc.es

Nuclear fission has been used as a tool for the study of nuclear properties since its discovery in 1939. A new approach was performed in the context of the R3B collaboration, at the FAIR facility, in which knockout reactions were used to induce fission in ^{238}U, which will allow to characterise the excitation energy of the process. The CALIFA calorimeter, a key part of the set-up, will be used to reconstruct the momentum of the two protons coming out the $(p, 2pf)$ reaction. Preliminary results show that kinematic variables are well reconstructed and in good agreement with theory.

Revisión de datos nucleares de ^{212}Po

Alejandro Martín Sánchez*, Raquel Mora Rodríguez

Departamento de Física, Universidad de Extremadura, 06006 Badajoz.

*e-mail: ams@unex.es

Rutherford and Woods [1] ya observaron en 1916 que unas pocas partículas alfa tenían un rango de unos 11,6 cm en aire, que era considerablemente mayor que el rango (8,6 cm) alcanzado por las bien conocidas partículas de 8,78437 MeV [2] emitidas por ^{212}Po, alcanzando el nivel fundamental de ^{208}Pb. Hoy en día es perfectamente conocido que estas partículas de largo alcance son emitidas desde los estados excitados de ^{212}Po. En este núcleo, la vida media parcial para desintegración alfa es comparable con su homónima para desintegración gamma, de tal manera que una pequeña fracción de los núcleos excitados de ^{212}Po decaerán directamente desde esos niveles excitados al nivel fundamental del ^{208}Pb. Las energías e intensidades de estos grupos de partículas de largo alcance ("long-range alpha-particles") fueron recopiladas por Rytz [3]. Se han realizado muy pocas revisiones de estos resultados [4], y los valores iniciales son prácticamente los que siguen vigentes desde entonces, incluso en las compilaciones de datos revisados más recientemente [5].

En nuestro laboratorio se han llevado a cabo nuevas medidas, chequeando los valores de las energías y las intensidades. Estas mediciones se realizaron con espectrometría de partículas alfa de baja resolución en cámara de vacío. La fuente usada ha sido un disco colimado de ^{232}U (en equilibrio con sus hijos) con un área activa de 20 mm^2, fabricada por electrodeposición en el CIEMAT. Se utilizó un detector de silicio, tipo PIPS, marca Canberra, con 50 mm^2 de área activa. La distancia fuente-detector fue de 65 mm. Se tomaron cerca de 90 espectros con objeto de realizar un análisis estadístico adecuado de los resultados obtenidos.

El hecho de que haya pocos resultados experimentales del efecto estudiado puede deberse a las dificultades que se presentan en la medida de estas partículas. En primer lugar, aparece su escasez, ya que su número es al menos cuatro órdenes de magnitud más bajo respecto a las consideradas emisiones más "normales". Por otro lado, debido a la corta vida media del ^{212}Po, se producen sumas en coincidencia entre las emisiones alfa procedentes del estado fundamental, y las partículas beta procedentes de las emisiones de ^{212}Bi, haciendo muy difícil el estudio de la región del espectro por encima de la línea de 8,78437 MeV, lugar esperado de aparición de las partículas alfa de largo alcance [6]. Para tratar de evitar estas interferencias, se incluyó un potente imán entre la fuente y el detector. Los resultados experimentales alcanzados permiten chequear los valores existentes en las tablas de datos nucleares, junto con sus incertidumbres, estimadas éstas, por primera vez, únicamente de manera experimental. Esto es importante, porque en la actualidad, las incertidumbres mostradas en las tablas de datos nucleares son solamente las medias no ponderadas de ciertos valores existentes con anterioridad [7], pero nunca han sido estimadas de un modo directo, como se ha realizado ahora en nuestro laboratorio.

[1] R. D. Evans, *The atomic nucleus*, Krieger (1982).
[2] E. Browne, R. B. Firestone, *Table of radioactive isotopes*, New York (1986).
[3] A. Rytz, *J. Recherches Centre Natl.* **25**, 254 (1953).
[4] G. T. Emery, W. R. Kane, *Phys. Rev.* **118**, 755 (1960).
[5] M. J. Martin, *Nucl. Data Sheets* **108**, 1583 (2007).
[6] A. Martín Sánchez, F. Vera Tomé, C. J. Bland, *Nucl. Instrum. Methods Phys. A* **295**, 273 (1990).
[7] A. L. Nichols, *Table de radionucleides*, LNE-LNHB/CEA (2011).

Agradecimientos: Trabajo parcialmente financiado por la Junta de Extremadura y el Fondo Europeo de Desarrollo Regional a través de la Ayuda GR21002.

Correlation between optical density and particle density in passive PADC (CR-39) detectors for high fluences

F. Barranco Blázquez[1,*], L. Palenciano[1], M.C. Jiménez-Ramos[2,3], J. García López[2,4], M. Seimetz[1]

[1]*Instituto de Instrumentación para Imagen Molecular (i3M), CSIC-Universitat Politècnica de València, Valencia, Spain.*
[2]*Centro Nacional de Aceleradores (CNA), Universidad de Sevilla-J. Andalucía-CSIC, Sevilla, Spain.*
[3]*Departamento de Física Aplicada II, Universidad de Sevilla, Sevilla, Spain.*
[4]*Departamento de Física Atómica, Molecular y Nuclear, Universidad de Sevilla, Sevilla, Spain.*

*e-mail: fbarranco@i3m.upv.es

Preclinical research is witnessing the growing importance of determining as precisely as possible the radiation dose deposited by ultra-intense ion bunches. In view of this growth, the use of passive detectors with a wide dynamic range is gaining in value, as they are less prone to saturation effects, making them attractive for cross-calibration of real-time devices and radiation dose monitoring.

For this calibration, two types of passive detectors have been irradiated with proton pulses with a width of 100 μs and energy 0.8 MeV. These detectors are the transparent polymer polyallyl-diglycol-carbonate (PADC) (CR-39) and radiochromic films of EBT3-U material. As a higher sensitivity has been observed in PADC, it is the most suitable material for measuring individual particles with the microscope [1,2]. However, counting traces becomes quite difficult for densities higher than 10^7 p/cm^2 due to the overlap between the tracks left by protons passing through the material. For higher fluences than this, the optical density of the material (OD_{net}), measured from images taken with a flatbed optical scanner and the software *imageJ*, shows a correlation with the density of particles passing through the 1 cm^2 chips of the material.

PADC chips of type RS39 (Radosys) were irradiated to a maximum fluence of about 10^{11} p/cm^2, and the results show a correlation with the optical density of the material up to 10^{10} p/cm^2 approximately, after the realisation of different etching processes. These results were compared with the results obtained for the radiochromic films (EBT3-U) which were irradiated with 0.8 MeV protons. For these, it was also observed that the grey values of the uniformly irradiated areas showed correlation with the fluence up to 10^{11} p/cm^2. However, PADC shows a wider dynamic range for particle density.

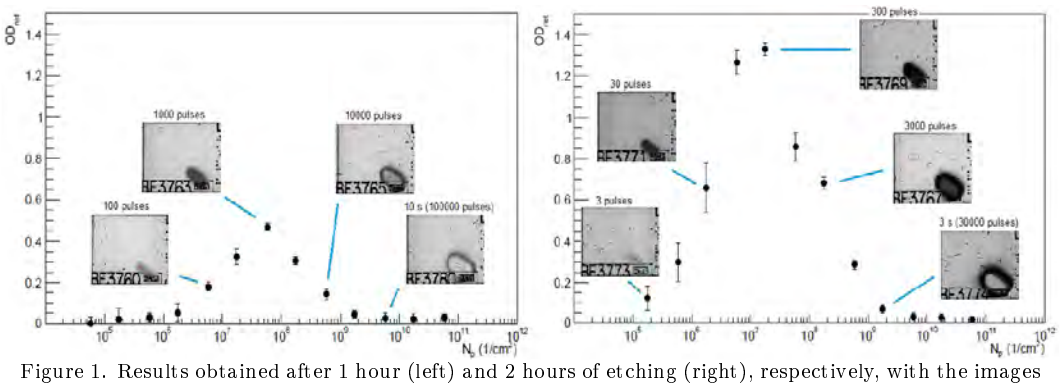

Figure 1. Results obtained after 1 hour (left) and 2 hours of etching (right), respectively, with the images obtained from the scanning of the chips.

[1] M. Seimetz, et al. *Phys. Med.* **76**, 72 (2020).
[2] M. Seimetz, et al. *Rev. Sci. Instrum.*, **89**, 023302 (2018).

Acknowledgements: Funded by Government of Spain, RTI2018-101578-B-C22, and by Generalitat Valenciana, AICO/2020/207. Co-financed by FEDER,IDIFEDER/2021/004, and Generalitat Valenciana, action EDGJID/2021/204.

Angular measurements on LGADs to study plasma effects using a Nuclear Microprobe

M.C. Jiménez Ramos[1,2,*], J. García López[1,3], A. García Osuna[1], I. Vila[4], E. Currás[4,5], R. Jaramillo[4], S. Hidalgo[6], G. Pellegrini[6]

[1]*CNA (U. Sevilla, J. Andalucia, CSIC), Av. Thomas A. Edison 7, 41092 Sevilla, Spain.*
[2]*Departamento de Física Aplicada II, Universidad de Sevilla, E-41012 Sevilla, Spain.*
[3]*Dept of Atomic, Molecular and Nuclear Physics. University of Sevilla. Av. Reina Mercedes s/n. 41012 Sevilla, Spain.*
[4]*Instituto de Física de Cantabria IFCA-CSIC-UC, Santander, Spain.*
[5]*Solid State Detector Group, CERN, Genéve, Switzerland.*
[6]*Centro Nacional de Microelectrónica, IMB-CNM-CSIC, Barcelona, Spain.*

*e-mail: mcyjr@us.es

The study of a Low Gain Avalanche Detector (LGAD) has been carried out by Ion Beam Induced Charge (IBIC) and Time Resolved Ion Beam Induced Charge (TRIBIC) using the nuclear microbeam line of the Centro Nacional de Aceleradores (CNA). For that purpose, a 3 MeV H ion beam was employed, and the results were compared to that obtained by the Transition Current Technique (TCT) using an infrared laser at the SSD laboratory at CERN and at the Clean Room of the Physics Institute of Cantabria (IFCA). Although the charge collection time is the same for both techniques, near the onset voltage the shape of the induced current pulses is significatively different. Moreover, the values of the absolute gain curve are considerably higher when measured by TCT. This gain suppression is related to the shielding effects of the electric field in the multiplication layer, which depend on the generated carrier density. Therefore, in order to study how the plasma effects change with the generated carrier density, experiments have been carried out by varying the proton incidence angle from 0° to 85°.

In this talk, the gain curves for all angles will be shown. The results indicate that when mean ionization density projected on the multiplication layer is minimum (50°) the measured gain is maximum. Also, at very large angles (> 70°) the electron path in the multiplication layer is the dominant factor for the gain suppression. TRIBIC results will also be shown, from which some conclusions can be drawn about the decrease in the hole gain and plasma effects outside the multiplication layer when the Bragg peak falls inside the detector.

Study of decay properties for La to Nd nuclei (A∼160) relevant for the formation of the r-process rare-earth peak

M. Pallàs[1,*], A. Tarifeño-Saldivia[3,1], G. G. Kiss[2], J. L. Tain[3], A. Tolosa-Delgado[4,3], A. Vitéz-Sveiczer[2], F.Calviño[1] for the BRIKEN collaboration[5]

[1]*Institut de Tècniques Energètiques (INTE), Universitat Politècnica de Catalunya (UPC), Spain.*
[2]*Institute for Nuclear Research (Atomki), Hungary.*
[3]*Instituto de Física Corpuscular (IFIC), Spain.*
[4]*Department of Physics, University of Jyväskylä, Finland.*
[5]*www.wiki.edu.ac.uk/display/BRIKEN/Home*

max.pallas@upc.edu

Around half of the nuclei heavier than iron are created via the rapid neutron capture process (r-process). For nuclear masses $A > 100$, there are two main peaks in the r-process elemental solar system abundances, located at $A \sim 130$ and $A \sim 195$, which are associated with the neutron shell closure during the $(n, \gamma) \leftrightarrow (\gamma, n)$ equilibrium. In contrast, the rare-earth peak (REP) is a small - but clear - peak around mass $A = 160$, which originates from the freeze-out during the late phases after neutron exhaustion. The formation of the REP offers a unique probe for the study of the late-time conditions on the r-process site. According to theoretical models and sensitivity studies, half-lives ($T_{1/2}$) and beta-delayed neutron emission probabilities (P_n) of very neutron-rich nuclei for $55 \leq Z \leq 64$ are the most influential ones on the formation of the REP [1,2]. The BRIKEN project [3,4] has been in operation from 2016 up to 2021 at the Radioactive Isotope Beam Factory (RIBF) in the RIKEN Nishina Center. BRIKEN has performed an ambitious measurement program of beta-decay properties of nuclei on the path of the r-process. The overall expected outcome of the BRIKEN project is about 120 new half-lives and 300 new measurements of single and multiple beta-delayed neutron emitters. Moreover, the BRIKEN-REP experiment has recently measured $T_{1/2}$ and P_n-values of nuclei from Ba to Eu (A $\sim$ 160), belonging to the region which is the most influential to the REP formation [5,6]. In this work, we discuss the status of the BRIKEN-REP experiment and present the first experimental results of new P_{1n}-values and $T_{1/2}$ for nuclei in the region from La to Nd.

[1] M. R. Mumpower et al , *Phys. Rev. C* **85**, 045801 (2012).
[2] A. Arcones and G. Martinez Pinedo , *Phys. Rev. C* **83**, 045809 (2011).
[3] J.L. Tain et. al , *Acta physica polonica B* **49(03)**, 417 − 428 (2018).
[4] A. Tolosa-Delgado et. al , *NIM A* **925**, 133 − 147 (2019).
[5] G. Kiss et al , *RIKEN Accel. Prog. Rep.* **53**, 33. (2020).
[6] A. Tarifeño-Saldivia et al , *RIKEN Accel. Prog. Rep.* **54**, 27. (2021).

Acknowledgements: This work has been supported by the Spanish Ministerio de Economía y Competitividad under Grants nos. FPA2014-52823-C2-1-P, FPA2014-52823-C2-2-P, FPA2017-83946-C2-1-P, FPA2017-83946-C2-2-P and grants from Ministerio de Ciencia e Innovacion nos PID2019-104714GB-C21 and PID2019-104714GB-C22.

β Decay Spectra Measurement for the Study of the Reactor Antineutrino Anomaly.

J. Agramunt[1], **G. A. Alcalá**[1,*], A. Algora[1,2], A. Beloeuvre[3], E. Bonnet[3], S. Bouvier[3], M. Estienne[3], D. Etasse[4], M. Fallot[3], L. Giot[3], A. Laureau[3], A. Porta[3], J.-S. Stutzmann[3], J. A. Victoria[1], and M. Yohannes[3].

[1]*Instituto de Física Corpuscular (IFIC), València, Spain.* [2]*Institute for Nuclear Research (Atomki), Debrecen, Hungary.* [3]*SUBATECH, CNRS/IN2P3, IMT Atlantique, Nantes Université, Nantes, France.* [4]*LPC Caen, CNRS/IN2P3, Caen, France.*

*e-mail: galcala@ific.uv.es

The Reactor Antineutrino Anomaly (RAA) has been a topic of great interest for the physics community in recent years [1]. The generally accepted Huber-Muller conversion model [2,3] to calculate the reactor's $\bar{\nu}$ spectrum has raised several questions about the experimental results and the different approximations used. In view of this, improved measurements of nuclear data of relevant isotopes plus the use of the Summation Calculation method [4] for the determination of the $\bar{\nu}$ spectrum brings a plausible alternative way of calculation. Critical calculations of this spectrum using standard databases' β feedings can suffer from the Pandemonium Effect problem, which can be solved by applying the Total Absorption Gamma Spectroscopy (TAGS) method [5].

The decay of only a relatively small number of neutron rich fission products contribute the most to the reactor $\bar{\nu}$ spectrum in the energy region where the anomaly is stronger [6]. Therefore, with the objective to directly determine the shapes of these β decay spectra, experimental campaigns have been carried out in the IGISOL facility at Jyväskylä with newly developed telescope detectors. Several β decay spectra of utmost relevance for the study of the RAA were measured, and more measurments are being planned.

This presentation is aimed to introduce the problem of the RAA and how the determination of the $\bar{\nu}$ spectrum is improved with the use of the Summation method with TAGS β feedings. Developed computational tools required for this study will be presented. Some preliminary results of the analysis of the data will be shown as well.

[1] G. Mention et al., *Physical Review D* **83**, 073006 (2011).
[2] P. Huber, *Physical Review C* **84**, 24617 (2011); *Physical Review C* **85**, 029901 (2012).
[3] T. A. Muller et al., *Physical Review C - Nuclear Physics* **83**, 054615 (2011).
[4] M. Estienne et al., *Physical Review Letters* **123**, 022502 (2019).
[5] A. Algora et al., *European Physical Journal A* **57**, 85 (2021).
[6] L. Hayen et al., *Physical Review C* **100**, 054323 (2019).

Acknowledgements: This work is supported by the Ministry of Science and Innovation of Spain via the grant PID2019-104714GB-C21.

Behaviour of particle detectors in a laser-driven neutron source

M. A. Millán-Callado[1,2,*], C. Guerrero[1,2], A. Alejo[3], S. Assenbaum[4], J. Benlliure[3], R. Beyer[5], B. Fernández[1,2], E. Griesmayer[6,7,8], A. R. Junghans[5], J. Kohl[9], F. Kroll[4], I. Prencipe[4], J. M. Quesada[1], C. Rödel[9], T. Rodríguez-González[1,2], S. Scheuren[9], U. Schramm[4], S. Urlass[5], C. Weiss[6,8], K. Zeil[4]

[1]*Dpt. Física Atómica, Molecular y Nuclear (FAMN), Facultad de Física. Universidad de Sevilla (US), Av. de la Reina Mercedes, S/N, 41012 Seville, Spain.*
[2]*Centro Nacional de Aceleradores (CNA, US - Junta de Andalucía - CSIC), C/ Tomás Alba Edison, 7. 41092. Seville, Spain.*
[3]*Instituto Galego de Física de Altas Enerxías, Universidad de Santiago de Compostela (IGFAE-USC), Rúa de Xoaquín Díaz de Rábago, 15705 Santiago de Compostela, A Coruña, Spain.*
[4]*Institute of Radiation Physics, Dpt. Laser Particle Acceleration, Helmholtz-Zentrum Dresden-Rosendorf (HZDR), 620, Bautzner Landstraße 400, 01328 Dresden, Germany.*
[5]*Institute of Radiation Physics, Dpt. Nuclear Physics, Helmholtz-Zentrum Dresden-Rosendorf (HZDR), 620, Bautzner Landstraße 400, 01328 Dresden, Germany.*
[6]*CIVIDEC Instrumentation GmbH, Schottengasse 3A/1/41, 1010 Wien, Austria.*
[7]*Faculty of Electrical Engineering and Information Technology, Technische Universität Wien, Gußhausstraße 25-29, 1040 Wien, Austria.*
[8]*Atominstitut, Technische Universität Wien, Stadionallee 2, 1020 Wien, Austria.*
[9]*Institute for Nuclear Physics, Technische Universität Darmstadt, S2|14, Schloßgartenstraße 9, 64289 Darmstadt, Germany.*

*e-mail: mmillan5@us.es

High power (~ PW) ultrashort pulse (~ fs) lasers are emerging as a promising alternative to conventional accelerators as compact sources of secondary radiation, including the production of neutron beams. These neutron beams, suitable for time-of-flight (TOF) experiments, can be characterized by time resolution, intensity per pulse, and frequency or repetition rate. In this context, short-pulse and high instantaneous flux laser-driven neutron sources (LDNS) are particularly attractive for nuclear physics applications based on the TOF technique.

Neutrons produced using this alternative method could reach higher instantaneous neutron fluxes than conventional neutron sources. However, it is necessary to characterize the experimental conditions associated with this type of sources, since the potential applications of these laser-driven neutrons rely on the performance of nuclear physics detectors in the environment produced by the laser-plasma interaction, which affects the response of the detectors commonly used in this type of measurements.

This work reports the preliminary results of an experimental campaign carried out in autumn 2021 at the DRACO laser facility (PW) of the Helmholtz Center Dresden Rossendorf (HZDR) in Dresden, Germany, with the objective of studying the feasibility of carrying out TOF nuclear reaction measurements in the harsh environment of a LDNS. The experiment consisted of characterizing and optimizing the response of different neutron detectors to these conditions under different ion acceleration and neutron production configurations.

While previous work has been performed either with high repetition rate but low power, or with high power (PW) but low repetition (single-shot mode); in DRACO we have succeeded in producing high-repetition neutron beams (~200 shots per day) in a high-power system. The production of a high-frequency beam has allowed us to use a low-efficiency detector, i.e: a diamond detector, to measure individual signals produced by fast neutron interactions, which is the first step towards neutron-induced reaction experiments in an LDNS.

β-delayed neutron spectroscopy of ^{85}As with MONSTER

A. Pérez de Rada[1,*], V. Alcayne[1], D. Cano-Ott[1], T. Martinez[1], E. Mendoza[1], J. Plaza[1], A. Sanchez-Caballero[1], D. Villamarin[1], J. Äystö[2], A. Jokinen[2], A. Kankainen[2], H. Penttilä[2], S. Rinta-Antila[2], J. Agramunt[3], A. Algora[3], C. Domingo-Pardo[3], J. Lerendegui-Marco[3,7], B. Rubio[3], J.L. Taín[3], K. Banerjee[4], C. Bhattacharya[4], P. Roy[4], F. Calviño[5], G. Cortés[5], C. Delafosse[6,2], I. Matea[6]

[1]*Centro de Investigaciones Energéticas, Medioambientales y Tecnológicas (CIEMAT), E-28040 Madrid, Spain.* [2]*JYFL, The Accelerator Laboratory of the Department of Physics, University of Jyväskylä, FI-40014 Jyväskylä, Finland.* [3]*Instituto de Física Corpuscular, CSIC-Universidad de Valencia, E-46071 Valencia, Spain.* [4]*Variable Energy Cyclotron Centre (VECC), IN-700064 Kolkata, India.* [5]*Universitat Politècnica de Catalunya (UPC), Departamento de Física, E-08034 Barcelona, Spain.* [6]*IJCLab, Université Paris-Saclay, CNRS/IN2P3, FR-91405 Orsay Cedex, France.* [7]*Universidad de Sevilla, Facultad de Física, E-41012 Sevilla, Spain.*
*e-mail: alberto.rada@ciemat.es

A better quantitative understanding of β-delayed neutron emission rates and spectra is relevant for nuclear structure, astrophysics, and reactor applications: β-delayed neutrons provide valuable information on the β-decay process, are needed in network calculations for understanding the stellar nucleosynthesis process, and can improve the understanding of the kinematics and safety of new reactor concepts loaded with new types of fuels. The field has experienced an increased activity during the last decades [1] thanks to the advances in nuclear experimental techniques and the radioactive ion beam facilities. More accurate measurements of β-delayed neutron emission properties like the emission probability, β-feeding, and energy spectrum from individual precursors are being made with advanced neutron detectors [2, 3, 4], digital data acquisition systems [5], and high intensity ion beams [6-9].

The β-delayed neutron emission in the ^{85}As decay has been measured at the Ion Guide Isotope Separator On-Line (IGISOL) facility [9] of the JYFL Accelerator Laboratory of the University of Jyväskylä. The ^{85}As isotopes were produced by proton-induced fission reactions in ^{238}U, separated from the rest of the fission fragments with IGISOL, and implanted onto a tape. The complete decay has been studied with the help of a complex setup which consists of a plastic scintillator detector for the emitted β-particles, a HPGe Clover and four $LaBr_3$ detectors for the emitted γ-rays, and the **MO**dular **N**eutron **S**pectrome**TER** (MONSTER) [4, 10] for the detection of the emitted neutrons. MONSTER consists of an array of 48 cylindrical cells of 200 mm diameter and 50 mm height, filled with BC501A or EJ301 scintillating liquid. Each cell is coupled through a light guide of 31 mm thickness to a R4144 or R11833 PMT. The neutron energy is determined by the time-of-flight technique, using the signals from the plastic detector and MONSTER as the start and stop signals, respectively.

In this conference, we report the results obtained from the measurement at JYFL. The β-delayed neutron energy distribution of the ^{85}As β-decay has been determined by unfolding the time-of-flight spectrum with the iterative Bayesian unfolding method [11], and their partial branching ratios to the excited states in the final nucleus by applying β-n-γ coincidences. We also compare the results of this work to existing data [12, 13].

[1] P. Dimitriou *et al.*, *Nuclear Data Sheets* **173**, 144-238 (2021).
[2] A. Buţă *et al.*, *Nucl. Instrum. and Methods A* **455**, 412-423 (2000).
[3] C. Matei *et al.*, *Proceedings of the 10th International Symposium on Nuclei in the Cosmos, 138, Proceedings of Science*, 1-5 (2008).
[4] A.R. Garcia *et al.*, *JINST* **7**, C05012 (2012).
[5] D. Villamarin *et al.*, In preparation.
[6] W.F. Henning *et al.*, *GSI publication*, (2001).
[7] H. Okuno *et al.*, *Prog. Theor. Exp. Phys.*, 03C002 (2012).
[8] R. Catherall *et al.*, *Nucl. Instrum. and Methods B* **317**, 204 (2013).
[9] I.D. Moore *et al.*, *Nucl. Instrum. and Methods B* **317**, 208 (2013).
[10] T. Martinez *et al.*, *Nuclear Data Sheets* **120**, 78 (2014).
[11] G. D'Agostini, *Nucl. Instrum. and Methods A* **362**, 487 (1995).
[12] K.-L. Kratz *et al.*, *Nucl. Phys. A* **317**, 335 (1979).
[13] D. Rudstam *et al.*, *At. Data and Nucl. Data Tables* **53**, 1 (1993).

Investigation of ^{130}Sn populated in the β decay of isomerically-purified ^{130}In isomers

J.R. Murias[1,*], J. Benito[1], L. M. Fraile[1], A. Korgul[2], M. Piersa,[2], E. Adamska[2], N. Andreyev[3,4], R. Álvarez-Rodríguez[5], A. E. Barzakh[6], G. Benzoni[7], T. Berry[8], M. J. G. Borge[9,10], M. Carmona[1], K. Chrysalidis[9], C. Costache[1]1, G. Cubiss[9,3], T. Day Goodacre[9,12], H. De Witte[9,13], D. V. Fedorov[6], V. N. Fedosseev[9], G. Fernández-Martínez[1]4, A. Fijałkowska[2], M. Fila,[2], H. Fynbo[1]5, D. Galaviz[1]6, P. Galve[1], M. García-Díez[1], P. T. Greenlees[17,18], R. Grzywacz[19,20], L. J. Harkness-Brennan[2]1, C. Henrich[2]2, M. Huyse[1]3, P. Ibáñez[1], A. Illana[13,23], Z. Janas[2], J. Jolie[2]4, D. S. Judson[2]1, V. Karayonchev[2]4, M. Kicińska-Habior[2], J. Konki[17,18], J. Kurcewicz[9], I. Lazarus[2]5, . Lică[9,11], A. López-Montes[1], M. Lund[1]5, H. Mach[2]6, M. Madurga[9,19], I. Marroquín[1]0, B. Marsh[9], M. C. Martínez[1], C. Mazzocchi[2], N. Mărginean[1]1, R. Mărginean[1]1, K. Miernik[2], C. Mihai[1]1, R. E. Mihai[1]1, E. Nácher[2]7, A. Negret[1]1, B. Olaizola[2]8, R. D. Page[2]1, S. V. Paulauskas[1]9, S. Pascu[1]1, A. Perea[1]0, V. Pucknell[2]5, P. Rahkila[17,18], C. Raison[3], E. Rapisarda[9], J.-M. Régis[2]4, K. Rezynkina[1]3, F. Rotaru,[1]1, S. Rothe[9], D. Sánchez-Parcerisa[1,29], V. Sánchez-Tembleque[1], K. Schomacker[2]4, G. S. Simpson[3]0, Ch. Sotty[10,11], L. Stan[1]1, M. Stănoiu[1]1, M. Stryjczyk[2,13], O. Tengblad[1]0, A. Turturica[1]1, J. M. Udías[1], P. Van Duppen[1]3, V. Vedia[1], A. Villa-Abaunza[1], S. Viñals[1]0, W. B. Walters[3]1, R. Wadsworth[3], N. Warr [24]

(IDS Collaboration)

[1]*Grupo de Física Nuclear and IPARCOS, Universidad Complutense de Madrid, CEI Moncloa, E-28040 Madrid, Spain.* [2]*Faculty of Physics, University of Warsaw, PL 02-093 Warsaw, Poland.* [3]*Department of Physics, University of York, York, YO10 5DD, United Kingdom.* [4]*Advanced Science Research Center (ASRC), Japan Atomic Energy Agency, Tokai-mura, Japan.* [5]*Escuela Técnica Superior de Arquitectura, Universidad Politécnica de Madrid, E-28040 Madrid, Spain.* [6]*Petersburg Nuclear Physics Institute, NRC Kurchatov Institute, 188300 Gatchina, Russia.* [7]*Istituto Nazionale di Fisica Nucleare, Sezione di Milano, I-20133 Milano, Italy.* [8]*Department of Physics, University of Surrey, Guildford GU2 7XH, United Kingdom.* [9]*CERN, CH-1211 Geneva 23, Switzerland.* [10]*Instituto de Estructura de la Materia, CSIC, E-28040 Madrid, Spain.* [11]*"Horia Hulubei" National Institute of Physics and Nuclear Engineering, RO-077125 Bucharest, Romania.* [12]*School of Physics and Astronomy, The University of Manchester, Manchester, United Kingdom.* [13]*Instituut voor Kern-en Stralingsfysica, KU Leuven, B-3001 Leuven, Belgium.* [14]*Institut für Kernphysik, Technische Universität Darmstadt, Germany.* [15]*Department of Physics and Astronomy, Aarhus University, DK-8000 Aarhus C, Denmark.* [16]*LIP and Faculty of Sciences, University of Lisbon, 1000-149 Lisbon, Portugal.* [17]*University of Jyväskylä, Department of Physics, P.O. Box 35, FI-40014 Jyväskylä, Finland.* [18]*Helsinki Institute of Physics, University of Helsinki, FIN-00014 Helsinki, Finland.* [19]*Department of Physics and Astronomy, University of Tennessee, Knoxville, Tennessee 37996, USA.* [20]*Physics Division, Oak Ridge National Laboratory, Oak Ridge, Tennessee 37831, USA.* [21]*Department of Physics, Oliver Lodge Laboratory, University of Liverpool, Liverpool L69 7ZE, United Kingdom.* [22]*Institut für Kernphysik, Technische Universität Darmstadt, 64289 Darmstadt, Germany.* [23]*Instituto Nazionale di Fisica Nucleare, Laboratori Nazionali di Legnaro, I-35020 Legnaro, Italy.* [24]*Institut für Kernphysik, Universität zu Köln, D-50937 Köln, Germany.* [25]*STFC Daresbury, Daresbury, Warrington WA4 4AD, United Kingdom.* [26]*National Centre for Nuclear Research, PL 02-093 Warsaw, Poland.* [27]*Instituto de Física Corpuscular, CSIC Universidad de Valencia, E-46071 Valencia, Spain.* [28]*TRIUMF, 4004 Wesbrook Mall, Vancouver, British Columbia, V6T 2A3 Canada.* [29]*Sedecal Molecular Imaging, E-28110 Algete (Madrid), Spain.* [30]*LPSC, IN2P3-CNRS/Université Grenoble Alpes, Grenoble Cedex F-38026, France.* [31]*Department of Chemistry, University of Maryland, Maryland 20742, USA.*

*e-mail: javiro02@ucm.es

The understanding of the evolution of shell structure far from the β-stability line is one of the major challenges in nuclear structure. Neutron-rich nuclei with a number of protons and neutrons close to

magic numbers are an ideal testing ground for shell model calculations. The structure of the even-even nucleus ^{130}Sn (Z=50, N=80), in the vicinity of ^{132}Sn (N=82) shell closure [1], is interesting from this viewpoint. Expected neutron-neutron coupling in ^{130}Sn arise from the shell-model configurations in the region, with two neutrons bellow the N=82 gap.

In this work we will report on the IS610 experiment carried out at the ISOLDE Decay Station (IDS) located at the ISOLDE facility at CERN. The experiment was aimed at completing the known level scheme as well as measuring excited level lifetimes. The ^{130}Sn structure was populated in the β decay of ^{130}In, produced as a fission product of a UC_x target. Indium diffused out of the target, were ionized by the Resonance Ionization Laser Ion Source (RILIS) and separated in mass. We took advantage of the isomeric selection capabilities of RILIS to enhance the ionization of the three known ^{130}In β decaying isomers to individually study their decay.

Gamma spectroscopy using high-resolution HPGe detectors has been employed to the construct the level scheme. For the measurement of level lifetimes the Advanced Time-Delayed $\beta\gamma\gamma$(t) method [2] was used. It makes use of electronic coincidences between fast scintillators to measure time differences between the population and de-excitation of nuclear levels. For that purpose we use fast β plastic and γ $LaBr_3$(Ce) scintillator detectors. The knowledge of the level scheme and the half-lives allows us to extract transition probabilities that make it possible to compare with theoretical calculations.

An extended level scheme of ^{130}Sn compared to the previous work [4] has been obtained. Level lifetimes for some of the low-lying states have also been obtained. We will present the new spectroscopic results and a comparison to recent shell model calculations.

[1] J. Benito, L. M. Fraile, A. Korgul et al., *Phys. Rev. C*, **102**, 014328, (2020).
[2] H. Mach, R.L. Gill and M. Moszyński, *Nucl. Instrum. Methods Phys. Res. A*, **280**, 49-72, (1989).
[4] B. Fogelberg, K. Heyde, J. Sau et al. *Nuclear Physics A*, **352**, 157-180, (1981).

Acknowledgements: This work was funded by projects RTI2018-098868-B-I00, FPA2015-65035-P, FPA-64969-P and FPA2017-87568-P (Spanish MCIN/AEI/FEDER), UMO-2015/18/E/ST2/00217, UMO-2015/18/M/ST2/00523 and UMO-2019/33/N/ST2/03023 (Polish National Science Center), CERN/FIS-NUC/0004/2015 (Portuguese FCT), 05P18PKCIA (German BMBF), CERN/ISOLDE (Romanian IFA), GOA/2015/010 (BOF KU Leuven) and ENSAR2 654002 (EU H2020).

Proton-induced cross sections of β+ isotopes of interest in PET range verification

Teresa Rodríguez González[1,2*], Carlos Guerrero[1,2], Claus Maximilian Bäcker[4,5,6,7], Julia Bauer[8], Christian Bäumer[4,5,6,7,9], Javier Balibrea Correa[10], Stephan Brons[8], C. Domingo-Pardo[10], **M. del Carmen Jiménez Ramos**[2,3,**], Jorge Lerendegui Marco[1,10], Ion Ladarescu[10], M. de los Ángeles Millán Callado[1,2], José Manuel Quesada[1]

[1]*University of Sevilla, Atomic, Molecular and Nuclear Physics, Sevilla, Spain.*
[2]*Centro Nacional de Aceleradores, Sevilla, Spain.*
[3]*University of Sevilla, Department of Applied Physics II, ETSA, Sevilla, Spain.*
[4]*TU Dortmund University, Department of Physics, Dortmund, Germany.*
[5]*University Hospital Essen, Essen, Germany.*
[6]*West German Cancer Centre, Essen, Germany.*
[7]*West German Proton Therapy Centre Essen, Essen, Germany.*
[8]*Heidelberg Ion-Beam Therapy Centre HIT, Department of Radiation Oncology, Heidelberg Germany.*
[9]*German Cancer Consortium DKTK, German Cancer Consortium DKTK, Heidelberg, Germany.*
[10]*Instituto de Física Corpuscular, CSIC-University of Valencia, Valencia, Spain.*

*e-mail: mrodriguezg@us.es
**e-mail: mcyjr@us.es

In PET-based beam range verification for particle therapy, new measurements and evaluations of the reaction cross-sections producing β^+ emitters are required in order to compare the measured and simulated activity distribution in the patient.

We have conducted a comprehensive measurement campaign at several irradiation facilities using different ion types in the therapeutic energy regime and different PET imaging technologies to detect short-lived (online PET monitoring) and long-lived (offline PET monitoring) radionuclides. The following experimental data will be presented:

a) The proton-induced production of the long-lived ^{11}C ($t_{1/2}$=20 min), ^{13}N ($t_{1/2}$=9.9 min) and ^{15}O ($t_{1/2}$=2 min) isotopes produced in the main elements of the human body (C, N and O) were measured at the Centro Nacional de Aceleradores (CNA) up to 20 MeV, and at the West German Proton Therapy Center (WPE) from 30 up to 200 MeV. The employed method combines the activation of an array of thin foils with the induced activity measurement using a clinical PET scanner. The carbon-induced production of ^{11}C was obtained at Heidelberg Ion Therapy Center (HIT) up to 400 MeV/u measuring the activation in graphite foils with NaI scintillation detectors.

b) The proton-induced cross-sections of the short-lived ^{12}N ($t_{1/2}$=11 ms) in C, ^{38m}K ($t_{1/2}$=0.92 s) in Ca and ^{29}P ($t_{1/2}$=4 s) in P up to 200 MeV and the carbon-induced cross-sections of ^{12}N and ^{10}C ($t_{1/2}$=19 s) in C up to 400 MeV/u were measured at HIT. The experiments consist in the activation of pure targets and "online" acquisition with $LaBr_3$ scintillation detectors operating in coincidence.

The results from these experimental campaigns will be presented and the relevance of the new data for PET range verification will be discussed.

^{46}Mn beta-decay experimental studies and its connection with CCSN

D. Godos-Valencia[1,*], L. Acosta[1], P. Ascher[2], B. Blank[2], J. Giovinazzo[2], F. de Oliveira[3], A. M. Sánchez-Benítez[4]

[1]*Instituto de Física, Universidad Nacional Autónoma de México, Mexico.* [2]*LP21-Bordeaux France,* [3]*GANIL, France.* [4]*CEAFMC, Universidad de Huelva, Spain.*

*e-mail: dgodosv@gmail.com

Stars with initial mass greater than 8 $M_\odot$ end their lives through a Core Collapse Supernova (CCSN) explosion. Besides, ^{44}Ti nucleosynthesis takes place in CCSN; making this nucleus a good gamma astronomy tracer for Super Nova (SN) events due to the characteristic gamma rays emitted on its decay chain. Furthermore, the comparison between observations and models of the synthetized ^{44}Ti in CCSN gives important constrains to the models. In the later, reaction networks are used for modelling nucleosynthesis occurring in the last stages of those stars with thermonuclear reaction rates as its inputs [1,2,3].

Unfortunately, a direct measurement of the cross section for a given thermonuclear reaction is extremely difficult in the current laboratories worldwide. Therefore, indirect methods can be used for this purpose, especially when the reaction rate is dominated by a narrow isolated resonance. In this context, beta-delayed proton emission is very useful with (p,γ) reactions involving low and medium mass proton-rich radioactive nuclei. That is a consequence of the fact that in those reactions narrow isolated resonances are likely to occur [1,4].

In this work we present the preliminary results of analysing the ^{46}Mn decay channel as a way to study the ^{45}V(p,γ)^{46}Cr reaction. This is due to the thought that nucleosynthesis of ^{44}Ti in CCSN explosions is quite sensitive to that reaction [5]. The ^{46}Mn was selected among other species in the cocktail beam delivered by LISE fragment separator at GANIL (Caen, France) in order to study its beta decay and the excited states of his daughter nucleus ^{46}Cr. We present the proton and gamma emission peaks related to the ^{46}Mn decay and compare them with the work from references [6,7].

Figure 1. ^{46}Mn decay proton energies spectra comparison. The curves in: green shows [7] results multiplied by 20; red shows [6] results multiplied by 2; and blue shows our results. Some interesting structures can be seen only in our work.

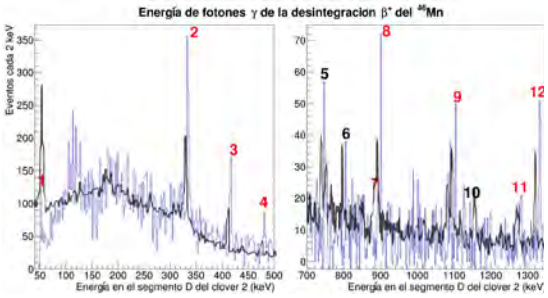

Figure 2. ^{46}Mn decay gamma energies spectra comparison. The curves in: black shows [6] results divided by a factor of 4 (left) and 2 (right); blue shows our results. More structures can be seen in our work.

[1] C. Illiadis, *Nuclear Physics of Stars*, Wiley-VCH (2007).
[2] A. Heger, C.L. Fryer, S.E. Woosley, N. Langer, and D.H. Hartmann, *ApJ* **591**, 288 (2003).
[3] C. Giunti, and K.C. Wook, *Fundamentals of Neutrino Physics and Astrophysics*, Oxford University Press (2007).
[4] L. Trache, E. Simmons, et al., *AIP Conference Proceedings* **1409**, 67 (2011).
[5] L.-S. The, D.D. Clayton, L. Jin, and B.S. Meyer, *ApJ* **504**, 500 (1998).
[6] C. Dossat, N. Adimi, et al., *Nuclear Physics A* **792**, 18 (2007).
[7] J. Giovinazzo, B. Blank, et al., *Eur. Phys. J. A* **10**, 73 (2001).

Acknowledgements: This work is supported by DGAPA-UNAM IN107820 and CONACyT 314857 projects.

Quasielastic neutrino-nucleus scattering within realistic nuclear model and Monte Carlo event generator

J. García-Marcos*, R. González-Jiménez, J. M. Udías

Grupo de Física Nuclear, Departamento de Estructura de la Materia, Física Térmica y Electrónica, Facultad de Ciencias Físicas, Universidad Complutense de Madrid, CEI Moncloa, Madrid 28040, Spain.

*e-mail: javier31@ucm.es

Neutrino oscillation experiments are essential to reach key goals in neutrino physics such as measuring CP-symmetry violation phase, neutrino mixing angles, and determining neutrino mass ordering, as well as searching physics beyond the Standard Model. These objectives require severe accuracy when evaluating the neutrino oscillation probability, which depends, among other parameters, on the neutrino energy. In current and future generation of oscillation experiments (T2K, DUNE, NOvA...) the neutrino beams used are not monoenergetic. Thus, in order to reduce systematic errors, the focus is on the interaction between neutrinos and targets, which are made of complex nuclei such as ^{12}C, ^{16}O or ^{40}Ar. These are the reasons why a deep study of neutrino-nucleus scattering is needed [1].

The main interaction mechanism in the neutrino-nucleus scattering when the energy of the neutrinos is up to 1 GeV is the so-called quasielastic (QE) scattering, where an incoming neutrino scatters off a bounded nucleon. This region is the core of neutrino energy distribution for several neutrino oscillation experiments such as T2K [1,2]. The way nuclei are described via different nuclear models is the main challenge we face when trying to extract information from these sorts of processes.

In this study, we consider the state-of-the-art spectral function, the so-called Rome spectral function (RSF) as our nuclear model [3]. The RSF provides a realistic description of the initial states of the nucleons inside the nucleus and gives us the probability of finding a nucleon with certain energy and momentum. Since the phase space of this process is vast, Monte Carlo (MC) generator is chosen so as to have a more efficient way of calculating our results. MC code generates randomly millions of possible kinematics belonging to phase space. Then, via acceptance-rejection method, the phase space is filled with all allowed kinematic configurations. The main advantage of this method is that only one run of the code is enough. At that point, results can be acquired just performing the corresponding computations.

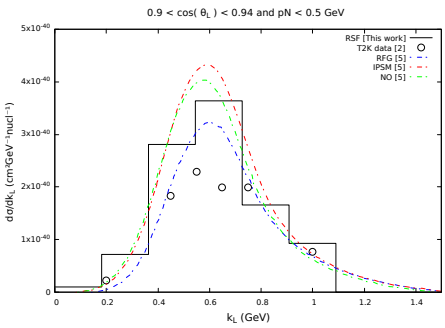

Figure 1. The T2K CC0π inclusive $\nu_\mu-^{12}$C cross section for RSF model, compared with experimental data [4], and other models [5].

This work is meant to be the benchmark for highly-developed analysis, using more sophisticated nuclear models such as the so-called relativistic mean field (RMF) model [4]. In such manner, we compare our results, either for inclusive and semi-inclusive differential cross sections, with recent data from the T2K (ν_μ on ^{12}C) [2]. We also compare our results with the up-to-date predictions obtained in Ref. [5], where three different nuclear models are used (see Fig. 1). Discrepancies between models and data come from other interaction mechanisms (mainly final state interactions and 2p2h) and Pauli blocking effects [6] that are not being taken into account in this work and contribute to experimental data.

[1] L. Alvarez-Ruso *et al.*, *Progress in Particle and Nuclear Physics* **100** (2018)
[2] K. Abe *et al.* (The T2K Collaboration), *Phys. Rev. D* **98**, 032003 (2018).
[3] O. Benhar, *et al.*, *Nuclear Physics A* **579** 493 (1994); O. Benhar *et al.*, *Phys. Rev. D* **72**, 053005 (2005).
[4] R. González-Jiménez *et al.*, *Phys. Rev. C* **105**, 025502 (2022)
[5] J.M. Franco-Patino *et al.*, *Phys. Rev. D* **104** 073008 (2021)
[6] R. González-Jiménez *et al.*, *Phys. Rev. C* **100**, 045501 (2019)

Acknowledgements: This work was supported by the Madrid Government under the Multiannual Agreement with Complutense University in the line Program to Stimulate Research for Young Doctors in the context of the V PRICIT (Regional Programme of Research and Technological Innovation), Project PR65/19-22430 (J.G.-M. and R.G.-J.) and RTI2018-098868-B-100 (MCIU/AEI,FEDER,EU) (J.M.U.).

Unified radiochemical method to determine ^{129}I by AMS in different matrix analysed in oceanographic studies

Victoria Lérida-Toro[1,*], Unai Abascal[1], María Villa-Alfageme[1,3], Santiago Hurtado[3], Jessica Klar[4], Natalie Hicks[5], José María López-Gutiérrez[1,2]

[1]*Centro Nacional de Aceleradores (Universidad de Sevilla, CSIC, Junta de Andalucía), Spain.* [2]*Dpto. Física Aplicada I, EPS, Universidad de Sevilla, Spain.* [3]*Dpto. Física Aplicada II, ETSIE, Universidad de Sevilla, Spain.* [4]*Université de Perpignan UPVD – CEFREM, France.* [5]*School of Biological Sciences, University of Essex, UK.*

*e-mail: vlerida@us.es

^{129}I is a long-lived radioisotope ($t_{1/2}$=15,7·10^6 years) whose origin is mainly anthropogenic. Its main sources are i) fallout from nuclear test carried out in 1945-1980, ii) nuclear accidents and iii) discharges from Nuclear Fuel Reprocessing Plants (NFRPs) [1]. Iodine is present in all environmental compartments and is conservative in water. This facts, together its long half-life and its continuous release in documented amount from NFRPs, make this radionuclide an excellent ocean tracer [2].

In oceanographic studies some samples of different matrix are analysed apart from seawater. For example, algae and mussel are frequently used as bioindicators. The impact of the radioactive contamination in aquatic systems is often recorded in sediments. These, depending on their biogeochemical behaviour, can give detailed information on the history of the discharges from the sources and the environmental processes related to the transportation of the radionuclides to the sediment.

For some long-lived radioisotopes as ^{129}I, only high sensitivity techniques as Accelerator Mass Spectrometry (AMS) (Figure 1) can measure it concentration at environmental levels [3]. To determine ^{129}I in environmental samples, application of a specific radiochemical methods to extract iodine different species from the matrix is needed. The isolation of the problem isotope is necessary in order to obtain the isotope in the appropriate form (silver iodide, AgI) for the measurement and reduce interferents as much as possible.

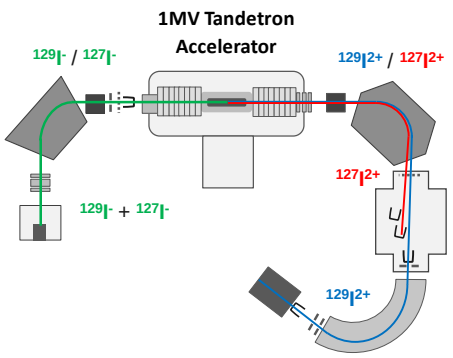

Figure 1. Spanish Accelerator for Radionuclide Analysis (SARA), the CNA AMS system.

The proposed radiochemical method consists of: a) pre-treatment depending on the sample matrix (filtering for seawater and microwave digestion for solid samples), b) redox process to decompose organic matter and adjust all iodine species oxidation status, c) iodine purification by a double extraction (first in an organic solvent and then in a reducing solution), d) silver iodide precipitation and e) cathode preparation for AMS measurement. Microwave digestion is a fast method to prepare solid samples and reduce cross contamination to a minimum.

In this work, a unified radiochemical method to determine ^{129}I by AMS in solid and liquid environmental samples has been applied in seawater from Namibian coast and core sediments of different texture from Celtic Sea. ^{129}I concentration measurement values range between (0.19-7.16)·10^{12} at./kg for sediment cores and between (0.75-1.45)·10^7 at./kg for seawater. These results have made it possible to evaluate the sources of ^{129}I the sampled areas. We found that the greatest influence in the Celtic Sea is the Sellafield NFRP and the main source of ^{129}I in the North of Benguela ecosystem is global fallout. As a conclusion, it can be noted that proposed radiochemical method is effective for the preparation of environmental samples of different matrices and with significantly variable ^{129}I concentrations.

[1] Raisbeck, G. M., y Yiou, F., ^{129}I in the oceans: origins and applications, *Sci. Total Environ.* **237–238**, 31 (1999).
[2] Karcher, M., Smith, J., Kauker, F., Gerdes, R., y Smethie, W., Recent changes in Arctic Ocean circulation revealed by ^{129}I observations and modeling, *J. Geophys. Res. Ocean.* **117** (2012).
[3] García-León, M., Accelerator Mass Spectrometry (AMS) in Radioecology, *J. Environ. Radioact*, **186**, 116 (2018).

Neutron spectrometry with HENSA: from underground physics to space weather applications

Ariel Tarifeño-Saldivia[1,*], on behalf of the HENSA collaboration[2]

[1]*Instituto de Física Corpuscular (IFIC), CSIC-UV, Catedrático José Beltrán, 2, E-46980 Paterna, Spain.*
[2]*https://www.hensaproject.org/home/about-hensa/collaboration*

*e-mail: atarisal@ific.uv.es

In underground facilities neutrons are produced from nuclear reactions induced by the intrinsic radioactivity of the materials in the rock and cavity walls. These radiogenic neutrons constitute a background which is a limiting factor for low counting rate experiments in astrophysics, dark matter and neutrino searches. Therefore, a proper characterization of the spectral distribution of radiogenic neutrons is required in order to properly assess or mitigate the neutron background component affecting experiments in underground facilities. On the other hand, neutrons are continuously produced as a secondary radiation from cosmic-ray interactions in the upper atmosphere of our planet. This component is the main contribution to the ambient neutron background observed at ground level or high altitudes. The measurement of cosmic-ray neutrons is connected with different fields such as environmental radioactivity, single event upsets (SEUs) in microelectronics, the physics of cosmic-rays and space weather.

In this contribution the High Efficiency Neutron Spectrometry Array (HENSA) will be presented. HENSA is a state-of-the-art detection system for neutron background spectrometry in low radioactivity facilities, such as underground laboratories, and for the measurement of secondary neutrons produced by cosmic-rays. The HENSA spectrometer has a spectral sensitivity 5-15 times larger than conventional spectrometers in a wide neutron energy range spanning from thermal up to GeV's. For cosmic-ray neutrons, HENSA provides near real-time measurements of the neutron spectrum on a time scale of tens of minutes up to few hours, thus enabling possible applications in space weather as a neutron monitor with spectral sensitivity. Since 2019 HENSA is being used for a long-term characterization of the neutron background at the Canfranc Underground Laboratory (LSC), which includes continuous measurements in hall A and hall B. Moreover, in 2020 HENSA has been used to map the cosmic-ray neutron background along the spanish territory during quiet solar conditions at the beginning of the solar cycle #25. Currently, a new version of HENSA, called HENSA++, is being developed at IFIC for space weather applications. The status of the HENSA project (www.hensaproject.org) and future perspectives will be discussed in this talk.

Study of multi-nucleon knockout reactions of exotic nuclei in the region of Sn

Martina Feijoo Fontán* and R3B collaboration

Física Atómica, Molecular e Nuclear, Universidade de Santiago de Compostela, Spain.

*e-mail: martina.feijoo.fontan@usc.es

The experimental data collected during the S515 experiment performed by R3B collaboration at GSI/FAIR represent a great opportunity to obtain nucleon knockout cross sections of exotic nuclei around 132Sn. These cross sections can be used to extract information about short-range correlations (SRCs), which emerge from pairs of nucleons having large relative momentum compared to their centre-of-mass momentum [1]. Recently, several works based on inclusive measurements [2,3] have shown that these SRCs could reduce the single nucleon knockout cross sections by around 50%, depending on the neutron excess (N/Z) of the initial projectile. The S515 data could help us to go further in this investigation because we could correlate the knockout cross sections of one and two nucleons with the number of protons and neutrons detected by CALIFA and NeuLAND and perform complete kinematical studies to separate between SRC events and others involving evaporation of particles. At the moment, the identification of the fragments between FRS and Cave C is done for the 124Sn settings (136Xe fragmentation), as well as charge calibrations for the LOS and R3B-MUSIC detectors and energy calibration for CALIFA crystals. Thus, the resulting yields for different incoming energies and targets can be compared.

[1] M. Duer et al., *Nature* **560**, 620 (2018).
[2] J. Díaz-Cortés et al., *Physics Letters B* **811**, 135962 (2020).
[3] V. Vaquero et al., *Physics Letters B* **795**, 356 (2019).

Measurement of $^{27}Al(\alpha,n)^{30}P$ thick target neutron yields at CMAM using the miniBELEN-10A neutron counter

N. Mont-Geli[1,*], A. Tarifeño-Saldivia[3], F. Calviño[1], L.M. Fraile[2], J.L. Taín[3], A. Perea[8], G. Cortés[1], M. Pallàs[1], E. Nácher[3], G. García[4], S. Viñals[4], V. Alcayne[5], A. Algora[3], J. Balibrea-Correa[3], J. Benito[2], M.J.G. Borge[8], J.A. Briz[8], D. Cano-Ott[5], A. De Blas[1], C. Domingo-Pardo[3], B. Fernández[6,7], R. García[1], J. Gómez-Camacho[6,7], E.M. González-Romero[5], C. Guerrero[6,7], J. Lerendegui-Marco[3], M. Llanos[2], T. Martínez[5], E. Mendoza[5], J.R. Murias[2], S.E.A. Orrigo[3], A. Pérez de Rada[5], V. Pesudo[5], J. Plaza[5], J.M. Quesada[6], A. Sánchez[5], V. Sánchez-Tembleque[2], R. Santorelli[5], O. Tengblad[8], A. Tolosa-Delgado[9], J.M. Udías[2], D. Villamarín[5]

[1]*Institut de Tècniques Energètiques (INTE), Universitat Politècnica de Catalunya (UPC), E-08028 Barcelona, Spain.*
[2]*Grupo de Física Nuclear (GFN) and IPARCOS, Universidad Complutense (UCM), E-28040 Madrid, Spain.*
[3]*Instituto de Física Corpuscular (IFIC), CSIC, E-46071 Valencia, Spain.*
[4]*Centro de Micro-Análisis de Materiales (CMAM), Universidad Autónoma de Madrid (UAM), E-28049 Madrid, Spain.*
[5]*Centro de Investigaciones Energéticas, Medioambientales y Tecnológicas (CIEMAT), E-28040 Madrid, Spain.*
[6]*Dpto. Física Atómica, Molecular y Nuclear, Universidad de Sevilla (US), E-41012 Sevilla, Spain.*
[7]*Centro Nacional de Aceleradores CNA (U. Sevilla - J. Andalucía - CSIC), E-41092 Sevilla, Spain.*
[8]*Instituto de Estructura de la Materia (IEM), CSIC, E-28049 Madrid, Spain.*
[9]*University of Jyväskylä, Department of Physics, PO Box 35, FI-40014, Jyväskylä, Finland.*

*e-mail: nil.mont@upc.edu

Neutron production through α-induced nuclear reactions is relevant in several fields. Specifically, (α,n) reactions are interesting in nuclear astrophysics as a source of neutrons for the slow neutron capture nucleosynthesis (the s-process) [1] and in the α-particles capture process (the α-process) [2, 3]. Other fields of interest include the neutron-induced background in underground laboratories [4] and in nuclear facilities such as nuclear reactors and particle accelerators [5]. Currently, evaluated data is only available for a limited number of isotopes and the databases present large discrepancies in some cases of interest.

The Measurement of Alpha Neutron Yields and spectra (MANY) collaboration is a coordinated effort by several Spanish research groups with the aim to carry out measurements of (α,xn) reactions yields, cross-sections and neutron spectra. The project relies on the exploitation of the existing infrastructure in Spain, in particular, the α-beams produced by the accelerators at CMAM [6] and CNA [7], and the use of neutron detection systems such as miniBELEN [8], a 4π counter with a nearly flat response up to 10 MeV based on the use of ^{3}He thermal neutrons counters and a high-density polyethylene moderator, and MONSTER [9,10], a time-of-flight spectrometer based on the use of BC501/EJ301 liquid scintillation modules. Both systems are complemented by γ-spectroscopy measurements using an array of fast $LaBr_3(Ce)$ scintillation detectors of the FATIMA type [11] with angular resolution capabilities. All instruments are coupled to high performance digital electronics.

In this work we report the results of the measurement of thick target total neutron yields and cross-sections from the $^{27}Al(\alpha,n)^{30}P$ reaction using miniBELEN. This measurement has been part of the commissioning of miniBELEN and the 45º beam-line at CMAM for the MANY program in (α,n) reactions.

[1] J.L. Tain *et al.*, *J. Phys.: Conf. Ser.* **665**, 012031 (2010).
[2] S.E. Woosley and R.D. Hoffmann, *Astrophys. J.* **395**, 202 - 239 (1992).
[3] J. Bliss *et al.*, *J. Phys. G.: Nucl. Part. Phys.* **44**, 054003 (2017).
[4] A. Bettini, *Nucl. Instrum. Methods* A **626–627**, S64 (2010).
[5] T. Murata and K. Shibata, *J. Nucl. Sci. Technol*. **39**, 76 (2002).
[6] A. Redondo-Cubero *et al.*, *Eur. Phys. J. Plus* **136**, 175 (2021).
[7] J. Gómez-Camacho *et al.*, *Eur. Phys. J. Plus* **136**, 273 (2021).
[8] N. Mont i Geli, *A novel modular neutron detector for (α,n) reactions: design and experimental validation*, Master thesis, U. de Sevilla, 2020.
[9] A.R. Garcia et al., *JINST* **7** C05012 (2012).
[10] T. Martinez *et al.*, *Nuclear Data Sheets* **120** (2014) 78.
[11] V. Vedia *et al.*, *Nucl. Instrum. Meth. A* **857** (2017) 98.

Acknowledgements: This work has been supported by the Spanish Ministerio de Economía y Competitividad under grants FPA2017-83946-C2-1 & C2-2 and PID2019-104714GB-C21 & C22.

Realistic treatment of nuclear structure in the neutrino-nucleus interaction

T. Franco-Munoz*, R. González-Jiménez, J.M. Udías

Grupo de Física Nuclear, Departamento de Estructura de la Materia, Física Térmica y Electrónica, Facultad de ciencias Físicas, Universidad Complutense de Madrid and IPARCOS, CEI Moncloa, Madrid 28040, Spain.

*e-mail: taniafra@ucm.es

An unprecedented activity has been unleashed in recent years to determine neutrino properties and their interactions. It has been firmly established that neutrinos oscillate and hence are massive particles. Some of the oscillation parameters, such as the neutrino mixing angles, have been measured with some precision, but other properties remain to be determined, such as their masses or the phase that quantifies the possible charge-parity violation. These are some of the goals of the new generation of accelerator-based neutrino oscillation experiments NOvA, DUNE and HyperKamiokande, with which neutrino physics enters a new 'Precision Era' [1].

The fact that all neutrino oscillation experiments use complex nuclei as target material in the detectors, for example mineral oils, water or liquid argon, complicates the analysis of the results since nuclear effects must be considered. In the energy region covered by the neutrino oscillation experiments, the neutrino-nucleus scattering cross section is not very precisely known, so that it is currently one of the largest contributions to the error [2]. This is what makes the study of neutrino-nucleus interactions a hot topic and brings theoretical nuclear physics to the stage.

Among all the reaction mechanisms that take place in neutrino experiments, we focus on the quasielastic channel (QE), where the scattering off a bound nucleon which is knocked out from the nucleus occurs. This process is studied within a realistic nuclear framework, using a state of the art relativistic mean-field based model for the description of the nuclear dynamics and final state interactions within a quantum mechanical framework (see [3] and references there in). Residual interactions between the bound nucleons through pion exchange are also included. We extend the usual treatment of QE scattering, based on a one-body current operator, by incorporating a two-body meson-exchange current (MEC) one. In this work, MEC include the dominant Delta-resonance mechanism (excitation of the $\Delta(1232)$ resonance and its subsequent decay into $N\pi$) and the background contributions deduced from the chiral perturbation theory Lagrangian of the pion-nucleon system [4].

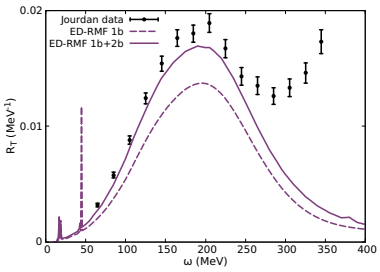

Figure 1. ^{12}C electromagnetic transverse response using the ED-RMF model to describe the final nucleon. The transferred momentum q is 570 MeV/c.

The connection of electron scattering experiments with neutrino scattering allows to scrutiny the available theoretical models by a first comparison to electron scattering data. Then, in our work [5], we compare our calculation of the electromagnetic responses of the ^{12}C nucleus with the available experimental data. We find that the effect of the two-body currents is only significant in the transverse channel, where the response is increased up to a 34%, leading to an improved description of the data compared to the one-body case (Fig. 1). The key contribution of this work is the incorporation of the two-body meson exchange current contribution.

[1] L. Alvarez-Ruso et al., *Progress in Particle and Nuclear Physics* **100**, 1-68 (2018).
[2] K. Abe et al. (T2K Collaboration), *arXiv:1607.08004* (2016).
[3] R. González-Jiménez et al. *Phys. Rev. D* **97**, 013004 (2018).
[4] S. Scherer and M. R. Schindler, *Quantum Chromodynamics and Chiral Symmetry in A Primer for Chiral Perturbation Theory. Lecture Notes in Physics*, **830**. Springer, Berlin, Heidelberg (2011).
[5] T. Franco-Munoz et al., *arXiv:2203.09996* (2022).

Acknowledgements: This work was supported by the Madrid Government under the Multiannual Agreement with Complutense University in the line Program to Stimulate Research for Young Doctors in the context of the V PRICIT (Regional Programme of Research and Technological Innovation), Project PR65/19-22430 (T.F.-M. and R.G.-J.) and RTI2018-098868-B-100 (MCIU/AEI,FEDER,EU) (JMU). The computations of this work were performed in Brigit, the HPC server of the Universidad Complutense de Madrid.

Quantum simulation and machine learned analysis of an extended Agassi model

Álvaro Sáiz[1,*], José-Enrique García-Ramos[2,3], José Miguel Arias[2,4], Lucas Lamata[4], Pedro Pérez-Fernández[1,2]

[1] *Dpto. de Física Aplicada III, Escuela Técnica Superior de Ingeniería, Universidad de Sevilla, Sevilla, Spain.*
[2] *Instituto Carlos I de Física Teórica y Computacional, Universidad de Granada, Granada, Spain.*
[3] *Departamento de Ciencias Integradas y Centro de Estudios Avanzados en Física, Matemática y Computación, Universidad de Huelva, 21071 Huelva, Spain.*
[4] *Departamento de Física Atómica, Molecular y Nuclear, Facultad de Física, Universidad de Sevilla, Sevilla, Spain.*

*e-mail: asaiz@us.es

Summary In this work, we study an extended Agassi model, which describes a many-body system in Nuclear Physics. It is a two-level system that includes a combination of long range monopole-monopole and short range pairing interactions. It presents a very rich quantum phase diagram that gives rise to several quantum phase transitions (QPTs) of different character, making it of great interest in the field of QPTs. We present the aforementioned model, propose an experimental setup for its quantum simulation and analyze its QPTs using machine learning tools.

The model The Agassi model [1] is a two-level system consisting of N interacting fermions, with each of the levels having a Ω degeneracy. The labeling for the single particle states are $\sigma = 1$ for the upper level and $\sigma = -1$ for the lower one. In this work an extended Agassi model is considered, introduced in [2], which includes a more general pairing interaction. Its Hamiltonian is written as

$$H = \varepsilon J^0 - g \sum_{\sigma,\sigma'=-1,1} A^\dagger_\sigma A_{\sigma'} - \frac{V}{2}\left[\left(J^+\right)^2 + \left(J^-\right)^2\right] - 2hA^\dagger_0 A_0. \tag{1}$$

With three parameters g, V and h that specify the quantum phase of the system. For its quantum simulation, we apply a Jordan-Wigner mapping that maps the Hamiltonian into spinless fermion operators. This leaves the Hamiltonian as a sum of Kronecker products of Pauli matrices, which can be simulated through single qubit gates and so-called Mølmer-Sørensen quantum gates.

Quantum Phase Transition analysis We study, for a system of size N=8, a correlation function between sites i, j, which is expressed as: $C(i,j)_{\alpha,\beta} = \langle \sigma^\alpha_i \otimes \sigma^\beta_j \rangle - \langle \sigma^\alpha_i \rangle \langle \sigma^\beta_j \rangle$, where $\alpha,\ \beta = x,\ y$ or z and σ represents the corresponding Pauli matrix. In previous works it was shown that the time dynamics of these correlation functions, evolving from a generic initial state, hold information about the quantum phase of the system [3]. Furthermore, for a digital experimental simulation of the model, where the time evolution is not exact and instead follows Trotterized dynamics, this information is conserved (and even enhanced), even for a small amount of Trotter steps.

To extract the quantum phase of the system, a convolutional neural network (CNN) was trained with classically computed data of the exactly solvable Agassi model and then used to predict another set of computed data. The results are showed in Fig. (1), both using the exact evolution and the Trotter expansion. This CNN accurately predicted the quantum phase of the system in 98.69% (categorical accuracy) of the test cases for the exact evolution. Using the Trotterized evolution with only 6 Trotter steps, the CNN was capable of obtaining a categorical accuracy of 99.21% [4].

Another benefit of the CNN is that it can predict the values of the parameters g, V and h, renamed as $V = \frac{\varepsilon\chi}{3}, g = \frac{\varepsilon\Sigma}{3}, h = \frac{\varepsilon\Lambda}{3}$ for convenience. Fig. (2) shows the predicted values of Σ for the same points of the phase space showed on Fig. (1). The outlier in the left panel (exact evolution) corresponds to the point $\Sigma = 0.3$ where the network shows a greater uncertainty (Fig. 1), but still predicts the correct phase. This kind of outliers disappears for the case where the Trotterized evolution was used, showing an enhanced performance. The predicted values lie within the real ones considering the mean squared error (mse), which is in any case smaller than the step of 0.1 used in Σ.

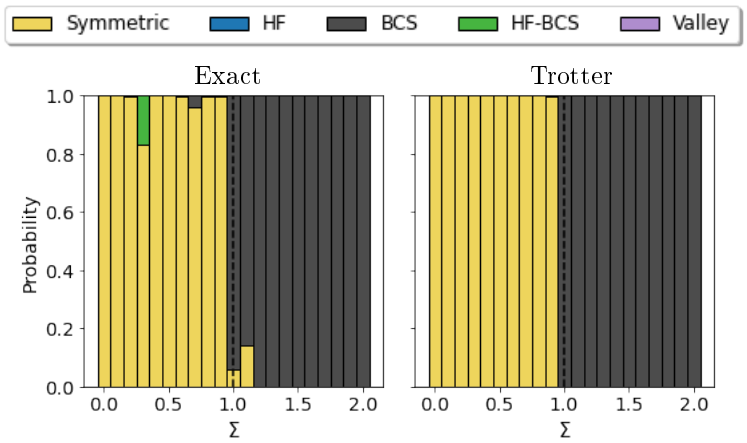

Figure 1. Quantum phase prediction of the system via the Convolutional Neural Network applied to the $\sigma_z(1,2)$ correlation function. The panels show the predicted probability of the system being in a given phase for specific values of the parameter Σ. Each color corresponds to one of the five possible phases. Left panels correspond to the results using the exact time evolution, while right ones using the Trotter approach with $n_T = 6$ Trotter steps. In both cases, the initial state $| \downarrow_1 \downarrow_2 \downarrow_3 \downarrow_4 \uparrow_5 \uparrow_6 \uparrow_7 \uparrow_8 \rangle$ is used. The phase s predicted across the line $\chi = 0.5$ and $\Lambda = 0.5$ moving from $\Sigma = 0$ (symmetric phase) to $\Sigma = 2$ (BCS phase). The theoretical critical point between these phases is $\Sigma = 1$, where a sudden change in the predicted phase is observed.

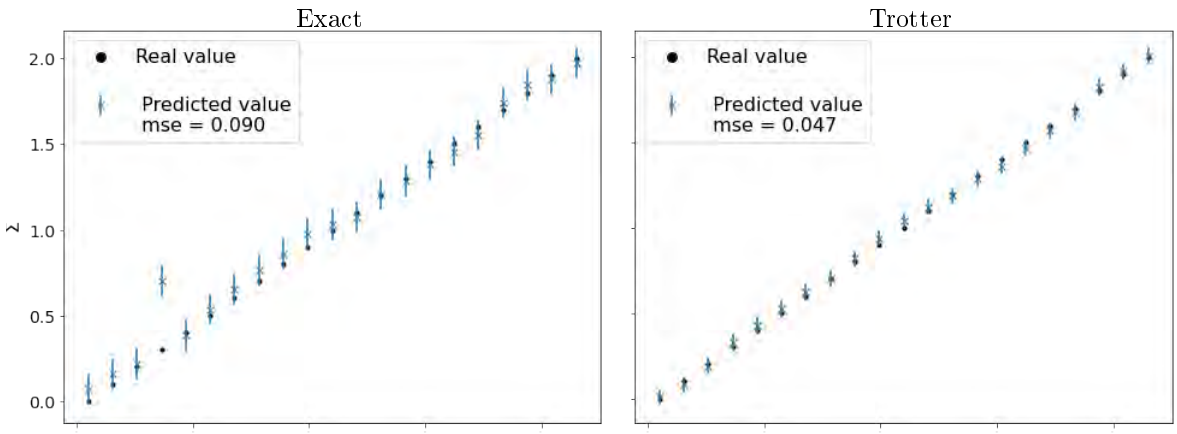

Figure 2. Predicted values of $\Sigma = \frac{3g}{\varepsilon}$ for the same initial state and the same line of the phase space showed on Fig. 1. Real target values represented by black dots, predicted values represented with blue crosses with errorbars showing the mean squared error (mse) of the prediction.

[1] D. Agassi, *Validity of the BCS and RPA approximations in the pairing-plus-monopole solvable model.* Nuclear Physics A, vol. 116, no. 1, pp. 49-71, (1968)

[2] J. E. García-Ramos, J. Dukelsky, Pérez-Fernández, and J. M. Arias, *Phase diagram of an extended Agassi model*, Physical Review C, vol. 97, no. 5, (May 2018).

[3] P. Pérez-Fernández, J. M. Arias, J. E. García-Ramos, and L. Lamata, *A digital quantum simulation of the Agassi model*, submitted to PLB (2021).

[4] A. Sáiz, J. E. García-Ramos, J. M. Arias, L. Lamata, P. Pérez-Fernández, *Quantum Simulations of an Extended Agassi Model in Trapped Ions using Machine Learning*, (work in progress)

Ampliando horizontes: interdisciplinariedad, física general e investigación novel

Presentaciones orales

Lunes 11/07:

15:30-15:45 Welcome and introduction.

15:45-16:00 Alejandro Pozas-Kerstjens (Instituto de Ciencias Matemáticas, CSIC-UAM UC3M-UCM / Dpto. de Análisis Matemático, Univ. Complutense). *Physics solutions to machine learning privacy leaks*

16:00-16:15 Consuelo Guardiola Salmerón (Centro Nacional de Microelectrónica IMB-CNM, CSIC). *High-resolution beam monitoring with 3D-microdetectors*

16:15-16:30 Miguel Ángel Ramos Ruiz (Centro de Microanálisis de Materiales, UAM / Inst. Nicolás Cabrera / IFIMAC). *CMAM: an ion-beam accelerator for multidisciplinary science*

16:30-16:45 María de los Ángeles Millán Callado (Dpto. de Física Atómica, Molecular y Nuclear, Univ. de Sevilla / Centro Nacional de Aceleradores, CSIC-US-Junta de Andalucía). *Image and CT capabilities at Centro Nacional de Aceleradores*

16:45-17:00 Diego Delgado Bueno (Dpto. de Matemáticas, Universidad de León). *Conserved magnitudes in flatwater canoeing*

17:00-17:30 **Pósteres y café**.

18:00-18:15 Ángel Jesús Murcia Gil (Instituto de Física Teórica, UAM-CSIC). *A universal feature of charged entanglement entropy*

18:15-18:30 José María Cámara Zapata (Centro de Investigación e Innovación Agroalimentaria y Agroambiental, Univ. Miguel Hernández). *Greenhouse dehumidification through dynamic overhead ventilation*

18:30-18:45 Pedro Hernández Cascales (Dpto. de Física, Univ. de Murcia). *Morphology of multi-wavelength selected AGN Host-Galaxies*

18:45-19:00 Carlos Yanguas Durán (Dpto. de Automática, Univ. de Alcalá). *Automatic solar burst detection and classification*

Pósteres

- Rosa Cibrián (Universitat de València). *Evaluación del paisaje sonoro de un evento patrimonial en entorno abierto: El Tribunal de las Aguas de Valencia*
- Milagros F. Morcillo Arencibia (Universidad de Córdoba). *Computational study of the Hydrogen molecule inside a C60 fullerene cage*
- Ricard Kirchner (Universidad Politécnica de Catalunya). *Análisis de la invariancia de escala fractal de series temporales de concentración aérea máxima de polen*

Physics solutions to machine learning privacy leaks

Alejandro Pozas-Kerstjens[1,2,*], Senaida Hernández-Santana[3], José Ramón Pareja Monturiol[1,2], Marco Castrillón López[4], Giannicola Scarpa[5], Carlos E. González-Guillén[3], David Pérez-García[1,2]

[1]*Instituto de Ciencias Matemáticas (CSIC-UAM-UC3M-UCM), 28049 Madrid, Spain.* [2]*Departamento de Análisis Matemático, Universidad Complutense de Madrid, 28040 Madrid, Spain.* [3]*Departamento de Matemática Aplicada a la Ingeniería Industrial, Universidad Politécnica de Madrid, Madrid, 28006, Spain.* [4]*Departamento de Álgebra, Geometría y Topología, Universidad Complutense de Madrid, Madrid, 28040, Spain.* [5]*Escuela Técnica Superior de Ingeniería de Sistemas Informáticos, Universidad Politécnica de Madrid, Madrid, 28031, Spain.*

*e-mail: physics@alexpozas.com

For already some years machine learning techniques are being applied in multiple areas of physics in order to attempt to solve difficult problems. The influence goes also in the opposite direction, since tools developed within the realm of physics offer an invaluable perspective on the dynamics of machine learning algorithms. However, despite notable exceptions, the impact of physics in the design of machine learning algorithms is still arguably limited. In this work, we point at physics as a crucial source of inspiration for better machine learning algorithms, especially if one cares about privacy.

First, we identify a new type of privacy leak that involves global properties of the data used for training. Concretely, if the data used for training a machine learning algorithm is imbalanced in some of its features, this imbalance can be detected by only looking at the trained model's parameters, *even if the feature is completely irrelevant for the task* that the algorithm intends to perform. We show that standard neural networks are vulnerable to such privacy leak. Moreover, the state-of-the-art protection mechanisms in machine learning [1] focus on hiding the presence of concrete datapoints in the training dataset. The new vulnerability affects global biases, so it is, a priori, resistant to this protection.

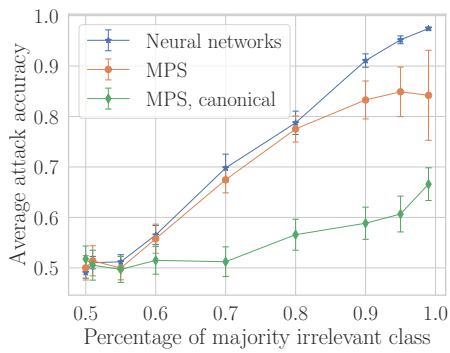

Figure 1. Accuracy of attacks attempting to predict properties of a training dataset consisting of medical records. Importantly, the MPS not expressed in canonical form are vulnerable in a similar way to the neural networks, but the canonical-form MPS achieve a high degree of security.

Second, we make an important connection between privacy and physics. We rigorously prove [2] that robustness to this new vulnerability can be achieved if one can characterize and access the equivalents of a trained model under gauge transformations. Gauge symmetry is a central concept in many areas of physics, ranging from relativity to particle physics. We illustrate the power of gauge symmetry in machine learning by formally proving and showing in practice that matrix product state architectures (MPS) are robust to the vulnerability described (see Figure 1). MPS are inspired by the theory of efficient representation of quantum many-body systems [3], and its use in machine learning is recently showing competitive, and in certain cases better [4], results than standard approaches. Importantly, robustness to the vulnerability discovered is inherent in MPS. This means that, in contrast with traditional solutions for privacy in machine learning [1], in MPS the protection does not impact the performance of the model.

Given the growing expertise in training tensor networks and the recent interest in tensor-based reformulations of popular machine learning architectures, these results imply that, after all, one may not need to make a choice between accuracy in prediction and ensuring the privacy of the information processed when using machine learning on sensitive data. More importantly, they point to physics as a very promising source of inspiration for better machine learning algorithms and architectures.

[1] C. Dwork, F. McSherry, K. Nissim, and A. Smith, *J. Priv. Confid.* **7**, 17 (2017).
[2] A. Pozas-Kerstjens *et al.*, arXiv:2202.12319 (2022).
[3] F. Verstraete, V. Murg, and J. I. Cirac, *Adv. Phys.* **57**, 143 (2008).
[4] J. Wang, C. Roberts, G. Vidal, and S. Leichenauer, arXiv:2006.02516 (2020).

High-resolution beam monitoring with 3D-microdetectors

D. Bachiller-Perea[1], C. Fleta[2], F. Gómez[3], **C. Guardiola**[2,*]

[1]*Université Paris-Saclay, CNRS/IN2P3, IJCLab, 91405 Orsay, France.*
[2]*Centro Nacional de Microelectrónica (IMB–CNM, CSIC), Bellaterra, 08193, Spain.*
[3]*Dep. de Física de Partículas, Universidad de Santiago de Compostela, 15782, Spain.*

*e-mail: consuelo.guardiola@imb-cnm.csic.es

The present work reports on the measurements performed at the Accélérateur Linéaire et Tandem à Orsay (ALTO) facility with the first multi-arrays of microdosimeters with the highest radiation sensitive surface covered so far. The sensors are based on new silicon-based radiation detectors with a novel 3D cylindrical architecture [1]. Each system consists of arrays of independent microdetectors covering 2 mm x 2 mm and 0.4 mm x 12 cm areas, which are arranged in layouts of 11x11 microdetectors and 3x3 multi-arrays, respectively (Fig. 1). We have performed proton irradiations at several energies to compare the performance of the two systems (Fig. 2). The unit-cell of both arrays is a 3D cylindrical diode with a 25 mm diameter and 20 µm thick. Measurements were carried out by irradiating the two detection systems with monoenergetic proton beams from 6 to 20 MeV at clinical-equivalent fluence rates. The microdosimetry quantities were obtained with a spatial resolution of 200 µm and 600 µm for the 11x11 system and for the 3x3 multi-array system, respectively (Fig. 3). Experimental results were compared with Monte Carlo simulations and an overall good agreement was found (Fig. 4). The good performance of both microdetector arrays demonstrates that this architecture can be employed as a multipurpose device for beam monitoring in particle accelerators.

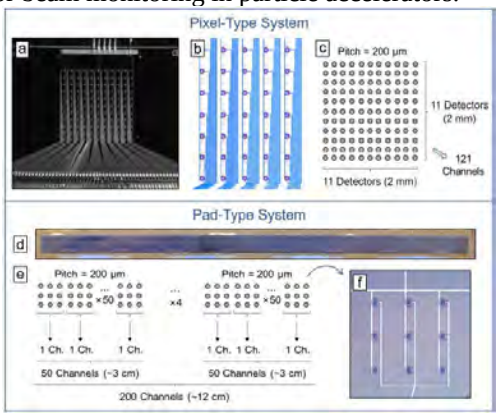

Figure 1. a) Optical image of the 11x11 pixel array. b) Detail of the pixel layout. c) Sketch of the pixel array. d) Photograph of the eight pad-type arrays stacked laterally covering a 12 cm length. e) Sketch of the pad-type array. f) Optical image of one of the 3x3 cells.

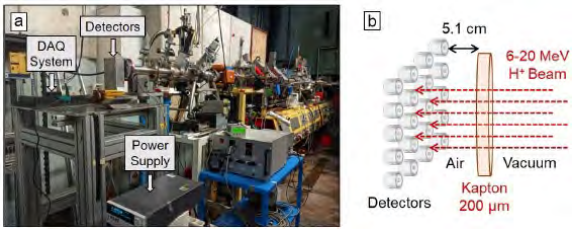

Figure 2. a) Photograph of the experimental setup used for the irradiations at the beamline 410 of ALTO. The distance between the front face of the detectors and the exit window of the beamline was 5.1 cm. b) Sketch of the irradiation configuration.

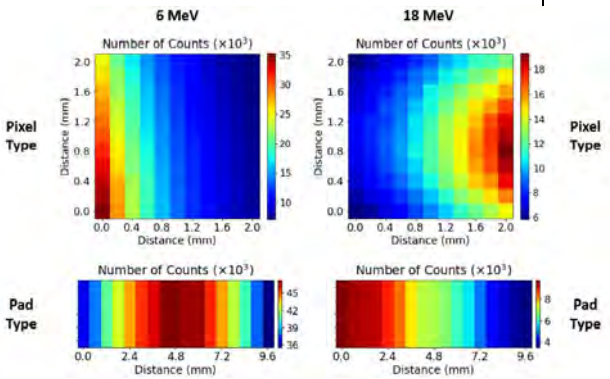

Figure 3. Number of counts measured with 6 and 18 MeV proton beams. Top: pixel-type system. Bottom: 1 cm representative region of the pad-type system (not to scale).

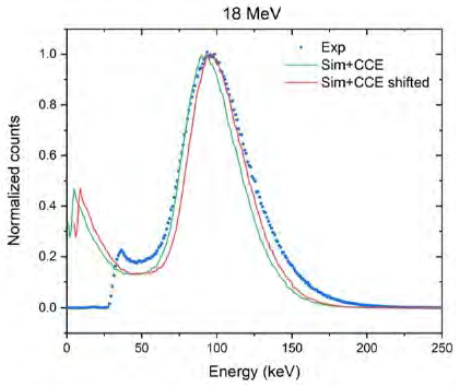

Figure 4. Experimental energy spectra (blue), Monte Carlo simulations of the spectra (green and red) for 18 MeV proton beams.

[1] Guardiola C., et al., *Applied Physics Letters* **107**, 023505 (2015).
[2] Bachiller-Perea D. et al., accepted in *Scientific Reports* 10.21203/rs.3.rs-1107731/v1.

CMAM: an ion-beam accelerator for multidisciplinary science

Miguel A. Ramos[1,2,3,*], Silvia Viñals[1], Nuria Gordillo[1,2,4], Andrés Redondo-Cubero[1,2,4], Gastón García[1]

[1]*Centro de Microanálisis de Materiales (CMAM), Universidad Autónoma de Madrid, 28049 Madrid, Spain.* [2]*Instituto "Nicolás Cabrera", Universidad Autónoma de Madrid, 28049 Madrid, Spain.* [3]*Departamento de Física de la Materia Condensada, Condensed Matter Physics Center (IFIMAC), Universidad Autónoma de Madrid, 28049 Madrid, Spain.* [4]*Departamento de Física Aplicada, Universidad Autónoma de Madrid, 28049 Madrid, Spain.*

*e-mail: miguel.ramos@uam.es

The Center for Micro-Analysis of Materials (CMAM) [1] at Universidad Autónoma de Madrid (UAM) is an ion beam facility equipped with a 5 MV tandem accelerator and six beam-lines implementing different techniques for analysis and modification of materials at the nanoscale [2]. CMAM operates on the basis of combining a dynamical own scientific program by ascribed scientists with an open user access system, all supported by a team of scientists, technologists and technicians. Recently, the facility has been recognized by the incorporation to the Spanish ICTS (Instalaciones Científico-Técnicas Singulares) map, where it will work in coordination with the CNA (Seville) facility, as a two-node distributed research infrastructure.

The beamlines available at CMAM offer very interesting opportunities to the scientific and industrial communities, making available different ion-beam analysis techniques (such as RBS, ERD, PIXE, PIGE and NRA) and opening the possibility to modify the properties of materials by ion irradiation. Practically any ion species of the periodic table may be accelerated and beam energies may reach 10 MeV for protons, 15 MeV for He and several tens of MeV for mid-mass or heavy ions, reaching the 40-50 MeV range.

Among the many fields in which scientific activities at CMAM may be featured, we have chosen two: (i) irradiation studies for biomedical applications, and (ii) processing of materials for quantum technologies.

(i) Proton beams are an extremely attractive tool for oncological radiotherapy. The beam energies necessary for clinical practice are much higher than those available at CMAM, but 10 MeV protons are ideal for radiobiology experiments in cells culture. During the last few years, CMAM has been increasingly collaborating with different user groups, performing irradiation experiments of different biological samples and under different beam conditions.

(ii) Some of the materials of interest for quantum technologies are very good candidates for processing techniques based on ion beam irradiation. Specifically, we are interested in irradiating diamond crystals, either to produce boron-doped diamond (which can be a superconductor) or nitrogen-vacancy centers (which act as sensitive color centers, useful for magnetometry). We are also exploring the possibility to fabricate amorphous bismuth-antimony films, which could potentially be topological superconductors.

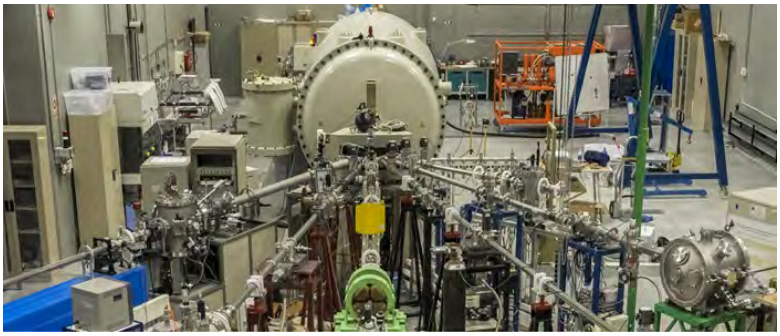

Figure 1. Panoramic view of the CMAM experimental hall.

[1] https://www.cmam.uam.es/
[2] A. Redondo-Cubero et al., *Eur. Phys. J. Plus* **136**, 175 (2021).

Image and CT capabilities at Centro Nacional de Aceleradores

E. M. García-Zamora[2], **M. A. Millán-Callado**[1,2,*], F.J. Ager[1,3], B. Fernández[1,2], C. Guerrero[1,2], M. C. Jiménez-Ramos[2], P. Martín-Holgado[2], Y. Morilla[2], M. A. Respaldiza[1,2], T. Rodríguez-González[1,2], J. Gómez[1,2], J. M. Quesada[1]

[1]*Dpt. Física Atómica, Molecular y Nuclear (FAMN), Facultad de Física. Universidad de Sevilla (US), Av. de la Reina Mercedes, s/n, 41012 Seville, Spain.*
[2]*Centro Nacional de Aceleradores (CSIC-US-Junta de Andalucía), C/ Tomás Alba Edison, 7. 41092. Seville, Spain.*
[3]*Dpt. Física Aplicada I, Escuela Politécnica Superior. Universidad de Sevilla (US), Av. de la Reina Mercedes, s/n, 41012 Seville, Spain.*

*e-mail: mmillan5@us.es

Centro Nacional de Aceleradores (CNA) is a singular scientific-technical facility located in the Isla de la Cartuja Scientific-Technological Park, Seville. Its installations include a 3MV Tandem accelerator, in which the first accelerator-based neutron source in Spain is installed, a 18/9 MeV Cyclotron accelerator and a ^{60}Co irradiator. In addition to these, CNA also has a clinical PET/CT scanner and portatile X-ray tubes used for studies in X-ray fluorescence.

Since 2018, a number of imaging campaigns have been carried out at the CNA installations, taking advantage of the different irradiation sources, in order to assess their potential for image analysis techniques and its complementarity. In this context, commercially available cameras, scintillators and CCD image sensors have been utilised to perform radiography with X-rays, gamma rays and thermal and fast neutrons.

In this work, the experimental setup optimization is presented, both in image resolution and image quality, as well as exposure time of the final images. The preliminary results of non-destructive testing applied to archaeological object dummies and cultural heritage objects are also shown.

Recently, a commercial rotating turntable, which allows us to perform computed tomography, has also been purchased. This technique has been successfully applied, both with gamma rays and neutrons, to cultural heritage objects and cultural heritage dummies.

Conserved magnitudes in flatwater canoeing

Diego Delgado Bueno

Departamento de Matemáticas, Universidad de León, Spain.

e-mail: ddelb@unileon.es

The field research in flatwater canoeing is developing hardware able of collect synchronized data of acceleration, velocity and applied force versus time, at high sample rates and with good precision. Some months ago we have proposed one dimensional mathematical model for kayak propulsion [1]. This model is supported in a few input constants and in the functional description of the paddler applied force. The so mentioned analysis of field data demonstrates that two conserved magnitudes appear, the average force to stroke frequency ratio,

$$\frac{< f >}{\nu},$$

and the squared asymptotic velocity to stroke frequency ratio.

$$\frac{v_\infty^2}{\nu}$$

Where ν represents the stroke frequency. From the results of our model, it could be deduced a relation between both magnitudes through the drag coefficient, and to develop one to reach an interesting merit figure to estimate paddler competence and efficiency. The product of the average force integrated over the water phase times the water phase duration, written as:

$$< f >_w \cdot t_w$$

A conserved magnitude as well. Expression that could be reduced, by introducing the integral expression for the average, to reach.

$$\int_0^{t_w} f(t) \cdot dt$$

That in geometrical terms means that average force integrated over the water phase is conserved as stroke frequency increase (and the water phase logically decreased). This merit figure could be a valuable estimator of paddler competence as we will show.

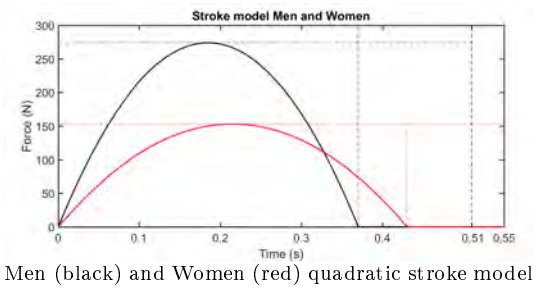

Men (black) and Women (red) quadratic stroke model for maximum frequency. Stroke based on data from Gomes et al. [2].

[1] Delgado, D., Ruiz, C., *Applied Sciences* **11**, (2021).
[2] Gomes, B. B., Ramos, N. V., Conceição, F. A., Sanders, R. H., Vaz, M. A., Vilas-Boas, J. P., *Journal of Applied Biomechanics* **31**, (4) (2015).

A universal feature of charged entanglement entropy

Pablo Bueno[1], Pablo A. Cano[2], **Ángel Murcia**[3,*], Alberto Rivadulla Sánchez[4,5]

[1]*CERN, Theoretical Physics Department, CH-1211 Geneva 23, Switzerland.*
[2]*Instituut voor Theoretische Fysica, KU Leuven. Celestijnenlaan 200D, B-3001 Leuven, Belgium.*
[3]*Instituto de Física Teórica UAM/CSIC. C/ Nicolás Cabrera 13-15, C.U. Cantoblanco, E-28049 Madrid, Spain.*
[4]*Departamento de Física de Partículas, Universidade de Santiago de Compostela, E-15782 Santiago de Compostela, Spain.*
[5]*Instituto Galego de Física de Altas Enerxías (IGFAE), Universidade de Santiago de Compostela, E-15782 Santiago de Compostela, Spain.*

*e-mail: angel.murcia@csic.es

Rényi entropies, S_n, admit a natural generalization in the presence of global symmetries. These "charged Rényi entropies" are functions of the chemical potential μ conjugate to the charge contained in the entangling region and reduce to the usual notions as $\mu \to 0$. For $n = 1$, this provides a notion of charged entanglement entropy. In this letter we prove that for a general $d(\geq 3)$-dimensional CFT, the leading correction to the uncharged entanglement entropy across a spherical entangling surface is quadratic in the chemical potential, positive definite, and universally controlled (up to fixed d-dependent constants) by the coefficients C_J and a_2. These fully characterize, for a given theory, the current correlators $\langle JJ \rangle$ and $\langle TJJ \rangle$, as well as the energy flux measured at infinity produced by the insertion of the current operator. Our result is motivated by analytic holographic calculations for a special class of higher-curvature gravities coupled to a $(d-2)$-form in general dimensions as well as for free-fields in $d = 4$. A proof for general theories and dimensions follows from previously known universal identities involving the magnetic response of twist operators introduced in `arXiv:1310.4180` and basic thermodynamic relations.

Greenhouse dehumidification through dynamic overhead ventilation

J. M. Cámara-Zapata*, C. Rocamora, H. Puerto

[1]*Centro de Investigación e Innovación Agroalimentaria y Agroambiental (CIAGRO), Universidad Miguel Hernández.*

*e-mail: jm.camara@umh.es

High environmental humidity is one of the main problems of greenhouse plant production. When the temperature is low, condensation occurs on the interior surfaces, which modifies the optical properties of the cover material and, consequently, can alter photosynthetic activity. Plant transpiration is also affected, and with it, calcium uptake, hormone distribution, ion pumping, and the opening and closing of stomata, reducing CO2 uptake and crop yield. In addition, the risk of cryptogamic diseases is increased, which is why it is necessary to intensify the treatments with pesticides, with the consequent risk to the health of the consumer. With the purpose of contributing to improve the economic and environmental profitability of greenhouse plant production, the prototype of an environmental humidity control device consisting of an overhead mechanical ventilation system has been used. The results show an important reduction of the specific humidity inside the greenhouse.

Figure 1 shows the evolution of the properties most affected by the operation of the system, the specific humidity (ω, g_{vapor} $kg_{dry\ air}^{-1}$) and the vapor pressure deficit (DPV, kPa). The central black box represents the test interval of February 2, 2022.

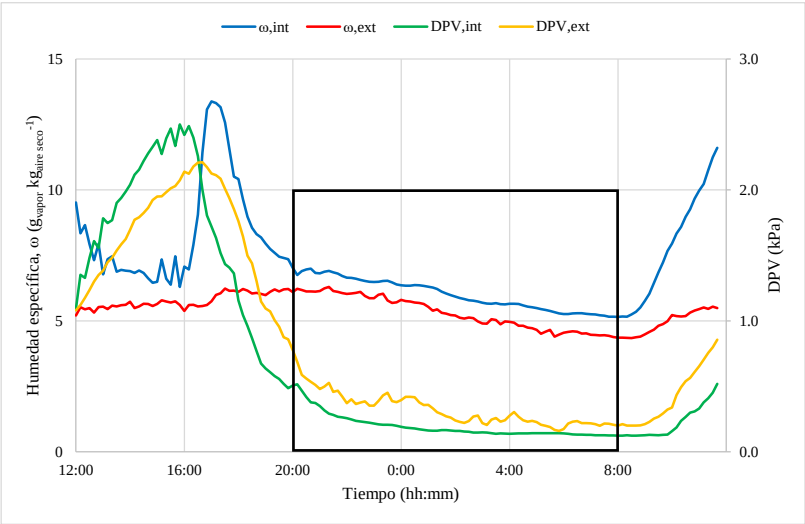

Figure 1. Evolution of specific humidity (g kg^{-1}) and vapor pressure deficit (VPD, kPa) indoors and outdoors on February 2, 2022.

Morphology of multi-wavelength selected AGN Host-Galaxies

Diego Tuccillo[1], **Pedro Hernández Cascales**[2,*], Francisco Carrera Troyano[1], Javier Bussons Gordo[2]

[1]*IFCA: Galaxies and AGNs, Av. de los Castros, 39005 Santander, Cantabria, Spain.* [2] *UM:Department of Physics, C.Campus Universitario, 5, 30100 Murcia, Spain.*

*e-mail: pedro.hernandezc@um.es

Over recent years, fundamental relationships between the Active Galactic Nuclei(AGN) and their host galaxies properties have been found, catching the attention of the scientific community on the connection between galaxy evolution and AGN activity. It is now clear that understanding this connection is critical in any attempt to map out the evolutionary pathways of both galaxies and AGN over cosmic time. In this context the study of the galaxy morphology represents one of the most accessible indicators of the galaxy physical structure and can provide valuable clues about star formation and interaction histories. In these studies, high-quality multi-wavelength data are essential to disentangle real co-evolutionary properties from bias due to selection effects and poor statistics.

In this work we study the morphological properties of galaxies hosting AGN compared to those of non active galaxies. In particular we investigate if there is a relationship between the spectral range used in AGN selection and the morphology of the host galaxy.

We identified a sample of 466 AGN in the GOODS-SOUTH CANDELS field, selected with methods based on their emission properties in different wavebands, including:optical variability, X-ray selection, infrared-selection, radio-selection. Different samples of AGN have been compared with each other and with samples of non active galaxies matched in redshift and magnitude.

The results show a notable difference between the non morphological magnitudes of active and non-active galaxies. They equally show that AGN-hosting galaxies tend to have an spheroidal bulge, this effect is mainly present in AGN identified via X-rays. Finally, results also show that non-active galaxies are irregular more frequently. In view of these results, there seems to be a relationship between the presence of an AGN and it's hosting galaxy morphology.

Acknowledgements: I would like to thank my tutors Diego, Francisco y Javier for all their help and patience with me. They have helped me to discover a wonderful field. I would also like to thank my family and friends whose support has been essential not only to complete this work but for my every day life.

Automatic solar burst detection and classification

Carlos Yanguas

Automation Department, Campus Universitario, Ctra. Madrid-Barcelona km, 33, 600, 28805 Alcalá de Henares

e-mail: carlos.yanguas@edu.uah.es

Radio bursts from the solar corona provide information to predict space weather hazards. These risks are due to the fact that this phenomenon will cause interference to our radio wave signal and affect the electromagnetic spectrum on earth, which could doom the entire line of communications, including the operation of satellites, the navigation system, the Global Positioning System (GPS), the international power grid and many more.

Since solar radio emissions are in the low frequency range, the detector system consists of a low frequency receiver, in our case the Compact Low Cost Low Frequency Astronomical Instrument for Spectroscopy and Transportable Observatory (CALLISTO).

Based on the morphology and drift rates in the dynamic spectrograms, there are five primary types of radio bursts, type I, type II, type III, type III, type IV and type V as well as other complex bursts that are often observed in the solar corona. Given the importance of this phenomenon and recent technological advances, regular monitoring of radio bursts has increased and large observational data sets have been produced. Therefore, their manual identification and classification is a difficult task implying great human effort for their detection and classification.

In this work, a system for automatic detection and classification of these solar events based on deep neural networks has been devised. Specifically, YOLO in its version four, has been trained with solar events reported since 2020 through manual labeling of solar events, resulting in a model that allows detecting solar events on high-contrast spectrograms generated with typical operations such as background removal. This whole process also has the advantage that it has been developed with open source tools, minimizing the cost of the system.

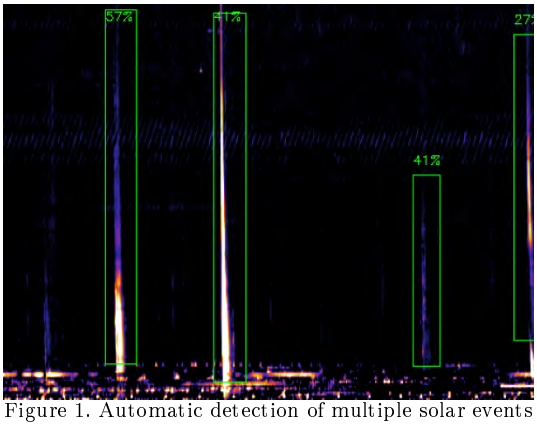

Figure 1. Automatic detection of multiple solar events by YOLO.

This work has been funded by the Junta de Comunidades de Castilla-La Mancha and the European Union (reference: SBPLY/19/180501/000237). With the collaboration of PCTCLM.

Acknowledgements: To the entire CELESTINA project team, especially Manuel Prieto, Javier Bussons and Mario Fernández.

Evaluación del paisaje sonoro de un evento patrimonial en entorno abierto: El Tribunal de las Aguas de Valencia

Elena Díaz[3], **Rosa Cibrian**[1,*], Jaume Segura[2], Alicia Giménez[3]

[1]*Dpt Fisiología, Universitat de València.* [2]*Dpt Informática, ETSE-Universitat de València.* [3]*Dpt Física Aplicada, ETSII-Universitat Politècnica de València.*

*e-mail: rosa.m.cibrian@uv.es

La evaluación acústica de entornos interiores es habitual en la aplicación de la acústica virtual. Además, en el estudio de edificios del patrimonio cultural, es una herramienta útil, pero no es tan común en la descripción de ambientes acústicos de eventos en ambientes exteriores. En este trabajose estudia el entorno acústico del Tribunal de las Aguas de Valencia (España). Se analiza desde la perspectiva del paisaje sonoro, caracterizando la fuente sonora y valorando la respuesta subjetiva.

El Tribunal de las Aguas es una antigua institución dedicada a regular y dirimir los conflictos en la gestión de los recursos hídricos de las acequias de Valencia y alrededores. Las sentencias de este tribunal tienen validez jurídica en el territorio valenciano, y constituyen una parte del antiguo Derecho Civil Valenciano que actualmente se está tratando de recuperar en el ámbito jurisprudencial.

La simulación acústica se realizó a partir del modelado del entorno y su ajuste a partir de la medida acústica realizada en el entorno de este evento, que es Patrimonio Inmaterial por UNESCO. Además, se caracterizó en la cámara anecóica de la UPV, una de las principales fuentes sonoras en este evento, que es el alguacil que anuncia a los participantes y se integró en el programa de simulación acústica ODEON (https://github.com/ACUSVIRT/Tribunal). El estudio acústico permitió generar una auralización dinámica a partir de la interpolación de diferentes respuestas impulsivas en un recorrido prefijado. Junto con la simulación acústica y la auralización generada se realizó un modelado visual para la navegación por el entorno y su integración se puede observar en el vídeo https://www.youtube.com/watch?v=JHOxuCvG7n8&t=21s[1]. Además, se realizó la evaluación de la respuesta subjetiva a partir de una encuesta pública basada en el "protocolo sueco de calidad del paisaje sonoro" [2]. Las estadísticas obtenidas (en escala Likert, donde 1 es "muy de acuerdo" y 5 es "muy en desacuerdo") en relación al "protocolo sueco", para las valoraciones del paisaje sonoro percibido por los encuestados muestran que, en general, aunque los oyentes perciben el paisaje sonoro como poco molesto (4,03/1,37), poco caótico (4,19/1,05) y ligeramente emocionante (3,42/1,27) debido a la reverberación percibida, lo interpretan como monótono (2,26/1,25) y poco activo (2,46/1,48), ya que en nuestro caso el evento auralizado sólo presenta una fuente sonora principal (alguacil), pero con reverberación interpolada en cada posición.

(a) (b)

Figura 2. (a) Vista general de la simulación visual del Tribunal de las Aguas. (b) Detalle de la representación de una sesióndel Tribunal de las Aguas.

[1] Díaz-Rubio, E.; Segura-Garcia, J.; Fayos-Jordan, R.; Cerdá, S.; Cibrián, R.M.; Giménez-Pérez, A., Sounds- cape Evaluation of a Heritage Event in an Open Environment: The Water Tribunal of the Plain of Valencia (Spain). *Appl. Sci.* **12**, 4292 (2022).
[2] Axelsson, O.; Nilsson, M.E.; Berglund, B., The Swedish soundscape-quality protocol, *J. Acoust. Soc. Am.* **131**, 3476 (2012).

Acknowledgements: Esta investigación ha sido parcialmente financiada por el Ministerio de Ciencia, Innovación y Universidades de España, subvención número BIA2016-76957-C3-3-R y por la Universitat de Valencia con la beca UV-INV-AE-1550319.

Computational study of the Hydrogen molecule inside a C_{60} fullerene cage

Milagros F. Morcillo Arencibia[1,*], José Manuel Alcaraz-Pelegrina[1], Juan M. Randazzo[2], Antonio J. Sarsa Rubio[1]

[1] *Departamento de Física, Universidad de Córdoba, España.* [2] *Consejo Nacional de Investigaciones Científicas y Técnicas, Argentina.*

*e-mail: f22moarm@uco.es

Endohedrally confined systems have been a subject of great interest during the recent rears [1, 2]. Besides a few exceptions [3, 4], spherical confinement is considered to study the system, i. e. the system is around the center of the spherical potential.

In this work we address the problem of the Hydrogen molecule under off-centered spherical confinement using two different spherical coordinate systems: a) the one associated to the confining cavity, and b) the one related to the Coulomb charge of the molecule. Off-centered treatment implies that the potential which is not centered needs to be analysed through a partial wave expansion approach.

The purpose of this study is the characterization of the convergence behaviour of the electronic ground state energie of the Hydrogen molecule as a function of the displacement in each one of the aforementioned approximations. A combination of two Woods-Saxon potentials is used to model a C_{60} fullerene cage as the confining environment [5].

Our results show a better performance of the second approach. In Figure 1 we plot the energy of the ground state energy of the H_2 molecule as a function of the position of the centre of the confining cavity, R_{OC}, for different maximum number of partial waves, L, in the expansion. A good accuracy of the energy is obtained from $L = 2$ onwards in the full range of positions of the cavity. The minimum energy coincides with the nuclei close to the structure of the confining cage, therefore the molecule is likely to tend to be in that location.

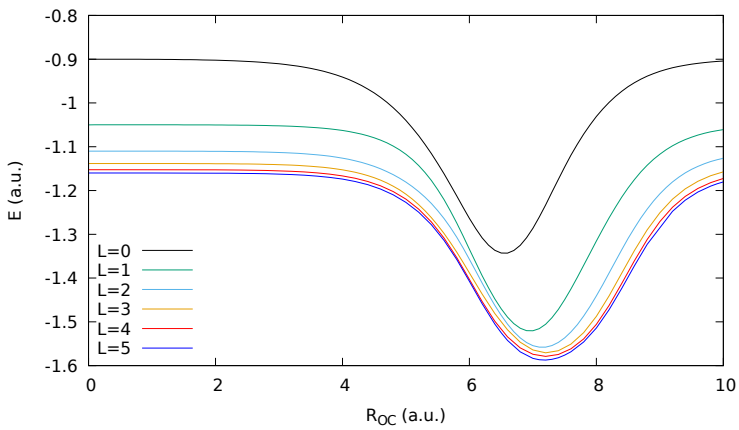

Figure 1. Convergence of the ground state energy of the confined Hydrogen molecule with moving nuclei as a function of the displacement and for different partial waves.

[1] K.D. Sen, *Electronic Structure of Quantum Confined Atoms and Molecules*, Springer-Verlag (2014).
[2] V. Aquilanti et al., *Eur. Phys. J. D - Topical Issue: Atoms and Molecules in a Confined Environment*, Springer Nature (2021).
[3] M. Neek-Amal, G. Tayebirad, R. Asgari, *J. Phys. B: At. Mol. Opt. Phys.* **40**, 1509 (2007).
[4] J.M. Randazzo, C.A. Ríos, *J. Phys. B: At. Mol. Opt. Phys.* **49**, 235003 (2016).
[5] C. Martínez-Flores, *Phys. Lett. A* **386**, 126988 (2021).

Acknowledgements: This work was partially supported by the Spanish Ministerio de Ciencia e Innovación under contract PID2020-114807GB-I00, the Junta de Andalucía grant FQM378 and the Universidad de Córdoba under a grant from the program "Plan Propio de Investigación 2019". M.F.M.A. acknowledges partial support by a Ph.D fellowship from the Spanish Ministerio de Universidades under grant FPU16/05950.

Análisis de la invariancia de escala fractal de series temporales de concentración aérea máxima de polen

Ricard Kirchner[1,*], Raúl Rodríguez-Solà[2], M. Carmen Casas-Castillo[1], Marta Alarcón[3], Cristina Periago[3], Jordina Belmonte[4,5]

[1]*Departmento de Física, ESEIAAT, Universitat Politècnica de Catalunya, Colom 1, 08222 Terrassa (Barcelona), Spain.*
[2]*Departmento de Física, ETSEIB, Universitat Politècnica de Catalunya, Avda. Diagonal 647, 08028 Barcelona.*
[3]*Departmento de Física, EEBE, Universitat Politècnica de Catalunya, Eduard Maristany 16, 08019 Barcelona.*
[4]*Dept. de Biología Animal, de Biología Vegetal y de Ecología, Universitat Autònoma de Bellaterra, 08193 Bellaterra.*
[5]*Institut de Ciències I Tecnologia Ambientals (ICTA-UAB), Universitat Autònoma de Bellaterra, 08193 Bellaterra.*

*e-mail: ricard.kirchner@upc.edu

En la naturaleza es común observar estructuras que al dividirlas en partes, éstas tienen una forma similar al total original. A éste fenómeno se le conoce como auto-similitud fractal y se dice que dichas estructuras muestran invariancia de escala. A diferencia de los fractales matemáticos en los que las partes son una copia exacta de la totalidad, en los procesos naturales la auto-similitud fractal suele tener un carácter estadístico. El desarrollo de teorías basadas en la invariancia de las propiedades de un sistema dinámico a través de las escalas ha permitido que algunos patrones naturales que aparecen extremadamente complejos puedan mostrar una simplicidad subyacente que facilita su estudio. Por ejemplo, el proceso de la generación de lluvia, como en el caso de otros fenómenos atmosféricos, se considera un complejo proceso dinámico no lineal que puede resultar más sencillo de analizar estudiando las relaciones de escala de una de sus posibles manifestaciones, las series temporales de intensidad.

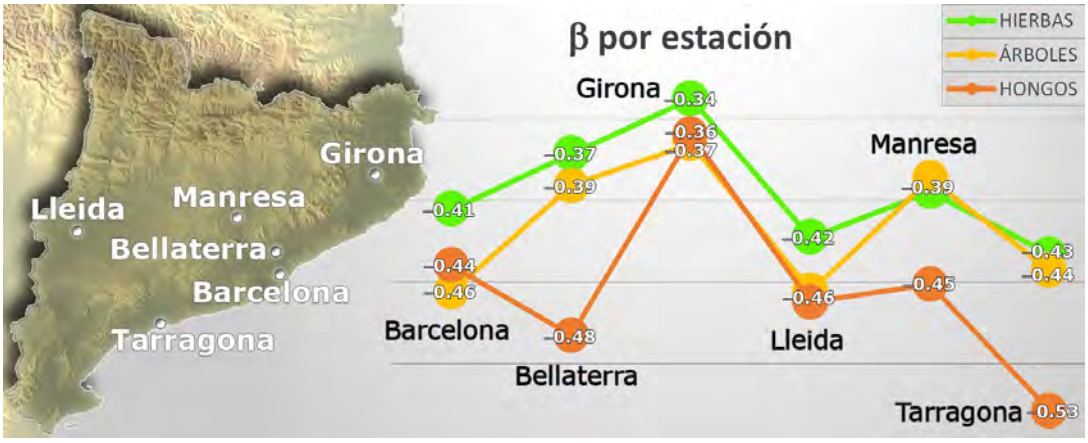

Figura 1. Valores medios del parámetro de escala simple β en estaciones aerobiológicas de Catalunya.

De una manera análoga, en este trabajo se han analizado las relaciones de escala simple de las series temporales de concentración aérea máxima de polen y esporas de varias especies, medidas en seis estaciones aerobiológicas de Catalunya, con el fin de simplificar el estudio de procesos tan complejos como la polinización y la esporulación. Introduciendo la magnitud I_t para una cierta escala temporal t, calculada como la concentración máxima dividida por la duración de la medida, esta magnitud satisface una relación de escala simple si se puede describir mediante una distribución estadística que resulta idéntica para los dos miembros de la ecuación $I_t = \lambda^{\beta q} I_{\lambda t}$, en la cual λ es la relación de escala y q el orden de sus momentos estadísticos. Si el parámetro de escala β ha mostrado ser un buen indicador de la irregularidad del régimen pluviométrico, con valores cercanos al límite inferior de -1 en el caso de registros muy irregulares y más altos conforme aumenta la regularidad [1], para la concentración aérea máxima de polen los valores medios por localidad que se muestran en la Fig.1 resultan ligeramente más altos para las especies herbáceas que para el que procede de árboles, siendo los menores los correspondientes a las esporas. También se ha encontrado correlación entre β y el promedio y el coeficiente de variación de la suma de concentraciones diarias en un año, APIn, en cada estación.

[1] Casas-Castillo MC, Rodríguez-Solà R, Llabrés- Brustenga A, García-Marín AP, Estévez J, Navarro X. A Simple Scaling Analysis of Rainfall in Andalusia (Spain) under Different Precipitation Regimes, *Water* **14**, 1303 (2022). https://doi.org/10.3390/w14081303.

Otros actos

Grupo de estudiantes

Martes 12/07:

15:30-17:00 Mesa redonda. *Estudiantes de física por España*

Diana Andrés Bautista (Instituto de Instrumentación para Imagen Molecular, UPV).

Laura Pérez Molina (Centro de Investigaciones Energéticas, Medioambientales y Tecnológicas, CIEMAT).

Rodrigo Martín Hernández (Universidad de Salamanca).

Pablo Sánchez Palencia (Universidad Politécnica de Madrid).

Victoria Vedia (TRIUMF, British Columbia, Canada).

Moderador: Pedro Villalba González (University of British Columbia)

Premios de DFMC-GEFES

Jueves 14/07:

16:00-16:15 Antonio Benítez, Experimental thesis award 2020-2021. *Spin-orbit phenomena in proximitized graphene*

16:15-16:30 Adolfo Otero, Theoretical thesis award (ex-aequo) 2020-2021. *Interplay between Ferromagnetic and Charge Density Wave orders in Transition Metal Dichalcogenides*

16:30-16:45 Ricardo Ortiz, Theoretical thesis award (ex-aequo) 2020-2021. *Electronic and spin properties of open- shell nanographenes*

16:45-17:00 Nicolás Agrait (on behalf of Laura Rincón García), Experimental thesis award 2019-2020. *Quantum thermopower of single-molecule junctions*

17:00-18:00 **Café**.

18:00-18:15 Juan Camilo López Carreño, Theoretical thesis award 2019-2020. *Exciting with Quantum Light*

18:15-18:30 Eva Cortés, Best article 2020-2021. *Observation of Yu-Shiba-Rusinov states in superconducting graphene*

18:30-18:45 Javier Argüello Luengo, Best article 2019-2020. *Simulating quantum chemistry using ultracold atoms*

Real
Sociedad
Española de
Física

R.S.E.F.

XXXVIII
Reunión Bienal
Murcia, 11-15 julio 2022
Real Sociedad Española de Física